Medical Radiology

Diagnostic Imaging

A.L. Baert
M.F. Reiser
H. Hricak
M. Knauth

D. Prayer
Editor

Fetal MRI

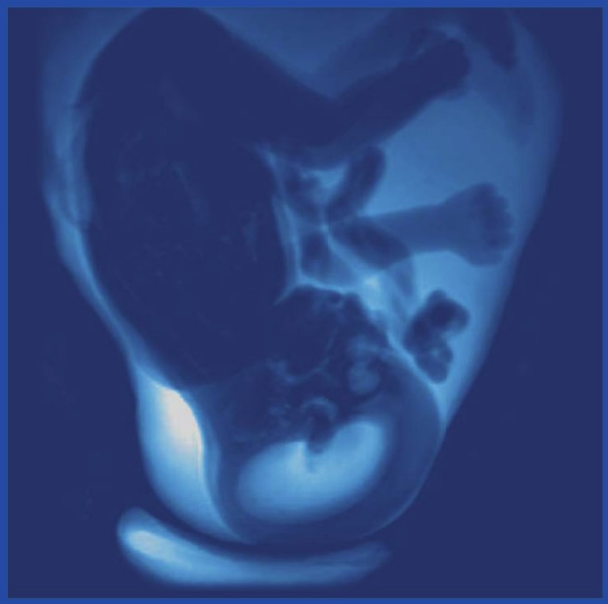

Springer

Medical Radiology

Diagnostic Imaging

Series Editors

For further volumes:
http:/www.springer.com/series/4354

Medical Radiology

Diagnostic Imaging

Editorial Board

Daniela Prayer (Ed.)

Fetal MRI

Foreword by
Albert L. Baert

Springer

Editor
Prof. Daniela Prayer
Medizinische Universität Wien
Klinik für Radiodiagnostik
Währinger Gürtel 18-20
1090 Wien
Österreich
daniela.prayer@meduniwien.ac.at

ISSN: 0942-5373

ISBN: 978-3-540-73270-9 e-ISBN: 978-3-540-73271-6

DOI: 10.1007/978-3-540-73271-6

Springer Heidelberg Dordrecht London New York

Library of Congress Control Number: 2011921700

Cover design: eStudioCalamar, Figueres/Berlin

Printed on acid-free paper

Springer is part of Springer Science+Business Media (www.springer.com)

Foreword I

It is my great pleasure and privilege to introduce another volume, published in our book series: "Medical Radiology – Diagnostic Imaging," whose aim is to focus on cutting-edge developments in the field of medical imaging.

Fetal MRI is without doubt one of the most exciting applications in clinical MRI imaging. It offers superb and frequently unique anatomical information on several organs of the fetus such as the brain and the heart without the need for ionizing radiation.

Recent technical progress in equipment design, as well as in computer hardware and software laid the base for the development of fetal MRI as a clinical tool for routine radiological imaging.

The editor of this new volume – Dr. D. Prayer – is a pioneer and an internationally leading expert in the methodology and clinical applications of fetal MRI. She is well known for her excellent publications on translational research as well as clinical studies on fetal MRI. For the preparation of this book excellent contributions are provided not only by members of the fetal MRI team at the University hospital in Vienna but also by other internationally recognized experts in the field.

This book is the first handbook to offer a state-of-the art and comprehensive overview of the meticulous examination techniques and the specific sequences, which are essential for optimal image quality in fetal imaging. It further covers in depth all its current clinical applications as well as the safety issues.

The clear and informative text, the numerous well-chosen illustrations of superb technical quality, as well as the traditional Springer excellent standards of design and layout make this outstanding work a reference handbook for both certified general and pediatric radiologists. Also radiologists in training will find it very useful to improve their knowledge and their skills. Referring physicians such as gynecologists-obstetricians and pediatricians will benefit from it in order to better organize the clinical management of their patients.

It is my sincere wish and my firm conviction that this unique book will meet great success with the readership of our book series Medical Radiology – Diagnostic Imaging.

Leuven, Belgium — Albert L. Baert

Foreword II

Fetal MRI has made remarkable progress. Fifteen years ago, every case was a challenge: either the parent of the fetus (or both) required sedation; the mother needed to take shallow breaths for 2–3 min or try to hold her breath for the duration of an imaging sequence (while the radiologist and technologist held *their* breaths, hoping the fetus would not move). The development of the much faster half-Fourier acquisition single-shot sequences (HASTE, SSFSE) allowed images to be acquired in 1 s this revolutionized fetal imaging and made it practical for use in both medical centers and community hospitals. The addition of echo-planar techniques to evaluate for hemorrhage and diffusion-weighted imaging to assess for acute injury as well as for normal white matter development has made fetal MRI a flexible and highly useful tool in the assessment of normal fetal development and the detection of fetal disease. Moreover, the use of fetal MRI to assess fetal movements, thereby evaluating function as well as anatomy, has made fetal imaging a tool for understanding behavioral development, as is discussed in Chap. 9, by Drs. Einspieler and Prechtl.

This timely book by Dr. Prayer and her colleagues discusses many aspect of fetal imaging, from technical considerations to underlying developmental anatomy and pathophysiology to basics of fetal neurology. The technical aspects are very important to proper fetal imaging, and it is quite appropriate that four chapters be devoted to that topic. In addition, Chap. 5, which discusses the psychological state of the mother, will remind the imaging physician of the sensitivity required to properly perform one's role in any situation dealing with pregnancy. All organ systems are covered in the chapters of this book and all are written by physicians with both academic and practical experience. Importantly, the book goes beyond details of imaging the fetus. Chapter 23 discusses placental development and placental pathology, reminding us that the health of the placenta is strongly related to the health of the fetus. Chapter 24 deals with the difficult situation of multiplet pregnancies, which can create significant imaging, in addition to management, problems. Chapter 26 discusses postmortem MRI of the fetus, which is becoming an important tool for management of subsequent pregnancies, as it helps to establish a diagnosis in situations where autopsy is not possible. The book closes with a chapter on the impact of maternal diseases on pregnancy.

Overall, Dr. Prayer and her colleagues cover a wide range of timely and important topics. Although some of these are (currently) mainly of research interest, most are critical for proper diagnosis and management of fetal and maternal disorders. This book is another outstanding contribution to the growing field of prenatal diagnosis.

San Francisco, USA — A. James Barkovich

Preface

Driven by the ongoing technical and scientific progress, fetal MR imaging has evolved from an exclusively experimental prenatal imaging modality to a clinically important tool, which impacts decision making in the field of pre- and perinatal medicine. Nowadays, specialists involved in prenatal diagnosis are challenged with the demand to perform fetal MR examinations without the availability of basic reference with respect to methods, indications, MR appearance of maturing fetal and extrafetal organs, and pathological changes of intrauterine contents.

The aim of this book is to provide basic information about fetal MRI not only for the examiners but also for the referring clinicians. MR methods are described in detail and safety aspects are discussed. The prerequisites of fetal MRI are described including patient preparation as well as the appropriate selection of MR parameters for the respective clinical questions. In order to fully exploit the potential of this modality, the MR characteristics of normal and pathological organ development are described on various MR sequences, including advanced MR imaging techniques with illustration by numerous figures. The possibilities of intrauterine surgical therapy are described using the example of treatment of congenital diaphragmatic hernia. For better understanding of normal and pathological brain development, the histological basis of early human brain maturation is provided. Different aspects of fetal neuroimaging are discussed comprising ultrasound and MR approaches. Information that may help with interpretation of MR findings and their possible prognostic significance are summarized in chapters on genetics, maternal disease with possible impact on pregnancy, and postmortem MRI. In addition advice is given on how to treat postmortem specimens in order to obtain useful diagnostic clues. All authors have been working scientifically and practically in the field. Thus the reader should receive well-grounded information on each topic.

I would like to express my sincere gratitude to all the authors who contributed their work. In addition I would like to thank all colleagues, technicians, and students at my department who supplied their knowledge and time to get this project done.

I do hope that this book will become a companion for all who work in the field of prenatal diagnosis, and that it will provide helpful practical advice regarding the indications and performance of fetal MRI as well as the interpretation of findings.

Vienna, Austria — Daniela Prayer

Contents

Indications for Fetal MRI

Daniela Prayer, Peter C. Brugger, and Ulrika Asenbaum

Contents

Abstract

› Indications to perform fetal magnetic resonance imaging (MRI) can result from inadequate ultrasound assessment and/or intrinsic ultrasound disadvantages, compared to MRI, or can be associated with suspected malformative and/or acquired changes, and changes of extrafetal organs suspected or diagnosed by ultrasound. In addition, indications for fetal MRI can result from maternal or family history, and screening. MRI should be performed at the earliest time, an accurate diagnosis can be made, and, for special clinical questions, acutely or within 48 h. The highest MRI quality is required for fetal MRI. Absolute or relative contraindications should be considered before performing the MRI.

D. Prayer (✉) and U. Asenbaum
University Clinics for Radiodiagnostics, Medical University of Vienna, Währinger Gürtel 18-20, 1090 Vienna, Austria
e-mail: daniela.prayer@meduniwien.ac.at; ulrika.asenbaum@meduniwien.ac.at

P.C. Brugger
Integrative Morphology Group, Center of Anatomy and Cell Biology, Medical University of Vienna, Waehringerstrasse 13, 1090 Vienna, Austria
e-mail: peter.brugger@meduniwien.ac.at

D. Prayer (ed.), *Fetal MRI*, Medical Radiology,
DOI: 10.1007/174_2010_24, © Springer-Verlag Berlin Heidelberg 2011

1 Introduction

"Modern" fetal MRI, beginning with the availability of T2-weighted ultrafast sequences (Levine et al. 1996) was primarily used for the examination of the fetal brain (Stazzone et al. 2000). T2-weighted contrast provides an excellent delineation between fluid (such as cerebrospinal fluid (CSF) and tissue (the developing brain)). Thus, sulcation/gyration, configuration, and width of

the CSF spaces and deviations thereof, were studied first (Girard et al. 1995; Garel 2006). With the development of more contrasts (T1, diffusion, echoplanar) (Brugger et al. 2006), the MRI investigation of organs apart from the brain also became feasible (Hubbard et al. 1999; Shinmoto et al. 2000; Liu et al. 2001; Breysem et al. 2003; Levine et al. 2003; Osada et al. 2004; Gorincour et al. 2005; Kitano et al. 2005; Brugger and Prayer 2006; Kasprian et al. 2006; Prayer and Brugger 2007; Savelli et al. 2007).

Indications to perform fetal MRI may be divided into ultrasound (US)-related problems, confirmation/additional information for previously diagnosed or suspected pathologies, "specific" screening, which is related to a known genetic anomaly, pathologies that may lead to acute brain changes that might not be detectable by US, and assessment of lung development, especially in impending preterm birth (Kasprian et al. 2006).

2 MRI Indications When There are Ultrasound-Related Problems

2.1 Maternal Conditions

In cases, where the mother is obese, an elevated body mass index (BMI) might interfere with image quality on US. However, using MRI, examination of obese pregnant women may result in a poor image quality as well, as the receptor elements of the coil will be too distant from the region of interest. In addition, the use of a wrap-around coil will not be possible, and the built-in body coil does not allow a comparable image quality. However, in such cases, MRI usually provides more image detail than US (Fig. 1). Maternal abdominal scarring or dense hairs on the abdomen, sometimes a problem with US, are not difficulties for MRI.

2.2 Maternal/Fetal Conditions

MRI image quality is not impaired by oligohydramnios or anhydramnios. Furthermore, fetal position is unimportant. However, polyhydramnios may be associated with MRI imaging problems, as these fetuses tend to move more than those with a normal or a reduced amount of amniotic fluid. In addition, the fetus itself will be further away from the coil, and the circumference of the maternal abdomen will be large, resulting in problems as discussed above (Fig. 1).

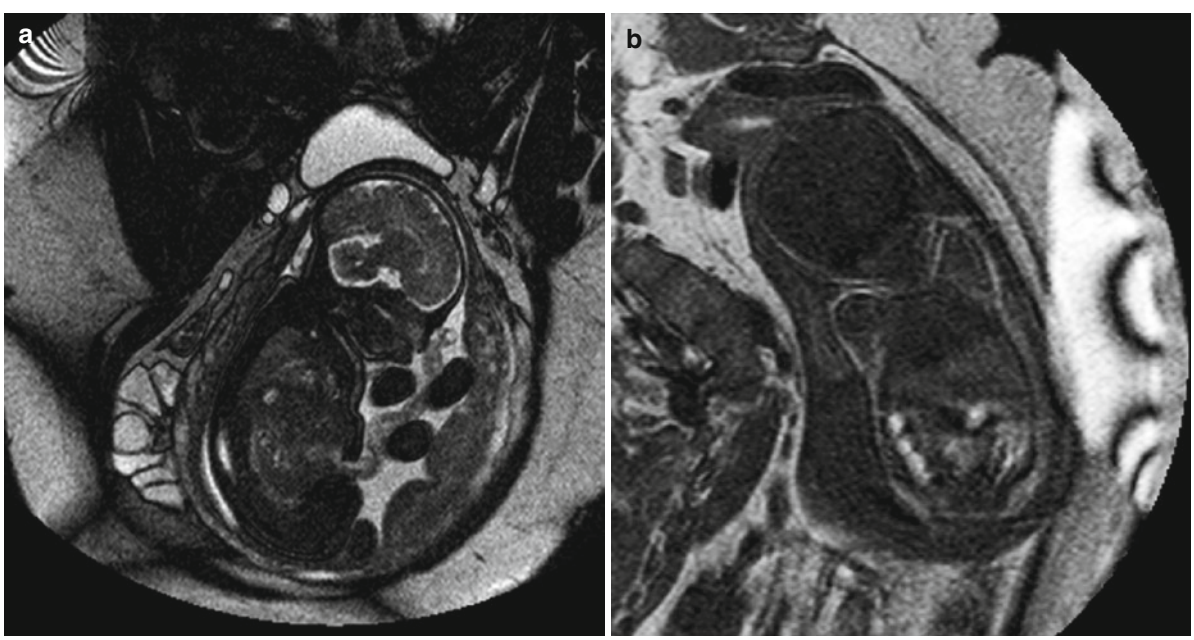

Fig. 1 Mother with high BMI at GW 35+5. Despite the reduced image quality, fetal structures can be evaluated sufficiently. (**a**) Sagittal T2-weighted image. (**b**) Coronal T1-weighted image with a fold-over artifact (*right lateral border* of the figure)

2.3 General Method-Related Conditions

US assessment uses a sector-shaped field of view that does not exceed a certain size. Thus, especially in the later second trimester, and in the third trimester, it is not possible to visualize the fetus as a whole at one time. This may impair, for instance, assessment of fetal behavior (de Vries et al. 1985).

3 MRI Indications When There are Sonographically Diagnosed or Suspected Pathologies

3.1 Cerebral Malformations

Gross malformations are readily detected by US (Angtuaco et al. 1994), most during the first trimester, when MRI is not used (American College of Obstetricians and Gynecologists 1995). Malformations of cortical development have also been reportedly visualized by US (Toi et al. 2004; Malinger et al. 2006). However, diagnosis of lissencephaly before the onset of gyration can be difficult. In that case, MRI may be helpful in demonstrating pathologic lamination of the brain mantle (Fig. 2). In addition, brainstem deformities, which are a salient feature of lissencephaly, can be easily delineated with MRI. Focal cortical dysplasia may not manifest itself before the late second trimester (Fig. 3). Other malformations, involving small structures, such as the olfactory bulbs, could be recognized earlier (Azoulay et al. 2006). Arachnoidal cysts may grow, and eventually obstruct CSF spaces and/or compress tissue that might undergo damage. These situations can be recognized with MRI. Preterm delivery to drain such cysts extrauterinely might be a consequence. Uni- or bilateral ventricular enlargement of more than 15 mm may be associated with any malformative or acquired pathology (Tauscher 2008). In isolated ventriculomegaly, smaller than 15 mm, the presence of a pathology is not likely (Tauscher 2008).

3.2 Cerebral Acquired Pathologies

Recent ischemic lesions (the presence of which may be indirectly indicated by deterioration of Doppler values

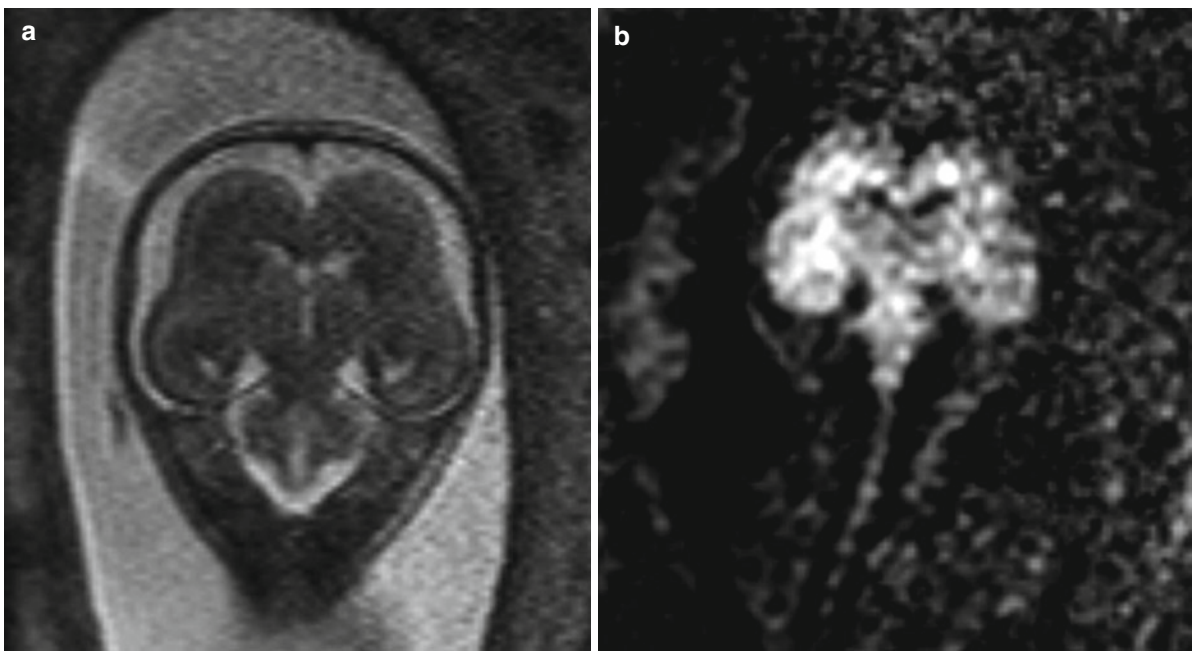

Fig. 2 Coronal T2-weighted images (**a**) and diffusion-weighted images (**b**) showing the disturbed lamination and too shallow insula indentation indicating the presence of lissencephaly I at GW 24 + 3

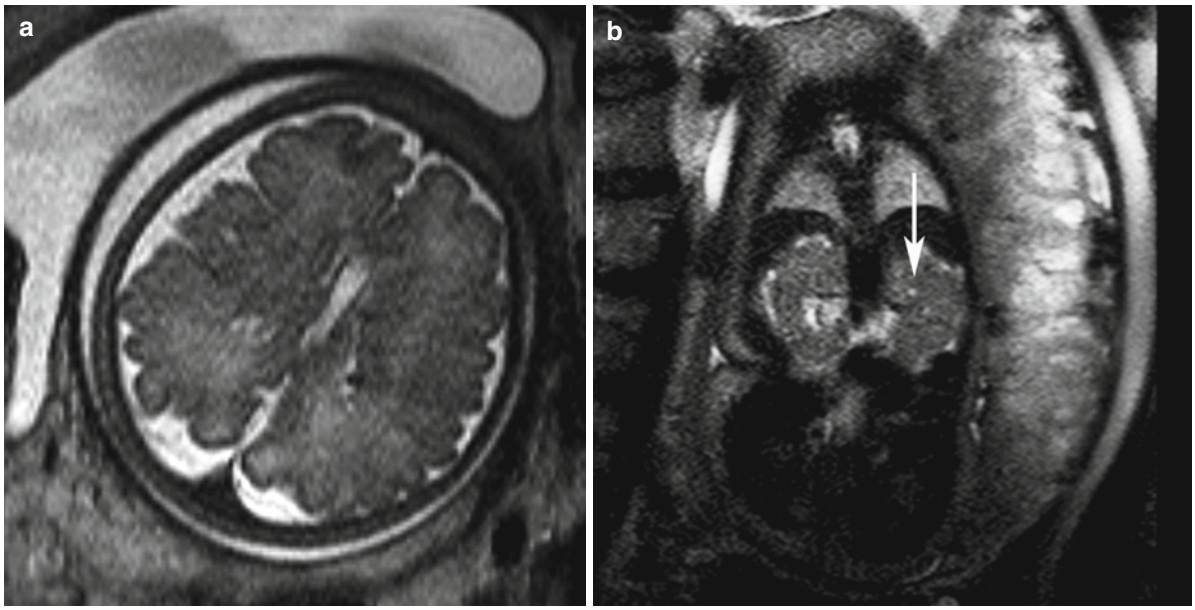

Fig. 3 Bourneville Pringle syndrome at GW 33+1. (**a**) Subependymal nodules, right frontal focal cortical dysplasia (axial T2-weighted image); (**b**) the kidneys with small cysts (*arrow*, coronal T2-weighted image)

in the medial cerebral artery, as has been described in growth-restricted fetuses (Mari and Hanif 2008)) appear bright on diffusion-weighted images before showing T2-weighted signal changes. Acute hemorrhage will display a signal loss on T2*, EPI-, and, to a lesser degree, also on T2-weighted sequences (Prayer et al. 2006). Brain edema will lead to a blurring of intracerebral signals on all sequences, obscuring lamination or no longer providing the delineation of premyelinating/myelinating structures (Fig. 4). In addition, inner and outer CSF spaces will become narrow. In case of cystic defects that are seen by US, MRI may point toward the acquired etiology by showing blood breakdown products (Fig. 5). While US can readily detect blood clots, hemorrhagic fluid might not be resolved. MRI identification of blood-breakdown products can also be helpful in cases of aqueduct stenosis (Fig. 6), when blood clots are identified or excluded as an underlying reason. Calcified lesions are detected more sensitively by US.

3.3 Metabolic Assessment of the Fetal Brain

Proton spectroscopy provides an insight into the metabolic changes associated with normal brain development (Kok et al. 2002). Deviations thereof may be recognized, and can provide insights into pathological processes associated with hypoxic ischemic injury (Garel 2006).

3.4 Extracerebral Pathologies

3.4.1 Malformations and Tumors Involving Single Organs or Organ Systems

Face

Clefts may involve only the lips or may include the maxilla and the soft and hard palate (Robson and Barnewolt 2004). Those involving just the hard palate, without involvement of surface structures, are easily missed by US (Fig. 7). MRI has been shown to provide additional information in the workup of facial clefts (Mailath-Pokorny et al. 2009). The tongue and its movements are readily identified. However, it should be noted that tongue hyperplasia, which leads to protrusion, might be present only from the late second trimester onward (Fig. 8). Malformations of the inner ear are detectable, as the fluid-filled cochlea and semicircular canals can be seen even in 20-week fetuses. Eyes (form, size, orbital content, intraocular distance) may be equally well determined by MRI as by US.

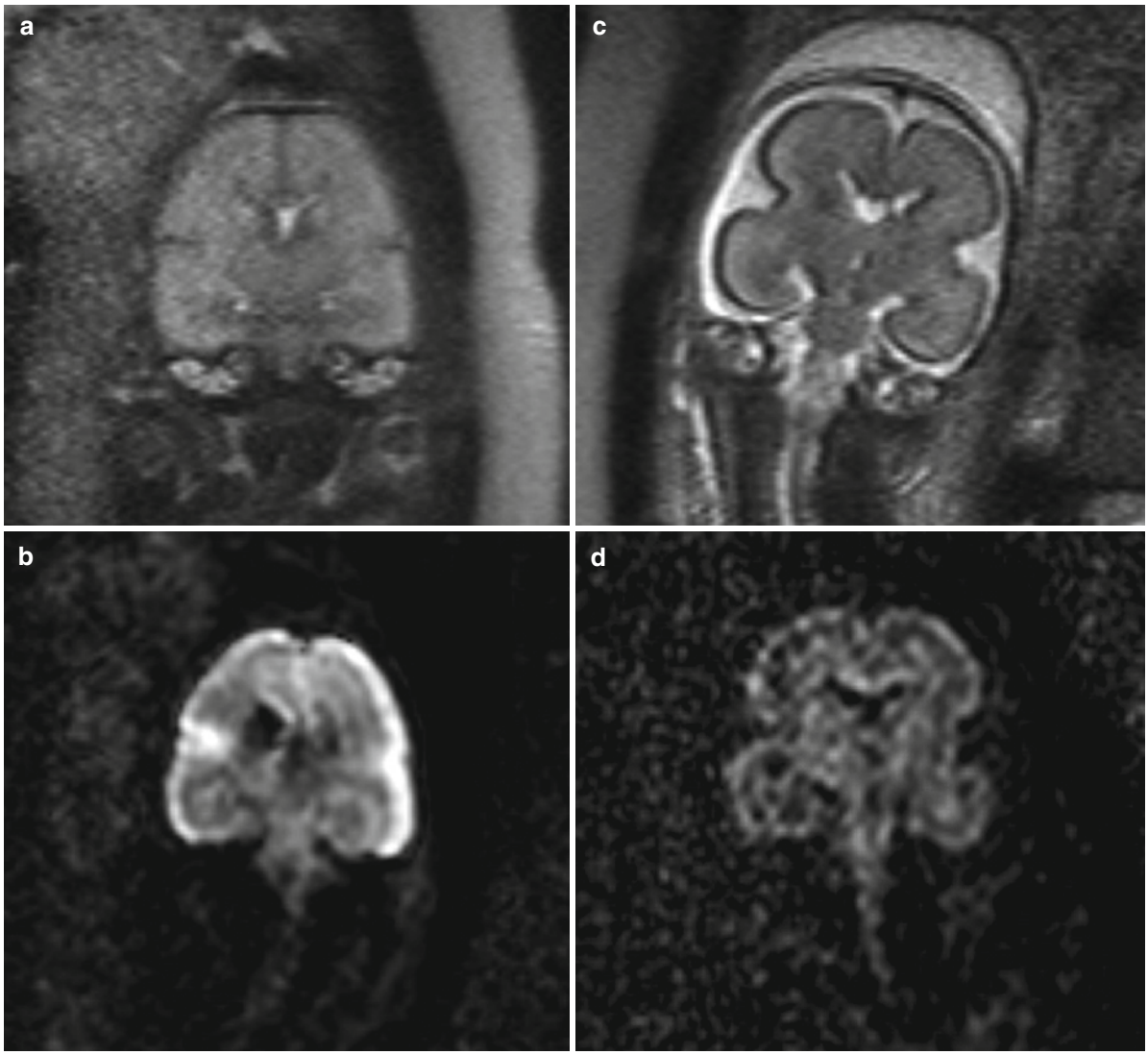

Fig. 4 (**a**, **b**) Global brain edema at GW 24+3; (**c**, **d**) normal subjects at GW 24+1 (**a**, **c**) coronal T2-weighted images. (**b**, **d**) coronal diffusion-weighted isotropic images. Lamination of the brain parenchyma cannot be delineated (**a**, **b**) in contrast to (**c**, **d**). Outer CSF spaces are consumed (**a**, **b**). Edema of the cortical plate in **b** (hyperintense signal)

Dacryocystoceles are detectable using MRI (Brugger and Prayer 2008).

Neck

Spaceoccupying lesions in this region tend to narrow and/or displace the trachea and/or the esophagus. Narrowing or displacement of the trachea carries the possible necessity of an ex utero intrapartum treatment (EXIT) procedure. In such cases, MRI has been shown to be able to locate the position of the trachea (Prayer and Brugger 2007). In case of esophageal obstruction, US will be able to describe only a small or undetectable stomach and polyhydramnios. MRI can be expected to prove the presence of a pouch sign in the esophagus in such cases (Fig. 9). In addition, MRI might be able to identify a small fluid-filled stomach by the characteristic appearance of its mucosa. With regard to the differential diagnoses of neck tumors, MRI may help in differentiating cystic (hem) angiolymphomas from teratomas (Fig. 10). The visualization of the carotids and jugular veins allows identification of pathologies, such as, for instance,

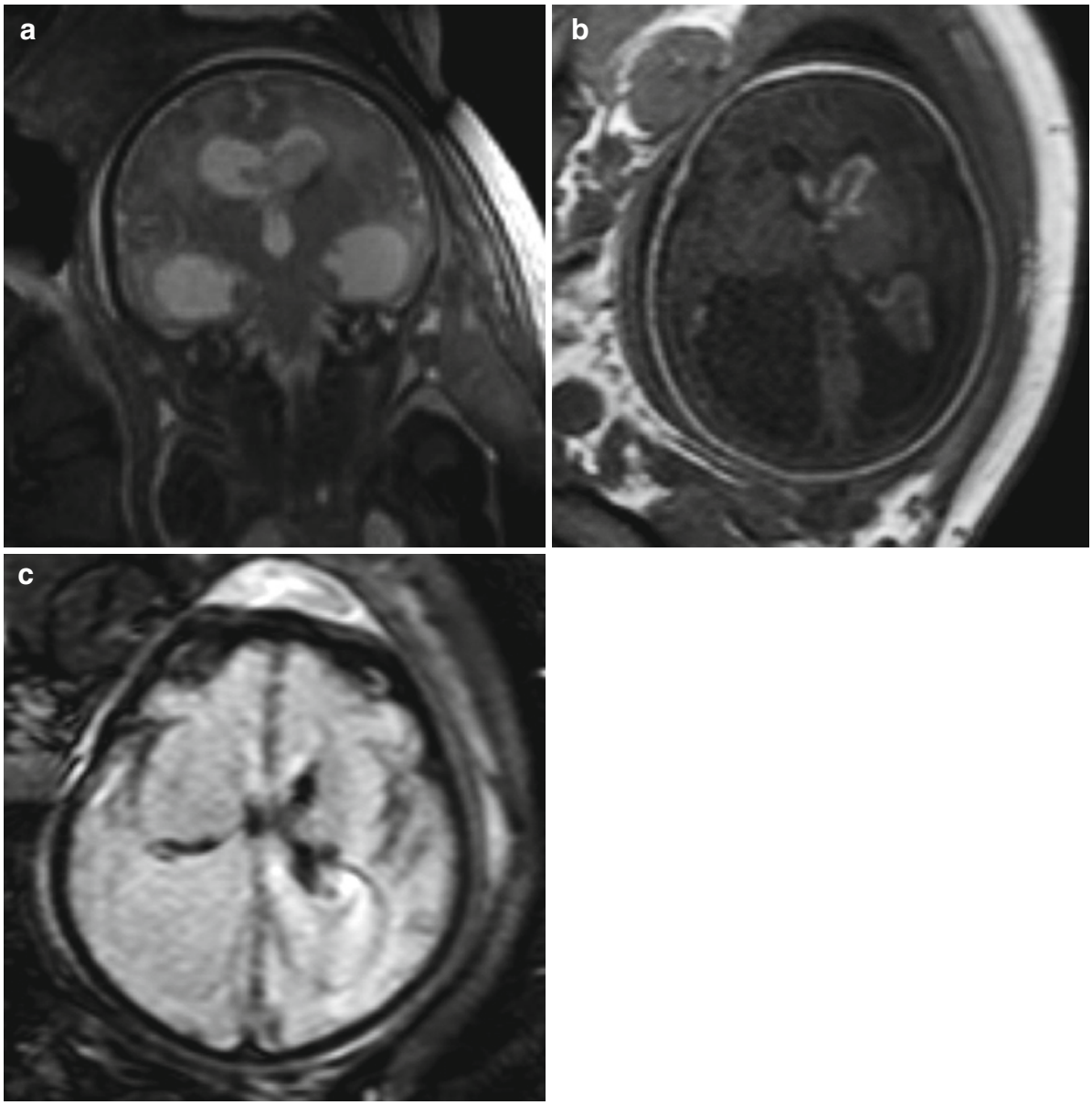

Fig. 5 Posthemorrhagic hydrocephalus at GW 36+6. Wide ventricles and blood-breakdown products adjacent to the ependyma (hypointense T2-weighted images) (**a**, coronal), and on the EPI sequence (**c**, axial), and hyperintense on T1-weighted images (**b**, axial)

wide jugular veins in the presence of a Galeni aneurysm (Fig. 11).

Thorax

Intrapulmonary malformations, such as congenital cystic adenomatoid malformations (CCAM), sequestrations, and bronchogenic cysts, can be readily differentiated from each other. MRI-based lung volumetry enables determination of the percentage of normal lung tissue in such cases. Follow-up studies may provide a clue to the relative growth of the lesion with respect to the normal lung. Cardiac malformations are currently not an indication to perform a fetal MRI. However, the position and diameter of the great

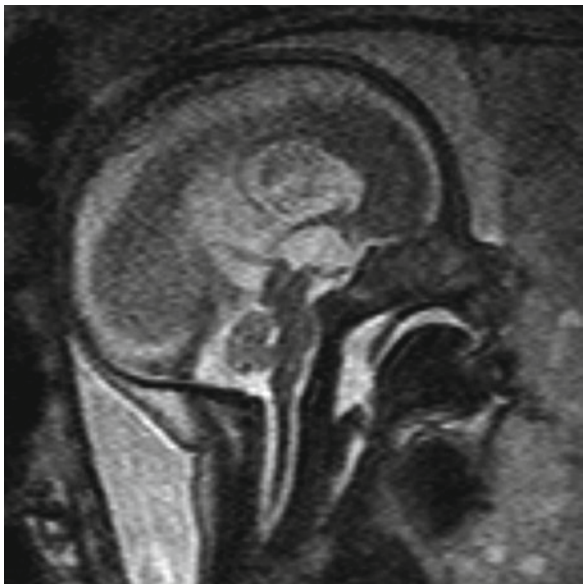

Fig. 6 Aqueduct stenosis with typical v-shaped configuration of the aqueduct in the cranial aspect (median sagittal T2-weighted sequence). Blood-breakdown products are not shown

vessels may be better determined with MRI than with US (Fig. 12). The thymus is difficult to delineate in second trimester fetuses: thus, the early detection of Di George syndrome (Chaoui et al. 2002) is not an indication to perform MRI.

Small and Large Bowels

Due to their age-dependent fluid or meconium filling, bowel loops can be identified. Thus, displacement, malrotation, changes of the luminal width, or agenesis can be recognized (Prayer and Brugger 2007). In case of enlargement, the visualization of peristaltic waves may allow the identification of the involved part of the bowel. Poststenotic widened parts often show abnormal meconium signals (T1-weighted not as bright as usual) (Fig. 13).

Liver and Spleen

As the liver can be clearly differentiated by its characteristic T1- and T2-weighted appearance compared to its surroundings, its position, size, and configuration can also be assessed. This is important in case of abnormal symmetry, indicating the presence of heterotaxy, or displacement into the thorax in congenital diaphragmatic hernia (Cannie et al. 2008). Pathological signals may be present, for instance in liver cirrhosis (Brugger and Prayer 2006) or in hemochromatosis (Marti-Bonmati et al. 1994; Coakley et al. 1999). Identification of the gall bladder is possible, regardless of its contents, because sludge,

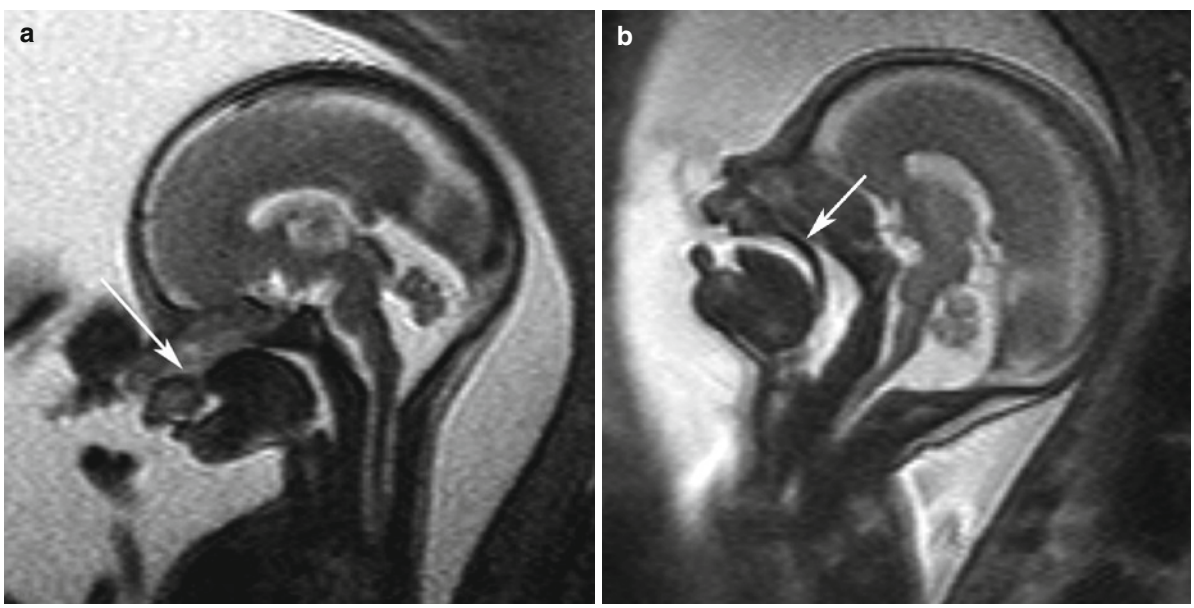

Fig. 7 Isolated hard palate cleft. Median sagittal T2-weighted-image (**a**) GW 24 + 0, hard palate absent (*arrow*), (**b**) GW 24 + 1, hard palate present (*arrow*)

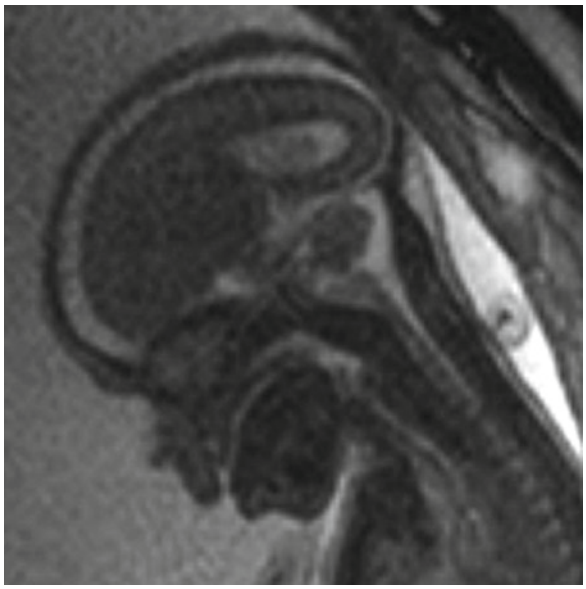

Fig. 8 Beckwidth–Wiedemann syndrome at GW 32+6: protruding tongue (median sagittal T2-weighted image)

which may prevent the identification of the gallbladder on US, shows characteristic signals on MRI (Brugger and Prayer 2006). Identification of the spleen(s) is required in heterotaxy, as the absence of a spleen might be associated with a worse prognosis than the presence of multiple spleens (Applegate et al. 1999).

Urogenital System

The identification of misplaced kidneys on US might be difficult in young fetuses (Poutamo et al. 2000; Cassart et al. 2004). Due to their appearance on diffusion-weighted images (Witzani et al. 2006), MRI can show kidneys at any fetal age (Fig. 14). This is especially important in case of oligohydramnios or anhydramnios, where US assessment is impaired. Ureters and the urethra can be identified when widened (Fig. 15). The bladder itself might have to be differentiated from other cysts, which can usually be accomplished successfully. In assessment of the genitals, MRI has no advantage compared to US. One exception to this is the delineation of complicated ovarian cysts (with intracystic hemorrhage, indicating torsion). They may present with signals typical of structures that contain blood breakdown products (Fig. 16).

Cysts and Tumors

Cysts may be a part of any malformation or of a tumor. The determination of the originating organ and the respective signals may help with differential diagnoses.

Thus, a bronchogenic cyst may display different signals from amniotic fluid, allowing differentiation from a CCAM cyst. Tumors may have a characteristic MRI appearance, such as, for instance, the wheel-like structure of a hepatoblastoma. Teratomas have cystic and solid parts, and lymph (hem) angiomas are primarily cystic with rare intracystic hemorrhages. Neuroblastomas are known to prefer certain localizations (Siegel and Jaju 2008) and display a rather solid appearance.

Musculoskeletal System

Using special sequences (based on EPI imaging), the parts of the bony skeleton can be identified with MRI. Based on the knowledge of the temporal appearance of the ossification centers, the presence of a skeletal dysplasia can be recognized. Whether MRI might be more sensitive in these cases than US, has yet to be proven. In case of spina bifida, the defect can be identified. By visualizing the neural structures at the same time, a differential diagnosis between the types of dysraphic malformation can be achieved. With increasing gestational age, skeletal muscles become isointense to bone. In case of muscle dystrophy, they may have different signals (Fig. 17).

3.4.2 Complex Pathologies

Complex pathologies may have a genetical background. Thus, one of the main tasks for MRI is the definition or exclusion of the presence of a syndrome with a known prognosis. From the MRI point of view, this means that in any case of pathology, the whole fetus must be examined. Malformations of the brain and face, may indicate, for instance the presence of trisomy 13 (Nemec et al. 2009). In case of certain abdominal pathologies, the lower spinal situation must be clarified to exclude or prove a caudal regression syndrome complex (Ertl-Wagner and

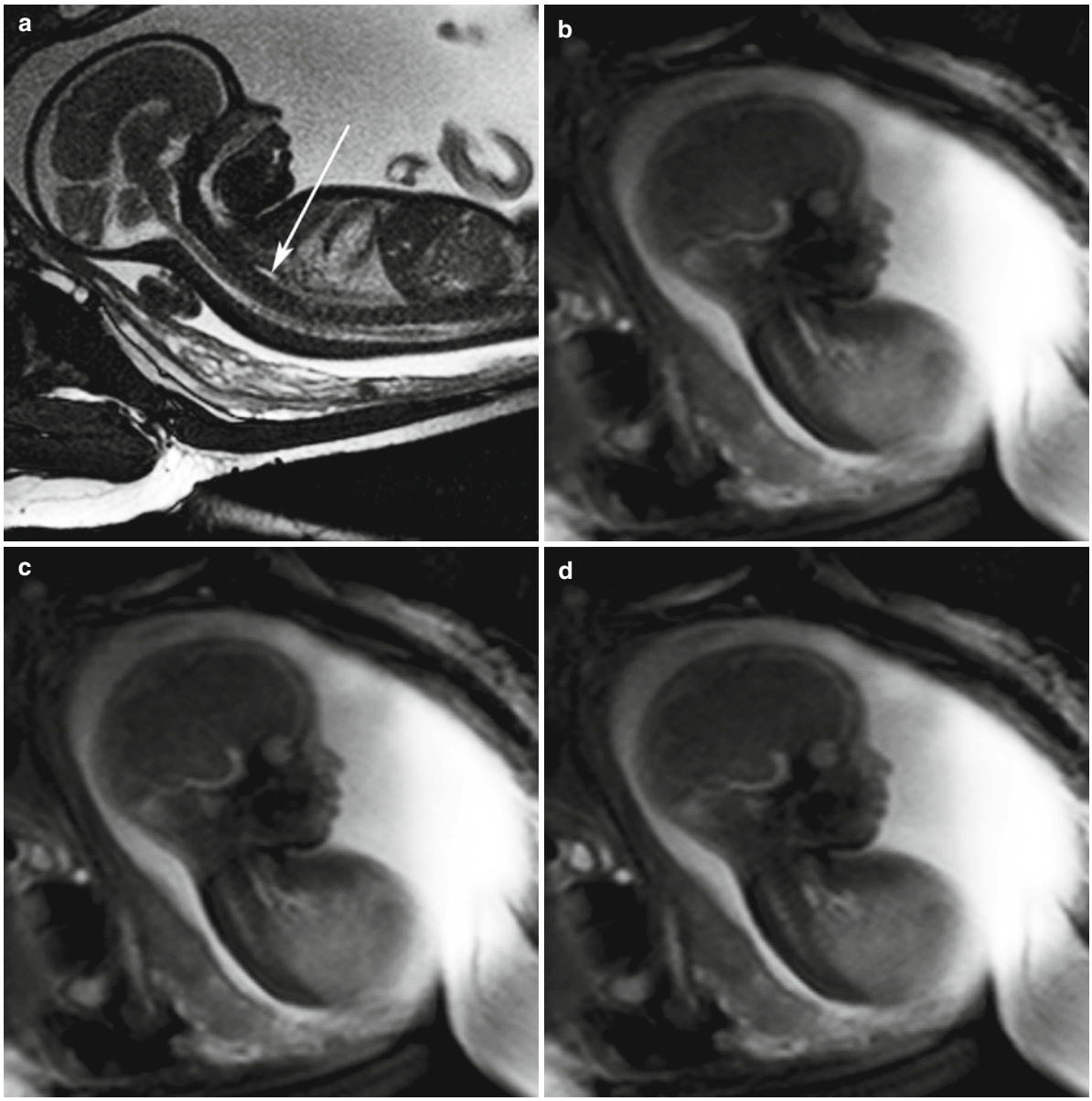

Fig. 9 Pouch sign in the esophagus at GW 30 + 5. (**a**) Median sagittal SSFP, showing a pouch sign (*arrow*). (**b–d**) Sagittal snap-shots from a dynamic sequence proving the pouch sign

Reiser 2001). However, organ systems that are not immediately adjacent to the respective region also must be screened: a "double bubble," indicating duodenal stenosis may be found in the context of a lissencephaly syndrome (de Rijk-van Andel et al. 1990). Pathologies of the kidney that result in deficient production of urine may be associated with pulmonary hypoplasia (Vanderheyden et al. 2003).

3.4.3 Intrauterine Growth Restriction

Underlying reasons for intrauterine growth restriction (IUGR) are multiple (Bernstein and Divon 1997). MRI may identify changes in the placenta (mainly its thickness and structure) in such cases (Fig. 18), and thus, rule out other etiologies. In addition, in IUGR, fetuses at risk for impending

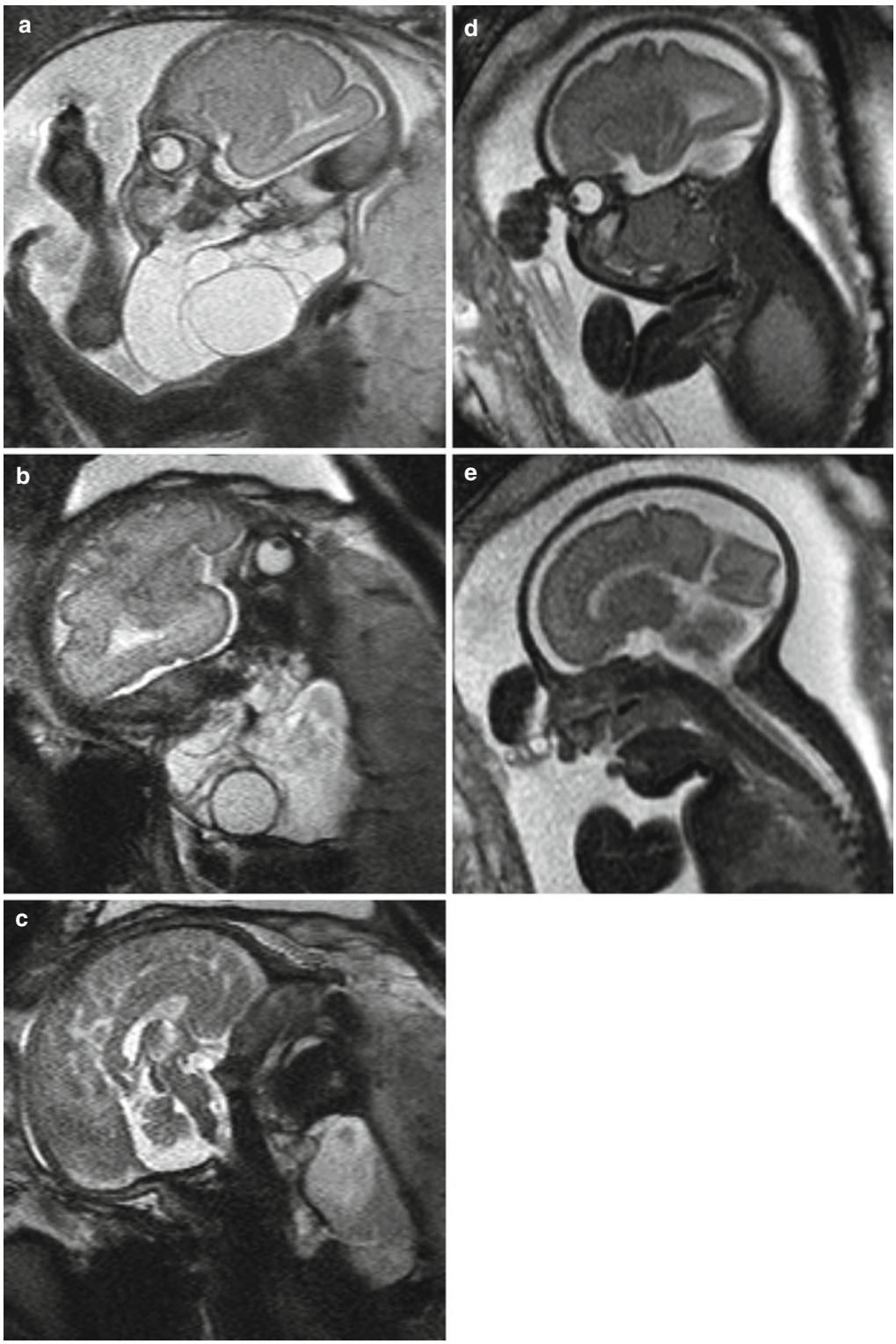

Fig. 10 (**a–c**) Parasagittal sections on T2-weighted images showing a multicystic, spaceoccupying lesion corresponding to lymphangioma at GW 29 + 2. (**d**, **e**) Parasagittal sections on T2-weighted images showing a solid space occupying lesion corresponding to a teratoma at GW 29 + 3

Fig. 11 Vena Galeni aneurysm at GW 26+0: parasagittal T2-weighted image, showing aneurysmatic structures intracerebrally (*arrowheads*), enlarged jugular vein (*arrow*), and enlarged heart

Fig. 12 Parasagittal SSFP image showing right common carotid artery (*arrow*) at GW 26+2

Fig. 13 Coronal T1-weighted image at GW 28+1, showing enlarged bowel-loops (*arrow*) without normal hyperintense signal of meconium (atresia)

premature birth, body-volume-related lung volumes may be determined by means of MRI volumetry.

3.4.4 Pathologies of Extrafetal Organs

The number of vessels, the length of the umbilical cord, the tortuosity, and the thickness of the Wharton`s jelly can be assessed, but do not represent special MRI indications. Pathologies involving the cord, for example a hernia into the cord, may be recognized. With regard to the amniotic fluid, its signals on MRI sequences show the presence or absence of intraamniotic hemorrhage (Fig. 19). The size, configuration, and intrinsic structure of the placenta can be seen (Gowland 2005; Blaicher et al. 2006; Linduska et al. 2009). Certain changes can be assigned to defined pathologies as described in placental specimens (Linduska et al. 2009). However, to date, the direct relationship between the (extent of) pathological changes and their impact on fetal development and/or well being is unclear. Tumors of the uterine wall or originating from the placenta may be identified. In

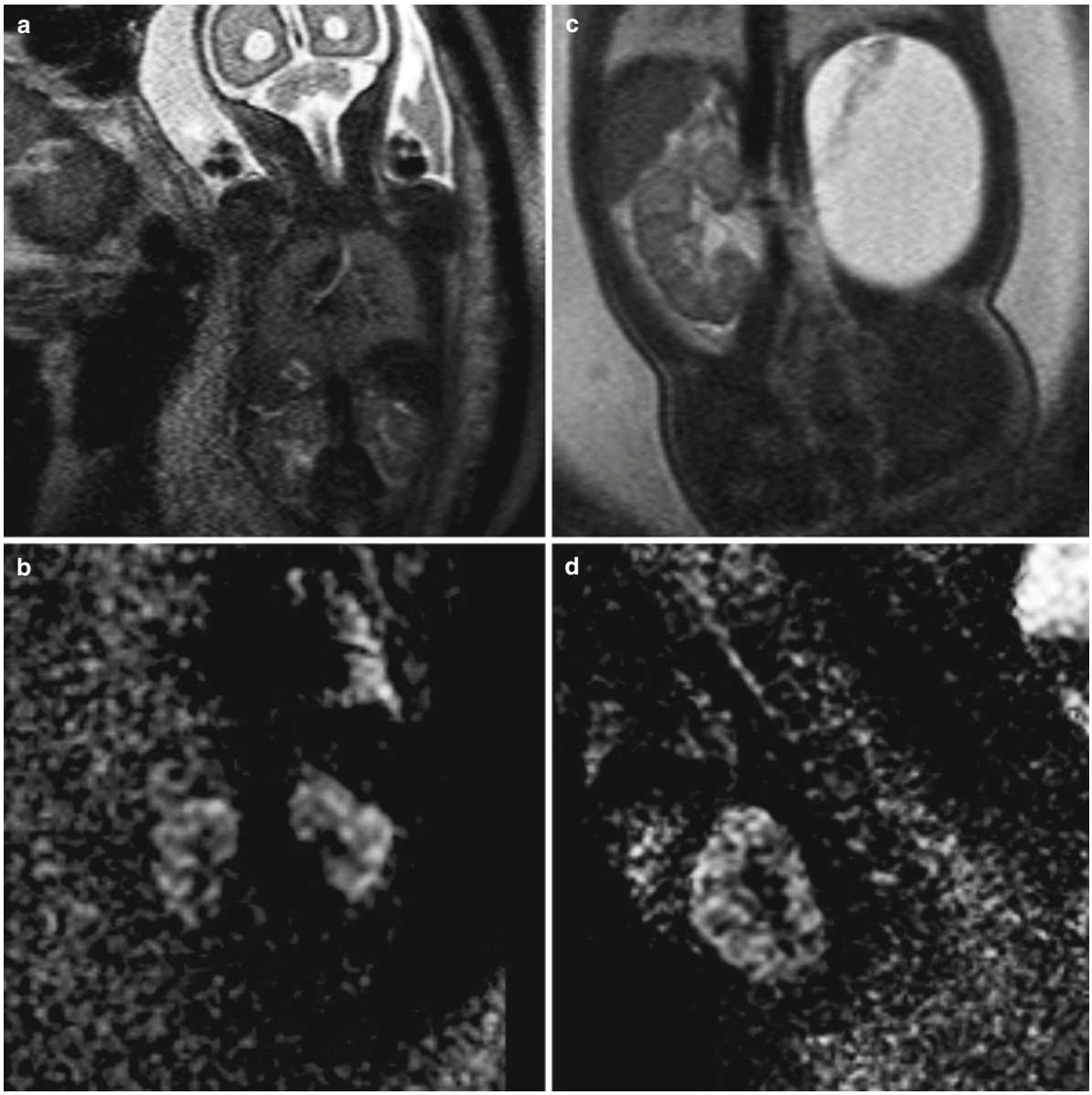

Fig. 14 DWI can show kidneys at any fetal age. (**a**, **c**) Coronal T2-weighted images; (**b**, **d**) DWI. (**a**, **b**) Normal kidneys at GW 24 + 1. (**c**, **d**) Cystic structures in location of the left kidney. On DWI, only the right kidney is present (GW 32 + 2)

case of placenta increta or percreta, contrast-enhanced sequences reportedly provide usable information (Palacios Jaraquemada and Bruno 2000). However, as the impact of MRI contrast media on the fetal kidneys is still unclear, indications for contrast-media administrations should be considered carefully (Prayer and Brugger 2007).

3.4.5 Feto-Fetal Transfusion Syndrome

Feto-fetal transfusion syndrome (FFTS) results from transfusion of blood between one twin (the donor) and the other twin (the recipient) via placental vascular anastomoses. The diagnosis of FFTS is based on ultrasound criteria (Huber and Hecher 2004).

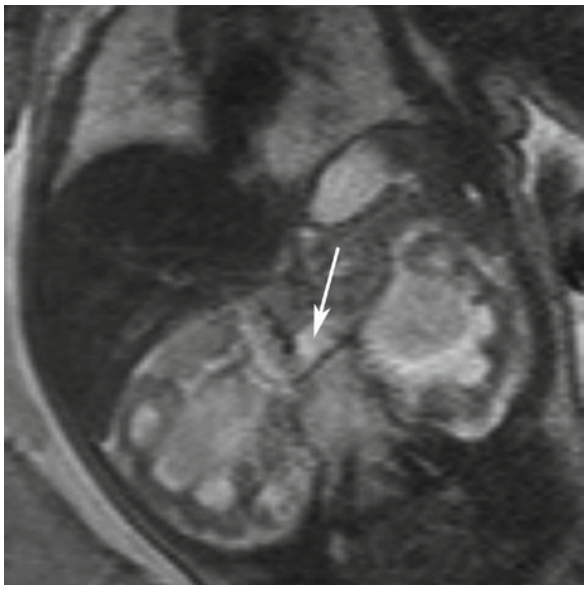

Fig. 15 Ureters and urethra can be identified when widened. Coronal T2-weighted image showing wide renal pelvis and enlarged ureters (*arrow*)

However, these criteria are associated with the consequences of already manifest FFTS. Early diagnosis, achieved with MRI, must focus on placental changes. Although FFTS is not yet an indication for MRI, it may become one, once noninvasive placental perfusion techniques are validated for this purpose (Gowland 2005).

4 Indications Resulting from Familial/ Maternal History

4.1 Suspect Familial Genetic Syndromes

In the case of one or more family members with certain malformations, a genetic background may be supposed (even in the absence of proof of such a defect). Some entities, as, for instance, the wide spectrum of corpus callosum agenesis may occur with or without chromosomal aberration (Paul et al. 2007).

4.2 Previous History of Unclear Abortions or Stillbirths

In cases of unclear abortions or stillbirths, various reasons must be considered. A screening of the fetus and extrafetal organs is necessary. The latter may identify, for instance, placental pathology, pointing

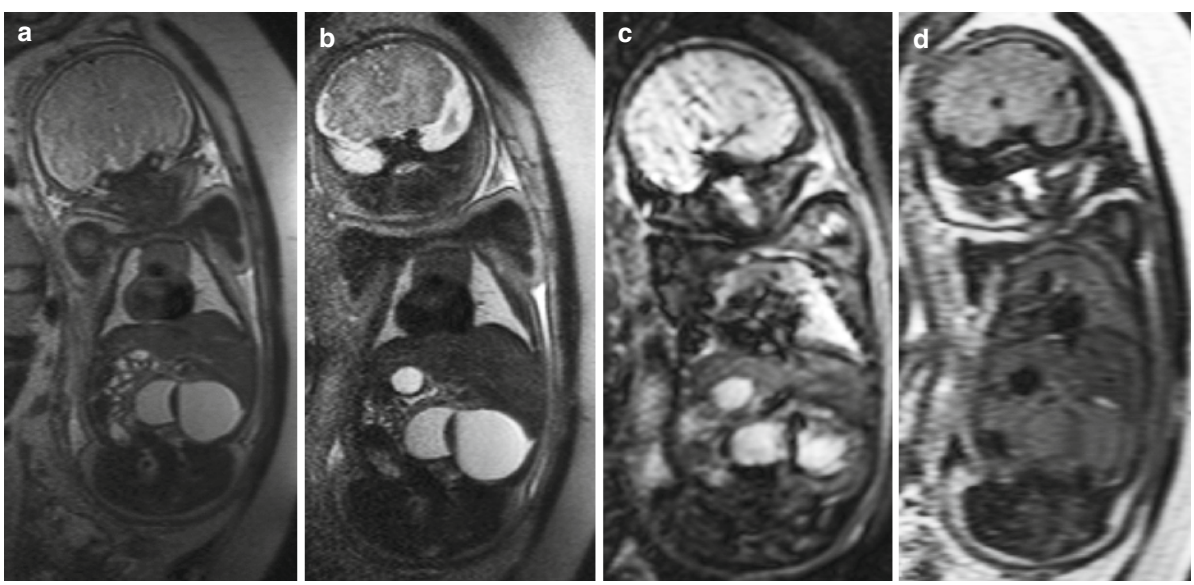

Fig. 16 Ovarian cysts. Coronal T2-weighted image (**a**, **b**), EPI (**c**), and T1 FLAIR (**d**) images show hemorrhage into an ovarian cyst. Notice the fluid level (**a–c**) and the bright signals compared to the content of the stomach (**d**)

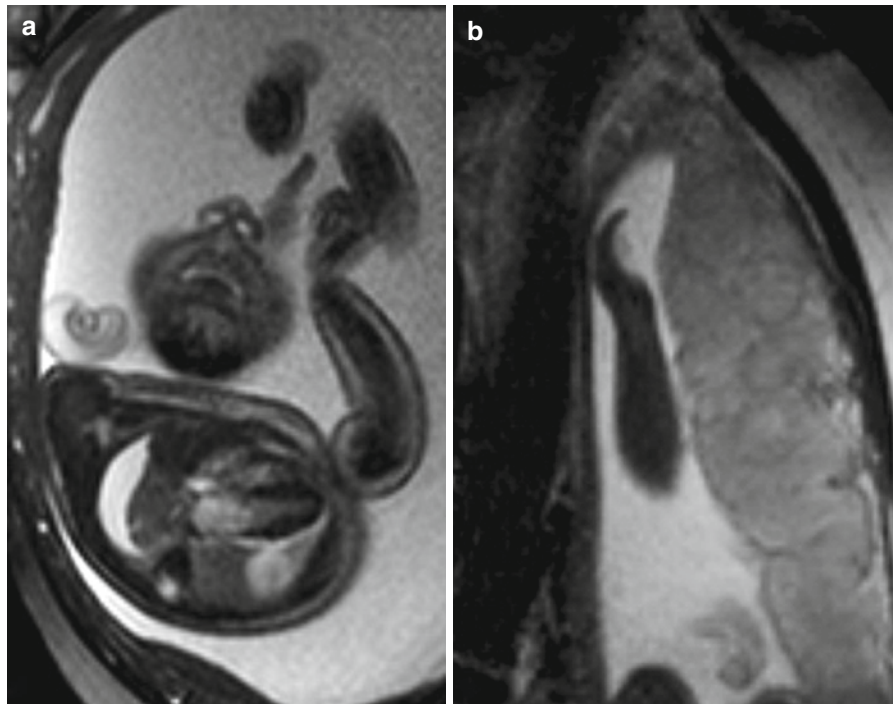

Fig. 17 (**a**) T2-weighted image (GW 30+0) showing abnormal brightness of the muscles (arm) compared with (**b**) (GW 29+1). Notice pleural effusions and abnormal hypointense signal of the lungs in (**a**)

Fig. 18 IUGR at GW 22+2 with edematous thickened placenta. T2-weighted section through the placenta showing retroplacental hematoma (*arrow*)

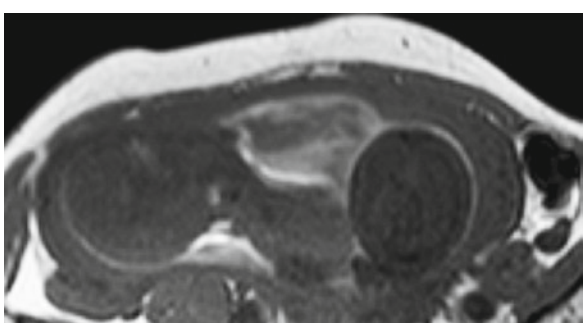

Fig. 19 Intraamniotic hemorrhage at GW 22+2. T1-weighted image showing abnormal hyperintensity of the amnion fluid

toward a maternal disease associated with impairment of placental function.

4.3 Chronic Maternal Disease Possibly Interfering with Successful Pregnancy

Lupus erythematosus (LE), antiphospholipid antibody syndrome, and similar diseases are known to interfere with placentation and/or placental maturation (Meroni et al. 2004; Blaicher et al. 2006). In such cases, the placenta, in particular, should be evaluated by MRI. Findings associated with LE include infarction, edema, and intervillous thomoboses (Surita et al. 2007), all of which may be depicted using MRI (Linduska et al. 2009). IUGR is the usual consequence of placental damage. Metabolic diseases, such as, for instance, hypothyroidism may have an impact on fetal brain development (Pemberton et al. 2005).

4.4 Acute Maternal Problems

Cardiorespiratory arrest, metabolic coma, high blood levels of anticoagulants (de Laveaucoupet et al. 2001; Chan et al. 2003; Lee et al. 2003), intoxication

(Bookstein et al. 2002; Riley and McGee 2005; von Mandach 2005), and similar situations may compromise the fetus (de Laveaucoupet et al. 2001). In these cases, MRI may be used to screen for fetal brain lesions. Maternal infection may be transmitted to the fetus via the placenta and may lead to CNS and extra-CNS lesions (Prayer et al. in press).

4.5 Trauma

Traumatic events with a mechanical impact on the maternal abdomen may lead to fetal damage either directly, or based on hemorrhage into the uterus, or via hypovolemia of the mother, leading to a drop in oxygen delivery (Chames and Pearlman 2008). MRI may also demonstrate acute changes as well as those with delayed onset resulting from reduced oxygen supply (Brunel et al. 2004).

4.6 Screening

A prenatal screening method must be able to visualize any fetal and extrafetal structure, in a manner comparable to US. These requirements are fulfilled by MRI. However, MRI is not currently used for screening purposes due to its still restricted availability and relatively high costs, compared with routine US.

5 When Should MRI Be Done?

5.1 With Respect to Gestational Age

In many countries, the time when a legal abortion may be performed ends at gestational week 24. Thus, a definite diagnosis of a certain pathology should be made as soon as possible. However, some changes might manifest themselves only later (as, for instance, focal cortical dysplasia). In other cases, morphological signs of a syndrome may be partly present in the early second trimester, but the full-blown picture may not be recognizable before the third trimester. In Beckwith–Wiedemann syndrome, the omphalocele may be diagnosed early, but the enlargement of organs will not be visible before the late second or early third trimester (Fig. 8). Late (third trimester) examinations should be performed in cases of a planned EXIT procedure or expected postnatal instability of the newborn, not allowing an immediate postnatal MRI or CT (Mittermayer et al. 2005; Prayer and Brugger 2007).

5.2 Triage

Generally, fetal MRI should be performed as soon as possible after the indication has been defined, or, in case of special questions, as soon as a conclusive answer is expected to be provided by MRI. An acute MRI indication is present in case of suspected impending acute brain damage to the fetus (mostly indicated by rapidly declining ACM Doppler values). Relatively acute (within 24–48 h) MRI should be done with PROM between GW 24 and 28/29 to determine the state of lung maturation (Pataraia 2008).

5.3 Indications Derived from the Referring Physician and MRI Center

Indications to perform MRI will vary with the quality of available previous US examinations. In countries where referral to MRI is performed exclusively by a level III US center (American College of Obstetricians and Gynecologists 1995), only a few clinical questions may remain unanswered by US. In contrast, more MRI examinations may be required in regions where MRI is more easily accessed than level III ultrasound and/or, for instance, dedicated neuro-ultrasound (Pistorius et al. 2008). Presently, MRI is performed at different levels as no quality criteria for fetal MRI have been defined as yet. This may lead to uncertainty about whether MRI might prove to be useful for certain clinical questions. The indications discussed above were selected based on the premise of the availability of high-level MRI (Prayer et al. 2004).

6 Contraindications

6.1 Absolute Contraindications

These are the same as for any MRI-examination, such as, for instance, a pacemaker (Shellock and Spinazzi 2008). MRI should also not be done in case of uninhabitable labor.

6.2 Relative Contraindications

Claustrophobia may prevent the completion of an MRI examination. In these cases, maternal sedation with diazepam or flunitrazepam may help (Sonigo et al. 1998; Girard et al. 2003). The presence of a person who can accompany the patient during the procedure has also proved to be beneficial. Another relative contraindication may result if the parents-to-be cannot draw any conclusions from the expected results of the MRI, or if they do not want the examination to be performed for any reason.

References

American College of Obstetricians and Gynecologists (1995) Guidelines for diagnostic imaging during pregnancy. The American College of Obstetricians and Gynecologists. Int J Gynaecol Obstet 51:288–291

Angtuaco EE, Angtuaco TL, Angtuaco EJ (1994) Prenatal diagnosis of central nervous system abnormalities. Curr Probl Diagn Radiol 23:69–99

Applegate K, Goske M, Pierce G, Murphy D (1999) Situs revisited: imaging of the heterotaxy syndrome. Radiographics 19:837–852, discussion 853–854

Azoulay R, Fallet-Bianco C, Garel C, Grabar S, Kalifa G, Adamsbaum C (2006) MRI of the olfactory bulbs and sulci in human fetuses. Pediatr Radiol 36:97–107

Bernstein PS, Divon MY (1997) Etiologies of fetal growth restriction. Clin Obstet Gynecol 40:723–729

Blaicher W, Brugger PC, Mittermayer C, Schwindt J, Deutinger J, Bernaschek G, Prayer D (2006) Magnetic resonance imaging of the normal placenta. Eur J Radiol 57:256–260

Bookstein FL, Sampson PD, Connor PD, Streissguth AP (2002) Midline corpus callosum is a neuroanatomical focus of fetal alcohol damage. Anat Rec 269:162–174

Breysem L, Bosmans H, Dymarkowski S, Schoubroeck DV, Witters I, Deprest J, Demaerel P, Vanbeckevoort D, Vanhole C, Casaer P, Smet M (2003) The value of fast MR imaging as an adjunct to ultrasound in prenatal diagnosis. Eur Radiol 13:1538–1548

Brugger PC, Prayer D (2006) Fetal abdominal magnetic resonance imaging. Eur J Radiol 57:278–293

Brugger PC, Prayer D (2008) Magnetic resonance imaging of the developing efferent lacrimal pathways and pathogenesis of congenital dacrycystoceles (abstract). Eur Radiol 18:231

Brugger PC, Stuhr F, Lindner C, Prayer D (2006) Methods of fetal MR: beyond T2-weighted imaging. Eur J Radiol 57:172–181

Brunel H, Girard N, Confort-Gouny S, Viola A, Chaumoitre K, D'Ercole C, Figarella-Branger D, Raybaud C, Cozzone P, Panuel M (2004) Fetal brain injury. J Neuroradiol 31:123–137

Cannie M, Jani J, Chaffiotte C, Vaast P, Deruelle P, Houfflin-Debarge V, Dymarkowski S, Deprest J (2008) Quantification of intrathoracic liver herniation by magnetic resonance imaging and prediction of postnatal survival in fetuses with congenital diaphragmatic hernia. Ultrasound Obstet Gynecol 32:627–632

Cassart M, Massez A, Metens T, Rypens F, Lambot MA, Hall M, Avni FE (2004) Complementary role of MRI after sonography in assessing bilateral urinary tract anomalies in the fetus. AJR Am J Roentgenol 182:689–695

Chames MC, Pearlman MD (2008) Trauma during pregnancy: outcomes and clinical management. Clin Obstet Gynecol 51:398–408

Chan KY, Gilbert-Barness E, Tiller G (2003) Warfarin embryopathy. Pediatr Pathol Mol Med 22:277–283

Chaoui R, Kalache K, Heling K, Tennstedt C, Bommer C, Körner H (2002) Absent or hypoplastic thymus on ultrasound: a marker for deletion 22q11.2 in fetal cardiac defects. Ultrasound Obstet Gynecol 20:546–552

Coakley FV, Hricak H, Filly RA, Barkovich AJ, Harrison MR (1999) Complex fetal disorders: effect of MR imaging on management–preliminary clinical experience. Radiology 213:691–696

de Laveaucoupet J, Audibert F, Guis F, Rambaud C, Suarez B, Boithias-Guerot C, Musset D (2001) Fetal magnetic resonance imaging (MRI) of ischemic brain injury. Prenat Diagn 21:729–736

de Rijk-van Andel JF, Arts WF, Barth PG, Loonen MC (1990) Diagnostic features and clinical signs of 21 patients with lissencephaly type 1. Dev Med Child Neurol 32:707–717

de Vries JI, Visser GH, Prechtl HF (1985) The emergence of fetal behavior. II. Quantitative aspects. Early Hum Dev 12:99–120

Ertl-Wagner BB, Reiser MF (2001) Congenital spinal malformations. Radiologe 41:1048–1055

Garel C (2006) New advances in fetal MR neuroimaging. Pediatr Radiol 36:621–625

Girard N, Raybaud C, Poncet M (1995) In vivo MR study of brain maturation in normal fetuses. AJNR Am J Neuroradiol 16:407–413

Girard N, Gire C, Sigaudy S, Porcu G, d'Ercole C, Figarella-Branger D, Raybaud C, Confort-Gouny S (2003) MR imaging of acquired fetal brain disorders. Childs Nerv Syst 19:490–500

Gorincour G, Bouvenot J, Mourot MG, Sonigo P, Chaumoitre K, Garel C, Guibaud L, Rypens F, Avni F, Cassart M, Maugey-Laulom B, Bourliere-Najean B, Brunelle F, Durand C, Eurin D (2005) Prenatal prognosis of congenital diaphragmatic hernia using magnetic resonance imaging measurement of fetal lung volume. Ultrasound Obstet Gynecol 26:738–744

Gowland P (2005) Placental MRI. Semin Fetal Neonatal Med 10:485–490

Hubbard AM, Crombleholme TM, Adzick NS, Coleman BG, Howell LJ, Meyer JS, Flake AW (1999) Prenatal MRI evaluation of congenital diaphragmatic hernia. Am J Perinatol 16:407–413

Huber A, Hecher K (2004) How can we diagnose and manage twin-twin transfusion syndrome? Best Pract Res Clin Obstet Gynaecol 18:543–556

Kasprian G, Balassy C, Brugger PC, Prayer D (2006) MRI of normal and pathological fetal lung development. Eur J Radiol 57:261–270

Kitano Y, Nakagawa S, Kuroda T, Honna T, Itoh Y, Nakamura T, Morikawa N, Shimizu N, Kashima K, Hayashi S, Sago H (2005) Liver position in fetal congenital diaphragmatic hernia retains a prognostic value in the era of lung-protective strategy. J Pediatr Surg 40:1827–1832

Kok RD, van den Berg PP, van den Bergh AJ, Nijland R, Heerschap A (2002) Maturation of the human fetal brain as observed by 1H MR spectroscopy. Magn Reson Med 48:611–616

Lee HC, Cho SY, Lee HJ, Kim CJ, Park JS, Chi JG (2003) Warfarin-associated fetal intracranial hemorrhage: a case report. J Korean Med Sci 18:764–767

Levine D, Hatabu H, Gaa J, Atkinson MW, Edelman RR (1996) Fetal anatomy revealed with fast MR sequences. AJR Am J Roentgenol 167:905–908

Levine D, Barnewolt CE, Mehta TS, Trop I, Estroff J, Wong G (2003) Fetal thoracic abnormalities: MR imaging. Radiology 228:379–388

Linduska N, Dekan S, Messerschmidt A, Kasprian G, Brugger PC, Chalubinski K, Weber M, Prayer D (2009) Placental pathologies in fetal MRI with pathohistological correlation. Placenta 30:555–559

Liu X, Ashtari M, Leonidas JC, Chan Y (2001) Magnetic resonance imaging of the fetus in congenital intrathoracic disorders: preliminary observations. Pediatr Radiol 31:435–439

Mailath-Pokorny M, Krampl E, Watzinger F, Brugger PC, Prayer D (2009) The role of magnetic resonance imaging in prenatal diagnosis of facial clefts. Eur Radiol 19(suppl 1):S486

Malinger G, Lev D, Lerman-Sagie T (2006) Normal and abnormal fetal brain development during the third trimester as demonstrated by neurosonography. Eur J Radiol 57:226–232

Mari G, Hanif F (2008) Fetal Doppler: umbilical artery, middle cerebral artery, and venous system. Semin Perinatol 32:253–257

Marti-Bonmati L, Baamonde A, Poyatos CR, Monteagudo E (1994) Prenatal diagnosis of idiopathic neonatal hemochromatosis with MRI. Abdom Imaging 19:55–56

Meroni PL, di Simone N, Testoni C, D'Asta M, Acaia B, Caruso A (2004) Antiphospholipid antibodies as cause of pregnancy loss. Lupus 13:649–652

Mittermayer C, Brugger PC, Lee A, Horcher E, Hayde M, Bernaschek G, Prayer D (2005) Prenatal magnetic resonance imaging as a useful adjunctive to ultrasound-enhanced diagnosis in case of a giant fetal tumor of the neck. Ultraschall Med 26:46–50

Nemec SF, Brugger PC, Koelblinger C, Czerny D, Prayer D (2009) The face predicts the brain: The association of facial malformations and brain anomalies in fetuses with trisomy 13 in fetal MRI. Eur Radiol 19(suppl 1):S225

Osada H, Kaku K, Masuda K, Iitsuka Y, Seki K, Sekiya S (2004) Quantitative and qualitative evaluations of fetal lung with MR imaging. Radiology 231:887–892

Palacios Jaraquemada JM, Bruno C (2000) Gadolinium-enhanced MR imaging in the differential diagnosis of placenta accreta and placenta percreta. Radiology 216:610–611

Pataraia A (2008) Fetal lung development in premature rupture of membranes. Thesis, University Clinics for Radiology, Medical University Vienna, Vienna

Paul LK, Brown WS, Adolphs R, Tyszka JM, Richards LJ, Mukherjee P, Sherr EH (2007) Agenesis of the corpus callosum: genetic, developmental, and functional aspects of connectivity. Nat Rev Neurosci 8:287–299

Pemberton HN, Franklyn JA, Kilby MD (2005) Thyroid hormones and fetal brain development. Minerva Ginecol 57:367–378

Pistorius LR, Hellmann PM, Visser GH, Malinger G, Prayer D (2008) Fetal neuroimaging: ultrasound, MRI, or both? Obstet Gynecol Surv 63:733–745

Poutamo J, Vanninen R, Partanen K, Kirkinen P (2000) Diagnosing fetal urinary tract abnormalities: benefits of MRI compared to ultrasonography. Acta Obstet Gynecol Scand 79:65–71

Prayer D, Brugger PC (2007) Investigation of normal organ development with fetal MRI. Eur Radiol 17:2458–2471

Prayer D, Brugger PC, Prayer L (2004) Fetal MRI: techniques and protocols. Pediatr Radiol 34:685–693

Prayer D, Brugger PC, Kasprian G, Witzani L, Helmer H, Dietrich W, Eppel W, Langer M (2006) MRI of fetal acquired brain lesions. Eur J Radiol 57:233–249

Prayer D, Kasprian G, Ribeiro V, Brugger P, Malinger G (2009) MRI of fetal brain infection. In: Pediatric Neuroimaging, Expert Consult-Online and Print (Expert Radiology,) Charles Raybaud, Mauricio Castillo, James G Smirniotopoulos, Soonmee Cha, Eds, released Oct 13th, 2010-09-01

Riley EP, McGee CL (2005) Fetal alcohol spectrum disorders: an overview with emphasis on changes in brain and behavior. Exp Biol Med (Maywood) 230:357–365

Robson CD, Barnewolt CE (2004) MR imaging of fetal head and neck anomalies. Neuroimaging Clin N Am 14:273–291, viii

Savelli S, Di Maurizio M, Perrone A, Tesei J, Francioso A, Angeletti M, La Barbera L, Ballesio L, de Felice C, Porfiri LM, Manganaro L (2007) MRI with diffusion-weighted imaging (DWI) and apparent diffusion coefficient (ADC) assessment in the evaluation of normal and abnormal fetal kidneys: preliminary experience. Prenat Diagn 27: 1104–1111

Shellock FG, Spinazzi A (2008) MRI safety update 2008: part 2, screening patients for MRI. AJR Am J Roentgenol 191: 1140–1149

Shinmoto H, Kashima K, Yuasa Y, Tanimoto A, Morikawa Y, Ishimoto H, Yoshimura Y, Hiramatsu K (2000) MR imaging of non-CNS fetal abnormalities: a pictorial essay. Radiographics 20:1227–1243

Siegel MJ, Jaju A (2008) MR imaging of neuroblastic masses. Magn Reson Imaging Clin N Am 16:499–513, vi

Sonigo PC, Rypens FF, Carteret M, Delezoide AL, Brunelle FO (1998) MR imaging of fetal cerebral anomalies. Pediatr Radiol 28:212–222

Stazzone M, Hubbard A, Bilaniuk L, Harty M, Meyer J, Zimmerman R, Mahboubi S (2000) Ultrafast MR imaging of the normal posterior fossa in fetuses. AJR Am J Roentgenol 175:835–839

Surita FG, Parpinelli MA, Yonehara E, Krupa F, Cecatti JG (2007) Systemic lupus erythematosus and pregnancy: clinical evolution, maternal and perinatal outcomes, and placental findings. Sao Paulo Med J 125:91–95

Tauscher V (2008). Fetal cerebral ventriculomegaly—prenatal diagnosis, associated malformations and postpartal outcome. Thesis, Department for Gynaecology and Obstetrics, Medical University Vienna, Vienna

Toi A, Lister W, Fong K (2004) How early are fetal cerebral sulci visible at prenatal ultrasound and what is the normal pattern of early fetal sulcal development? Ultrasound Obstet Gynecol 24:706–715

Vanderheyden T, Kumar S, Fisk NM (2003) Fetal renal impairment. Semin Neonatol 8:279–289

von Mandach U (2005) Drug use in pregnancy. Ther Umsch 62:29–35

Witzani L, Brugger PC, Hormann M, Kasprian G, Csapone-Balassy C, Prayer D (2006) Normal renal development investigated with fetal MRI. Eur J Radiol 57:294–302

How to Shorten MRI Sequences

Guiding Choices for High Speed Imaging

Matthew Clemence

Contents

Abstract

› MRI offers an unrivaled method for detailed anatomical imaging with a high degree of flexibility in the image contrasts which may be generated. However, this flexibility comes at the cost of considerable complexity in the determination of the optimum sequence for any given application. It is rare, however, that an imaging task is created from scratch; often an MR sequence needs to be modified in response to a clinical challenge. For fetal imaging, this is most often to compensate for motion in utero. This chapter seeks to present to the non-MRI specialist the consequences and trade-offs encountered when modifying scan procedures, to provide a background and common ground for the development of fetal imaging protocols.

1 Introduction

It is always possible to make an MR imaging sequence faster; however, like the restaurant that offered on its menu "Good, Cheap, Fast – Pick any two," Magnetic Resonance Imaging (MRI) is similarly constrained, but in this case our options are "High quality, High resolution, Fast – Pick any two." It is an unfortunate fact that MRI is a signal limited method of imaging, and unlike other techniques, there are limited strategies available to raise the baseline amount of signal

M. Clemence
Philips Healthcare Clinical Science, Guildford Business Park, Surrey, GU21 8XH, UK
e-mail: matthew.clemence@philips.com

D. Prayer (ed.), *Fetal MRI*, Medical Radiology,
DOI: 10.1007/174_2010_96, © Springer-Verlag Berlin Heidelberg 2011

available. Methods where the body is probed using an outside source and the information is created through the interaction of that source with tissues, such as X-ray, CT, and PET, the intensity of the outside source can easily be increased within biological safety limits. In contrast, MRI induces the subject under study to generate and emit its own intrinsic signal which is very weak. As such, for high quality imaging, almost by definition, the imaging process will take an extended period of time.

The development of MRI, again in comparison with X-ray and CT, has taken place in a culture where image quality has often been evaluated through the surrogate measure of signal to noise ratio (SNR). This has been possible as MRI, without the use of ionizing radiation, has not often been constrained by scan time, the practical limit often being that of patient tolerance. Imaging sessions up to 1 h are not uncommon and may be even longer in the research arena, especially with healthy volunteers. X-ray and CT methods have always strived to reduce the dose on patient safety grounds, and hence their design criterion could be crudely phrased as "What is the worst (SNR) image I can use clinically." In contrast, MRI has typically been driven by "What is the best (SNR) image I can collect in the time available." This difference in strategy has led to very different approaches to the design of imaging sequences and their clinical practice.

Neglecting for a moment the trend to higher field strengths, the development of MRI to the clinical tool that it is today has been driven by the many strategies created to make the most of the limited signal available, through either hardware improvements or more complex imaging schemes ("pulse sequences"). In addition, advances in computing and reconstruction methods allow clinically useful images to be created with less data and reduced artifacts. In this chapter, I hope to provide an overview of many of these strategies and their impacts on speed, quality, and resolution, along with references where more detailed explanations can be found. However, it should be borne in mind that it is difficult to treat these strategies fully independently as they are highly coupled. The implementation of parallel imaging is a case in point, where advances in electronic design, and possibly more importantly hardware cost reductions, allowed duplication of the receiver sections of the MRI system. This has, in turn, opened up new possibilities for the creation of images from less data and hence in a shorter time. Ultimately, this has led to new sequences and corresponding changes in workflow being possible, for example, what previously may have required many minutes to acquire could now be covered in a breath-hold mitigating many of the motion issues, which the original imaging sequences were designed to eliminate.

As a physicist, I am often consulted on issues of protocol optimization, and to a user coming into MR from other modalities it can be bewildering to be confronted with the large parameter space available on a modern MR system. Given that a typical basic image will be determined by the four underlying magnetic properties (T_1, T_2, T_2*, proton density) in conjunction with secondary physiological parameters (such as diffusion, perfusion, flow) and any image represents a mix of these in varying ratios depending upon the timing of acquisitions, system specification (such as gradient performance), and interactions with natural motions, it is easy to see that sometimes seemingly small changes can lead to dramatic changes in image quality. Add to this the fondness of the MRI community for acronyms and differences in terminology between manufacturers, it can be difficult to know where to begin the conversation. The main aim of this chapter is therefore to try and bring some order to this process and help provide guidance on the likely impact of changes.

It is rare that an imaging protocol has to be created from scratch. All MRI systems are provided with comprehensive libraries of protocols and therefore it can be assumed that for a desired contrast, a protocol with good image quality is available, but which needs to be modified for speed, resolution, or artifact reduction in a particular clinical case. Given such a starting point, for each type of sequence it is possible to create a set of strategies for protocol modification and their impact on image quality, which unfortunately is almost inevitably (except in a few special cases) downward. As a result, the corresponding clinical decision is to determine what level of image degradation can be tolerated in order to answer the clinical question under study.

To that end I will cover first of all the motivations behind trying to achieve faster sequences, then give an overview of the sequences that are intrinsically fast and hence give a good starting point for further optimizations. Thirdly, present the different methods of sequence time reduction with discussions of

their likely visual impact. Finally, provide a brief overview of other newer strategies for speed increases offered by higher field strengths and parallel imaging technology.

One final point, however, is that one needs to start from the right place, recognizing the limitations inherent in a given MRI system. Technological development in MRI is still a major part of system design and new products and technologies appear annually. It is inevitable that for demanding applications, (fetal, cardiac, fMRI, diffusion methods) the largest increases come from having the latest electronics, a highly specified system, particularly the radiofrequency and gradients subsystems.

2 Image Quality and Resolution

A key aspect of any discussion on protocol optimization relies on a shared understanding of what aspect of the final image production is important. As has been indicated previously, for some applications this might be related to high SNR where subtle changes in signal intensity are to be detected, whereas in other areas a low artifact level may be important as it could be confused with pathology, and of course these criteria must be determined for each individual clinical area.

Where higher resolution is the target criterion it must be borne in mind that the final resolution achieved by the MR imaging process can easily be misinterpreted. Section on Image Production will expand on this area, but at this stage it is important to realize that the quoted resolution of MRI scan when viewed may not reflect the actual resolution acquired. Most scanners will allow two definitions of resolution to be made, one corresponding to the output image sent to storage and another which reflects the acquisition of the data from which the image is formed. As these two figures may be different, the data may be acquired at a lower resolution and interpolated (or otherwise reformatted) into the final target resolution of the image. Additional factors, such as physiological motion, may render the target resolution impossible to achieve. For example, when imaging the adult brain, the pulsatile motion of the tissue can cause displacements on the millimeter scale. The interpretation of the underlying resolution of imaging is that this can be difficult to determine as it depends subtly on the relationship to the time variation of the motion, the length of the scan, and the method by which the data is collected. These points must be taken into account when attempting to re-create or compare results taken from the literature.

3 Motion Control in MRI, Why Fast Imaging is Necessary

The demand for fast imaging is principally driven from two directions; the tolerance of the total scan time in the clinical environment (for either clinical or financial reasons) and imaging in the presence of motion. For the former, there is recognition that a certain set of imaging methods must be used to answer a clinical need. It is always preferable to perform this process in the most time efficient manner, whether it be for patient tolerance or issues of cost, income generation, etc. However, in this case, it is simply a tradeoff between image quality and time. It can be assumed that the imaging process will work in all cases. However, for motion control, this is no longer the case. If a single imaging scan may take several minutes to acquire the data for a given volume of interest, then any motion of the subject under study during that time will have an adverse effect on the resultant image. The effects may be as simple as blurring, or may introduce structured artifacts, which may be mistaken for anatomy or pathology. If the scan cannot be made motion tolerant, then the resultant scan will be nondiagnostic (Fig. 1).

Motion can be an issue in many clinical areas, whether due to patient restlessness, illness, age or discomfort, or where subject motion is a key part of the biological process under study, as in the case of cardiac and fetal imaging.

It is convenient to break physiological motion into four classes, each of which corresponds to a different set of compensating imaging strategies. They are, with typical examples

(a) Bulk unidirectional motion (e.g., Blood flow)
(b) Periodic motion (e.g., the cardiac muscle)
(c) Random constant motion (e.g., the bowels, restless patients)
(d) Random rare motion (e.g., a cough or spasm)

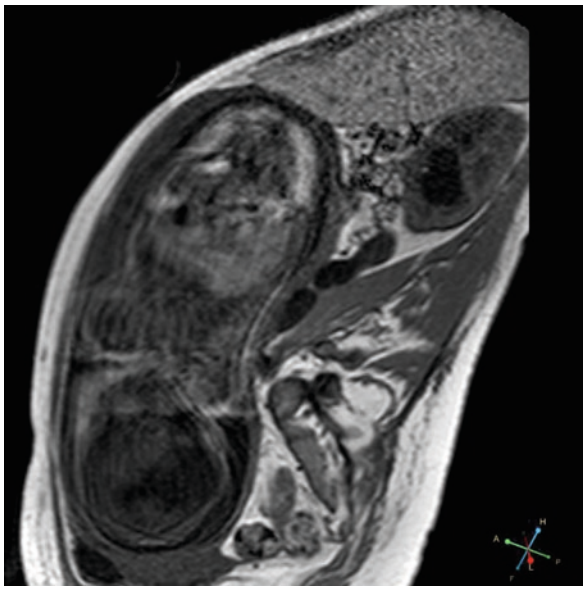

Fig. 1 Example of fetal motion during scan acquisition (scan time 22 s). 1.5 T TE 5.0 ms T_R 136 ms FA 80FOV 320 mm Slice 5.0 mm parallel imaging factor (SENSE) 1.5 acquired matrix 256×166 (Image courtesy D Prayer, AKH Vienna)

In MRI, several approaches have been developed to address each of the cases above, for example, time averaging of the data, synchronization of the acquisition to the motion, or ignoring the data when motion takes place (either in real time or by simple reacquisition), depending upon which of these cases we seek to deal with. Of course, paradoxically some of these strategies seek to minimize the artifact level through *extension* of the imaging time.

Cardiac cine imaging is probably the most familiar area where MRI produces what appears to be data with a high temporal resolution with each cine frame often representing an acquisition window of typically 1/20 s; however, this apparent high speed is an illusion. To achieve this, the scanner exploits the periodic nature of the cardiac cycle and the fact that MR images are built up from many measurements. Given this, and the fact that the electrocardiogram can be reliably measured in the MR scanner, it is possible to synchronize these two processes and acquire the images gradually over many heart beats; an approach which cannot be applied to cases c and d above. This leaves us with either motion averaging, which leads to blurred images in the same way a long exposure photograph blurs the passersby on a busy street, or truly snapshot imaging.

4 Image Production

In order to appreciate the impact of sequence changes, an understanding is required of how an MRI system creates an image from the raw signal and how this influences the time required for data acquisition. While sufficient overview will be presented here, for a complete description of this process the reader is referred to one of the many excellent text books on the subject for more detailed descriptions (for example, McRobbie et al. 2003).

4.1 The Image as Information

One approach is to consider that an image represents knowledge about an object represented as discrete points or pixels. The creation of an image is therefore a process of collecting information; for each point in space a measurement of a tissue property is made and translated to gray scale for display. This knowledge requires time to collect, and how efficiently we can collect that information is a distinguishing characteristic of different imaging modalities. It is important to make the distinction that this is a separate concept from measuring signal. Areas of the image may well be empty but this still represents the knowledge that the object does not extend into this area and therefore time is required to collect that information. What is significant in this formulation is that it is not necessary to collect all of this information as part of the scan. If some details of the object under study are known in advance, that knowledge can be incorporated into the scanning process reducing the amount of information collected at scan time, hence reducing the overall scan time. This use of prior knowledge is one of the key concepts behind parallel imaging.

Clinically, an image will be specified in terms of its field of view (FOV) and spatial resolution and hence we can describe our final image in terms of a matrix of data (usually square in the final production) consisting of a $n \times n$ matrix of points. As a consequence, this leads to the simplest form of imaging speed up, that is, simply to collect less data – either by reduction of the FOV (at constant resolution) or increasing the pixel size (at constant FOV) or a combination of both. In terms of the image/information formulation introduced above, this trivial case may be seen as introducing prior knowledge of either the

object's physical extent, or the minimum detectable size that is clinically relevant and using that prior information to collect less data.

4.2 Image Production in MRI

For MRI, compared to other imaging modalities, the image is not directly produced from the received signal, but via an intermediate form often referred to as k-space. The final image and k-space are related through a mathematical transformation, the Fourier transformation and this relationship underpins how data reduction and MRI parameters affect the final image.

MRI signal and k-space are so closely related such that the recorded MRI signal *is* the data required to fill in k-space. Whereas most imaging modalities build up an image directly over time, MRI builds up the k-space data over time and then produces the final image through a Fourier reconstruction. A key property of this relationship is that different parts of the k-space data correspond to properties of the whole image, more formally local changes in k-space correspond to nonlocal changes in the final image.

The first MRI parameter to consider is the repetition time, T_R. For the simplest class of imaging sequences – this defines time between the individual imaging experiments from which the image is formed. For conventional imaging sequences (conveniently defined here as those which collect one line of k-space per T_R), this directly controls the total imaging time; n lines of k-space will require $n \times T_R$ seconds to produce one image. As k-space is filled line by line, the two different axis of the resultant image are not equivalent. The two directions can be referred to the frequency encoded (or read) axis and the phase encoded axis. The MRI experiment collects a line of k-space along the frequency encoded axis in one T_R, with subsequent T_R intervals filling up k-space along the phase encoded axis. If we assume for a moment that the T_R is fixed because of the contrast we desire in the image, it can be appreciated that our simple approach of reducing the FOV, or resolution translates directly to collecting less lines of k-space, and hence requires less time for acquisition. All advanced acceleration methods are based upon collecting less lines of k-space and attempting to mitigate the effect that it has on the final image.

4.3 Summary

- Acquisition speed up in MRI depends upon collecting lines of k-space in a time efficient manner or collecting less lines overall.
- Collect the minimum amount of data for the clinical application by ensuring the FOV is as small as possible and the resolution is the largest acceptable.
- If the FOV is rectangular, try to ensure the shortest dimension corresponds to the phase encoding (or foldover) direction as this ensures the minimum number of lines of k-space is acquired.

5 Fast Imaging Sequences

There is only a limited amount of reduction to imaging speed that can be obtained through data reduction as a certain minimum image quality has to be maintained. Much of the recent progress in MRI has been the development of naturally fast imaging sequences. It is unfortunate that these methods are referred to by several different names in the literature depending upon the manufacturer and implementation. I will where possible use generic names and highlight equivalents where necessary.

5.1 Fast Imaging with Reduced T_R

The first class of fast imaging schemes arose from the simple observation that if the T_R could be reduced, the overall imaging time would drop; however, this adversely affects the available signal. How the MRI signal evolves with time is tissue-specific and variations in this evolution are exploited to develop tissue specific contrast in the image. Wherever an image is built up over many successive MR measurements, this evolution or *relaxation* has to be taken into account to ensure that there is both sufficient MR signal from which to form the image and also that the signal differences between tissues is suitable for the clinical application.

It is convenient to divide the source MR signal into two components. The first represents the pool of available signal which can be used to form a line of k-space. This signal is not detected directly but is converted to

the second, detectable signal pool through the interaction of specific radio frequency (RF) pulses on the subject. This first source pool, referred to as the longitudinal or z-magnetization, grows back to its equilibrium value (M_o) with a characteristic time T_1 according to the equation $M_z = M_o(1 - \exp(-t/T_1))$. For the majority of clinically relevant tissues, this characteristic time is typically 50–1,500 ms. If it is desired to get the maximum signal in each of the measurements, we must acquire the data fully relaxed, in other words our T_R must be several seconds. Given that a typical image may require around $200 \times T_R$, the source of the extended imaging times for MRI becomes clear.

It would therefore be desirable to reduce the T_R to shorten the acquisition times. Some shortening is beneficial as it introduces contrast in the image between tissues with differing T_1 relaxation times. However, if the T_R is chosen to be very short compared to the T_1 of the tissue under study, then there is insufficient time for new signal to develop before the next line of k-space is collected, and hence signal to noise in the final image drops. The solution, introduced in the sequence "FLASH" (Haase et al. 1986) is to reduce the amount of signal converted in each T_R through manipulation of the excitation RF pulses. For conventional imaging, the excitation pulse has a flip angle of 90° fully converting the pool of available signal into the detectable form. In the modified scheme, this flip angle is reduced only partially converting the available pool. This reduces the amount of signal for each line of k-space, but crucially leaves a significant amount of magnetization in the pool for the next T_R. For a given T_1 and T_R there is an optimum RF pulse flip angle which will produce the maximum SNR in the image. A side effect is that tissues with different T_1 will have different intensities so that this method produces a T_1 weighted image with the shorter the T_R leading to reduced SNR but more T_1 weighting. Modern implementations (variously named as Spoiled GRASS, SPGR, T_1-FFE, FLASH) can achieve repetition times as short as 2–10 ms such that an entire image may be collected in subsecond times with sufficient SNR and contrast to be clinically useful (Fig. 2).

These sequences, where repeated RF pulses produce and maintain a balance between the creation of new magnetization through T_1 processes and the transfer of that magnetization into useful signal form common group of methods referred to as steady state imaging. Once the steady state is achieved, the imaging can proceed for as long as required, leading to a high degree of flexibility in trading off imaging time for spatial resolution or multiple collections for averaging purposes. Another advantage is that as long as the T_R is kept constant, sequence adjustments will have a minimal effect on the contrast in the final image.

5.2 Fast Imaging Through Signal Recycling

Having explored the restrictions introduced by manipulating the source pool of signal, all of the other fast imaging methods explore the possibility of reusing the second, detectable, pool of signal after a line of k-space has been acquired. This second pool, referred to as the transverse- or *xy*-magnetization, decays away to zero after excitation with its own characteristic time constant. There are several mechanisms of decay, but it is convenient to combine them into a single time constant denoted T_2^*. The transverse signal, S, may be described with a exponential decay equation $S = S_0 \exp(-t/T_2^*)$. This time constant is again tissue-specific and represents the decay due to a combination of effects, magnetic susceptibility, magnetic field uniformity, as well as the intrinsic properties of the tissue. The consequence is that after a line of k-space has been acquired, many of these processes can be reversed such that, as long as T_2^* decay has not eliminated the signal entirely, significant signal can remain.

One of the first attempts to use this signal productively was proposed in the sequence FISP (Fast Imaging with Steady State Precession) (Oppelt et al. 1986).

In conventional spoiled gradient echo imaging, the steady state is only maintained in the longitudinal pool of magnetization, any remaining signal is deliberately removed (or "spoiled"). This approach had to be taken due to limitations in hardware performance on earlier systems that prevented the constructive build-up of the transverse steady state without introducing artifacts in the final image. These artifacts most commonly appear as dark bands across the image where instead of signal adding constructively to produce an enhanced signal level, variations due to small changes in the magnet homogeneity led to the signal adding destructively and leading to zero signal in these areas. Improvements in magnet specification and gradient design have in recent years allowed this sequence to become practical in its original form. Unfortunately, over time the term FISP has become associated with other steady state methods

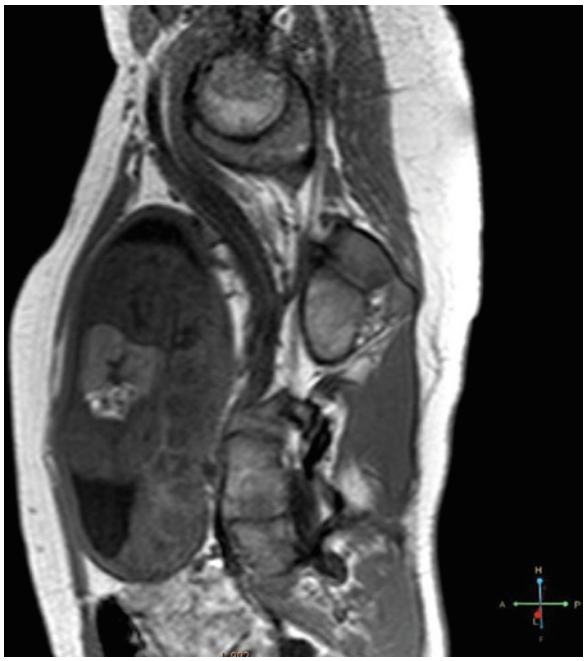

Fig. 2 Example large field of view T_1 weighted spoiled gradient echo image. 1.5 T T_E 5.0 ms T_R 125 ms FA 80 FOV 400 mm Slice 5.0 mm acquired matrix 208×114 (interpolated 256×256) (Image courtesy D Prayer, AKH Vienna)

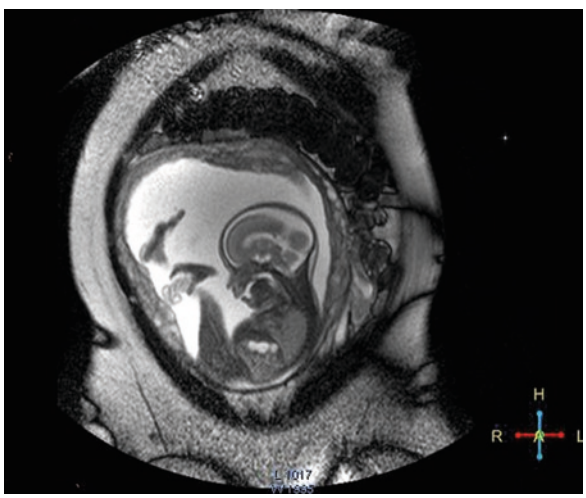

Fig. 3 Example large field of view bSSFP image – note the high signal intensity from fluids and presence of banding artifacts at periphery of image. 1.5 T T_E 2.9 ms T_R 5.8 ms FA 70 FOV 400 mm Slice 6.0 mm acquired matrix 272×218 (interpolated 512×512) (Image courtesy P Gowland, University of Nottingham, UK)

and so now this method goes under various names such as True-FISP, balanced FFE or Fiesta to distinguish it from the earlier techniques. These balanced steady state methods (bSSFP) have the advantage of much higher signal to noise than conventional spoiled gradient echo imaging but can be marred by the presence of the residual striping artifacts in large fields of view. The contrast in a bSSFP image (Fig. 3) looks superficially to be similar to that of a T_2 weighted image (in that fluid is bright); however, some caution in interpretation is required. Due to the fact that the final signal is a product of both a steady state in both the transverse and longitudinal pools, the final contrast is proportional to T_2/T_1

5.3 Fast Imaging Through Signal Refocusing

In the previous techniques, the signal has been derived by maintenance of a steady state through the balance of signal created through T_1 processes matching the signal decay during measurement. As such these scans use low flip angle RF pulses and start with a lower available signal, but can maintain that signal indefinitely. Returning to where we began with conventional imaging, an alternative approach to fast imaging can instead use the high flip angles of conventional imaging, and hence start with a large initial signal, but by using further manipulations to employ that signal as efficiently as possible during the T_2 decay period. This family of sequences, often referred to as turbo sequences, are characterized by collecting more than one line of k-space per repetition time. It may be desirable because of contrast considerations to extend the $T_{R,}$ but as we have seen this extends the overall imaging time; by filling more lines of k-space per T_R that time can be used more efficiently. This method is often presented to the user in the form of a "Turbo factor," which indicates how many lines of k-space per excitation pulse will be collected and thus directly relates to the scan time reduction achieved.

As was stated earlier, the transverse signal decays away due several mechanisms. This family of T_2-like effects, all of which affect the transverse signal pool are due to magnetic field inhomogeneities, both intrinsic to the tissue and from the external magnetic field, the imaging process itself as well as the true T_2 decay. Only this latter mechanism, being random in nature, is irreversible and represents the ultimate limit on how long the signal in a tissue may be detected. Typical tissues have a T_2 in the range of 10–400 ms, with fluids

having T_2 relaxation times upward of seconds. If it were possible to undo the effects of the other decay mechanisms, the signal is available for considerably longer than it takes to collect a single line of k-space and hence there is scope for more efficient scanning.

There are two methods for restoring the signal, spin echo, and gradient recalled echo methods. The former uses refocusing (180°) RF pulses to reverse both imaging and field-based decays leading to signal whose amplitude is purely dependant on T_2. Gradient recalled methods only reverse the effects of the imaging process and in this case the field inhomogeneity effects remain. This decay, represented by T_2^*, is a combination of the effects of the main magnet field homogeneity ("shim"), and tissue-induced field variations (susceptibility) is faster than T_2 and limits the amount of time available for data collection in gradient echo methods.

The first implementation of these methods using RF refocusing was originally referred to as RARE (Hennig et al. 1986) but is generally referred to as Turbo Spin Echo (TSE) or Fast Spin Echo (FSE). Its key characteristic is the high signal to noise of a conventional T_2 weighted imaging sequence; but given that m lines of k-space are acquired per T_R, the final image is acquired m times faster. It must be remembered, however, that T_2 decay is occurring throughout the echo train, which leads to different lines of k-space having different T_2 weightings. One advantage of this is that, by selecting which lines of k-space are acquired at different times after the initial excitation, the degree of T_2 weighting in the final image can be controlled without changing the overall imaging time. However, if the decay is significant over the whole scan, this can lead to blurring of the final image with tissues with a short T_2 relaxation time being more blurred than those tissues or fluids with long relaxation times. A second problem with TSE sequences is that there are strict safety limits on the amount of radiofrequency power, which can be put into a patient, specified in terms of a Specific Absorption Rate or SAR. The refocusing RF pulses require a high power and so the speed of these sequences may be SAR limited, particularly at higher field strengths.

The natural extension of this method is to collect the entire image with one excitation with a TSE turbo factor equal to the number of k-space lines required. This would be a true single shot method, but even with high performance gradients it is difficult to collect all of the data within the T_2 decay curve. To achieve true single shot imaging with TSE it is therefore necessary to aggressively reduce the amount of data collected, using partial k-space methods described earlier. Combining these techniques produces the HASTE sequence (Half Fourier Acquisition Single Shot Turbo Spin Echo) and may be referred to variously as SSH-TSE and SSH-FSE depending upon the reduction methods used (Fig. 4).

The third and final class of high speed imaging methods is the gradient recalled echo method. As with the TSE methods above, multiple lines of k-space are acquired per primary excitation but instead of using refocusing RF pulses, only the effects due to the imaging reversed by simply reversing the applied magnetic gradients. The signal will be recalled as those parts of the object which experienced a higher field will now experience a lower field and vice versa. As long as care is taken that the data is suitably reversed before use, this gradient recalled echo may be used for further lines of k-space.

In comparison with the TSE sequence, this has the advantage that no further RF pulses are required hence saving time and also SAR is not a limiting factor. However, now the signal is decaying with T_2* rather than T_2, a much shorter process. As a result, these images are much lower in SNR and have a much higher sensitivity to distortion from the imperfections in the main field and tissue susceptibility differences.

As with the TSE methods, the ultimate extension of this method is to collect the entire image with one single shot excitation with the number of gradient echoes equal

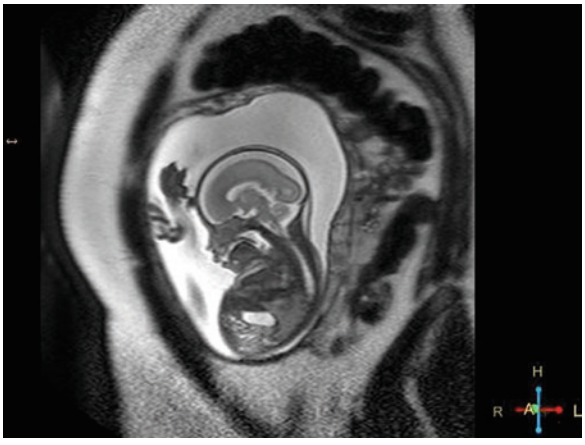

Fig. 4 Example large field of view sshTSE (HASTE) image – note the sharp edges on bright fluids but reduced sharpness on other tissues due to long echo train lengths 1.5 T T_E 120 ms T_R 8.3 s FA 90 FOV 300 mm Slice 4.5 mm echo train length 100 acquired matrix 272×167 (Image courtesy P Gowland, University of Nottingham, UK)

to the number of lines of k-space required for the entire image. In order to achieve the required number of gradient reversals within the T_2^* decay curve (typically <200 ms), high performance gradients are required in the MRI system to achieve artifact free imaging.

This method, Echo Planar Imaging (EPI) (Mansfield and Maudsley 1977), represents the fastest possible imaging method providing subsecond imaging times. The image quality however suffers due to distortions, low signal from short T_2^* tissues (muscle, liver) and requires high performance gradient systems to achieve. For certain applications, however, particularly diffusion imaging and fMRI, EPI represents the only practical method of obtaining the images free of motion artifacts (Fig. 5). The high performance gradients required for this sequence also generate a large amount of acoustic noise which may be of concern. Some of the shortcomings of EPI may be addressed if extreme speed is not required, by collecting the image in several segments or shots. It is important that the subject under study does not exhibit motion between the shots otherwise severe artifacts can be generated. Therefore, where SNR is sufficient, parallel imaging methods (see section on Parallel Imaging) are preferred

5.4 Hybrid Sequences

While sequences such as turbo spin echo, SPGR, EPI, and SSFP are often described as separate imaging methods with their own artifacts, it is often useful to consider them as a continuum of sequences. If we consider an image requiring n lines of k-space, for example, and gradient echo methods, a simple 2DFT is at one end of the spectrum with one gradient echo per RF excitation pulse and n repetitions with EPI at the other end with a n gradient echoes per RF excitation pulse and one repetition. Similarly for spin echo methods with single shot TSE as the extreme (n 180° pulses per excitation pulse). The advantages and disadvantages of TSE methods are low distortion, high SNR but with high SAR which are complementary to those of the gradient echo methods so it is reasonable to suggest that these techniques may be combined. The resulting sequence GRASE (Gradient Spin Echo) (Oshio and Feinberg 1991) introduces a small number of gradient echoes at each spin echo location. This has the effect of reducing the number of 180° pulses required for a single scan, reducing both SAR and scan time, while introducing some T_2* weighting putting the SAR, susceptibility and distortion performance between that of TSE sequences and EPI methods.

5.5 Summary

- FLASH gradient echo methods generate fast imaging T_1 weighted imaging through reduced T_R. For each T_R and T_1, there exists an optimum RF flip angle setting for maximum signal. For long T_1 and short T_R, signal is reduced.

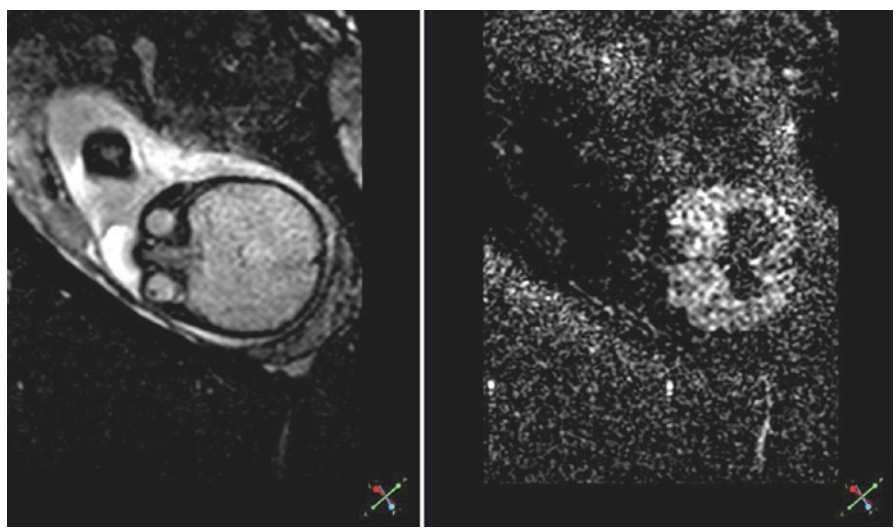

Fig. 5 Example SE-EPI (with and without diffusion weighting). Note Low SNR in all tissues with short T_2^*. 1.5 T T_E 125 ms, T_R 1.4 s FA 90; SPIR fat suppression FOV 250 mm × 190 mm EPI echo train length 81 (Image courtesy D Prayer; AKH Vienna)

- True-FISP methods improve on the SNR from FLASH methods at the risk increased banding artifacts. T_R must be kept short (and equal to $2 \times T_E$) for maximum SNR and artifact free imaging.
- Single Shot TSE sequences collect the entire image within the T_2 decay of the tissue under study. Caution needs to be used as the blurring is tissue-specific and can be significant in tissues with short T_2 but with the appearance of sharpness in long T_2 areas such as the amniotic fluid or CSF. Often limited by SAR power constraints due to the large RF duty cycle required.
- EPI sequences collect the entire image within the T_2^* decay, so most suitable for tissues with long T_2^* such as the central nervous system. Susceptibility distortions are prominent and acoustic noise may be an issue.
- GRASE hybrid sequences trade of the benefits and disadvantages of TSE and EPI sequences with performance levels between the two.

6 Parallel Imaging

The most significant advance in imaging technology in recent years has been the implementation and availability of parallel imaging methods whereby the receiving system forms a key part of the image generation process rather than merely being an antenna for the MR signal. In early MR systems, a single RF antenna was used both for generation of the RF pulses and also the reception of the subsequent MR signal. It was essential that the field generated by such antennae were as spatially uniform as possible so that the RF pulses were well defined throughout the object under study as this directly impacted image uniformity and the contrast developed in the image. However, it soon became obvious that significant gains in performance could be obtained by separating out these two functions. A single uniform transmission coil, typically built into the bore of the magnet, combined with many smaller, higher sensitivity receive coils which could be placed closer to the body has now become the universal approach. Initially, the receive arrays were constructed such that the signals from each element could be combined electronically to approximate a uniform coil response to preserve the uniformity of the final image. However, this method required the relative spatial position of coils to be fixed and sacrificed the flexibility of arbitrary receive coil placement. Once the idea of a deliberately nonuniform response field was accepted, a new approach to image acceleration became possible.

Returning to the concept that image production is the collection of information about the distribution of signal, this idea can be extended to incorporate information from other sources in addition to the single imaging experiment. In fact, the idea that prior knowledge allows the imaging experiment to be shortened has already been introduced when we consider the effect FOV has on imaging time. By using the *prior information* that there is no signal from certain areas (obtained from a survey image, for example) we can tailor the FOV, and hence the acquisition time, to the object under study. This can be powerfully extended if the following conditions are met.

(a) The signals from each of the receive elements can be recorded as a separate image rather than combined electronically (multiple independent channels).
(b) The receive coil sensitivity patterns are maximally different.
(c) The receive coil sensitivity patterns are known in advance.
(d) All parts of the final image can be picked up by at least one coil.

By comparing at the relative signal intensity of the same part of the image in all of the different channels and knowing the sensitivity patterns we gain prior knowledge of the spatial distribution of the signal. As these sensitivity patterns can be collected in advance, this has the possibility of significantly reducing the data collection burden during the actual imaging scan, and hence shortening imaging times.

These methods have developed to a high level of maturity, and implementations are available on all major MRI systems. Parallel imaging may however be implemented in several different ways each with their own, as MR developments tend to be, acronyms; most notably either in image space (SENSE) (Pruessmann et al. 1999) or k-space (SMASH) (Sodickson and Manning 1997) with many variations based on these initial methods. In typical implementations of both techniques, a new parameter is presented to allow the user to reduce the number of phase encoding steps by some factor and hence reduce the scan time, with the loss of some SNR in the final image as less data is being used to create the final result. The actual acceleration achievable without artifact is heavily dependent

upon the number of channels, the protocol and available SNR. In addition, the time taken to collect the reference data may have to be taken into account depending on whether the implementation incorporates this process in the actual scan or can be instructed to collect it in advance. Where the image- and k-space methods differ is in how the images degrade and the appearance artifact levels when the acceleration is pushed beyond practical limits. Whereas for conventional imaging the drop in image quality is predictable and often smoothly variable, parallel imaging methods can suddenly introduce highly spatial variable noise characteristics and unusual foldover artifacts with small changes in SNR or planning. This is most noticeable as noise enhancement in the center of images where none of the receive coils have a good sensitivity. This leads to the undesirable side effect that the performance of a protocol may become very dependent upon patient size as the receiver coils are further apart. Other issues, such as foldover restrictions may limit the general applicability of parallel imaging in fetal imaging. It is typical in fetal imaging that some image foldover, or wrap, will occur due to the difficulty in planning a suitable image plane. In general, this artifact will occur at the edges of the FOV and not interfere with the diagnostic quality of the scan. If image based parallel imaging is used in the presence of foldover, depending upon the factor and obliqueness, this artifact can be moved into critical parts of the image as shown in Fig. 6.

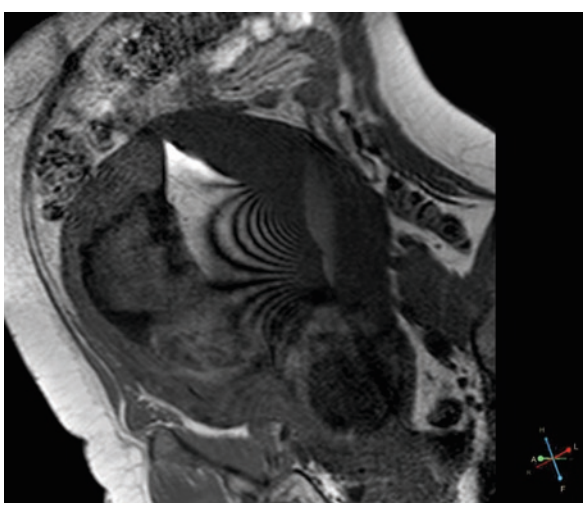

Fig. 6 Example gradient echo image showing foldover artifact from image- based parallel imaging with a too restrictive field of view (Image courtesy P Gowland, University of Nottingham, UK)

However, as parallel imaging has been incorporated into routine scan protocols what has emerged is that rather than simply a technique which may be used to accelerate imaging, with a commensurate drop in SNR, it has become a method by which freedom to modify other, more desirable, aspects of the protocol becomes possible. By reducing the number of phase encoding steps acquired, more time becomes available, which may be utilized in other ways. For example, for TSE methods, echo times may be reduced, increasing the available SNR which may compensate for that lost by applying parallel imaging, leading to a scan which is both of faster and higher quality. For echo planar methods this reduction can also lead to improved distortion characteristics for diffusion methods. Alternatively, the overall protocol acquisition time can be kept constant and the reduced number of lines of k-space collected with lower bandwidths improving SNR, but at the cost of increased distortion and longer echo times.

6.1 Summary

- Parallel imaging is a general method for reducing the amount of k-space data which is required to produce an image by simultaneous data collection on multiple separate channels. However, this can introduce artifacts if too little data is collected for a given protocol.
- Most commonly used at moderate levels for faster scanning but with a drop in SNR.
- The time freed up by the data reduction can instead be flexibly traded off against other parameters such as SNR (by reducing acquisition bandwidths), and echo time.
- EPI sequences can benefit greatly from parallel imaging through both the reduction in echo time (leading to more signal) and also the improved distortion characteristics of the shorter scan.
- Planning and FOV limitations may be required depending upon the implementations.

7 High Field Imaging at 3.0 T

MRI is unfortunately a signal limited imaging modality, a point which has impacted upon all of the techniques we have described previously. The baseline, maximum equilibrium signal available is limited due to the low magnetization, which is present in the

hydrogen nucleus under normal conditions. While there are methods of temporarily increasing the pool of available signal, usually referred to as enhanced- or hyper-polarization, these methods are not generally applicable to the bulk source of signal in the human body. However, the polarization is proportional to the strength of the main magnetic field of the magnet and while 1.5 T remain the most common field strength, 3.0 T systems and higher are becoming widely available. It is tempting to think of 3.0 T systems simply in terms of enhanced signal, and while the advantages of having twice the signal available would appear at first sight to make the move to 3.0 T an obvious one, there are several other effects which must be taken into account. As a consequence, it is important that protocols are designed afresh when moving to higher field systems as the relaxation times, SAR, and artifact levels are all modified and can lead to different strategies to be required. It should also be noted that there may be national guidelines and regulatory issues which will have to be followed for routine clinical scanning at higher field strengths for fetal imaging.

7.1 Physical Limitations of 3.0 T Imaging, SAR, and Susceptibility

A by-product of the method of inducing the sample under study to generate the visible MR signal, the application of RF pulses, is heat. This heat, if applied unchecked, would lead to large temperature rises within the tissues and consequent cell damage. As a result, there are strict regulatory limits placed upon the temperature rise of tissues when scanning. This is translated into a measure of SAR and is calculated in terms of W/kg of the tissue exposed. The consequence of this is that there is a limit to the number and power of RF pulses that may be played out in unit time, which is counter to many of the strategies for fast imaging. This limit is present at all field strengths; however, as the field increases, more heat is generated for the same requested RF performance and so as field strengths increase scan protocols can become increasingly SAR limited. TSE sequences suffer most from this effect due to the high number 180° of refocusing pulses required, with gradient echo next and EPI methods affected the least. The practical upshot is that if a high SAR protocol is translated unchanged from 1.5 T to 3.0 T, it is probable that the minimum T_R achievable will be longer; consequently, the scan may not be possible, the image contrast changes, or motion will again become an issue due to the extended scan duration. Fortunately, the data reduction strategies already considered (parallel imaging, partial k-space scanning) will reduce the RF burden but will also cost some of that hard-won SNR gained by going to the higher field strength.

A second effect of the higher field strength is that distortions, both in the RF field and main magnetic field, will also become more significant. The consequence is that image artifacts at tissue boundaries (gradient echo methods), geometric distortions (echo planar methods), fat suppression methods, and, image homogeneity all require greater performance for the same image quality at 3.0 T. To address some of these issues, technical advances such as inhomogeneity-tolerant methods for fat suppression, high channel count coils, and advanced post-processing have been developed at 3.0 T, many of which have also trickled down to 1.5 T systems.

7.2 New Developments in 3.0 T Imaging, RF Homogeneity, and Multi-transmit

It has previously been discussed that the move to 3.0 T is not a panacea for improved image quality in all areas. The limitations of SAR have already been highlighted but there is also a more subtle problem with the interaction between the patient and the system, that of RF homogeneity. The goal of MRI is to produce a diagnostic image with both a uniform intensity across the FOV and, almost more importantly, a uniform contrast response. To achieve this, early MR systems were designed around a hardware RF coil system (so called "birdcage" coils), which had a uniform response field throughout the sensitive volume. With advent of parallel imaging, the receive side of the system was made deliberately nonuniform and image homogeneity restored as a by-product of the parallel imaging method. However, all of these methods assume that the transmit field of the system remains uniform, that is, the requested RF flip angle is the same throughout the FOV. As a result most modern scanners use a two coil solution – a uniform "body coil," often built into the fabric of the scanner, to produce the homogeneous transmit field, and the separate receive coil array for multichannel imaging. The assumption of transmit

uniformity is required for many aspects of the imaging process, not least that the contrast developed in the image is the same no matter where in the image one is looking. The difficulty is that if a conductive object is placed in the RF field, the human body being a fine example, the RF field is distorted and low and high spots can be generated. As well is the impact this variation has on the image quality, the high spots induced also have an impact on the SAR performance of the protocol. This effect is present at all field strengths and at 1.5 T and below is often tolerable in all but the most exacting circumstances; but like many properties of MRI, gets worse at increasing field strength. While much improvement can be gained through protocol design (to limit the effects of flip angle sensitivity) and also in system design, for example, by assuming a default patient and changing the body coil design to compensate, there are limits to the applicability of these methods as they depend upon the size and shape of the patient. Fetal imaging, with the dramatic body changes induced in the mother, and the presence of a large amount of conductive fluid, often shows the effects of RF inhomogeneity dramatically.

The solution currently being developed and starting to become available clinically is to apply more control to the transmit field in an analogous way to the changes introduced to the receive field by parallel imaging. By splitting the single body coil into many individually controllable elements, the RF field can be adjusted to compensate for the variations induced on a patient by patient basis. This is, at the time of writing, a method under rapid development and early results demonstrate clear advantages for fetal imaging with improvements in image quality and, as adjustments are made on a patient by patient basis, also improve consistency across patients. Figure 7 shows an example comparison for a single shot spin echo sequence at 3.0 T. For the normal single channel excitation system (A), it is clear that the image homogeneity and contrast is reduced in the center of the image due to the large patient size and presence of the amniotic fluid. With multichannel adjustment, (B) much of the image quality is restored.

A second benefit is improved SAR control due to the measurement and adaptation of the RF field. Currently, SAR is predicted in software on a protocol by protocol basis and has to take into account the presence of worst-case variations in the field induced by all patients, leading to a more conservative model than may actually be required for a specific patient. By measuring and adapting the transmit field, faster imaging can be achieved more easily in the SAR limited case. For the future, it is expected that these methods, with greater and more flexible control of the transmit field through the use of more independent transmit channels will be able to be employed as flexibly as parallel imaging has come to be used. Whereas parallel imaging was originally developed for speed, it has become a general parameter which may be traded off against SNR, distortion, echo times, etc. Similarly, the user may choose to run a higher SAR sequence but control the homogeneity over a small defined region, for example, quantitative MRI. The availability of multichannel transmit systems outside of the research

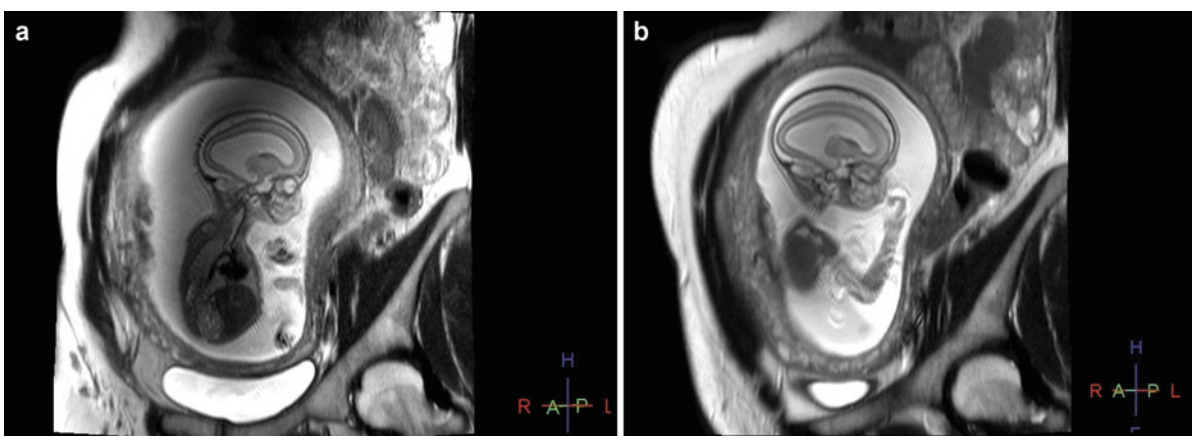

Fig. 7 3.0 T Multichannel transmit (ssh-SE T_E 120 ms) (Images courtesy Fletcher Allen Heathcare Centre, University of Vermont, Philips Healthcare Best NL)

arena is just beginning and development, especially in high field applications is expected to be rapid.

8 Conclusion

Protocol optimization, particularly in challenging clinical imaging areas, is always a task of trading off benefits with disadvantages. Clinical guidance will determine what level of image quality, artifact and contrast is acceptable for a given application and with less important aspects sacrificed to compensate. For any given system, reduction in imaging time will nearly always result in a compromise between resolution and SNR. New developments in parallel imaging and multichannel transmit technology, in conjunction with higher field strengths are delivering new parameter spaces and SNR improvements, allowing improved image quality and consistency in these challenging clinical areas.

References

Haase A, Frahm J, Matthaei D, Hänicke W, Merboldt KD (1986) FLASH imaging: rapid NMR imaging using low flip angle pulses. J Magn Reson 67:258–266

Hennig J, Nauerth A, Friedburg H (1986) RARE imaging: a fast imaging method for clinical MR. Magn Reson Med 3:823–833

Mansfield P, Maudsley AA (1977) Planar spin imaging. J Magn Reson 27:101

McRobbie D. et al. (2003) MRI, From picture to proton. Cambridge University Press

Pruessmann KP, Weiger M, Scheidegger MB, Boesiger P (1999) SENSE: sensitivity encoding for fast MRI. Magn Reson Med 42(5):952–962

Oppelt A, Graumann R, Barfuss H, Fisher H, Hartl W, Schajor W (1986) FISP – a new fast MRI sequence. Electromedica 54(1):15–18

Oshio K, Feinberg DA (1991) GRASE (Gradient-and Spin-Echo) imaging: a novel fast MRI technique. Magn Reson Med 20:344–349

Sodickson DK, Manning WJ (1997) Simultaneous acquisition of spatial harmonics (SMASH): fastimaging with radiofrequency coil arrays. Magn Reson Med 38(4):591–603

Fetal MRI at Higher Field Strength

Andreas Stadlbauer and Daniela Prayer

Contents

Abstract

› While fetal MRI has become a routine method at field strengths up to 1.5 T, the use of higher field strength is at an early stage. A higher signal-to-noise ratio is accompanied by a higher energy deposition. In addition, parameters of sequences have to be adjusted to achieve useful contrasts. Susceptibility effects and certain artifacts that increase with higher field strength have to be considered. The same is true for certain artifacts that maybe negligible at lower field strength. Special measures have to be taken to grant maternal and fetal safety. Due to the high resolution, MR imaging at 3 T is currently the method of choice in postmortem fetal imaging.

1 Introduction

At the introduction of magnetic resonance imaging (MRI) into clinical practice in the late1970s, the most MR systems on the market operated at a magnetic field strength of ≤0.6 T. In these early days of MRI, a necessity for the development of more powerful magnets for imaging of parts of the body beyond the brain was commonly not seen. The first 1.5 T MR systems were introduced in 1982 and became the predominant magnetic field strength used for clinical high-quality MR imaging in the late 1980. At that time, MR scanners operating at 1.5 T were named "high-field systems." The first 3.0 T whole-body MR systems were developed in the early 1990s. Due to practical reasons, e.g.,

A. Stadlbauer (✉)
MR Physics Group, Department of Radiology,
Landesklinikum St. Poelten, Propst Fuehrer Strasse 4,
3100 St. Poelten, Austria and
Department of Neurosurgery, University of Erlangen-Nürnberg,
Schwabachanlage 6, 91054 Erlangen, Germany
e-mail: andi@nmr.at

D. Prayer
Department of Radiology, Medical University of Vienna,
Waehringer Gürtel 18–20, 1090 Vienna, Austria
e-mail: daniela.prayer@meduniwien.ac.at

D. Prayer (ed.) *Fetal MRI*, Medical Radiology,
DOI: 10.1007/174_2010_27, © Springer-Verlag Berlin Heidelberg 2011

inadequacies in radiofrequency (RF) coil design and protocols, installations of these systems remained limited to academic institutions for research till the beginning of the new century. However, a multiplicity of publications demonstrated improvements at 3.0 T in anatomical imaging (Duewell et al. 1996; Fujii et al. 1998; Ugurbil et al. 1993; Vinitski and Griffey 1991), MR spectroscopy (MRS) (Barfuss et al. 1990; Hetherington et al. 1995), and functional MRI (fMRI) (Jesmanowicz et al. 1998; Kruger et al. 2001; Menon et al. 1995; Thulborn 1999) – only a small sample of papers are presented here – compared with 1.5 T.

Safety guidelines of the Food and Drug Administration (FDA) which limited the magnetic field strength that may be used for diagnostic purposes were expanded from 2.0 to 4.0 T in 2002. The FDA limit for magnetic field for MR imaging applications in human subjects is currently at 8.0 T. Since that time and due to technological advances occurred meanwhile, 3.0 T whole-body MR systems have been introduced into clinical practice in increasing numbers and are the "high-field systems" of today, while MR systems operating at field strengths of below 1.5 T have generally lost popularity and are limited now to open designs.

The main argument for purchasing a 3.0 T MR system, besides commercial considerations (i.e., strategic marketing and to stay competitive), is the expected improvement in image quality due to increased signal-to-noise ratio (SNR) of up to twofold (Edelstein et al. 1986) compared to 1.5 T. This gain in SNR can be used directly to improve the image quality or traded for improved temporal or spatial resolution, or both. However, the transition to higher field strength was accompanied with new challenges, such as increases in RF power deposition (i.e., specific absorption rate, SAR), T1 relaxation times, RF effects, susceptibility effects, and chemical shift effects.

As mentioned above, important technological developments occurred besides the shift to the use of higher field main magnetic field strengths. These advances in MR technology include the development of phased array surface coils consisting of 4–16 or more coil elements, increased number and bandwidth of receiver channels, improvements in gradient performance, and innovative and accelerated acquisition techniques (Hussain et al. 2005).

The purpose of the first part of this chapter is to review and discuss the opportunities and challenges of MR imaging in the abdomen at high magnetic field strength, i.e., 3.0 T in context of this chapter. The second part addresses the potential and limitations of 3.0 T MRI for the use in fetal diagnostics.

2 Opportunities and Challenges of Abdominal MR Imaging at Higher Field Strength

The increase of strength of the main magnetic field (B_0), e.g., from 1.5 to 3.0 T, influences several physical parameters which are essential for the quality of the MR images. Most of the physical effects of the higher magnetic field strength are not solely beneficial or disadvantageous, but represent rather two sides of the same coin. It is important to see these changes of the physical parameters in connection with the type of MR application. Therefore, a discussion about opportunities and challenges rather than advantages and disadvantages of MR imaging at higher field strength is preferable. This section describes the changes of the most important physical parameters and their effects on MR imaging at higher field strength.

2.1 Signal-to-Noise Ratio

The SNR describes the signal strength of a tissue or a part of the body on the MR image relative to the background noise, which is defined as the mean standard deviation of the signal strength in the background of the image. The SNR is proportional to the net spin vector, also named as net magnetization. This net magnetization is defined as the difference between the number of spins aligned parallel and antiparallel to the main magnetic field, respectively, and increases almost linearly with increasing main magnetic field strength (Hoult and Phil 2000; Wen et al. 1997). At 1.5 T and under in vivo conditions (i.e., body temperature), five out of one million spins are additionally aligned along the magnetic field. This number, and hence the net magnetization, is double at 3.0 T, which creates the potential for a doubling of the derived signal. Since noise is independent of field strength and based on the arguments mentioned above, the SNR at 3.0 T should be double that at 1.5 T.

However, the SNR of an MR image depends not only on the field strength alone, but also on several of other parameters, e.g., the number of hydrogen spins per voxel volume (i.e., spatial resolution), acquisition time, receiver bandwidth, and the environment of the spins (i.e., relaxation effects). Equation (1) represents a simplified correlation between the SNR in spin-echo (SE) sequences and these parameters (Edelstein et al. 1986):

$$\mathrm{SNR}_{\mathrm{SE}} \propto B_0 \cdot V \cdot \sqrt{\frac{N_{\mathrm{ex}} \cdot N_{\mathrm{ph}}}{\mathrm{BW}}} \cdot (1 - e^{-\mathrm{TR}/T1}) \cdot e^{-\mathrm{TE}/T2}. \quad (1)$$

B_0 is the strength of the static magnetic field, V is the volume of a voxel, N_{ex} is the number of excitations, N_{ph} is the number of phase-encoding lines in k-space, and BW is the receiver bandwidth. The product of N_{ex} and N_{ph} is a measure of the image acquisition time. The two factors including exponential functions consider the effects of relaxation: TR and TE are the repetition and the echo time, T1 and T2 are the relaxation times, respectively. The equation for gradient-echo sequences is very similar, but showed two additional factors to account for flip angels <90° used for excitation and those <180° used for refocusing (Edelstein et al. 1986). Based on this formula, SNR is proportional to the main magnetic field strength, the voxel volume, the square root of the data acquisition time divided by the receiver bandwidth, and some tissue- (T1 and T2 relaxation time) and sequence-specific (TR and TE) terms. Provided that the other parameters in Eq (1) remain constant, the SNR at 3.0 T is really double that at 1.5 T. However, in real life these factors are usually affected by the field strength and tend unfortunately to counteract the benefit in SNR. At higher field strengths, the two most important effects, which lead to a limitation of the SNR advantage, are the increases in tissue T1 relaxation time values and the increased deposition of RF energy (i.e., SAR). The corrections to overcome these and other obstacles, which will be described in more detail in the following sections of this chapter, are mostly associated with a loss in SNR. The realized gain in SNR for abdominal MRI at 3.0 T over that at 1.5 T was reported to be between 0.8 and 5.6-fold (Merkle and Dale 2006; Merkle et al. 2006). Within a particular examination, the higher SNR afforded by higher field strength can be exploited in several different ways: to reduce acquisition time at a given spatial resolution or vice versa and variable combinations of the two.

A second aspect of SNR at higher field strength has to be discussed in this context. The beneficial increase in SNR at 3.0 T is associated with an increased noticeability of artifacts. Bernstein et al. (2006) called this phenomenon an increased artifact-to-noise ratio (ANR) due to the increased SNR. Some artifacts are masked by the noise on the image at 1.5 T. They are either not conspicuous or at least not troublesome because their intensity level is comparatively low. The increased ANR at higher field strength is associated with an increased background contrast and hence an increased detectability of the artifact. A typical example is Gibbs ringing (or truncation artifact) which tends to be more prominent at 3.0 T (Amartur and Haacke 1991; Dietrich et al. 2008). Gibbs ringing arises when the acquired raw data are clipped at the edges of k-space. In this case the signal intensities are significant over the level of noise at the border of k-space due to the increased SNR at higher field strength. Strategies to reduce or overcome the artifact are either to increase the spatial resolution, which is associated with an increase in measurement time and a decrease in SNR (see eq. 1), or the application of an apodization filter (e.g., Hanning filter).

2.2 B_0 Homogeneity and Susceptibility Effects

The homogeneity of the main (static) magnetic field (B_0) is a fundamental concern during the design and implementation of many magnetic resonance experiments, especially for echo planar imaging (EPI), steady-state free precession (SSFP), and localized MRS. The B_0 homogeneity has influence on the distribution of the resonance frequency of the protons and the linearity of the magnetic field gradients required for spatial encoding. The homogeneity depends on the passive and active shimming (a procedure to improve homogeneity) of the magnet, the composition and geometry of the object or subject under investigation, and any foreign (metal) objects in the subject or the scanner. At 3.0 T, it is more challenging to obtain a sufficient homogeneity of the main magnetic field. This kind of magnets requires more and high-order shimming.

A heterogeneous magnetic field, also known as "poor shimming of the magnet," leads to different effects: (a) the dispersion of the resonance frequency

of the spins within a single voxel leads to an increased dephasing of the magnetization and a decrease in T2* relaxation time, which is also a measure for signal loss due to B_0 inhomogeneity (Haacke et al. 1989; Yablonskiy and Haacke 1994). In MRS experiments the line width of the peaks, i.e., the width of the metabolic signal in the MR spectrum, is increased and may cause a worse spectral resolution due to overlapping peaks. Further, water and lipid suppression may be ineffective and resulted in poor quality of the spectrum; (b) Stronger variations of the resonance frequency cause, on the one hand, intravoxel dephasing, which is associated with signal attenuation and geometric distortions, especially at EPI sequences (Merboldt et al. 2000; Ojemann et al. 1997). SSFP sequences are also very sensitive to off-resonance effects which can cause banding artifacts (Wieben et al. 2008). Figure 1 shows examples for massive banding artifacts in SSFP sequences measured at a woman with a triplet pregnancy. On the other hand, these frequency variations result in mismatch of the excitation frequency of chemically selective radiofrequency (RF) pulses. This leads to an incomplete fat saturation for the application of frequency-selective (spectral) fat suppression.

An interesting point is the fact that the B_0 homogeneity of the empty magnet is very high, but substantially reduced by positioning of the patient inside the magnet because of the patient's susceptibility. Magnetic susceptibility is the extent to which a material becomes magnetized when exposed to a magnetic field. The susceptibility varies substantially for different materials. A distinction is drawn between diamagnetic materials like water and biological tissue, which weaken the external magnetic field and have negative susceptibility; paramagnetic substances like gadolinium and titanium with positive susceptibility, which show an enhancement of field strength inside the material; and ferromagnetic materials (e.g., iron) with a strong positive susceptibility. The susceptibility of air is approximately zero. As a consequence of the differences in magnetic properties of the materials, additional magnetic fields of different strength are superposed to the originally very homogenous main magnetic field and lead to partly drastic decrease in field homogeneity. Microscopic magnetic field gradients and variations occur around the interface of regions with different susceptibility (i.e., bone – soft tissue; or air – soft tissue) and lead to the so-called susceptibility artifacts. As susceptibility of a material is proportional to field strength, the worsening effect on the field homogeneity as well as the microscopic field variations at 3.0 T is double that at 1.5 T. On the other hand, this effect is exploited at 3.0 T in improving the sensitivity of MR imaging sequences to the presence of hemorrhage and mineralization (Frayne et al. 2003).

A variety of protocol manipulations are available to minimize the influence of susceptibility artifacts:

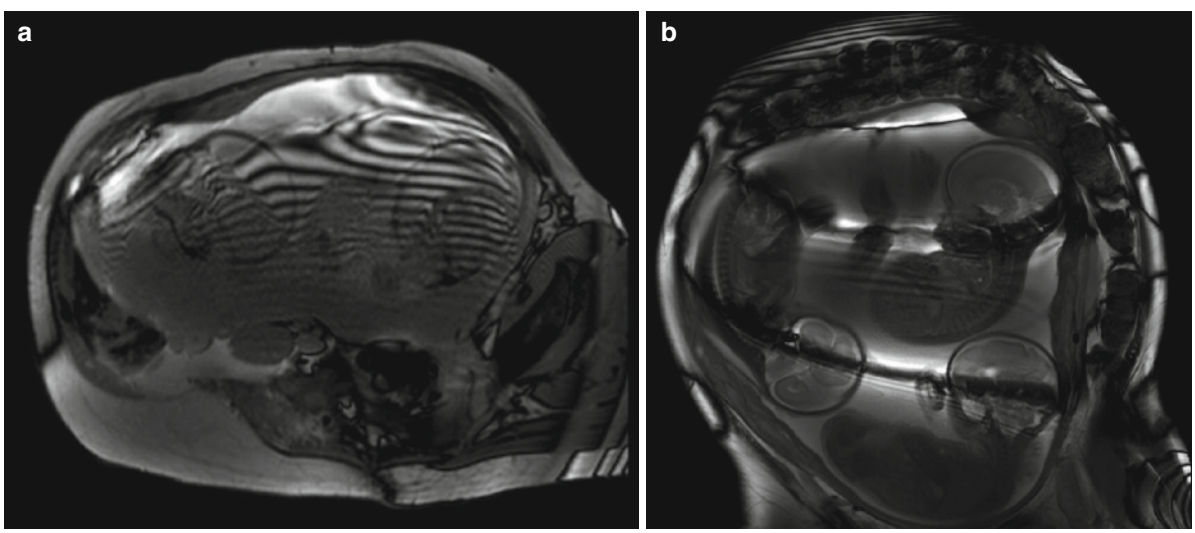

Fig. 1 Bending artifact in fetal MRI at higher field strength. Axial (**a**) and coronal (**b**) image of band-shaped signal losses (banding artifact) in steady-state free precession (SSFP) sequences due to B_0 inhomogeneities in a woman with a triplet pregnancy at 22 weeks of gestation measured at 3.0 T

shorter TE and/or increased receiver bandwidth, reductions in voxel size, or better shimming of the main magnetic field. The higher SNR that is afforded by 3.0 T also allows for the implementation of parallel imaging techniques within echo planar imaging, which shortens echo trains and helps to reduce these artifacts. An alternative method is the view-angle tilting method which is not widely used at the moment at 3.0 T, but has the drawback of increased image blurring (Butts et al. 2005; Cho et al. 1988).

2.3 Larmor Frequency and Chemical Shift

Larmor frequency (resonance frequency) linearly increases with magnetic field strength. At 1.5 T, the Larmor frequency of protons is 63.9 MHz and doubles to 127.8 MHz at 3.0 T. The higher resonance frequency is associated with both advantages (e.g., higher spectral resolution in MRS applications) and difficulties (e.g., increased chemical shift artifacts). Furthermore, the RF coils have to be tuned to the Larmor frequency of the MR system; hence, RF coils of a 1.5 T system cannot be used at 3.0 T.

Chemical shift artifacts are due to the difference in resonance frequency between water and fat. This difference is proportional to field strength, i.e., it is about 225 MHz at 1.5 T and 450 MHz at 3.0 T. A distinction is drawn between the chemical shift artifact of the first and the second kind. The chemical shift artifact of the first kind is a misregistration artifact and occurs only in frequency encoding and slice selection direction due to the slight difference between the precessional frequency of protons in water and fat, respectively. In other words, the proton spins of water at one location precess at the same frequency as the proton spins of fat at another location. Consequently, the images arise from the water and the fat signals are superposed and shifted in frequency direction which leads to a hyperintense line at one side and a hypointense line on the opposite side of the organ. The width of the lines increases with field strength. The artifact can be reduced by increasing the receiver bandwidth (Hussain et al. 2005); however, this strategy is related with a reduction of the SNR. Alternatively, the view-angle tilting mentioned above or a fat-suppression technique can be helpful, which in turn leads to an increase of acquisition time and/or an increase in RF deposition (SAR). The increased chemical shift between water and fat, however, has the advantage of more effective spectral fat suppression.

The difference in Larmor frequency between water and fat is associated with a reduction of the time period until proton spins of water and fat precess in phase, i.e., it is reduced from 4.6 ms at 1.5 T to 2.3 ms at 3.0 T. This effect of higher field strength is known as the chemical shift artifact of the second kind. It is advantageous for MR imaging in the abdomen of opposed-phase echoes, which are used for fat suppression. The shortening of the in-phase period allows for a reduction of echo time and hence a reduction in acquisition time and artifacts. However, it might be a problem for pulse sequences that use in-phase echo times due to a more challenging timing of the RF pulses.

An important point regarding the RF pulses of imaging sequences at 3.0 T represents the fact that the RF pulses also have to match the higher resonance frequency. A higher frequency of the RF pulses is equivalent to a shorter wavelength of the RF pulses which is associated with today's most important challenges and technical difficulties related to abdominal MR imaging at higher field strength: increased inhomogeneities of the B_1 field, stronger heating of tissue due to increased RF deposition and SAR, and standing wave effects. These challenges and effects will be the topic of the following subsection.

2.4 B_1 Homogeneity, Standing Wave Effect, and RF Deposition

The RF field used in MR imaging is also referred to as B_1 field and its strength increases proportionally with main magnetic field strength. The purpose of the B_1 field is to excite the spins and create an MR signal that can be detected by a receiver coil. The wavelength of the RF field in air is approximately 468 cm at 1.5 T and 234 cm at 3.0 T. The dielectric constant (ε_r) is an important physical parameter in context of in vivo MR imaging. The higher the dielectric constant of a medium, the slower the speed of light through it and the shorter the wavelength becomes. The dielectric constant of air and water is about 1 and 80, respectively; that of human tissue can be assessed between 10 and 100 (Gabriel et al. 1996a, b, c). The wavelength in a medium is reduced by a factor calculated as the inverse of the square root of the dielectric constant,

i.e., $1/\sqrt{\varepsilon_r}$ (Tanenbaum 2006). This effect reduces the RF wavelength at 3.0 T from 234 cm in air to about 30 cm in water-containing tissue (Haacke et al. 1999). The wavelength of the RF field at 3.0 T is in the same scale as the size of the field-of-view (FOV) used in many abdominal MRI applications. As a result, regional brightening and signal loss due to constructive and destructive interference of the standing waves can be observed. These artifacts are called standing waves effects (formerly incorrectly called "dielectric resonance effect") (Collins et al. 2005) and tend to be more pronounced with increasing FOV as required in fetal MR imaging. A related artifact, which is known as conductivity artifact (Merkle et al. 2006), is caused by the interaction of the (rapidly changing) RF field and highly conductive tissue or liquids in the body. The RF field induces a circulating electric current, which on its part creates induced magnetic fields that oppose the change of the original magnetic field due to the Lenz's law. In other words, the induced circulating current acts like an electromagnet that attenuates the causing RF field. The more conductive the medium, the stronger is the opposing effect and the greater is the reduction of amplitude and dissipation of energy of the RF field. Therefore, large amounts of highly conductive amniotic or ascitic fluid can cause a substantial shielding effect and requires more RF power for compensation which in turn increases SAR.

These two effects, the standing wave artifact and the conductivity artifact, combine to cause particularly strong artifacts for abdominal MR imaging, especially in pregnant women at a late stage of gestation or women with a multiple pregnancy. Figure 2 shows an example for the combination of the standing wave and the conductivity artifact for a woman with a triplet pregnancy.

A simple method to reduce B_1 inhomogeneity and wave-related artifacts is to use multichannel phased array receive coils, which have a stronger B_1-sensitivity near the body surface and might partially counteract the standing wave and conductivity artifact. However, especially in abdominal MR imaging, the artifacts persist and image quality is not acceptable. Another possibility for correction, which is commercially available, is a B_1 receive-field correction that uses low-resolution maps from the body and surface coils can be applied (Narayana et al. 1988). These corrections go by various names, such as constant level appearance (CLEAR), phased array uniformity enhancement (PURE), and prescan normalization. However, these methods are postprocessing corrections and do not compensate for B_1 inhomogeneity. Improvement of RF penetration by positioning an additional "RF cushion" with high dielectric constant on the abdomen of the patient has been demonstrated (Franklin et al. 2008). However, this is not an acceptable and feasible solution, especially for pregnant women.

A promising and more advanced technique for compensation B_1 inhomogeneities uses multichannel transmission body coils (Vernickel et al. 2007), which allows for application of methods such as active shimming of the RF field (Ullmann et al. 2005) and local excitation in combination with parallel transmission methods (Zhu 2004), e.g., transmit sensitivity encoding (transmit SENSE) (Katscher et al. 2003). This technology was under intensive development during the last years and the first commercially available MR system was introduced recently (Achieva 3.0 T TX, Philips Medical Systems).

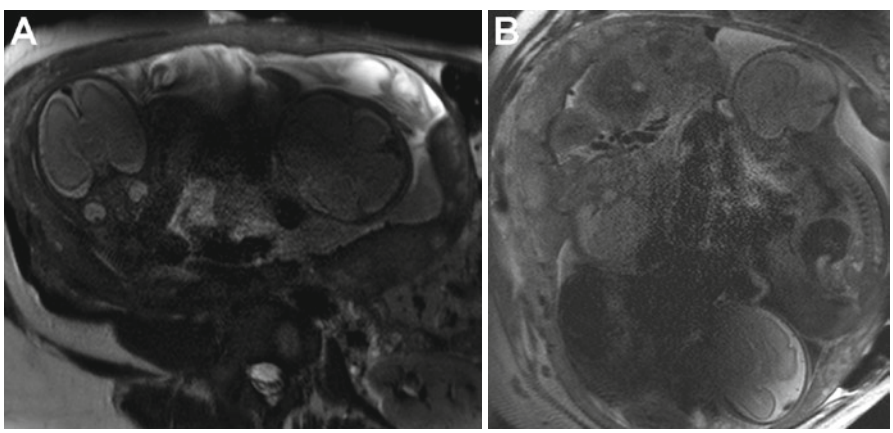

Fig. 2 Standing wave and conductivity artifact in fetal MRI at higher field strength. Axial (**a**) and coronal (**b**) image of a combined appearance of the standing wave and the conductivity artifact in T2-weighted turbo spin-echo (TSE) sequences in a woman with a triplet pregnancy at 22 weeks of gestation measured at 3.0 T

The SAR is a measure for the energy deposited in tissue by the RF pulses, or in other words, for the energy which is transferred via the RF flied into the patient's body where it generates heat. The SAR increases quadratically with the resonance frequency (i.e., the B_1 field strength) and the flip angle of the RF pulse. Among other factors, it additionally depends on the duty cycle of the RF pulses (i.e., the ratio between the RF pulse duration and the time period between two consecutive pulses), on the bandwidth of the RF pulses, and on the size and the position of the patient (Bernstein et al. 2006; Kuhl et al. 2008; Soher et al. 2007). The correlation between SAR and the bandwidth of the RF pulses is critical, because an increase of the bandwidth was recommended as favorable strategy to overcome susceptibility and chemical shift effects at the higher field strength. A doubling of the bandwidth of the RF pulses in combination with the inherent increase in SAR due to the higher B_1 field strength leads to a factor of eight for the net increase in SAR going from 1.5 to 3.0 T. In addition, the situation in pregnant women is twofold problematic. First, the standing wave artifact tends to be more pronounced and can result in inhomogeneous power deposition and formation of localized "hot spots" near or even in the fetus. Second, the huge amount of amniotic fluid leads to a greater RF field attenuation due to the conductivity artifact, and in turn, to an increased RF power for compensation in order to maintain signal intensity and image quality. However, an increase of the RF power is not possible when operating at the SAR limits. These effects and the relevance of the pregnancy-related SAR problems increase with increasing week of gestation. Therefore, intensified effort to cope with the increasing RF deposition, especially at late stage of gestation, is necessary. In an interesting study by Hand et al. (2006), the authors used an electromagnetic solver based on the time domain finite integration technique in combination with an anatomically realistic model of a pregnant woman at 28 weeks of gestation to predict SAR values in the mother and the fetus for 3.0 T MR systems. They found that the highest local SAR occurs in the mother. The maximum local SAR in the fetus was approximately 50–70% of that in the mother and occurred in a limb. This was due to the fact that relatively high SAR was exposed within the amniotic fluid and placenta close to the fetal limb. They concluded that their results suggest that control of the maternal maximum local SAR, rather than the whole-body averaged SAR, is required to comply with U.S. Food and Drug Administration (FDA) and International Commission on Non-Ionizing Radiation Protection (ICNIRP) guidelines.

The SAR as a limiting factor will be most relevant for RF-intensive MR protocols like turbo spin-echo (TSE), SSFP, or fat-saturated sequences. Conventional strategies to reduce increased RF deposition at 3.0 T compared to 1.5 T include protocol adjustment such as an increase of TR, decrease in the number of slices, decrease of the flip angle of the RF pulses, shorten the echo train length, and/or increase of inter echo spacing. However, all proposed solutions are associated with undesired penalties like increase in image acquisition time, reduction of anatomical coverage, changes in image contrast, and reduction of the gain in SNR at 3.0 T.

Parallel imaging (Griswold et al. 2002; Pruessmann et al. 1999) is a powerful method for reduction of SAR levels. These techniques allow for a reduction of the number of phase-encoding steps and shortening of image acquisition time, thereby leading to a reduction of RF energy absorbed and less tissue heating. A reduction factor (R) of two yields to a twofold reduction of RF deposition. However, an inherent drawback of all parallel imaging techniques is a decrease in SNR ($R=2$ reduces SNR by 40%), which is at least partly compensated by the higher signal at 3.0 T. Please refer to Chap. 2 for more details about the parallel imaging techniques.

More innovative modifications in pulse sequence design use different strategies for modulations of the flip angle of the refocusing pulses in TSE or gradient-echo sequences; these include flip angle sweep, hyperechoes, and transition between pseudo-steady states (TRAPS). Flip angle sweep (Morakkabati-Spitz et al. 2006) uses a successive reduction of the refocusing flip angle starting from the usual angle (e.g., 180°) to a much lower value (e.g., 130°) over the echo train. However, small refocusing angles give rise to the formation and interferences of the so-called stimulated echoes, and the prolongation of T1 relaxation times at 3.0 T (see next subsection for more detail) may lead to a mixed T1/T2 contrast, which has to be considered during interpretation of the images. A more advanced spin refocusing strategy uses varying flip angles and varying pulse phases which are symmetrically arranged around a central 180° pulse to completely refocus magnetization. This leads to the formation of echoes, thus hyperechoes (Hennig and Scheffler 2001; Weigel and Hennig 2006), and allows to preserve SNR as in conventional TSE sequences at simultaneous

reduction of SAR (up to 70–90%). Hyperechoes are complex signals consisting of several sources of magnetization, including transverse magnetization, longitudinal magnetization, and stimulated echo components of individual RF pulses; additionally, relaxation and diffusion effects have to be considered as well (Hussain et al. 2005). A drawback of hyperechoes is the fact that the echo time has to be increased to obtain T2 contrast which is similar to that provided by standard fast SE sequences. The TRAPS approach is based on the observation that once a static pseudo-steady state for a given refocusing flip angle is established, the maximum attainable signal is extremely robust against variations of the flip angles of the refocusing pulses. This technique allows for a significant reduction in RF power deposition for TSE sequences, by using higher flip angles only for the central part of k-space (Hennig et al. 2003).

2.5 Relaxation Time Effects

The longitudinal relaxation time T1 of many tissues increases with increasing strength main magnetic field but does not follow a simple mathematical correlation (Bottomley et al. 1984; de Bazelaire et al. 2004; Stanisz et al. 2005). T1 relaxation, which is also known as spin-lattice relaxation, describes the recovery process of the longitudinal magnetization by transfer of energy between the excited spins (protons in case of MR imaging) and the surrounding structure (also named as lattice, following the terminology of solid-state physics). The easier the energy transfer between the spins and the lattice occurs, the faster the longitudinal magnetization is recovered and the shorter is T1. As the strength of the main field B_0 increases, the resonance frequency of the spins as well as the energy which is required for a spin flip process (from parallel to antiparallel) also increases and, hence, the efficiency of the energy transfer decreases. This results in longer T1 relaxation times at 3.0 T. The reported results for the degree of T1 increase from 1.5 to 3.0 T demonstrates a wide range of measured changes, between up to 40% increase in skeletal muscle and up to 73% increase in kidney (Stanisz et al. 2005). The problems that are related to the increase in T1 relaxation times are a decrease in image SNR (please refer to the Sect. 2.1), a decrease in image contrast, and an increase in conspicuity of certain artifacts. Examples for a decreased image contrast at 3.0 T because of a different degree of T1 prolongation of two tissues are the gray matter-to-white matter contrast in MR imaging of the brain and the kidney-to-liver contrast in abdominal MR imaging. The increase in conspicuity of certain artifacts is related to the fact that the T1 relaxation time increases only by 10–20% [P4:3,43]. Therefore, the lipid signal remains stronger compared to the signal of other tissues at 3.0 T, leading to increased artifacts such as chemical shift artifacts or Gibbs ringing (Soher et al. 2007).

On the other hand, it was accepted that the transverse relaxation time T2 is mostly independent of the main magnetic field strength (Bernstein et al. 2006; Bottomley et al. 1984). T2 is the time constant for the decay of the transverse magnetization due to spin–spin interactions, hence also called spin–spin relaxation time. However, more recent studies (de Bazelaire et al. 2004; Gold et al. 2004; Stanisz et al. 2005) suggest a small but statistically insignificant decrease of T2 relaxation time in certain tissues by 10–15% as the field strength is increased from 1.5 to 3.0 T. Therefore and due to the afore-mentioned increased susceptibility effects at higher field strength, the apparent transverse relaxation time T2* decreases at 3.0 T. T2* is not a tissue-specific parameter like T1 or T2. Besides the T2 relaxation time, field inhomogeneities and susceptibility effects are included in T2*. To the best of our knowledge, changes in relaxation times for fetal MR imaging at 3.0 T are not published thus far, but are assumed to be comparable in scale with the described effects.

These changes in relaxation times lead to the fact that the contrast between various tissues on MR images measured at 3.0 T cannot be the same as known from standard 1.5 T MR images. Several changes of parameters (i.e., repetition time, receiver bandwidth, etc.) of the pulse sequences are available for compensation.

2.6 Safety Concerns and Acoustic Noise

Little specific data about safety issues in fetal MR imaging at higher field strength are available. In general, it is assumed that a higher magnetic field strength is related to an increased torque on ferromagnetic implants, increased risk of RF burns from RF coils or echocardiogram leads, and an increase in acoustic noise. The latter two are of special interest in fetal MR imaging. Careful handling of RF coils and other medical equipment (e.g., to avoid direct contact between the coil and patient's

skin) will be the best strategy to avoid RF burns. The noise level, on the other hand, increases with field strength and the higher performance of the gradient system used at higher field strengths (the noise occurs during the quick current alterations in the gradient coils) (Foster et al. 2000). Passive approaches, such as earplugs or headphones, are sufficient to protect the mother from the high acoustic noise levels. However, for protection of the fetus, a reduction in gradient performance and/or acoustically shielded vacuum-based bore liners are required (Tanenbaum 2006).

3 Fetal MR Imaging at Higher Field Strength

In consideration of the challenges that are connected with fetal MR imaging at higher magnetic field strengths and are described in the previous section, the question for reasonableness is legitimate. On the other hand, the chance to obtain increased SNR at higher field strength, which can be used for higher spatial resolution or faster imaging, is of course an issue of interest in fetal MR imaging. Therefore, research groups are busy with tuning of MR sequences as well as development of new MR hardware to take up the challenges. Initial experiences from a pilot study at the Department of Radiology of Medical University of Vienna demonstrated, however, that the way from 1.5 to 3.0 T in fetal MR imaging is challenging and not straight forward. Promising results from the first four patients are presented in the following two subsections of this chapter. All women had premature amniorrhexis which helps to reduce the intensity of the standing wave and the conductivity artifact. All measurements were performed on 3.0 T clinical whole-body MR scanners (Achieva, Philips Medical Systems, Best, The Netherlands or TRIO, Siemens Medical Solutions, Erlangen, Germany) using multichannel surface coils.

3.1 Fetal Diffusion-Weighted MR Imaging

Diffusion-weighted MR imaging (DWI) is a method for detection of the Brownian motion of water molecules and provides information about tissue structure and intra/extracellular space (Le Bihan et al. 2006). DWI sequences measure the signal attenuation which occurred due to diffusion of water molecules. The observed signal decay can be used to calculate the diffusion properties or the apparent diffusion coefficient (ADC).The essential parameters for the "diffusivity weighting" are the strength and timing of the diffusion gradients and can be expressed with the so-called "*b*-factor." One basic rule of DWI is: the higher the *b*-factor, the stronger the "diffusion-weighting" and the signal drop-off in areas with higher diffusion in the images, but the lower the SNR of the DWI data.

Except for the problems related to a low SNR, long acquisition time, vulnerability to motion of the fetus due to breathing of the mother as well as diffusion mimicking signal attenuations due to blood flow in the capillaries have to be resolved first before fetal DWI is feasible. The use of parallel imaging techniques in combination with an MR system working at 3.0 T and multichannels receiver may help overcome some of these difficulties. The higher SNR at 3.0 T allows for application of higher *b* values, which in turn are more sensitive to diffusion and less sensitive to transverse relaxation time (T2) and perfusion-related motion. In general, the quality of DWI images measured at 3.0 T is superior to that of diffusion-weighted (DW) images obtained at 1.5 T. However, the magnetic field inhomogeneities that degrade DW images are worse at 3.0 T. Figure 3 shows an example of a DWI examination of the brain of a fetus at 3.0 T.

The DWIBS approach (DWIBS stands for DW whole-body imaging with background body signal suppression) was developed by Takahara et al. (2004). DWIBS is a new technology of body DW MRI acquiring multiple, thin axial slices with a high number of signal averages during free breathing and STIR (short TI inversion recovery) fat suppression, which provides high-spatial-resolution images of various regions of the body and can be useful in detecting malignancies in the whole body. The usefulness of DWIBS for the detection of thoracic and abdominal lesions has been demonstrated in a few reports (Bohlscheid et al. 2008; Komori et al. 2007; Murtz et al. 2007; Stadlbauer et al. 2009). A study by Takahara et al. (2008) used DWIBS to introduce and assess DW MR neurography for imaging of the brachial plexus. Figure 4 shows an example of the application of the DWIBS technique for visualization of the spinal cord of a fetus.

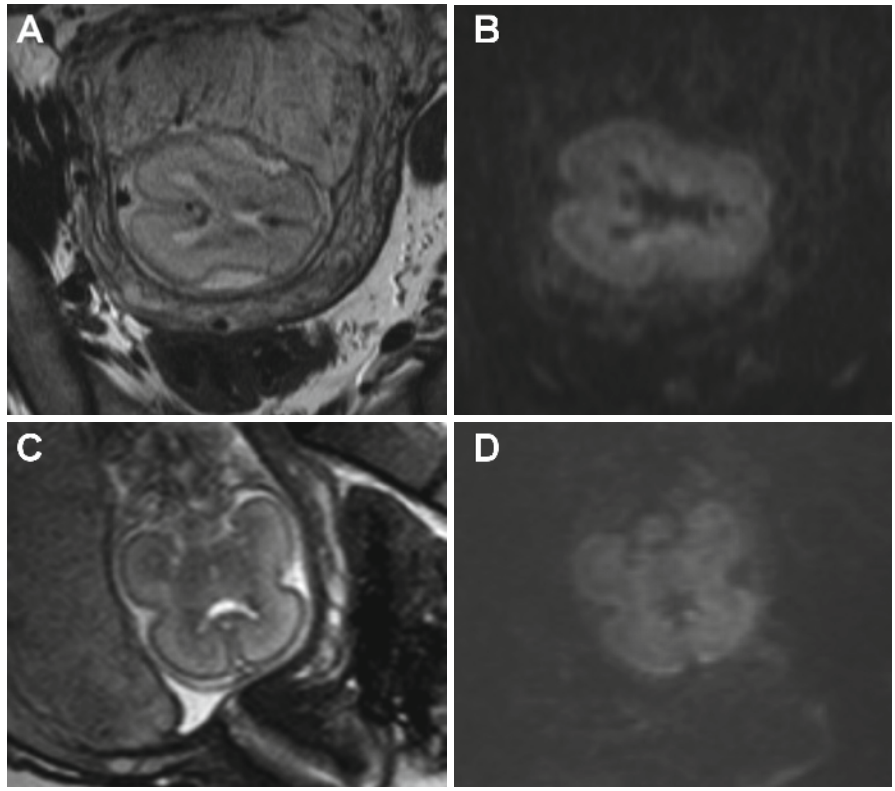

Fig. 3 Fetal diffusion-weighted MR imaging (DWI) at 3.0 T. Axial (**a**) and coronal (**c**) balanced steady-state free precession (balanced SSFP) images of a normally developed fetal brain (21 weeks of gestation). Corresponding axial (**b**) and coronal (**d**) DWI images measured with a *b*-value of 700 s/mm^2, an in-plane resolution of 1.3 × 1.3 mm^2, a slice thickness of 4 mm, and a TE/TR of 92/2,200 ms, respectively

Depending on the anatomical region, diffusion can occur unrestricted and equal in magnitude in all spatial directions, which is referred to as isotropic diffusion. However, mobility of water in biological tissue can show a preferred direction by structures, e.g., restriction of diffusion by myelinated sheets of nerve fibers, which is referred to as anisotropic diffusion. The conventional DWI method provides information about the magnitude of water diffusion but not about its direction.

Diffusion tensor MR imaging (DTI) allows for the measurement of anisotropic diffusion of water molecules in tissues such as white brain matter and provides insight into the microstructure of tissues (Le Bihan et al. 2001) with the use of diffusion gradients in at least six directions. DTI shows clinical application for preoperative planning of brain tumor surgery to differentiate peritumoral edema from tumor border, to assess tumor infiltration into white-matter tracts, and to visualize and localize the major white-matter tracts (Cruz and Sorensen 2006). This strategy can help to avoid injuries to normal and/or functionally important brain areas. Application of DWI and DTI is more problematic in regions outside of the brain, e.g., due to increased motion and susceptibility artifacts. However, these methods may provide helpful information regarding the development of the brain parenchyma and brain structures in a fetus as well as about the nature and extent of pathologies in several organs, which is currently a field of clinical investigations.

In general, DTI data are evaluated by calculating parametric maps of fractional anisotropy (FA) and mean diffusivity (MD) that describe the directionality and magnitude of water diffusion, respectively. Fiber tracking enables reconstruction of white matter pathways in three dimensions with the use of a mathematical algorithm for comparison of orientations of water diffusion anisotropy on a voxel-by-voxel basis. Reconstructed fiber bundles may be evaluated visually or with qualitative assessment. Figure 5 shows an example of a DTI examination and subsequent postprocessing using Fiber tracking of the DTI data of a fetus.

3.2 Fetal MR Venography

MR venography is a noninvasive imaging method for investigation of the vasculature of the human brain.

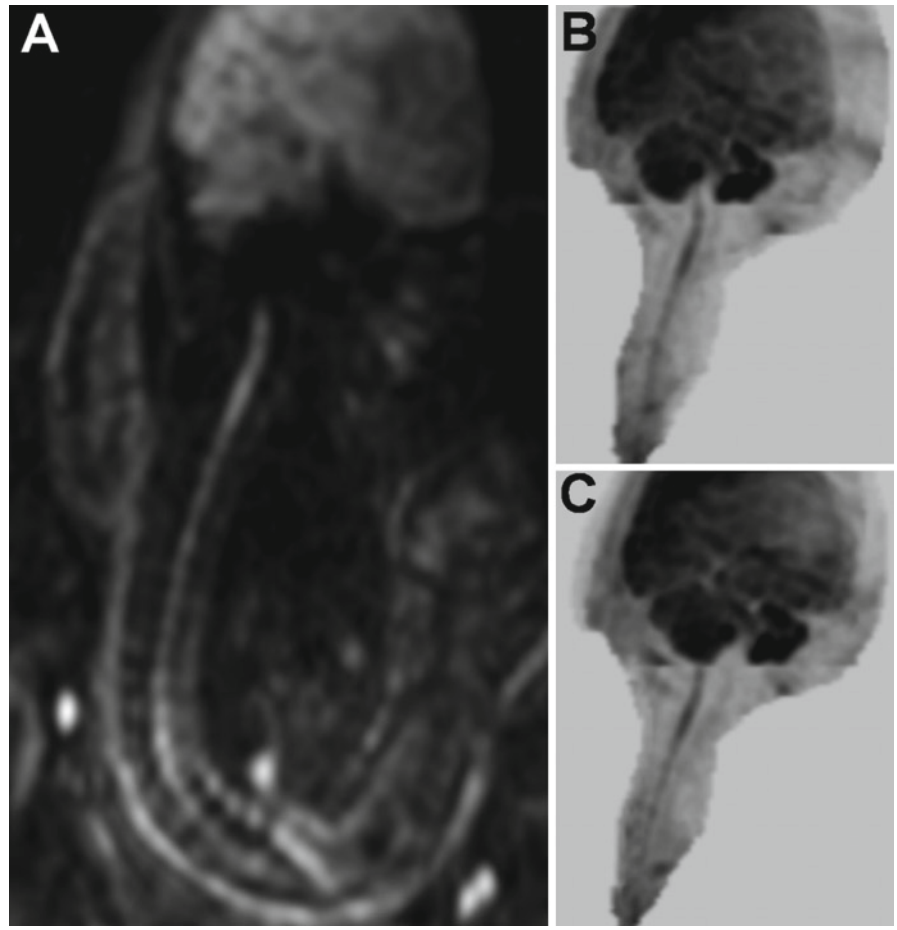

Fig. 4 Fetal diffusion-weighted whole-body imaging with background body signal suppression (DWIBS) at 3.0 T. Sagittal DWIBS image (**a**) of a fetus (30 weeks of gestation) measured with a *b*-value of 1,000 s/mm^2, an in-plane resolution of 1.5 × 1.5 mm^2, a slice thickness of 5 mm, and a TE/TR of 58/2,238 ms, respectively. Oblique sagittal maximum intensity projection (MIP) reconstructions and inversion of gray-scale for the DWIBS data (**b**) and (**c**)

A 3D gradient echo imaging technique to visualize venous structures has been introduced by Reichenbach et al. (1997, 1998). The underlying contrast mechanism of this method is based on the fact that the level of blood oxygenation of venous blood is smaller compared to arterial blood. The iron atom of deoxygenated hemoglobin contains four unpaired electrons and is paramagnetic for that reason. On the other hand, in oxygenated hemoglobin an oxygen molecule is attached to the iron atom, which leads to the fact that the electrons are not unpaired any longer, and consequently, the iron atom is diamagnetic. As described above, diamagnetic materials have negative susceptibility and weaken the external magnetic field, whereas paramagnetic substances have positive susceptibility. The paramagnetic nature of deoxygenated venous blood leads to magnetic field inhomogeneities and thus serves as a contrast media. These field inhomogeneities result in two effects: (a) a reduction of T2* (Li et al. 1998; Thulborn et al. 1982) and (b) a phase difference between the venous vessel and its surroundings (Gomori et al. 1987; Hoogenraad et al. 1998). In other words, the difference in oxygenation level between arterial and venous blood is associated with a difference in the bulk magnetic susceptibility of the blood in the vessel. Therefore, the intensity of this blood oxygenation level dependent (BOLD) susceptibility effect (or artifact) is higher at higher field strengths (Ogawa and Lee 1990; Turner et al. 1993) and MR venography benefits in general from higher field strengths. Figure 6 gives an example for an MR venography examination of a fetus and demonstrates the results of the subsequent postprocessing using minimum intensity projection of the MR venography data.

3.3 Postmortem Fetal MR Imaging

Solely MR studies at higher magnetic field strength (>1.5 T) on postmortem specimen of fetal brains were

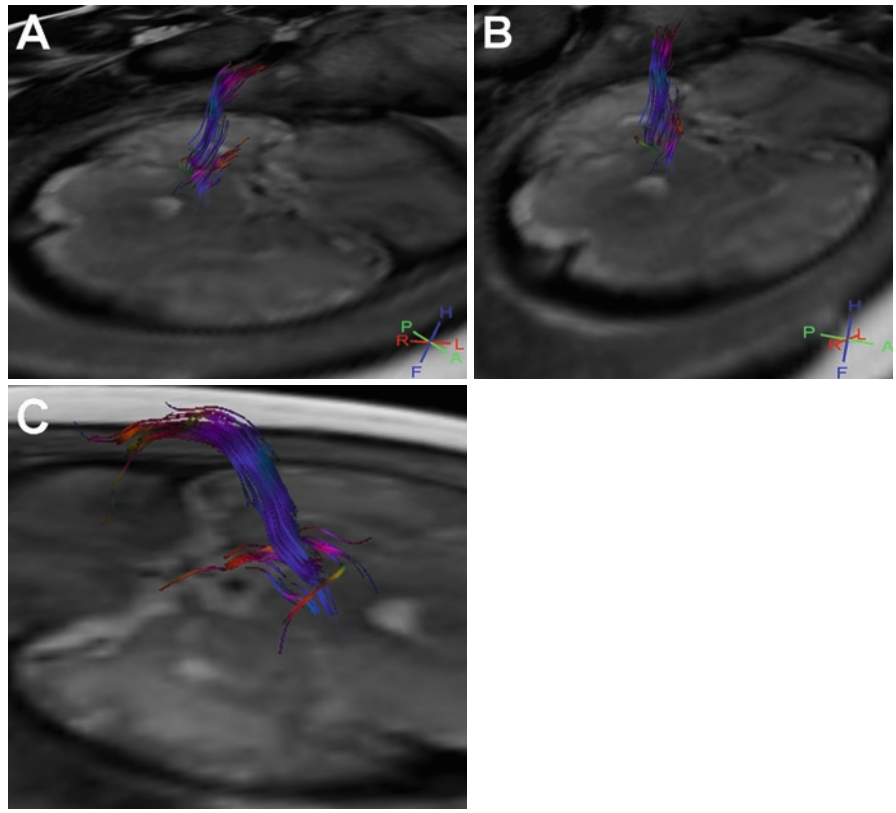

Fig. 5 Fetal diffusion tensor MR imaging (DTI) and fiber tracking at 3.0 T. Three-dimensional reconstruction of parts of the pyramidal tract as a result of a fiber tracking procedure of the DTI data using the FACT (fiber assignment by continuous tracking) algorithm. Reconstructed fiber tracts and DTI data were coregistered to transversal T2-weighted TSE images and depicted in (**a–c**) in three different projections. DTI data were measured on a normally developed fetal brain (30 weeks of gestation) using the following parameters: *b* values of 0 and 1,000 s/mm^2, diffusion gradients in 15 directions, in-plane resolution of 0.8×0.8 mm^2, slice thickness of 2.5 mm, and TE/TR of 55/4,100 ms

published in the literature so far. Sbarbati and coworkers (Sbarbati et al. 2004) investigated seven cadaveric human fetuses of gestational ages ranging from the 12th to the 16th week by acquiring 2D- and 3D T1- and T2-weighted MR images at a magnetic field strength of 4.7 T. The purpose of this study was to evaluate brain morphology in situ and to describe dynamics of brain development during an important period of fetal morphogenesis. MRI data were evaluated by 3D reconstruction and calculation of the thickness of the cortex in both hemispheres. The findings of the MR experiments were compared with histological sections obtained from ten paraffin-embedded brains from fetus of corresponding gestational age. The results of the 3D reconstruction of the MRI data demonstrated the increasing degree of maturation of the brains in terms of fronto-occipital distance, bitemporal distance, and occipital angle in all the fetuses and were quite similar to those provided by necropsy but with an absence of mechanical artifacts. A spatial in-plane resolution of 0.12×0.12 mm^2 voxel was sufficient for a detailed detection of five cortical layers and to visualize the subplate and marginal zones on T2-weighted MR images. The authors demonstrated with their paper the utility of MRI for studying brain development. They conclude that MR imaging with high spatial resolution at high field strength provides quantitative profiling of fetal brain, which allows for the calculation of important morphological parameters.

In a study by Huang et al. (2006) the authors acquired DTI data of postmortem fetal brain samples measured at 4.7 T. They evaluated the growth status of various white matter tracts on cross-sections at 19–20th gestational weeks and compared the findings with in vivo MR examinations of brains of 0-month-old neonates and 5- to 6-year-old children at 1.5 T. Limbic, commissural, association, and projection white matter tracts and gray matter structures were three-dimensionally reconstructed. They performed a quantitative characterization of these structures to assess their dynamic changes. Huang and coworkers found that the overall pattern of the time courses for the development of different white matter is that limbic fibers develop first and association fibers last and commissural and projection fibers are

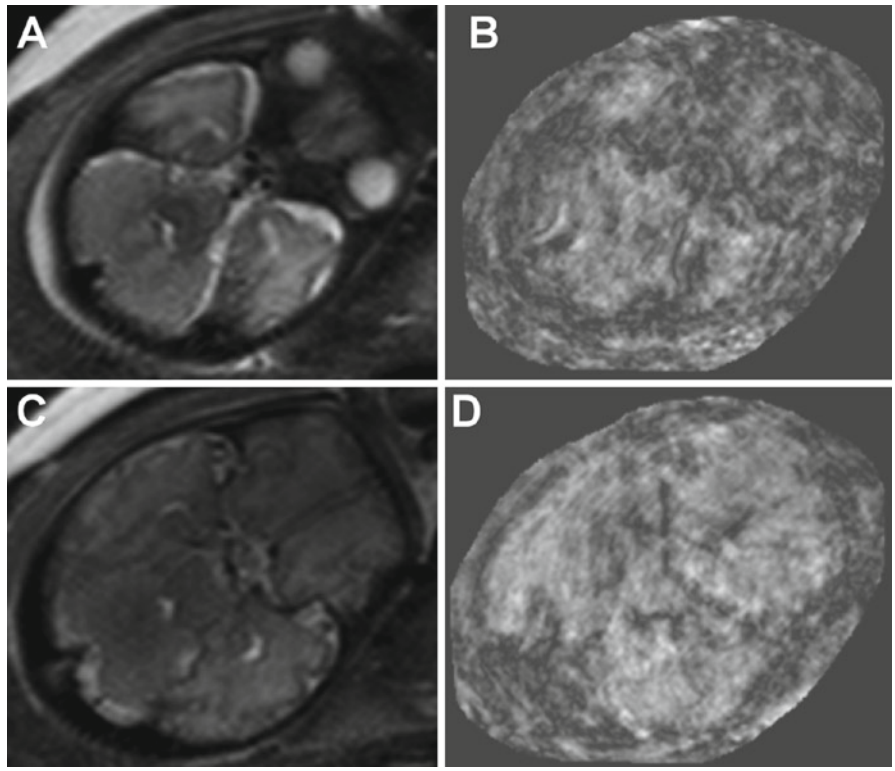

Fig. 6 Fetal MR venography at 3.0 T. Axial T2-weighted TSE images (**a**, **c**) of a normally developed fetal brain (30 weeks of gestation). Corresponding axial MR venography images after minimum intensity projection (mIP) reconstructions (**b**, **d**). MR venography data were measured using the following parameters: in-plane resolution of 0.45×0.45 mm^2, slice thickness of 2 mm, and TE/TR of 27/19 ms

forming from anterior to posterior part of the brain. Most white matter tracts have already formed at 0 month of age. They conclude that 3D DTI data of the human brain could be a valuable anatomical reference for diagnostic radiology of premature newborns as well as for basic human development studies.

Ren et al. (2006) analyzed midline glial and commissural development in postmortem human fetal brains ranging from 13 to 20 weeks of gestation using both DTI and immunohistochemistry. Fetal brains of between 14 and 16 weeks of gestation were scanned in a MR scanner working at field strength of 11.7 T. Brains of 17 weeks or older fetuses were scanned at 4.7 T. Their data show the morphological development of multiple forebrain commissures/decussations, including the corpus callosum, anterior commissure, hippocampal commissure, and the optic chiasm. Furthermore, they were able to demonstrate that mechanisms regulating callosal formation in the developing human brain are very similar to their findings of previous study about the developing mouse forebrain. Histological analyses performed in their studies showed that all the midline glial populations as well as structures analogous to the subcallosal sling and cingulate pioneering axons, which mediate callosal axon guidance in mouse, are also present during human brain development. They concluded from their data that similar mechanisms and molecules required for midline commissure formation operate during both mouse and human brain development. Therefore, the mouse is an excellent model system for studying normal and pathological commissural formation in human brain development.

References

Amartur S, Haacke EM (1991) Modified iterative model based on data extrapolation method to reduce Gibbs ringing. J Magn Reson Imaging 1:307–317

Barfuss H, Fischer H, Hentschel D, Ladebeck R, Oppelt A, Wittig R, Duerr W, Oppelt R (1990) In vivo magnetic resonance imaging and spectroscopy of humans with a 4 T whole-body magnet. NMR Biomed 3:31–45

Bernstein MA, Huston J III, Ward HA (2006) Imaging artifacts at 3.0T. J Magn Reson Imaging 24:735–746

Bohlscheid A, Nuss D, Lieser S, Busch HP (2008) Tumor search with diffusion-weighted imaging–first experience. Rofo 180:302–309

Bottomley PA, Foster TH, Argersinger RE, Pfeifer LM (1984) A review of normal tissue hydrogen NMR relaxation times and

relaxation mechanisms from 1-100 MHz: dependence on tissue type, NMR frequency, temperature, species, excision, and age. Med Phys 11:425–448

Butts K, Pauly JM, Gold GE (2005) Reduction of blurring in view angle tilting MRI. Magn Reson Med 53:418–424

Cho ZH, Kim DJ, Kim YK (1988) Total inhomogeneity correction including chemical shifts and susceptibility by view angle tilting. Med Phys 15:7–11

Collins CM, Liu W, Schreiber W, Yang QX, Smith MB (2005) Central brightening due to constructive interference with, without, and despite dielectric resonance. J Magn Reson Imaging 21:192–196

Cruz LC Jr, Sorensen AG (2006) Diffusion tensor magnetic resonance imaging of brain tumors. Magn Reson Imaging Clin N Am 14:183–202

de Bazelaire CM, Duhamel GD, Rofsky NM, Alsop DC (2004) MR imaging relaxation times of abdominal and pelvic tissues measured in vivo at 3.0 T: preliminary results. Radiology 230:652–659

Dietrich O, Reiser MF, Schoenberg SO (2008) Artifacts in 3-T MRI: physical background and reduction strategies. Eur J Radiol 65:29–35

Duewell S, Wolff SD, Wen H, Balaban RS, Jezzard P (1996) MR imaging contrast in human brain tissue: assessment and optimization at 4 T. Radiology 199:780–786

Edelstein WA, Glover GH, Hardy CJ, Redington RW (1986) The intrinsic signal-to-noise ratio in NMR imaging. Magn Reson Med 3:604–618

Foster JR, Hall DA, Summerfield AQ, Palmer AR, Bowtell RW (2000) Sound-level measurements and calculations of safe noise dosage during EPI at 3 T. J Magn Reson Imaging 12:157–163

Franklin KM, Dale BM, Merkle EM (2008) Improvement in B1-inhomogeneity artifacts in the abdomen at 3T MR imaging using a radiofrequency cushion. J Magn Reson Imaging 27:1443–1447

Frayne R, Goodyear BG, Dickhoff P, Lauzon ML, Sevick RJ (2003) Magnetic resonance imaging at 3.0 Tesla: challenges and advantages in clinical neurological imaging. Invest Radiol 38:385–402

Fujii Y, Nakayama N, Nakada T (1998) High-resolution T2-reversed magnetic resonance imaging on a high magnetic field system. Technical note. J Neurosurg 89:492–495

Gabriel C, Gabriel S, Corthout E (1996a) The dielectric properties of biological tissues: I. Literature survey. Phys Med Biol 41:2231–2249

Gabriel S, Lau RW, Gabriel C (1996b) The dielectric properties of biological tissues: III. Parametric models for the dielectric spectrum of tissues. Phys Med Biol 41: 2271–2293

Gabriel S, Lau RW, Gabriel C (1996c) The dielectric properties of biological tissues: II. Measurements in the frequency range 10 Hz to 20 GHz. Phys Med Biol 41:2251–2269

Gold GE, Han E, Stainsby J, Wright G, Brittain J, Beaulieu C (2004) Musculoskeletal MRI at 3.0 T: relaxation times and image contrast. AJR Am J Roentgenol 183:343–351

Gomori JM, Grossman RI, Yu-Ip C, Asakura T (1987) NMR relaxation times of blood: dependence on field strength, oxidation state, and cell integrity. J Comput Assist Tomogr 11: 684–690

Griswold MA, Jakob PM, Heidemann RM, Nittka M, Jellus V, Wang J, Kiefer B, Haase A (2002) Generalized autocalibrating partially parallel acquisitions (GRAPPA). Magn Reson Med 47:1202–1210

Haacke EM, Tkach JA, Parrish TB (1989) Reduction of T2* dephasing in gradient field-echo imaging. Radiology 170: 457–462

Haacke EM, Brown RW, Thompson MR, Venkatesan R (1999) Magnetic resonance imaging - physical principles and sequence design, 1st edn. Wiley, New York

Hand JW, Li Y, Thomas EL, Rutherford MA, Hajnal JV (2006) Prediction of specific absorption rate in mother and fetus associated with MRI examinations during pregnancy. Magn Reson Med 55:883–893

Hennig J, Scheffler K (2001) Hyperechoes. Magn Reson Med 46:6–12

Hennig J, Weigel M, Scheffler K (2003) Multiecho sequences with variable refocusing flip angles: optimization of signal behavior using smooth transitions between pseudo steady states (TRAPS). Magn Reson Med 49:527–535

Hetherington H, Kuzniecky R, Pan J, Mason G, Morawetz R, Harris C, Faught E, Vaughan T, Pohost G (1995) Proton nuclear magnetic resonance spectroscopic imaging of human temporal lobe epilepsy at 4.1 T. Ann Neurol 38:396–404

Hoogenraad FG, Reichenbach JR, Haacke EM, Lai S, Kuppusamy K, Sprenger M (1998) In vivo measurement of changes in venous blood-oxygenation with high resolution functional MRI at 0.95 tesla by measuring changes in susceptibility and velocity. Magn Reson Med 39:97–107

Hoult DI, Phil D (2000) Sensitivity and power deposition in a high-field imaging experiment. J Magn Reson Imaging 12:46–67

Huang H, Zhang J, Wakana S, Zhang W, Ren T, Richards LJ, Yarowsky P, Donohue P, Graham E, van Zijl PC, Mori S (2006) White and gray matter development in human fetal, newborn and pediatric brains. Neuroimage 33:27–38

Hussain SM, Wielopolski PA, Martin DR (2005) Abdominal magnetic resonance imaging at 3.0 T: problem or a promise for the future? Top Magn Reson Imaging 16:325–335

Jesmanowicz A, Bandettini PA, Hyde JS (1998) Single-shot half k-space high-resolution gradient-recalled EPI for fMRI at 3 Tesla. Magn Reson Med 40:754–762

Katscher U, Bornert P, Leussler C, van den Brink JS (2003) Transmit SENSE. Magn Reson Med 49:144–150

Komori T, Narabayashi I, Matsumura K, Matsuki M, Akagi H, Ogura Y, Aga F, Adachi I (2007) 2-[Fluorine-18]-fluoro-2-deoxy-D-glucose positron emission tomography/computed tomography versus whole-body diffusion-weighted MRI for detection of malignant lesions: initial experience. Ann Nucl Med 21:209–215

Kruger G, Kastrup A, Glover GH (2001) Neuroimaging at 1.5 T and 3.0 T: comparison of oxygenation-sensitive magnetic resonance imaging. Magn Reson Med 45:595–604

Kuhl CK, Traber F, Schild HH (2008) Whole-body high-field-strength (3.0-T) MR imaging in clinical practice. Part I. Technical considerations and clinical applications. Radiology 246:675–696

Le Bihan D, Mangin JF, Poupon C, Clark CA, Pappata S, Molko N, Chabriat H (2001) Diffusion tensor imaging: concepts and applications. J Magn Reson Imaging 13:534–546

Le Bihan D, Poupon C, Amadon A, Lethimonnier F (2006) Artifacts and pitfalls in diffusion MRI. J Magn Reson Imaging 24:478–488

Li D, Waight DJ, Wang Y (1998) In vivo correlation between blood T2* and oxygen saturation. J Magn Reson Imaging 8:1236–1239

Menon RS, Ogawa S, Hu X, Strupp JP, Anderson P, Ugurbil K (1995) BOLD based functional MRI at 4 Tesla includes a capillary bed contribution: echo-planar imaging correlates with previous optical imaging using intrinsic signals. Magn Reson Med 33:453–459

Merboldt KD, Finsterbusch J, Frahm J (2000) Reducing inhomogeneity artifacts in functional MRI of human brain activation-thin sections vs gradient compensation. J Magn Reson 145:184–191

Merkle EM, Dale BM (2006) Abdominal MRI at 3.0 T: the basics revisited. AJR Am J Roentgenol 186:1524–1532

Merkle EM, Dale BM, Paulson EK (2006) Abdominal MR imaging at 3T. Magn Reson Imaging Clin N Am 14:17–26

Morakkabati-Spitz N, Schild HH, Kuhl CK, Lutterbey G, von Falkenhausen M, Traber F, Gieseke J (2006) Female pelvis: MR imaging at 3.0 T with sensitivity encoding and flip-angle sweep technique. Radiology 241:538–545

Murtz P, Krautmacher C, Traber F, Gieseke J, Schild HH, Willinek WA (2007) Diffusion-weighted whole-body MR imaging with background body signal suppression: a feasibility study at 3.0 Tesla. Eur Radiol 17:3031–3037

Narayana PA, Brey WW, Kulkarni MV, Sievenpiper CL (1988) Compensation for surface coil sensitivity variation in magnetic resonance imaging. Magn Reson Imaging 6:271–274

Ogawa S, Lee TM (1990) Magnetic resonance imaging of blood vessels at high fields: in vivo and in vitro measurements and image simulation. Magn Reson Med 16:9–18

Ojemann JG, Akbudak E, Snyder AZ, McKinstry RC, Raichle ME, Conturo TE (1997) Anatomic localization and quantitative analysis of gradient refocused echo-planar fMRI susceptibility artifacts. Neuroimage 6:156–167

Pruessmann KP, Weiger M, Scheidegger MB, Boesiger P (1999) SENSE: sensitivity encoding for fast MRI. Magn Reson Med 42:952–962

Reichenbach JR, Venkatesan R, Schillinger DJ, Kido DK, Haacke EM (1997) Small vessels in the human brain: MR venography with deoxyhemoglobin as an intrinsic contrast agent. Radiology 204:272–277

Reichenbach JR, Essig M, Haacke EM, Lee BC, Przetak C, Kaiser WA, Schad LR (1998) High-resolution venography of the brain using magnetic resonance imaging. MAGMA 6:62–69

Ren T, Anderson A, Shen WB, Huang H, Plachez C, Zhang J, Mori S, Kinsman SL, Richards LJ (2006) Imaging, anatomical, and molecular analysis of callosal formation in the developing human fetal brain. Anat Rec A Discov Mol Cell Evol Biol 288:191–204

Sbarbati A, Pizzini F, Fabene PF, Nicolato E, Marzola P, Calderan L, Simonati A, Longo L, Osculati A, Beltramello A (2004) Cerebral cortex three-dimensional profiling in human fetuses by magnetic resonance imaging. J Anat 204:465–474

Soher BJ, Dale BM, Merkle EM (2007) A review of MR physics: 3T versus 1.5T. Magn Reson Imaging Clin N Am 15:277–290, v

Stadlbauer A, Bernt R, Gruber S, Bogner W, Pinker K, van der Riet W, Haller J, Salomonowitz E (2009) Diffusion-weighted MR imaging with background body signal suppression (DWIBS) for the diagnosis of malignant and benign breast lesions. Eur Radiol 19:2349–2356

Stanisz GJ, Odrobina EE, Pun J, Escaravage M, Graham SJ, Bronskill MJ, Henkelman RM (2005) T1, T2 relaxation and magnetization transfer in tissue at 3T. Magn Reson Med 54:507–512

Takahara T, Imai Y, Yamashita T, Yasuda S, Nasu S, Van Cauteren M (2004) Diffusion weighted whole body imaging with background body signal suppression (DWIBS): technical improvement using free breathing, STIR and high resolution 3D display. Radiat Med 22:275–282

Takahara T, Hendrikse J, Yamashita T, Mali WP, Kwee TC, Imai Y, Luijten PR (2008) Diffusion-weighted MR neurography of the brachial plexus: feasibility study. Radiology 249:653–660

Tanenbaum LN (2006) Clinical 3T MR imaging: mastering the challenges. Magn Reson Imaging Clin N Am 14:1–15

Thulborn KR (1999) Clinical rationale for very-high-field (3.0 Tesla) functional magnetic resonance imaging. Top Magn Reson Imaging 10:37–50

Thulborn KR, Waterton JC, Matthews PM, Radda GK (1982) Oxygenation dependence of the transverse relaxation time of water protons in whole blood at high field. Biochim Biophys Acta 714:265–270

Turner R, Jezzard P, Wen H, Kwong KK, Le Bihan D, Zeffiro T, Balaban RS (1993) Functional mapping of the human visual cortex at 4 and 1.5 tesla using deoxygenation contrast EPI. Magn Reson Med 29:277–279

Ugurbil K, Garwood M, Ellermann J, Hendrich K, Hinke R, Hu X, Kim SG, Menon R, Merkle H, Ogawa S et al (1993) Imaging at high magnetic fields: initial experiences at 4 T. Magn Reson Q 9:259–277

Ullmann P, Junge S, Wick M, Seifert F, Ruhm W, Hennig J (2005) Experimental analysis of parallel excitation using dedicated coil setups and simultaneous RF transmission on multiple channels. Magn Reson Med 54:994–1001

Vernickel P, Roschmann P, Findeklee C, Ludeke KM, Leussler C, Overweg J, Katscher U, Grasslin I, Schunemann K (2007) Eight-channel transmit/receive body MRI coil at 3T. Magn Reson Med 58:381–389

Vinitski S, Griffey RH (1991) MR image contrast at high field strength. J Magn Reson Imaging 1:451–456

Weigel M, Hennig J (2006) Contrast behavior and relaxation effects of conventional and hyperecho-turbo spin echo sequences at 1.5 and 3 T. Magn Reson Med 55:826–835

Wen H, Denison TJ, Singerman RW, Balaban RS (1997) The intrinsic signal-to-noise ratio in human cardiac imaging at 1.5, 3, and 4 T. J Magn Reson 125:65–71

Wieben O, Francois C, Reeder SB (2008) Cardiac MRI of ischemic heart disease at 3 T: potential and challenges. Eur J Radiol 65:15–28

Yablonskiy DA, Haacke EM (1994) Theory of NMR signal behavior in magnetically inhomogeneous tissues: the static dephasing regime. Magn Reson Med 32:749–763

Zhu Y (2004) Parallel excitation with an array of transmit coils. Magn Reson Med 51:775–784

Safety of Fetal MRI Scanning

Penny Gowland

Contents

Abstract

› MRI uses a variety of different magnetic fields to produce images. These all interact with the body in some way. This chapter considers how they interact with the fetus in particular, and whether they pose any risk to the fetus. It also considers practical aspects of MR scanning that can cause problems for the mother or fetus.

1 Introduction

This book demonstrates that fetal magnetic resonance imaging (MRI) can provide major benefits in the management of pregnancy and fetal development. However, given that many MRI developments are relatively recent, it remains important to balance these benefits against any possible risks that MRI may pose to the fetus. As for all subjects being scanned with MRI, there are three areas of concern with regard to safety of the fetus and indeed that of the mother and the MR worker. These are the static field used to polarize the nuclear magnetization and provide high signal-to-noise ratio in the MR data, the time-varying (approximately kilo Hertz) magnetic fields arising from the switched magnetic field gradients used for image encoding, and the radiofrequency (RF) fields used to excite the nuclear spin signal to obtain a signal. Each

P. Gowland
Sir Peter Mansfield Magnetic Resonance Centre,
University of Nottingham, Nottingham, UK
e-mail: penny.gowland@nottingham.ac.uk

D. Prayer (ed.), *Fetal MRI*, Medical Radiology,
DOI: 10.1007/174_2010_122, © Springer-Verlag Berlin Heidelberg 2011

of these fields will be considered in turn in terms of the possible risks to the health of the fetus. Following that, reviews of studies into outcomes of children scanned as fetuses will be presented. Finally, some other factors that could affect the well-being of the fetus will be discussed.

2 Static Field

In the MR safety literature, the term "projectile effect" is often used to describe the acceleration of ferromagnetic materials within the vicinity of the stray field of the magnet, and it is unquestionably the case that this effect is the primary danger associated with MRI. Accelerated metal objects can obviously cause serious injury and this risk is likely to be somewhat increased when scanning pregnant women because it is likely that other healthcare professionals and partners may accompany the subject to the scan and even into the scan room. However, this risk should be mitigated by careful staff training, scanner room layout, and adherence to appropriate local working rules (Kanal et al. 2002, 2004).

Associated with this is the risk of torques or translational forces on metal objects in the body, or the risks to the functioning of medical implants. With some exceptions (body piercing), these risks are less likely to be an issue in young pregnant subjects than in older patients, but nonetheless all subjects must be carefully screened to determine whether they have any foreign objects in their body.

Large (>2 T) static magnetic fields (or movements in such fields) are known to affect sensory organs, leading to a perception of vertigo, a metallic taste in the mouth and in some instances phosphenes, although these effects are apparently transient and not associated with any risks to health (Glover et al. 2007). These effects are most pronounced when moving rapidly through a spatially varying magnetic field, and so as the mother is likely to be moving slowly when climbing onto the bed these effects are unlikely to be a problem for a pregnant woman at normal clinical field strengths. At very high fields (>16 T) it is possible that the force on a blood (a conducting fluid) moving in a magnetic field (the magnetohydrodynamic effect), might become significant, initially leading to compensatory changes in blood pressure in the adult, but there is no consistent evidence that any clinically significant change can be detected at the field strengths currently used (Kinouchi et al. 1996). Therefore, this will also not be a problem for the fetus at the field strengths currently used, though on going to higher field strength it should be noted that the fetus may be more sensitive to this effect than the adult for a number of reasons. First, the fetus can be lying randomly orientated with respect to the direction of the static field, and hence, unlike the adult in most current scanner configurations, it could be aligned in such a way that the direction of flow is perpendicular to the magnetic field (which is the worst-case scenario that was assumed in the study by Kinouchi et al.) Furthermore, the fetus has a similar aortic blood flow velocity to the adult (Marsal et al. 1984), which will determine the force on the blood, but has a somewhat lower blood pressure so any compensatory action may need to be relatively greater.

There have been a number of reviews of the effects of static fields on embryo development over the last few years. There is evidence that magnetic fields can alter the early division of the frog embryo probably due to variations in the magnetic susceptibility of the different components of a cell involved in division, but this effect does not persist to impede later development (Denegre et al. 1998). There have been a number of studies suggesting that magnetic fields can interfere with the chick embryo development, but these effects are less consistently reported in mammals (HPA 2008; ICNIRP 2009a, b). Overall, it is concluded that no adverse effects have been consistently demonstrated but that more studies are required particularly at fields about 1 T.

There is no consistent evidence that magnetic fields are mutagenic, although there are a few studies suggesting that magnetic fields may act synergistically with other mutagenic agents such as x-rays (Nakahara et al. 2002) or chemicals. The mechanism for such an interaction has not been elucidated but could be related to altered DNA repair mechanisms in a strong magnetic field.

3 Gradients

The gradients used in MRI are varied with time during the scanning session, and hence induce electric currents within the human body, which vary at approximately 1 kHz. It is well known that rapid

changes or large field gradients can cause peripheral nerve stimulation (PNS) in adults, and this occurs well below the threshold at which cardiac defibrillation occurs. The PNS thresholds for a scanner are generally determined empirically in adults, and there is a possibility that the different geometry of a pregnant woman could lead to an increased risk of PNS in certain circumstances, although this would be unpleasant rather than risky at the levels obtained on a clinical scanner, and extremely unlikely if the scanner is run in the international electrotechnical commission (IEC) Normal exposure Level. The fetus is contained within the body where the induced currents will be lower. Nonetheless, it is sensible to restrict scanning to the Normal level to reduce the risk of PNS in the mother.

However, a more significant concern is that the gradients are also responsible for the loud acoustic noise associated with MRI that can reach 120 dB_A. Because of this high noise level, all subjects should be advised to wear ear protection while being scanned, but there is a concern whether the sound intensity level could be damaging to the fetal ear. There are two routes for noise transmission to the fetus, airborne noise transmitted through the maternal body wall, and mechanical vibrations transmitted to the fetal ear because the mother is lying in contact with (is mechanically coupled to) the scanner bed. However, the noise level reaching the fetal cochlear is significantly reduced because the fetus is insulated by the mother's abdominal wall and amniotic fluid which attenuate the noise in a frequency-dependent manner (higher frequencies are attenuated, lower frequencies can be somewhat amplified) and because the fetal ear is filled with amniotic fluid preventing the normal amplification of sound by the ear (Glover et al. 1995; Richards et al. 1992). Furthermore, the sound exposure is relatively brief compared to typical occupational sound exposures. Therefore, it is not expected that acoustic noise will be a significant problem for fetal hearing. It should be noted that the noise levels involved certainly exceed noise levels that, if applied persistently through pregnancy, can lead to poor pregnancy outcome, presumably due to maternal stress (Etzel et al. 1997).

To reduce fetal and maternal noise exposure, the mother should be given adequate hearing protection herself and should be mechanically isolated from the bed by using dense mattresses, and loud pulse sequences should be avoided if alternatives exist. The acoustic noise is expected to increase with magnetic field strength, although in practice it is also significantly affected by the design of the scanner and couch and also by the design of the scanner hall.

4 Radiofrequency (RF) Fields

The established risk associated with RF fields is that of heat deposition, both global heat load and focal heating potentially leading to local burns. Heating is a particular concern for fetuses since temperature rises are known to be teratogenic (Edwards 2006). There have been a few experimental studies of MRI heating of the fetus, for instance measuring the temperature rise in the uterus of a pregnant pig. These studies found no change in temperature for the sequences used at the time (Levine et al. 2001).

It should be noted that the most significant source of RF burns in the adult is due to contact with extraneous electrical conductors (including metal implants, ECG leads, and RF coils leads), close contact with the RF coils, and conduction loops setup through the skin (e.g., by allowing skin of the shins or thighs to touch). None of these sources of localized burning are likely to be a problem for the fetuses.

The models of RF deposition used to control the RF output of the scanners are generally based on models of the nonpregnant adult, and so recently there have been a number of studies aimed at modeling typical RF deposition (Specific Absorption Rate, SAR) within the fetuses and pregnant mother from MR scanners (Hand et al. 2006; Shamsi et al. 2006). These studies generally agree that the highest local peak of SAR is to be found in the mother with the ratio of fetal peak SAR to maternal peak SAR increasing with field strength and that maternal local SAR limits will be exceeded if the scanner is only set to limit whole body exposure. However, SAR is not really the parameter of interest; the biologically important parameter is temperature rise.

It is difficult to predict the fetal temperature rise for a given SAR from the standard models applied to adults since the fetal and maternal circulations are independent of each other. Adult limits to RF power deposition assume that there are good routes for heat loss via the skin (that the scanner bore temperature is less than 24°C, that the humidity is less than 60%, and that the subject is not covered with blankets) whereas

this route is impaired for the fetus since it is contained within the mother's abdomen which is at 37°C. This means that the only route for heat loss from the fetus is across the placenta, and to a lesser extent by conduction through the amniotic fluid (Gowland and De Wilde 2008). Fortunately, Hand et al. (2010) have recently attempted to account for this by modeling the temperature rise in the fetus due to RF exposure, and their results suggest that if the scanner is operated in the IEC normal mode (<2 W/kg whole body exposure) then the fetal SAR and temperature rises will be within international safety limits, but in case of a whole body SAR exposure of 2 W/kg for periods of 7.5 min, the fetal temperature may rise above 38°C. Therefore, it would seem unwise to scan fetuses above the Normal SAR level until further information becomes available. It would also be sensible to design fetal imaging protocols to limit fetal temperature rise by interleaving the higher SAR sequences (e.g., HASTE) with lower SAR sequences (e.g., EPI).

Unfortunately, rapid imaging sequences are required to reduce the impact of fetal motion on image quality, such as half fourier acquisition single shot turbo spin echo (HASTE) and even balanced turbo field echo (bTFE) tend to be high SAR sequences, although with more rapid acceleration factors becoming available with 32 channel abdominal or pelvic coils, this may become less of a problem. In our lab as a precautionary measure, we never exceed the first controlled level of RF exposure when scanning fetuses. A practical consequence of this is that we have only scanned at 1.5 T and not attempted to scan at 3 T since our experience suggests that this will only be achieved successfully with our current hardware by going to the first controlled level.

5 Outcome Studies

There are disappointingly few of studies following up fetuses exposed to MRI in utero. There have been a number of studies of fetal well-being during MRI procedures, monitored using MR compatible cardiotocograph (CTG) systems. These studies showed no evidence that MRI changed the fetal heart rate or fetal movements (Poutamo et al. 1998; Vadeyar et al. 2000; Michel et al. 2003). A study of the birth weight of infants scanned with echo planar MRI at 0.5 T (which therefore had relatively low RF exposure but relatively high noise level exposure) showed that there was no evidence of MRI causing reduced fetal growth; there was some evidence of earlier delivery for the fetuses scanned with MRI, but this was attributed to increased intervention in the group of subjects who were scanned (Myers et al. 1998). When the same infants were followed up at 9 months, the only differences found compared to the control group were a small decrease in length and a small increase in gross motor function (Clements et al. 2000). A separate group of fetuses who had similar exposures were followed up at 3 years, and found no effects of MR exposure (Baker et al. 1994). In a study of children aged up to 9 years old who had been scanned as fetuses, no adverse effects of MRI scanning could be observed (Kok et al. 2004). There have been few studies of the pregnancy outcomes of MR workers, although an early study found no major reproductive hazard associated with MRI work (Kanal et al. 1993).

One common question is how early in gestation can the fetus safely be scanned? There is no data on the risks of exposure during the first trimester though it is probably sensible to avoid scanning in that period since the fetus is more vulnerable to teratogenic insults during that period. Furthermore, heat loss may be even more compromised before placental blood flow becomes properly established.

6 Other Issues Related to MR Scanning and the Well-being of the Fetus

Finally, it is not only the magnetic fields of an MR scanner that will impact on the well-being of the fetus and mother during an MR scan. Obviously, it is important to avoid any unnecessary stress for the mother of undergoing a fetal MRI scan, and as with all clinical procedures, this can be mitigated by careful subject handling (Duncan et al. 1996).

It is also important to bear in mind the relatively high risk of aortocaval compression if the mother lies flat on her back when heavily pregnant. Aortocaval compression causes hypotension to the mother and makes her feel unwell and nauseous and also leads to reduced uteroplacental blood flow. Ideally, subjects should be scanned in the left lateral position, but this is rarely feasible. However, simply elevating the right hip by 15–20

cm generally eliminates the problem. Unfortunately, for most scanner designs this lifts the mother away from the RF coil. The mother must be closely monitored during scanning (via the intercom) to ensure she is not experiencing this symptom.

There is some evidence that some MR contrast agents can cross the human placenta and reach the fetus (Brunelli et al. 2008). In the light of the recent evidence that MR contrast agents are associated with nephrogenic systemic fibrosis (NSF) it would seem prudent to apply the utmost caution before using MR contrast agents in pregnancy, considering in particular the stability of the chelate. Toxicity tests in embryos must consider the biological half-life of the contrast agent in the human amniotic sac.

In conclusion, there have been a number of recent reviews of the effects of MRI and its associated fields on fetal development, which have concluded that there is no apparent risk to human fetal development (Juutilainen 2005). Although it is important to be extremely careful when undertaking any procedure on a fetus, there are no apparent risks associated with fetal MRI, and this procedure must be balanced against the potential advantages of undertaking the scan.

References

Baker PN, Johnson IR, Harvey PR, Gowland PA, Mansfield P (1994) A 3-year follow-up of children imaged in-utero with echo-planar magnetic-resonance. Am J Obstet Gynecol 170(1):32–33

Brunelli R, Masselli G, Gualdi G, De Spirito M, Aarasassi T, Perrone G, De Pratti V, Arpe SD, Anceschi MM (2008) Gadolinium-enhanced MRI mapping of placental perfusion in normal and IUGR pregnancies. Am J Obstet Gynecol 199(6):470

Clements H, Duncan KR, Fielding K, Gowland PA, Johnson IR, Baker PN (2000) Infants exposed to MRI inutero have a normal paediatric assessment at 9 months of age. Br J Radiol 73(866):190–194

Denegre JM, Valles JM, Lin K, Jordan WB, Mowry KL (1998) Cleavage planes in frog eggs are altered by strong magnetic fields. Proc Natl Acad Sci USA 95(25):14729–14732

Duncan K, Baker PN, Johnson IR, Gowland P (1996) Treat patients with kindness during magnetic resonance imaging. Br Med J 312(7043):1421–1421

Edwards MJ (2006) Hyperthermia and fever during pregnancy. Birth Defects Res A Clin Mol Teratol 76(7):507–516

Etzel RA, Balk SJ, Bearer CF, Miller MD, Shea KM, Simon PR (1997) Noise: a hazard for the fetus and newborn. Pediatrics 100(4):724–727

Glover P, Hykin J, Gowland P, Wright J, Johnson I, Mansfield P (1995) An assessment of the intrauterine sound intensity level during obstetric echo-planar magnetic-resonance-imaging. Br J Radiol 68(814):1090–1094

Glover PM, Cavin I, Qian W, Bowtell R, Gowland PA (2007) Magnetic-field-induced vertigo: a theoretical and experimental investigation. Bioelectromagnetics 28(5):349–361

Gowland PA, De Wilde J (2008) Temperature increase in the fetus due to radio frequency exposure during magnetic resonance scanning. Phys Med Biol 53(21):L15–L18

Hand JW, Li Y, Thomas EL, Rutherford MA, Hajnal JV (2006) Prediction of specific absorption rate in mother and fetus associated with MRI examinations during pregnancy. Magn Reson Med 55(4):883–893

Hand JW, Li Y, Hajnal JV (2010) Numerical study of RF exposure and the resulting temperature rise in the foetus during a magnetic resonance procedure. Phys Med Biol 55(4): 913–930

HPA (2008) Static magnetic fields (RCE-6). HPA-Advisory Group on Non-Ionising Radiation, Chilton

ICNIRP (2009a) Guidelines on limits of exposure to static magnetic fields. Health Phys 96(4):504–514

ICNIRP (2009b) Amendment to the ICNIRP "Statement on medical magnetic resonance (MR) procedures: protection of patients". Health Phys 97(3):259–261

Juutilainen J (2005) Developmental effects of electromagnetic fields. Bioelectromagnetics Suppl 7:S107–S115

Kanal E, Gillen J, Evans JA, Savitz DA, Shellock FG (1993) Survey of reproductive health among female MR workers. Radiology 187(2):395–399

Kanal E, Borgstede JP, Barkovich AJ, Bell C, Bradley WG, Felmlee JP, Froelich JW, Kaminski EM, Keeler EK, Lester JW, Scoumis EA, Zaremba LA, Zinninger MD (2002) American College of Radiology white paper on MR safety. Am J Roentgenol 178:1335–1347

Kanal E, Borgstede JP, Barkovich AJ, Bell C, Bradley WG, Etheridge S, Felmlee JP, Froelich JW, Hayden J, Kaminski EM, Lester JW, Scoumis EA, Zaremba LA, Zinninger MD (2004) American College of Radiology White Paper on MR Safety.2004 Updates and Revisions. Am J Roentgenol 182(5):1111–1114

Kinouchi Y, Yamaguchi H, Tenforde TS (1996) Theoretical analysis of magnetic field interactions with aortic blood flow. Bioelectromagnetics 17(1):21–32

Kok RD, de Vries MM, Heerschap A, van den Berg PP (2004) Absence of harmful effects of magnetic resonance exposure at 1.5 T inutero during the third trimester of pregnancy: a follow-up study. Magn Reson Imaging 22(6): 851–854

Levine D, Zuo C, Faro CB, Chen Q (2001) Potential heating effect in the gravid uterus during MR HASTE imaging. J Magn Reson Imaging 13(6):856–861

Marsal K, Lindblad A, Lingman G, Eiknes SH (1984) Blood-flow in the fetal descending aorta – intrinsic-factors affecting fetal blood-flow, i.e. fetal breathing movements and cardiac-arrhythmia. Ultrasound Med Biol 10(3): 339–348

Michel SCA, Rake A, Keller TM, Huch R, Konig V, Seifert B, Marincek B, Kubik-Huch RA (2003) Fetal cardiographic monitoring during 1.5-T MR imaging. Am J Roentgenol 180(4):1159–1164

Myers C, Duncan KR, Gowland PA, Johnson IR, Baker PN (1998) Failure to detect intrauterine growth restriction following inutero exposure to MRI. Br J Radiol 71(845): 549–551

Nakahara T, Yaguchi H, Yoshida M, Miyakoshi J (2002) Effects of exposure of CHO-K1 cells to a 10 T static magnetic field. Radiology 224(3):817–822

Poutamo J, Partanen K, Vanninen R, Vainio P, Kirkinen P (1998) MRI does not change fetal cardiotocographic parameters. Prenat Diagn 18(11):1149–1154

Richards DS, Frentzen B, Gerhardt KJ, McCann ME, Abrams RM (1992) Sound levels in the human uterus. Obstet Gynecol 80(2):186–190

Shamsi S, Wu DG, Chen J, Liu R, Kainz W (2006) SAR evaluation of pregnant woman models in 64 MHz MRI birdcage coil. IEEE MTT S Int Microw Symp Dig 1–5:225–228

Vadeyar SH, Moore RJ, Strachan BK, Gowland PA, Shakespeare SA, James DK, Johnson IR, Baker PN (2000) Effect of fetal magnetic resonance imaging on fetal heart rate patterns. Am J Obstet Gynecol 182(3):666–669

The Psychic State of the Pregnant Woman and Prenatal Diagnostic Procedures

Katharina Leithner

Contents

Abstract

- Prenatal procedures have a major impact on a woman's psychological experience during pregnancy. Generally, women expect a confirmation of their expectation of a healthy child during ultrasonography. The detection of a fetal abnormality is a considerably stressful situation. The active decision to terminate a wanted pregnancy following an adverse prenatal diagnosis as well as any loss of a pregnancy, frequently result in acute feelings of grief, despair, and guilt, and may also cause severe long-term psychological sequelae.
- Invasive procedures are often linked with anxiety about losing the baby and may confront women and their partners with a moral dilemma about terminating the pregnancy. This seems even more evident for multiple pregnancies, which may expose couples to the question of selective feticide or multifetal pregnancy reduction.
- Psychological support, from the first suspicion of a fetal abnormality, and during the prenatal diagnostic process and after the termination of a pregnancy, is needed to help women and their partners.

Abbreviations

CVS	Chorionic villus sampling
MFPR	Multifetal pregnancy reduction
MRI	Magnetic resonance imaging

K. Leithner
Department of Psychoanalysis and Psychotherapy, Medical University Vienna, Währinger Gürtel 18–20, 1090 Vienna, Austria
e-mail: katharina.leithner@meduniwien.ac.at

D. Prayer (ed.), *Fetal MRI*, Medical Radiology,
DOI: 10.1007/174_2010_28, © Springer-Verlag Berlin Heidelberg 2011

1 Introduction

The field of prenatal procedures has not only radically changed our strategies in dealing with pregnancies at a medical level, but also has changed the pregnant woman's view about fetal life. Women seeing their unborn child on the screen are often struck by the sudden reality of the living body within them. Registration of the heartbeat and fetal measurements during ultrasonography help to develop a real image of the unborn child. Direct visualization of the unborn child increases the mother's attachment to the child. In addition, this visualization has changed the maternal/parental attitude toward termination of pregnancy, fetal death, or detection of a fetal abnormality even more dramatic. Technological advances seem to have increased women's anxieties as well as their belief in all-powerful medicine to prevent any mishaps. Pregnancy is more often experienced as a time of particular vulnerability and the fetus has now become a "patient." This seems to be even more prevalent in twin pregnancies. Ultrasound and other prenatal procedures, such as fetal MRI, are of particular relevance for twin pregnancies, as these are monitored more frequently and this increases maternal anxiety, and dependency on the medical system (Piontelli 2000).

The use of different prenatal procedures offers the opportunity to detect fetal pathology, but therapeutic options are limited when chromosomal anomalies or severe malformations or acquired changes become evident. The active decision to terminate a wanted pregnancy following an adverse prenatal diagnosis, as well as any loss of a pregnancy (i.e., stillbirth or perinatal death of the child), frequently results in acute feelings of grief, despair, and guilt, and may also cause severe long-term psychological sequelae (Demyttenaere et al. 1995; Grossmann 1987; Lilford et al. 1994; Lloyd and Laurence 1985; Salvesen et al. 1997).

2 Affective State of Women Following a Prenatal Diagnosis

2.1 Acute Psychic Stress

The emotional attachment to a fetus develops much earlier than has been assumed (Beutel 1991; Beutel et al. 1992). Women already have fantasies of a child and its very specific attributes even before the event of an intact pregnancy (Zeanah et al. 1985). Miscarriage, fetal death, preterm delivery, or termination due to medical reasons is connected with psychic stress both for the women and their partners (Weiner 1992; Dyregov and Matthiesen 1987a; Condon 1987). The psychological impact of miscarriages is often underestimated by the medical system or by the partner. As a consequence, women are alone with their grief.

It has been shown that even a suspect prenatal pathology is a traumatic event for the woman and her partner. Depression rates of women who receive a prenatal diagnosis of a fetal abnormality correspond to those of women with major depression episodes. Older women in particular, women who are nulliparous, who have high trait anxiety levels, and women who use negative coping strategies are at risk for developing psychological problems after the prenatal diagnosis of a fetal abnormality (Leithner et al. 2004).

The loss of an unborn child hits a woman at a psychologically and psychobiologically vulnerable phase (Beutel 1991). Several authors emphasize the need for mourning to enable the detachment from the deceased child in order to regain the ability to reestablish relationships with other persons (Weiner 1992; Dyregov and Matthiesen 1987b; Beutel 1996). However, data about predictive factors for mourning reactions and the associated patterns of mourning after an adverse prenatal diagnosis are limited and somewhat contradictory (Kirkley-Best and Kellner 1982; Schütt et al. 2001).

The number of preceding losses and advanced pregnancy were found to influence the course and severity of mourning reactions (Beutel 1991; Toedter et al. 1988; Kennell et al. 1970; LaRoche et al. 1984). Some studies found an increase in anxiety, somatic, and socio-economic stress, and adverse coping strategies in women with a pregnancy loss in their history (Läpple and Lukesch 1988). Former, unprocessed losses have also been suggested to be a risk factor for a poor psychological outcome, as well as a negative image of oneself, and problematic relations to one's children (Turco 1981; Pines 1990).

In two studies, women who had already had children before a stillbirth were found to have a better psychological outcome (Kirkley-Best and Kellner 1982; Läpple and Lukesch 1988), although this finding was not replicated in other studies (Toedter et al. 1988; LaRoche et al. 1984). Moreover, advanced maternal

age has been linked to decreased mourning (Beutel 1991; Toedter et al. 1988). We found that older women with a history of prenatal incidents are more at risk for developing depressive reactions, because advanced age is associated with an increased risk of losing a child during a subsequent pregnancy (Leithner et al. 2004). In some women, work may serve as a distraction, and workplace social networks may provide some support in the crisis situation of a prenatal diagnosis of fetal pathology or loss of pregnancy. Other studies have reported that women who had to work showed less improvement of their poor affective state, than women who did not work (Leithner et al. 2004).

The importance of social support has been stressed in some studies (Toedter et al. 1988; LaRoche et al. 1984). An individually perceived deficit in social support is found to be a predictor for a severe grief reaction, which is associated with social withdrawal, feelings of distrust, and hostility (Beutel 1991).

The results of coping research indicate a relationship between negative coping strategies and increased psychological discomfort (Läpple and Lukesch 1988). Factors such as self-consciousness, a supportive family background, higher education, and a satisfying working situation seem to promote efficient coping strategies "acitve-cognitive" and "behavior-orientated" coping) (Moos 1988). Active behavior, problem analysis, acceptance, emotional relief, an optimistic attitude, and the application of diverse strategies were described as effective coping strategies, while passivity, resignation, self-accusation, rumination, and suppression of emotions were classified as unsuitable strategies (Heim 1988; Becker 1985).

The variance in perinatal grief was related to inadequacy as a personality trait and negative life-events were found to have a significantly more negative impact on anxious individuals than on nonanxious persons (Rapee et al. 1990; Hunfeld et al. 1995). These findings correspond to our results that high trait anxiety levels were found to be a predictor for a negative psychological outcome (Leithner et al. 2004).

The mere suspicion of having any prenatal problem may have a tremendous emotional impact on pregnant women, regardless of the actual obstetric diagnosis and its medical outcome. A prenatal diagnosis always means the loss of the "imaginary child" (Soulé 1990). The "imaginary child" is built on conscious and unconscious wishes, expectations, fantasies, and hopes of the parents-to-be. In the course of ultrasound investigation or prenatal examinations of the fetus, imagined and actual children of the parents-to-be meet for the first time. At least, after birth, the integration of the "imaginary child" of each parent with the "real" baby must take place to allow acceptance and bonding with the baby. A major discrepancy caused by a prenatal problem or a fetal malformation between the "imaginary" child and the "real" baby makes this process much more difficult. Between the "imaginary," perfect child and the "real" child with a prenatal problem lies a gap that is difficult to overcome. The process of integration depends on the parents' abilities to gradually give up their "imaginary child" in order to accept their "real" child with its appearance, temperament, and sex. When the child has a prenatal problem or a malformation, this process requires mourning for the loss of an "imaginary" healthy child.

2.2 Long-Term Consequences

Women are very disappointed when doctors or the social environment cannot deal with the personal meaning of the loss. The experience of a termination of pregnancy due to a "medical reason" (fetal malformation, genetic problems) may be accompanied by severe psychological trauma and the fear that the reproductive functions have been damaged. This emotional crisis situation may persist over a long period of time (Beutel et al. 1996). The predominant use of depressive coping strategies, such as resignation, passivity, self-accusation, and repression, may lead to serious psychic problems (Moos 1988; Muthny et al. 1992; Cuisinier et al. 1996; Demyttenaere et al. 1995).

Long-lasting negative psychological and social reactions occur more frequently following the termination of pregnancies due to genetic problems than abortions due to social indications (Donnai et al. 1981). Women who decide to terminate a desired pregnancy represent a high-risk group for depression or for social withdrawal (Jörgensen et al. 1985). One in five women develops an adjustment disorder with increasing somatic symptoms, a depressed mood, and continual occupation with the loss 1 year after the abortion (Beutel et al. 1993).

Repeated miscarriages, particularly when they are linked to unresolved mourning and long-lasting

depression, frequently lead to a decrease in self-esteem and hate of the female body (Pines 1990; Leon 1990; Kennell et al. 1970). Factors that have a negative influence on the duration and the degree of the mourning reaction are related to the duration of pregnancy, the absence of children, miscarriages, the lack of a social support system, the mental attitude of the women toward pregnancy, and the psychic representation of the pregnancy and previously unresolved mourning situations and a negative self-representation (Kirkley-Best and Kellner 1982; Condon 1987; Lilford et al. 1994; Lloyd and Laurence 1985).

2.3 Psychological Interventions

The importance of psychological/psychotherapeutic help for women and couples following the prenatal diagnosis of a fetal malformation is clearly mentioned in the literature (Salvesen et al. 1997; Langer et al. 1988).

The patient–doctor relationship is frequently characterized by ambivalent emotions. Feelings of gratefulness, reproach, grief, and aggression may exist at the same time, which makes the situation of professionals working in the field of obstetrics and prenatal care precarious (Knapp and Peppers 1979; Hall et al. 2003). After an adverse prenatal incident, women frequently complain about a lack of emotional support and sufficient information from health care professionals (Nikcevic et al. 1998; Hamilton 1989; Jörgensen et al. 1985; Leschot et al. 1982; Radestad et al. 1996). When fetal death or miscarriage occurs, the women's needs during the initial phase of the grieving process are great (Seibel and Graves 1980). Moreover, adverse prenatal incidents are tragedies experienced by the medical staff as well. Adequate supervision services may help to ensure that interactions with the patient do not become routine and impersonal (Prettyman and Cordle 1992).

Physicians may fill some of the patients' immediate needs by supplying sufficient medical information about the cause and circumstances of the prenatal incident (Leithner et al. 2006). As a matter of course, everyday life at a hospital can hardly provide a sufficient setting to answer all the needs of these highly traumatized patients. The implementation of communication training, which has proven to be effective in teaching physicians to address psychological issues and concerns (Hall et al. 2003; Van Dulmen et al. 2003; Sollner et al. 1998; Langewitz et al. 1998), may enhance the chances for a more satisfying interaction for all parties involved.

Psychological support should be available to all women who are referred to a department of prenatal care. Short-term psychological treatment has been shown to be sufficient for the majority of women, but access to long-term psychotherapy should be facilitated. Involved therapists should be able to apply various psychological techniques, depending on diagnostic findings and the subjective needs of a patient. To avoid a negative psychological outcome, psychological techniques should focus on the patient's potential use of negative coping strategies (Leithner et al. 2002).

2.4 Satisfaction with Prenatal Care

During a prenatal procedure, women are in a fragile psychic state. The importance of the subjective experiences of prenatal procedures as a determinant factor for satisfaction with the received care has been clearly shown (Leithner et al. 2006). Several findings indicate that up to 35% of women attending a prenatal care unit complain about the paucity of information and the lack of emotional support (Nikcevic et al. 1998; Hamilton 1989; Leschot et al. 1982; Friedman 1989; Helström and Victor 1987; Dyregov and Matthiesen 1987a; Beutel 1996; White-Van-Mourik et al. 1992). In a follow-up study of 20 patients after pregnancy termination because of genetic indications, women reported that they felt unprepared for their diagnosis and complained about the communication style of physicians (Leschot et al. 1982). Similarly, in a follow-up investigation in women after a second trimester termination of pregnancy due to fetal abnormality, women complained about a lack of understanding, silence about the termination of pregnancy, indifference, and disapproval (White-Van-Mourik et al. 1992). Generally, women's dissatisfaction with treatment in the hospital is reported to be between 13% and 35% (Hamilton 1989; Friedman 1989). However, there may be different expectations toward certain subgroups of professionals working in primary care. Nurses and midwives were found to demonstrate a greater tendency to promote the patient's autonomy by making less direct

recommendations about prenatal decisions than obstetricians (Bernhardt et al. 1998).

3 Prenatal Diagnostic Procedures

In general, attitudes concerning prenatal procedures are reported to be positive in the majority of pregnant women. Women were found to be informed about the procedure of screening (29%–65%) tests, but had little knowledge about the purpose of tracing fetal malformations (30%–43%) or the limitations of screening tests (Dahl et al. 2006a). Van den Berg et al. (2005) showed that screening in a context where it is not part of routine prenatal care resulted in lower up-take rates and different reasons for accepting or declining screening tests than in a context in which screening is offered routinely. Accepting prenatal screening is often not the result of an informed decision, but is rather perceived as self-evident when prenatal screening is part of the customary prenatal care (Green et al. 2004).

Dahl et al. (2006b) found that the content of provided information only rarely includes details that would enable informed choice, and lacks detailed and balanced information. Prenatal tests are often issued in an uncomplicated and positive manner. Information (e.g., group counseling, individual counseling, and information leaflets) can improve the level of knowledge without raising anxiety (Dahl et al. 2006b).

3.1 Ultrasonography

The diagnostic benefits of ultrasound scanning in pregnancy are well documented, but little attention has been paid to the psychological impact of prenatal diagnostic procedures (Levi 1998). It has been reported that the majority of women who undergo routine ultrasound examination exhibit positive feelings toward scanning and accept the procedure rather uncritically (Whynes 2002).

Ultrasound is considered a benign procedure that allows the baby to be seen (van den Berg et al. 2005). Kowalcek et al. (2002) found that the invasiveness of the prenatal method does not influence the subjective mood within the meaning of depressive irritations. They found higher rates of depressive reactions in mothers and fathers before diagnostic ultrasound compared to invasive procedures (amniocentesis or chorionic villus sampling (CVS)). The sonographic visualization of the fetus often is the father-to-be's first contact with the baby, thus probably explaining the high levels of depressive reactions during ultrasound. Müller et al. (2006) showed that offering nuchal translucency screening for Down syndrome does not increase anxiety levels.

Generally, pregnant women expect the confirmation of their expectation of a healthy child and the removal of any uncertainty about fetal problems or malformations during ultrasound. Therefore, routine ultrasound is mainly perceived as a positive and reassuring experience for the parents-to-be.

3.2 Invasive Procedures

3.2.1 Amniocentesis and Chorionic Villus Sampling

Raphael-Leff (2005) describes amniocentesis as a live event and not as a medical procedure. The procedure is followed by a long wait for a "verdict," associated with the risk of a possible miscarriage.

In addition to the sense of endangering the fetus by the procedure, the woman knows that the result might expose her to a dilemma about a decision that will affect the rest of her life.

Typically, 53% of women are anxious about miscarriage, and 78% are anxious before the examination (Endres 1989). Women who undergo amniocentesis were found to be more anxious and showed more negative attitudes toward the baby than women who did not undergo amniocentesis (Marteau et al. 1992). Previous experience with prenatal testing, increased risk of a birth anomaly, and favorable attitudes toward abortion were found to be associated with increased precounseling anxiety (Tercyak et al. 2001). Earlier gestational age, as seen in women having CVS, does not go along with lower levels of stress (Kowalcek et al. 2002). Several studies showed that women were most worried about miscarriage and fetal injury due to the procedure and about test outcome (Cederholm et al. 1999; Beeson and Globus 1979). These factors, of significant importance to women, should be considered in preinformation and genetic counseling.

3.2.2 Termination of Pregnancy

The detection of a fetal malformation, and the subsequent management by termination of the pregnancy, presents a challenge to the medical staff as well as to the woman and her partner. Support is needed from the first suspicion of a fetal malformation, during the prenatal diagnostic process, and during the waiting for the test results. After receiving positive results, the couple needs help about the decision and, after termination of pregnancy, the woman and her partner need psychological help to resolve the mourning process as well as support in case of a subsequent pregnancy (Elder and Laurence 1991).

3.2.3 Multiple Pregnancies

A woman expecting two or more babies must meet greater physiological and psychological demands during pregnancy. The risk of preterm labor, lower birth weight, and perinatal mortality are increased, and the woman is more often exposed to prenatal screening procedures than in a singleton pregnancy. Psychologically, the mother-to-be must integrate the reality of two or more babies. The woman is confronted with the necessity to bond with two babies, knowing, at the same time, about the high risk of losing one fetus during pregnancy. Apart from the physiological and psychological strains of a multiple pregnancy, the detection of a serious abnormality in one twin or the question of multifetal pregnancy reduction (MFPR) in higher-order pregnancies after infertility treatment may generate anxiety, fear, and moral dilemmas for the parents-to-be.

Selective Feticide

The main predictor of whether a woman will terminate a pregnancy in singleton pregnancies is the severity of fetal malformation (Evans et al. 1996). A selective feticide in a twin pregnancy is very different from termination of a singleton pregnancy, as the pregnancy continues with the dead fetus (Bryan 2005). Data on fantasies and long-term consequences for parents-to be and the surviving child after selective feticide is still lacking. Many parents have not heard of selective feticide before faced with that situation. Apart from the moral dilemma for the parents-to-be, there is often a limited time frame to come to an acceptable decision. Professionals need to be aware of their own moral feelings concerning feticide, and the management of these cases essentially requires good communication between all parties involved (Bryan 2005).

Multifetal Pregnancy Reduction

Fortunately, the number of MFPR has dramatically decreased in the last several years due to restriction on the numbers of transferred embryos. MFPR is always a distressing experience for parents (Bryan 2002). The main feelings associated with the reduction are anxiety, sadness, grief, and guilt (Bergh et al. 1999). Moreover, the psychological trauma of an MFPR may reinforce stress due to prolonged fertility treatment, low self-esteem, and a feeling of failure (McKinney et al. 1996). Britt et al. (2002) reported that the moral dilemma for couples in multiple pregnancies may lie in the fact that no fetal abnormality is found, which probably makes the decision for MFPR even more difficult. Consequently, the detection of a fetal abnormality in one fetus may be met with relief rather than despair.

Follow-up studies showed that many women suffered from guilt and grief during the first year after MFPR, but the majority felt that they had made the right decision (Schreiner-Engel et al. 1995). Psychological support should be available, not only during the decision process or the ongoing pregnancy after the reduction, but also in the longer term.

3.3 Fetal Magnetic Resonance Imaging

Data about the psychological experiences of fetal magnetic resonance imaging (MRI) is rare. Michel et al. (2002) investigated the psychological reactions of 15 pregnant women and 15 nonpregnant controls undergoing pelvimetry, and compared patient acceptability between open 0.5-T and closed 1.5-T MR systems. Thirty-three percent of pregnant women in both systems reported fear of fetal harm independent of the pre-information provided by their gynecologists about possible MRI-induced risks. The noise during an MRI examination, in particular, has been mentioned as a major disturbing factor, even though there are phantom studies that MR room noise of 120 dB falls to below 90 dB in utero (Glover et al. 1995), comparable to the

baseline noise from 72 to 88 dB of the aorta, to which the fetus is physiologically exposed daily (Smith et al. 1990). Scan time was only a minor determinant of overall satisfaction with MRI.

With regard to psychological reactions during MRI procedures in general, we know that prevalence rates for claustrophobic reactions during scanning are between 5% and 10% in the general population (Mackenzie et al. 1995; Kilborn and Labbé 1990; Friday and Kubal 1990). Anxiety reactions were found in up to 37% of the patients undergoing scanning procedures (Katz et al. 1994; Melendez and McCrank 1993). A long examination time, high noise level, and temperature are found to be predictive for developing problems during MRI (Quirk et al. 1989; Mackenzie et al. 1995). Anxious patients who stated that they were worried by technical apparatus before the examination are at risk for developing problems during scanning (Thorp et al. 1990; Dantendorfer et al. 1997). The degree of information provided by the referring doctor has a major impact on a patient's experience of MRI. Information folders are often not understood by the targeted patient population (Quirk et al. 1989). Intervention strategies to increase a patient's ability to cope with these procedures, which have been discussed in literature, include detailed patient information using special folders or information material, video demonstration, or support by an accompanying person during the examination (Tillier et al. 1997; Nozzolillo et al. 1991; Thorp et al. 1990).

Garel (2008) reported that women felt greater levels of anxiety before fetal MRI than before ultrasonography, and she concluded that fetal MRI has a potentially negative psychological effect on the patient that should be considered in the decision for this prenatal procedure.

We performed a study on the psychological experiences of fetal MRI examinations (Leithner et al. 2008). Although fetal MRI was well accepted in our sample, women were found to experience considerable stress immediately before scanning, which decreased to normal anxiety levels after the scan. Major distressing factors for the pregnant women were physical restraint, noise level, duration of the examination, and anxiety for the baby. The severity of the referral diagnosis showed an increasing effect on anxiety levels.

In contrast to ultrasound examinations, women do not see their baby during scanning: thus, immediate reassurance of the baby's health is not possible. Generally, women are alone in the examination room without the opportunity to see the medical staff, which probably makes the situation for the women even more frightening. The presence of the partner during MRI may be a relief for some women, because fetal MRI is a rather new procedure in prenatal medicine, and women are often not well prepared about the course and the circumstances of the examination procedure.

According to our experiences, pregnant women referred because of a suspicion of a prenatal diagnosis are already in a considerably stressful situation. Women need adequate pre-information to prepare them for the special situation of an MRI examination. This pre-information should stress the restricted body movement, the high temperature, the noise level, and the duration of the examination. Women should also be informed about the safety of their baby during MRI. Remaining insecurities and anxieties concerning the baby's health should be addressed by the referring physician.

3.4 Checklist Before Any Prenatal Diagnostic Procedure

- Explain the reason for the performance of ultrasound or MRI and make sure the pregnant woman/ parents-to-be have understood the explanation.
- In case the examination might have consequences on the further management of the pregnancy (premature C-section, prenatal therapy, EXIT (ex utero-intrapartum) procedure, postnatal surgery, pregnancy termination), counseling by a team (referring obstetrician, surgeon, neonatologist, psychologist…) will be necessary.
- MRI examination requires a written patient information and a signed consent.
- The pregnant woman/ parents-to-be should be informed prior to the examination when a definite written report will be available. Especially in case of MRI, this might take some time if measurements, such as lung volumetry have to be performed.

References

Becker P (1985) Bewältigungsverhalten und psychische Gesundheit. Z f Klein Psychol 14:169–184

Beeson D, Globus MS (1979) Anxiety engendered by amniocentesis. Birth Defects 15:191–197

Bergh C, Möller A, Nilsson L et al (1999) Obstetric outcome and psychological follow-up of pregnancies after embryo reduction. Hum Reprod 14:2170–2175

Bernhardt BA, Geller GS, Doksum T et al (1998) Prenatal genetic testing: content of discussions between obstetric providers and pregnant women. Obstet Gynecol 91:648–655

Beutel M (1991) Zur Psychobiologie von Trauer und Verlustverarbeitung - neuere immunologische und endokrinologische Zugangswege und Befunde. Psychother Med Psychol 41:267–277

Beutel M (1996) Der frühe Verlust eines Kindes: Bewältigung und Hilfe bei Fehl-, Totgeburten und Fehlbildungen. Verlag für angewandte Psychologie, Göttingen

Beutel M, Deckardt R, Schaudig K et al (1992) Trauer, Depressivität und Angst nach einem Spontanabort - Eine Studie über systematische Erfassung und Einflußfaktoren. Psychother Med Psychol 42:158–166

Beutel M, Deckardt R, Schaudig K et al (1993) Chronische Trauer nach einem Spontanabort: Ergebnisse einer Längsschnittstudie nach 13 Monaten. Psychother Psychosom Med Psychol 43:411–419

Beutel M, Willner H, Deckhardt R et al (1996) Similarities and differences in couples' grief reactions following a miscarriage: results from a longitudinal study. J Psychosom Res 40:245–253

Britt DW, Risinger ST, Mans MK et al (2002) Devastation and relief: conflicting meanings of detected fetal anomalies. Ultrasound Obstet Gynecol 20:1–5

Bryan E (2002) Loss in higher multiple pregnancies and multifetal pregnancy reduction. Twin Res 5:169–174

Bryan E (2005) Psychological aspects of prenatal diagnosis and its indications in multiple pregnancies. Prenat Diagn 25: 827–834

Cederholm M, Axelsson O, Sjödén P-O (1999) Women's knowledge, concerns, and psychological reactions before undergoing an invasive procedure for prenatal karyotyping. Ultrasound Obstet Gynecol 14:267–272

Condon JT (1987) Prevention of emotional disability following stillbirth. N Z J Obstet Gynaecol 27:323–329

Cuisinier M, Janssen H, De Graauw C et al (1996) Pregnancy following miscarriage: course of grief and some determining factors. J Psychosom Obstet Gynecol 17:168–174

Dahl K, Kesmodel U, Hividman L et al (2006a) Informed consent: attitudes, knowledge, and information concerning prenatal examinations. Acta Obstet Gynecol Scand 85: 1414–1419

Dahl K, Kesmodel U, Hividman L et al (2006b) Informed consent: providing information about prenatal examinations. Acta Obstet Gynecol Scand 85:1420–1425

Dantendorfer K, Amering M, Bankier A et al (1997) A study of the effects of patient anxiety, perceptions, and equipment on motion artifacts in magnetic resonance imaging. Magn Reson Imaging 15:301–306

Demyttenaere K, Maes A, Nijs P et al (1995) Coping style and preterm labor. J Psychosom Obstet Gynecol 16:109–115

Donnai P, Charles N, Harris R (1981) Attitudes of parents after "genetic" termination of pregnancy. Brit Med J 282: 621–622

Dyregov A, Matthiesen SB (1987a) Similarities and differences in mothers' and fathers' grief following the death of an infant. Scand J Psychol 28:1–15

Dyregov A, Matthiesen SB (1987b) Anxiety and vulnerability in parents following the death of an infant. Scand J Psychol 28:16–25

Elder SH, Laurence KM (1991) The impact of supportive intervention after second trimester termination of pregnancy for fetal abnormality. Prenat Diagn 11:47–54

Endres M (1989) The psychological effects of antenatal diagnosis on pregnancy. In: Fedor-Freybergh P, Vogel MLV (eds) Prenatal and perinatal psychology and medicine: encounter with the unborn. Parthenon, Lancaster

Evans MI, Sobiecki MA, Krivchenia EL et al (1996) Parental decisions to terminate/continue following abnormal cytogenetic prenatal diagnosis: "what" is still more important than "when". Am J Mel Genet 61:353–355

Friday PJ, Kubal WS (1990) Magnetic resonance imaging: improved patient tolerance utilizing medical hypnosis. Am J Clin Hypn 33:80–84

Friedman T (1989) Women's experiences of general practitioner management of miscarriage. J R Coll Gen Pract 39:456–458

Garel C (2008) Fetal MRI: what is the future? Ultrasound Obstet Gynecol 31:123–128

Glover P, Hykin J, Gowland P et al (1995) An assessment of the intrauterine sound intensity level during obstetric echo-planar magnetic resonance imaging. Br J Radiol 814: 1090–1094

Green JM, Hewison J, Bekker HL et al (2004) Psychosocial aspects of genetic screening of pregnant women and newborns: a systematic review. Health Technol Assess 8:1–124

Grossmann K (1987) Trauerarbeit nach Verlust des Kindes. In: Prill HJ, Stauber M, Teichmann A (eds) Psychosomatische Gynäkologie und Geburtshilfe. Springer, Berlin, pp 32–47

Hall S, Abramsky L, Marteau TM (2003) Health professionals' reports of information given to parents following the prenatal diagnosis of sex chromosome anomalies and outcome of pregnancies: a pilot study. Prenat Diag 23:535–538

Hamilton SM (1989) Should follow-up be provided after miscarriage? Br J Obstet Gynaecol 96:743–745

Heim E (1988) Coping und Adaptivität. Gibt es geeignetes oder ungeeignetes Coping? Psychother Med Psychol 38:8–18

Helström L, Victor A (1987) Information and emotional support for women after miscarriage. J Psychosom Obstet Gynecol 7:93–98

Hunfeld JAM, Wladimiroff JW, Verhage F et al (1995) Previous stress and acute psychological defense as predictors of perinatal grief – an exploratory study. Soc Sci Med 40:829–835

Jörgensen C, Uddenber N, Ursing I (1985) Ultrasound diagnosis of fetal malformation in the second trimester. J Psychosom Obstet Gynecol 4:31–40

Katz RC, Wilson L, Frazer N (1994) Anxiety and its determinants in patients undergoing magnetic resonance imaging. J Behav Ther Exp Psychiatry 25:131–134

Kennell JH, Slyter H, Klaus MH (1970) The mourning response of parents to the death of a newborn infant. N Engl J Med 283:344–349

Kilborn LC, Labbé EE (1990) Magnetic resonance imaging scanning procedures: development of phobic response during scan and at one-month follow-up. J Behav Med 13: 391–401

Kirkley-Best E, Kellner KR (1982) The forgotten grief: a review of the psychology of stillbirth. Am J Orthopsychiatry 52: 420–429

Knapp RJ, Peppers LG (1979) Doctor-patient relationships in fetal/infant death encounters. J Med Educ 54:775–780
Kowalcek I, Mühlhoff A, Bachmann S et al (2002) Depressive reactions and stress related to prenatal medicine procedures. Ultrasound Obstet Gynecol 19:18–23
Langer M, Ringler M, Reinold E (1988) Psychological effects of ultrasound examinations: changes of body perception and child image in pregnancy. J Psychosom Obstet Gynecol 8:199–208
Langewitz WA, Eich P, Kiss A et al (1998) Improving communication skills-a randomized controlled behaviorally oriented intervention study for residents in internal medicine. Psychosom Med 60:268–276
Läpple M, Lukesch H (1988) Psychische und psychosoziale Faktoren sowie relevante therapeutische Massnahmen bei Spontanaborten und rezidivierenden Spontanaborten bzw. habituellen Aborten. Zentbl Gynäkol 110:1185–1194
LaRoche C, Lalinec-Michauld M, Engelsmann F et al (1984) Grief reactions to perinatal death – a follow-up study. Can J Psychiatry 29:14–19
Leithner K, Maar A, Maritsch F (2002) Experiences with a psychological help service for women following a prenatal diagnosis: results of a follow-up study. J Psychosom Obstet Gynecol 23:183–192
Leithner K, Maar A, Fischer-Kern M et al (2004) Affective state of women following a prenatal diagnosis: predictors of a negative psychological outcome. Ultrasound Obstet Gynecol 23:240–246
Leithner K, Hilger E, Fischer-Kern M et al (2006) Prenatal care: the patient's perspective. A qualitative study. Prenat Diagn 26:931–937
Leithner K, Pörnbacher S, Assem-Hilger E et al (2008) Psychological reactions in women undergoing fetal magnetic resonance imaging. Obstet Gynecol 111:396–402
Leon IG (1990) When a baby dies. Yale University Press, New Haven
Leschot NJ, Verjaal M, Treffers PE (1982) Therapeutic abortion on genetic indications – a detailed follow-up study of 20 patients. J Psychosom Obstet Gynecol 1–2:47–56
Levi S (1998) Routine ultrasound screening of congenital abnormalities. An overview of the European experience. Ann N Y Acad Sci 9:86–98
Lilford RJ, Stratton P, Godsil S et al (1994) A randomized trial of routine versus selective counseling in perinatal bereavement from congenital disease. Br J Obstet Gynaecol 101:291–296
Lloyd J, Laurence KM (1985) Sequelae and support after termination of pregnancy for fetal malformation. Br Med J 290: 907–990
Mackenzie R, Sims C, Owens RG et al (1995) Patients' perceptions of magnetic resonance imaging. Clin Radiol 50: 137–143
Marteau TM, Kidd J, Cook R et al (1992) Psychological effects of having amniocentesis: are these due to the procedure, the risk or the behavior? J Psychosom Res 36:395–402
McKinney MK, Tuber SB, Downey JI et al (1996) Multifetal pregnancy reduction: psychodynamic implications. Psychiatry 59:393–407
Melendez JC, McCrank E (1993) Anxiety-related reactions associated with magnetic resonance imaging examinations. JAMA 27:745–747
Michel SC, Rake A, Götzmann L et al (2002) Pelvimetry and patient acceptability compared between open 0.5-T and closed 1.5-T MR systems. Eur Radiol 12:2898–2905
Moos RH (1988) Coping: Konzepte und Meßverfahren. Z Psychosom Med Psychoanal 3:207–225
Müller MA, Bleker OP, Bonsel GJ et al (2006) Nuchal translucency screening and anxiety levels in pregnancy and puerperium. Ultrasound Obstet Gynecol 27:357–361
Muthny FA, Bechtel M, Spaete M (1992) Laienätiologien und Krankheitsverarbeitung bei schweren körperlichen Erkrankungen. Psychother Psychosom Med Psychol 42: 41–53
Nikcevic AV, Tunkel SA, Nicolaides KH (1998) Psychological outcomes following missed abortions and provision of follow-up care. Ultrasound Obstet Gynecol 11:123–128
Nozzolillo R, Ercolani P, Giovagnoni A et al (1991) Reazioni psicologiche di pazienti sottoposti a imaging con risonanza magnetica. Radiol Med 81:601–604
Pines D (1990) Schwangerschaft, Fehlgeburt und Abtreibung: eine psychoanalytische Perspektive. Zschr f psychoanal Theorie und Praxis 5:311–321
Piontelli A (2000) 'Is there something wrong': the impact of technology in pregnancy. In: Raphael-Leff J (ed) 'Spilt milk' perinatal loss and breakdown. Institute of Psychoanalysis, London, pp 39–52
Prettyman RJ, Cordle C (1992) Psychological aspects of miscarriage: attitudes of primary health care team. Br J Gen Pract 42:97–99
Quirk ME, Letendre AJ, Ciottone RA et al (1989) Anxiety in patients undergoing MR imaging. Radiology 170:463–466
Radestad I, Steineck G, Nordin C et al (1996) Psychological complications after stillbirth – influence of memories and immediate management: population-based study. BMJ 312:1505–1508
Rapee RM, Litwin EM, Barlow DH (1990) Impact of live events on subjects with panic disorder and on comparison subjects. Am J Psychiatry 147:640–644
Raphael-Leff J (2005) Psychological process of childbearing, 4th edn. Anna Freud Center, London
Salvesen KA, Oyen L, Schmidt N et al (1997) Comparison of long-term psychological responses of women after pregnancy termination due to fetal anomalies and after perinatal loss. Ultrasound Obstet Gynecol 9:80–85
Schreiner-Engel P, Walther N, Mindes J et al (1995) First-trimester multifetal pregnancy reduction: acute and persistent psychologic reactions. Am J Obstet Gynecol 172: 541–547
Schütt K, Kersting A, Ohrmann P et al (2001) Schwangerschaftsabbruch aus fetaler Indikation – Ein traumatisches Ereignis? Zentralbl Gynäkol 123:37–41
Seibel M, Graves WL (1980) The psychological implications of spontaneous abortions. J Reprod Med 25:161–165
Smith CV, Satt B, Phelan JP et al (1990) Intrauterine sound levels: intrapartum assessment with an intrauterine microphone. Am J Perinatol 4:312–315
Sollner W, Zingg-Schir M, Rumpold G et al (1998) Need for supportive counseling- the professionals' versus the patients' perspective. A survey in a representative sample of 236 melanoma patients. Psychother Psychosom 67:94–104
Soulé M (1990) Das Kind im Kopf – das imaginäre Kind. Sein strukturierender Wert im Austausch zwischen Mutter und

Kind. In: Stork J (ed) Neue Wege im Verständnis der allerfrühesten Entwicklung des Kindes. Erkenntnisse der Psychopathologie des Säuglingsalters. Frommann-holzboog, Stuttgart-Bad Cannstatt, pp 20–80

Tercyak KP, Bennett Johnson S, Roberts SF et al (2001) Psychological response to prenatal genetic counseling and amniocentesis. Patient Educ Couns 43:73–84

Thorp D, Owens RG, Whitehouse G et al (1990) Subjective experiences of magnetic resonance imaging. Clin Radiol 41:276–278

Tillier P, Leclet H, Malgouyres A et al (1997) Le comportement psychologique des patients en IRM: analyse, propositions d'amélioration et apport de l'appareillage à aimant ouvert. J Radiol 78:433–437

Toedter L, Lasker J, Alhadeff J (1988) The perinatal grief scale: development and initial validation. Am J Orthopsychiat 58:435–449

Turco R (1981) The treatment of unresolved grief following loss of an infant. Am J Obstet Gynecol 141:503–507

van den Berg M, Timmermans DRM, Kleinveld JH et al (2005) Accepting or declining the offer of prenatal screening for congenital defects: test uptake and women's reasons. Prenat Diagn 25:84–90

Van Dulmen S, Nubling M, Langewitz W (2003) Doctor's responses to patient's concerns; an exploration of communication sequences in gynecology. Epidemiol Psychiatr Soc 12:98–102

Weiner H (1992) Perturbing the organism. University of Chicago Press, Chicago

White-Van-Mourik MCA, Connor JM, Ferguson-Smith MA (1992) The psychosocial sequelae of a second-trimester termination of pregnancy for fetal abnormality. Prenat Diagn 12:189–204

Whynes DK (2002) Receipt of information and women's attitudes toward ultrasound scanning during pregnancy. Ultrasound Obstet Gynecol 19:7–12

Zeanah CH, Keener M, Stewart L et al (1985) Prenatal perception of infant personality. J Am Acad Child Psychiatry 24:204–210

Methods of Fetal MRI

Peter C. Brugger

Contents

P.C. Brugger
Integrative Morphology Group, Center of Anatomy and Cell Biology, Medical University of Vienna, Waehringerstrasse 13, 1090 Vienna, Austria
e-mail: peter.brugger@meduniwien.ac.at

D. Prayer (ed.), *Fetal MRI*, Medical Radiology,
DOI: 10.1007/174_2010_29, © Springer-Verlag Berlin Heidelberg 2011

Abstract

› Fetal magnetic resonance imaging (MRI) differs in many respects from a postnatal MRI study. The operator has no influence on the position of the fetus, only by proper positioning and repositioning of the surface coil, and/or the pregnant woman, may optimal imaging conditions be achieved. Without using sedation, fetal movements and positional changes make fetal MRI a sort of interactive imaging, with the goal being to acquire a series of continuous, correctly oriented images as quickly as possible. As structures to be imaged are very small, high-quality images are essential for depicting detailed anatomy and pathology. Therefore, a balance between resolution, field of view, slice thickness, and acquisition time must be found. In addition to T2-weighted sequences, several ultrafast sequences are now available that can provide additional information about specific organs or pathologies.

1 Introduction

Since its introduction in the early 1980s, the development of ultrafast sequences and improvements in scanner and coil technology have led to an increased use of fetal MRI (see also Chap. 1). At present, fetal MRI studies are typically performed on a 1.5-T system using phased-array surface coils with 4–8 elements. For experience at higher field strengths, the reader is referred to Chap. 5, and safety issues are discussed in Chap. 6.

2 Differences from Postnatal MRI

Fetal MRI differs in many respects from postnatal MR studies. First, the operator has no influence on fetal position. Second, structures to be imaged are very small and the fetus may be far away from the coil elements. In addition, without sedation, fetal movements may interfere with image acquisition, making fetal MRI a sort of interactive imaging. While there is no influence on the position of the fetus, coil geometry and image quality can be improved by repositioning the coil and/or the pregnant woman. This is of particular importance in larger fetuses and in cases of increased maternal abdominal circumference (Fig. 1).

3 Age-Related Differences

As fetal MRI is usually performed after the 19th gestational week (GW), it covers a time period of more than 20 weeks, in which the fetus grows considerably in size and fetal weight increases by approximately ten times. Apart from the time a given pathology may be detectable, imaging a small fetus is different from imaging a fetus close to term. However, imaging smaller fetuses is an important issue since legal abortion in many countries is only possible before 24 GW.

In young fetuses, imaging is complicated by the small dimensions and the more frequent fetal general movements, and, in advanced stages of pregnancy, the fetus becomes relatively large with respect to the coil. As the

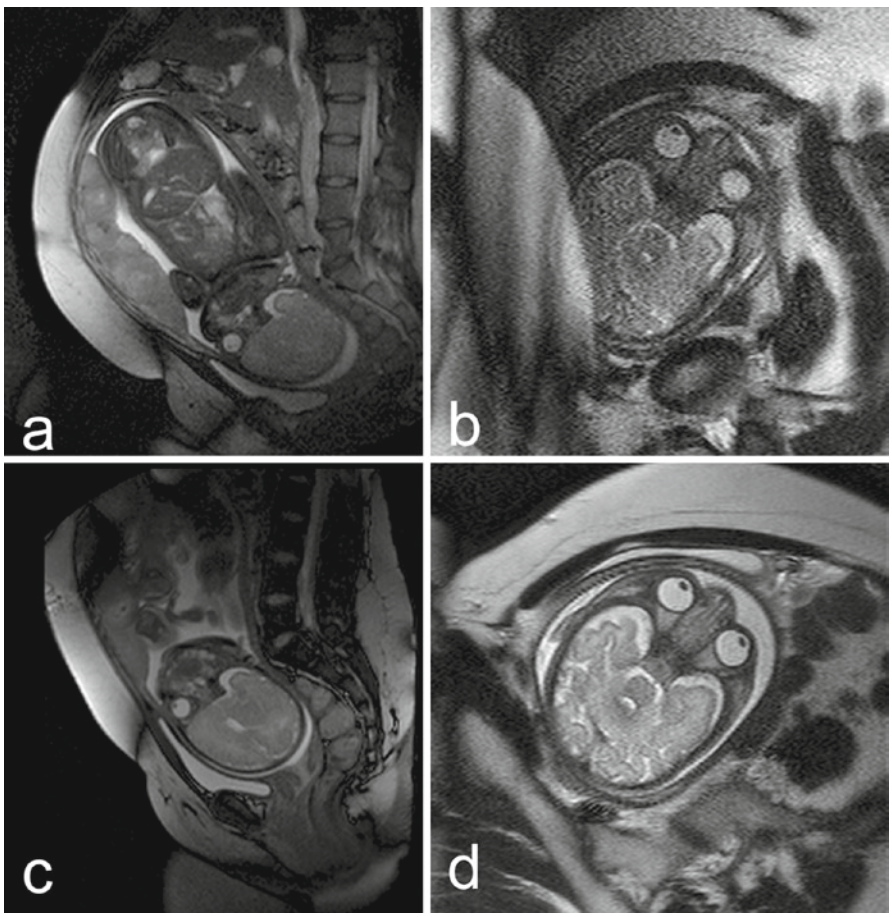

Fig. 1 Repositioning of the coil improves image quality. (**a**) Fetus at 35 + 1 GW. Sagittal image of the initial SSFP survey with center of the coil on the fetal body. (**b**) Low image quality of the resulting axial T2-weighted image through the fetal head. (**c**) SSFP survey with the coil moved more caudally. (**d**) Improved image quality of the axial T2-weighted image through the fetal head

signal-to-noise ratio of the coil decreases toward the edge zones, repositioning of the coil becomes necessary to obtain high-quality images of the fetus. Moreover, the increasing abdominal circumference of the expectant woman also increases the distance between the fetus and the coil elements.

4 Fetal MRI is Whole-Body MRI

Up to 27/28 GW, the relatively small fetal size allows imaging of the whole fetus without repositioning of the coil, although, due to non-alignment of the fetal head with respect to the fetal body, it is usually necessary to image the head and body separately. Assessment of the whole fetal body is particularly important in cases of complex malformations, because diagnosis may only be established by summing up the findings in various organ systems. In addition, extrafetal structures, such as the placenta and umbilical cord, should also be assessed. It is, therefore, advantageous to cover the whole uterus with one sequence to determine the site of umbilical cord insertion.

5 Survey Scan

A steady-state free-precession (SSFP) survey scan yields a total of 42 images in three orthogonal planes of the maternal body in 26 s (Table 1; Fig. 2). It shows the actual position of the fetus and enables a determination about whether the region of interest is within the center of the coil (Figs. 1 and 2). If this is not the case, the coil should be repositioned to guarantee optimal image quality.

The survey scan is more than a simple localizer. Depending on the way the fetus is sectioned, many anatomical details and gross pathologies can be seen on these images. Since the position of the pregnant woman in the scanner is known, as well as the fetuses' position relative to her, the survey scan is also useful for assessing the visceral situs in the fetus. It also provides information on the size and position of the placenta and cervix and the amount of amniotic fluid. Since the scan is planned orthogonal to the body of the pregnant woman, maternal anatomy is also depicted.

6 Planning Sequences and Orientation

Basically, sequences in fetal MRI are planned assuming that the fetus will still be in the same position as on the previous scan. Using the most recent acquisitions in three planes as the basis for the subsequent sequences, the next sequence should be planned immediately after the start of one sequence, so little time elapses between two acquisitions. Although, during the study, there is usually little time to look at the images, one should scroll through the most recent images, look for additional pathologies, and think of sequences that might supply further information.

As the fetus is usually oriented oblique to the standard planes of the pregnant woman, the directions provided by the scanner do not apply to the fetus. Moreover, the orientation of the image plane through the fetus in relation to the pregnant woman also must be taken into account in order to avoid fold-over artifacts. As more or less pronounced changes in fetal position are the rule during the study, appropriate corrections must be made. A keen knowledge of fetal anatomy and spatial imagination are essential in making these corrections.

In planning sequences through the fetal head, the orientation of the axial and frontal planes perpendicular or parallel to the brainstem or the floor of the fourth ventricle is recommended. The interhemispheric fissure and/or the cranial base may be used for proper alignment. These structures can be recognized in smaller fetuses and may be identified even on oblique planes of the survey, or, if fetal motion occurred during the previous acquisition.

Sagittal planes through the fetal head only pose a problem when there is kyphosis of the cranial base. In frontal planes, the superior sagittal sinus can serve as a pointer. Every attempt should be made to acquire an exact median plane, with the tip of the nose, the infundibulum, the aqueduct, and the vermis on one image. An uneven number of slices makes this easier.

Unlike in postnatal whole-body MRI, the long axis of the fetal body is rarely straight, corresponding to the supine position in postnatal imaging. Rather, the long axis usually presents with various degrees of flexion in sagittal and/or frontal planes, or even rotation along its long axis. Consequently, exact orthogonal planes are a compromise. Frontal planes are most useful when there is lateral flexion, as neither strictly orthogonal, sagittal, or axial planes can be planned. Acquisition of exact

Table1 Imaging parameters of sequences used in fetal MRI (1.5 T, Philips, Gyroscan, Best, The Netherlands)

Sequence	FOV (mm)	Matrix	Slice Thickness/ Gap (mm)	TR (ms)	TE (ms)	Acquired Voxel Size (mm)	Reconstructed Voxel Size (mm)	Flip Angle (degree)	Number of Slices	Acquisition Time (s)	NSA
SSFP Survey	400	224×209	7.0	3.13	1.56	1.79/1.79/7.00	1.56/1.57/7.0	60	42	26.2	1
T2 SSH TSE	200	256×153	4.0/0.4 4.0/−1.0	∞	140	0.78/1.18 /4.00	0.78/0.78/4.0	90	18	16.0	1
T2 SSH TSE	230	256×153	4.0/0.4 4.0/−1.0	∞	140	0.90/1.36/4.00	0.90/0.90/4.0	90	18	16.0	1
T2 SSH TSE	200	256×153	4.0/0.4 4.0/−1.0	∞	100	0.78/1.18 /4.00	0.78/0.78/4.0	90	18	13.5	1
T2 SSH TSE	300	256×153	4.0/0.4.0	∞	100	1.17/1.78/4.00	1.17/1.17/4.0	90	18	13.5	1
T2 SSH TSE	275	320×255	4.0/0.4.0	∞	250	0.86/1.08/4.00	0.54/0.54/4.0	90	17	13.5	1
T2 SSH TSE	345	256×148	4.0/0.4.0	∞	80	1.35/2.11/4.00	1.35/1.35/4.00	90	25	21.0	1
SSH MRCP	260	256×205	40–50	8000	800	0.98/1.22/40.0	0.98/0.98/40.0	90	1	<1	1
T1 FFE	325	208×165	5.0/0.5 4.0/0.0	∞	4.6	1.27/1.96/5.00	1.27/1.27/5.0	80	15	15.6	1
SSFP	260	192×219	6.0/−3.0 5.0/−2.5	∞	∞	1.35/1.19/6.00	1.02/1.02/6.0	80	25	20.9	1
SSFP	300	192×255	6.0/−3.0 5.0/−2.5	∞	∞	1.56/1.17/6.00	1.17/1.17/6.0	90	20	21.9	1
SSFP dynamic	320	176×110	7–50	∞	∞	1.82/2.31/7–50.0	1.25/1.25/30.0	60	200	33.6	1
FLAIR	240	192×68	4.0/0.4.0	7000	140	1.35/3.82/4.00	1.02/1.02/4.00	90	18	21.0	2
SSH GRE EPI	230	160×95	4.0	3000	53	1.44/2.42/4.00	0.90/0.90/4.0	90	19	12.0	2
DWI ($b=700$)	250	128×81	5.0	1470	125	1.95/2.31/5.00	0.98/0.98/5.0	90	16	20.1	1
DTI ($b=1{,}000$)	230	112×67	5.0	1649	90	2.05/2.66/5.00	1.80/1.81/5.0	90	12	113	2

FOV field of view; *TR* relaxation time; *TE* echo time; *ms* milliseconds; *NSA* number of signals acquired; *SSFP* steady-state free-precession

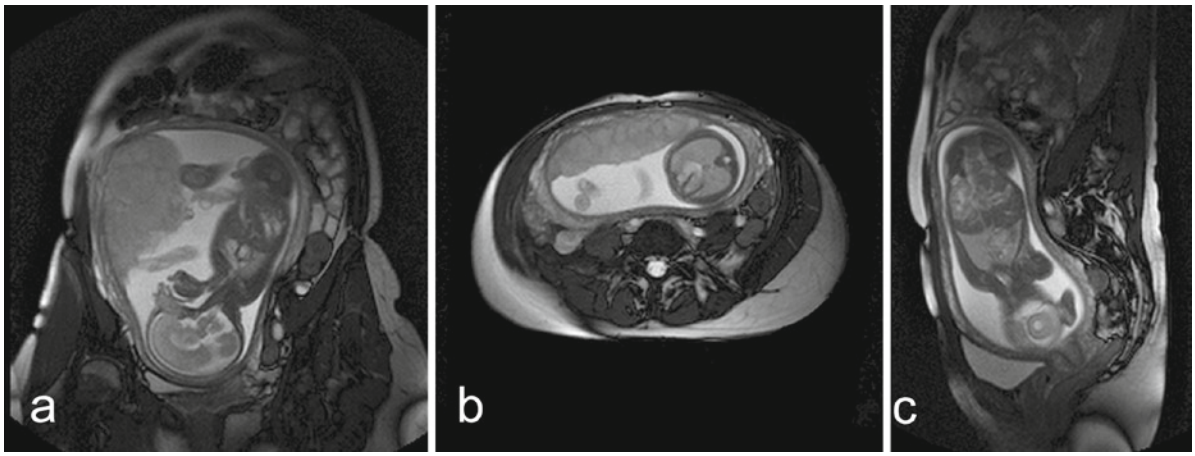

Fig. 2 Selected images of an SSFP survey scan of a fetus at 26+4 GW. (**a**) Frontal image through the pregnant woman provides a sagittal section through the fetal head and allows assessing the male external genitalia. (**b**) Axial image showing the anterior positioned placenta also yields an axial slice through the fetal thorax, depicting the heart and lungs. (**c**) Sagittal image showing the position of the cervix

sagittal planes may also be complicated when the trunk has an oblique elliptical cross section. This frequently happens in cases where there is little amniotic fluid, as when the fetal body is squeezed between the uterine walls and/or placenta. Moreover, in most fetal positions, sagittal images will also include the fetal extremities. Although neither sagittal nor frontal planes will be exactly orthogonal in many cases, fewer images are needed compared to axial planes. Acquisition of axial images through the whole fetal body results in longer acquisition times, as more images are required. This is especially true in larger fetuses in which acquisition of an axial stack may last longer than 1 min.

In case of pronounced flexion of the fetus (curl up position), the fetal thorax and abdomen may have to be imaged separately to obtain axial images, or the acquisition of a radial stack may be indicated.

In general, it is helpful to plan different sequences in the same plane to facilitate comparison of signal intensities of organs or lesions (Fig. 6).

7 Movements

7.1 Fetal Movements

Without sedation, fetal movements will occur during a fetal MRI study. The different patterns of fetal movements and their changes with gestational age are discussed in Chap. 13. As fetal activity is subject to a circadian rhythm (Ehrström 1984), the time when MR is performed might have an impact on imaging. However, while more than half the fetal MRI studies at our institution are made between 7 and 8 o'clock in the morning—a time when a minor peak in fetal activity is reported (Ehrström 1984)—fetal movements are only rarely a problem. Although no constant pattern can be recognized when fetal movements occur during a study, they tend to be rare at the beginning of the study. As imaging focuses on the fetal head or trunk in most cases, the more frequent extremity movements are less of a problem.

Episodes of fetal movements usually last for several minutes, while continuous fetal bulk motion is the exception. Usually, it is possible to continue imaging by repeating sequences in the most amenable plane (e.g., perpendicular to the rotational axis). In doing so, several sequences may be necessary to obtain the desired section plane. In case of persistent fetal bulk motion, dynamic SSFP sequences enable the monitoring of fetal movements and determining when they stop. As a last resort, a new survey scan may become necessary.

In general, fetal movements will depend on gestational age and the space available, and thus, will be more pronounced in younger fetuses and in cases of polyhydramnios. While oligohydramnios restricts fetal movements, the impact of maternal breathing movements on positional changes of the fetus increases, as excursions of the diaphragm or the anterior abdominal wall are directly translated onto the fetus.

7.2 Maternal Breathing Movements

The effect of maternal breathing movements is best demonstrated either by using dynamic sequences or by reformatting a stack of images (Fig. 3). Their impact on dislocation of the fetus depends on fetal position and the amount of amniotic fluid present. Furthermore, in larger fetuses, it is more likely that the fetus is in contact with the uterus, the placenta, or the anterior abdominal wall. Abdominal breathing leads to an anterior–posterior dislocation of the fetus being more pronounced in the cranial half of the uterus, while diaphragmatic breathing movements cause a cranio-caudal shifting. To prevent breathing movements that affect the accuracy of volumetry, sequences acquired for volumetrical purposes should be performed during maternal breath-hold.

7.2.1 Image Acquisition During Maternal Breath-Hold

With regard to maternal breathing movements, fetal MRI faces problems similar to abdominal MRI. In our experience, image acquisition in maternal breath-hold is primarily indicated when using T1-weighted sequences, which are performed in a single breath-hold lasting for 16 s. Other situations in which maternal breath-hold is advisable include oligohydramnios, when the region of interest is subject to maternal breathing movements, especially when volumetry should be performed.

8 Resolution

Dealing with small structures makes resolution an important issue in fetal MRI, as visualization of anatomical and pathological detail depends, in large part, on the spatial resolution of the images and the dimensions of the structure under consideration.

8.1 In-Plane Resolution: Less is More

At least on 1.5-T magnets, the optimal pixel size appears to be on the order of 0.7–0.8 mm. Figure 4 demonstrates that a higher acquisition matrix does not

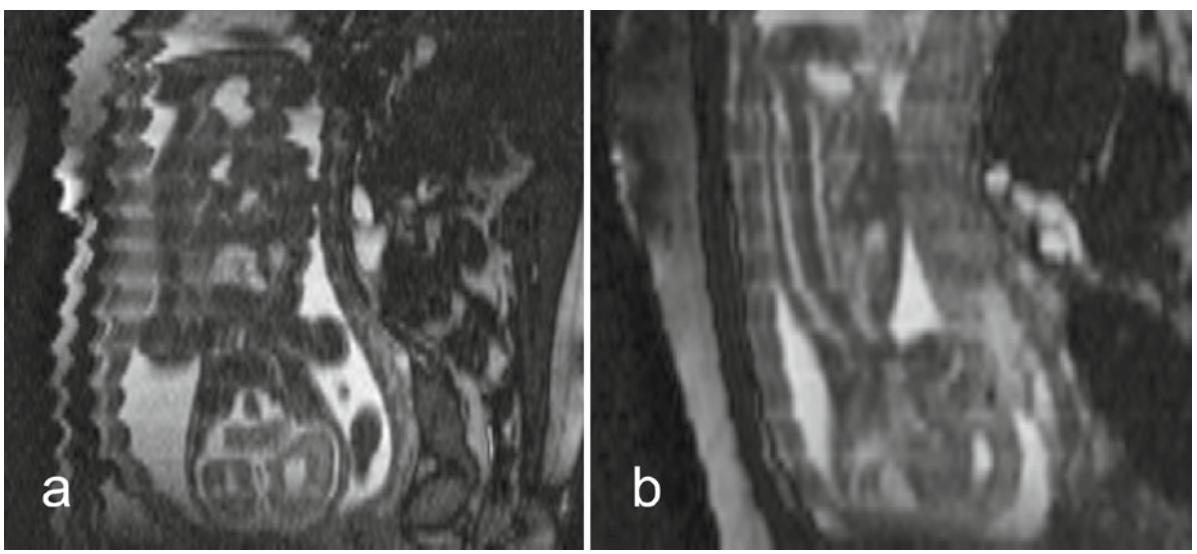

Fig. 3 Visualization of maternal breathing in fetuses with a cephalic presentation. (**a**) Fetus at 27 GW. Reformatted image from an axial stack of 84 SSFP images demonstrates maternal breathing movements during the acquisition: the outline of the pregnant woman's ventral abdominal wall looks like a saw-blade. Note that the effect of breathing on the fetus is most pronounced where the fetal body is in contact with the maternal abdominal wall. (**b**) Reformatted image from an axial stack of 55 SSFP images (2.5 mm distance between slices) in a fetus at 17 + 3 GW. No maternal breathing is evident. The reformatted image allows identification of the fetal spinal canal and aorta

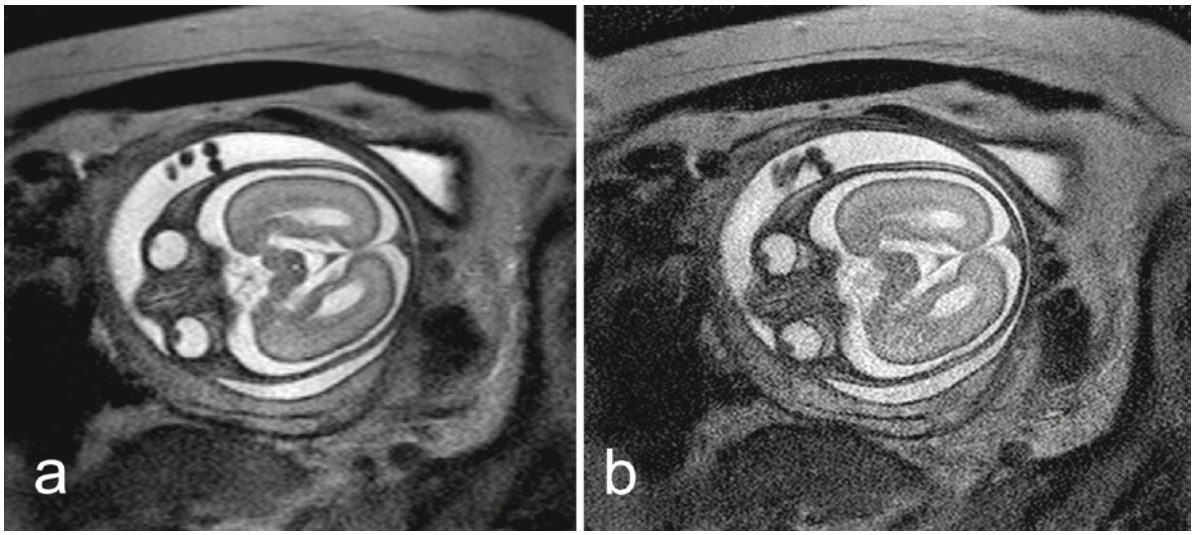

Fig. 4 In-plane resolution and image quality: Corresponding axial T2-weighted images (FOV 200 mm, slice thickness 4.0 mm, gap 0.4 mm) through the head of GW 25+0 fetus. (**a**) Acquired voxel size 0.78×1.18 mm, reconstructed voxel size 0.78 mm. Acquisition time for 18 images was 16 s. (**b**) Acquired voxel size 0.6×0.7 mm, reconstructed voxel size 0.48 mm. Acquisition time for 18 images increased to 22.4 s. Note that neither the optic structures nor the internal carotids and the patent aqueduct can be neatly discerned on the "higher resolution" image

lead to better image quality, but results in more grainy images that veil anatomical detail. While voxel size should be adapted to the size of the fetus or the organ in question, the FOV should be adjusted to maternal body habitus to avoid fold-over artifacts (Fig. 5). However, the larger FOV increases acquisition time, and therefore, the likelihood of fetal motion occurring during the acquisition.

8.2 Slice Thickness

Minimum slice thickness is limited by an increased signal-to-noise ratio. While a 4 mm slice thickness is usually sufficient in larger fetuses, thinner slices are appropriate in smaller fetuses. Using over continuous slices in fetuses less than 25 GW, T2-weighted sequences may be acquired with a distance between

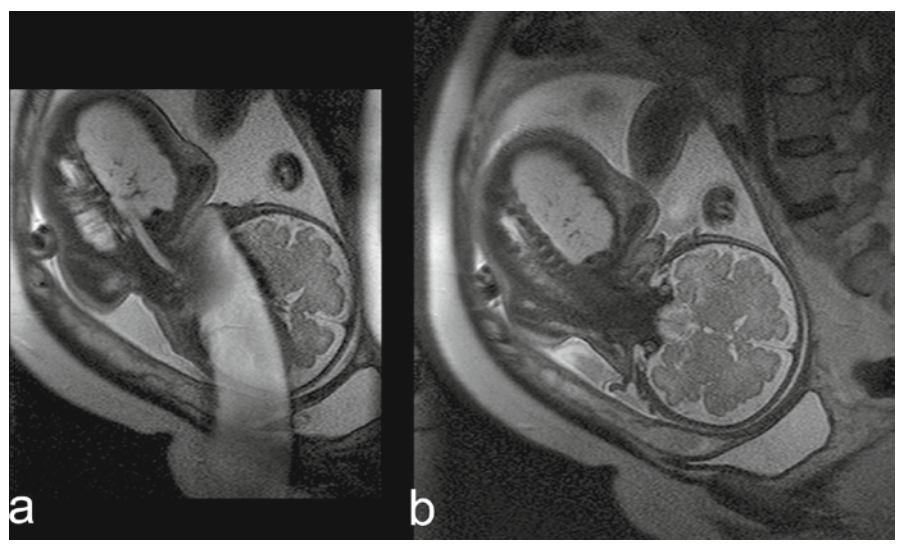

Fig. 5 Frontal T2-weighted images through the fetal head (35+4 GW). (**a**) Typical fold-over artifact using a FOV of 230 mm (stack of 32 images acquired in 23 s). (**b**) Same sequence and resolution: The larger FOV (300 mm) eliminates the artifact, but increases acquisition time to 32 s

slices of 3 mm, and SSFP sequences with a distance of 2.5 mm. T1-weighted sequences may be acquired with a 4 mm slice thickness without gap.

9 Sequences

To date, many so-called ultrafast sequences are available in fetal MRI (Fig. 6). Typically, the acquisition of 18–25 images takes 14–22 s. Sequence parameters will depend on the type of scanner used; those set forth in Table 1 are based on the author's experience with a 1.5 T Gyroscan (Philips, Best, The Netherlands).

9.1 T2-Weighted Sequences

High-resolution T2-weighted TSE sequences (Table 1) are the mainstay in prenatal MRI to depict normal and pathologic fetal anatomy. Provided there is sufficient contrast and using the right section plane structures, a size of 1.5–2 mm can be depicted (Fig. 7). The presence of amniotic fluid around the fetus provides a perfect contrast to the fetal surface. As most fetal body cavities are also fluid-filled, the nasal and oral cavities and the middle and inner ear can be demonstrated. The fetal stomach and, with advancing gestation, the intestines, are fluid-filled (Fig. 6). The same holds true for the trachea, gallbladder, the renal pelvis, and the urinary bladder.

The physiologically wide external cerebrospinal fluid spaces allow delineation of the cerebral surface and developing gyration (Fig. 7).

The T2-weighted signal intensity of the fetal lungs increases with advancing gestation and is used to assess fetal lung maturation (c.f. Chap. 16).

Vessels surrounded by fluid (extracorporeal umbilical vessels, intracranial arteries, veins, and sinuses) or hyperintense tissues (lung vessels in later stages of gestation) can be depicted using T2-weighted TSE sequences.

T2-weighted imaging with longer echo times enhances contrast and is helpful in demonstrating the intrinsic structure of cystic lesions (e.g., congenital cystic adenomatoid malformations of the lungs).

As a matter of fact, assessment of the fetal surface is limited in cases of pronounced oligohydramnios, while this does not impair visualization of the internal details.

9.2 Thick-Slab Imaging

MR fetography was introduced by Terakoshi et al. (2000) as an alternative to single-shot, fast spin echo MR imaging. While these authors used maximum intensity projections of heavily T2-weighted sequences, today thick-slab acquisitions with a slice thickness of 30–50 mm are used to image the fetus (Table 1; Fig. 8a). Images obtained in this way provide a three-dimensional impression of the fetus and its surroundings. In planning this sequence, intrauterine geometry

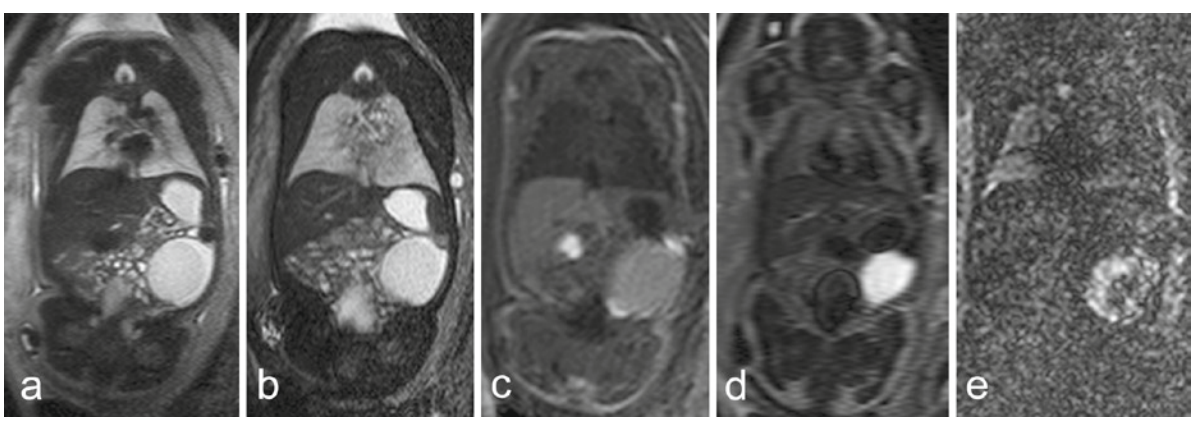

Fig. 6 Corresponding frontal images of different sequences from a female fetus at 36+4 GW with a left-sided ovarian cyst. (**a**) T2-weighted image. (**b**) SSFP image. (**c**) T1-weighted image. (**d**) FLAIR image. (**e**) Diffusion-weighted isotropic image. The hemorrhagic nature of the cystic content is most conspicuous on the FLAIR image

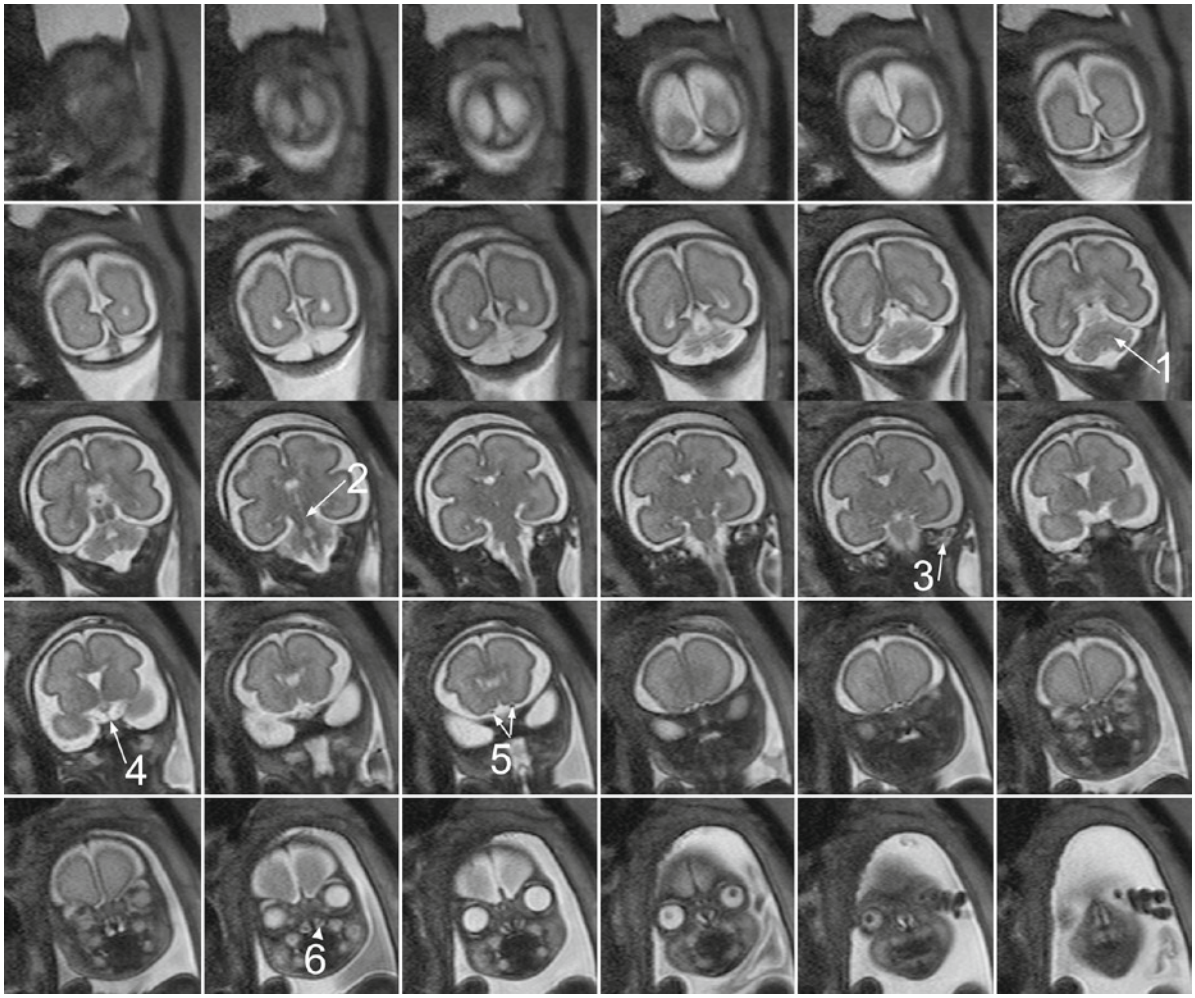

Fig. 7 Set of continuous T2-weighted images (distance between slices, 3 mm) through the fetal head at 26+6 GW. Anatomical details, such as the dentate nuclei (*1*), aqueduct (*2*), ear ossicles (*3*), infundibulum (*4*), olfactory tracts (*5*), and inferior nasal conchae (*6*), can be recognized

must be taken into account in order to avoid projection of the uterine wall or placenta into the image. Maximum slice thickness is, therefore, limited by intrauterine geometry. Another limitation is that at least some amniotic fluid has to be present.

Transparency is increased by shorter echo times, or, alternatively, by using SSFP sequences, which can also be acquired in the thick-slab mode (Fig. 8b). The spatial impression is increased when several images are planned as a radial stack along the long axis of the fetus. With regard to radial acquisition, SSFP sequences are faster, as they have a much shorter preparation phase.

While, in a given case, much information can be drawn from thick-slab images, they cannot substitute for "normal" sequences, which are still necessary for further evaluation. However, this kind of imaging is especially helpful to parents and those who are not familiar with sectional anatomy.

9.3 Steady-State Free-Precession Sequences

While principally providing information similar to that of T2-TSE sequences, steady-state free-precession (SSFP) sequences (Table 1) have the advantage

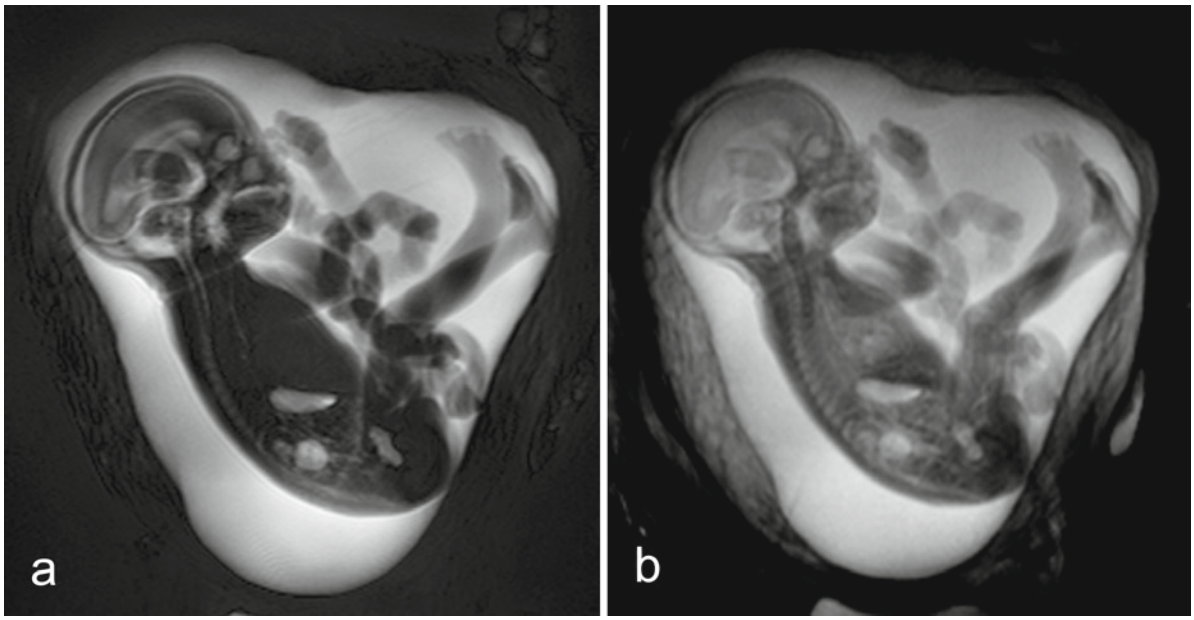

Fig. 8 Sagittal thick-slab acquisitions (40 mm slice thickness) of a fetus at 23 + 1 GW with moderate hydronephrosis. (**a**) T2-weighted image (TE 800 ms). (**b**) Corresponding SSFP image, which is more translucent

that images are immediately reconstructed during acquisition, thus providing "online" information. This makes it easier to determine the latest fetal position in case the fetus moved during the acquisition. SSFP sequences are superior to T2-TSE sequences in visualizing vessels, especially when these are surrounded by dense tissues (e.g., hepatic veins, neck vessels) (Figs. 2 and 9). To date, they are the only sequences to demonstrate fetal cardiac anatomy in greater detail (c.f. Chap. 18).

9.4 T1-Weighted Sequences

Fast low angle shot (FLASH) sequences benefit from acquisition during maternal breath-hold. Parallel imaging allows the acquisition of 15 images in less than 16 s, but makes these sequences prone to artifacts. Usually, 15 images (5.0/0.5 mm slice thickness/gap) are sufficient to cover the whole fetal body in a frontal plane (Table 1). As fewer slices are needed in younger fetuses (<24 GW), slice thickness may be reduced to 4 mm (without gap), increasing the resolution along the *z*-axis at the same time.

T1-weighted sequences allow selectively the demonstration of the fetal pituitary, thyroid (Chap. 19), and liver. These sequences are vital in fetal abdominal imaging, as meconium within the bowels is characterized by T1-weighted hyperintensity (Fig. 10; Chap. 27). Fat suppression is usually not necessary, since adipose tissues develop only with advancing gestation. However, fetal lipomas, such as corpus callosum lipomas (Kim et al. 2002), can be identified in the third trimester. Ossified parts of the skeleton are hypointense and become more clearly visible closer to term (Fig. 11c). Moreover, hemorrhage and even diluted blood (Verswijvel et al. 2002) can be demonstrated using T1-weighted sequences.

9.5 Echoplanar Imaging

Echoplanar sequences (Table 1) allow a rather selective visualization of the fetal skeleton: bones appear hypointense while the cartilaginous parts of the skeleton are hyperintense (Fig. 11). However, with advancing gestation, the contrast between fetal long bones and the surrounding muscles becomes less pronounced. While most organs present with intermediate signal intensity,

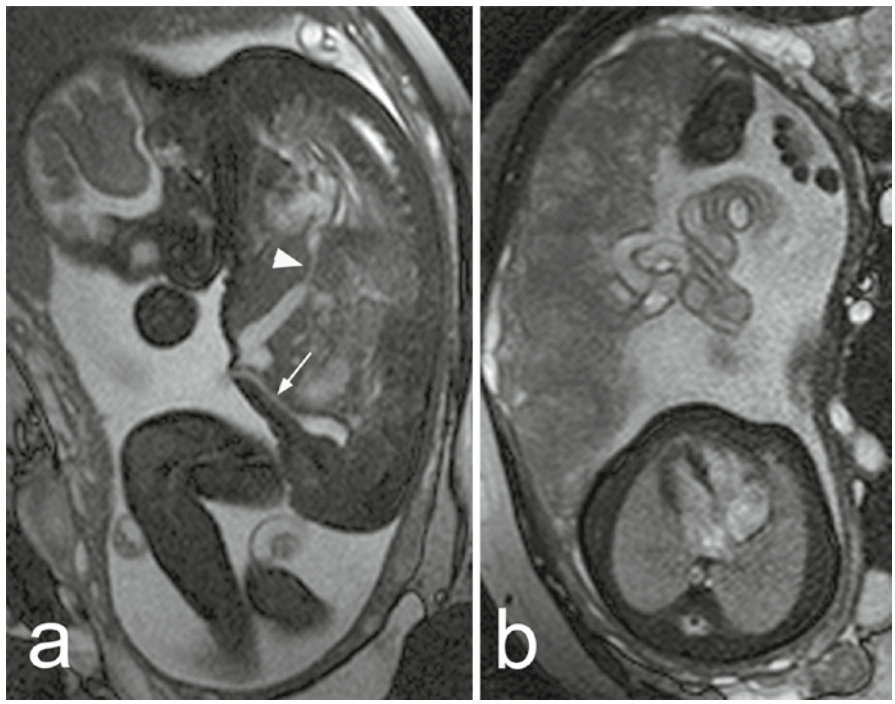

Fig. 9 (**a**) Sagittal SSFP image (fetus at 31 GW) shows the intraabdominal portion of the umbilical vein, its continuity with the ductus venosus (*arrowhead*), and the hepatic vein draining into the right atrium; umbilical artery (*small arrow*). (**b**) Axial SSFP image (2.5 mm distance between slices) through the thorax of a fetus at 30 + 4 GW shows the heart, aorta, and azygos vein, as well as the umbilical cord insertion

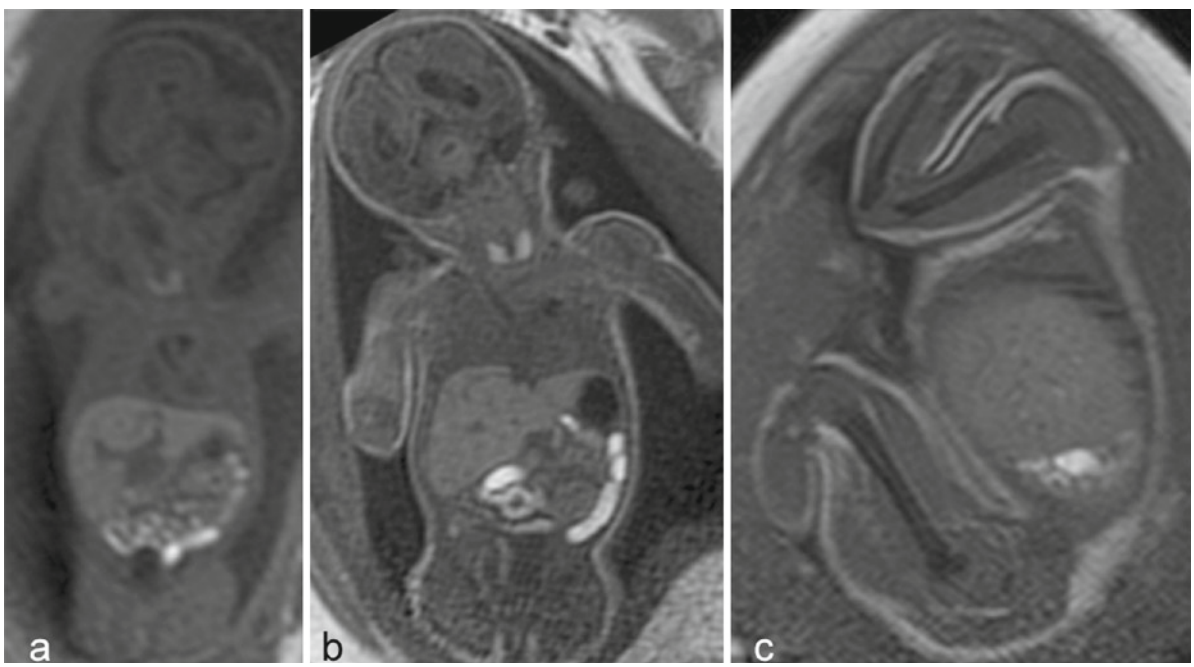

Fig. 10 T1-weighted images. (**a**) Frontal image of a fetus at 22 + 0 GW. (**b**) Fetus at 31 + 0 GW. The liver and thyroid display hyperintense signal intensity, and meconium within the fetal bowels shows marked T1-weighted hyperintensity. The subcutaneous fat layer is evident in (**b**). (**c**) Sagittal T1-weighted image of a fetus at 37 + 3 GW shows well-developed subcutaneous adipose tissues, and the fetal long bones are distinguished by their marked hypointense signal from the muscles, showing intermediate signal intensity

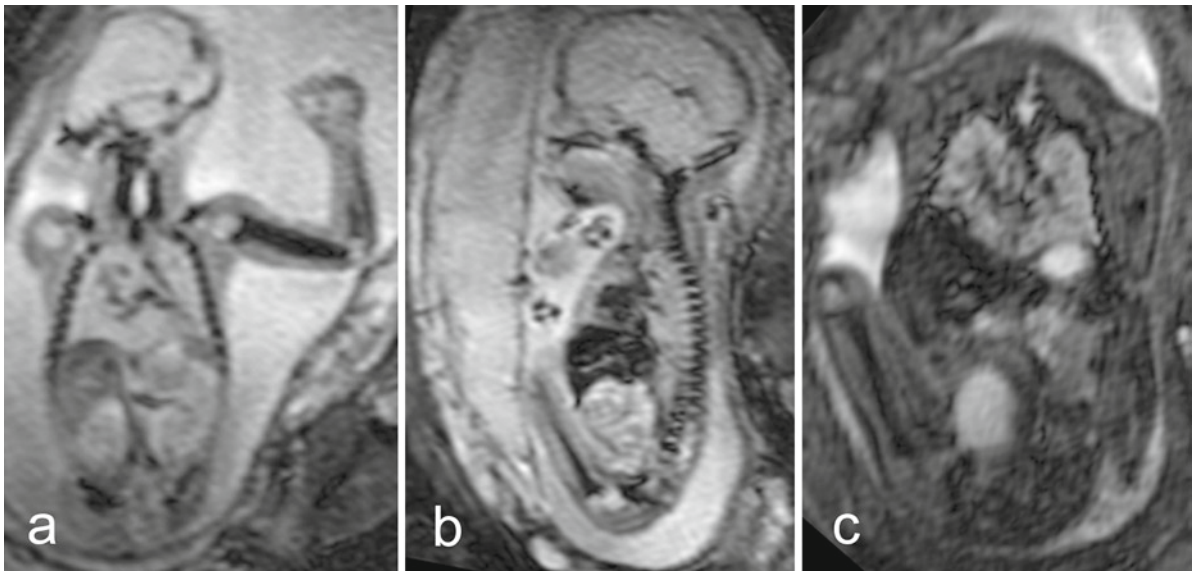

Fig. 11 Echoplanar images. (**a**) Frontal image in a 22+0 GW fetus. (**b**) Sagittal image in a 22+5 GW fetus. The hypointense-appearing fetal bones contrast well against the surrounding structures, and the cartilaginous parts of the skeleton are hyperintense. (**c**) Frontal image in a 31+5 GW fetus demonstrates the decreasing contrast between bone and muscle

the fetal liver usually has hypointense signal characteristics. Furthermore, flow void makes vessels and the heart appear hypointense. The normal placenta usually displays intermediate to hyperintense signal intensity, which decreases with advancing gestation. Echoplanar sequences are also instrumental in demonstrating blood breakdown products, especially when these no longer present as T1-weighted hyperintense lesions.

9.6 Diffusion-Weighted Imaging

Diffusion-weighted sequences are acquired with a *b*-value of 700 and with three phase-encoding directions (Table 1). Figure 12 shows the effect of different b values on imaging in the fetal brain. With regard to the image quality of diffusion-weighted sequences, it is important that the region of interest is in the center of the coil, especially in larger fetuses. With diffusion-weighted imaging (DWI), fiber tracts of the fetal brain, the kidneys, and teeth buds can be selectively demonstrated. For reasons yet to be determined, the whole fetus (except for the liver) displays diffusion-weighted hyperintensity in the earlier stages of gestation (up to 21/22 GW).

Moreover, it is possible to demonstrate ischemic lesions of the white matter with DWI (Baldoli et al. 2002; Guimiot et al. 2008). DWI has also been used to assess the normal and abnormal developing kidneys

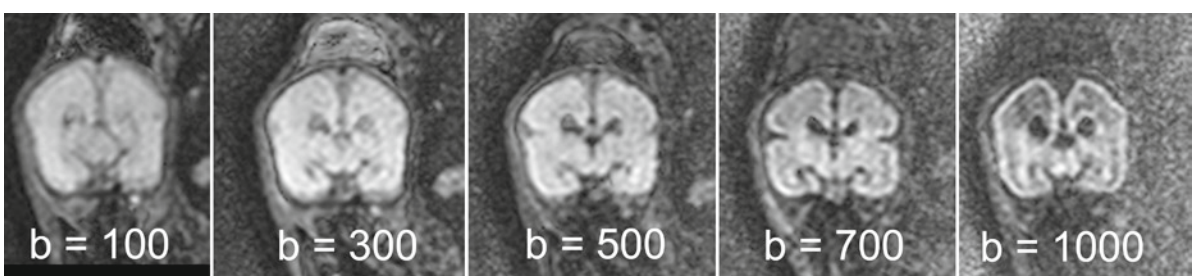

Fig. 12 Corresponding frontal diffusion-weighted images through the head of a fetus at 27+1 GW. With increasing *b*-value, the internal organization of the brain parenchyma becomes evident

(Witzani et al. 2006; Chaumoitre et al. 2007; Savelli et al. 2007). Recently, diffusion tensor imaging using 32 non-collinear diffusion gradient encoding directions has also been applied in utero (Kasprian et al. 2008) (c.f. Chap. 11), allowing demonstration of major fiber tracts of the fetal brain in utero.

9.7 Dynamic Sequences

When there are pronounced fetal movements, the acquisition time of ultrafast sequences is too long and dynamic sequences are the only way to monitor the fetus. We acquire dynamic SSFP sequences with six frames per seconds (fps) and an in-plane resolution of 1.82×2.31 mm, with slice thickness ranging from 8 to 50 mm, depending on the issue at hand (Table 1). As in other thick-slab acquisitions, the maximum slice thickness is limited by the intrauterine space available. With 6 fps, the temporal resolution is high enough to be called real time, as the animated images result in a movie as long as the original acquisition time and show smooth fetal movements. Apart from capturing fetal general movements, dynamic scans are useful in demonstrating intrinsic fetal movements, such as swallowing (Fig. 13), bowel peristalsis, breathing movements, and the beating heart (c.f. Chap. 18).

9.8 FLAIR Sequence

Fluid-attenuated inversion recovery (FLAIR) sequences (Table 1) may provide supplementary information on the content of cystic lesions and in cases of hemorrhage (Fig. 6), and may offer possibilities for staging hemorrhage. As they are also flow-sensitive, moving fluids (e.g., in the pharynx) appear hyperintense.

10 Spectroscopy

In recent years, spectroscopy has been performed in the fetal setting, primarily to further assess the fetal brain (Kok et al. 2002; Heerschap et al. 2003; Girard et al. 2006a, b) (see Chap. 12), but also to study fetal lung maturation and its effects on the composition of amniotic fluid (Fenton et al. 2000; Clifton et al. 2006; Kim et al. 2008).

However, without fetal sedation, the long acquisition time (up to 5 min) may interfere with the successful acquisition of a spectrum. Nevertheless, readable spectra can be obtained in 73.3% of cases (Kulemann et al. 2009). In addition to fetal movements, the size and position of the voxel are important. Fetal brain spectroscopy may be complicated when there is little brain left, or when the fetus is in a breech presentation.

11 Three-Dimensional Dataset

Under ideal conditions, a continuous set of images devoid of fetal motion may be acquired, which is the prerequisite for volumetry and offers possibilities for reconstruction.

11.1 Volumetry

Volumetry of the fetus or fetal organs is being performed more often, especially to determine the size of the fetal

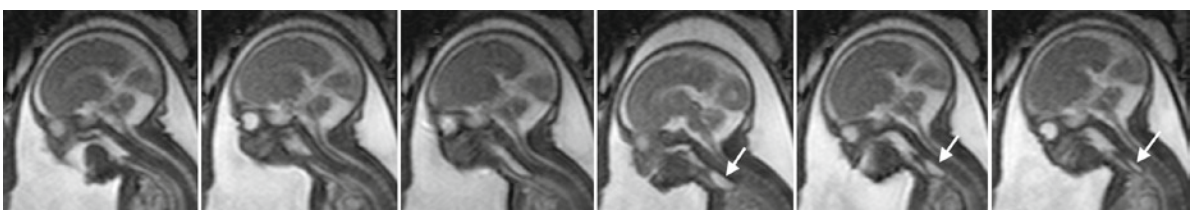

Fig. 13 Selected frames from a dynamic SSFP sequence that demonstrates swallowing in a fetus, with esophageal atresia, at 28+0 GW. The characteristic pouch sign (*arrow*) becomes apparent on the fourth image from the *left*

lungs in normal and pathological conditions (Kasprian et al. 2006; Ward et al. 2006) (see also Chap. 16). The region of interest is manually segmented on each slice, and its total area is multiplied by the distance between slices to compute the volume of an organ. Because of manual segmentation, volumetry is time-consuming. Depending on the size of the organ (lungs or liver), volumetry requires between 10 and 15 min; determining the total fetal body volume requires up to half an hour, depending on fetal size and the orientation of the stack, i.e., the number of slices (Cannie et al. 2006).

Since a continuous and nearly motion-free stack of images is essential for accurate volumetry, the sequence should be acquired during maternal breath-hold, especially when the fetus is vertically positioned. In that case, dislocation of the fetus along its vertical axis during acquisition of an axial stack may lead to images showing the same anatomy, or a cross section may be missed. This will lead to inaccuracies in volume determination. Therefore, the volumetry sequence should be checked for possible discontinuities that may affect volumetry. If this is the case, the sequence should be repeated.

The accuracy of volumetry will also depend on the size of the organ and on the section plane.

Choosing the plane with the least partial volume effects (e.g., axial for lungs) (Jani et al. 2005) will minimize this error. In general, it would appear that fetal MRI volumetry tends to overestimate organ volumes (lungs, liver) when compared to post-mortem organ volumetry (Jani et al. 2005).

11.2 Reconstruction

The acquisition of a continuous three-dimensional dataset covering the whole fetus would allow re-slicing of the stack of images in any desired section plane. However, the spatial resolution of such reformatted images is currently limited by the relatively large slice thickness, especially in smaller fetuses (Fig. 3). Recently, methods have been developed to produce self-consistent 3D volume images, even when motion occurs during the acquisition (Rousseau et al. 2006; Jiang 2008).

A motion-free dataset would also allow the creation of so-called three-dimensional reconstructions of the fetus (Fig. 14). However, this sort of reconstruction is rather time-consuming and the actual benefit remains to be determined.

12 Difficulties in Imaging

Difficulties in imaging an unsedated fetus usually result from fetal movements that complicate the acquisition of a continuous set of images, which are necessary to follow structures through the stack of images. Fortunately, constant fetal bulk movements throughout the study are infrequent.

It is commonly believed that, unlike ultrasound, MRI is not affected by maternal and fetal conditions, such as obesity and oligohydramnios. This calls for some

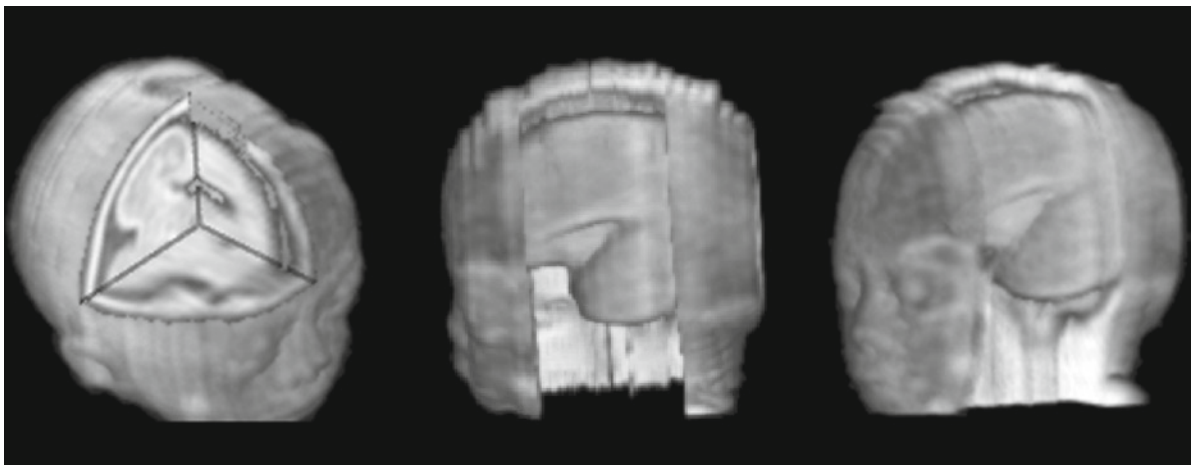

Fig. 14 Different views of a so-called "three-dimensional" reconstruction of the fetal head and brain at 24+2 GW, based on an inverted T2-weighted sequence acquired in the frontal plane. Note the irregular outline of the scalp due to manual segmentation in those areas where the head was in contact with the uterus

discussion, as these conditions can have an impact on image quality. Most notably, maternal overweight can pose problems for fetal MRI. While the table weight limit of 150 kg is less of a problem, the abdominal circumference in the supine position is more important, since it determines whether the pregnant woman fits into the bore of the magnet. While the gantry size differs between various types of magnets, in our experience, the upper limit of abdominal circumference in the supine position is about 135 cm. In such cases, the phased-array surface coil may not fit and the integral Q-body coil must be used, which leads to poorer image quality.

Abdominal circumference is also increased by marked polyhydramnios or multiple pregnancy. In polyhydramnios, apart from more space available for fetal movements, the fetus may be far away from the coil elements. In most cases, coil geometry can be improved by positioning the pregnant woman in the lateral decubitus position, which may bring the fetus closer to the coil elements.

By the end of pregnancy, pregnant women frequently do not tolerate the supine position well, and thus, have to be imaged in the lateral decubitus position. This, however, may be complicated or impossible when the pelvic width of the pregnant woman exceeds the height of the MRI gantry. When the fetal head requires examination, further problems may arise, since fetuses close to term usually have their head engaged within the lesser pelvis. This central position increases the distance of the fetal head from the fixed coil elements, which are now positioned at the maternal hip. Furthermore, placing the ventral coil elements above the pubic symphysis is difficult in the lateral decubitus position, because the thighs are flexed at the hip. This leads to an unfavorable coil geometry for imaging the fetal head. To complicate matters further, fetuses older than 34/35 GW, despite the little space available, tend to show pronounced head movements.

In fact, imaging multiple pregnancies is a challenge, especially when both fetuses need to be studied. Only rarely are the fetuses positioned, relative to each other, in such a way as to enable imaging of both in the same orthogonal plane. Moreover, movements of one fetus may be transferred to the co-twin. In feto-fetal transfusion syndrome, the acceptor presents with polyhydramnios and usually shows abundant movements, while the stuck twin, depending on its position within the uterus, may be subject to maternal breathing movements.

References

Baldoli C, Righini A, Parazzini C, Scotti G, Triulzi F (2002) Demonstration of acute ischemic lesions in the fetal brain by diffusion magnetic resonance imaging. Ann Neurol 52:243–246

Cannie M, Jani JC, De Keyzer F, Devlieger R, Van Schoubroeck D, Witters I, Marchal G, Dymarkowski S, Deprest JA (2006) Fetal body volume: use of MR imaging to quantify relative lung volume in fetuses suspected of having pulmonary hypoplasia. Radiology 241:847–853

Chaumoitre K, Colavolpe N, Shojai R, Sarran A, D' Ercole C, Panuel M (2007) Diffusion-weighted magnetic resonance imaging with apparent diffusion coefficient (ADC) determination in normal and pathological fetal kidneys. Ultrasound Obstet Gynecol 29:22–31

Clifton MS, Joe BN, Zektzer AS, Kurhanewicz J, Vigneron DB, Coakley FV, Nobuhara KK, Swanson MG (2006) Feasibility of magnetic resonance spectroscopy for evaluating fetal lung maturity. J Pediatr Surg 41:768–773

Ehrström C (1984) Circadian rhythm of fetal movements. Acta Obstet Gynecol Scand 63:539–541

Fenton BW, Lin CS, Ascher S, Macedonia C (2000) Magnetic resonance spectroscopy to detect lecithin in amniotic fluid and fetal lung. Obstet Gynecol 95:457–460

Girard N, Fogliarini C, Viola A, Confort-Gouny S, Fur YL, Viout P, Chapon F, Levrier O, Cozzone P (2006a) MRS of normal and impaired fetal brain development. Eur J Radiol 57:217–225

Girard N, Gouny SC, Viola A, Le Fur Y, Viout P, Chaumoitre K, D'Ercole C, Gire C, Figarella-Branger D, Cozzone PJ (2006b) Assessment of normal fetal brain maturation in utero by proton magnetic resonance spectroscopy. Magn Reson Med 56:768–775

Guimiot F, Garel C, Fallet-Bianco C, Menez F, Khung-Savatovsky S, Oury JF, Sebag G, Delezoide AL (2008) Contribution of diffusion-weighted imaging in the evaluation of diffuse white matter ischemic lesions in fetuses: correlations with fetopathologic findings. AJNR Am J Neuroradiol 29:110–115

Heerschap A, Kok RD, van den Berg PP (2003) Antenatal proton MR spectroscopy of the human brain in vivo. Childs Nerv Syst 19:418–421

Jani J, Breysem L, Maes F, Boulvain M, Roubliova X, Lewi L, Vaast P, Biard JM, Cannie M, Deprest J (2005) Accuracy of magnetic resonance imaging for measuring fetal sheep lungs and other organs. Ultrasound Obstet Gynecol 25:270–276

Jiang S (2008) Magnetic resonance imaging of the brain in moving subjects. Application to fetal, neonatal and adult brain studies. PhD Thesis, Imperial College London

Kasprian G, Balassy C, Brugger PC, Prayer D (2006) MRI of normal and pathological fetal lung development. Eur J Radiol 57:261–270

Kasprian G, Brugger PC, Weber M, Krssak M, Krampl E, Herold C, Prayer D (2008) In utero tractography of fetal white matter development. Neuroimage 43:213–224

Kim DH, Vahidi K, Caughey AB, Coakley FV, Vigneron DB, Kurhanewicz J, Mow B, Joe BN (2008) In vivo (1)H magnetic resonance spectroscopy of amniotic fluid and fetal lung at 1.5 T: technical challenges. J Magn Reson Imaging 28:1033–1038

Kim TH, Joh JH, Kim MY, Kim YM, Han KS (2002) Fetal pericallosal lipoma: US and MR findings. Korean J Radiol 3: 140–143

Kok RD, van den Berg PP, van den Bergh AJ, Nijland R, Heerschap A (2002) Maturation of the human fetal brain as observed by 1H MR spectroscopy. Magn Reson Med 48:611–616

Kulemann V, Brugger PC, Pugash D, Weber M, Prayer D (2009) Magnetic Resonance Spectroscopy of the fetal brain - does it work without sedation? ASNR 47th Annual Meeting 2009, Vancouver, Abstract book

Rousseau F, Glenn OA, Iordanova B, Rodriguez-Carranza C, Vigneron DB, Barkovich JA, Studholme C (2006) Registration-based approach for reconstruction of high-resolution in utero fetal MR brain images. Acad Radiol 13:1072–1081

Savelli S, Di Maurizio M, Perrone A, Tesei J, Francioso A, Angeletti M, La Barbera L, Ballesio L, de Felice C, Porfiri LM, Manganaro L (2007) MRI with diffusion-weighted imaging (DWI) and apparent diffusion coefficient (ADC) assessment in the evaluation of normal and abnormal fetal kidneys: preliminary experience. Prenat Diagn 27:1104–1111

Terakoshi H, Uchiyama K, Era K, Oishi S, Osone F, Futami T (2000) MR fetography. A new MR technique for imaging of the fetus. Jpn J of Magn Reson Med 20:138–149

Verswijvel G, Grieten M, Gyselaers W, Van Holsbeke C, Vandevenne J, Horvath M, Gelin G, Palmers Y (2002) MRI in the assessment of pregnancy-related intrauterine bleeding: a valuable adjunct to ultrasound? Jbr-Btr 85: 189–192

Ward VL, Nishino M, Hatabu H, Estroff JA, Barnewolt CE, Feldman HA, Levine D (2006) Fetal lung volume measurements: determination with MR imaging - effect of various factors. Radiology 240:187–193

Witzani L, Brugger PC, Hörmann M, Kasprian G, Csapone-Balassy C, Prayer D (2006) Normal renal development investigated with fetal MRI. Eur J Radiol 57:294–302

Prenatal Development of the Human Fetal Telencephalon

Miloš Judaš

Contents

M. Judaš
Section of Developmental Neuroscience,
Department of Neuroscience,
Croatian Institute for Brain Research,
University of Zagreb School of Medicine, Šalata 12,
Zagreb 10000, Croatia
e-mail: mjudas@hiim.hr

D. Prayer (ed.), *Fetal MRI*, Medical Radiology,
DOI: 10.1007/174_2010_119, © Springer-Verlag Berlin Heidelberg 2011

Abstract

› Human corticogenesis is perhaps the most complex process in the realm of biology, and also displays some unique (species-specific) features. There are major and clinically relevant differences in cortical development between rodents and humans, and they are reflected in the structure and function of the brain at every hierarchical level, from genes and cells to large neuronal assemblies and functional systems. For example, in comparison to rodents, the human cortex displays dramatically expanded fetal subplate zone, more complex and hugely expanded subventricular zone, significantly different process of initial cortical formation, more complex and diverse radial glial cells, Cajal–Retzius cells, and the subpial granular layer, as well as other unique transient fetal structures and/or features. These phylogenetic novelties contribute to the introduction of species-specific cell types (especially cortical interneurons), new cytoarchitectonic areas, and new patterns of connectivity and transmitter/receptor composition. Therefore, human-specific features of human brain are highly relevant for understanding the etiology of developmental brain disorders and for advancing their diagnostics and treatment. Fortunately, new noninvasive methods from neurohistology, neuroimaging, and genomics are making the human brain accessible for direct and detailed study as never before, and the number of these new and powerful methods for analyzing human brain development is rapidly increasing.

1 Introduction

It is common knowledge that structure and function of the human fetal telencephalon display a number of transient features. However, what is exactly transient in the developing brain? The first and the simplest answer, of course, is that everything is transient, because the brain continuously changes and reorganizes as its developmental program enfolds in the interaction with other organ systems, the pregnant mother and the environment. However, from the viewpoint of a practicing clinician, it is important to note that the concept of transient has two different meanings.

> First, there are transient appearances: any growing cell, architectonic/modular structure or organ changes as it grows, so that at each developmental age its appearance is transient (in the sense that what was seen before is no longer recognized as such). But, appearances are deceiving – if something changes its appearance, it does not cease to exist. For example, both ventricular and subventricular zones disappear (as cytoarchitectonically observable entities) but all neurons and glia generated in these zones simply move to another place and happily continue to exist.
>
> Second, there are cells (and by extension, architectonic entities) that really cease to exist after a while, because they die by apoptosis, that is, normal and developmentally programmed cell death. Such cells or structures deserve to be named transient sensu stricto – but, in fact, there are quite a few such cells or structures in the developing human brain.

Thus, so-called transient embryonic or fetal cells, structures, neuronal circuits (and, by extension, transient electrophysiological and behavioral phenomena) simply represent a fleeting and protean reflections of the basic fact of life: that the human embryo or fetus is a living organism, which cleverly and adaptively uses and re-shuffles all available resources during its long and autopoietic (self-assembling) journey to the maturity. Therefore, although the term transient is deeply entrenched in the current literature, it would be appropriate to use more neutral (and accurate) terms, such as age- or stage-specific, or characteristic for a specified developmental window. For example, the so-called transient subplate zone, when fully formed, is indeed recognizable as a distinct architectonic entity during the developmental window extending approximately from 13 postconceptional weeks (PCW) until birth. However, its first constituent neurons actually appeared much earlier (at 7 or 8 PCW), and the majority of them will continue to exist throughout the postnatal lifespan as so-called interstitial white matter neurons.

With this in mind, let us embark on a quick journey through the complex and ever-changing landscape of human brain development. Due to the limits of space, we will obviously unveil just the tip of the iceberg of the underlying bewildering variety of molecular and

cellular interactions and histogenetic processes. If the reader nevertheless finds this chapter (and especially its reference list) too long and crowded with expert details, but endures to its end, he or she will hopefully realize that the integration of the wealth of descriptive data provided by classical human neuroanatomy with data pouring from recent molecular biological, genetic, genomic and neuroimaging studies is, in fact, the order of the day. Namely, although the large majority of recent breakthroughs in the field of developmental neurobiology have originated from studies of experimental models (especially genetically modified mice), it becomes increasingly evident that "the proper study of mankind is man" – to use the famous dictum of the nineteenth-century English poet. Finally, it should be noted that this chapter is focused on prenatal development, but human brain continues to develop long after birth (Fig. 1).

2 Brain Development in the Embryonic Period Proper: Carnegie Stages 8–23 (Embryonic Days E23–E56)

As pointed out by leading authorities (O'Rahilly and Müller 1999), prenatal age is always postfertilizational by definition (or, as an acceptable alternative, postovulatory, postconceptional). Menstrual weeks are convenient in obstetrics but are not age; the ambiguous term gestational age should never be used, because three different starting points are possible: the last menstrual period, ovulation and/or fertilization, and implantation. Unfortunately, the term gestational age/gestational weeks continues to plague many current publications. In this chapter, as in all of our studies, I use the term postconceptional weeks, PCW to encompass both proper terms (postfertilizational and postovulatory). When appropriate or unavoidable, I also use embryonic days (E – e.g., E43) or postnatal days (P – e.g., P7), because it is the only way age is measured in prenatal and postnatal development of experimental animals, such as rhesus monkeys (in which the gestation period is 165 days). Finally, the most useful measurement in both embryonic and fetal development is the greatest length (GL, taken as a caliper length without inclusion of the flexed lower limbs; it is replaced after birth by the sitting height), while the crown–rump length (CRL) is frequently similar and commonly cited but less reliable measurement (O'Rahilly and Müller 1984). At 4.5 PCW, the GL is about 5 mm, and at the end of the embryonic period proper (at 8 PCW) it is approximately 30 mm, while body weight is about 2–3 g (O'Rahilly and Müller 1999).

The staging used for describing the development of the human embryonic brain is the internationally accepted Carnegie system (for comprehensive summary, see O'Rahilly and Müller 1999, 2006). In the Carnegie system the embryonic period proper occupies the first 8 PCW and is subdivided into 23 morphological Carnegie stages based on both external and internal morphological criteria. At present, morphological staging is limited to the embryonic period proper, because no fully satisfactory staging system has yet been devised for the fetal period (O'Rahilly and Müller 1999; but, see Sect. 3.2 for alternative approaches).

The human prenatal life is usually divided into embryonic (first 8 PCW) and fetal periods (9 PCW to birth). The duration of prenatal life is generally about 38 PCW, the mean being 264 days. The range 35–40 PCW is considered to indicate an infant at term. Commonly used figures at birth are about 335 mm for the GL (exclusive of the lower limbs) and about 500 mm for the crown-heel length (O'Rahilly and Müller 1999). The biparietal diameter is approximately 95 mm, the head circumference is of the order of 350 mm, the body weight at birth varies from 2,500 to 4,000 g or more (with an average of about 3,350 g), and the brain weight ranges from about 300–400 g (O'Rahilly and Müller 1999).

Another convenient way to consider prenatal life is in terms of trimesters: (1) the first trimester (including the embryonic period proper – up to about 30 mm GL) extends to some 90 or 100 mm GL; (2) the second trimester (mid-fetal period) proceeds to about 250 mm GL; and (3) the third trimester continues until birth (very approximately 335 mm GL). While the work of O'Rahilly and Müller has been predominantly restricted to the embryonic period, they offered the following classification of the postembryonic (fetal) phase (O'Rahilly and Müller 1999):

1. In the first trimester (after the embryonic period), an early postembryonic phase (approximately 30–50 mm in GL, 8–9 PCW);
2. The later postembryonic phase of the first trimester (approximately 50–100 mm in GL, 9–13 PCW);
3. The second trimester (approximately 100–250 mm in GL, 13–26 PCW); and
4. The third trimester and the newborn (approximately 250–335 mm in GL, 26 PCW to birth).

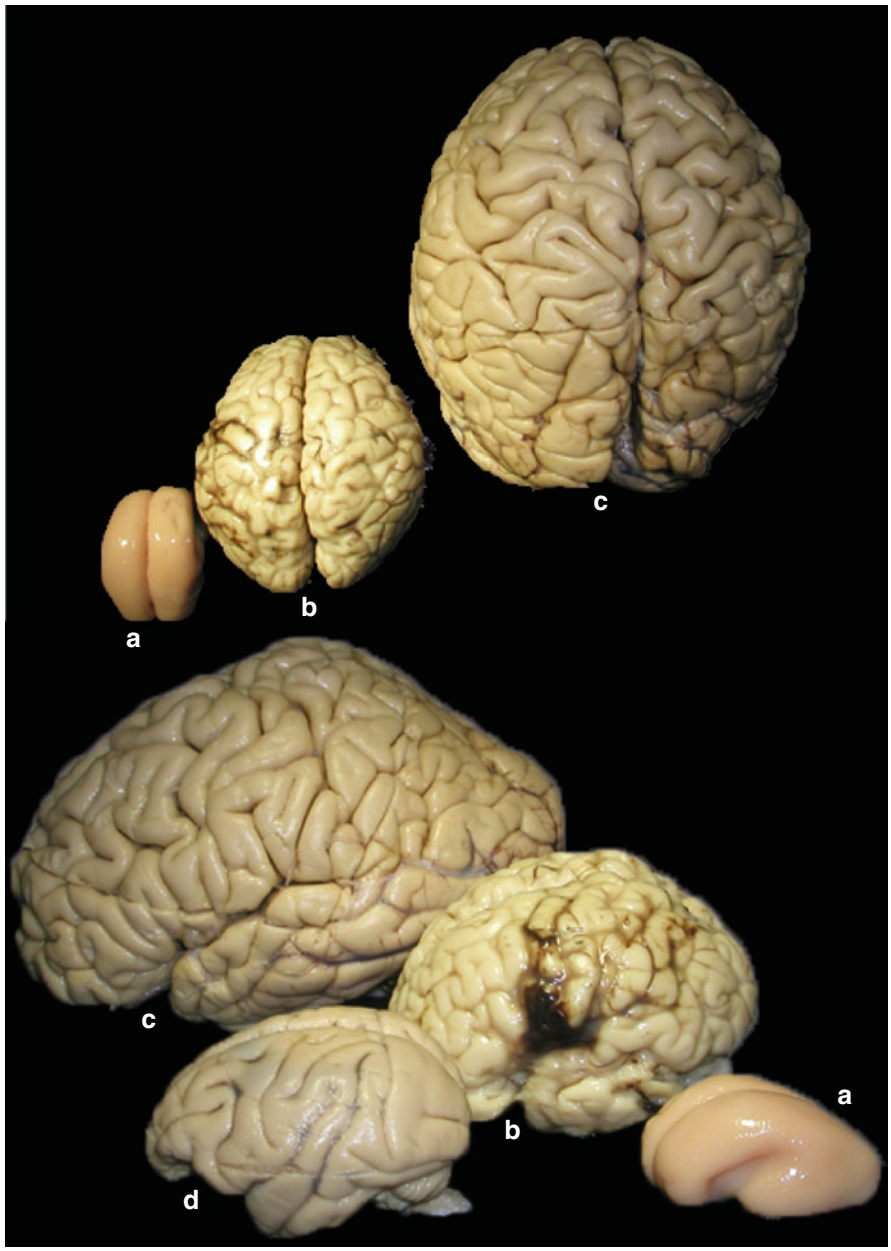

Fig. 1 Comparison of morphological and volumetric development of human brain in an 18-week-old fetus (**a**), newborn (**b**), and adult (**c**) in dorsal (*upper row*) and lateral view (*lower row*). Note that the brain of the adult rhesus monkey (**d**, *Macaca rhesus*) is intermediate in size between mid-term and newborn human brain. Note also that a huge part of human brain growth occurs postnatally (from cca. 380 g of brain mass in newborn to cca. 1,350 g in adult)

As we will see in the subsequent section, this classification has largely been superseded by more advanced ones (Sidman and Rakic 1973, 1982; Kostović 1990a, b; Kostović and Judaš 1994, 1995, 2009; Kostović et al. 2008).

In the following paragraphs, we provide synopsis of key events in the development of human embryonic brain, as described in the original publications of Ronan O'Rahilly and Fabiola Müller and, when needed, corrected in the second and third edition of their atlas (O'Rahilly and Müller 1999, 2006).

Carnegie stage 8: *approximately 1–1.5 mm in GL, 3 PCW, E23* (O'Rahilly and Müller 1981): at least in some specimens, the neural groove can be detected in

the neural plate as a very shallow sulcus bounded by faint neural folds. This is the first visible sign of the future nervous system, and it is of interest that the primordium of the brain appears before the heart or any other organs become visible.

Carnegie stage 9: *approximately 1.5–2.5 mm in GL, E26* (Müller and O'Rahilly 1983): the three major divisions of the brain (prosencephalon, mesencephalon, and rhombencephalon) are distinguishable in the folds of the completely open neural groove; no neural tube has yet formed, and "brain vesicles" are not present; the otic discs are first visible at this stage as the first indication of the (internal) ears.

Carnegie stage 10: *approximately 2–3.5 mm in GL, E29* (Müller and O'Rahilly 1985): a portion of neural tube is formed; the diencephalon consists of the future thalamic region and an optic portion; optic primordia are visible for the first time and connected by the chiasmatic plate; the lateral parts of the forebrain beyond the chiasmatic plate belong to the telencephalon medium or impar which is the first part of the telencephalon to appear at this stage.

Carnegie stage 11: *approximately 2.5–4.5 mm in GL, E30* (Müller and O'Rahilly 1986): the rostral (cephalic) neuropore closes during this stage; the floor of the telencephalon medium becomes distinct as the future lamina terminalis and commissural plate; the optic vesicle is being formed; notochordal and neural axial structures are still closely related.

Carnegie stage 12: *approximately 3–5 mm in GL, E31* (Müller and O'Rahilly 1987): the caudal neuropore closes and its final site is at the level of somitic pair 31; the beginning of secondary neurulation; the mesencephalon consists of two neuromeres (M1 and M2) and the rhombomeres have important relations to the cranial ganglia; the first nerve fibers are differentiating.

Carnegie stage 13: *approximately 4–6 mm in GL, E32, 4–5 PCW* (Müller and O'Rahilly 1988a): both neuropores are closed, so that the closed neural tube finally appears; the retinal and lens discs are beginning to develop; the adenohypophysial pouch is distinct; three diencephalic neuromeres (D1, parencephalon, synencephalon) are present; the isthmus rhombencephali is visible; a marginal zone is distinguishable in the wall of the mesencephalon and rhombencephalon; the first indication of the cerebellum appears in rhombomere Rh.1.

Carnegie stage 14: *approximately 5–7 mm in GL, E33, 5 PCW* (Müller and O'Rahilly 1988b): the future cerebral hemispheres become identifiable during this stage and are delimited from the telencephalon medium by the torus hemisphericus internally and by the ditelencephalic sulcus externally; the pontine flexure appears; the cerebellum is formed by the alar plate of the isthmus as well as by that of rhombomere 1; blood vessels now penetrate the wall of the brain.

Carnegie stage 15: *approximately 7–9 mm in GL, E35, 5 PCW* (Müller and O'Rahilly 1988c): the medial ganglionic eminence has appeared in the previous stage and it is diencephalic; the lateral ganglionic eminence, which now appears, is telencephalic; the wall of the diencephalon presents five longitudinal zones (epithalamus, dorsal thalamus, ventral thalamus, subthalamus, and hypothalamus); the primordium of the epiphysis cerebri is beginning; the hippocampal thickening is distinct on each side of the lamina terminalis; most cranial nerves are present; axodendritic synapses have been detected in the cervical region of the spinal cord (Okado 1981).

Carnegie stage 16: *approximately 8–11 mm in GL, E37* (Müller and O'Rahilly 1989a): the presence of the hippocampal thickening and other histological features makes possible a distinction among archipallium, paleopallium, and neopallium; the primordial plexiform layer can be discerned at the periphery of the amygdaloid area; olfactory fibers enter the wall of the brain at the site of the future olfactory bulb, and the future olfactory tubercle is detectable; the evagination of the neurohypophysis is now becoming distinct. Up to and including stage 16 the neocortical part of the cerebral hemispheres is avascular, although it is already surrounded by a prominent perineural vascular process (Marin-Padilla 1988b).

Carnegie stage 17: *approximately 11–14 mm in GL, E40, 6 PCW* (Müller and O'Rahilly 1989b): due to the rostral and caudodorsal growth of the cerebral hemispheres the longitudinal fissure deepens, and the vessels of the future choroid plexus develop in it; the olfactory bulb and tubercle become outlined; the amygdaloid area contains one or two nuclei; the first indication of a septal nucleus is recognizable; the hemispheric stalk unites the cerebral hemispheres with the ventral thalamus and the medial ganglionic eminence; the telencephalon begins to overlap the diencephalon; the interventricular foramina begin to develop.

Carnegie stage 18: *approximately 13–17 mm in GL, E42, 6 PCW* (Müller and O'Rahilly 1990a): the cerebral hemispheres are slightly flattened in the future insular region; the C-shaped hippocampus, accompanied by the

area dentata, reaches the olfactory region; the lateral ganglionic eminence is distinct; the red nucleus is present and the substantia nigra is beginning to develop; choroid plexuses develop in the lateral as well as in the fourth ventricle, so that the production of cerebrospinal fluid sensu stricto can now begin. The primordial plexiform layer extends over most of the cerebral hemispheres (see later sections). Tracts present at stage 18 include the stria medullaris thalami, mamillothalamic tract, medial and lateral tectobulbar, dentatorubral, and the tractus solitarius.

Carnegie stage 19: *approximately 16–18 mm in GL, E44, 6–7 PCW* (Müller and O'Rahilly 1990a): the embryo now has a recognizably human face; the olfactory nerve, bulb, and tubercle are well developed; the nucleus accumbens appears; the cerebral hemispheres have grown rostrally; optic fibers arrive in the chiasmatic plate; many bundles are identifiable, including the thalamostriatal tract (Stammbündel of His or lateral prosencephalic fasciculus) and the stria medullaris thalami.

Carnegie stage 20: *approximately 18–22 mm in GL, E47, 7 PCW* (Müller and O'Rahilly 1990a, b): the choroid plexuses of the lateral ventricles are at the "club-shaped" phase; optic and habenular commissures develop; the medial septal nucleus and the nucleus of the diagonal band are differentiating; important fiber connections of the olfactory system are now identifiable; the intrinsic vascularization of the neocortex begins.

Carnegie stage 21: *approximately 22–24 mm in GL, E50, 7–8 PCW* (Müller and O'Rahilly 1990b): very important stage, characterized by *the first appearance of the cortical plate*, adjacent to the lateral ganglionic eminence; the transition from the hemisphere to the diencephalon is the hemispheric stalk (Hemisphärenstiel of Hochstetter) which contains a thick bundle of fibers, the lateral prosencephalic fasciculus (Stammbündel of His); the internal capsule, however, is not yet present in the absence of the appropriate neocortical connections; the subthalamic nucleus and the globus pallidus are distinguishable; the circulus arteriosus of Willis is now complete.

Carnegie stage 22: *approximately 23–28 mm in GL, E52, 7.5–8 PCW* (Müller and O'Rahilly 1990b): the internal capsule and its connections to the neopallium are now present; the primordium of the claustrum develops as a condensed stream of neurons that extends from the area caudal to the olfactory bulb and along the lateral ganglionic eminence to the future insular region; the cortical plate extends over half the surface of the neopallium; the inferior horn of the lateral ventricle is evident; the sulcus terminalis is the internal boundary between telencephalon and diencephalon.

Carnegie stage 23: *approximately 27–31 mm in GL, E56, 8 PCW* (Müller and O'Rahilly 1980, 1990a, 1990b; O'Rahilly and Müller 1990): this stage is also very important because it is the close of the embryonic period proper. The cortical plate covers almost the whole neopallial surface; the hippocampus has reached the temporal pole; the insula appears as an indented area; the primordia of the caudate nucleus and the putamen are recognizable, and the globus pallidus externus has moved from its diencephalic into a telencephalic position; the anterior commissure begins to develop in the commissural plate; the telencephalon and the diencephalon are not fused; the optic tract reaches the ventral portion of the lateral geniculate body; the inferior and the superior cerebellar peduncles are distinguishable; the presence of the pyramidal decussation is noted for the first time; the choroid plexus at this time has become lobular.

3 Spatiotemporal (Architectonic) Framework for Analyzing Corticogenesis: Transient Embryonic and Fetal Zones and Developmental Staging Systems

The aim of this section is to provide a general spatiotemporal framework for analyzing histogenetic processes in the developing human telencephalon and for correlating these events with features observed in images obtained by in vivo in utero or in vitro fetal MRI.

There are few atlases which provide systematic illustrations of Nissl-stained and serially sectioned human fetal brains (Feess-Higgins and Larroche 1987). Recently published atlases based on the Carnegie, Minot and Yakovlev Collection contain hundreds of microphotographs of the best quality, but unfortunately these illustrations are provided with descriptions and terminology that are appropriate for the developing rodent, but not human brain (Bayer and Altman 2002,

2004, 2005, 2006, 2008). However, there are also presently largely neglected but very important and excellently illustrated classical monographs (Retzius 1896; His 1904; Hochstetter 1919, 1923, 1929, 1934, 1939; Barbé 1938; Bartelmez and Dekaban 1962; Richter 1965; Kahle 1969; Windle 1970) including the series of monographs published by LeRoy Conel on the early postnatal development (birth to 6 years) of the human cerebral cortex (Conel 1939, 1941, 1947, 1951, 1955, 1959, 1963, 1967).

3.1 Boulder Committee System and Its Revisions

During embryonic and fetal periods, the telencephalic wall consists of several architectonic zones that do not exist in the mature brain. Upon the recommendation of the Boulder Committee (appointed by the American Association of Anatomists), these zones have been generally adopted as a generic description for basic histogenetic processes and developmental events for the entire vertebrate central nervous system (Boulder Committee 1970; Rakic 1982; Bystron et al. 2008; Rakic et al. 2009). However, between the initial proposal (Boulder Committee 1970) and the latest revision (Bystron et al. 2008), a number of important developments occurred which prompted subsequent revisions of the basic scheme. One such major development was the discovery of the subplate zone in the human fetal brain (Kostović and Molliver 1974). A separate line of criticism was initiated by Miguel Marin-Padilla who introduced the concept of the primordial plexiform layer (PPL) initially based on his studies of fetal cat cortex (Marin-Padilla 1971, 1972, 1978) and subsequently extended to the initial development of the human cerebral cortex (Marin-Padilla 1983; Marin-Padilla and Marin-Padilla 1982; for review, see Marin-Padilla 1984, 1988a, 1992, 1998). This concept was soon extended to rodents (Rickmann et al. 1977; Bayer and Altman 1990) and in fact remains the dominant concept in studies on cortical development in rodents and carnivora (e.g., Bayer and Altman 1991; Allendoerfer and Shatz 1994; Kanold and Luhmann 2010). However, it should be noted that significant revisions of the initial Boulder scheme were primarily driven by subsequent discoveries made in brains of humans and nonhuman primates and not in rodents (see below). For example, recent studies have revealed new types of transient neurons and proliferative cells outside the classical neurepithelium, new routes of cellular migration, and additional cellular compartments (Smart et al. 2002; Zecevic et al. 2005; Bystron et al. 2005, 2006; Carney et al. 2007; Rakic et al. 2009).

3.2 The System of Poliakov as Revised by Sidman and Rakic and Further Developed by Kostović

With respect to the development of the human fetal brain, there is another approach to developmental staging which combines the legacy of the Boulder Committee with older tradition stemming from the Russian architectonic school. The Russian neuroanatomist G.I. Poliakov (Poliakov 1949, 1959, 1961, 1965, 1979) developed a staging system which was adopted and slightly modified by Richard L. Sidman and Pasko Rakic in their highly influential reviews (Sidman and Rakic 1973, 1982; Rakic 1982). Poliakov divided the entire human prenatal cortical development into three major periods: (1) an early period of migration and consolidation (2nd to 4th fetal month), (2) a middle or transitional period of pre-differentiation of cortical layers (4th to 6th fetal month), and (3) a late period of final differentiation of cortical layers (6th month to birth). He furthermore divided his early period into four stages of cortical plate development, which he described as: (a) initial formation, (b) primary consolidation, (c) migratory-consolidating differentiation, and (d) secondary consolidation. Sidman and Rakic (1973, 1982) adopted that scheme and supplemented it with additional data from their own material. The latest version of their description of Poljakov's four stages, with inclusion of equivalent embryonic days in rhesus monkeys (Rakic et al. 2009: pp 20), is as follows:

Stage I: Initial formation of the cortical plate (6–10 PCW; E40–E54 in monkey)
Stage II: Primary condensation of the cortical plate (10–11 PCW; E55–E59 in monkey)
Stage III: Bilaminate cortical plate (11–13 PCW; E59–E64 in monkey)
Stage IV: Secondary condensation (13–15 PCW; E64–E75 in monkey)

However, after the discovery of the subplate zone (Kostovic and Molliver 1974), it soon became obvious that stage III in fact corresponds to the subplate formation stage or stage of the "second" cortical plate (Kostovic and Rakic 1990). See Fig. 2.

The radial columnar arrangement of cells (so-called ontogenetic columns; Rakic 1988, 1995) is a prominent feature of the early fetal cortical plate (Kostović-Knežević et al. 1978; Krmpotić-Nemanić et al. 1984; Kostovic and Rakic 1990). In the prospective somatosensory cortex of human fetuses aged 9–11 PCW (31–65 mm CRL) the cortical plate appeared as the condensed, darkly stained and clearly delineated zone with pronounced radial (columnar) orientation of its cells (Kostović-Knežević et al. 1978). However, as the fetus develops from 9 to 11 PCW, there are increasingly distinct differences between the superficial and the deep part of the cortical plate (Fig. 2): while the superficial CP remains characterized by predominantly radial orientation of both cell somata and processes, the cells and their processes in the deep CP become more loosely packed due to the enlarged intercellular space and the presence of numerous processes without radial orientation (Kostović-Knežević et al. 1978; Kostovic and Rakic 1990). This decrease in cell density and variability of cell arrangement and orientations becomes more pronounced during the formation of the subplate zone at 13–15 PCW (Krmpotić-Nemanić et al. 1984; Kostovic and Rakic 1990).

Starting from the above described Poliakov-Sidman-Rakic-Kostovic classification, and thanks to the availability of a unique resource – the Zagreb Collection of human brains located at the Croatian Institute of Brain Research (Kostović et al. 1991a; Judaš et al. 2010c) – our research group gradually developed the most detailed classification of human fetal cortical development, as described in a number of previous reviews (Kostović 1990a, b; Kostović and Judaš 1994, 1995, 2009; Kostović et al. 2008). The reader may wish to consult these reviews for a detailed description and numerous illustrations; the aim of this section is just to point out essential facts relevant for the understanding of subsequent sections.

Embryonic and fetal zones of the telencephalic wall are concentric architectonic compartments that represent a spatial framework for temporal analysis of specific histogenetic events, such as neuronal proliferation, migration, axonal pathfinding, synaptogenesis, dendritic differentiation and establishment of transient and permanent cortical neuronal circuitry and input–output connections (Fig. 2). In the human fetal telencephalon, their development peaks during the midgestation (15–24 PCW), that is, the period of the so-called typical fetal lamination pattern (Fig. 3) when all zones are present and well developed. From ventricular to the pial surface, these zones are: the ventricular zone (VZ) and the subventricular zone (SVZ), the intermediate zone (IZ), the subplate zone (SP), the cortical plate (CP), and the marginal zone (MZ).

The proliferation of cortical progenitors occurs in VZ and SVZ, initially by symmetric mitotic divisions (when one cortical progenitor cell divides to give rise to two other cortical progenitor cells). However, at 7 PCW, some progenitors begin to enter asymmetric mitotic divisions (when one progenitor cell divides to give rise to another progenitor cell and one young postmitotic neuron which will divide never again). This marks the beginning of cortical neurogenesis. Young postmitotic neurons migrate from VZ (along radial glial guides; see below) toward the pia, and their accumulation below the MZ leads to the initial formation of the CP at 7–8 PCW. While principal cortical output neurons (pyramidal neurons) are generated

Fig. 2 Sequential development of transient embryonic and fetal zones in the neocortical (pallial) wall of the human fetal telencephalon, from 8 to 18 PCW. Note that the cortical plate (CP) displays two periods of sharp delineation: the stage of primary consolidation of the CP (at 8–10 PCW) and the stage of secondary consolidation of the CP (from 15 PCW onward). These two periods are separated by the subplate formation (SPF) stage (12–15 PCW). The formation of the subplate zone is a protracted process, which begins with the formation of the presubplate (asterisk at 10 PCW), and continues during 12, 13, and 14 PCW through merging and reorganization of the deep part of the initial cortical plate (CP2/SPF) and numerous additional subplate neurons accumulating below it (SPF at 14 PCW). Note that during this period the upper part of the CP (CP1) remains compact and with strictly radially oriented cells, while its deeper part becomes rarified and looses its radial arrangement of cells (CP2). As the SP develops at the interface of CP and IZ, during the subplate formation stage it can be also subdivided into its upper part (SPU, i.e., CP2) and lower part (SPL). At 18 PCW, the typical fetal lamination pattern is fully established, and the SP becomes the thickest part of neocortical anlage as well as of the entire telencephalic wall. Note also the well-developed subpial granular layer (*arrow*) at 15 PCW. For further details, see text

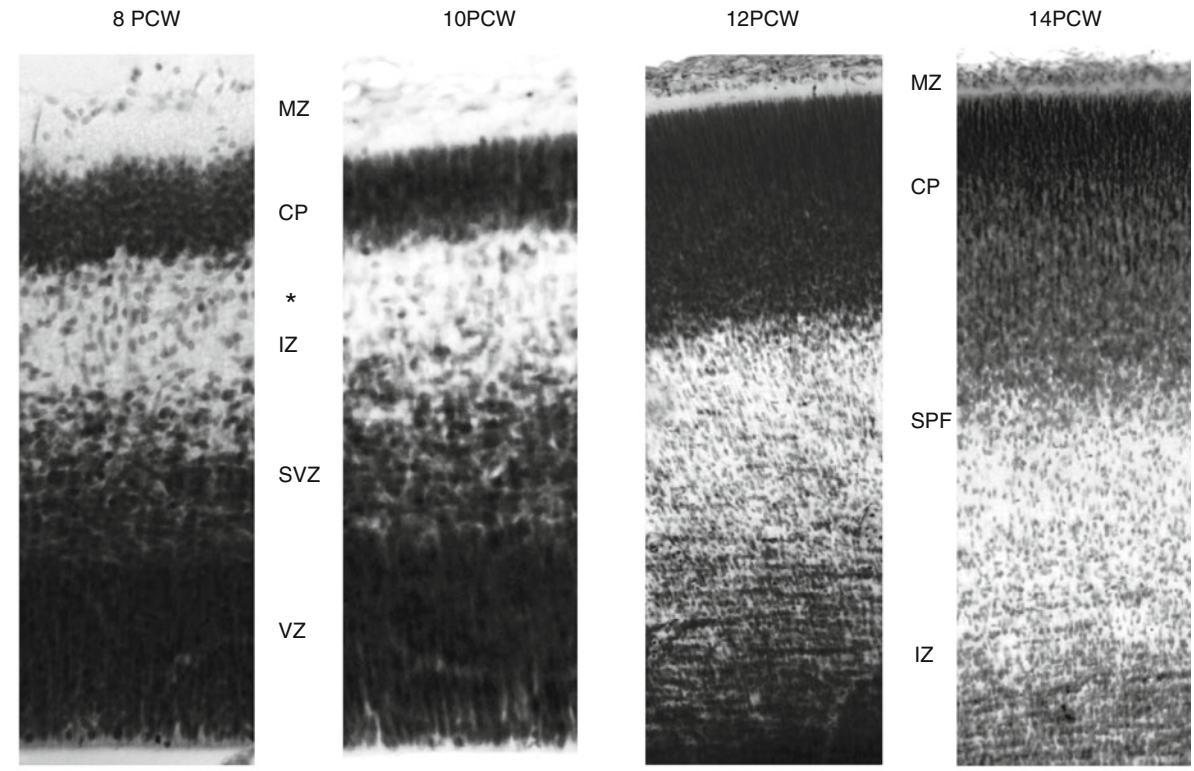
8 PCW
10PCW
12PCW
14PCW
MZ
CP
*
IZ
SVZ
VZ
MZ
CP
SPF
IZ

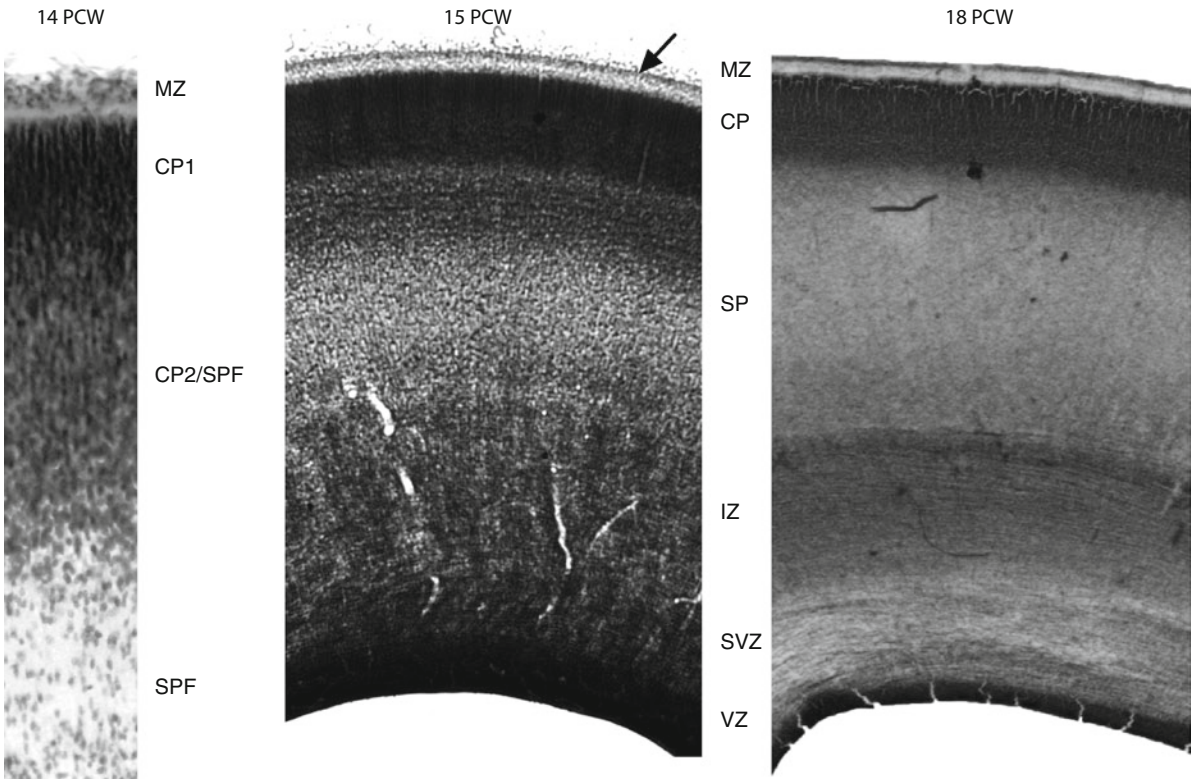
14 PCW
15 PCW
18 PCW
MZ
CP1
CP2/SPF
SPF
MZ
CP
SP
IZ
SVZ
VZ

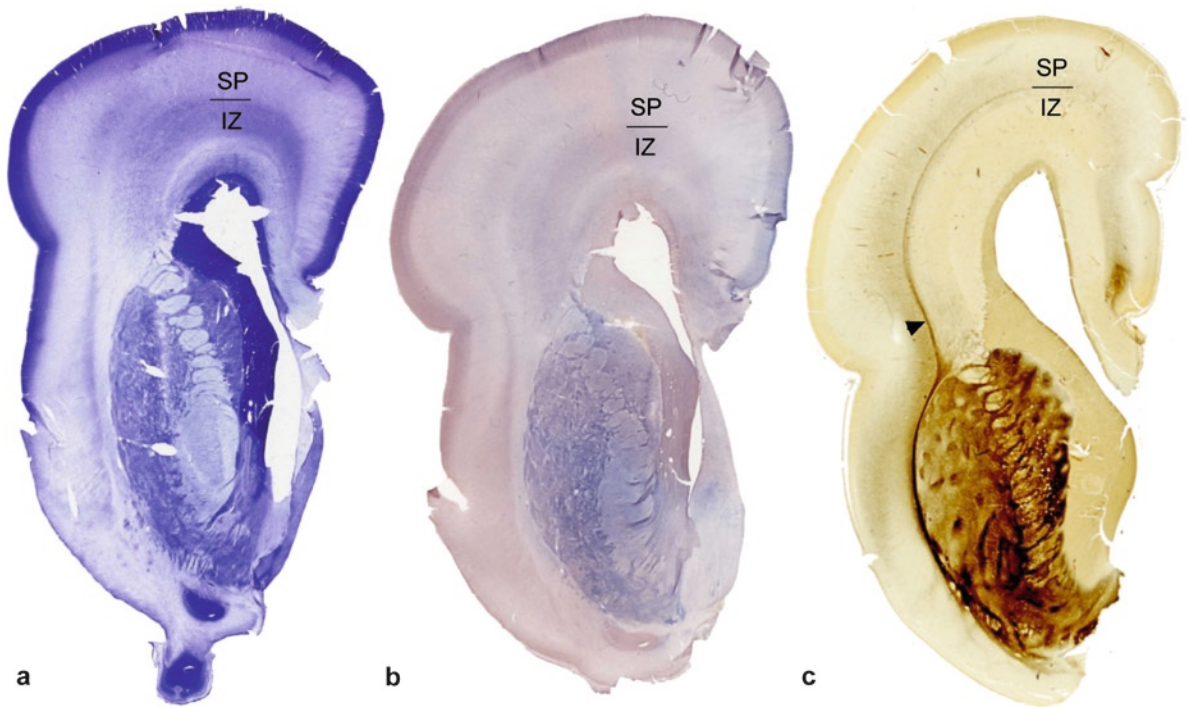

Fig. 3 Typical fetal lamination pattern at 18/19 PCW, as illustrated by Nissl staining (**a**), NADPH-diaphorase histochemistry (**b**), and AChE-histochemistry (**c**). Note that the external capsule (*arrowhead* in **c**) represents the outermost part of the fetal white matter (i.e., intermediate zone, IZ) and serves as an excellent marker for the border between the IZ and the subplate (SP), because its position is clearly recognizable in all three types of staining (and directly visualized by AChE-histochemistry). Note also the huge ganglionic eminence capping the developing caudate nucleus

within the VZ and reach the CP by radial migration, cortical interneurons are generated in both pallial SVZ and subpallial ganglionic eminence (together with neurons of basal ganglia) and reach the CP by tangential migration (for details, see Sect. 6.2.2).

However, two other important fetal zones are interposed between VZ/SVZ and the CP: the intermediate zone (IZ) and the subplate zone (SP). The IZ has a dual role: (a) it is a compartment through which all cortical neurons have to migrate (either radially or tangentially) in order to reach their final destination in the CP (or the SP), and (b) it is the major compartment through which all cortical efferent and afferent (output–input) axonal pathways have to grow and navigate in order to reach their target region/area. The subplate (SP) is the most prominent transient compartment of the fetal neocortical anlage, which contains numerous early differentiated projection (glutamatergic) neurons and local (GABAergic and peptidergic) interneurons and serves as a waiting compartment for growing cortical afferents (Rakic 1977; Kostovic and Rakic 1990). Thus, it is the major site of synaptogenesis in the midfetal brain and contains diverse and transient neuronal circuits which represent a neurobiological basis for transient electrophysiological and behavioral phenomena in fetuses and early preterm infants (for review, see Kostović and Judaš 2002a, b, 2006, 2007, 2010). The SP circuits are also connected with another early population of well differentiated cells – Cajal–Retzius cells situated in the MZ. It also contains an abundant hydrophilic extracellular matrix which enables its easy visualization on fetal MRI (Kostović et al. 2002a; see Fig. 4).

Thus, an important take-home message is that, during midgestation (and, at least in future associative cortical regions, until birth) the human fetal telencephalic wall can be divided in three major regions: (a) the neocortical anlage which consists of the marginal zone (MZ), the cortical plate (CP) and the subplate (SP); (b) the intermediate zone (IZ) which represents the fetal white matter, and (c) proliferative ventricular/subventricular zones (VZ/SVZ), including the ganglionic eminence (which is greatly enlarged part of the VZ).

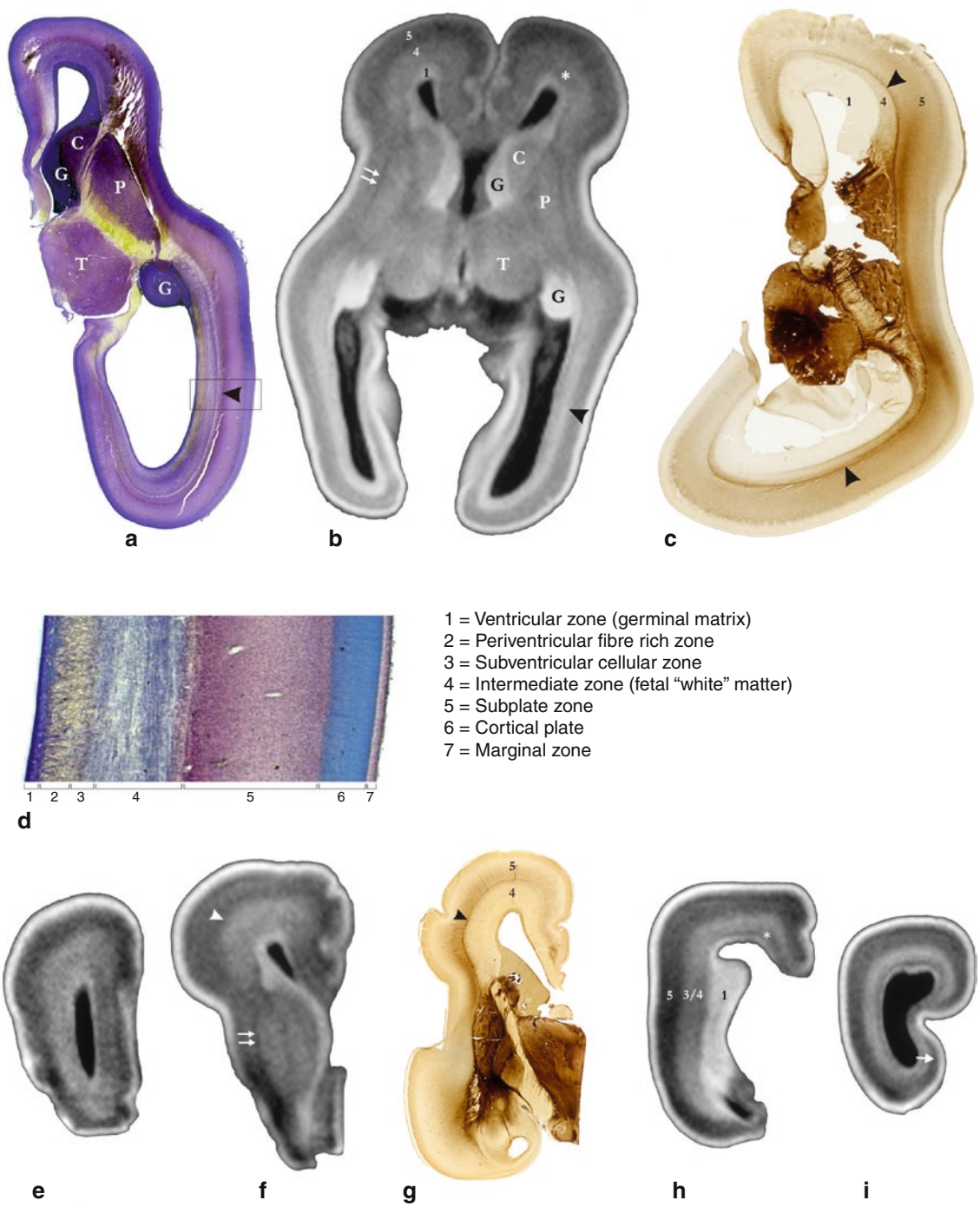

Fig. 4 At 18 PCW, the histological, histochemical, and MRI sections reveal a transient pattern of lamination in the cerebral wall. Low-power views of brains sectioned (**a**–**c**) horizontally and (**e**–**i**) coronally and stained with (**a**, **d**) cresyl violet Nissl staining, (**c**, **g**) AChE-histochemistry or (**b**, **e**, **f**, **h**, **i**) displayed on 3-D GRE T1-weighted MRI sections. For the horizontal sections anterior is to the top and for the coronal sections medial is to the right and dorsal is to the top. The box in (**a**) corresponds to the higher power view in (**d**) (*C*, caudate nucleus; *G*, ganglionic eminence; *P*, putamen; *T*, thalamus). The asterisk in (**b**, **h**) indicates the periventricular fiber-rich zone as seen on T1-weighted images, the *arrowheads* in (**a**–**c**, **f**, **g**) indicate the external capsule or its position, the *arrow* in (**i**) indicates the wedge-shaped narrowing of the subplate zone in the prospective primary visual cortex, and the *double arrows* in (**b**, **f**) indicate the position of the external capsule in the MRI sections (From (Kostovic et al. 2002a). With permission)

The MZ represents a future cortical layer I, while CP will differentiate into future cortical layers II–VI. While the SP will subsequently disappear as an architectonic compartment, the majority of subplate neurons will survive as interstitial neurons of the gyral white matter in the adult brain (or become partly incorporated in the deepest part of the layer VI; see Sect. 7.2). As the SP at its developmental peak (25–30 PCW) is four to five times thicker than the CP, the neocortical anlage occupies the entire outer half of the fetal telencephalic wall, while the fetal white matter (IZ) occupies deep periventricular regions (Figs. 3 and 4).

4 Histologically Defined Fetal Zones Can Be Successfully Traced by MRI in Vitro and in Vivo

Recent advances in MRI technology have opened new vistas for both in vivo and in vitro studies of human brain development (Chung et al. 2009; Ment et al. 2009; Kostovic and Vasung 2009; Lodygensky et al. 2010). Fetal MRI provides a precise insight into brain structure and thus allows the correlation with functional maturation and facilitates early detection of brain damage (Rutherford et al. 2005; Ment et al. 2009). The MRI is also important in the postnatal follow-up of neurodevelopmental outcome in preterm infants at risk (Counsell and Boardman 2005; Ment et al. 2009). Thus, a close correlation of in vivo MR images with histological images of the fetal brain has became a necessity for a proper neurobiological interpretation of normal and disturbed human brain development. An in vitro MRI analysis of postmortem human fetal brain specimens represents a convenient first step in bridging the gap between histogenesis and in vivo MRI (Kostović and Vasung 2009). The layered appearance of the fetal cerebral wall was already observed in early MRI studies (Girard and Raybaud 1992; Girard et al. 1995; Chong et al. 1996; Brisse et al. 1997; Childs et al. 1998, 2001; Sbarbati et al. 1998; Hüppi et al. 1998; Felderhoff-Mueser et al. 1999; Lan et al. 2000; Hüppi et al. 2001; Garel et al. 2001). In a pioneering study, we demonstrated the full correspondence between fetal architectonic zones and corresponding MR images between 15 and 36 PCW (Kostović et al. 2002a; Judaš et al. 2005; Radoš et al. 2006). We demonstrated that changes in the MRI lamination pattern of the human fetal cerebral wall are predominantly caused by changes in the subplate zone (Fig. 4) and that SP can be easily visualized in MR images due to its abundance of the hydrophilic extracellular matrix (Kostović et al. 2002a; for review, see Judaš et al. 2003a). These findings were subsequently confirmed and extended in both in vitro and in vivo MRI studies of the human fetal brain, including those which used a more advanced diffusion tensor imaging (McKinstry et al. 2002; Maas et al. 2004; Gupta et al. 2005; Prayer et al. 2006; Perkins et al. 2008; Dubois et al. 2008a, b; Trivedi et al. 2009; Widjaja et al. 2010; Kasprian et al. 2010).

5 There Are Major and Clinically Relevant Differences in Cortical Development Between Rodents and Humans

Rats and mice cannot speak, write or read or suffer from schizophrenia, but we can. While everybody wants to know what distinguishes the human brain from that of other animals, most neuroscientists study nonhuman species and leave the human and comparative neuroanatomy to a small group of devotees. Thus, neuroscientists rely on studies of nonhuman species for understanding human brain organization. This emphasis on studies of model animals, which comes to us from the biomedical research tradition and from experimental psychology, has become the accepted approach to biomedicine (Preuss 2009). The underlying assumption has been that there are basic features of brain organization that are widely shared across animals and that eventual differences are minor and unimportant (Preuss 2009). As a paragon for that approach may serve a long ago disproved but still widely cited study claiming that there is the "basic uniformity in the structure of neocortex" (Rockel et al. 1980). As pointed out in a recent review (Preuss 2009: pp 61): "The science we have built, centered on the model-animal paradigm and supported by biomedical funding agencies, is in important respects the wrong kind of science for elucidating the structure, functions, and diseases of the human brain…. I am not suggesting that we abandon our model species, but rather that those species are not enough."

There are a myriad of significant differences between rodents and humans (or, for that matter, even between humans and chimpanzees) in the structure and function of the brain at every hierarchical level, from genes and cells to large neuronal assemblies and functional systems (for a comprehensive review, see Kaas and Preuss 2007). There are large differences in number and varieties of cortical interneurons and specializations of the cortical microstructure of humans (DeFelipe et al. 2002, 2007; Hof and Sherwood 2007; Sherwood and Hof 2007). There are pronounced specializations of the neocortical pyramidal cell during primate evolution (Elston 2003, 2007) including pyramidal neurons which express calretinin (Hof et al. 2001); significant cortical area and species differences in dendritic spine morphology (Benavides-Piccione et al. 2002); primate-specific patterns of cortical commissural connections (Doty 2007); uniquely human patterns of organization within the primary visual cortex (Preuss et al. 1999; Preuss and Coleman 2002) and lateralization of minicolumns in the planum temporale (Buxhoeveden et al. 2001); special types of large, spindle-shaped layer V pyramidal neurons (Von Economo neurons) in the anterior cingulate and frontoinsular human cortex (Von Economo and Koskinas 1925; Von Economo 1926; Nimchinsky et al. 1995, 1999; Allman et al. 2002, 2005); and even hominoid specializations of the density and morphologies of cholinergic (Raghanti et al. 2008a) and serotonergic (Raghanti et al. 2008b) fibers in frontal cortex or a human-specific gene in microglia (Hayakawa et al. 2005).

The bourgeoning field of comparative genomics has convincingly demonstrated that the genetic specializations of human beings turn out to be far more extensive than expected, and include not only changes in gene sequences and gene expression, but also rearrangements, duplications, and losses of blocks of DNA (Eichler et al. 2001; Johnson et al. 2001; Gagneux and Varki 2001; Enard et al. 2002a, b; Cáceres 2003; Clark et al. 2003; Gu and Gu 2003; Hsieh et al. 2003; Preuss et al. 2004; Uddin et al. 2004; Bustamante et al. 2005; Cheng et al. 2005; Evans et al. 2005; Mekel-Bobrov et al. 2005; Khaitovich et al. 2005; Varki and Altheide 2005; Arbiza et al. 2006; Bailey and Eichler 2006; Berezikov et al. 2006; Donaldson and Gottgens 2006; Harris and Meyer 2006; Oldham et al. 2006; Popesco et al. 2006; Sikela 2006; Varki 2006; Cáceres et al. 2007; Calarco et al. 2007; Spiteri et al. 2007; Vernes et al. 2007; Zhang et al. 2007; for review see Varki et al. 2008; Preuss 2009).

Even the so-called essential genes (considered responsible for survival) give different phenotypes in different species, and about 20% of mouse orthologs of human-essential genes are nonessential in mice (Liao and Zhang 2008). The recent data in humans (Johnson et al. 2009) have uncovered an order of magnitude of greater transcriptional differences between neocortical areas than has been obtained in comparable studies in rodents (Kudo et al. 2007; Mühlfriedel et al. 2007). For example, the gene *contactin associated protein-like 2* (*CNTNAP2*), previously studied for its role in autism and specific language impairment (Arking et al. 2008; Alarcón et al. 2008; Bakkaloglu et al. 2008; Vernes et al. 2007, 2008), is selectively and highly enriched in the orbital prefrontal cortex, an area involved in regulation of social behavior in humans and has no comparable analogue in rodents. The mouse homologue *Cntnap2* has not been found to be expressed in any areal pattern or gradient in the mouse brain at any stage of development (Abrahams et al. 2007). This is an example of how unique structures and gene expression patterns that give rise to abilities, such as language, are also involved in disorders, such as autism, for which there is no accepted mouse model (Levitt 2005; Rakic 2009).

In the field of developmental neurobiology, the vast majority of published work has focused on rodent cortical development (Ragsdale and Grove 2001; Alvarez-Buylla et al. 2001; O'Leary and Nakagawa 2002; Kriegstein and Parnavelas 2003; Kriegstein and Noctor 2004; Rakic 2006a; O'Leary et al. 2007; Molyneaux et al. 2007; Rakic et al. 2009; Preuss 2009). Indeed, the mouse may be regarded as an unexcelled model for studying development of the cerebral cortex (Rakic 2000). While the basic principles of cortical development in all mammals are similar (Rakic et al. 2009), the modifications of developmental events during evolution produce not only quantitative but also qualitative changes (Preuss 2009; Rakic et al. 2009). Thus, it should be not surprising that the large primate cerebral cortex displays much more complex development and has some distinct features not observed in commonly used laboratory animals (Rakic 2006a). The human brain has different cell-cycle kinetics during cortical neurogenesis (Kornack 2000; Kornack and Rakic 1998) and longer developmental period, larger size, and evolutionary new areas with enlarged corticocortical layers II and III (Hill and Walsh 2005).

There are also a number of major differences between rodents and humans with respect to the brain development itself. For example, human cortex displays dramatically expanded subplate zone (Kostovic and Rakic 1990; see Sect. 7.2); more complex and hugely expanded SVZ (Smart et al. 2002; Zecevic et al. 2005; see Sect. 6.2.2); very prominent subpial granular layer (see Sect. 7.1.2) and significantly different process of initial cortical formation (Bystron et al. 2008; see Sect. 6.1); more complex and diverse Cajal–Retzius cells (Meyer 2010; see Sect. 7.1.1); particularly prominent and morphologically and functionally more diverse radial glial cells (Rakic 2003a, b; see Sect. 6.2.1); significantly different gradients of gene expression in the developing cortex (see Sect. 7.3.3); and several unique transient fetal structures and/or features (see Sect. 7.5). In terms of neurogenesis, one important difference deserves to be pointed out already in this section: humans have greatly expanded SVZ (Sidman and Rakic 1973, 1982; Kostovic and Rakic 1990; Smart et al. 2002; Zecevic et al. 2005) as well as the mitotically active subpial granular layer in the marginal zone (Zecevic and Rakic 2001). In comparison to rodents, these phylogenetic novelties contribute to the introduction of species-specific cell types (especially cortical interneurons; see Sect. 6.2.2), new cytoarchitectonic fields, and the pattern of connectivity and transmitter/receptor composition that needs to be taken into account if we are to understand the etiology of congenital malformations in humans (Rakic 2006a; Rakic et al. 2009).

For example, fewer than four extra rounds of symmetric cell divisions during the initial proliferation in the VZ can account for the ten-fold difference in size of the cortical surface between monkeys and humans (Rakic 1995, 2006a). In contrast, the 1,000-fold difference between the size of the cerebral cortex in mouse and human can be achieved by less than seven extra symmetrical divisions in the VZ before the onset of corticogenesis (Rakic 2006a). Indeed, such changes were experimentally confirmed in mice in which production of proliferative units has been increased either by reduction in programmed cell death (Kuida et al. 1996; Haydar et al. 1999) or through an increase in production (Chenn and Walsh 2003).

In conclusion, the traditional model-animal research paradigm (focused almost exclusively on rodents) does not offer a solid foundation for understanding what is human-specific in the human brain and human mind. However, new methods from histology, neuroimaging, and genomics share the common feature of being non-invasive and are thus making the human brain finally accessible for direct, detailed study and enable direct comparisons of humans with any other species (Preuss 2009). Thus, the time is ripe for bridging the gap between the treasure of data provided in classical human neuroanatomy and molecular biology and genomics, by taking advantage of these modern approaches and creating a foundation for new, integrative neuroscience of human brain development.

6 The Complexity and Unique Features of the Human Corticogenesis

Brain development is a complex and long process which involves sequential expression of genes, cascades of multiple molecular pathways, and continuous interactions among heterogeneous classes of cells (Rakic 2006a; Rakic et al. 2009; Preuss 2009). Modern and powerful methodological approaches, such as genomics and neuroimaging, offer unprecedented possibilities for getting new insights into development of the human brain, which, unlike in rodents, remains inaccessible for experimental approaches, for obvious ethical reasons. The complexity and unique features of human corticogenesis are evident at all major stages of cortical development: the initial formation of the neocortical anlage at the embryonic preplate stage; the pronounced heterogeneity of neuronal and glial progenitor pools in both VZ and SVZ (including the ganglionic eminence); the huge development and phylogenetically new features of both the SVZ and the subplate; distinct features of radial glial cells; multiple origins of Cajal–Retzius cells and the subpial granular layer; and other features mentioned in the following paragraphs.

6.1 The Embryonic (Preplate) Stage and the Initial Formation of the Neocortical Anlage

Over the past three decades, modern histological and/or molecular biological methods have been used to analyze the initial formation of the neocortical anlage (so-called preplate stage) during the human embryonic

period proper (Carnegie stages 12–22, E31–E51, 4–8 PCW) or during the initial development of the neocortical plate and the pre-subplate (8–10 PCW) in a rapidly increasing number of studies (Molliver et al. 1973; Kostović-Knežević et al. 1978; Larroche et al. 1981; Larroche 1981; Larroche and Houcine 1982; Marin-Padilla 1983; Krmpotić-Nemanić et al. 1984; Kostović 1986; Kostovic and Rakic 1990; Kostović et al. 1993; Zecevic 1993, 2004; Zecevic and Rakic 2001; Rakic and Zecevic 2003a; Zecevic et al. 1999, 2005; Meyer et al. 2000, 2002b, 2003; Bystron et al. 2005, 2006; Howard et al. 2006; Carney et al. 2007; Cabrera-Socorro et al. 2007; Bayatti et al. 2008a, b; Ip et al. 2010; Kerwin et al. 2010; Verney et al. 2010).

These studies revealed a previously unsuspected complexity of the early neocortical anlage in humans (for review, see Bystron et al. 2008) and clearly demonstrated that the concept of the primordial plexiform layer as introduced by Miguel Marin-Padilla (Marin-Padilla 1971, 1972, 1978, 1983, 1988a; Marin-Padilla and Marin-Padilla 1982) was overly simplified and that it at best can only be applied to the developing brains of rodents and carnivora. For example, at 4–7 PCW, a widespread network of precocious MAP2-immunoreactive cells, with long, nonaxonal processes, are present in the human preplate before the appearance of the cortical plate (Bystron et al. 2005). These cells seem to be generated outside the cerebral wall rather than in the local VZ and the first thalamocortical axons and axons of preplate cells extend across the striato-cortical boundary before the arrival of the first cortical plate neurons (Bystron et al. 2005). In a subsequent study, the same group described a distinctive, widespread population of neurons (predecessor cells) situated beneath the pial surface of the human embryonic forebrain even before complete closure of the neural tube (Bystron et al. 2006). These predecessor cells invade the cortical primordium by tangential migration from the subpallium and precede all other known cell types of the developing cortex, because they are neither Cajal–Retzius cells nor interneurons of basal origin (Bystron et al. 2006). Thus, in human forebrain, unlike rodent, predecessor cells migrate into the cortical primordium from the subpallium even before local neurogenesis has begun and no equivalent of predecessor cells has been described in any other species (Bystron et al. 2005, 2006; Carney et al. 2007); in addition, there are also other human-specific and tangentially migrating cell types (Bystron et al. 2008).

6.2 The Heterogeneity of Neuronal and Glial Progenitor Pools

The past decade has wittnessed a number of important discoveries which revealed a hitherto unexpected complexity and heterogeneity of neuronal and glial progenitor pools in the telencephalon of mammals, including humans: (1) it was discovered that radial glia not only serves as guide for radially migrating neurons but also represents a neural stem cell which produces both astrocytes and neurons; (2) it has been demonstrated that cortical principal (pyramidal) neurons as well as interneurons originate from multiple and separate proliferative pools; (3) newly generated neurons arrive to the cortex by multiple radial and tangential migratory routes; (4) there are major differences between rodents and primates in both the diversity of origins and migratory routes of cortical neurons; and (5) there are major differences between rodents and humans with respect to the clinically important question of adult neurogenesis. Thus, in the developing mammalian telencephalon, there are several classes of progenitors that can produce distinct neuronal subclasses with considerable species-specific differences in their relative proportions (Rakic et al. 2009). These differences are controlled by genes that act on the progenitor cells at or prior to their exit from their cell's mitotic cycle (Shirasaki and Pfaff 2002) and thus generate a different outcome, depending on the given evolutionary context (Rakic 2003a, b). In the following sections, we focus on several key topics which illustrate why data obtained in rodents in most cases simply cannot be meaningfully extrapolated to the developing human telencephalon.

6.2.1 Radial Glial Cell: Just a Radial Guide for Migratory Neurons, or Mother of Them All?

There are several excellent reviews on the long history of radial glia (Bentivoglio and Mazzarello 1999) and their developmental and evolutionary adaptations (Cameron and Rakic 1991; Rakic 2003a, b). It is important to recognize at least three separate developmental roles of these cells: (1) their role as temporary guides for radially migrating neurons; (2) their role as precursors of astrocytes; (3) their role as neural stem

cells, including their putative role as multipotent stem cells in the adult brain (see Sect. 6.2.2).

Radial Glial Fibers as Guides for Radial Migration of Neurons

In studies combining the use of Golgi impregnation and electron microscopy in the monkey developing cortex, Pasko Rakic discovered that radial glial cells serve as guides for radial migration of young postmitotic neurons on their journey from the VZ to the cortical plate (Rakic 1971, 1972). The glial nature of these radial fibers was assumed on the basis of the morphological criteria (Rakic 1971, 1972; Schmechel and Rakic 1979a) and confirmed by early immunocytochemical studies in both monkey (Levitt and Rakic 1980; Levitt et al. 1981) and human brain (Choi and Lapham 1978; Choi 1986). In the human and macaque fetal cerebrum during the course of corticogenesis, radial glial cells contain glial fibrillary acidic protein (GFAP) and are distinctly different from GFAP-negative cells (Antanitus et al. 1976; Choi and Lapham 1978; Levitt and Rakic 1980; Levitt et al. 1981, 1983; Choi 1986; Kadhim et al. 1988; DeAzevedo et al. 2003). The intermediate filament vimentin is also a helpful marker for the identification of radial glia as a separate cell line in primates, since the adjacent neuronal cells are vimentin-negative (Rakic 2003a, b). Unlike in primates, radial glial cells in rodents are not GFAP-positive until the completion of corticoneurogenesis (Cameron and Rakic 1991) and the change in their developmental phenotype is indicated by a substitution from vimentin to GFAP (for review, see Rakic 2003a, b). In primates, radial glial cells express both GFAP and vimentin throughout at least two-thirds of gestation (Antanitus et al. 1976; Choi and Lapham 1978; Levitt et al. 1981; Choi 1986; Sasaki et al. 1988; Stagaard and Mollgard 1989; Gould et al. 1990; Wilkinson et al. 1990; Sarnat 1992; Honig et al. 1996; Zecevic et al. 1999; DeAzevedo et al. 2003).

In addition, human and monkey radial glial cells display much more complex and diverse morphological features in comparison to rodents – such as, lamellate expansions and cone-shaped endfeet forming a continuous glia limitans component of the pial surface. In fact, radial glial cells reach the peak in size and phenotypic differentiation in the human fetal forebrain (Rakic 2003a, b). As the size of the cerebral wall expands during evolution, radial glial scaffolding also becomes more differentiated, more permanent, and functionally more significant – that is, radial glial cells have undergone substantial evolutionary transformation (Schmechel and Rakic 1979a, b; Levitt and Rakic 1980; Levitt et al. 1981, 1983; Rakic 2003a, b). There are important structural, molecular, and functional differences in radial glia between different regions within the same species as well as between the same regions of different species (Rakic 2003a, b). For example, the length of the radial glial fiber in the macaque monkey cerebrum toward the end of corticoneurogenesis may reach 3–7 mm (Rakic 1972) and at this stage in the primate forebrain, many radial glial cells stop transiently to divide while their shaft serves as scaffolding for a cohort of migrating neurons (Schmechel and Rakic 1979a, b). In the fetal human cerebral wall several generations of GFAP-negative migrating neurons can be aligned along a single GFAP-positive radial glial shaft, and the number of thus associated neurons increases with the gestational age (Rakic 2003a, b). For example, in the wide intermediate zone of the human fetus during midgestation, as many as 30 generations of migrating neurons can be simultaneously aligned along the single radial glial shaft (Sidman and Rakic 1973, 1982).

Thus, this radial glial scaffolding may be particularly important in the primate fetal cerebrum, where a large SVZ supplies a bulk of interneurons at the late developmental stages, thus contributing to evolutionary and developmental cortical expansion (Letinic et al. 2002; Smart et al. 2002; Zecevic 2004; Kriegstein et al. 2006). The fate of the radial glial cells depends on the context and functional requirements, which differ between species (Rakic 2003a, b).

Radial Glia as Precursor of Astrocytes

In most mammals the telencephalic radial glial cells are transient, and disappear or transform into astrocytes with the completion of cortical development (Schmechel and Rakic 1979a, b; Kadhim et al. 1988; Wilkinson et al. 1990; DeAzevedo et al. 2003; Rakic 2003a, b). During the early embryonic and fetal development, the pial contacts of these cells are multiple, connected by tight junctions, and each one terminates in a characteristic endfoot process covered with basal lamina material (Marin-Padilla 1995). The apposed

and basal lamina-covered endfeet of these radial cells constitute the primordium of neocortical external glial limiting membrane, which is perforated and subsequently reformed only at specific sites by entering meningeal blood vessels and olfactory axons (Marin-Padilla 1985, 1988b; Krisch 1988; Marin-Padilla and Amieva 1989).

In the fetal brains of monkeys and humans, radial glial cells become transformed into fibrous (white matter) and/or protoplasmic (gray matter) astrocytes (Choi and Lapham 1978; Schmechel and Rakic 1979a; Levitt and Rakic 1980; Eckenhoff and Rakic 1984; Choi 1986; Marin-Padilla 1995). The first fibrous astrocytes in the neocortex are those of the SVZ and the subplate and their appearance parallels the early vascularization of these zones (Marin-Padilla 1995). However, modified radial glial cells may be found in some regions of the adult nervous system – for example, Bergmann glial cells of the cerebellum, Müller cells of the retina, tanycytes of the hypothalamus (Rakic 2003a, b).

Radial Glia as Neural Stem Cells

While it has been known for a long time that the primary radial glial phenotype (as defined by Cameron and Rakic 1991) can revert to the neuroepithelial form and generate neurons, recent studies in rodents provided direct evidence that radial glia give origin to cortical neurons (Malatesta et al. 2000, 2003; Noctor et al. 2001, 2002; Tamamaki et al. 2001; Hartfuss et al. 2001; Tramontin et al. 2003; Gal et al. 2006; for review, see Barres 1999; Alvarez-Buylla et al. 2001; Parnavelas and Nadarajah 2001; Campbell and Götz 2002; Gaiano and Fishell 2002; Fishell and Kriegstein 2003; Weissman et al. 2003; Götz and Huttner 2005). Thus, the daughter cells (i.e., young postmitotic neurons) are guided by the radial fibers of their mother's cells to the appropriate location in the cortical plate (Noctor et al. 2001; Rakic 2003a, b). The protein Numb is a crucial player in maintaining the adhesiveness of radial glia in the VZ, preventing premature detachment and subsequent astrogliogenesis (Rasin et al. 2007). In contrast, Notch functions cell-autonomously to maintain the radial glial cell fate while the proneural genes antagonize Notch signaling to promote neuronal differentiation and subsequent migration (Breunig et al. 2007b). Furthermore, the daughter neuronal cell stimulates Notch signaling in the radial glial mother cell to maintain the neurogenic VZ niche and migratory scaffold (Yoon et al. 2008).

Multipotent astrocytic stem cell has also been identified in fetal and adult mouse brain (Laywell et al. 2000). More recent observations have indicated the existence of a transit-amplifying cell that populates both the VZ and SVZ. These cells are considered dedicated neuronal progenitors derived from the parent radial glial cells that do not inherit the pial fiber (Noctor et al. 2004; Gal et al. 2006; Martinez-Cerdeno et al. 2006). There are radial glial cells that span the entire neocortical cerebral wall as well as short neural precursors (SNPs) with basal processes of variable length that are retracted during mitotic division (Gal et al. 2006). While SNPs are marked by their preferential expression of the tubulin alpha-1 promoter, radial glial cells instead express the glutamate astrocyte-specific transporter (GLAST) and brain lipid-binding protein promoters (Gal et al. 2006). Thus, radial glial cells can give rise to both neuron and astrocytic progenitors that each can produce several generations of dedicated progenitors before their terminal differentiation (Rakic 2006a). Multipotential progenitors have also been recognized in the human fetal brain: human embryonic stem cells produce separate neuron- and glia-restricted precursors in vitro (Carpenter et al. 2001); molecular phenotyping of neurospheres obtained from fetal human brain revealed glial and neuronal classes of cells (Suslov et al. 2002; Kim et al. 2006); glial cells from the human fetal lateral ganglionic eminence in vitro produce either glia or neurons (Skogh et al. 2001); and in the human brain radial glia can directly produce neurons (Weissman et al. 2003; Mo et al. 2007; Hansen et al. 2010). Multipotent astrocytic stem cells have also been identified in the adult human brain (Kirschenbaum et al. 1994; Kukekov et al. 2002; Sanai et al. 2004).

In human VZ and SVZ already at 5–6 PCW (Carnegie stages 14–15), three major cell types are observed (Zecevic 2004): (a) most proliferating VZ cells are labeled with radial glial markers such as vimentin, GFAP, and GLAST antibodies; (b) a subpopulation of these cells also express the neuronal markers β III-tubulin, MAP-2, and phosphorylated neurofilament SMI-31, in addition to the stem cell marker nestin, which indicates their multipotential capacity; and (c) some VZ cells that immunoreact only with neuronal markers, which indicates the emergence of restricted neuronal progenitors. All three classes are proliferative and share common

radial morphology with attachments to the VZ and pial surface (Zecevic 2004). Thus, multipotential progenitors coexist with restricted neuronal progenitors and radial glial cells during initial human corticogenesis, demonstrating that the diversification of cells in human VZ and overlying SVZ begins earlier and is more pronounced than in rodents (Zecevic 2004; Howard et al. 2006). However, radial cells double labeled with glial and neuronal markers cease to be present in human fetuses of 10 PCW and older (DeAzevedo et al. 2003; Zecevic 2004). In a subsequent study, it was confirmed that restricted neuronal progenitor cells divide simultaneously with radial glial cells in the human embryonic VZ at the onset of cortical neurogenesis, that at midgestation radial glial cells proliferate not only in the VZ, but throughout various regions of the telencephalic wall, and that several subtypes of radial glial cells can be distinguished on the basis of their antigen content (Howard et al. 2006). In a recent in vitro study, Mo et al. (2007) provided the first direct evidence that radial glial cells in the human cerebral cortex serve as neuronal progenitors and that diverse populations of cortical progenitor cells (including multipotent radial glia and neuron-restricted progenitors) contribute differentially to cortical neurogenesis at the second trimester of gestation (Mo et al. 2007). In contrast to mouse, it seems that radial glia in human do not generate all, or even the majority, of cortical neurons during midgestation – an additional progenitor subtype (restricted neuronal progenitors) is contributing to neuronal population of the human cerebral cortex (Piper et al. 2001; Howard et al. 2006; Mo et al. 2007).

6.2.2 Pallial Versus Subpallial Origin of Cortical Neurons and the Evolutionary Expansion of the Subventricular Zone

The Rodent Story: Pyramidal Neurons from Pallial Ventricular Zone and Interneurons from the Subpallial Ganglionic Eminence

Initial studies in rodents offered a simple and attractive concept: while all cortical glutamatergic pyramidal neurons originate from the pallial VZ and reach cortical plate by radial migration, all cortical GABAergic interneurons originate from the subpallial ganglionic eminence and reach the cortex by tangential migration through deep IZ/SVZ or through the superficial MZ (DeDiego et al. 1994; Tamamaki et al. 1997; Anderson et al. 2001, 2002; Parnavelas 2000; Marin and Rubenstein 2001, 2003; Nadarajah and Parnavelas 2002; Polleux et al. 2002; Nery et al. 2002; Kriegstein and Parnavelas 2003; Kriegstein and Noctor 2004; Xu et al. 2004; Wonders and Anderson 2005; for review see Métin et al. 2006; Hernández-Miranda et al. 2010). Cortical interneurons originate from several sources and migrate via distinct and independent tangential streams to reach their final destination (Ang et al. 2003; Marin and Rubenstein 2003). In rodents, the majority of cortical interneurons originate in the medial ganglionic eminence from progenitors that express ventral (subpallial) transcription factors *Dlx2*, *Nkx2.1*, *Lhx6* and *Mash1* (Xu et al. 2004).

The Human Story: Cortical Interneurons Predominantly from Pallial VZ/SVZ

Unlike in rodents, many GABAergic cortical interneurons are generated in pallial VZ/SVZ in monkeys (Petanjek et al. 2009) and humans (Letinic et al. 2002; Rakic and Zecevic 2003a; Fertuzinhos et al. 2009; for review, see Jones 2009). In the human, most of the cortical interneurons originate in the VZ/SVZ of the dorsal telencephalon subjacent to a given area (Letinic et al. 2002). This is particularly evident in the primary visual cortex, which in monkeys and humans contains a significantly larger number of interneurons than the adjacent areas (Smart et al. 2002; Lukaszewicz et al. 2005). In humans, a distinct lineage of neocortical GABAergic neurons that express *Dlx1/2* and *Mash1* transcription factors and originate from the neocortical VZ/SVZ comprise about two-thirds of the neocortical GABAergic neurons, while the remaining third originate from the ganglionic eminence (Letinic et al. 2002; Rakic and Zecevic 2003a). The expression of Nkx2.1 mRNA and protein was also demonstrated in human neocortical VZ/SVZ from 5 PCW until midgestation (Rakic and Zecevic 2003a).

Evolutionary Expansion of the Subventricular Zone in Primates and Humans

It is now generally accepted that, in addition to multipotential radial glial cells, the telencephalic proliferative

centers (VZ, SVZ, ganglionic eminence) also contain more restricted neuronal and glial cell progenitors. Initial studies in monkeys (Levitt and Rakic 1980; Levitt et al. 1981, 1983) as well as in humans (Carpenter et al. 2001; Letinic et al. 2002; DeAzevedo et al. 2003) demonstrated the existence of at least two separate stem cell lines in the VZ and a highly expanded SVZ: one glial and the other neuronal. For example, cells isolated from the human VZ/SVZ even at early fetal stages generate separate neuron-restricted and glia-restricted precursors (Carpenter et al. 2001). There are multiple divisions of human neuronal stem cell progenitors in the VZ/SVZ before they begin radial migration to the neocortex (Letinic et al. 2002).

An expansion of cortical progenitor cell number during evolution must have contributed to the increase in size of the human brain (Rakic 1995, 2009; Molnár et al. 2006; Dehay and Kennedy 2007; Fish et al. 2008; Abdel-Mannan et al. 2008). The evolution of primate and human neocortex is associated with enormous increase in size of the SVZ and the subplate (Kostovic and Rakic 1990; Smart et al. 2002; Kriegstein et al. 2006; Martinez-Cerdeno et al. 2006).

In humans, the SVZ appears as the secondary proliferative zone at 7–8 PCW (Sidman and Rakic 1982; Zecevic 1993). The SVZ in primates, including humans, produce mostly interneurons (Letinic et al. 2002; Rakic 2003a) and late generated subplate neurons (Smart et al. 2002; Zecevic et al. 2005) and glial cells (Rakic 2003a), including oligodendrocyte progenitors (Zecevic et al. 2005) and eventually in the adult cerebrum transforms into the subependymal zone (SEZ) which produces mostly glial cells (Lewis 1968; McDermott and Lantos 1990; Sanai et al. 2004). In the adult human brain, mature ependyma serves as an important barrier between CSF and brain parenchyma (Bruni 1998), and human ependymal cells were studied by immunohistological methods and electron microscopy (Gould and Howard 1987; Gould et al. 1990) and always described as the lining of the ventricular cavity (Roessmann et al. 1980; Gould et al. 1990).

The adult human SVZ represents a niche of neural stem cells, displays unique features and its architecture and function differs significantly from that described in other mammals (Quinones-Hinojosa et al. 2006). It is composed of four layers: a monolayer of ependymal cells (layer I), a hypocellular gap (layer II), a ribbon of cells (layer III) composed of astrocytes, and a transitional (layer IV) zone into the brain parenchyma (Quinones-Hinojosa et al. 2006). It contains three distinct types of astrocytes (which differ significantly from those described in rodent brain) and a group of displaced ependymal cells. Unlike rodents and non-human primates, adult human GFAP-positive SVZ astrocytes are separated from the ependyma by the hypocellular gap, and the adult human SVZ appears to be devoid of chain migration of large numbers of newly formed young neurons (Quinones-Hinojosa et al. 2006).

Radial glial cells in the VZ generate intermediate progenitor cells that migrate into the SVZ and further proliferate to increase neuronal number (Haubensak et al. 2004; Noctor et al. 2004; Fietz et al. 2010). In the human brain, a substantial fraction of interneurons originates locally, in the pallial VZ/SVZ (Letinic et al. 2002; Rakic and Zecevic 2003a; Zecevic 2004). Furthermore, oligodendrocytes and astrocytes (Back et al. 2001; Rakic and Zecevic 2003b; Zecevic 2004; Jakovcevski and Zecevic 2005a, b; Jakovcevski et al. 2009) and stem-like cells (Flax et al. 1998; Vescovi et al. 1999; Ourednik et al. 2001) are generated and reside in the human fetal SVZ. It should be noted that hypoxic-ischemic injury in prematurely born infants frequently damages the SVZ (Judaš et al. 2005; McQuillen and Ferriero 2005; Volpe 2009).

A distinguishing feature of primate corticogenesis is the appearance of the outer SVZ (OSVZ) during midgestation (Smart et al. 2002; Kostović et al. 2002a; Zecevic et al. 2005; Fish et al. 2008; Fietz et al. 2010). Cell divisions in both the OSVZ and the VZ coincide with the major wave of cortical neurogenesis, suggesting that OSVZ cells produce neurons (Lukaszewicz et al. 2005). Unlike in rodents, cells expressing the transcription factor PAX6 are found in the OSVZ of human and primate cortex (Fish et al. 2008; Bayatti et al. 2008a; Mo et al. 2007). Neuronal proliferation in the human SVZ between 18 and 24 PCW is important for generation of upper cortical layers, because at that time the SVZ remains the only proliferative zone (Zecevic et al. 2005) while during the cortical expansion in the last trimester a threefold increase in the number of cells takes place (Badsberg Samuelsen et al. 2003).

Hansen et al. (2010) recently described classes of radial glia-like (neural stem) cells and transit-amplifying (intermediate progenitor) cells in the human OSVZ

that contribute significantly to neurogenesis. OSVZ radial glia-like cells show unusual cell cycle behaviors that further distinguish them from traditional RG cells (Hansen et al. 2010). Large numbers of radial glia-like cells and intermediate progenitor cells populate the human OSVZ; OSVZ radial glia-like cells have a long basal process but, surprisingly, are non-epithelial as they lack contact with the ventricular surface. They undergo proliferative divisions and self-renewing asymmetric divisions to generate neuronal progenitor cells that can proliferate further. The inhibition of Notch signaling in OSVZ progenitor cells induces their neuronal differentiation. This novel finding that OSVZ progenitors undergo expansive proliferative divisions contrasts with observations of the rodent SVZ – in which intermediate progenitor cells usually divide only once – and provides a new cellular basis for understanding the evolutionary expansion of surface area in human cortex (Hansen et al. 2010; Kriegstein et al. 2006; Martinez-Cerdeno et al. 2006). These results indicate a new mechanism for cortical expansion outside the VZ through the addition of radial columns arising from the OSVZ – the establishment of non-ventricular radial glia–like cells may have been a critical evolutionary advance underlying increased cortical size and complexity in the human brain (Hansen et al. 2010).

There Is No Firm Evidence for Adult Neurogenesis in the Cerebral Cortex of Monkeys and Humans

In the adult mammalian brain, neurogenesis persists in two germinal regions: the SVZ on the walls of the lateral ventricle (Lois and Alvarez-Buylla 1994; Alvarez-Buylla and Garcia-Verdugo 2002; Alvarez-Buylla and Lim 2004) and the subgranular layer of the hippocampal dentate gyrus (Kempermann 2002). In rodents, SVZ astrocytes function as primary progenitors which generate intermediate precursors that function as transit amplifying cells for the generation of large number of new neurons.

Granule cell formation has been found in small numbers in the dentate gyrus of adult monkeys (Kornack and Rakic 1999) and some studies purported to show that there is a long-lasting postnatal granule cell proliferation in the dentate gyrus of both monkey (Gould et al. 1998, 1999a) and the human hippocampus (Murell et al. 1996; Eriksson et al. 1998; Roy et al. 2000). However, only one of these studies indicated granule cell formation in the adult human dentate gyrus (Eriksson et al. 1998), while the other two reports were based on in vitro studies (Murell et al. 1996; Roy et al. 2000). Even these authors later suggested that adult-generated hippocampal and neocortical neurons in macaques have a transient existence (Gould et al. 2001). Furthermore, neurogenesis was not changed in the resected hippocampi of epileptic patients (Seress et al. 2001; Heinrich et al. 2006; Fahrner et al. 2007), and human brain after stroke and irradiation displays very limited possibilities for neuronal repair (Price 2001; Snyder and Park 2002; Arvidsson et al. 2002), in spite of isolated report that adult neurogenesis may occur after stroke (Jin et al. 2006). Adult neurogenesis was also suggested to occur in the monkey striatum (Bedard et al. 2006) and amygdala and adjoining cortex (Bernier et al. 2002). The rostral migratory stream of newly generated neurons (which differentiate into interneurons of the olfactory bulb) has been demonstrated in the brain of adult rodents (Lois and Alvarez-Buylla 1994) and adult monkeys (Kornack and Rakic 2001a; Pencea et al. 2001), but does not occur in adult human brain (Sanai et al. 2004; however, see Bédard and Parent 2004). However, SVZ astrocytes isolated from the adult human brain can function as neural stem cells and can generate new neurons in vitro (Sanai et al. 2004). Previous study observed PSA-NCAM-positive (presumably migrating) cells in the human SVZ of children less than 1 year old, but also did not see similar clusters in adult specimens (Weickert et al. 2000).

Similarly, one initial study suggested neurogenesis for the adult primate neocortex (Gould et al. 1999b), but subsequent studies clearly demonstrated that neurogenesis in the primate and human neocortex is an early prenatal phenomenon (Korr and Schmitz 1999; Kornack and Rakic 2001b; Rakic 1998, 2002a, b, 2006b; Koketsu et al. 2003; Spalding et al. 2005; Bhardwaj et al. 2006; Breunig et al. 2007a). One can safely conclude that there is no firm data to support the claim that neurogenesis would occur in the adult human brain in general, which is in accordance with classical reports on limits of neurogenesis in primates as a form of evolutionary adaptation (Rakic 1985). Pasko Rakic proposed that a stable population of cortical neurons

that lasts throughout the life span has evolved to enable storage of long-term memory and retention of learned experience (Rakic 1985, 2006a, b).

7 The Transformation of the Neocortical Anlage into the Six-Layered Neocortex and Development of the Cortical Map

The transformation of fetal neocortical anlage into the adult six-layered neocortex is a very protracted process, starting during the last trimester and extending to at least 3 or 4 years after birth. This transformation in fact consists of sequential reorganizational events (accompanied by corresponding transient electrophysiological and behavioral phenomena) and, importantly, encompasses the perinatal period in which both transient and permanent cortical circuitry elements coexist (Kostović and Judaš 2006, 2007, 2010). These reorganizational events affect all three major compartments of the fetal neocortical anlage: (1) the marginal zone (with significant changes in Cajal–Retzius neurons and other small neurons, and disappearance of the subpial granular layer); (2) the cortical plate (with gradual appearance of Brodmann's six-layered ontogenetic Grundtypus, intense morphological and chemical differentiation of cortical neurons and ever increasing intensity of synaptogenesis); and (3) the subplate zone, which after birth gradually disappears as a recognizable architectonic entity, but many of its neurons survive into adulthood as the so-called subcortical white matter interstitial neurons (for review, see Judaš et al. 2010a, b). These major reorganizational events enable the final regional and areal differentiation and specification of the cortical map and occur in parallel with increasing myelinization of the cortical white matter. In addition, during the same perinatal period a number of other transient fetal structures (some of which seem to be human-specific) disappear – such as the ganglionic eminence, the gangliothalamic body, the perireticular nucleus, certain transient populations of intracallosal and subcallosal neurons, and so forth (see Sect. 7.5). As the last trimester is also the period of prematurely born babies, which frequently suffer from hypoxic-ischemic brain damage and thus are at risk for poor neurodevelopmental outcome (Leviton and Gressens 2007; Miller and Ferriero 2009; Volpe 2009), it is obvious that the detailed knowledge of these perinatal and postnatal reorganizational events is of great clinical significance – especially if these events can be visualized and used as in vivo biomarkers in modern neuroimaging studies (Ment et al. 2009). Such knowledge is also vital for understanding and (hopefully) managing brain reorganization after pre- and perinatal brain lesions (for review, see Staudt 2010).

7.1 The Transformation of the Marginal Zone into the Neocortical Layer I

7.1.1 The Origin and Fate of Cajal–Retzius Cells

The Cajal–Retzius cells are a special population of large neurons in the fetal marginal zone and the future cortical layer I (Krmpotić-Nemanić et al. 1987; Meyer and Gonzalez-Hernandez 1993; Verney and Derer 1995; Meyer and Goffinet 1998; Meyer and Wahle 1999; Meyer et al. 2000, 2002a, 2003; Abraham et al. 2004a; Cabrera-Socorro et al. 2007; Meyer 2010). They have important functions in the initial establishment of cortical lamination and transient neuronal circuitry of the fetal cortex and they secrete an extracellular matrix glycoprotein reelin (for review see Meyer et al. 1999; Tissir and Goffinet 2003; Meyer 2010). For example, autosomal recessive lissencephaly is associated with human reelin (*RELN*) gene mutations (Hong et al. 2000). The main site of origin of Cajal–Retzius cells destined for the neocortex is the cortical hem (Grove and Tole 1999; Ragsdale and Grove 2001), a putative signaling center at the interface of the prospective hippocampus and the choroid plexus, which is most highly developed in the human brain (Abu-Khalil et al. 2004; Meyer 2010). Additional populations of Cajal–Retzius cells may derive from the thalamic eminence in the ventral thalamus and from the amygdalar hem (Meyer 2010).

The Cajal–Retzius cells may represent a rare example of truly transient fetal neurons, because recent studies indicate that they degenerate and undergo cell death when cortical migration is completed (Meyer 2010); however, this is by no means a generally shared opinion, and the debate on their supposed postnatal existence continues for almost a century (e.g., Marin-Padilla 1984, 1988a, 1992, 1998; Martin et al. 1999).

The first Cajal–Retzius cells in the human neocortical anlage have been observed already at 7 PCW (Larroche 1981; Larroche and Houcine 1982) in the early preplate; they express reelin and continue to increase in number after the appearance of the cortical plate (Meyer 2010).

Some NPY-positive Cajal–Retzius cells can be observed in the human marginal zone already at 14 PCW, but they become quite rare from 36 PCW onward (Uylings and Delalle 1997). At midgestation, most Cajal–Retzius cells in humans are reported to contain calbindin-D28k and calretinin (Verney and Derer 1995; Yan et al. 1997) while only few of them contain parvalbumin (Verney and Derer 1995; Cao et al. 1996). In the human newborn, neocortical layer I contains parvalbumin-positive Cajal–Retzius cells, and many of them display clear signs of degeneration (Ding et al. 2000). There is also a plexus of horizontal parvalbumin-positive fibers in deep layer I, and many small neurons of the layer I also contain parvalbumin (Ding et al. 2000). Finally, human Cajal–Retzius cells are unique because they specifically express the RNA gene *human accelerated regions 1F* (*HAR1F*), part of a region of the human genome that has shown a significant evolutionary acceleration since the divergence of humans and chimpanzees (Pollard et al. 2006).

7.1.2 The Origin and Fate of the Subpial Granular Layer

The subpial granular layer (SGL) is a transient layer composed of small granular cells located within the fetal marginal zone (MZ) and is usually considered specific to human or primate cortex (Brun 1965; Gadisseux et al. 1992; Sidman and Rakic 1982; Bystron et al. 2008; Rakic 2009; for review see Judaš and Pletikos 2010). While it has been frequently stated that the SGL has been recognized only in man, it should be noted that the SGL is also well developed in the fetal monkey cerebral cortex (Zecevic and Rakic 2001); has been observed in fetal brains of sheep, cow, dog, and cat (Ranke 1910; Sanides and Sas 1970); and it has recently been described even in the developing cortex of rodents (Meyer et al. 1998; Jiménez et al. 2003). Nevertheless, it remains true that the SGL is the most prominent (and present during the longest prenatal period) in the human fetal brain. In the human fetal brain, the SGL originates in the paleocortical region at the end of the first trimester of gestation, spreads over the entire cerebral surface during the following 2 months, and disappears progressively during the third trimester (Brun 1965). It seems that the SGL is formed by an extension of the olfactory SVZ (Gadisseux et al. 1992), that is, the prepiriform region of the human fetal basal forebrain (Meyer and Wahle 1999; Meyer et al. 1999), and spreads from this localized fountainhead over the entire neocortex through tangential, subpial migration (Brun 1965; Gadisseux et al. 1992). At least some small neurons of the fetal marginal zone (including probably at least some SGL cells) are generated in the olfactory placode and olfactory primordium, both in humans (Meyer and Wahle 1999) and in monkeys (Zecevic and Rakic 2001). The usual explanation for the gradual disappearance of the SGL is that its cells migrate inwardly into the cortical plate, thus supplementing the cortical contingent of interneurons (Brun 1965; Gadisseux et al. 1992). However, it is worth noting that at least some of the SGL cells degenerate (Gadisseux et al. 1992) and that after 30 PCW the naturally occurring cell death is an active mechanism contributing to the disappearance of SGL cells, but not the Cajal–Retzius cells (Spreafico et al. 1999).

The SGL is clearly not present during the early human preplate stage (4–8 PCW, that is, Carnegie stages 12–22, or embryonic days E31–E51) or during the initial formation of the neocortical plate (8–10 PCW), as demonstrated in a number of studies (Larroche 1981; Marin-Padilla 1983; Zecevic 1993; Zecevic et al. 1999; Meyer et al. 2000, 2002b, 2003; Bystron et al. 2005, 2006). However, when exactly the SGL appears in the human fetal brain remains a somewhat debatable topic. It has been suggested that the SGL appears around 11 PCW (Zecevic and Milosevic 1997; Bystron et al. 2008), or at 12 PCW (Gadisseux et al. 1992), or 14 PCW (Meyer and Goffinet 1998; Meyer et al. 1999), or 15 PCW (Marin-Padilla 1995). The SGL is said to be most prominent from 17 to 26 PCW (Brun 1965), or from 16 to 24 PCW (Meyer and Gonzalez-Hernandez 1993; Meyer and Goffinet 1998; Meyer and Wahle 1999), or fully developed by 25 PCW but already starts to disappear by 26 PCW (Marin-Padilla 1995). The SGL is supposed to disappear by 27–29 PCW (Rakic and Zecevic 2003a), by 28–30 PCW (Meyer and Gonzalez-Hernandez 1993), by 31 PCW (Spreafico et al. 1999), by 35 PCW (Gadisseux et al. 1992; Marin-Padilla 1995), or simply around the end of gestation (Brun 1965).

While some have interpreted SGL cells as glial precursors destined to layer I (Marin-Padilla 1995), a number of subsequent histochemical and immunohistochemical studies demonstrated that most, if not all, SGL cells are indeed neurons (Gadisseux et al. 1992; Meyer and Gonzalez-Hernandez 1993; Meyer and Wahle 1999; Spreafico et al. 1999). The SGL cells are positive for neuronal marker MAP2 and negative for a glial marker GFAP (Gadisseux et al. 1992).

What is the exact developmental fate and possible function of transient SGL cells? According to the traditional interpretation, the SGL in cats, monkeys and humans produces neurons that may descend to the underlying cortical plate and thus contribute to the wealth of interneurons in certain cortical areas (Brun 1965; Zecevic and Milosevic 1997; Zecevic and Rakic 2001).

Another group of researchers proposed that SGL cells basically represent a precursor pool for subsequent development of two main types of Cajal–Retzius cells (Meyer and Goffinet 1998; Meyer et al. 1999). The same group also demonstrated that human fetal SGL cells also express the gene *doublecortin – DCX* (Meyer et al. 2002a). However, it does not seem likely that Cajal–Retzius cells are derived from the SGL, since most of them are already present in the marginal zone before the transient SGL develops (Sidman and Rakic 1982; Zecevic and Rakic 2001). An autoradiographic study in rhesus monkeys (Zecevic and Rakic 2001) also demonstrated that, unlike in rodents, neurons of layer I are generated during the entire 2 month period of corticogenesis. The large Cajal–Retzius cells (which express reelin and calretinin but not GABA) are generated first (E38–E50), while smaller, GABAergic neurons are generated from E43 to E94. These late-generated layer I cells are imported from outside sources such as the olfactory primordium and ganglionic eminence and via a massive SGL that may also supply some GABAergic neurons to the subjacent cortical plate (Zecevic and Rakic 2001). This study demonstrated that in monkey the SGL appears only after the large Cajal–Retzius cells have been generated, and thus the SGL in primates contributes mostly to the later-generated layer I neurons (Zecevic and Rakic 2001). In addition, a recent study using both classical interneuron markers (calretinin, calbindin, and GABA) as well as transcription factors (*NKX2.1* and *DLX* – markers indicating subcortical, i.e., ganglionic eminence origin) demonstrated that the human SGL between 17 and 22 PCW contained a population of small interneurons that originated mainly in the lateral ganglionic eminence/olfactory region, since the majority of these cells were double-labeled with DLX/GABA and rarely with NKX2.1/GABA (Rakic and Zecevic 2003a). But some of these cells also originated from the cortical SVZ (Rakic and Zecevic 2003a), indicating that neurons in the human cortical layer I are heterogeneous, with more complex origin and migratory routes than in rodents.

According to the analysis of our own material, the subpial granular layer develops around 13 PCW, starts to disappear after 28 PCW, and is not visible at 34 PCW (Kostović et al. 2004). It should be noted that the marginal zone of the human neocortex between 18 and 28 PCW displays a very complex six-layered organization (Kostović et al. 2004) and starting from the pia to the cortical plate, the following layers can be distinguished: (1) cell-poor marginal stripe (Randstreifen), (2) the SGL, (3) marginal zone proper, (4) stratum lucidum, (5) deep granular layer, and (6) stratum radiatum.

In conclusion, both the marginal zone and the SGL in the human fetal telencephalon have a complex cell composition, which may change over time. The subpopulations of interneurons that originate in the SGL may be involved in human cortical disorders that do not occur or cannot be mimicked in mice (Rakic 2009). Thus, the developmental fate of the human SGL certainly requires further studies.

7.2 The Dissolution of the Subplate Zone and Postnatal Persistence of Subplate/Interstitial Neurons

As already mentioned, the subplate zone appears at the beginning of the early fetal period, reaches its peak during midgestation, and its dissolution begins during the last third of gestation; however, it remains present under the prefrontal association cortex up to 6 postnatal months (Kostovic and Rakic 1990; Kostovic 1990a, b, b; for an extensive review see Judaš et al. 2010a, b). However, the dissolution of the subplate does not mean that its neurons disappear after fulfilling their presumed prenatal developmental roles. In fact, a large number of these cells survive for a life-time as so-called interstitial white matter neurons (Kostovic and Rakic 1980; for review see Suárez-Solá et al. 2009;

Judaš et al. 2010a, b). In this section our primary goal is to draw attention to a pronounced diversity of morphological and molecular phenotypes of fetal subplate and postnatal interstitial neurons. Various functional roles of the subplate zone were subject of many previous reviews in both experimental animals (Allendoerfer and Shatz 1994; Friedlander and Torres-Reveron 2009; Kanold and Luhmann 2010) and in human brain (Kostović 1990b; Kostović and Judaš 2002a, 2006, 2007, 2010).

7.2.1 Morphological Phenotypes and Projections of Subplate and Interstitial Neurons

We already published a detailed description of morphological differentiation and growth of human subplate neurons, from 10.5 PCW to early postnatal period on the basis of Golgi-stained material (Mrzljak et al. 1988, 1990, 1992; Kostovic and Rakic 1980, 1990). We also used NADPH-d histochemistry which offers a Golgi-like staining of many subplate neurons (Judaš et al. 1999) and postnatal interstitial neurons (Judaš et al. 2010b).

At 10.5 PCW the primordial human subplate contains rich rootlike arborization of descending processes of deep cortical plate neurons as well as more differentiated polymorphous subplate and bipolar neurons (Mrzljak et al. 1988). These polymorphous neurons have two or three dendrites protruding from oval or irregularly shaped cell bodies and branching several times, with axons which either ascend toward the CP or (less frequently) descend toward the IZ. At 13.5–15 PCW, the subplate consists of an upper part (with horizontally spaced rows of cells) which incorporates the primordial subplate of the previous stage, and the pale lower part which displays a fibrillar organization. The subplate neurons are more differentiated, polymorphous, variably oriented, with more branched dendrites and axons which usually run toward the CP. Horizontally oriented neurons are most frequent at the interface of the CP and the upper SP (Mrzljak et al. 1988). Between 17 and 25 PCW, the subplate is the most prominent part of the neocortical anlage and appears as a wide homogeneous zone, and different types of subplate neurons appear within it for the first time: fusiform, pyramidal, inverted pyramidal, and polymorphous (Mrzljak et al. 1988, 1990). Around 20 or 21 PCW, another cell type appears – large, multipolar neurons with three to five long dendrites and axons which either ascend or descend or remain horizontally oriented. From 17 PCW onward, the most frequent Golgi-impregnated subplate neurons were inverted pyramidal neurons with axons ascending toward the CP (Mrzljak et al. 1988). Between 26 and 29 PCW, the subplate remains the widest cortical zone with a rich population of various types of neurons, the polymorphous and fusiform being impregnated most frequently at all depths of the subplate, while large multipolar neurons were usually observed in its superficial part. Between 32 and 34 PCW, subplate neurons displayed a further dendritic differentiation, although the subplate zone is already significantly diminished in size. Subplate neurons displayed varicosities and growth-cone-like terminal tips on dendrites and short, newly formed branches arising from the main dendrites, and it was not possible to demonstrate degeneration of subplate neurons that could parallel the reduction in depth of the subplate zone (Mrzljak et al. 1988). In addition, around 36 PCW another interneuron type appeared in the subplate zone – a small type of neuron with strictly local axonal arborization which probably corresponds to the neurogliaform cell of Ramón y Cajal (Mrzljak et al. 1990). Finally, in the newborn child rather numerous subplate neurons are present below the developing layer VI, although the subplate zone is largely dissolved. However, while all types of subplate neurons could be observed within the 1 mm below the layer VI in the crowns of gyri, at the bottom of sulci the fusiform and bipolar forms predominated (Kostovic and Rakic 1980; Mrzljak et al. 1988).

Thus, the intensive differentiation of subplate neurons into five neuronal types (in the human dorsolateral prefrontal cortex) between 17 and 25 PCW coincides with the ingrowth of afferent fibers into the subplate zone. However, the subplate neurons continue with further dendritic growth even after afferent fibers have relocated to the cortical plate and acquire spine-like protrusions on dendrites during the last trimester of fetal life. In fact, their dendrites continue to grow even after birth and at early postnatal age (Mrzljak et al. 1992). In a quantitative Golgi analysis of 157 subplate neurons it was found that their dendrites grow continuously and their dendritic trees increase in size from the earliest stages studied (13.5 PCW) to the second postnatal month (Mrzljak et al. 1992).

Fusiform neurons with very long dendrites were the most frequently impregnated interstitial cell type in the gyral white matter after birth, and a constant increase of spine number was observed in these neurons between 1 and 7 postnatal month (Mrzljak et al. 1990). In addition, slightly modified pyramidal neurons and multipolar nonpyramidal interstitial neurons are present in the postnatal gyral white matter. While most of them were healthy-looking, some neighboring neurons had disrupted dendrites.

So, an important finding of these studies has been the continuation of dendritic growth and differentiation of new neuronal types in the subplate in the preterm, newborn and early infant (Mrzljak et al. 1988, 1990, 1992). A rich morphological diversity of subplate neuronal types has also been documented in the monkey (Kostovic and Rakic 1980, 1990).

7.2.2 Molecular Phenotypes of Subplate and Interstial Neurons

The neurochemical diversity of subplate neurons surpasses the diversity of their morphological types. Just in the human cortex, the following neurotransmitters, neuropeptides, transmitter-related enzymes and other specific molecular markers have thus far been demonstrated in the subplate neurons and their descendants in the adult brain, the interstitial neurons: GABA (Yan et al. 1992; Zecevic and Milosevic 1997), somatostatin (Kostović et al. 1991b), neuropeptide Y (Uylings and Delalle 1997; Delalle et al. 1997; Wai et al. 2004; Bayatti et al. 2008a), acetylcholinesterase (Kostovic and Rakic 1980), NADPH-diaphorase i.e., nitric oxide synthase (Yan et al. 1996; Yan and Ribak 1997; Judaš et al. 1999, 2010b; Downen et al. 1999; DeAzevedo et al. 2002), MAP2 (Sims et al. 1988; Honig et al. 1996; Bayatti et al. 2008a, b), p75 low affinity nerve growth factor (NGF) receptor (Kordower and Mufson 1992), plasma proteins albumin, prealbumin, transferrin and alpha-fetoprotein (Mollgard and Jacobsen 1984; Mollgard et al. 1984, 1988; Dziegielewska et al. 1993a, b; Saunders et al. 1991, 2008; Wang et al. 2010), transcription factor *Tbr1* (Bayatti et al. 2008a, b; Suárez-Solá et al. 2009; Ip et al. 2010), reelin (Suárez-Solá et al. 2009), calbindin (Yan et al. 1997; Suárez-Solá et al. 2009), calretinin (Suárez-Solá et al. 2009), parvalbumin (Honig et al. 1996), GAP-43 (Benowitz et al. 1989; Honig et al. 1996; Bayatti et al. 2008a, b), nicotinic acetylcholine receptors (Schröder et al. 2001), various glutamate receptors (Talos et al. 2006), vesicular GABA transporter vGAT and synaptophysin (Bayatti et al. 2008a, b), a potassium/chloride cotransporter KCC2 (Bayatti et al. 2008a, b; Wang et al. 2010), a marker for nonphosphorylated neurofilament high molecular weight SMI 32 (Ang et al. 1991; Haynes et al. 2005).

GABAergic neurons were also demonstrated in the subplate zone of the monkey (Huntley et al. 1988; Meinecke and Rakic 1992), as well as $GABA_A$ receptors (Meinecke and Rakic 1992; Huntley et al. 1990). The GABA labeling in neurons beneath the cortical plate appears very early – as early as embryonic days E45–E50 in the monkey (Meinecke and Rakic 1992) or the 14th week of gestation in the human (Yan et al. 1992). Finally, choline-acetyltransferase-immunoreactive subplate neurons were observed in fetal monkey cortex (Hendry et al. 1987a), and monkey subplate and interstitial neurons also contain a variety of neuropeptides: neuropeptide Y (Huntley et al. 1988; Hayashi et al. 1989; Kuljis and Rakic 1989), cholecystokinin (Hayashi et al. 1989), somatostatin (Huntley et al. 1988; Yamashita et al. 1989), substance P (Yamashita et al. 1990) and VIP (Benson et al. 1991).

The presence of a significant population of nitrinergic neurons in the fetal white matter (Judaš et al. 1999) and within the adult subcortical white matter has been reported in almost all studies of the mammalian neocortex and their molecular phenotypes have been investigated in a number of co-localization studies (for extensive review, see Judaš et al. 1999, 2010b). In the human cortex, the majority of nitrinergic interstitial neurons co-express somatostatin and neuropeptide Y. About 70% of nitrinergic interstitial neurons in the subcortical white matter of monkey and human neocortex also contain muscarinic m2-receptors, and approximately 90% of these cells were rich in acetylcholinesterase (Smiley et al. 1998). Nitrinergic axons often form perivascular fiber networks and contact blood vessels (DeFelipe 1993). Thus, it has been frequently suggested that nitrinergic subcortical interstitial neurons are involved in local regulation of cortical microvascular circulation (Estrada and DeFelipe 1998; Suárez-Solá et al. 2009).

7.3 The Transformation of the Cortical Plate into Neocortical Layers II – VI

7.3.1 The Maturation of Morphological and Molecular Phenotypes of Neocortical Neurons

The detailed description of development of several hundreds of distinct morphological and molecular phenotypes of cortical neurons would require a book in itself. The reader may wish to consult our detailed descriptions based on the use of Golgi impregnations (Mrzljak et al. 1988, 1990, 1992) and NADPH-diaphorase histochemistry which also provides a Golgi-like staining of nitrinergic cortical neurons (Judaš et al. 1999, 2010b). In this section, I will rather focus on two topics: (a) a life-span development of prefrontal cortical neurons (Petanjek et al. 2008), and (b) those few studies describing development of neuropeptides (Kostović et al. 1991b; Delalle et al. 1997; Uylings and Delalle 1997; Bayatti et al. 2008a, b; Wang et al. 2010) and calcium-binding proteins (Cao et al. 1996; Yan et al. 1997; Letinic and Kostovic 1998) in the human cerebral cortex.

In a recent quantitative study, we analyzed the postnatal development and lifespan alterations in basal dendrites of large layer IIIC and layer V pyramidal neurons in human prefrontal cortex (Petanjek et al. 2008). The major findings of this study can be summarized as follows. First, both classes of neurons displayed a rapid dendritic growth during the first postnatal months. Second, after a more than year-long "dormant" period of only fine dendritic rearrangement, layer IIIC pyramidal neurons displayed a second period of dendritic growth, starting at the end of the second year and continuing in the third year. Thus, layer IIIC pyramidal neurons (which are the major source of long corticocortical associative connections) appear to show a biphasic pattern of postnatal dendritic development. Finally, subtler forms of dendritic organization were noted until late adolescence and adulthood. In other words, both corticocortical layer IIIC neurons and subcortically projecting layer V neurons in the human prefrontal cortex continue their maturation during the rapid cognitive development in preschool children as well as in the period of protracted cognitive maturation during puberty and adolescence (Petanjek et al. 2008).

Neurons expressing the neuropeptide Y (NPY) display very protracted maturation in the human prefrontal cortex (Delalle et al. 1997; Uylings and Delalle 1997). In the fetal cortex, the majority of NPY neurons were found in the subplate zone (where they appeared already at 14 PCW), and during the first postnatal year subcortical interstitial neurons (surviving remnants of the subplate) also represented the majority of cortical NPY neurons (Delalle et al. 1997). The density of NPY neurons transiently increased within the cortex between 4 and 7 years, and the adult pattern of relatively low density of cortical NPY neurons was reached from about 8 years (Delalle et al. 1997). It is interesting to note that, while at 14 PCW NPY neurons appeared predominantly in the deep subplate, at 28 PCW, the upper subplate contained significantly more NPY neurons than the deep subplate (Delalle et al. 1997); this shift may occur even earlier, during midgestation (Bayatti et al. 2008a; Wang et al. 2010). Very few NPY neurons are present in the CP and SVZ at 15 PCW, but their density increased in all fetal zones from 17 PCW onward (Delalle et al. 1997).

The earliest somatostatin-immunoreactive cells of the human fetal frontal cortex appear in the subplate at 22 PCW (Kostović et al. 1991b). Around 32 PCW the number of somatostatin neurons increases at the interface between the subplate and the cortical plate, but the newborn cortex shows a decline in the overall number of deep somatostatin neurons in parallel with the increase of their numbers in superficial cortical layers (Kostović et al. 1991b).

Calcium-binding proteins calbindin and parvalbumin appear in the human visual cortex prenatally, already at midgestation (parvalbumin; Cao et al. 1996) or in the case of calbindin mainly from 26 PCW onward (Yan et al. 1997), and develop in an inside-out fashion. However, while calbindin expression was consistently high in the visual cortex of newborn, the peak of parvalbumin development occurred only after the second postnatal month (Letinic and Kostovic 1998). Moreover, there was a postnatal reorganization in cortical calbindin expression: the neonatal pattern of high calbindin in layers IV-VI was transformed during infancy and childhood into an adult pattern of high calbindin in layer II, but low calbindin in layer IV and infragranular layers (Letinic and Kostovic 1998). Finally, it should be noted that the development of acetylcholinesterase activity in cortical pyramidal neurons continues until young adulthood (Kostović et al. 1988).

7.3.2 The Development of Brodmann's Ontogenetic Six-Layered Grundtypus and Cytoarchitectonic Differentiation of the Cortical Map

Korbinian Brodmann (Brodmann 1906) was first to note that cytoarchitectonic regional and areal differentiation of the human neocortex begins at 6–8 months of intrauterine life (depending on the region) and occurs by various modifications of the initial (tectogenetic) six-layered Grundtypus (Fig. 5). All cortical areas which develop from this initial six-layered basic type belong to the isocortex (that is, neocortex), while the remaining areas which start to develop from different laminar arrangements belong to the allocortex (that is, paleocortex, archicortex, and several transitional – mesocortical – types between them and the isocortex, such as peripaleocortex, periarchicortex, proisocortex). While this concept over the past century has been criticized on various grounds, it still serves as the basis for recognizing six major neocortical layers (with a number of sublayers). However, Brodmann's initial conception of the allocortex has been substantially modified in studies of Maximilian Rose (Rose 1926, 1927) and I.N. Filimonov (Filimonov 1957), and many others.

Substantial differences in tempo and mode of the prenatal cytoarchitectonic differentiation of isocortical vs. allocortical areas were already noted in classical studies on development of the human brain (His 1904; Brodmann 1906; Hochstetter 1919; Hines 1922; Von Economo and Koskinas 1925; Rose 1926,1927; Filimonov 1957; Macchi 1951; Humphrey 1966, 1967; Yakovlev 1968; Kahle 1969).

While regional and areal differentiation of the neocortex is relatively late perinatal and postnatal event (Kostović 1990a, b; Kostović and Judaš 1995, 2009), cytoarchitectonic specialization and area-specific differentiation of the prospective entorhinal cortex appear surprisingly early in the human fetuses (Kostović et al. 1993). Entorhinal area-specific large neurons appear already at 10 PCW, concomitantly with the appearance of a one-cell-thick layer at the interface between the CP and the marginal zone and with multilaminated spread of the deep part of the CP. This is the earliest sign of area-specific cytoarchitectonic differentiation of all pallial regions characterized by the presence of the typical cortical plate (Kostović et al. 1993). The first subareal differentiation within the entorhinal region begins at 13 PCW with uneven development of fiber-rich lamina dissecans and the appearance of characteristic cell islands of the prospective cortical layer II (Kostović et al. 1993). Similar early development of the hippocampal formation was also noted in several recent studies (Kostović et al. 1989a; Arnold and Trojanowski 1996a, b; Hevner and Kinney 1996; Zaidel 1999; Abrahám et al. 2004a, b). However, it should be noted that although hippocampal formation begins to develop very early in comparison to the neocortex, its entire development is nevertheless a protracted process and neuronal connectivity in the human hippocampus reaches an adultlike complexity between 2nd and 8th postnatal years (Seress and Mrzljak 1992; Seress et al. 2001; Abrahám and Meyer 2003; for an excellent review, see Seress and Abrahám 2008).

With respect to neocortex, due to the limits of space we provide only a brief overview, mainly to point out that neocortical maturation lasts at least two decades after birth. The prospective premotor cortical belt begins to differentiate toward the end of the human fetal life, but its areal specification continues well after birth (Kostović et al. 1987). Between 15 and 26 PCW, the entire frontal cortex displays typical fetal lamination pattern, and regional architectonic differences are more related to maturational gradients than to the areal specification itself. Between 26 and 32 PCW, Brodmann's six-layered Grundtypus and the first regional differentiation appear in the lateral frontal cortex (Fig. 5), but perinatal period is characterized by a notable cytoarchitectonic reorganization and areal parcellation is completed only after birth (Kostović et al. 1987; Kostović 1990a, b; Kostović and Judaš 2009). Typical cytoarchitectonic features of the human auditory cortex also develop during the early postnatal period (Krmpotić-Nemanić et al. 1984, 1988). We recently demonstrated that magnopyramidality (as a key cytoarchitectonic feature of Broca's speech region of the left hemisphere) of area 45 develops between 8 and 12 postnatal months in area 45, and between 8 and 14 months in area 44 (Judaš and Cepanec 2007; Cepanec 2009). These findings indicate that significant cytoarchitectonic changes of fronto-opercular cortex occur at the end of the first postnatal year, in parallel with major developmental changes in language processing/comprehension and production, speech, and other aspects of communication (Cepanec 2009).

Regional and areal specification of the cerebral cortex is also closely related to development of cortical gyri and sulci and corticocortical connections (see Sects. 7.4 and 8.3).

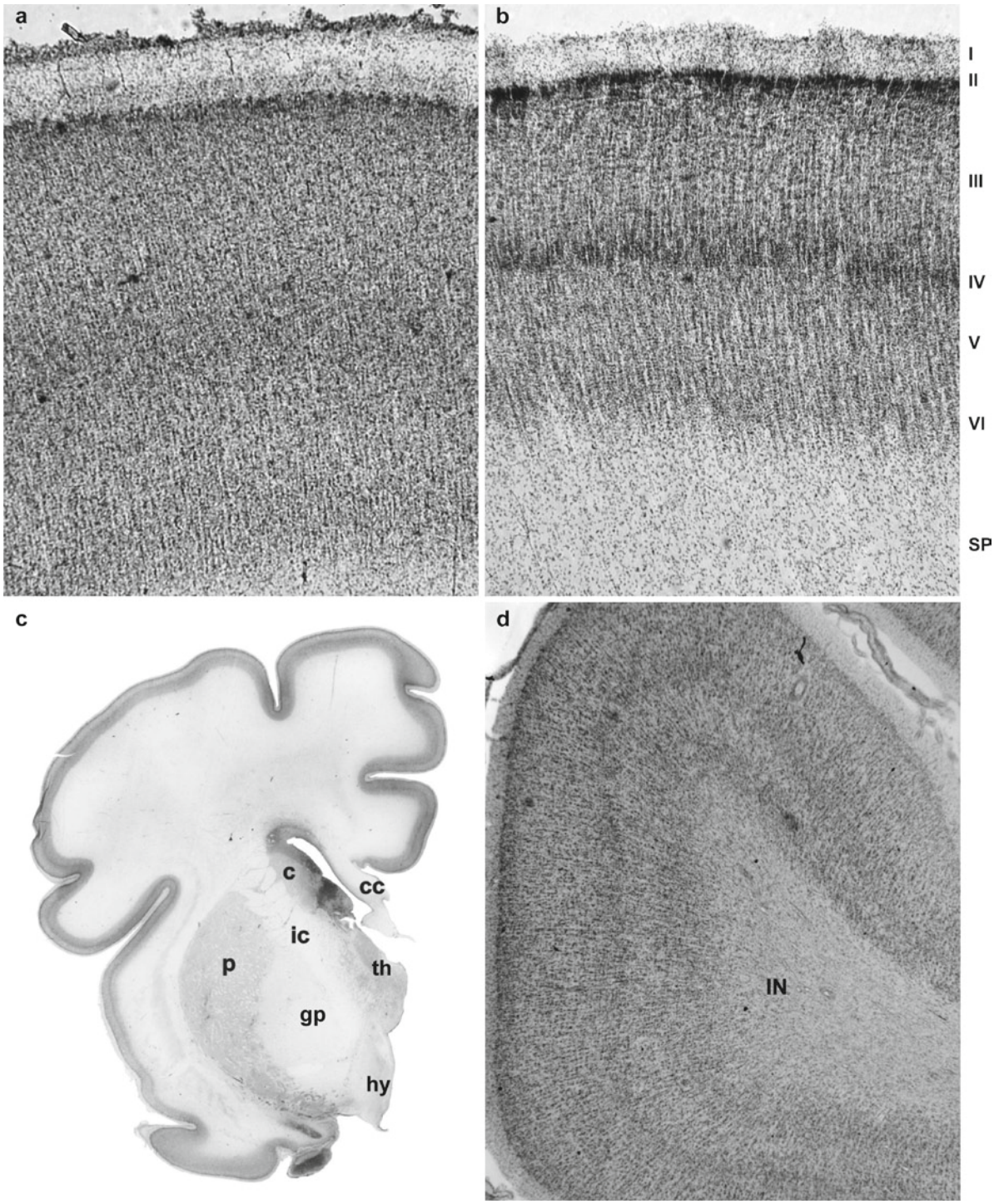

Fig. 5 During the last third of gestation, Brodmann's ontogenetic six-layered Grundtypus gradually develops within the neocortical plate. While at 28 PCW (**a**) its development is just beginning and the lamination is barely recognizable (one can clearly recognize only the uppermost dark band in the CP as the future layer II, a zone of small granular cells in the middle as the future layer IV and the paler band below it as the developing layer V), the Grundtypus is already fully developed at 36 PCW (**b**), after the onset of gyrification (**c** – low power view of Nissl stained section at 36 PCW; note the lamination within the cortical plate). In a 9-month-old infant (**d**) the neocortex is still immature in spite of its adult–like laminar appearance, because dendritic growth of cortical neurons continues during the second and third year after birth (see text) (*I–VI*, developing neocortical layers; *c*, caudate nucleus; *cc*, corpus callosum; *gp*, globus pallidus; *Hy*, hypothalamus; *ic*, internal capsule; *p*, putamen; *Th*, thalamus). IN (in **d**) denotes numerous interstitial neurons in the subcortical white matter, especially within the gyral crowns

7.3.3 The Development of the Cortical Map as Revealed by Recent Molecular and Genetic Studies

Regional and areal differentiation of the cerebral cortex can be revealed even before the appearance of Brodmann's Grundtypus, indicating that it does not depend exclusively on extrinsic afferent input but is largely determined in the cortical protomap (Rakic 1988, 1995; Smart et al. 2002; Lukasziewicz et al. 2005; Dehay and Kennedy 2007; Rakic et al. 2009). Differences between primary and associative visual cortical areas in the human and monkey fetuses can be revealed even by AChE-histochemistry (Kostovic and Rakic 1984, 1990). The development of correct topological connections in early enucleated monkeys indicates that basic connections and chemoarchitectonic characteristics can form in the absence of afferent input (Rakic 1988; Rakic et al. 1991; Dehay et al. 1991, 1993; Kennedy and Dehay 1993; Dehay and Kennedy 2007).

Previous work in rodents has identified a number of transcription factors expressed in gradients across the neocortex that appear to control cortical parcellation (Grove and Tole 1999; Bishop et al. 2000; Monuki and Walsh 2001; Ragsdale and Grove 2001; Fukuchi-Shimogori and Grove 2001; Muzio et al. 2002; O'Leary and Nakagawa 2002; Hamasaki et al. 2004; Molnár et al. 2006; O'Leary et al. 2007; Kim et al. 2007; Kudo et al. 2007). Changes in expression of morphoregulatory molecules can even shift anterior/posterior areal boundaries in the developing rodent neocortex (Fukuchi-Shimogori and Grove 2001).

However, there are few such studies in primates or humans. In fetal rhesus monkey, the gradients or region-specific distribution of various morphoregulatory molecules in the embryonic cerebral wall also contribute to the formation of specified axonal pathways and parcellation of cortical areas (Donoghue and Rakic 1999; Sestan et al. 2001; Watakabe et al. 2007). Several recent studies performed on embryonic and fetal human material have indicated that even with respect to gradients of gene expression there are significant differences between rodents and humans (Lako et al. 1998; Abu-Khalil et al. 2004; Lindsay and Copp 2005; Lindsay et al. 2005; Sarma et al. 2005; Bayatti et al. 2008a, b; for review see Kerwin et al. 2010; Ip et al. 2010; Wang et al. 2010). Especially interesting are findings from recent studies on the role of *WNT* and *BMP* genes in the establishment of dorso–ventral (Lako et al. 1998; Patapoutian and Reichardt 2000; Abu-Khalil et al. 2004) and left-right polarity axis (Gebbia et al. 1997; Geschwind and Miller 2001; Yost 2001) in human embryos because the functional specialization of the human cerebral cortex for language depends on the asymmetric development of cerebral hemispheres.

7.4 The Development of the Human Cortical Gyrification

According to the radial unit hypothesis (Rakic 1988, 1995), the surface area of the cortex is determined by the number of radial units in the protomap formed during the phase of symmetrical divisions, while the cortical thickness is determined by number of asymmetrical divisions within radial units. Greater surface area equates to a larger amount of cortical gray matter and thus greater computational power (White and Hilgetag 2008), and the phylogenetic increase in the surface area of the human brain has far exceeded growth in the cortical thickness (Welker 1990). For example, in comparison to macaque monkeys, the surface area of the human brain is approximately ten times greater (see Fig. 1), whereas the human cortex is only twice as thick (Rakic 1995). The convoluted human cortex is about three times as large as the inner surface of the skull (Welker 1990; Van Essen 1997; Hilgetag and Barbas 2005, 2006; Toro and Burnod 2005). It also appears that gyrification is strongly related to absolute increases in brain size, because prosimian and primate brains of up to 10 cm^3 volume are generally lissencephalic, while for larger volumes there is a close correlation between the degree of gyrification and absolute brain size (Zilles et al. 1989; White and Hilgetag 2008).

The development of gyri and sulci is also closely related to the ingrowth of thalamocortical afferents (White et al. 2002) and especially to the amount and diversity of long and short commissural and ipsilateral corticocortical fibers (Kostovic and Rakic 1990; Price et al. 2006). This notion is also supported by experimental findings in rhesus monkeys, in which local and remote changes of gyrification have been observed after experimental white matter lesions in the developing animal (Goldman-Rakic 1980; Goldman-Rakic and Rakic 1984).

While most visible changes in brain morphology occur primarily during the third trimester (between 24 and 38 PCW, see Fig. 1) and continue during the first few years after birth (Retzius 1896; Chi et al. 1977; Sidman and Rakic 1982; Feess-Higgins and Larroche 1987; Kostović 1990b; Leuba and Kraftsik 1994; Naidich et al. 1994; Armstrong et al. 1995; Bayer and Altman 2004; Dubois et al. 2008a, b), more subtle brain changes (e.g., density changes of cells within the neuropil, dendritic and synaptic alterations, an increase in myelination) can be seen throughout childhood and adolescence, even into early to middle adulthood (White and Hilgetag 2008). For example, there are life-span changes of dendrites and dendritic spines (Jacobs et al. 1997). The so-called gyrification index (Zilles et al. 1988, 1989) increases dramatically during the third trimester of fetal life, then remains relatively constant throughout development (Armstrong et al. 1995; but see Magnotta et al. 1999 for different interpretation).

The brain surface morphology continues to change as well during the adolescence and adult life (Jernigan and Tallal 1990; Jernigan et al. 1991a, b; Pfefferbaum et al. 1994; Caviness et al. 1996; Giedd et al. 1996a, b, 1999a; Sowell et al. 1999a, b, 2001a, b, 2002a, b, 2003, 2004a, b; Giedd 2004; Gogtay et al. 2004; Shaw et al. 2006; for review, see Lenroot and Giedd 2006; O'Hare and Sowell 2008). During that period, the gyri become steeper and the sulci develop a broader appearance (White and Hilgetag 2008). Thus, the processes of gyrification lead to systematic morphologic differences in different cortical regions and areas, affecting overall thickness, lamination and cellular morphology (Kostovic and Rakic 1990; Welker 1990; Van Essen 1997; Hilgetag and Barbas 2005, 2006; Toro and Burnod 2005). The potential clinical relevance of these observations lies in the fact that systematic differences have been observed in white matter as well as gyrification between normal subjects and patients with a variety of developmental, neurological or mental disorders (for review, see White and Hilgetag 2008; Rakic 2009).

There is a significant cortical sulcal variability in children (Sowell et al. 2002a, b) and adults (Narr et al. 2001). There is also a sexual dimorphism (Giedd et al. 1997; De Bellis et al. 2001), with the female cerebral cortex more strongly convoluted than the male cortex (Luders et al. 2004). The surface morphology of the human brain displays much greater variability than brain volume or subcortical brain regions (Bartley et al. 1997; White et al. 2002). In monozygotic twins, the deeper and developmentally earlier sulci are more highly correlated than the tertiary sulci (Lohmann et al. 1999). However, it should be noted that in monozygotic twins the majority of the morphologic variance between the brain surface morphology was a result of random environmental effects, while brain size appeared to be strongly determined by genetic factors (Bartley et al. 1997; Thompson et al. 2001; White et al. 2002). In addition, monozygotic twins discordant for handedness exhibited differing degrees of asymmetry of the planum temporale (Steinmetz et al. 1995).

Finally, it should be noted that neurobiological mechanisms underlying the development of cortical gyri and sulci are as yet unknown. Accordingly, there are several concurrent theories, such as the theory that the gyri form as a result of active growth of specific brain regions (Le Gros Clark 1945) or various mechanical theories of gyrification which assume the physical self-organization of the brain (Richman et al. 1975; Van Essen 1997; Hilgetag and Barbas 2005, 2006; Toro and Burnod 2005; for an excellent review, see Welker 1990).

7.5 Other Transient and/or Human-Specific Structures and Populations of Neurons

7.5.1 The Corpus Gangliothalamicum

The corpus gangliothalamicum is a transient structure located beneath the surface of the pulvinar adjacent to the telo-diencephalic sulcus in human fetuses between 15 and 34 PCW (Rakic and Sidman 1969; Letinić and Kostović 1997; Letinic and Rakic 2001). In Nissl-stained sections, the gangliothalamic body is a thin cellular layer situated beneath the thalamic surface near the telo-diencephalic junction, and in Golgi- and MAP2-stained sections it is a stream of mostly bipolar cells extending from the ganglionic eminence to the medial thalamus (Letinić and Kostović 1997). It was subsequently shown that this structure is composed of tangentially migrating GABAergic interneurons from the ganglionic eminence to the pulvinar and lateral posterior nucleus of the thalamus, because these migrating neurons are GAD- and Dlx-positive and guided by

homotypic-neurophilic cues (Letinic and Rakic 2001). The corpus gangliothalamicum and its migrating cells could not be identified in any nonhuman species so far examined including rodents, carnivores and even nonhuman primates (Clowry et al. 2010).

7.5.2 The Perireticular Nucleus

The internal capsule of the human fetus contains a large number of distinct interstitial neurons which express MAP2, somatostatin, calbindin-D28k, AChE, and p75 low-affinity NGF receptor (Letinić and Kostović 1996a). This cell population corresponds to the perireticular nucleus (Mitrofanis and Guillery 1993; Earle and Mitrofanis 1996) previously described in the rat (Mitrofanis and Baker 1993; Adams and Baker 1995), cat, and ferret (Clemence and Mitrofanis 1992; Mitrofanis 1994). The number of neurons in the human perireticular nucleus gradually increased up to 32 PCW (Tulay et al. 2004), but subsequently the nucleus rapidly decreases in size during early infancy (Tulay et al. 2004; Letinić and Kostović 1996a) and few cells are apparent in the 1-year-old infant (Letinić and Kostović 1996a).

7.5.3 Intracallosal and Subcallosal Neurons

Transient cells are also present in the human fetal subcallosal zone, which occupies a paramedian territory situated between the developing corpus callosum dorsally and bundles of the fornix ventrally (Kostović et al. 2002b). The midline portion of this subcallosal region is the part of the septohippocampal continuum and corresponds to the nucleus septohippocampalis, while the left and right paramedian portions contain radial glial cells and continue directly into the SVZ of the dorsal neocortical telencephalic wall. In other words, paramedian subcallosal zones represent a dorsal allocortical counterpart of the SVZ (Kostović et al. 2002b). Transient fetal presence of neurons and glial cells in the subcallosal zone suggests that they may be involved in the guidance of callosal axons, while the cells of the septohippocampal continuum may have a pivotal role in the bidirectional growth of fornix system fibers (Kostović et al. 2002b; Jovanov-Milošević et al. 2009). Furthermore, we recently described a separate population of fetal intracallosal neurons, which remain to be present even in the postnatal human corpus callosum as a special subset of interstitial neurons (Jovanov-Milošević et al. 2010).

7.5.4 Transient Patterns in the Human Fetal Striatum and Amygdala

Transient patterns of organization are also notable in the human fetal striatum, as revealed by calbindin-D28k expression (Letinić and Kostović 1996b) or by compartmentalization of NADPH-diaphorase staining (Sajin et al. 1992) and AChE-staining and Nissl staining (Vukšić et al. 2008). In the human fetus, the developing lateral amygdaloid nucleus (which is the largest and most differentiated of all nuclei in the amygdaloid complex of man) displays a transient presence of discrete cytoarchitectonic units which are especially prominent between 12.5 and 16 PCW (Nikolić and Kostović 1986).

7.5.5 Nucleus Subputaminalis (Ayala)

Giuseppe Ayala was first to describe the nucleus subputaminalis, that is, a small magnocellular group of neurons located within the rostrolateral extension of the basal forebrain in the human and chimpanzee brain (Ayala 1915, 1924). We recently demonstrated that the nucleus subputaminalis is a special subgroup of cholinergic magnocellular neurons (Šimić et al. 1999). On the basis of their location and projection trajectory, these cholinergic neurons are probably connected with the frontal cortical speech area and may be human specific since they were not described in nonhuman primates (Šimić et al. 1999).

8 The Development of Cortical Synapses, Input–Output Connectivity and Intracortical Neuronal Circuitry

The synaptogenesis, morphological and chemical maturation of cortical neurons, and the development of cortical circuitry are all tightly related to ingrowth of cortical afferents and outgrowth of cortical efferent projections (Mrzljak et al. 1988, 1990, 1992; Kostović 1990a, b; Kostović and Judaš 2002a, 2006, 2007, 2010; Kostović and Jovanov-Milošević 2006). While all of

these processes begin prenatally, most of them continue and even intensify during the first two postnatal years, and some of them (for example, synaptogenesis, fine reorganization of dendritic spines, and terminal dendritic and axonal arborizations) in fact continue throughout the life-span, reaching the adult steady-state dynamical equilibrium during the third decade (for review, see Petanjek et al. 2008; Kostović et al. 2008; Kostović and Judaš 2009; Rakic et al. 2009).

8.1 *Synaptogenesis Begins during the Initial Formation of the Cortical Plate, Intensifies during the Third Trimester and Even More after Birth, Reaches its Peak in Early Childhood, and Then Slowly Diminishes until the Third Decade of Life*

8.1.1 Initial Synaptogenesis (8–20 PCW) is Bilaminar and Occurs outside the Cortical Plate, within the Marginal and the Subplate Zone

The study of synaptogenesis was instrumental in the initial discovery of the human subplate zone (Kostović and Molliver 1974; for review, see Judaš et al. 2010a). The first synapses appear in the neocortical anlage very early – in the marginal zone at 7 PCW, that is, in a 20 mm CRL human embryo (Larroche 1981; Larroche and Houcine 1982), or at 8 PCW, concurrently with the formation of the cortical plate (Molliver et al. 1973; Zecevic 1998). It is important to note that the initial distribution of early synapses is bilaminar – they are situated above and below the cortical plate but not within it (Molliver et al. 1973). This early bilaminar synaptogenesis in the neocortex has been confirmed in subsequent studies of 10 PCW-old human fetuses (Povlishock 1976; Larroche et al. 1981). In fact, in the human dorsolateral (motor-sensory) pallium, between 8.5 and 18 PCW synapses are present above and below the cortical plate, but never within it (Molliver et al. 1973). At 15 PCW, the E.M. of the subplate revealed a band of swollen processes and an increased extracellular space; all the synapses were presumably axo-dendritic and asymmetric (Molliver et al. 1973). From its initial formation (between 10 and 15 PCW) until 23/24 PCW, the SP represents the major site of neocortical synaptogenesis. The synaptogenesis also starts in the human cingulate subplate as early as 11 PCW (Kostović and Krmpotić 1976). Early bilaminar synaptogenesis was also demonstrated above and below the hippocampal cortical plate in 15 and 16.5 PCW human fetuses (Kostović et al. 1989a). However, in contrast to the neocortex (where the majority of early synapses were present in the subplate zone), the hippocampal archicortex displayed the prevalence of early synaptogenesis in the superficial marginal zone (Kostović et al. 1989a).

8.1.2 The Synaptogenesis within the Cortical Plate (Ca. 23 PCW Onward) Begins with Relocation of Waiting Afferents from the Subplate into the Cortical Plate

The earliest synapses found within the cortical plate were at 23 PCW – but the onset of synapse formation within the CP cannot be precisely dated because no fetuses from 19 to 22 PCW were analyzed (Molliver et al. 1973). The synaptogenesis within the CP occurs progressively in a deep-to-superficial fashion from 23/24 PCW onward, when thalamocortical and other afferent axons start to relocate from the "waiting" compartment of the subplate into the cortical plate (Kostović and Judaš 2002a, 2010). Thus, intense synaptogenesis within the cortical plate occurs in parallel to the ingrowth of cortical afferents as well as an intense dendritic differentiation of CP neurons; both processes intensify during the last trimester (Mrzljak et al. 1988, 1990, 1992; Kostović and Judaš 2002a, 2010). However, it is important to note that both synaptogenesis and neuronal differentiation are predominantly postnatal processes, which start during the last trimester but continue for several years after birth. Similarly, the myelination begins during the last trimester, but reaches its peak during the first and second postnatal year and continues until adulthood (see Sect. 8.6).

8.1.3 The Postnatal Continuation of Synaptogenesis: Rapid Initial Overproduction and Protracted Elimination of Supernumerary Synapses

Cortical synaptogenesis in primates, and particularly in the human, is a prolonged postnatal process that involves overproduction of axons, synapses and dendritic spines and their later elimination in response to

environmental influences (Rakic et al. 1994; Bourgeois et al. 2000; Rakic et al. 2009; Kostovic and Judas 2009, 2010). In the macaque monkey, the synaptogenesis peaks after birth and lasts at least 3–4 years (Bourgeois et al. 2000), and in the human it lasts at least 15–19 years (Huttenlocher 1979; Huttenlocher et al. 1982; Huttenlocher and Dabholkar 1997; Rakic et al. 2009) and probably extends into the third decade (Petanjek et al. 2008; Kostović et al. 2008; Kostović and Judaš 2009, 2010). In the rhesus monkey, during the first 2–3 postnatal months, synaptic density increases rapidly and reaches a peak that is about two times higher than in the adult and remains well above the adult level throughout infancy and adolescence (for review, see Rakic et al. 1994; Bourgeois et al. 2000). Pasko Rakic and collaborators calculated that in the visual cortex (single hemisphere) of the rhesus monkey during puberty about 1.8×10^{11} synapses are lost – meaning that during this period about 2,500 synapses were lost each second (Bouergeois et al. 2000; Rakic et al. 2009). Nevertheless, because of concurrent overproduction of synapses, the net number still remains above the adult value. The density of major neurotransmitter receptors in the monkey cortex also reaches its peak between 2 and 4 months of age and then declines to the adult level during the period of sexual maturation (Lidow et al. 1991).

Postnatal synaptogenesis is not restricted to neocortical layers I–VI, but also continues on interstitial white matter neurons (Kostovic and Rakic 1980, 1990) which are surviving subplate neurons (for review, see Judaš et al. 2010a, b). Synaptic junctions are observed on both the perikarya and dendrites of interstitial neurons, but the number of synapses on the perikaryon is relatively low (Kostovic and Rakic 1980). The number of axosomatic synapses decreases with age in parallel with an increase in the number of synapses on the dendrites (Kostovic and Rakic 1980). Axosomatic synapses were both symmetrical and asymmetrical, and both types lack dense core vesicles but contain round and clear vesicles. Axodendritic synapses were asymmetrical, with clear round vesicles and their number increased during postnatal maturation (Kostovic and Rakic 1980). Therefore, Kostovic and Rakic (1980) proposed that axons forming asymmetrical synapses may originate from thalamus or other cortical areas (or even from monoaminergic brain stem neurons), while axons forming symmetrical synapses may arise from nearby interstitial cells, that is, from local circuit neurons. The polymorphic interstitial neurons situated immediately subjacent to the cortex might also receive a local circuit input from overlying cortical cells.

8.2 Cortical Afferents Initially Navigate through the Intermediate Zone, Then Establish Temporary Synapses in the Waiting Compartment of the Subplate Zone, and Finally Relocate into the Cortical Plate

Before cortical afferent axons can reach the appropriate target cells within the cortical plate, they first have to navigate through the intermediate zone and then wait (that is, establish temporary synapses) in the subplate zone. All that occurs while neurons of the cortical plate are still being generated in VZ/SVZ and migrate through the intermediate and subplate zone. Thus, one can expect that the subplate zone is not only the waiting compartment for ingrowing afferents but also enables important signaling interactions between these afferents and migrating cortical neurons before they reach the cortical plate. The midgestation represents a crucial period for these interactions, because cortical afferents accumulate and wait in the subplate between 15 and 23 PCW, and relocate to the cortical plate approximately between 24 and 28 PCW – to be precise, that occurs at least with thalamocortical and cholinergic afferents, while corticocortical connectivity displays much more protracted development (see below).

As already stated, the fetal white matter occupies the inner (periventricular) half of the telencephalic wall, and consists predominantly of the intermediate zone (Fig. 6). However, it should be noted that in the human fetal brain a significant contingent of input and/or output connections also grows through the SVZ (Kostovic et al. 2002a; Smart et al. 2002; Judaš et al. 2005; Rakic 2009). The fetal white matter is composed of a number of different contingents of growing axons: (1) noradrenergic, dopaminergic, and serotoninergic afferents from the brain stem; (2) histaminergic afferents from the hypothalamus; (3) cholinergic afferents from the basal forebrain; (4) thalamocortical afferents; (5) afferents from amygdala and claustrum; (6) corticofugal efferent projections to thalamus, striatum, claustrum, amygdala, and various brain stem and

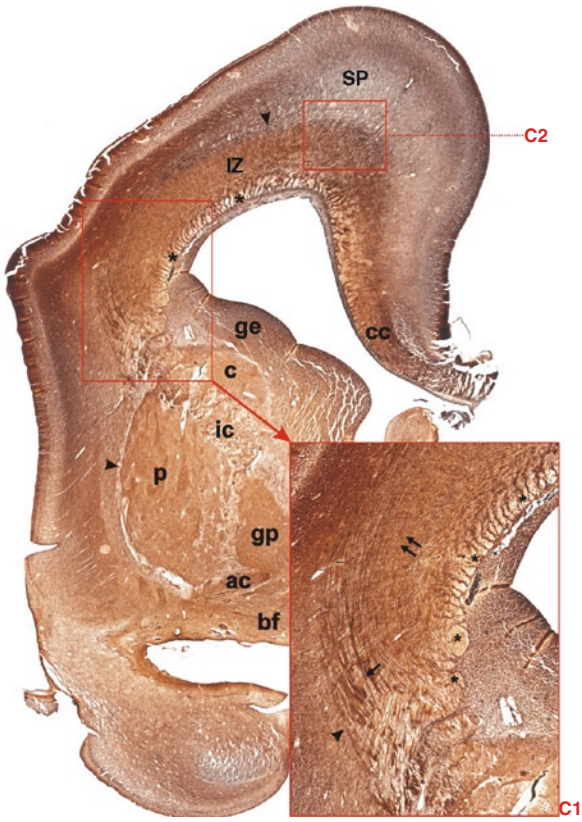

Fig. 6 The coronal section through the telencephalon at 18 PCW, Gallyas silver impregnation by means of physical development. Note that fiber bundles and their crossings are located in the fetal white matter, that is, in the periventricular region (C1, C2, and *asterisks*), and the intermediate zone (IZ), whereas the subplate zone (SP) is characterized by a loose ("isotropic") argirophylic network of fibers. The fetal white matter consists of tangentially stratified fiber bundles such as external capsule (*arrowheads*), corpus callosum radiation (cc), thalamocortical projection fibers (*arrow*), and the deep system (*double arrows*, see insert C1). In addition, a prominent periventricular system of unstained and transversely or obliquely cut fiber bundles (*row of asterisks*) is situated in the subventricular zone (*a*, amygdala; *ac*, anterior commissure; *bf*, basal forebrain; *c*, caudate nucleus; *C1*, *C2*, crossroad areas; *cc*, corpus callosum; *ge*, ganglionic eminence; *gp*, globus pallidus; *ic*, internal capsule; *iz*, intermediate zone; *p*, putamen; *sp*, subplate zone; *th*, thalamus) (From Judaš et al. (2005). With permission)

spinal cord targets; and (7) last, but not least, the huge amount of corticocortical (ipsilateral and commissural/callosal) fibers. At the same time, the fetal white matter contains radially and tangentially migrating neurons, oligodendrocyte precursors and developing astrocytes.

While some of those axonal systems are relatively well studied in both human and monkey fetuses (e.g., thalamocortical, monoaminergic, cholinergic, corticospinal, commissural and some long ipsilateral corticocortical projections), very few data are available on development of corticostriatal, corticothalamic, and short corticocortical projections, while there are simply no available data on development of potentially important bidirectional connections between cortex and amygdala or claustrum, as well as histaminergic hypothalamic projections.

These growing axons in the human fetal white matter can be visualized by a variety of classical and modern approaches: any modification of classical Weigert method (Yakovlev and Lecourse 1967), Bielschowsky's silver impregnation to identify the intensely argyrophilic neurofilaments (Haynes et al. 2005), Gallyas silver impregnation by means of physical development (Judaš et al. 2005), histochemical staining with Luxol-fast-blue for myelin (Brody et al. 1987; Kinney et al. 1988, 1994), acetylcholinesterase (AChE) histochemistry (Kostovic and Goldman-Rakic 1983; Kostovic and Rakic 1984, 1990; Kostovic 1986), or immunocytochemical visualization of growth associated protein GAP-43 which is a marker of axonal growth and elongation (Milosevic et al. 1995; Kanazir et al. 1996; Honig et al. 1996; Haynes et al. 2005), anti-SMI 312, a pan-marker of neurofilaments (Sasaki et al. 1988; Haynes et al. 2005), anti-SMI 32, a marker for nonphosphorylated neurofilament high molecular weight – NFH (Ang et al. 1991; Haynes et al. 2005), anti-SMI 31 which stains phosphorylated NFH and is used as a marker of axonal maturity (Verney and Derer 1995; Zecevic et al. 1999; Haynes et al. 2005), myelin basic protein (MBP) immunocytochemistry (Back et al. 2001, 2002; Jakovcevski and Zecevic 2005a; Haynes et al. 2005), synaptophysin or SNAP25 (Judaš et al. 2005; Vasung et al. 2010a, b) or even DiI tracing method on postmortem material (Burkhalter 1993; Burkhalter et al. 1993; DeAzevedo et al. 1997; Hevner 2005).

Most of these methods are useful for a general analysis of axonal growth, but only few of them enable visualization of specific projection system; for example, AChE-histochemistry for thalamocortical afferents (Kostovic and Rakic 1984, 1990) or cholinergic basal forebrain afferents (Kostović 1986), and immunocytochemical visualization of catecholaminergic (Verney 1999) or serotoninergic afferents (Verney et al. 2002). For example, GAP-43 fibers (which probably corresponded to monoaminergic afferents) were

observed in human embryos as early as 4 PCW (Milosevic et al. 1995). Honig et al. (1996) demonstrated that between 14 and 22 PCW the GAP-43 immunoreactivity was prominent in the subplate and marginal zone neuropil and in the fibers running near the VZ, while GAP-43 fibers appeared in the cortical plate from 22 PCW onward. Similarly, Haynes et al. (2005) noted the highest level of GAP-43 expression from 21 to 64 PCW. On the other hand, anti-SMI 312 stained axons as early as 23 PCW, anti-SMI 31 showed relatively low levels of staining from 24 to 34 PCW, and anti-SMI 32 primarily stained neuronal cell bodies (Haynes et al. 2005).

8.2.1 MRI Tractography Enables the in Vivo Analysis of Growing Cortical Pathways

Over the past decade the development of MRI tractography, such as diffusion tensor imaging (Hüppi et al. 1998, 2001; Prayer et al. 2001; Prayer and Prayer 2003; Hüppi and Dubois 2006; Chung et al. 2009; Ment et al. 2009; Lodygensky et al. 2010) has increasingly enabled the visualization and analysis of growing axonal pathways in the human fetal brain (Berman et al. 2005; Bui et al. 2006; Huang et al. 2006, 2009; Counsell et al. 2007; Dubois et al. 2008c; Kasprian et al. 2008; Kim et al. 2008; Aeby et al. 2009). In an initial MRI-histological correlation study of 15 to 36 PCW human fetuses, we demonstrated the presence of periventricular fiber crossroads rich in extracellular matrix and axonal guidance molecules (Judaš et al. 2005). These periventricular crossroads of growing cortical pathways (Figs. 6 and 8) represent a hitherto unrecognized and vulnerable cellular and topographic target in which combined damage of association-commissural and projection fibers may explain the complexity of cognitive, sensory, and motor deficit in survivors of periventricular white matter lesions (Judaš et al. 2005). We recently succeeded in combining histological approaches with diffusion tensor imaging to investigate prenatal development of human fronto-limbic pathways (Vasung et al. 2010a) and to demonstrate the existence of early, prominent and hitherto undescribed periventricular fiber system which is related to ganglionic eminence and striatum and contains forerunners of adult associative and projection cortical pathways (Vasung et al. 2010b). This periventricular system of growing pathways appears in the early fetal period (10–13 PCW), and in the midfetal period (15–18 PCW) already consists of four major components: the corpus callosum, the fronto-occipital fascicle, the fronto-pontine pathway, and the subcallosal fascicle of Muratoff (Vasung et al. 2010b).

8.2.2 The Development of Catecholaminergic and Serotoninergic Cortical Afferents

The presence of monoaminergic cell bodies at 7 PCW (Olson et al. 1973) and early ingrowth of monoaminergic afferents to the human telencephalic wall at 12 PCW were demonstrated already in classical histochemical studies (Nobin and Björklund 1973; Olson et al. 1973). Later immunocytochemical studies have confirmed and expanded these findings. The tyrosin hydroxylase (TH) immunoreactive catecholaminergic groups of neurons are present in human embryos at 4.5–6 PCW (Puelles and Verney 1998; Freeman et al. 1991; Verney et al. 1991; Zecevic and Verney 1995; Ugrumov et al. 1996; Almqvist et al. 1996). At the end of the embryonic period, TH-positive (dopaminergic) axons run through the central tegmental tract from the medulla oblongata to the mesencephalon, and together with those from locus coeruleus and dopaminergic axons from substantia nigra and ventral tegmental area form the medial forebrain bundle (Zecevic and Verney 1995; Puelles and Verney 1998). No TH-positive fibers penetrate the primordial plexiform layer at 6 PCW, but when the cortical plate starts to form at 7/8 PCW, the first TH positive fibers penetrate the lateral frontal cortex (Verney 1999). These fibers run in the intermediate zone, below the cortical plate, and few fibers are also present in the marginal zone. Thus, the arrival of catecholaminergic axons coincides with the formation of the cortical plate (Zecevic and Verney 1995; Verney 1999). Noradrenergic (dopamine-beta-hydroxylase-immunoreactive, DBH-ir) axons penetrate the telencephalic wall in a pattern similar to dopaminergic axons and at the same time (Zecevic and Verney 1995; Verney 1999). The dopaminergic and noradrenergic axons penetrate the subplate before other afferents and their waiting period (before the penetration into the cortical plate) in the subplate lasts for about one month (Verney 1999). Therefore, it is also probable that the first synapses observed above and below the cortical plate at 7 or 8 PCW (Molliver et al. 1973; Larroche and Houcine 1982) in fact belong to catecholaminergic

axons. There is also a rostrocaudal gradient of penetration of catecholaminergic axons, so that at 13 PCW they invade occipital subplate while at the same time they already penetrate the cortical plate in the frontal region, mostly ascending from fibers in the subplate and only rarely descending from the marginal zone (Zecevic and Verney 1995; Verney 1999).

At 20–24 PCW, there is a widespread dopaminergic and noradrenergic innervation of the frontal cortex (Verney et al. 1993), with the densest dopaminergic innervation in the anlage of the motor and cingulate and insular cortices. Noradrenergic afferents are less numerous than dopaminergic in all cortical areas studied (Verney et al. 1993; Verney 1999). In all areas, the upper subplate and the deep cortical plate are densely innervated by catecholaminergic axons, whereas fewer axons are present in the molecular zone and intermediate zone (Verney 1999). However, the development of dopaminergic innervation continues in the cortex long after birth. For example, in rhesus monkeys prefrontal cortex a transient sprouting of dopaminergic fibers was observed during postnatal development with a peak at adolescence and a decrease in adulthood (Rosenberg and Lewis 1995).

The development of cortical serotoninergic innervation was studied in human embryos and fetuses by immunocytochemistry of the vesicular monoamine transporter (VMAT2 – a general monoaminergic marker) and the high-affinity serotonin transporter (SERT) which is a marker of the serotoninergic axons (Verney et al. 2002). The serotonergic fibers from brainstem raphe nuclei appeared as thick varicose fibers in the medial forebrain bundle, where they were less numerous than the VMAT2-immunoreactive axons (Verney et al. 2002). However, they displayed a similar developmental sequence as dopaminergic and noradrenergic fibers: they reached the cortical anlage at 8 PCW, reached the subplate at 10 PCW, and started to penetrate the cortical plate at 13 PCW (Verney et al. 2002). However, it should be noted that at 12–14 PCW, SERT-immunolabeled fibers were observed in the rostral and caudal limbs of the internal capsule that do not correspond to serotoninergic fibers, but do coincide with the calbindin D28k-labeled thalamocortical fiber tracts (Verney et al. 2002).

The early embryonic appearance of serotoninergic axons has also been reported in the entorhinal cortex of the rhesus monkey (Berger et al. 1993), and in monkey the serotonin terminal network matures very rapidly during early postnatal life, contrary to the protracted development of the dopaminergic innervation (Lambe et al. 2000).

8.2.3 The Development of Cholinergic Cortical Afferents

In the human fetus, the first sign of histochemical differentiation of the basal telencephalon is the appearance of a dark AChE-reactive spot situated between the developing striatum and basal telencephalic surface as early as 9 PCW (Kostović 1986). At 10.5 PCW, the nucleus basalis complex significantly increases, and strongly AChE-reactive neuropil occupies the sublenticular, diagonal and septal areas, while one well developed AChE-reactive fiber bundle extends through the external capsule toward the neocortical anlage (but does not reach it yet) and another fiber bundle runs through the precommissural septum toward the medial limbic cortex. At 15 PCW, the first AChE-reactive cells appear in the nucleus basalis complex, while its cholinergic fibers via the external capsule penetrate into the intermediate zone of frontal, temporal, parietal and occipital lobes (Kostović 1986). Between 15 and 18 PCW, cholinergic afferents spread through the IZ, and between 18 and 22 PCW they accumulate in the subplate. Between 22 and 30 PCW, cholinergic fibers gradually penetrate into the cortical plate and strong AChE-reactivity can be observed in the deep cortical plate and the marginal zone (Fig. 7).

8.2.4 The Development of Thalamocortical System

The subplate zone represents a waiting compartment for thalamocortical afferents in rhesus monkey visual cortex (Rakic 1977), human and monkey visual cortex (Kostovic and Rakic 1984), human and monkey prefrontal cortex (Kostović and Goldman-Rakic 1983), human and monkey somatosensory cortex (Kostović and Rakic 1990), and human auditory cortex (Krmpotić-Nemanić et al. 1983). The projection from pulvinar to the associative visual cortex enters the subplate at 17–20 PCW in humans (E60–E79 in rhesus monkeys), waits in the subplate at 21–25 PCW (E80–E99 in rhesus monkeys) and begins to penetrate the CP towards the end of this period (23/24 PCW), and finally relocates into the CP at 26–34 PCW (E100–E124 in rhesus

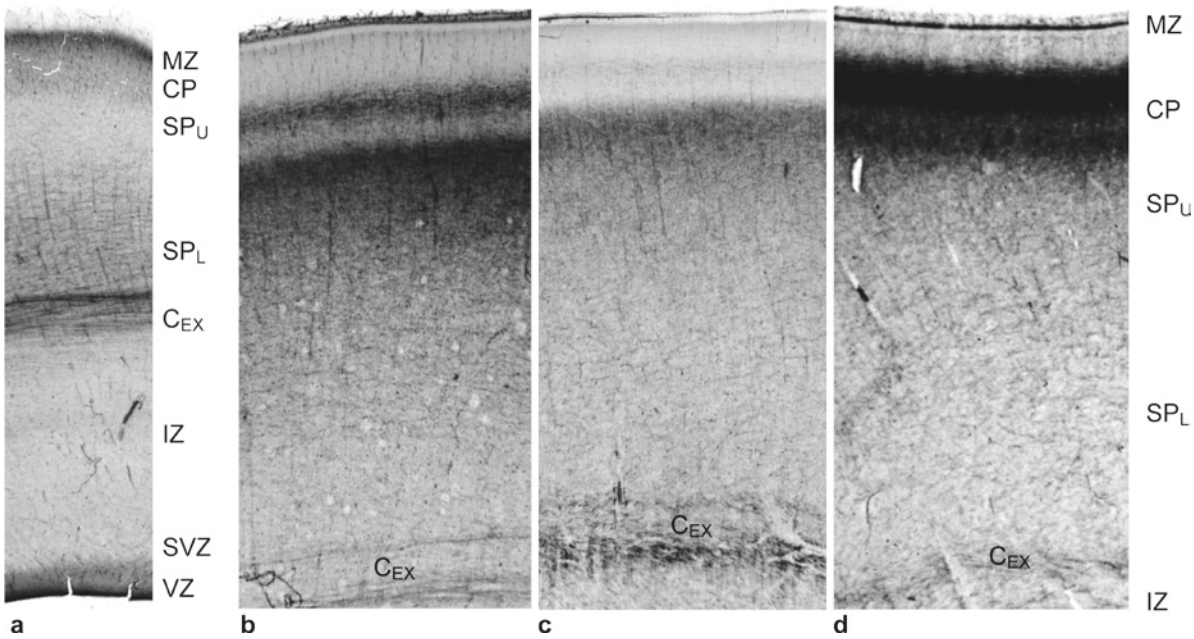

Fig. 7 Development of thalamocortical (thalamic MD nucleus to prefrontal cortex) projection between 19 and 28 PCW. At 19 PCW (**a**), thalamocortical afferents "wait" in the lower part of the subplate zone (SP_L). At 23 PCW (**b**), afferents relocated to the upper subplate (SP_U) and started to penetrate the deep part of the cortical plate (CP). At 26 PCW (**c**), the majority of afferents already relocated to the CP, and at 28 PCW (**d**) they are all within the CP. Cex – the external capsule, which demarcates the border between the subplate and the intermediate zone (IZ). For details, see text

monkeys) (Kostovic and Rakic 1984). The projection from the mediodorsal nucleus to the frontal cortex (Kostovic and Goldman-Rakic 1983) accumulates in the subplate between 16 and 18 PCW, shifts to the superficial part of the subplate at 19 PCW, and by 23–24 PCW enters the cortical plate (Fig. 7); from 28 PCW onward the AChE staining within the cortical plate spreads and exhibits a laminar pattern in which two intense bands of activity in prospective layers III and V are separated by a pale, thin band corresponding to future layer IV (Kostovic and Goldman-Rakic 1983; see also Fig. 7).

8.3 The Development of Commissural and Ipsilateral Corticocortical Connectivity

The ipsilateral and contralateral corticocortical connections arrive last and remain the longest in the subplate zone; they also represent the largest proportion of axons in the subplate in both monkeys and humans (Kostovic and Rakic 1990).

8.3.1 The Development of Forebrain Commissures

The forebrain commissures of primates consist of the corpus callosum, anterior commissure, hippocampal commissure, and the basal telencephalic commissure (LaMantia and Rakic 1990a). Unlike in most eutherian mammals (in which the anterior commissure is primarily an interhemispheric pathway for the olfactory system), in monkeys the few olfactory fibers are concentrated in the basal telencephalic commissure (LaMantia and Rakic 1990a). Again, unlike in most mammals, the dorsal hippocampal commissure has very limited connections to Ammon's horn, and instead includes substantial connections from entorhinal cortex, presubiculum, and parahippocampal gyrus (Amaral et al. 1984; Demeter et al. 1985, 1990). In the adult rhesus monkey, the anterior commissure has 3.15 million fibers, while the corpus callosum has 56 million fibers (LaMantia and Rakic 1990a, 1994). In the adult human, the anterior commissure has 2.4–4.16 million of fibers, of which about 66% are myelinated (Tomasch 1957). The number of fibers in the adult human corpus callosum varies from 200 to 350 million

with a mean value of about 250 million (Blinkov and Chernyshev 1936).

The forebrain commissures are unmyelinated at birth, progress gradually with myelination during childhood and adolescence, but still leave a substantial proportion of interhemispheric fibers unmyelinated in adults (Yakovlev and Lecourse 1967; Aboitiz et al. 1996; Doty 2007). For example, 70–94% of callosal axons (depending on region) are myelinated in rhesus monkeys (LaMantia and Rakic 1990a), while in humans 84% are myelinated in the genu and 95% elsewhere in the corpus callosum (Aboitiz et al. 1992). The protracted course of myelination and growth of the human corpus callosum until at least 20 years of age has been confirmed in recent MRI studies (Pujol et al. 1993; Rauch and Jenkins 1994; Giedd et al. 1996c, 1999b; Keshavan et al. 2002).

Another important feature of the primate cortex is the existence of acallosal areas. The primary visual cortex lacks interhemispheric connections in rhesus monkeys (Dehay et al. 1988; Chalupa et al. 1989), chimpanzees (Bailey et al. 1941) and humans (Clarke and Miklossy 1990). Similar acallosal regions are present in monkey motor and somatosensory cortical areas representing the hand and foot (Killackey et al. 1983; Killackey and Chalupa 1986; Rouiller et al. 1994). In addition, the density of callosal cells and terminals varies widely across the cortex, to give a patchy appearance in most mammals (Doty 2007), including humans (Clarke and Miklossy 1990).

In the human brain, the anterior commissure is crossing the midline already at 9 PCW (Bayer and Altman 2006). The corpus callosum also appears quite early at 11–12 PCW (Rakic and Yakovlev 1968), simultaneously with the emergence of the subplate (Kostović and Krmpotić 1976; Kostovic and Rakic 1990). However, a recent imaging, anatomical, and molecular analysis of callosal formation in human fetal brains ranging from 13 to 20 PCW (Ren et al. 2006) suggested that callosal axons do not cross a fused midline until 14 PCW, and no discernable corpus callosum, or even midline fusion, was observed at 13 PCW (Ren et al. 2006). The number of axons in the human corpus callosum increases from 13,000 at 10 PCW to 144 millions in the child aged 5 months (Luttenberg 1965).

In the human fetal brain between 25 and 32 PCW, the cingulate cortex contains callosally projecting neurons both in the cortical plate and in the subplate (DeAzevedo et al. 1997). These subplate callosal cells are smooth neurons of diverse dendritic morphology (radially oriented, horizontally oriented, multipolar, inverted pyramids), distributed widely throughout the subplate depth, while those in the cortical plate are spiny pyramidal cells with well developed basal dendrites and apical dendrites that consistently ramify within the marginal zone (DeAzevedo et al. 1997).

In the rhesus monkey, some fetal subplate neurons send callosal and association projections (Goldman-Rakic 1982; Schwartz and Goldman-Rakic 1982, 1991; Schwartz et al. 1991) and early growing callosal and association fibers wait in the subplate (Goldman-Rakic 1982). Experimental studies in the monkey have shown that commissural corticocortical fibers reside in the subplate zone between embryonic days E100 and E123 (Goldman-Rakic 1982). In addition, some subplate neurons transiently send their axons through the corpus callosum (Schwartz et al. 1991). In the monkey, callosal axons are at birth three times more numerous than in the adult (LaMantia and Rakic 1990b) and the final number is achieved by the process of competitive elimination during the early postnatal period (Chalupa and Killackey 1989; LaMantia and Rakic 1990b). A newborn rhesus monkey has almost 200 million callosal axons compared to less than 50 million in the adult (LaMantia and Rakic 1990b). The axons are lost at the rate of about 8 million per day or 50 per second during the first 3 weeks after birth. Thereafter, they are lost at an estimated rate of half a million per day or 5 per second until the adult value is reached (LaMantia and Rakic 1990b). Interestingly, this huge loss of callosal axons occurs in parallel with the major overproduction of cortical synapses in the rhesus monkey (Bourgeois et al. 2000). Similarly, the anterior commissure in rhesus monkeys contains 11 million fibers in newborns, but only about 3 million fibers in adults (LaMantia and Rakic 1994). Thus, there is a considerable postnatal reorganization of corticocortical connectivity. Since in the human cortex waiting associative and commissural pathways are major constituents of the subplate zone after 28 PCW (Kostovic and Rakic 1990), and since the development proceeds in humans more slowly than in the monkey, we expect that this protracted postnatal reorganization of corticocortical connectivity is even more pronounced in the human brain.

8.3.2 The Development of Ipsilateral Corticocortical Connectivity

There are few available data on the development of ipsilateral corticocortical connections in monkeys and no such data in humans. As already mentioned, in the rhesus monkey some fetal subplate neurons send callosal and association projections (Goldman-Rakic 1982; Schwartz and Goldman-Rakic 1982,1991; Schwartz et al. 1991) and early growing callosal and association fibers wait in the subplate (Goldman-Rakic 1982). Ipsilateral corticocortical fibers wait in the subplate zone for several weeks before entering the cortical plate (Schwartz and Goldman-Rakic 1982; Schwartz et al. 1991).

Adultlike projections from inferior temporal areas TE and TEO to orbitofrontal cortical areas have been described in one-week-old macaques (Webster et al. 1991). However, monkey inferotemporal cortex displays an extended period of postnatal development and may not be functionally mature until the end of the first year (Rodman 1994); moreover, cortical inputs and outputs of the inferotemporal cortex undergo considerable refinement of transient connections during the first postnatal months (Webster et al. 1991; Rodman 1994).

8.4 The Development of Cortical Efferent Projection Systems

While the development of corticospinal projection is relatively well studied in both monkeys and humans, there are very few data on development of other cortico-subcortical efferent projections in the human fetal brain. By using both MRI-histological correlation and DTI, we have recently provided a preliminary evidence on prenatal development of human corticostriate projections (Kostović et al. 2002a; Judaš et al. 2005; Vukšić et al. 2008) and frontopontine pathways (Vasung et al. 2010b).

In monkeys, functional corticospinal projections to alpha-motoneurons are not established until the first appearance of fine manipulative skills at 3 postnatal months (for review, see Armand et al. 1996, 1997). However, functional human corticospinal projections seem to develop prenatally, although their development was not associated with a significant developmental milestone of motor behavior (Eyre et al. 2000).

In humans, corticospinal axons reach the decussation area at 10 PCW, gradually cross the midline and complete the decussation by 17 PCW (Ten Donkelaar et al. 2004; Ramakers 2005). The lumbosacral area is reached by 29 PCW, but growth cones do not enter spinal cord gray matter for several weeks (Ten Donkelaar et al. 2004). The corticospinal tract is the last of the major descending fiber systems to enter the human spinal cord (Humphrey 1960; Tanaka et al. 1995; Grever et al. 1996; Weidenheim et al. 1992, 1993, 1996). According to a recent study (Eyre et al. 2000), corticospinal axons reach the cervical spinal cord by 24 PCW, by 27 PCW they are still growing, and by 33 PCW they increasingly penetrate the spinal gray matter. The progressive outgrowth of axons from the intermediate gray matter toward the dorsal and ventral horns is characteristic of corticospinal tract development in both monkeys (Galea and Darian-Smith 1995; Olivier et al. 1997) and humans (Eyre et al. 2000). The pathway length from cortex to spinal segment C5 in human newborns at term is 13–14 cm (Eyre et al. 1991). In man, group Ia afferents establish a monosynaptic projection to alpha-motoneurons early in fetal development (Okado 1981; Okado and Kojima 1984; Konstantinidou et al. 1995) and Eyre et al. (2000) have provided a compelling physiological evidence for the prenatal establishment of monosynaptic corticospinal projections to both alpha-motoneurons and group Ia inhibitory interneurons in human fetuses. Finally, significant levels of high affinity NMDA glutamate receptors are transiently expressed in man in the ventral horn from 24 PCW to 2 months postnatally, indicating that a critical period for plasticity in alpha-motoneuron development is also likely to occur in man in the perinatal period. Thus, monosynaptic corticomotoneuronal projections preceded the appearance of relatively independent finger movements by at least 12 months (Eyre et al. 2000). While initial corticospinal projections are bilateral, the ongoing normal development is characterized by a gradual weakening of ipsilateral projections, in parallel with strengthening of contralateral projections (Eyre et al. 2001). Finally, corticospinal system in humans displays a high degree of perinatal and early postnatal plasticity (Eyre et al. 2001, 2007; Staudt et al. 2002, 2004, 2006; for review, see Eyre 2007; Staudt 2007, 2010).

8.5 The Development of Bidirectional Pathways Connecting Cortex with the Amygdala and Claustrum

In distinction to caudate nucleus and putamen, which receive cortical input but have only subcortical outputs, the claustrum and amygdala are both bidirectionally connected with the cerebral cortex (Swanson and Petrovich 1998; Aggleton 2000). The amygdala and its cortical connections have an important role in development of social cognition (for review, see Bauman and Amaral 2008). While there are studies on prenatal cytoarchitectonic development of the human amygdala (Humphrey 1968; Nikolić and Kostović 1986; Müller and O'Rahilly 2006), there are no information on development of its connectivity. In rhesus monkeys, the neurogenesis of amygdala occurs between E33 and E65 (Kordower et al. 1992). This makes the amygdaloid complex, like the magnocellular basal forebrain (Kordower and Rakic 1990), among the earliest developing structures of the primate telencephalon; interestingly, the neurogenesis of the monkey hippocampus also begins at E33 (Rakic and Nowakowski 1981). By two weeks of postnatal age, macaque amygdalocortical connections already closely resemble those in the mature monkeys (Bauman and Amaral 2008). Adultlike projections from inferior temporal areas TE and TEO to both amygdala and orbitofrontal areas have also been described in one-week-old macaques (Webster et al. 1991); the distribution of opiate receptors within the amygdala and cingulate cortex is comparable to adult patterns as early as one week of age (Bachevalier et al. 1986) while the pattern of serotoninergic innervation of monkey amygdala resembles the adult within the first postnatal month (Bauman and Amaral 2008). Thus, several regions implicated in social processing appear to mature very early in postnatal development and may play a critical role in the emergence of species-typical social behavior (Bauman and Amaral 2008). On the other hand, monkey inferotemporal cortex displays an extended period of postnatal development and may not be functionally mature until the end of the first year (Rodman 1994); moreover, cortical inputs and outputs of the inferotemporal cortex undergo considerable refinement of transient connections during the first postnatal months (Webster et al. 1991; Rodman 1994). In the macaque inferotemporal cortex, response selectivity to faces appears already within the second month of life (Rodman 1994; Rodman et al. 1991, 1993), and infant monkeys that sustained damage to the inferior temporal visual area TE within the first postnatal month display less social contact compared to controls at 6 months of age, but do not show deficits in other aspects of social behavior such as eye contact and approach/withdrawal (Bachevalier et al. 2001). In addition, neonatal amygdala damage leads to pronounced changes in fear behaviors or deficits in social development (for review, see Bachevalier 1994, 1996). On the other hand, macaques that are reared in a social environment and receive selective amygdala lesions at two weeks of age do not demonstrate profound impairments in social development within the first year of life (Bauman et al. 2004a, b) but over time these amygdala-lesioned monkeys displayed changes, such as decreased social dominance, which may be due to an inability to regulate fear responses (Bauman et al. 2006). Finally, in this context it should be noted that neonatal temporal lobe lesions have been associated with delayed maturation of the prefrontal cortex (Bertolino et al. 1997). Obviously, developmental data on human cortico-amygdala connectivity are sorely needed and this topic represents an important challenge for future MRI tractography studies.

8.6 The Transformation of the Fetal into Adult White Matter and Protracted Postnatal Myelination

The transformation of the fetal white matter (the intermediate zone) occurs gradually during the third trimester, in parallel with gradual dissolution of the subplate and the SVZ, and continues postnatally. The period spanning the last prenatal and at least first six postnatal months is characterized by significant fiber-architectonic changes, that is, reorganization of the white matter, especially at the cortical/white matter interface (Hüppi et al. 1998, 2001; Prayer et al. 2001; McKinstry et al. 2002; Berman et al. 2005; Huang et al. 2006). This reorganization is related to the onset of myelination, the postnatal persistence of the subplate (at least in the associative cortical regions – Kostović et al. 2002a), the appearance of tertiary gyri and sulci (probably related to the protracted

development of short corticocortical connections, that is, Meynert's U-fibers), and probably a host of other, as yet poorly investigated factors, such as changes in microvascular network, changes in the molecular profile of the extracellular matrix, development of white matter astrocytes, and so forth. The myelination starts shortly before birth, but continues for at least two or three decades (see below).

8.6.1 Prenatal Development of Oligodendroglia in the Human Telencephalon

In a series of recent studies, Nada Zecevic and collaborators offered a detailed analysis of an early oligodendrocyte specification (Rakic and Zecevic 2003b; Filipovic et al. 2003; Jakovcevski and Zecevic 2005a, b), the onset of myelination (Jakovcevski et al. 2007), in vitro studies on the capacity of radial glia cells to generate oligodendrocytes (Mo and Zecevic 2009), interactions of oligodendrocyte progenitors with other cell types (Filipovic and Zecevic 2005, 2008) and interactions between oligodendrocytes and axons before the onset of myelination (Jakovcevski et al. 2007). For a recent review, see Jakovcevski et al. (2009). These studies demonstrated that oligodendrocyte development begins during the second trimester and progresses toward birth and further into adulthood (Rivkin et al. 1995; Back et al. 2001, 2002; Rakic and Zecevic 2003b; Jakovcevski and Zecevic 2005b). Early oligodendrocyte progenitor cells express the platelet derived growth factor receptor alpha (PDGFRα) and NG2 proteoglycans and display typical morphology with few ramified processes (Jakovcevski and Zecevic 2005b). They appear at 10 PCW, but increase in number only around 15 PCW when they are most numerous in the ganglionic eminence and in the cortical VZ/SVZ (Jakovcevski et al. 2009). By midgestation (19–22 PCW), oligodendrocyte precursor cells invade the dorsal telencephalic wall and the cortical plate, but remain most numerous in the SVZ until 24 PCW (Jakovcevski and Zecevic 2005b). Late oligodendrocyte precursor cells display O4 immunoreactivity, whereas pre-myelinating oligodendrocytes are reactive to O1 antibody (Jakovcevski et al. 2009). At 20–22 PCW, O4 and O1 cells are especially numerous in the subplate which indicates that the subplate may be important for maturation of oligodendrocytes (Rakic and Zecevic 2003b; Jakovcevski and Zecevic 2005b). The subplate during midgestation also attracts numerous GFAP-positive astrocytes (Zecevic 2004). Further maturation of oligodendrocytes is marked by the expression of myelin basic protein (MBP) and proteolipid protein (PLP). While MBP was observed already at 5 PCW, this expression was attributed to Golli/MBP splice variants (Zecevic et al. 1998; Tosic et al. 2002; Filipovic et al. 2002, 2003). In the telencephalon, first MBP-positive cells were found at 18 PCW, scattered through the intermediate zone (Back et al. 2001; Jakovcevski and Zecevic 2005b). It should be noted that the human fetal forebrain is characterized by a ventro-dorsal gradient in the oligodendrocyte precursor cell density (Rakic and Zecevic 2003b; Jakovcevski and Zecevic 2005a, b) and in the extent of myelination (Jakovcevski et al. 2007). Moreover, human cortical oligodendrocytes originate from multiple sites, such as ganglionic eminence and SVZ (Rakic and Zecevic 2003b; Jakovcevski and Zecevic 2005a, b). Transcription factors that are necessary and sufficient for generation of oligodendrocytes and for myelination are *Olig* genes, and *Olig2* is expressed in all MBP-positive cells in the human fetal forebrain at midgestation, and in around 50% of early oligodendrocyte progenitors in the SVZ (Jakovcevski and Zecevic 2005a). However, a subpopulation of MAP2-positive neuronal progenitors in the SVZ also expresses *Olig2* during midgestation (but not later), which suggests existence of a common progenitor cell for oligodendrocytes and at least some neuronal classes in the human telencephalon (Jakovcevski and Zecevic 2005a). Indeed, *Olig1* was colocalized in vimentin-positive radial glial cells, which are multiple neural progenitors (Mo et al. 2007; Mo and Zecevic 2009). Another important finding was that, in contrast to rodents where chemokine CXCL1 directly induces oligodendrocyte proliferation, in human fetal brain CXCL1 acts indirectly, through astrocyte secretion of interleukin IL-6, to increase oligodendrocyte proliferation (Filipovic and Zecevic 2008; Jakovcevski et al. 2009). It should also be noted that at midgestation numerous early oligodendrocyte precursor cells still persist in the SVZ. This is clinically relevant because it indicates prolonged proliferation of oligodendrocytes in the human fetal brain that can compensate for minor defects after hypoxic-ischemic periventricular damage (Jakovcevski and Zecevic 2005b).

8.6.2 The Onset and Progression of Myelination in the Human Telencephalon

Myelination in the human brain progresses over several decades, which is much longer than a complete lifespan of the commonly studied animals (Jakovcevski et al. 2009). For example, by 3–6 months, subcortical regions of the macaque brain are well myelinated, and most cortical regions contain some myelin, but cortical layers continue to acquire myelin until at least 3.5 years of age in macaque monkeys (Gibson 1991). The myelination of axons within inferotemporal cortex has not reached adultlike levels in 7-month-old macaque monkeys (Rodman 1994), while myelination within the macaque orbitofrontal cortex may take 1–2 years to reach adultlike levels (Gibson 1991).

Before myelination is initiated, oligodendrocyte precursors transform first to pre-myelinating oligodendrocytes and then into mature myelin-producing cells. In humans there is a clear dissociation between the time of oligodendrocyte differentiation and the beginning of myelination in the fetal forebrain (Back et al. 2001; Jakovcevski and Zecevic 2005b).

In the existing literature, the estimates of the onset of myelination in the human telencephalon vary widely, from 17 PCW (Yakovlev and Lecourse 1967; Tosic et al. 2002) to 30 PCW (Back et al. 2001) or even to the postnatal period (Kinney et al. 1994). At 20 PCW, myelinated axons were observed in the diencephalon, but they could not be observed in the telencephalon either by immunohistochemistry or electron microscopy (Jakovcevski and Zecevic 2005b). In the forebrain, first myelin sheaths detected by MBP-immunohistochemistry were present in the thalamus at 22 PCW (Jakovcevski and Zecevic 2005b). According to another study, the onset of myelination as seen by MBP expression, was postnatal at 54 PCW, with progression to adult-like staining by 72–92 PCW (Haynes et al. 2005).

8.6.3 The Importance of Myelination for a Proper Interpretation of MRI Findings in Brains of Children and Adolescents

The protracted and progressive postnatal myelination is quite important for proper interpretation of in vivo MRI studies of cortical volume and thickness during childhood, adolescence, and adulthood. Already Kaes (1907), by analyzing cortical thickness in myeloarchitectonic sections throughout the lifespan (3 months to 97 years of age), demonstrated the progressive spread of intracortical myelination into frontal and parietal cortices during the first four decades of life. This increase in myelin content in deep cortical layers leads to the apparent cortical thinning, especially when observed by MRI because nonmyelinated axons would appear more like gray matter at a gross level in MRI. This effect of late myelinization is much more significant than the often invoked effects of postnatal synaptic pruning and cell loss; in other words, the apparent thinning of cortex (loss of gray matter density) probably results from increased myelination (for review, see O'Hare and Sowell 2008). Similarly, a 95% increase in the extent of myelination relative to brain weight between the first and second decades of life has been observed within the superior dissecant lamina of the entorhinal cortex (Benes et al. 1994). Reductions in synaptic density are unlikely to account for the large volume decreases in the cortex observed throughout development; the balance between the decreasing number of neurons and the increasing size of glial cells attributable to myelination seems to be primarily responsible for determining the overall cortical thickness (Giedd et al. 1996a). However, it should be noted that a current consensus is that cortical neurons are generally preserved during adolescence and adulthood with at most a 10% reduction in neuronal numbers (Peters et al. 1998).

Initial quantitative structural MRI studies reported that children aged 8–10 years had significantly more cortical gray matter than young adults, although young adults had larger total brain volumes (Jernigan and Tallal 1990), and that the timing of gray matter loss displays regional differences (Jernigan et al. 1991a, b). The decrease in the cortical volume during development (along with concomitant increases in white matter) has been reported in subsequent studies (Pfefferbaum et al. 1994), especially in the dorsal associative frontal and parietal cortices (Giedd et al. 1999a; Sowell et al. 1999a, 2001a, b, 2002a, 2003). In another study, the postadolescent gray matter loss was localized to large regions of the dorsal, mesial, and orbitofrontal cortex, with relatively little gray matter loss in the parietal lobes (Sowell et al. 1999b). There is an initial increase in cortical density that peaks between 10 and 12 years, depending on gender, in both frontal and parietal lobes, and thereafter declines during the

adolescent and postadolescent periods (Giedd et al. 1999a; Gogtay et al. 2004). Thus, it has been concluded that there are regionally specific patterns of gray matter loss during late childhood and adolescence. In contrast, ventral temporal cortex changes less dramatically between childhood and adolescence (Giedd et al. 1999a; Sowell et al. 2002a). Finally, significant age-related increases in white matter density were observed in the motor and language-related cortical regions (Paus et al. 1999) and small increases in cortical gray matter density between childhood and young adulthood have been observed in bilateral posterior perisylvian regions (Sowell et al. 2002b, 2003, 2004a, b) and in the left inferior frontal sulcus, that is, Broca's area (Sowell et al. 2004a, b). More recent studies measured the cortical thickness (instead of cortical gray matter density) across development and revealed statistically significant cortical thinning of approximately 0.15–0.30 mm per year, most prominently in right dorsal frontal and bilateral parietal regions (Sowell et al. 2002a, b, 2003, 2004a, b). On the other hand, significant increases in cortical thickness (approximately 0.10–0.15 mm per year) were observed in frontal and temporal language regions (O'Hare and Sowell 2008). Recent MRI studies also suggested that there are significant relationships between frontal lobe structure and general intellectual functioning (Thompson et al. 2001; Toga and Thompson 2005; Shaw et al. 2006). In conclusion, a number of recent studies have consistently demonstrated a decrease in gray matter volume starting in late childhood or early adolescence and progressing into late adulthood – with notable exception of language-related cortical areas (Caviness et al. 1996; Giedd et al. 1996a, b; De Bellis et al. 2001; Sowell et al. 2002a, 2003, 2004a, b; Giedd 2004; Gogtay et al. 2004; Lenroot and Giedd 2006; O'Hare and Sowell 2008).

9 Concluding Remarks and Clinical Implications

As illustrated in Sect. 5 (and in most other sections of this chapter), there are profound and clinically relevant differences in cortical development between rodents and humans. There are numerous evolutionary modifications of developmental events that produce not only quantitative changes, such as the number of neurons and columns or timing and sequence of cellular events, but also qualitative ones (for example, the elaboration of new neuronal types, addition of specialized cytoarchitectonic areas and formation of new connections (Rakic et al. 2009)). Analyzing species-specific differences in the timing, sequence, and phenotypic differentiation could provide insight into the pathogenesis of cortical abnormalities and cortical evolution (Levitt 2003; Rakic et al. 2009; Preuss 2009). Thus, neither the genetic, the cellular, nor the circuitry basis of human cortical uniqueness can be deciphered by studying exclusively rodents (Rakic et al. 2009; Preuss 2009). Animal models are therefore not sufficient and appropriate human studies and human model systems are necessary.

For example, unlike in rodents, the SVZ in the human contributes the majority of interneurons to the neocortex (see Sect. 6.2.2). Thus, the modifications in the expression pattern of transcription factors in the forebrain may underlie species-specific programs for the generation of distinct lineages of cortical interneurons that may be differentially affected in genetic and acquired disorders related to neuronal migration (Jones 1997; Lewis 2000; Gleeson and Walsh 2000; Ross and Walsh 2001; Rakic 2003a, b; Hevner 2007; Guerrini et al. 2008). For example, a species-specific difference was discovered in the effect of the deletion of doublecortin (*Dbx*) mutation, which was found to have a profound effect on neuronal migration in the human telencephalon but does not affect formation and neurogenetic gradients of the mouse cerebral cortex (Corbo et al. 2002). There are already many examples of how unique structures and gene expression patterns that give rise to abilities, such as language, are also involved in disorders, such as autism, for which there is no accepted mouse model (Levitt 2005; Rakic 2009). As the development of human brain circuitry depends on the diversity and precise spatiotemporal regulation of its transcriptome (Johnson et al. 2009), and symptoms of many neurological and mental disorders are dramatically influenced by pre-existing regional molecular profiles and neuronal circuitry (Morrison and Hof 1997; Levitt 2005), such disorders are at least in part defined during development by differential gene expression determining regional differences in neuronal circuits (Johnson et al. 2009). The detailed and up-to-date knowledge on human cortical development is also highly relevant for understanding and analyzing the neurobiological basis and developmental origin of

major neurological and mental disorders, such as schizophrenia, (for review, see Kostović et al. 2010) or Down's syndrome (Vukšić et al. 2002), as well as developmental brain disorders such as lissencephaly (Judaš et al. 2009) and holoprosencephaly (Judaš et al. 2003b; Fertuzinhos et al. 2009).

Fortunately, new noninvasive methods from histology, neuroimaging, and genomics are making the human brain accessible for direct, detailed study as never before and we shoud use these methods not only to analyze human brain development, but to directly compare humans to other species (Preuss 2009). We should also increasingly use the correlation between the improving imaging and more diverse histological studies to aid clinicopathological diagnosis (Kostović and Vasung 2009; Vasung et al. 2010a, b; Wang et al. 2010). The number of new and powerful methods for analyzing human brain development is rapidly increasing. For example, one can use gene chips and human genome microarrays, rtPCR and cell culture (Ip et al. 2010), or purify specific subpopulations of developing human cortical cells, such as radial glia, in culture (Mo et al. 2007; Mo and Zecevic 2008). Another important goal is to establish the molecular taxonomy of diverse neuronal types, as a first step in identifying the subpopulations that may have very different roles during development and in various pathologies (Hevner 2007; Hoerder-Suabedissen et al. 2009). Such studies already opened the way for selective recognition of different subpopulations of neurons in experimental rodents (Hoerder-Suabedissen et al. 2009; Osheroff and Hatten 2009; Ayoub and Kostovic 2009) and we need similar studies to focus on the origins, categories, and functional roles of human cortical neurons. Combining knowledge of cell-type specific gene expression with modern imaging methods will enable a better understanding of neuropathologies involving cerebral cortex – for example, by selectively manipulating these cells in animal models and analyzing them in human histological slides (Wang et al. 2010). Another important step in this direction is represented by a development of the three-dimensional (3D) HUDSEN Atlas (http://www.hudsen.org) for studying gene expression in the embryonic human brain at Carnegie stages 12–23 (Lindsay and Copp 2005; Lindsay et al. 2005; Sarma et al. 2005; for review, see Kerwin et al. 2010).

The functional significance of transient fetal circuitry and the pivotal role of the subplate zone has already been extensively reviewed in both experimental model animals (Kanold and Luhmann 2010) and in humans (Kostović et al. 1995; Kostović and Judaš 2006, 2007, 2010). The subplate is involved in plasticity after perinatal hypoxic-ischemic lesion (Kostović et al. 1989b) and plays a major role in current interpretations of pathogenesis of this major pathology of prematurely born infants (McQuillen and Ferriero 2005; Leviton and Gressens 2007; Mathur and Inder 2009; Ment et al. 2009; Miller and Ferriero 2009; Volpe 2009). The reader may find extensive descriptions and analyses in the above mentioned reviews, but I wish to conclude this chapter by pointing out two specific features of late prenatal and perinatal human brain, one related to the complexity of the periventricular fetal white matter, and another to the pivotal role of the subplate zone.

The complexity of the structure of the fetal white matter as well as continuously changing variability of its cellular and axonal contents are bewildering (Fig. 8). In addition to numerous and variable contingents of growing axons (see Sects. 8.2–8.6), the fetal white matter (that is, the IZ and the subjacent outer SVZ) contain different populations of cells: radially migrating cortical projection neurons, radially and tangentially migrating cortical interneurons, various types of neuronal progenitor cells (see Sect. 6.2), early developing oligodendrocytes and astrocytes, a complex extracellular matrix (Kostović et al. 2002a), and at least six major crossroads of developing cortical pathways (Judaš et al. 2005). No wonder that hypoxic-ischemic lesions can cause a huge variety of neurodevelopmental outcomes, and we are just beginning to unveil the unprecedented complexity of these developmental processes and interactions (Leviton and Gressens 2007; Miller and Ferriero 2009; Ment et al. 2009; Volpe 2009; Staudt 2007, 2010).

As illustrated in preceding sections, histogenetic processes in the human fetal and perinatal brain are protracted and significantly overlap, but the subplate zone represents a playground for the majority of important events during that developmental window. Therefore, the human perinatal period is characterized by simultaneous existence of two separate (but interconnected) types of cortical circuitry organization: (a) transient fetal circuitry, centered at the subplate zone, and (b) immature but progressively developing permanent cortical circuitry, centered at the cortical plate (that is, developing cortical layers I–VI). Thus, the developing human cortex passes through three major

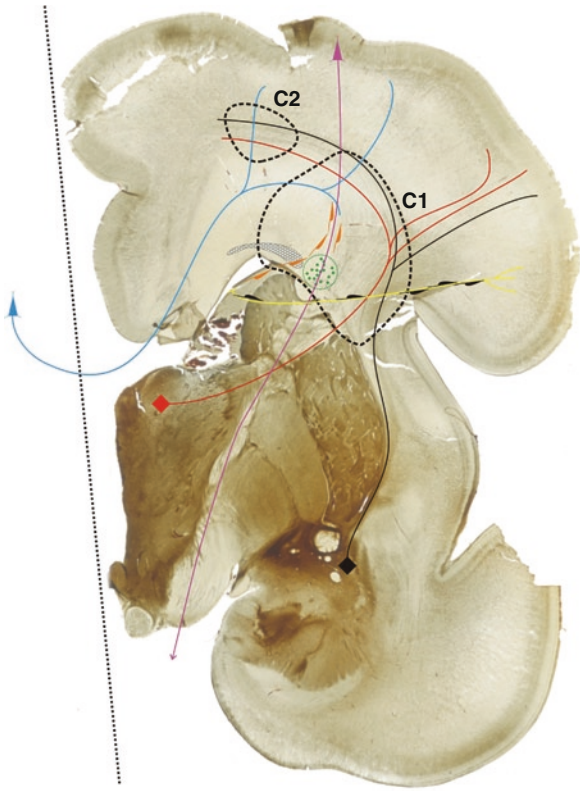

Fig. 8 Summary diagram, superposed on AChE-stained coronal section through a telencephalon of 28-week-old human fetus constructed on the basis of our data and evidence from current literature. Thick *black dashed lines* delineate the first (C1) and second (C2) frontal crossroad area. The honeycomb pattern area denotes the deep periventricular system of fiber bundles; and *circle with green dots* developing fronto-occipital system, both containing SNAP-25 immunoreactive fibers. *Colored lines* denote systems of projection, association and commissural fibers passing through the crossroads (with triangles or quadrangles depicting cell bodies of origin), as follows: black – basal forebrain afferents; red – thalamocortical afferents; blue – callosal fibers; violet – corticofugal efferents. Note that both radially migrating neurons (*black profiles* along the yellow radial glial fiber) and tangentially migrating neurons (*orange profiles*) pass through the major crossroad (C1) area, which is located at the main predilection site of hypoxic-ischemic lesion in preterm infants (From Judaš et al. (2005). With permission)

stages of functional development (Kostović and Judaš 2006, 2007, 2010; see also Vanhatalo and Kaila 2006; Vanhatalo et al. 2005; Milh et al. 2007): (1) initial fetal circuitry which is endogeneously (spontaneously) driven, (2) perinatal dual circuitry (co-existence of endogeneously driven SP-centered transient circuitry with developing CP-centered permanent circuitry) and (3) postnatally established permanent (externally driven) cortical circuitry.

Acknowledgment This work has been supported by Croatian Ministry of Science, Education and Sport Grant No. 108-1081870-1878 (to M.J.) and Unity Through Knowledge Fund (UKF) grant (director Ivica Kostović). The technical assistance of Mihovil Pletikos in preparation of illustrations is gratefully acknowledged.

References

Abdel-Mannan O, Cheung A, Molnár Z (2008) Evolution of cortical neurogenesis. Brain Res Bull 75(2–4):398–404

Aboitiz F, Scheibel AB, Fisher RS, Zaidel E (1992) Fiber composition of the human corpus callosum. Brain Res 598: 143–153

Aboitiz F, Rodriguez E, Olivares R, Zaidel E (1996) Age-related changes in fibre composition of the human corpus callosum: sex differences. NeuroReport 7:1761–1764

Abrahám H, Meyer G (2003) Reelin-expressing neurons in the postnatal and adult human hippocampal formation. Hippocampus 13:715–727

Abrahám H, Perez-Garcia CG, Meyer G (2004a) p73 and reelin in Cajal-Retzius cells of the developing human hippocampal formation. Cereb Cortex 14:484–495

Abrahám H, Tornóczky T, Kosztolányi G, Seress L (2004b) Cell proliferation correlates with the postconceptual and not with the postnatal age in the hippocampal dentate gyrus, temporal neocortex and cerebellar cortex of preterm infants. Early Hum Dev 78:29–43

Abrahams BS, Tentler D, Perederiy JV, Oldham MC, Coppola G, Geschwind DH (2007) Genome wide analyses of human perisylvian cerebral cortical patterning. Proc Natl Acad Sci USA 104(45):17849–17854

Abu-Khalil A, Fu L, Grove EA, Zecevic N, Geschwind DH (2004) *Wnt* genes define distinct boundaries in the developing human brain: implications for human forebrain patterning. J Comp Neurol 474:276–288

Adams NC, Baker GE (1995) Cells of the perireticular nucleus project to the developing neocortex of the rat. J Comp Neurol 359:613–626

Aeby A, Liu Y, De Tiege X, Denolin V, David P, Balériaux D, Kavec M, Metens T, Van Bogaert P (2009) Maturation of thalamic radiations between 34 and 41 weeks' gestation: a combined voxel-based study and probabilistic tractography with diffusion tensor imaging. Am J Neuroradiol 30:1780–1786

Aggleton JP (ed) (2000) The amygdala: a functional analysis. Oxford University Press, New York

Alarcón M, Abrahams BS, Stone JL, Duvall JA, Perederiy JV, Bomar JM, Sebat J, Wigler M, Martin CL, Ledbetter DH, Nelson SF, Cantor RM, Geschwind DH (2008) Linkage, association and gene-expression analyses identify *CNTNAP2* as an autism-susceptibility gene. Am J Hum Genet 82(1): 150–159

Allendoerfer KL, Shatz CJ (1994) The subplate, a transient neocortical structure: its role in the development of connections between thalamus and cortex. Annu Rev Neurosci 17: 185–218

Allman J, Hakeem A, Watson K (2002) Two phylogenetic specializations in the human brain. Neuroscientist 8:335–346

Allman JM, Watson KK, Tetreault NA, Hakeem AY (2005) Intuition and autism: a possible role for Von Economo neurons. Trends Cogn Sci 9:367–373

Almqvist PM, Akesson E, Wahlberg LU, Pschera H, Seiger A, Sundstrom E (1996) First trimester of the human nigrostriatal dopamine system. Exp Neurol 139:227–237

Alvarez-Buylla A, Garcia-Verdugo JM (2002) Neurogenesis in adult subventricular zone. J Neurosci 22:629–634

Alvarez-Buylla A, Lim DA (2004) For the long run: maintaining germinal niches in the adult brain. Neuron 41:683–686

Alvarez-Buylla A, Garcia-Verdugo JM, Tramontin AD (2001) A unified hypothesis on the lineage of neural stem cells. Nat Rev Neurosci 2:287–293

Amaral DG, Insausti R, Cowan WM (1984) The commissural connections of the monkey hippocampal formation. J Comp Neurol 224:307–336

Anderson SA, Marín O, Horn C, Jennings K, Rubenstein JL (2001) Distinct cortical migrations from the medial and lateral ganglionic eminences. Development 128:353–363

Anderson SA, Kaznowski CE, Horn C, Rubenstein JLR, McConnell SK (2002) Distinct origins of neocortical projection neurons and interneurons in vivo. Cereb Cortex 12: 702–709

Ang LC, Munoz DG, Shul D, George DH (1991) SMI-32 immunoreactivity in human striate cortex during postnatal development. Dev Brain Res 61(1):103–109

Ang ESBC, Haydar TF, Gluncic V, Rakic P (2003) Four dimensional migratory coordinates of GABAergic neurons in the developing cerebral cortex. J Neurosci 23:5805–5815

Antanitus DS, Choi BH, Lapham LW (1976) The demonstration of glial fibrillary acidic protein in the cerebrum of the human fetus by indirect immunofluorescence. Brain Res 103:613–616

Arbiza L, Dopazo J, Dopazo H (2006) Positive selection, relaxation, and acceleration in the evolution of the human and chimp genome. PLoS Comput Biol 2(4):e38

Arking DE, Cutler DJ, Brune CW, Teslovich TM, West K, Ikeda M, Rea A, Guy M, Lin S, Cook EH, Chakravarti A (2008) A common genetic variant in the neurexin superfamily member *CNTNAP2* increases familial risk of autism. Am J Hum Genet 82(1):160–164

Armand J, Olivier E, Edgley SA, Lemon RN (1996) The structure and function of the developing corticospinal tract: some key issues. In: Wing AM, Haggard P, Flanagan JR (eds) Hand and brain: the neurophysiology and psychology of hand movements. Academic, San Diego, pp 125–143

Armand J, Olivier E, Edgley SA, Lemon RN (1997) Postnatal development of corticospinal projections from motor cortex to the cervical enlargement in the macaque monkey. J Neurosci 17:251–266

Armstrong E, Schleicher A, Omran H, Curtis M, Zilles K (1995) The ontogeny of human gyrification. Cereb Cortex 5:56–63

Arnold SE, Trojanowski JQ (1996a) Human fetal hippocampal development. I. Cytoarchitecture, myeloarchitecture, and neuronal morphologic features. J Comp Neurol 367:274–292

Arnold SE, Trojanowski JQ (1996b) Human fetal hippocampal development. II. The neuronal cytoskeleton. J Comp Neurol 367:293–307

Arvidsson A, Collin T, Kirik D, Kokaia Z, Lindvall O (2002) Neuronal replacement from endogenous precursors in the adult brain after stroke. Nat Med 8:963–970

Ayala G (1915) A hitherto undifferentiated nucleus in the forebrain (nucleus subputaminalis). Brain 37:433–438

Ayala G (1924) Weitere Untersuchungen über den Nucleus subputaminalis. J Psychol Neurol 30:285–299

Ayoub AE, Kostovic I (2009) New horizons for the subplate zone and its pioneering neurons. Cereb Cortex 19:1705–1707

Bachevalier J (1994) Medial temporal lobe structures and autism – a review of clinical and experimental findings. Neuropsychologia 32:627–648

Bachevalier J (1996) Medial temporal lobe and autism – a putative animal model in primates. J Autism Dev Disord 26: 217–220

Bachevalier J, Ungerleider LG, O'Neill JB, Friedman DP (1986) Regional distribution of (^{3}H) naloxone binding in the brain of a newborn rhesus monkey. Brain Res 390:302–308

Bachevalier J, Malkova L, Mishkin M (2001) Effects of selective neonatal temporal lobe lesions on socioemotional behavior in infant rhesus monkeys (*Macaca mulatta*). Behav Neurosci 115:545–559

Back SA, Luo NL, Borenstein NS, Levine JM, Volpe JJ, Kinney HC (2001) Late oligodendrocyte progenitors coincide with the developmental window of vulnerability for human perinatal white matter injury. J Neurosci 21:1302–1312

Back SA, Han BH, Luo NL, Chricton CA, Xanthaudakis S, Tam J, Arvin KL, Holtzman DM (2002) Selective vulnerability of late oligodendrocyte progenitors to hypoxia-ischemia. J Neurosci 22:455–463

Badsberg GS, Bonde KL, Bogdanovic N, Laursen H, Graem N, Falk JL, Pakkenberg B (2003) The changing number of cells in the human fetal forebrain and its subdivisions: a stereological analysis. Cereb Cortex 13(2):115–122

Bailey JA, Eichler EE (2006) Primate segmental duplications: crucibles of evolution, diversity and disease. Nat Rev Genet 7(7):552–564

Bailey P, Garol HW, McCulloch WS (1941) Cortical origin and distribution of corpus callosum and anterior commissure in chimpanzee (*Pan satyrus*). J Neurophysiol 4:564–571

Bakkaloglu B, O'Roak BJ, Louvi A, Gupta AR, Abelson JF, Morgan TM, Chawarska K, Klin A, Ercan-Sencicek AG, Stillman AA, Tanriover G, Abrahams BS, Duvall JA, Robbins EM, Geschwind DH, Biederer T, Gunel M, Lifton RP, State MW (2008) Molecular cytogenetic analysis and resequencing of contactin associated protein-like 2 in autism spectrum disorders. Am J Hum Genet 82(1):165–173

Barbé A (1938) Recherches sur l'embryologie du systeme nerveux central de l'homme. Masson, Paris

Barres BA (1999) New role of glia: generation of neurons! Cell 97:667–670

Bartelmez GW, Dekaban AS (1962) The early development of the human brain. Contrib Embryol Carnegie Inst 37:13–32

Bartley AJ, Jones DW, Weinberger DR (1997) Genetic variability of human brain size and cortical gyral patterns. Brain 120:257–269

Bauman MD, Amaral DG (2008) Neurodevelopment of social cognition. In: Nelson CA, Luciana M (eds) Handbook of developmental cognitive neuroscience, 2nd edn. A Bradford Book, The MIT Press, Cambridge, pp 161–186

Bauman MD, Lavenex P, Mason WA, Capitanio JP, Amaral DG (2004a) The development of mother-infant interactions after neonatal amygdala lesions in rhesus monkeys. J Neurosci 24(3):711–721

Bauman MD, Lavenex P, Mason WA, Capitanio JP, Amaral DG (2004b) The development of social behavior following neonatal amygdala lesions in rhesus monkeys. J Cogn Neurosci 16:1388–1411

Bauman MD, Toscano JE, Mason WA, Lavenex P, Amaral DG (2006) The expression of social dominance following neonatal lesions of the amygdala or hippocampus in rhesus monkeys (*Macaca mulatta*). Behav Neurosci 120:749–760

Bayatti N, Moss JA, Sun L, Ambrose P, Ward JF, Lindsay S, Clowry GJ (2008a) A molecular neuroanatomical study of the developing human neocortex from 8 to 17 postconceptional weeks revealing the early differentiation of the subplate and subventricular zone. Cereb Cortex 18:1536–1548

Bayatti N, Sarma S, Shaw C, Eyre JA, Vouyiouklis DA, Lindsay S, Clowry GJ (2008b) Progressive loss of *PAX6*, *TBR2*, *NEUROD* and *TBR1* mRNA gradients correlates with translocation of *EMX2* to the cortical plate during human cortical development. Eur J Neurosci 28:1449–1456

Bayer SA, Altman J (1990) Development of layer I and the subplate in the rat neocortex. Exp Neurol 107:48–62

Bayer SA, Altman J (1991) Neocortical development. Raven Press, New York

Bayer SA, Altman J (2002) Atlas of human central nervous system development, Vol 1: The Spinal Cord from Gestational Week 4 to the 4th Postnatal Month. CRC Press, Boca Raton, 287 pp

Bayer SA, Altman J (2004) Atlas of human central nervous system development, Vol 2: The human brain during the third trimester. CRC Press, Boca Raton, 383pp

Bayer SA, Altman J (2005) Atlas of human central nervous system development, Vol 3: The human brain during the second trimester. CRC Press (Taylor & Francis Group), Boca Raton, 369 pp

Bayer SA, Altman J (2006) Atlas of human central nervous system development, Vol 4: The human brain during the late first trimester. CRC Press (Taylor & Francis Group), Boca Raton, 576 pp

Bayer SA, Altman J (2008) Atlas of human central nervous system development, Vol 5: The human brain during the early first trimester. CRC Press (Taylor & Francis Group), Boca Raton

Bédard A, Parent A (2004) Evidence of newly generated neurons in the human olfactory bulb. Dev Brain Res 151:159–168

Bédard A, Gravel AC, Parent A (2006) Chemical characterization of newly generated neurons in the striatum of adult primates. Exp Brain Res 170(4):501–512

Benavides-Piccione R, Ballesteros-Yanez I, DeFelipe J, Yuste R (2002) Cortical area and species differences in dendritic spine morphology. J Neurocytol 31(3–5):337–346

Benes FM, Turtle M, Khan Y, Farol P (1994) Myelination of a key relay zone in the hippocampal formation occurs in the human brain during childhood, adolescence, and adulthood. Arch Gen Psychiatry 51:477–484

Benowitz LI, Perrone-Bizzozero NI, Finklestein SP, Bird ED (1989) Localization of the growth-associated phosphoprotein GAP-43 (B-50, F1) in the human cerebral cortex. J Neurosci 9:990–995

Benson DL, Isakson PJ, Jones EG (1991) In situ hybridization reveals VIP precursor mRNA-containing neurons in monkey and rat neocortex. Mol Brain Res 9:169–174

Bentivoglio M, Mazzarello P (1999) The history of radial glia. Brain Res Bull 49:305–315

Berezikov E, Thuemmler F, van Laake LW, Kondova I, Bontrop R, Cuppen E, Plasterk RH (2006) Diversity of microRNAs in human and chimpanzee brain. Nat Genet 38(12): 1375–1377

Berger B, Alvarez C, Goldman-Rakic PS (1993) Neurochemical development of the hippocampal region in the fetal rhesus monkey. I. Early appearance of peptides, calcium-binding proteins, DARPP-32, and monoamine innervation in the entorhinal cortex during the first half of gestation (E47 to E90). Hippocampus 3:279–305

Berman JI, Mukherjee P, Partridge SC, Miller SP, Ferriero DM, Barkovich AJ, Vigneron DB, Henry RG (2005) Quantitative diffusion tensor MRI fiber tractography of sensorimotor white matter development in premature infants. Neuroimage 27:862–871

Bernier PJ, Bedard A, Vinet J, Levesque M, Parent A (2002) Newly generated neurons in the amygdala and adjoining cortex of adult primates. Proc Natl Acad Sci USA 99(17):11464–11469

Bertolino A, Saunders RC, Mattay VS, Bachevalier J, Frank JA, Weinberger DR (1997) Altered development of prefrontal neurons in rhesus monkeys with neonatal mesial temporolimbic lesions: a proton magnetic resonance spectroscopic imaging study. Cereb Cortex 7:740–748

Bhardwaj RD, Curtis MA, Spalding KL, Buchholz BA, Fink D, Björk-Eriksson T, Nordborg C, Gage FH, Druid H, Eriksson PS, Frisén J (2006) Neocortical neurogenesis in humans is restricted to development. Proc Natl Acad Sci USA 103(33):12564–12568

Bishop KM, Goudreau G, O'Leary DD (2000) Regulation of area identitiy in the mammalian neocortex by *Emx2* and *Pax6*. Science 288:344–349

Blinkov SM, Chernyshev AS (1936) Variations in the Human Corpus callosum. Collection in Honor of P.I. Emdin. Rostov on Don, pp. 381–387 (in Russian)

Boulder Committee (1970) Embryonic vertebrate central nervous system: revised terminology. Anat Rec 166:257–262

Bourgeois JP, Goldman-Rakic PS, Rakic P (2000) Formation, elimination and stabilization of synapses in the primate cerebral cortex. In: Gazzaniga MS (ed) Cognitive neuroscience: a handbook for the field. MIT Press, Cambridge, pp 23–32

Breunig JJ, Arellano JI, Macklis JD, Rakic P (2007a) Everything that glitters isn't gold: a critical review of postnatal neural precursor analyses. Cell Stem Cell 1(6):612–627

Breunig JJ, Silbereis J, Vaccarino FM, Šestan N, Rakic P (2007b) Notch regulates cell fate and dendritic morphology of newborn neurons in the postnatal dentate gyrus. Proc Natl Acad Sci USA 104(51):20558–20563

Brisse H, Fallet C, Sebag G, Nessmann C, Blot P, Hassan M (1997) Supratentorial parenchyma in the developing fetal brain: in vitro MR study with histologic comparison. Am J Neuroradiol 18:1491–1497

Brodmann K (1906) Beiträge zur histologischen Lokalisation der Grosshirnrinde. V. Mitteilung: Ueber den allgemeinen Bauplan des Cortex pallii bei den Mammaliern und zwei homologe Rindenfelder im besonderen. Zugleich ein Beitrag zur Furchenlehre (Mit 298 Textfiguren). J Psychol Neurol Ergänzungsheft 6:275–400

Brody BA, Kinney HC, Kloman AS, Gilles FH (1987) Sequence of central nervous system myelination in human infancy. I. An autopsy study of myelination. J Neuropathol Exp Neurol 46:283–301

Brun A (1965) The subpial granular layer of the foetal cerebral cortex in man. Its ontogeny and significance in congenital cortical malformations. Acta Pathol Microbiol Scand 13(suppl 179):1–98

Bruni JE (1998) Ependymal development, proliferation, and functions: a review. Microsc Res Tech 41:2–13

Bui T, Daire JL, Chalard F, Zaccaria I, Alberti C, Elmaleh M, Garel C, Luton D, Blanc N, Sebag G (2006) Microstructural development of human brain assessed in utero by diffusion tensor imaging. Pediatr Radiol 36:1133–1140

Burkhalter A (1993) Development of forward and feedback connections between areas V1 and V2 of human visual cortex. Cereb Cortex 3:476–487

Burkhalter A, Bernardo KL, Charles V (1993) Development of local circuits in human visual cortex. J Neurosci 13: 1916–1931

Bustamante CD, Fledel-Alon A, Williamson S, Nielsen R, Hubisz MT, Glanowski S, Tanenbaum DM, White TJ, Sninsky JJ, Hernandez RD, Civello D, Adams MD, Cargill M, Clark AG (2005) Natural selection on protein-coding genes in the human genome. Nature 437:1153–1157

Buxhoeveden DP, Switala AE, Litaker M, Roy E, Casanova MF (2001) Lateralization of minicolumns in human planum temporale is absent in nonhuman primate cortex. Brain Behav Evol 57:349–358

Bystron I, Molnár Z, Otellin V, Blakemore C (2005) Tangential networks of precocious neurons and early axonal outgrowth in the embryonic human forebrain. J Neurosci 25:2781–2792

Bystron I, Rakic P, Molnár Z, Blakemore C (2006) The first neurons of the human cerebral cortex. Nat Neurosci 9:880–886

Bystron I, Blakemore C, Rakic P (2008) Development of human cerebral cortex: Boulder Committee revisited. Nat Rev Neurosci 9:110–122

Cabrera-Socorro A, Hernandez-Acosta NC, Gonzalez-Gomez M et al (2007) Comparative aspects of p73 and reelin expression in Cajal-Retzius cells and the cortical hem in lizard, mouse and human. Brain Res 1132:59–70

Cáceres M (2003) Elevated gene expression levels distinguish human from non-human primate brains. Proc Natl Acad Sci USA 100(22):13030–13035

Cáceres M, Suwyn C, Maddox M, Thomas JW, Preuss TM (2007) Increased cortical expression of two synaptogenic thrombospondins in human brain evolution. Cereb Cortex 17(10):2312–2321

Calarco JA, Xing Y, Cáceres M, Calarco JP, Xiao X, Pan Q, Lee C, Preuss TM, Blencowe BJ (2007) Global analysis of alternative splicing differences between humans and chimpanzees. Genes Dev 21(22):2963–2975

Cameron RS, Rakic P (1991) Glial cell lineage in the cerebral cortex: a review and synthesis. Glia 4:124–137

Campbell K, Götz M (2002) Radial glia: multi-purpose cells for vertebrate brain development. Trends Neurosci 25:235–238

Cao QL, Yan XX, Luo XG, Garey LJ (1996) Prenatal development of parvalbumin immunoreactivity in the human striate cortex. Cereb Cortex 6:620–630

Carney RSE, Bystron I, López-Bendito G, Molnár Z (2007) Comparative analysis of extraventricular mitoses at early stages of cortical development in rat and human. Brain Struct Funct 212(1):37–54

Carpenter MK, Inokuma MS, Denham J, Mujtaba T, Chiu CP, Rao MS (2001) Enrichment of neurons and neural precursors from human embryonic stem cells. Exp Neurol 172(2):383–397

Caviness VS Jr, Kennedy DN, Richelme C, Rademacher J, Filipek PA (1996) The human brain age 7-11 years: a volumetric analysis based on magnetic resonance images. Cereb Cortex 6:726–736

Cepanec M (2009) Quantitative analysis of the cytoarchitectonics of the fronto-opercular area in the human brain in prenatal, prelinguistic and early linguistic period. D.Sc. Thesis, University of Zagreb (Croatia), 350 pp

Chalupa LM, Killackey HP (1989) Process elimination underlies ontogenetic change in the distribution of callosal projection neurons in the postcentral gyrus of the fetal rhesus monkey. Proc Natl Acad Sci USA 86:1076–1079

Chalupa LM, Killackey HP, Snider CJ, Lia B (1989) Callosal projection neurons in area 17 of the fetal rhesus monkey. Dev Brain Res 46:303–308

Cheng Z, Ventura M, She X, Khaitovich P, Graves T, Osoegawa K, Church D, DeJong P, Wilson RK, Pääbo S, Rocchi M, Eichler EE (2005) A genome-wide comparison of recent chimpanzee and human segmental duplications. Nature 437:88–93

Chenn A, Walsh CA (2003) Increased neuronal production, enlarged forebrains and cytoarchitectural distortions in beta-catenin over-expressing transgenic mice. Cereb Cortex 13:599–606

Chi JG, Dooling EC, Gilles FH (1977) Gyral development of the human brain. Ann Neurol 1:86–93

Childs AM, Ramenghi LA, Evans DJ, Ridgeway J, Saysell M, Martinez D, Arthur R, Tanner S, Levene MI (1998) MR features of developing periventricular white matter in preterm infants: evidence of glial cell migration. Am J Neuroradiol 19:971–976

Childs AM, Ramenghi LA, Cornette L, Tanner SF, Arthur RJ, Martinez D, Levene MI (2001) Cerebral maturation in premature infants: quantitative assessment using MR imaging. Am J Neuroradiol 22:1577–1582

Choi BH (1986) Glial fibrillary acid protein in radial glia of early human fetal cerebrum: a light and electron immunocytochemical study. J Neuropathol Exp Neurol 45:408–418

Choi BH, Lapham LW (1978) Radial glia in the human fetal cerebrum: a combined Golgi, immunofluorescent and electron microscopic study. Brain Res 148:295–311

Chong BW, Babcook CJ, Salamat MS, Nemzek W, Kroeker D, Ellis WG (1996) A magnetic resonance template for normal neuronal migration in the fetus. Neurosurgery 39: 110–116

Chung R, Kasprian G, Brugger PC, Prayer D (2009) The current state and future of fetal imaging. Clin Perinatol 36:685–699

Clark AG, Glanowski S, Nielsen R, Thomas PD, Kejariwal A, Todd MA, Tanenbaum DM, Civello D, Lu F, Murphy B, Ferriera S, Wang G, Zheng X, White TJ, Sninsky JJ, Adams MD, Cargill M (2003) Inferring nonneutral evolution from human-chimp-mouse orthologous gene trios. Science 302: 1960–1963

Clarke S, Miklossy J (1990) Occipital cortex in man: organization of callosal connections, related myelo- and cytoarchitecture,

and putative boundaries of functional visual areas. J Comp Neurol 298:188–214
Clemence AE, Mitrofanis J (1992) Cytoarchitectonic heterogeneities in the thalamic reticular nucleus of cats and ferrets. J Comp Neurol 322:167–181
Clowry G, Molnár Z, Rakic P (2010) Renewed focus on the developing human neocortex. J Anat 217:276–288
Conel JL (1939) The postnatal development of the human cerebral cortex, vol I: The cortex of the newborn. Harvard University Press, Cambridge
Conel JL (1941) The postnatal development of the human cerebral cortex, vol II: The cortex of the one-month infant. Harvard University Press, Cambridge
Conel JL (1947) The postnatal development of the human cerebral cortex, vol III: The cortex of the three-month infant. Harvard University Press, Cambridge
Conel JL (1951) The postnatal development of the human cerebral cortex, vol IV: The cortex of the six-month infant. Harvard University Press, Cambridge
Conel JL (1955) The postnatal development of the human cerebral cortex, vol V: The cortex of the fifteen-month infant. Harvard University Press, Cambridge
Conel JL (1959) The postnatal development of the human cerebral cortex, vol VI: The cortex of the twenty-four-month infant. Harvard University Press, Cambridge
Conel JL (1963) The postnatal development of the human cerebral cortex, vol VII: The cortex of a four year old child. Harvard University Press, Cambridge
Conel JL (1967) The postnatal development of the human cerebral cortex, vol VIII: The cortex of a six year old child. Harvard University Press, Cambridge
Corbo JC, Deuel TA, Long JM, LaPorte P, Tsai E, Wynshaw-Boris A, Walsh CA (2002) Doublecortin is required in mice for lamination of the hippocampus but not the neocortex. J Neurosci 22:7548–7557
Counsell SJ, Boardman JP (2005) Differential brain growth in the infant born preterm: current knowledge and future developments from brain imaging. Semin Fetal Neonatal Med 10:403–410
Counsell SJ, Dyet LE, Larkman DJ, Nunes RG, Boardman JP, Allsop JM, Fitzpatrick J, Srinivasan L, Cowan FM, Hajnal JV, Rutherford MA, Edwards AD (2007) Thalamo-cortical connectivity in children born preterm mapped using probabilistic magnetic resonance tractography. Neuroimage 34:896–904
De Bellis MD, Keshavan MS, Beers SR, Hall J, Frustaci K, Masalehdan A, Noll J, Boring AM (2001) Sex differences in brain maturation during childhood and adolescence. Cereb Cortex 11(6):552–557
DeAzevedo LC, Hedin-Pereira C, Lent R (1997) Callosal neurons in cingulate cortical plate and subplate of human fetuses. J Comp Neurol 386:60–70
DeAzevedo LC, Hedin-Pereira C, Lent R (2002) Diaphorase-positive neurons in the cingulate cortex of human fetuses during the second half of gestation. Anat Embryol 205:29–35
DeAzevedo LC, Fallet C, Moura-Neto V, Daumas-Duport C, Hedin-Pereira C, Lent R (2003) Cortical radial glial cells in human fetuses: depth-correlated transformation into astrocytes. J Neurobiol 55(3):288–298
DeDiego I, Smith-Fernandez A, Fairén A (1994) Cortical cells that migrate beyond area boundaries: characterization of an early neuronal population in the lower intermediate zone of prenatal rats. Eur J Neurosci 6:983–997
DeFelipe J (1993) A study of NADPH diaphorase-positive axonal plexuses in the human temporal cortex. Brain Res 615:342–346
DeFelipe J, Alonso-Nanclares L, Arellano JI (2002) Microstructure of the neocortex: comparative aspects. J Neurocytol 31:299–316
DeFelipe J, Alonso-Nanclares L, Arellano J, Ballesteros-Yánez I, Benavides-Piccione R, Munoz A (2007) Specializations of the cortical microstructure of humans. In: Kaas JH, Preuss TM (eds) Evolution of nervous system, vol 4: Primates. Elsevier, Oxford, pp 167–190
Dehay C, Kennedy H (2007) Cell-cycle control and cortical development. Nat Rev Neurosci 8:438–450
Dehay C, Kennedy H, Bullier J, Berland M (1988) Absence of interhemispheric connections of area 17 during development in the monkey. Nature 331:348–350
Dehay C, Horsburgh G, Berland M, Killackey H, Kennedy H (1991) The effects of bilateral enucleation in primate fetus on the parcellation of visual cortex. Dev Brain Res 62:137–141
Dehay C, Giroud P, Berland M, Smart I, Kennedy H (1993) Modulation of the cell cycle contributes to the parcellation of the primate visual cortex. Nature 366:464–466
Delalle I, Evers P, Kostović I, Uylings HBM (1997) Laminar distribution of neuropeptide Y-immunoreactive neurons in human prefrontal cortex during development. J Comp Neurol 379:515–522
Demeter S, Rosene DL, Van Hoesen GW (1985) Interhemispheric pathways of the hippocampal formation, presubiculum, and entorhinal and posterior parahippocampal cortices in the rhesus monkey: the structure and organization of the hippocampal commissures. J Comp Neurol 233:30–47
Demeter S, Rosene DL, Van Hoesen GW (1990) Fields of origin and pathways of the interhemispheric commissures in the temporal lobe of macaques. J Comp Neurol 302:29–53
Ding SL, Rockland KS, Zheng DS (2000) Parvalbumin immunoreactive Cajal-Retzius and non Cajal-Retzius neurons in layer I of different cortical regions of human newborn. Anat Embryol 201(5):407–417
Donaldson I, Gottgens B (2006) Evolution of candidate transcriptional regulatory motifs since the human-chimpanzee divergence. Genome Biol 7(6):R52
Donoghue MJ, Rakic P (1999) Molecular evidence for the early specification of presumptive functional domains in the embryonic primate cerebral cortex. J Neurosci 19:5967–5979
Doty RW (2007) Cortical commissural connections in Primates. In: Kaas JH, Preuss TM (eds) Evolution of nervous systems, vol 4: Primates. Elsevier, Amsterdam, pp 277–289
Downen M, Zhao ML, Lee P, Weidenheim KM, Dickson DW, Lee SC (1999) Neuronal nitric oxide synthase expression in developing and adult human CNS. J Neuropathol Exp Neurol 58:12–21
Dubois J, Benders M, Borradori-Tolsa C, Cachia A, Lazeyras F, Ha-Vinh RL, Sizonenko SV, Warfield SK, Mangin JF, Hüppi PS (2008a) Primary cortical folding in the human newborn: an early marker of later functional development. Brain 131:2028–2041
Dubois J, Benders M, Cachia A, Lazeyras F, Ha-Vinh RL, Sizonenko SV, Borradori-Tolsa C, Mangin JF, Hüppi PS

(2008b) Mapping the early cortical folding process in the preterm newborn brain. Cereb Cortex 18:1444–1454

Dubois J, Dehaene-Lambertz G, Perrin M, Mangin JF, Cointepas Y, Duchesnay E, Le Bihan D, Hertz-Pannier L (2008c) Asynchrony of the early maturation of white matter bundles in healthy infants: quantitative landmarks revealed noninvasively by diffusion tensor imaging. Hum Brain Mapp 29:14–27

Dziegielewska KM, Bell JE, Matthews N, Mollgard K, Saunders NR (1993a) Zn-binding globulin in human fetal brain and liver: a marker for passive blood/CSF transfer of protein. Neuropathol Appl Neurobiol 19:82–90

Dziegielewska KM, Reader M, Matthews N, Brown WM, Mollgard K, Saunders NR (1993b) Synthesis of the foetal protein fetuin by early developing neurons in the immature neocortex. J Neurocytol 22:266–272

Earle KL, Mitrofanis J (1996) Genesis and fate of the perireticular thalamic nucleus during early development. J Comp Neurol 367:246–263

Eckenhoff M, Rakic P (1984) Radial organization of the hippocampal dentate gyrus: a Golgi, ultrastructural and immunohistochemical analysis in the developing rhesus monkey. J Comp Neurol 223:1–21

Eichler EE, Johnson ME, Alkan C, Tuzun E, Sahinalp C, Misceo D, Archidiacono N, Rocchi M (2001) Divergent origins and concerted expansion of two segmental duplications on chromosome 16. J Hered 92(6):462–468

Elston GN (2003) Cortex, cognition and the cell: new insights into the pyramidal neuron and prefrontal function. Cereb Cortex 13:1124–1138

Elston GN (2007) Specialization of the neocortical pyramidal cell during primate evolution. In: Kaas JH, Preuss TM (eds) Evolution of nervous systems, vol 4: Primates. Elsevier, Oxford, pp 191–242

Enard W, Khaitovich P, Klose J, Zollner S, Heissig F, Giavalisco P, Nieselt-Struwe K, Muchmore E, Varki A, Ravid R, Doxiadis GM, Bontrop RE, Pääbo S (2002a) Intra- and interspecific variation in primate gene expression patterns. Science 296:340–343

Enard W, Przeworski M, Fisher SE, Lai CSL, Wiebe V, Kitano T, Monaco AP, Pääbo S (2002b) Molecular evolution of *FOXP2*, a gene involved in speech and language. Nature 418:869–872

Eriksson PS, Perfilieva E, Björk-Eriksson T, Alborn AM, Nordborg C, Peterson DA, Gage FH (1998) Neurogenesis in the adult human hippocampus. Nat Med 4(11):1313–1317

Estrada C, DeFelipe J (1998) Nitric oxide-producing neurons in the neocortex, morphological and functional relationship with intraparenchymal microvasculature. Cereb Cortex 8:193–203

Evans PD, Gilbert SL, Mekel-Bobrov N, Vallender EJ, Anderson JR, Vaez-Azizi LM, Tishkoff SA, Hudson RR, Lahn BT (2005) Microcephalin, a gene regulating brain size, continues to evolve adaptively in humans. Science 309:1717–1720

Eyre JA (2007) Corticospinal tract development and its plasticity after perinatal injury. Neurosci Biobehav Rev 31:1136–1149

Eyre JA, Miller S, Ramesh V (1991) Constancy of central conduction delays during development in man: investigation of motor and somatosensory pathways. J Physiol Lond 434:441–452

Eyre JA, Miller S, Clowry GJ, Conway E, Watts C (2000) Functional cortical projections are established in the human foetus permitting cortical involvement in the development of spinal motor centres. Brain 123:51–64

Eyre JA, Taylor JP, Villagra F, Smith M, Miller S (2001) Evidence of activity-dependent withdrawal of corticospinal projections during human development. Neurology 57(9): 1543–1554

Eyre JA, Smith M, Dabydeen L, Clowry GJ, Petacchi E, Battini R, Guzzetta A, Cioni G (2007) Is hemiplegic cerebral palsy equivalent to amblyopia of the corticospinal system? Ann Neurol 62(5):493–503

Fahrner A, Kann G, Flubacher A, Heinrich C, Freiman TM, Zentner J, Frotscher M, Haas CA (2007) Granule cell dispersion is not accompanied by enhanced neurogenesis in temporal lobe epilepsy patients. Exp Neurol 203: 320–332

Feess-Higgins A, Larroche JC (1987) Le développement du cerveau foetal humain. Atlas anatomique. Masson – INSERM-CNRS, Paris

Felderhoff-Mueser U, Rutherford MA, Squier WV, Cox P, Maalouf EF, Counsell SJ, Bydder GM, Edwards AD (1999) Relationship between MR imaging and histopathologic findings of the brain in extremely sick preterm infants. Am J Neuroradiol 20:1349–1357

Fertuzinhos S, Krsnik Ž, Kawasawa YI, Rašin MR, Kwan KY, Chen JG, Judaš M, Hayashi M, Šestan N (2009) Selective depletion of molecularly defined cortical interneurons in human holoprosencephaly with severe striatal hypoplasia. Cereb Cortex 19:2196–2207

Fietz SA, Kelava I, Vogt J, Wilsch-Brauninger M, Stenzel D, Fish JL, Corbeil D, Riehn A, Distler W, Nitsch R, Huttner WB (2010) OSVZ progenitors of human and ferret neocortex are epithelial-like and expand by integrin signaling. Nat Neurosci 13(6):690–699

Filimonov IN (1957) A rational subdivision of the cerebral cortex. Arch Neurol Psychiat (Chic) 58:296–311

Filipovic R, Zecevic N (2005) Interaction between microglia and oligodendrocyte cell progenitors involves Golli proteins. Ann NY Acad Sci 1048:166–174

Filipovic R, Zecevic N (2008) The effect of CXCL1 on human fetal oligodendrocyte progenitor cells. Glia 56:1–15

Filipovic R, Rakic S, Zecevic N (2002) Expression of Golli proteins in adult human brain and multiple sclerosis lesions. J Neuroimmunol 127:1–12

Filipovic R, Jakovcevski I, Zecevic N (2003) Expression pattern of GRO-α and CXCR2 in the human fetal brain and multiple sclerosis lesions. Dev Neurosci 25:279–290

Fish JL, Dehay C, Kennedy H, Huttner WB (2008) Making bigger brains: the evolution of neural-progenitor-cell division. J Cell Sci 121(Pt 17):2783–2793

Fishell G, Kriegstein AR (2003) Neurons from radial glia: the consequences of asymmetric inheritance. Curr Opin Neurobiol 13:34–41

Flax JD, Aurora S, Yang C, Simonin C, Wills AM, Billinghurst LL, Jendoubi M, Sidman RL, Wolfe JH, Kim SU, Snyder EY (1998) Engraftable human neural stem cells respond to developmental cues, replace neurons, and express foreign genes. Nat Biotechnol 16(11):1033–1039

Freeman TB, Spence MS, Boss BD, Spector DH, Strecker RE, Olanow CW, Kordower JH (1991) Development of dopaminergic neurons in the human substantia nigra. Exp Neurol 113:344–353

Friedlander MJ, Torres-Reveron J (2009) The changing roles of neurons in the cortical subplate. Front Neuroanat 3:15 (Vol. 3, article 15, pp. 1-8)

Fukuchi-Shimogori T, Grove EA (2001) Neocortex patterning by the secreted signaling molecule FGF8. Science 294:1071–1074

Gadisseux JF, Goffinet AM, Lyon G, Evrard P (1992) The human transient subpial granular layer: an optical, immunohistochemical, and ultrastructural analysis. J Comp Neurol 324:94–114

Gagneux P, Varki A (2001) Genetic differences between humans and great apes. Mol Phylogenet Evol 18:2–13

Gaiano N, Fishell G (2002) The role of notch in promoting glial and neural stem cell fates. Annu Rev Neurosci 25:471–490

Gal JS, Morozov YM, Ayoub AE, Chatterjee M, Rakic P, Haydar TF (2006) Molecular and morphological heterogeneity of neural precursors in the mouse neocortical proliferative zones. J Neurosci 26(3):1045–1056

Galea MP, Darian-Smith I (1995) Postnatal maturation of the direct corticospinal projections in the macaque monkey. Cereb Cortex 5:518–540

Garel C, Chantrel E, Brisse H, Elmaleh M, Luton D, Oury JF, Sebag G, Hassan M (2001) Fetal cerebral cortex: normal gestational landmarks identified using prenatal MR imaging. Am J Neuroradiol 22:184–189

Gebbia M, Ferrero GB, Pilia G, Bassi MT, Aylsworth A, Penman-Splitt M, Bird LM, Bamforth JS, Burn J, Schlessinger D, Nelson DL, Casey B (1997) X-linked situs abnormalities result from mutations in *ZIC3*. Nat Genet 17:305–308

Geschwind DH, Miller B (2001) Molecular approaches to cerebral laterality: development and neurodegeneration. Am J Med Genet 101(4):370–381

Gibson KR (1991) Myelination and behavioral development: A comparative perspective on questions of neoteny, altriciality and intelligence. In: Gibson KR, Peterson AC (eds) Brain maturation and cognitive development: comparative and cross-cultural perspectives. Aldine De Gruyter, New York, pp 29–63

Giedd JN (2004) Structural magnetic resonance imaging of the adolescent brain. Ann NY Acad Sci 1021:77–85

Giedd JN, Snell JW, Lange N, Rajapakse JC, Casey BJ, Kozuch PL, Vaituzis AC, Vauss YC, Hamburger SD, Kaysen D, Rapoport JL (1996a) Quantitative magnetic resonance imaging of human brain development: ages 4-18. Cereb Cortex 6:551–560

Giedd JN, Vaituzis AC, Hamburger SD, Lange N, Rajapakse JC, Kaysen D, Vauss YC, Rapoport JL (1996b) Quantitative MRI of the temporal lobe, amygdala, and hippocampus in normal human development: ages 4-18 years. J Comp Neurol 366:223–230

Giedd JN, Rumsey JM, Castellanos FX, Rajapakse JC, Kaysen D, Vaituzis AC, Vauss YC, Hamburger SD, Rapoport JL (1996c) A quantitative MRI study of the corpus callosum in children and adolescents. Dev Brain Res 91(2):274–280

Giedd JN, Castellanos FX, Rajapakse JC, Vaituzis AC, Rapoport JL (1997) Sexual dimorphism of the developing human brain. Prog Neuropsychopharmacol Biol Psychiatry 21: 1185–1201

Giedd JN, Blumenthal J, Jeffries NO, Castellanos FX, Liu H, Zijdenbos A, Paus T, Evans AC, Rapoport JL (1999a) Brain development during childhood and adolescence: a longitudinal MRI study. Nat Neurosci 2:861–863

Giedd JN, Blumenthal J, Jeffries NO, Rajapakse JC, Vaituzis AC, Lin H, Berry YC, Tobin M, Nelson J, Castellanos FX (1999b) Development of the human corpus callosum during childhood and adolescence: a longitudinal MRI study. Prog Neuropsychopharmacol Biol Psychiatry 23:571–588

Girard NJ, Raybaud CA (1992) In vivo MRI of fetal brain cellular migration. J Comp Assist Tomogr 16:265–267

Girard NJ, Raybaud CA, Poncet M (1995) In vivo MR study of brain maturation in normal fetuses. Am J Neuroradiol 16:407–413

Gleeson JG, Walsh CA (2000) Neuronal migration disorders: from genetic diseases to developmental mechanisms. Trends Neurosci 23:352–359

Gogtay N, Giedd JN, Lusk L, Hayashi KM, Greenstein DK, Vaituzis AC, Nugent TF, Herman D, Clasen LS, Toga AW, Rapoport JL, Thompson PM (2004) Dynamic mapping of human cortical development during childhood through early adulthood. Proc Natl Acad Sci USA 101:8174–8179

Goldman-Rakic PS (1980) Morphological consequences of prenatal injury to the primate brain. Prog Brain Res 53:1–19

Goldman-Rakic PS (1982) Neuronal development and plasticity of association cortex in primates. Neurosci Res Program Bull 20:520–532

Goldman-Rakic PS, Rakic P (1984) Experimental modification of gyral patterns. In: Geschwind N, Galaburda A (eds) Cerebral dominance. Harvard University Press, Cambridge, pp 179–192

Götz M, Huttner WB (2005) The cell biology of neurogenesis. Nat Rev Mol Cell Biol 6:777–788

Gould SJ, Howard S (1987) An immunohistochemical study of the germinal layer in the late gestation human fetal brain. Neuropathol Appl Neurobiol 13(6):421–437

Gould SJ, Howard S, Papadaki L (1990) The development of ependyma in the human fetal brain: an immunohistological and electron microscopy study. Dev Brain Res 55(2):255–267

Gould E, Tanapat P, McEwen BS, Flügge G, Fuchs E (1998) Proliferation of granule cell precursors in the dentate gyrus of adult monkeys is diminished by stress. Proc Natl Acad Sci USA 95(6):3168–3171

Gould E, Reeves AJ, Fallah M, Tapanat P, Gross CG, Fuchs E (1999a) Hippocampal neurogenesis in adult old world primates. Proc Natl Acad Sci USA 96(9):5263–5267

Gould E, Reeves AJ, Graziano MSA, Gross CG (1999b) Neurogenesis in the neocortex of adult primates. Science 286:548–552

Gould E, Vail N, Wagers M, Gross CG (2001) Adult-generated hippocampal and neocortical neurons in macaques have a transient existence. Proc Natl Acad Sci USA 98(19): 10910–10917

Grever WE, Chiu FC, Tricoche M, Rashbaum WK, Weidenheim KM, Lyman WD (1996) Quantification of myelin basic protein in the human fetal spinal cord during midtrimester of gestation. J Comp Neurol 376:306–314

Grove EA, Tole S (1999) Patterning events and specification signals in the developing hippocampus. Cereb Cortex 9: 551–561

Gu J, Gu X (2003) Induced gene expression in human brain after the split from chimpanzee. Trends Genet 19(2):63–65

Guerrini R, Dobyns WB, Barkovich JA (2008) Abnormal development of the human cerebral cortex: genetics, functional consequences and treatment options. Trends Neurosci 31(3): 154–162

Gupta RK, Hasan KM, Trivedi R, Pradhan M, Das V, Parikh NA, Narayana PA (2005) Diffusion tensor imaging of the developing human cerebrum. J Neurosci Res 81:172–178

Hamasaki T, Leingartner A, Ringstedt T, O'Leary DD (2004) *EMX2* regulates sizes and positioning of the primary sensory and motor areas in neocortex by direct specification of cortical progenitors. Neuron 43(3):359–372

Hansen DV, Lui JH, Parker PR, Kriegstein AR (2010) Neurogenic radial glia in the outer subventricular zone of human neocortex. Nature 464:554–561

Harris EE, Meyer D (2006) The molecular signature of selection underlying human adaptations. Yearb Phys Anthropol 49:89–130

Hartfuss E, Galli R, Heins N, Götz M (2001) Characterization of CNS precursor subtypes and radial glia. Dev Biol 229: 15–30

Haubensak W, Attardo A, Denk W, Huttner WB (2004) Neurons arise in the basal neuroepithelium of the early mammalian telencephalon: a major site of neurogenesis. Proc Natl Acad Sci USA 101(9):3196–3201

Hayakawa T, Angata T, Lewis AL, Mikkelsen TS, Varki NM, Varki A (2005) A human-specific gene in microglia. Science 309:1693

Hayashi M, Yamashita A, Shimizu K, Oshima K (1989) Ontogeny of cholecystokinin-8 and glutamic acid decarboxylase in cerebral neocortex of macaque monkey. Exp Brain Res 74:249–255

Haydar TF, Kuan CY, Flavell RA, Rakic P (1999) The role of cell death in regulating the size and shape of the mammalian forebrain. Cereb Cortex 9:621–626

Haynes RL, Borenstein NS, Desilva TM, Folkerth RD, Liu LG, Volpe JJ, Kinney HC (2005) Axonal development in the cerebral white matter of the human fetus and infant. J Comp Neurol 484:156–167

Heinrich C, Nitta N, Flubacher A, Muller M, Fahrner A, Kirsch M, Freiman T, Susuki F, Depaulis A, Frotscher M, Haas CA (2006) Reelin deficiency and displacement of mature neurons, but not neurogenesis, underlie the formation of granule cell dispersion in the epileptic hippocampus. J Neurosci 26:4701–4703

Hendry SH, Jones EG, Killackey HP, Chalupa LM (1987a) Choline acetyltransferase-immunoreactive neurons in fetal monkey cerebral cortex. Brain Res 465:311–317

Hernández-Miranda LR, Parnavelas JG, Chiara F (2010) Molecules and mechanisms involved in the generation and migration of cortical interneurons. ASN Neuro 2(2):art:e00031. doi:10.1042/AN20090053

Hevner RF (2005) Development of connections in the human visual system during fetal midgestation: a Dil-tracing study. J Neuropathol Exp Neurol 59:385–392

Hevner RF (2007) Layer-specific markers as probes for neuron type identity in human neocortex and malformations of cortical development. J Neuropathol Exp Neurol 66(2): 101–109

Hevner RF, Kinney HC (1996) Reciprocal entorhinal-hippocampal connections established by human fetal midgestation. J Comp Neurol 372(3):384–394

Hilgetag CC, Barbas H (2005) Developmental mechanics of the primate cerebral cortex. Anat Embryol 210:411–417

Hilgetag CC, Barbas H (2006) Role of mechanical factors in the morphology of the primate cerebral cortex. PLoS Comput Biol 2:e22

Hill RS, Walsh CA (2005) Molecular insights into human brain evolution. Nature 437:64–67

Hines M (1922) Studies in the growth and differentiation of the telencephalon in man: the fissura hippocampi. J Comp Neurol 34:73–171

His W (1904) Die Entwickelung des menschlichen Gehirns während der ersten Monate. Untersuchungsergebnisse. Hirzel, Leipzig

Hochstetter F (1919) Beiträge zur Entwicklungsgeschichte des menschlichen Gehirns. I. Teil. Deuticke, Wien

Hochstetter F (1923) Beiträge zur Entwicklungsgeschichte des menschlichen Gehirns. II. Teil, 1. Lieferung. Die Entwicklung der Zirbeldrüse. Deuticke, Wien

Hochstetter F (1929) Beiträge zur Entwicklungsgeschichte des menschlichen Gehirns. II. Teil, 3. Lieferung. Die Entwicklung des Mittel- und Rautenhirns. Deuticke, Wien

Hochstetter F (1934) Ueber die Entwicklung und Differenzierung der Hüllen des Rückenmarkes beim Menschen. Morphol Jahrb 74:1–104

Hochstetter F (1939) Ueber die Entwicklung und Differenzierung der Hüllen des menschlichen Gehirnes. Morphol Jahrb 83:359–494

Hoerder-Suabedissen A, Wang WZ, Lee S, Davies KE, Goffinet AM, Rakic S, Parnavelas J, Reim K, Nicolić M, Paulsen O, Molnár Z (2009) Novel markers reveal subpopulations of subplate neurons in the murine cerebral cortex. Cereb Cortex 19:1738–1750

Hof PR, Sherwood CC (2007) The evolution of neuron classes in the neocortex of mammals. In: Kaas JH, Krubitzer LA (eds) Evolution of nervous systems, vol 3: Mammals. Elsevier, Oxford, pp 113–124

Hof PR, Nimchinsky EA, Perl DP, Erwin JM (2001) An unusual population of pyramidal neurons in the anterior cingulate cortex of hominids contains the calcium-binding protein calretinin. Neurosci Lett 307:139–142

Hong SE, Shugart YY, Huang DT, Shahwan SA, Grant PE, Hourihane JOB, Martin NDT, Walsh CA (2000) Autosomal recessive lissencephaly with cerebellar hypoplasia is associated with human *RELN* mutations. Nat Genet 26(1):93–96 (erratum in Nat Genet 27(2):225, 2001)

Honig LS, Herrmann K, Shatz CJ (1996) Developmental changes revealed by immunohistochemical markers in human cerebral cortex. Cereb Cortex 6:794–806

Howard B, Chen Y, Zecevic N (2006) Cortical progenitor cells in the developing human telencephalon. Glia 53:57–66

Hsieh WP, Chu TM, Wolfinger RD, Gibson G (2003) Mixed-model reanalysis of primate data suggests tissue and species biases in oligonucleotide-based gene expression profiles. Genetics 165(2):747–757

Huang H, Zhang J, Wakana S, Zhang W, Ren T, Richards LJ, Yarowsky P, Donohue P, Graham E, van Zijl PCM, Mori S (2006) White and gray matter development in human fetal, newborn and pediatric brains. Neuroimage 33: 27–38

Huang H, Xue R, Zhang J, Ren T, Richards LJ, Yarowsky P, Miller MI, Mori S (2009) Anatomical characterization of

human fetal brain development with diffusion tensor magnetic resonance imaging. J Neurosci 29:4263–4273
Humphrey T (1960) The development of the pyramidal tracts in human fetuses, correlated with cortical differentiation. In: Tower DB, Schade JP (eds) Structure and function of the cerebral cortex. Elsevier, Amsterdam, pp 93–103
Humphrey T (1966) The development of the human hippocampal formation correlated with some aspects of its phylogenetic history. In: Hassler R, Stephan H (eds) Evolution of the forebrain. Plenum Press, New York, pp 104–116
Humphrey T (1967) The development of the human hippocampal fissure. J Anat 101:655–676
Humphrey T (1968) The development of the human amygdala during early embryonic life. J Comp Neurol 132:135–165
Huntley GW, Hendry SH, Killackey HP, Chalupa LM, Jones EG (1988) Temporal sequence of neurotransmitter expression by developing neurons of fetal monkey visual cortex. Brain Res 471:69–96
Huntley GW, deBlas AL, Jones EG (1990) GABA-A receptor immunoreactivity in adult and developing monkey sensorymotor cortex. Exp Brain Res 82:519–535
Hüppi PS, Dubois J (2006) Diffusion tensor imaging of brain development. Semin Fetal Neonatal Med 11:489–497
Hüppi PS, Maier SE, Peled S, Zientara GP, Barnes PD, Jolesz FA, Volpe JJ (1998) Microstructural development of human newborn cerebral white matter assessed in vivo by diffusion tensor magnetic resonance imaging. Pediatr Res 44:584–590
Hüppi PS, Murphy B, Maier SE, Zientara GP, Inder TE, Barnes PD, Kikinis R, Jolesz FA, Volpe JJ (2001) Microstructural brain development after perinatal cerebral white matter injury assessed by diffusion tensor magnetic resonance imaging. Pediatrics 107:455–460
Huttenlocher PR (1979) Synaptic density in human frontal cortex. Developmental changes and effects of aging. Brain Res 163:195–205
Huttenlocher PR, Dabholkar AS (1997) Regional differences in synaptogenesis in human cerebral cortex. J Comp Neurol 387:167–178
Huttenlocher PR, De Courten C, Garey LJ, Van der Loos H (1982) Synaptogenesis in human visual cortex – evidence for synapse elimination during normal development. Neurosci Lett 33:247–252
Ip BK, Wappler I, Peters H, Lindsay S, Clowry GJ, Bayatti N (2010) Investigating gradients of gene expression involved in early human cortical development. J Anat 217:300–311
Jacobs B, Driscoll L, Schall M (1997) Life-span dendritic and spine changes in areas 10 and 18 of human cortex: a quantitative golgi study. J Comp Neurol 386:661–680
Jakovcevski I, Zecevic N (2005a) Olig transcription factors are expressed in oligodendrocyte and neuronal cells in human fetal CNS. J Neurosci 25:10064–10073
Jakovcevski I, Zecevic N (2005b) Sequence of oligodendrocyte development in the human fetal telencephalon. Glia 49: 480–491
Jakovcevski I, Mo Z, Zecevic N (2007) Down-regulation of the axonal polysialic acid-neural cell adhesion molecule expression coincides with the onset of myelination in the human fetal forebrain. Neuroscience 149:328–337
Jakovcevski I, Filipovic R, Mo Z, Rakic S, Zecevic N (2009) Oligodendrocyte development and the onset of myelination in the human fetal brain. Front Neuroanat 3(5):1–15
Jernigan TL, Tallal P (1990) Late childhood changes in brain morphology observable with MRI. Dev Med Child Neurol 32:379–385
Jernigan TL, Trauner DA, Hesselink JR, Tallal PA (1991a) Maturation of human cerebrum observed in vivo during adolescence. Brain 114:2037–2049
Jernigan TL, Archibald SL, Berhow MT, Sowell ER, Foster DS, Hesselink JR (1991b) Cerebral structure on MRI. Part I: localization of age-related changes. Biol Psychiatry 29: 55–67
Jiménez D, Rivera R, López-Mascaraque L, De Carlos JA (2003) Origin of the cortical layer I in rodents. Dev Neurosci 25: 105–115
Jin K, Wang X, Xie L, Mao XO, Zhu W, Wang Y, Shen J, Mao Y, Banwait S, Greenberg DA (2006) Evidence for stroke-induced neurogenesis in the human brain. Proc Natl Acad Sci USA 103(35):13198–13202
Johnson ME, Viggiano L, Bailey JA, Abdul-Rauf M, Goodwin G, Rocchi M, Eichler EE (2001) Positive selection of a gene family during the emergence of humans and African apes. Nature 413:514–519
Johnson MB, Kawasawa YI, Mason CE, Krsnik Ž, Coppola G, Bogdanović D, Geschwind DH, Mane SM, State MW, Šestan N (2009) Functional and evolutionary insights into human brain development through global transcriptome analysis. Neuron 62:494–509
Jones EG (1997) Cortical development and thalamic pathology in schizophrenia. Schizophr Bull 23:483–501
Jones EG (2009) The origins of cortical interneurons: mouse vs. monkey and human. Cereb Cortex 19:1953–1956
Jovanov-Milošević N, Čuljat M, Kostović I (2009) Growth of the human corpus callosum: modular and laminar morphogenetic zones. Front Neuroanat 3:1–10
Jovanov-Milošević N, Petanjek Z, Petrović D, Judaš M, Kostović I (2010) Morphology, molecular phenotypes and distribution of neurons in developing human corpus callosum. Eur J Neurosci 32:1423–1432
Judaš M, Cepanec M (2007) Adult structure and development of the human fronto-opercular cerebral cortex (Broca's region). Clin Linguist Phon 21:975–989
Judaš M, Pletikos M (2010) The discovery of the subpial granular layer in the human cerebral cortex. Transl Neurosci 1(3):255–260
Judaš M, Šestan N, Kostović I (1999) Nitrinergic neurons in the developing and adult human telencephalon: transient and permanent patterns of expression in comparison to other mammals. Microsc Res Techn 45:401–419
Judaš M, Milošević NJ, Rašin MR, Heffer-Lauc M, Kostović I (2003a) Complex patterns and simple architects: molecular guidance cues for developing axonal pathways in the telencephalon. Prog Mol Subcell Biol 32:1–32
Judaš M, Rašin MR, Krušlin B, Kostović K, Jukić D, Petanjek Z, Kostović I (2003b) Dendritic overgrowth and alterations in laminar phenotypes of neocortical neurons in the newborn with semilobar holoprosencephaly. Brain Dev 25: 32–39
Judaš M, Radoš M, Jovanov-Milošević N, Hrabač P, Štern-Padovan R, Kostović I (2005) Structural, immunocytochemical, and MR imaging properties of periventricular crossroads of growing cortical pathways in preterm infants. Am J Neuroradiol 26:2671–2784

Judaš M, Sedmak G, Radoš M, Sarnavka V, Fumić K, Willer T, Gross C, Hehr U, Strahl S, Ćuk M, Barić I (2009) POMT1-Associated Walker-Warburg syndrome: a disorder of dendritic development of neocortical neurons. Neuropediatrics 40:6–14

Judaš M, Sedmak G, Pletikos M (2010a) Early history of subplate and interstitial neurons: from Theodor Meynert (1867) to the discovery of the subplate zone (1974). J Anat 217:344–367

Judaš M, Sedmak G, Pletikos M, Jovanov-Milošević N (2010b) Populations of subplate and interstitial neurons in fetal and adult human telencephalon. J Anat 217:381–399

Judaš M, Šimić G, Petanjek Z, Jovanov-Milošević N, Pletikos M, Vasung L, Kostović I (2010c) Zagreb Collection of human brains: unique, versatile but underexploited added value resource for neuroscience community. Ann N Y Acad Sci (in press)

Kaas JH, Preuss TM (eds) (2007) Evolution of nervous systems, vol 4: Primates. Elsevier, Amsterdam, p 730

Kadhim HJ, Gadisseux JF, Evrard P (1988) Topographical and cytological evolution of the glial phase during prenatal development of the human brain: histochemical and electron microscopic study. J Neuropathol Exp Neurol 47:166–188

Kaes T (1907) Die Grosshirnrinde des Menschen in ihrem Massen und in ihrem Fasergehalt. Fischer, Jena

Kahle W (1969) Die Entwicklung der menschlichen Grosshirnhemisphäre. Springer, Berlin, p 116

Kanazir S, Ruzdijic S, Vukosavic S, Ivkovic S, Milosevic A, Zecevic N, Lj R (1996) GAP-43 mRNA expression in early development of human nervous system. Mol Brain Res 38:145–155

Kanold PO, Luhmann HJ (2010) The subplate and early cortical circuits. Annu Rev Neurosci 33:23–48

Kasprian G, Brugger PC, Weber M, Krssák M, Krampl E, Herold C, Prayer D (2008) In utero tractography of fetal white matter development. Neuroimage 43:213–224

Kasprian G, Langs G, Brugger PC, Bittner M, Weber M, Arantes M, Prayer D (2010) The prenatal origin of hemispheric asymmetry: an in utero neuroimaging study. Cereb Cortex. doi:10.1093/cercor/bhq179

Kempermann G (2002) Why new neurons? Possible functions for adult hippocampal neurogenesis. J Neurosci 22(3):635–638

Kennedy H, Dehay C (1993) Cortical specification of mice and men. Cereb Cortex 3:171–186

Kerwin J, Yang Y, Merchan P, Sarma S, Thompson J, Wang X, Sandoval J, Puelles L, Baldock R, Lindsay S (2010) The HUDSEN Atlas: a three-dimensional (3D) spatial framework for studying gene expression in the developing human brain. J Anat 217:289–299

Keshavan MS, Diwadkar VA, DeBellis M, Dick E, Kotwal R, Rosenberg DR, Sweeney JA, Minshew N, Pettegrew JW (2002) Development of the corpus callosum in childhood, adolescence and early adulthood. Life Sci 70:1909–1922

Khaitovich P, Hellmann I, Enard W, Nowick K, Leinweber M, Franz H, Weiss G, Lachmann M, Pääbo S (2005) Parallel patterns of evolution in the genomes and transcriptomes of humans and chimpanzees. Science 309:1850–1854

Killackey HP, Chalupa LM (1986) Ontogenetic change in the distribution of callosal projection neurons in the postcentral gyrus of the fetal rhesus monkey. J Comp Neurol 244: 331–348

Killackey HP, Gould HJ III, Cusick CG, Pons TP, Kaas JH (1983) The relation of corpus callosum connections to architectonic fields and body surface maps in sensorimotor cortex of new and old world monkeys. J Comp Neurol 219: 384–419

Kim HT, Kim IS, Lee IS, Lee JP, Snyder EY, Park KI (2006) Human neurospheres derived from the fetal central nervous system are regionally and temporally specified but are not committed. Exp Neurol 199(1):222–235

Kim SY, Chung HS, Sun W, Kim H (2007) Spatiotemporal expression pattern of non-clustered protocadherin family members in the developing rat brain. Neuroscience 147(4): 996–1021

Kim DH, Chung SW, Vigneron DB, Barkovich AJ, Glenn OA (2008) Diffusion-weighted imaging of the fetal brain *in vivo*. Magn Res Med 59:216–220

Kinney HC, Brody BA, Kloman AS, Gilles FH (1988) Sequence of central nervous system myelination in human infancy. II. Patterns of myelination in autopsied infants. J Neuropathol Exp Neurol 47:217–234

Kinney HC, Karthigasan J, Borenshteyn NI, Flax JD, Kirschner DA (1994) Myelination in the developing human brain: biochemical correlates. Neurochem Res 19:983–996

Kirschenbaum B, Nedergaard M, Preuss A, Barami K, Fraser RA, Goldman SA (1994) In-vitro neuronal production and differentiation by precursor cells derived from the adult human forebrain. Cereb Cortex 4:576–589

Koketsu D, Mikami A, Miyamoto Y, Hisatsune T (2003) Nonrenewal of neurons in the cerebral neocortex of adult Macaque monkeys. J Neurosci 23(3):937–942

Konstantinidou AD, Silos-Santiago I, Flaris N, Snider WD (1995) Development of the primary afferent projection in human spinal cord. J Comp Neurol 354:11–12

Kordower JH, Mufson EJ (1992) Nerve growth factor receptor-immunoreactive neurons within the developing human cortex. J Comp Neurol 323:25–41

Kordower JH, Rakic P (1990) Neurogenesis of the magnocellular basal forebrain nuclei in the rhesus monkey. J Comp Neurol 292:637–653

Kordower JH, Piecinski P, Rakic P (1992) Neurogenesis of the amygdaloid nuclear complex in the rhesus monkey. Dev Brain Res 68:9–15

Kornack DR (2000) Neurogenesis and the evolution of cortical diversity: mode, tempo, and partitioning during development and persistence in adulthood. Brain Behav Evol 55(6):336–344

Kornack DR, Rakic P (1998) Changes in cell-cycle kinetics during the development and evolution of primate neocortex. Proc Natl Acad Sci USA 95:1242–1246

Kornack DR, Rakic P (1999) Continuation of neurogenesis in the hippocampus of the adult macaque monkey. Proc Natl Acad Sci USA 96(10):5768–5773

Kornack DR, Rakic P (2001a) The generation, migration, and differentiation of olfactory neurons in the adult primate brain. Proc Natl Acad Sci USA 98(8):4752–4757

Kornack DR, Rakic P (2001b) Cell proliferation without neurogenesis in adult primate neocortex. Science 294: 2127–2130

Korr H, Schmitz C (1999) Facts and fictions regarding postnatal neurogenesis in the developing human cerebral cortex. J Theor Biol 200:291–297

Kostović I (1986) Prenatal development of nucleus basalis complex and related fiber systems in man: a histochemical study. Neuroscience 17:1047–1077

Kostović I (1990a) Zentralnervensystem. In: Hinrichsen KV (ed) Humanembryologie. Springer, Berlin/Heidelberg, pp 381–448

Kostović I (1990b) Structural and histochemical reorganization of the human prefrontal cortex during perinatal and postnatal life. Prog Brain Res 85:223–240

Kostovic I, Goldman-Rakic PS (1983) Transient cholinesterase staining in the mediodorsal nucleus of the thalamus and its connections in the developing human and monkey brain. J Comp Neurol 219:431–447

Kostović I, Jovanov-Milošević N (2006) The development of cerebral connections during the first 20-45 weeks' gestation. Semin Fetal Neonatal Med 11:415–422

Kostović I, Judaš M (1994) Prenatal and perinatal development of the human cerebral cortex. In: Kurjak A, Chervenak FA (eds) Fetus as a Patient. Parthenon Publishing Group, Casterton, pp 35–55

Kostović I, Judaš M (1995) Prenatal development of the cerebral cortex. In: Chervenak FA, Kurjak A, Comstock CH (eds) Ultrasound and the fetal brain (Progress in obstetric and gynecological sonography series). The Parthenon Publishing Group, New York/London, pp 1–26

Kostović I, Judaš M (2002a) Correlation between the sequential ingrowth of afferents and transient patterns of cortical lamination in preterm infants. Anat Rec 267:1–6

Kostović I, Judaš M (2002b) The role of the subplate zone in the structural plasticity of the developing human cerebral cortex. Neuroembryology 1:145–153

Kostović I, Judaš M (2006) Prolonged coexistence of transient and permanent circuitry elements in the developing cerebral cortex of fetuses and preterm infants. Dev Med Child Neurol 48:388–393

Kostović I, Judaš M (2007) Transient patterns of cortical lamination during prenatal life: do they have implications for treatment? Neurosci Biobehav Rev 31:1157–1168

Kostović I, Judaš M (2009) Early development of neuronal circuitry of the human prefrontal cortex. In: Gazzaniga MS (ed) The cognitive neurosciences, 4th edn. A Bradford Book, The MIT Press, Cambridge/London, pp 29–47

Kostović I, Judaš M (2010) The development of the subplate and thalamocortical connections in the human foetal brain. Acta Paediatr 99:1119–1127

Kostović I, Krmpotić J (1976) Early prenatal ontogenesis of the neuronal connections in the interhemispheric cortex of the human gyrus cinguli. Verh Anat Ges 70:305–316

Kostović I, Molliver ME (1974) A new interpretation of the laminar development of cerebral cortex: synaptogenesis in different layers of neopallium in the human fetus. Anat Rec 178:395

Kostovic I, Rakic P (1980) Cytology and time of origin of interstitial neurons in the white matter in infant and adult human and monkey telencephalon. J Neurocytol 9:219–242

Kostovic I, Rakic P (1984) Development of prestriate visual projections in the monkey and human fetal cerebrum revealed by transient cholinesterase staining. J Neurosci 4:25–42

Kostovic I, Rakic P (1990) Developmental history of the transient subplate zone in the visual and somatosensory cortex of the macaque monkey and human brain. J Comp Neurol 297:441–470

Kostović I, Vasung L (2009) Insights from in vitro fetal magnetic resonance imaging of cerebral development. Semin Perinatol 33:220–233

Kostović I, Judaš M, Bogdanović N (1987) Perinatal cytoarchitectonic development of the prospective "premotor" cortical belt in man. Verh Anat Ges 81:533–534

Kostović I, Škavić J, Strinović D (1988) Acetylcholinesterase in the human frontal associative cortex during the period of cognitive development: early laminar shifts and late innervation of pyramidal neurons. Neurosci Lett 90:107–112

Kostović I, Seress L, Mrzljak L, Judaš M (1989a) Early onset of synapse formation in the human hippocampus: a correlation with Nissl-Golgi architectonics in 15- and 16.5-week-old foetuses. Neuroscience 30:105–116

Kostović I, Lukinović N, Judaš M, Bogdanović N, Mrzljak L, Zečević D, Kubat M (1989b) Structural basis of the developmental plasticity in the human cerebral cortex: the role of the transient subplate zone. Metab Brain Dis 4:17–23

Kostović I, Judaš M, Lj K-K, Šimić G, Delalle I, Chudy D, Šajin B, Petanjek Z (1991a) Zagreb research collection of human brains for developmental neurobiologists and clinical neuroscientists. Int J Dev Biol 35:215–230

Kostović I, Štefulj-Fučić A, Mrzljak L, Jukić S, Delalle I (1991b) Prenatal and perinatal development of the somatostatin-immunoreactive neurons in the human prefrontal cortex. Neurosci Lett 124:153–156

Kostović I, Petanjek Z, Judaš M (1993) Early areal differentiation of the human cerebral cortex: entorhinal area. Hippocampus 3:447–458

Kostović I, Judaš M, Petanjek Z, Šimić G (1995) Ontogenesis of goal-directed behavior: anatomo-functional considerations. Int J Psychophysiol 19:85–102

Kostović I, Judaš M, Radoš M, Hrabač P (2002a) Laminar organization of the human fetal cerebrum revealed by histochemical markers and magnetic resonance imaging. Cereb Cortex 12:536–544

Kostović I, Rašin MR, Petanjek Z, Judaš M (2002b) Morphological characteristics of the cells in the subcallosal zone (Nucleus septohippocampalis) of the human fetus. Neuroembryology 1:97–104

Kostović I, Jovanov-Milošević N, Krsnik Ž, Petanjek Z, Judaš M (2004) Laminar organization of the marginal zone in the human fetal cortex. Neuroembryology 3:19–26

Kostović I, Judaš M, Petanjek Z (2008) Structural development of the human prefrontal cortex. In: Nelson CA, Luciana M (eds) Handbook of developmental cognitive neuroscience, 2nd edn. A Bradford Book, The MIT Press, Cambridge/London, pp 213–235

Kostović I, Judaš M, Sedmak G (2010) Developmental history of the subplate zone, subplate neurons and interstitial white matter neurons: relevance for schizophrenia. Int J Dev Neurosci. doi:10.1016/ijdevneu.2010.09.005

Kriegstein AR, Noctor SC (2004) Patterns of neuronal migration in the embryonic cortex. Trends Neurosci 27:392–399

Kriegstein AR, Parnavelas JG (2003) Changing concepts of cortical development. Cereb Cortex 13:541–699

Kriegstein A, Noctor S, Martinez-Cerdeno V (2006) Patterns of neural stem and progenitor cell division may underlie evolutionary cortical expansion. Nat Rev Neurosci 7:883–890

Krisch B (1988) Ultrastructure of the meninges at the site of penetration of veins through the dura mater, with particular

reference to Pacchionian granulations. Cell Tissue Res 251:621–631
Krmpotić-Nemanić J, Kostović I, Kelović Z, Nemanić D, Mrzljak L (1983) Development of the human fetal auditory cortex: growth of afferent fibres. Acta Anat 116:69–73
Krmpotić-Nemanić J, Kostović I, Nemanić Đ (1984) Prenatal and perinatal development of radial cell columns in the human auditory cortex. Acta Otolaryngol (Stockh) 97: 489–495
Krmpotić-Nemanić J, Kostović I, Vidić Z, Nemanić D, Kostović-Knežević LJ (1987) Development of Cajal-Retzius cells in the human auditory cortex. Acta Otolaryngol (Stockh) 103:477–480
Krmpotić-Nemanić J, Kostović I, Bogdanović N, Fučić A, Judaš M (1988) Cytoarchitectonic parameters of developmental capacity of the human associative auditory cortex during postnatal life. Acta Otolaryngol (Stockh) 105:463–466
Kudo LC, Karsten SL, Chen J, Levitt P, Geschwind DH (2007) Genetic analysis of anterior posterior expression gradients in the developing mammalian forebrain. Cereb Cortex 17(9): 2108–2122
Kuida K, Zheng TS, Na S, Kuang CY, Yang D, Karasuyama H, Rakic P, Flavell RA (1996) Decreased apoptosis in the brain and premature lethality in CPP32-deficient mice. Nature 384:368–372
Kukekov VG, Laywell ED, Suslov O, Davies K, Scheffler B, Thomas LB, O'Brien TF, Kusakabe M, Steindler DA (2002) Multipotent stem/progenitor cells with similar properties arise from two neurogenic regions of adult human brain. Exp Neurol 156(2):333–344
Kuljis RO, Rakic P (1989) Distribution of neuropeptide Y-containing perikarya and axons in various neocortical areas in the macaque monkey. J Comp Neurol 280:383–392
Lako M, Lindsay S, Bullen P, Wilson DI, Robson SC, Strachan T (1998) A novel mammalian *wnt* gene, *WNT8B*, shows brain-restricted expression in early development, with sharply delimited expression boundaries in the developing forebrain. Hum Mol Genet 7(5):813–822
LaMantia AS, Rakic P (1990a) Cytological and quantitative characteristics of four cerebral commissures in the rhesus monkey. J Comp Neurol 291:520–537
LaMantia AS, Rakic P (1990b) Axon overproduction and elimination in the corpus callosum of the developing rhesus monkey. J Neurosci 10:2156–2175
LaMantia AS, Rakic P (1994) Axon overproduction and elimination in the anterior commissure of the developing rhesus monkey. J Comp Neurol 340:328–336
Lambe EK, Krimer LS, Goldman-Rakic PS (2000) Differential postnatal development of catecholamine and serotonin inputs to identified neurons in prefrontal cortex of rhesus monkey. J Neurosci 20:8780–8787
Lan LM, Yamashita Y, Tang Y, Sugahara T, Takahashi M, Ohba T, Okamura H (2000) Normal fetal brain development: MR imaging with a half-Fourier rapid acquisition with relaxation enhancement sequence. Radiology 215:205–210
Larroche JC (1981) The marginal layer in the neocortex of a 7 week-old human embryo. A light and electron microscopic study. Anat Embryol 162:301–312
Larroche JC, Houcine O (1982) Le néo-cortex chez l'embryon et le foetus humain. Apport du microscope électronique et du Golgi. Reprod Nutr Dév 22(1B):163–170
Larroche JC, Privat A, Jardin L (1981) Some fine structures of the human fetal brain. In: Monset-Couchard M, Minkowski A (eds) Physiological and biochemical basis for perinatal medicine. S. Karger, Basel, pp 350–358
Laywell ED, Rakic P, Kukekov VG, Holland EC, Steindler D (2000) Identification of a multipotent astrocytic stem cell in the immature and adult mouse brain. Proc Natl Acad Sci USA 97(25):13883–13888
LeGros WEC (1945) Deformation patterns of the cerebral cortex. In: LeGros WEC, Medawar PB (eds) Essays on growth and form. Oxford University Press, Oxford, pp 1–23
Lenroot RK, Giedd JN (2006) Brain development in children and adolescents: insights from anatomical magnetic resonance imaging. Neurosci Biobehav Rev 30:718–729
Letinic K, Kostovic I (1998) Postnatal development of calcium-binding proteins calbindin and parvalbumin in human visual cortex. Cereb Cortex 8:660–669
Letinić K, Kostović I (1996a) Transient neuron population of the internal capsule in the developing human cerebrum. NeuroReport 7:2159–2162
Letinić K, Kostović I (1996b) Transient patterns of calbindin-D28k expression in the developing striatum of man. Neurosci Lett 220:211–214
Letinić K, Kostović I (1997) Transient fetal structure, the gangliothalamic body, connects telencephalic germinal zone with all thalamic regions in the developing human brain. J Comp Neurol 381:1–23
Letinic K, Rakic P (2001) Telencephalic origin of human thalamic GABAergic neurons. Nat Neurosci 4:931–936
Letinic K, Zoncu R, Rakic P (2002) Origin of GABAergic neurons in the human neocortex. Nature 417:645–649
Leuba G, Kraftsik R (1994) Changes in volume, surface estimate, three-dimensional shape and total number of neurons of the human primary visual cortex from midgestation until old age. Anat Embryol 190:351–366
Leviton A, Gressens P (2007) Neuronal damage accompanies perinatal white-matter damage. Trends Neurosci 30:473–477
Levitt P (2003) Structural and functional maturation of the developing primate brain. J Pediatr 143(4):S35–S45
Levitt P (2005) Developmental neurobiology and clinical disorders: lost in translation? Neuron 46(3):407–412
Levitt P, Rakic P (1980) Immunoperoxidase localization of glial fibrillary acid protein in radial glial cells and astrocytes of the developing rhesus monkey brain. J Comp Neurol 193: 815–840
Levitt P, Cooper ML, Rakic P (1981) Coexistence of neural and glial precursor cells in the cerebral ventricular zone of the fetal monkey: an ultrastructural immunoperoxidase analysis. J Neurosci 1:27–39
Levitt P, Cooper ML, Rakic P (1983) Early divergence and changing proportions of neuronal and glial precursors cells in the primate cerebral ventricular zone. Dev Biol 96: 472–484
Lewis PD (1968) Mitotic activity in the primate subependymal layer and the genesis of gliomas. Nature 217:974–975
Lewis DA (2000) GABAergic local circuit neurons and prefrontal cortical dysfunction in schizophrenia. Brain Res Rev 31:270–276
Liao BY, Zhang J (2008) Null mutations in human and mouse orthologs frequently result in different phenotypes. Proc Natl Acad Sci USA 105(19):6987–6992

Lidow M, Goldman-Rakic PS, Rakic P (1991) Synchronized overproduction of neurotransmitter receptors in diverse regions of the primate cerebral cortex. Proc Natl Acad Sci USA 88:10218–10221

Lindsay S, Copp AJ (2005) MRC-Wellcome Trust Human Developmental Biology Resource: enabling studies of human developmental gene expression. Trends Genet 21: 586–590

Lindsay S, Sarma S, Martinez-de-la-Torre M, Kerwin J, Scott M, Luis JF, Baldock R, Puelles L (2005) Anatomical and gene expression mapping of the ventral pallium in a three-dimensional model of developing human brain. Neuroscience 136:625–632

LJ K-K, Kostović I, Krmpotić-Nemanić J, Kelović Z, Vuković B (1978) The cortical plate of the human neocortex during the early fetal period (at 31–65 mm CRL). Verh Anat Ges 72:721–723

Lodygensky GA, Vasung L, Sizonenko SV, Hüppi P (2010) Neuroimaging of cortical development and brain connectivity in human newborns and animal models. J Anat 217: 418–428

Lohmann G, Von Cramon DY, Steinmetz H (1999) Sulcal variability of twins. Cereb Cortex 9:754–763

Lois C, Alvarez-Buylla A (1994) Long-distance neuronal migration in the adult mammalian brain. Science 264: 1145–1148

Luders E, Narr KL, Thompson PM, Rex DE, Jäncke L, Steinmetz H, Toga AW (2004) Gender differences in cortical complexity. Nat Neurosci 7:799–800

Lukaszewicz A, Savatier P, Cortay V, Giroud P, Huissoud C, Berland M, Kennedy H, Dehay C (2005) G1 phase regulation, area-specific cell cycle control, and cytoarchitectonics in the primate cortex. Neuron 47:353–364

Luttenberg J (1965) Contribution to the fetal ontogenesis of the corpus callosum in man. Folia Morphol 13:136–144

Maas LC, Mukherjee P, Carballido-Gamio J, Veeraraghavan S, Miller SP, Partridge SC, Henry RG, Barkovich AJ, Vigneron DB (2004) Early laminar organization of the human cerebrum demonstrated with diffusion tensor imaging in extremely premature infants. Neuroimage 22:1134–1140

Macchi G (1951) The ontogenetic development of the olfactory telencephalon in man. J Comp Neurol 95:245–305

Magnotta VA, Andreasen NC, Schultz SK, Harris G, Cizadlo T, Heckel D, Nopoulos P, Flaum M (1999) Quantitative in vivo measurement of gyrification in the human brain: changes associated with aging. Cereb Cortex 9(2):151–160

Malatesta P, Hartfuss E, Götz M (2000) Isolation of radial glial cells by fluorescent-activated cell sorting reveals a neuronal lineage. Development 127:5253–5263

Malatesta P, Hack MA, Hartfuss E, Kettenmann H, Klinkert W, Kirchhoff F, Götz M (2003) Neuronal or glial progeny: regional differences in radial glia fate. Neuron 37:751–764

Marin O, Rubenstein JL (2001) A long, remarkable journey: tangential migration in the telencephalon. Nat Rev Neurosci 2:780–790

Marin O, Rubenstein JL (2003) Cell migration in the forebrain. Annu Rev Neurosci 26:441–483

Marin-Padilla M (1971) Early prenatal ontogenesis of the cerebral cortex (neocortex) of the cat (*Felis domestica*). A Golgi study. I. The primordial neocortical organization. Z Anat Entwicklungsgesch 134:117–145

Marin-Padilla M (1972) Prenatal ontogenetic history of the principal neurons of the neocortex of the cat (*Felis domestica*). A golgi study. II. Developmental differences and their significances. Z Anat Entwicklungsgesch 136:125–142

Marin-Padilla M (1978) Dual origin of the mammalian neocortex and evolution of the cortical plate. Anat Embryol 152:109–126

Marin-Padilla M (1983) Structural organization of the human cerebral cortex prior to the appearance of the cortical plate. Anat Embryol 168:21–40

Marin-Padilla M (1984) Neurons of layer I. A developmental study. In: Peters A, Jones EG (eds) Cerebral cortex, vol 1: Cellular components of cerebral cortex. Plenum Press, New York, pp 447–478

Marin-Padilla M (1985) Early vascularization of the embryonic cerebral cortex. Golgi and electron microscopic studies. J Comp Neurol 241:237–249

Marin-Padilla M (1988a) Early ontogenesis of the human cerebral cortex. In: Peters A, Jones EG (eds) Cerebral cortex, vol 7: Development and maturation of cerebral cortex. Plenum Press, New York, pp 1–34

Marin-Padilla M (1988b) Embryonic vascularization of the mammalian cerebral cortex. In: Peters A, Jones EG (eds) Cerebral cortex, vol 7: Development and maturation of cerebral cortex. Plenum Press, New York, pp 479–509

Marin-Padilla M (1992) Ontogenesis of the pyramidal cell of the mammalian neocortex and developmental cytoarchitectonics: a unifying theory. J Comp Neurol 321: 223–240

Marin-Padilla M (1995) Prenatal development of fibrous (white matter), protoplasmic (gray matter), and layer I astrocytes in the human cerebral cortex: a Golgi study. J Comp Neurol 357:554–572

Marin-Padilla M (1998) Cajal-Retzius cells and the development of the neocortex. Trends Neurosci 21:64–71

Marin-Padilla M, Amieva MR (1989) Early neurogenesis of the mouse olfactory nerve: Golgi and electron microscopic studies. J Comp Neurol 288:339–352

Marin-Padilla M, Marin-Padilla T (1982) Origin, prenatal development and structural organization of layer I of the human cerebral (motor) cortex. A Golgi study. Anat Embryol 164: 161–206

Martin R, Gutierrez A, Penafiel A, Marin-Padilla M, de la Calle A (1999) Persistence of Cajal-Retzius cells in the adult human cerebral cortex. An immunohistochemical study. Histol Histopathol 14(2):487–490

Martinez-Cerdeno V, Noctor SC, Kriegstein AR (2006) The role of intermediate progenitor cells in the evolutionary expansion of the cerebral cortex. Cereb Cortex 16(Suppl 1): i152–i161

Mathur A, Inder T (2009) Magnetic resonance imaging – insights into brain injury and outcomes in premature infants. J Commun Disord 42:248–255

McDermott KW, Lantos PL (1990) Cell proliferation in the subependymal layer of the postnatal marmoset, *Callithrix jacchus*. Dev Brain Res 57(2):269–277

McKinstry RC, Mathur A, Miller JH, Ozcan A, Snyder AZ, Schefft GL, Almli CR, Shiran SI, Conturo TE, Neil JJ (2002) Radial organization of developing preterm human cerebral cortex revealed by non-invasive water diffusion anisotropy MRI. Cereb Cortex 12:1237–1243

McQuillen PS, Ferriero DM (2005) Perinatal subplate neurons injury: implications for cortical development and plasticity. Brain Pathol 15:250–260

Meinecke DL, Rakic P (1992) Expression of GABA and $GABA_A$ receptors by neurons of the subplate zone in developing primate occipital cortex: evidence for transient local circuits. J Comp Neurol 317:91–101

Mekel-Bobrov N, Gilbert SL, Evans PD, Vallender EJ, Anderson JR, Hudson RR, Tishkoff SA, Lahn BT (2005) Ongoing adaptive evolution of ASPM, a brain size determinant in *Homo sapiens*. Science 309:1720–1722

Ment LR, Hirtz D, Hüppi PS (2009) Imaging biomarkers of outcome in the developing preterm brain. Lancet Neurol 8:1042–1055

Métin C, Baudoin JP, Rakić S, Parnavelas JG (2006) Cell and molecular mechanisms involved in the migration of cortical interneurons. Eur J Neurosci 23:894–900

Meyer G (2010) Building a human cortex: the evolutionary differentiation of Cajal-Retzius cells and the cortical hem. J Anat 217:334–343

Meyer G, Goffinet AM (1998) Prenatal development of reelin-immunoreactive neurons in the human neocortex. J Comp Neurol 397:29–40

Meyer G, Gonzalez-Hernandez T (1993) Developmental changes in layer I of the human neocortex during prenatal life: a DiI-tracing and AChE and NADPH-d histochemistry study. J Comp Neurol 338:317–336

Meyer G, Wahle P (1999) The paleocortical ventricle is the origin of reelin-expressing neurons in the marginal zone of the fetal human neocortex. Eur J Neurosci 11:3937–3944

Meyer G, Soria JM, Martínez-Galán JR, Martin-Clemente B, Fairén A (1998) Different origins and developmental histories of transient neurons in the marginal zone of the fetal and neonatal rat cortex. J Comp Neurol 397:493–518

Meyer G, Goffinet AM, Fairén A (1999) What is a Cajal-Retzius cell? A reassessment of a classical cell type based on recent observations in the developing neocortex. Cereb Cortex 9:765–775

Meyer G, Schaaps JP, Moreau L, Goffinet AM (2000) Embryonic and early fetal development of the human neocortex. J Neurosci 20:1858–1868

Meyer G, Perez-Garcia CG, Gleeson JG (2002a) Selective expression of doublecortin and LIS1 in developing human cortex suggests unique modes of neuronal movement. Cereb Cortex 12:1225–1236

Meyer G, Perez-Garcia CG, Abraham H, Caput D (2002b) Expression of p73 and reelin in the developing human cortex. J Neurosci 15:4973–4986

Meyer G, de Lambert CR, Goffinet AM, Wahle P (2003) Disabled-1 mRNA and protein expression in developing human cortex. Eur J Neurosci 17:517–525

Milh M, Kaminska A, Huon C, Lapillonne A, Ben-Ari Y, Khazipov R (2007) Rapid cortical oscillations and early motor activity in premature human neonate. Cereb Cortex 17:1582–1594

Miller SP, Ferriero DM (2009) From selective vulnerability to connectivity: insights from newborn brain imaging. Trends Neurosci 32:496–505

Milosevic A, Kanazir S, Zecevic N (1995) Immunocytochemical localization of growth-associated protein GAP-43 in early human development. Dev Brain Res 84:282–286

Mitrofanis J (1994) Development of the pathway from the reticular and perireticular nuclei to the thalamus in ferrets: a DiI study. Eur J Neurosci 6:1864–1882

Mitrofanis J, Baker GE (1993) Development of the thalamic reticular and perireticular nuclei in rats and their relationship to the course of growing corticofugal and corticopetal axons. J Comp Neurol 388:575–587

Mitrofanis J, Guillery RW (1993) New views of the thalamic reticular nucleus in the adult and the developing brain. Trends Neurosci 16:240–245

Mo Z, Zecevic N (2008) Is pax6 critical for neurogenesis in the human fetal brain? Cereb Cortex 18:1455–1465

Mo Z, Zecevic N (2009) Human fetal radial glia cells generate oligodendrocytes in vitro. Glia 57:490–498

Mo Z, Moore AR, Filipovic R, Ogawa Y, Kazuhiro I, Antic SD, Zecevic N (2007) Human cortical neurons originate from radial glia and neuron-restricted progenitors. J Neurosci 27:4132–4145

Mollgard K, Jacobsen M (1984) Immunohistochemical identification of some plasma proteins in human embryonic and fetal forebrain with particular reference to the development of the neocortex. Dev Brain Res 13:497–502

Mollgard K, Reynolds ML, Jacobsen M, Dziegielewska KM, Saunders NR (1984) Differential immunocytochemical staining for fetuin and transferrin in the developing cortical plate. J Neurocytol 13:L497–502

Mollgard K, Dziegielewska KM, Saunders NR, Zakut H, Soreq H (1988) Synthesis and localization of plasma proteins in the developing human brain. Integrity of the fetal blood-brain barrier to endogenous proteins of hepatic origin. Dev Biol 128:207–221

Molliver ME, Kostović I, Van der Loos H (1973) The development of synapses in cerebral cortex of the human fetus. Brain Res 50:403–407

Molnár Z, Métin C, Stoykova A, Tarabykin V, Price DJ, Francis F, Meyer G, Dehay C, Kennedy H (2006) Comparative aspects of cerebral cortical development. Eur J Neurosci 23(4):921–934

Molyneaux BJ, Arlotta P, Menezes JR, Macklis JD (2007) Neuronal subtype specification in the cerebral cortex. Nat Rev Neurosci 8:427–437

Monuki ES, Walsh CA (2001) Mechanisms of cerebral cortical patterning in mice and humans. Nat Neurosci 4: 1199–1206

Morrison JH, Hof PR (1997) Life and death of neurons in the aging brain. Science 278:412–419

Mrzljak L, Uylings HBM, Kostović I, Van Eden CG (1988) Prenatal development of neurons in the human prefrontal cortex: I. A qualitative golgi study. J Comp Neurol 271: 355–386

Mrzljak L, Uylings HBM, Van Eden CG, Judaš M (1990) Neuronal development in human prefrontal cortex in prenatal and postnatal stages. Prog Brain Res 85:185–222

Mrzljak L, Uylings HBM, Kostović I, Van Eden CG (1992) Prenatal development of neurons in the human prefrontal cortex. II. A quantitative Golgi study. J Comp Neurol 316: 485–496

Mühlfriedel S, Kirsch F, Gruss P, Chowdhury K, Stoykova A (2007) Novel genes differentially expressed in cortical regions during late neurogenesis. Eur J Neurosci 26: 33–50

Müller F, O'Rahilly R (1980) The human chondrocranium at the end of the embryonic period proper, with particular reference to the nervous system. Am J Anat 159:33–58

Müller F, O'Rahilly R (1983) The first appearance of the major divisions of the human brain at stage 9. Anat Embryol 168:419–432

Müller F, O'Rahilly R (1985) The first appearance of the neural tube and optic primordium in the human embryo at stage 10. Anat Embryol 172:157–169

Müller F, O'Rahilly R (1986) The development of the human brain and the closure of the rostral neuropore at stage 11. Anat Embryol 175:205–222

Müller F, O'Rahilly R (1987) The development of the human brain, the closure of the caudal neuropore, and the beginning of secondary neurulation at stage 12. Anat Embryol 176:413–430

Müller F, O'Rahilly R (1988a) The development of the human brain from a closed neural tube at stage 13. Anat Embryol 177:203–224

Müller F, O'Rahilly R (1988b) The first appearance of the future cerebral hemispheres in the human embryo at stage 14. Anat Embryol 177:495–511

Müller F, O'Rahilly R (1988c) The development of the brain, including the longitudinal zoning in the diencephalon at stage 15. Anat Embryol 179:55–71

Müller F, O'Rahilly R (1989a) The human brain at stage 16, including the initial evagination of the neurohypophysis. Anat Embryol 179:551–569

Müller F, O'Rahilly R (1989b) The human brain at stage 17, including the appearance of the future olfactory bulb and the first amygdaloid nuclei. Anat Embryol 179:353–369

Müller F, O'Rahilly R (1990a) The human brain at stages 18–20, including the choroid plexuses and the amygdaloid and septal nuclei. Anat Embryol 182:285–306

Müller F, O'Rahilly R (1990b) The human brain at stages 21–23, with particular reference to the cerebral cortical plate and to the development of the cerebellum. Anat Embryol 182: 375–400

Müller F, O'Rahilly R (2006) The amygdaloid complex and the medial and lateral ventricular eminences in staged human embryos. J Anat 208:547–564

Murell W, Bushell GR, Livesey J, McGrath J, McDonald KPA, Bates PR, Mackay-Sim A (1996) Neurogenesis in adult human. NeuroReport 7:1189–1194

Muzio L, DiBenedetto B, Stoykova A, Boncinelli E, Gruss P, Mallamaci A (2002) *Emx2* and *Pax6* control regionalization of the pre-neuronogenic cortical primordium. Cereb Cortex 12(2):129–139

Nadarajah B, Parnavelas JG (2002) Modes of neuronal migration in the developing cerebral cortex. Nat Rev Neurosci 3:423–432

Naidich TP, Grant JL, Altman N, Zimmerman RA, Birchansky SB, Braffman B, Daniel JL (1994) The developing cerebral surface. Preliminary report on the patterns of sulcal and gyral maturation – anatomy, ultrasound, and magnetic resonance imaging. Neuroimaging Clin N Am 4(2): 201–240

Narr KL, Thompson PM, Sharma T, Moussai J, Zoumalan C, Rayman J, Toga AW (2001) Three-dimensional mapping of gyral shape and cortical surface asymmetries in schizophrenia: gender effects. Am J Psychiatry 158:244–255

Nery S, Fishell G, Corbin JG (2002) The caudal ganglionic eminence is a source of distinct cortical and subcortical cell populations. Nat Neurosci 5:1279–1287

Nikolić I, Kostović I (1986) Development of the lateral amygdaloid nucleus in the human fetus: transient presence of discrete cytoarchitectonic units. Anat Embryol 174:355–360

Nimchinsky EA, Vogt B, Morrison J, Hof P (1995) Spindle neurons of the human anterior cingulate cortex. J Comp Neurol 355:27–37

Nimchinsky EA, Gilissen E, Allman JM, Perl DP, Erwin JM, Hof PR (1999) A neuronal morphologic type unique to humans and great apes. Proc Natl Acad Sci USA 96: 5268–5273

Nobin A, Björklund A (1973) Topography of the monoamine neuron systems in the human brain as revealed in fetuses. Acta Physiol Scand Suppl 388:1–40

Noctor SC, Flint AC, Weissman TA, Dammerman RS, Kriegstein AR (2001) Neurons derived from radial glial cells establish radial units in neocortex. Nature 409:714–720

Noctor SC, Flint AC, Weissman TA, Wong WS, Clinton BK, Kriegstein AR (2002) Dividing precursor cells of the embryonic cortical ventricular zone have morphological and molecular characteristics of radial glia. J Neurosci 22: 3161–3173

Noctor SC, Martinez-Cerdeno V, Ivic L, Kriegstein AR (2004) Cortical neurons arise in symmetric and asymmetric division zones and migrate through specific phases. Nat Neurosci 7:136–144

O'Hare ED, Sowell ER (2008) Imaging developmental changes in gray and white matter in the human brain. In: Nelson CA, Luciana M (eds) Handbook of developmental cognitive neuroscience, 2nd edn. A Bradford Book, The MIT Press, Cambridge/London, pp 23–38

Okado N (1981) Onset of synapse formation in the human spinal cord. J Comp Neurol 201:211–219

Okado N, Kojima T (1984) Ontogeny of the central nervous system: neurogenesis, fibre connection, synaptogenesis and myelination in the spinal cord. In: Prechtl HFR (ed) Continuity of neural functions from prenatal life to postnatal life. Spastics International Medical, London, pp 31–45

Oldham MC, Horvath S, Geschwind DH (2006) Conservation and evolution of gene coexpression networks in human and chimpanzee brains. Proc Natl Acad Sci USA 103(47): 17973–17978

O'Leary DD, Nakagawa Y (2002) Patterning centers, regulatory genes and extrinsic mechanisms controlling arealization of the neocortex. Curr Opin Neurobiol 12:14–25

O'Leary DD, Chou SJ, Sahara S (2007) Area patterning of the mammalian cortex. Neuron 56(2):252–269

Olivier E, Edgley SA, Armand J, Lemon RN (1997) An electrophysiological study of the postnatal development of the corticospinal system in the macaque monkey. J Neurosci 17:267–276

Olson L, Boreus LO, Seiger A (1973) Histochemical demonstration and mapping of 5-hydroxytryptamine- and catecholamine-containing neuron systems in the human fetal brain. Z Anat Entwickl Gesch 139:259–282

O'Rahilly R, Müller F (1981) The first appearance of the human nervous system at stage 8. Anat Embryol 163:1–13

O'Rahilly R, Müller F (1984) Embryonic length and cerebral landmarks in staged human embryos. Anat Rec 209: 265–271

O'Rahilly R, Müller F (1990) Ventricular system and choroid plexuses of the human brain during the embryonic period proper. Am J Anat 189:285–302

O'Rahilly R, Müller F (1999) The embryonic human brain. An atlas of developmental stages, 2nd edn. Wiley-Liss, New York, p 454

O'Rahilly R, Müller F (2006) The embryonic human brain. An atlas of developmental stages, 3rd edn. Wiley-Liss, New York, p 358

Osheroff H, Hatten ME (2009) Gene expression profiling of preplate neurons destined for the subplate: genes involved in transcription, axon extension, neurotransmitter regulation, steroid hormone signaling, and neuronal survival. Cereb Cortex 19:i126–i134

Ourednik V, Ourednik J, Flax JD, Zawada WM, Hutt C, Yang C, Park KI, Kim SU, Sidman RL, Freed CR, Snyder EY (2001) Segregation of human neural stem cells in the developing primate forebrain. Science 293:1820–1824

Parnavelas JG (2000) The origin and migration of cortical neurons: new vistas. Trends Neurosci 23:126–131

Parnavelas JG, Nadarajah B (2001) Radial glia cells: are they really glia? Neuron 31:881–884

Patapoutian A, Reichardt LF (2000) Roles of Wnt proteins in neural development and maintenance. Curr Opin Neurobiol 10:392–399

Paus T, Zijdenbos A, Worsley K, Collins DL, Blumenthal J, Giedd JN, Rapoport JL, Evans AE (1999) Structural maturation of neural pathways in children and adolescents: in vivo study. Science 283:1908–1911

Pencea V, Bingaman KD, Freedman LJ, Luskin MB (2001) Neurogenesis in the subventricular zone and rostral migratory stream of the neonatal and adult primate forebrain. Exp Neurol 172(1):1–16

Perkins L, Hughes E, Srinivasan L, Allsop J, Glover A, Kumar S, Fisk N, Rutherford M (2008) Exploring cortical subplate evolution using magnetic resonance imaging of the fetal brain. Dev Neurosci 30:211–220

Petanjek Z, Judaš M, Kostović I, Uylings HBM (2008) Lifespan alterations of basal dendritic trees of pyramidal neurons in the human prefrontal cortex: a layer-specific pattern. Cereb Cortex 18:915–929

Petanjek Z, Berger B, Esclapez M (2009) Origins of cortical GABAergic neurons in the cynomolgus monkey. Cereb Cortex 19:249–262

Peters A, Morrison JH, Rosene DL, Hyman BT (1998) Are neurons lost from the primate cerebral cortex during normal aging? Cereb Cortex 8:295–300

Pfefferbaum A, Mathalon DH, Sullivan EV, Rawles JM, Zipursky RB, Lim KO (1994) A quantitative magnetic resonance imaging study of changes in brain morphology from infancy to late adulthood. Arch Neurol 51:874–887

Piper DR, Mujtaba T, Keyoung H, Roy NS, Goldman SA, Rao MS, Lucero MT (2001) Identification and characterization of neuronal precursors and their progeny from human fetal tissue. J Neurosci Res 66(3):356–368

Poliakov GI (1949) Structural organization of the human cerebral cortex during its ontogenetic development. In: Sarkisov SA, Filimonov IN, Preobrazhenskaya NS (eds) Cytoarchitectonics of the human cerebral cortex. Medgiz, Moscow, pp 33–91 (in Russian)

Poliakov GI (1959) Progressive neuron differentiation of the human cerebral cortex in ontogenesis. In: Sarkisov SA, Preobrazhenskaya NS (eds) Development of the central nervous system: onto- and phylogenesis of the cerebral cortex and subcortical structures. Medgiz, Moscow, pp 11–26 (in Russian)

Poliakov GI (1961) Some results of research into the development of the neuronal structure of the cortical ends of the analyzers in man. J Comp Neurol 117:197–212

Poliakov GI (1965) Development of the cerebral neocortex during first half of intrauterine life. In: Sarkisov SA (ed) Development of the child's brain. Meditsina, Leningrad, pp 22–52 (in Russian)

Poliakow GI (1979) Entwicklung der Neuronen der menschlichen Grosshirnrinde (Herausgegeben von B. Schönheit). VEB Georg Thieme, Leipzig, 320 pp

Pollard KS, Salama SR, Lambert N, Lambot MA, Coppens S, Pedersen JS, Katzman S, King B, Onodera C, Siepel A, Kern AD, Dehay C, Igel H, Ares M, Vanderhaeghen P, Haussler D (2006) An RNA gene expressed during cortical development evolved rapidly in humans. Nature 443:167–172

Polleux F, Whitford KL, Dijkhuizen PA, Vitalis T, Ghosh A (2002) Control of cortical interneuron migration by neurotrophins and p13-kinase signaling. Development 129:3147–3160

Popesco MC, MacLaren EJ, Hopkins J, Dumas L, Cox M, Meltesen L, McGavran L, Wyckoff GJ, Sikela JM (2006) Human lineage-specific amplification, selection, and neuronal expression of DUF1220 domains. Science 313: 1304–1307

Povlishock JT (1976) The fine structure of the axons and growth cones of the human fetal cerebral cortex. Brain Res 114:379–389

Prayer D, Prayer L (2003) Diffusion-weighted magnetic resonance imaging of cerebral white matter development. Eur J Radiol 45:235–243

Prayer D, Barkovich AJ, Kirschner DA, Prayer LM, Roberts TP, Kucharczyk J, Moseley ME (2001) Visualization of nonstructural changes in early white matter development on diffusion-weighted MR images: evidence supporting premyelination anisotropy. Am J Neuroradiol 22: 1572–1576

Prayer D, Kasprian C, Krampl E, Ulm B, Witzani L, Prayer L, Brugger PC (2006) MRI of normal fetal brain development. Eur J Radiol 57:199–216

Preuss TM (2009) The cognitive neuroscience of human uniqueness. In: Gazzaniga MS (ed) The cognitive neurosciences, 4th edn. A Bradford Book, The MIT Press, Cambridge/ London, pp 49–66

Preuss TM, Coleman GQ (2002) Human-specific organization of primary visual cortex: alternating compartments of dense Cat-301 and calbinding immunoreactivity in layer 4A. Cereb Cortex 12:671–691

Preuss TM, Qi H, Kaas JH (1999) Distinctive compartmental organization of human primary visual cortex. Proc Natl Acad Sci USA 96:11601–11606

Preuss TM, Cáceres M, Oldham MC, Geschwind DH (2004) Human brain evolution: insights from microarrays. Nat Rev Genet 5:850–860

Price J (2001) Neuronal stem cells – where are you? Nat Med 7:998–999
Price DJ, Kennedy H, Dehay C, Zhou L, Mercier M, Jossin Y, Goffinet AM, Tissir F, Blakey D, Molnár Z (2006) The development of cortical connections. Eur J Neurosci 23: 910–920
Puelles L, Verney C (1998) Early neuromeric distribution of tyrosine-immunoreactive neurons in human embryos. J Comp Neurol 394:283–308
Pujol J, Vendrell P, Junque C, Marti-Vilalta JL, Capdevila A (1993) When does human brain development end? Evidence of corpus callosum growth up to adulthood. Ann Neurol 34:71–75
Quinones-Hinojosa A, Sanai N, Soriano-Navarro M, Gonzalez-Perez O, Mirzadeh Z, Gil-Perotin S, Romero-Rodriguez R, Berger MS, Garcia-Verdugo JM, Alvarez-Buylla A (2006) Cellular composition and cytoarchitecture of the adult human subventricular zone: a niche of neural stem cells. J Comp Neurol 494:415–434
Radoš M, Judaš M, Kostović I (2006) In vitro MRI of brain development. Eur J Radiol 57:187–198
Raghanti MA, Stimpson CD, Marcinkiewicz JL, Erwin JM, Hof PR, Sherwood CC (2008a) Cholinergic innervation of the frontal cortex: differences among humans, chimpanzees, and macaque monkeys. J Comp Neurol 506(3):409–424
Raghanti MA, Stimpson CD, Marcinkiewicz JL, Erwin JM, Hof PR, Sherwood CC (2008b) Differences in cortical serotonergic innervation among humans, chimpanzees, and macaque monkeys: a comparative study. Cereb Cortex 18(3):584–597
Ragsdale CW, Grove EA (2001) Patterning the mammalian cerebral cortex. Curr Opin Neurobiol 11:50–58
Rakic P (1971) Guidance of neurons migrating in the fetal monkey neocortex. Brain Res 33:471–476
Rakic P (1972) Mode of cell migration to the superficial layers of fetal monkey neocortex. J Comp Neurol 145:61–84
Rakic P (1977) Prenatal development of the visual system in the rhesus monkey. Philos Trans R Soc Lond B 278:245–260
Rakic P (1982) Early developmental events: cell lineages, acquisition of neuronal positions, and areal and laminar development. Neurosci Res Program Bull 20:439–451
Rakic P (1985) Limits of neurogenesis in primates. Science 227:1054–1056
Rakic P (1988) Specification of cerebral cortical areas. Science 241:170–176
Rakic P (1995) A small step for the cell: a giant leap for mankind – a hypothesis of neocortical expansion during evolution. Trends Neurosci 18:383–388
Rakic P (1998) Young neurons for old brains? Nat Neurosci 1(8):645–647
Rakic P (2000) Advantages of the mouse model: From spontaneous to induced mutations. In: Goffinet A, Rakic P (eds) The mouse brain development. Springer-Verlag, Berlin, pp 1–19
Rakic P (2002a) Neurogenesis in adult primate neocortex: an evaluation of the evidence. Nat Rev Neurosci 3:65–71
Rakic P (2002b) Pre and post-developmental neurogenesis in primates. Clin Neurosci Res 2(1–2):29–39
Rakic P (2003a) Developmental and evolutionary adaptations of cortical radial glia. Cereb Cortex 13:541–549
Rakic P (2003b) Elusive radial glial cells: historical and evolutionary perspective. Glia 43:19–32
Rakic P (2006a) A century of progress in corticoneurogenesis: from silver impregnation to genetic engineering. Cereb Cortex 16:i3–i17
Rakic P (2006b) No more cortical neurons for you. Science 313:928–929
Rakic P (2009) Evolution of the neocortex: a perspective from developmental biology. Nat Rev Neurosci 10:724–735
Rakic P, Nowakowski RS (1981) The time of origin of neurons in the hippocampal region of the rhesus monkey. J Comp Neurol 196:99–128
Rakic P, Sidman RL (1969) Telencephalic origin of pulvinar neurons in the fetal human brain. Z Anat Entwickl Gesch 129:53–82
Rakic P, Yakovlev PI (1968) Development of the corpus callosum and cavum septi in man. J Comp Neurol 132:45–72
Rakic S, Zecevic N (2003a) Emerging complexity of layer I in human cerebral cortex. Cereb Cortex 13:1072–1083
Rakic S, Zecevic N (2003b) Early oligodendrocyte progenitor cells in the human fetal telencephalon. Glia 41:117–127
Rakic P, Suner I, Williams RW (1991) A novel cytoarchitectonic area induced experimentally within the primate visual cortex. Proc Natl Acad Sci USA 88:2083–2087
Rakic P, Bourgeois JP, Goldman-Rakic PS (1994) Synaptic development of the cerebral cortex: implications for learning, memory, and mental illness. Prog Brain Res 102: 227–243
Rakic P, Arellano JI, Breunig J (2009) Development of the primate cerebral cortex. In: Gazzaniga MS (ed) The cognitive neurosciences, 4th edn. A Bradford Book, The MIT Press, Cambridge/London, pp 7–28
Ramakers GJA (2005) Neuronal network formation in human cerebral cortex. Prog Brain Res 147:3–14
Ranke O (1910) Beiträge zur Kenntnis der normalen und pathologischen Hirnrindenbildung. Beitr Pathol Anat 47:51–125
Rasin MR, Gazula VR, Breunig JJ, Kwan KY, Johnson MB, Liu-Chen S, Li HS, Jan LY, Jan YN, Rakic P, Sestan N (2007) Numb and Numb1 are required for maintenance of cadherin-based adhesion and polarity of neural progenitors. Nat Neurosci 10(7):819–827
Rauch RA, Jenkins JR (1994) Analysis of cross-sectional area measurements of the corpus callosum adjusted for brain size in male and female subjects from childhood to adulthood. Behav Brain Res 64:65–78
Ren T, Anderson A, Shen WB, Huang H, Plachez C, Zhang J, Mori S, Kinsman SL, Richards LJ (2006) Imaging, anatomical, and molecular analysis of callosal formation in the developing human fetal brain. Anat Rec A Discov Mol Cell Evol Biol 288A(2):191–204
Retzius G (1896) Das Menschenhirn. Studien in der makroskopischen Morphologie. Text und Atlas. Norstedt, Stockholm
Richman DP, Stewart RM, Hutchinson JW, Caviness VS Jr (1975) Mechanical model of brain convolutional development. Science 189:18–21
Richter E (1965) Die Entwicklung des Globus pallidus und des Corpus subthalamicum. Monogr Gesamtgeb Neurol Psychiat Berlin 108:1–132
Rickmann M, Chronwall BM, Wolff JR (1977) On the development of non-pyramidal neurons and axons outside the cortical plate: the early marginal zone as a pallial anlage. Anat Embryol 151:285–307

Rivkin MJ, Flax J, Mozell R, Osathanondh R, Volpe JJ, Villa-Komaroff L (1995) Oligodendroglial development in human fetal cerebrum. Ann Neurol 38(1):92–101

Rockel AJ, Hiorns RW, Powell TP (1980) The basic uniformity in structure of the neocortex. Brain 103:221–244

Rodman HR (1994) Development of inferior temporal cortex in the monkey. Cereb Cortex 4:484–498

Rodman HR, Skelly JP, Gross CG (1991) Stimulus selectivity and state dependence of activity in inferior temporal cortex of infant monkeys. Proc Natl Acad Sci USA 88: 7572–7575

Rodman HR, Scalaidhe SP, Gross CG (1993) Response properties of neurons in temporal cortical visual areas of infant monkeys. J Neurophysiol 70:1115–1136

Roessmann U, Velasco ME, Sindely SD, Gambetti P (1980) Glial fibrillary acidic protein (GFAP) in ependymal cells during development. An immunocytochemical study. Brain Res 200:13–21

Rose M (1926) Der Allocortex bei Tier und Mensch. I. Teil (Mit 21 Textabbildungen und 30 Doppeltafeln). J Psychol Neurol 34:1–111

Rose M (1927) Die sogenannte Riechrinde beim Menschen und beim Affen. II. Teil des "Allocortex bei Tier und Mensch" (Mit 13 Textabbildungen und 35 Doppeltafeln). J Psychol Neurol 34:261–401

Rosenberg DR, Lewis DA (1995) Postnatal maturation of the dopaminergic innervation of monkey prefrontal and motor cortices: a tyrosine hydroxylase immunohistochemical analysis. J Comp Neurol 358:383–400

Ross ME, Walsh CA (2001) Human brain malformations and their lessons for neuronal migration. Annu Rev Neurosci 24:1041–1070

Rouiller EM, Babalian A, Kazennikov O, Moret V, Yu XH, Wiesendanger M (1994) Transcallosal connections of the distal forelimb representations of the primary and supplementary motor cortical areas in macaque monkeys. Exp Brain Res 102:227–243

Roy NS, Wang S, Jiang L, Kang J, Benraiss A, Harrison-Restelli C, Fraser RA, Couldwell WT, Kawaguchi A, Okano H, Nedergaard M, Goldman SA (2000) In vitro neurogenesis by progenitor cells isolated from the adult human hippocampus. Nat Med 6:271–277

Rutherford MA, Ward P, Malamatentiou C (2005) Advanced MR techniques in the term-born neonate with perinatal brain injury. Semin Fetal Neonatal Med 10:445–460

Sajin B, Sestan N, Dmitrović B (1992) Compartmentalization of NADPH-diaphorase staining in the developing human striatum. Neurosci Lett 140:117–120

Sanai N, Tramontin AD, Qulnones-Hinojosa A, Barbaro NM, Gupta N, Kunwar S, Lawton MT, McDermott MW, Parsa AT, Garcia JMV, Berger MS, Alvarez-Buylla A (2004) Unique astrocyte ribbon in adult human brain contains neural stem cells but lacks chain migration. Nature 427: 740–744

Sanides F, Sas E (1970) Persistence of horizontal cells of the Cajal foetal type and of the subpial granular layer in parts of the mammalian paleocortex. Ztschr Mikrosk Anat Forsch 82:570–588

Sarma S, Kerwin J, Puelles L, Scott M, Strachan T, Feng G, Sharpe J, Davidson D, Baldock R, Lindsay S (2005) 3D modelling, gene expression mapping and post-mapping image analysis in the developing human brain. Brain Res Bull 66:449–453

Sarnat HB (1992) Regional differentiation of the human fetal ependyma: immunocytochemical markers. J Neuropathol Exp Neurol 51(1):58–75

Sasaki A, Hirato J, Nakazato Y, Ishida Y (1988) Immunohistochemical study of the early human fetal brain. Acta Neuropathol 76(2): 128–134

Saunders NR, Dziegielewska KM, Mollgard K (1991) The importance of the blood-brain barrier in fetuses and embryos. Trends Neurosci 14:14–15

Saunders NR, Ek CJ, Habgood MD, Dziegielewska KM (2008) Barriers in the brain: a renaissance? Trends Neurosci 31(6): 279–286

Sbarbati A, Marzola P, Simonati A, Nicolato E, Osculati F (1998) High-field magnetic resonance imaging of the developing human brain from the 10th to the 16th week of gestational age. Acta Anat 163:39–46

Schmechel DE, Rakic P (1979a) Arrested proliferation of radial glial cells during midgestation in rhesus monkey. Nature 277:303–305

Schmechel D, Rakic P (1979b) A Golgi study of radial glia cells in developing monkey telencephalon: morphogenesis and transformation into astrocytes. Anat Embryol 156: 115–152

Schröder H, Schütz U, Burghaus L, Lindstrom J, Kuryatov A, Monteggia L, de Vos RA, van Noort G, Wevers A, Nowacki S, Happich E, Moser N, Arneric SP, Maelicke A (2001) Expression of the alpha4 isoform of the nicotinic acetylcholine receptor in the fetal human cerebral cortex. Dev Brain Res 132:33–45

Schwartz ML, Goldman-Rakic PS (1982) Single cortical neurones have axon collaterals to ipsilateral and contralateral cortex in fetal and adult primates. Nature 299:154–156

Schwartz ML, Goldman-Rakic PS (1991) Prenatal specification of callosal connections in rhesus monkey. J Comp Neurol 307:144–162

Schwartz ML, Rakic P, Goldman-Rakic PS (1991) Early phenotype expression of cortical neurons: evidence that a subclass of migratory neurons have callosal axons. Proc Natl Acad Sci USA 88:1354–1358

Seress L, Abrahám H (2008) Pre- and postnatal morphological development of the human hippocampal formation. In: Nelson CA, Luciana M (eds) Handbook of developmental cognitive neuroscience, 2nd edn. A Bradford Book, The MIT Press, Cambridge/London, pp 187–211

Seress L, Mrzljak L (1992) Postnatal development of mossy cells in the human dentate gyrus: a light microscopic Golgi study. Hippocampus 2:127–142

Seress L, Abrahám H, Tornóczky T, Kosztolányi G (2001) Cell formation in the human hippocampal formation from midgestation to the late postnatal period. Neuroscience 105: 831–843

Sestan N, Rakic P, Donoghue MJ (2001) Independent parcellation of the embryonic visual cortex and thalamus revealed by combinatorial *Eph/ephrin* gene expression. Curr Biol 11:39–43

Shaw P, Greenstein D, Lerch J, Clasen L, Lenroot R, Gogtay N, Evans A, Rapoport J, Giedd J (2006) Intellectual ability and cortical development in children and adolescents. Nature 440:676–679

Sherwood C, Hof P (2007) The evolution of neuron types and cortical histology in apes and humans. In: Kaas J, Preuss TM (eds) Evolution of nervous systems, vol 4: Primates. Elsevier, Oxford, pp 355–378

Shirasaki R, Pfaff SL (2002) Transcriptional codes and the control of neuronal identity. Annu Rev Neurosci 25:251–281

Sidman RL, Rakic P (1973) Neuronal migration, with special reference to developing human brain: a review. Brain Res 62:1–35

Sidman RL, Rakic P (1982) Development of the human central nervous system. In: Haymaker W, Adams RD (eds) Histology and histopathology of the nervous system. C.C. Thomas Publisher, Springfield, pp 3–145

Sikela JM (2006) The jewels of our genome: the search for the genomic changes underlying the evolutionarily unique capacities of the human brain. PLoS Genet 2(5):646–655

Šimić G, Mrzljak L, Fučić A, Winblad B, Lovrić H, Kostović I (1999) Nucleus subputaminalis (Ayala): the still disregarded magnocellular component of the basal forebrain may be human specific and connected with the cortical speech area. Neuroscience 89:73–89

Sims KB, Crandall JE, Kosik KS, Williams RS (1988) Microtubule-associated protein 2 (MAP2) immunoreractivity in human fetal neocortex. Brain Res 449:192–200

Skogh C, Eriksson C, Kokaia M, Meijer LU, Wictorin K, Campbell K (2001) Generation of regionally specified neurons in expanded glial cultures derived from the mouse and human lateral ganglionic eminence. Mol Cell Neurosci 17(5):811–820

Smart IHM, Dehay C, Giroud P, Berland M, Kennedy H (2002) Unique morphological features of the proliferative zones and postmitotic compartments of the neural epithelium give rise to striate and extrastriate cortex in the monkey. Cereb Cortex 12:37–53

Smiley JF, Levey AI, Mesulam MM (1998) Infracortical interstitial cells concurrently expressing M2-muscarinic receptors, acetylcholinesterase and nicotinamide adenine dinucleotide phosphate-diaphorase in the human and monkey cerebral cortex. Neuroscience 84:755–769

Snyder EY, Park KI (2002) Limitations in brain repair. Nat Med 7:928–930

Sowell ER, Thompson PM, Holmes CJ, Batth R, Jernigan TL, Toga AW (1999a) Localizing age-related changes in brain structure between childhood and adolescence using statistical parametric mapping. Neuroimage 9:587–597

Sowell ER, Thompson PM, Holmes CJ, Jernigan TL, Toga AW (1999b) In vivo evidence for post-adolescent brain maturation in frontal and striatal regions. Nat Neurosci 2:859–861

Sowell ER, Thompson PM, Tessner KD, Toga AW (2001a) Mapping continued brain growth and gray matter density reduction in dorsal frontal cortex: inverse relationships during postadolescent brain maturation. J Neurosci 21:8819–8829

Sowell ER, Delis D, Stiles J, Jernigan TL (2001b) Improved memory functioning and frontal lobe maturation between childhood and adolescence: a structural MRI study. J Int Neuropsychol Soc 7:312–322

Sowell ER, Thompson PM, Rex D, Kornsand D, Tessner KD, Jernigan TL, Toga AW (2002a) Mapping sulcal pattern asymmetry and local cortical surface gray matter distribution in vivo: maturation in perisylvian cortices. Cereb Cortex 12(1):17–26

Sowell ER, Trauner DA, Gamst A, Jernigan TL (2002b) Development of cortical and subcortical brain structures in childhood and adolescence: a structural MRI study. Dev Med Child Neurol 44:4–16

Sowell ER, Peterson BS, Thompson PM, Welcome SE, Henkenius AL, Toga AW (2003) Mapping cortical change across the human life span. Nat Neurosci 6:309–315

Sowell ER, Thompson PM, Leonard CM, Welcome SE, Kan E, Toga AW (2004a) Longitudinal mapping of cortical thickness and brain growth in normal children. J Neurosci 24:8223–8231

Sowell ER, Thompson PM, Toga AW (2004b) Mapping changes in the human cortex throughout the span of life. Neuroscientist 10:372–392

Spalding KL, Bhardwaj RD, Buchholz BA, Druid H, Frisén J (2005) Retrospective birth dating of cells in humans. Cell 122(1):133–143

Spiteri E, Konopka G, Coppola G, Bomar J, Oldham M, Ou J, Vernes SC, Fisher SE, Ren B, Geschwind DH (2007) Identification of the transcriptional targets of *FOXP2*, a gene linked to speech and language, in developing human brain. Am J Hum Genet 81(6):1144–1157

Spreafico R, Arcelli P, Frassoni C, Canetti P, Giaccone G, Rizzuti T, Mastrangelo M, Bentivoglio M (1999) Development of layer I of the human cerebral cortex after midgestation: architectonic findings, immunocytochemical identification of neurons and glia, and in situ labeling of apoptotic cells. J Comp Neurol 410:126–142

Stagaard M, Mollgard K (1989) The developing neuroepithelium in human embryonic and fetal brain studied with vimentin-immunocytochemistry. Anat Embryol 180: 17–28

Staudt M (2007) (Re-)organization of the developing human brain following periventricular white matter lesions. Neurosci Biobehav Rev 31:1150–1156

Staudt M (2010) Reorganization after pre- and perinatal brain lesions. J Anat 217:469–474

Staudt M, Grodd W, Gerloff C, Erb M, Stitz J, Krageloh-Mann I (2002) Two types of ipsilateral reorganization in congenital hemiparesis: a TMS and fMRI study. Brain 125(Pt 10): 2222–2237

Staudt M, Gerloff C, Grodd W, Holthausen H, Niemann G, Krageloh-Mann I (2004) Reorganization in congenital hemiparesis acquired at different gestational ages. Ann Neurol 56(6):854–863

Staudt M, Erb M, Braun C, Gerloff C, Grodd W, Krageloh-Mann I (2006) Extensive peri-lesional connectivity in congenital hemiparesis. Neurology 66(5):771–771

Steinmetz H, Herzog A, Schlaug G, Huang Y, Jäncke L (1995) Brain (A)symmetry in monozygotic twins. Cereb Cortex 5:296–300

Suárez-Solá ML, González-Delgado FJ, Pueyo-Morlans M, Medina-Bolivar OC, Hernández-Acosta NC, González-Gomez M, Meyer G (2009) Neurons in the white matter of the adult human neocortex. Front Neuroanat 3:1–7

Suslov ON, Kukekov VG, Ignatova TN, Steindler DA (2002) Neural stem cell heterogeneity demonstrated by molecular phenotyping of clonal neurospheres. Proc Natl Acad Sci USA 99(22):14506–14511

Swanson LW, Petrovich GD (1998) What is the amygdala? Trends Neurosci 21:323–331

Talos DM, Follett PL, Folkerth RD, Fishman RE, Trachtenberg FL, Volpe JJ, Jensen FE (2006) Developmental regulation of α-amino-3-hydroxy-5-methyl-4-isoxazole-propionic acid receptor subunit expression in forebrain and relationship to regional susceptibility to hypoxic/ischemic injury. II. Human cerebral white matter and cortex. J Comp Neurol 497: 61–77

Tamamaki N, Fujimori KE, Takauji R (1997) Origin and route of tangentially migrating neurons in the developing neocortical intermediate zone. J Neurosci 17:8313–8323

Tamamaki N, Nakamura K, Okamoto K, Kaneko T (2001) Radial glia is a progenitor of neocortical neurons in the developing cerebral cortex. Neurosci Res 41:51–60

Tanaka S, Mito T, Takashima S (1995) Progress of myelination in the human fetal spinal nerve roots, spinal cord and brainstem with myelin basic protein immunohistochemistry. Early Hum Dev 41:49–59

Ten Donkelaar HJ, Lmmens M, Wesseling P, Hori A, Keyser A, Rotteveel J (2004) Development and malformations of the human pyramidal tract. J Neurol 251:1429–1442

Thompson PM, Cannon TD, Narr KL, Van Erp T, Poutanen VP, Huttunen M, Lonnqvist J, Standertskjold-Nordenstam CG, Kaprio J, Khaledy M, Dail R, Zoumalan CI, Toga AW (2001) Genetic influences on brain structure. Nat Neurosci 4: 1253–1258

Tissir F, Goffinet AM (2003) Reelin and brain development. Nat Rev Neurosci 4:496–505

Toga AW, Thompson PM (2005) Genetics of brain structure and intelligence. Annu Rev Neurosci 28:1–23

Tomasch J (1957) A quantitative analysis of the human anterior commissure. Acta Anat 30:902–906

Toro R, Burnod Y (2005) A morphogenetic model for the development of cortical convolutions. Cereb Cortex 15(12): 1900–1913

Tosic M, Rakic S, Matthieu JM, Zecevic N (2002) Identification of Golli and Myelin basic proteins in human brain during early development. Glia 37:219–228

Tramontin AD, Garcia-Verdugo J, Lim DA, Alvarez-Buylla A (2003) Postnatal development of radial glia and the ventricular zone (VZ): a continuum of the neural stem cell compartment. Cereb Cortex 13(6):580–587

Trivedi R, Husain N, Rathore RKS, Saksena S, Srivastava S, Malik GK, Das V, Pradhan M, Pandey CM, Gupta RK (2009) Correlation of diffusion tensor imaging with histology in the developing human frontal cerebrum. Dev Neurosci 31:487–496

Tulay CM, Elevli L, Duman U, Sarimehmetoglu A, Cavdar S (2004) Morphological study of the perireticular nucleus in human fetal brains. J Anat 205(1):57–63

Uddin M, Wildman DE, Liu GZ, Xu WB, Johnson RM, Hof PR, Kapatos G, Grossman LI, Goodman M (2004) Sister grouping of chimpanzees and humans as revealed by genome-wide phylogenetic analysis of brain gene expression profiles. Proc Natl Acad Sci USA 101(9):2957–2962

Ugrumov M, Proshlyakova E, Sapronova A, Popov A (1996) Development of the mesencephalic and diencephalic catecholamine systems in human fetuses: uptake and release of catecholamines *in vitro*. Neurosci Lett 212:29–32

Uylings HBM, Delalle I (1997) Morphology of neuropeptide Y-immunoreactive neurons and fibres in human prefrontal cortex during prenatal and postnatal development. J Comp Neurol 379:523–540

Van Essen DC (1997) A tension-based theory of morphogenesis and compact wiring in the central nervous system. Nature 385:313–318

Vanhatalo S, Kaila K (2006) Development of neonatal EEG activity: from phenomenology to physiology. Semin Fetal Neonatal Med 11:471–478

Vanhatalo S, Palvas JM, Andersson S, Rivera C, Voipio J, Kaila K (2005) Slow endogenous activity transients and developmental expression of KCC2 in the immature human cortex. Eur J Neurosci 22:2799–2804

Varki A (2006) Nothing in glycobiology makes sense, except in the light of evolution. Cell 126(5):841–845

Varki A, Altheide TK (2005) Comparing the human and chimpanzee genomes: Searching for needles in a haystack. Genome Res 15(12):1746–1758, erratum: Genome Res 19(12):2343-2343, 2009

Varki A, Geschwind DH, Eichler EE (2008) Explaining human uniqueness: genome interactions with environment, behaviour and culture. Nat Rev Genet 9:749–763

Vasung L, Huang H, Jovanov-Milošević N, Pletikos M, Mori S, Kostović I (2010a) Development of axonal pathways in the human fetal fronto-limbic brain: histochemical characterization and diffusion tensor imaging. J Anat 217:400–417

Vasung L, Jovanov-Milošević N, Pletikos M, Mori S, Judaš M, Kostović I (2010b) Prominent periventricular fiber system related to ganglionic eminence and striatum in the human fetal cerebrum. Brain Struct Funct. doi:10.1007/s00429-010-0279-4

Vernes SC, Spiteri E, Nicod J, Groszer M, Taylor JM, Davies KE, Geschwind DH, Fisher SE (2007) High-throughput analysis of promoter occupancy reveals direct neural targets of *FOXP2*, a gene mutated in speech and language disorders. Am J Hum Genet 81:1232–1250

Vernes SC, Newbury DF, Abrahams BS, Winchester L, Nicod J, Groszer M, Alarcón M, Olivier PL, Davies KE, Geschwind DH, Monaco AP, Fisher SE (2008) A functional genetic link between distinct developmental language disorders. N Engl J Med 359:2337–2345

Verney C (1999) Distribution of the catecholaminergic neurons in the central nervous system of human embryos and fetuses. Microsc Res Techn 46:24–47

Verney C, Derer P (1995) Cajal-Retzius neurons in human cerebral cortex at midgestation show immunoreactivity for neurofilament and calcium-binding proteins. J Comp Neurol 359:144–153

Verney C, Zecevic N, Nikovic B, Alvarez C, Berger B (1991) Early evidence of catecholaminergic cell groups in 5- and 6-week-old human embryos using tyrosine-hydroxylase immunocytochemistry. Neurosci Lett 131:121–124

Verney C, Milošević A, Alvarez C, Berger B (1993) Immunocytochemical evidence of well-developed dopaminergic and noradrenergic innervations in the frontal cerebral cortex of human fetuses at midgestation. J Comp Neurol 336:331–344

Verney C, Lebrand C, Gaspar P (2002) Changing distribution of monoaminergic markers in the developing human cerebral cortex with special emphasis on the serotonin transporter. Anat Rec 267:87–93

Verney C, Monier A, Fallet-Bianco C, Gressens P (2010) Early microglial colonization of the human forebrain and possible involvement in periventricular white-matter injury of preterm infants. J Anat 217:436–448

Vescovi AL, Parati EA, Gritti A, Poulin P, Ferrario M, Wanke E, Frolichsthal-Schoeller P, Cova L, Arcellana-Pantililo M, Colombo A, Galli R (1999) Isolation and cloning of multipotential stem cells from the embryonic human CNS and establishment of transplantable human neural stem cell lines by epigenic stimulation. Exp Neurol 156(1):71–83

Volpe JJ (2009) Brain injury in premature infants: a complex amalgam of destructive and developmental disturbances. Lancet Neurol 8:110–124

Von Economo C (1926) Eine neue Art Spezialzellen des Lobus cinguli und Lobus insulae. Z Ges Neurol Psychiatr 100: 706–712

Von Economo C, Koskinas GN (1925) Die Cytoarchitektonik der Hirnrinde des erwachsenen Menschen. Verlag von Julius Springer, Wien

Vukšić M, Petanjek Z, Rašin MR, Kostović I (2002) Perinatal growth of prefrontal layer III pyramids in Down syndrome. Pediat Neurol 27(1):36–38

Vukšić M, Radoš M, Kostović I (2008) Structural basis of developmental plasticity in the corticostriatal system. Coll Antropol 32(suppl 1):155–159

Wai SM, Kindler PM, Lam ET, Zhang A, Yew DT (2004) Distribution of neuropeptide Y-immunoreactive neurons in human prefrontal cortex during development. Cell Mol Neurobiol 24:667–684

Wang WZ, Hoerder-Suabedissen A, Oeschger FM, Bayatti N, Ip BK, Lindsay S, Supramaniam V, Srinivasan L, Rutherford M, Mollgard K, Clowry GJ, Molnár Z (2010) Subplate in the developing cortex of mouse and human. J Anat 217: 368–380

Watakabe A, Ichinohe N, Ohsawa S, Hashikawa T, Komatsu Y, Rockland KS, Yamamori T (2007) Comparative analysis of layer-specific genes in mammalian neocortex. Cereb Cortex 17:1918–1933

Webster MJ, Ungerleider LG, Bachevalier J (1991) Connections of inferior temporal areas TE and TEO with medial temporal-lobe structures in infant and adult monkeys. J Neurosci 11:1095–1116

Weickert CS, Webster MJ, Colvin SM, Herman MM, Hyde TM, Weinberger DR, Kleinman JE (2000) Localization of epidermal growth factor receptors and putative neuroblasts in human subependymal zone. J Comp Neurol 423(3):359–372

Weidenheim KM, Kress Y, Epshteyn I, Rashbaum WK, Lyman WD (1992) Early myelination in the human fetal lumbosacral spinal cord: characterization by light and electron microscopy. J Neuropathol Exp Neurol 51:142–149

Weidenheim KM, Epshteyn I, Rashbaum WK, Lyman WD (1993) Neuroanatomical localization of myelin basic protein in the late first and early second trimester human foetal spinal cord and brainstem. J Neurocytol 22:507–516

Weidenheim KM, Bodhireddy SR, Rashbaum WK, Lyman WD (1996) Temporal and spatial expression of major myelin proteins in the human fetal spinal cord during the second trimester. J Neuropathol Exp Neurol 55:734–745

Weissman T, Noctor SC, Clinton BK, Honig LS, Kriegstein AR (2003) Neurogenic radial glial cells in reptile, rodent and human: from mitosis to migration. Cereb Cortex 13(6): 550–559

Welker W (1990) Why does cerebral cortex fissure and fold? In: Jones EG, Peters A (eds) Cerebral cortex, vol 8B: Comparative structure and evolution of cerebral cortex, Part II. Plenum Press, New York/London, pp 3–136

White T, Hilgetag CC (2008) Gyrification and development of the human brain. In: Nelson CA, Luciana M (eds) Handbook of developmental cognitive neuroscience, 2nd edn. A Bradford Book, The MIT Press, Cambridge/London, pp 39–50

White T, Andreasen NC, Nopoulos P (2002) Brain volumes and surface morphology in monozygotic twins. Cereb Cortex 12:486–493

Widjaja E, Geibprasert S, Mahmoodabadi SZ, Blaser S, Brown NE, Shannon P (2010) Alteration of human fetal subplate layer and intermediate zone during normal development on MR and diffusion tensor imaging. Am J Neuroradiol 31(6):1091–1099

Wilkinson W, Hume R, Strange R, Bell JE (1990) Glial and neuronal differentiation in the human fetal brain 9–23 weeks of gestation. Neuropathol Appl Neurobiol 16:193–204

Windle WF (1970) Development of neural elements in human embryos of four to seven weeks gestation. Exp Neurol 28(suppl 5):44–83

Wonders C, Anderson SA (2005) Beyond migration: *Dlx1* regulates interneuron differentiation. Nat Neurosci 8:979–981

Xu Q, Cobos I, De la Cruz E, Rubenstein JL, Anderson SA (2004) Origins of cortical interneuron subtypes. J Neurosci 24(11):2612–2622

Yakovlev PI (1968) Telencephalon "impar", "semipar", and "totopar". Morphogenetic, tectogenetic, and architectonic definitions. Int J Neurol 6:245–259

Yakovlev PI, Lecourse AR (1967) The myelinogenetic cycles in regional maturation of the brain. In: Minkowsky A (ed) Regional development of the brain in early life. Blackwell, Oxford, pp 3–70

Yamashita A, Hayashi M, Shimizu K, Oshima K (1989) Ontogeny of somatostatin in cerebral cortex of macaque monkey: an immunohistochemical study. Dev Brain Res 45:103–111

Yamashita A, Shimizu K, Hayashi M (1990) Ontogeny of substance P-immunoreactive structures in the primate cerebral neocortex. Dev Brain Res 57:197–207

Yan XX, Ribak CE (1997) Prenatal development of nicotinamide adenine dinucleotide phosphate-diaphorase activity in the human hippocampal formation. Hippocampus 7:215–231

Yan XX, Zheng DS, Garey LJ (1992) Prenatal development of GABA-immunoreactive neurons in the human striate cortex. Dev Brain Res 65:191–204

Yan XX, Garey LJ, Jen LS (1996) Prenatal development of NADPH-diaphorase-reactive neurons in human frontal cortex. Cereb Cortex 6:737–745

Yan XX, Cao QL, Luo XG, Garey LJ (1997) Prenatal development of calbindin D-28k in human visual cortex. Cereb Cortex 7:67–62

Yoon KJ, Koo BK, Im SK, Jeong HW, Ghim J, Kwon MC, Moon JS, Miyata T, Kong YY (2008) Mind bomb 1-expressing intermediate progenitors generate notch signaling to maintain radial glial cells. Neuron 58:519–531

Yost HJ (2001) Establishment of left-right asymmetry. Int Rev Cytol 203:357–381

Zaidel DW (1999) Quantitative morphology of human hippocampus early neuron development. Anat Rec 254:87–91

Zecevic N (1993) Cellular composition of the telencephalic wall in human embryos. Early Hum Dev 32:131–149

Zecevic N (1998) Synaptogenesis in layer I of the human cerebral cortex in the first half of gestation. Cereb Cortex 8:245–252

Zecevic N (2004) Specific characteristic of radial glia in the human fetal telencephalon. Glia 48:27–35

Zecevic N, Milosevic A (1997) Initial development of γ-aminobutyric acid immunoreactivity in the human cerebral cortex. J Comp Neurol 380:495–506

Zecevic N, Rakic P (2001) Development of layer I neurons in the primate cerebral cortex. J Neurosci 21:5607–5619

Zecevic N, Verney C (1995) Development of catecholamine neurons in human embryos and fetuses, with special emphasis of the innervation of the cerebral cortex. J Comp Neurol 351:509–535

Zecevic N, Andjelkovic A, Matthieu JM, Tosic M (1998) Myelin basic protein is expressed in the human embryonic CNS. Dev Brain Res 105:97–108

Zecevic N, Milosevic A, Rakic S, Marin-Padilla M (1999) Early development and composition of the human primordial plexiform layer: an immunohistochemical study. J Comp Neurol 412:241–254

Zecevic N, Chen Y, Filipovic R (2005) Contributions of cortical subventricular zone to the development of the human cerebral cortex. J Comp Neurol 491:109–122

Zhang R, Peng Y, Wang W, Su B (2007) Rapid evolution of an X-linked microRNA cluster in primates. Genome Res 17:612–617

Zilles K, Armstrong E, Schleicher A, Kretschmann HJ (1988) The human pattern of gyrification in the cerebral cortex. Anat Embryol 179:173–179

Zilles K, Armstrong E, Moser KH, Schleicher A, Stephan H (1989) Gyrification in the cerebral cortex of primates. Brain Behav Evol 34:143–150

Fetal MRI of Normal Brain Development

Denise Pugash, Ursula Nemec, Peter C. Brugger, and Daniela Prayer

Contents

Abstract

› The fetal brain is substantially different from the neonatal brain in terms of its structure and connectivity. Fetal MRI, beginning at 16–18 GW (gestational weeks), can be used to study fetal brain development and maturation in vivo. T2-weighted (T2W), T1-weighted (T1W), and diffusion-weighted (DW) imaging sequences can be used primarily to demonstrate morphology, parenchymal lamination, sulcation and gyration, the width of the subarachnoid spaces, and the size and shape of the midline structures. It is essential to understand MR signal changes associated with maturation, including the appearance and disappearance of transient structures,

D. Pugash (✉)
Departments of Radiology and Obstetrics and Gynecology, Division of Maternal-Fetal Medicine,
British Columbia Women's Hospital and
University of British Columbia, 1T48 - 4500 Oak Street
Vancouver, Canada V6H 3N1
e-mail: dpugash@cw.bc.ca

U. Nemec and D. Prayer
University Clinics of Radiodiagnostics and Medical University of Vienna, Waehringerguertel 18-20, 1090, Wien, Austria
e-mail: daniela.prayer@meduniwien.ac.at

P.C. Brugger
Integrative Morphology Group, Centre of Anatomy and Cell Biology, Medical University of Vienna, Waehringerstrasse 13, 1090, Vienna, Austria
e-mail: peter.brugger@meduniwien.ac.at

D. Prayer (ed.), *Fetal MRI*, Medical Radiology,
DOI: 10.1007/174_2010_116, © Springer-Verlag Berlin Heidelberg 2011

the underlying histological development of the fetal brain as well as the timing of development of landmarks in maturation in order to interpret normal and abnormal findings. It is the basis for understanding how neurogenetic development can be disrupted during vulnerable periods by different pathological processes, and how genetically controlled events in development correlate with functional development. The maturational stages of the fetal cerebral cortex, white matter, temporal lobe, and cerebellum, including structures that appear transiently in the developing brain as shown by various MR sequences, will be reviewed in this chapter.

1 Introduction

Ultrasound remains the primary imaging method of choice in the first and early second trimesters and has been used to demonstrate landmarks in the development of the brain, and in particular developmental timing of sulcation of the cortical mantle (Toi et al. 2004). Newer generation technology is beginning to allow visualization of individual zones of cortical development (Fig. 1). However, the ability to visualize the entire brain is inherently limited due to the physical impedance of the cranial vault. MRI can, in contrast, provide information both about gross anatomical structures as well as histological microstructure.

Histological changes in tissue composition result in decreased water content and increased cell density (the latter mainly in the gray matter), which are reflected in shortening of T1 and T2 relaxation times, and correspondingly increased T1-weighted (T1W) signal intensity and decreased T2-weighted (T2W) signal intensity. Secondly, differences in microanatomical structures can be demonstrated by diffusion-weighted (DW) anisotropy, as well as premyelination of axons which affect the appearance of structures on DW sequences. Sequences used must provide optimal contrast at the respective gestational ages, and must reflect tissue properties such as cell density and impending myelination. In addition, proton spectroscopy can provide metabolic information, and assessment of fetal movement can be correlated with functional development of neural structures.

Imaging of the fetal brain has been done from the beginning of in vivo MRI (Daffos et al. 1988), relying upon the T2-weighted contrast between CSF spaces and brain which allowed accurate assessment of the development of the brain surface. This permitted the assessment of timing of normal sulcation and gyration (Garel et al. 2001).

Subsequently, in vitro studies of fetal brain development recognized that the fetal brain parenchyma before about 28 gestational weeks (GW) had a different appearance of cortical layering than that of older

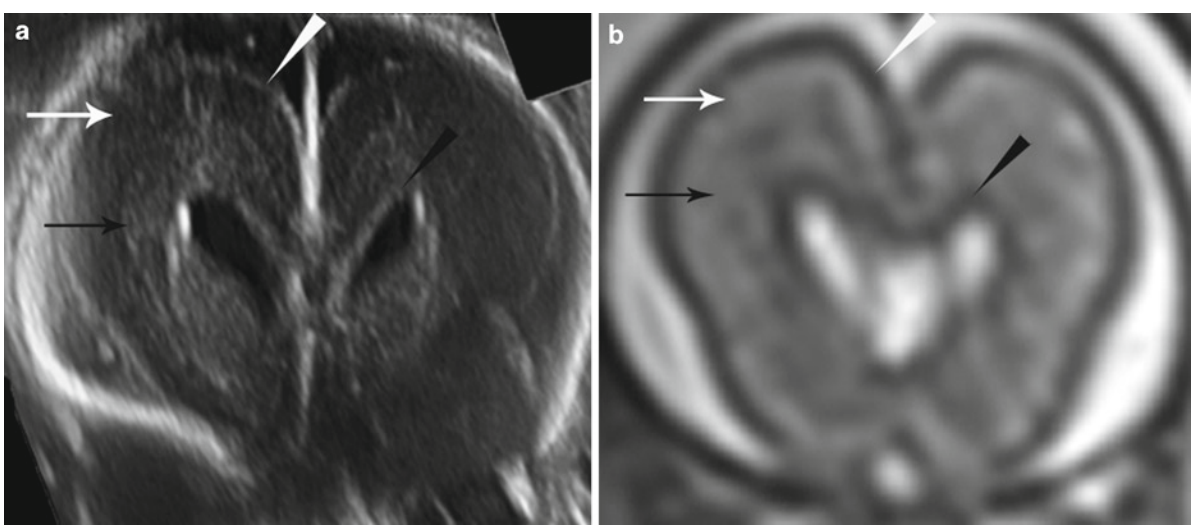

Fig. 1 Coronal view through the frontal horns using ultrasound at 19+3 GW (**a**) and T2-weighted MRI at 21 GW (**b**). High-resolution ultrasound technology allows visualization of individual zones of cortical development. However, the ability to visualize the entire brain is limited due to ossification of the cranial vault. Visible layers include the ventricular zone (*black arrowheads*), the intermediate zone (*black arrows*), the subplate (*white arrows*), and the cortical plate (*white arrowheads*)

fetuses (Kostovic et al. 2002). The morphological characterization of the different layers of the fetal brain parenchyma before 28 GW requires high-resolution T2-weighted contrast and/or diffusion-weighted information. T1-weighted contrast was shown to visualize regions of higher cell density, compared with surrounding structures (Brugger et al. 2006). Based on anisotropy that is present already in premyelinating white matter tracts (Wimberger et al. 1995), diffusion-tensor imaging and fibertracking can be performed (Kasprian et al. 2008). In addition, patterns of normal fetal movement and behavior have been defined, and can be documented using dynamic MR techniques.

2 Supratentorial Cortical Development

The primitive cerebral hemispheres are first seen at about 5 GW (3 GW after conception) as bilateral vesicles that protrude from the sides of the telencephalon in the area of the foramina of Monro (Muller and O'Rahilly 1988). The forebrain consists of the dorsal telencephalon or pallium which develops into the cerebral cortex and hippocampus, and the ventral telencephalon or subpallium which gives rise to the striatum and globus pallidus. The diencephalon gives rise to the thalamus and hypothalamus. In the initial stages, the wall of the cerebral vesicles is composed of a single layer of neuroepithelial cells (Marin-Padilla 1990). The cerebral vesicles grow and expand as neuroepithelial cells, located in the germinal ventricular zone, divide to form future cortical neurons beginning at 5 GW (Fishell et al. 1993; Levitt 2003). Layers of cells develop in the vesicles as they expand, forming the germinal matrices which are the origin of cells that will form the cerebral cortices. Initially, the germinal matrices are composed of a single zone, the ventricular zone. These cells are direct descendents of the neural plate, and differentiate into glial cells and neuroblasts (Brazel et al. 2003). The cortical plate begins to appear after the seventh gestational (fifth postconception) week, in the lateral aspect of the hemispheric wall (Bystron et al. 2006). At this stage, the forebrain wall contains two layers. The deeper layer consists of neuroepithelial cells and is termed the ventricular zone or germinal matrix. The more superficial layer is the preplate, which gives rise to the future cortex.

The vesicular walls are thin and are joined by the lamina terminalis in the midline. Cortical predecessor cells are thought to originate from the basal telencephalon, and migrate tangentially to the pia, arriving before cells from the ventricular zone begin radial migration to the preplate (Bystron et al. 2006). The cortical predecessor cells join neurons formed in the ventricular zone which migrate radially into the preplate, as well as Cajal–Retzius cells and neurons that have arrived by means of tangential migration (Bystron et al. 2008). The ventricular zone subsequently generates the first postmitotic or "pioneer" neurons that migrate radially into the preplate, dividing the preplate into two zones, the superficial marginal zone and the deeper subplate zone (Super and Uylings 2001). The outermost portion of the cortical plate is the marginal zone, and will become the future layer 1 of the mature cerebral cortex (Marin-Padilla 1990). Layer 1 also results from the first postmitotic cells from the ventricular zone (Samuelsen et al. 2003). It influences the laminar organization of the future cerebral cortex (ten Donkelaar 2000). This coincides with the end of the embryonic period and the beginning of the fetal period.

The germinal ventricular zone is the source of cells during embryonic and early fetal life. However, the subventricular zone, which is formed by the ventricular zone, increasingly becomes the source of neurons and glial cells when the ventricular zone begins to disappear in the third trimester (Brazel et al. 2003).

The ventricular zone generates waves of postmitotic neurons which migrate along radial glial cells, and form individual layers of neocortex. The ventricular zone produces deep-layer neurons of the future six-layer cortex, and the subventricular zone generates more superficially located neurons (Zecevic 1993). Layer 6 forms between the subplate and Cajal–Retzius cells. Layer 5 then forms between layer 6 and the marginal zone, resulting in formation of the cortex in an inside-out fashion (Marin-Padilla 1990).

Subsequently, the subventricular germinal zone develops laterally, separate from the ventricular zone, and is located between the ventricular zone and the intermediate zone. It also contains GABAergic interneurons originating in the lateral ganglionic eminence (in the third ventricular walls). These migrate tangentially to the walls of the lateral ventricles before

radial migration to the developing neocortex (Letinic et al. 2002; Marin and Rubenstein 2003). Migration to the developing cortex is complete for the most part by 26 GW (Marin-Padilla 1990). It is therefore evident that neuronal migration is occurring at a gestational age when fetal imaging is performed for clinical purposes.

There are four distinct areas within the ventricular/subventricular zone which include the medial, lateral, and caudal ganglionic eminences; and the neocortical subventricular zone. The ganglionic eminences are focal areas of thickening in the ventricular/subventricular zone which protrude into and shape the lateral ventricles (Brazel et al. 2003). The ganglionic eminences give rise to neurons which form the transient gangliothalamic body, parts of the amygdala, the basal nucleus of Meynert, the basal ganglia, and the thalamus (Letinic and Kostovic 1997; Ulfig 2002).

After 17 GW, the brain contains seven histological layers that are visible on in vitro MR images (Kostovic et al. 2002). These layers mature and evolve in thickness and number until 36 GW. At 18 GW, the ventricles appear prominent relative to the thickness of the cortex (Farrell et al. 1994). As gestation progresses, the thickness of the cortical mantle increases relative to the ventricle while the ventricular size remains unchanged (Prayer et al. 2006). As the basal ganglia enlarge, the ventricles assume their typical configuration. There is, therefore/subsequently, a relative decrease in size of the ventricles between 18 and 24 GW. Sulcation and gyration subsequently contribute to growth and increased thickness of the cortical mantle (Prayer et al. 2006) (Fig. 2).

Before 20 GW, a cortical plate forms within the preplate and gives rise to cortical layers 2–4 (Marin-Padilla 1998). Neurons migrate in radial as well as tangential fashion, with an exponential increase in numbers of cells (Corbin et al. 2001; Samuelsen et al. 2003; Fogliarini et al. 2005). The subplate zone, also known as layer 7 of the developing cortex, is visible beneath the cortical plate, and is a transient structure that is widest at 22 GW and cannot be delineated on fetal MR after 30 GW (Kostovic et al. 2002). It is formed when the preplate is divided by radial migration of streams of neurons from the ventricular zone. Neurons in the subplate are derived from the deepest layer of the preplate and are among the oldest population in the forebrain. The subplate contains a heterogeneous population of neurons with abundant extracellular matrix containing neurotransmitters and transient synapses (Bystron et al. 2008). Within the subplate layer, neurons are able to form temporary circuits between

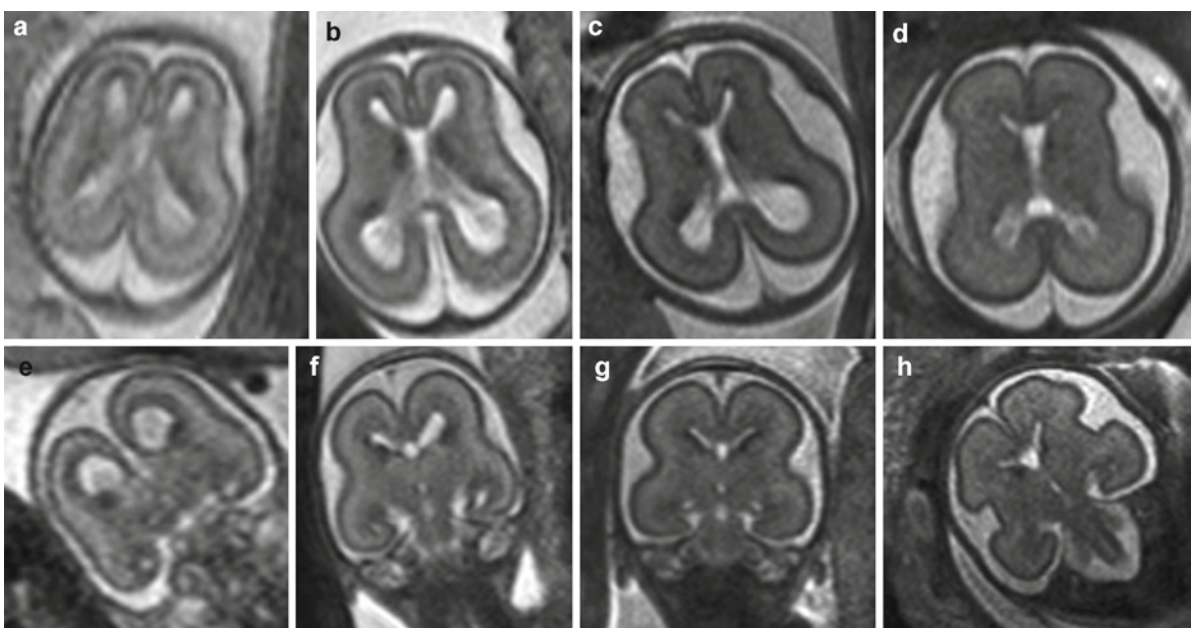

Fig. 2 Axial (*upper line*) and coronal (*lower line*) T2-weighted sequences of fetuses at 18+1 (**a**, **e**), 20+4 (**b**, **f**), 22+1 (**c, g**), and 24+0 (**d**, **h**) GW. Note the width of the ventricles and the thin brain parenchyma in the 18 GW fetus (**a, e**). Later, the thickness of the cortical mantle increases whereas the size of the ventricles decreases (**b–d, f–h**)

thalamus and cortex (Arber 2004). Cells are derived from the ventricular zone, the marginal zone, and the cortical plate (Kostovic et al. 1995).

Numerous functions have been attributed to the subplate zone, including that of an accumulation and waiting area for axons predetermined to synapse in the developing cortex, while their target cells migrate to the cortical plate, after which the axonal connections are established. This is important in the development of thalamocortical and other cortical afferent connections (Sur and Rubenstein 2005). The fetal white matter (external capsule fibers of the intermediate zone) forms the inferior border of the subplate (Kostovic et al. 2002). Subplate thickness varies in different locations of the brain. As axons move from the subplate to synapse in the cortex, the subplate progressively disappears after 34–36 GW (Kostovic and Jovanov-Milosevic 2008). The extracellular content of the subplate also decreases (Rados et al. 2006). Some cells persist as interstitial neurons in the subcortical white matter (Kostovic and Jovanov-Milosevic 2008).

In beginning of the preterm phase (26–33 GW), the subplate is very thick and can be easily distinguished from the cortical plate. After 34–36 GW, the subplate becomes thin and less well delineated from the cortical plate (Kostovic and Vasung 2009). The function of the subplate at this stage is related to the development of thalamocortical synaptic connections that form the first sensory circuitry which may be involved, for instance, in early pain processing (Lowery et al. 2007). Synaptogenesis increases with the development of the subplate (Kostovic et al. 1995). Due to the formation of specific axon-target interactions, neurons are "locked into position" once migration is complete (Samuelsen et al. 2003).

2.1 MRI Findings of Supratentorial Cortical Development

At 16 GW, in vitro, three layers can be differentiated in the cortical mantle by MRI, with the innermost and outermost layer appearing bright on T1-weighted and diffusion-weighted, and dark on T2W images. The intermediate layer shows relatively low signal on T1W images and high signal on T2W images compared to the inner and outer layers, corresponding to the intermediate zone which contains sparse neuroglial cells (Brisse et al. 1997). These layers, representing the ventricular/periventricular/subventricular zone, subplate and cortical plate (Kostovic et al. 2002), are difficult to delineate in vivo before GW 17–18. The intermediate zone, seen as a band between the ventricular/periventricular/subventricular zone, is usually detectable with intermediate signals of the respective sequence at the level of the frontal horns. After 17–18 GW, the cerebral mantle appears multilayered on in vitro as well as in vivo MR images until about 28–30 GW (Girard and Raybaud 1992; Chong et al. 1996; Brisse et al. 1997; Kostovic et al. 2002; Garel et al. 2003, 2004; Glenn and Barkovich 2006; Prayer et al. 2006) (Fig. 3). These layers are described as follows:

1. Ventricular zone – On T2W images, the germinal zone is hypointense, whereas, on T1W images it is hyperintense due to the high density of cell nuclei (Kinoshita et al. 2001; Maas et al. 2004) (Fig. 3a–d). It is of high signal intensity on DW images and is associated with a low ADC and medium-graded fractional anisotropy on scans of preterm neonates (Maas et al. 2004). The band of high signal intensity on DW source images, correlating with a dark band on ADC maps, corresponds with the intermediate, subventricular, periventricular, and germinal zone (Maas et al. 2004). (Fig. 3e). The hyperintensity may be due to high cell density as well as microvascularity which is more prevalent in the germinal zone than any other part of the developing brain (Ballabh et al. 2004), as well as the lack of radial organization (Maas et al. 2004).
2. Subventricular zone – The subventricular zone is thick in the frontal area and can be differentiated from other layers (Zecevic et al. 1999) (Fig. 3b). The subventricular zone contains germinal matrix that increases cell production as the ventricular zone disappears.
3. Intermediate zone – The intermediate zone is of slightly lower T1 signal intensity relative to the subplate layer (Widjaja et al. 2010a), between the subplate and the subventricular zone. (Fogliarini et al. 2005) (Fig. 3d). Together with the subventricular zone, it appears as a band of somewhat hypointense T2 signal subplate layer relative to ventricular zone and cortex (Fig. 3a–c). The intermediate zone contains axonal strata (Kostovic and Judas 2002) containing migratory neurons and glial cells, which results in moderate signal intensity on both T1 and T2W images (Kostovic and Vasung 2009) (Fig. 3a, d).

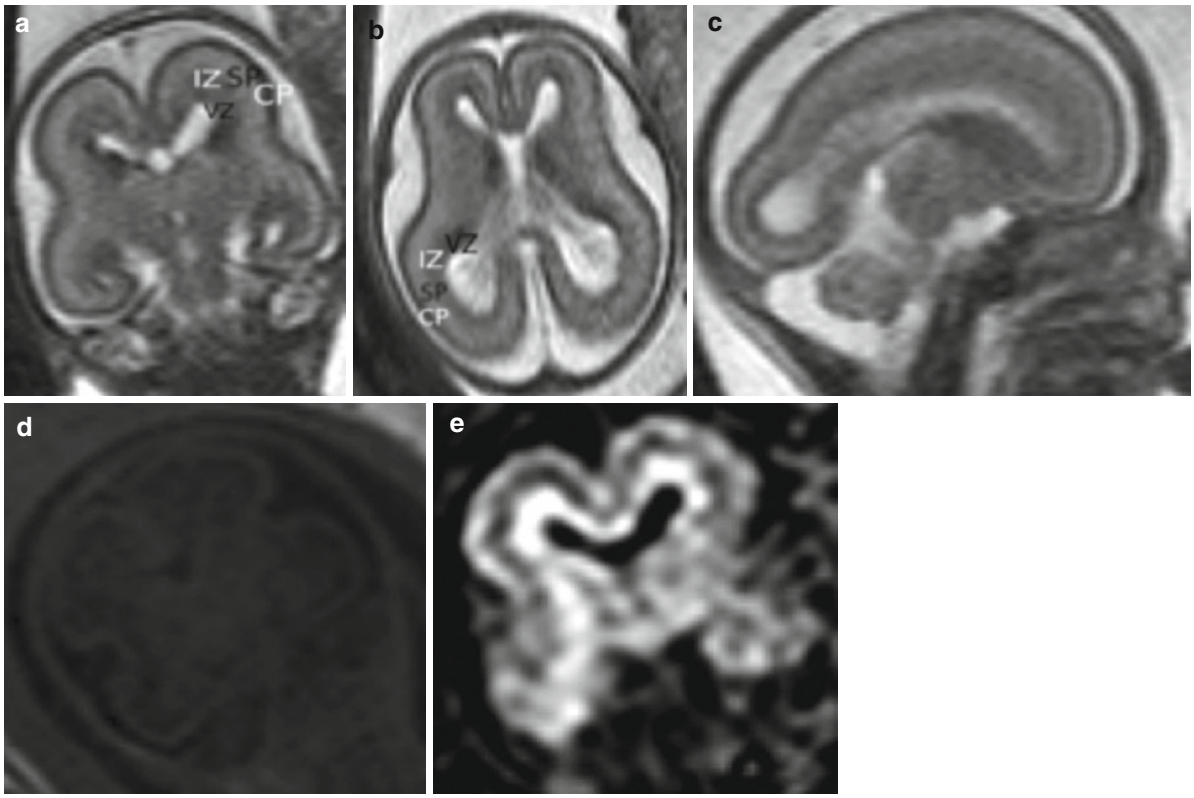

Fig. 3 T2-weighted sequences of a 20+4 GW fetus ((**a**) coronal T2 (**b**) axial T2 (**c**) sagittal). Note the layered organization of the fetal brain. The cortical plate (*CP*) appears hypointense, the subplate (*SP*) is hyperintense. The slim hypointense intermediate zone (IZ) and the hypointense ventricular zone (*VZ*) follow. On T1-weighted images the cortical plate is hypointense ((**d**) coronal). On diffusion-weighted sequences ((**e**) coronal), the cortical plate appears anisotropic

4. Subplate – The subplate zone has high water content due to extracellular matrix (Kostovic et al. 2002). On T2W images, the subplate is hyperintense (Fig. 3a–c), and it is hypointense to the cortical plate on T1W images (Fig. 3d). The subplate is hypointense on DW source images, and does not show evidence of anisotropy (Fig. 3e). These typical findings may be due to the amount of extracellular matrix and by the presence of axons that are not uniformly aligned and do not allow anisotropic behavior. The subplate band is thinner on DW images than on T2W sequences. (Fig. 3a, e). This reflects the inhomogeneity of the subplate due to fiber bundles which curve as they emerge from the thalamus (Prayer et al. 2006).
5. Cortical plate – The developing cortex appears hypointense on T2W images and hyperintense on T1W sequences relative to the subplate (Fig. 3a–d). On DW sequences, the cortical plate shows anisotropic behavior since it contains radially oriented migrating neurons (McKinstry et al. 2002; Maas et al. 2004) (Fig. 3e).

The layered appearance of the brain persists until around 28 GW, when decreasing T2W hyperintensity and increasing hypointensity of the subplate zone becomes isointense to the intermediate zone, and thus cannot be differentiated (Fig. 4). Alteration in lamination between 20 and 25 GW is due to gradual reduction in high T1 signal intensity and increase in low T2 signal intensity from about 22 weeks, found in both postmortem brains as well as antenatal T2W images (Widjaja et al. 2010b). This occurs prior to the histological disappearance of the subplate zone. The change in signal properties is most likely due to decreased water content of the extracellular matrix due to increased cellularity as axons "wait" in the upper subplate zone before moving to the more superficial developing cortex, as well as increased thickness of deep projecting fibers (Rados et al. 2006). The subplate

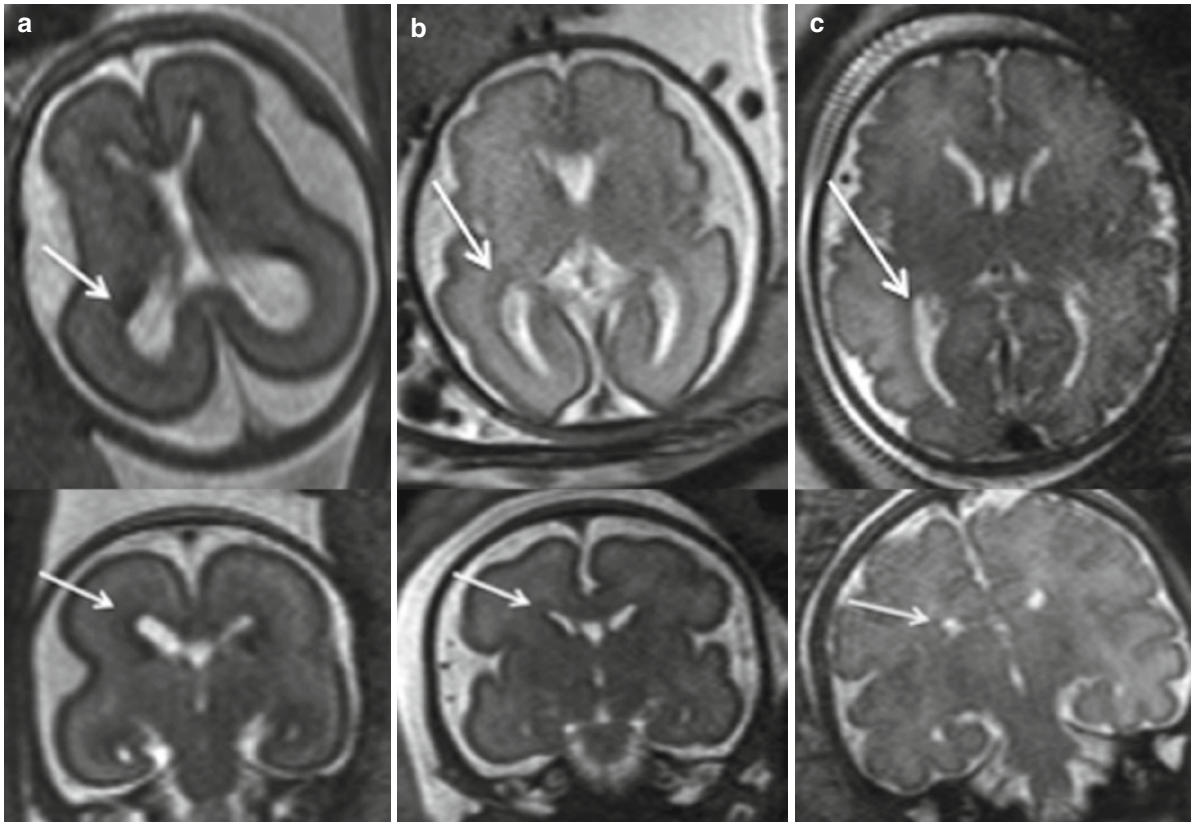

Fig. 4 T2-weighted fetal images at 20+4 (**a**), 28+1 (**b**), and 36+6 (**c**) GW. Upper images are in the axial plane, lower images are coronal. The subplate becomes isointense to the intermediate zone with increasing gestational age and cannot be differentiated. *Arrows* indicate areas where the subplate persists longest

persists longest in the frontal and temporal lobes on histological studies, and this has been observed in vivo as well (Rutherford et al. 2008) (Fig. 4).

Changes in cortical mantle development are also reflected in DW images. Mean diffusivity decreases in white matter with increasing gestational age and cortical thickening, due to synaptogenesis (Prayer and Prayer 2003; Bui et al. 2006; Manganaro et al. 2007; Schneider et al. 2007, 2009). Anisotropy disappears first in the central areas, then occipital cortex, and persists in the frontal and temporal areas until 35 GW (McKinstry et al. 2002; Maas et al. 2004; Fogliarini et al. 2005) (Fig. 5). DW imaging has also shown evidence of faster maturation of the right-sided frontal cortex relative to the left side, based on different values of fractional anisotropy (Gupta et al. 2005).

The appearances of the developing brain as well as biometric norms have been evaluated in a number of studies (Garel et al. 2003; Parazzini et al. 2008; Chung et al. 2009; Tilea et al. 2009).

3 Normal Sulcation and Gyration

Proposed hypotheses to explain the mechanisms of sulcal formation include sulcation resulting from cortical growth (Toro and Burnod 2005), variable growth between inner and outer cortical layers, and mechanical pulling by tethered axonal and glial fibers (Van Essen 1997; Hilgetag and Barbas 2005). Gyral development is most rapid in areas of sensory and visual pathways, which are the first areas to myelinate (Barkovich et al. 1988). Since sulcation is more predictable and uniform in areas of basic function such as motor and visual cortex, and more variable in areas of higher cortical function, sulcal formation may be related to variability and complexity of cortical connections (Fischl et al. 2008). Asymmetry in sulcation between right and left hemispheres, for example, with the left Sylvian fissure being longer than the right, has been noted both postmortem in fetuses (Chi et al. 1977) as well as on fetal MRI (Prayer et al. 2006; Chung

et al. 2009; Kasprian et al. 2010). Gyral development is later in the frontobasal, frontopolar, and anterior temporal areas, which are also slower to myelinate and to become metabolically mature (Penrice et al. 1996).

Cortical gyration occurs relatively late in fetal life. In the first half of gestation, the brain has a smooth, lissencephalic surface (Fig. 6a, b). In the second half of pregnancy, the brain surface gradually becomes more complex with a specific pattern of rapid development of gyri and sulci in the third trimester. Sulcation has been divided into 3 groups based on time of appearance and individual variability: primary, secondary, and tertiary. Primary sulci develop in parallel with the growth of the cerebral hemispheres, and are thought to reflect normal neurogenesis and orderly neuronal migration. The development of secondary sulci occurs at the same time as synaptogenesis begins to develop in the cortical plate.

Developmental appearance and localization of primary sulci are characterized by major cellular proliferative events. The appearance of the primary sulci coincides with thalamocortical axons reaching their destinations in the cortical plate (Kostovic and Judas 2002). As the cortex matures, the fissures and sulci become deeper, and the gyri expand. After 24–26 GW, gyration accelerates, and long corticocortical connections become established, characterized by the appearance of secondary sulci. (Kostovic 1990; Kostovic and Judas 2002, 2006). Tertiary sulcation begins after 28 GW (Garel et al. 2004; Fogliarini et al. 2005). At term and after birth, short corticocortical fibers reach their targets and the brain biomes highly convoluted with the development of highly variable tertiary sulci (Kostovic 1990; Kostovic and Judas 2002, 2006).

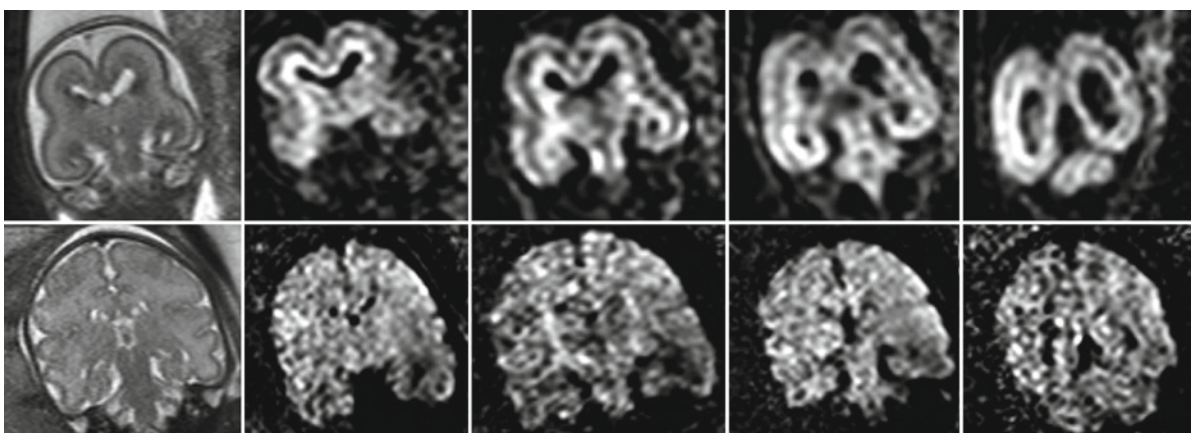

Fig. 5 Coronal diffusion-weighted sequences of fetuses at 20+4 GW (*upper*) and at 36+6 GW (*lower*). On the left are similar T2-weighted sequences. Note the changes in cortical mantle, particularly the disappearance of anisotropy and of the different layers (*lower line*)

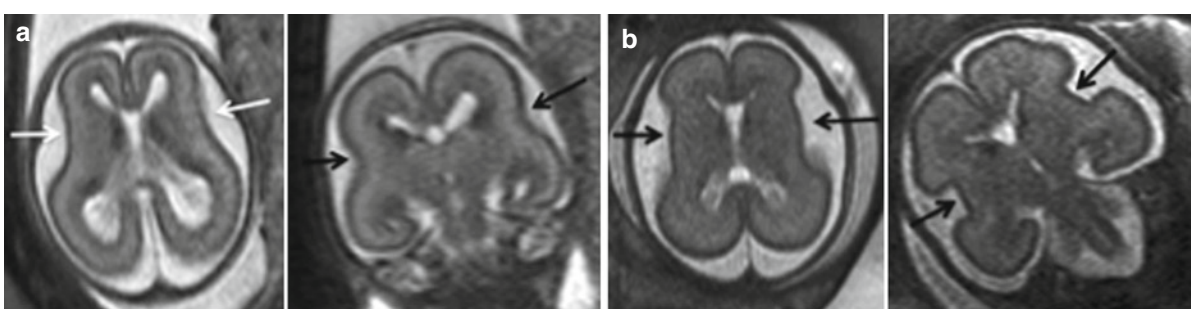

Fig. 6 T2-weighted sequences of fetuses at 20+4 GW ((**a**) left image, axial; right image, coronal) and at 24+0 GW ((**b**) left image, axial; right, coronal). Before 24 GW, the brain is agyric, and only the widely open obtusely angled Sylvian fissures can be recognized (*arrows*)

Since the appearance and development of sulci in the fetal brain follows a predictable pattern, the degree of sulcation may be used as an indicator of gestational age-related cortical development, both at autopsy and in vivo with fetal MRI (Chi et al. 1977; Dorovini-Zis and Dolman 1977; Garel et al. 2001, 2003). However, there is no clear consensus as to whether external landmarks of sulcation are reliable for gestational age estimation (Kostovic and Vasung 2009). This may in part be ascribed to inaccuracies in dating the autopsy specimens themselves in studies in which comparisons are based, different techniques for examining the fetal brains, and limited numbers of specimens in the studies. In particular, some postmortem studies of brain maturation rely on last menstrual period as the sole criterion of gestational age. One study (Chi et al. 1977) included specimens with a gestational age of 44 GW, which in itself probably reflects substantial errors in dating pregnancies. Moreover, delayed sulcation of 2–3 GW in twins before 32 GW as compared to singleton gestations, as well as asymmetry of maturation of the hemispheres, with the sulci appearing 1–2 GW earlier on the left side than the right side, introduces further error in establishing gestational age. Sulcation on fetal MRI appears to temporally lag by an average of two GW when compared with autopsy specimens (Levine and Barnes 1999; Garel et al. 2001, 2003). Comparisons may also be discrepant due to limitations in resolution of fetal MRI due to minimum voxel size and partial volume averaging (Chung et al. 2009). Also, there is a 2-week difference in when a sulcus can be detected initially, and when it can be recognized in 75% of fetuses (Garel et al. 2001). Cortical maturation has been assessed using sonography in both preterm neonates (van der Knaap et al. 1996; Dubois et al. 2008)and in the antenatal population (Toi et al. 2004).

3.1 MRI Appearance of Sulcation

Cortical gyration begins to be visible on MR images at 18 GW, starting with the shallow bitemporal indentations of the future Sylvian fissures. Before 24 GW, the brain is agyric apart from the widely open, obtusely angled Sylvian fissures (Fig. 6). The brain is very small and the cortex is extremely thin, therefore thin imaging sections are required (3 mm or less). By 23 GW, Sylvian fissures are more angular, and the parietooccipital sulcus and the callosal sulcus are detected in 75% of fetuses (Garel et al. 2001, 2003, 2004) (Fig. 7). The calcarine sulcus is visible by 24–25 GW in 75% of fetuses, and the central sulcus by 26 GW in 75%. The precentral and postcentral gyri can be identified in 75% by 27 and 28 GW, respectively. All primary and some secondary sulci are visible on fetal MRI by 34 GW (Garel et al. 2001, 2003; Garel 2004; Garel et al. 2004). Since very little sulcation is present prior to 24 GW, a suspected sulcal abnormality should be assessed later in gestation, ideally after 28 GW, when most of the primary sulci should be visible.

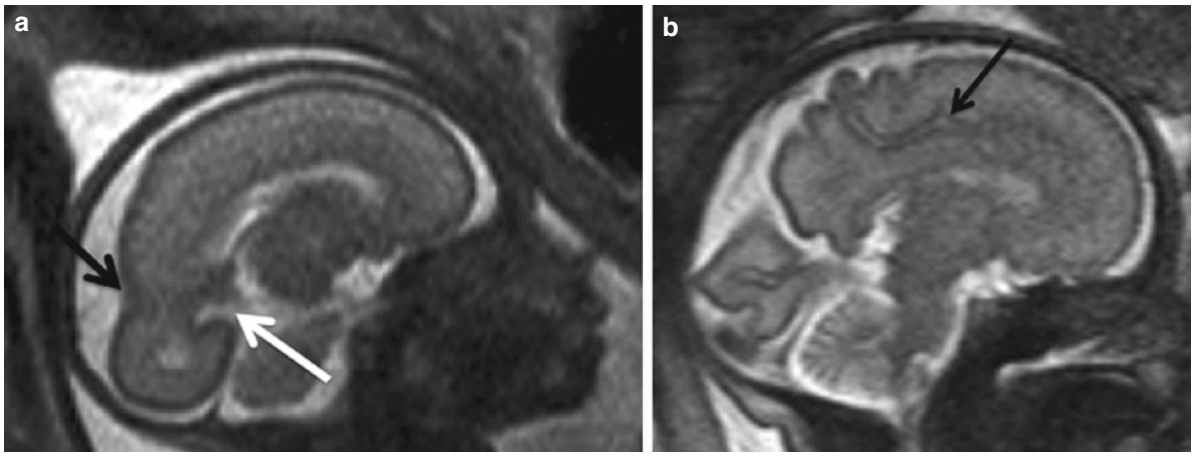

Fig. 7 Sagittal T2-weighted sequences of a fetus at 24+0 GW (**a**) and 32+0 GW (**b**). On image (**a**) the parieto-occipital sulcus (*black arrow*) and the calcarine sulcus (*white arrow*) are visible. Note the cingulate gyrus on image (**b**)

4 Development of the Temporal Lobe

A primordial hippocampus and hippocampal fissure begin to develop on the medial aspect of the telencephalon from the dorsal part of the lamina reuniens of His and can be identified histologically in the ninth GW (Rakic and Yakovlev 1968). Hippocampal cells originate from the ventricular zone of the dorsal forebrain and migrate radially to establish the temporal lobe. In addition, cells arise from the ganglionic eminence of the ventral forebrain and migrate tangentially to the cortical plate of the developing hippocampus, which is formed in an "inside-out manner" (Marin and Rubenstein 2003).

At 17–24 GW, the hippocampal formation displays a characteristic convoluted appearance and progressive narrowing of the cortical plate (Rados et al. 2006). In vitro, the hippocampal formation is the only part of the cerebral cortex in which the marginal zone is thick enough to be visualized by MRI. The increased thickness is due to transiently enlarged extracellular spaces, similar to that in the transient subplate zone elsewhere (Kostovic 1990). It forms a thin stripe of low signal on T1W images superficial to the hippocampal cortical plate which has high signal intensity (Rados et al. 2006). At 13–14 GW, on in vitro MR, the unfolded hippocampus surrounds the widely open hippocampal sulcus (hippocampal fissure) on the medial surface of the temporal lobe (Kier et al. 1997). At 15–16 GW, the dentate gyrus and cornu ammonis begin to fold inward. The hippocampal sulcus remains open, and the parahippocampal gyrus is larger and more medial in position. By 18–20 GW, the hippocampus begins to assume a more adult configuration, with the dentate gyrus and cornu ammonis folded within the temporal lobe (Fig. 8). The hippocampal sulcus is narrow and separates the closely apposed hippocampus and subiculum (Kier et al. 1997).

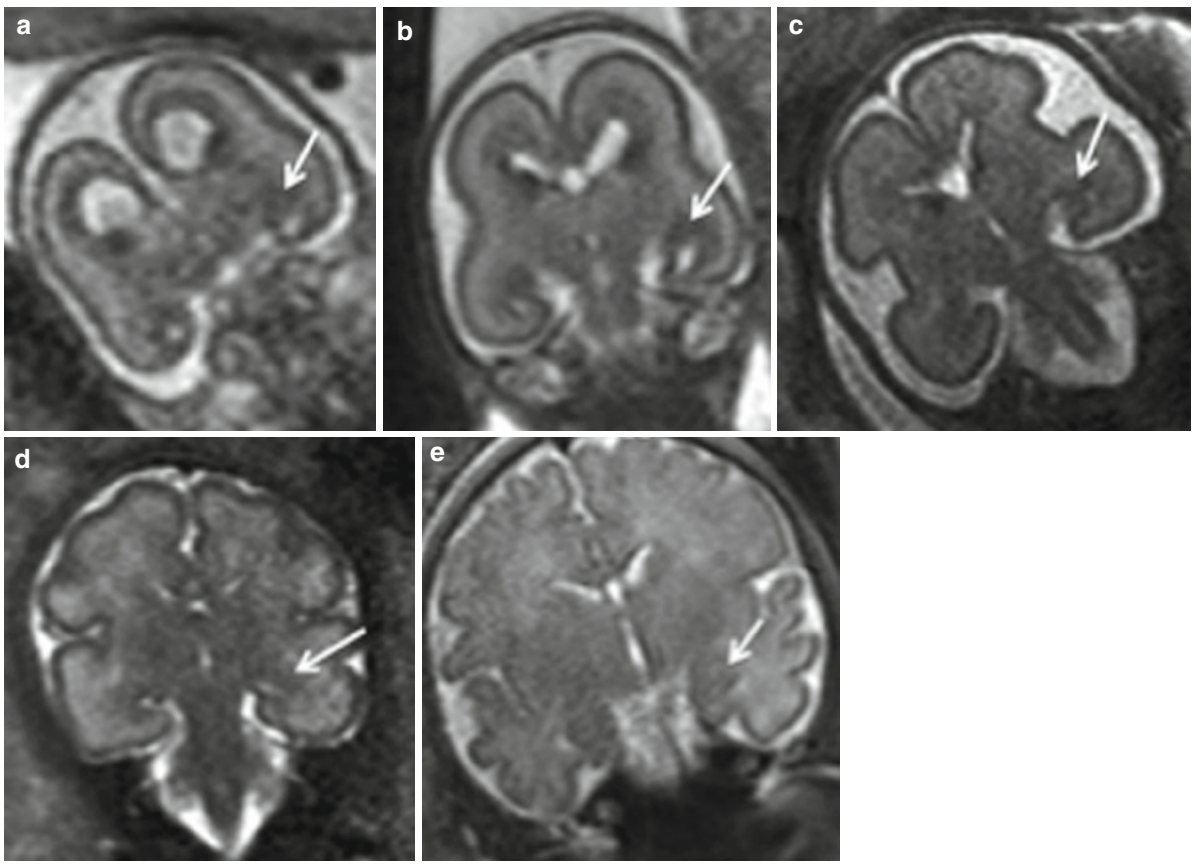

Fig. 8 Development of the hippocampus in coronal T2-weighted sequences of fetuses at (**a**) 18+1, (**b**) 20+4, (**c**) 24+3, (**d**) 31+1, and (**e**) 36+6. Note the hypointensity of the hippocampus and amygdaloid complex (*white arrows*). First the hippocampus shows a vertical position (S-shaped), and then it rotates and appears as a horizontal structure. Note also the development of the hippocampal sulcus (**c**–**e**)

At 15 GW, the hippocampus has the appearance of an upright "S" shape. Between 15 and 24 GW, there is cell proliferation and horizontal migration (Arnold and Trojanowski 1996). The vertical orientation of the hippocampus undergoes progressive rotation until 22–24 GW when it appears more horizontal and inferomedial position in the temporal horn. Subsequently, the volume of the hippocampus increases due to increased numbers of glial and endothelial cell components.

Fornical connections occur as early as 10–11 GW with the exchange of fibers across the midline (Raybaud 2010). In the third trimester, hippocampal fiber connections are established as the hippocampal network matures. Gamma-aminobutyric acid (GABA)ergic interneurons are thought to play an excitatory role in the maturation of the hippocampal network (Ben-Ari et al. 2004). Activity in the hippocampal or neocortical networks is present in late gestation in primates (Khazipov et al. 2001).

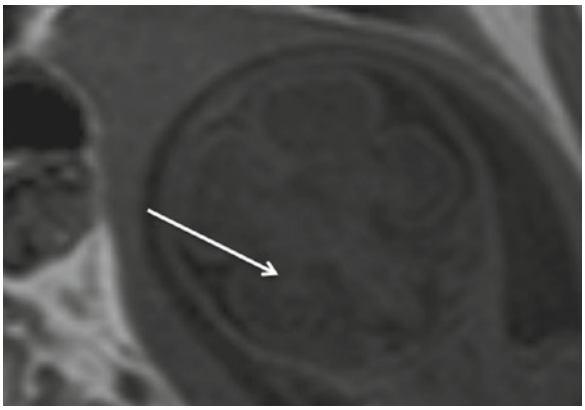

Fig. 9 Coronal T1-weighted sequence of a fetus (24+0 GW). The hippocampus appears as a hyperintense structure (*white arrow*)

4.1 MRI Findings of Temporal Lobe Development

In vitro, the hippocampus is a hypointense structure along the medial surface of the temporal lobe on T2W sequences, adjacent to the hippocampal sulcus (Kier et al. 1997) (Fig. 8). The hippocampus has a thick marginal zone, visible as a zone of T2W hyperintensity and low T1W intensity on postmortem images (Rados et al. 2006).

Coronal T2W images can provide information about hippocampal development in vivo (Kasprian 2006). At 18 GW, the hippocampus is hypointense and has a slim "S-shaped" appearance. The hippocampal sulcus appears as a deep horizontal indentation between the parahippocampal gyrus and the forming cornu ammonis (Prayer et al. 2006). (Fig. 8c–e). The medial border of the hippocampal sulcus fuses around 20 GW. The process may be incomplete and leave residual cysts (Bronen and Cheung 1991; Sasaki et al. 1993). Coronal T2W images between 20 and 24 GW demonstrate the growth and changing morphology of the hippocampus. Initially, the hippocampus is vertically oriented, and progressively becomes more horizontal by 22–24 GW (Fig. 8a–c). The degree of rotation of the hippocampus can be measured on fetal MR images by using the hippocampal infolding angle, which increases with gestational age (Righini et al. 2006). After 24 GW, the hippocampus appears as a horizontally oriented structure at the medial ventricular border of the temporal horn (Prayer et al. 2006) (Fig. 8d, e). Subsequently, the hippocampus increases in thickness and volume. Hyperintense signal is visible throughout all areas on axial T1W sequences (Fig. 9). This probably is a result of the increasing glial, endothelial, and neuronal cellularity (Prayer et al. 2006). A focal area of T2W hyperintensity develops in the temporopolar white matter around 28 GW (Prayer et al. 2006), correlating with the development of the amygdalocortical connections and temporal cortical plate (Fig. 8).

Gyration of the temporal lobe begins after 24 GW. The superior temporal sulcus serves as a landmark for gyral development and correlates well with gestational age in anatomical studies (Larroche 1981). At 25 GW, the posterior part of the superior temporal gyrus develops (Chi et al. 1977) (Fig. 10b), and by 32–34 GW, its formation is complete (Kasprian 2006). Concurrent with, or subsequent to, the appearance of the superior temporal gyrus, the collateral sulcus develops (Fig. 10a), and all primary sulci are visible by 34 GW (Garel et al. 2001).

The amygdaloid complex has a hypointense appearance rostral to the temporal horn of the lateral ventricle on coronal T2W images at 18 GW. The amygdala appears hyperintense on T1W images and persists through term. These signal intensities most likely result from cellularity (Prayer et al. 2006). At 1.5 T, T2W MR resolution is not adequate to delineate the hypointense

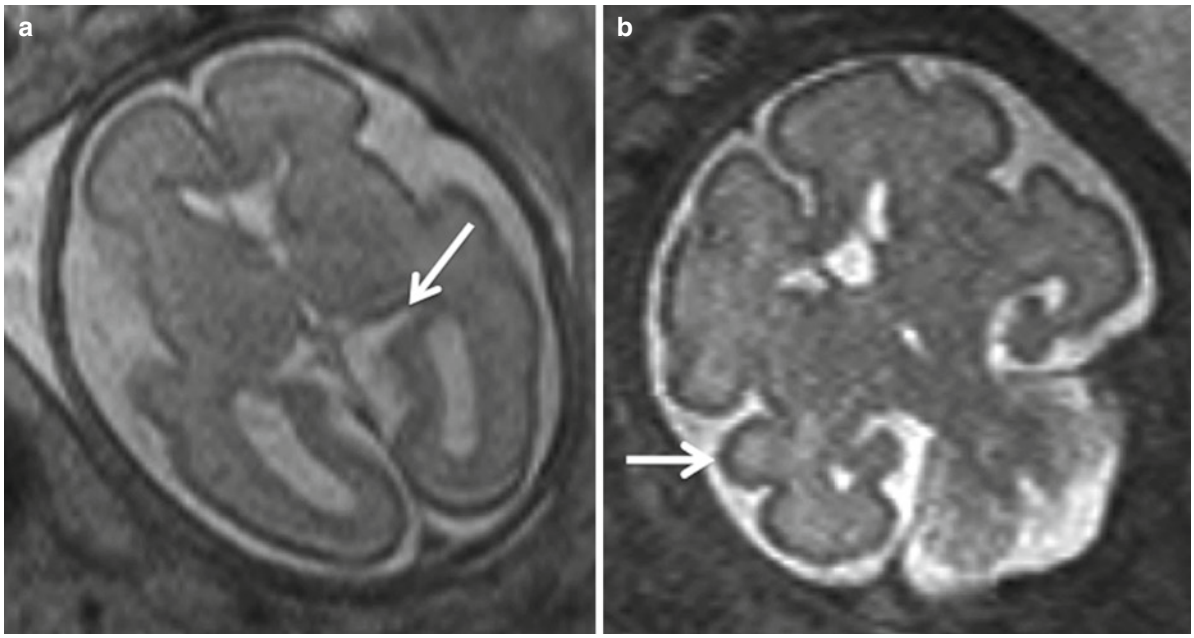

Fig. 10 T2-weighted sequences of fetuses at 24+4 GW (**a**) – axial; and at 25+4GW (**b**) – coronal. On the left image the collateral sulcus is visible (*white arrow*). On the right, the T2-weighted image shows the developing superior temporal gyrus (*white arrow*)

ganglionic eminence inferiorly. Before 31 GW, the amygdala, piriform cortex, and hippocampal head appear as a continuous zone of hypointensity in the medial temporopolar area on axial T2W sequences (Fig. 11). When formation of the anterior temporal lobe gyri begins at 31 GW, growth of the temporal lateral neocortex displaces this area more posteromedially within the temporal lobe (Prayer et al. 2006).

5 Transient Structures in the Fetal Brain

The appearances of transient structures in the fetal brain are critical steps in normal brain development. Transient structures include the subplate (as discussed above), the perireticular nucleus, the gangliothalamic body, and periventricular crossroads (Letinic and Kostovic 1997; Kostovic and Judas 1998; Ulfig 2000; Prayer et al. 2006).

The perireticular nucleus contains neurons that function as guideposts that direct corticothalamic fibers toward the dorsal thalamus and corticofugal fibers toward the brainstem (Ulfig 2000). Pioneer axons originate in the internal capsule and move to the thalamus, and may provide a framework for thalamocortical connections (Coleman and Mitrofanis 1999). The perireticular nucleus involutes due to cell

Fig. 11 Axial T2-weighted sequence of a fetus at 29+5 GW. Note the focal area of hyperintensity in the temporopolar white matter (*white arrow*). There is also a continuous zone of hypointensity in the medial temporopolar area which is formed by the amygdala, piriform cortex and hippocampal head before 31 GW (*black arrow*)

apoptosis or migration (Earle and Mitrofanis 1996) and displacement due to expansion of the fibers of the internal capsule (Tulay et al. 2004). The gangliothalamic body exists between 15 and 34 GW and represents a stream of migrating neurons between the ganglionic eminence and the pulvinar thalami. It regresses most likely as a result of cell migration (Letinic and Kostovic 1997).

Periventricular crossroads are special areas of periventricular white matter where growing fibers encounter axonal guidance molecules during growth. Crossroads result from a transiently increased content of extracellular matrix in association with radial and tangential migration of immature fibers (Judas et al. 2005). They are most prominent in the frontal lobe anterolateral to the frontal horn of the lateral ventricles.

5.1 MRI Findings of Transient Structures

The ganglionic eminence is visible on in vitro MRI scans at 10 GW (Brisse et al. 1997). The volume increases until about 26 GW, at which point it begins to diminish, persisting the longest in the superior ganglionic eminence (Kinoshita et al. 2001; Ulfig 2000). The gangliothalamic body is isointense to the adjacent gray matter nuclei and ganglionic eminence on MR images. Lack of DW anisotropy may be due to the nonlinear direction of the stream of migrating neurons (Prayer et al. 2006). The MRI appearances of periventricular crossroads will be discussed in the following sections.

6 White Matter Development

Prospective white matter develops from the second wave of postmitotic cells generated by cells in the ventricular zone. It appears between the ventricular zone and the marginal zone and therefore is termed the intermediate zone (Kostovic and Judas 2002; Samuelsen et al. 2003). The intermediate zone contains growing axonal pathways and oligodendrocyte progenitors. Neuronal migration and growth of axons take place principally in the intermediate zone (fetal white matter) and the subplate zone between the intermediate zone and the cortical plate (Rakic 2004). Growing thalamocortical fibers within transient zones and cortical afferent axons are distributed in the intermediate zone (fetal white matter). They also form an extensive system that involves the subplate zone and periventricular fiber-rich zone (Kostovic and Judas 2002; Judas et al. 2005). Collections of growing axons exhibit two morphological patterns: a laminar arrangement (Kostovic and Judas 2002) and periventricular crossroads (Judas et al. 2005). The cell number of the intermediate zone increases by a factor of 3.8 between 13 and 20 GW (Samuelsen et al. 2003). Since postmitotic neurons need several weeks to reach their final destination, as many as 30 generations of neurons can be simultaneously aligned along a single radial glial shaft within the wide intermediate zone (Rakic 2003). Tangential migration also occurs perpendicular to the radial glia (Menezes et al. 2002). A pathway for migration of callosal axons may also be provided by neurons at the

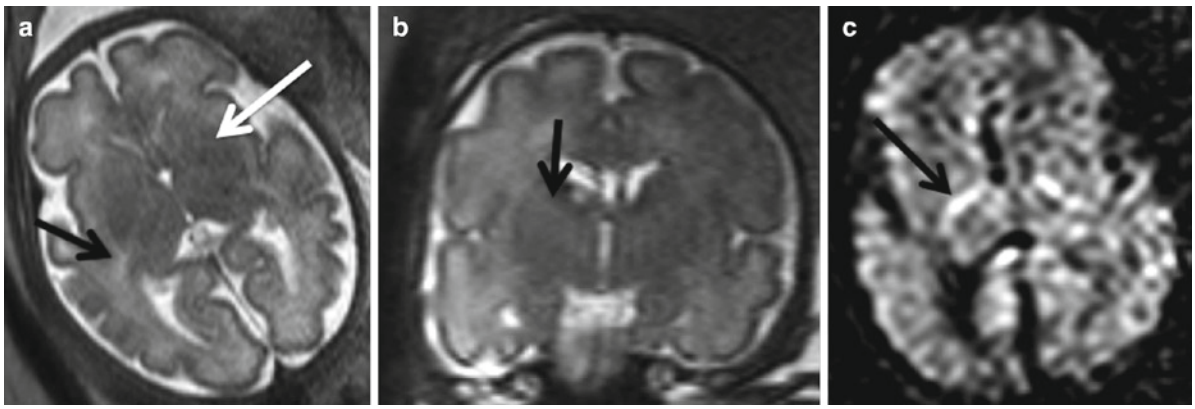

Fig. 12 Axial (**a**) and coronal (**b**) T2-weighted sequence of a fetus at 32+5. Note the hyperintensity of internal capsule (*black arrows*). A small lesion is present to the right of the arrow in image (**b**). The gray nuclei appear more hypointense on T2-weighted images in comparison to the internal capsule (*white arrow*). (**c**) Axial diffusion-weighted sequence of a fetus at 32+5 GW. Note the anisotropic posterior crus of the internal capsule that can be detected as early as 22 GW

border between the subventricular zone and the intermediate zone (Del Rio et al. 2000).

Fetal white matter development is also characterized by prominent areas of extracellular matrix in periventricular areas where there are numerous crossing fibers, known as periventricular crossroads (Judas et al. 2005). These areas of crossing efferent, afferent, associative, and callosal fibers are characterized by abundant hydrophilic extracellular matrix which contain axonal guidance material (see above). Originally described in preterm neonates (Battin et al. 1998), they have a "cap-like" appearance on MR images. Crossroads may also be identified adjacent to the caudal portion of the ganglionic eminence, lateral to the posterior crus of the internal capsule, and appear similar to those in the frontal and occipital region between 20 and 30 GW. Crossroads appear hypointense relative to white matter on T1W images and hyperintense on T2W images, and are seen in the frontal and occipital white matter. They become visible around 24 GW and persist throughout gestation. These are visible on fetal MR images by about 22 GW, and are "slightly hyperintense" on T2W images and "slightly hypointense" on T1W images relative to the intermediate zone (Kostovic and Judas 2002). These have been described in six locations: the main crossroad at the lateral margin of the frontal horn and body of the lateral ventricle, the frontal crossroad along the dorsal aspect of the lateral ventricle, a frontal crossroad inferolateral to the frontal horn and ventral to the putamen, the occipital crossroad lateral to the atrium and occipital horn, the parietal crossroad anterolateral to the atrium and centered over the retrolenticular internal capsule (the "Wetterwinkel" (Prayer et al. 2005) (Fig. 13), and the temporal crossroad anterolateral to the temporal horn (Judas et al. 2005) (Fig. 11).

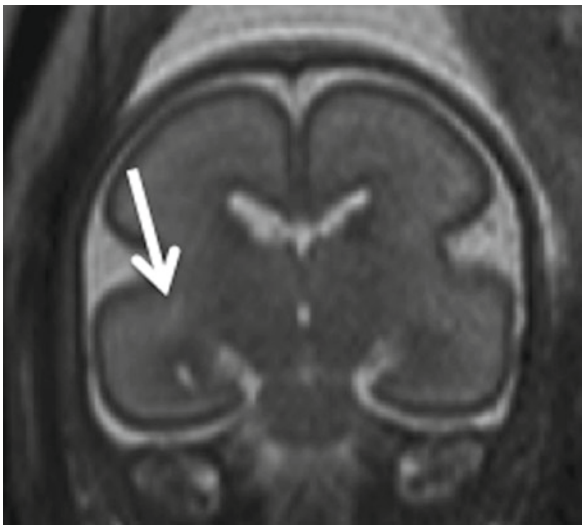

Fig. 13 Coronal T2-weighted sequence of a fetus at 23+0 GW. Crossroads appear hypointense relative to white matter on T1W images and hyperintense on T2W images. Note the triangular crossroad the so-called Wetterwinkel (*white arrow*)

6.1 White Matter Tract Formation

Neural connectivity depends on the directed growth of axons (Richards et al. 1997). The internal capsule is visible in the late embryonic period at the time of preplate formation, and is shaped by emerging thalamic axons (Molnar and Blakemore 1995; O'Rahilly and Muller 1999). However, before 20 GW it is a potential space that contains undifferentiated blast cells (Tulay et al. 2004). The axons that form the internal capsule are mainly derived from the subplate (Koester and O'Leary 1994). At 12–15 GW, three fiber systems are visible: the corpus callosum, the fornix, and the cerebral stalk, which contains all the projection fibers of the developing internal capsule including thalamocortical fibers (Rados et al. 2006).

Axons that form the pyramidal tracts in the late embryonic period also come from the subplate (ten Donkelaar 2000). Decussation of the pyramidal tract is complete by 17 GW, myelination is present at 25 GW, and corticospinal tract fibers reach the spinal cord by 24 GW (Eyre et al. 2000).

From 17 to 24 GW, the corpus callosum, the fornix, the internal capsule, and the external capsule continue to grow and develop. The growing fiber tracts intersect at the periventricular crossroads (Judas et al. 2005). From 24 to 32 GW, the corona radiata develops, and all major segments of the cerebral white matter can be identified (Kostovic and Judas 2002). These include the corpus callosum, the peduncular part of the corona radiata, the centrum semiovale, and gyral white matter. Between 32 weeks and term, the internal capsule becomes well-defined due to the onset of myelination. Gyral white matter becomes well-developed.

Myelination occurs predominantly postnatally (Counsell et al. 2002) in a craniocaudad and centrifugal fashion (Garel et al. 2003; Kinney 2005). Although there is evidence of myelination in the spinal cord as early as

15–21 GW (Grever et al. 1996), the first histological evidence of brain myelination occurs at 21 GW in the brainstem and internal capsule (Shiraishi et al. 2003) and in the thalamus at 22 GW (Jakovcevski and Zecevic 2005). The number of immature oligodendrocytes increases about 3 months prior to the onset of myelination, referred to as myelination gliosis (Girard et al. 1991). At 20 GW, premyelination changes occur when oligodendrocyte progenitors transform into oligodendrocytes. There are three phases of myelination: "premyelin sheath" formation by immature oligodendrocytes; formation of a "transitional sheath," which contains myelin basic protein which is characteristic of mature myelin; and formation of a mature myelin sheath, which contains myelin basic protein (Back et al. 2002).

6.2 MRI of White Matter Development

On T1W postmortem MR images, the subplate has lower signal intensity than the intermediate zone. Postmortem and T2W images display higher signal intensity in the subplate compared with the intermediate zone. This correlates with histological changes of decreased extracellular matrix and increased cellularity in the subplate layer. Antenatal T2W images show similar findings (Widjaja et al. 2010b). On DW sequences, there is no anisotropy due to microstructural changes of the differing fiber pathways across the zones (Prayer et al. 2006; Widjaja et al. 2010a). After 27 GW, water content in the subplate decreases, and the interface between the intermediate zone and the subplate becomes less distinct. In vivo, the internal capsule is hyperintense on T2W images and hypointense relative to the basal ganglia on T1W images. After 28 GW in the preterm neonate (Counsell et al. 2002) and 30th week in the fetal brain (Garel et al. 2003), the posterior limb of the internal capsule becomes T2W hypointense and T1W hyperintense (Fig. 12a, b). DW anisotropy can be detected in the posterior crus as early as 22 GW (Prayer et al. 2006) (Fig. 12c). In preterm neonate brains, the posterior crus shows lower mean diffusivity and higher fractional anisotropy than other unmyelinated white matter tracts (Partridge et al. 2004). Signal changes can be ascribed to increased cell density related to the perireticular nucleus neurons and glial cells or due to alignment of the neurons, creating an asymmetrical environment (Prayer et al. 2006).

Premyelinating changes in the corticospinal tract, the longitudinal fasciculus at the level of the brainstem, the internal capsule, the CC, and the optic chiasm can be recognized on DW imaging (Wimberger et al. 1995; Prayer and Prayer 2003; Partridge et al. 2004) (Fig. 14). White matter tract anisotropy precedes myelination, probably due to histological changes as the axons develop and tracts mature, and to the establishment of an axon potential (Huppi et al. 1998) which promotes differentiation of immature oligodendrocytes and stimulates myelination (Fields 2004).

The technique of diffusion tensor imaging (DTI), by measuring the directionality of diffusion, allows a three-dimensional reconstruction of tissue microstructure and thus can depict the architecture of the developing fetal brain (Le Bihan et al. 1986). The DTI technique has been used to study and quantify white matter maturation and development (Huppi et al. 1998; Childs et al. 2001; Mukherjee et al. 2002; Zhai et al. 2003; Maas et al. 2004; Partridge et al. 2004; Berman et al. 2005; Partridge et al. 2005; Yoo et al. 2005; Bui et al. 2006; Huang et al. 2006; Anjari et al. 2007; Dubois et al. 2008). DTI sequence optimization permits the in utero acquisition of data on unsedated fetuses, allowing visualization of corticospinal and callosal pathways in 40% of cases (Kasprian et al. 2008) (Fig. 15). DTI detects regions of intermingling callosal and craniocaudal pathways anterolaterally to the anterior horns of the lateral ventricles. These correlate with the periventricular "caps" (Battin 2001) seen on T2W images which correspond with the periventricular crossroads described both histologically and on postmortem studies.

7 Development of the Corpus Callosum

At 10 GW, the interhemispheric fissure contains meninx primitiva, and deepens, resulting in a cleft in the dorsal lamina reuniens and formation of the sulcus medianus telencephali medii (Rakic and Yakovlev 1968). The sulci are close together at the edge of the cortical plate (Rakic and Yakovlev 1968) at the corticoseptal boundary which is genetically predetermined (Hankin and Silver 1988; Shu and Richards 2001; Shu et al. 2003; Richards et al. 2004; Shen et al. 2006). A glial sling is formed by medial migration of glial and possibly neuronal cells from

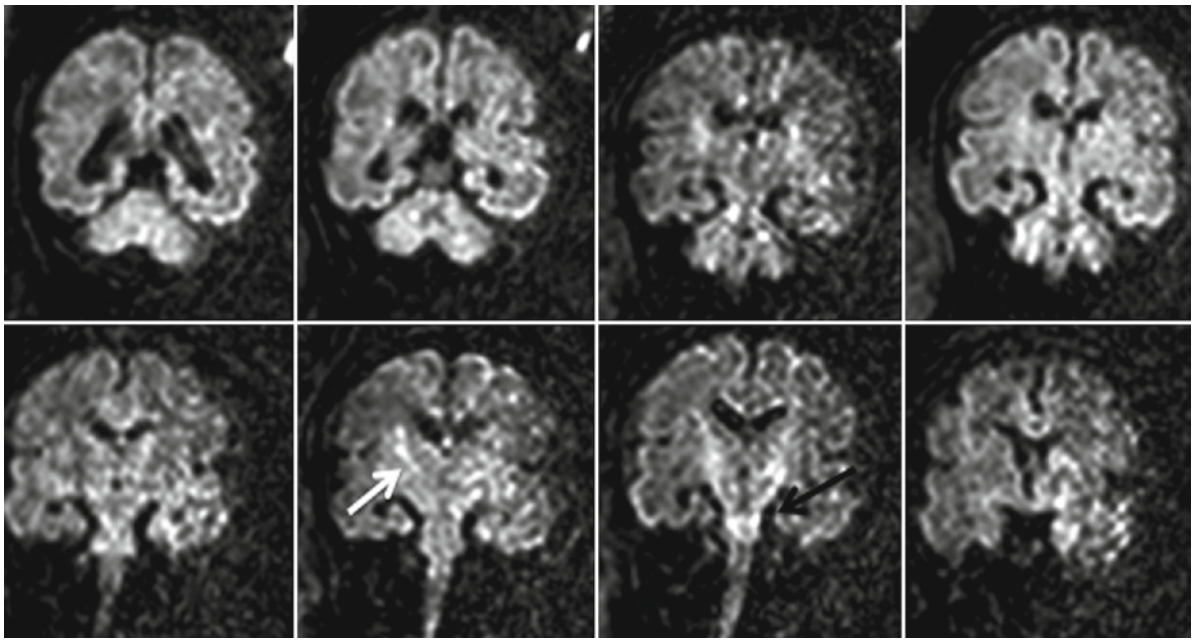

Fig. 14 Premyelinating changes can be recognized on coronal diffusion-weighted images at GW 34+0. Note the anisotropy of the internal capsule (*white arrow*) and of the longitudinal fasciculus at the level of the brainstem

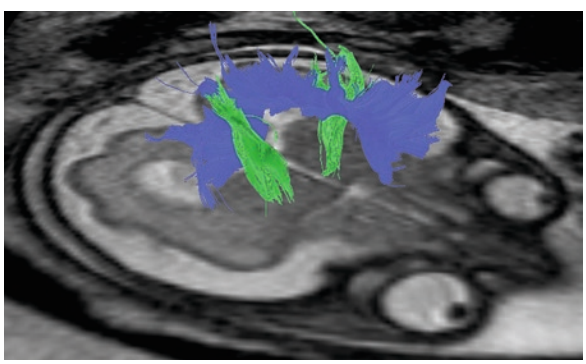

Fig. 15 Diffusion tensor imaging sequence optimization allows the in utero acquisition of data on unsedated fetuses, allowing visualization of corticospinal and callosal pathways at GW 28+2

the subventricular zone toward the midline at around 12 GW (Rakic and Yakovlev 1968; Silver et al. 1982; Katz et al. 1983; Hankin and Silver 1988; Shu and Richards 2001; Shu et al. 2003; Richards et al. 2004) (Lent et al. 2005; Ren et al. 2006). The glial sling forms an interhemispheric bridge that supports the crossing of the first pioneer axons at 12–13 GW (Rakic and Yakovlev 1968). If the glial sling is not present, the callosal fibers do not cross and instead extend parallel to the midline (Silver et al. 1982). Further guidance of axons across the midline is provided by two other glial structures: the indusium griseum and the glial wedge (Shu and Richards 2001; Richards 2002; Shu et al. 2003; Richards et al. 2004). These structures repel pioneer axons initially from the cingulate cortex (Koester and O'Leary 1994; Richards 2002) and direct them toward the glial sling and the midline. Axons are guided across the midline to homologous regions in the contralateral hemisphere by a variety of guidance molecules, transcription factors, and morphogens that are chemoattractive and chemorepulsive (Richards et al. 1997; Richards 2002; Judas et al. 2005; Plachez and Richards 2005; Shen et al. 2006; Lindwall et al. 2007). Subsequently, neocortical axons join them in a process that occurs within GW 13 (Rakic and Yakovlev 1968). Neocortical commisural axons from the anterior hemisphere arrive by means of the pioneer callosal fibers and the glial sling, while those from the posterior neocortex cross along the hippocampal commissure (Raybaud 2010). Both anterior and posterior sections continue to grow and fuse and all parts of the corpus callosum are fused and complete by GW 14 or 15 (Kier and Truwit 1996, 1997). At this point, the corpus callosum is short but grows by addition of fibers as the cortex develops and connectivity increases until after birth (Raybaud 2010). Rather than developing from front

to back as has been postulated, it appears that in humans, due to disproportionate growth of the frontal lobes, there is a corresponding increase in anterior callosal fibers (Huang et al. 2009). This causes the splenium and hippocampal fissure to be shifted posteriorly into position above the posterior third ventricle and tectal plate (Raybaud 2010).

The splenium of the corpus callosum becomes prominent by 18–19 GW (Ren et al. 2006) and the overall shape of the corpus callosum is established by GW 20 (Raybaud 2010). At this stage the cross-sectional area is only 5% of that of a 5-year-old child, and in neonatal life prior to myelinization is 50% of the size (Huang et al. 2006; Jovanov-Milosevic et al. 2009). The corpus callosum enlarges in a proportional fashion to the cortical growth and complexity in utero by the addition of fibers (Raybaud 2010).

7.1 MRI of Development of the Corpus Callosum

The corpus callosum is seen on T2W images in the midline sagittal plane as a horizontal thin curvilinear C-shaped hypointense structure (relative to the subplate) at the superior margin of the cavum septi pellucidi (Fig. 16a). It increases in length and thickness with gestational age. Normative values for callosal length are available (Garel 2004; Parazzini et al. 2008; Chung et al. 2009; Tilea et al. 2009). Diffusion tensor imaging with fiber-tracking has been used to demonstrate callosal fibers and trajectories (Kasprian et al. 2008) (Fig. 16b).

8 Normal Development of the Ventricular System

The ventricular walls are composed of cells of the ventricular zone (germinal matrix). It is the innermost layer of the developing cerebral cortex. It is thickest early in gestation, regressing in the third trimester(Fig. 2). A single layer of ependymal cells lines the ventricular walls by 28 GW. Germinal matrix cells persist in the roof of the temporal horn and in the occipital horn lateral wall until 33 GW, and persist later in the caudothalamic groove (Kinoshita et al. 2001; Bystron et al. 2008).

8.1 MRI of the Ventricular System

The ventricular zone is visible on MR images as a dark band on T2W sequences and a bright band on T1W sequences (Fig. 3a–d). The diameter of the atria of the lateral ventricles remains constant from 15 to 35 GW, but particularly on MR images, appears more prominent

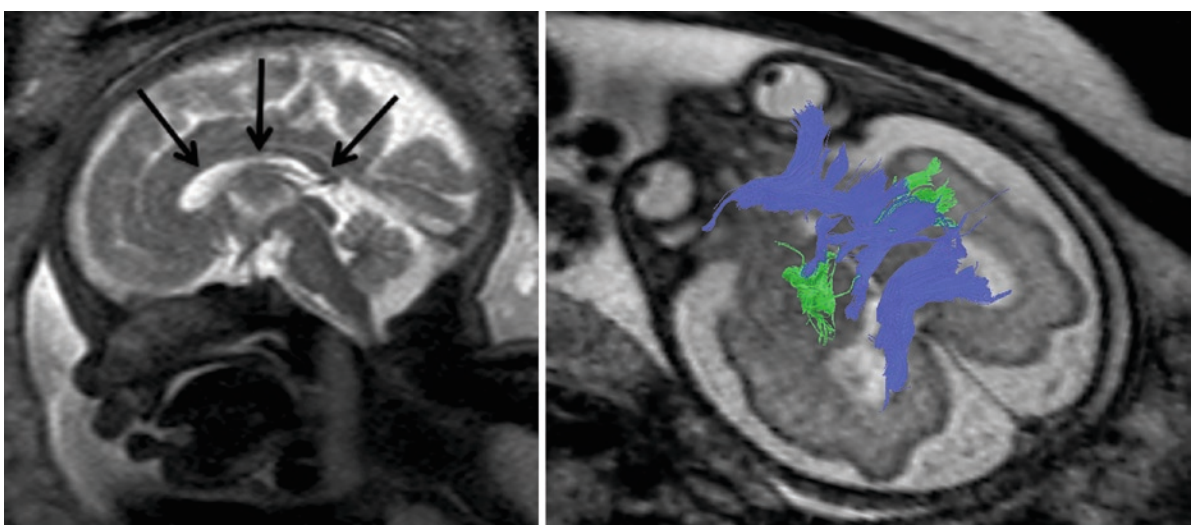

Fig. 16 (**a**) Sagittal T2-weighted sequence of a fetus at GW 32. The corpus callosum can be identified as a horizontal thin C-shaped hypointense structure (*black arrows*). (**b**) Diffusion tensor imaging with fiber-tracking at 28+2 GW can be used to demonstrate callosal fibers and trajectories

in early gestation due to the relative paucity of brain parenchyma relative to ventricular size at early gestational ages (Prayer et al. 2006) (Fig. 2). Sonographic studies have reported mean atrial diameters in the axial plane of 5.4–7.6 mm at the posterior margin of the glomus in the axial plane (Cardoza and Filly 1988; Alagappan et al. 1994; Filly and Goldstein 1994). Normative values have been reported using MRI, and mean values are comparable to sonographic studies (Levine et al. 2002; Twickler et al. 2002; Parazzini et al. 2008; Chung et al. 2009). However, the normal range of ventricular measurements is considerably more variable and may be significantly greater with MRI in the axial plane between 18 and 25 GW. Measurements in normal fetuses in this age group may exceed the normal sonographic upper limit of 10 mm, most likely related to artifacts related to motion, slice thickness, pulse sequences, screen pixels, and small size of target objects (Chung et al. 2009). In the coronal plane, at a median gestational age of 32 GW, sonographic and MRI ventricular measurements were shown to correlate well (Garel and Alberti 2006). The cavum septi pellucidi is visible until fusion of the septal leaves occurs near birth (Fig. 17).

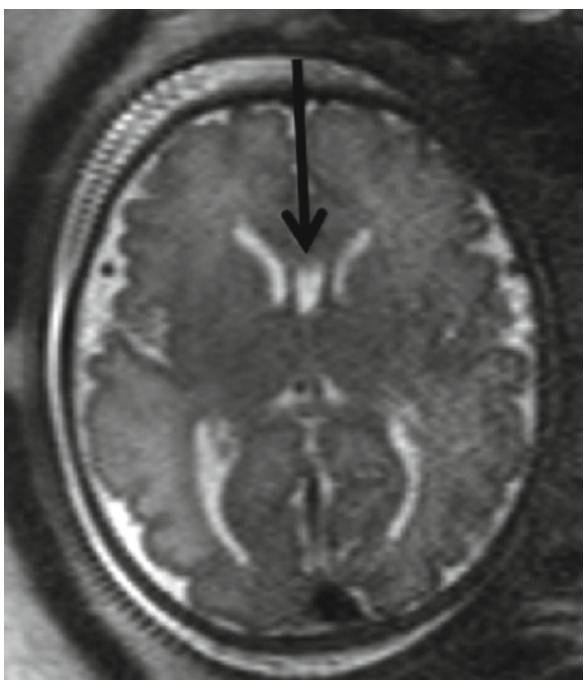

Fig. 17 Axial T2-weighted sequence of a fetus at 35+1 GW. The image shows cavum septi pellucidi that is visible until the fusion of the septi near term

9 Development of the Deep Gray Nuclei

During the embryonic period, the striatum (caudate and putamen) and globus pallidus arise from the medial and lateral ganglionic eminences that represent the germinal matrix areas of the ventral forebrain (Marin and Rubenstein 2003). Thalamic cells are derived from the germinal matrix lining the diencephalon (Rakic and Yakovlev 1968; Kostovic 1990; Petanjek et al. 2008). Between 17 and 37 GW, thalamic cells are derived from the gangliothalamic body, which extends from the ganglionic eminence to the thalamus. The gangliothalamic body is the source of gamma-aminobutyric acid–producing cells that migrate tangentially to the thalamus (Letinic and Rakic 2001; Petanjek et al. 2008).

9.1 MRI Findings of the Deep Gray Nuclei Development

Early in gestation, the deep gray nuclei are isointense to slightly hypointense relative to white matter on T2W sequences. After 28 GW, they appear more hyperintense on T1W sequences (Garel 2004) and more hypointense on T2W images relative to the internal capsule (Fig. 12) (Lan et al. 2000). Diffusion-weighted images show a decline in mean diffusivity in the basal ganglia and thalamus with advancing gestational age (Righini et al. 2003; Manganaro et al. 2007; Schneider et al. 2007, 2009). In addition, the pituitary stalk can be detected on axial, coronal, or sagittal T2W images beginning at 16 GW (Righini et al. 2009; Schmook et al. 2010) (Fig. 18). The pituitary gland can be detected on T1W sequences after 16 GW, with the detection rate and size increasing with gestational age (Schmook et al. 2010).

10 Cerebellar Development

Cerebellar development begins in the fifth to sixth GW, and continues after birth (ten Donkelaar et al. 2003; ten Donkelaar and Lammens 2009). Maturation of the cerebellum occurs later than that of the telencephalon (Simonati et al. 1999). The initial phase of cerebellar development consists of differentiation from the hindbrain as it originates from the metencephalon (rhombencephalon) and mesencephalon (midbrain). The pontine

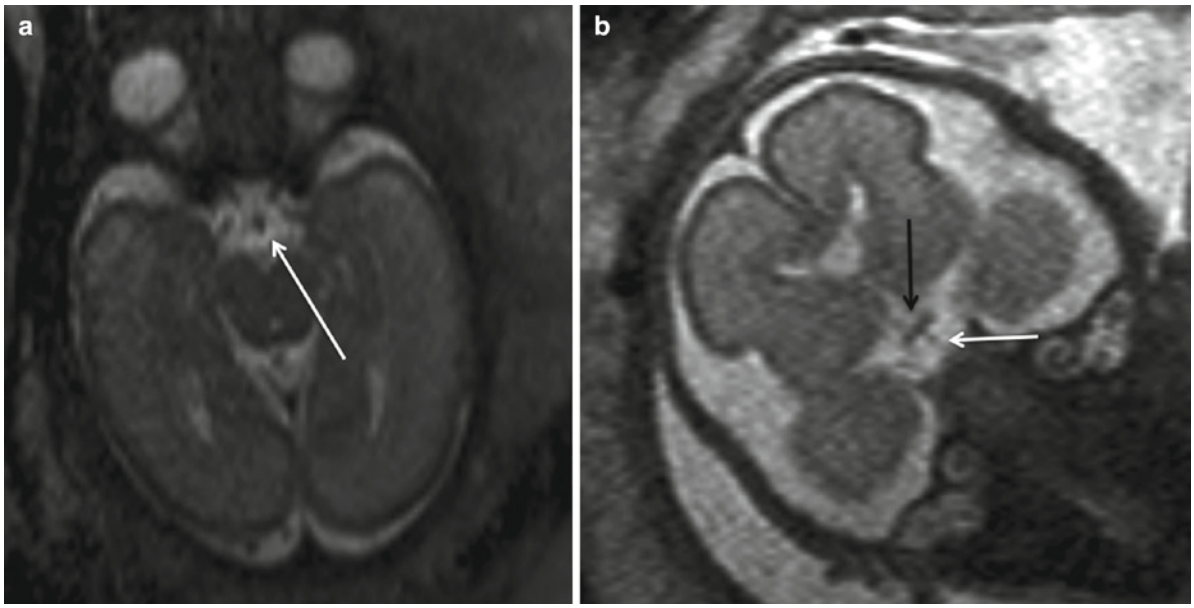

Fig. 18 (**a**) Axial and (**b**) coronal T2-weighted sequences of a fetus at 24+0 GW. The pituitary stalk (*white arrows*) can be seen on T2-weighted images beginning at 16 GW as well as the optic chiasm (*black arrow*)

flexure develops at the same time as the cerebellar hemispheres (Nakayama and Yamada 1999). The isthmic organizer, a region in the caudal mesencephalon, is situated at the border between the midbrain and hind-brain, and coordinates development of the cerebellum and pons (Nakayama and Yamada 1999; Basson et al. 2008). Initial development of the cerebellum is from neuroepithelial cells in the ventricular zone (Larroche 1981).

The second cerebellar developmental phase is cell production in two germinal matrix zones that disappear after birth which are believed to be the source of cerebellar neurons, the ventricular zone, and the rhombic lips (Hynes et al. 1986). The first region is the ventricular zone in the roof of the fourth ventricle, from which originate initially Purkinje cells and deep cerebellar neurons, and subsequently basket cells, stellate cells, and Golgi cells (ten Donkelaar et al. 2003; Sotelo 2004). Cells migrate from the ventricular zone toward the sparsely cellular outer marginal layer to form the intermediate zone at 5–10 GW (Larroche 1981). The internal granular layer develops by migration in a radial fashion (Hynes et al. 1986). The external granular layer, the second germinal zone develops between the 9th and 13th GW and originates by means of tangential migration from the rhombic lips (Larroche 1981) which are more dorsolaterally located in the metencephalon between the roof plate and the dorsal neuroepithelium at the caudal aspect of the fourth ventricle (Sotelo 2004). The rostral rhombic lip neuroepithelium gives rise to migrating cells which begin to move to the surface at 11–13 GW in a second wave, which becomes the granule cell layer after birth (Hynes et al. 1986). Pontine nuclei and the inferior olivary nucleus arise from the caudal portion (Nakayama and Yamada 1999; Sotelo 2004).

The third phase of cerebellar development begins in the 16th GW and involves inward migration of the granule cells, which persists throughout fetal life (Nakayama and Yamada 1999; ten Donkelaar et al. 2003).

The lamina dissecans is visible between 20 and 32 GW as a transient zone of migrating cells (Sidman and Rakic 1973; Nakayama and Yamada 1999). It separates the external granular cell layer from the deep internal granular cell layer (Larroche 1981; Abraham et al. 2001). The highest rate of proliferation occurs in this zone between 28 and 34 GW (Abraham et al. 2001). The lamina dissecans disappears from the flocculus and subsequently from the hemispheres while the Purkinje cell layer becomes more prominent along the outer surface of the lamina dissecans as it disappears. Postnatally, the external granular layer disappears around 10 months of age, leaving three layers of cerebellar cortex (Larroche 1981).

In the fourth phase of cerebellar development, there is further cell differentiation and development of neuronal circuits and cerebellar function (ten Donkelaar et al. 2003).

Anatomically, the first area to form is the flocculonodular lobe (Adamsbaum et al. 2005) and the first fissure to appear is the posterolateral fissure at 12–13 GW. The primary fissure develops at 14–15 GW, and is deepest in the midline. Prepyramidal, preculminate, and precentral fissures are seen at 15–16 GW. The horizontal fissure is visible by 21 GW (Adamsbaum et al. 2005). Foliation of the vermis begins at 14 GW. The deep gray matter nuclei of the cerebellum originate from the ventricular zone. The dentate nuclei may be detected by 11 GW (Yamaguchi and Goto 1997) to 16 GW (Mihajlovic and Zecevic 1986). The vermis is formed at the time of the fusion of the cerebellar hemispheres at the end of the 8th GW. The cerebellar hemispheres grow faster than the vermis and attain a mature morphology by 22 GW.

10.1 MRI of Cerebellar Development

The small size of cerebellar structures precludes early visualization of some structures and therefore MR appearances are delayed relative to histological development. In vitro MR can demonstrate the rhombencephalic vesicle (primitive fourth ventricle) after 10 GW (Chong et al. 1997). The transverse cerebellar diameter increases during gestation and can be measured using fetal MRI (Chung et al. 2009). Vermian normative biometric data are also available (Garel et al. 2003; Triulzi et al. 2005; Parazzini et al. 2008; Tilea et al. 2009). The fetal cerebellum has an extremely high cell density and therefore appears hypointense on T2W, hyperintense on T1W, and bright on diffusion-weighted images (Fig. 19). The lack of anisotropy is probably due to the different direction of migrating neuronal pathways (Prayer and Prayer 2003; Prayer et al. 2006) (Fig. 20). Mean diffusivity decreases with gestational age (Schneider et al. 2007, 2009). The hemispheres appear multilayered after 20 GW (Fig. 20). T2 hypointensity and T1 hyperintensity in the central area represent deep gray nuclei surrounded by T2 hyperintense tissue with T2 hypointense cortex which includes the deep granular layer (Chong et al. 1997; Adamsbaum et al. 2005; Triulzi et al. 2005) (Fig. 21). T2 hypointensity deep in the cerebellar hemispheres has been attributed to the cell-dense dentate nucleus and is best seen on sagittal images from 21 GW (Adamsbaum et al. 2005). Gyration of the dentate nucleus, after 30 GW, is hypointense on T2W images, relative to the hyperintense core (Prayer et al. 2006) (Fig. 19b, c).

The vermis encloses the fourth ventricle by 20 GW (Adamsbaum et al. 2005). The vermis is optimally assessed on thin midline sagittal T2W sections as well as axial and coronal planes. The primary fissure is visible on midline sagittal images by 25–26 GW and beginning as early as 20–21 GW (Fig. 16), with other fissures appearing subsequently (Figs. 16 and 24). Optimal image quality is critical to their visibility (Adamsbaum et al. 2005). The distal tips of the cerebellar foliae are focally hypointense on T2W images, which could be due to a higher density of Purkinje cells in the periphery (Isumi et al. 1997) (Fig. 21). Vermian foliae can be differentiated on T2W images at 24 GW and hemispheric foliae by 30 GW (Triulzi et al. 2005) (Fig. 22). The flocculonodular lobule is hypointense on T2W images by 30–31 GW (Triulzi et al. 2005) (Fig. 23).

11 Brainstem Development

The brainstem forms between 6 and 7 GW and matures in a caudal to rostral direction. The medulla develops from the myelencephalon and develops and functions earlier than the pons and midbrain (Joseph 2000). The brainstem continues to develop throughout gestation and continues postnatally until about 6 months after birth. Descending motor tracts as well as the nuclei of cranial nerves VIII–XII are located within the medulla. The nucleus of the solitary tract is located in the dorsal aspect of the medulla and has a craniocaudad orientation.

11.1 MRI Appearance of Brainstem Development

Both the nucleus of the solitary tract and the corticospinal tract are visible after 18 GW. On T2W images, the ascending sensory tracts are hypointense due to cell density and myelination (Prayer et al. 2006). The pyramidal tract is relatively hyperintense. Both tracts are not sufficiently different in contrast on T1-weighted images to be visualized. The inferior cerebellar peduncles are hypointense on T2W images after 32 GW (Triulzi et al. 2005). However, on diffusion-weighted images, both structures demonstrate anisotropy (Fig. 27).

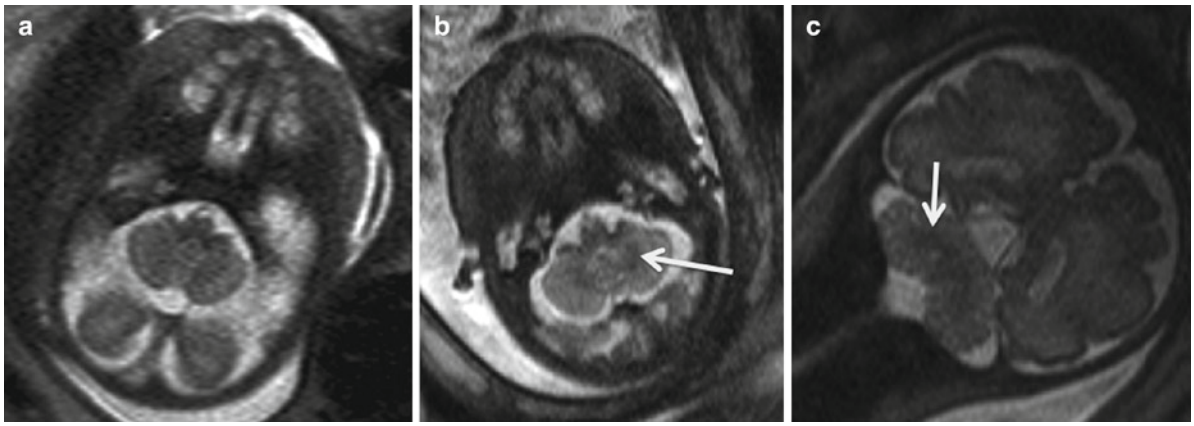

Fig. 19 (**a**) Axial T2-weighted sequence of a fetus at 28 GW. The cerebellar hemispheres appear multilayered. Axial T2-weighted sequence (**b**) and coronal T2-weighted sequence (**c**) of fetuses at 32+4 and 32+5GW. The gyration of the dentate nucleus shows hypointensity compared to the hyperintense core (*white arrow*)

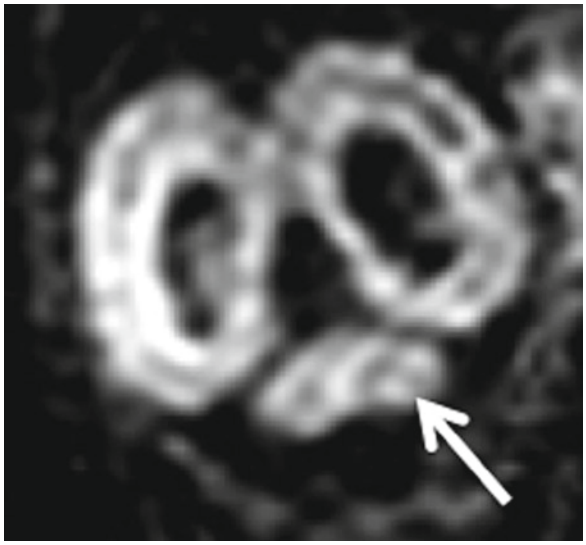

Fig. 20 Coronal diffusion-weighted sequence of a fetus at 20+4 GW. The cerebellum appears isotropic on diffusion-weighted images. The lack of anisotropy is probably due to the different directions of migrating neuronal pathways

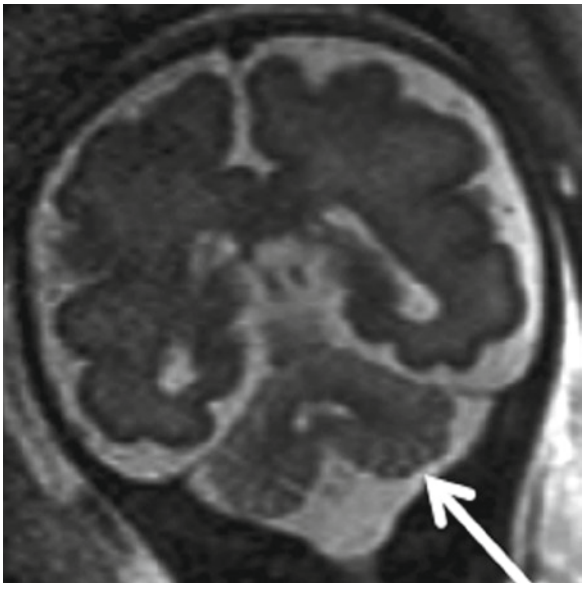

Fig. 21 Coronal T2-weighted sequence of a fetus at 26+0 GW. The distal tips of the cerebellar foliae are focally hypointense on T2-weighted images, which could be due to a higher density of Purkinje cells in the periphery

12 Development of the Pons

The pons develops after the medulla at around 8 GW (Joseph 2000). Structures within the pons include the nuclei of cranial nerves V–VIII, the tegmentum, the raphe nucleus, the locus coeruleus, and the medial longitudinal fasciculus. Pontine functions such as reactivity to acoustic and vibratory stimulation begin to develop after 26 GW (Joseph 2000).

12.1 MRI of Development of the Pons

The dorsal part of the pons is hypointense on T2W and hyperintense on T1W images after 24 GW (Girard et al. 1995; Adamsbaum et al. 2005; Triulzi et al. 2005) (Fig. 24). The ventral part maintains hyperintensity on T2W and hypointensity on T1W images until birth (Chong et al. 1997; Counsell et al.

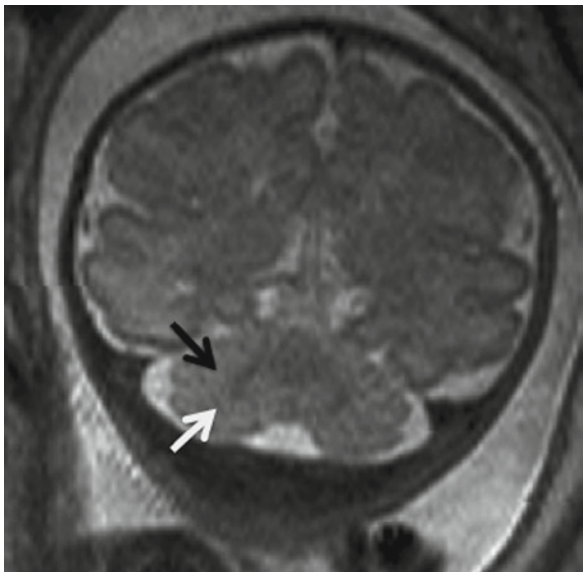

Fig. 22 Coronal T2-weighted of a fetus at 34+1 GW. The foliae of the cerebellar hemispheres can be discriminated, as well as the anterior lobe (*black arrow*) and posterior lobe (*white arrow*)

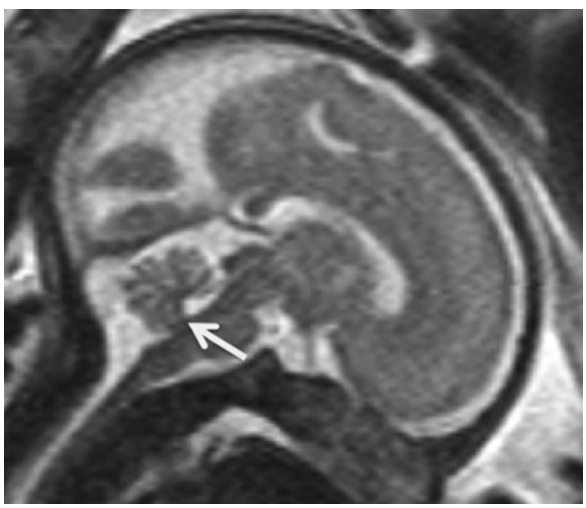

Fig. 23 Sagittal T2-weighted sequence of a fetus at 28+5 GW. The flocculonodular lobe can be identified because of its hypointensity (*white arrow*)

2002). On DW images, the pons is homogeneously hyperintense with no anisotropy (Prayer et al. 2006). Mean diffusivity of the pons decreases with increasing gestational age (Schneider et al. 2007; Schneider et al. 2009).

Fig. 24 Sagittal T2-weighted sequence of a fetus at 24+0 GW. Note the hypointensity of the dorsal part of the pons (*white arrow*)

13 Development of the Midbrain

The midbrain contains the substantia nigra, the inferior and superior colliculi, nuclei of cranial nerves III–VI, and the continuation of pontine structures (Joseph 2000). Auditory pathways develop and mature in fetal life with early maturation in the inferior colliculi, which are a "relay station" for auditory stimuli. After 18 GW, development in the inferior colliculi accelerates, then slows after 33 GW as Nissl bodies mature (Nara et al. 1996).

13.1 MRI of Development of the Midbrain

The inferior colliculi appear hypointense on T2W images as early 16 GW and reliably after 20 GW but are not seen well on other sequences due to their small size (Fig. 25). The dorsal midbrain appears hypointense on T2W and hyperintense on T1W images after 34 GW (Girard et al. 1995; Stazzone

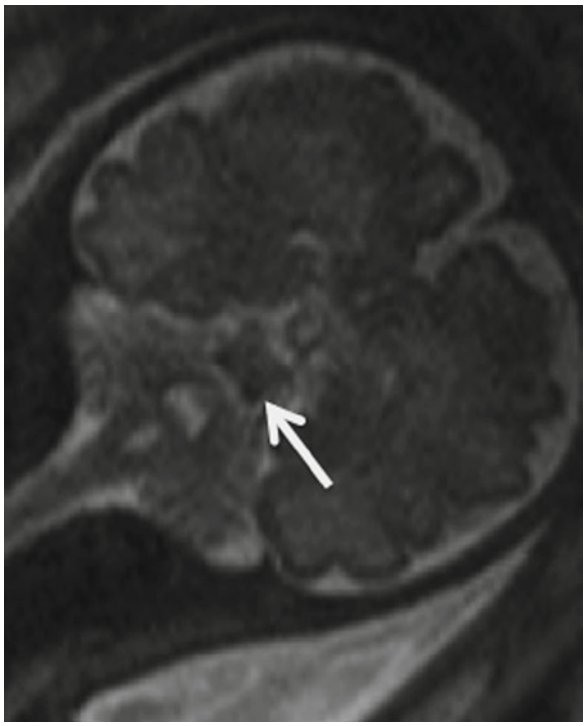

Fig. 25 Coronal T2-weighted sequence of a fetus (32+4 GW). The inferior colliculi appear hypointense (*white arrow*). They cannot be seen well on other sequences because of their small size

Fig. 26 Axial T2-weighted sequence of a fetus at 32+4 GW. The dorsal midbrain appears hypointense in T2W sequences with advanced gestational age (*black arrow*)

et al. 2000) (Fig. 26). Myelination begins between 20 and 24 GW. By 28 GW, the inferior and superior cerebellar peduncles appear as hypointense structures on T2W images (Fig. 27a), and anisotropic on DW sequences (Prayer et al. 2006) (Fig. 27b).

14 Fetal Behavior

Evaluation of behavior is a potentially useful indicator of normal CNS development and potential pathology, since fetal movement requires appropriate neuromuscular development and metabolism (Sparling et al. 1999; Olesen and Svare 2004). Further discussion of fetal behavior can be found in the chapter "Phylogeny and Ontogeny of Early Fetal Behavior" by Einspieler and Prechtl.

14.1 MRI and Fetal Behavior

Fetal movement can be documented using dynamic MR sequences (Prayer et al. 2006). Sequences of 30 s length can be obtained during a scan of 30–45 min and allow assessment of fetal behavior (Fig. 28). However, due to the short duration of observation, it is not possible to conclude definitively that fetal movement is absent, or to confirm reliably that abnormal behavior is present (Prayer et al. 2006).

15 Conclusion

Normal brain development can be assessed with MRI both morphologically as well as functionally in terms of fetal movement. In order to assess processes that interfere with developmental steps and the morphological changes that result from them, it is essential to first understand and recognize and interpret the normal developmental stages and to be familiar with MR appearances of normal brain development including the appearance and disappearance of transient structures.

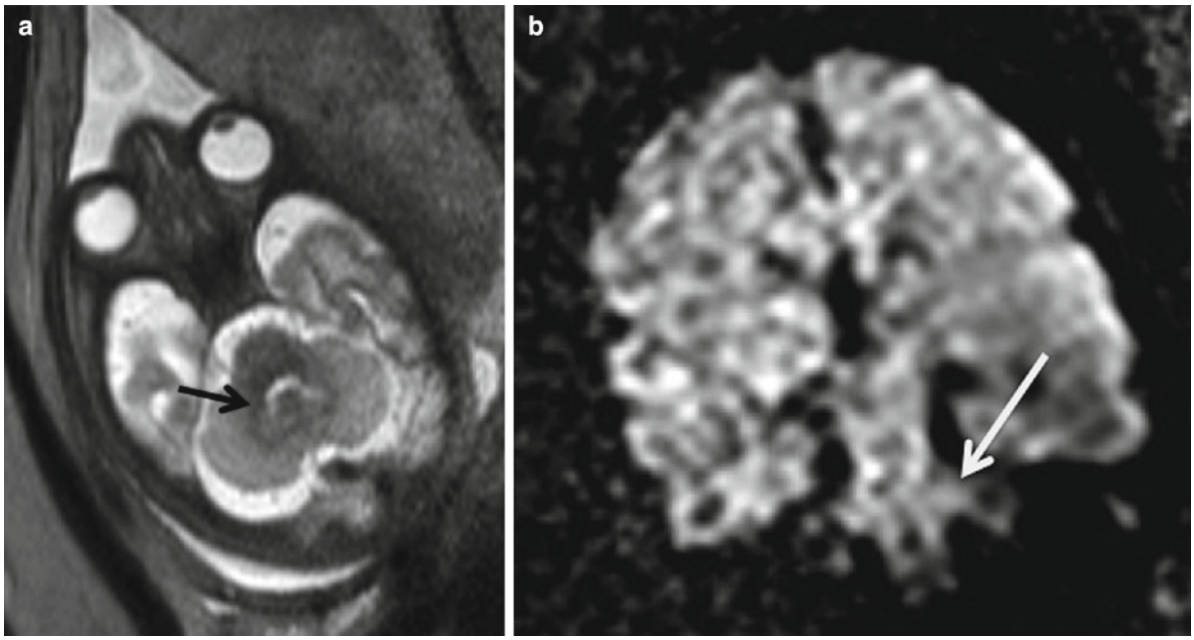

Fig. 27 (**a**) Axial T2-weighted sequence of a fetus (32+5 GW). At 28 GW, the inferior and superior cerebellar peduncles appear hypointense (*black arrow*) relative to the cerebellar hemispheres. (**b**) Coronal diffusion-weighted sequence of a fetus at 36+6 GW. The inferior cerebellar peduncles appear anisotropic (*white arrow*) whereas they are hypointense on T2-weighted images

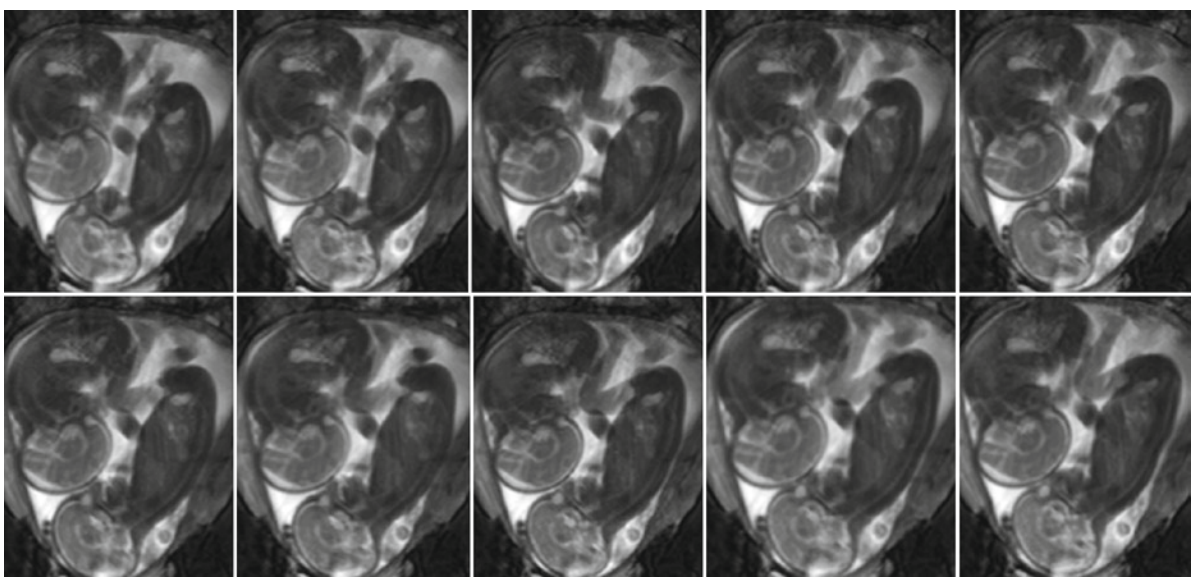

Fig. 28 Dynamic sequence of twins at 28+5 GW. Random movement of the limbs, swallowing and tongue movement is detectable. "Mouthing" is thought to be essential to motor speech development

References

Abraham H, Tornoczky T et al (2001) Cell formation in the cortical layers of the developing human cerebellum. Int J Dev Neurosci 19(1):53–62

Adamsbaum C, Moutard ML et al (2005) MRI of the fetal posterior fossa. Pediatr Radiol 35(2):124–140

Alagappan R, Browning PD et al (1994) Distal lateral ventricular atrium: reevaluation of normal range. Radiology 193(2): 405–408

Anjari M, Srinivasan L et al (2007) Diffusion tensor imaging with tract-based spatial statistics reveals local white matter abnormalities in preterm infants. Neuroimage 35(3):1021–1027

Arber S (2004) Subplate neurons: bridging the gap to function in the cortex. Trends Neurosci 27(3):111–113

Arnold SE, Trojanowski JQ (1996) Human fetal hippocampal development: I. Cytoarchitecture, myeloarchitecture, and neuronal morphologic features. J Comp Neurol 367(2): 274–292

Back SA, Luo NL et al (2002) Arrested oligodendrocyte lineage progression during human cerebral white matter development: dissociation between the timing of progenitor differentiation and myelinogenesis. J Neuropathol Exp Neurol 61(2):197–211

Ballabh P, Braun A et al (2004) Anatomic analysis of blood vessels in germinal matrix, cerebral cortex, and white matter in developing infants. Pediatr Res 56(1):117–124

Barkovich AJ, Kjos BO et al (1988) Normal maturation of the neonatal and infant brain: MR imaging at 1.5 T. Radiology 166(1 Pt 1):173–180

Basson MA, Echevarria D et al (2008) Specific regions within the embryonic midbrain and cerebellum require different levels of FGF signaling during development. Development 135(5):889–898

Battin M., Rutherford MA, (2001). MRI of the Fetal Brain. MA, Rutherford, Saunders Ltd.: 36–45

Battin MR, Maalouf EF et al (1998) Magnetic resonance imaging of the brain in very preterm infants: visualization of the germinal matrix, early myelination, and cortical folding. Pediatrics 101(6):957–962

Ben-Ari Y, Khalilov I et al (2004) Interneurons set the tune of developing networks. Trends Neurosci 27(7):422–427

Berman JI, Mukherjee P et al (2005) Quantitative diffusion tensor MRI fiber tractography of sensorimotor white matter development in premature infants. Neuroimage 27(4):862–871

Brazel CY, Romanko MJ et al (2003) Roles of the mammalian subventricular zone in brain development. Prog Neurobiol 69(1):49–69

Brisse H, Fallet C et al (1997) Supratentorial parenchyma in the developing fetal brain: in vitro MR study with histologic comparison. AJNR Am J Neuroradiol 18(8):1491–1497

Bronen RA, Cheung G (1991) MRI of the temporal lobe: normal variations, with special reference toward epilepsy. Magn Reson Imaging 9(4):501–507

Brugger PC, Stuhr F et al (2006) Methods of fetal MR: beyond T2-weighted imaging. Eur J Radiol 57(2):172–181

Bui T, Daire JL et al (2006) Microstructural development of human brain assessed in utero by diffusion tensor imaging. Pediatr Radiol 36(11):1133–1140

Bystron I, Rakic P et al (2006) The first neurons of the human cerebral cortex. Nat Neurosci 9(7):880–886

Bystron I, Blakemore C et al (2008) Development of the human cerebral cortex: Boulder Committee revisited. Nat Rev Neurosci 9(2):110–122

Cardoza GR, Goldstein RB, Filly RA (1988) Exclusion of fetal ventriculomegaly with a single measurement: the width of the lateral ventricular atrium. Radiology 169(3):711–714

Chi JG, Dooling EC et al (1977) Gyral development of the human brain. Ann Neurol 1(1):86–93

Childs AM, Ramenghi LA et al (2001) Cerebral maturation in premature infants: quantitative assessment using MR imaging. AJNR Am J Neuroradiol 22(8):1577–1582

Chong BW, Babcook CJ et al (1996) A magnetic resonance template for normal neuronal migration in the fetus. Neurosurgery 39(1):110–116

Chong BW, Babcook CJ et al (1997) A magnetic resonance template for normal cerebellar development in the human fetus. Neurosurgery 41(4):924–928, discussion 928-9

Chung R, Kasprian G et al (2009) The current state and future of fetal imaging. Clin Perinatol 36(3):685–699

Coleman KA, Mitrofanis J (1999) Does the perireticular thalamic nucleus project to the neocortex? Anat Embryol (Berl) 200(5):521–531

Corbin JG, Nery S et al (2001) Telencephalic cells take a tangent: non-radial migration in the mammalian forebrain. Nat Neurosci 4(Suppl):1177–1182

Counsell SJ, Maalouf EF et al (2002) MR imaging assessment of myelination in the very preterm brain. AJNR Am J Neuroradiol 23(5):872–881

Daffos F, Forestier F et al (1988) Fetal curarization for prenatal magnetic resonance imaging. Prenat Diagn 8(4):312–314

Del Rio JA, Martinez A et al (2000) Developmental history of the subplate and developing white matter in the murine neocortex. Neuronal organization and relationship with the main afferent systems at embryonic and perinatal stages. Cereb Cortex 10(8):784–801

Dorovini-Zis K, Dolman CL (1977) Gestational development of brain. Arch Pathol Lab Med 101(4):192–195

Dubois J, Benders M et al (2008) Mapping the early cortical folding process in the preterm newborn brain. Cereb Cortex 18(6):1444–1454

Earle KL, Mitrofanis J (1996) Genesis and fate of the perireticular thalamic nucleus during early development. J Comp Neurol 367(2):246–263

Eyre JA, Miller S et al (2000) Functional corticospinal projections are established prenatally in the human foetus permitting involvement in the development of spinal motor centres. Brain 123(Pt 1):51–64

Farrell TA, Hertzberg BS et al (1994) Fetal lateral ventricles: reassessment of normal values for atrial diameter at US. Radiology 193(2):409–411

Fields RD (2004) Volume transmission in activity-dependent regulation of myelinating glia. Neurochem Int 45(4):503–509

Filly RA, Goldstein RB (1994) The fetal ventricular atrium: fourth down and 10 mm to go. Radiology 193(2): 315–317

Fischl B, Rajendran N et al (2008) Cortical folding patterns and predicting cytoarchitecture. Cereb Cortex 18(8): 1973–1980

Fishell G, Mason CA et al (1993) Dispersion of neural progenitors within the germinal zones of the forebrain. Nature 362(6421):636–638

Fogliarini C, Chaumoitre K et al (2005) Assessment of cortical maturation with prenatal MRI. Part I: Normal cortical maturation. Eur Radiol 15(8):1671–1685

Garel C (2004) MRI of the fetal brain: normal development and cerebral pathologies. Springer-Verlag, Berlin Heidelberg

Garel C, Alberti C (2006) Coronal measurement of the fetal lateral ventricles: comparison between ultrasonography and magnetic resonance imaging. Ultrasound Obstet Gynecol 27(1):23–27

Garel C, Chantrel E et al (2001) Fetal cerebral cortex: normal gestational landmarks identified using prenatal MR imaging. AJNR Am J Neuroradiol 22(1):184–189

Garel C, Chantrel E et al (2003) Fetal MRI: normal gestational landmarks for cerebral biometry, gyration and myelination. Childs Nerv Syst 19(7–8):422–425

Garel C, Delezoide AL et al (2004) Contribution of fetal MR imaging in the evaluation of cerebral ischemic lesions. AJNR Am J Neuroradiol 25(9):1563–1568

Girard NJ, Raybaud CA (1992) In vivo MRI of fetal brain cellular migration. J Comput Assist Tomogr 16(2):265–267

Girard N, Raybaud C et al (1991) MRI study of brain myelination. J Neuroradiol 18(4):291–307

Girard N, Raybaud C et al (1995) In vivo MR study of brain maturation in normal fetuses. AJNR Am J Neuroradiol 16(2):407–413

Glenn OA, Barkovich AJ (2006) Magnetic resonance imaging of the fetal brain and spine: an increasingly important tool in prenatal diagnosis, part 1. AJNR Am J Neuroradiol 27(8):1604–1611

Grever WE, Chiu FC et al (1996) Quantification of myelin basic protein in the human fetal spinal cord during the midtrimester of gestation. J Comp Neurol 376(2):306–314

Gupta RK, Hasan KM et al (2005) Diffusion tensor imaging of the developing human cerebrum. J Neurosci Res 81(2):172–178

Hankin MH, Silver J (1988) Development of intersecting CNS fiber tracts: the corpus callosum and its perforating fiber pathway. J Comp Neurol 272(2):177–190

Hilgetag CC, Barbas H (2005) Developmental mechanics of the primate cerebral cortex. Anat Embryol (Berl) 210(5–6):411–417

Hofer S, Frahm J (2006) Topography of the human corpus callosum revisited–comprehensive fiber tractography using diffusion tensor magnetic resonance imaging. Neuroimage 32(3):989–994

Huang H, Zhang J et al (2006) White and gray matter development in human fetal, newborn and pediatric brains. Neuroimage 33(1):27–38

Huang H, Xue R et al (2009) Anatomical characterization of human fetal brain development with diffusion tensor magnetic resonance imaging. J Neurosci 29(13):4263–4273

Huppi PS, Maier SE et al (1998) Microstructural development of human newborn cerebral white matter assessed in vivo by diffusion tensor magnetic resonance imaging. Pediatr Res 44(4):584–590

Hynes RO, Patel R et al (1986) Migration of neuroblasts along preexisting axonal tracts during prenatal cerebellar development. J Neurosci 6(3):867–876

Isumi H, Mizuguchi M et al (1997) Differential development of the human cerebellar vermis: immunohistochemical and morphometrical evaluation. Brain Dev 19(4): 254–257

Jakovcevski I, Zecevic N (2005) Olig transcription factors are expressed in oligodendrocyte and neuronal cells in human fetal CNS. J Neurosci 25(44):10064–10073

Joseph R (2000) Fetal brain behavior and cognitive development. Dev Rev 20:81–98

Jovanov-Milosevic N, Culjat M et al (2009) Growth of the human corpus callosum: modular and laminar morphogenetic zones. Front Neuroanat 3:6

Judas M, Rados M et al (2005) Structural, immunocytochemical, and mr imaging properties of periventricular crossroads of growing cortical pathways in preterm infants. AJNR Am J Neuroradiol 26(10):2671–2684

Kasprian G (2006) Growth and development of the fetal temporal lobe in vivo. Medical University of Vienna, Vienna

Kasprian G, Brugger PC et al (2008) In utero tractography of fetal white matter development. Neuroimage 43(2): 213–224

Kasprian G, Langs G et al (2010) The prenatal origin of hemispheric asymmetry: an in utero neuroimaging study. Cereb Cortex. [Epub ahead of print]

Katz MJ, Lasek RJ et al (1983) Ontophyletics of the nervous system: development of the corpus callosum and evolution of axon tracts. Proc Natl Acad Sci USA 80(19): 5936–5940

Khazipov R, Esclapez M et al (2001) Early development of neuronal activity in the primate hippocampus in utero. J Neurosci 21(24):9770–9781

Kier EL, Truwit CL (1996) The normal and abnormal genu of the corpus callosum: an evolutionary, embryologic, anatomic, and MR analysis. AJNR Am J Neuroradiol 17(9): 1631–1641

Kier EL, Truwit CL (1997) The lamina rostralis: modification of concepts concerning the anatomy, embryology, and MR appearance of the rostrum of the corpus callosum. AJNR Am J Neuroradiol 18(4):715–722

Kier EL, Kim JH et al (1997) Embryology of the human fetal hippocampus: MR imaging, anatomy, and histology. AJNR Am J Neuroradiol 18(3):525–532

Kinney HC (2005) Human myelination and perinatal white matter disorders. J Neurol Sci 228(2):190–192

Kinoshita Y, Okudera T et al (2001) Volumetric analysis of the germinal matrix and lateral ventricles performed using MR images of postmortem fetuses. AJNR Am J Neuroradiol 22(2):382–388

Koester SE, O'Leary DD (1994) Axons of early generated neurons in cingulate cortex pioneer the corpus callosum. J Neurosci 14(11 Pt 1):6608–6620

Kostovic I (1990) Structural and histochemical reorganization of the human prefrontal cortex during perinatal and postnatal life. Prog Brain Res 85:223–239, discussion 239–240

Kostovic I, Jovanov-Milosevic N (2008) Subplate zone of the human brain: historical perspective and new concepts. Coll Antropol 32(Suppl 1):3–8

Kostovic I, Judas M (1998) Transient patterns of organization of the human fetal brain. Croat Med J 39(2):107–114
Kostovic I, Judas M (2002) Correlation between the sequential ingrowth of afferents and transient patterns of cortical lamination in preterm infants. Anat Rec 267(1):1–6
Kostovic I, Judas M (2006) Prolonged coexistence of transient and permanent circuitry elements in the developing cerebral cortex of fetuses and preterm infants. Dev Med Child Neurol 48(5):388–393
Kostovic I, Vasung L (2009) Insights from in vitro fetal magnetic resonance imaging of cerebral development. Semin Perinatol 33(4):220–233
Kostovic I, Judas M et al (1995) Ontogenesis of goal-directed behavior: anatomo-functional considerations. Int J Psychophysiol 19(2):85–102
Kostovic I, Judas M et al (2002) Laminar organization of the human fetal cerebrum revealed by histochemical markers and magnetic resonance imaging. Cereb Cortex 12(5): 536–544
Lan LM, Yamashita Y et al (2000) Normal fetal brain development: MR imaging with a half-Fourier rapid acquisition with relaxation enhancement sequence. Radiology 215(1):205–210
Larroche JC (1981) Morphological criteria of central nervous system development in the human foetus. J Neuroradiol 8(2):93–108
Le Bihan D, Breton E, Lallemand D, Grenier P, Cabanis E, Laval-Jeantet M (1986) MR imaging of intravoxel incoherent motions: application to diffusion and perfusion in neurologic disorders. Radiology 161(2):401–407
Lent R, Uziel D et al (2005) Cellular and molecular tunnels surrounding the forebrain commissures of human fetuses. J Comp Neurol 483(4):375–382
Letinic K, Kostovic I (1997) Transient fetal structure, the gangliothalamic body, connects telencephalic germinal zone with all thalamic regions in the developing human brain. J Comp Neurol 384(3):373–395
Letinic K, Rakic P (2001) Telencephalic origin of human thalamic GABAergic neurons. Nat Neurosci 4(9):931–936
Letinic K, Zoncu R et al (2002) Origin of GABAergic neurons in the human neocortex. Nature 417(6889):645–649
Levine D, Barnes PD (1999) Cortical maturation in normal and abnormal fetuses as assessed with prenatal MR imaging. Radiology 210(3):751–758
Levine D, Trop I et al (2002) MR imaging appearance of fetal cerebral ventricular morphology. Radiology 223(3): 652–660
Levitt P (2003) Structural and functional maturation of the developing primate brain. J Pediatr 143(4 Suppl):S35–S45
Lindwall C, Fothergill T et al (2007) Commissure formation in the mammalian forebrain. Curr Opin Neurobiol 17(1):3–14
Lowery CL, Hardman MP et al (2007) Neurodevelopmental changes of fetal pain. Semin Perinatol 31(5):275–282
Maas LC, Mukherjee P et al (2004) Early laminar organization of the human cerebrum demonstrated with diffusion tensor imaging in extremely premature infants. Neuroimage 22(3): 1134–1140
Manganaro L, Perrone A et al (2007) Evaluation of normal brain development by prenatal MR imaging. Radiol Med 112(3):444–455
Marin O, Rubenstein JL (2003) Cell migration in the forebrain. Annu Rev Neurosci 26:441–483
Marin-Padilla M (1990) Three-dimensional structural organization of layer I of the human cerebral cortex: a Golgi study. J Comp Neurol 299(1):89–105
Marin-Padilla M (1998) Cajal-Retzius cells and the development of the neocortex. Trends Neurosci 21(2):64–71
McKinstry RC, Mathur A et al (2002) Radial organization of developing preterm human cerebral cortex revealed by noninvasive water diffusion anisotropy MRI. Cereb Cortex 12(12):1237–1243
Menezes JR, Marins M et al (2002) Cell migration in the postnatal subventricular zone. Braz J Med Biol Res 35(12): 1411–1421
Mihajlovic P, Zecevic N (1986) Development of the human dentate nucleus. Hum Neurobiol 5(3):189–197
Molnar Z, Blakemore C (1995) How do thalamic axons find their way to the cortex? Trends Neurosci 18(9):389–397
Mukherjee P, Miller JH et al (2002) Diffusion-tensor MR imaging of gray and white matter development during normal human brain maturation. AJNR Am J Neuroradiol 23(9): 1445–1456
Muller F, O'Rahilly R (1988) The first appearance of the future cerebral hemispheres in the human embryo at stage 14. Anat Embryol (Berl) 177(6):495–511
Nakayama T, Yamada R (1999) MR imaging of the posterior fossa structures of human embryos and fetuses. Radiat Med 17(2):105–114
Nara T, Goto N et al (1996) Morphometric development of the human fetal auditory system: inferior collicular nucleus. Brain Dev 18(1):35–39
Olesen AG, Svare JA (2004) Decreased fetal movements: background, assessment, and clinical management. Acta Obstet Gynecol Scand 83(9):818–826
O'Rahilly R, Muller F (1999) Minireview: summary of the initial development of the human nervous system. Teratology 60(1):39–41
Parazzini C, Righini A et al (2008) Prenatal magnetic resonance imaging: brain normal linear biometric values below 24 gestational weeks. Neuroradiology 50(10):877–883
Partridge SC, Mukherjee P et al (2004) Diffusion tensor imaging: serial quantitation of white matter tract maturity in premature newborns. Neuroimage 22(3):1302–1314
Partridge SC, Mukherjee P et al (2005) Tractography-based quantitation of diffusion tensor imaging parameters in white matter tracts of preterm newborns. J Magn Reson Imaging 22(4):467–474
Penrice J, Cady EB et al (1996) Proton magnetic resonance spectroscopy of the brain in normal preterm and term infants, and early changes after perinatal hypoxia-ischemia. Pediatr Res 40(1):6–14
Petanjek Z, Dujmovic A et al (2008) Distinct origin of GABAergic neurons in forebrain of man, nonhuman primates and lower mammals. Coll Antropol 32(Suppl 1):9–17
Plachez C, Richards LJ (2005) Mechanisms of axon guidance in the developing nervous system. Curr Top Dev Biol 69: 267–346
Prayer D, Prayer L (2003) Diffusion-weighted magnetic resonance imaging of cerebral white matter development. Eur J Radiol 45(3):235–243
Prayer D, Brugger PC et al (2005) Triangular crossroads: a "Wetterwinkel" of the fetal brain. American Society of Neuroradiology, Toronto

Prayer D, Kasprian G et al (2006) MRI of normal fetal brain development. Eur J Radiol 57(2):199–216
Rados M, Judas M et al (2006) In vitro MRI of brain development. Eur J Radiol 57(2):187–198
Rakic P (2003) Developmental and evolutionary adaptations of cortical radial glia. Cereb Cortex 13(6):541–549
Rakic P (2004) Neuroscience. Genetic control of cortical convolutions. Science 303(5666):1983–1984
Rakic P, Yakovlev PI (1968) Development of the corpus callosum and cavum septi in man. J Comp Neurol 132(1):45–72
Raybaud C (2010) The corpus callosum, the other great forebrain commissures, and the septum pellucidum: anatomy, development, and malformation. Neuroradiology 52(6):447–477
Ren T, Anderson A et al (2006) Imaging, anatomical, and molecular analysis of callosal formation in the developing human fetal brain. Anat Rec A Discov Mol Cell Evol Biol 288(2):191–204
Richards LJ (2002) Axonal pathfinding mechanisms at the cortical midline and in the development of the corpus callosum. Braz J Med Biol Res 35(12):1431–1439
Richards LJ, Koester SE et al (1997) Directed growth of early cortical axons is influenced by a chemoattractant released from an intermediate target. J Neurosci 17(7): 2445–2458
Richards LJ, Plachez C et al (2004) Mechanisms regulating the development of the corpus callosum and its agenesis in mouse and human. Clin Genet 66(4):276–289
Righini A, Bianchini E et al (2003) Apparent diffusion coefficient determination in normal fetal brain: a prenatal MR imaging study. AJNR Am J Neuroradiol 24(5):799–804
Righini A, Zirpoli S et al (2006) Hippocampal infolding angle changes during brain development assessed by prenatal MR imaging. AJNR Am J Neuroradiol 27(10): 2093–2097
Righini A, Parazzini C et al (2009) Prenatal MR imaging of the normal pituitary stalk. AJNR Am J Neuroradiol 30(5): 1014–1016
Rutherford M, Jiang S et al (2008) MR imaging methods for assessing fetal brain development. Dev Neurobiol 68(6): 700–711
Samuelsen GB, Larsen KB et al (2003) The changing number of cells in the human fetal forebrain and its subdivisions: a stereological analysis. Cereb Cortex 13(2):115–122
Sasaki M, Sone M et al (1993) Hippocampal sulcus remnant: potential cause of change in signal intensity in the hippocampus. Radiology 188(3):743–746
Schmook MT, Brugger PC et al (2010) Forebrain development in fetal MRI: evaluation of anatomical landmarks before gestational week 27. Neuroradiology 52(6):495–504
Schneider JF, Confort-Gouny S et al (2007) Diffusion-weighted imaging in normal fetal brain maturation. Eur Radiol 17(9):2422–2429
Schneider MM, Berman JI et al (2009) Normative apparent diffusion coefficient values in the developing fetal brain. AJNR Am J Neuroradiol 30(9):1799–1803
Shen WB, Plachez C et al (2006) Identification of candidate genes at the corticoseptal boundary during development. Gene Expr Patterns 6(5):471–481
Shiraishi K, Itoh M et al (2003) Myelination of a fetus with Pelizaeus-Merzbacher disease: immunopathological study. Ann Neurol 54(2):259–262
Shu T, Richards LJ (2001) Cortical axon guidance by the glial wedge during the development of the corpus callosum. J Neurosci 21(8):2749–2758
Shu T, Puche AC et al (2003) Development of midline glial populations at the corticoseptal boundary. J Neurobiol 57(1):81–94
Sidman RL, Rakic P (1973) Neuronal migration, with special reference to developing human brain: a review. Brain Res 62(1):1–35
Silver J, Lorenz SE et al (1982) Axonal guidance during development of the great cerebral commissures: descriptive and experimental studies, in vivo, on the role of preformed glial pathways. J Comp Neurol 210(1):10–29
Simonati A, Tosati C et al (1999) Cell proliferation and death: morphological evidence during corticogenesis in the developing human brain. Microsc Res Tech 45(6):341–352
Sotelo C (2004) Cellular and genetic regulation of the development of the cerebellar system. Prog Neurobiol 72(5):295–339
Sparling JW, Van Tol J et al (1999) Fetal and neonatal hand movement. Phys Ther 79(1):24–39
Stazzone MM, Hubbard AM et al (2000) Ultrafast MR imaging of the normal posterior fossa in fetuses. AJR Am J Roentgenol 175(3):835–839
Super H, Uylings HB (2001) The early differentiation of the neocortex: a hypothesis on neocortical evolution. Cereb Cortex 11(12):1101–1109
Sur M, Rubenstein JL (2005) Patterning and plasticity of the cerebral cortex. Science 310(5749):805–810
ten Donkelaar HJ (2000) Major events in the development of the forebrain. Eur J Morphol 38(5):301–308
ten Donkelaar HJ, Lammens M (2009) Development of the human cerebellum and its disorders. Clin Perinatol 36(3): 513–530
ten Donkelaar HJ, Lammens M et al (2003) Development and developmental disorders of the human cerebellum. J Neurol 250(9):1025–1036
Tilea B, Alberti C et al (2009) Cerebral biometry in fetal magnetic resonance imaging: new reference data. Ultrasound Obstet Gynecol 33(2):173–181
Toi A, Lister WS et al (2004) How early are fetal cerebral sulci visible at prenatal ultrasound and what is the normal pattern of early fetal sulcal development? Ultrasound Obstet Gynecol 24(7):706–715
Toro R, Burnod Y (2005) A morphogenetic model for the development of cortical convolutions. Cereb Cortex 15(12):1900–1913
Triulzi F, Parazzini C et al (2005) MRI of fetal and neonatal cerebellar development. Semin Fetal Neonatal Med 10(5):411–420
Tulay CM, Elevli L et al (2004) Morphological study of the perireticular nucleus in human fetal brains. J Anat 205(1): 57–63
Twickler DM, Reichel T et al (2002) Fetal central nervous system ventricle and cisterna magna measurements by magnetic resonance imaging. Am J Obstet Gynecol 187(4):927–931
Ulfig N (2000) The ganglionic eminence – new vistas. Trends Neurosci 23(11):530
Ulfig N (2002) The ganglionic eminence – a putative intermediate target of amygdaloid connections. Brain Res Dev Brain Res 139(2):313–318
van der Knaap MS, van Wezel-Meijler G et al (1996) Normal gyration and sulcation in preterm and term neonates: appearance on MR images. Radiology 200(2):389–396

Van Essen DC (1997) A tension-based theory of morphogenesis and compact wiring in the central nervous system. Nature 385(6614):313–318

Widjaja E, Geibprasert S et al (2010a) Alteration of human fetal subplate layer and intermediate zone during normal development on MR and diffusion tensor imaging. AJNR Am J Neuroradiol 31(6):1091–1099

Widjaja E, Geibprasert S et al (2010b) Corroboration of normal and abnormal fetal cerebral lamination on postmortem MR imaging with postmortem examination. AJNR Am J Neuroradiol 0: ajnr.A2193v1-0

Wimberger DM, Roberts TP et al (1995) Identification of "premyelination" by diffusion-weighted MRI. J Comput Assist Tomogr 19(1):28–33

Yamaguchi K, Goto N (1997) Three-dimensional structure of the human cerebellar dentate nucleus: a computerized reconstruction study. Anat Embryol (Berl) 196(4):343–348

Yoo SS, Park HJ et al (2005) In vivo visualization of white matter fiber tracts of preterm- and term-infant brains with diffusion tensor magnetic resonance imaging. Invest Radiol 40(2):110–115

Zecevic N (1993) Cellular composition of the telencephalic wall in human embryos. Early Hum Dev 32(2–3): 131–149

Zecevic N, Milosevic A et al (1999) Early development and composition of the human primordial plexiform layer: An immunohistochemical study. J Comp Neurol 412(2): 241–254

Zhai G, Lin W et al (2003) Comparisons of regional white matter diffusion in healthy neonates and adults performed with a 3.0-T head-only MR imaging unit. Radiology 229(3): 673–681

Fetal Movements. Though They May Be Spontaneous, Yet There is Method in Them

Christa Einspieler and Heinz F.R. Prechtl

Contents

Abstract

- The spontaneous movements of the newborn infant have a long prenatal history: from 7 weeks and 2 days onward, the human embryo moves.
- Already 2–3 weeks later, the spontaneously generated motility shows a rich repertoire of coordinated and identifiable patterns.
- Once a movement pattern is stabilized, it remains present for at least until term, but usually for longer, sometimes even for life.
- Embryonic and fetal movements are necessary for the proper development of the skeletal, muscular, and neural systems, or vice versa; normal fetal development requires adequate fetal activity.
- Hence, function is an integral part of normal development, and the prenatal use of an (albeit immature) structure is necessary for the continuing and normal development of the very structure.

1 Introduction

The English-German physiologist William T. Preyer (1841–1897) placed a stethoscope on the mother's abdomen and thus "heard" the fetal movements. He concluded that the movements were definitely present by a gestational age of 12 weeks, but most probably earlier. Furthermore, Preyer was convinced that those early movements were spontaneously generated (Preyer 1885). A few years later, also the obstetrician Ahlfeld, who recorded fetal breathing

C. Einspieler (✉) and H.F.R. Prechtl
Institute of Physiology, Center for Physiological Medicine, Medical University of Graz, Harrachgasse 21, 8010 Graz, Austria
e-mail: christa.einspieler@medunigraz.at

D. Prayer (ed.), *Fetal MRI*, Medical Radiology,
DOI: 10.1007/174_2010_18, © Springer-Verlag Berlin Heidelberg 2011

movements by means of a kymograph, considered those movements to be spontaneously generated (Ahlfeld 1888). However, the phenomenon of spontaneous movements was not yet pursued, since, at that time, scientists were convinced that such movements had to be evoked (Coghill 1929; Barcroft and Barron 1939). In his studies on exteriorized embryos and fetuses, Davenport Hooker observed movements without any evident prior tactile stimulation, and described them as "a spontaneous reflex for which the stimulus was not yet known" (Hooker 1952).

The first sonar studies of fetal movements, although not yet real time, were reported by the Viennese obstetrician Emil Reinold in 1971. He got the impression that fetal movements were actually comparable to the darting movements of fish. He further stated that it is not before the 10th week of gestation that fetal movements were forceful enough to alter the position of the fetal body. And, lastly, he came to the conclusion that the observed movements of the fetus were spontaneous rather than caused by external influences (Reinold 1971). Nowadays, we have extensive experimental evidence that embryonic and fetal movements are endogenously generated, and that motor output to the developing muscles can occur even in the absence of sensory input (Hamburger et al. 1966; Oppenheim 1982; for a review: Einspieler et al. 2004, 2010).

With the advent of real-time ultrasound scanners, an attempt was made to determine the age at which fetal movements first occur. Van Dongen and Goudie (1980) observed embryos with a crown-rump length of 5–12 mm, and saw the heart pulsating at 6 weeks' gestation, with tiny movements occurring in one pole of the embryo at 7–8 weeks of age. At that time, the door has opened to both the behavioral and the neurological assessment of the human fetus (Ianniruberto and Tajani 1981; de Vries et al. 1982; Nijhuis et al. 1982). Today, dynamic fetal MRI allows an additional detailed behavioral observation of the fetus (Prayer and Brugger 2007).

From a methodological point of view, our studies on fetal behavior come very close to the approach of developmental neurology, where the observation of movement patterns, of their quantity and, above all, their quality, serves as a basis for the investigation of neural development and for the assessment of the condition of the nervous system (Prechtl 1990, 2001; Einspieler et al. 2004).

2 The First Body Movements

Hippocrates (460–370 BC) already suspected that fetal movements might set in a few weeks earlier than the expectant mother feels them. More precisely, he suggested that the fetus could start moving as soon as 70–90 days after conception, which corresponds to a gestational age of 12–15 weeks (Needham 1959).

Owing to recent transvaginal ultrasound recordings following in vitro fertilization, we by now know that the earliest body movements occur at 7 weeks and 2 days (Lüchinger et al. 2008). They consist of slow, small, noncomplex sideward bending of the head or the rump or both, sometimes accompanied by a little activity in the arms or legs a few days later. A week later, speed and amplitude of the movements start to vary to some degree, although no variation in sequence or direction can be seen as yet. By 10 weeks' gestation, the duration of this sideward bending increases to 5 s, while at the same time, its frequency of occurrence decreases.

Coinciding with the appearance of the first movements, axodendritic synapses are rapidly formed in the cervical spinal cord – initially between interneurons and motoneurons, then between afferent fibers and interneurons. In the lateral motor column, axodendritic synapses increase from one synapse per 200 μm^2 at 8 weeks to 10 synapses at 9 weeks (Okado 1981).

3 Startles and General Movements

By 8–10 weeks' gestation, movements emerge in the entire body (de Vries et al. 1982). They can be either quick and forceful, i.e., in the form of startles, or slower and more complex. The latter are referred to as general movements (Prechtl et al. 1979), which comprise the rotation of the thorax, partial rotation of the head, and displacement of the limbs. As startles promote a displacement of the thorax, they often induce a general movement (Lüchinger et al. 2008). It would seem plausible, therefore, that the simultaneous ontogenetic onset of these two movement patterns (Table 1) has an adaptive function.

A startle is initiated in the limbs and spreads to the neck and trunk. Depending on whether the initial limb posture is extended or flexed, the limbs either flex or

Table 1 The first occurrence of specific spontaneous embryonic and fetal movement patterns

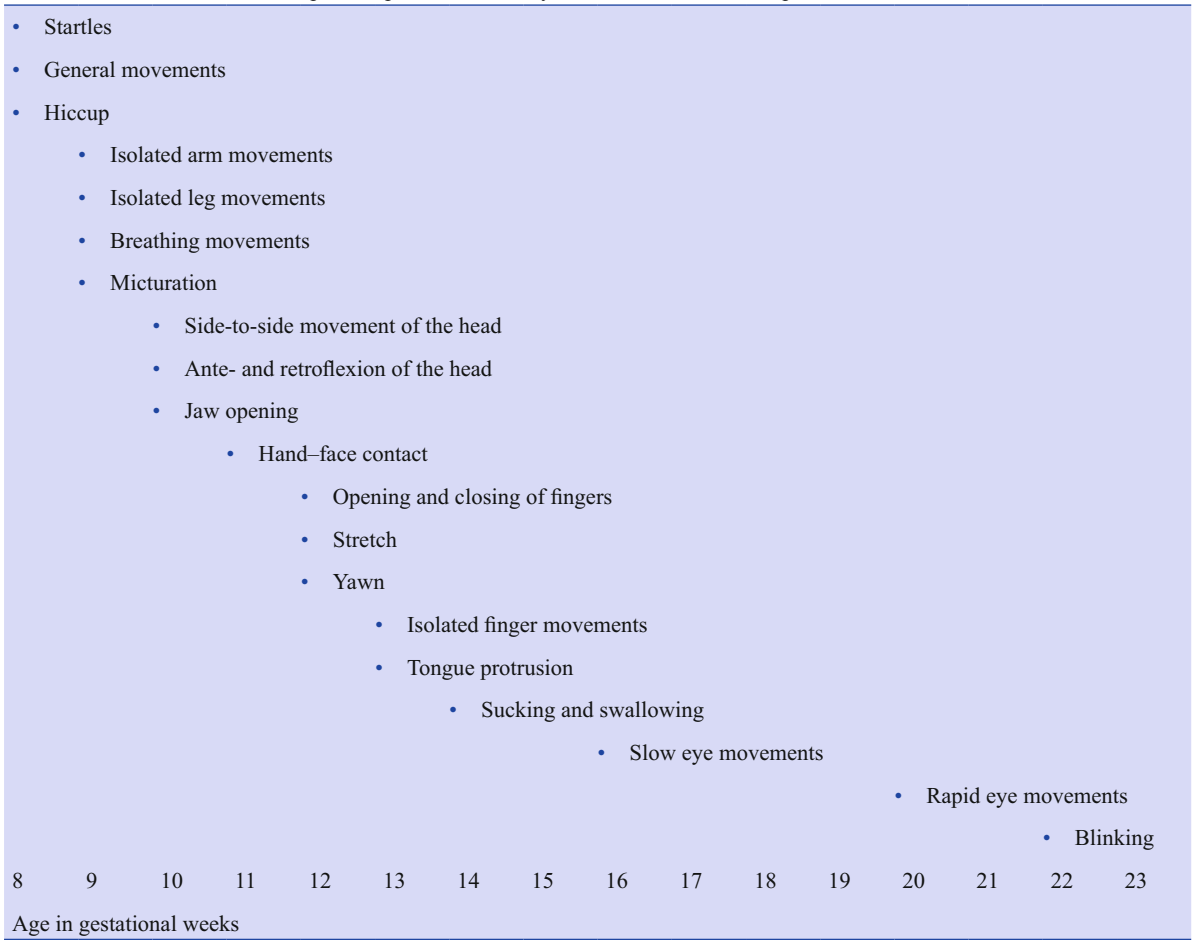

extend, respectively. With progressing gestational age, startles increasingly set out from flexed extremities, resulting in an extension of the limbs (de Vries et al. 1982; Roodenburg et al. 1991).

General movements comprise the entire body and manifest themselves in a variable sequence of arm, leg, neck, and trunk movements. They appear and cease gradually and vary in intensity and speed (Prechtl 1990, 2001; Einspieler et al. 2004). Rotations and frequent slight variations of the direction of motion make them look complex but smooth.

From 9.5 weeks' gestation onward, the majority of general movements show a substantial degree of variation not only in speed, amplitude, and direction but also in the sequence of the participating body parts. At this early stage, the sideward bending of the head and rump still coexists with general movements (Lüchinger et al. 2008). At 10–12 weeks gestational age, the general movements become more forceful, albeit smooth in appearance. They frequently cause a shift in the fetal position. After 12 weeks, they come and go, but vary more in speed and amplitude, lasting up to 5 min. However variable these movements may be, they are always graceful and fluent in character (Einspieler and Prechtl 2005; Einspieler et al. 2010).

General movements increase during the first weeks of pregnancy; then they reach a plateau and remain at this level for the first two trimesters, only to decrease again around term (Roodenburg et al. 1991; ten Hof et al. 1999). Although the space within the uterus becomes increasingly limited during the end of pregnancy, it seems more likely that the decrease of general movements is a result of the central nervous system development. Interestingly enough, the incidence of

general movements also decreases in low-risk preterm infants until term age, even though there is no space limitation (Prechtl et al. 1979).

3.1 Minimal Structures are Capable of Generating Well-Organized Movements

The synaptic innervation of cervical motoneurons only sets in at 8–9 weeks' gestation (Okado and Kojima 1984; Konstantinidou et al., 1995), when startles and general movements emerge. By the end of week 10, the number of axodendritic synapses on the motoneurons has increased about eightfold, while axosomatic synapses only increase at 14–15 weeks (Okado and Kojima 1984). The first appearance of definite myelinated fibers is in the lateral portion of the ventral marginal layer at 12 weeks' gestation (Okado 1982). The differentiation of skeletal muscles is yet at an early phase as well, as it is even several weeks after the onset of general movements (Fidziańska and Goebel 1991).

Observations on anencephalic fetuses have demonstrated that minimal neural structures are sufficient to generate fetal movements. Isolated arm movements, breathing movements, and hiccups can be seen, although only fetal meninges, glial tissue, ectopic motoneurones, and dorsal ganglia are present at the level of the spinal cord (Visser et al. 1985). However, the quality of the movements is abnormal. It is clear, therefore, that a normal fetal nervous system, albeit age-specifically still poorly developed, is needed in order for movements to be executed normally.

3.2 Abnormal General Movements

The variability and complexity of general movements is an indicator for the integrity of the young nervous system (Prechtl and Einspieler 1997). If the nervous system is impaired, general movements become monotonous and repetitive; they loose their fluent appearance and become fragmented, jerky, and abrupt. This can be observed in fetuses with prenatally acquired leukomalacia (Prechtl 1997), in fetuses exposed to antiepileptic drugs (Swartjes et al. 1992), in fetuses of mothers with type-I-diabetes (Kainer et al. 1997), or in growth-retarded fetuses, especially after the occurrence of abnormalities in the fetal heart rate (Bekedam et al. 1985; Sival et al. 1992).

Fetuses with brain malformations have usually forceful and abrupt general movements with large amplitude. Anencephalic fetuses, for example, have also an abnormal temporal patterning: the excessive activity is either scattered throughout the observation time or movements occur in burst–pause patterns (Visser et al. 1985; Kurauchi et al. 1995).

Interestingly, fetuses with spina bifida do show leg movements of an even normal quality (Sival et al. 1997). Also, postnatally – during the first 2 days of life – movements can be normal, especially if the meningomyelocele is caudal from L3. Only thereafter, leg movements become abnormal until they disappear (Sival et al. 2006).

4 Specific Motor Patterns of the Limbs

One might assume that, at this early stage, isolated movements should be more difficult to produce for the nervous system than global motor activity while, in fact, the isolated movements of particular limbs emerge only a few days after the general movements (de Vries et al. 1982; Prechtl 2001). And, here is yet another unexpected finding: it has traditionally been taken for granted that the early ontogenetic process goes from cranial to caudal (Saint-Anne Dargassies 1979). Although this assumption is primarily based on stimulation experiments (Hooker 1952), the motor system does not follow that rule: isolated arm and isolated leg movements emerge at the same time, at 9–10 weeks (Table 1). It is a fact, however, that isolated arm movements occur more frequently than isolated leg movements, which certainly biases the results of short-lasting recordings (Prechtl 2001; Einspieler et al. 2010).

4.1 Arm, Hand and Finger Movements

Isolated arm movements, rapid or slow, may involve extension, flexion, external or internal rotation, abduction or adduction of an arm without movement in other

body parts. Fast, jerky arm movements can either appear as single events (twitches) or as rhythmical movements at a rate of 3–4 per second (clonus). Cloni only appear after 14 weeks, but are rare even then (de Vries et al. 1982).

Fetuses start to clench and unclench their fists at 12–13 weeks' gestation (Ianniruberto and Tajani 1981). Isolated movements of one or more fingers appear from 13 to 14 weeks onward (Pooh and Ogura 2004). Some hand postures resemble postnatal hand gestures (Fig. 1).

From 11 to 13 weeks' gestation onward, the hand regularly touches the head, face, and mouth (Ianniruberto and Tajani 1981). These contacts are most frequent between 14 and 20 weeks, before decreasing again (van Tol-Geerdink et al. 1995). The hand slowly touches the face, with the fingers extending and flexing. Insertion of finger(s) into the mouth, occasionally even thumb-sucking, is observable.

There are several case reports of third-trimester fetuses who grasp (Fig. 2), manipulate, and even squeeze the umbilical cord. Partial or intermittent complete cord occlusion alters the blood flow in the umbilical cord, increases the afterload, and decreases

Fig. 1 MRI print of a 27-week-old fetus with pointing index finger

Fig. 2 MRI prints of a 27-week-old fetus grasping the umbilical cord

the fetal oxygen content (Ball and Parer 1992), which results in increased vagal activity causing variable fetal heart rate decelerations by up to 15–60 beats per minute (Petrikovsky and Kaplan 1993; Habek et al. 2006). Such a significant heart rate deceleration may result in diminished fetal cardiac output due to a poorly developed Frank-Starling mechanism at low fetal heart rates. Any hypoperfusion thus engendered is likely to be transient, however, because the brainstem-mediated grasp reflex would soon be abolished due to sustained hypoperfusion of the fetal central nervous system. Still, it sometimes takes a motor provocation test (vibroacoustic stimulation) for the fetus to release the umbilical cord. On release, heart rate decelerations disappear immediately (Heyl and Rath 1996).

4.2 Leg Movements

Isolated leg movements, rapid or slow, may involve extension, flexion, external or internal rotation, abduction or adduction of a leg without movements in other body parts (de Vries et al. 1982). A sporadic kick can be of sufficient strength to displace the fetus from its resting position. Slow leg movements are rare. Fast and jerky leg movements occur either as a single event (twitch) or as rhythmical movements at a rate of 3–4 per second (clonus). Leg twitches and cloni occur not only as isolated phenomena but may also be superimposed on general movements or, in fact, precede them.

The so-called stepping movements, as observed after birth are most probably a remnant of a specific fetal function, namely alternating leg movements, which enable the fetus to change the position (Prechtl 2001).

5 Diaphragmatic Movements

The formation of the diaphragm sets in at 8 weeks' gestation and is completed by 10 weeks (Wells 1954), providing the anatomical substrate for the onset of hiccups and breathing movements. While motoneurons need a critical number of functional synapses in order to discharge spontaneously, phrenic motoneurons in the cervical region seem to possess sufficient synapse contacts to produce hiccup by as early as 8 weeks (de Vries et al. 1982). Fetal breathing movements typically follow 2–4 weeks later (de Vries et al. 1982), although they can sometimes even be observed as soon as 8–9 weeks (Lüchinger et al. 2008).

The developmental trends of both motor patterns are quite different, with fetal hiccups being the predominant type of diaphragmatic movements up until 26–30 weeks and fetal breathing movements predominating thereafter (Pillai and James 1990). The observation that hiccups decrease with advancing gestational age suggests that brain development may have an inhibitory effect on the hiccup. This assumption is corroborated by the finding that growth retarded or otherwise compromised fetuses hiccup more often than normally growing fetuses (Bots et al. 1978; James et al. 1995).

5.1 Hiccups

Pregnant women do usually notice fetal hiccups, which are forceful and jerky diaphragmatic contractions characterized by a sudden and abrupt displacement of the thorax and abdomen (de Vries et al. 1982; Zheng et al. 1998). Hiccups are often followed by passive limb or head movements, sometimes by both. Typically, hiccups occur episodically, in regular succession, at an interval of 2–3 s. Such hiccup spells can last up to 10 min (van Woerden et al. 1989). During fetal hiccups, the umbilical artery flow can be transiently reduced or even reversed (Levi et al. 2000), but this is not associated with an adverse fetal outcome (Mueller and Sipes 1993).

5.2 Breathing Movements

Fetal breathing movements emerge at 8–12 weeks (de Vries et al. 1982; Lüchinger et al. 2008). They are paradoxical in nature: inspiratory movements consist of fluent movements of the diaphragm in caudal direction, making the anterior chest move inward and the abdominal wall move outward (de Vries et al. 1982; Maršál et al. 1984). The displacement of the diaphragm in the caudal direction varies in amplitude and lasts no longer than 1 s. In normal fetuses, chest wall movements are generally 2–5 mm in amplitude, abdominal wall movements 3–8 mm (Patrick et al. 1978).

Breathing movements vary from superficial and rapid to deep and slow (Roodenburg et al. 1991). Such rapid and irregular ones (both in rate and amplitude) account for more than 90% of all breathing movements, while slow, deep inspiratory movements like sighs or gasps, or respiratory efforts that resemble grunting, coughing, or panting, are less frequent (Cosmi et al. 2001). Yet another type is shallow fetal breathing movements (Piontelli 2006), a form of superficial and regular breathing movements characterized by low synergistic outward excursions of the thorax and the abdomen. Shallow fetal breathing movements are noticed from 12 weeks onward; they increase until 16 weeks and then level off.

Lung development depends on normal fetal breathing movements. Surgical procedures that prevent breathing movements in fetal lambs cause severe lung hypoplasia (Wigglesworth and Desai 1982). Aside from lung growth, fetal breathing movements are also required for lung maturation. If they are abnormal, surfactant-active material is only partially released into the alveolar or amniotic fluid (Dornan et al. 1984). Moreover, fetal breathing movements appear to be required for the accomplishment of the morphological differentiation of type I and type II pneumocytes (Inanlou et al. 2005).

There are a number of (patho)physiological conditions that affect fetal breathing movements (Table 2). Among them, a high maternal plasma glucose concentration causes an increase of fetal breathing movements (Harper et al. 1987). Even around term, when fetal breathing movements are usually almost absent, they can increase by 25% after intravenous administration of glucose to the mother (Divon et al. 1985). Also, fetuses of diabetic mothers show more breathing movements than normal fetuses (Mulder and Visser 1991).

Table 2 Physiological reasons and pathophysiological conditions that result in an increase or decrease of fetal breathing movements

	Increase	Decrease
Physiological reasons	Glucose intake	Labor
	Diurnal variation: early morning	Diurnal variation: late evening
		Maternal fasting
Pathological conditions	Maternal diabetes	Smoking
	Maternal hypercapnia	Alcohol
		Methadone
		Maternal hyperventilation
		Severe fetal hypoxia
		Preterm rupture of the membranes

6 Specific Motor Patterns of the Head

Side-to-side movements of the head set in at 10–11 weeks' gestation (de Vries et al. 1982). They are usually characterized by slow speed and may cover a range of approximately 160°. At times, such head movements come along with hand-to-face contact. Quite often, side-to-side movements succeed each other, incidentally reaching a rhythmical pattern over a longer period. Prechtl (1989) regards these rhythmical side-to-side movements, which are slightly irregular in nature, as the basis of rooting. In the newborn, rooting gradually comes under tactile control and develops into an oriented turning response of the head and mouth toward the eliciting stimulus (Prechtl 1958).

Retroflexion of the head is usually carried out at a slow pace, but can sometimes also be quick and jerky, resembling a twitch. The displacement of the head varies in amplitude; wide displacement may cause overextension of the fetal spine. The head may remain retroflexed from a few seconds to more than a minute. Sometimes, retroflexion of the head is part of a stretch or yawn. It emerges at 10–11 weeks (Table 1) and can occur up to 12 times per hour, especially during the second half of pregnancy (de Vries et al. 1982; Roodenburg et al. 1991).

Anteflexion of the head is carried out at a slow pace and sometimes occurs along with hand-to-mouth contact. After birth at term, it takes 4–5 months for the anteflexion of the head to reoccur, so the movement in utero appears to be due to the buoyancy effect in the amniotic fluid (Prechtl 2001).

6.1 Movements of the Jaw

Spontaneous jaw movements emerge at 10–11 weeks' gestation (van Dongen and Goudie 1980). At this age, the masseter muscle is still mainly composed of irregularly arranged myotubes, and the motor endplate is as

yet simple and undeveloped (Ezure 1996). Until up to 15 weeks' gestation, single wide opening of the jaw is more common than later (de Vries et al. 1982).

Rhythmical mouthing shows a developmental trend diametrically opposed to that of general movements. Its incidence increases progressively during the last 10 weeks of gestation (D'Elia et al. 2001). By now, the myotubes in the masseter muscle have disappeared and the muscle is composed solely of muscle fibers (Ezure 1996). Once fetal behavioral states are established, clusters of regular mouthing occur – in the absence of other motor activities – during behavioral state 1F, or quiet sleep (D'Elia et al. 2001). Rhythmical mouthing movements like sucking can entrain a sinusoidal-like fetal heart rate pattern that coincides with the oscillation frequency of the mouthing cluster. This might deceive the clinician, since a sinusoidal fetal heart rate can also reflect an underlying pathology like fetal anemia or acute blood loss (Nijhuis 2003).

At 13–14 weeks' gestation, mouth opening with tongue protrusion may occur (Ianniruberto and Tajani 1981). It is known from experiments on mice that tongue movements are required for a normal development of the palate (Walker and Quarles 1962). In the human fetus, tongue expulsion, tongue thrust, or tongue click can occasionally be observed during the second half of pregnancy (Roodenburg et al. 1991; Yigiter and Kavak 2006). Most of the tongue protrusions can be observed during behavioral state 2F, or active sleep (van Woerden et al. 1988).

By means of 3D-ultrasound, various facial expressions can be distinguished, such as smiling movements (Campbell 2002), full extension of the lips in a pout or scowling (Yan et al. 2006). Usually, 3D-recordings are carried out during the last trimester, which is why the early ontogeny of these facial expressions is not yet known.

6.2 Eye Movements

By means of transabdominal ultrasound scanning, the fetal lens can be seen at 14 weeks' gestation (de Elejalde and Elejalde 1985). Displacement of the lenses indicates (1) slow, rolling eye movements, or (2) rapid, more regular eye movements (Prechtl and Nijhuis 1983). Eye movements begin to consolidate at about 24 weeks – a tendency that becomes more distinct henceforth as the consolidation grows into a long-term cluster of rapid eye movements from around 30 weeks onward (Bots et al. 1981; Koyanagi et al. 1993). Bear in mind, however, that it is extremely difficult – and sometimes impossible – to assess eye movements while the fetus is performing general movements or head rotations.

From 23 to 26 weeks onward, opening and closing of the eyelids can be observed (Campbell 2002). Repeated blinking is associated with the central dopaminergic system (Karson 1982). It occurs during the last weeks of pregnancy at a frequency of 6 ± 2 blinks per hour (Petrikovsky et al. 2003).

7 Stretches and Yawns: Life-Long Motor Patterns

One striking phenomenon in fetal motor development is the early emergence of stretches and yawns. They both can be observed from 12 weeks onward (de Vries et al. 1982), but even more interesting is the fact that they continue to exist throughout life with virtually no change in form or pattern.

A stretch consists of the following components: marked extension of the trunk, retroflexion of the head, and elevation of the arms in outward rotation. The pattern lasts for several seconds and only occurs in the form of isolated events. Sometimes a stretch is accompanied by a short-lasting heart rate deceleration.

Yawning is a phylogenetically old, stereotyped event in humans and animals (Darwin 1872). It is considered to be indicative of fatigue, drowsiness, or boredom, although research has found no support of these popular hypotheses. In fact, neither elevated carbon dioxide nor a depressed oxygen level in the blood increases yawning; and, reversely, breathing pure oxygen does not decrease yawning either (Provine et al. 1987). As for the fetus, yawning is not associated with fetal hypoxia (Sepulveda and Mangiamarchi 1995). The most curious, if least understood, aspect of human yawning is its contagiousness: people who witness or even just think about yawning cannot help but yawn themselves, which is not so much a case of imitation – since the mirror-neuron system is not involved – as an automatically released behavioral act (Schürmann et al. 2005).

A fetal yawn starts with a slow, usually wide and prolonged opening of the jaw and a simultaneous downward moving of the tongue as well as a retroflexion of the head, sometimes accompanied by limb stretching. After reaching its maximum opening, the mouth remains open for a few seconds. The third part of the complex yawning movement consists in shutting the mouth quickly and returning to the initial position. Once a yawn is under way, there seems to be no way back. Fetal yawning is accompanied by a flow of fluid between the amniotic cavity and the fetal airway (Masuzaki et al. 1996).

The physiological function of yawning is still a subject of speculation. Some consider it to be a protective mechanism that prevents alveolar collapse (Sepulveda and Mangiamarchi 1995). Others regard it as a spreading activation of facial motor patterning (Giganti et al. 2002). The powerful muscular contraction caused by yawning could also release arousal by activation of the locus coeruleus, to which the cranial nerves send retroprojections (Saper et al. 2001). Still others consider yawning a mechanism for thermoregulation, providing compensatory cooling when other provisions fail to operate favorably (Gallup and Gallup 2008).

8 Sucking and Swallowing

We know from ultrasound recordings that from 14 weeks onward (Table 1), rhythmical bursts of regular jaw opening and closing at a rate of about 1–2 per second can be followed by swallowing movements, which indicates that the fetus is drinking amniotic fluid (de Vries et al. 1982). Sucking and swallowing increase as pregnancy progresses. By 34 weeks, most healthy fetuses can suck and swallow well enough to sustain nutritional needs via the oral route, if born at this early age (da Costa et al. 2008). During the final weeks of life, sucking increases, as does the amount of amniotic fluid swallowed: starting from 2 to 7 mL per day, the fetus swallows 450–500 mL per day by the end of pregnancy (Bosma 1986).

Swallowing is both preparatory and functional. It is preparatory in the sense that the neonate must be capable of ingesting food actively; and it is functional in that fetal swallowing – along with urine flow and intramembraneous resorption of fluids – is one of the main regulators of the amniotic fluid volume (Bacchi Modena and Fieni 2004). Moreover, swallowing is considered to enhance the growth and development of the mandibula (Sherer et al. 1995) as well as the gastrointestinal tract (Grassi et al. 2005).

9 Diurnal Variations of Fetal Activities

As early as by 20–22 weeks' gestation, fetal activity shows a diurnal variation with peaks of activity in the late evening (Patrick et al. 1982; de Vries et al. 1987; de Vries and Fong 2006). It is, above all, the increase in breathing movements during the afternoon that accounts for this diurnal variation. Head retroflexion and jaw opening also occur more often in the afternoon and in the evening than in the morning. Since the percentage of general movements per hour basically remains constant throughout the day, general movements account for 50% of the total activity during the morning hours, but only for 30% during the evening hours.

At midgestation, diurnal variation of the basal fetal heart rate, which is closely related to the maternal heart rate variation, sets in as well (de Vries et al. 1987). The underlying mechanism of this biological clock is poorly understood and caution is required in determining causal links. The suprachiasmatic nuclei in the anterior hypothalamus also seem to play an essential role in generating diurnal rhythms in early development (Lunshof et al. 1997). Furthermore, maternal factors – especially maternal glucocorticoid levels – may play an important role, since heart rates of anencephalic fetuses with an aplasia rostral of the medulla oblongata show diurnal oscillations (Muro et al. 1998).

10 Continuity of Motor Patterns from Prenatal to Postnatal Life

While birth is an environmental discontinuity *par excellence,* the motor repertoire displays an impressive continuity from intrauterine to extrauterine life (Prechtl 1984). The comparison of a third-trimester-fetus with a preterm infant of the same age reveals that their movements are pretty much the same in spite of the fact that the respective environmental influences are quite different in terms of gravity, spatial constriction, and perceptual information. Neither preterm infants nor preterm fetuses change their motor repertoire in a

way that would indicate functional reorganization around term age (Prechtl 1985).

Some movements like stretches or yawns maintain their pattern throughout life, whereas other patterns such as general movements or sucking change at the end of the second month postterm (Hopkins and Prechtl 1984; Iwayama and Eishima 1997; Einspieler et al. 2004). Anteflexion of the head and upward extension of the legs disappear temporarily after birth, only to reappear 15–18 weeks later.

A set of endogenously generated motor patterns gradually comes under afferent control after birth (Prechtl 1984, 2001). Rooting is an outstanding example: a rhythmical side-to-side head movement in the fetus, it aligns with the stimulated perioral area in the young infant. While, in the fetus, sucking movements are endogenously generated, they need to be triggered after birth in the actual feeding situation. Hence, it is a matter of vital biological adaptation that rooting and sucking are elicited in the proper feeding situation, which now is initiated by the caregiver. Other examples of endogenously generated motor patterns that need to come under sensory control are breathing movements and smiling movements.

11 Why Does the Fetus Move in the First Place?

There is more and more evidence that embryonic and fetal movements are necessary for the proper development of the skeletal, muscular, and neural systems, or vice versa, that normal fetal development requires adequate fetal activity. Function is an integral part of normal development, and the prenatal use of an (albeit immature) structure is necessary for the continuing and normal development of the very structure.

If the neuromuscular activity underlying the movement is silenced pharmacologically or by disease, the population of the spinal motoneurons, the distribution of neurotransmitter receptors on the muscle fibers, and the pattern of neuromuscular synaptic contacts develop abnormally (Pena and Shokeir 1974; Oppenheim 1981; Moessinger 1983).

The number of motoneurons undergoing genetically determined cell death (apoptosis) is closely related to muscle activity. Chick embryos immobilized by means of neuromuscular blocking agents show an increase of motoneurons in the brachial and lumbar lateral motor columns that would otherwise degenerate. When administration of the immobilizing agents is stopped, allowing the embryo's motility to return to control level, the excess neurons undergo a delayed cell death and the total cell number falls below control level (Oppenheim et al. 2003). On the other hand, there is a delay in the disappearance of early multiple motor endplates when muscle activity is reduced by means of tenotomy in young rats (Benoit and Changeux 1975). Conversely, this disappearance is accelerated when muscle activity is increased by way of electrical stimulation of the corresponding nerve (O'Brien et al. 1978).

In the context of the human fetal akinesia deformation sequence, it has been reported that, in one and the same fetus, a partial absence of movements results in contractures or hypoplasia in the respective regions (e.g., upper limbs, part of the face, thorax), while the active regions (e.g., lower limbs) develop normally (Tongsong et al. 2000).

In addition to common genetic regulatory programs required for organogenesis, mechanical forces generated in the embryo or fetus also have an influence on how the differentiating tissues respond to gene instructions. Lack or impairment of such physical forces changes the state of the organs (Inanlou et al. 2005).

Fetal movements continuously change the position of the fetus – when, for example, the trunk follows a rotation of the head, or when the fetus somersaults backward with the help of alternating leg movements. These active – and frequent – changes of the intrauterine position prevent adhesions and local stasis of the blood, especially in the early fetus, whose skin is very fragile (Visser and Prechtl 1988).

References

Ahlfeld F (1888) Über bisher noch nicht beschriebene intrauterine Bewegungen des Kindes. Verhandl Dt Gesell Gynäkol 2:203–210

Bacchi Modena A, Fieni S (2004) Amniotic fluid dynamics. Acta Bio Med Ateneo Parmense 75(suppl):11–13

Ball RH, Parer JT (1992) The physiological mechanisms of variable decelerations. Am J Obstet Gynecol 166:1683–1689

Barcroft J, Barron DH (1939) Movement in the mammalian fetus. In: Asher L, Spiro K (eds) Ergebnisse der Physiologie. München, Bergmann Verlag

Bekedam DJ, Visser GHA, de Vries JIP, Prechtl HFR (1985) Motor behavior of the growth retarded fetus. Early Hum Dev 12:155–165

Benoit P, Changeux JP (1975) Consequences of tenotomy on the evolution of multi-innervation in developing rat soleus muscle. Brain Res 99:354–358

Bosma JF (1986) Development of feeding. Clin Nutr 5:210–218

Bots RSGM, Broeders GHB, Farman DJ, Haverkorn MJ, Stolte LAM (1978) Fetal breathing movements in the growth-retarded human fetus: a multiscan M-mode echofetographic study. Eur J Obstet Gynecol Reprod Biol 8:21–29

Bots RSGM, Nijhuis JG, Martin CB, Prechtl HFR (1981) Human fetal eye movements: detection in utero by means of ultrasonography. Early Hum Dev 5:87–94

Campbell S (2002) 4D, or not 4D: that is the question. Ultrasound Obstet Gynecol 19:1–4

Coghill GE (1929) Anatomy and the problem of behavior. Cambridge University Press, Cambridge

Cosmi EV, Cosmi E, La Torre R (2001) The effects of fetal breathing movements on the utero-fetal-placental circulation. Early Pregn 5:51–52

da Costa SP, van den Engel-Hoek L, Bos AF (2008) Sucking and swallowing in infants and diagnostic tools. J Perinatol 28:247–257

Darwin C (1872/1920) The expressions of the emotions in man and animals. Appleton, NewYork

de Elejalde MM, Elejalde BR (1985) Ultrasonographic visualization of the fetal eye. J Craniofac Genet Dev Biol 5:319–326

D'Elia A, Pighetti M, Moccia G, Santangelo N (2001) Spontaneous motor activity in normal fetuses. Early Hum Dev 65:139–147

de Vries JIP, Fong BF (2006) Normal fetal motility: an overview. Ultrasound Obstet Gynecol 27:701–711

de Vries JIP, Visser GHA, Prechtl HFR (1982) The emergence of fetal behavior. I. Qualitative aspects. Early Hum Dev 7:301–322

de Vries JIP, Visser GHA, Mulder EJH, Prechtl HFR (1987) Diurnal and other variations in fetal movements and other heart rate patterns. Early Hum Dev 15:99–114

Divon MY, Zimmer EZ, Yeh SY, Vilenski A, Sarna Z, Paldi E, Platt LD (1985) Effect of maternal intravenous glucose administration on fetal heart rate patterns and fetal breathing. Am J Perinatol 2:292–294

Dornan JC, Ritchie JWK, Meban C (1984) Fetal breathing movements and lung maturation in the congenitally abnormal human fetus. J Dev Physiol 6:367–374

Einspieler C, Prechtl HFR (2005) Prechtl's assessment of general movements: a diagnostic tool for the functional assessment of the young nervous system. Ment Retard Dev Disabil Res Rev 11:61–67

Einspieler C, Prechtl HFR, Bos AF, Ferrari F, Cioni G (2004) Prechtl's method on the qualitative assessment of general movements in preterm, term, and young infants. Clin Dev Med 167. Cambridge University Press, Cambridge

Einspieler C, Prayer D, Prechtl HFR (2010) The behavioral repertoire of the human fetus. An approach in the context of developmental neurology. Clin Dev Med. Mac Keith Press, London; distributed by Wiley-Blackwell

Ezure H (1996) Development of the motor endplates in the masseter muscle in the human fetus. Ann Anat 178:15–23

Fidziańska A, Goebel HH (1991) Human ontogenesis. 3. Cell death in fetal muscle. Acta Neuropathol 81:572–577

Gallup AC, Gallup GG Jr (2008) Yawning and thermoregulation. Physiol Behav 95:10–16

Giganti F, Hayes MJ, Akilesh MR, Salzarulo P (2002) Yawning and behavioral states in premature infants. Dev Psychobiol 41:289–293

Grassi R, Farina R, Floriani I, Amodio F, Romano S (2005) Assessment of fetal swallowing with gray-scale and color Doppler sonography. Am J Radiol 185:1322–1327

Habek D, Kulaš SR, Rosso M, Popović PD, Ugljarević M (2006) 3D-Ultrasound detection of fetal grasping of the umbilical cord and fetal outcome. Fetal Diagn Ther 21:332–333

Hamburger V, Wenger E, Oppenheim R (1966) Motility in the absence of sensory input. J Exp Zool 162:133–160

Harper MA, Meis PJ, Rose JC, Swain M, Burns J, Kardon B (1987) Human fetal breathing response to intravenous glucose is directly related to gestational age. Am J Obstet Gynceol 157:1403–1405

Heyl W, Rath W (1996) Intrapartum therapy-resistant fetal bradycardia-color Doppler sonographic diagnosis of umbilical cord compression due to fetal grasping. Z Geburtshilfe Neonatol 200:30–32

Hooker D (1952) The prenatal origin of behavior. University of Kansa Press, Lawrence

Hopkins B, Prechtl HFR (1984) A qualitative approach to the development of movements during early infancy. In: Prechtl HFR (ed) Continuity of neural functions from prenatal to postnatal life. Clin Dev Med 94. Blackwell, Lippincott, Oxford, Philadelphia

Ianniruberto A, Tajani E (1981) Ultrasonographic study of fetal movements. Sem Perinatol 5:175–181

Inanlou MR, Baguma-Nibasheka M, Kablar B (2005) The role of fetal breathing-like movements in lung organogenesis. Histol Histopathol 20:1261–1266

Iwayama K, Eishima M (1997) Neonatal sucking behavior and its development until 14 months. Early Hum Dev 47:1–9

James DJ, Pillai M, Smoleniec J (1995) Neurobehavioral development in the human fetus. In: Lecanuet JP, Fifer WP, Krasnegor NA, Smotherman WP (eds) Fetal development. A psychobiological perspective. Lawrence Erlbaum, Hillsdale, Hove

Kainer F, Prechtl HFR, Engele H, Einspieler C (1997) Assessment of the quality of general movements in fetuses and infants of women with type-1 diabetes mellitus. Early Hum Dev 50:13–25

Karson CN (1982) Spontaneous eye blink rates and dopaminergic system. Brain 106:643–653

Konstantinidou AD, Silos-Santiago I, Flaris N, Snider WD (1995) Development of the primary afferent projection in human spinal cord. J Comp Neurol 354:11–12

Koyanagi T, Horimoto N, Takashima T, Satoh S, Maeda H, Nakano H (1993) Ontogenesis of ultradian rhythm in the human fetus, observed through the alternation of eye movement and no eye movement periods. J Reprod Infant Psychol 11:129–134

Kurauchi O, Ohno Y, Mizutani S, Tomoda Y (1995) Longitudinal monitoring of fetal behaviour in twins when one is anencephalic. Obstet Gynecol 86:672–674

Levi A, Benvenisti O, David D (2000) Significant beat-to-beat hemodynamic changes in fetal circulation: a consequence of abrupt intrathoracic pressure variation induced by hiccup. J Am Soc Echocardiogr 13:295–299

Lüchinger AB, Hadders-Algra M, van Kan CM, de Vries JIP (2008) Fetal onset of general movements. Pediatr Res 63:191–195

Lunshof S, Boer K, van Hoffen G, Wolf H, Mirmiran M (1997) The diurnal rhythm in fetal heart rate in a twin pregnancy with discordant anencephaly: comparison with three normal twin pregnancies. Early Hum Dev 48:47–57

Maršál K, Lindblad A, Lingman G, Eik-Nes SH (1984) Blood flow in the fetal descending aorta; intrinsic factors affecting fetal blood flow, i.e., fetal breathing movements and cardiac arrhythmia. Ultrasound Biol 10:339–348

Masuzaki H, Masuzaki M, Ishimaru T (1996) Color Doppler imaging of fetal yawning. Ultrasound Obstet Gynecol 8:355–360

Moessinger AC (1983) Fetal akinesia deformation sequence: an animal model. Pediatr 72:857–863

Mueller GM, Sipes SL (1993) Isolated reversed umbilical arterial blood flow on Doppler ultrasonography and fetal hiccups. J Ultrasound Med 12:541–643

Mulder EJH, Visser GHA (1991) Growth and motor development in fetuses of women with type 1 diabetes. II. Emergence of specific motor pattern. Early Hum Dev 25:107–115

Muro M, Shono H, Ito Y, Sugimori H (1998) Diurnal variation in baseline heart rate of anencephalic fetuses. Psychiatry Clin Neurosci 52:173–174

Needham J (1959) A history of embryology. Cambridge University Press, Cambridge

Nijhuis JG (2003) Fetal behavior. Neurobiol Aging 24:S41–S46

Nijhuis JG, Prechtl HFR, Martin CB, Bots RSGM (1982) Are there behavioral states in the human fetus? Early Hum Dev 6:177–195

O'Brien RAD, Ôstberg AJC, Vrbová G (1978) Observations on the elimination of polyneural innervation in developing mammalian skeletal muscle. J Physiol 282:571–582

Okado N (1981) Onset of synapse formation in the human spinal cord. J Comp Neurol 201:211–219

Okado N (1982) Early myelin formation and glia cell development in the human spinal cord. Anat Rec 202:483–490

Okado N, Kojima T (1984) Ontogeny of the central nervous system: neurogenesis, fiber connection, synaptogenesis, and myelination in the spinal cord. In: Prechtl HFR (ed) Continuity of neural functions from prenatal to postnatal life. Clin Dev Med 94. Blackwell, Lippincott, Oxford, Philadelphia

Oppenheim RW (1981) Ontogenetic adaptations and retrogressive processes in the development of the nervous system and behavior: a neuroembryological perspective. In: Connolly KJ, Prechtl HFR (eds) Maturation and development: biological and psychological perspectives. Clin Dev Med 77/78. Heinemann, Lippincott, London, Philadelphia

Oppenheim RW (1982) The neuroembryological study of behavior: progress, problems, perspectives. In: Hunt RK (ed) Neural development. Part III. Curr Top Dev Biol 17. Academic, New York

Oppenheim RW, Calderó J, Cuitat D, Esquerda J, Ayala V, Prevette D, Wang S (2003) Rescue of developing spinal motorneurons from programmes cell death by the $GABA_A$ agonist muscimol acts by blockade of neuromuscular activity and increased intramuscular nerve branching. Mol Cell Neurosci 22:331–343

Patrick J, Fetherston W, Vick H, Voegelin R (1978) Human fetal breathing movements and gross fetal body movements at weeks 34 to 35 gestation. Am J Obstet Gynecol 130:693–699

Patrick J, Campbell K, Carmichael L, Natale R, Richardson B (1982) Patterns of gross fetal body movements over 24-hour observation intervals during the last 10 weeks of pregnancy. Am J Obstet Gynecol 146:363–371

Pena SDJ, Shokeir MHK (1974) Syndrome of camptodactyly, multiple ankyloses, facial anomalies, and pulmonary hypoplasia: a lethal condition. J Pediatr 85:373–375

Petrikovsky BM, Kaplan GP (1993) Fetal grasping of the umbilical cord causing variable fetal heart rate decelerations. J Clin Ultrasound 21:642–644

Petrikovsky BM, Kaplan GP, Holsten N (2003) Eyelid movements in normal human fetuses. J Clin Ultrasound 31:299–301

Pillai M, James D (1990) Development of human fetal behavior: a review. Fetal Diagn Ther 5:15–32

Piontelli A (2006) On the onset of human fetal behavior. In: Manca M (ed) Psychoanalysis and neuroscience. Springer, Mailand

Pooh RK, Ogura T (2004) Normal and abnormal fetal hand positioning and movement in early pregnancy detected by three- and four-dimensional ultrasound. Ultrasound Rev Obstet Gynecol 4:46–51

Prayer D, Brugger PC (2007) Investigation of normal organ development with fetal MRI. Eur Radiol 17:2458–2471

Prechtl HFR (1958) The directed head turning response and allied movements of the human baby. Behaviour 13:212–242

Prechtl HFR (1984) Continuity and change in early neural development. In: Prechtl HFR (ed) Continuity of neural functions from prenatal to postnatal life. Clin Dev Med 94. Blackwell, Lippincott, Oxford, Philadelphia

Prechtl HFR (1985) Ultrasound studies of human fetal behavior. Early Hum Dev 12:91–98

Prechtl HFR (1989) Fetal behavior. In: Hill A, Volpe JJ (eds) Fetal neurology. Raven, New York

Prechtl HFR (1990) Qualitative changes of spontaneous movements in fetus and preterm infants are a marker of neurological dysfunction. Early Hum Dev 23:151–159

Prechtl HFR (1997) The importance of fetal movements. In: Connolly KJ, Forssberg H (eds) Neurophysiology and psychology of motor development. Clin Dev Med 143/144. Cambridge University Press, Cambridge

Prechtl HFR (2001) Prenatal and postnatal development of human motor behavior. In: Kalverboer AF, Gramsbergen A (eds) Handbook of brain and behavior in human development. Kluwer Academic, Dordrecht

Prechtl HFR, Einspieler C (1997) Is neurological assessment of the fetus possible? Eur J Obstet Gynecol Reprod Biol 75:81–84

Prechtl HFR, Nijhuis JG (1983) Eye movements in the human fetus and newborn. Behav Brain Res 10:119–124

Prechtl HFR, Fargel JW, Weinmann HM, Bakker HH (1979) Postures, motility, and respiration of low-risk preterm infants. Dev Med Child Neurol 21:3–27

Preyer W (1885) Spezielle Physiologie des Embryo. Grieben, Leipzig

Provine RR, Tate BL, Geldmacher LL (1987) Yawning: No effect of 3–5 % CO_2, 100 % O_2, and exercise. Behav Neural Biol 48:382–393

Reinold E (1971) Beobachtung fetaler Aktivität in der ersten Hälfte der Gravidität mit dem Ultraschall. Pädiat Pädol 6:274–279

Roodenburg PJ, Wladimiroff JW, van Es A, Prechtl HFR (1991) Classification and quantitative aspects of fetal movements during the second half of normal pregnancy. Early Hum Dev 25:19–35

Saint-Anne Dargassies S (1979) Normal and pathological fetal behavior as seen through neurological study of the premature newborn. Contrib Gynecol Obstet 6:42–49

Saper CB, Chou TC, Scammell TE (2001) The sleep switch: hypothalamic control of sleep and wakefulness. Trends Neurosci 24:726–731

Schürmann M, Hesse MD, Stephan KE, Saarela M, Zilles K, Hari R, Fink GR (2005) Yearning to yawn: the neural basis of contagious yawning. Neuroimage 24:1260–1264

Sepulveda W, Mangiamarchi M (1995) Fetal yawning. Ultrasound Obstet Gynecol 5:57–59

Sherer DM, Metlay LA, Woods JR Jr (1995) Lack of mandibular movement manifested by absent fetal swallowing: a possible factor in the pathogenesis of micrognathia. Am J Perinatol 12:30–33

Sival DA, Visser GHA, Prechtl HFR (1992) The effect of intrauterine growth retardation on the quality of general movements in the human fetus. Early Hum Dev 28:119–132

Sival DA, Begeer JH, Staal-Schreinemachers AL, Vos-Niel JM, Beekhuis JR, Prechtl HFR (1997) Perinatal motor behavior and neurological outcome in spina bifida aperta. Early Hum Dev 50:27–37

Sival DA, Brouwer OF, Bruggink JLM, Vles JSH, Staal-Schreinemachers AL, Sollie KM, Sauer PJJ, Bos AF (2006) Movement analysis in neonates with spina bifida aperta. Early Hum Dev 82:227–234

Swartjes JM, van Geijn HP, Meinardi H, van Woerden EE, Mantel R (1992) Fetal motility and chronic exposure to antiepileptic drugs. Eur J Obstet Gynecol Reprod Biol 16:37–45

ten Hof J, Nijhuis IJM, Nijhuis JG, Narayan H, Taylor DJ, Visser GHA, Mulder EJH (1999) Quantitative analysis of fetal general movements: methodological considerations. Early Hum Dev 56:57–73

Tongsong T, Chanprapaph P, Khunamornpong S (2000) Prenatal ultrasound of regional akinesia with Pena-Shokier phenotype. Prenat Diagn 20:422–425

van Dongen LGR, Goudie EG (1980) Fetal movement patterns in the first trimester of pregnancy. Br J Obstet Gynaecol 87:191–193

van Tol-Geerdink JJ, Sparling JW, Chescheir NC (1995) The development of hand movements in utero. Am J Obstet Gynecol 172:351

van Woerden EE, van Geijn HPM, Caron FJM, van der Valk AW, Swartjes JM, Arts NF (1988) Fetal mouth movements during behavioural states 1F and 2F. Eur J Obstet Gynecol Reprod Biol 29:97–105

van Woerden EE, van Geijn HP, Caron FJM, Mantel R, Swartjes JM, Arts NF (1989) Fetal hiccups; characteristics and relation to fetal heart rate. Eur J Obstet Gynecol Reprod Biol 30:209–216

Visser GHA, Prechtl HFR (1988) Movements and behavioral states in the human fetus. In: Jones CT (ed) Fetal and neonatal development. Perinatology Press, Ithaca

Visser GHA, Laurini RN, de Vries JIP, Bekedam DJ, Prechtl HFR (1985) Abnormal motor behavior in anencephalic fetuses. Early Hum Dev 12:173–182

Walker BE, Quarles J (1962) Palate development in mouse fetuses after tongue removal. Arch Oral Biol 21:405–412

Wells LJ (1954) Development of the human diaphragm and pleural sacs. Contr Embryol Carneg Inst 35:107–134

Wigglesworth JS, Desai R (1982) Is fetal respiratory function a major determinant of perinatal survival? Lancet 1(8266): 264–267

Yan F, Dai SY, Akther N, Kuno A, Yanagihara T, Hata T (2006) Four-dimensional sonographic assessment of fetal facial expression early in the third trimester 94:108–113

Yigiter AB, Kavak ZN (2006) Normal standards of fetal behavior assessed by four-dimensional sonography. J Matern Fetal Neonat Med 19:707–721

Zheng YT, Sampson MB, Soper R (1998) The significance of umbilical vein Doppler changes during fetal hiccups. J Matern Fetal Invest 8:89–91

The Fetal Neurology Clinic – A Multidisciplinary Approach

The Edith Wolfson Medical Center Experience

Gustavo Malinger, Dorit Lev, and Tally Lerman-Sagie

Contents

Abstract

› Fetal neurology, formerly describing observations on prematurely born babies, has become an adjunct to morphological assessment of the developing nervous system on prenatal imaging studies. A multidisciplinary approach has provided the best results.

1 Introduction

The study of fetal neurodevelopment raised interest and controversy since ancient times. As late as the first half of the twentieth century, the predominant concept was that neurological and psychological development starts after birth (deMause 1982). Following scientific observations on newborns delivered prematurely, the notion of fetal neurological function gained quick acceptance (Vaughn 1975). In the 1980s, the group led by Professor Prechtl used ultrasound to study fetal behavioral states (Nijhuis et al. 1982; de Vries et al. 1982) and fetal eye movements (Bots et al. 1981) and founded the basis of a new field of research: Fetal Neurology (Prechtl 1988).

G. Malinger (✉)
Fetal Neurology Clinic, Division of Prenatal Diagnosis, Edith Wolfson Medical Center, Sackler School of Medicine, Tel Aviv University
e-mail: gmalinger@gmail.com

D. Lev
Fetal Neurology Clinic, Genetics Institute,Edith Wolfson Medical Center, Sackler School of Medicine, Tel Aviv University
e-mail: dorlev@post.tau.ac.il

T. Lerman-Sagie
Fetal Neurology Clinic, Division of Pediatric Neurology, Edith Wolfson Medical Center, Sackler School of Medicine, Tel Aviv University
e-mail: asagie@post.tau.ac.il

D. Prayer (ed.), *Fetal MRI*, Medical Radiology,
DOI: 10.1007/174_2010_95, © Springer-Verlag Berlin Heidelberg 2011

Advances in the field of Fetal Neurology were possible due to two separate but interacting factors: (a) the improvement in fetal imaging due to the development of high frequency ultrasound probes, the use of the transvaginal approach, and the introduction of magnetic resonance as a complementary imaging technique; (b) the creation of multidisciplinary groups of experts from different fields that were able to integrate their knowledge for the benefit of the unborn patients and their families.

The Fetal Neurology Clinic at Wolfson Medical Center in Israel represents one example of such an approach. Similar clinics are now actively working in many countries (Italy, France, Spain, Colombia, Chile, and the USA).

The purpose of this chapter is to present the clinical approach of The Fetal Neurology Clinic at Wolfson Medical Center to the fetus with suspected neurological pathology and the methods we use for accurate parental counseling.

2 Early Steps Toward the Opening of a New Fetal Neurology Clinic

2.1 The Team

The success of a new FNC depends on the commitment and dedication of the participants. The initial team should include a specialist in fetal imaging, a geneticist, and a pediatric neurologist. We consider the participation of a social worker or a psychologist extremely important to help families cope with the serious dilemmas they are confronted with during and following counseling. Other specialists (Table 1) can participate on a routine basis, but more often will be invited to participate according to the specific findings on fetal imaging.

A reliable database that includes image files as well as demographic and, clinical information should be created from the beginning – for research and follow-up purposes.

It is also important that the pediatric neurologist who participates in the Fetal Neurology Clinic be able to follow the patients after birth and offer early intervention when needed.

In countries where termination of pregnancy is allowed, it is imperative to do an autopsy and study the brain by a pediatric pathologist with special expertise in fetal brain development.

Table 1 The fetal neurology clinic-participating disciplines

Initial team
Dedicated neurosonography
Pediatric neurology
Genetics
Clinic coordinator
Additional disciplines
Social service or psychology
Perinatology
Neonatology
Pediatric neuradiology
Pediatric neurosurgery
Perinatal pathology
Pediatric cardiology

2.2 Training in Fetal Neuroimaging

Currently we are not aware of any fellowship programs dedicated to fetal neuroimaging. Obstetric programs provide training in prenatal diagnosis based mainly on the use of ultrasound, and radiology programs usually concentrate on Pediatric imaging with little or no emphasis on fetal neurosonography and fetal MRI.

Historically, training in fetal neuroimaging developed on an individual, self-learning basis. During the last 10 years, dedicated courses on Fetal Neuroimaging have been available at different venues but self-training based on trial and error continues to be important. Articles and textbooks are useful in the process of understanding normal and pathologic fetal anatomy (Naidich et al. 1986; Volpe 2008a; b) and can enable learning from the experience of other centers in order to supply accurate counseling. In order to achieve proficiency in fetal neuroimaging, the ultrasonographers and pediatric neuroradiologists who work in the field of fetal neurology should study in established centers with a good work volume for a period of at least 6 months, and receive hands-on experience.

Fetal dedicated neurosonography (Malinger et al. 1993; Timor-Tritsch and Monteagudo 1996; Malinger et al. 2003; Malinger et al. 2006; Malinger and Pilu 2009; ISUOG guidelines 2007) relies on the multiplanar approach of the brain, and it should be clear that the use of standard axial planes is inadequate for the diagnosis of complex pathologies (Malinger et al. 2002, 2007). Furthermore, the dynamic maturation of the fetal brain

throughout pregnancy, particularly the formation of the cortex, corpus callosum, and cerebellum should be understood and kept in mind in order to avoid possible diagnostic errors (Fong et al. 2004; Cohen-Sacher et al. 2006; Malinger et al. 2009).

2.3 Fetal Neurology Clinic Setup

Almost from the start, 15 years ago, the FNC is conducted on a weekly basis with active participation of staff from the Prenatal Diagnosis and Pediatric Neurology Units, and the Genetics Institute. The participants are exclusively committed to the task. The appointments are usually scheduled by the patients or their treating physicians and they are asked to send all the relevant information to the program's coordinator. A list of the scheduled patients with a short history indicating the reason for the consultation and the data regarding imaging findings and or familiar history is e-mailed, two or three days in advance to all the FNC members, including those that do not participate on a regular basis. This allows the physicians to prepare themselves and have the opportunity to review the relevant literature. In urgent cases, an ad hoc meeting may be summoned without delay.

Upon arrival, the patients fill a form that includes demographic and pregnancy-related data, thereafter an introductory talk with the family and a complete medical intake are conducted.

The US examination includes biometry measurements and the performance of a detailed multiplanar neurosonographic examination. When indicated and technically possible, an anatomical full body scan is also performed. It should be mentioned that more than 50% of the examinations are performed during the third trimester with the well-known limitations of US at that time.

A tentative diagnosis is usually given after the initial examination and compared with the referral diagnosis. It is important to mention that currently 30% of the referrals are evaluated following the performance of fetal brain MRI.

The presence of all the relevant specialists in situ enables to provide the family with a unified diagnosis, and counseling regarding prognosis and management including recommendations for further tests (i.e., fetal echocardiography, TORCH, amniocentesis, genetic tests) and follow-up. When considered necessary, the social worker is asked to participate in this part of the discussion. The social worker will accompany the family during the stressful pregnancy until after delivery.

A complete and detailed report including annexed images is provided to the family and in most cases a follow-up visit is scheduled. During these visits new information and results of pertinent tests are obtained, a full neurosonographic examination is performed and compared to the previous US or when available to the MRI. The parents are counseled according to the new findings and test results.

When the patients are referred for either fetal MRI or neurosurgical consultations, the referral is usually done by physician to physician direct communication by phone or e-mail. Following termination of pregnancy, the fetus is delivered to a pediatric pathologist with special expertise in fetal brain development after discussion of the relevant findings and full documentation.

Delivered babies are first examined close to birth by the pediatric neurologist and geneticist and then followed routinely in the pediatric neurology clinic. When the family opts for termination of pregnancy the team reconvenes with the parents, after the autopsy results have been received and provides genetic counseling and recommendations regarding future tests and pregnancies.

3 Fetal Neurosonography

The fetal neurosonography technique has been extensively reported (Malinger et al. 1993; Timor-Tritsch and Monteagudo 1996; Malinger et al. 2003; Malinger et al. 2006; ISUOG guidelines 2007; Malinger and Pilu 2009), we will present a short description accompanied by demonstrative images.

A complete fetal neurosonographic examination depicts the brain in three orthogonal planes: axial, coronal, and sagittal. The examination is performed using transabdominal probes, when the fetus is in breech presentation and a combination of transabdominal and transvaginal probes for fetuses in vertex presentation. Although the use of 3D volume acquisitions has been proposed as an alternative (Pilu et al. 2006) we believe that at present in cases with suspected brain pathologies, the study should be done using the 2D technique.

The axial planes are the same as used for the basic examination of the brain: transventricular, transthalamic, and transcerebellar (Fig 1).

The transventricular plane enables visualization and measurement of the distal lateral ventricle width (LVW). LVW should be measured by positioning the calipers (in–in) at the level of the atrium and perpendicular to the median wall of the ventricle (ISUOG guidelines 2007). We also recommend obtaining an image of the proximal ventricle, when it is of normal size we do not measure the LVW of this ventricle.

The transthalamic plane is used to measure the HC and BPD and to depict the cavum septi pellucidi and the zone of the third ventricle.

The transcerebellar plane focuses on the visualization of the cerebellum and cisterna magna with the measurement of the transcerebellar diameter and the width of the cisterna magna.

Coronal planes are depicted by moving the transducer in a ventro-dorsal direction through the anterior fontanel, the sagittal suture, and the posterior fontanel. In this way, parallel views of each of the planes are obtained. Although the whole brain is scanned, four main planes have been described: transfrontal, transcaudal, transthalamic, and transcerebellar (Fig. 2). The transfrontal plane enables visualization of the frontal horns, the interhemispheric fissure, and during the third trimester depiction of the main frontal sulci. The transcaudal plane shows the presence of the anterior part of the CC and the CSP and its relationship with the lateral ventricles. The transthalamic plane is useful for the visualization of the 3rd ventricle and the insula; the lateral ventricles, CC, and CSP are also visualized. The transcerebellar plane depicts the occipital horns of the lateral ventricles, the tentorium, and the cerebellar hemispheres with the usually more echogenic vermis in the midline. Special attention should be given to the echogenicity of the periventricular zone, looking specifically for the presence of echogenicities, cystic changes, or an irregular ventricular wall. The coronal planes are also useful in the demonstration of the middle cerebral arteries and the presence of the optic chiasm (Fig. 3).

The sagittal planes are obtained while rotating the transducer 90° from any of the coronal views. The depiction of the brain is best when obtaining these planes through the anterior fontanel, but all the other placements, through the metopic suture, sagittal suture, or posterior fontanel also produce good quality pictures. Failure to visualize the brain structures through these points should raise the suspicion of craniosynostosis. We generally obtain a midsagittal and two parasagittal views, one for each ventricle.

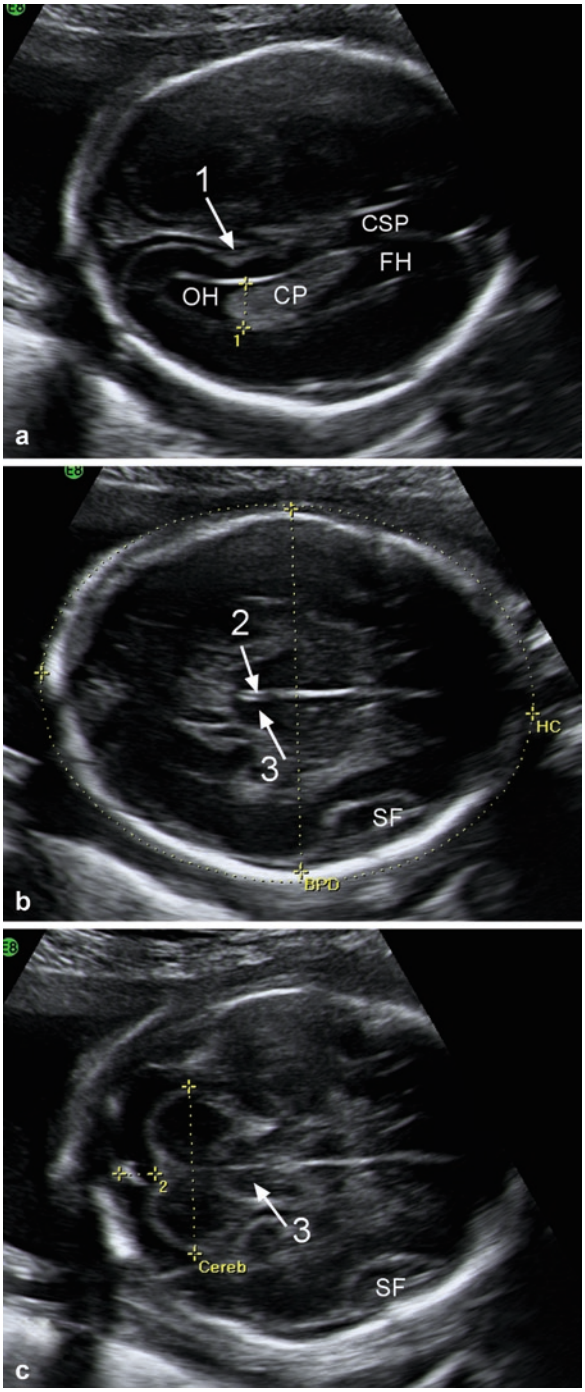

Fig. 1 Transabdominal axial planes at 23 weeks of gestation. (**a**) Transcentricular, (**b**) transthalamic,and (**c**) transcerebellar. Parieto-occipital fissure (1), aqueduct (2), middle cerebellar peduncles (3). Frontal (FH) and occipital OH lateral ventricle horns; choroid plexus (CP); cavum septi pellucidi (CSP); Sylvian fissure (SF). The yellow calipers are measuring the LVW (1 in (**a**)); the biparietal diameter (BPD) and head circumference (HC) (**b**) and the transverse cerebellar diameter (cereb) and cisterna magna width (2 in (**c**)) Note the poor visualization of the proximal cerebral hemisphere

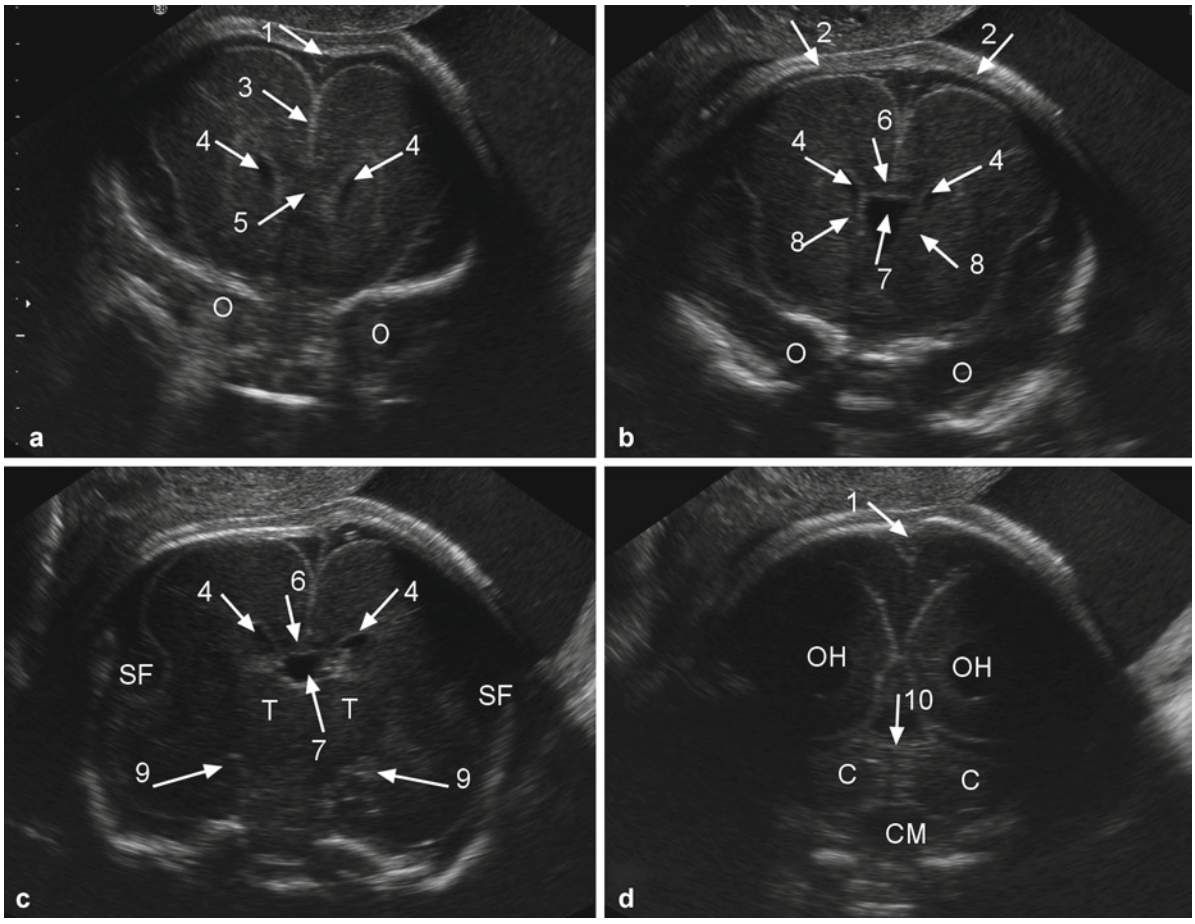

Fig. 2 Transvaginal coronal planes at 23 weeks of gestation. (**a**) Transfrontal, (**b**) transcaudate, (**c**) transthalamic, and (**d**) transcerebellar. Superior sagittal sinus (1), parietal bones and anterior fontanel (2), interhemispheic fissure (3), frontal horns of the lateral ventricles (4), genu (5) and body (6) of the corpus callosum, cavum septi pellucidi (7), caudate nucleus (8), hippocampus (9), cerebellar vermis (10). Orbits (O), Sylvian fissure (SF), occipital horns (OH), cerebellar hemispheres (C), cisterna magna (CM)

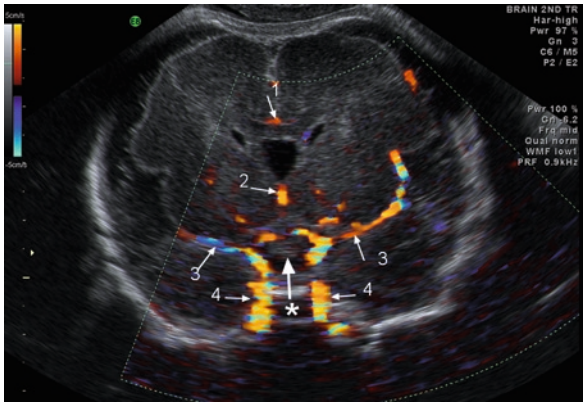

Fig. 3 Transvaginal transthalamic coronal plane at 26 weeks of gestation showing the optic chiasm (*). Callosal arteries (1), anterior cerebral artery (2), middle cerebral arteries (3), carotid arteries (4)

The midsagittal view depicts the midline structures: the corpus callosum, with the CSP and the cavum vergae and the cerebellar vermis, 4th ventricle, pons and surrounding cisterns (Fig. 4).

The parasagittal views show the lateral ventricle and the surrounding basal ganglia and brain parenchyma (Fig. 5).

4 Indications for Referral to Wolfson FNC

The indications for referral to the FNC can be divided into two groups (Table 2): screening of patients with a family history of congenital neurological disease, or exposure to possible teratogens; and evaluation of

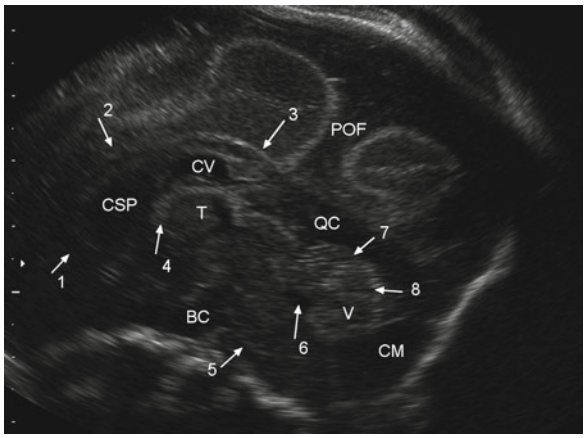

Fig. 4 Transvaginal median plane obtained through the sagittal suture at 23 weeks of gestation. Genu (1), body (2), and splenium (3) of the corpus callosum, choroid plexus of the 3rd ventricle (4), pons (5), 4th ventricle (6), primary (7) and secondary (8) vermian fissures. Cavun septi pellucidi (CSP), cavum vergae (CV), basal (BC), quadrageminal (QC) and magna (CM) cisterns; cerebellar vermis (V) and parieto-occipital fissure (POF)

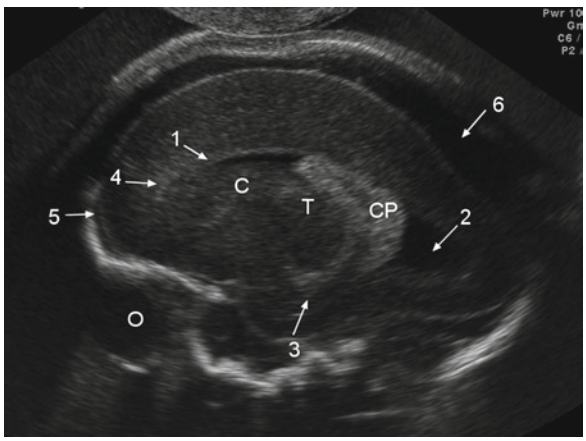

Fig. 5 Transvaginal parasagittal plane at the level of the lateral ventricles at 23 weeks of gestation. Frontal (1), occipital (2) and temporal (3) horns of the lateral ventricle; hyperechogenic normal periventricular zone (4); subarachnoid space, note the normal differences in cerebrospinal fluid between the frontal (5) and occipital (6) regions. Orbit (O), caudate (C), thalamus (T), choroid plexus (CP)

fetuses with suspected anomalies, either involving the CNS or other organs.

In the first group, it is particularly important to have maximal information regarding the affected family member or the possible teratogenic agent before starting the US examination. In cases with a known diagnosis in a family member, it is mandatory to know the inheritance of the disease and to obtain a detailed clinical synopsis of the expected findings. It is sometimes necessary for the pediatric neurologist/geneticist to evaluate the affected child. It should be remembered that some important signs of the disorder may not always be present or amenable to diagnosis during pregnancy (examples: postnatal microcephaly or brain findings associated with tuberous sclerosis).

The second group of indications includes fetuses with suspected anomalies usually diagnosed during routine or targeted examinations at referring centers.

The more frequent diagnoses evaluated at the FNC include: mild ventriculomegaly, either symmetric or asymmetric; fetuses with small or large head circumferences; suspicion of callosal or vermian anomalies. Cases of serious early developing malformations such as anencephaly, holoprosencephaly, and open neural tube defects are rarely seen.

Table 2 Indications for referral to the fetal neurology clinic

Family history of potentially recurrent CNS anomaly
Family history of an undiagnosed CNS malformation
Fetus at risk of intrauterine infection involving the CNS
Follow-up of maternal abdominal trauma (3 weeks after trauma)
Maternal epilepsy
Medications or drug consumption of substances known to produce CNS anomalies
Suspected CNS anomaly
Patient with apparently isolated non-CNS anomaly
Fetal growth restriction (below 5th percentile)
Hydramnios (AFI > 30)
Fetuses with known chromosomal aberrations
Fetuses with known anemia
Twin to twin transfusion
Single twin demise

5 Indications for Fetal MRI

Our indications for referral to Fetal MRI are not based on a routine protocol; we try to individualize our decisions taking into consideration:

1. The degree of diagnostic certainty reached by the US examination.
2. The willingness of the family to modify the proposed management in case of a different MRI diagnosis.
3. When it is obvious that the US examination cannot provide a diagnosis (due to a specific etiology or due to technical difficulties).
4. When the families need confirmation of the dire finding by another modality in order to make decisions regarding the continuation of pregnancy.
5. When MRI can give additional information regarding cortical malformations.

We believe that the option to perform a full body MRI examination late in pregnancy, following the diagnosis of an apparently isolated malformation, will become in the future one of the main indications for fetal MRI, particularly in countries that permit late termination of pregnancy.

References

deMause L (1982) The Fetal Origins of History In *Foundations of Psychohistory*. Creative Roots, Inc, New York, p 247

Vaughn HG Jr (1975) Electrophysiological analysis of regional cortical maturation. Biol Psychiatry 10:513–526

Nijhuis JG, Prechtl HF, Martin CB Jr, Bots RS (1982) Are there behavioural states in the human fetus? Early Hum Dev 6:177–195

de Vries JI, Visser GH, Prechtl HF (1982) The emergence of fetal behaviour. I. Qualitative aspects. Early Hum Dev 7:301–322

Bots RS, Nijhuis JG, Martin CB Jr, Prechtl HF (1981) Human fetal eye movements: detection in utero by ultrasonography. Early Hum Dev 5:87–94

Prechtl HF (1988) Developmental neurology of the fetus. Baillières Clin Obstet Gynaecol 2:21–36

Naidich TP, Yousefzadeh DK, Gusnard DA (1986) Sonography of the normal neonatal head. Supratentorial structures: state-of-the-art imaging. Neuroradiology 28:408–427

Volpe JJ (2008a) Neural tube formation and prosencephalic development. In: Neurology of the newborn. Saunders, Philadelphia, pp 3–50

Volpe JJ (2008b) Neuronal proliferation, migration, organization, and myelinization. In: Neurology of the newborn. Saunders, Philadelphia, pp 51–118

Malinger G, Katz A, Zakut H (1993) Transvaginal fetal neurosonography. Supratentorial structures. Isr J Obstet Gynecol 4:1–5

Timor-Tritsch IE, Monteagudo A (1996) Transvaginal fetal neurosonography: standardization of the planes and sections by anatomic landmarks. Ultrasound Obstet Gynecol 8:42–47

Malinger G, Lev D, Lerman-Sagie T (2003) Assessment of fetal intracranial pathologies first demonstrated late in pregnancy: cell proliferation disorders. Reprod Biol Endocrinol 1:110

Malinger G, Lev D, Lerman-Sagie T (2006) Normal and abnormal fetal brain development during the third trimester as demonstrated by neurosonography. Eur J Radiol 57:226–232

Malinger G, Pilu G (2009) Sonography of the central nervous system. In: Rodech CH, Whittle MJ (eds) Fetal medicine. Basic science and clinical practice. Elsevier, London

ISUOG guidelines (2007) Sonographic examination of the fetal central nervous system: guidelines for performing the basic examination and the fetal neurosonogram. Ultrasound Obstet Gynecol 29:109–116

Malinger G, Lerman-Sagie T, Watemberg N, Rotmensch S, Lev D, Glezerman M (2002) A normal second-trimester ultrasound does not exclude intracranial structural pathology. Ultrasound Obstet Gyneco 20:51–56

Malinger G, Kidron D, Schreiber L, Ben-Sira L, Hoffmann C, Lev D, Lerman-Sagie T (2007) Prenatal diagnosis of malformations of cortical development by dedicated neurosonography. Ultrasound Obstet Gynecol 29:178–191

Cohen-Sacher B, Lerman-Sagie T, Lev D, Malinger G (2006) Developmental milestones of the fetal cerebral cortex. A longitudinal sonographic study. Ultrasound Obstet Gynecol 27:494–502

Fong KW, Ghai S, Toi A, Blaser S, Winsor EJ, Chitayat D (2004) Prenatal ultrasound findings of lissencephaly associated with Miller–Dieker syndrome and comparison with pre- and postnatal magnetic resonance imaging. Ultrasound Obstet Gynecol 24:716–723

Malinger G, Lev D, Lerman-Sagie T (2009) The fetal cerebellum. Pitfalls in diagnosis and management. Prenat Diagn 29:372–380

Pilu G, Segata M, Ghi T, Carletti A, Perolo A, Santini D, Bonasoni P, Tani G, Rizzo N (2006) Diagnosis of midline anomalies of the fetal brain with the three-dimensional median view. Ultrasound Obstet Gynecol 27:522–529

Fetal Neuroimaging: Ultrasound or MRI?

Lou Pistorius

Contents

Abstract

› Ultrasound (US) is the imaging method of choice before 20 weeks of gestation, as screening modality, where repeated examinations are required and where magnetic resonance imaging (MRI) is contraindicated or has failed. In the right hands, US appears to be the equal of MRI in most instances of fetal cerebral pathology. MRI is preferred where US would be expected to be difficult, such as a very obese patient and in instances where acute asphyxia or cerebral tuberous sclerosis is suspected. A combination of US and MRI is preferred for possible fetal central nervous system complications related to congenital cytomegaloviral infection, trauma, bleeding, tumors, or cerebellar bleeding or telangiectasia. Whichever modality is used, the final diagnosis of complex central nervous system pathology should be made in a multidisciplinary setting.

1 Introduction

The ability to visualize the fetal brain has undergone almost incredible development in the last few decades. In the 1960s, fetal visualization with US (ultrasound) started with A-mode US imaging, with which a graph is displayed on which the distance between different tissues can be measured. This made it possible to measure the biparietal diameter, and indeed, to diagnose hydrocephalus. A decade later, B-mode ("brightness-mode") US enabled the display of two-dimensional (2D) cross-sectional images of the fetal brain (Pasto and Kurtz 1986).

L. Pistorius
Department Obstetrics, University Medical Centre Utrecht, Lund Avenue 6, 3584 EA Utrecht, The Netherlands
e-mail: l.pistorius@umcutrecht.nl

D. Prayer (ed.), *Fetal MRI*, Medical Radiology,
DOI: 10.1007/174_2010_17, © Springer-Verlag Berlin Heidelberg 2011

Fig. 1 Ultrasound at 8 weeks demonstrating normal cerebral ventricles

Subsequently, the resolution of US equipment has improved to the point that it is possible, among others, to visualize the early embryonic development of the central nervous system in vivo (Blaas et al. 1995; Kim et al. 2008; Pistorius et al. 2009; Timor-Tritsch et al. 1990) (Fig. 1) and to demonstrate details of structures such as the corpus callosum from a gestational age of 16 weeks (Achiron and Achiron 2001) and the optic chiasm from a gestational age of 22 weeks (Bault 2006).

Prenatal MRI (magnetic resonance imaging) has also developed at a rapid pace, from the "tissue characterization information that complements the superior anatomic detail of US" of the 1980s (McCarthy et al. 1985) to arguably "the optimal method for depicting the specific abnormalities that characterize each type of malformation of the brain in the fetus" (Raybaud et al. 2003).

This raises the question: Is MRI the optimal method and inherently superior to US for the assessment of the fetal brain, or is "dedicated neurosonography equal to MRI in the diagnosis of fetal brain anomalies"? Malinger et al. (2004a).

2 Technical Aspects

To answer the question, we should first have a look at the means of image generation, in which US and MRI differ completely. With US, an image is generated when ultrasound waves are reflected from the interface between tissues with different sound conducting characteristics. The image, therefore, depends on how the specific tissue or object conducts sound and can be modified by the ultrasound frequency (Whittingham 2007). With MRI, an image is generated by aligning magnetically active nuclei (such as hydrogen nuclei, i.e., protons) in a magnetic field and then applying a radiofrequency pulse that knocks the nuclei out of

alignment. As the nuclei recover their alignment, they emit a radio signal that is converted into an image. The image, therefore, depends on the tissue's fat and water content and proton density and can be modified by manipulating the repetition time (the interval between different radiofrequency pulses) and echo time (the interval between applying an radiofrequency pulse and measuring the returning radio signal) (Bitar et al. 2006).

The minimal US examination of the fetal brain comprises transabdominal US with which images are obtained in an axial plane. It is usually possible to obtain coronal and sagittal planes as well on transabdominal US examination. The ability to visualize these planes might be enhanced with the use of three-dimensional (3D) US (Kalache et al. 2006; Monteagudo et al. 2000; Pilu et al. 2006) and can certainly be obtained with high resolution transvaginal US when the fetus is in a cephalic presentation (Malinger et al. 2007a). Although the use of transvaginal US in pregnancy is well accepted by patients (Clement et al. 2003) and the ability to visualize cerebral structures is dramatically better than with transabdominal ultrasound (Monteagudo et al. 1993; Timor-Tritsch and Monteagudo 1996) (Fig. 2), this approach has not yet become a standard practice. This may be due to the reluctance of radiologists, who are familiar with the complexities of brain anatomy, to use transvaginal sonography and, on the other hand, to obstetricians' unfamiliarity with the relatively complex brain anatomy and pathology. There is no direct comparison between the acceptability and psychotrauma of transvaginal US and MRI in pregnancy, but available data suggest that more than 95% of patients find either method acceptable (Clement et al. 2003; Leithner et al. 2008).

With fetal MRI, T2-weighted imaging (T2-WI) is typically used to demonstrate fetal anatomy. T1-weighted imaging (T1-WI) is useful to depict the cortical plate, brain stem, and basal ganglia in late gestation and is also useful to detect blood, calcifications, or lipomas (Kusaka et al. 2005).

MRI is also negatively affected by obesity, but possibly less than US. Morbidly obese patients weighing more than 150 kg cannot be examined with traditional MRI equipment and have to be examined with a vertical open or large bore cylindrical system.

Both US and MRI are regarded as safe in pregnancy (Reddy et al. 2008). It makes sense to avoid unnecessary US exposure and to stick to the ALARA ("as low as reasonably achievable") principle (Abramowicz

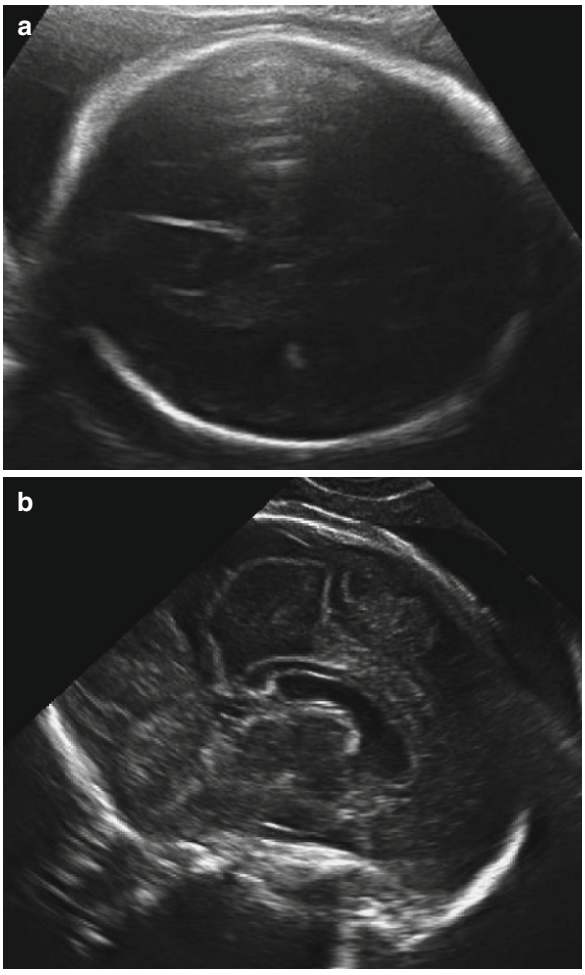

Fig. 2 Ultrasound at 30 weeks. (**a**) Limited visualization with transabdominal ultrasound: axial section. (**b**) Improved visualization with transvaginal ultrasound: sagittal section depicting corpus callosum and median sulci

2007) as the use of techniques using color and spectral Doppler US imaging is associated with an increased fetal exposure to ultrasound energy. Results of animal studies demonstrating a small effect on neuronal migration in mice fetuses that had been exposed to US for more than 30 min daily have recently caused concern (Ang et al. 2006). In a similar vein, there is currently insufficient reassurance about the use of 3 T (as compared to 1.5 T) MRI apparatus during pregnancy and about the use of MRI during the first trimester of pregnancy (Chen et al. 2008).

A synergistic effect between the two imaging modalities would be expected, given the different ways in which images are generated with US and MRI.

When reviewing the available literature on the diagnostic value of US and MRI in fetal neuroimaging, it is, however, difficult to determine when either modality would be appropriate, or when the two could best be combined to optimize the ability to diagnose a fetal central nervous system lesion (Pistorius et al. 2008). Many publications are hampered by an obvious bias by comparing a diagnosis made in primary care by US with a tertiary diagnosis by MRI, often after a long interval, with only few reports on a comparison between high quality ultrasound and high quality MRI (Levine et al. 2003; Malinger et al. 2004a).

Having said that, an attempt will be made to discuss the relative merits of each modality in structural and functional evaluation of the fetal central nervous system.

3 Structural Fetal Evaluation

3.1 Failure of Dorsal Induction

Dorsal induction involves the formation of the neural tube and occurs from 5 to 6 (postmenstrual) weeks of gestation (van der Knaap and Valk 1988). Failure of this process gives rise to neural tube defects.

US imaging is an effective means of screening for neural tube defects with anencephaly reliably diagnosed by US by 10–14 weeks' gestation (Johnson et al. 1997) and spina bifida reliably diagnosed by 20 gestational weeks (Dashe et al. 2006; Grandjean et al. 1999). In case of a spina bifida, US and MRI are equally accurate to determine the lesion height, one of the most important prognostic parameters (Aaronson et al. 2003) (Fig. 3). The functional neurological level might differ from the anatomical level by as much as six vertebral levels (Vossen et al. 2008), and therefore, neither US nor MRI could predict final neurological outcome accurately. Where an encephalocele is diagnosed by US, MRI (or more detailed neurosonography) can be of value to diagnose additional abnormalities (Doherty et al. 2005).

3.2 Failure of Ventral Induction

Ventral induction takes place from 7 to 12 (postmenstrual) weeks of gestation. The rostral end of the neural tube forms the prosencephalon, mesencephalon, and rhombencephalon. The prosencephalon divides into the telencephalon and diencephalon from which the lateral hemispheres and the third ventricle develop, respectively. The mesencephalon develops into the midbrain. The rhombencephalon divides into the metencephalon, from which the pons and cerebellum develop, and the myelencephalon, from which the medulla oblongata develops. Failure of ventral induction gives rise to conditions such as holoprosencephaly, vermian aplasia, and Dandy-Walker syndrome (van der Knaap and Valk 1988).

There are reports of MRI demonstrating holoprosencephaly after this diagnosed was missed by US

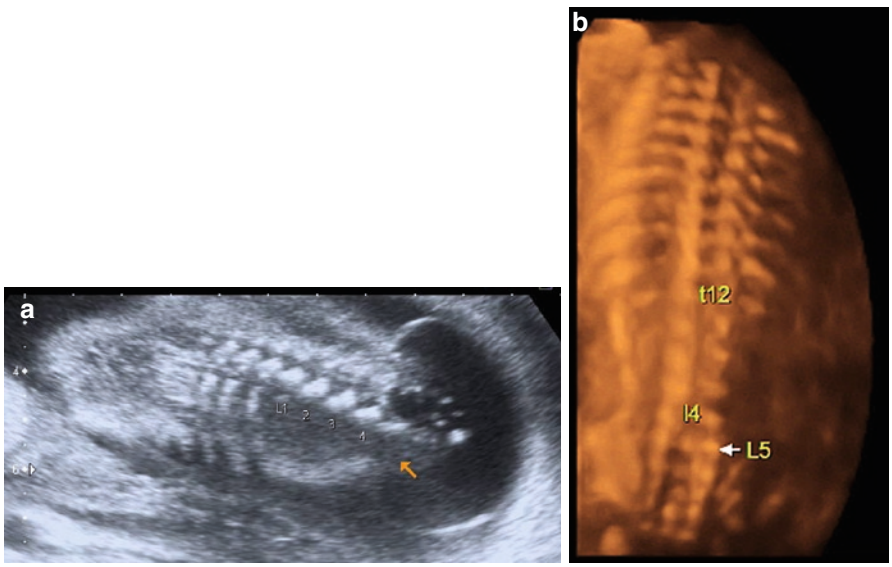

Fig. 3 Evaluation of level of spina bifida. (**a**) Two-dimensional ultrasound. (**b**) Three-dimensional ultrasound

Fig. 4 Ultrasound at 12 weeks demonstrating holoprosencephaly with fused thalami and single ventricle

examination of fetuses with ventriculomegaly in the second trimester (Twickler et al. 2003; Whitby et al. 2004). This might reflect the quality of the US examination, as it is possible to diagnose holoprosencephaly with US in the first trimester (Sepulveda et al. 2004; Timor-Tritsch et al. 2008) (Fig. 4).

The corpus callosum can be measured in detail with transvaginal US from 16 weeks (Achiron and Achiron 2001; Malinger and Zakut 1993), whereas it is difficult to visualize with MRI before myelination (Levine et al. 2006). The pericallosal arteries can also be visualized with Doppler ultrasound to facilitate the diagnosis of partial or complete agenesis of the corpus callosum (Volpe et al. 2006). Despite these technical advantages, US has commonly been less effective than MRI at diagnosing agenesis of the corpus callosum (D'ercole et al. 1998; Frates et al. 2004; Ismail et al. 2002; Levine et al. 2003; Sonigo et al. 1998; Twickler et al. 2003; Wald et al. 2004; Whitby et al. 2004). On the other hand, studies in which the corpus callosum was evaluated with US on a midsagittal view, US was as good as or better than MRI to diagnose abnormalities of the corpus callosum (Malinger et al. 2004a; Pilu et al. 2006; Volpe et al. 2006).

Posterior fossa lesions can be difficult to visualize on US, especially in late pregnancy (Fig. 5), and transvaginal or 3D US can be necessary to distinguish between conditions such as vermian rotation or hypoplasia (Paladini and Volpe 2006; Pilu et al. 2000, 2006; Vinals et al. 2005; Zalel et al. 2006). The specificity of less detailed US is much lower (Wald et al. 2004) when compared to MRI (Tilea et al. 2007). MRI has also been useful in the diagnosis of posterior fossa cysts (Ismail et al. 2002; Sonigo et al. 1998) and pontine abnormalities (Frates et al. 2004; Glenn et al. 2005). With either imaging modality, an accurate anatomical description and classification of

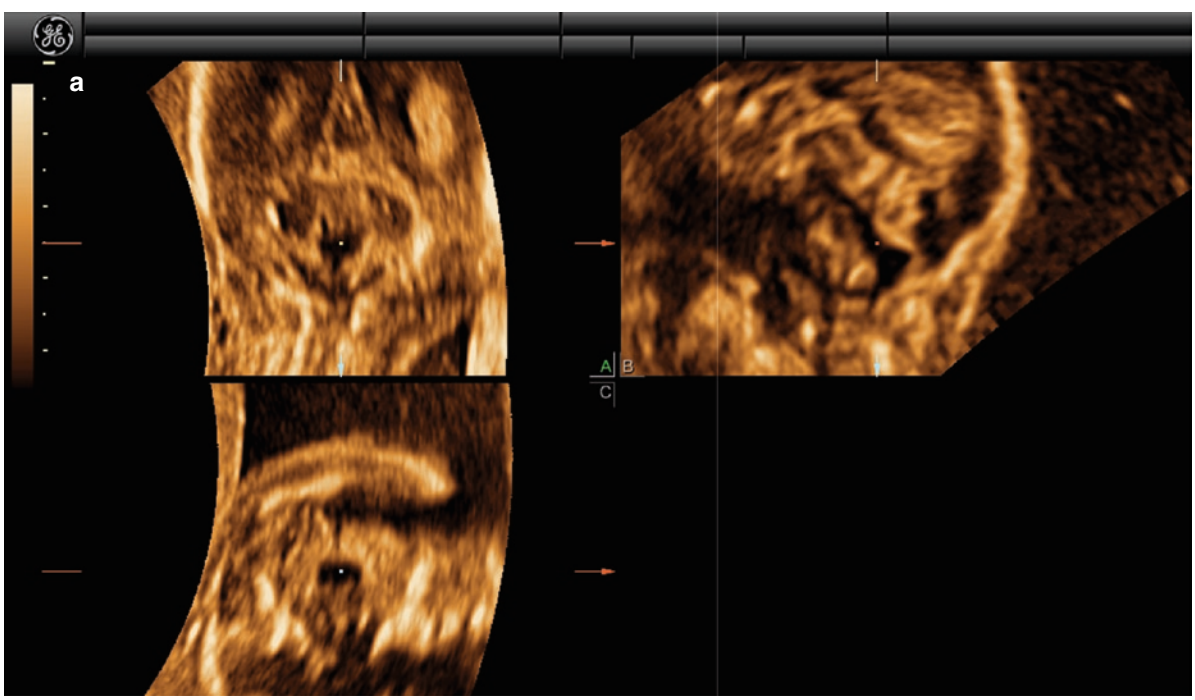

Fig. 5 Fetus with persisting Blake's pouch. (**a**) Ultrasound at 33 weeks. (**b**) MRI at 33 weeks. (**c**) Postnatal MRI

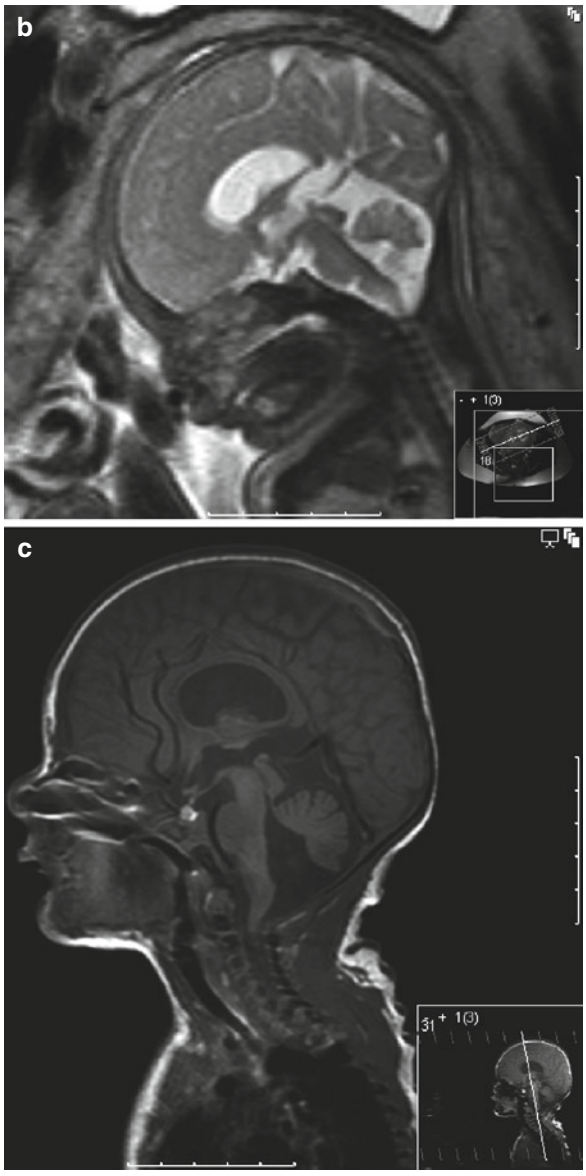

Fig. 5 (contined)

an abnormality is essential to allow refined prenatal counseling with regard to neurodevelopmental prognosis (Guibaud and des Portes 2006).

Although craniosynostosis can be diagnosed with 2D US (Delahaye et al. 2003; Ghi et al. 2002), 3D US can be helpful in the diagnosis by demonstrating the frontal and metopic sutures (Benacerraf et al. 2000; Faro et al. 2005, 2006; Krakow et al. 2001). MRI can be of value, especially in excluding associated cerebral pathology (Fjortoft et al. 2007).

3.3 Failure of Neuronal Proliferation, Differentiation, and Histogenesis

Neuronal proliferation, differentiation, and histogenesis mainly occur from 8 to 24 (postmenstrual) weeks and continue until postnatal life. Disorders of these events lead to conditions such as micrencephaly, megalencephaly, Von Recklinghausen disease and congenital tumors, and vascular malformations of the nervous system (van der Knaap and Valk 1988).

Microcephaly is easily detected with US. In less severe cases, the ratio of the frontal lobe to the cerebellum (Persutte et al. 1997) and assessment of cerebral blood flow with Doppler ultrasound (Pilu et al. 1998) can aid the diagnosis. In more severe cases, it is difficult to examine the intracranial content with US because the fontanelles are very small (Fig. 6), and MRI may be

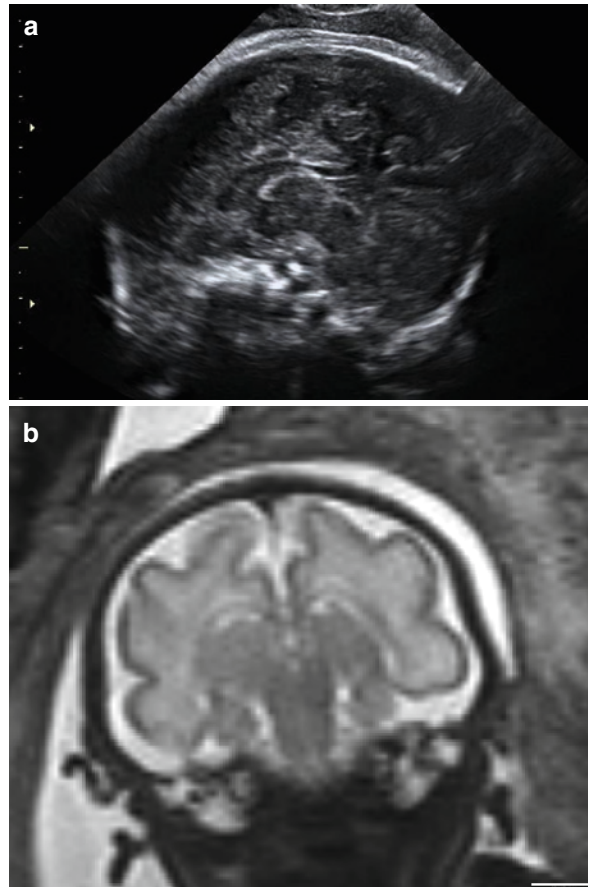

Fig. 6 Fetus with microcephaly. (**a**) Ultrasound: suboptimal visualization despite transvaginal approach. (**b**) MRI demonstrating increased subarachnoid space and delayed gyral development

needed to arrive at a specific diagnosis as microcephaly is a description, not a diagnosis (Raybaud et al. 2003).

MRI can demonstrate the increased cellularity (Agid et al. 2006) and accelerated myelination (Yuh et al. 1994) in fetuses with suspected hemimegalencephaly. It is important to realize that some degree of cerebral asymmetry occurs normally. Anatomical studies demonstrate up to 20% asymmetry, and there is also evidence of functional (de Vries and Fong 2006) and structural asymmetry on prenatal US (Hering-Hanit et al. 2001) and MRI (Kasprian 2006).

Different aspects of intracranial tumors can be assessed with US and MRI. Doppler US is useful to demonstrate the increased blood flow in highly vascularized tumors (Pinto et al. 1999), and MRI can be useful to determine the cellularity (Mascalchi et al. 2005) and fat content (of lipomas), distinguish tumors from hematomas, and diagnose areas of bleeding or necrosis (Woodward et al. 2005).

MRI is also a valuable tool to detect the periventricular, cortical, and subcortical nodules of tuberous sclerosis which are difficult to detect with ultrasound. The question usually arises in fetuses where cardiac rhabdomyomata are detected on US (Levine et al. 2000; Sonigo et al. 1996) (Fig. 7).

As with microcephaly, ventriculomegaly is the description of a condition which can be caused by many different genetic and acquired etiological factors.

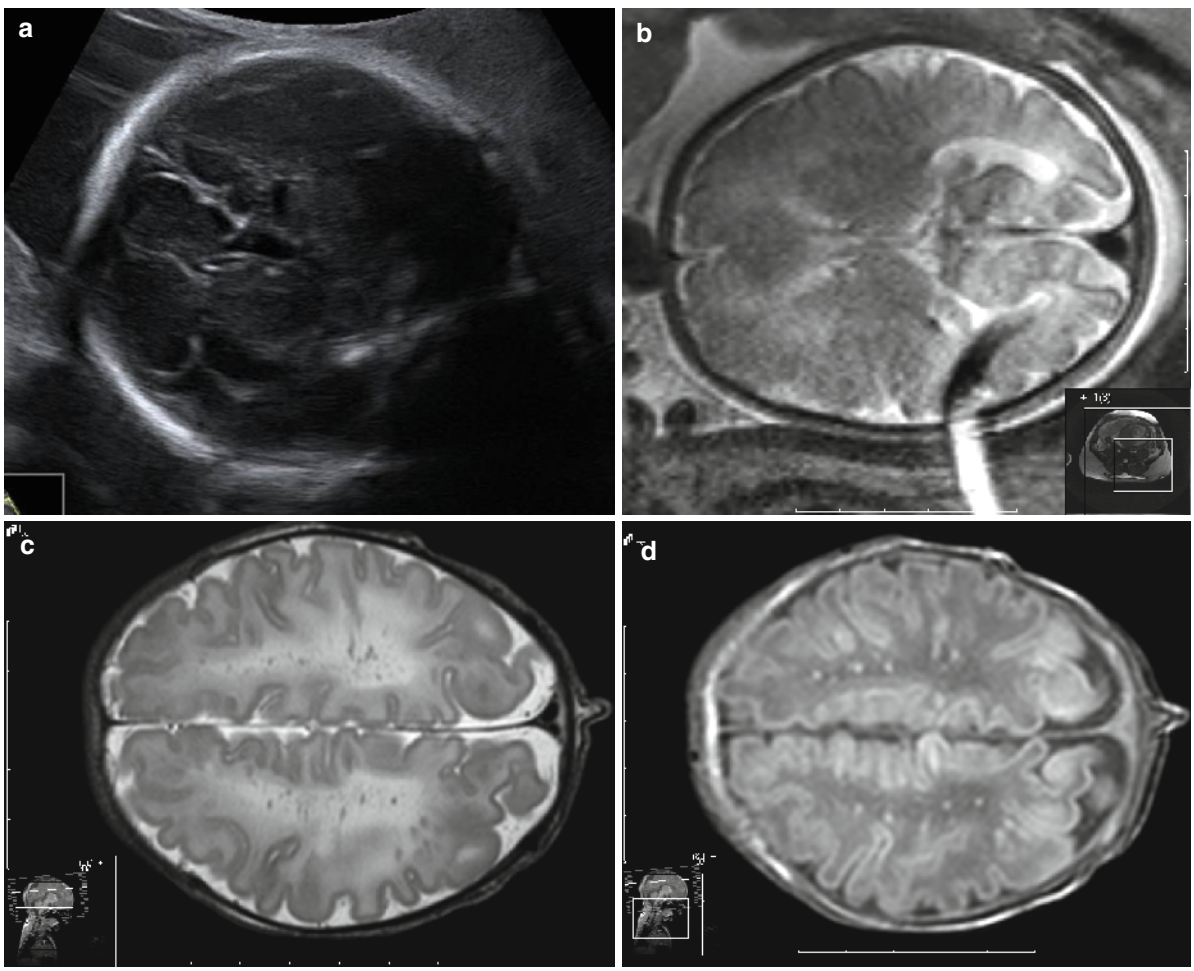

Fig. 7 Fetus with rhabdomyoma and tuberous sclerosis. (**a**) Ultrasound at 31 weeks demonstrating suspicious periventricular nodules. (**b**) T2-weighted MRI at 31 weeks demonstrating hypointense subependymal nodules. (**c**) T2-weighted postnatal MRI demonstrating multiple hypointense subependymal nodules. (**d**) T1-weighted postnatal MRI demonstrating multiple hyperintense subependymal nodules

With US, aqueduct stenosis is a diagnosis of exclusion where no signs of intraventricular bleeding or other cerebral pathology are seen in a fetus with dilated lateral and third ventricles and a small fourth ventricle. US is an excellent means to screen for ventriculomegaly by demonstrating the lateral ventricle in the axial plane, and the ventricular measurements done by ultrasound and MRI correlate well (Garel and Alberti 2006). It is common to find additional diagnosis such as malformations of cortical development, periventricular leukomalacia, or intracranial hemorrhage on MRI after an US diagnosis of ventriculomegaly (Breysem et al. 2003; Canapicchi et al. 1998; Simon et al. 2000; Valsky et al. 2004) . On the other hand, these conditions can be diagnosed by US as well (Hashimoto et al. 1999; Kalache et al. 2006; Malinger et al. 2002; Timor-Tritsch and Monteagudo 2003), and the difference in diagnostic accuracy between US and MRI might reflect the expertise of the operator and interpreter rather than the technical advantage of the imaging method (Malinger et al. 2004b).

3.4 Failure of Neuronal Migration

Neurons migrate from the ventricular and periventricular areas where they originate toward the cortex and deep nuclei from 12 to 24 (postmenstrual) weeks. Migrational disorders include lissencephaly,

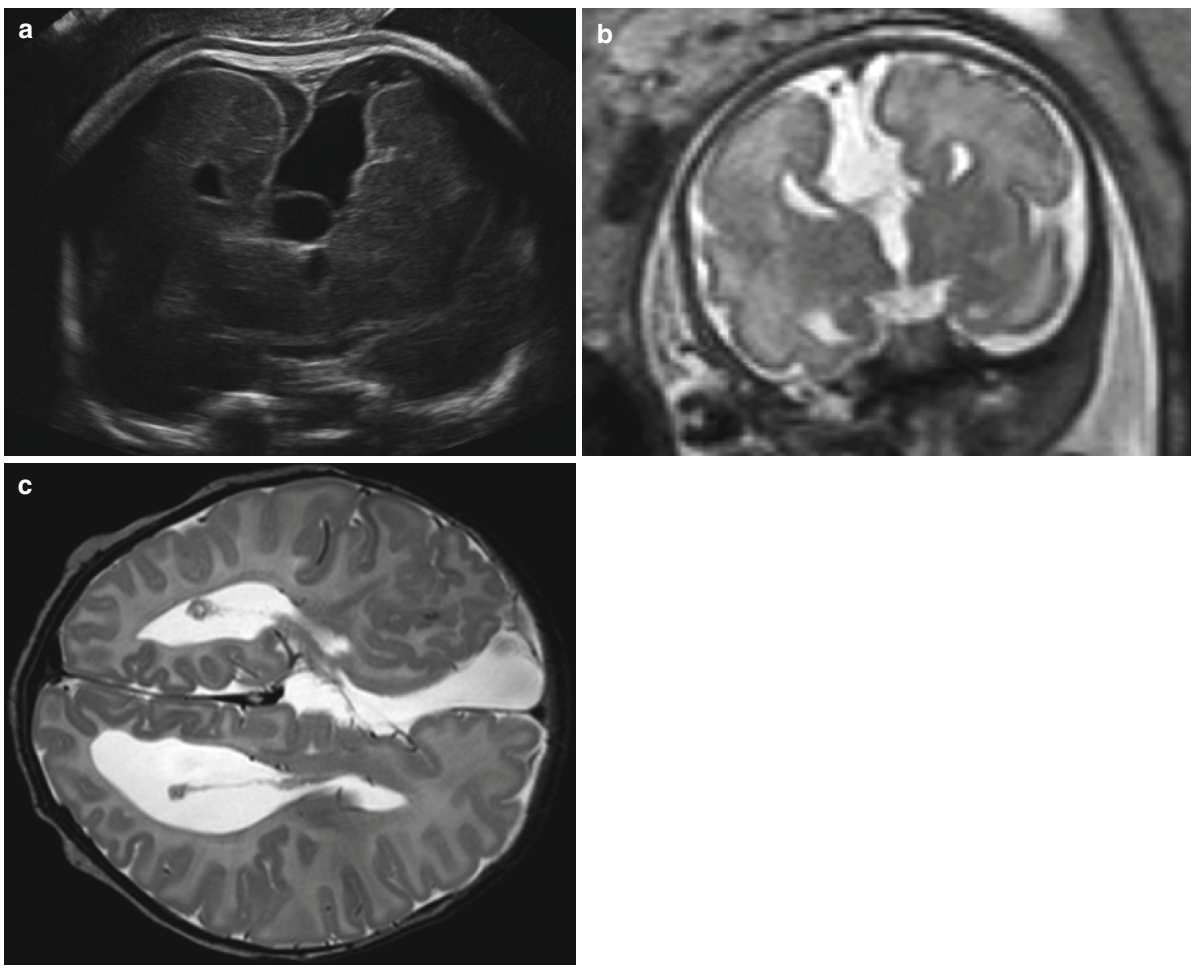

Fig. 8 Imaging of abnormal cortical development associated with corpus callosum agenesis and midline cyst. (**a**) Ultrasound at 20 weeks demonstrating agenesis of corpus callosum, cystic structure, and suspicion of abnormal cortical development. (**b**) MRI at 32 weeks. (**c**) Postnatal MRI

schizencephaly, polymicrogyria, pachygyria, and neuronal heterotopia (van der Knaap and Valk 1988).

With MRI, it is possible to evaluate both cortical gyration and sulcation and neuronal migration, as seen with the transient multilayered appearance of the cortex (Fogliarini et al. 2005a; Kostovic et al. 2002; Prayer et al. 2006b). MRI has indeed been considered necessary for the prenatal diagnosis of malformations of cortical development, as this diagnosis is often not suspected in fetuses with an US diagnosis of ventriculomegaly (Fogliarini et al. 2005b; Sonigo et al. 1998; Twickler et al. 2003).

On the other hand, US has been instrumental in detecting malformations of cortical development, such as polimicrogyria which later became evident in an area of increased echogenicity (Delle Urban et al. 2004). It might be that malformations of cortical development are infrequently diagnosed with US because it is not actively searched for with US, either because of a lack of knowledge or because of the belief that it is not visible anyway. In support of this, it was possible to diagnose delayed cortical development on prenatal US images in a retrospective study of infants with Miller-Dieker syndrome (Fong et al. 2004). In a prospective study of 24 fetuses with abnormal cortical development, it was also possible to diagnose abnormal cortical development with US with the same accuracy as with MRI (Malinger et al. 2007b) (Fig. 8).

3.5 Failure of Myelination

Myelination starts in the early third trimester of pregnancy and continues into adult life (van der Knaap and Valk 1988). Myelination-corresponding signals can be seen on MRI from around 30 weeks, sometime after myelin's histological appearance. White matter tracts can be imaged with diffusion-weighted imaging thanks to the anisotropy caused by premyelin sheaths and the formation of an axon potential (Prayer et al. 2006b). With diffusion tensor imaging and tractography, the 3D appearance of sensorimotor and callosal trajectories can also be visualized from as early as 18 gestational weeks (Kasprian et al. 2008).

Failure of myelination is usually diagnosed postnatally, unless it is associated with structural abnormalities, such as the delayed cortical development associated with Zellweger's disease (Prayer et al. 2006a) or when invasive testing is performed due to a known familial gene defect.

3.6 Acquired Lesions

With US, cerebral abnormalities can be seen up to 2 weeks after the death of a monochorial cotwin (Simonazzi et al. 2006). With MRI, ischemia can be seen as a hyperintense signal on diffusion-weighted imaging and reduced ADC (Righini et al. 2003) within hours after an insult (Baldoli et al. 2002; Drobyshevsky et al. 2007; Mascalchi et al. 2005). Subsequently, the ischemia could lead to subcortical leukomalacia which could be visualized as increased signals on T2-WI or decreased signals on T1-WI (Girard et al. 2003), or to porencephalic cysts (Ozduman et al. 2004). The latter can be seen with US and MRI, as can schizencephaly, periventricular leukomalacia, and other parenchymal lesions (Breysem et al. 2003; Ismail et al. 2002; Vimercati et al. 1999; Wagenvoort et al. 2000; Whitby et al. 2004; Gelder-Hasker et al. 2003). The synergy between US and MRI can be useful in diagnosing fetal brain death (Otsubo et al. 1999).

The diagnosis of congenital infections such as cytomegalovirus is a good example of the synergy between US and MRI. With US, borderline ventriculomegaly and more specific signs such as a hyperechogenic periventricular germinal matrix, parenchymal and cerebellar calcifications, and striatal vasculopathy might be seen, and MRI can add information on abnormal gyration and cerebellar hypoplasia. The development of US and MRI signs is a very dynamic process (Guibaud et al. 2004; Malinger et al. 2003; Picone et al. 2008).

Trauma might precede fetal pathology such as schizencephaly, vermian hemorrhage, and epidural bleeding (Ellestad et al. 2004; Mancini et al. 2001). The exact prevalence and progression of fetal central nervous system pathology and neurodevelopmental abnormalities after maternal trauma is largely unknown.

Intraventricular hemorrhage can be seen on ultrasound as a mass with irregular echogenicity, which can lead to the development of ventriculomegaly with an increased echogenicity of the ventricular walls (Ghi et al. 2003). MRI might aid in the diagnosis of germinal matrix and intraventricular bleeding even without a mass effect such as seen in grade I hemorrhage, by the specific pattern (a central hypointense area surrounded by a hyperintense area on T1-WI and mixed hypo and isointensity on T2-WI) or by visualizing the T2 hypointense signal caused by hemosiderin (Morioka et al. 2006; Ramenghi et al. 2005).

Both cerebellar hemorrhage and cerebellar telangiectasia, conditions with very different prognoses, appear

echogenic on US, but can be distinguished by means of MRI as hemorrhage shows up hyperintense on T1 and hopointense on T2-WI, and telangiectasia demonstrates no mass effect and isointensity on both T1 and T2-WI (Gorincour et al. 2006; Guibaud et al. 2003).

4 Functional Fetal Evaluation

Structural evaluation of the fetal central nervous system has been refined over the years to the point that further refinement of diagnostic abilities probably lie in the field of functional evaluation, i.e., to move from a structural examination to a fetal neurological examination.

Fetal cerebral blood flow can be evaluated with power or color Doppler US. This can help to demonstrate vascular lesions such as a vascular malformation or an aneurysm of the vein of Galen (Chaoui et al. 2001; Hartung et al. 2003) even without obvious abnormalities on gray scale imaging (Fig. 9). Decreased regional flow in the circle of Willis or carotid artery can also help to determine the origin of pathology such as schizencephaly (Suchet 1994). Neonatally, middle cerebral arterial flow has been used to aid the diagnosis of raised intracranial pressure (Hanlo et al. 1995). The prenatal use of middle cerebral artery flow indices is not widely used for this indication, although it is generally used in the management of growth-restricted fetuses (Baschat and Hecher 2004). There are some indications that cerebral venous flow might be useful in this regard (Pooh et al. 1999).

Cerebral flow can also be evaluated with MRI. The relative amount of deoxyhemoglobin can be detected

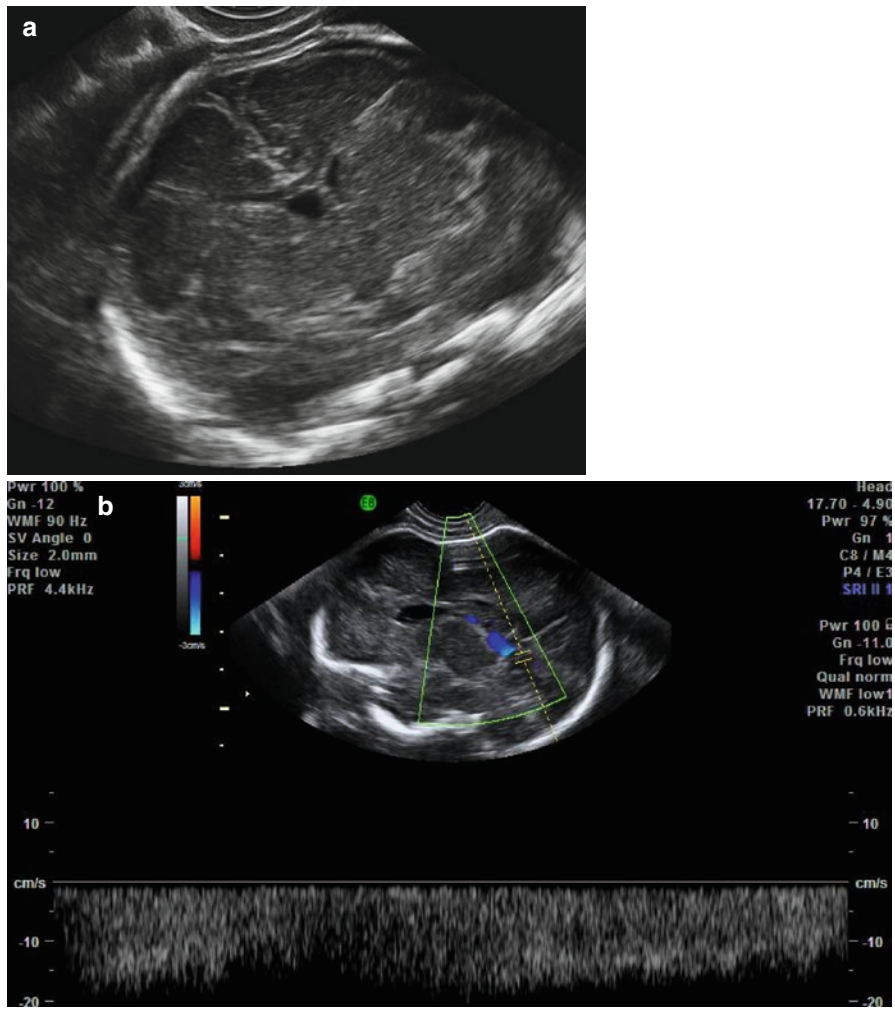

Fig. 9 Fetus with arteriovenous malformation. (**a**) Ultrasound at 27 weeks without obvious malformation. (**b**) Color Doppler ultrasound at 27 weeks with increased flow through arteriovenous malformation

with BOLD (blood oxygen level-dependent) (Wedegartner et al. 2006) imaging. This can be used to map brain activity, also in utero, in response to prerecorded nursery rhymes (Hykin et al. 1999), music (Moore et al. 2001), visual (Fulford et al. 2003), or vibro-acoustic stimuli (Fulford et al. 2004). Similar results as with adult functional MRI (fMRI) are obtained, with a stronger BOLD signal seen prenatally (Gowland and Fulford 2004). Dynamic fMRI sequences might also be possible (Pisani et al. 2007). It has also been shown in a sheep model that BOLD sequences could be used to monitor oxyhemoglobin concentrations during maternal hypoxia (Wedegartner et al. 2002, 2006). Whether it is possible to translate this to the human fetus using 1.5 T apparatus remains to be seen (Levine 2006). pO_2 might also be measured by means of quantitative images of fluid oxygenation on standard single-shot fast-spin echo (SSFSE) sequences (Zaharchuk et al. 2006).

Furthermore, it is eminently possible to evaluate fetal movement patterns, which provide some functional information about the fetal brain (de Vries and Fong 2006). Assessment of fetal movements by US has been well described a decade and a half ago (Marsal 1983), and more recently, using MRI (Brugger et al. 2006; Guo et al. 2006). Fetal memory, or at least habituation, has even been demonstrated by evaluating the fetal response to auditory stimuli by means of real-time ultrasound and cardiotocography (van Heteren et al. 2000).

Abnormal movement patterns are highly specific, but unfortunately insensitive indicators of fetal cerebral pathology (de Vries and Fong 2007; Salihagic-Kadic et al. 2005; Koyanagi et al. 1993). Although there are many reports of the usefulness of assessing the movement patterns of a fetus with possible or definitive nervous system pathology, it is not yet part of standard neurosonography (Malinger et al. 2007a). It is time-consuming, requiring an hour or more to accurately evaluate fetal movements (de Vries and Fong 2007; Sival et al. 1992), and probably requiring more than one assessment (Nijhuis 2003) and standardization for the diurnal rhythm and maternal food and medication intake and possible pathology (Salisbury et al. 2005) before one could draw any conclusions. Automated actigraphy has been used to minimize the labor intensity of fetal movement assessment, with some varying success (de Wit and Nijhuis 2003; Dipietro et al. 2002; Maeda et al. 2006).

Magnetic resonance might prove to be especially useful to evaluate fetal movements in late pregnancy and oligohydramnion, when the ability to visualize fetal activity with ultrasound is restricted. It has been estimated that a three observation period of 30 s, each during the MR examination time of 30–45 min, would be sufficient to assess fetal general movements qualitatively (Olesen and Svare 2004; Prayer et al. 2006b), but it remains to be seen whether this small sample would be sufficiently representative.

Another imaging method which might in future be of much greater clinical value is MRS (magnetic resonance spectroscopy), with which it is possible to measure relative and even absolute levels of specific substances (Girard et al. 2006). It is feasible, but difficult (Fenton et al. 2001), to measure fetal brain lactate (Roelants-van Rijn et al. 2004) and other metabolites such as inositol, which was found to be decreased in fetuses with hydrocephalus (Kok et al. 2003). MRS also has potential applications in diagnosing asphyxia. In congenital disorders of metabolism, the maternal metabolism could compensate for the abnormal fetal metabolism, with false negative results (Robinson et al. 2001).

5 Diagnostic Aspects

Imaging does not equate diagnosis. Many studies affirm the value of a multidisciplinary discussion (Hagmann et al. 2008; Levine et al. 2003; Malinger et al. 2004a) and it would appear that this is where the real strength lies: not in the choice between US or MRI, but in using each modality to its maximum capability and arriving at a final diagnosis during a multidisciplinary discussion.

References

Aaronson OS, Hernanz-Schulman M, Bruner JP, Reed GW, Tulipan NB (2003) Myelomeningocele: prenatal evaluation–comparison between transabdominal US and MR imaging. Radiology 227:839–843

Abramowicz JS (2007) Prenatal exposure to ultrasound waves: is there a risk? Ultrasound Obstet Gynecol 29:363–367

Achiron R, Achiron A (2001) Development of the human fetal corpus callosum: a high-resolution, cross-sectional sonographic study. Ultrasound Obstet Gynecol 18:343–347

Agid R, Lieberman S, Nadjari M, Gomori JM (2006) Prenatal MR diffusion-weighted imaging in a fetus with hemimegalencephaly. Pediatr Radiol 36:138–140

Ang ES Jr, Gluncic V, Duque A, Schafer ME, Rakic P (2006) Prenatal exposure to ultrasound waves impacts neuronal migration in mice. Proc Natl Acad Sci U S A 103:12903–12910

Baldoli C, Righini A, Parazzini C, Scotti G, Triulzi F (2002) Demonstration of acute ischemic lesions in the fetal brain by diffusion magnetic resonance imaging. Ann Neurol 52: 243–246

Baschat AA, Hecher K (2004) Fetal growth restriction due to placental disease. Semin Perinatol 28:67–80

Bault JP (2006) Visualization of the fetal optic chiasma using three-dimensional ultrasound imaging. Ultrasound Obstet Gynecol 28:862–864

Benacerraf BR, Spiro R, Mitchell AG (2000) Using three-dimensional ultrasound to detect craniosynostosis in a fetus with Pfeiffer syndrome. Ultrasound Obstet Gynecol 16:391–394

Bitar R, Leung G, Perng R, Tadros S, Moody AR, Sarrazin J, McGregor C, Christakis M, Symons S, Nelson A, Roberts TP (2006) MR pulse sequences: what every radiologist wants to know but is afraid to ask. Radiographics 26:513–537

Blaas HG, Eik-Nes SH, Kiserud T, Hellevik LR (1995) Early development of the hindbrain: a longi-tudinal ultrasound study from 7 to 12 weeks of gestation. Ultrasound Obstet Gynecol 5:151–160

Breysem L, Bosmans H, Dymarkowski S, Schoubroeck DV, Witters I, Deprest J, Demaerel P, Vanbeckevoort D, Vanhole C, Casaer P, Smet M (2003) The value of fast MR imaging as an adjunct to ultrasound in prenatal diagnosis. Eur Radiol 13:1538–1548

Brugger PC, Stuhr F, Lindner C, Prayer D (2006) Methods of fetal MR: beyond T2-weighted imaging. Eur J Radiol 57:172–181

Canapicchi R, Cioni G, Strigini FA, Abbruzzese A, Bartalena L, Lencioni G (1998) Prenatal diagnosis of periventricular hemorrhage by fetal brain magnetic resonance imaging. Childs Nerv Syst 14:689–692

Chaoui R, Kalache KD, Hartung J (2001) Application of three-dimensional power Doppler ultrasound in prenatal diagnosis. Ultrasound Obstet Gynecol 17:22–29

Chen MM, Coakley FV, Kaimal A, Laros RK Jr (2008) Guidelines for computed tomography and magnetic resonance imaging use during pregnancy and lactation. Obstet Gynecol 112: 333–340

Clement S, Candy B, Heath V, To M, Nicolaides KH (2003) Transvaginal ultrasound in pregnancy: its acceptability to women and maternal psychological morbidity. Ultrasound Obstet Gynecol 22:508–514

D'ercole C, Girard N, Cravello L, Boubli L, Potier A, Raybaud C, Blanc B (1998) Prenatal diagnosis of fetal corpus callosum agenesis by ultrasonography and magnetic resonance imaging. Prenat Diagn 18:247–253

Dashe JS, Twickler DM, Santos-Ramos R, McIntire DD, Ramus RM (2006) Alpha-fetoprotein detection of neural tube defects and the impact of standard ultrasound. Am J Obstet Gynecol 195:1623–1628

de Vries JI, Fong BF (2006) Normal fetal motility: an overview. Ultrasound Obstet Gynecol 27:701–711

de Vries JI, Fong BF (2007) Changes in fetal motility as a result of congenital disorders: an overview. Ultrasound Obstet Gynecol 29:590–599

de Wit AC, Nijhuis JG (2003) Validity of the Hewlett-Packard actograph in detecting fetal movements. Ultrasound Obstet Gynecol 22:152–156

Delahaye S, Bernard JP, Renier D, Ville Y (2003) Prenatal ultrasound diagnosis of fetal craniosynostosis. Ultrasound Obstet Gynecol 21:347–353

Delle Urban LA, Righini A, Rustico M, Triulzi F, Nicolini U (2004) Prenatal ultrasound detection of bilateral focal polymicrogyria. Prenat Diagn 24:808–811

Dipietro JA, Bornstein MH, Costigan KA, Pressman EK, Hahn CS, Painter K, Smith BA, Yi LJ (2002) What does fetal movement predict about behavior during the first two years of life? Dev Psychobiol 40:358–371

Doherty D, Glass IA, Siebert JR, Strouse PJ, Parisi MA, Shaw DW, Chance PF, Barr M Jr, Nyberg D (2005) Prenatal diagnosis in pregnancies at risk for Joubert syndrome by ultrasound and MRI. Prenat Diagn 25:442–447

Drobyshevsky A, Derrick M, Prasad PV, Ji X, Englof I, Tan S (2007) Fetal brain magnetic resonance imaging response acutely to hypoxia-ischemia predicts postnatal outcome. Ann Neurol 61:307–314

Ellestad SC, Shelton S, James AH (2004) Prenatal diagnosis of a trauma-related fetal epidural hematoma. Obstet Gynecol 104:1298–1300

Faro C, Benoit B, Wegrzyn P, Chaoui R, Nicolaides KH (2005) Three-dimensional sonographic description of the fetal frontal bones and metopic suture. Ultrasound Obstet Gynecol 26:618–621

Faro C, Chaoui R, Wegrzyn P, Levaillant JM, Benoit B, Nicolaides KH (2006) Metopic suture in fetuses with Apert syndrome at 22–27 weeks of gestation. Ultrasound Obstet Gynecol 27:28–33

Fenton BW, Lin CS, Macedonia C, Schellinger D, Ascher S (2001) The fetus at term: in utero volume-selected proton MR spectroscopy with a breath-hold technique–a feasibility study. Radiology 219:563–566

Fjortoft MI, Sevely A, Boetto S, Kessler S, Sarramon MF, Rolland M (2007) Prenatal diagnosis of craniosynostosis: value of MR imaging. Neuroradiology 49:515–521

Fogliarini C, Chaumoitre K, Chapon F, Fernandez C, Levrier O, Figarella-Branger D, Girard N (2005a) Assessment of cortical maturation with prenatal MRI. Part I: normal cortical maturation. Eur Radiol 15:1671–1685

Fogliarini C, Chaumoitre K, Chapon F, Fernandez C, Levrier O, Figarella-Branger D, Girard N (2005b) Assessment of cortical maturation with prenatal MRI: part II: abnormalities of cortical maturation. Eur Radiol 15:1781–1789

Fong KW, Ghai S, Toi A, Blaser S, Winsor EJ, Chitayat D (2004) Prenatal ultrasound findings of lissencephaly associated with Miller-Dieker syndrome and comparison with pre- and postnatal magnetic resonance imaging. Ultrasound Obstet Gynecol 24:716–723

Frates MC, Kumar AJ, Benson CB, Ward VL, Tempany CM (2004) Fetal anomalies: comparison of MR imaging and US for diagnosis. Radiology 232:398–404

Fulford J, Vadeyar SH, Dodampahala SH, Moore RJ, Young P, Baker PN, James DK, Gowland PA (2003) Fetal brain activity in response to a visual stimulus. Hum Brain Mapp 20: 239–245

Fulford J, Vadeyar SH, Dodampahala SH, Ong S, Moore RJ, Baker PN, James DK, Gowland P (2004) Fetal brain activity and hemodynamic response to a vibroacoustic stimulus. Hum Brain Mapp 22:116–121

Garel C, Alberti C (2006) Coronal measurement of the fetal lateral ventricles: comparison between ultrasonography and magnetic resonance imaging. Ultrasound Obstet Gynecol 27: 23–27

Gelder-Hasker MR, Wezel-Meijler G, de Groot L, van Geijn HP, de Vries JI (2003) Peri- and intra-ventricular cerebral sonography in second- and third-trimester high-risk fetuses: a comparison with neonatal ultrasound and relation to neurological development. Ultrasound Obstet Gynecol 22:110–120

Ghi T, Perolo A, Banzi C, Contratti G, Valeri B, Savelli L, Morselli GP, Bovicelli L, Pilu G (2002) Two-dimensional ultrasound is accurate in the diagnosis of fetal craniofacial malformation. Ultrasound Obstet Gynecol 19:543–551

Ghi T, Simonazzi G, Perolo A, Savelli L, Sandri F, Bernardi B, Santini D, Bovicelli L, Pilu G (2003) Outcome of antenatally diagnosed intracranial hemorrhage: case series and review of the literature. Ultrasound Obstet Gynecol 22:121–130

Girard N, Gire C, Sigaudy S, Porcu G, D'ercole C, Figarella-Branger D, Raybaud C, Confort-Gouny S (2003) MR imaging of acquired fetal brain disorders. Childs Nerv Syst 19: 490–500

Girard N, Fogliarini C, Viola A, Confort-Gouny S, Fur YL, Viout P, Chapon F, Levrier O, Cozzone P (2006) MRS of normal and impaired fetal brain development. Eur J Radiol 57:217–225

Glenn OA, Goldstein RB, Li KC, Young SJ, Norton ME, Busse RF, Goldberg JD, Barkovich AJ (2005) Fetal magnetic resonance imaging in the evaluation of fetuses referred for sonographically suspected abnormalities of the corpus callosum. J Ultrasound Med 24:791–804

Gorincour G, Rypens F, Lapierre C, Costa T, Audibert F, Robitaille Y (2006) Fetal magnetic resonance imaging in the prenatal diagnosis of cerebellar hemorrhage. Ultrasound Obstet Gynecol 27:78–80

Gowland P, Fulford J (2004) Initial experiences of performing fetal fMRI. Exp Neurol 190(suppl 1):S22–S27

Grandjean H, Larroque D, Levi S (1999) The performance of routine ultrasonographic screening of pregnancies in the Eurofetus Study. Am J Obstet Gynecol 181:446–454

Guibaud L, des Portes V (2006) Plea for an anatomical approach to abnormalities of the posterior fossa in prenatal diagnosis. Ultrasound Obstet Gynecol 27:477–481

Guibaud L, Garel C, Annie B, Pascal G, Francois V, Vavasseur C, Oury JF, Pracros JP (2003) Prenatal diagnosis of capillary telangiectasia of the cerebellum–ultrasound and MRI features. Prenat Diagn 23:791–796

Guibaud L, Attia-Sobol J, Buenerd A, Foray P, Jacquet C, Champion F, Arnould P, Pracros JP, Golfier F (2004) Focal sonographic periventricular pattern associated with mild ventriculomegaly in foetal cytomegalic infection revealing cytomegalic encephalitis in the third trimester of pregnancy. Prenat Diagn 24:727–732

Guo WY, Ono S, Oi S, Shen SH, Wong TT, Chung HW, Hung JH (2006) Dynamic motion analysis of fetuses with central nervous system disorders by cine magnetic resonance imaging using fast imaging employing steady-state acquisition and parallel imaging: a preliminary result. J Neurosurg 105:94–100

Hagmann CF, Robertson NJ, Leung WC, Chong KW, Chitty LS (2008) Foetal brain imaging: ultra-sound or MRI. A comparison between magnetic resonance imaging and a dedicated multidisciplinary neurosonographic opinion. Acta Paediatr 97:414–419

Hanlo PW, Gooskens RH, Nijhuis IJ, Faber JA, Peters RJ, van Huffelen AC, Tulleken CA, Willemse J (1995) Value of transcranial Doppler indices in predicting raised ICP in infantile hydrocephalus. A study with review of the literature. Childs Nerv Syst 11:595–603

Hartung J, Heling KS, Rake A, Zimmer C, Chaoui R (2003) Detection of an aneurysm of the vein of Galen following signs of cardiac overload in a 22-week old fetus. Prenat Diagn 23:901–903

Hashimoto I, Tada K, Nakatsuka M, Nakata T, Inoue N, Takata M, Kudo T, Joja I (1999) Fetal hydrocephalus secondary to intraventricular hemorrhage diagnosed by ultrasonography and in utero fast magnetic resonance imaging. A case report. Fetal Diagn Ther 14:248–253

Hering-Hanit R, Achiron R, Lipitz S, Achiron A (2001) Asymmetry of fetal cerebral hemispheres: in utero ultrasound study. Arch Dis Child Fetal Neonatal Ed 85: F194–F196

Hykin J, Moore R, Duncan K, Clare S, Baker P, Johnson I, Bowtell R, Mansfield P, Gowland P (1999) Fetal brain activity demonstrated by functional magnetic resonance imaging. Lancet 354:645–646

Ismail KM, Ashworth JR, Martin WL, Chapman S, McHugo J, Whittle MJ, Kilby MD (2002) Fetal magnetic resonance imaging in prenatal diagnosis of central nervous system abnormalities: 3-year experience. J Matern Fetal Neonatal Med 12:185–190

Johnson SP, Sebire NJ, Snijders RJ, Tunkel S, Nicolaides KH (1997) Ultrasound screening for anen-cephaly at 10–14 weeks of gestation. Ultrasound Obstet Gynecol 9:14–16

Kalache KD, Eder K, Esser T, Proquitte H, Stoltenburg-Didinger G, Hartung JP, Bamberg C (2006) Three-dimensional ultrasonographic reslicing of the fetal brain to assist prenatal diagnosis of central nervous system anomalies. J Ultrasound Med 25:509–514

Kasprian G (2006) Growth and development of the fetal temporal lobe in vivo. Thesis/Dissertation, Medical University of Vienna, Austria

Kasprian G, Brugger PC, Weber M, Krssak M, Krampl E, Herold C, Prayer D (2008) In utero tractography of fetal white matter development. Neuroimage 43:213–224

Kim MS, Jeanty P, Turner C, Benoit B (2008) Three-dimensional sonographic evaluations of embryonic brain development. J Ultrasound Med 27:119–124

Kok RD, Steegers-Theunissen RP, Eskes TK, Heerschap A, van den Berg PP (2003) Decreased relative brain tissue levels of inositol in fetal hydrocephalus. Am J Obstet Gynecol 188: 978–980

Kostovic I, Judas M, Rados M, Hrabac P (2002) Laminar organization of the human fetal cerebrum revealed by histochemical markers and magnetic resonance imaging. Cereb Cortex 12:536–544

Koyanagi T, Horimoto N, Maeda H, Kukita J, Minami T, Ueda K, Nakano H (1993) Abnormal behavioral patterns in the human fetus at term: correlation with lesion sites in the central nervous system after birth. J Child Neurol 8:19–26

Krakow D, Santulli T, Platt LD (2001) Use of three-dimensional ultrasonography in differentiating craniosynostosis from severe fetal molding. J Ultrasound Med 20:427–431

Kusaka Y, Luedemann W, Oi S, Shwardfegar R, Samii M (2005) Fetal arachnoid cyst of the quadrigeminal cistern in MRI and ultrasound. Childs Nerv Syst 21:1065–1066

Leithner K, Pornbacher S, Assem-Hilger E, Krampl E, Ponocny-Seliger E, Prayer D (2008) Psychological reactions in

women undergoing fetal magnetic resonance imaging. Obstet Gynecol 111:396–402
Levine D (2006) Science to practice: can MR oxygenation imaging be used to assess at-risk pregnancies? Radiology 238: 765–766
Levine D, Barnes P, Korf B, Edelman R (2000) Tuberous sclerosis in the fetus: second-trimester diagnosis of subependymal tubers with ultrafast MR imaging. AJR Am J Roentgenol 175:1067–1069
Levine D, Barnes PD, Robertson RR, Wong G, Mehta TS (2003) Fast MR imaging of fetal central nervous system abnormalities. Radiology 229:51–61
Levine D, Cavazos C, Kazan-Tannus JF, McKenzie CA, Dialani V, Robson CD, Robertson RL, Poussaint TY, Busse RF, Rofsky NM (2006) Evaluation of real-time single-shot fast spin-echo MRI for visualization of the fetal midline corpus callosum and secondary palate. AJR Am J Roentgenol 187:1505–1511
Maeda K, Morokuma S, Yoshida S, Ito T, Pooh RK, Serizawa M (2006) Fetal behavior analyzed by ultrasonic actocardiogram in cases with central nervous system lesions. J Perinat Med 34:398–403
Malinger G, Zakut H (1993) The corpus callosum: normal fetal development as shown by transvaginal sonography. AJR Am J Roentgenol 161:1041–1043
Malinger G, Lev D, Lerman-Sagie T (2002) Is fetal magnetic resonance imaging superior to neurosonography for detection of brain anomalies? Ultrasound Obstet Gynecol 20: 317–321
Malinger G, Lev D, Zahalka N, Ben Aroia Z, Watemberg N, Kidron D, Sira LB, Lerman-Sagie TF et al (2003) Cytomegalovirus infection of the brain: the spectrum of sonographic findings. AJNR Am J Neuroradiol 24:28–32
Malinger G, Ben Sira L, Lev D, Ben Aroya Z, Kidron D, Lerman-Sagie T (2004a) Fetal brain imaging: a comparison between magnetic resonance imaging and dedicated neurosonography. Ultrasound Obstet Gynecol 23:333–340
Malinger G, Lev D, Lerman-Sagie T (2004b) Fetal central nervous system: MR imaging versus dedi-cated US–need for prospective, blind, comparative studies. Radiology 232:306–307
Malinger G, Monteagudo A, Pilu G, Timor-Tritsch IE, Toi A (2007a) Sonographic examination of the fetal central nervous system: guidelines for performing the 'basic examination' and the 'fetal neurosonogram'. Ultrasound Obstet Gynecol 29:109–116
Malinger G, Kidron D, Schreiber L, Ben Sira L, Hoffmann C, Lev D, Lerman-Sagie T (2007b) Prenatal diagnosis of malformations of cortical development by dedicated neurosonography. Ultrasound Obstet Gynecol 29:178–191
Mancini J, Lethel V, Hugonenq C, Chabrol B (2001) Brain injuries in early foetal life: consequences for brain development. Dev Med Child Neurol 43:52–55
Marsal K (1983) Ultrasonic assessment of fetal activity. Clin Obstet Gynaecol 10:541–563
Mascalchi M, Filippi M, Floris R, Fonda C, Gasparotti R, Villari N (2005) Diffusion-weighted MR of the brain: methodology and clinical application. Radiol Med (Torino) 109:155–197
McCarthy SM, Filly RA, Stark DD, Hricak H, Brant-Zawadzki MN, Callen PW, Higgins CB (1985) Obstetrical magnetic resonance imaging: fetal anatomy. Radiology 154:427–432
Monteagudo A, Timor-Tritsch IE, Moomjy M (1993) Nomograms of the fetal lateral ventricles using transvaginal sonography. J Ultrasound Med 12:265–269
Monteagudo A, Timor-Tritsch IE, Mayberry P (2000) Three-dimensional transvaginal neurosonography of the fetal brain: 'navigating' in the volume scan. Ultrasound Obstet Gynecol 16:307–313
Moore RJ, Vadeyar S, Fulford J, Tyler DJ, Gribben C, Baker PN, James D, Gowland PA (2001) An-tenatal determination of fetal brain activity in response to an acoustic stimulus using functional magnetic resonance imaging. Hum Brain Mapp 12:94–99
Morioka T, Hashiguchi K, Nagata S, Miyagi Y, Mihara F, Hikino S, Tsukimori K, Sasaki T (2006) Fetal germinal matrix and intraventricular hemorrhage. Pediatr Neurosurg 42:354–361
Nijhuis JG (2003) Fetal behavior. Neurobiol Aging 24(suppl 1):S41–S46
Olesen AG, Svare JA (2004) Decreased fetal movements: background, assessment, and clinical management. Acta Obstet Gynecol Scand 83:818–826
Otsubo Y, Yoneyama Y, Sawa R, Suzuki S, Araki T (1999) Fetal brain death and Dandy-Walker malformation. Prenat Diagn 19:777–779
Ozduman K, Pober BR, Barnes P, Copel JA, Ogle EA, Duncan CC, Ment LR (2004) Fetal stroke. Pediatr Neurol 30:151–162
Paladini D, Volpe P (2006) Posterior fossa and vermian morphometry in the characterization of fetal cerebellar abnormalities: a prospective three-dimensional ultrasound study. Ultrasound Obstet Gynecol 27:482–489
Pasto ME, Kurtz AB (1986) Ultrasonography of the normal fetal brain. Neuroradiology 28:380–385
Persutte WH, Coury A, Hobbins JC (1997) Correlation of fetal frontal lobe and transcerebellar diameter measurements: the utility of a new prenatal sonographic technique. Ultrasound Obstet Gynecol 10:94–97
Picone O, Simon I, Benachi A, Brunelle F, Sonigo P (2008) Comparison between ultrasound and magnetic resonance imaging in assessment of fetal cytomegalovirus infection. Prenat Diagn 28:753–758
Pilu G, Falco P, Milano V, Perolo A, Bovicelli L (1998) Prenatal diagnosis of microcephaly assisted by vaginal sonography and power Doppler. Ultrasound Obstet Gynecol 11:357–360
Pilu G, Visentin A, Valeri B (2000) The Dandy-Walker complex and fetal sonography. Ultrasound Obstet Gynecol 16: 115–117
Pilu G, Segata M, Ghi T, Carletti A, Perolo A, Santini D, Bonasoni P, Tani G, Rizzo N (2006) Diagnosis of midline anomalies of the fetal brain with the three-dimensional median view. Ultrasound Obstet Gynecol 27:522–529
Pinto V, Meo F, Loiudice L, D'Addario V (1999) Prenatal sonographic imaging of an immature intracranial teratoma. Fetal Diagn Ther 14:220–222
Pisani L, Bammer R, Glover G (2007) Restricted field of view magnetic resonance imaging of a dynamic time series. Magn Reson Med 57:297–307
Pistorius LR, Hellmann PM, Visser GH, Malinger G, Prayer D (2008) Fetal neuroimaging: ultrasound, MRI, or both? Obstet Gynecol Surv 63:733–745

Pistorius L, Stoutenbeek P, Visser GH (2009) First trimester neurosonoembryology with automated follicle tracking: preliminary findings. J Matern Fetal Neonatal Med 22:1–3

Pooh RK, Pooh KH, Nakagawa Y, Maeda K, Fukui R, Aono T (1999) Transvaginal Doppler assessment of fetal intracranial venous flow. Obstet Gynecol 93:697–701

Prayer D, Brugger PC, Kasprian G, Witzani L, Helmer H, Dietrich W, Eppel W, Langer M (2006a) MRI of fetal acquired brain lesions. Eur J Radiol 57:233–249

Prayer D, Kasprian G, Krampl E, Ulm B, Witzani L, Prayer L, Brugger PC (2006b) MRI of normal fetal brain development. Eur J Radiol 57:199–216

Ramenghi LA, Fumagalli M, Righini A, Triulzi F, Kustermann A, Mosca F (2005) Thrombophilia and fetal germinal matrix-intraventricular hemorrhage: does it matter? Ultrasound Obstet Gynecol 26:574–576

Raybaud C, Levrier O, Brunel H, Girard N, Farnarier P (2003) MR imaging of fetal brain malformations. Childs Nerv Syst 19:455–470

Reddy UM, Filly RA, Copel JA (2008) Prenatal imaging: ultrasonography and magnetic resonance imaging. Obstet Gynecol 112:145–157

Righini A, Bianchini E, Parazzini C, Gementi P, Ramenghi L, Baldoli C, Nicolini U, Mosca F, Triulzi F (2003) Apparent diffusion coefficient determination in normal fetal brain: a prenatal MR imaging study. AJNR Am J Neuroradiol 24: 799–804

Robinson JN, Norwitz ER, Mulkern R, Brown SA, Rybicki F, Tempany CM (2001) Prenatal diagnosis of pyruvate dehydrogenase deficiency using magnetic resonance imaging. Prenat Diagn 21:1053–1056

Roelants-van Rijn AM, Groenendaal F, Stoutenbeek P, van der Grond J (2004) Lactate in the foetal brain: detection and implications. Acta Paediatr 93:937–940

Salihagic-Kadic A, Kurjak A, Medic M, Andonotopo W, Azumendi G (2005) New data about embryonic and fetal neurodevelopment and behavior obtained by 3D and 4D sonography. J Perinat Med 33:478–490

Salisbury AL, Fallone MD, Lester B (2005) Neurobehavioral assessment from fetus to infant: the NICU Network Neurobehavioral Scale and the Fetal Neurobehavior Coding Scale. Ment Retard Dev Disabil Res Rev 11:14–20

Sepulveda W, Dezerega V, Be C (2004) First-trimester sonographic diagnosis of holoprosencephaly: value of the "butterfly" sign. J Ultrasound Med 23:761–765

Simon EM, Goldstein RB, Coakley FV, Filly RA, Broderick KC, Musci TJ, Barkovich AJ (2000) Fast MR imaging of fetal CNS anomalies in utero. AJNR Am J Neuroradiol 21:1688–1698

Simonazzi G, Segata M, Ghi T, Sandri F, Ancora G, Bernardi B, Tani G, Rizzo N, Santini D, Bonasoni P, Pilu G (2006) Accurate neurosonographic prediction of brain injury in the surviving fetus after the death of a monochorionic cotwin. Ultrasound Obstet Gynecol 27:517–521

Sival DA, Visser GH, Prechtl HF (1992) The effect of intrauterine growth retardation on the quality of general movements in the human fetus. Early Hum Dev 28:119–132

Sonigo P, Elmaleh A, Fermont L, Delezoide AL, Mirlesse V, Brunelle F (1996) Prenatal MRI diagnosis of fetal cerebral tuberous sclerosis. Pediatr Radiol 26:1–4

Sonigo PC, Rypens FF, Carteret M, Delezoide AL, Brunelle FO (1998) MR imaging of fetal cerebral anomalies. Pediatr Radiol 28:212–222

Suchet IB (1994) Schizencephaly: antenatal and postnatal assessment with colour-flow Doppler imaging. Can Assoc Radiol J 45:193–200

Tilea B, Delezoide AL, Khung-Savatovski S, Guimiot F, Vuillard E, Oury JF, Garel C (2007) Comparison between magnetic resonance imaging and fetopathology in the evaluation of fetal posterior fossa non-cystic abnormalities. Ultrasound Obstet Gynecol 29:651–659

Timor-Tritsch IE, Monteagudo A (1996) Transvaginal fetal neurosonography: standardization of the planes and sections by anatomic landmarks. Ultrasound Obstet Gynecol 8:42–47

Timor-Tritsch IE, Monteagudo A (2003) Magnetic resonance imaging versus ultrasound for fetal central nervous system abnormalities. Am J Obstet Gynecol 189:1210–1211

Timor-Tritsch IE, Peisner DB, Raju S (1990) Sonoembryology: an organ-oriented approach using a high-frequency vaginal probe. J Clin Ultrasound 18:286–298

Timor-Tritsch IE, Monteagudo A, Santos R (2008) Three-dimensional inversion rendering in the first- and early second-trimester fetal brain: its use in holoprosencephaly. Ultrasound Obstet Gynecol 32:744–750

Twickler DM, Magee KP, Caire J, Zaretsky M, Fleckenstein JL, Ramus RM (2003) Second-opinion magnetic resonance imaging for suspected fetal central nervous system abnormalities. Am J Obstet Gynecol 188:492–496

Valsky DV, Ben Sira L, Porat S, Yanai N, Lewin A, Nadjari M, Gomori JM, Yagel S (2004) The role of magnetic resonance imaging in the evaluation of isolated mild ventriculomegaly. J Ultrasound Med 23:519–523

van der Knaap MS, Valk J (1988) Classification of congenital abnormalities of the CNS. AJNR Am J Neuroradiol 9: 315–326

Van der Vossen , Pistorius LR, Mulder EJ, Platenkamp M, Stoutenbeek P, Visser GH, Gooskens RH (2009) The role of prenatal ultrasound in predicting survival and mental and motor functioning in children with spina bifida. Ultrasound Obstet Gynecol 34(3):253–258

van Heteren CF, Boekkooi PF, Jongsma HW, Nijhuis JG (2000) Fetal learning and memory. Lancet 356:1169–1170

Vimercati A, Greco P, Vera L, Resta M, Selvaggi L (1999) The diagnostic role of "in utero" magnetic resonance imaging. J Perinat Med 27:303–308

Vinals F, Munoz M, Naveas R, Shalper J, Giuliano A (2005) The fetal cerebellar vermis: anatomy and biometric assessment using volume contrast imaging in the C-plane (VCI-C). Ultrasound Obstet Gynecol 26:622–627

Volpe P, Paladini D, Resta M, Stanziano A, Salvatore M, Quarantelli M, De Robertis V, Buonadonna AL, Caruso G, Gentile M (2006) Characteristics, associations and outcome of partial agenesis of the corpus callosum in the fetus. Ultrasound Obstet Gynecol 27:509–516

Wagenvoort AM, Bekker MN, Go AT, Vandenbussche FP, van Buchem MA, Valk J, van Vugt JM (2000) Ultrafast scan magnetic resonance in prenatal diagnosis. Fetal Diagn Ther 15:364–372

Wald M, Lawrenz K, Deutinger J, Weninger M (2004) Verification of anomalies of the central nervous system

detected by prenatal ultrasound. Ultraschall Med 25: 214–217

Wedegartner U, Tchirikov M, Koch M, Adam G, Schroder H (2002) Functional magnetic resonance imaging (fMRI) for fetal oxygenation during maternal hypoxia: initial results. Rofo 174:700–703

Wedegartner U, Tchirikov M, Schafer S, Priest AN, Kooijman H, Adam G, Schroder HJ (2006) Func-tional MR imaging: comparison of BOLD signal intensity changes in fetal organs with fetal and maternal oxyhemoglobin saturation during hypoxia in sheep. Radiology 238:872–880

Whitby EH, Paley MN, Sprigg A, Rutter S, Davies NP, Wilkinson ID, Griffiths PD (2004) Comparison of ultrasound and magnetic resonance imaging in 100 singleton pregnancies with suspected brain abnormalities. BJOG 111:784–792

Whittingham TA (2007) Medical diagnostic applications and sources. Prog Biophys Mol Biol 93:84–110

Woodward PJ, Sohaey R, Kennedy A, Koeller KK (2005) From the archives of the AFIP: a comprehensive review of fetal tumors with pathologic correlation. Radiographics 25:215–242

Yuh WT, Nguyen HD, Fisher DJ, Tali ET, Gao F, Simonson TM, Kao SC, Weiner CP (1994) MR of fetal central nervous system abnormalities. AJNR Am J Neuroradiol 15:459–464

Zaharchuk G, Busse RF, Rosenthal G, Manley GT, Glenn OA, Dillon WP (2006) Noninvasive oxygen partial pressure measurement of human body fluids in vivo using magnetic resonance imaging. Acad Radiol 13:1016–1024

Zalel Y, Gilboa Y, Gabis L, Ben-Sira L, Hoffman C, Wiener Y, Achiron R (2006) Rotation of the vermis as a cause of enlarged cisterna magna on prenatal imaging. Ultrasound Obstet Gynecol 27:490–493

MRI of the Normal Fetal Lung

Gregor Kasprian

Contents

Abstract

› Perinatal survival crucially depends on a sufficiently sized and functionally well-developed cardiopulmonary system. Especially, the stage of lung development and the biochemical and structural maturity of the fetal lung are the most important determinants for survival and after birth. Since our understanding of the complexity of the processes influencing lung growth has substantially improved, this knowledge can now be translated into clinical science. Fetal MR has opened a new exciting field in the prenatal assessment of lung maturity, since it noninvasively provides important data on the size, structure, and biochemical maturity of the fetal lung. In order to confidently diagnose developmental pathologies of the growing respiratory system and evaluate their impact on extrauterine life, it is of utmost importance to be fully aware of the potential and limitations of new MR imaging methods in the characterization of normal fetal lung development.

1 Normal Fetal Lung Development

As most of the fetal organs, the structure and morphology of the fetal lung change during development. The tissue composition of this organ is variable even at later stages of intrauterine life. This is mirrored by the changing appearance of fetal lung tissue on different MR sequences. Currently, the principles of human fetal lung development are understood and the microscopic

G. Kasprian
Department of Radiology, Medical University of Vienna,
Währinger Gürtel 18-20, 1090 Vienna, Austria
e-mail: gregor.kasprian@meduniwien.ac.at

D. Prayer (ed.), *Fetal MRI*, Medical Radiology,
DOI: 10.1007/174_2010_19, © Springer-Verlag Berlin Heidelberg 2011

appearance of the organ well described. However, since it is impossible to perform correlations between MR and histology in normally developing fetuses, the microstructural background for the MR appearance of the fetal lung is rather hypothetical. Still, by knowing the principles of fetal lung development on a histological and anatomical basis, a reasonable interpretation of fetal MR images and the confident detection of abnormalities are possible. Figure 1 schematically illustrates the overlapping histological stages of fetal lung development and the major changes seen on different MR sequences.

During the first trimester, the developing lung resembles structurally and functionally more an exophytic gland than a parenchymatous organ. By 26 embryonic days, two lung buds bulge out of the ventrolateral wall of the primitive foregut (Burri 1997) and mark the onset of growth of the primordial airways. Shortly after this event, the first vascular structures appear and surround the tubular appearing airways (Hall et al. 2002). By 6 GW, all lobar bronchi are generated and the trachea is coated by a single layer of smooth muscle. The further dividing primordial pathways serve as a template for the accompanying pulmonary vasculature. Besides the early developing pulmonary veins and arteries, the bronchial arteries appear later at 8 GW.

Dichotomous airway branching mainly occurs in the following pseudoglandular stage of lung development between 10 and 14 GW, with all conducting airways developed by 16 GW (Reid 1977; Thurlbeck 1988). At this stage, the fetal lung appears as tubular structure with poorly differentiated cellular lining (Fig. 1).

The processes influencing lung growth during the following canalicular stage substantially determine the postnatal viability of the developing fetus. Structurally, the canalicular stage is characterized by widening of the airway lumina, growth of the respiratory airways, and most importantly, flattening and massive angiogenesis at the future gas-exchanging developing alveolar structures, accompanied by rapid growth of the distal pulmonary vasculature. These structural changes are driven by a variety of factors, of which mechanical forces begin to play an increasingly important role. In the past decades these factors have been identified in several animal studies. Now this knowledge serves as important scientific background for clinical prenatal MR imaging studies, since the canalicular stage is the first stage of lung development, which can be routinely assessed by fetal MR (after 18 GW).

The developmental physiology of the fetal lung in the second trimester, and especially before 24 GW, is dominated by the mechanical effects of permanent

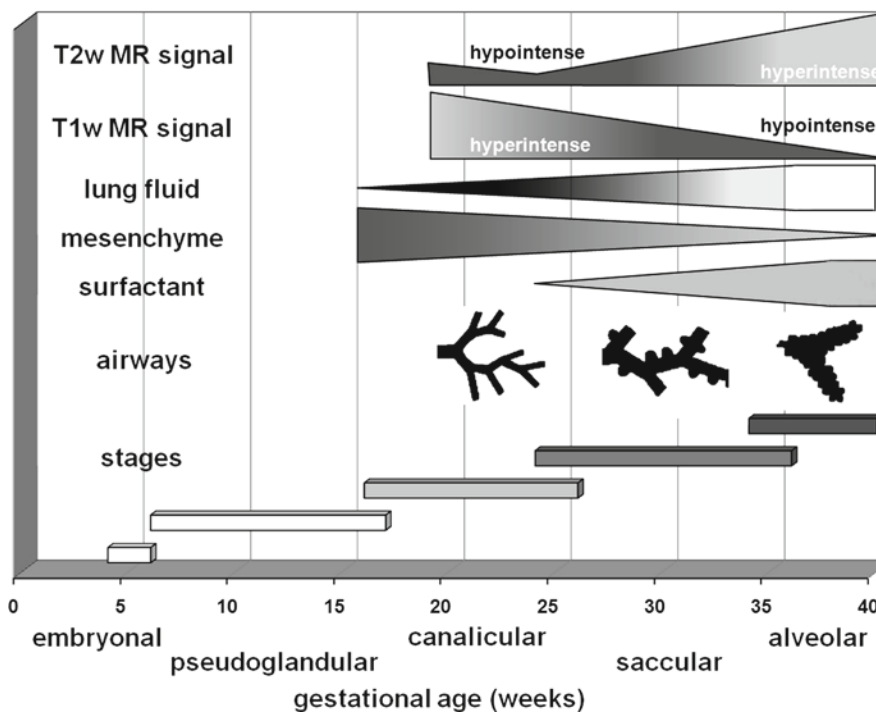

Fig. 1 Schematic illustration of the histologically defined stages of lung development and the major events in fetal lung maturation. The upper rows show the changes of MR signal characteristics on T1- and T2-weighted sequences during development between 18 GW and birth

secretion of lung fluid by the bronchopulmonary epithelium by means of a chloride-dependent transport mechanism (McCray et al. 1992) (Fig. 1). The large amount of lung fluid produced daily (48–100 mL/day), contributing to 30% of amniotic fluid volume (Brace et al. 1994), requires well-regulated clearance mechanisms (Kotecha 2000). The clearance of lung fluid is granted through fetal breathing movements, cyclic contractions of the diaphragm (Harding and Hooper 1996), and phasic contractions of the fetal airways, which are present throughout pregnancy (Schittny et al. 2000) and generated by pacemaker cells in the bronchial smooth muscle (Jesudason et al. 2005). However, lung fluid efflux is limited by a high laryngeal pressure during phases of fetal apnea. According to the long periods of fetal apnea during the second trimester, the retained lung fluid accumulates and builds up a transpulmonary pressure gradient. This mechanical key stimulus induces proliferation and differentiation of alveocytes (Scott et al. 1993) and additionally leads to apoptosis of mesenchymal fibroblasts. Additionally, mechanical stretch on alveocytes (Sanchez-Esteban et al. 2002), mainly induced by the pressure gradient in combination with fetal breathing movements (Inanlou et al. 2005), facilitates later surfactant production and release.

Concordantly with the differentiation of the epithelial lung structures, the pulmonary vasculature forms. The development of the vessel wall of fetal pulmonary arteries, which is twice as thick as in the adult (Hislop and Reid 1973), indirectly controls the high vascular resistance of the pulmonary vasculature during fetal development. The muscle cells of the pulmonary artery muscle layer are derived from three sources – the bronchial smooth muscle during the embryonal stage, the pulmonary mesenchyme during later stages of lung growth, and finally from endothelial cells, whereas the muscular wall of the pulmonary veins is exclusively derived from the pulmonary mesenchyme (Hall et al. 2002).

By 24 GW, the fetal lung has reached a degree of structural maturity, which allows extremely preterm children to survive under intensive respiratory support. As a consequence of the aforementioned complex mechanisms, the terminal airways have further developed, and histologically, the saccular stage of lung development has been reached. Still, the important process of "biochemical" lung maturation has not yet begun. The advanced differentiation of type 2 alveocytes enables their cellular organelles to produce surfactant, which can be readily detected in the amniotic fluid of the majority of fetuses by 30 GW (Odom and Ballard 1997) (Fig. 1).

By 30 GW, the structural development of the fetal lung is by far incomplete, since the first alveolar structures are now appearing (Fig. 1). Alveoles are uniformly present in the lungs at 36 GW (Langston et al. 1984), but continue to increase in number, with over 85% of alveoles formed (Thurlbeck 1982), particularly during the first 2 years (Burri 1997) after birth.

2 MRI of the Developing Fetal Lung

Since the beginning of fetal MR imaging (Smith et al. 1983), the assessment of the maturity and size of the developing respiratory system has been of great interest (Powell et al. 1988). Particularly the advance of ultrafast MR imaging sequences has attracted the scientific and clinical interest in this technique. Nowadays, MR offers a detailed visualization of the thoracic organs irrespective of conditions, which are known to interfere with sonographic image quality, such as maternal obesity, advanced rib ossification, or oligo/anhydramnios. According to the ability to characterize chemical tissue properties, fetal MR gains insights into the biochemical and microstructural maturation of the lung. Further improvements in the acquisition speed of MR sequences and in the correction of motion artifacts by advanced postprocessing methods promise to boost the diagnostic impact of MRI on the perinatal management of fetuses at risk for lethal or life-threatening pulmonary hypoplasia.

2.1 MR Assessment of Fetal Lung Structure

During development, the pulmonary tissue is subject to substantial structural changes. Most notably, the mesenchyme and interstitial tissues between the forming saccules and alveoles undergo apoptotic changes and continuously disappear (Fig. 1). Together with angiogenesis, this leads to an approximation of future air spaces and pulmonary capillaries. Subsequently, the alveolar-capillary barrier thins and guarantees an efficient and sufficient gas exchange after birth.

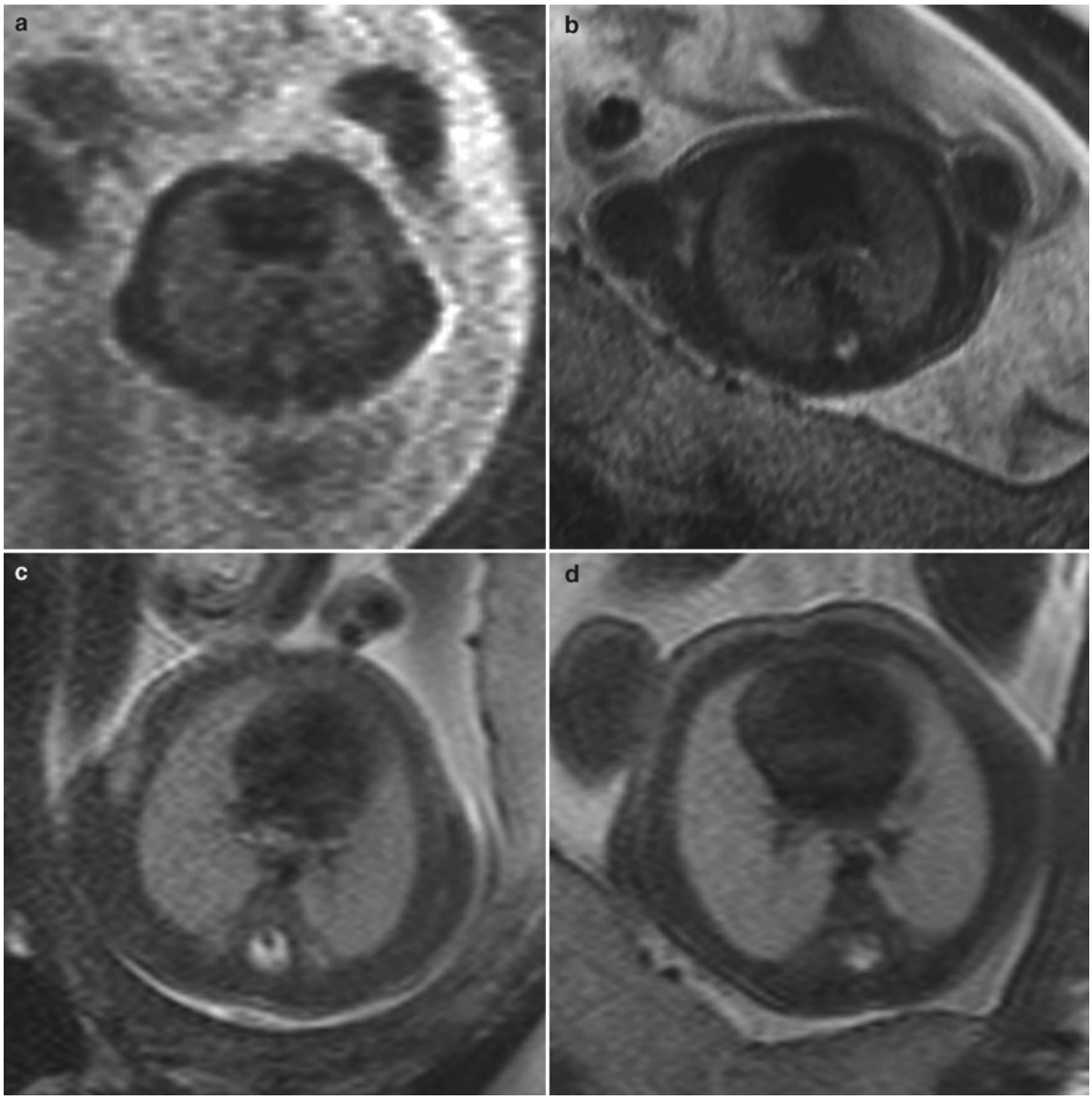

Fig. 2 Axial T2-weighted sequences of the fetal thorax, at the level of the tracheal bifurcation at 15 (**a**), 21 (**b**), 25 (**c**), and 31 (**d**) GW. Note the initial intermediate signal intensity of the fetal lung, decreasing during the canalicular stage with the lowest signal intensity between 19 and 23 GW (**b**). Afterwards, the T2-weighted signal increases substantially

These developmental changes of lung structure can be visualized by ultrasound and MRI. According to the decrease in tissue density, especially during the canalicular and saccular stages of lung development, the sonographic appearance of the fetal lung parallels this process by changes in the lung tissue echogenicity. At 22 and 23 GW, the mean gray value of the fetal lung on T2-weighted and T1-weighted sequences equals that of the fetal liver (Fig. 2). Between 24 and 31 GW, the lungs linearly become darker and less echogenic, and finally, increase in echogenicity in the last weeks before birth (Tekesin et al. 2004). However, no single sonographic feature has been found to significantly correlate with the biochemical maturity of the fetal lung (Cayea et al. 1985).

Since MRI is based on the visualization of magnetic properties of molecules and tissues, particularly those

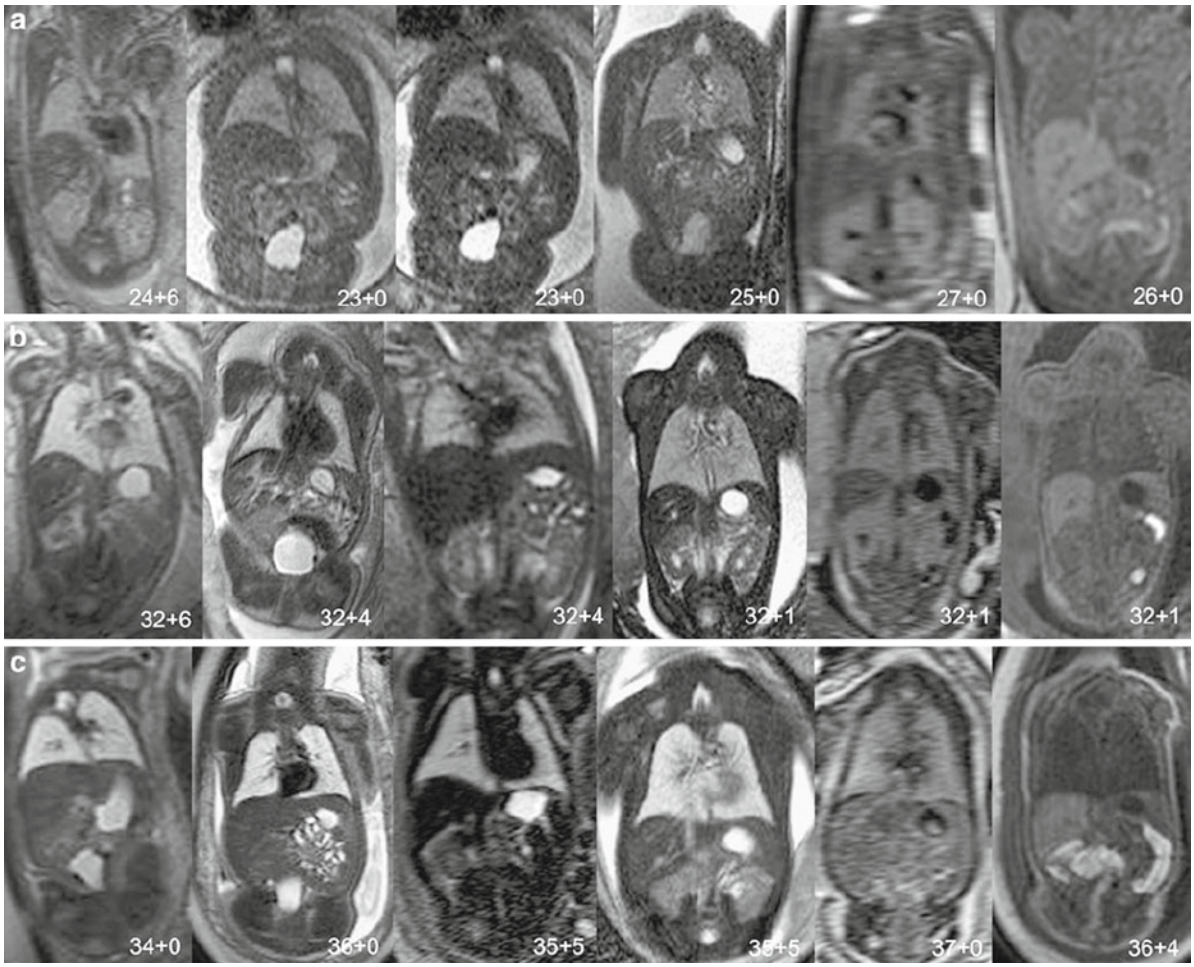

Fig. 3 Image examples of the six evaluated sequences of fetuses of three different age groups: (**a**) 23–26 weeks, (**b**): 32+1–32+ 6 weeks, and (**c**): 34–37 weeks of gestation. The increasing signal intensities on all T2-weighted sequences and on FLAIR and the decreasing signal intensity on T1-weighted sequence are demonstrated during the course of pregnancy. (Copyright Balassy et al. 2007)

rich in protons, it is an ideal tool to gain data on the chemical composition of a certain organ or tissue type. Thus, MR allows us to noninvasively examine the correlates of the aforementioned structural and biochemical developmental processes leading to a functionally mature lung. This is mainly achieved by the use of a variety of different imaging sequences.

Nowadays, the T2-weighted single-shot fast spin echo sequence is the most commonly used MR sequence in the assessment of the fetus in general. Using an optimized field of view and a rapid acquisition (approximately 20 s) by implementing acceleration factors, this sequence can be acquired with a slice thickness of as low as 3 mm in fetuses aged 17 GW and older.

At the beginning of the canalicular stage (17 GW), the fetal lung is visualized by T2-weighted sequences with an intermediate signal intensity, modestly hypointense to amniotic fluid and clearly hyperintense to muscle and to liver (Figs. 2–4). Using T2-weighted sequences, the anatomy of the lungs, grossly showing their characteristic morphological organ shape, the trachea and hilar structures, which are mostly fluid-filled at this stage, are successfully visualized (Figs. 5–7). Occasionally and inconsistently, the fluid-filled esophagus can be seen as well as fluid-filled structure, especially at the level of the hiatus (Fig. 5).

Whereas T1-weighted sequences are less efficient in depicting the pulmonary anatomy, they initially provide

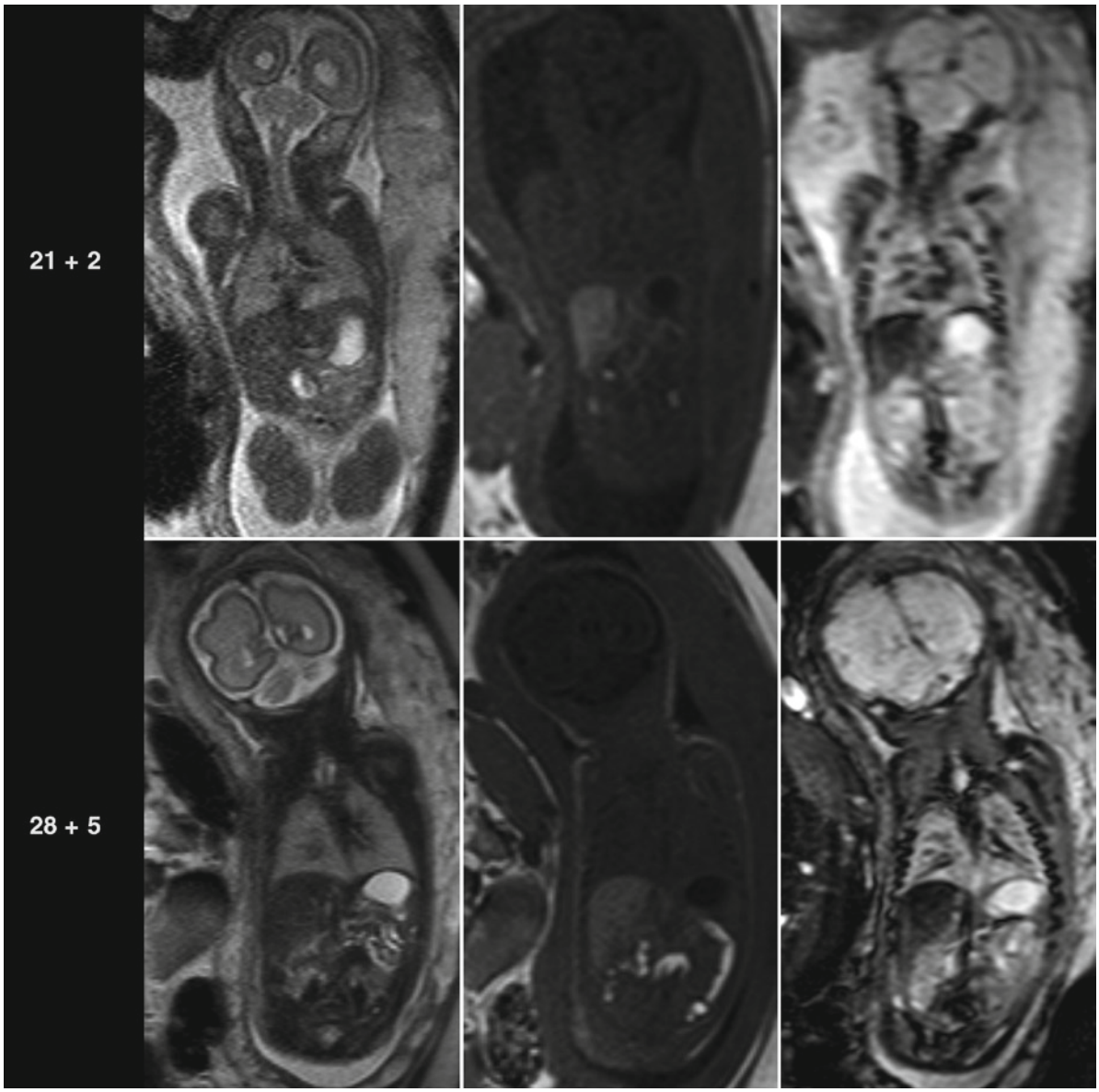

Fig. 4 The changing imaging characteristics of the fetal lung and liver between 21 and 28 GW in a longitudinal study of the same fetus: increase of the lung signal intensity and slight decrease of the liver signal intensity, visible on T2- (*left row*) and less evidently on echo-planar sequences (*right row*). The signal changes occur vice versa on T1-weighted sequences (*middle*)

a stable, intermediate signal intensity of the pulmonary tissue (Figs. 3, 4, and 6). These imaging characteristics may be related to the high amount of protein and lipid rich interstitial mesenchyme and the comparably low amount of free intraluminal lung fluid.

It is commonly accepted that the brightness of the fetal lung parenchyma on T2-weighted sequences increases with gestational age (Duncan et al. 1999a, b; Kuwashima et al. 2001; Levine et al. 2003; Balassy et al. 2004; Keller et al. 2004; Osada et al. 2004; Brewerton et al. 2005). This effect can be detected at different echo times, but its visual perception is greatest using echo times longer than 120 ms (Fig. 2) (Balassy et al. 2007).

In the last decade it was hoped that the properties of FLAIR (long tau inversion recovery) sequences, to attenuate the signal of the unbound water fraction, can be used to evaluate the level of lung maturity and

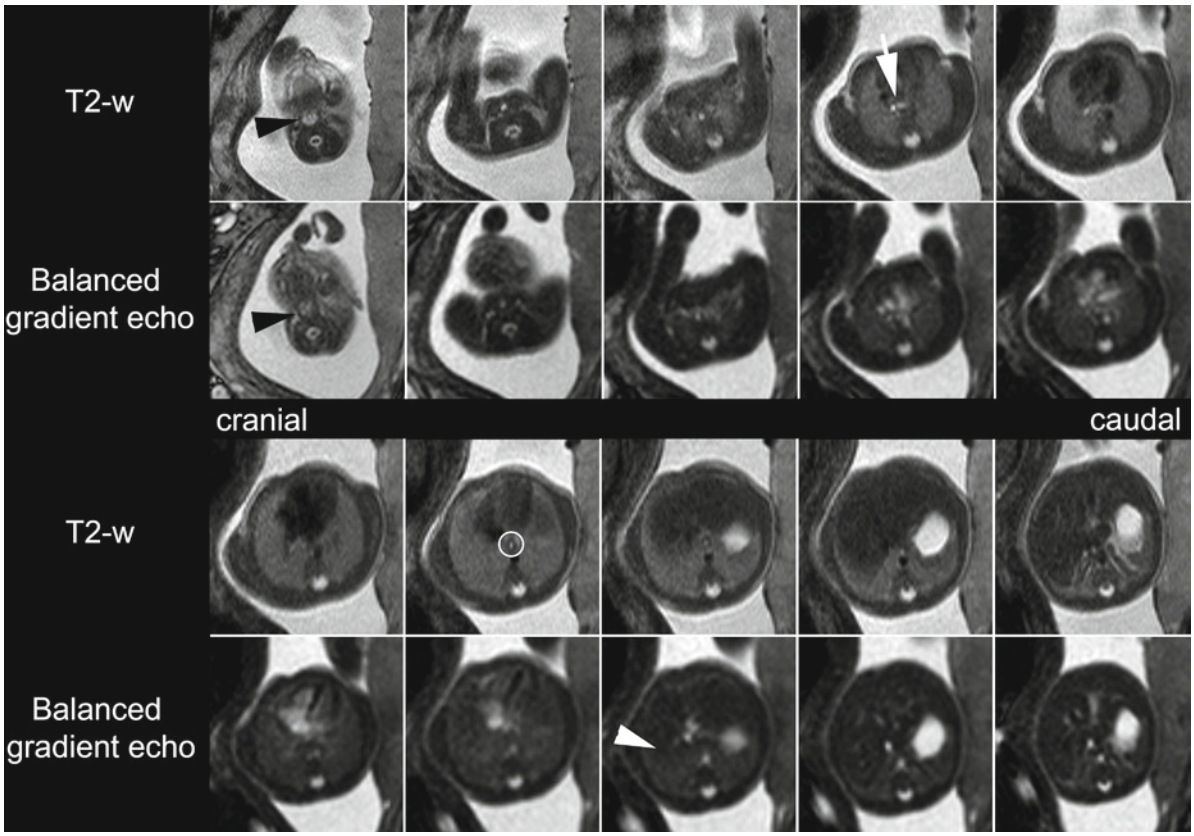

Fig. 5 Comparative scheme of axial T2-weighted and balanced gradient echo sequences in the visualization of the fetal thorax at 21 GW: the fetal respiratory tract is visualized from laryngeal level (*black arrowheads*) to the tracheal bifurcation (*white arrow*) and the fluid-filled main bronchi. The esophagus can be frequently seen on T2-weighted sequences at the level of the hiatus (*circle*). Note the less clear delineation between lung and liver tissue on balanced gradient echo sequences

potentially elaborate the contribution of surfactant to the lung signal. As with T2-weighted sequences, the signal of the lung parenchyma was found to increase (Balassy et al. 2007). Unfortunately, FLAIR imaging is very sensitive to motion and thus often provides artifact degraded data with abnormally high or low lung signals. Additionally, the effect of age-dependent signal increase is less perceptible on these sequences.

T1-weighted sequences can often be successfully acquired during maternal breath hold providing a robust signal, which can be most consistently quantified. It has been concordantly demonstrated that the T1-weighted signal of the fetal lung is declining during the canalicular and saccular stage of lung growth (between 20 and 30 GW, Figs. 3, 4, and 6) (Duncan et al. 1999a, b; Balassy et al. 2007).

Before birth, the fetal lung displays a very characteristic homogenous bright appearance on T2-weighted images and profound hypointensity on T1-weighted sequences.

The physiologic background behind the changing MR signal properties of the growing lung is complex and may not be attributed to a single maturational mechanism. Actually it is appreciated that the MR characteristics of the pulmonary parenchyma relate to a variety of structural and biochemical developmental processes and indirectly reflect the maturational state of the fetal lung (Fig. 1).

Currently, the theoretic concept assumes that the lung signal increase on T2-weighted sequences and decrease on T1 weighted sequences is mainly influenced by the changing amount of lung fluid and the larger fraction of unbound protons at later gestational ages (Sedin et al. 2000). As fetal lung fluid production serves as a key stimulus for lung growth (described above and proven by a MR study in fetal sheep

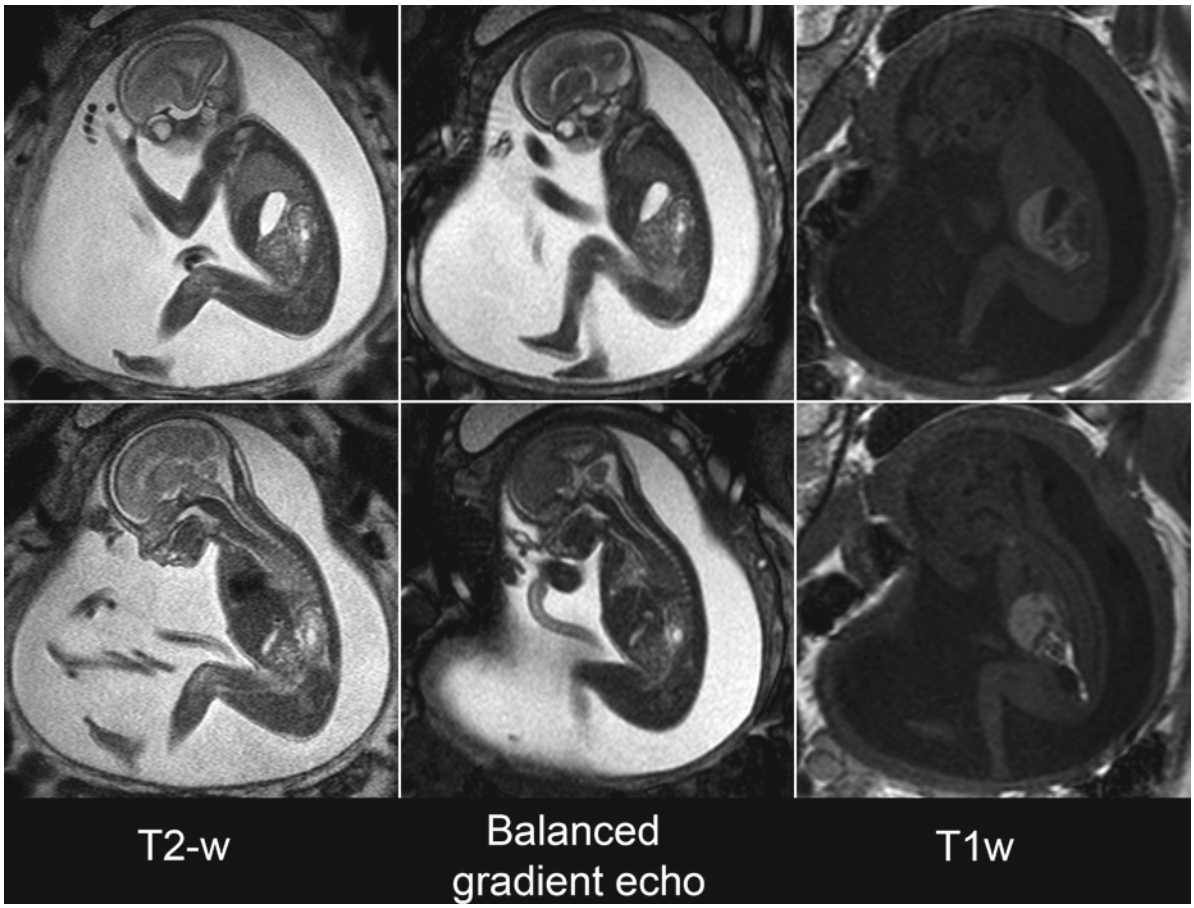

Fig. 6 Parasagittal and median/parasagittal sequences of a fetus aged 21 GW. Note the relations between the signals of the lungs, the fluid-filled stomach, and the liver. At this stage, the trachea can be nicely delineated in its entire course

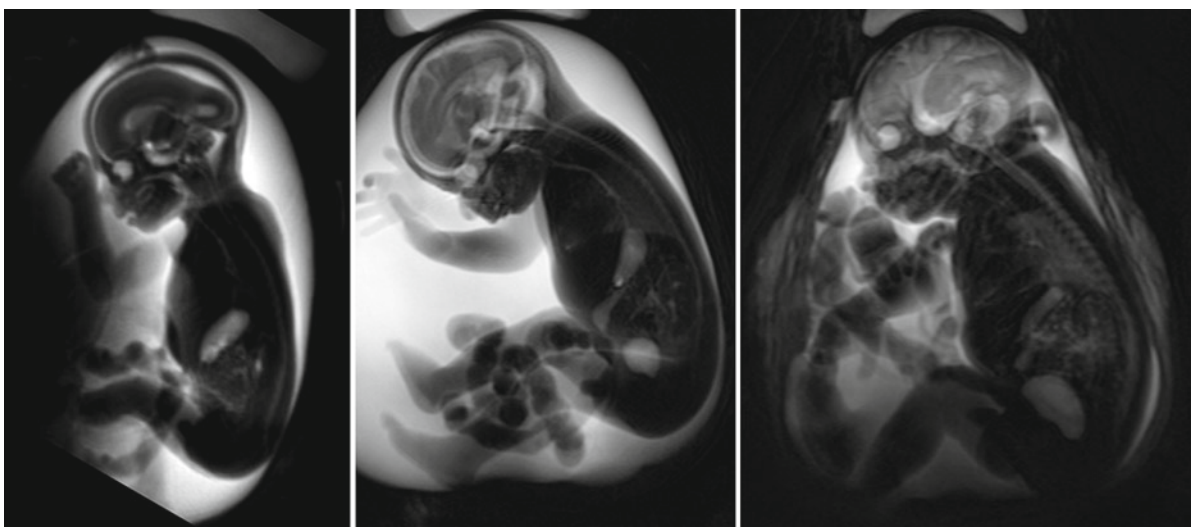

Fig. 7 Sagittal thick slab T2-weighted sequences at 22, 25, and 29 GW: Note the hyperintense depiction of the trachea, especially at early stages of lung development. Moreover, the fetal lungs have increased in signal intensity

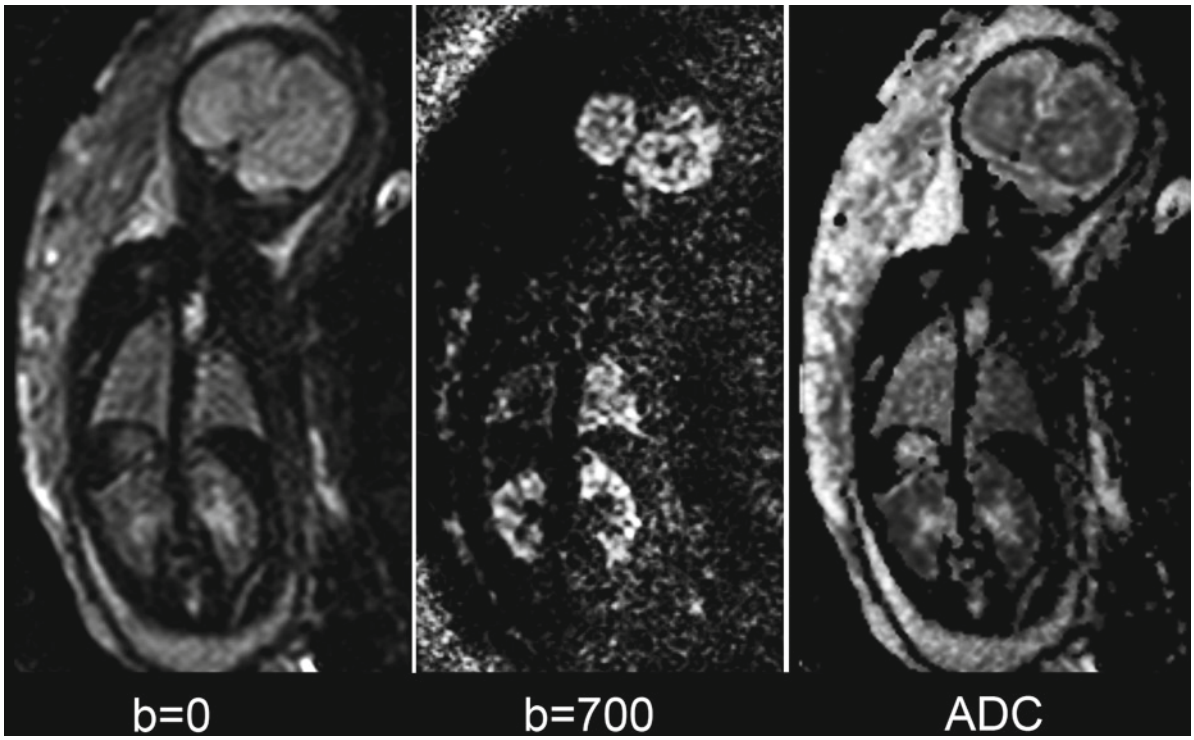

Fig. 8 Coronal diffusion-weighted sequence with *b*-values of 0 and 700 s/mm². The signal characteristics of the fetal lungs on diffusion-weighted images are inconsistent in their developmental appearances as well as in their anatomic variation. Note the low ADC values of the cerebral cortex, the kidneys, and the side differences in ADC and diffusivity values between the right and left lung

(Wedegaertner et al. 2004)), its noninvasive evaluation by fetal MR allows an estimation of the actual growth potential of the fetal lung.

The decreasing amount of interstitial tissue and mesenchyme (Fig. 1) is leading to a lower amount of the overall lipid and protein content of the lung, mirroring the process of alveolar-capillary barrier thinning. This may particularly affect the signal on T1-weighted sequences resulting in a lower signal in structurally more mature lungs (Sedin et al. 2000; Osada et al. 2004; Balassy et al. 2007). Besides microstructural changes, the generation of surfactant after 24 GW may influence the lung signal. According to the chemical composition of surfactant (90% phospholipids and 10% proteins), it affects the MR appearance of the fetal lung parenchyma; however, it is still unclear if its quantity and concentration are high enough to visually contribute to the MR signal of the fetal lung on any of the used sequences.

Vasculogenesis and growth of the distal capillary bed importantly affect the state of maturity of the fetal cardiopulmonary system. Still, the exact impact of these processes on the signal intensity of the fetal lung is not yet known. Basically, the fetal lung remains a low flow, high resistance vascular network throughout pregnancy. By the 20th week of gestation, only 13% of the cardiac output supplies the lung, doubling until 30 GW and then remaining constant (Rasanen et al. 1996).

Recently, diffusion-weighted sequences have also been used to monitor lung maturation (Fig. 8). Some works found a significant linear increase in the apparent diffusion coefficient (ADC) during pregnancy and related this finding mainly to hemodynamic changes and vasculogenesis (Moore et al. 2001, Manganaro et al. 2008). Others did not find any age-dependent changes of lung diffusion parameters, but detected their regional variation as expression of the local heterogeneity of fetal lung tissue (Fig. 8) (Balassy et al. 2008), possibly reflecting the apicobasal gradient of structural lung maturity reported in animal studies (Zeltner et al. 1990) and human fetuses (Laudy and Wladimiroff 2000). Since diffusion-weighted imaging

is highly susceptible to motion, the high variability of diffusion measurements may be explained by technical limitations. Before no more consistent data on this subject are available, diffusion-weighted imaging of the fetal lung remains of theoretical use.

Basically, a variety of developmental processes are contributing to the appearance of the fetal lung on MRI. As yet, not enough animal data are available to confidently link a certain maturational factor to the lung signal changes of the lungs. However, an abnormally low signal on T2-weighted sequences and an abnormally high signal on T1-weighted sequences is always an indicator of abnormal or even immaturity.

2.2 Quantification of Fetal Lung Signal Intensities

Several attempts have been made to quantify the MR signal changes of the fetal lung in order to objectify abnormal signal properties of the fetal lung. After the first relaxation time measurements by Duncan et al. (Duncan et al. 1999a, b) using time- consuming multiecho sequences, more recent studies focused on the quantification of lung signals by direct measurement of the lung signal intensity. Since the absolute SI values showed a high variability, lung signal intensity ratios between lung and liver signals were calculated in order to achieve more stable values (Keller et al. 2004; Osada et al. 2004; Balassy et al. 2007). As hematopoietic organ, the fetal liver does not provide a stable MR signal during the second and third trimester (Balassy et al. 2004; Keller et al. 2004), and therefore, cannot serve as an optimal reference organ. Thus, none of the following studies in larger cohorts and especially in younger fetuses (under 24 GW) was successful in defining age-dependent absolute reference values, which could be clinically used to identify abnormal lung growth (Keller et al. 2004; Osada et al. 2004; Brewerton et al. 2005). Still, several experiences show that the quantification of fetal lung signal intensity increases sensitivity in the detection of pulmonary hypoplasia, especially when combined with fetal lung volumetry (Ikeda et al. 2000; Kuwashima et al. 2001, Kasprian et al. 2006; Balassy et al. 2004; Brewerton et al. 2005). Therefore, future work will aim to develop fast multiecho sequences, which allow the absolute organ-independent lung signal measurement techniques.

2.3 Surfactant Detection by MR Spectroscopy

Surfactant, chemically, is mainly composed of proteins (10%) and phospholipids (90%), including mainly phosphatidylcholine (lecitihin, 70%) and lesser amounts of phosphytidylglycerol, phosphatidylethanolamine, and phosphatidylinositol. So far only invasive testing of the lecithin/sphingomyelin ratio in amniotic fluid samples after amniocentesis could provide in vivo and in utero data on the state of surfactant production and "biochemical" fetal lung maturity (Krieglsteiner et al. 1976). Due to the ability of MR spectroscopy to noninvasively detect and quantify the chemical compounds of fluids and tissues in vivo, the potential of this technique has been realized early (Nelson et al. 1987) and, despite great technical challenges, it is still hoped to be of great value in the assessment of fetal lung maturity.

Using single voxel H^1 spectroscopy, the quantification of surfactant in vivo basically followed two strategies: either the point-resolved spectroscopy (PRESS) box was placed in amniotic fluid pockets or directly in the pulmonary tissue of the fetus (Fenton et al. 2001; Clifton et al. 2006; Kim et al. 2008).

The attempt of detecting surfactant in amniotic fluid has the advantage of being less affected by fetal motion. In earlier ex vivo studies, a broad profile of chemical compounds has been found in amniotic fluid samples, comprising creatinine, glucose, organic acids (acetate, citrate, and lactate), and several amino acids (valine, alanine, histidine, tyrosine, phenylalanine, leucine, and isoleucine) (McGowan et al. 1993; Sims et al. 1993, Nelson et al., 1987). However, according to the low concentrations of choline in amniotic fluid, the possibility of detecting surfactant in vivo at a clinical 1.5 T scanner has been doubted (McGowan et al. 1993; Sims et al. 1993).

A recent 11.5 T ex vivo MR spectroscopy study managed to consistently detect the main compound of surfactant – phosphatidylcholine – in amniotic fluid with the characteristic peak at 3.2 ppm and found a progressive increase in the choline/creatine ratio during the second and third trimester of pregnancy (Clifton et al. 2006). Actually, only sporadic experiences of in utero and in vivo choline detection in amniotic fluid and in the fetal lung at clinical 1.5 T MR scanner are available. They have been successfully performed exclusively in late pregnancy (>35 GW), thus being of almost no clinical use at this developmental stage

(Fenton et al. 2001; Clifton et al. 2006; Kim et al. 2008).

Generally, caution is necessary when interpreting in utero spectroscopy results. Apart from the low signal-to-noise ratio in clinical scanning, the signals arising from the target tissues may be contaminated especially by lipids from maternal or fetal fatty tissue and consequently cause false-positive or -negative results (Kok et al. 2002, Kim, et al 2008). Therefore, clinical in utero spectroscopy is rather a matter of ongoing MR research (particularly at higher field strengths), then a reliable instrument in the assessment of fetal lung maturity.

Although different approaches in the noninvasive assessment of fetal lung maturity are currently under investigation, the subjective assessment of the fetal lung signals on different MR sequences by a physician with experience in fetal MR imaging seems to be the most reliable strategy to assess fetal lung development.

The visual qualitative assessment of the signal intensities of the fetal lung should be part of each fetal MR examination, since it allows a quick and sensitive marker for the detection of pulmonary hypoplasia.

2.4 *Quantification of Fetal Pulmonary Volume*

The postnatal viability of a fetus requires a sufficient surface area of the gas-exchanging alveolar epithelium. Currently, there is no in vivo method available to directly or indirectly assess this parameter. The lung volume of a fetus does not necessarily correlate with the actual potential of pulmonary oxygen uptake, thus its quantification does only allow an estimate of future respiratory outcome. Actually, it constitutes the most important prognostic parameter for postnatal respiratory outcome, measureable by noninvasive prenatal imaging techniques.

As clinical tool, quantification fetal lung volume is essentially feasible in the age period between 17 and 30 GW. Earlier than 17 GW, the organ size is very small and the utility as a prognostic parameter is limited. As pregnancy advances, the fetal lung usually reaches a certain level of microstructural and biochemical maturity, which seems to compensate for a small organ size. This is reflected by the fact that later than 30 GW normal fetal lung volume shows a wide range of individual variability without any major impact on postnatal lung function.

Estimation of fetal lung size is helpful in any condition, where pulmonary hypoplasia must be suspected (see Chap. 27). Both methods – prenatal sonography and fetal MR – technically allow the 2D and 3D assessment of fetal lung size. As the postmortem quantification of the pulmonary volume is hampered by postmortem lung collapse and tissue degradation, it cannot serve as reasonable "gold standard." Therefore, the direct comparison of the accuracy of these methods is hardly possible.

2.4.1 2D Fetal Lung Biometry

2D Biometry is the most timesaving way to assess fetal lung size and has been frequently applied by ultrasound studies in order to detect pulmonary hypoplasia. Sonographic measurements were initially confined to biometry of the fetal thorax, by measuring the thoracic circumference (Thompson and Makowski 1971; Nimrod et al. 1986; Fong et al. 1988; Songster et al. 1989). As the quantification of thoracic circumference includes contribution from all thoracic organs, this method was associated with a low specificity, which could not be improved by determination of the fetal thoracic area and subtraction of the measured heart area (Vintzileos et al. 1989). Finally, it had to be noted that the measurement of chest circumference without any additional diameter of the fetal lung was not sufficiently accurate to predict pulmonary hypoplasia (Merz et al. 1999). Thus, it became clear that the only way to raise the sensitivity and specificity of prenatal biometry methods was to restrict the measurements to the fetal lung and avoid the inclusion of other thoracic organs.

The value of linear 2D measurements of certain diameters of the fetal lung (mostly at the level of the four-chamber view) seems to depend on the etiology of pulmonary hypoplasia. Several studies could show that the lung-to-head ratio (see paragraph CDH) is a quick and useful parameter in predicting lethality of left-sided CDH (Metkus et al. 1996; Sbragia et al. 2000; Jani et al. 2006) and has been used in the inclusion criteria for FETO. Still, the clinical evidence for this tool as independent predictor of outcome in CDH is unclear (Heling et al. 2005; Ba'ath et al. 2007).

In pulmonary hypoplasia secondary to other conditions, such as PROM, hydrothorax, thoracic lesions,

and renal failure, the results of 2D lung biometry (lung length, transverse diameter, and sagittal diameter) are not reliable (Heling et al. 2001; Gerards et al. 2008).

Therefore, and according to the multiplanar capabilities of fetal MR, the examiner should take advantage of the possibility of 3D organ volume quantification and avoid linear measurements in any case or situation where pulmonary hypoplasia is suspected.

2.4.2 Clinical Evidence for Fetal Lung Volumetry as Diagnostic Test

Depending on the indication, the technique of fetal lung volumetry is currently in stage II and III of Gluud and Gluud's four-stage assessment of diagnostic tests (Gluud and Gluud 2005), meaning that normal reference values have been established, but evaluations of the accuracy of the test are still ongoing. Clinical evidence that a method is suitable to predict perinatal survival in certain conditions requires the assessment in all four stages including randomized intervention trials and large cohort studies, which determine the clinical effects of the respective test (stage IV). Due to the traditionally small cohort sizes in fetal MR studies, it will require some time to establish fetal lung volumetry as reliable test for pulmonary hypoplasia in a variety of conditions, although the most recent results in certain pathologies (such as CDH) are promising.

2.4.3 Method of Fetal Lung Volumetry

Background

Recently, several groups reported normal reference values of fetal lung volumes between 18 and 37 GW (Table 1). Except for some specialized prenatal care centers, this method has not been accepted as standard in the detection and quantification of pulmonary hypoplasia. This is mainly due to the complicated and time-consuming postprocessing, as well as the need for the involvement of an examiner, experienced in fetal anatomy and the technique of MR volumetry. Automated, computerized lung volume quantification (Thayyil et al. 2008) would help to overcome some of these problems. Currently, it is difficult to automatically create appropriate masks, which accurately define the organ boundaries and prevent the inclusion of other organs, mainly due to the inhomogeneous signal properties of the fetal lung, which are often overlapping with extrapulmonary structures. Additionally, the changing signal characteristics of the fetal lungs, especially in the condition of hypoplasia, would lead to inconsistent and unreliable results. Therefore, the manual tracing method is actually the only and most reliable tool in the fetal MR biometry of fetal lung volumes. Still, its accuracy and diagnostic value depend on skill and experience of the examiner. This can be easily and quickly achieved, as the anatomy of the fetal lung is visualized in an unequivocal way (Figure 4, 5, 6).

Procedure of Fetal Lung Volumetry

The Sequences

The consistency and validity of MR volumetry data crucially depend on the quality of the image raw data. In case of suspected pulmonary hypoplasia, at least one high-quality MR sequence covering the entire fetal thorax, without evident fetal motion artifacts, must be acquired. Generally, it has been shown that the axial slice orientation offers the most accurate measurement data (Tanigaki et al. 2004; Jani et al. 2005; Ward et al. 2006; Busing et al. 2008). Sagittal and coronal measurement planes are acceptable as well (Ward et al. 2006), but according to their smaller slice number, they may underestimate the total lung volume (Jani et al. 2005; Busing et al. 2008). In order to compare the measured individual data with the fetal lung volumetry reference data available in literature, it has to be acknowledged that the majority of studies chose the axial slice orientation as reference for the volumetry procedure.

Another important factor is the choice of the imaging sequence. Accurate lung volumetry demands a low slice thickness and a small field of view, respecting a reasonable acquisition time to avoid movement artifacts. In literature, two types of sequences are mainly described as a basis for fetal MR volumetry: T2w (single-shot turbo or fast spin echo/HASTE or RARE sequences) and balanced gradient echo (steady-state free precession/true FISP/FIESTA) sequences. In Fig. 5, the differences in the visualization of the fetal

Table 1 Summary of so far published larger MR lung volumetry studies. The different postprocessing and volumetry tools and the sequence characteristics as well as the source (case number) of volumetry data is outlined

Study	Field strength, sequence	Slice thickness (mm)	Matrix/in-plane resolution	Case number	Age range	Method	Time required
Duncan et al. 1999a, b	0.5 T single-shot echo-planar sequence	7	128×128	56, no abnormalities	19 GW-term	n.n.	
Coakley et al. 2000	1.5 T, single-shot RARE	4–6	256×160–256	46, cerebral malformations included	18–32 GW	PACS (Impax; Agfa), free-form region-of-interest tool	30 min
Rypens et al. 2001	1.5 T, T2-weighted fast spin echo	3–5	1.2×1.5 mm in-plane resolution	215, no abnormalities	21–38 GW; (mean: 31GW)	n.n.	10 min
Williams et al. 2004	1.5 T, single-shot rapid acquisition with relaxation enhancement sequence	4–6	256×160–256	91	18–38 GW (mean: 24 GW)	PACS (Impax; Agfa), free-form region-of-interest tool	
Keller et al. 2004	1.5 T, T2w single-shot fast spin-echo imaging	3, 5 gap	256×256	35, normal	22–42 GW; (mean: 31.6±6.5 GW)	Workstation (Unix; Silicon Graphics), segmentation and 3D modeling software (ProVision Version 3.0b; Algotec)	
Ward et al. 2006	1.5 T, T2w single-shot fast spin-echo imaging	4–6	128–256 or 256–512	30, no thoracic abnormalities, body malformations included	17–36 GW	Workstation (Advantage, version 2.0; GE Medical Systems)	48–77 s
Kasprian et al. 2006	1.5 T, T2w single-shot fast spin-echo imaging	3 and 4.4, 0.4 gap	200, 230 or 300; 0.9×0.9 mm in-plane resolution	106, abnormalities included	18–38 GW	ImageJ (NIH, http://rsbweb.nih.gov/ij/)	20 min
Gerards et al. 2007	1.5 T, HASTE sequences	5	1.4×1.4 mm in-plane resolution	10, longitudinal	24–34 GW	n.n	
Cannie et al. 2008	1.5 T, T2w single-shot fast spin-echo imaging	4	173×256; 1.8×1.5 in-plane resolution	200, abnormalities included, twin pregnancy included (n=41)	16–40 GW	PACS (Impax; Agfa), free-form region-of-interest tool	20±4 min

lung are graphically compared. Both have advantages and limitations:

T2w Sequences (Fig. 5) have the advantage to:

(a) Provide an excellent contrast between the high-signal lung tissue and the surrounding structures (particularly, when using long echo times – >120 ms).
(b) Offer an exact delineation between pulmonary tissue and vascular structures at the hilum.
(c) Allow the reliable identification of fetal pulmonary parenchyma even in cases of severe pulmonary hypoplasia and in pathological conditions, where the fetal thoracic anatomy is unclear.

Have the disadvantage to:

(a) Be limited by a rather greater slice thickness. However, a slice thickness between 3 and 4.5 mm should be achieved (Kasprian et al. 2006) and is commonly used in the reference literature (Jani et al. 2005; Cannie et al. 2006; Busing et al. 2008).

Balanced gradient echo sequences (steady-state free precession/true FISP/FIESTA) (Fig. 5) have the advantage to:

(a) Be more robust against motion artifacts.
(b) Offer a smaller slice thickness (consistently 3 mm, see Chap. 29).
(c) Show the anatomy of thoracic blood vessels and the fetal heart in more detail, than T2-w sequences.

and have the disadvantage to

(a) Allow a less distinct delineation of the pulmonary parenchyma, which appears more isointense to the thoracic wall and mediastinal structures. Consequently, they seem to rather underestimate the "real" fetal lung volume (Busing et al. 2008)
(b) Prevent the detailed differentiation between pathological and normal lung tissue (for instance, in cases of congenital cystic adenomatoid malformations –CCAM)

Mainly, the choice of the sequence has to follow practical considerations. Basically, T2-weighted sequences may be currently the most reasonable fetal lung imaging sequence choice, as most of the reference data are based on T2-weighted data. In cases of considerable motion artifacts, balanced gradient echo sequences may be more efficient in providing an artifact-free image dataset, but are limited in the comparison with available reference data. According to the low resolution (large field of view and the longer acquisition times), T1- and T2-FLAIR weighted sequences currently play no role in MR lung volumetry.

In addition to the choice of sequence type, the matrix and slice thickness have to be optimized (see Chap. 29 and Table 1). Currently, a matrix of 256 and a slice thickness between 3 and 5 mm should be achieved.

Almost always occurring motion artifacts substantially limit image data quality, and in certain cases, the use of maternal and fetal sedation constitutes the only possibility to reduce them. As any kind of in utero pharmacological intervention should be used in a restrictive way, other strategies to limit fetal motion have to be exploited. Especially, sequence acquisition using maternal breath hold does not only limit maternal motion, but also reduce fetal breathing movements (Meyberg-Solomayer et al. 2007).

Data Preparation and Measurement Procedure

The postprocessing of fetal imaging data is always a debate of personal habits and individual opinions. There are many software packages (commercially or freely) available (see Table 1) which allow a quantification of body or organ volumes. According to the semiautomated technique, the postprocessing software does not impact the volumetry data quality, but may influence the speed of the postprocessing workflow.

In order to achieve the most reliable results, it is important to rule out movement as a major source of error in fetal lung volumetry (Fig. 9). For obvious reasons, the detection of motion-degraded images should be already performed by the time of sequence acquisition as this may guarantee at least one axial sequence of acceptable quality for volumetry. This mainly applies to artifacts caused by fetal motion, as they are easily detectable.

However, maternal breathing movements may result in significant motion of the fetus in the craniocaudal axis and thereby to the repeated acquisition of one slice position. Especially, while assessing axial images, this bias is difficult to realize. A fast and secure way to prevent this error is the reconstruction of the sequence in the coronal and sagittal plane (Fig. 9). Most of the available image processing software packages provide a multiplanar reconstruction tool, which is easily accessible. The appearance of large "steps" of the fetal thoracic body contour in the reconstructed image may serve as a good indicator of maternal or fetal motion (Fig. 9). In this way, misregistrations of the volumetry data may be avoided and accuracy of the measurements improved.

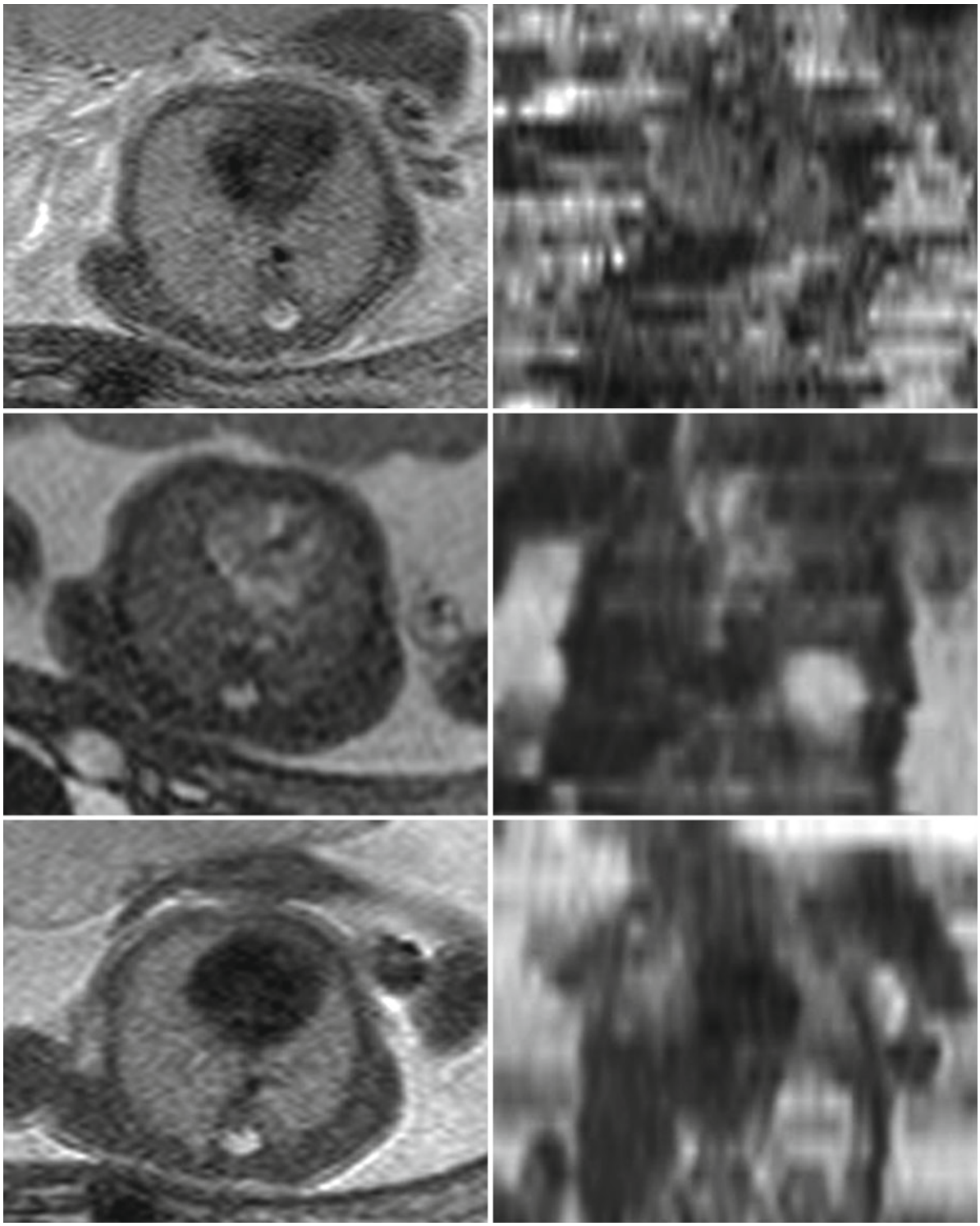

Fig. 9 The problem of fetal motion in fetal lung volumetry: multiplanar reconstruction of the original data sensitively detects fetal and/or maternal motion, even if the in-plane/axial image appears of quite good quality (*upper row*). Repeated acquisition of T2-weighted sequences increases the chance of a nonmotion-degraded dataset with a smooth reconstruction (*lower row*)

Fig. 10 In order to consistently measure the fetal lung volume, the segmentation of the pulmonary parenchyma has to follow certain rules. For instance, the hilar structures have to be avoided

The manual delineation of the pleural contours of the fetal lung is still the most reliable way to segment this organ. The clear delineation of fetal pulmonary tissue may be challenging in certain anatomical regions. In order to compare the volumetry data with the reference literature, the hilar structures (pulmonary vessels, bronchial airways) should be avoided (Fig. 10). Segmentation of the lung base is often challenged by partial volume artifacts (due to the diaphragmatic domes). Additionally, the hyperintense adrenal cortex and retroperitoneal fat make it difficult to differentiate between the bordering tissue types (Fig. 5). A consistent way to measure in this area is important as incorrect segmentation at the lung base causes the greatest error.

2.4.4 Reference Data of Fetal Lung Volumes

Table 1 provides an overview of the currently available reference data of fetal lung volumes. Fig. 11 shows the (quadratic regression) growth curves of three MR studies with a study population over 100 cases (Rypens et al. 2001; Cannie et al. 2006; Kasprian et al. 2006). These studies used comparable methods concerning imaging parameters and postprocessing methods. The major limitation in these studies is the inclusion of fetuses with (mostly) cerebral abnormalities.

In order to apply the volumetry results in the assessment of pulmonary hypoplasia, the volumetry results have to be correlated to a reference, such as gestational age (Rypens et al. 2001; Kasprian et al. 2006) or fetal body volume (Cannie et al. 2008). As total body volume shows the closest correlation with fetal lung volume (Cannie et al. 2008), this additional measurement may be acquired as well. However, total body volume quantification is time-consuming and currently it is not clear if this additional effort has a clinical impact. Nevertheless, especially in conditions in which total body volume is reduced as well (IUGR, syndromes, complex malformations), this approach is beneficial and more sensitive in the detection of lethal pulmonary hypoplasia.

Figure 11 shows a comparison of the mean values of fetal lung volumes between 18 and 38 GW, determined by 3 MR studies (Rypens et al. 2001; Kasprian et al. 2006; Cannie et al. 2008) in at least more than 106 (Kasprian et al. 2006) and a maximum of 215 (Rypens et al. 2001) cases and a overall case number of 521 cases. All studies used a comparable measurement and imaging technique (Table 1) leading to a standard variation between the age-related mean values of overall and between 18 and 32 GW. These data may be used as initial reference data.

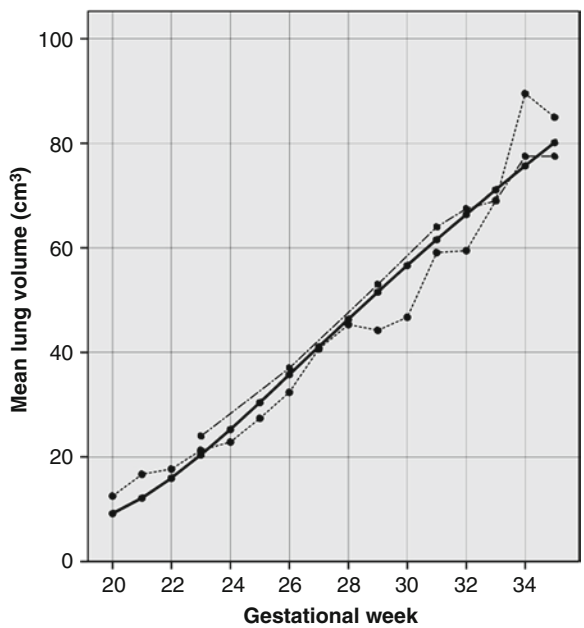

Fig. 11 Summary of the age-related mean values of the pulmonary volumes derived from three MR studies with the largest study population(Cannie et al. (2006, 2008): *line*, Rypens et al. (2001): *semi dashed line*, Kasprian et al. (2006): *dotted line*)

For a number of reasons, the assessment of lung volume as a prognostic determinant of later pulmonary function is especially valuable before 27 GW. First, variations in lung volume can be physiologically compensated more easily after and the functional consequences of a small lung size are more detrimental before this fetal age. Second, the impact of these data on perinatal management is much greater at earlier gestational ages. Third, at 18–27 GW, the anatomical variability of lung size is much less evident compared to older fetuses leading to a lower standard deviation. However, volumetry is generally more inaccurate in small organ sizes leading to a certain examiner-dependent variability.

The diagnostic utility of fetal lung volumetry reference data in different pathologies is discussed in Chap. 26.

3 MR Assessment of Fetal Breathing Movements

Over 120 years ago, Ahlfeld (1888) and Weber (1888) described see-saw movements in the umbilical region of the mother and attributed them to fetal breathing movements. Nowadays, these movements have been widely noticed as early expression of the maturing central nervous system and are frequently used as biological marker of fetal wellbeing (Trudinger et al. 1979). Moreover, they importantly contribute to the structural and biochemical maturation of the fetal lung. In the complete absence of fetal breathing movements, type 2 pneumocytes are unable to compile, store, and release surfactant, and type 1 pneumocytes are unable to flatten and optimize gas exchange (Inanlou et al. 2005).

Using sonography, fetal breathing movements can be observed from 10 GW onwards (de Vries et al. 1982). Initially, fetal breathing movements are observed infrequently (Natale et al. 1988). During second and third trimester development, their incidence, frequency, and pattern change. Before 20 GW, fetal breathing movements are dominated by abdominal movements with typical "see-saw" configurative changes of the fetal trunk, then followed by more extensive chest movements, and finally nasal fluid flow is detected sonographically (Cosmi et al. 2003), constituting the sonographic equivalent of frequent diaphragmatic contractions or the result of contractions of the airway smooth muscle (Badalian et al. 1996). Before 32 GW, the breathing cycle is short and periodic and finally gets more uniform and regular before birth (Trudinger and Knight 1980).

When encountered during fetal MR studies, fetal breathing movements are mostly causing motion artifacts and thereby reducing image quality and the accuracy of fetal lung volumetry. However, using dynamic sequences (Prayer et al. 2006), fetal breathing movements can be visualized during repeated intervals of 200 s of observation/image acquisition time. Since comparably long periods of apnea (14 min (Natale et al. 1988) to 122 min (Rayburn 1995)) have been reported in normal fetuses, the current observational window offered by MRI is too small to allow their conclusive assessment. However, in fetal MR studies complicated by severe fetal motion, the application of dynamic MR sequences adds information on the biophysical state of the fetus. Mainly two types of abnormal fetal breathing movements have been reported in various fetal pathologies: hyperkinetic and hypokinetic movements (de Vries and Fong 2007). Poor/hypokinetic fetal breathing movements seem to be a nonspecific movement pattern encountered in numerous fetal pathologies. Conversely, hyperkinetic breathing motion with high-speed, large amplitudes may be a more specific phenomenon as it has been observed in tracheal atresia (Baarsma et al. 1993).

Although the importance of fetal MR in monitoring fetal breathing movements is definitely limited by the short observation time, the dynamic MR examination of the fetus offers insights into the fetal breathing pattern, which may be used in the holistic assessment of fetal abnormalities.

References

Ahlfeld F (1888) Über bisher noch nicht beschriebene intrauterine Bewegungen des Kindes. Verhandlungen der Deutschen Gesellschaft für Gynäkologie, 2. Versammlung, Halle

Ba'ath ME, Jesudason EC, Losty PD (2007) How useful is the lung-to-head ratio in predicting outcome in the fetus with congenital diaphragmatic hernia? A systematic review and meta-analysis. Ultrasound Obstet Gynecol 30:897–906

Baarsma R, Bekedam DJ, Visser GH (1993) Qualitative abnormal fetal breathing movements, associated with tracheal atresia. Early Hum Dev 32:63–69

Badalian SS, Fox HE, Zimmer EZ, Fifer WP, Stark RI (1996) Patterns of perinasal fluid flow and contractions of the diaphragm in the human fetus. Ultrasound Obstet Gynecol 8:109–113

Balassy C, Brugger PC, Csapo B, Mittermayer C, Kasprian G, Prayer D (2004) In vivo investigation of fetal lung maturation with MRI. Eur Radiol 14:220–221

Balassy C, Kasprian G, Brugger PC, Weber M, Csapo B, Mittermayer C, Hormann M, Prayer D (2007) MRI investigation of normal fetal lung maturation using signal intensities on different imaging sequences. Eur Radiol 17:835–842

Balassy C, Kasprian G, Brugger PC, Csapo B, Weber M, Hormann M, Bankier A, Bammer R, Herold CJ, Prayer D (2008) Diffusion-weighted MR imaging of the normal fetal lung. Eur Radiol 18:700–706

Brace RA, Wlodek ME, Cock ML, Harding R (1994) Swallowing of lung liquid and amniotic fluid by the ovine fetus under normoxic and hypoxic conditions. Am J Obstet Gynecol 171:764–770

Brewerton LJ, Chari RS, Liang Y, Bhargava R (2005) Fetal lung-to-liver signal intensity ratio at MR imaging: development of a normal scale and possible role in predicting pulmonary hypoplasia in utero. Radiology 235:1005–1010. Epub 2005 Apr 1021

Burri PH (1997) Structural Aspects of Prenatal and Postnatal Development and Growth of the Lung. In: McDonald JA (ed) Lung growth and development. Marcel Dekker, New York, pp 1–35

Busing KA, Kilian AK, Schaible T, Debus A, Weiss C, Neff KW (2008) Reliability and validity of MR image lung volume measurement in fetuses with congenital diaphragmatic hernia and in vitro lung models. Radiology 246:553–561

Cannie M, Jani JC, De Keyzer F, Devlieger R, Van Schoubroeck D, Witters I, Marchal G, Dymarkowski S, Deprest JA (2006) Fetal body volume: use at MR imaging to quantify relative lung volume in fetuses suspected of having pulmonary hypoplasia. Radiology 241:847–853

Cannie MM, Jani JC, Van Kerkhove F, Meerschaert J, De Keyzer F, Lewi L, Deprest JA, Dymarkowski S (2008) Fetal body volume at MR imaging to quantify total fetal lung volume: normal ranges. Radiology 247:197–203

Cayea PD, Grant DC, Doubilet PM, Jones TB (1985) Prediction of fetal lung maturity: inaccuracy of study using conventional ultrasound instruments. Radiology 155:473–475

Clifton MS, Joe BN, Zektzer AS, Kurhanewicz J, Vigneron DB, Coakley FV, Nobuhara KK, Swanson MG (2006) Feasibility of magnetic resonance spectroscopy for evaluating fetal lung maturity. J Pediatr Surg 41:768–773

Coakley FV, Lopoo JB, Lu Y, Hricak H, Albanese CT, Harrison MR, Filly RA (2000) Normal and hypoplastic fetal lungs: volumetric assessment with prenatal single-shot rapid acquisition with relaxation enhancement MR imaging. Radiology 216:107–111

Cosmi EV, Anceschi MM, Cosmi E, Piazze JJ, La Torre R (2003) Ultrasonographic patterns of fetal breathing movements in normal pregnancy. Int J Gynaecol Obstet 80:285–290

de Vries JI, Fong BF (2007) Changes in fetal motility as a result of congenital disorders: an overview. Ultrasound Obstet Gynecol 29:590–599

de Vries JI, Visser GH, Prechtl HF (1982) The emergence of fetal behaviour. I. Qualitative aspects. Early Hum Dev 7:301–322

Duncan KR, Gowland PA, Freeman A, Moore R, Baker PN, Johnson IR (1999a) The changes in magnetic resonance properties of the fetal lungs: a first result and a potential tool for the non-invasive in utero demonstration of fetal lung maturation. Br J Obstet Gynaecol 106:122–125

Duncan KR, Gowland PA, Moore RJ, Baker PN, Johnson IR (1999b) Assessment of fetal lung growth in utero with echo-planar MR imaging. Radiology 210:197–200

Fenton BW, Lin CS, Macedonia C, Schellinger D, Ascher S (2001) The fetus at term: in utero volume-selected proton MR spectroscopy with a breath-hold technique–a feasibility study. Radiology 219:563–566

Fong K, Ohlsson A, Zalev A (1988) Fetal thoracic circumference: a prospective cross-sectional study with real-time ultrasound. Am J Obstet Gynecol 158:1154–1160

Gerards FA, Twisk JW, Bakker M, Barkhof F, van Vugt JM (2007) Fetal lung volume: three-dimensional ultrasonography compared with magnetic resonance imaging. Ultrasound Obstet Gynecol 29:533–536

Gerards FA, Twisk JW, Fetter WP, Wijnaendts LC, van Vugt JM (2008) Predicting pulmonary hypoplasia with 2- or 3-dimensional ultrasonography in complicated pregnancies. Am J Obstet Gynecol 198(140):e141–e146

Gluud C, Gluud LL (2005) Evidence based diagnostics. BMJ 330:724–726

Hall SM, Hislop AA, Haworth SG (2002) Origin, differentiation, and maturation of human pulmonary veins. Am J Respir Cell Mol Biol 26:333–340

Harding R, Hooper SB (1996) Regulation of lung expansion and lung growth before birth. J Appl Physiol 81:209–224

Heling KS, Tennstedt C, Chaoui R, Kalache KD, Hartung J, Bollmann R (2001) Reliability of prenatal sonographic lung biometry in the diagnosis of pulmonary hypoplasia. Prenat Diagn 21:649–657

Heling KS, Wauer RR, Hammer H, Bollmann R, Chaoui R (2005) Reliability of the lung-to-head ratio in predicting outcome and neonatal ventilation parameters in fetuses with congenital diaphragmatic hernia. Ultrasound Obstet Gynecol 25:112–118

Hislop A, Reid L (1973) Lung development in relation to gas exchange capacity. Bull Physiopathol Respir (Nancy) 9:1317–1343

Ikeda K, Hokuto I, Mori K, Hayashida S, Tokieda K, Tanigaki S, Tanaka M, Yuasa Y (2000) Intrauterine MRI with single-shot fast-spin echo imaging showed different signal intensities in hypoplastic lungs. J Perinat Med 28:151–154

Inanlou MR, Baguma-Nibasheka M, Kablar B (2005) The role of fetal breathing-like movements in lung organogenesis. Histol Histopathol 20:1261–1266

Jani J, Breysem L, Maes F, Boulvain M, Roubliova X, Lewi L, Vaast P, Biard JM, Cannie M, Deprest J (2005) Accuracy of magnetic resonance imaging for measuring fetal sheep lungs and other organs. Ultrasound Obstet Gynecol 25:270–276

Jani J, Keller RL, Benachi A, Nicolaides KH, Favre R, Gratacos E, Laudy J, Eisenberg V, Eggink A, Vaast P, Deprest J (2006) Prenatal prediction of survival in isolated left-sided diaphragmatic hernia. Ultrasound Obstet Gynecol 27:18–22

Jesudason EC, Smith NP, Connell MG, Spiller DG, White MR, Fernig DG, Losty PD (2005) Developing rat lung has a sided pacemaker region for morphogenesis-related airway peristalsis. Am J Respir Cell Mol Biol 32:118–127. Epub 2004 Dec 2002

Kasprian G, Balassy C, Brugger PC, Prayer D (2006) MRI of normal and pathological fetal lung development. Eur J Radiol 57:261–270

Keller TM, Rake A, Michel SC, Seifert B, Wisser J, Marincek B, Kubik-Huch RA (2004) MR assessment of fetal lung

development using lung volumes and signal intensities. Eur Radiol 14:984–989. Epub 2004 Mar 2011

Kim DH, Vahidi K, Caughey AB, Coakley FV, Vigneron DB, Kurhanewicz J, Mow B, Joe BN (2008) In vivo (1)H magnetic resonance spectroscopy of amniotic fluid and fetal lung at 1.5 T: technical challenges. J Magn Reson Imaging 28: 1033–1038

Kok RD, van den Berg PP, van den Bergh AJ, Nijland R, Heerschap A (2002) MR spectroscopy in the human fetus. Radiology 223:584; author reply 584–585

Kotecha S (2000) Lung growth for beginners. Paediatr Respir Rev 1:308–313

Krieglsteiner P, Schneider R, Kopcke H, Tolle W, Johannigmann J, Blumel G (1976) Prenatal prediction of respiratory distress syndrome. Measurement of surface properties and Lecithin/Sphingomyelin ratio in human amniotic fluid. J Perinat Med 4:261–270

Kuwashima S, Nishimura G, Iimura F, Kohno T, Watanabe H, Kohno A, Fujioka M (2001) Low-intensity fetal lungs on MRI may suggest the diagnosis of pulmonary hypoplasia. Pediatr Radiol 31:669–672

Langston C, Kida K, Reed M, Thurlbeck WM (1984) Human lung growth in late gestation and in the neonate. Am Rev Respir Dis 129:607–613

Laudy JA, Wladimiroff JW (2000) The fetal lung. 1: Developmental aspects. Ultrasound Obstet Gynecol 16:284–290

Levine D, Barnewolt CE, Mehta TS, Trop I, Estroff J, Wong G (2003) Fetal thoracic abnormalities: MR imaging. Radiology 228:379–388. Epub 2003 Jun 23

Manganaro L, Perrone A, Sassi S, Fierro F, Savelli S, Di Maurizio M, Tomei A, Francioso A, La Barbera L, Giancotti A, Ballesio L (2008) Diffusion-weighted MR imaging and apparent diffusion coefficient of the normal fetal lung: preliminary experience. Prenat Diagn 28: 745–748

McCray PB Jr, Bettencourt JD, Bastacky J (1992) Developing bronchopulmonary epithelium of the human fetus secretes fluid. Am J Physiol 262:L270–L279

McGowan PE, Reglinski J, Wilson R, Walker JJ, Wisdoms S, McKillop JH (1993) Quantitative 1H-NMR analysis of amniotic fluid. J Pharm Biomed Anal 11:629–632

Merz E, Miric-Tesanic D, Bahlmann F, Weber G, Hallermann C (1999) Prenatal sonographic chest and lung measurements for predicting severe pulmonary hypoplasia. Prenat Diagn 19:614–619

Metkus AP, Filly RA, Stringer MD, Harrison MR, Adzick NS (1996) Sonographic predictors of survival in fetal diaphragmatic hernia. J Pediatr Surg 31:148–151; discussion 151–142

Meyberg-Solomayer GC, Wallwiener D, Solomayer E (2007) Maternal breath-holding and the valsalva maneuver: methods to overcome fetal breathing movements during Doppler sonography. Ultrasound Med Biol 33:1586–1591

Moore RJ, Strachan B, Tyler DJ, Baker PN, Gowland PA (2001) In vivo diffusion measurements as an indication of fetal lung maturation using echo planar imaging at 0.5T. Magn Reson Med 45:247–253

Natale R, Nasello-Paterson C, Connors G (1988) Patterns of fetal breathing activity in the human fetus at 24 to 28 weeks of gestation. Am J Obstet Gynecol 158:317–321

Nelson TR, Gillies RJ, Powell DA, Schrader MC, Manchester DK, Pretorius DH (1987) High resolution proton NMR spectroscopy of human amniotic fluid. Prenat Diagn 7: 363–372

Nimrod C, Davies D, Iwanicki S, Harder J, Persaud D, Nicholson S (1986) Ultrasound prediction of pulmonary hypoplasia. Obstet Gynecol 68:495–498

Odom MW, Ballard PL (1997) Developmental and hormonal regulation of the surfactant system. In: McDonald JA (ed) Lung growth and development. Marcel Dekker, New York, pp 495–575

Osada H, Kaku K, Masuda K, Iitsuka Y, Seki K, Sekiya S (2004) Quantitative and qualitative evaluations of fetal lung with MR imaging. Radiology 231:887–892. Epub 2004 Apr 2029

Powell MC, Worthington BS, Buckley JM, Symonds EM (1988) Magnetic resonance imaging (MRI) in obstetrics. II. Fetal anatomy. Br J Obstet Gynaecol 95:38–46

Prayer D, Kasprian G, Krampl E, Ulm B, Witzani L, Prayer L, Brugger PC (2006) MRI of normal fetal brain development. Eur J Radiol 57:199–216

Rasanen J, Wood DC, Weiner S, Ludomirski A, Huhta JC (1996) Role of the pulmonary circulation in the distribution of human fetal cardiac output during the second half of pregnancy. Circulation 94:1068–1073

Rayburn WF (1995) Fetal movement monitoring. Clin Obstet Gynecol 38:59–67

Reid L (1977) 1976 Edward B.D. Neuhauser lecture: the lung: growth and remodeling in health and disease. AJR Am J Roentgenol 129:777–788

Rypens F, Metens T, Rocourt N, Sonigo P, Brunelle F, Quere MP, Guibaud L, Maugey-Laulom B, Durand C, Avni FE, Eurin D (2001) Fetal lung volume: estimation at MR imaging-initial results. Radiology 219:236–241

Sanchez-Esteban J, Wang Y, Cicchiello LA, Rubin LP (2002) Cyclic mechanical stretch inhibits cell proliferation and induces apoptosis in fetal rat lung fibroblasts. Am J Physiol Lung Cell Mol Physiol 282:L448–L456

Sbragia L, Paek BW, Filly RA, Harrison MR, Farrell JA, Farmer DL, Albanese CT (2000) Congenital diaphragmatic hernia without herniation of the liver: does the lung-to-head ratio predict survival? J Ultrasound Med 19:845–848

Schittny JC, Miserocchi G, Sparrow MP (2000) Spontaneous peristaltic airway contractions propel lung liquid through the bronchial tree of intact and fetal lung explants. Am J Respir Cell Mol Biol 23:11–18

Scott JE, Yang SY, Stanik E, Anderson JE (1993) Influence of strain on [3H]thymidine incorporation, surfactant-related phospholipid synthesis, and cAMP levels in fetal type II alveolar cells. Am J Respir Cell Mol Biol 8:258–265

Sedin G, Bogner P, Berenyi E, Repa I, Nyul Z, Sulyok E (2000) Lung water and proton magnetic resonance relaxation in preterm and term rabbit pups: their relation to tissue hyaluronan. Pediatr Res 48:554–559

Sims CJ, Fujito DT, Burholt DR, Dadok J, Giles HR, Wilkinson DA (1993) Quantification of human amniotic fluid constituents by high resolution proton nuclear magnetic resonance (NMR) spectroscopy. Prenat Diagn 13:473–480

Smith FW, Adam AH, Phillips WD (1983) NMR imaging in pregnancy. Lancet 1:61–62

Songster GS, Gray DL, Crane JP (1989) Prenatal prediction of lethal pulmonary hypoplasia using ultrasonic fetal chest circumference. Obstet Gynecol 73:261–266

Tanigaki S, Miyakoshi K, Tanaka M, Hattori Y, Matsumoto T, Ueno K, Uehara K, Nishimura O, Minegishi K, Ishimoto H, Shinmoto H, Ikeda K, Yoshimura Y (2004) Pulmonary hypoplasia: prediction with use of ratio of MR imaging-measured

fetal lung volume to US-estimated fetal body weight. Radiology 232:767–772

Tekesin I, Anderer G, Hellmeyer L, Stein W, Kuhnert M, Schmidt S (2004) Assessment of fetal lung development by quantitative ultrasonic tissue characterization: a methodical study. Prenat Diagn 24:671–676

Thayyil S, Schievano S, Robertson NJ, Jones R, Chitty LS, Sebire NJ, Taylor AM (2008) A semi-automated method for non-invasive internal organ weight estimation by post-mortem magnetic resonance imaging in fetuses, newborns and children. Eur J Radiol 72:321–326

Thompson HE, Makowski EL (1971) Estimation of birth weight and gestational age. Obstet Gynecol 37:44–47

Thurlbeck WM (1982) Postnatal human lung growth. Thorax 37:564–571

Thurlbeck WM (1988) Lung growth. In: Thurlbeck WM (ed) Pathology of the lung. Georg Thieme, Stuttgart, pp 1–10

Trudinger BJ, Knight PC (1980) Fetal age and patterns of human fetal breathing movements. Am J Obstet Gynecol 137: 724–728

Trudinger BJ, Gordon YB, Grudzinskas JG, Hull MG, Lewis PJ, Arrans ME (1979) Fetal breathing movements and other tests of fetal wellbeing: a comparative evaluation. Br Med J 2:577–579

Vintzileos AM, Campbell WA, Rodis JF, Nochimson DJ, Pinette MG, Petrikovsky BM (1989) Comparison of six different ultrasonographic methods for predicting lethal fetal pulmonary hypoplasia. Am J Obstet Gynecol 161: 606–612

Ward VL, Nishino M, Hatabu H, Estroff JA, Barnewolt CE, Feldman HA, Levine D (2006) Fetal lung volume measurements: determination with MR imaging–effect of various factors. Radiology 240:187–193

Weber H (1888) Über physiologische Atmungsbewegungen des Kindes im Uterus. Thesis. Marburg/Lahn, University of Marburg

Wedegaertner U, Tchirikov M, Habermann C, Hecher K, Deprest J, Adam G, Schroeder HJ (2004) Fetal sheep with tracheal occlusion: monitoring lung development with MR imaging and B-mode US. Radiology 230:353–358. Epub 2003 Dec 2029

Williams G, Coakley FV, Qayyum A, Farmer DL, Joe BN, Filly RA (2004) Fetal relative lung volume: quantification by using prenatal MR imaging lung volumetry. Radiology 233:457–462. Epub 2004 Sep 30

Zeltner TB, Bertacchini M, Messerli A, Burri PH (1990) Morphometric estimation of regional differences in the rat lung. Exp Lung Res 16:145–158

The Skeleton and Musculature

Stefan F. Nemec, Peter C. Brugger, Gregor Kasprian, Ursula Nemec, John M. Graham Jr., and Daniela Prayer

Contents

Abstract

› Based upon innovations in sequence technology, initial results demonstrate the ability of prenatal magnetic resonance imaging (MRI) to visualize the skeleton and muscles. Serving as an adjunct to ultrasonography (US), MRI may be useful in differentiating isolated from complex musculoskeletal abnormalities with potential impact on perinatal management.

1 Introduction

Fetal magnetic resonance imaging (MRI) has become an increasingly used prenatal imaging method that can depict the whole fetus between the 18th gestational week (GW) and term and serves as an adjunct to ultrasound (US) in prenatal diagnosis (Garel 2008a, b; Prayer and Brugger 2007). Several studies underlined the advantages of MRI in demonstrating defects of the brain, lungs, complex syndromes, and conditions associated with reduction of amniotic fluid (Coakley et al. 2004; Glenn and Barkovich 2006a, b; Prayer and Brugger 2007).

However, until now, there is almost no literature describing the use of MRI for the diagnosis of fetal musculoskeletal abnormalities except for a few single reported cases (Applegate 2004). This chapter will demonstrate the preliminary results in the visualization of the musculoskeletal system, in utero, with fetal MRI, reflecting the authors' experience with this subject over the last 5 years. The imaging techniques are described and the potential impact of a prenatal MRI diagnosis is outlined.

S.F. Nemec (✉), G. Kasprian, U. Nemec, and D. Prayer
Department of Radiology/Division of Neuroradiology and Musculoskeletal Radiology, Medical University Vienna, Waehringer Guertel 18–20, A-1090 Vienna, Austria
e-mail: stefan.nemec@meduniwien.ac.at; daniela.prayer@meduniwien.ac.at

P.C. Brugger
Center of Anatomy and Cell Biology, Integrative Morphology Group, Medical University Vienna, Waehringerstrasse 13, A-1090 Vienna, Austria
e-mail: peter.brugger@meduniwien.ac.at

J.M. Graham Jr.
Medical Genetics Institute, Cedars Sinai Medical Center, 8700 Beverly Boulevard, PACT Suite 400, Los Angeles, CA 90048, USA

D. Prayer (ed.), *Fetal MRI*, Medical Radiology,
DOI: 10.1007/174_2010_58, © Springer-Verlag Berlin Heidelberg 2011

2 Imaging

2.1 General Aspects

In addition to T2-weighted (w) sequences depicting fetal anatomy and pathology at all gestational ages, additional imaging techniques such as echo planar imaging (EPI), thick-slab T2-w sequences, and dynamic steady-state free precession (SSFP) sequences are crucial in the visualization of the developing musculoskeletal system.

2.2 Echo Planar Imaging (EPI)

Fetal MRI has been described as "virtually blind to bones" (Brunelle 2001). This might be true for "conventional" T2-w sequences. In the meantime, EP sequences are available, allowing delineation of bony structures dependent on fetal age (Brugger et al. 2006). EP sequences are currently the only ones to depict the fetal skeleton with MRI before 27GW, as they demonstrate bone as hypointense structures and delineate the hyperintense cartilaginous epiphyses (Figs. 1 and 2). EPI provides a pronounced distinction between the bones and the adjacent muscles (Fig. 3). EPI overcomes motional artifacts found at conventional MRI by acquiring images in milliseconds (Mansfield et al. 1990). Otherwise, a low spatial resolution represents a limitation of these EP sequences.

2.3 Thick-Slab T2-w Sequences

Thick-slab T2-w images offer a global overview of fetal anatomy and pathology by generating a three-dimensional (3D) impression of the fetus (Brugger et al. 2006). Due to the large view-of-field the entire fetus can be visualized, even in the third trimester. Fetal proportions are more readily recognized, and defects can be captured in one image. This technique is useful in those fetuses in which an overall morphological impression is beneficial in the perception of fetal anomalies (e.g., fetal proportions, extremities, and arthrogryphosis) (Fig. 4).

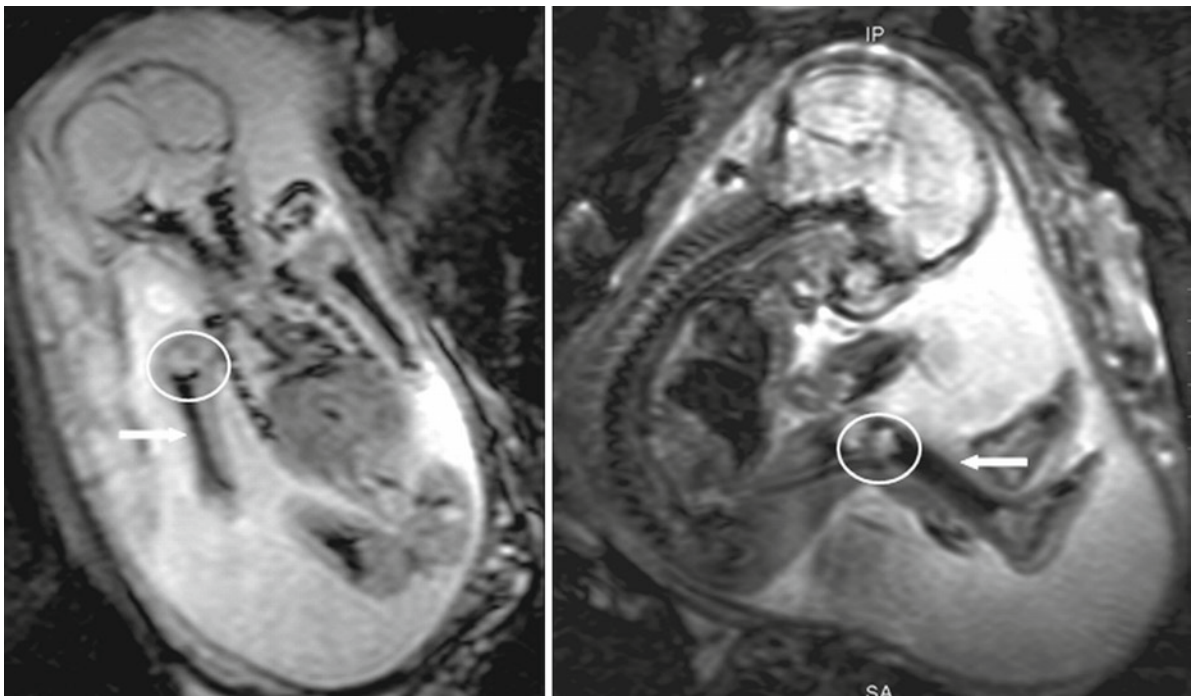

Fig. 1 Different Fetuses at 21 GW (*Left*) and 24 GW (*Right*). The EP-images demonstrate bone as hypointense structures (*arrows*) and hypointense epiphyses (*ellipses*)

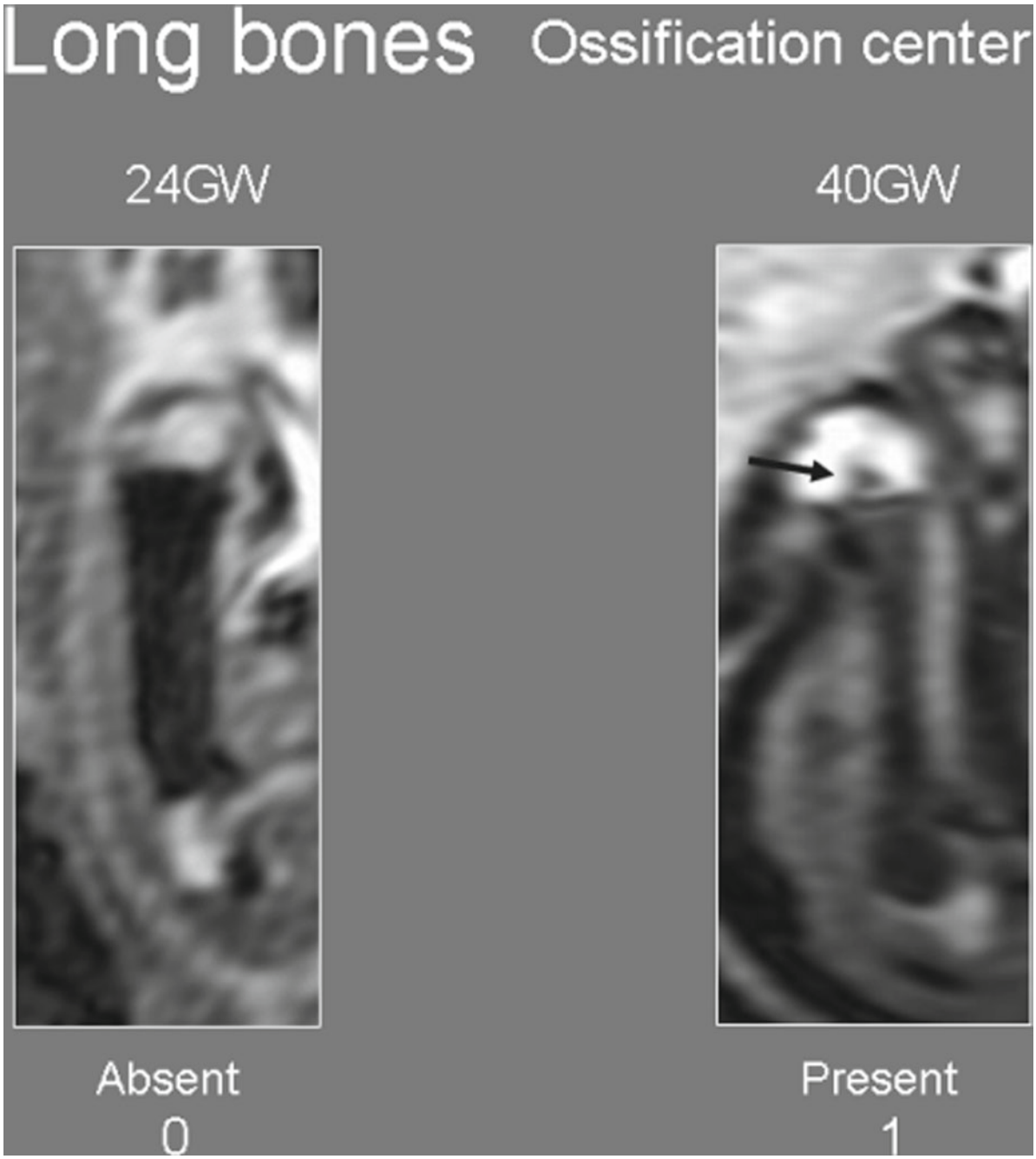

Fig. 2 Long bone development. The EP images demonstrate the course of bone development and ossification (*arrow*) at different gestational ages

The visualization of extremities on typical stacks of cross-sectional images may be impaired by motion artifacts and the missing continuity of the limb (Trop and Levine 2001). Thick-slab images enable the depiction of the limb as a whole demonstrating its shape and position. This may be helpful in cases of limb deformation (dwarfism, conditions that restrict movement either because of a neuromuscular disease or CNS malformation, or extrinsic reasons, such as amniotic bands). Overall, the use of thick-slab images can overcome the difficulties currently associated with 3D reconstructions of fetal MRI data, especially the time-consuming

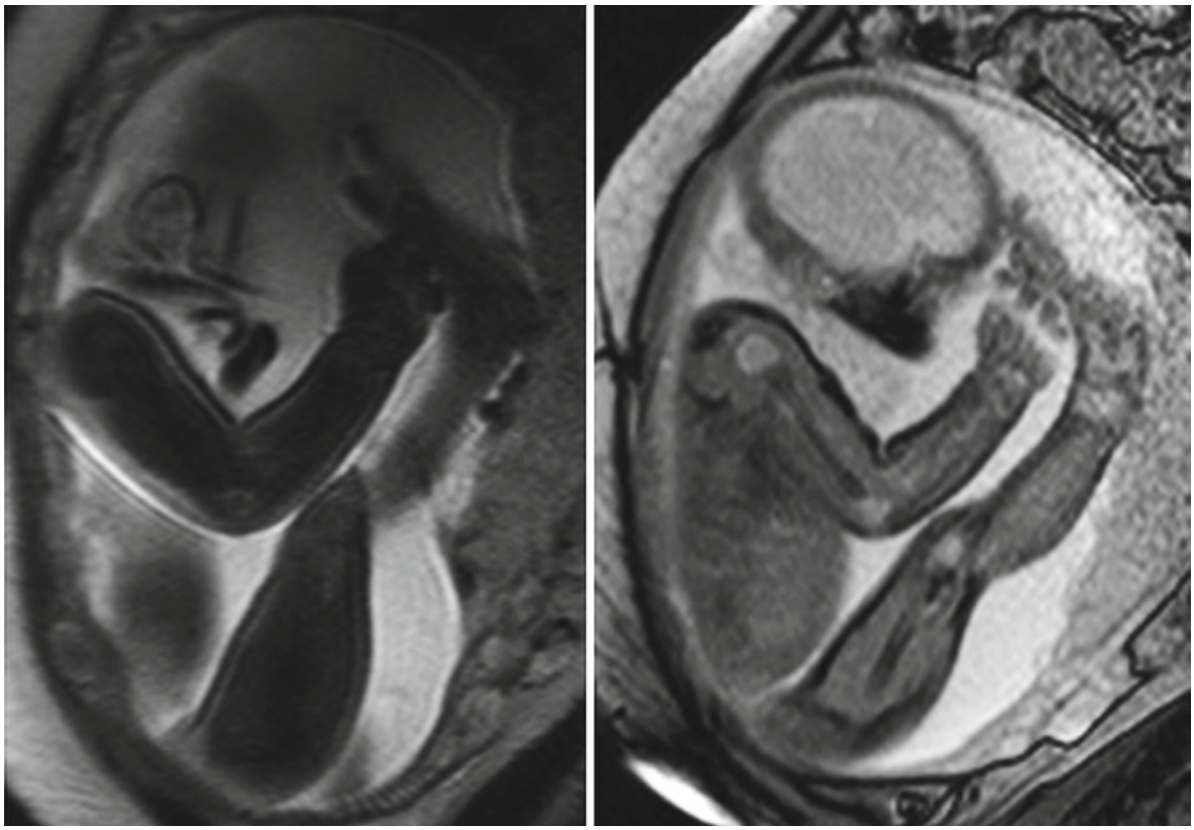

Fig. 3 Fetus at 32 + 1 GW comparison of sequences. *Left* The T2-w sequence provides only poor differentiation between bones and muscles of the extremities. *Right* Echo planar imaging (EPI) enables high contrast between the long bones and adjacent muscles

segmentation (Kubik-Huch et al. 2001; Levine 2001). Thus, the thick-slab method represents an alternative to 3D reconstructions.

2.4 Dynamic Sequences

Dynamic SSFP sequences with 4–6 frames per second and variable slice thickness allow assessment of fetal movements and provide online information. MRI may not capture both hands and feet if the fetus is moving in and out of the scanning plane. This restriction can be overcome by using dynamic sequences (Brugger et al. 2006; Pugash et al. 2008). A limb abnormality will be more obvious with movement on dynamic scans than on static images. Therefore, dynamic scans are instrumental in evaluating extremity malformations, which may otherwise be complicated, as fetal extremity movements are very common. Quantitative movement studies are currently not done using MRI (Prayer and Brugger 2007). As a consequence, one has to be cautious about diagnosing movement reduction based on 30–60 MRI studies. The movement pattern of the extremities should be assessed according to published US criteria (de Vries and Fong 2007). Modified US criteria (qualitative aspects of movements: reduced amplitude and speed, or number of participating body parts) might be used on MRI to diagnose generalized disorders of fetal motility (de Vries and Fong 2007). The fixed nature of an obvious extremity malpositioning should defined as the absence of changes of the extremity position in the dynamic sequences applied five times at about 5, 10, 15, 20, and 25 min during the course of the examination. To comprehend the extremity in toto, dynamic MRI studies should be evaluated only in combination with other musculoskeletal patterns, such as muscular relief and bone structures. This will be helpful to interpret the often

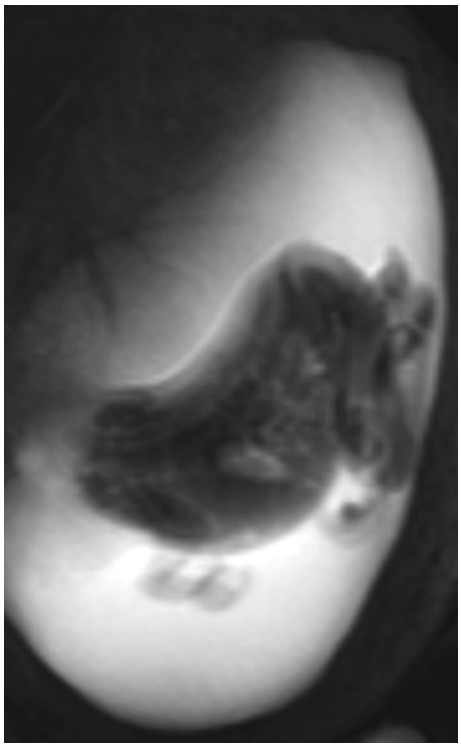

Fig. 4 Fetus at 18+4 GW with akinesia sequence. The thick-slab T2-w image features a hyperlordosis of the whole spine and fixed malpositioning of all extremities

Fig. 5 Fetus at 28 GW with severe craniofacial malformations in holoprosencephaly. The sagittal T2-w image delineates an abnormal (*arrow*) profile without regular shape of lips and nose

complex position of the fetal limbs, and to distinguish what may be a normal variant from a true abnormality. Permanent akinesia manifesting itself by a complete absence of motion, especially in combination with thin muscles, absence of swallowing movements, and presence of polyhydramnios, could be interpreted as a sign of (neuro) muscular disease.

3 The Fetal Face and Skull

3.1 Face

The fetal profile is usually best depicted on sagittal T2-w sequences. However, delineation of the fetal profile may be difficult in case of oligohydramnios. In older fetuses SSFP sequences may be helpful, as the chemical-shift artifact (as a consequence of the subcutaneous fat layer) produces a line allowing the delineation of the surface structures.

The assessment of the fetal face is important in cases of complex malformations (Suri 2005) (Fig. 5). Regarding the orbits, eyes and lens can be demonstrated early. Further orbital details can be delineated in older fetuses. A pathological interorbital distance can be measured and may point to midface malformation related to severe anomalies, such as holoprosencephaly. Conjugate eye gaze, interpreted as the functional output of normal upper brain-stem development, can be observed after 35 GW. Teeth buds may be recognized on T2-w images as well as diffusion-weighted sequences. The external ears should be screened for their presence, shape, and position. Since the fluid-filled inner ears are relatively large structures in the fetus, they can be delineated from 18 GW onward.

US accurately depicts a spectrum of head and neck anomalies, providing that the face and anterior neck are not obscured due to fetal position or bone. 3D techniques have been used to generate detailed images of surface anatomy. In optimal imaging circumstances, both 2DUS and 3DUS provide detailed images of cleft lip and anterior palate. US of the posterior palate may be technically challenging due to acoustic shadowing from the maxilla. In comparison,

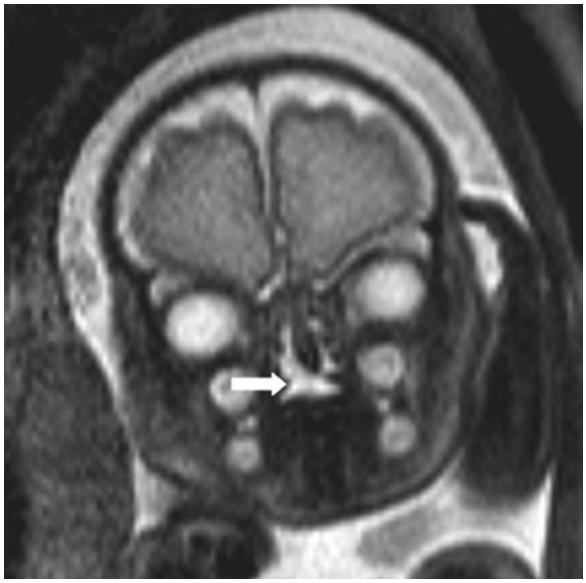

Fig. 6 Fetus at 29+2 GW with isolated cleft palate. The coronal T2-w image delineates a slight defect of the hard palate (*arrow*) of the right side with direct communication between oropharynx and nasopharynx

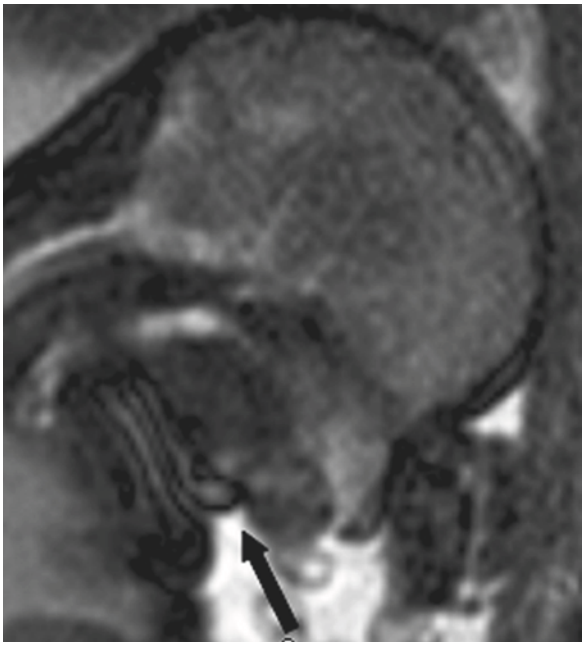

Fig. 7 Fetus at 30+9 GW with "mild" craniofacial malformation. The sagittal GE image delineates a profile with distinct retrognathia (*arrow*)

T2-w MRI demonstrates the posterior palate consistently, regardless of fetal position. MRI has been used to detect isolated cleft palate as well as clefts of both the primary and secondary palates (Fig. 6). Isolated cleft lip without osseous involvement may be more difficult to detect on MRI than on US, due to partial volume averaging in MRI. Other facial anomalies in which MRI findings have been described include other facial clefts, retrognathia, micrognathia, craniosynostosis, cephaloceles, vascular anomalies, tumors, microphthalmia, and other ocular and orbital abnormalities (Fig. 7) (Robson and Barnewolt 2004).

3.2 Skull

The size and shape of the fetal skull is usually known from a previous US study, but also excellently shown in MRI (Fig. 8). On MRI, the region of the craniocervical junction should be visualized with special respect to the width and content of the foramen magnum. On the one side, a narrow foramen magnum may occur within skeletal dysplasias, and on the other side, herniation of cerebellar structures can be observed in Chiari malformations.

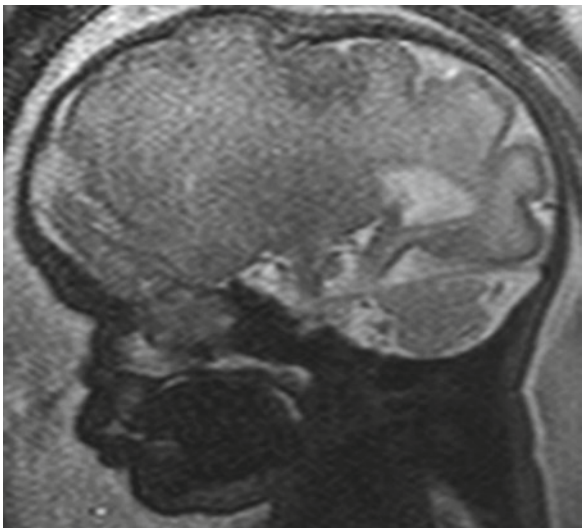

Fig. 8 Fetus at 26+1 GW with abnormal skull shape. The sagittal T2-w image shows a dolichocephaly because of craniosynostosis

In case of asymmetrical head enlargement, the presence/absence of associated cerebral malformations has to be proved. Encephaloceles have to be screened for their content (Fig. 9).

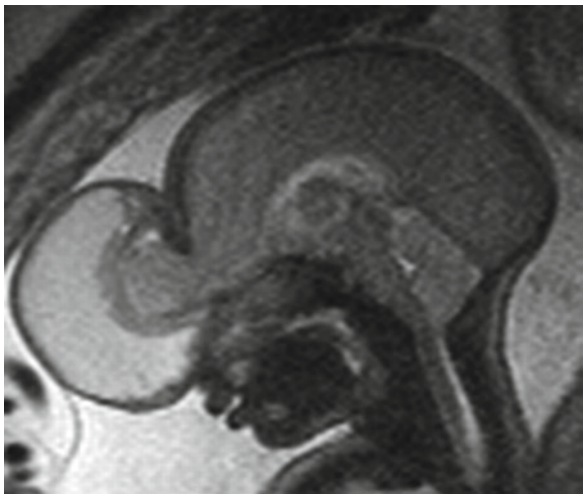

Fig. 9 Fetus at 32+2 GW with meningoencephalocele. The sagittal T2-w image shows a large frontal bony defect with herniation of the meninges and frontal lobes

Fig. 10 Fetus at 32 GW with Chiari-malformation type II. The sagittal T2-w image of the fetal body shows a broad lumbal meningomyelocele (*ellipses*)

4 The Musculoskeletal System

4.1 Fetal Surface and Proportions

Fetal surface contours depend on the nutritional state, amount of subcutaneous fat, muscle mass, integrity of the body wall, and facial features. The fetal skin contrasts well with the surrounding amniotic fluid. The subcutaneous fat layer becomes increasingly prominent with advancing gestation demonstrating characteristic T1-w hyperintensity during the third trimester. Assessment of the fetal surface should be performed on T2-w and thick-slab T2-w sequences (Brugger et al. 2006). The fetal surface may be altered by subcutaneous or intracorporal fluid collections such as, for instance, hydrops. Subcutaneous edema, restricted to the nuchal region, is seen with various etiologies and may also be the first stage of fetal hydrops (Haak and van Vugt 2003). As discontinuity of the body surface occurs most frequently in the median-sagittal plane (spina bifida and body stalk anomaly) (Smrcek et al. 2003), a visualization of the dorsal and ventral midline is required. Protruding organs and the contents of protruding cystic structures have to be characterized (Fig. 10). MRI enables the exact differentiation of open and closed spinal dysraphism in fetuses with a Chiari II malformation, potentially associated with TEV, which is of clinical significance as, in particular, patients with terminal myelocystoceles typically have no bowel or bladder control and poor lower-extremity function (Rossi et al. 2004). Furthermore, fetal proportions, which may be altered due to intrauterine growth restriction (IUGR) (Bamberg and Kalache 2004) or skeletal dysplasia are visualized best using thick-slab T2-w sequences (Fig. 4).

4.2 Bones

US is the method of choice for measuring long bones and observing subtle findings involving distal appendages such as abnormal finger position and polydactyly which can be also observed in fetal MRI (Fig. 11) (Paladini et al. 2010; Pugash et al. 2008). The extremities are particularly well suited to 3DUS. However, it may be difficult or impossible to sonographically assess all extremities on the dependent side of the fetus, or if amniotic fluid is severely reduced, or late in gestation. EPI sequences can be used to image fetal

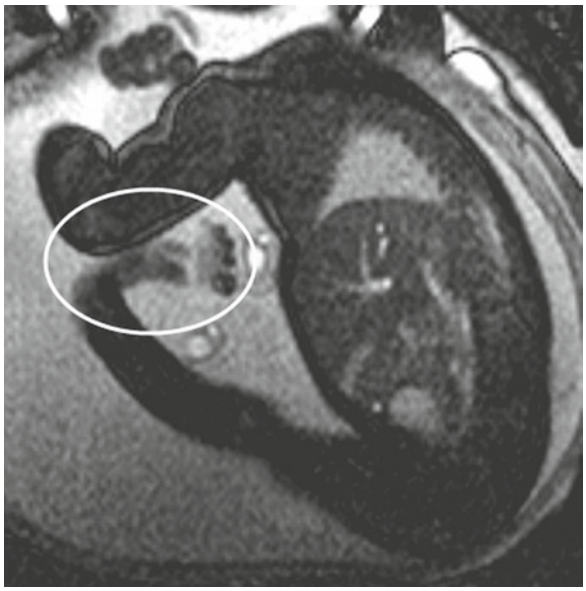

Fig. 11 Fetus at 31 GW with isolated foot deformity. The sagittal T2-w image shows a clubfoot

bone, and are useful to obtain an overview of thoracic size and skeletal development. In addition, details of the developing epiphysis may be recognized (Figs. 1 and 2) (Malinger et al. 2006; Prayer and Brugger 2007). Connolly et al. analyzed pathologic specimens of fetal pig femurs. The authors described the MRI appearances of the fetal pig femur at each trimester and with histologic analysis (Connolly et al. 2004). MRI depicted contour changes of the developing femoral intercondylar notch, changes in cartilage composition such as development of the epiphyseal ossification center, and changes in the signal intensity and shape of the bone and bone marrow (Connolly et al. 2004).

Congenital scoliosis is the most frequent congenital deformity of the spine (Fig. 12). Congenital curvatures are due to anomalous development of the vertebrae (failure of formation and/or segmentation). Congenital scoliosis is possibly related to an insult during embryological development, and associated malformations (heart, spinal cord, kidney) are frequently observed, which underlines the importance of a careful prenatal assessment (Arlet et al. 2003).

Furthermore, most fetuses with prenatally diagnosed hemivertebrae (Fig. 13) have additional anomalies, often syndromic, which affect the prognosis. Neonates with nonisolated hemivertebrae are more often delivered before term and have higher mortality rates (Wax et al. 2008).

Fig. 12 Fetus at 21+2 GW with spinal deformity. The sagittal T2-w image shows an undulating course of the spine referring to scoliosis

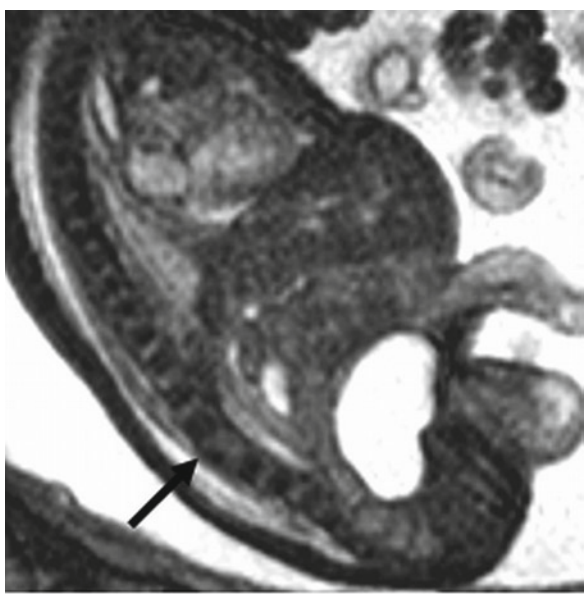

Fig. 13 Fetus at 30+4 GW with spinal abnormality. The T2-w image shows an incomplete vertebral body (*arrow*) of the lumbar spine referring to a hemivertebra

4.3 Muscles

MRI assessment of the musculature is based on direct imaging of muscle contours and structure and on recording of limb posture and movements. Regarding the structure, normal individual muscles (with few exceptions, e.g., the diaphragm, soft palate, and psoas major) cannot be delineated, as muscles display a homogenous T2-w hypointensity. This is especially true for skeletal muscles. However, tissue composition changes with advancing gestation as evidenced by EPI sequences. Using 3D ultrasound, the demonstration of the external shape of limbs requires time-intensive postprocessing (Kos et al. 2002). MRI can show the thickness and contours of the skeletal muscles, atrophy of which may point toward the presence of neuromuscular disease (Fig. 3) (Witters et al. 2002; von Kleist-Retzow et al. 2003). In addition, T1- and T2-w signals may be pathological (Prayer and Brugger 2007) (Fig. 14). It has been stated that impairment of muscle development and fiber differentiation must reach a critical stage, occurring relatively late in pregnancy, to result in significant changes in fetal motility and morphology (Mulder et al. 2001). However, abnormal muscular development may be observed with limb deformities, where an increase of connective tissue in the muscular compartments may change the shape and appearance of the muscular relief, with arthrogryposis, spinal muscular atrophy, or muscular dystrophy (Beals 2005; Yfantis et al. 2002). Newborns with neuromuscular disease may be diagnosed by their marked reduction of anti-gravity movements. Whether this may be observed in utero is not certain; on one hand, it has been concluded that gravity is present in the intrauterine environment (Sekulic et al. 2005); on the other hand, observation of intrauterine leg movements in cases with Chiari II malformations was not an indicator for postnatal leg function (Sival et al. 2004).

Fig. 14 Fetus at 32 GW with muscular atrophy. The sagittal T2-w image shows increased hyperintensity of the thigh musculature (*arrow*)

4.4 Complex Musculoskeletal Disorders

Extremity pathologies can be either isolated or accompanied by numerous other defects, such as certain genetic disorders or chromosomal syndromes resulting in significant pre- and postnatal morbidity and mortality (Keret et al. 2005; Mortier 2001). Prenatal diagnosis of musculoskeletal anomalies should be based on information assembled from imaging and from biochemical and genetic workups (Keret et al. 2005; Mortier 2001; Pagnotta et al. 1996). The prenatal diagnosis can serve as a prognostic tool and in counseling the parents (Keret et al. 2005; Mortier 2001).

When identifying a musculoskeletal abnormality, there is an absolute demand for careful assessment of the whole fetus, in particular the CNS, and for the detection of potential visceral abnormalities (Fig. 15) (Paladini et al. 2010; Prayer and Brugger 2007). The presence or absence of specific MRI findings will point toward a more accurate imaging diagnosis and will help to differentiate between an isolated and a complex pathology in syndromes or generalized musculoskeletal disorders. Acquired conditions such as amniotic bands that may also interfere with skeletal development should be primarily considered as the underlying pathology in case of isolated limb deficiency (Fig. 16) (Sentilhes et al. 2003).

Fig. 15 Fetus at 20 GW with. Chiari-malformations type II. The sagittal T2-w image shows severe deformatics of the lower extremities (*arrow*)

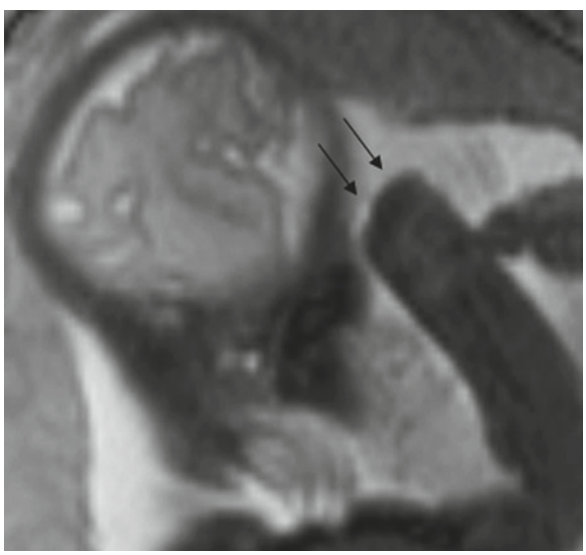

Fig. 16 Fetus at 32+3 GW with isolated limb deficiency. The sagittal T2-w sequence demonstrates a complete missing of the fingers of the right hand (*arrows*)

Fetal skeletal dysplasias are sometimes recognized by ultrasound. Published reports have described US as only moderately accurate in the detection of fetal musculoskeletal anomalies and as inaccurate in the diagnosis of specific skeletal dysplasias (Dugoff et al. 2000; Morcuende and Weinstein 2003) emphasizing the potential future role of MRI in the visualization of the skeleton (Fig. 17). Fetal MR imaging may help to

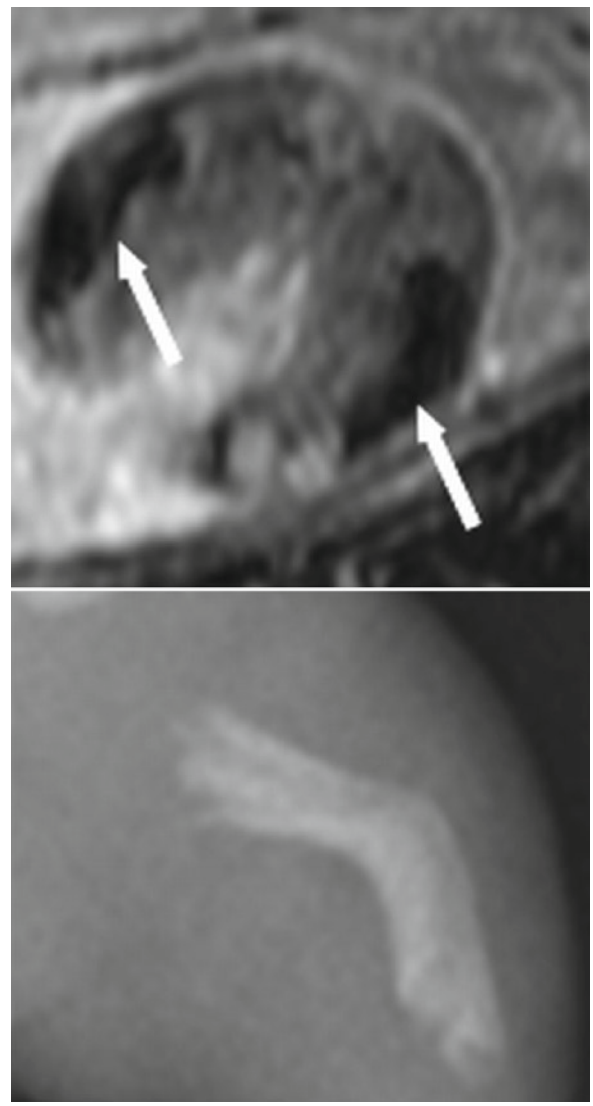

Fig. 17 Fetus at 22+6 GW with hypophosphatasia. *Top* The coronal EPI sequence through the thigh shows an abnormal curved shape of the femur (*arrow*) due to a severe bone mineralization disorder. *Bottom* The postmortem X-ray features the deformity of the femur

complement the use of molecular genetics to diagnose skeletal dysplasias.

References

Applegate KE (2004) Can MR imaging be used to characterize fetal musculoskeletal development? Radiology 233:305–306

Arlet V, Odent T, Aebi M (2003) Congenital scoliosis. Eur Spine J 12:456–463

Bamberg C, Kalache KD (2004) Prenatal diagnosis of fetal growth restriction. Semin Fetal Neonatal Med 9:387–394

Beals RK (2005) The distal arthrogryposes: a new classification of peripheral contractures. Clin Orthop Relat Res 435: 203–210

Brugger PC, Mittermayer C, Prayer D (2006) A new look at the fetus: thickslab T2-weighted sequences in fetal MRI. Eur J Radiol 57:182–186

Brunelle F (2001) Fetal imaging in a new era. Ultrasound Obstet Gynecol 18:91–95

Coakley FV, Glenn OA, Qayyum A, Barkovich AJ, Goldstein R, Filly RA (2004) Fetal MRI: a developing technique for the developing patient. AJR Am J Roentgenol 182: 243–252

Connolly SA, Jaramillo D, Hong JK, Shapiro F (2004) Skeletal development in fetal pig specimens: MR imaging of femur with histologic comparison. Radiology 233:505–514

de Vries JI, Fong BF (2007) Changes in fetal motility as a result of congenital disorders: an overview. Ultrasound Obstet Gynecol 29:590–599

Dugoff L, Thieme G, Hobbins JC (2000) Skeletal anomalies. Clin Perinatol 27:979–1005

Garel C (2008a) Imaging the fetus: when does MRI really help? Pediatr Radiol 38(Suppl 3):S467–S470

Garel C (2008b) Fetal MRI: what is the future? Ultrasound Obstet Gynecol 31:123–128

Glenn OA, Barkovich AJ (2006a) Magnetic resonance imaging of the fetal brain and spine: an increasingly important tool in prenatal diagnosis, part 1. AJNR Am J Neuroradiol 27: 1604–1611

Glenn OA, Barkovich J (2006b) Magnetic resonance imaging of the fetal brain and spine: an increasingly important tool in prenatal diagnosis: part 2. AJNR Am J Neuroradiol 27: 1807–1814

Haak MC, van Vugt JM (2003) Pathophysiology of increased nuchal translucency: a review of the literature. Hum Reprod Update 9:175–184

Keret D, Bronshtein M, Weintroub S (2005) Prenatal diagnosis of musculoskeletal anomalies. Clin Orthop Relat Res 434:8–15

Kos M, Hafner T, Funduk-Kurjak B, Bozek T, Kurjak A (2002) Limb deformities and three-dimensional ultrasound. J Perinat Med 30:40–47

Kubik-Huch RA, Wildermuth S, Cettuzzi L et al (2001) Fetus and uteroplacental unit: fast MR imaging with three-dimensional reconstruction and volumetry – feasibility study. Radiology 219:567–573

Levine D (2001) Three-dimensional fetal MR imaging: will it fulfill its promise? Radiology 219:313–315

Malinger G, Brugger PC, Prayer D (2006) Fetal MRI of the femur – preliminary results. Ultrasound Obstet Gynecol 27:593

Mansfield P, Stehling MK, Ordidge RJ et al (1990) Echo planar imaging of the human fetus in utero at 0.5 T. Br J Radiol 63:833–841

Morcuende JA, Weinstein SL (2003) Developmental skeletal anomalies. Birth Defects Res C Embryo Today 69: 197–207

Mortier GR (2001) The diagnosis of skeletal dysplasias: a multidisciplinary approach. Eur J Radiol 40:161–167

Mulder EJ, Nikkels PG, Visser GH (2001) Fetal akinesia deformation sequence: behavioral development in a case of congenital myopathy. Ultrasound Obstet Gynecol 18:253–257

Pagnotta G, Maffulli N, Aureli S, Maggi E, Mariani M, Yip KM (1996) Antenatal sonographic diagnosis of clubfoot: a six-year experience. Foot Ankle Surg 35:67–71

Paladini D, Greco E, Sglavo G, D'Armiento MR, Penner I, Nappi C (2010) Congenital anomalies of upper extremities: prenatal ultrasound diagnosis, significance, and outcome. Am J Obstet Gynecol 202(596):e1–e10

Prayer D, Brugger PC (2007) Investigation of normal organ development with fetal MRI. Eur Radiol 17: 2458–2471

Pugash D, Brugger PC, Bettelheim D, Prayer D (2008) Prenatal ultrasound and fetal MRI: the comparative value of each modality in prenatal diagnosis. Eur J Radiol 68: 214–226

Robson CD, Barnewolt CE (2004) MR imaging of fetal head and neck anomalies. Neuroimaging Clin N Am 14: 273–291

Rossi A, Biancheri R, Cama A et al (2004) Imaging in spine and spinal cord malformations. Eur J Radiol 50:177–200

Sekulic SR, Lukac DD, Naumovic NM (2005) The fetus cannot exercise like an stronaut: gravity loading is necessary for the physiological development during second half of pregnancy. Med Hypotheses 64:221–228

Sentilhes L, Verspyck E, Patrier S, Eurin D, Lechevallier J, Marpeau L (2003) Amniotic band syndrome: pathogenesis, prenatal diagnosis and neonatal management. J Gynecol Obstet Biol Reprod (Paris) 32:693–704

Sival DA, van Weerden TW, Vles JS, Timmer A, den Dunnen WF, Staal-Schreinemachers AL, Hoving EW, Sollie KM, Kranen-Mastenbroek VJ, Sauer PJ, Brouwer OF (2004) Neonatal loss of motor function in human spina bifida aperta. Pediatrics 114:427–434

Smrcek JM, Germer U, Krokowski M, Berg C, Krapp M, Geipel A, Gembruch U (2003) Prenatal ultrasound diagnosis and management of body stalk anomaly: analysis of nine singleton and two multiple pregnancies. Ultrasound Obstet Gynecol 21:322–328

Suri M (2005) Craniofacial syndromes. Semin Fetal Neonatal Med 10:243–257

Trop I, Levine D (2001) Normal fetal anatomy as visualized with fast magnetic resonance imaging. Top Magn Reson Imaging 12:3–17

von Kleist-Retzow JC, Cormier-Daire V, Viot G, Goldenberg A, Mardach B, Amiel J, Saada P, Dumez Y, Brunelle F, Saudubray JM, Chretien D, Rotig A, Rustin P, Munnich A, De Lonlay P (2003) Antenatal manifestations of mitochondrial respiratory chain deficiency. J Pediatr 143:208–212

Wax JR, Watson WJ, Miller RC, Ingardia CJ, Pinette MG, Cartin A, Grimes CK, Blackstone J (2008) Prenatal sonographic diagnosis of hemivertebrae: associations and outcomes. J Ultrasound Med 27:1023–1027

Witters I, Moerman P, Fryns JP (2002) Fetal akinesia deformation sequence: a study of 30 consecutive in utero diagnoses. Am J Med Genet 113:23–28

Yfantis H, Nonaka D, Castellani R, Harman C, Sun CC (2002) Heterogeneity in fetal akinesia deformation sequence (FADS): autopsy confirmation in three 20–21-week fetuses. Prenat Diagn 22:42–47

MRI of the Fetal Heart

Peter C. Brugger

Contents

Abstract

› Visualization of the fetal heart with MRI is complicated because of the small size of the fetal heart and the high heart rate of approximately 140 beats per minute. While conventional T2-weighted sequences only allow assessment of its size and position, steady-state free-precession sequences are currently the best way to image the fetal heart. The anatomical detail that can be depicted depends on fetal size and on section plane. However, as cardiac triggering is not possible in the fetal setting, the images are taken at random points in the fetal cardiac cycle. This leads to blurring and prevents exact visualization of the thin moving parts, such as the cusps and valves. This may be partly overcome by using dynamic sequences. While a variety of fetal cardiac malformations, especially those associated with cardiomegaly, can also be detected with MRI, its additional value in evaluating fetal cardiac pathologies remains to be determined.

1 Introduction

Without a doubt, ultrasound is the method of choice to visualize the fetal heart and to screen for possible cardiac defects (Budorick and Millman 2000). Although fetal magnetic resonance imaging (MRI) has become increasingly important as an adjunct to ultrasound in the past several years, there has been general agreement that MRI evaluation of the fetal heart

P.C. Brugger
Integrative Morphology Group, Center for Anatomy and Cell Biology, Medical University of Vienna, Waehringerstrasse 13, 1090 Vienna, Austria
e-mail: peter.brugger@meduniwien.ac.at

D. Prayer (ed.), *Fetal MRI*, Medical Radiology,
DOI: 10.1007/174_2010_20, © Springer-Verlag Berlin Heidelberg 2011

is limited (Levine et al. 1998; Amin et al. 1999; Huppert et al. 1999; Levine 2001; Trop and Levine 2001; Ertl-Wagner et al. 2002). The limitations of fetal cardiac MRI were thought to be due to fetal motion (Trop and Levine 2001), the fast-beating fetal heart (Amin et al. 1999), or were attributed to the fact that cardiac gating is not feasible (Levine 2001; Trop and Levine 2001; Ertl-Wagner et al. 2002; Glastonbury and Kennedy 2002). Accordingly, fetal MRI reports on cardiac malformations were scanty (Hata et al. 1995; Kivelitz et al. 2004; Mühler et al. 2004).

More recently, the feasibility of MRI to study the fetal heart was demonstrated using steady-state free-precession (SSFP) sequences (Fogel et al. 2005; Gorincour et al. 2007; Manganaro et al. 2008, 2009a, b; Saleem 2008; Savelli et al. 2009). The present chapter reviews fetal cardiac anatomy and summarizes the possibilities of fetal MRI to visualize the fetal heart in normal and pathological conditions.

2 Fetal Heart Anatomy

The major developmental steps of the heart have taken place by the end of embryonic period proper, and further prenatal development of the heart is basically an increase in size. This growth is very pronounced, as evidenced by the fact that the total heart weight increases more than 200-fold between 8 weeks and term (St John Sutton et al. 1984).

However, some developmental processes, involving chiefly the valvular apparatus, occur in the fetal period (Tandler 1913). The atrioventricular valves, with the chordae tendineae and papillary muscles, differentiate in the early fetal period and achieve a mature morphology after 14 weeks (Oosthoek et al. 1998a, b). The formation of the membranaceous part of the interventricular septum is paralleled by the liberation of the medial leaflet of the tricuspid valve from the muscular ventricular septum and takes place later in fetal development and in the early postnatal period (Allwork and Anderson 1979). By the fifth fetal month, the septal cusp of the tricuspidal valve is established, and at birth, both components of the membranous septum, atrioventricular and interventricular, are completely differentiated (Conte and Grieco 1984).

With the beginning of the fetal period, the leaflets of the semilunar valves become thinner and more delicate. Collagenous and elastic fibers appear in the developing valves and increase progressively in amount and in organization, and, by 19 gestational weeks (GW), the semilunar valves begin to adopt a mature structure (Maron and Hutchins 1974). The histologic structure of both the aortic and pulmonary valves, as well as the wall of the ascending aorta and pulmonary trunk, is identical until birth. Differences only become apparent after birth when the fetal type of circulation changes to the adult pattern (Maron and Hutchins 1974).

With respect to the thickness of the ventricular wall myocardium, there is conflicting evidence. While Oyer et al. (2004) and Arteaga-Martinez et al. (2009) reported the mean left ventricular wall thickness to be greater than the right throughout gestation, St John Sutton et al. (1984) found no differences between right and left ventricular sizes from 20 weeks gestation to term. According to Oyer et al. (2004, 2005), the wall thickness of the right and left ventricles, by 20 GW, averages 1.4 and 2.4 mm, respectively. Both dimensions increase to 3.6 and 4.2 mm at 40 GW.

The thickness of the membranous part of the interventricular septum increases from 0.6 mm around 19 GW to 1 mm at term (Figueira et al. 1991).

In the right atrium, the elliptical opening of the inferior vena cava is found close to the foramen ovale. The valve of the inferior vena cava is large in the fetus and is in continuity with the anterior limb of the limbus fossa ovalis, and directs most of the blood from the inferior vena cava toward the foramen ovale (Walmsley and Monkhouse 1988). The posterior wall of the right atrium shows a well-marked bending at the area of the intervenous tubercle. The axis of the superior vena cava passes over this tubercle and may be traced directly into the right atrioventricular opening (Brandt 1954). In contrast to the adult, the fetal right auricle is a voluminous cavity contributing to the filling capacity of the right atrium, with its well-differentiated pectinate muscles being considered to contribute to the expulsion of blood (Brandt 1954).

The atria are partly separated by the interatrial septum, which is formed by the septum primum and secundum. The foramen ovale connecting both atria has dimensions similar to those of the orifice of the

inferior vena cava (Patten et al. 1929). In anatomical specimens, the diameter of the foramen ovale reportedly increases from about 3.3 mm at 28 GW to about 3.7 mm at 36 GW (Amaral et al. 2007). Using ultrasound, Zielinsky et al. (2004) found the average diameter to be 5.06 ± 1.29 mm in fetuses of 20–40 GW.

The septum primum acts as a valve for the foramen ovale, closing it when atrial contractions occur. During diastole, the septum primum bulges into the left atrium, allowing maximal opening and right-to-left flow (Zielinsky et al. 2004; Amaral et al. 2007), thereby assuming the shape of a loose pocket (Kachalia et al. 1991). The blood flowing through the foramen ovale basically comes from the inferior vena cava. This is brought about by the topographical relationship of the septum secundum to the opening of the inferior vena cava. As the blood column in the inferior vena cava ascends, it hits the falciform inferior margin of the septum secundum (Crista dividens), and is thus divided into a greater part that is directed into the left atrium, and a smaller part that remains within the right atrium (Reiff 1976; Kiserud and Rasmussen 2001).

With regard to the left atrium, it has been pointed out that the process of incorporation of the pulmonary veins into its dorsal wall continues into the fetal period (Douglas et al. 2006).

Owing to this mode of development, the left atrial wall is thin.

With respect to the great vessels, the ductus arteriosus merits special attention. This relatively large vessel is the direct continuation of the pulmonary trunk and shunts blood to the descending aorta. It parallels the aortic arch and upper part of the descending aorta, running more directly antero-posterior as it bulges markedly to the left to terminate in the descending aorta about 1 cm distal to the origin of the left subclavian artery (Noback and Rehman 1941). The growth of the great vessels follows a linear function (Szpinda et al. 2006, 2007; Szpinda 2007). By 22 GW, the external diameters of both the ascending aorta and pulmonary trunk measure 4.2 mm (Castillo et al. 2005), and increase to 6.8 and 6.4 mm in the ninth month, respectively (Szpinda 2007). The minimum diameter of the ductus arteriosus at half the distance between its union with the aorta and the pulmonary artery measures about 1.8 mm by 20 GW (Castillo et al. 2005). The external diameter increases from 2.4 mm at GW 22 to 3.5 mm at GW 34, with its length increasing from 6.1 to 12.2 mm (Szpinda et al. 2007).

3 MR Imaging

3.1 General Considerations

By 20 GW the fetal heart may be considered a miniature of the adult. However, it is approximately the size of a thumbnail and its maximum axial cross-sectional area is about 270 mm^2. The problem faced by fetal cardiac MRI is best shown in Fig. 1. Basically, the sequences used in fetal MRI have a similar FOV and spatial resolution as in adult imaging, while the target is very much smaller.

With an in-plane resolution of 0.78 × 0.78 mm on T2-weighted sequences and 1.0 × 1.0 mm on SSFP sequences, the heart at 20 GW is represented by only 350 or 270 pixels, respectively. Moreover, slice thickness is a limiting factor in fetal cardiac MRI, as the rather large slice thickness of 3–4 mm leads to considerable volume averaging, considering the small size of the organ in younger fetuses. Due to its small

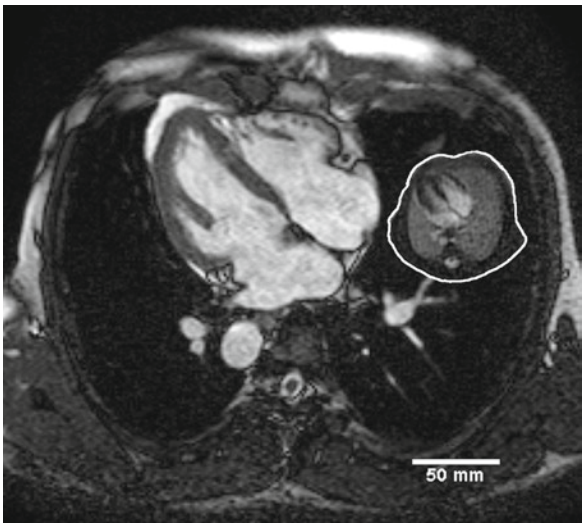

Fig. 1 Axial SSFP image through an adult thorax at the level of the heart, with a corresponding image of a 27 GW fetus inserted into the right adult lung (outlined in *white*). Both images brought to same scale

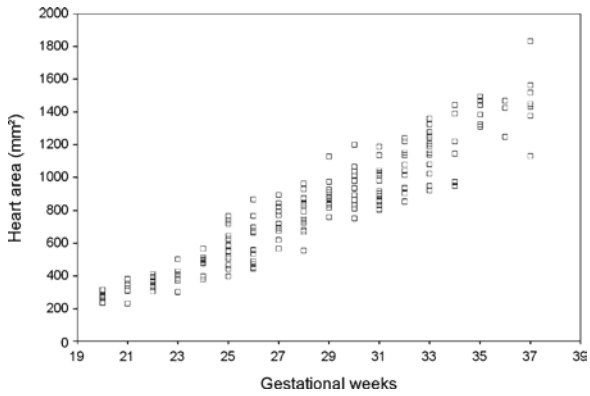

Fig. 2 Axial cross-sectional area (mm^2) of the fetal heart in relation to gestational age (personal data, $n = 180$)

vertical dimensions, the heart is present on only three to four images in the axial plane at 20 GW. However, as the dimensions of the fetal heart increase (Fig. 2), more detail will be seen in older fetuses.

Imaging is further complicated by the fast-beating fetal heart. Therefore, images are snapshots taken at random during the cardiac cycle, which frequently leads to blurring of the cardiac structures, even on SSFP sequences. While EKG triggering can be used in the experimental set-up, and has successfully been demonstrated in ovine fetuses (Yamamura et al. 2009), to date, it is not possible in the human fetus. The problem of cardiac motion may, in part, be overcome by using dynamic SSFP sequences with a reasonable in-plane resolution (c.f. Sect. 3.2.2). Furthermore, fetal movements make dedicated fetal cardiac MRI difficult. Due to the small size of the heart, correctly aligned planes are difficult to obtain, since even minor fetal movements will lead to an undesired imaging plane.

3.2 MRI Appearance of the Fetal Heart and Great Vessels

3.2.1 T2-Weighted Sequences

On conventional T2-weighted TSE sequences (FOV: 200–300 mm, TR: ∞/TE: 100–140 ms, flip angle 90°, slice thickness 3–4 mm, acquired in-plane resolution: 0.78 × 1.18–1.17 × 1.78 mm), the fetal heart appears as a homogenous, hypointense structure, and only its size and position can be evaluated (Fig. 3). Occasionally, the interventricular septum and myocardium can be distinguished (Fig. 3a), but, usually, differentiation between the myocardium and the ventricular cavities is not possible, except in cases of intrauterine fetal demise.

The great vessels in the superior mediastinum become better visible with advancing gestation, because the more hyperintense thymus then contrasts better with the hypointense-appearing vessels. The thoracic aorta and, less frequently, the azygos vein, can be demonstrated in the posterior mediastinum at the level of the heart. The pulmonary vessels are more easily recognized in older fetuses, as the signal intensity of the fetal lungs increases with advancing gestation.

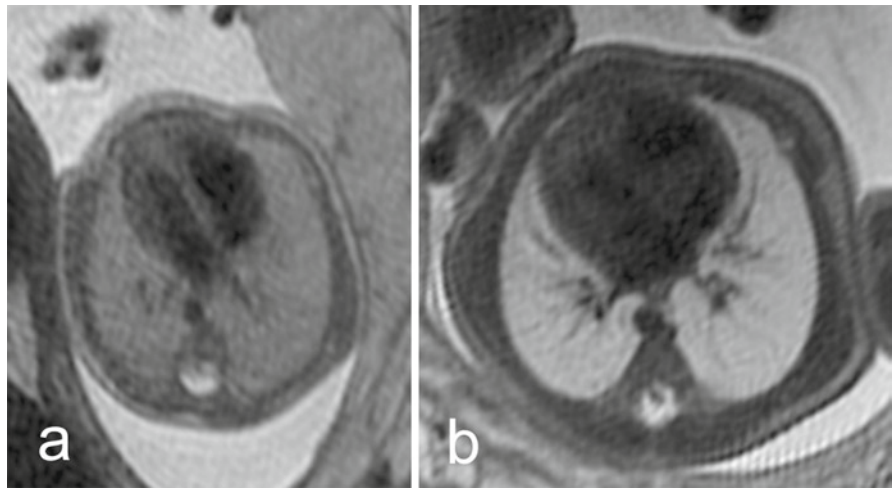

Fig. 3 Axial T2-weighted images through the fetal thorax at 23 + 0 GW (**a**) and 34 + 1 GW (**b**). The interventricular septum and myocardium are seen in (**a**). The thoracic aorta is seen descending on the left side in both fetuses. (**b**) The pulmonary veins are clearly depicted

3.2.2 Steady-State Free-Precession Sequences

SSFP sequences (FOV: 260–300 mm, TR/TE: ∞/∞; flip angle: 60–80°, slice thickness: 6/–3 mm, acquired in-plane resolution: 1.35 × 1.19 mm) allow visualization of the intrinsic anatomy of the fetal heart in greater detail. Overcontinuous slices (5–2.5 mm) may be of advantage when imaging smaller fetuses. Using SSFP sequences, flowing blood will appear variably hyperintense depending on the direction of blood flow in relation to the acquisition plane, and thus, provide contrast to the hypointense-appearing myocardium. The following descriptions are based on standard planes through the fetal body.

On axial sections through the fetal thorax, the heart is usually seen in the four-chamber view, with the ventricles of equal size (Figs. 4–6). The myocardium of the ventricles and the interventricular septum are well-delineated, although some blurring may occur due to cardiac motion. This also affects the thickness of the ventricular wall, which depends on the moment during the cardiac cycle when the image is acquired. The outline of the luminal side of the ventricular myocardium appears irregular, because the trabeculae carneae and papillary muscles project from the inner surface of the ventricle.

Since the muscular part of the interventricular septum is less affected by cardiac contractions, it is usually more clearly visible (Figs. 4–6). This enables

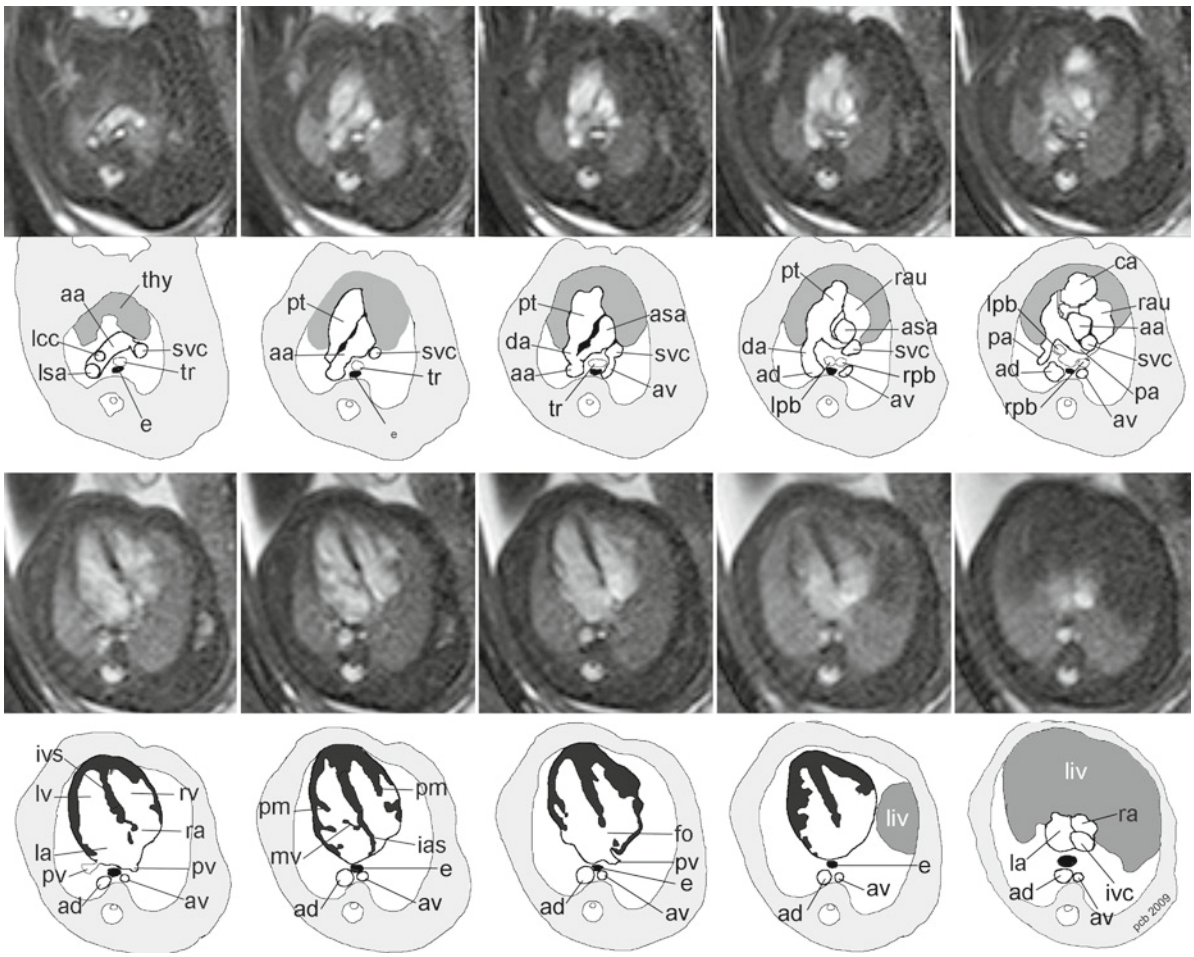

Fig. 4 Set of axial SSFP images through the fetal thorax at 29 + 5 GW, with 3 mm slice thickness, cranio-caudal migration and corresponding schematic drawings with legends: *aa* aortic arch; *ad* descending aorta; *asa* ascending aorta; *av* azygos vein; *ca* conus arteriosus; *da* ductus arteriosus; *e* esophagus; *fo* foramen ovale; *ias* interatrial septum; *ivs* interventricular septum; *ivc* inferior vena cava; *liv* liver; *lpb* left principal bronchus; *lv* left ventricle; *pt* pulmonary trunk, *pa* pulmonary artery; *pm* papillary muscle; *ra* right atrium; *rau* right auricle; *rpb* right principal bronchus; *rv* right ventricle; *svc* superior vena cava; *thy* thymus; *tr* trachea

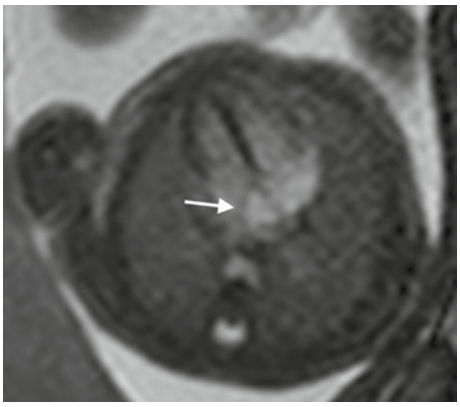

Fig. 5 Axial SSFP image of a fetus at 23+4 GW showing the interatrial septum and septum primum (*arrow*)

determination of the cardiac axis (angle between the midplane and the interventricular septum), which averages 41° on fetal MRI. Measurement of the cardiac axis allows identification of the deviations thereof, which are considered to be a marker for fetal cardiac and/or extracardiac anomalies (Shipp et al. 1995; Smith et al. 1995).

Unlike the ventricular myocardium, the atrial myocardium is extremely thin in most areas, and therefore, is difficult to demonstrate in younger fetuses, which is especially true for the left atrium. Likewise, the interatrial septum and foramen ovale may also be difficult to visualize. Demonstration of the septum primum is inconstant, but, on axial images, it may be seen as a C-shaped line bulging into the left atrium in diastole (Fig. 5).

Flow phenomena may be observed in the atria on axial SSFP images. Most frequently, the elliptical outline of the inferior vena cava and the blood flowing through it are seen as a hyperintense area in the dorsal parts of the right atrium (Fig. 6). Sometimes, the valve of the inferior vena cava may be recognized as its ventral boundary. Occasionally, the blood entering through the superior vena cava can also be traced to the right atrium. Then, two elliptical hyperintense areas may be recognized at the mid-level of the atria (Fig. 6c): a dorsally positioned blood column entering through the inferior vena cava and directed toward the foramen ovale by the valve of the inferior vena cava; and, ventro-lateral to this blood column, the blood flowing through the superior vena cava towards the right atrioventricular valve.

A similar flow artifact may be observed on the left side of the interatrial septum, which corresponds to that part of the inferior vena cava blood column that is divided by the crista dividens of the atrial septum.

While the atrioventricular openings are easy detectable, the cusps themselves are rarely clearly depicted. Due to their rapid movements and their delicate structure, compared to voxel size, which inevitably leads to considerable volume averaging, the cusps can only vaguely be identified as such. This also applies to the aortic and pulmonary valves. The papillary muscles may be discernible following 24 GW, and are best depicted in the short axis of the heart.

In fact, more details become visible in older fetuses (compare Fig. 5 with 6).

Frontal and sagittal planes through the fetal body will show different views of the fetal heart, depending on the cardiac axis. On frontal images, the right atrium with the superior and inferior venae cavae, as well as the left ventricle with its outflow tract, can usually be depicted (Fig. 7).

The great vessels may be identified in different section planes. On axial slices cranial to the heart, the so-called "three-vessel view" depicts the pulmonary trunk, the aortic arch, and the superior vena cava (Figs. 5 and 6), as well as the ductus arteriosus. In fact, delineation of these vessels is clearer in older fetuses. In a continuous set of images, the great vessels can be followed into the respective ventricles.

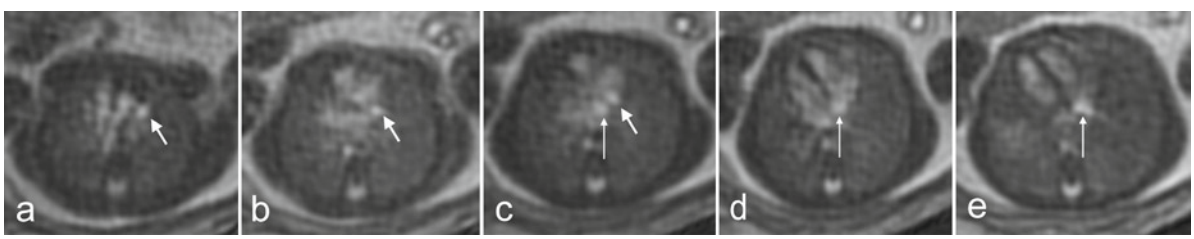

Fig. 6 (**a–e**) Sequential SSFP images (cranio-caudal migration) through the fetal thorax (23+4 GW), with 3-mm slice thickness that demonstrates the flow phenomena in the atria. The *short arrow* points to the blood stream entering through the superior vena cava, and the *long arrow* points to the blood column entering through the inferior vena cava

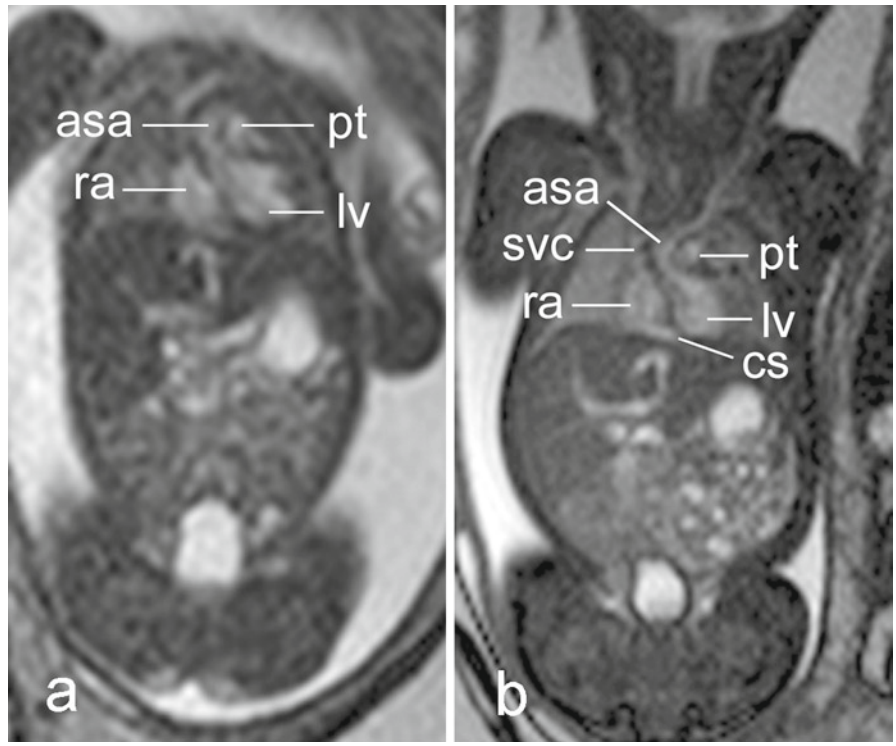

Fig. 7 Frontal SSFP images (through the fetal body), demonstrating the outflow tract of the left ventricle and great vessels. (**a**) Fetus at 21+5 GW. (**b**) Fetus at 28+6. The left ventricle and ascending aorta can be identified. Frontal images depict cardiac chambers and great vessels. *Asa* ascending aorta; *cs* coronary sinus; *lv* left ventricle; *pt* pulmonary trunk; *ra* right atrium; *svc* superior vena cava. The neck vessels in (**b**) in apparent continuity with the aorta, are, in fact, veins (due to volume averaging)

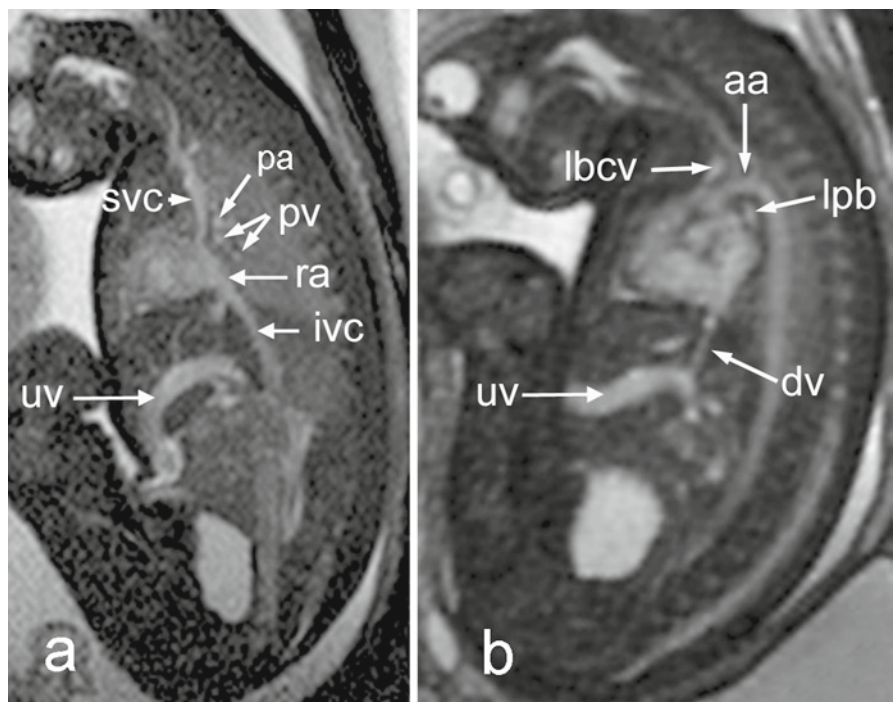

Fig. 8 (**a**) Sagittal SSFP image of a fetus at 29+4 GW, demonstrating the superior and inferior venae cavae entering the right atrium. Note the angle between the superior and inferior vena cava. (**b**) Oblique sagittal SSFP image of a fetus at 31+0 GW. *aa* aortic arch; *ao* aorta; *ivc* inferior vena cava; *lbcv* left brachiocephalic vein; *lpb* left principal bronchus; *pa* pulmonary artery; *pv* pulmonary veins; *svc* superior vena cava; *dv* ductus venosus; *uv* umbilical vein

While the pulmonary trunk is easy to demonstrate, the pulmonary arteries themselves are more difficult to visualize on axial images, but they may be identified by their topographical relationship to the principal bronchi on sagittal images in larger fetuses (Fig. 8).

As the pulmonary veins are surrounded by hyperintense lung tissue, they are easier to demonstrate on T2-weighted sequences (Fig. 3). On axial SSFP sequences, the pulmonary veins may only be visualized before they enter the left atrium (Fig. 4). The

superior and inferior vena cava usually can be demonstrated in all section planes (Figs 4 and 6–8).

Depending on the cardiac angle, the coronary sinus may be visualized on frontal images (Fig. 7b), since its terminal part travels in a nearly sagittal direction, and blood flow within the coronary sinus is directed perpendicular to the acquisition plane, and will, therefore, appear more hyperintense.

The coronary arteries cannot be demonstrated.

3.2.3 Dynamic Sequences

Since cardiac gating is not possible, dynamic sequences with high temporal and spatial resolution may be used to image the beating heart. Initial attempts were made using ungated echoplanar sequences (Mansfield et al. 1990). At present, dynamic SSFP sequences (FOV: 290–320 mm, TR/TE: 3,4/1,7; flip angle 60°, slice thickness: 6–10 mm, one signal acquired, acquired in-plane resolution: 1.82×2.31 mm), with up to six frames per second (i.e., about 135 ms to acquire one image), are used to demonstrate the beating heart. The temporal resolution is sufficient to visualize the systolic and diastolic phases of the cardiac cycle (Fig. 9). In order to smoothly document a whole cardiac cycle without cardiac triggering, approximately 18 fps would be necessary, which, at present, is not possible with a reasonable resolution. In fact, the mediocre resolution, and especially, the large slice thickness limit the demonstration of intrinsic details in smaller fetuses.

In addition to the details that can be seen on static SSFP sequences, the movements of the atrioventricular plane and the atrioventricular cusps may be seen in later stages of pregnancy (Fig. 9).

4 Cardiac Pathologies

While positional anomalies of the heart may also be seen on T2-weighted sequences, they can be better assessed on SSFP sequences, since the cardiac axis can also be demonstrated (Fig. 10).

Positional anomalies may be an isolated finding (e.g., simple dextrocardia, Fig. 10c), or may be caused by the mass effect of intrathoracic lesions, such as congenital cystic adenomatoid malformations of the lungs or congenital diaphragmatic hernias (Fig. 10d). However, they may also be part of more complex malformations, such as omphaloceles or heterotaxy syndromes. Atypical positions of the fetal heart not related to intrathoracic masses should prompt assessment of the visceral situs, which is best done on the survey scan. In fetuses with heterotaxy syndromes, the abdominal situs (symmetry of liver, absence or presence

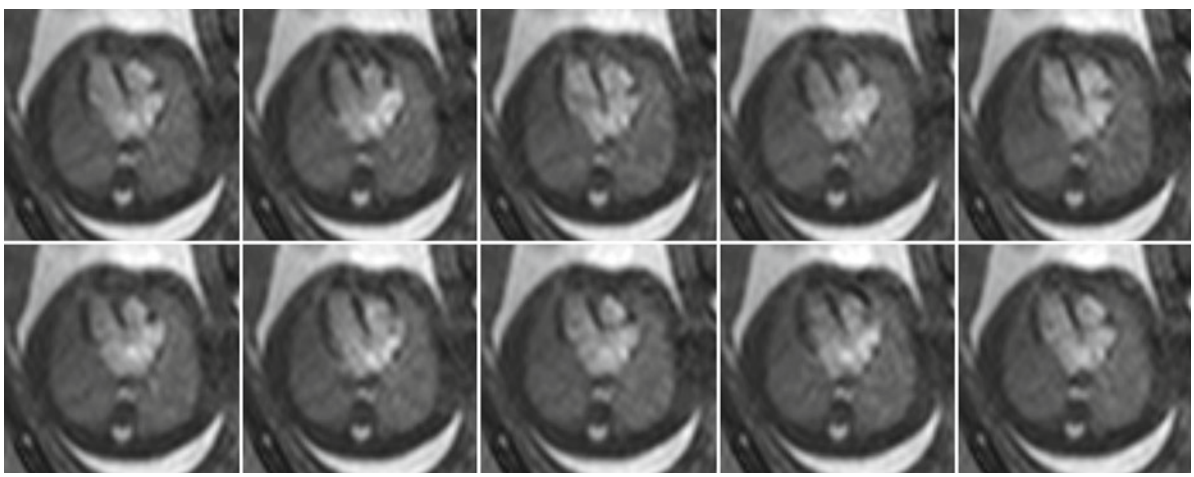

Fig. 9 Ten consecutive frames of a dynamic fetal cardiac MRI study (SSFP sequence, 5.3 frames per second, TR/TE 3,4/1,7; 8-mm slice thickness, FOV: 290 mm) in a fetus at 27 GW, four-chamber view. The hypointense myocardium (including the interventricular septum) contrasts with the more hyperintense blood within the heart. The atrio-ventricular valves are also discernible. Note also the changes in signal intensity of the blood flowing within the atria

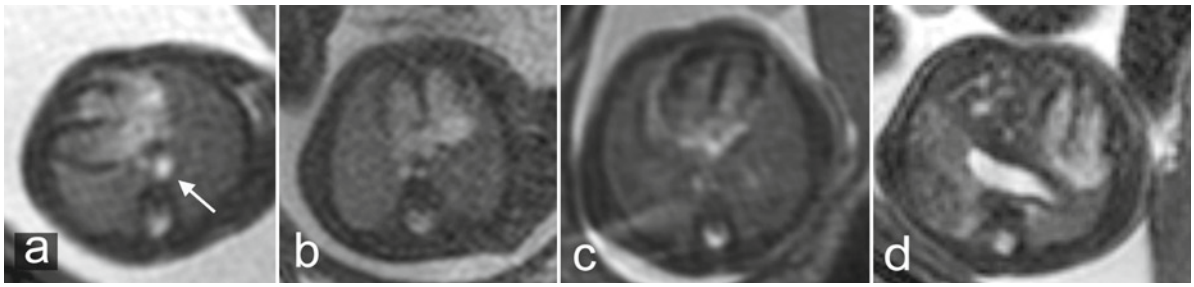

Fig. 10 Axial SSFP images showing anomalous positions of the fetal heart. (**a**) Fetus at 21 + 6 GW with omphalocele and a cardiac axis perpendicular (94°) to the median plane. The large vessel ventral to the thoracic spine is the azygos vein (*arrow*), since no infrahepatic inferior vena cava was present. (**b**) Nearly median-positioned heart in a fetus at 25 + 4 GW with omphalocele. (**c**) Dextrocardia in a fetus at 23 + 5 GW. (**d**) Left-sided congenital diaphragmatic hernia (24 + 0 GW) with intrathoracic stomach and left hepatic lobe, showing typical displacement of the heart to the right side

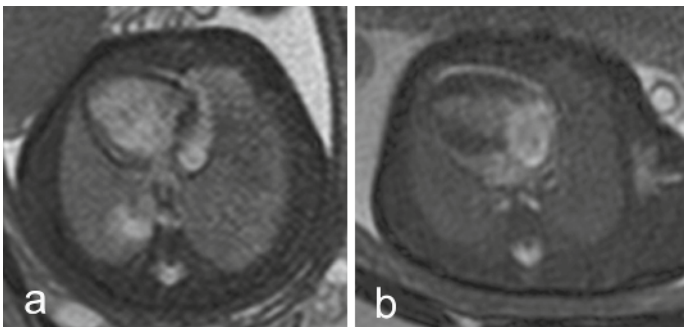

Fig. 11 (**a**) Axial SSFP image of a fetus at 32 GW with complex cardiac vitium (ultrasound diagnosis of tricuspidal atresia, transposition of the great arteries, hypoplastic right ventricle, and hypoplastic aortic arch). (**b**) Axial SSFP image of a fetus at 31 + 0 GW with hypoplastic left heart syndrome

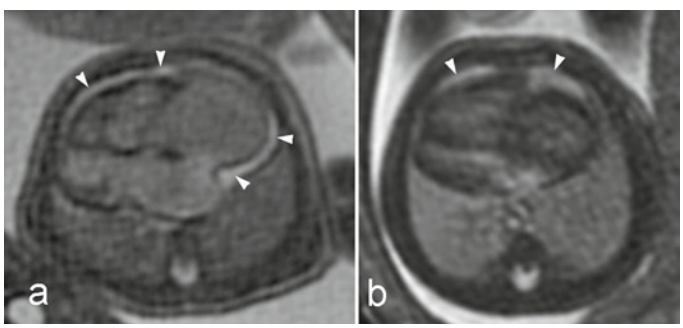

Fig. 12 Enlargement of the heart involving particularly the right atrium. (**a**) Fetus at 28 + 5 GW with an ultrasound diagnosis of pulmonary atresia with intact ventricular septum. On the axial SSFP image, the cardiac chambers appear with intermediate signal intensity, most probably due to turbulent flow. (**b**) Axial SSFP image of a fetus at 27 + 4 GW with tricuspidal dysplasia (ultrasound diagnosis) showing the enlarged right heart. The tricuspidal valve itself cannot be clearly demonstrated. Note also the pericardial effusion (*arrowheads*)

of spleen(s), the course of the hemiazygos/azygos veins, the presence of the infrahepatic segment of the inferior vena cava), and pulmonary anatomy (symmetry of the tracheal bifurcation and course of the principal bronchi) should be assessed.

Cardiac malformations associated with cardiomegaly and/or different sizes of the cardiac chambers (univentricular, hypoplastic left/right heart) are also easily recognized with fetal MRI (Figs. 11 and 12).

An enlarged heart that involves the right atrium, in particular, may be seen in fetuses with tricuspidal dysplasia or pulmonary atresia (Fig. 12), both of which have a similar appearance on MRI. Usually associated with an abnormal cardiac angle, the enlarged cardiac chambers present with homogenous and intermediate signal intensity, most probably due to compromised hemodynamics. However, further assessment of such cardiac pathologies with standard

fetal MRI is limited by the fact that the valves cannot be clearly depicted.

A further limitation in studying fetal cardiac pathologies is the difficulty in detecting ventricular and atrial septum defects. Given a slice thickness of 3 mm, smaller septal defects are unlikely to be depicted by fetal MRI. This also renders reliable proof of septal defects nearly impossible in younger fetuses. To date, only one case of a ventricular septum defect, located in the muscular part of the septum, has been reported in a 36 GW fetus with fetal MRI (Savelli et al. 2009).

An exception to the rule that the fetal heart is better imaged using SSFP sequences are, cardiac rhabdomyomas. By way of contrast, these are more easily recognized on T2-weighted sequences (Fig. 13a, b), since their T2-weighted hyperintensity contrasts well with the otherwise hypointense signal of the heart. On SSFP sequences, rhabdomyomas display only intermediate signal intensity and are thus less clearly identified. Other, although rare, cardiac tumors, include cardiac teratomas (Fig. 13c), which can be well-depicted by virtue of the massive pericardial effusions.

Anomalies of the great vessels, such as a hypoplastic aortic arch, coarctation of the aorta, or a persistent left superior vena cava, can be visualized in larger fetuses (Fig. 14).

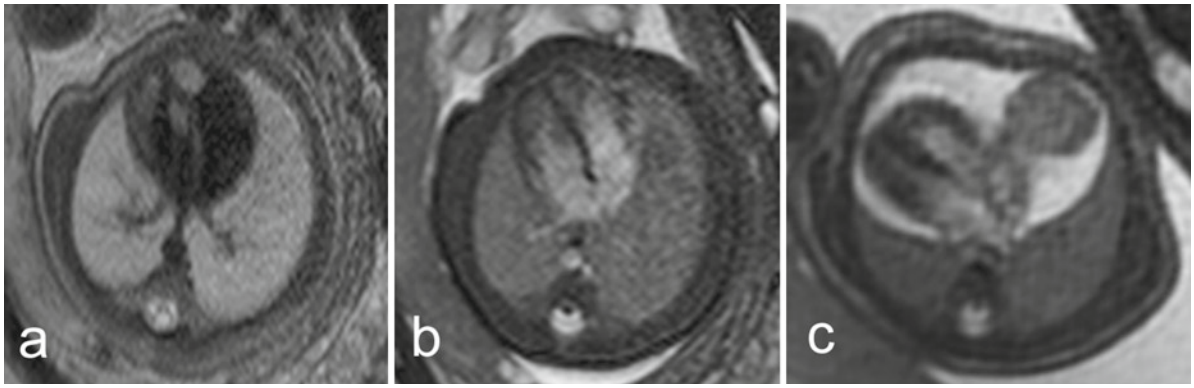

Fig. 13 Multiple cardiac rhabdomyomas in a fetus (29 + 4 GW) with tuberous sclerosis. (**a**) Axial T2-weighted image demonstrates the lesions as hyperintense areas. (**b**) Corresponding SSFP image in which the rhabdomyomas are less conspicuous. Note also that the pulmonary veins are better visualized on the T2-weighted image. (**c**) Axial SSFP image of a fetus at 28 + 0 GW with a cardiac teratoma emanating from the right atrium. The lesion is clearly demarcated because of the massive pericardial effusion

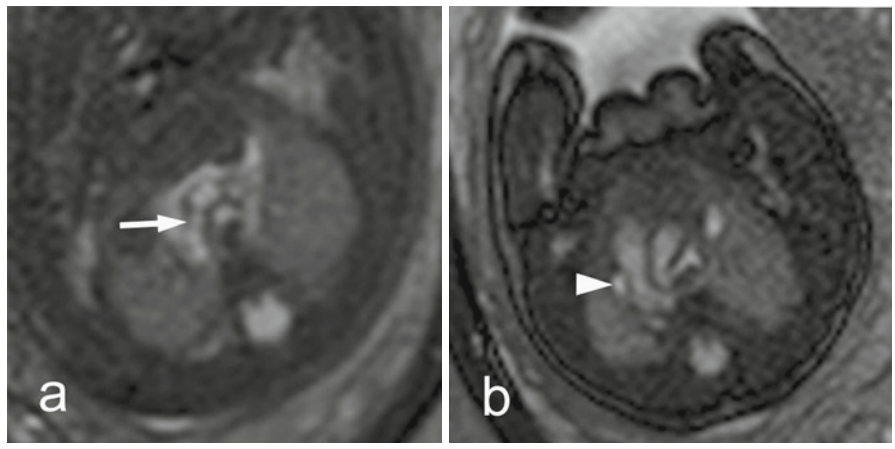

Fig. 14 (**a**) Axial SSFP image of a fetus at 28 + 5 GW with hypoplastic aortic arch (*arrow*). (**b**) Axial SSFP image of a fetus at 32 + 1 GW. Incidental finding of a persistent left superior vena cava (*arrowhead*)

References

Allwork SP, Anderson RH (1979) Developmental anatomy of the membranous part of the ventricular septum in the human heart. Br Heart J 41:275–280

Amaral HB, Zielinsky P, da Silveira AF, Costabeber I, Nicoloso LH, de Souza Filho OC, Salum M, Manica JL, Zanettini JS, Costabeber AM (2007) Morphological basis for the study of the interatrial septum in the human fetus. Arq Bras Cardiol 88:559–564

Amin RS, Nikolaidis P, Kawashima A, Kramer LA, Ernst RD (1999) Normal anatomy of the fetus at MR imaging. Radiographics 19(spec no):S201–S214

Arteaga-Martinez M, Halley-Castillo E, Garcia-Pelaez I, Villasis-Keever MA, Aguirre OM, Vizcaino-Alarcon A (2009) Morphometric study of the ventricular segment of the human fetal heart between 13 and 20 weeks' gestation. Fetal Pediatr Pathol 28:78–94

Brandt W (1954) Fetal circulation and the development of the prime movers of right atrioventricular ring in the human heart. Acta Anat (Basel) 22:216–227

Budorick NE, Millman SL (2000) New modalities for imaging the fetal heart. Semin Perinatol 24:352–359

Castillo EH, Arteaga-Martinez M, Garcia-Pelaez I, Villasis-Keever MA, Aguirre OM, Moran V, Vizcaino Alarcon A (2005) Morphometric study of the human fetal heart. I. Arterial segment. Clin Anat 18:260–268

Conte G, Grieco M (1984) Closure of the interventricular foramen and morphogenesis of the membranous septum and ventricular septal defects in the human heart. Anat Anz 155:39–55

Douglas YL, Jongbloed MR, Gittenberger-de Groot AC, Evers D, Dion RA, Voigt P, Bartelings MM, Schalij MJ, Ebels T, DeRuiter MC (2006) Histology of vascular myocardial wall of left atrial body after pulmonary venous incorporation. Am J Cardiol 97:662–670

Ertl-Wagner B, Lienemann A, Strauss A, Reiser MF (2002) Fetal magnetic resonance imaging: indications, technique, anatomical considerations and a review of fetal abnormalities. Eur Radiol 12:1931–1940

Figueira RR, Prates JC, Hayashi H (1991) Development of the pars membranacea septi interventricularis of the human heart. II. Thickness change. Arch Ital Anat Embriol 96:303–307

Fogel MA, Wilson RD, Flake A, Johnson M, Cohen D, McNeal G, Tian ZY, Rychik J (2005) Preliminary investigations into a new method of functional assessment of the fetal heart using a novel application of 'real-time' cardiac magnetic resonance imaging. Fetal Diagn Ther 20:475–480

Glastonbury CM, Kennedy AM (2002) Ultrafast MRI of the fetus. Australas Radiol 46:22–32

Gorincour G, Bourliere-Najean B, Bonello B, Fraisse A, Philip N, Potier A, Kreitmann B, Petit P (2007) Feasibility of fetal cardiac magnetic resonance imaging: preliminary experience. Ultrasound Obstet Gynecol 29:105–108

Hata K, Hata T, Manabe A, Kitao M (1995) Hypoplastic left heart syndrome: color Doppler sonographic and magnetic resonance imaging features in utero. Gynecol Obstet Invest 39:70–72

Huppert BJ, Brandt KR, Ramin KD, King BF (1999) Single-shot fast spin-echo MR imaging of the fetus: a pictorial essay. Radiographics 19(spec no):S215–S227

Kachalia P, Bowie JD, Adams DB, Carroll BA (1991) In utero sonographic appearance of the atrial septum primum and septum secundum. J Ultrasound Med 10:423–426

Kiserud T, Rasmussen S (2001) Ultrasound assessment of the fetal foramen ovale. Ultrasound Obstet Gynecol 17:119–124

Kivelitz DE, Mühler M, Rake A, Scheer I, Chaoui R (2004) MRI of cardiac rhabdomyoma in the fetus. Eur Radiol 14: 1513–1516

Levine D (2001) Ultrasound versus magnetic resonance imaging in fetal evaluation. Top Magn Reson Imaging 12:25–38

Levine D, Barnes PD, Sher S, Semelka RC, Li W, McArdle CR, Worawattanakul S, Edelman RR (1998) Fetal fast MR imaging: reproducibility, technical quality, and conspicuity of anatomy. Radiology 206:549–554

Manganaro L, Savelli S, Di Maurizio M, Perrone A, Tesei J, Francioso A, Angeletti M, Coratella F, Irimia D, Fierro F, Ventriglia F, Ballesio L (2008) Potential role of fetal cardiac evaluation with magnetic resonance imaging: preliminary experience. Prenat Diagn 28:148–156

Manganaro L, Savelli S, Di Maurizio M, Francioso A, Fierro F, Tomei A, Coratella F, Ballesio L, Ventriglia F (2009a) Fetal MRI of the cardiovascular system: role of steady-state free precession sequences for the evaluation of normal and pathological appearances. Radiol Med 114:852–870

Manganaro L, Savelli S, Di Maurizio M, Perrone A, Francioso A, La Barbera L, Totaro P, Fierro F, Tomei A, Coratella F, Giancotti A, Ballesio L, Ventriglia F (2009b) Assessment of congenital heart disease (CHD): is there a role for fetal magnetic resonance imaging (MRI)? Eur J Radiol 72:172–180

Mansfield P, Stehling MK, Ordidge RJ, Coxon R, Chapman B, Blamire A, Gibbs P, Johnson IR, Symonds EM, Worthington BS et al (1990) Echo planar imaging of the human fetus in utero at 0.5 T. Br J Radiol 63:833–841

Maron BJ, Hutchins GM (1974) The development of the semilunar valves in the human heart. Am J Pathol 74:331–344

Mühler MR, Rake A, Schwabe M, Chaoui R, Heling KS, Planke C, Lembcke A, Fischer T, Kivelitz D (2004) Truncus arteriosus communis in a midtrimester fetus: comparison of prenatal ultrasound and MRI with postmortem MRI and autopsy. Eur Radiol 14:2120–2124

Noback GJ, Rehman I (1941) The ductus arteriosus in the human fetus and newborn infant. Anat Rec 81:505–527

Oosthoek PW, Wenink AC, Vrolijk BC, Wisse LJ, DeRuiter MC, Poelmann RE, Gittenberger-de Groot AC (1998a) Development of the atrioventricular valve tension apparatus in the human heart. Anat Embryol (Berl) 198:317–329

Oosthoek PW, Wenink AC, Wisse LJ, Gittenberger-de Groot AC (1998b) Development of the papillary muscles of the mitral valve: morphogenetic background of parachute-like asymmetric mitral valves and other mitral valve anomalies. J Thorac Cardiovasc Surg 116:36–46

Oyer CE, Sung CJ, Friedman R, Hansen K, Paepe MD, Pinar H, Singer DB (2004) Reference values for valve circumferences and ventricular wall thicknesses of fetal and neonatal hearts. Pediatr Dev Pathol 7:499–505

Oyer CE, Sung CJ, Friedman R, Hansen K, Paepe MD, Pinar H, Singer DB (2005) Reference values for valve circumferences

and ventricular wall thicknesses of fetal and neonatal hearts. Erratum Pediatr Dev Pathol 8:139–140

Patten BM, Sommerfeld WA, Paff GH (1929) Functional limitations of the foramen ovale in the human foetal heart. Anat Rec 44:165–178

Reiff H (1976) Zur funktionellen Anatomie der venösen Einstrombahn ins menschliche fetale Herz. Basic Res Cardiol 71:199–209

Saleem SN (2008) Feasibility of MRI of the fetal heart with balanced steady-state free precession sequence along fetal body and cardiac planes. AJR Am J Roentgenol 191:1208–1215

Savelli S, Di Maurizio M, Francioso A, La Barbera L, Totaro P, Tomei A, Fierro F, Coratella F, Irimia D, Manganaro L (2009) Fetal mid-muscular ventricular septal defect: role of fetal cardio-vascular evaluation with magnetic resonance (MR) imaging and MR-angiography. Eur J Radiol Extra 69:e101–e103

Shipp TD, Bromley B, Hornberger LK, Nadel A, Benacerraf BR (1995) Levorotation of the fetal cardiac axis: a clue for the presence of congenital heart disease. Obstet Gynecol 85:97–102

Smith RS, Comstock CH, Kirk JS, Lee W (1995) Ultrasonographic left cardiac axis deviation: a marker for fetal anomalies. Obstet Gynecol 85:187–191

St John Sutton MG, Raichlen JS, Reichek N, Huff DS (1984) Quantitative assessment of right and left ventricular growth in the human fetal heart: a pathoanatomic study. Circulation 70:935–941

Szpinda M (2007) Morphometric study of the ascending aorta in human fetuses. Ann Anat 189:465–472

Szpinda M, Brazis P, Elminowska-Wenda G, Wisniewski M (2006) Morphometric study of the aortic and great pulmonary arterial pathways in human foetuses. Ann Anat 188: 25–31

Szpinda M, Szwesta A, Szpinda E (2007) Morphometric study of the ductus arteriosus during human development. Ann Anat 189:47–52

Tandler J (1913) Anatomie des Herzens. Gustav Fischer, Jena

Trop I, Levine D (2001) Normal fetal anatomy as visualized with fast magnetic resonance imaging. Top Magn Reson Imaging 12:3–17

Walmsley R, Monkhouse WS (1988) The heart of the newborn child: an anatomical study based upon transverse serial sections. J Anat 159:93–111

Yamamura J, Schnackenburg B, Kooijmann H, Frisch M, Hecher K, Adam G, Wedegärtner U (2009) High resolution MR imaging of the fetal heart with cardiac triggering: a feasibility study in the sheep fetus. European Journal of Radiology Extra 19:2383–2390

Zielinsky P, Sallum M, Satler F, Gus EI, Nicoloso LH, Manica JL, Piccoli AL Jr (2004) Mobility of the septum primum does not depend on the foramen ovale diameter in normal fetuses. Arq Bras Cardiol 83:304–307

MRI of the Fetal Endocrine Glands

Maria Theresa Schmook

Contents

Abstract

› Prenatal pathologies of the endocrine glands are generally rare, and reports in the literature about the use of fetal MRI for this purpose are still scarce. However, sonography and postnatal MR literature can help to assess the examination. For the pituitary gland, a T1w sequence is recommended to visualize the typical bright spot of the whole fetal gland. Possible pathologies include pituitary aplasia, duplication, ectopy, and transsphenoidal meningocele. The pineal gland is not demonstrable in fetal MRI. The thyroid gland is T1w hyperintense, and size can be measured, including screening for fetal goiter. In case of cervical teratoma or cystic hygroma, the position of the thyroid and trachea relative to the tumor should be assessed. The ovaries and undescended testes are usually not delineable. Fetal MRI is helpful in assessing ovarian cysts and possible complications, such as hemorrhage or torsion. In case of hydrocele, fetal MRI may be valuable in distinguishing simple from complex cases, the latter being associated with testicular torsion, inguinoscrotal hernia, or meconium periorchitis. For fetal MRI of the pancreas and adrenal glands, see Chapter 22.

1 Introduction

The following text provides an overview of the embryology, imaging features, and possible connatal pathologies of the pituitary, pineal, thyroid, and parathyroid glands

M.T. Schmook
Department of Radiology, Division of Neuroradiology and Musculoskeletal Radiology, Medical University of Vienna
Waehringer Guertel 18-20, 1090 Vienna, Austria
e-mail: maria.schmook@meduniwien.ac.at

D. Prayer (ed.), *Fetal MRI*, Medical Radiology,
DOI: 10.1007/174_2010_115, © Springer-Verlag Berlin Heidelberg 2011

and gonads in fetal MRI (the adrenal glands and pancreas are discussed in the chapter "MRI of the Fetal Abdomen"). However, prenatal pathologies of the endocrine glands are generally rare, and reports of cases that have been diagnosed with fetal MRI are still rare. As a consequence, the majority of considerations regarding the MR-based fetal diagnosis and detectability of such pathologies must remain theoretical and/or be based on the knowledge from postnatal MRI literature and sonography data. MR images of pathologies of the fetal endocrine glands are quite rare and cannot always be provided.

2 The Pituitary Gland

2.1 Embryology

According to traditional literature, the pituitary gland has two origins:

2.1.1 The Adenohypophysis

The adenohypophysis (anterior lobe) derives from the oral ectoderm. During gestational week (GW) 3, the roof of the stomodeum gives rise to Rathke's pouch, a diverticulum that grows upward and meets the infundibulum at about day 42. The anterior wall of the diverticulum develops into (1) the pars anterior, and another part grows around the infundibulum and forms (2) the pars tuberalis, and the posterior wall transforms to (3) the pars intermedia of the adenohypophysis. The lumen of the diverticulum shrinks to a residual (mostly unrecognizable) cleft due to surrounding cell proliferation. The diverticulum's stalk regresses, and the connection to the oral cavity is lost during GW 6 (Moore and Persaud 2008; Sadler and Drews 2008). An alternative theory hypothesizes a neuroectodermal origin of the anterior lobe, with the adenohypophysis originating from cells in the ventral neural ridge (Morton 1957; Zhu et al. 2005; Castillo 2005).

2.1.2 The Neurohypophysis

The neurohypophysis (posterior lobe of the pituitary gland) originates from the neuroectoderm. The ventral part (floor) of the diencephalon gives rise to the neurohypophyseal diverticulum, which grows downward and forms the infundibulum to meet the primordium of the adenohypophysis around day 42. The infundibulum then differentiates into (1) the median eminence, (2) the infundibular stalk, and (3) the pars nervosa of the neurohypophysis (Moore and Persaud 2008; Sadler and Drews 2008).

2.2 Imaging Features

For the evaluation of the pituitary gland with fetal MRI, a T1-weighted (T1w) sequence is recommended, and all available planes are suitable. The pituitary stalk is best depicted on T2w images, and all orthogonal planes are appropriate.

2.2.1 Imaging Features with T1 Weighting

On T1w images, the whole pituitary gland appears brightly hyperintense compared to brain tissue (e.g., the pons) and skull base (Fig. 1). In our experience, separation of the anterior and posterior lobe is not reliably possible in the fetus (Fig. 1b), and detectability of the pituitary is low before GW 21, and usually high (>85%) in the third trimester. Regarding pituitary *size*, the maximum diameter of the fetal pituitary gland (regardless of plane) increases with gestational age (GA) and ranges from 2 to 6 mm in the second trimester (Schmook et al. 2010) and up to 8 mm in the third trimester. The pituitary stalk may be delineable on T1w images, as it is slightly hyperintense to CSF.

2.2.2 Imaging Features with T2 Weighting

On T2w images, the pituitary gland shows a flat or convex border to the CSF space in the supracellar cistern. Delineation against the sellar walls and surrounding skull base is difficult and frequently not possible, as the hypophysis is iso- to only slightly hyperintense (Fig. 2b). The pituitary stalk is usually nicely depictable (especially after gestational week 21) as a thin hypointense thread (sagittal and coronal sequences, Fig. 2a, b) or dot (axial sequences, Fig. 2c) located in the median plane.

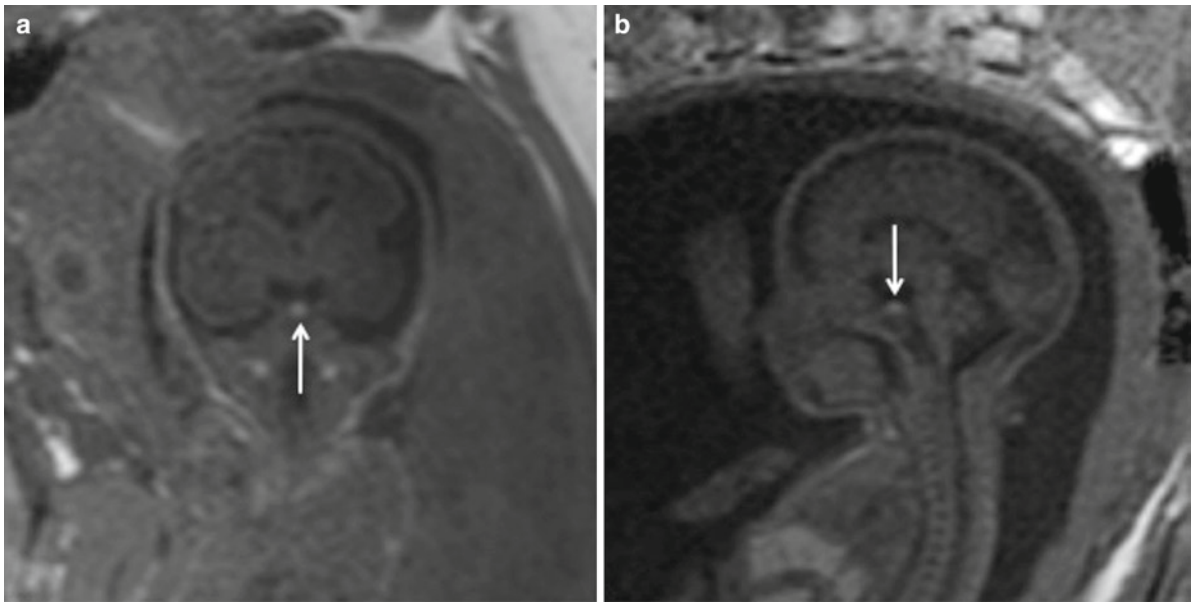

Fig. 1 Coronal (**a**) and sagittal (**b**) T1-weighted MR images of two different fetuses showing the typical bright spot (*arrows*) of the pituitary gland at GW 27 and 26, respectively

2.2.3 Why Is the Fetal Pituitary Gland Hyperintense on T1?

The T1 hyperintense signal contributed by the neurohypophysis correlates with its postnatal signal pattern, and is well known as the "bright spot" on T1w images, regardless of age. This is due to storage of the vasopressin–neurophysin complex (Colombo et al. 1987; Kurokawa et al. 1998; Lee et al. 2001) in the posterior lobe. The T1w hyperintense signal of the fetal anterior lobe differs from the hypointense signal in children and adults. Its hyperintensity in fetal age is believed to be related to histological changes, higher hormonal synthetic activity, the amount of endoplasmic reticulum (Cox and Elster 1991), the increased number of prolactin cells after week 25 (Asa et al. 1986; Kitamura et al. 2008), and/or the effect of placental estrogens (Kitamura et al. 2008). The signal change from hyper- to hypointense usually occurs within the first 6–8 weeks of postnatal life (Cox and Elster 1991; Dietrich et al. 1995).

2.2.4 Comparison of the Fetal with the Postnatal Pituitary Signal Pattern in Preterm Babies

With regard to the comparison of the prenatal signal pattern of the pituitary to the postnatal pituitary signal in preterm neonates, Argyropoulou et al. showed a negative correlation of the T1 signal of the pituitary gland of preterm children with chronological and corrected age. These authors also observed that the T1 hyperintense signal of the adenohypophysis (compared to the vermis white matter) of preterm babies may persist up to 2 months of the corrected age (Argyropoulou et al. 2004). Another study (Kitamura et al. 2008) that analyzed MRIs of preterm babies, imaged at term-equivalent age, found slightly different results. That study confirmed the significant negative correlation of the relative signal intensity (compared to the pons) of the anterior pituitary lobe of preterm babies with postnatal age, but not with gestational age at birth. They concluded that a nonhyperintense anterior pituitary is a normal finding in preterm babies when imaged near term.

2.3 Pathologies

2.3.1 Pituitary Aplasia

Pituitary aplasia is a very rare abnormality, especially when it is not part of a major brain anomaly, such as anencephaly. It may be associated with facial abnormalities, and boys may show hypoplastic external genitalia.

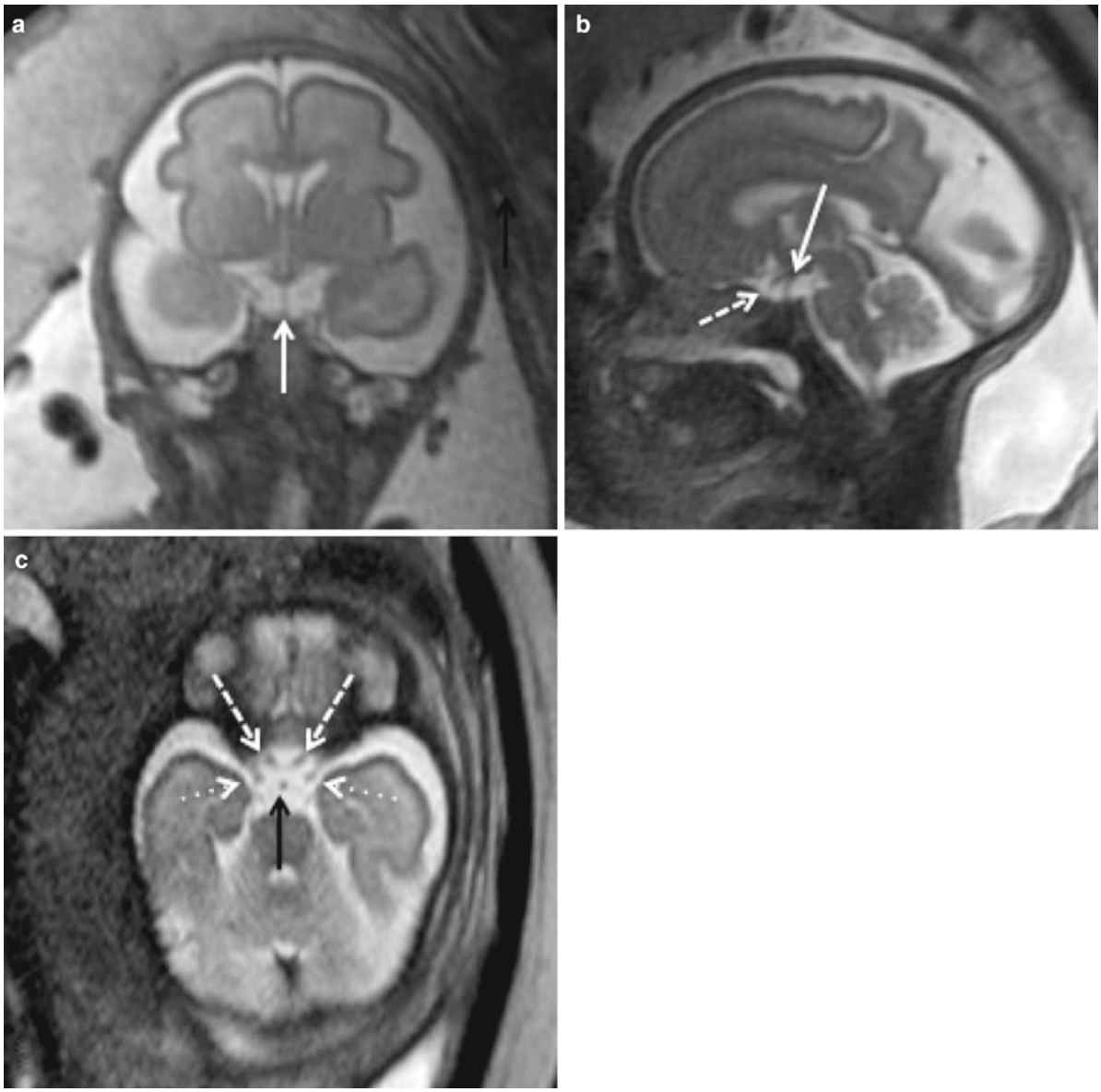

Fig. 2 T2-weighted MR images of three fetuses (GW 28, 32, and 29, respectively) showing the infundibulum as a thin thread in the coronal and sagittal plane (*white arrows in* (**a**) *and* (**b**)), and as a dot in the axial plane (*black arrow in* (**c**)). It can be clearly delineated from the chiasm/optical nerves (*dashed arrows in* (**b**), (**c**)) and the intradural segment of the internal carotid arteries (*dotted arrows in* (**c**)). In contrast to T1w images, the pituitary gland cannot be delineated against the sellar walls and skull base on T2 w images (**b**). Note that the fetal pineal gland is not depictable (**b**)

As it may lead to severe postnatal hypoglycemia due to neonatal panhypopituitarism (Cervantes et al. 2006), prenatal recognition is important.

This diagnosis should be considered when the hyperintense pituitary signal is missing on T1, and the infundibulum is not delineable on T2. In addition, the sella should be flat. Nevertheless, it should be noted that an absent pituitary bright spot does not automatically equal aplasia, as its detection is not always possible in all cases. Nevertheless, detection rates are high (>85%) in the third trimester. A follow-up examination at a later gestational age and/or postnatally could substantiate or undermine the suspicion.

2.3.2 Pituitary Duplication and Triplication

Pituitary duplication is an extremely rare malformation, and, to our knowledge, only postnatally diagnosed cases have been reported as yet. It can be associated with other abnormalities, such as facial dysmorphism, cleft palate, nasopharyngeal teratomas, agenesis of the corpus callosum, or basilary artery duplication (Kollias et al. 1995; Shroff et al. 2003; de Penna et al. 2005; Huismann et al. 2005). Diagnosis with fetal MRI seems possible, in principle, as the postnatally reported doubled (left and right paramedian) pituitary bright spot (T1), the doubled infundibulum (T2), and the associated thickening of the floor of the third ventricle should be delineable, at least at a later gestational age.

Pituitary triplication has been reported once in an infant (Manara et al. 2009).

2.3.3 Ectopia of the Posterior Pituitary Lobe

Ectopia of the posterior lobe can occur in isolation, or in association with other abnormalities, such as agenesis of the corpus callosum, the olfactory nerves (in Kallmann syndrome), septooptic dysplasia (including agenesis of the septum pellucidum), or lobar holoprosencephaly (Spampinato and Castillo 2005). Diagnosis of neurohypophyseal ectopy with fetal MRI seems possible at later gestational ages, but is highly dependent on the size of the posterior pituitary lobe, and on good T1w image quality. Theoretically, one would expect two pituitary bright spots on T1, one in the sellar region (regularly located fetal adenohypophysis) and one in an atypical suprasellar position (ectopic neurohypophysis, Fig. 3). Particularly if a case shows one of the associated malformations listed above, the position (and number) of the fetal pituitary bright spot(s) should be assessed carefully.

2.3.4 Transsphenoidal Meningoencephalocele

Due to their location, transsphenoidal meningoencephaloceles can affect the pituitary and infundibular position and form.

There are two subtypes of transsphenoidal meningoencephalocele, the intrasphenoidal and the truly transsphenoidal variant, the latter protruding into the nasopharynx (Jabre et al. 2000). This diagnosis should be suspected in fetal MRI when an atypical contour of the skull base is noticed on sagittal and coronal images, with a CSF-filled protrusion in the sellar and sphenoid region that may contain the (atypically located) pituitary bright spot, the infundibulum, the hypothalamus, the chiasm, or the anterior cerebral arteries. Associated abnormalities include corpus callosum agenesis and craniofacial midline defects (Jabre et al. 2000; Spampinato and Castillo 2005).

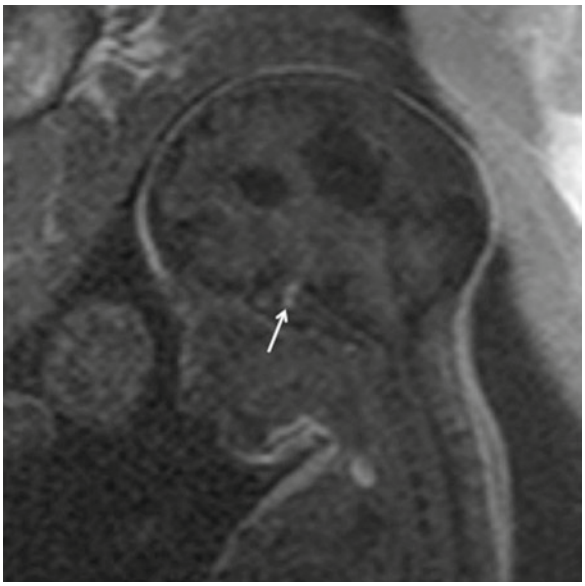

Fig. 3 Sagittal T1-weighted image of a fetus with holoprosencephaly, face dysmorphism, and omphalocele (GW 33+2) who presented with a doubled pituitary bright spot (*arrow*). Ectopy of the posterior pituitary lobe was suspected on the assumption that the second spot in the suprasellar region represented the ectopic neurohypophysis

2.3.5 Congenital Tumors

Apart from the fact that congenital CNS tumors are rare (10% of all fetal tumors), the suprasellar area is a possible location. Thus, the sella and the pituitary gland may be affected.

These tumors grow rapidly and may become huge, so that determination of their exact origin can be difficult. The mass is usually detected in the third trimester. It may be associated with other abnormalities, such as facial clefts, and can lead to

macrocephaly, hydrocephalus, and polyhydramnios (Woodward 2005 and Woodward et al. 2005). The prognosis is poor.

Possible entities include teratoma (which accounts for 50% of fetal intracranial tumors) and craniopharyngioma. Differentiation between tumor entities, especially between connatal teratoma and craniopharyngioma, is often impossible, as they both have cystic and solid components and T1w hyperintense areas (proteinaceous content in craniopharyngioma, fat in teratoma; methemoglobin in case of tumor hemorrhage, and calcification that may be T1w hyperintense). When the tumor is located suprasellarly, the chiasm and infundibulum usually cannot be delineated from the mass. Moreover, assessment of the presence and location of the pituitary bright spot is very limited, as it may be indistinguishable from T1w hyperintense tumor areas. See also chapter "Cerebral Acquired Disease".

2.3.6 Miscellaneous

Other possible pathologies of the pituitary and sella include a pharyngeal hypophysis, pituitary hypoplasia, or a persistent craniopharyngeal canal, but it is highly improbable that these diagnoses are possible with fetal MRI.

3 The Pineal Gland

3.1 Embryology

The pineal gland develops from the caudal part of the roof of the diencephalon, where the epithelium thickens and a median diverticulum is formed in GW 7, and then transformed into a solid structure by cell proliferation (Moore and Persaud 2008; Sadler and Drews 2008).

3.2 Imaging Features

The fetal pineal gland is usually not delineable with fetal MRI (Fig. 2b). The gland may be visible in later gestational weeks, in exceptional cases, on T2w sagittal images.

3.3 Pathologies

The pineal region is a possible location for fetal intracranial tumors, such as teratoma (see Sect. 2.3.5 "Congenital Tumors" and Chapter 18 "Cerebral Acquired Disease").

4 The Thyroid Gland

4.1 Embryology

The thyroid gland is of endodermal origin. At approximately day 24, a bud is formed in the floor of the primordial pharynx, directly caudal to the tuberculum impar of the tongue anlage. The bud's position will be later marked by the foramen cecum of the tongue. The thyroid primordium descends ventral to the hyoid bone and laryngeal cartilages to the neck, thus forming the thyroglossal duct. Anterior to the second and third tracheal ring, this duct gives rise to the primordial isthmus, which sprouts bilaterally to form the thyroid lobes. The definite localization and shape of the thyroid gland is accomplished at 7 weeks, and functional activity begins at about week 12 (Moore and Persaud 2008; Hinrichsen 1990). Maternal T4 can cross the placenta, and thus, contributes to fetal supply prenatally (Polak and Van Vliet 2010).

Transiently, the thyroglossal duct connects the tongue and the thyroid and degenerates later. The caudal part of the thyroglossal duct can persist and give rise to the pyramidal lobe, an accessory lobe located superior to the thyroid isthmus (Moore and Persaud 2008; Sadler and Drews 2008; Hinrichsen 1990).

The parafollicular, or C cells, originate from cells of the ultimobranchial body (a derivative of the fifth pharyngeal pouch) that wander into the thyroid anlage (Hinrichsen 1990; Fontaine 1979).

4.2 Imaging Features

For the assessment of the fetal thyroid gland, a coronal T1w sequence is recommended, as the gland contrasts well against the surrounding neck tissue, and a combined evaluation of its position, shape, and size (with regard to lobe length and transverse diameter) is possible. Additional measurements can be performed in the axial plane (if available).

4.2.1 Imaging Features with T1 Weighting

As fetal thyroid gland tissue is hyperintense on T1w sequences, the gland can be depicted as a T1w hyperintense structure bilateral and ventral to the trachea. The characteristic thyroidal shape, with its two lobes and isthmus, can be observed best in the coronal plane (Fig. 4a). An accessory pyramidal lobe is probably only delineable at later gestational ages, if it is prominent.

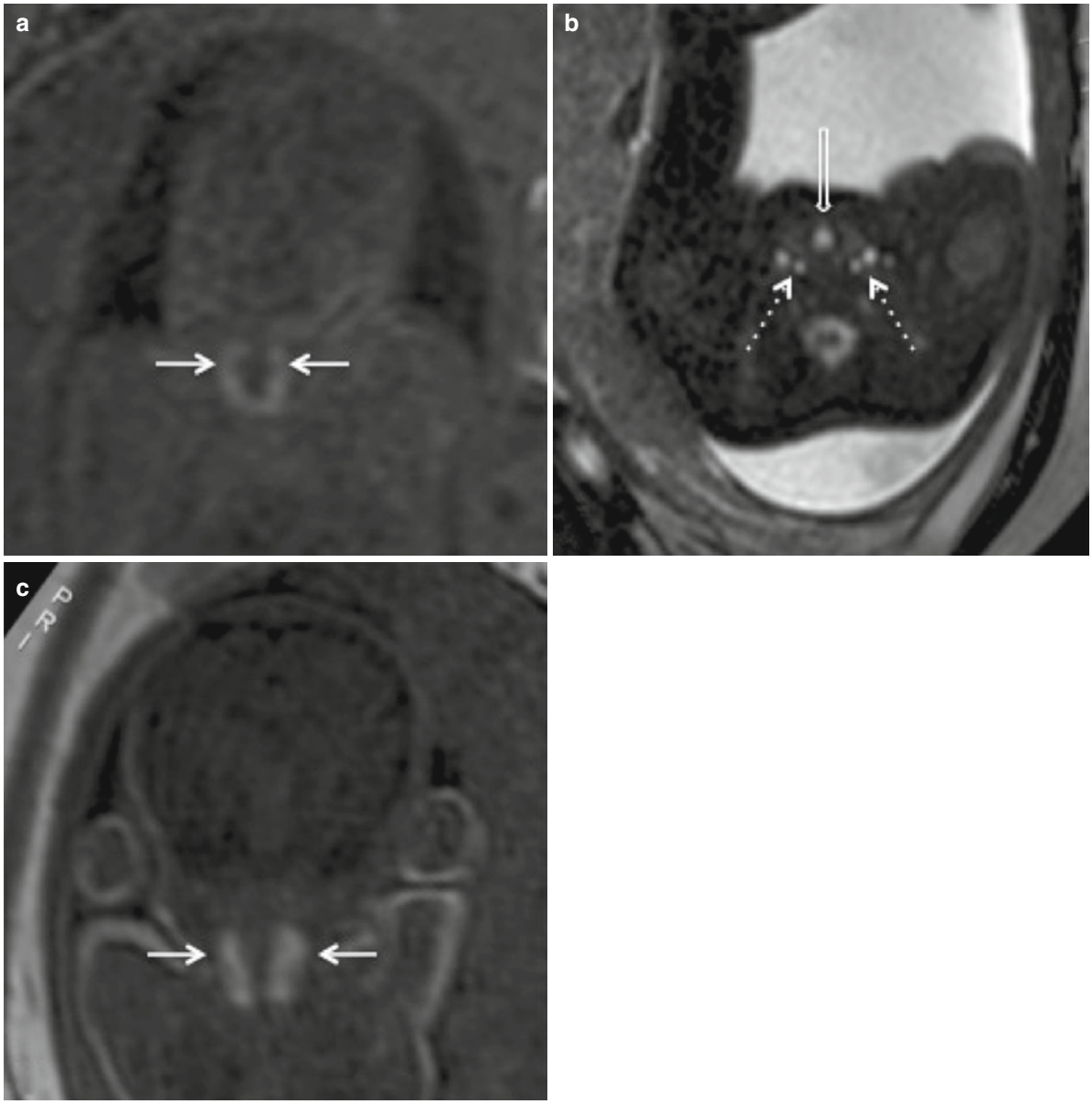

Fig. 4 The thyroid gland in fetal MRI: (**a**) Coronal T1w image with the *white arrows* pointing at the hyperintense lobes of a regularly sized thyroid gland at GW 27. (**b**) T2-weighted axial SSFE image showing the slightly hyperintense thyroid gland (GW 31). The *block arrow* points at the fluid-filled trachea, and the *dotted arrows* mark the hyperintense cervical vessels at the posterolateral border of the thyroid lobes. (**c**) Coronal T1w image of a fetal goiter at GW 28. This fetus suffered from fetal hyperhyreosis secondary to maternal Graves' disease. Compare the size of the enlarged thyroid gland (**c**) to the size of the thyroid gland in the normal case (**a**)

4.2.2 Imaging Features with T2 Weighting

On T2w images, the normal fetal thyroid gland is isointense to slightly hyperintense compared to the surrounding soft tissue, including the muscles. T2w sequences can help in visualizing the position of the thyroid relative to the fluid-filled trachea (axial plane) and the ventral contour of the neck (sagittal plane). In steady-state free precession (SSFP) sequences, the cervical vessels are hyperintense, and thus can serve as indirect markers for the posterolateral borders of the thyroid lobes (axial plane, Fig. 4b).

4.2.3 Thyroid Size

Thyroid size can be measured in the coronal and axial planes. To our knowledge, MR-based normal values for thyroid size, related to gestational age, are not yet available. Nevertheless, the literature provides thyroid measurements (including diameters and volume), normograms, and/or formulas based on sonography (Bernardes et al. 2008; Radaelli et al. 2002; Achiron et al. 1998; Ho and Metreweli 1998) and on autopsy (Cicekcibasi et al. 2007) For example, Cicekcibasi's study, based on autopsies of spontaneously aborted fetuses, found a mean lobe length of 8.8 mm (right lobe) and 8.5 mm (left lobe) in the second trimester, and 13.0 mm (right lobe) and 12.2 mm (left lobe) in the third trimester. The mean axial transverse diameter of the lobes increased from 4.6 mm in the second trimester to 6.6 mm (right lobe) and 5.9 mm (left lobe) in the third trimester, and the mean sagittal axial diameter increased from 2.8 mm (right lobe) and 2.9 mm (left lobe) to 3.1 mm (right and left lobe, respectively). Bernardes et al. provided normograms of the fetal thyroid area, the circumference and transverse diameter by gestational age, and the estimated fetal weight. They found a sonographically measured fetal thyroid transverse diameter (FTTD, distance between the *lateral* borders of the right and left lobe) from 1.19 cm at 22 weeks to 1.89 cm at 35 weeks (mean values), and defined a formula for normal FTTD, according to gestational age (GA): FTTD (cm) = 0.054 × GA (weeks). Ho et al. published a normogram for the normal fetal thyroid volume related to gestational age, and showed an exponential growth of the fetal thyroid, with the highest growth rate after GW 32. The fetal thyroid volume/estimated birth weight ratio was lower than postnatally.

The assessment of fetal thyroid size is especially important in mothers with a history of thyroid dysfunction. Monitoring is usually performed by sonography, but could also be done via fetal MRI.

4.3 Pathologies

Prenatal pathologies of the thyroid gland are generally rare. Nevertheless, diagnosis is important, as thyroxine plays a role in human growth and CNS development. Thus, congenital hypothyroidism represents a preventable cause of delayed physical and psychological development of the child. Undiagnosed fetal thyroid dysfunction may significantly increase morbidity and mortality.

4.3.1 Thyroid Agenesis

Thyroid agenesis and hemiagenesis are very rare, but could be suspected if there is a (globally or unilaterally) missing T1 hyperintense signal of the thyroid on fetal MRI in loco typico.

4.3.2 Ectopic and Accessory Thyroid Tissue

Ectopic thyroid tissue often represents the only thyroid tissue in an individual, and is mostly located lingually or sublingually. In fetal MRI, ectopy of the thyroid gland could be suspected if the T1 hyperintense signal of the thyroid tissue were absent, *and* could be localized in a clearly abnormal position along the thyroglossal duct.

Accessory thyroid tissue (in addition to a regularly located thyroid gland) may appear in the thymus or lateral to the thyroid cartilage. Its detection by fetal MRI is improbable due to its size.

4.3.3 Fetal Goiter

Enlargement of the fetal thyroid may be a sign of fetal thyroid dysfunction, and is often secondary to maternal thyroid dysfunction or medication. Fetal

hyperthyroidism can be due to transplacental passage of maternal thyroid-stimulating antibodies in Graves' disease. Fetal hypothyroidism can be the consequence of transplacental passage of maternal antithyroid medication (in maternal hyperthyreosis) or maternal thyrotropin-binding inhibitory immunoglobulin. In other cases, it may be due to endemic iodine deficiency, maternal lithium medication, and genetic defects in fetal thyroid biosynthesis (Woodward 2005; Nath et al. 2005).

In case of fetal struma, fetal MRI demonstrates an anterior neck mass with the typical thyroid form and contour, representing the enlarged gland. Large goiters can be recognized easily visually (Fig. 4c). However, moderate cases could be missed by visual assessment alone, so that comparison of measurements with normal values for the respective gestational age is needed (see Sect. 4.2.3), especially in cases of maternal thyroid dysfunction. Fetal goiters show the typical homogeneous T1 hyperintense signal of the thyroid, and the T2w signal has been described as intermediate (Karabulut et al. 2002), or as rather hyperintense compared to the musculature (Kondoh et al. 2004). In severe enlargement, compression of the trachea can occur, especially with regard to the transverse diameter (Agrawal et al. 2002, Shinmoto et al. 2000). In such a case, the fluid filling of the trachea would be narrowed or interrupted at the thyroid level. The anterior contour of the neck may become convex due to the goiter, and the cervical vessels may be displaced posteriorly. In voluminous struma, the cervical spine is hyperextended, which may lead to dystocia, so that a Cesarean may be the best choice.

Associated findings include polyhydramnios (if the fetal struma leads to swallowing difficulties), hydrops (due to vascular shunting within the enlarged gland or tachycardia in case of fetal hyperthyreosis), intrauterine growth retardation, accelerated (in fetal hyperthyroidism) or delayed (in fetal hypothyroidism) skeletal maturation, and, sometimes, ovarian cysts (in fetal hypothyroidism). Postnatally, respiratory distress may occur due to tracheal compression or tracheomalacia.

The prognosis for fetal goiter is good if it is treated by the optimization of maternal therapy or intraamniotic drug injections in severe cases (Koyuncu et al. 2010; Polak and Van Vliet 2010). Regular measuring of the fetal thyroid size may be one tool for monitoring the therapeutic effect, as improvement/normalization of thyroid size has been described in successful therapy (Nath et al. 2005). If the thyroid size remains the same or increases, these measurements may help to make the decision to proceed with invasive diagnostics, such as evaluation by cordocentesis (to assess fetal hormone levels), which has a known fetal mortality risk.

4.3.4 Cervical Tumors

General Considerations

In case of a cervical tumor, e.g., teratomas, fetal MRI can be helpful in assessing tumor extent, establishing the diagnosis, and assessing the position and patency of the adjacent anatomical structures. The position of the thyroid gland in relation to the tumor should be described, and the possibility of a thyroidal origin and/or involvement should be evaluated, although differentiation of the thyroid and T1 hyperintense tumor components may sometimes be difficult. Displacement of cervical vessels and displacement and/or obstruction of the trachea and esophagus should be mentioned (if delineable), as these details can be important for delivery mode and therapeutic strategies, including an EXIT (ex utero intrapartum treatment) procedure, and postnatal surgical planning (Mittermayer et al. 2005; Kathary et al. 2001; Bouchard et al. 2002; Suzuki et al. 1998).

Cervical Teratoma

The neck is the second most common site for teratomas after the sacrococcygeal region. Cervical teratomas occur sporadically and contain derivates of all three germ cell layers.

Such a tumor presents as a rapidly growing and often large anterior neck mass that frequently involves the thyroid gland, and may reach the mastoid cranially and the mediastinum caudally. It has solid and cystic components, and thus an often mixed signal intensity (Fig. 5), with intermediate solid parts, T2w hyperintense cysts, and (if large enough) T1w and T2w hyperintense fat (Woodward 2005). Calcifications are present in half of all cases and may lead to susceptibility effects in gradient echo EPI (echo planar imaging) sequences. However, identification of intratumoral calcifications can be difficult in fetal MRI, especially when calcifications are small, or in cases of coexistent hemorrhage (ultrasound is preferable for calcification assessment).

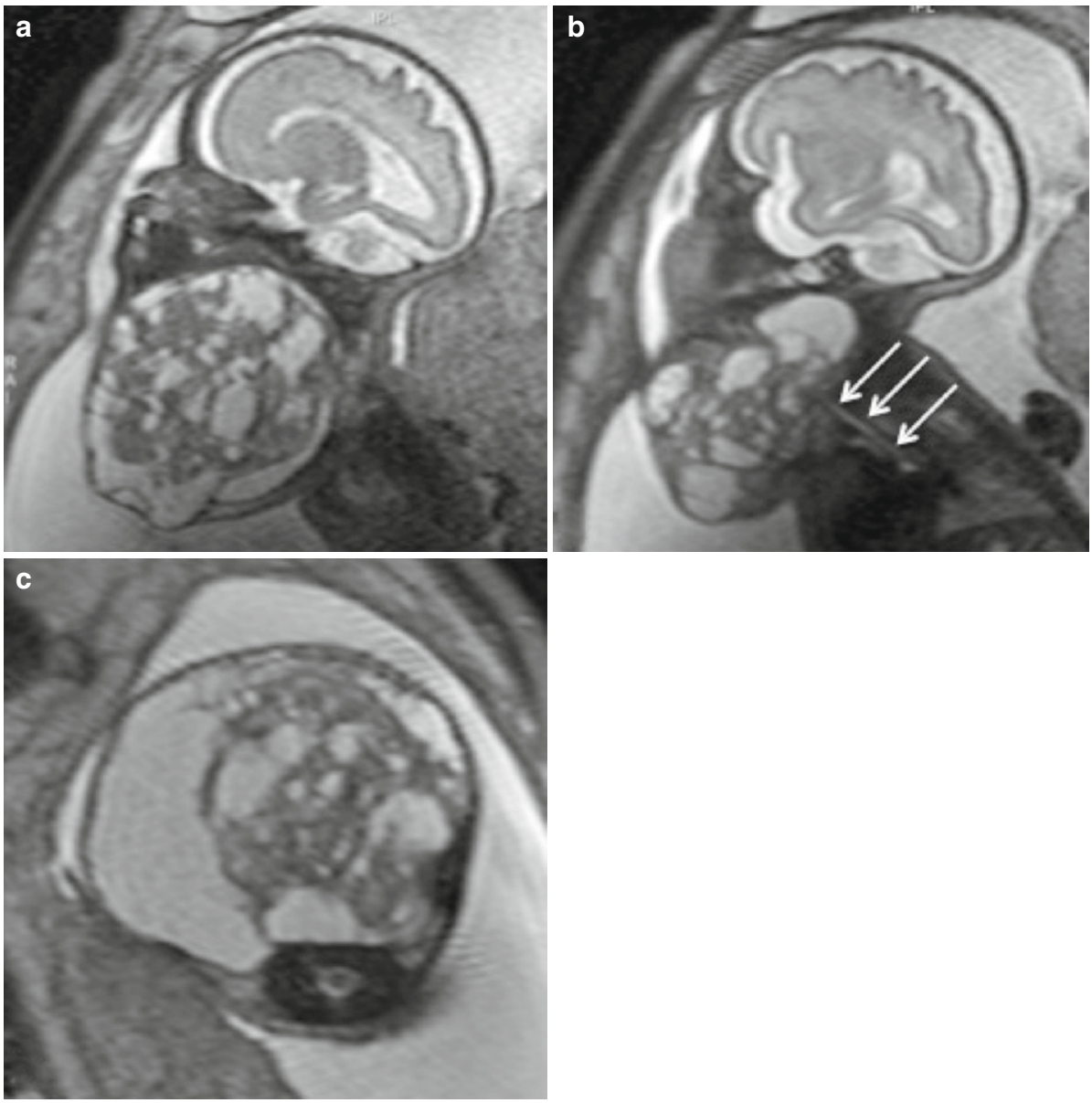

Fig. 5 Cervical teratoma at GW 29+5 (histology proven): Sagittal (**a**, **b**) and axial (**c**) T2-weighted MR images show a large anterior neck mass with cystic and solid components. Note the hyperextended neck (**a**, **b**). The trachea was only partly traceable and was displaced laterally (*arrows* in (b)). Tracheal obstruction was suspected and proved postnatally

Associated findings include a hyperextended neck (due to the anterior centered mass, this may lead to dystocia), polyhydramnios (due to esophageal obstruction and/or swallowing difficulties, which may lead to preterm labor), cardiac failure and hydrops, and distorted anatomy with displacement and compression of the larynx, trachea (Fig. 5a, b), and pharynx (Kathary et al. 2001; Mittermayer et al. 2005).

Untreated cervical teratomas have a poor prognosis in cases of airway obstruction. Mortality can be lowered by the EXIT procedure, which allows the airway to be secured, in many cases, by intubation or tracheostomy while placental support is maintained (Bouchard et al. 2002). Postnatally, tumor extirpation is performed. Monitoring of thyroid and parathyroid function is important, as these glands may be impaired by the tumor itself or by surgery (Kirchhoff et al. 2006).

Cystic Hygroma

A cystic hygroma is a lymphangioma that results from failed fusion of the primordial lymph sac with the central venous system, or from sequestered embryonic lymph sacs. It occurs genetically, and sporadically, and is associated with Turner syndrome, Down syndrome, Noonan syndrome, and fetal alcohol syndrome. Patients with cystic hygroma may also have concurrent cardiovascular anomalies (Ganapathy et al. 2004).

Cervical lesions are often located posteriorly, and, in these cases, the nuchal ligament can be delineable as a median sagittal septum within the hygroma. The masticator and submandibular space are other frequent sites. The size of cystic hygromas is variable, and they may become large masses. The characteristic imaging features of a hygroma include a uniloculated or multiseptated cystic mass that typically spreads transspatially without, or only slightly displacing, vessels and other anatomical structures (Fig. 6). The cystic compartments are T2w hyperintense, the thin septa hypointense (Fig. 6a). In case of hemorrhage, the content of the cysts may be T1w hyperintense and T2w partly hypointense, with fluid–fluid levels. Some lesions show venous vascular components. Airway obstruction may occur in airway mucosal lesions or in large lymphangiomas that encase and displace the trachea. Cystic hygromas can be associated with hydrops.

Therapy options include surgery (with a high recurrence rate due to incomplete surgical resection) and percutaneous sclerosing agents (in large transspatial lesions) (Woodward 2005; Harnsberger 2004). Spontaneous regression has been observed in 10–18% of cases (Ganapathy et al. 2004). Small cystic hygromas may transform into a thick nuchal fold.

Miscellaneous

Other cervical tumors and tumor-like lesions include the *hemangioma*, a cystic and solid anterolateral lesion that grows exophytically and usually does not lead to compression of adjacent organs. *Thyroglossal duct cysts* may be located anywhere along the thyroglossal duct, but are most often found below the hyoid bone as a median or slightly paramedian cystic mass. Prenatal diagnosis is extremely rare. *Branchial cleft cysts* are usually located anterolaterally. Fetal neuroblastomas are rarely located in the cervical region, as they are most often located within the adrenals. Neuroblastomas are complex cystic masses with thick septations and solid parts.

5 The Parathyroid Glands

5.1 Embryology

The two superior parathyroid glands originate from the dorsal part of the fourth pharyngeal pouch, whereas the two inferior parathyroid glands derive (like the thymus) from the dorsal bulbar parts of the third pharyngeal pouch. In the sixth GW, these pouch segments are unequally displaced caudally (those from the third pharyngeal pouch "outrun" those from the fourth pharyngeal pouch), and the primordial glands are finally located on the superior and inferior dorsal surface of both thyroid lobes (Moore and Persaud 2008; Hinrichsen 1990).

5.2 Imaging Features

The parathyroid glands are not delineable with fetal MRI. This is not surprising, as the parathyroids are minuscule prenatally, ranging from 0.14 mm in the second lunar month to 0.78 mm in the ninth lunar month (Pezerovic-Panijan et al. 1999).

5.3 Pathologies

Prenatal diagnosis of parathyroidal pathologies with fetal MRI is highly improbable. Because of the physiological minuteness of the fetal parathyroids, it is not possible to detect pathological changes of their number (supernumerary glands), location (ectopia), or their size (aplasia, hypoplasia, or hyperplasia) with fetal MRI. Even in cases of a large parathyroidal mass, it is unlikely that the parathyroidal origin of such a cervical mass could be recognized.

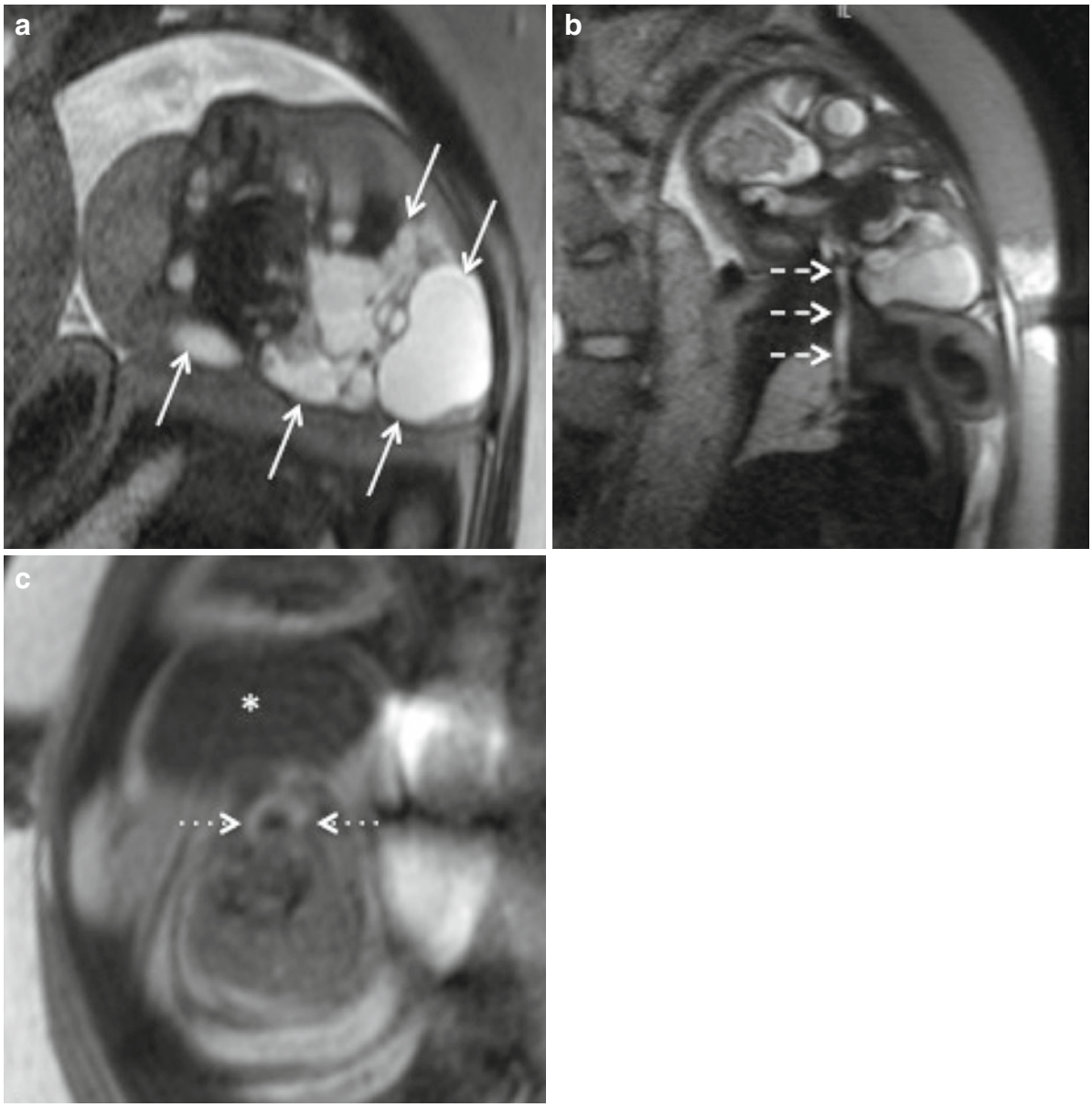

Fig. 6 MR images of a cystic hygroma (histology: cavernous lymphangioma) in a fetus at GW 37+2: Paraaxial (**a**) and oblique (**b**) T2w MR images demonstrate a multiseptated transspatial mass (*white arrows* in (**a**)) in the masticator, submandibular, and cervical regions. Note that the fluid-filled trachea is hardly distorted (*dashed arrows* in (**b**)). The thyroid gland could be identified in its regular position on a paraaxial T1w sequence (*dotted arrows* in (**c**)), despite artifacts. The *asterisk* marks an inferior cyst of the hygroma

Parathyroidal aplasia is part of DiGeorge syndrome, and thus can be indirectly suspected in case of thymus aplasia. Another genetic syndrome associated with primary hypoparathyroidism is HRD syndrome (hypoparathyroidism–retardation–dysmorphism, Kenny–Caffey Syndrome).

6 The Gonads

6.1 Embryology

The testicles and the ovaries develop at the posterior abdominal wall and derive from the mesothelium,

the underlying mesenchyme, and primordial germ cells.

6.1.1 Indifferent Gonads

In the sexually *indifferent stage of development*, the medial side of each mesonephros (a paired transient structure in renal development) thickens and forms the (equally paired) gonadal ridge in gestational week 5. Within the ridge, the epithelium builds the gonadal cords that grow into the underlying mesenchyme. In addition to this, the primordial germ cells migrate from the umbilicate vesicle along the dorsal mesentery of the hindgut to both gonadal ridges, reaching there in GW 6. Thus, the indifferent gonads are formed, being similar in both sexes and consisting of a cortex and a medulla (Moore and Persaud 2008, Sadler and Drews 2008).

6.1.2 Differentiation into Testicles or Ovaries

Differentiation into testicles or ovaries occurs in the seventh to eighth week.

In *genetically male* embryos, the Y chromosome directs testicular differentiation by expressing the testis-determining factor (TDF), coded by the SRY gene. The gonadal cords differentiate into seminiferous cords, which extend into the medulla, lose the connection to the surface epithelium, and form the tubuli seminiferi, tubuli recti, and rete testis. The (prepubertally solid) tubuli seminiferi are formed by Sertoli cells and spermatogonia: the Sertoli cells originate from cells of the surface epithelium and produce the Antimüllerian Hormone (AMH), and the spermatogonia differentiate from the primordial germ cells. The mesenchyme gives rise to the Leydig cells, which are stimulated by human chorionic gonadotropin to produce testosterone, and thereby, induce further male differentiation. Several mesonephric tubules are transformed into ductuli efferentes, which connect the rete testis with the duct of epididymis (Moore and Persaud 2008).

In *genetically female* individuals, the absence of the TDF leads to ovarian differentiation, which occurs slower than testicular differentiation. The gonadal cords extend into the medulla and form a rudimentary rete ovarii, but both structures degenerate. In contrast to males, the surface epithelium proliferates and gives rise to cortical cords, with extend into the mesenchyme and incorporate primordial germ cells. Together, they form primordial follicles. The primordial germ cells differentiate into oogonia, and some, further into primary oocytes. A part of the oogonia and primary oocytes degenerate, and around two million primary oocytes persist and remain in the diplotene of prophase 1. The surface epithelium flattens to a single layer of cells that lies on a thin capsule, the tunica albuginea (Moore and Persaud 2008; Sadler and Drews 2008).

6.1.3 Gonadal Descent

Testicular descent begins with an extraperitoneal relocation from the posterior abdominal wall to the deep inguinal rings, which are usually reached in GW 12. This movement is more a relative than an active movement due to elongation of the trunk, growth of the cranial part of the abdomen, and enlargement of the fetal pelvis. The subsequent passage through the inguinal canal usually occurs around gestational week 26–28. It is controlled by androgens and seems to be promoted by the increasing intraabdominal pressure and guided by the shortening gubernaculum, a ligament that is fixated cranially at the caudal pole of the gonads and caudally in the labioscrotal swellings. In week 33, the testicles have usually reached the scrotum. In 3–4% of full-term newborn males, the testes are still undescended or incompletely descended (Moore and Persaud 2008; Sadler and Drews 2008).

Accordingly, sonography studies reported an absence of testicular descent before gestational week 25/26. In GW 26, uni- or bilateral descent could be documented in 90% of cases, and bilateral descent was found in 93–97% of fetuses after 32 weeks (Birnholz 1983; Achiron et al. 1998). In cases of an apparently empty scrotum in late pregnancy, the possible differential diagnosis of ambiguous genitalia should be kept in mind.

Ovarian descent leads to a repositioning from the posterior abdominal wall to the pelvis. The gubernaculum becomes the ovarian ligament and the round ligament of the uterus (Moore and Persaud 2008).

6.2 Imaging Features

Fetal ovaries and undescended testes cannot usually be visualized with fetal MRI. The ovaries may become

demonstrable in case of ascites or, indirectly, in cases where there is a gonadal mass. Descended testes can be delineated as oval structures of intermediate signal intensity within the scrotum on T2w images (Fig. 7b). The scrotal septum is seen as a thin median hypointense line (Figs. 7a, b and 8b). The sonography literature provides a centile chart for the fetal scrotal size based on circumference measurements (Achiron et al. 1998).

6.3 Pathologies

6.3.1 Hydrocele & Associated Pathologies

Hydrocele, a fluid accumulation around the testes within the scrotum, can be found sonographically in about 15% of male fetuses, especially in the third trimester (Pretorius et al. 1998). It can occur if the processus vaginalis remains open, and thus communication of the scrotum with the peritoneal cavity is possible, and/or if intrascrotal fluid is not resorbed. Simple hydroceles are transient and usually resolve spontaneously (often perinatally). Complex hydroceles, which are much rarer, are associated with inguinal hernia, ascites and hydrops, meconium peritonitis, or testicular torsion (Woodward 2005).

A hydrocele is more frequently unilateral than bilateral. It presents as a T2w hyperintense fluid layer around the testicle(s) and can result in an enlargement of the scrotum (Fig. 8). Differentiation of a thin fluid layer from the scrotal wall may be more difficult in fetal MRI than in sonography, as the scrotal soft tissue itself can be relatively hyperintense on T2w images (Fig. 7). If the hydrocele is unilateral, the scrotal septum is deviated to the contralateral side. An altered signal pattern of the fluid, inhomogeneities, and septa, are suspicious for hemorrhage and may be an early indicator of *testicular torsion* and infarction. If testicular torsion has occurred, according to the sonographic literature, the affected testis would be acutely enlarged compared to the other side, the scrotal wall would be thickened, the scrotal septum (if delineable) deviated to the unaffected side, and a contralateral hydrocele could occur (Herman et al. 2002). Hemorrhagic fluid organized in two concentric compartments has been documented sonographically in a case of prenatal testicular torsion and been called the "double ring hemorrhage" (Herman et al. 2002). Subsequently, the affected testis may become atrophic and calcify (Woodward 2005). Generally, fetal testicular torsion is rare and

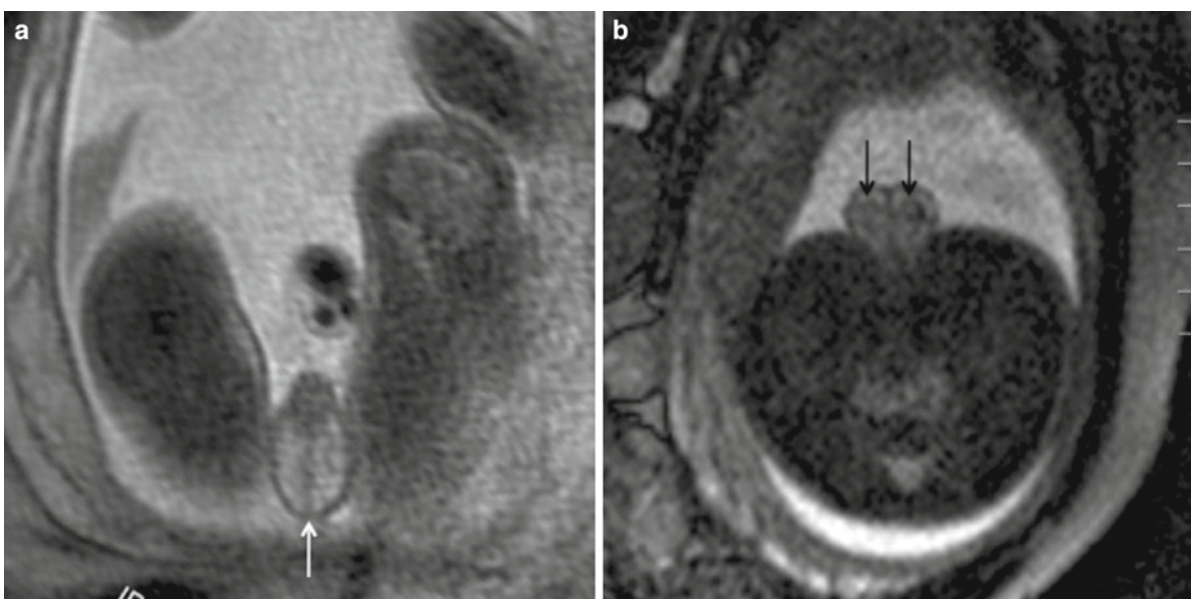

Fig. 7 (**a**) Axial T2-weighted MR image showing an empty scrotum in a fetus aged 22 weeks whose testes are undescended yet. The scrotal septum can be nicely delineated as a thin hypointense median line (*white arrow*). (**b**) Axial T2-weighted MR image of an older fetus with bilaterally descended testes (*black arrows*) at GW 31

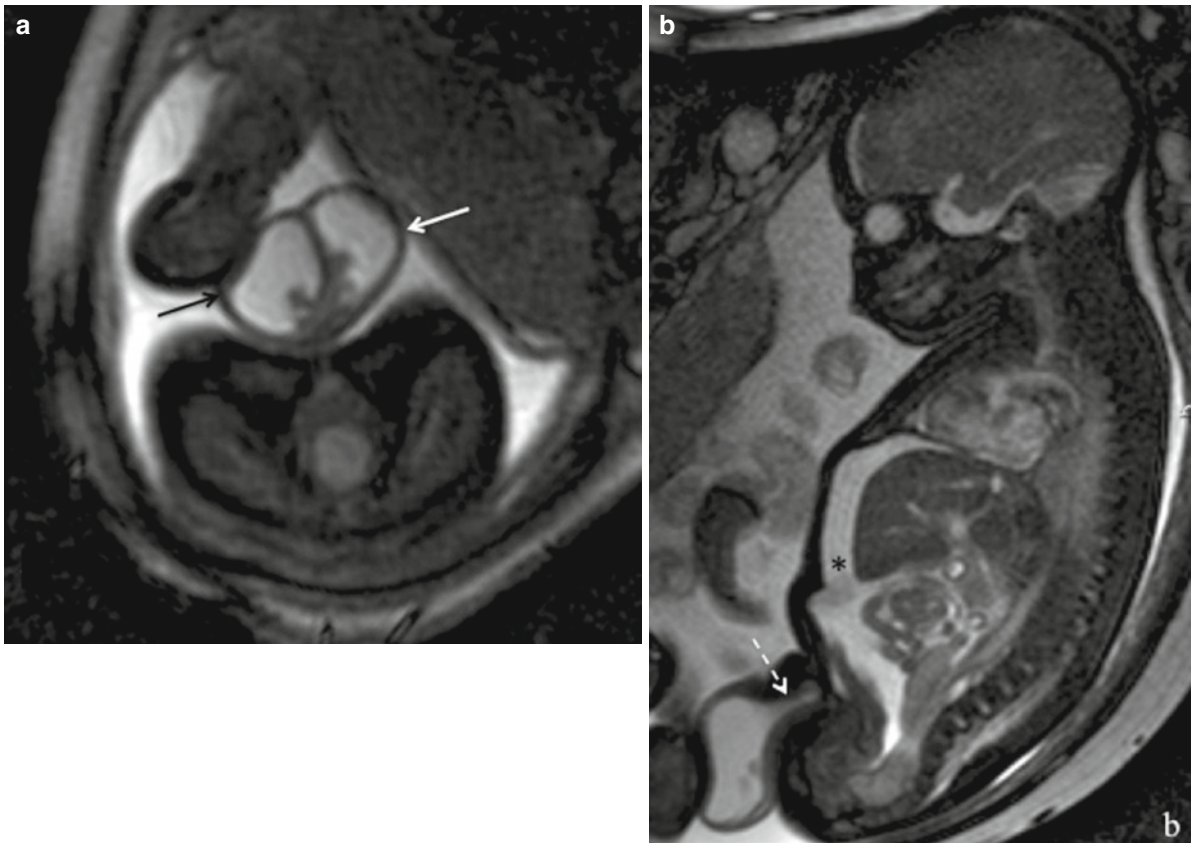

Fig. 8 Massive bilateral hydrocele in a fetus suffering from ascites (GW36+4). The T2-weighted axial MR image (**a**) shows the enlarged scrotum (*black and white arrow*). The scrotal septum is slightly deviated to the *left* side, and the testes seem atrophic (**a**). Note the fluid-filled patent processus vaginalis (*dashed arrow*) and the ascites (*asterisk*) in the paramedian sagittal T2-weighted image (**b**)

usually represents the extravaginal type. The affected testicle can rarely be saved if torsion occurred *in utero* (Woodward 2005).

Meconium peritonitis due to bowel perforation may spread via a patent processus vaginalis to the scrotum and result in *meconium periorchitis*, a rare entity. Meconium periorchitis may be accompanied by an enlarged scrotum, hydrocele, and a scrotal hematoma or mass (Regev et al. 2009). Theoretically, T1 hyperintensities might be seen within the scrotum due to meconium content, and scrotal and abdominal calcifications may be depictable with gradient echo EPI (echo planar imaging) sequences.

As mentioned, hydrocele may also occur in fetal *inguinoscrotal hernia*, which is rarely found prenatally. Associated bowel dilatation may be found in cases of bowel obstruction. Corresponding to sonographic findings (Frati et al. 2008), bowel movements of the herniated loops might be visualized within the enlarged scrotum with a movie sequence, presuming a sufficient resolution.

Testicular tumors, such as teratomas, are extremely rare prenatally and are usually located within the lower abdomen.

6.3.2 Ovarian Cysts

Ovarian cysts represent the most frequent type of abdominal cysts in female fetuses. They can arise if the fetal ovaries react to increased levels of maternal estrogen, placental chorionic gonadotropin, or fetal

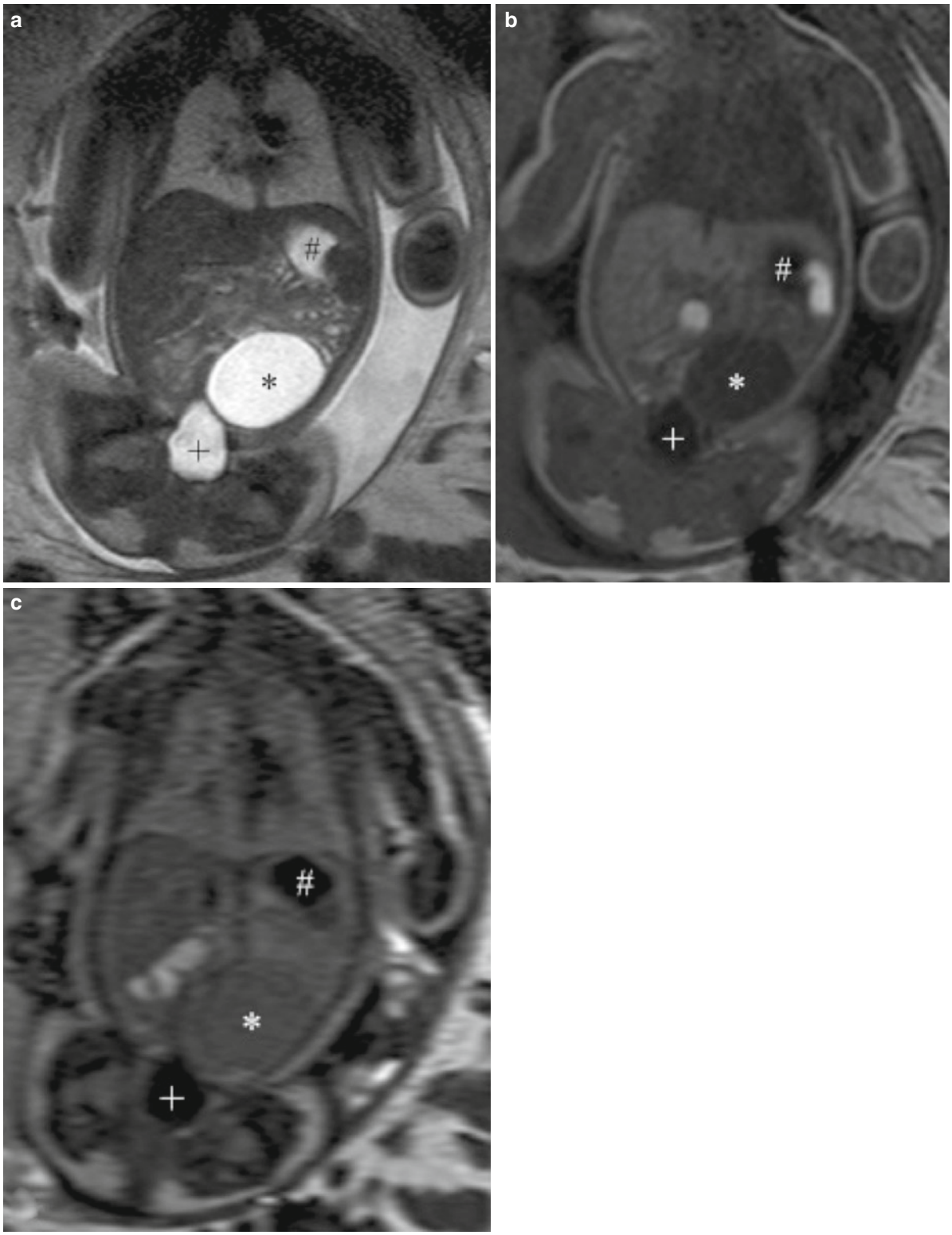

Fig. 9 Coronal MR images of a female fetus with a *left*-sided ovarian cyst (*asterisk*) at GW 33 + 3. Note that the cyst content is isointense to urine (bladder is marked with a "+") and the stomach contents (marked with a "#") in the T2w (**a**) and T1w (**b**) image, but hyperintense in the FLAIR image (**c**). This suggests proteinaceous or hemorrhagic cyst content

gonadotropins. The incidence is higher in diabetic mothers, preeclampsia, and rhesus incompatibility.

It is important to know that fetal ovarian cysts are not confined to the pelvis, but can extend superiorly or even be positioned in the middle or upper abdomen (Hörmann et al. 2005). Furthermore, they may be mobile and change position between different examinations (McEwing et al. 2003).

Ovarian cysts are usually an incidental finding in the third trimester and are more often unilateral than bilateral. They vary in size and may reach a diameter of up to 10 cm. In fetal MRI, an ovarian cyst presents as a uniloculated T2 hyperintense and T1 hypointense sharply demarcated cystic lesion (Fig. 9a, b). Occasionally, septations can be depicted, or a small secondary cyst at the inner side of the cyst wall, a specific feature that has been described as the "daughter cyst sign" in sonography literature (Quarello et al. 2003, Lee et al. 2000). In cases of cystic bleeding, the cyst content may become T2 hypointense, T1 hyperintense, and/or inhomogeneous, and clot formation may be visible. A FLAIR sequence is especially helpful, as it can reliably demonstrate the non-isointensity of the cyst content to urine in case of hemorrhage or proteinaceous content, even if the content is isointense on T2w images (Fig. 9), and fluid–fluid levels. These findings can also be a hint that there is cyst torsion. According to the sonographic literature, complications like intracystic hemorrhage and cyst torsion occur mainly in lesions larger than 5 cm, and have been reported in 35% of cases (Slodki and Respondek-Liberska 2007). In our experience, MRI has depicted hemorrhage in smaller lesions, as well. Rupture can occur, e.g., during labor, and result in ascites. Polyhydramnios is an associated finding in about 10% of cases (Woodward 2005).

Differential diagnoses are manifold, and include hydronephrosis, ureterocele, renal cysts, mesenteral cyst, duplication cyst, meconium pseudocyst, choledochal cyst, dilated bowels, hydrometrocolpos, and intraabdominal tumors, such as teratomas and adrenal cystic lesions. Therefore, abdominal organs should be systematically assessed with regard to delineation from the cystic lesion.

Fetal ovarian cysts that measure less than 5 cm usually resolve spontaneously, but sonographic monitoring is recommended (Slodki and Respondek-Liberska 2007). Alternatively, MRI follow-up is possible, especially when complications, such as hemorrhage, are suspected. In selected cases, prenatal fluid aspiration has been reported in cysts larger than 5 cm for decompression and to lower the risk of torsion (Crombleholme et al. 1997; Slodki and Respondek-Liberska 2007). Elective Cesarean may be the goal in such cases. Surgery is a postnatal therapeutic option, and has been reported in up to 40% of neonates with prenatally diagnosed ovarian cysts (Slodki and Respondek-Liberska 2007).

References

Achiron R, Pinhas-Hamiel O, Zalel Y, Rotstein Z, Lipitz S (1998) Development of fetal male gender: prenatal sonographic measurement of the scrotum and evaluation of testicular descent. Ultrasound Obstet Gynecol 11:242–245

Agrawal P, Ogilvy-Stuart A, Lees C (2002) Intrauterine diagnosis and management of congenital goitrous hypothyroidism. Ultrasound Obstet Gynecol 19:501–505

Argyropoulou MI, Xydis V, Kiortsis DN, Pantou K, Zikou A, Efremidis SC, Andronikou S (2004) Pituitary gland signal in pre-term infants during the first year of life: an MRI study. Neuroradiology 46:1031–1035

Asa SL, Kovacs K, Laszlo FA, Domokos I, Ezrin C (1986) Human fetal adenohypophysis. Histologic and immunocytochemical analysis. Neuroendocrinology 43(3):308–316

Bernardes LS, Ruano R, Sapienza AD, Maganha CA, Zugaib M (2008) Nomograms of fetal thyroid measurements estimated by 2-dimensional sonography. J Clin Ultrasound 36:193–199

Birnholz JC (1983) Determination of fetal sex. N Engl J Med 309:942–944

Bouchard S, Johnson M, Flake A, Howell L, Myers L, Aszick N, Crombleholme T (2002) The EXIT procedure: experience and outcome in 31 cases. J Pediatr Surg 37:418–426

Castillo M (2005) Pituitary gland: development, normal appearances, and magnetic resonance imaging protocols. Top Magn Reson Imaging 16:259–268

Cervantes LF, Altman N, Medina L (2006) Pituitary aplasia. Radiology 241:936–938

Cicekcibasi A, Salbacak A, Seker M, Taner Z, Tuncer I, Buyukmumcu M (2007) Developmental variations and clinical importance of the fetal thyroid gland. A morphometric study. Saudi Med J 28(4):524–528

Colombo N, Berry I, Kucharczyk J, Kucharczyk W, de Groot J, Larson T, Norman D, Newton TH (1987) Posterior pituitary gland: appearance on MR images in normal and pathologic states. Radiology 165:481–485

Cox TD, Elster AD (1991) Normal pituitary gland: changes in shape, size, and signal intensity during the 1st year of life at MR imaging. Radiology 179:721–724

Crombleholme TM, Craigo SD, Garnel S, D´Alton ME (1997) Fetal ovarian cyst decompression to prevent torsion. J Pediatr Surg 32(10):1447–1449

De Penna GC, Pimenta MP, Drummond J, Sarquis M, Martins J, de Campos RC, Dias EP (2005) Duplication of the

hypophysis associated with precocious puberty: presentation of two cases and review of pituitary embryogenesis. Arq Bras Endocrinol Metabol 49:323–327
Dietrich RB, Lis LE, Greensite FS, Pitt D (1995) Normal MR appearance of the pituitary gland in the first 2 years of life. Am J Neuroradiol 16:1413–1419
Fontaine J (1979) Multistep migration of calcitonin cell precursors during ontogeny of the mouse pharynx. Gen Comp Endocrinol 37:81–92
Frati A, Ducarme G, Vuillard E, Pecastaing A, Yver C, Pejoan H, Luton D (2008) Prenatal evaluation of a scrotal mass using a high-frequency probe in the diagnosis of inguinoscrotal hernia. Ultrasound Obstet Gynecol 32:949–950
Ganapathy R, Guven M, Sethna F, Vivekananda U, Thilaganathan B (2004) Natural history and outcome of prenatally diagnosed cystic hygroma. Prenat Diagn 24:965–968
Harnsberger H (2004) Diagnostic imaging: head & neck, 1st edn. Amyrsis, Salt Lake City
Herman A, Schvimer M, Tovbin J, Sandbank J, Bukovski I, Strauss S (2002) Antenatal sonographic diagnosis of testicular torsion. Ultrasound Obstet Gynecol 20:522–524
Hinrichsen K (1990) Humanembryologie: Lehrbuch und Atlas der vorgeburtlichen Entwicklung des Menschen. Springer, Berlin
Ho S, Metreweli C (1998) Normal fetal thyroid volume. Ultrasound Obstet Gynecol 11:118–122
Hörmann M, Brugger C, Ballasy C, Witzani L, Prayer D (2005) Fetal MRI of the urinary system. Eur J Radiol 57:303–311
Huismann T, Fischer U, Boltshauser E, Straube T, Gysin C (2005) Pituitary duplication and nasopharyngeal teratoma in a newborn: CT, MRI, US and correlative histopathological findings. Neuroradiology 47:558–561
Jabre A, Tabaddor R, Samaraweera R (2000) Transsphenoidal meningoencephalocele in adults. Surg Neurol 54:183–188
Karabulut N, Martin D, Yang M, Boyd B (2002) MR imaging findings in fetal goiter caused by maternal Graves disease. J Comput Assist Tomogr 26(4):538–540
Kathary N, Bulas D, Newman K, Schonberg R (2001) MRI imaging of fetal neck masses with airway compromise: utility in delivery planning. Pediatr Radiol 31:727–731
Kirchhoff M, Zimmermann B, Gundlach K, Henkel K (2006) Neonatales zervikales Teratom: Falldarstellung. Mund Kiefer Gesichtschir 10:259–262
Kitamura E, Miki Y, Kawai M, Itoh H, Yura S, Mori N, Sugimura K, Togashi K (2008) T1 signal intensity and height of the anterior pituitary in neonates: correlation with postnatal time. Am J Neuroradiol 29:1257–1260
Kollias S, Ball W, Prenger EC (1995) Review of the embryologic development of the pituitary gland and report of a hypophyseal duplication detected by MRI. Neuroradiology 37:3–12
Kondoh M, Miyazaki O, Imanishi Y, Hayakawa M, Aikyou M, Doi H (2004) Neonatal goiter with congenital thyroid dysfunction in two infants diagnosed by MRI. Pediatr Radiol 34:570–573
Koyuncu F, Tamay AG, Bugday S (2010) Intrauterine diagnosis and management of fetal goiter: a case report. J Clin Ultrasound 38(9):503–505
Kurokawa H, Fujisawa I, Nakano Y, Kimura H, Akagi K, Ikeda K, Uokawa K, Tanaka Y (1998) Posterior lobe of the pituitary gland: correlation between signal intensity on T1-weighted MR images and vasopressin concentration. Radiology 207:79–83
Lee HJ, Woo S, Kim J, Suh S (2000) Daughter cyst sign: a sonographic finding of ovarian cyst in neonates, infants, and young children. Am J Roentgenol 174:1013–1015
Lee MH, Choi HY, Sung YA, Lee JK (2001) High signal intensity of the posterior pituitary gland on T1-weighted MR images. Correlation with plasma vasopressin concentration to water deprivation. Acta Radiol 42:129–134
Manara R, Citton V, Rossetto M, Padoan A, D´Avella D (2009) Hypophyseal triplication: case report and embryologic considerations. AJNR Am J Neuroradiol 30(7):1328–1329
McEwing R, Hayward C, Furness M (2003) Foetal cystic abdominal masses. Australas Radiol 47:101–110
Mittermayer C, Brugger PC, Lee A, Horcher E, Hayde M, Bernaschek G, Prayer D (2005) Prenatal magnetic resonance imaging as a useful adjunctive to ultrasound-enhanced diagnosis in case of a giant foetal tumour of the neck. Ultraschall Med 26:46–50
Moore K, Persaud T (2008) The developing human: clinically oriented embryology, 8th edn. Saunders Elsevier, Philadelphia
Morton WR (1957) Duplication of the pituitary and stomatodaeal structures in a 38-week male infant. Arch Dis Child 32:135–141
Nath C, Oyelese Y, Yeo L, Chavez M, Kontopoulos V, Giannina G, Smulian J, Vintzileos A (2005) Picture of the month: three-dimensional sonography in the evaluation and management of fetal goiter. Ultrasound Obstet Gynecol 25: 312–314
Pezerovic-Panijan R, Grbesa D, Baneka L, Jezek D, Relja Z, Puljiz M, Banek T, Cavci*f*á J, Pezovi*f*á D (1999) Anthropological measurements of the skeleton and parathyroid glands growth during fetal development. Coll Antropol 23(2):737–744
Polak M, Van Vliet G (2010) Therapeutic approach to fetal thyroid disorders. Horm Res Paediatr 74:1–5
Pretorius D, Halsted M, Abels W, Catanzarie V, Kaplan G (1998) Hydroceles identified prenatally. J Ultrasound Med 17: 49–52
Quarello E, Gorincour G, Merrot T, Boubli L, DÉrcole C (2003) The daughter cyst sign: a sonographic clue to the diagnosis of fetal ovarian cyst. Ultrasound Obstet Gynecol 22:433–434
Radaelli T, Cetin I, Zamperini P, Ferrazzi E, Pardi G (2002) Intrauterine growth of normal thyroid. Gynecol Endocrinol 16:427–430
Regev RH, Markovich O, Arnon S, Bauer S, Dolfin T, Litmanovitz I (2009) Meconium periorchitis: intrauterine diagnosis and neonatal outcome: case reports and review of the literature. J Perinatol 29:585–587
Sadler T, Drews U (2008) Medizinische Embryologie: Die normale menschliche Entwicklung und ihre Fehlbildungen, 11th edn. Georg Thieme Verlag, Stuttgart/New York
Schmook MT, Brugger PC, Weber M, Kasprian G, Nemec S, Krampl-Bettelheim E, Prayer D (2010) Forebrain development in fetal MRI: evaluation of anatomical landmarks before gestational week 27. Neuroradiology 52: 495–504
Shinmoto H, Kashima K, Yuasa Y, Tanimoto A, Morikawa Y, Ishimoto H, Yoshimura Y, Hiramatsu K (2000) MR imaging of non-CNS fetal abnormalities: a pictorial essay. Radiographics 20:1227–1243

Shroff M, Blaser S, Jay V, Chitayat D, Armstrong D (2003) Basilar artery duplication associated with pituitary duplication: a new finding. Am J Neuroradiol 24:956–961

Slodki M, Respondek-Liberska M (2007) Fetal ovarian cysts – 420 cases from literature – metaanalysis 1984-2005. Ginekol Pol 78:324–328

Spampinato V, Castillo M (2005) Congenital pathology of the pituitary gland and parasellar region. Top Magn Reson Imaging 16:269–276

Suzuki N, Tsuchida Y, Takahashi A, Kuroiwa M, Ikeda H, Mohara J, Hatakeyama S, Koizumia T (1998) Prenatally diagnosed cystic lymphangioma in infants. J Pediatr Surg 33:1599–1604

Woodward P (2005) Diagnostic imaging: obstetrics, 1st edn. Amyrsis, Salt Lake City

Woodward P, Sohaey R, Kennedy A, Koeller K (2005) From the archives of the AFIP: a comprehensive review of fetal tumors with pathologic correlation. Radiographics 25:215–242

Zhu X, Lin CR, Prefontaine GG, Tollkuhn J, Rosenfeld MG (2005) Genetic control of pituitary development and hypopituitarism. Curr Opin Genet Dev 15:332–340

The Prenatal Diagnosis of Facial Clefts with Fetal MRI

Mariella Mailáth-Pokorny and Daniela Prayer

Contents

Abstract

› Orofacial clefts are among the most common congenital anomalies caused by abnormal facial development during gestation. As prenatal ultrasonography becomes a routine practice in pregnancy, antenatal detection of facial clefts is possible and improves adequate counseling of the prospective parents and planning of obstetrical and neonatal management. However, the prenatal detection rate, especially of isolated cleft palate, is low. Limitations of ultrasonography include acoustic shadowing from the surrounding structures, poor image quality in case of lack of amniotic fluid or maternal obesity, and limited soft tissue contrast. Fetal MRI is a valuable alternative to ultrasonography providing superior tissue contrast and imaging planes in any orientation regardless of the fetal lie and is increasingly used for detailed assessment of inconclusive sonographic findings.

› In this article, we describe our experience in evaluating the accuracy of both, prenatal ultrasound and magnetic resonance imaging in detecting the position and extent of a cleft as well as the presence of any associated anomalies.

M. Mailáth-Pokorny (✉)
Department of Obstetrics and Gynecology, Medical University of Vienna, Waehringer Guertel 18–20, 1090 Vienna, Austria
e-mail: mariella.mailath-pokorny@meduniwien.ac.at

D. Prayer
Department of Radiodiagnostics, Medical University of Vienna, Waehringer Guertel 18–20, 1090 Vienna, Austria
e-mail: daniela.prayer@meduniwien.ac.at

1 Introduction

The human face is formed from five facial primordia. The primary and secondary palate form independently, separated from each other by the incisive foramen (Stroustrup Smith et al. 2004). The primary palate is

D. Prayer (ed.), *Fetal MRI*, Medical Radiology,
DOI: 10.1007/174_2010_59, © Springer-Verlag Berlin Heidelberg 2011

formed by the midfacial prominences between 4 and 6 embryonic weeks, the secondary palate develops with the fusion of the maxilla, the palatine bones and the soft palate between 8 and 12 weeks of gestation (Ortiz-Posadas et al. 2001).

Orofacial clefts are congenital malformations caused by abnormal facial development during gestation. They are among the most common maxillofacial anomalies (Nyberg et al. 1992) occurring in about 1 per 600 to 1 per 1,000 (Schutte et al. 1999) live births.

On the basis of embryologic facial development, orofacial clefts can be divided into clefts of the primary palate, including the lips and the alveolus and clefts of the embryological secondary hard and soft palate (Kennely and Moran 2008) and are registered according to the extension either as isolated cleft lip or as cleft lip with cleft palate (Nyberg et al. 1995). Clefts can further be divided by the location and registered as unilateral, bilateral and midline. Midline facial clefts result from failure of the nasal processes to close and are associated with severe cerebral defects (Demircioglu et al. 2008) (Fig. 1).

The etiology of facial clefts is multifactorial with genetic and environmental factors (Murray 1995) with a higher prevalence in Orientals and a lower prevalence among Africans (Derijcke et al. 1996). Seventy percent of orofacial clefts are isolated and nonsyndromic (Gorlin et al. 2001). The remaining syndromic cases can be subdivided into clefts with chromosomal anomalies, like Trisomie 13 and 18 (Chmait et al. 2006), additional malformations (Berge et al. 2001; Stoll et al. 2000), or can be part of one of 350 Mendelian syndromes associated with clefting (Gorlin et al. 1971). The overall prognosis of facial clefts depends on the presence of associated anomalies or chromosomal defects (Perrotin et al. 2001).

The birth of a child with a cleft is associated with considerable anxiety for the affected families (Davalbhakta and Hall 2000). Although orofacial clefts are considered as only aesthetic malformations they encompass a variety of disorders and are notable for significant lifelong morbidity (Bender 2000). Prenatal detection on mid-trimester scan is possible and offers antenatal consultation with members of the craniomaxillofacial treatment team with focus on possible feeding, respiratory and ear problems and to predict the extent of surgery required after birth (Russell et al. 2008). Ultrasound is known as the primary screening modality for identifying cleft lip and cleft palate. However, the accurate visualization of isolated cleft palate with two-dimensional ultrasound remains difficult to assess, especially in low-risk patients. Additionally, sonographic findings can be inconclusive when information about the extent of the defect or

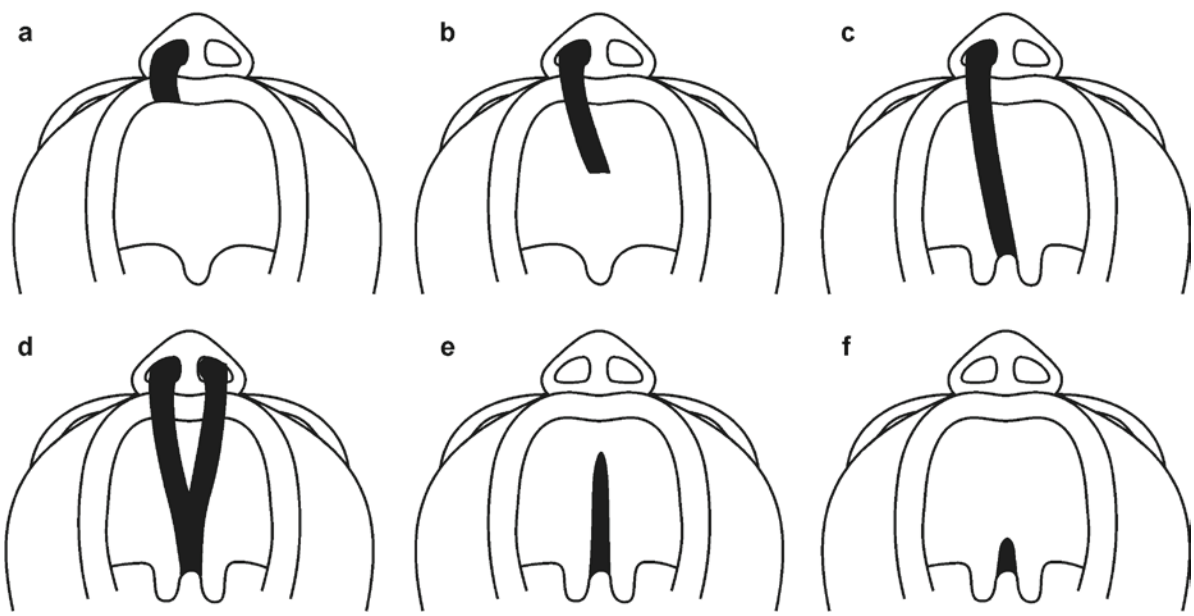

Fig. 1 View of the primary and secondary palate, showing different forms of facial clefting: unilateral cleft lip (**a**), unilateral cleft lip and alveolus (**b**), unilateral cleft lip and palate (**c**), bilateral cleft lip and palate (**d**), isolated cleft of the hard palate (**e**), and isolated cleft of the soft palate (**f**). Reproduced with permission from M. Mailáth-Pokorny et al. 2010

the presence of associated abnormalities is insufficient (Chitty et al. 1991).

Fetal MRI is a valuable method in the evaluation of inconclusive sonographic findings. High tissue contrast and imaging planes in any orientation provide a more precise survey of the fetal face and improve visualization of the secondary bony palate. Fetal MRI is especially useful to evaluate the extent of the structural defect as well as the presence of associated anomalies offering proper patient counseling and reduction of parental anxiety (Ghi et al. 2003).

2 Prenatal Diagnosis of Cleft Lip and Palate on Ultrasound (US)

Antenatal detection of facial clefts by high resolution ultrasound is possible (Shaikh et al. 2001) as the assessment of the fetal face is performed routinely during anatomical screening (Royal College of Obstetricians and Gynecologists Working Party 2000). However, the image quality can be limited by a small field of view and poor soft tissue contrast in case of obese patients or lack of amniotic fluid (Pugash et al. 2008). The detection rates of oral clefts by routine ultrasound examinations are variable (Offerdal et al. 2008). Clefts of the primary palate can be routinely detected during the first ultrasound examination. Sonographic visualization of the posterior hard palate is difficult, due to acoustic shadowing from the maxilla (Chmait et al. 2002), and the detection rate of isolated cleft palate is low. Several authors have reported the use of color doppler technique, showing abnormal oronasopharyngeal fluid dynamics (Sherer et al. 1993) or 3D sonography in order to avoid the problem of the maxillary shadowing and to obtain a higher detection rate (Ulm et al. 1998; Merz et al. 1997; Rotten and Levaillant 2004).

3 Prenatal Diagnosis of Cleft Lip and Palate on Fetal Magnetic Resonance Imaging (MRI)

Magnetic resonance imaging provides diagnostic accuracy in evaluating orofacial clefts of the primary and secondary palate (Ghi et al. 2003) and has several advantages over ultrasound (Pistorius et al. 2008). It is less limited by maternal body mass index, severe lack of amniotic fluid and position of the fetus than ultrasound. It has high soft- tissue resolution and allows multiplanar scanning and visualization of the posterior palate as well as the identification of any associated anomalies (Pugash et al. 2008).

The fetal MRI is performed on a 1.5 T superconducting unit using a five-element surface phased-array coil. T2 weighted, ultrafastspin-echo sequences, echo-planar sequences and steady-state free precession sequences with 2–4 mm slice sickness are obtained. The combination of three imaging planes of the fetal body is composed: Axial views at the level of the maxilla, coronal views at the level of the fetal lips and sagittal planes.

In the axial plane, the hard palate can be visualized in its entirety, as well as the soft tissue of the upper lip overlaying the maxilla and the alveolar ridge with the anterior six tooth buds (Fig. 2).

In the coronal plane, the continuity of the entire upper lip can be assessed (Fig. 3). A sagittal section shows the soft tissue profile of the fetal face and the posterior palate as a continuous straight echogenic line (Fig. 4). It is best visualized when amniotic fluid fills the fetal mouth.

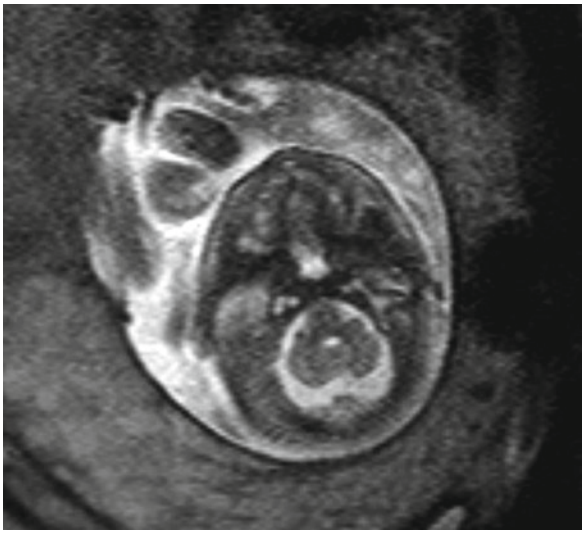

Fig. 2 T2 weighted axial image of the hard palate, the alveolar ridge with the anterior six tooth buds and the soft tissue of the upper lip overlaying the maxilla at 22 weeks gestational age

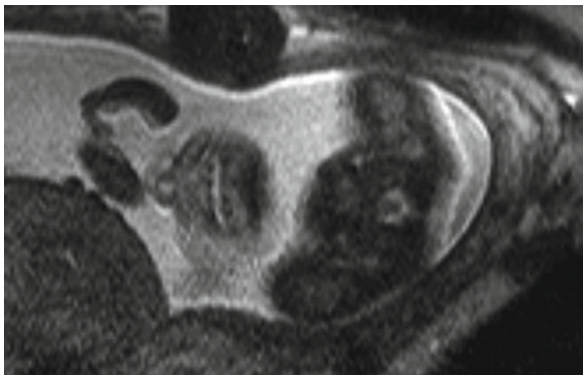

Fig. 3 T2 weighted coronal image with continuous upper lip at 24 weeks gestational age

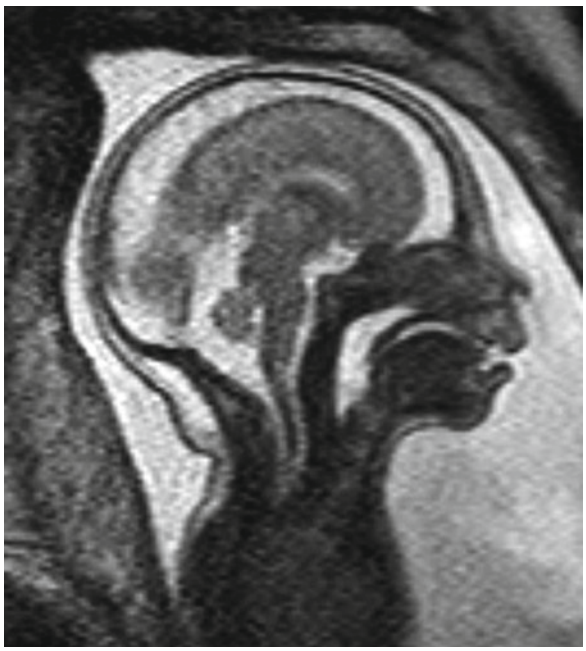

Fig. 4 T2 weighted sagittal section showing the soft tissue profile of the fetal face and the posterior palate as a continuous straight echogenic line at 25 weeks gestational age

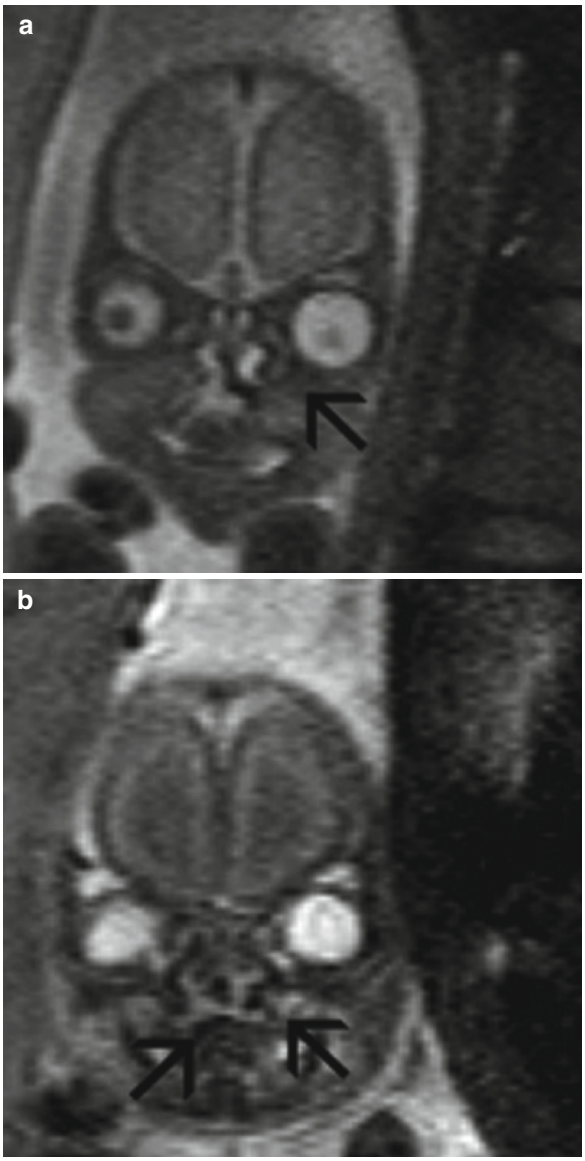

Fig. 5 T2 weighted coronal images of a unilateral facial cleft at 25 (**a**) and 22 (**b**) weeks gestational age

4 MRI Images of Clefts of the Primary and Secondary Palate

4.1 Cleft Lip and Alveolus

Twenty-five percent of clefts affect only the primary palate with good functional and aesthetic outcome (Bellis et al. 1999). Cleft primary palate is best visualized on MRI in the axial and coronal planes.

Axial views allow visualization of the labial skin line, the underlying orbicularis oris muscle and the deeper anatomy of the maxilla and are helpful to exclude involvement of the secondary palate, which is variable in isolated cleft lip. Coronal planes show the soft tissue of the fetal nose and the upper lip can be visualized (Fig. 5). A cleft lip is diagnosed if a hypoechoic defect is identified in the area of the musculus orbicularis oris. The underlying alveolar ridge shows no evidence of disruption. If the defect extends further into the primary

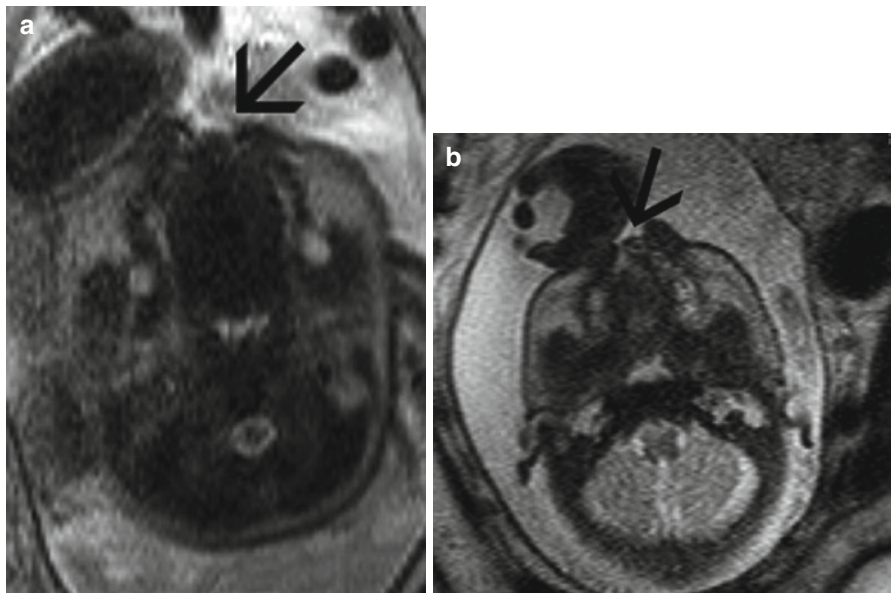

Fig. 6 T2 weighted image of a cleft primary palate with irregularly arranged upper tooth germs in the alveolar ridge at 35 (**a**) and 34 (**b**) weeks gestational age

palate, axial views show a disrupted irregular contour of the echogenic alveolar ridge with absent or irregularly arranged upper tooth germs (Fig. 6).

Additionally, the characteristic deviation of the nasal septum (the mid portion is bent to the side of the defect and the anterocaudal portion is deviated to the noncleft side) can be seen (Fig. 7).

4.2 Cleft Lip and Palate

Approximately 30% of fetuses with a complete cleft of the primary palate will also have a complete cleft of the secondary palate, whereas 45% of clefts only affect the secondary palate (Bellis et al. 1999). Clefts extending into the secondary palate are directly visible on MRI in the axial (Fig. 8) and sagittal planes (Fig. 9). Amniotic fluid is of high signal on T2-weighted images and allows visualization of the external fetal contour. When amniotic fluid fills the fetal mouth a clear identification of the oropharynx, tongue, and secondary palate as a curve of soft-tissue signal intensity is possible. A posterior cleft abnormality interrupts the continuity of the midline suture between the lateral palatine processes. Identification of protrusion of the intermaxillary segment can be helpful for the identification of bilateral cleft lip and palate (Fig. 10). The premaxillary protrusion develops because of uninhibited growth of the vomer and premaxillary bones and is best visualized on axial and midline sagittal views. Additional signs are missing tooth germs, a short columella and a flattened nose. Cleft soft palate in the absence of cleft lip is far less common than cleft lip and palate. Isolated cleft of the secondary palate is rarely identified on prenatal sonography but can be seen on fetal MRI (Fig. 11). Communication of the oro and nasopharynx in the expected region of the soft palate and fetal tongue movements, abnormally elevated in the oral cavity can be used as evidence of cleft secondary palate.

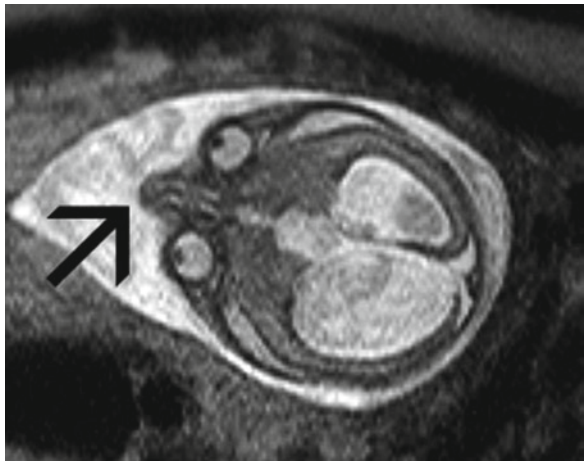

Fig. 7 T2 weighted axial image of cleft lip with cleft alveolus, showing the characteristic deviation of the nasal septum

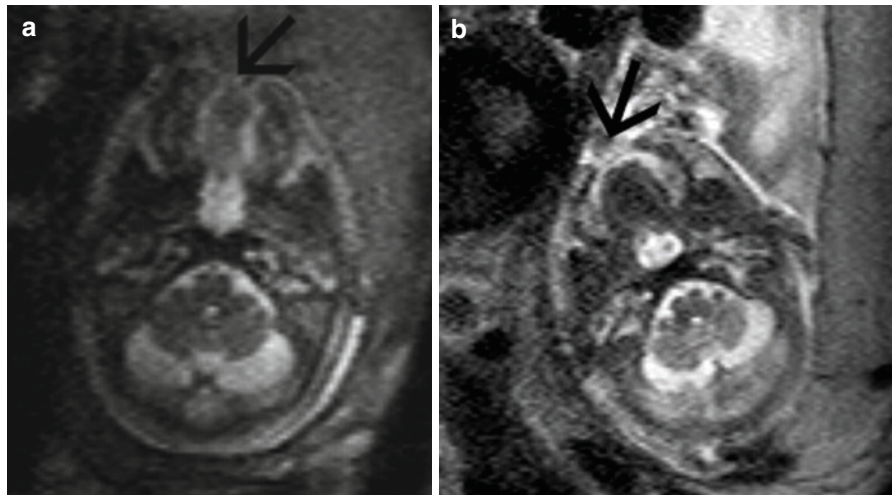

Fig. 8 T2 weighted axial images of a unilateral (**a**) and a bilateral (**b**) cleft lip and palate, both at 22 weeks gestational age

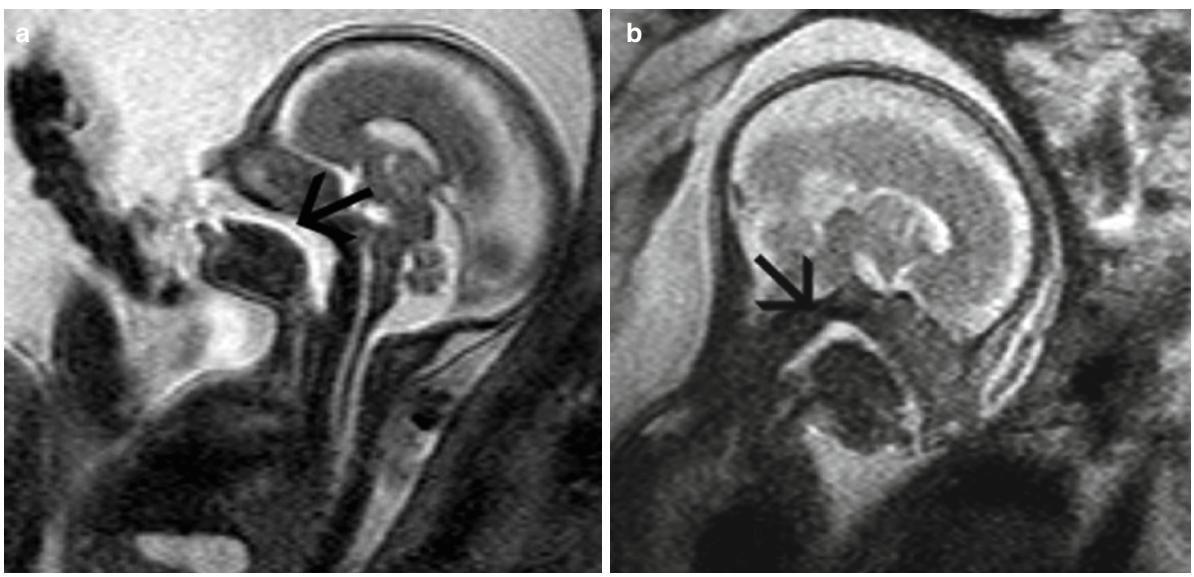

Fig. 9 T2 weighted sagittal MRI image of a complete cleft of the primary and secondary palate missing the hypointense layer of the hard palate at 20 (**a**) and 22 (**b**) weeks gestational age

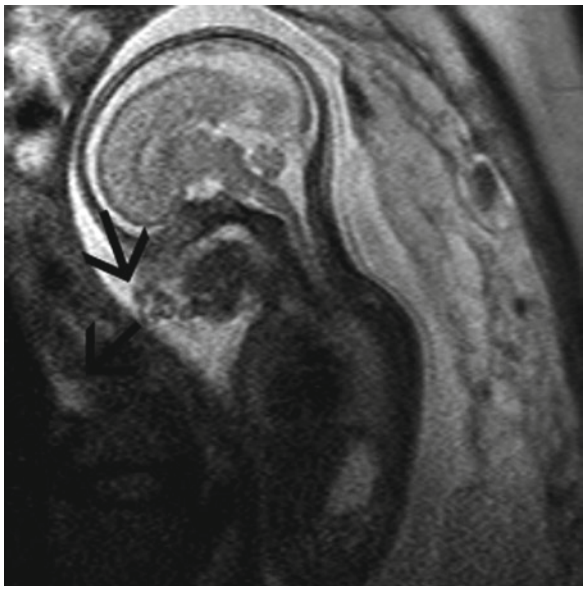

Fig. 10 Protrusion of the intermaxillary segment on the midline sagittal view

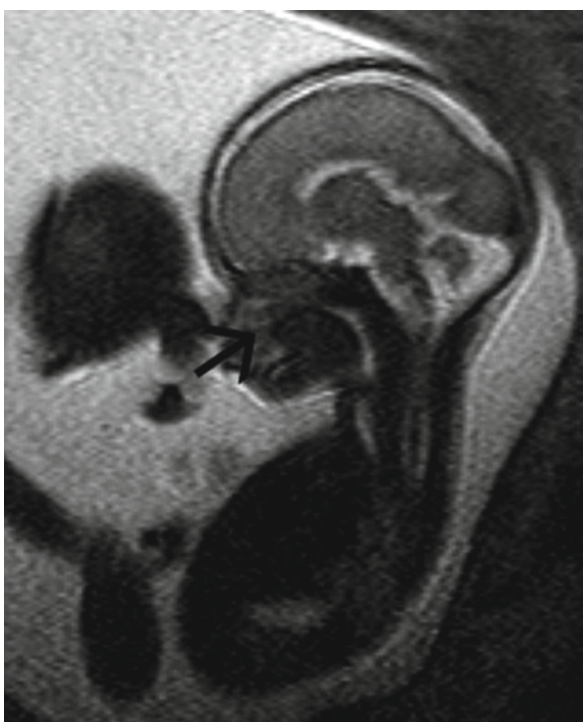

Fig. 11 T2 weighted sagittal image of an isolated cleft of the secondary palate

5 Future Development

The use of fetal MRI has improved the detection rate of facial anomalies in the early second trimester and is increasingly used for detailed assessment of complicated sonographic findings. Where standard sonography is limited due to fetal position or oligohydramnios, MRI succeeds to visualize the laterality of the cleft, the extension into the secondary palate, and the detection of isolated clefts improving prenatal parental counseling and postnatal therapeutic planning.

Fetal MRI enhances diagnostic accuracy and prepares the path for future fetal therapies (Prayer 2006). There has been some interest in open repair of facial clefts in utero with the advantage of scarless mucoperiostal healing in the fetus (Weinzweig et al. 2006; Stelnicki et al. 1999). Nevertheless, further research is needed to eliminate the need of further postnatal correction to achieve satisfactory final results (Papadopulos and Papadopoulos 2003).

References

Bellis, T.H., Orth, M., Wolgemuth, B.: The incidence of cleft lip and palate deformities in the south-east of Scotland. Br J Orthod **26**, 121–125 (1999)

Bender, P.L.: Genetics of cleft lip and palate. J Pediatr Nurs **15**, 242–249 (2000)

Berge, S.J., Palth, H., Van de Vondel, P.T., Appel, T., Niederhagen, B., Von Lindern, J.J., Reich, R.H., Hansmann, M.: Fetal cleft lip and palate: sonographic diagnosis, chromosomal abnormalities, associated anomalies and postnatal outcome in 70 fetuses. Ultrasound Obstet Gynecol **18**, 422–431 (2001)

Chmait, R., Pretorius, D., Jones, M., Hull, A., James, G., Nelson, T., Moore, T.: Prenatal evaluation of facial clefts with two-dimensional and adjunctive three-dimensional ultrasonography: a prospective trial. Am J Obstet Gynecol **187**, 946–949 (2002)

Chmait, R., Pretorius, D., Moore, T., Hull, A., James, G., Nelson, T., Jones, M.: Prenatal detection of associated anomalies in fetuses diagnosed with cleft lip with or without cleft palate in utero. Ultrasound Obstet Gynecol **27**, 173–176 (2006)

Chitty, L.S., Hunt, G.H., Moore, J., Loob, M.O.: Effectiveness of routine ultrasonography in detecting fetal structural abnormalities in low risk population. Br Med J **303**, 1165–1169 (1991)

Davalbhakta, A., Hall, P.N.: The impact of antenatal diagnosis on the effectiveness and timing of counseling for cleft lip and palate. Br J Plastic Surg **53**, 298–301 (2000)

Demircioglu, M., Kangesu, L., Ismail, A., Lake, E., Hughes, J., Wright, S., Sommerland, B.C.: Increasing accuracy of antenatal ultrasound diagnosis of cleft lip with or without cleft palate, in cases referred to the North Thames London Region. Ultrasound Obstet Gynecol **31**, 647–651 (2008)

Derijcke, A., Eerens, A., Carels, C.: The incidence of oral clefts: a review. Br J Oral Maxillofac Surg **34**, 488–494 (1996)

Ghi, T., Tani, G., Savelli, L., Colleoni, G.G., Pilu, G., Bovicelli, L.: Prenatal imaging of facial clefts by magnetic resonance imaging with emphasis on the posterior palate. Prenat Diagn **23**, 970–975 (2003)

Gorlin, R.J., Cervenka, J., Pruzansky, S.: Facial clefting and its syndromes. Birth Defects Orig Artic Ser **7**, 3–49 (1971)

Gorlin, R.J., Cohen, M.M., Hennekam, R.C.M.: Syndromes of the Head and Neck, 4th edn. Oxford University Press, New York (2001)

Kennely, M.M., Moran, P.: Directional power Doppler in the midsagittal plane as an aid to the prenatal diagnosis of cleft lip and palate. Prenat Diagn **28**, 56–58 (2008)

Mailáth-Pokorny, M., Worda, C., Krampl-Bettelheim, E., Watzinger, F., Brugger, P.C., Prayer, D.: What does magnetic resonance imaging add to the prenatal ultrasound diagnosis of facial clefts? Ultrasound Obstet Gynecol **36**, 445–451 (2010)

Merz, E., Weber, G., Bahlmann, F., Miric-Tesanic, D.: Application of transvaginal and abdominal three-dimensional ultrasound for the detection or exclusion of malformations of the fetal face. Ultrasound Obstet Gynecol **9**, 237–243 (1997)

Murray, J.C.: Face facts: Genes, environment, and clefts. Am J Hum Genet **57**, 227–232 (1995)

Nyberg, D.A., Mahony, B.S., Kramer, D.: Paranasal echogenic mass: sonographic sign of bilateral complete cleft lip and palate before 20 menstrual weeks. Radiology **184**, 757–759 (1992)

Nyberg, D.A., Sickler, G.K., Hegge, F.N., Kramer, D.J., Kropp, R.J.: Fetal cleft lip with and without cleft palate: US classification and correlation with outcome. Radiology **195**, 677–684 (1995)

Offerdal, K., Jebens, N., Syvertsen, T., Blaas, H.-G.K., Johansen, O.J., Eik-Nes, S.H.: Prenatal ultrasound detection of facial clefts: a prospective study of 49314 deliveries in a non-selected population in Norway. Ultrasound Obstet Gynecol **31**, 639–646 (2008)

Ortiz-Posadas, M.R., Vega-Alvarado, L.V., Maya-Behar, J.M.: A new approach to classify cleft lip and palate. Cleft Palate Craniofacial J **38**, 545–550 (2001)

Papadopulos, N.A., Papadopoulos, M.A.: Can intrauterine surgery improve the quality of life of cleft lip and palate patients? Hippokratia **7**, 59–80 (2003)

Perrotin, F., Mabille de Poncheville, L., Marret, H., Paillet, C., Lansac, J., Body, G.: Chromosomal defects and associated malformations in fetal cleft lip with or without cleft palate. Eur J Obstet Gynecol Reprod Biol **99**, 19–24 (2001)

Pistorius, L.R., Hellmann, P.M., Visser, G.H.A., Malinger, G., Prayer, D.: Fetal neuroimaging: Ultrasound, MRI, or both? Obstet Gynecol Surv **63**, 733–745 (2008)

Prayer, D.: Fetal MRI. Eur J Radiol **57**, 171 (2006)

Pugash, D., Brugger, P.C., Bettelheim, D., Prayer, D.: Prenatal ultrasound and fetal MRI: the comparative value of each modality in prenatal diagnosis. Eur J Radiol **68**, 214–226 (2008)

Rotten, D., Levaillant, J.M.: Two and three dimensional songraphic assessment of the fetal face: analysis of cleft lip, alveolus and palate. Ultrasound Obstet Gynecol **24**, 402–411 (2004)

Royal College of Obstetricians and Gynecologists Working Party: Routine Ultrasound Screening in Pregnancy-Protocol, Standards and Training. RCOG Press, London (2000)

Russell, K.A., Allen, V.M., Mac Donald, M.E., Smith, K., Dodds, L.: A population- based evaluation of antenatal diagnosis of orofacial clefts. Cleft Palate Cran J **45**, 148–153 (2008)

Schutte, B.C., Murray, J.C.: The many faces and factors of orofacial clefts. Hum Molec Genet **8**, 1853–1859 (1999)

Shaikh, D., Mercer, N.S., Sohan, K., Kyle, P., Soothill, P.W.: Prenatal diagnosis of cleft lip and palate. Br J Plast Surg **54**, 288–289 (2001)

Sherer, D.M., Abramowicz, J.S., Jaffe, R., Woods, R.: Cleft palate: confirmation of prenatal diagnosis by colour Doppler ultrasound. Prenat Diagn **13**, 953–956 (1993)

Stelnicki, E.J., Lee, S., Hoffman, W., Lopoo, J., Foster, R., Harrison, M.R., Longaker, M.T.: A long-term, controlled-outcome analysis of in utero versus neonatal cleft lip repair using an ovine model. Plast Reconstr Surg **104**, 607–615 (1999)

Stoll, C., Alembik, Y., Dott, B., Roth, M.P.: Associated malformations in cases with oral clefts. Cleft Palate Craniofacial J **37**, 41–47 (2000)

Stroustrup Smith, A., Estroff, J.A., Barnewolt, C.E., Mulliken, J.B., Levine, D.: Prenatal diagnosis of cleft lip and palate using MRI. AJR Am J Roentgenol **183**, 229–235 (2004)

Ulm, M.R., Kratochwil, A., Ulm, B., Aro, G., Bernaschek, G.: Three-dimensional ultrasound evaluation of fetal tooth germs. Ultrasound Obstet Gynecol **12**, 240–243 (1998)

Weinzweig, J., Panter, K.E., Seki, J., Pantaloni, M., Spangenberger, A., Harper, J.S.: The fetal cleft palate: IV. Midfacial growth and bony palatal development following in utero and neonatal repair of the congenital caprine model. Plast Reconstr Surg **118**, 81–93 (2006)

Cerebral Malformations

Daniela Prayer, Peter C. Brugger, Ursula Nemec,
Ruxandra Iulia Milos, Christian Mitter, and Gregor Kasprian

Contents

Abstract

› During the second trimester cerebral malformations may present with morphological features that are different from those that are seen in a more mature brain. Consequently, the chapter focuses on early detection of cerebral malformations. MR- sequences that might be useful for the detection of changes in fetal brain development are described. A schematic approach, including the assessment of lamination of the brain parenchyma, the appearance of deep gray matter structures, the width and shape of the ventricles and outer CSF spaces, the midline structures, and the cerebellum is suggested. Salient features of the second-trimester appearance of lissencephaly/polymicrogyria syndromes, holoprosencephaly (HPE), and commissural agenesis that may be detected early are discussed.

1 Introduction

A malformation is defined as an aberration of normal organ development occurring as a consequence of a genetic disposition, infection, exposition to a teratogenic agent, or sporadically (Schumacher 2004).

The true incidence of cerebral malformations is unknown. Postnatal data reflect only those that are compatible with development until birth. In a large Brazilian study, malformations occurred in 3.67% of lifebirths, 0.36% being related to the CNS (Guardiola et al. 2009). In 42.7% of children with ataxic form of congenital cerebral palsy, and in 2.1% with dyskinetic

D. Prayer (✉), U. Nemec,
R.I. Milos, C. Mitter, and G. Kasprian
Division of Neuroradiology and Musculokeletal Radiology,
Department of Radiology, Medical University Vienna,
Währinger Gürtel 18-20, Vienna, Austria
e-mail: daniela.prayer@meduniwien.ac.at

P.C. Brugger
Center of Anatomy and Cell Biology,
Medical University of Vienna,
Waehringerstrasse 13 1090 Vienna, Austria
e-mail: peter.brugger@meduniwien.ac.at

D. Prayer (ed.), *Fetal MRI*, Medical Radiology,
DOI: 10.1007/174_2010_117, © Springer-Verlag Berlin Heidelberg 2011

form of congenital cerebral palsy, a cerebral anomaly was diagnosed (Rankin et al. 2010). However, in this number, acquired injury may be included in these figures (Rankin et al. 2010). Neonatal autopsies found malformations in 4.27% with a predominance of females with respect to not further specified cerebral malformations (Noronha et al. 2001).

Regarding involvement of fetal MRI in the diagnosis of cerebral malformations the following facts will have to be considered:

1. The most severe anomalies of neurulation, such as exencephaly/anencephaly, and craniorachischisis (Greene and Copp 2009) will only rarely be seen, as these can readily be diagnosed by early ultrasound (Blaas and Eik-Nes 2009). In most cases, the pregnancy will be terminated based on ultrasound findings.
2. Between gestational weeks (GW) 18 and 28 a certain malformation may have a different appearance than known from postnatal studies. In addition, malformations may change their appearance (Bronshtein and Wiener 1991).
3. At that time anomalies of cortical formation, such as polymicrogyria, might not yet be present.
4. The proof of a malformation, such as corpus callosum agenesis, does not rule out an underlying disease completely. Infections and metabolic disease might also be considered in some cases, see next chapter.

MR morphology of malformations in the middle and late third trimester is comparable to the postnatal one. The latter was described in detail in multiple books and publications (Barkovich 2005; Tortori-Donati 2005). Consequently, this chapter will focus on second trimester appearance, especially on malformations of cortical development.

2 Sequences to Visualize Cerebral Malformations

Description of pathoanatomy relies in most cases on high-quality T2-weighted contrast, allowing an equal assessment of the brain surface and parenchyma. Slice thickness will vary between 3 and 4 mm. Resolution of the aqueduct may require thinner slices. Diffusion-weighted images can help with delineation of unmyelinated white matter tracts (Prayer et al. 2001), which can be defined in greater detail using diffusion tensor imaging (Kasprian et al. 2008). T1-weighted images are important to delineate the pituitary gland (Schmook et al. 2010). In addition, they may be helpful in identifying regions of abnormal cell density, as, for instance, focal cortical dysplasia. Echoplanar images depict subventricular nodules. Furthermore, they may be helpful with the visualization of vascular pathology. The protocol should consist of strictly orthogonal sections, as asymmetries cannot be diagnosed unequivocally otherwise.

3 Schematic Approach to the MR Diagnosis of Cerebral Malformations

Basic information about the head size and the shape of the bony skull are usually provided by previous ultrasound; these findings may determine the indication for MRI. In case of suspect celes, MRI is usually asked to describe the content (Saleem et al. 2009) (Fig. 1).

It has been proved as useful to look at the fetal brain on MR studies following a certain scheme, in order to recognize any change that might contribute to an accurate diagnosis (Table 1).

In any case, the assessment of the fetal face and head should be part of the MR examination. With respect to malformations involving the face and brain at the same time (Dubourg et al. 2007; Pavone et al. 2010) the following structures should be evaluated for their presence, configuration, position, and integrity: forehead, ears, orbits, eyes, nose, jaw, palate, teeth, lips, and chin. In addition, the profile should be assessed, as some syndromes are associated with certain dysmorphic changes (Kjaer et al. 2001; Boog et al. 2004).

4 Pathological Appearance of Morphological Structures

4.1 Ventricles

Abnormal width of the lateral ventricles may be the first sign of developmental anomalies. Isolated symmetrical borderline ventriculomegaly (up to 15 mm ventricular width) has been found to be associated with

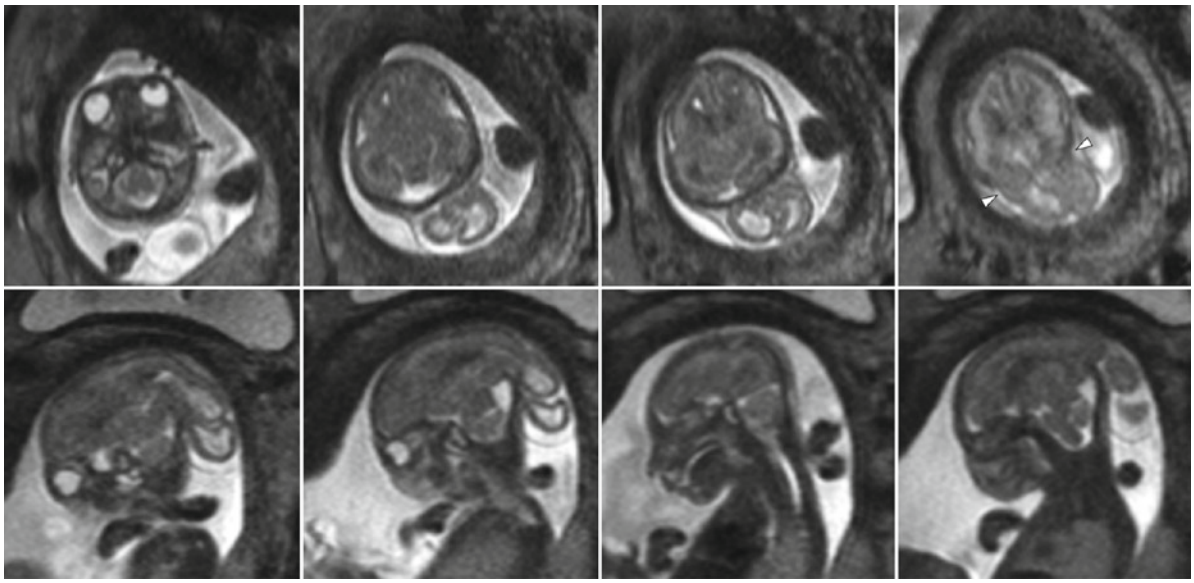

Fig. 1 Axial (*upper panel*) and corresponding sagittal (*lower panel*) sections of T2-weighted sequences in a fetus aged 19+4 gestational weeks (*GW*) demonstrate parietooccipital bilaterally a sac with herniated brain parenchyma (*white arrowheads*), consistent with a meningoencephalocele. Note the relationship between face and skull

a good prognosis (Simioli et al. 2009). However, malformations have been described in such cases too, especially in case of a ventricle width of more than 12 mm (Pilu et al. 1999). The percentage of morphological and/or postnatal developmental abnormalities is based on the outcome of pregnancies (Pilu et al. 1999; Simioli et al. 2009), meaning at that time it was known whether the ventriculomegaly was isolated or part of a malformation. On admission to fetal MRI, this is unknown, as it is exactly the indication to perform the MRI. In such cases the stage of cortical folding, lamination of the brain parenchyma (Widjaja et al. 2009), the pons and cerebellum (Ghai et al. 2006) should be screened for anomalies associated with lissencephaly (Fig. 3). The shape of the widened lateral ventricles may also point toward the underlying etiology (Levine et al. 2002). Colpocephaly is associated with corpus callosum agenesis (Figs. 3 and 4); pointed posterior horns are seen in Chiari II malformation (Callen and Filly 2008) (Fig. 5), and widened posterior horns combined with a widened, v-shaped third ventricle occur in aqueduct stenosis (Fig. 6). Ventriculomegaly (caused by a lack of tissue) has to be differentiated from hydrocephalus (occurring as a consequence of impaired cerebrospinal fluid circulation).

Unilateral ventriculomegaly is rather seen with acquired changes than with malformations. However, in some cases as, for instance, plexus cysts (Fig. 7), unilateral malformation of cortical development, obliteration of the foramen of Monroe by giant cell astrocytoma (Durfee et al. 2001), imperforate foramen of Monroe (Senat et al. 2001), or asymmetric manifestation of colpocephaly, one lateral ventricle may be wider than the other. In hemimegalencephaly, the ventricle on the side of the malformed hemisphere is usually wider than the contralateral one (Fig. 8), thus this condition should not be mixed up with an intrauterine brain tumor. A tumor will compress the ipsilateral ventricle.

Separation of the lateral ventricles may be incomplete to some degree or completely missing. The differential diagnosis between malformations such as absence of the septum pellucidum or holoprosencephaly (HPE), and secondary destruction of the midline septum as a consequence of hydrocephalus can be done in most cases (Malinger et al. 2005). The following morphological signs point toward the presence of a malformation: the septum pellucidum cannot be seen with bullhorn-shaped frontal horns, the most anterior parts of the ventricles are unseparated (in case of lobar or semilobar HPE), a complete cleavage of the hemispheres is missing, the thalami are not separated (Fig. 9), schizencephalic clefts are present, and an additional facial malformation can be proved (Malinger et al. 2005).

Table 1 Schematic approach to the diagnosis of cerebral malformations in the second trimester

Structure	Feature
Lateral ventricles	Symmetry, width, shape, separation, displacement, content, delineation
Third ventricle	Width, shape, displacement, content, delineation
Aqueduct	Patency
Fourth ventricle	Presence, width, shape, displacement, content, delineation
Ventricular zone, ganglionic eminences	Presence, symmetry, width, signals on respective sequences
Intermediate zone	Age-related delineation (Widjaja E et al. 2010a), signals
Subplate	Age-related delineation (Widjaja E et al. 2010a), signals, borders
Cortical plate	Delineation, gyration, sulcation
Basal ganglia and thalami	Delineation, symmetry, signals
Internal capsule	Delineation, signals
Tracts[a] (Corticospinal, frontopontine tracts, Probst bundles in case of suspect callosal agenesis) (Fig. 2)	Presence, deviation
Subarachnoid and subdural space	Width, configuration
Midline structures (interhemispheric fissure, falx, corpus callosum, septum pellucidum, tectum, brainstem) and cerebellum	Presence, shape, size, signals, displacement
Small intracranial structures (chiasm, infundibulum, pituitary) (Schmook et al. 2010)	Presence
Abnormal structures (vessels, subependymal nodules)	Presence, size, shape, signals

[a]In case of availability of tractography

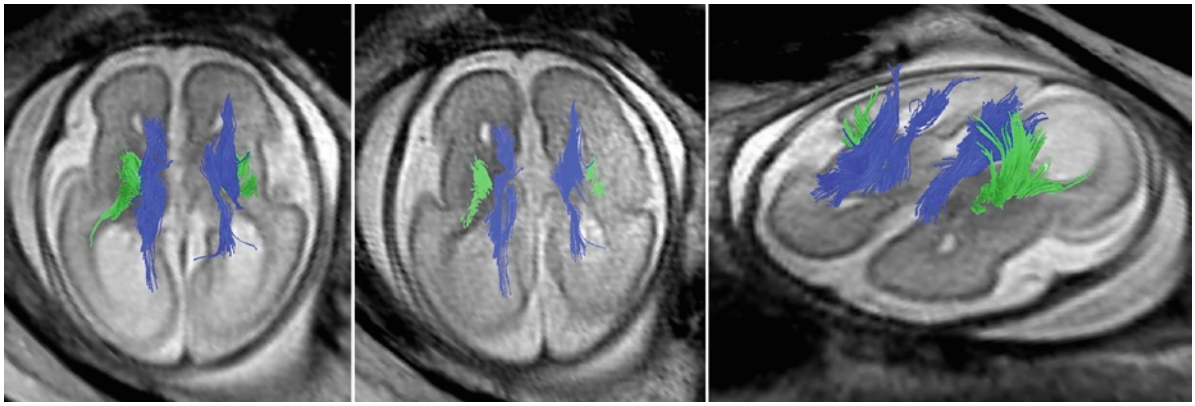

Fig. 2 Diffusion tensor tractography coregistered with the axial T2-weighted sequence in a fetus aged 22 GW with callosal agenesis showing bilaterally the Probst bundles (*in blue*) and the sensimotor trajectories (*in green*)

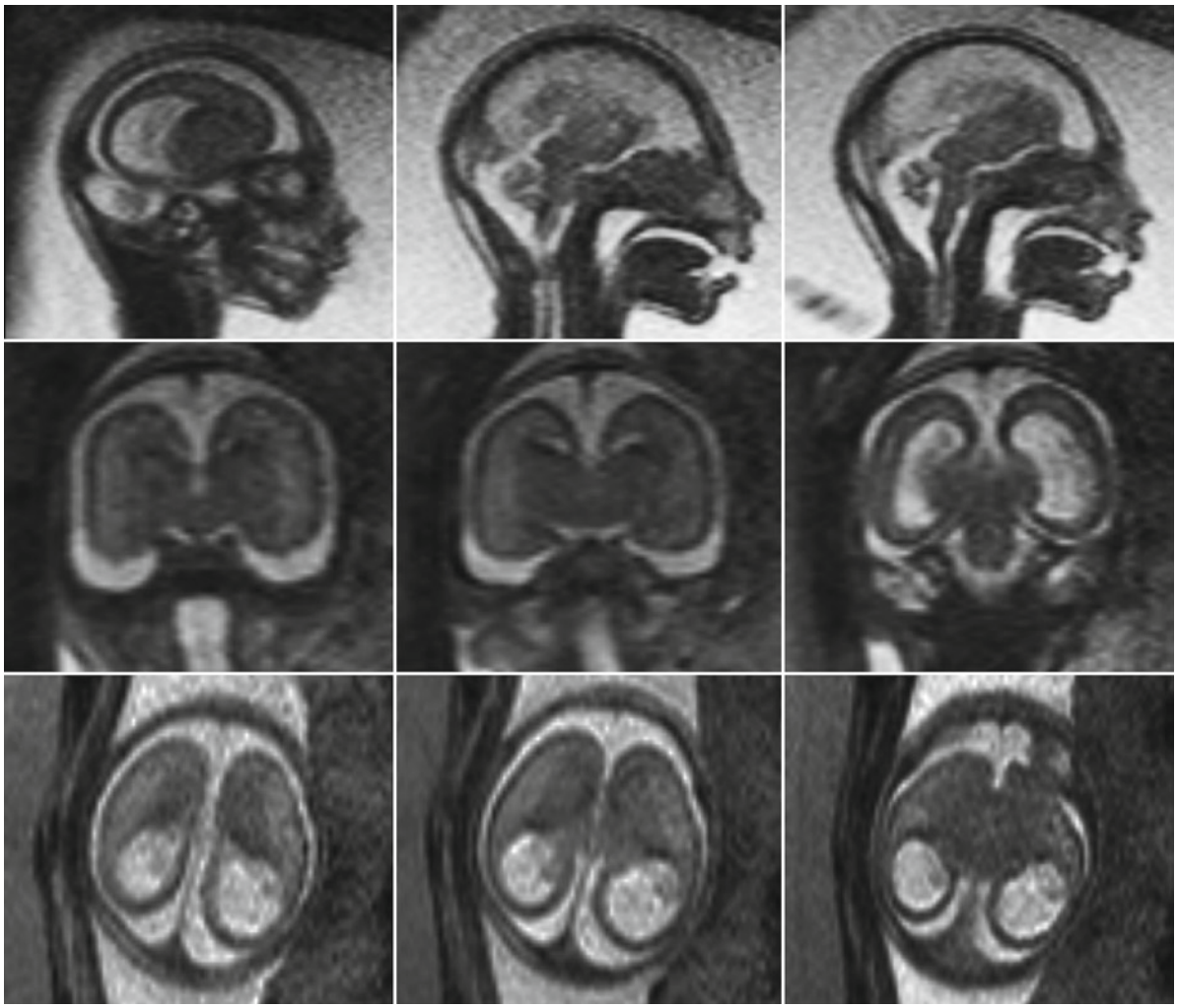

Fig. 3 Sagittal (*upper panel*), coronal (*middle panel*), and axial (*lower panel*) sections of T2-weighted sequences in a fetus aged 23+5 GW with microlissencephaly and corpus callosum agenesis. Note the microcephaly, the total absence of gyration, even the insular indentation is missing, the hypoplastic pons and cerebellum, as well as the absence of the corpus callosum

While irregular ventricular borders are mainly seen with early-onset periventricular leukomalacia, in case of associated callosal agenesis they may point toward Aicardi syndrome (Raybaud 2010).

V-shaped widening of the third ventricle in the frontal plane is usually a morphologic feature of narrowing of the aqueduct (Pasquier et al. 2009) (Fig. 6). Either there is a stenosis, which is a reduction of the lumen of the aqueduct, or an obliteration that implies the complete disappearance of the aqueductal lumen due to the fusion of the walls (Wagner et al. 2003).

During embryonic development, the aqueduct is wide, narrowing continuously to reach the normal width by GW 14. On imaging studies, a hydrocephalus, caused by aqueduct obliteration, usually does not become apparent until 18–20 GW (Senat et al. 2001). The so-called dysgenetic aqueduct stenosis/obstruction (Oi 2003) is thought to be the consequence of overgrown or hypertrophied parenchyma in the midbrain (Oi 2003). The complete occlusion of the aqueduct might be prevented by secretion of the subcommissural organ (Wagner et al. 2003), which is located in the

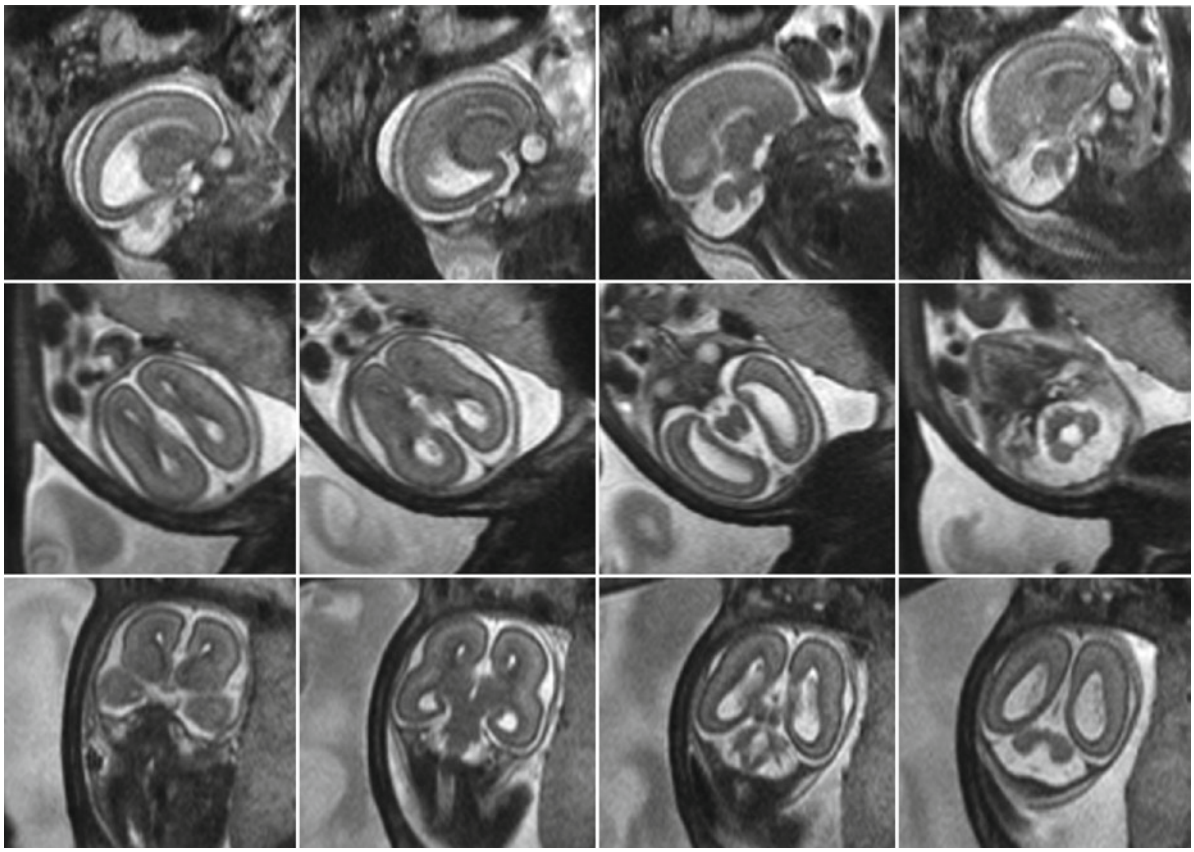

Fig. 4 Sagittal (*upper panel*) and corresponding axial (*middle panel*) and coronal (*lower panel*) sections of T2-weighted sequences in a 23 GW old fetus showing colpocephalic configuration of the lateral ventricles, as sign of callosal agenesis, small cerebellar hemispheres, and preserved laminar organization of the brain parenchyma, in contrast to the fetus in Fig. 3 (fetuses in Figs. 3 and 4 have comparable ages). Shallow insular indentation

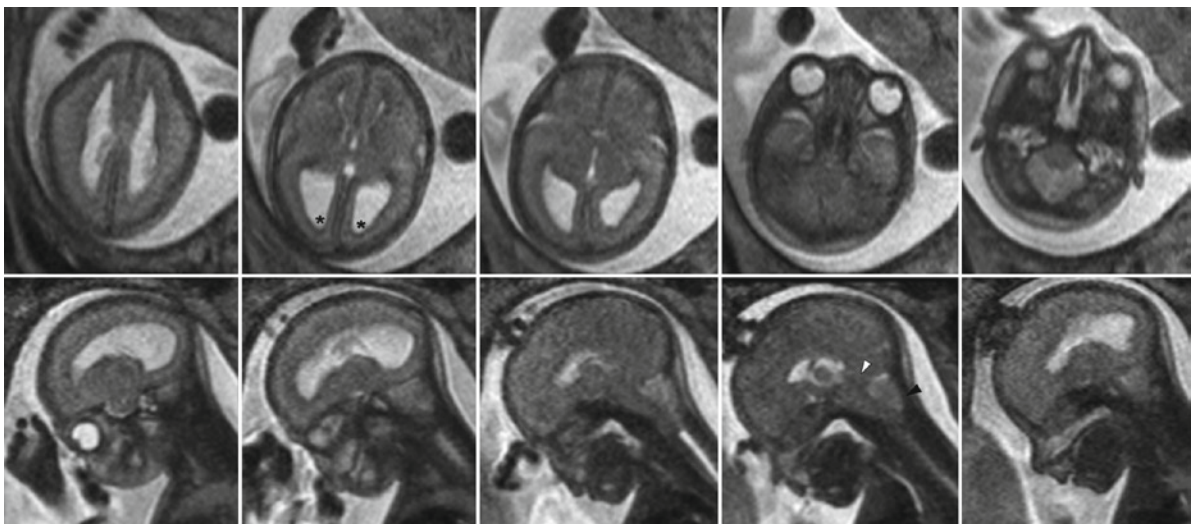

Fig. 5 Axial (*upper panel*) and sagittal (*lower panel*) sections of T2-weighted sequences in a 23+6 GW old fetus with Chiari II malformation. Note the typical lemonhead form (*first image upper panel*), the small posterior fossa, the tectal elongation (*white arrowhead*), the absence of a fourth ventricle, the herniation of the vermis (*black arrowhead*), and the pointed rather than rounded posterior horns (*black asterisks*)

anterior wall of the rostral part of the aqueduct. This location has been described as the primary site of aqueduct obliteration (Oi 2003; Wagner et al. 2003). The described mechanism has been implicated into the manifestation of X-linked hydrocephalus, which accounts for approximately 5–10% of males with non-syndromic congenital hydrocephalus (Schrander-Stumpel and Vos 2004, updated 2006). Hydrocephalus may also occur as part of a complex malformation, such as Chiari malformations, Dandy–Walker complex, vein of Galen malformation, midline hyperplasia with malformation of the fornical system, and other midline abnormalities such as cysts (Schrander-Stumpel and Vos 2004, updated 2006). Cytogenetically, trisomies (13, 18, 9) or triploidy may be associated with hydrocephalus. On fetal MRI, an impatent aqueduct combined with symmetrical supratentorial widening of the ventricles may point toward the presence of impairment of CSF movement (Fig. 6). In contrast to postnatal studies, macrocephaly is not present in all cases. The brain parenchyma may be compressed and hyperintense on diffusion-weighted images (Fig. 10). As a fast T2-weighted FLAIR sequence is not available yet, periventricular zones of disturbed CSF resorption cannot be identified. The outer CSF spaces may be narrow or even consumed. Gyri, if already built, may be flattened. Suspecting hydrocephalus with a genetic background, it should be tried to get a tractography of the corticospinal tracts: in this condition, they may be hypolastic or absent (Senat et al. 2001).

On ultrasound, the (future) fourth ventricle may be delineated as early as at 7 GW (Blaas and Eik-Nes 2009). At the time when fetal MRI is performed it already has its typical diamond shape in a sagittal plane. In Chiari II malformation, the fourth ventricle may be not delineable or slit-like. Cystic deformation of the fourth ventricle is a hallmark of the Dandy–Walker complex (Figs. 11 and 12). Membranes at the level of the foramen of Magendie, as associated with Blake's pouch (Calabrò et al. 2000), may be difficult to identify. The hallmark in this type of malformation is an increased tegmento-vermian angle (Garel 2010) with a wide opening of the fourth ventricle outlet. In case of a convexity of the anterior floor of the fourth ventricle, a molar-tooth

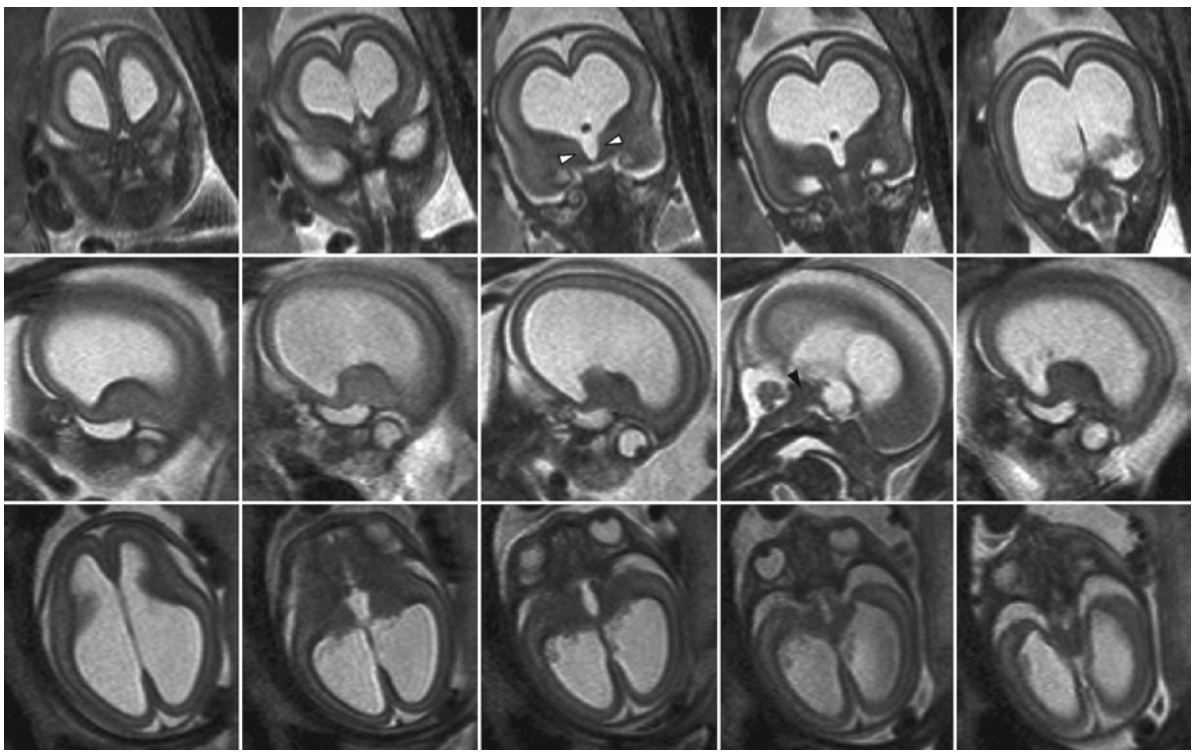

Fig. 6 Coronal (*upper panel*), sagittal (*middle panel*), and axial (*lower panel*) sections of T2-weighted sequences in a fetus aged 20+4 GW depicting symmetrically enlarged lateral ventricles with a v-shaped third ventricle (*white arrowheads*). On the sagittal image, the lumen of the aqueduct cannot be identified (*black arrowhead*). This constellation of findings is characteristic for aqueduct stenosis/obstruction

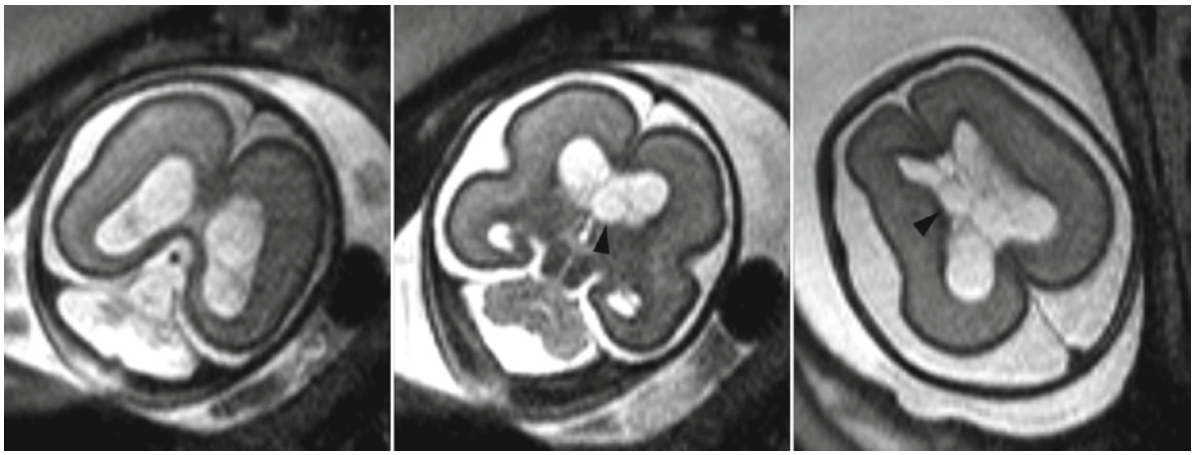

Fig. 7 T2-weighted sequences (two coronal sections and one axial) of a fetus aged 21+5 GW showing multiple, almost CSF-isointense cystic structures in both lateral ventricles with discrete hypointense wall (*black arrowheads*), that represent multiple choroid plexus cysts, probably responsible for the slight ventriculomegaly

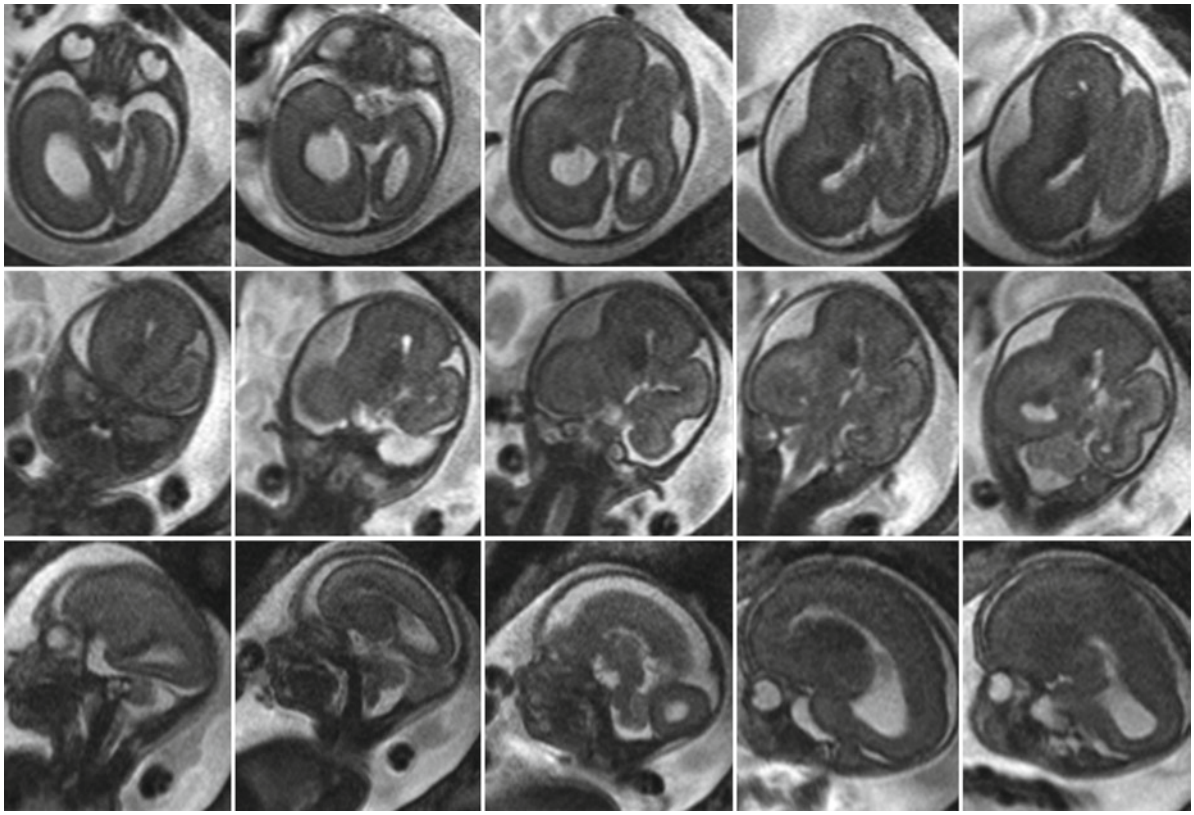

Fig. 8 Axial (*upper panel*), coronal (*middle panel*), and sagittal (*lower panel*) sections of T2-weighted sequences in a fetus aged 21+6 GW with hemimegalencephaly demonstrating an obvious asymmetry of the cerebral hemispheres with the lateral ventricle on the malformed hemisphere clearly wider than the contralateral one. In addition, the laminar organization of the enlarged hemisphere is deranged

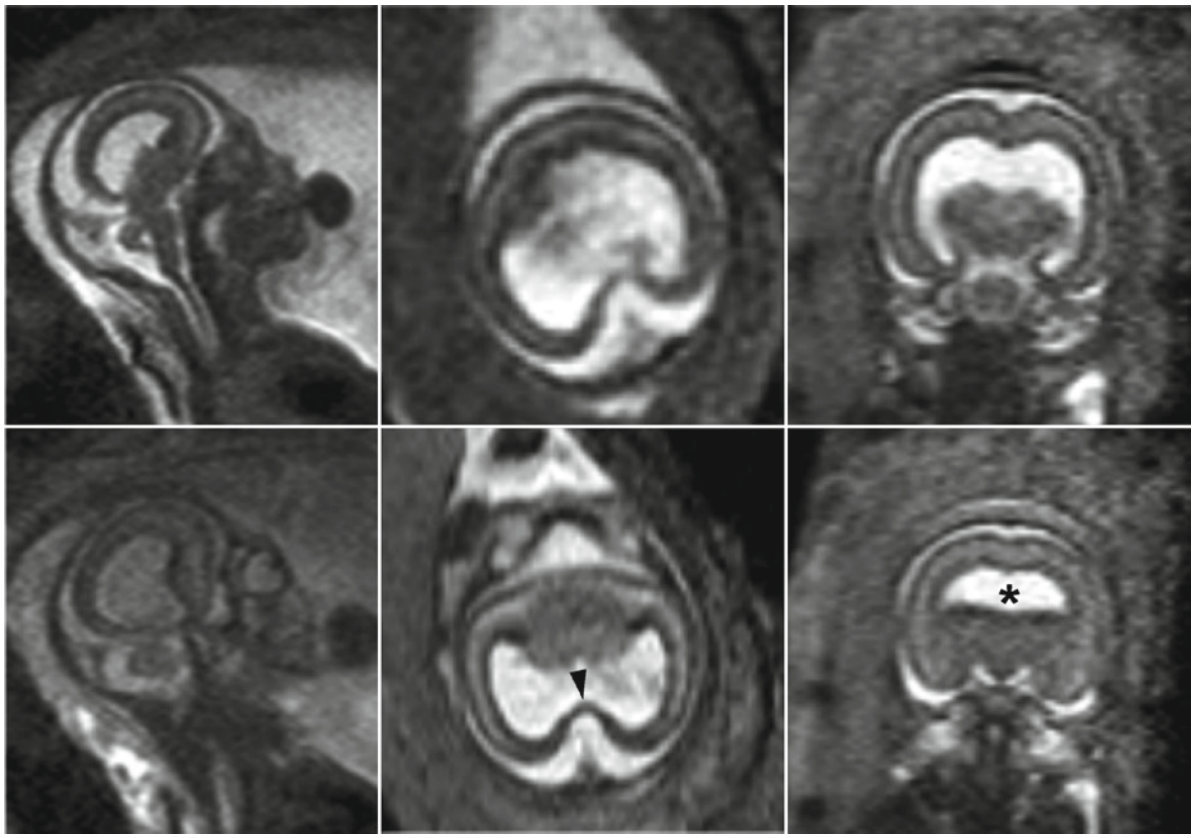

Fig. 9 Sagittal (*left column*) and corresponding axial (*middle column*) and coronal (*right column*) sections of T2-weighted sequences in a fetus aged 18+1 GW with semilobar holoprosencephaly showing the absence of the septum pellucidum, partial ventricular fusion (*asterisk*), partial separation of the cerebral hemispheres posteriorly (*black arrowhead*), non-cleavage of the thalamus, and hypotelorism. In addition, the brainstem and the cerebellum are hypoplastic. Note the regular delineation of the inner ear (*images on the right side*, *upper and lower panel*), and of the pituitary stalk, (*right image lower panel*)

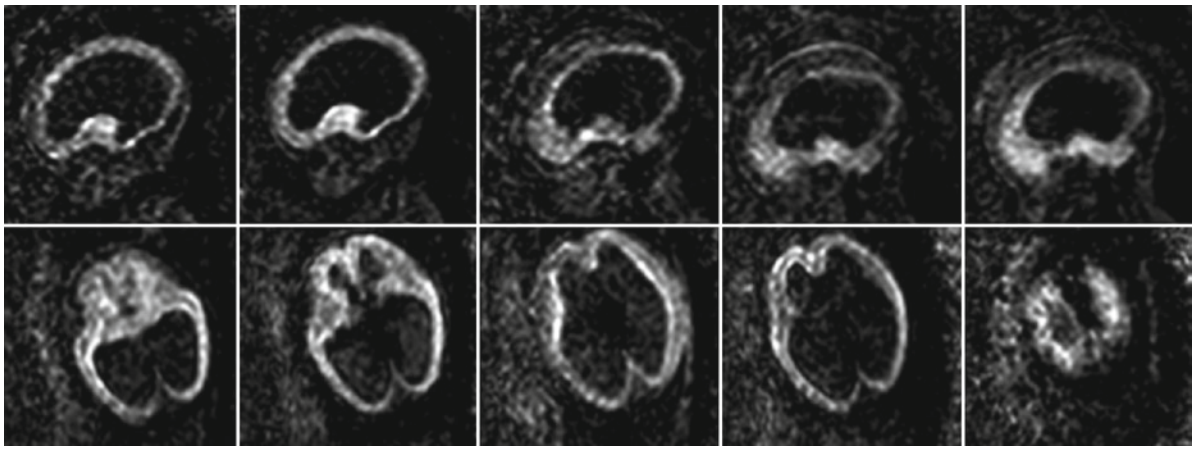

Fig. 10 Sagittal (*upper panel*) and axial (*lower panel*) diffusion-weighted sequences in a 21+4 GW old fetus. Because of the compression through the considerable enlargement of the ventricular system, the brain parenchyma loses its normal laminar signal and becomes homogeneously hyperintense in the posterior aspects of the brain

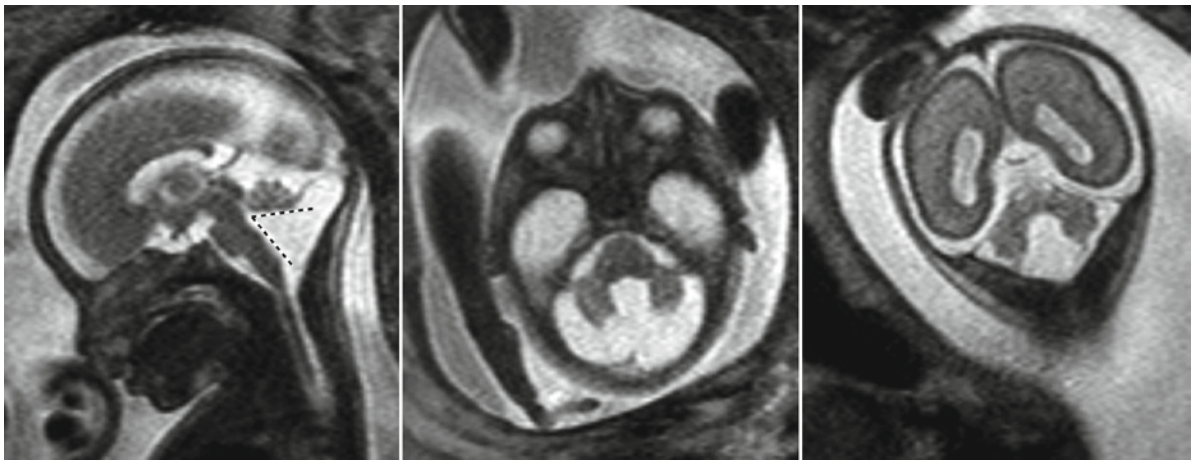

Fig. 11 Midline sagittal, axial, and coronal T2-weighted sequences of a fetus aged 22+4 GW with Dandy–Walker malformation. Note the cystic enlargement of the fourth ventricle with upwardly displacement of the tentorium and torcula and an uprotated vermis with an increased tegmento-vermian angle (*dotted angle*)

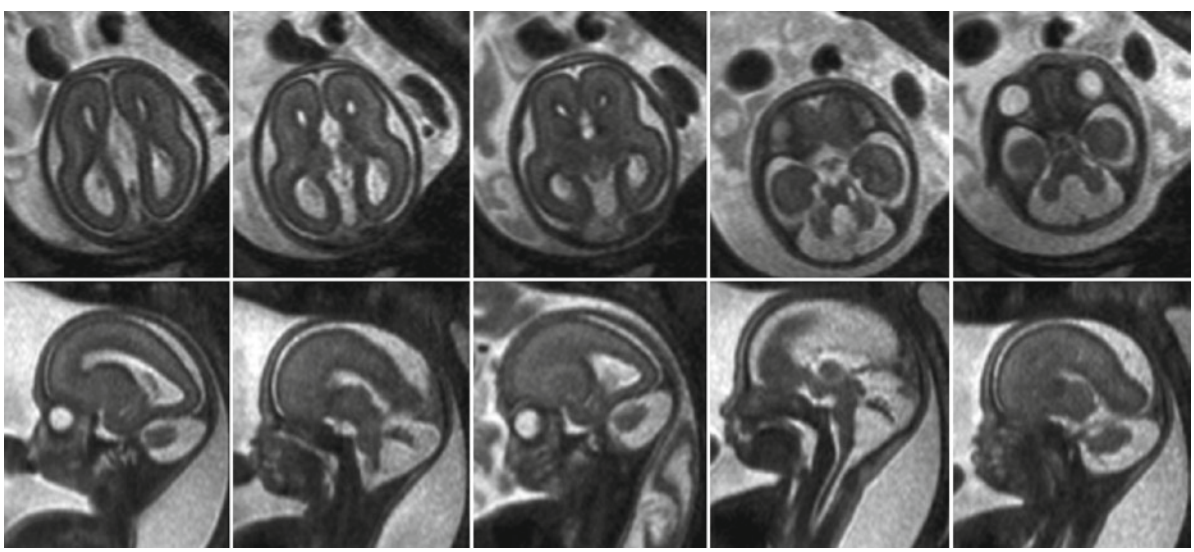

Fig. 12 Axial (*upper panel*) and sagittal (*lower panel*) sections of T2-weighted sequences in a 22+2 GW old fetus with corpus callosum agenesis and Dandy–Walker malformation. Note the absence of the corpus callosum with typically separated frontal horns, and the colpocephalic configuration of the lateral ventricles, indicative of callosal agenesis, as well as the widening of the fourth ventricle, an increased tegmento-vermian angle and high torcular, consistent with a Dandy–Walker malformation

malformation has to be suspected that can already be seen in GW 22 (Saleem and Zaki 2010). The characteristical shape of the fourth ventricle in such cases has been described to be umbrella-like (Spampinato et al. 2008). Partial vermian agenesis will lead to an abnormally wide connection of the fourth ventricle with the cisterna magna (Guibaud and des Portes 2006).

4.2 Lamination of the Brain Parenchyma

The ventricular and subventricular zone with its ganglionic eminences, the intermediate zone, subplate, and cortical plate can be delineated on MR images in vitro (Kostovic and Vasung 2009) and in vivo (Prayer et al. 2006). These zones have been found to have age-related

signals and dimensions (Perkins et al. 2008; Widjaja E et al. 2010a). Deviations from the normal lamination have been seen, for instance, in cases with lissencephaly (Widjaja E et al. 2010b) (Fig. 3). Regarding the cortical plate, a lack of sulci that are known to be present at a certain time, may indicate a malformation of cortical development (Ghai et al. 2006). The too shallow indentation of the insular cistern may be a subtle sign of lissencephaly before GW24 (Figs. 3 and 4). Gyri, usually irregularly configured and which appear prematurely, may be a sign of polymicrogyria (Dhombres et al. 2008) or cobblestone cortex. Attention should also be paid to the symmetry of the hemispheres. Sulcation and gyration is normally not completely symmetrical (Chung et al. 2009). Especially in the temporal lobe, in most fetuses the gyration of the right side is ahead to that on the left (Kasprian et al. 2010). In case of lissencephaly, the temporal lobe development may be (abnormally) symmetrical.

4.3 Basal Ganglia and Thalami

Basal ganglia and thalami can be delineated from unmyelinated white matter by their relative T1-weighted hyperintensity and T2-weighted hypointensity. On diffusion-weighted source images they also appear slightly hyperintense. Thus partial or complete fusion, the hallmark of holoprosencephalies (Hahn and Barnes 2010), can be recognized (Fig. 9).

4.4 Internal Capsule and White Matter Tracts

In the second trimester, the internal capsule is an unmyelinated white matter structure that is T2-weighted hyperintense, T1-weighted hypointense, but may display bright signals on anisotropy images as early as in GW 20 (Prayer et al. 2006). Based on the anisotropical behavior of unmyelinated white matter tracts, tractography is possible (Kasprian et al. 2008). The presence/absence/hypoplasia of certain white matter tracts may have an impact on diagnosis and prognosis, respectively (ten Donkelaar et al. 2004; Raybaud and Di Rocco 2007). Missing/hypoplastic corticospinal tracts may be found in microcephaly and L1CAM mutations (ten Donkelaar et al. 1999, 2004). Disorganization of the corticospinal tract was seen in Kallmann syndrome (Koenigkam-Santos et al. 2010). A wrong course of the pyramidal tracts (missing decussation) has been described in Joubert syndrome (Spampinato et al. 2008). In malformations of cortical development, fiber tracts may also deviate from their normal course (Lim et al. 2005) or be hypoplastic (Widjaja et al. 2007). Regarding partial or complete callosal agenesis, proof of the presence of Probst bundles secures the diagnosis (Fig. 2). In addition, aberrant bundles, as the sigmoid bundle, may be found in partial callosal agenesis (Utsunomiya H et al. 2006a). The proof of such pathological connectivity may have implications on future neuropsychological developments (Wahl M et al. 2009).

4.5 Subdural and Subarachnoid Space

In contrast to postnatally, the subdural space can be seen in fetuses. It is a few millimeter wide fluid-filled compartment that can be distinguished from the subarachnoid space that lies interiorly, by a lack of crossing vessels. Arachnoidal cysts result from a localized splitting of the arachnoid membrane with fluid accumulation in between (Starkman et al. 1958). Consequently, within the cyst no vessels are seen. Arachnoidal cysts have certain predilection sites (Sommer and Smit 1997), for instance, the temporal poles, or the region around the pineal gland (Fig. 13). In case of bilateral temporal location, the differential diagnosis includes glutaric aciduria with short temporal lobes (Righini et al. 2010). Infratentorial arachnoid cysts will have to be differentiated from cystic malformations of the posterior fossa (Hayward 2009; Parisi and Dobyns 2003). Retro or infracerebellar cysts may compress the cerebellum and displace the tentorium cerebelli, with the insertion of the tentorium cerebelli and torcula usually remaining in normal position (in contrast to malformations of the Dandy–Walker complex) (Guibaud 2004). However, in rare cases, also infratentorial arachnoid cysts may be also associated with upwardly displaced tentorium and torcula (Utsunomiya H et al. 2006b). Another differential diagnostic feature between an infratentorial arachnoid cyst and a Dandy–Walker malformation is the enlarged fourth ventricle and uprotated vermis in the latter (Figs. 11 and 12). In contrast, in arachnoid cysts, the vermis and fourth ventricle are primarily normal, but may be compressed or and/or dislocated. In megacisterna magna, the arachnoid membrane is normally formed, tentorium and torcula are in regular position, the anatomical borders of the posterior fossa are preserved (Utsunomiya H et al. 2006b), and

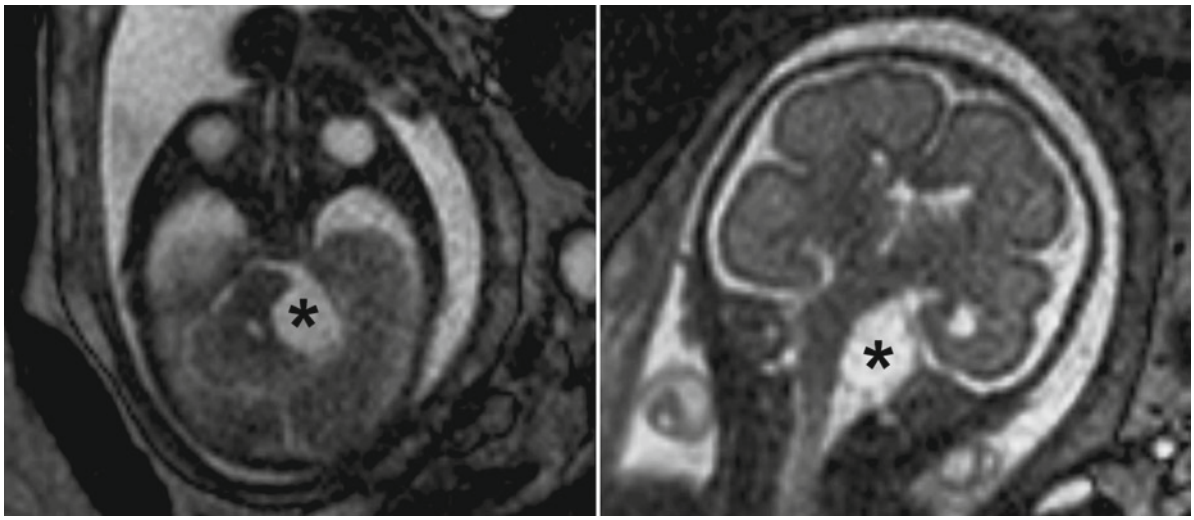

Fig. 13 Arachnoidal cyst compressing the brainstem (*asterisk*). The aqueduct is open, but follow-up examinations (at least with ultrasound) are necessary, as occlusive hydrocephalus may develop

the cerebellar falx is present and normally positioned. As the cerebellum continues to grow even postnatally, the fetal cisterna magna normally appears always larger than in the adult. However, enlargement of the cisterna magna may also be simulated by cerebellar hypoplasia (Forzano et al. 2007).

4.6 Midline Structures and Cerebellum

The interhemispheric fissure can readily be identified at the time when fetal MRI is done (Schmook et al. 2010). (Partial) absence of the interhemispheric fissure, and, more frequently, of the falx may point toward the presence of holoprosencephaly (HPE) (Volpe et al. 2009), or commissural agenesis (Raybaud 2010).

Even if other commissures are formed prior to the corpus callosum (Raybaud 2010), the latter is the only one that can be visualized on fetal MR studies regularly. The other commissures are usually too small to be delineated from the surrounding parenchyma. At GW 17/18, the corpus callosum is already formed in its whole extension (Raybaud 2010). Thus, non-visualization of the corpus callosum, or parts of it, has to be interpreted as pathological. As the contrast between the unmyelinated corpus callosum and the adjacent structures may be low on T2-weighted images, anisotropic diffusion-weighted images and tractography are helpful (Fig. 2). In contrast to the third trimester, radial gyri (Volpe et al. 2009), indicating the malpositioned cingular gyrus in callosal agenesis, will not be seen before GW 28. MR diagnosis of callosal agenesis is based on proving the complete/partial absence of the corpus callosum, and on demonstrating Probst bundles, or the sigmoid bundle respectively (Wahl M et al. 2009; Utsunomiya H et al. 2006a). Looking at malformations of corpus callosum, its development has to be considered as bicentrical: the lamina rostralis is the earliest part to develop, and thus always present in partial callosal agenesis involving the genu and splenium (Kier and Truwit 1997). At the same time, a more posterior part of the future body is formed at the level of the hippocampal commissure (Richards et al. 2004). The beaked segment of the rostrum develops at the same time as the genu (Kier and Truwit 1997). Complete callosal agenesis has been described as a white matter heterotopia rather than a lack of a commisure, as non-crossing fibers, the bundle of Probst is seen frequently (Raybaud 2010). Partial agenesis of the corpus callosum may affect different parts; consequently, these malformations should not be interpreted as minor forms of callosal agenesis, but as different entities (Raybaud 2010).

The septum pellucidum is located above the lamina rostralis, closing the medial aspect of and separating the lateral ventricles (Raybaud 2010). The cavum septi pellucidi is a space between the septal leaves, tela choroidea, and corpus callosum (Raybaud 2010). The absence of a cavum septi pellucidi on prenatal ultrasound is regarded as unspecific marker of various midline abnormalities (Winter et al. 2010). This has less

importance in fetal MRI, as the respective anatomical structures can be visualized directly. A posterior recess between the splenium and hippocampal commissure is called a cavum vergae (Raybaud 2010).The septum pellucidum is present before the corpus callosum in a primitive form. A dysplastic or missing septum pellucidum may be part of various syndromes (Raybaud 2010). This finding should initiate a careful screening for associated anomalies, especially involving the chiasm and pituitary (Schmook et al. 2010), and for schizencephalic clefts (Maeda et al. 2009).

Abnormal presentation of the tectum is a hallmark of the Chiari II malformation (Callen et al. 2009) (Fig. 5). In addition, a thickened tectum has been described in Aicardi malformation (Hopkins et al. 2008), a misshaped tectum is part of tectocerebellar dysraphism (Anik et al. 2010). Fused midbrain colliculi may be seen in rhombencephalosynapsis (Parisi and Dobyns 2003).

Measurements of the cerebellar structures should be done in any case of a suspect cystic or noncystic cerebellar malformation (Tilea et al. 2009). In addition, the shape of the cerebellum should be assessed: in rhombencephalosynapsis, for instance, the hemispheres are fused as a consequence of agenesis or hypoplasia of the vermis, mostly affecting its anterior part (Utsunomiya et al. 1998). The dentate nuclei lie adjacent to each other and thus may be visible on a midline sagittal slice. Elongated superior cerebellar peduncles are the result of vermian hypoplasia, leading to the characteristic molar-tooth pattern (Parisi 2009; Saleem and Zaki 2010). Upward distortion of the vermis is one of the landmarks of Dandy–Walker malformation (ten Donkelaar HL et al. 2003; Adamsbaum C et al. 2005; Parisi and Dobyns 2003). In such cases, the shape of the vermis may give a clue to intellectual outcome (Klein et al. 2003); the prognosis is estimated to be better if the normal lobulation is preserved (Boddaert et al. 2003; Bolduc and Limperopoulos 2009) (Figs. 11 and 12). Hypoplasia of the inferior vermis characterizes a short vermis with otherwise normal remaining cerebellar and supratentorial structures (Limperopoulos et al. 2006). However, different degrees of vermian hypoplasia are invariably present in type II lissencephalies (Aida et al. 1996; Barkovich 1998). Cerebellar hypoplasia refers to a small, but otherwise normal cerebellum, and may be unilateral or bilateral, involving the hemispheres with or without the vermis (Limperopoulos et al. 2006; Parisi and Dobyns 2003) (Fig. 4). As unilateral forms may be a sequelae of acquired conditions or a sign of disruption (Poretti et al. 2009; Barkovich et al. 2009), only the bilateral form will be considered here. Isolated cerebellar hypoplasia is rather the exception than the rule (Tilea et al. 2007). Cerebellar dysplasia is characterized by an impairment of cerebellar cell maturation (Patel and Barkovich 2002; Bolduc and Limperopoulos 2009). Cerebellar dysplasia is histiologically found in up to 85% of newborns without other structural abnormalities (Rorke et al. 1968). Heterotopia, disorders of folie formation, and disturbance of cortical layering were frequently seen in presence of genetic abnormalities (Soto-Ares et al. 2000). However, as a consequence of the limited resolution of fetal MRI, mainly disorders of foliation will be recognized, as these may interfere with the overall shape of the cerebellum. The primary fissure can be used as a landmark for normal cerebellar proportions (Zalel et al. 2009). In cerebellar dysplasia, the normal proportions will be distorted. A hypoplastic/dysplastic cerebellum is a constant morphological feature in type I and type II lissencephalies (Fallet-Bianco et al. 2008) (Fig. 3). In lissencephalies type I, the cerebellar involvement is usually less pronounced than in type II lissencephalies (Dobyns 2010). However, a heterogeneous group of lissencephalies with smooth cortex or pachygyria has been identified that is associated with marked cerebellar hypoplasia/dysplasia, including vermis and hemispheres (Ross et al. 2001), the so-called LCH type (lissencephaly with cerebellar hypoplasia) (Ross et al. 2001). There, cerebellar abnormalities are characterized by absent or defective foliation (Forman MS et al. 2005), a feature that might be detectable in prenatal MRI, of course depending on the extent of pathological changes and gestational age. Genetically, for instance, defects encoding the extracellular matrix protein reelin also belong to these groups (Forman MS et al. 2005). In Fukuyama congenital muscle dystrophy, a disease within the lissencephaly type II spectrum, cerebellar polymicrogyria leading to disorganized foliation and cysts are leading morphological symptoms (Aida et al. 1996). However, as the cysts may be small, they might not be identifiable prenatally. To date, prenatal diagnosis of Fukuyama has been done only by haplotype analysis using fetal DNA from chorionic villus sampling (Saito 2006). Cerebellar cysts have also been found in muscle-eye brain disease (Barkovich 1998). In addition, also certain muscle dystrophies with defective dystroglycan glycosylation present with cerebellar cysts (Clement et al. 2008). Cerebellar hypomyelination is a postnatal feature of Walker–Warburg syndrome (Barkovich 1998), but cannot be proved in fetuses, as at that time the cerebellum is not myelinated anyway.

Disorders of glycosylation are a group of inherited disorders caused by defects in the synthesis and processing of the asparagines (ASN)-linked oligosaccharides of glycoproteins (Jaeken and Matthijs 2007). One salient feature is a small cerebellum that may be present shortly after birth (Jaeken and Matthijs 2007). Prenatal cerebellar atrophy due to such a disorder has not yet been described; in fetuses, hydrops fetalis was seen (van de Kamp et al. 2007).

The shape and dimensions of the pons can be determined as well on ultrasound as on MRI (Achiron et al. 2004; Tilea et al. 2009). Pathological changes of the pons include hypoplasia and dysplasia: the latter one may appear as flattened anterior part (Longman et al. 2004), or z-shaped form (Barkovich 1998; Ross et al. 2001; Fallet-Bianco et al. 2008; Barkovich et al. 2009) (Fig. 3). Hypoplasia may be the consequence of the absence of corticospinal tracts. This feature is not specific for lissencephalies and might, for instance, also be seen in holoprosencephaly. In muscle eye brain disease and Walker–Warburg syndrome, the pons may show a midline cleft (Jissendi-Tchofo et al. 2009).

Pontocerebellar hypoplasia (PCH) is characterized by a small and/or dysplastic cerebellum and pons. The different forms may be associated with supratentorial atrophy, and/or motor neuron defects, and/or optic atrophy (Barth 2000), and/or mitochondrial defects (de Koning et al. 1999). In addition to these forms, also the so-called CASK (calcium/calmodulin-dependent serine protein kinase)-mutations (Takanashi et al. 2010) may lead to PCH. These syndromes are combined with microcephaly, but normally sized corpus callosum (Takanashi et al. 2010). It is not clear whether isolated PCH can be diagnosed prenatally: indirect signs are polyhydramnios and/or microcephaly (Barth 2000).

4.7 Abnormal Structures

1. Pathological vascular structures comprise vascular malformations, such as the vein of Galen aneurysmal malformations (VGAMs) (Mighell et al. 2009) (Fig. 14). These malformations are arteriovenous malformations originating from the choroidal system that develop in the early embryonic stage (Geibprasert et al. 2010). As a consequence of arteriovenous fistula the aneurismal sac is filled (Brunelle 1997). The drainage usually occurs via the straight sinus, which will eventually become enlarged. Prenatally they can be identified readily by ultrasound as well as by MRI (Brunelle 1997; Geibprasert et al. 2010). The same is true for malformations of the dural sinus (McInnes et al. 2009). Pial arteriovenous malformations (Ozanne et al. 2007) and arteriovenous fistula can also be found apart from VGAMs, which may be associated with metameric syndromes (Bun et al. 2009). Complications include steal phenomena, ischemia or perfusion failure due to congestive heart failure, atrophy of adjacent structures due to compression, and whole brain atrophy (Brunelle 1997; Geibprasert et al. 2010). The so-called melting brain (Ozanne et al. 2007) is a hydrovenous disorder leading to malnourishment of tissue (Ozanne et al. 2007).
2. Subependymal nodules may correspond either to subependymal heterotopia or to manifestations of tuberous sclerosis (TS). In the latter one, MRI is usually performed in case of a sonographical proof of cardiac rhabdomyomas. Subependymal nodules and/or giant cell astrocytomas can be visualized from around gestational week 30 (Mühler et al. 2007). Hussain et al. diagnosed a giant cell astrocytoma near the loco typico, near the foramen of Monroe on fetal MRI (Hussain et al. 2006). However, before that time it may not be possible to estimate the full extent of TS-associated cerebral changes (Fig. 15). The differential diagnosis between subependymal nodules and heterotopia may be difficult, as nodules do calcify only after birth, and contrast-media information is usually not available prenatally. However, the MR visualization of heterotopia has been possible already in gestational week 23 (Mitchell et al. 2000).

5 Diagnosis of Selected Syndromes in the Second Trimester

In order to facilitate diagnoses of lissencephalies, holoprosencephalies, and commissural agenesis, tables (Tables 2, 3, 4, and 5) are provided that include the most important information related to the respective pathology. As most criteria are unspecific, the accuracy of a diagnosis increases with the fulfilled number of mentioned criteria. Specific criteria are printed in bold. However, the absence of a "specific" criterion does not exclude a certain diagnosis.

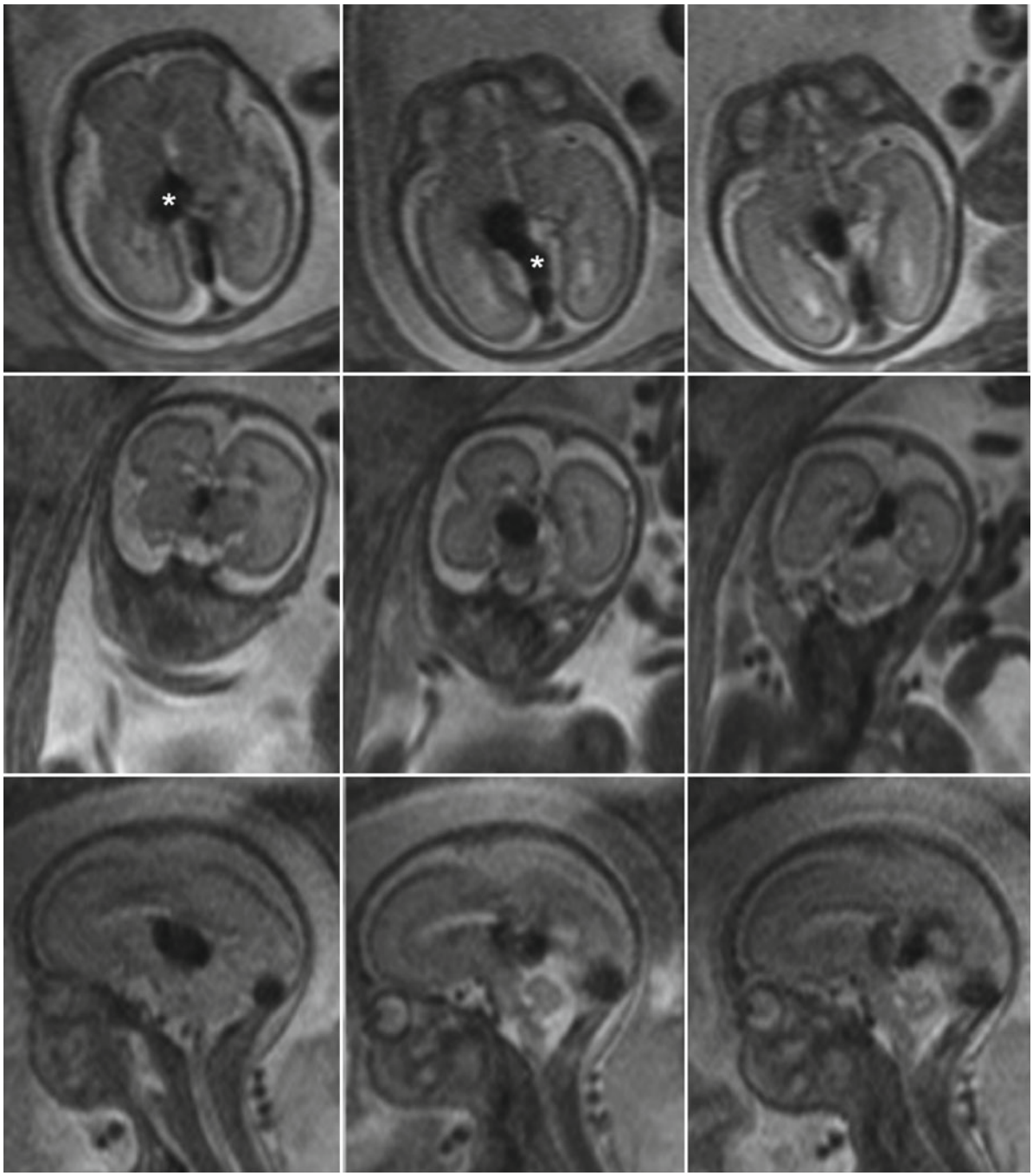

Fig. 14 Axial (*upper panel*), coronal (*middle panel*), and sagittal (*lower panel*) sections of T2-weighted sequences in a fetus aged 26 GW showing an aneurysmal dilatation of the vein of Galen, of the straight sinus (*white asterisks*) and of the jugular veins (*most right image middle panel*)

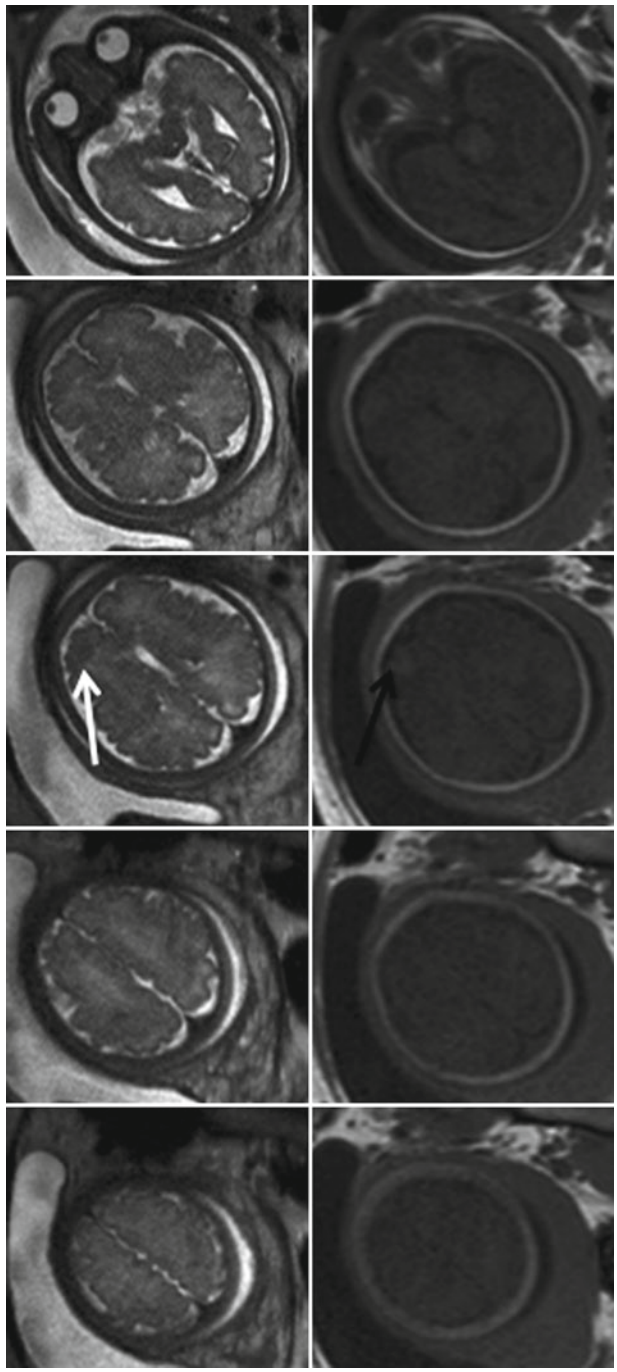

Fig. 15 Axial sections of T2-weighted sequence (*upper panel*), and corresponding T1-weighted sequence (*lower panel*) of a fetus aged 33+6 GW with tuberous sclerosis (TS). Note the focal cortical dysplasia in the frontal lobe, which is hypointense on the T2-weighted sequence (*white arrow*) and hyperintense on the T1-weighted sequence (*black arrow*). In addition, subependymal nodules are visible (T2-weighted hypointense, *middle image*). These changes had not been present at the MRI in GW 22. Notice the delineation of the optic chiasm (*most right image upper panel*), and the hyperintense pituitary, (*most right image lower panel*)

5.1 Lissencephalies/Polymicrogyria Syndromes (Chang et al. 2004)

Table 2 Indications for MRI and frequent MR findings in second trimester lissencephaly

Frequent indications	Microcephaly, (borderline) ventriculomegaly, small cerebellum on US, lissencephaly in previous pregnancy, genetic disposition
MRI supratentorial	Ventriculomegaly, **disordered lamination** (small subplate, not age-related appearance of the ventricular/subventricular zones), **shallow insular indentation**, absence of age-related gyri and sulci, irregular gyri and sulci, absent corpus callosum
MRI infratentorial	Hypoplastic cerebellum, hypoplastic/dysplastic pons, **z-shaped pons in lissencephalies type II**
MRI face	Tall, prominent forehead, hypertelorism, short nose, thickened upper lip (lissencephaly type I) (Allanson et al. 1998)
MRI extra CNS	Omphalocele (Chitayat et al. 1997), ambiguous genitalia

5.2 Holoprosencephalies

Table 3 Indications for MRI and frequent MR findings in second trimester holoprosencephaly

Frequent indications	"Irregular" ventriculomegaly, and/or facial cleft, and/or missing septum pellucidum on US (Winter et al. 2010)
MRI supratentorial	Complete or partial **monoventricle,** complete or partial **thalamic fusion**, missing or incomplete falx, missing olfactory bulbs, malformations of cortical development
MRI infratentorial	Rhombencephalosynapsis, Dandy–Walker continuum, vermian agenesis (Blazer et al. 1997)
MRI face	Hypotelorism, anophthalmia/microophthalmia, flat nasal bridge, absent nasal septum, flat nasal tip, bilateral cleft lip with median process representing the philtrum–premaxilla anlage, midline cleft (lip and/or palate), single median incisor (Nanni et al. 2001)
MRI extra CNS	Cardiac malformations, polydactyly, clinodactyly, ectrodactyly (Vilain et al. 2009)

5.3 Commissural Agenesis

The only commissure that may be found reliably prenatally is the corpus callosum. The anterior and hippocampal commissures may be visible in selected cases. However, the absence of any interhemispheric connection can be detected easily on fetal MR images.

Table 4 Indications for MRI and frequent MR findings in second trimester commissural agenesis

Frequent indications	(Mild) ventriculomegaly, missing septum pellucidum (Winter et al. 2010), displaced pericallosal artery on US
MRI supratentorial	**Missing corpus callosum, colpocephaly, proof of Probst bundles or a sigmoid bundle using tractography**, midline cysts, hydrocephalus, malformations of cortical development, lipoma, arachnoidal cyst, hippocampal malrotation, defective falx, plexus cysts, holoprosencephaly (HPE)
MRI infratentorial	Chiari II, rhombencephalosynapsis, aqueduct stenosis, for instance, in X-linked hydrocephalus, Dandy–Walker complex, vermian hypogenesis
MRI face	Eye abnormalities in Aicardi Mowat–Wilson syndrome, unspecific facial dysmorphism, see Table 3
MRI extra CNS	As agenesis, or hypoplasia, or dysgenesis of the corpus callosum may be parts of various complex malformations (Schell-Apacik et al. 2008), a meticulous examination of all fetal organs is required in such cases. Selected syndromes with involvement of the corpus callosum are summarized in Table 5.

Table 5 Main morphological changes associated with callosal agenesis

Syndrome	Main morphological findings apart from callosal abnormalities
Acrocallosal	Macrocephaly, hypertolorism, polydactyly, hallux duplication
Aicardi	Plexus cyst, plexus papilloma, microphthalmia, chorioretinopathy, tumors
Andermann	Facial dysmorphism, syndactyly, high-arched palate, skoliosis
Genitopatellar	Prominent nose, high nasal bridge, micrognathia, pulmonary hypoplasia, renal abnormalities, hypospadia, absent patellae, hip-and-foot deformities
MASA (mental retardation, aphasia, shuffling gait, and adducted thumbs)	Aqueduct stenosis, hydrocephalus, misshaped tectum, dysplastic cerebellum, adducted thumbs, skoliosis
Mowat–Wilson	Distinctive facial features, Hirschsprung disease, genitourinary anomalies (particularly hypospadias in males), congenital heart defects (abnormalities of the pulmonary arteries and/or valves), and eye defects (microphthalmia and Axenfeld anomaly) (Schell-Apacik et al. 2008)
Meckel–Gruber	Encephalocele, polydactyly, polycystic kidneys
Oculocerebrocutaneous	Malformations of cortical development, skin appendages, microphthalmia, anophthalmia, facial cleft, vertebral anomalies, cardiac malformation
Donnai–Barrow	Hypertelorism, prominent eyes, diaphragmatic hernia, omphalocele (Chassaing et al. 2003)
Fryns	Congenital diaphragmatic hernia, pulmonary hypoplasia, craniofacial changes (Slavotinek 2004)
Fetal alcohol spectrum disorders	Hypoplastic cerebellum (Spadoni et al. 2007)
Toriello–Carey	Retrognathia, laryngeal and cardiac anomalies, brachydactyly (Aftimos and McGaughran 2001)

The morphological changes that may be associated with callosal agenesis that are mentioned in Table 5 are restricted to those that have been described or are detectable on prenatal imaging studies.

In conclusion, the diagnosis of malformations in the second trimester is a challenge for MRI.

However, most of the syndromes bearing an unfavorable prognosis will be recognized in case high-quality images are available. In the future, the inclusion of tractography will help with more accurate diagnosis and contribute to better prenatal counseling.

References

Achiron R, Kivilevitch Z, Lipitz S, Gamzu R, Almog B, Zalel Y (2004) Development of the human fetal pons: in utero ultrasonographic study. Ultrasound Obstet Gynecol 24:506–510

Adamsbaum C, Moutard ML, Andre C, Merzoug V, Ferey S, Quere MP, Lewin F, Fallet-Bianco C (2005) MRI of the fetal posterior fossa. Pediatr Radiol 35:124–140

Aftimos S, McGaughran J (2001) Toriello-Carey syndrome: case report with additional findings. Am J Med Genet 98:273–276

Aida N, Tamagawa K, Takada K, Yagishita A, Kobayashi N, Chikumaru K, Iwamoto H (1996) Brain MR in Fukuyama congenital muscular dystrophy. AJNR Am J Neuroradiol 17:605–613

Allanson JE, Ledbetter DH, Dobyns WB (1998) Classical lissencephaly syndromes: does the face reflect the brain? J Med Genet 35:920–923

Anik I, Koc K, Anik Y, Yildiz DK, Ceylan S (2010) Tectocerebellar dysraphism with vermian encephalocele. J Child Neurol [Epub ahead of print]

Barkovich AJ (1998) Neuroimaging manifestations and classification of congenital muscular dystrophies. AJNR Am J Neuroradiol 19:1389–1396

Barkovich AJ (2005) Pediatric neuroimaging, 4th edn. Lippincott Williams & Wilkins, Philadelphia

Barkovich AJ, Millen KJ, Dobyns WB (2009) A developmental and genetic classification for midbrain-hindbrain malformations. Brain 132:3199–3230

Barth PG (2000) Pontocerebellar hypoplasia – how many types? Eur J Paediatr Neurol 4:161–162

Blaas HG, Eik-Nes SH (2009) Sonoembryology and early prenatal diagnosis of neural anomalies. Prenat Diagn 29: 312–325

Blazer S, Berant M, Sujov PO, Zimmer EZ, Bronshtein M (1997) Prenatal sonographic diagnosis of vermal agenesis. Prenat Diagn 17:907–911

Boddaert N, Klein O, Ferguson N, Sonigo P, Parisot D, Hertz-Pannier L, Baraton J, Emond S, Simon I, Chigot V, Schmit P, Pierre-Kahn

A, Brunelle F (2003) Intellectual prognosis of the Dandy-Walker malformation in children: the importance of vermian lobulation. Neuroradiology 45:320–324

Bolduc ME, Limperopoulos C (2009) Neurodevelopmental outcomes in children with cerebellar malformations: a systematic review. Dev Med Child Neurol 51:256–267

Boog G, Le Vaillant C, Collet M, Dupré PF, Parent P, Bongain A, Benoit B, Trastour C (2004) Prenatal sonographic patterns in six cases of Wolf-Hirschhorn (4p-)syndrome. Fetal Diagn Ther 19:421–430

Bronshtein M, Wiener Z (1991) Early transvaginal sonographic diagnosis of alobar holoprosencephaly. Prenat Diagn 11:459–462

Brunelle F (1997) Arteriovenous malformation of the vein of Galen in children. Pediatr Radiol 27:501–513

Bun YY, Ming CK, Ming CH, Ling CY, Ming CC (2009) Endovascular treatment of a neonate with dural arteriovenous fistula and other features suggestive of cerebrofacial arteriovenous metameric syndromes. Childs Nerv Syst 25:383–387

Calabrò F, Arcuri T, Jinkins JR (2000) Blake's pouch cyst: an entity within the Dandy-Walker continuum. Neuroradiology 42:290–295

Callen AL, Filly RA (2008) Supratentorial abnormalities in the Chiari II malformation, I: the ventricular "point". J Ultrasound Med 27:33–38

Callen AL, Stengel JW, Filly RA (2009) Supratentorial abnormalities in the Chiari II malformation, II: tectal morphologic changes. J Ultrasound Med 28:29–35

Chang BS, Piao X, Giannini C, Cascino GD, Scheffer I, Woods CG, Topcu M, Tezcan K, Bodell A, Leventer RJ, Barkovich AJ, Grant PE, Walsh CA (2004) Bilateral generalized polymicrogyria (BGP): a distinct syndrome of cortical malformation. Neurology 25:1722–1728

Chassaing N, Lacombe D, Carles D, Calvas P, Saura R, Bieth E (2003) Donnai-Barrow syndrome: four additional patients. Am J Med Genet A 121A:258–262

Chitayat D, Toi A, Babul R, Blaser S, Moola S, Yarkoni D, Sermer M, Johnson JA, Vasjar J, Teshima I (1997) Omphalocele in Miller-Dieker syndrome: expanding the phenotype. Am J Med Genet A 69:293–298

Chung R, Kasprian G, Brugger PC, Prayer D (2009) The current state and future of fetal imaging. Clin Perinatol 36:685–699

Clement E, Mercuri E, Godfrey C, Smith J, Robb S, Kinali M, Straub V, Bushby K, Manzur A, Talim B, Cowan F, Quinlivan R, Klein A, Longman C, McWilliam R, Topaloglu H, Mein R, Abbs S, North K, Barkovich AJ, Rutherford M, Muntoni F (2008) Brain involvement in muscular dystrophies with defective dystroglycan glycosylation. Ann Neurol 64:573–582

de Koning TJ, de Vries LS, Groenendaal F, Ruitenbeek W, Jansen GH, Poll-The BT, Barth PG (1999) Pontocerebellar hypoplasia associated with respiratory-chain defects. Neuropediatrics 30:93–95

Dhombres F, Nahama-Allouche C, Gelot A, Jouannic JM, de Villemeur TB, Saint-Frison MH, le Pointe HD, Garel C (2008) Prenatal ultrasonographic diagnosis of polymicrogyria. Ultrasound Obstet Gynecol 32:951–954

Dobyns WB (2010) The clinical patterns and molecular genetics of lissencephaly and subcortical band heterotopia. Epilepsia 51:5–9

Dubourg C, Bendavid C, Pasquier L, Henry C, Odent S, David V (2007) Holoprosencephaly. Orphanet J Rare Dis 2:8

Durfee SM, Kim FM, Benson CB (2001) Postnatal outcome of fetuses with the prenatal diagnosis of asymmetric hydrocephalus. J Ultrasound Med 20:263–268

Fallet-Bianco C, Loeuillet L, Poirier K, Loget P, Chapon F, Pasquier L, Saillour Y, Beldjord C, Chelly J, Francis F (2008) Neuropathological phenotype of a distinct form of lissencephaly associated with mutations in TUBA1A. Brain 131:2304–2320

Forman MS, Squier W, Dobyns WB, Golden JA (2005) Genotypically defined lissencephalies show distinct pathologies. J Neuropathol Exp Neurol 64:847–857

Forzano F, Mansour S, Ierullo A, Homfray T, Thilaganathan B (2007) Posterior fossa malformation in fetuses: a report of 56 further cases and a review of the literature. Prenat Diagn 27:495–501

Garel C (2010) Posterior fossa malformations: main features and limits in prenatal diagnosis. Pediatr Radiol 40:1038–1045

Geibprasert S, Krings T, Armstrong D, Terbrugge KG, Raybaud CA (2010) Predicting factors for the follow-up outcome and management decisions in vein of Galen aneurysmal malformations. Childs Nerv Syst 26:35–46

Ghai S, Fong KW, Toi A, Chitayat D, Pantazi S, Blaser S (2006) Prenatal US and MR imaging findings of lissencephaly: review of fetal cerebral sulcal development. Radiographics 26:389–405

Greene ND, Copp AJ (2009) Development of the vertebrate central nervous system: formation of the neural tube. Prenat Diagn 29:303–311

Guardiola A, Koltermann V, Aguiar PM, Grossi SP, Fleck V, Pereira EC, Pellanda L (2009) Neurological congenital malformations in a tertiary hospital in south Brazil. Arq Neuropsiquiatr 67:807–811

Guibaud L (2004) Practical approach to prenatal posterior fossa abnormalities using MRI. Pediatr Radiol 34:700–711

Guibaud L, des Portes V (2006) Plea for an anatomical approach to abnormalities of the posterior fossa in prenatal diagnosis. Ultrasound Obstet Gynecol 5:477–481

Hahn JS, Barnes PD (2010) Neuroimaging advances in holoprosencephaly: refining the spectrum of the midline malformation. Am J Med Genet C Semin Med Genet 15:120–132

Hayward R (2009) Postnatal management and outcome for fetal-diagnosed intra-cerebral cystic masses and tumours. Prenat Diagn 29:396–401

Hopkins B, Sutton VR, Lewis RA, Van den Veyver I, Clark G (2008) Neuroimaging aspects of Aicardi syndrome. Am J Med Genet A 15:2871–2878

Hussain N, Curran A, Pilling D, Malluci CL, Ladusans EJ, Alfirevic Z, Pizer B (2006) Congenital subependymal giant cell astrocytoma diagnosed on fetal MRI. Arch Dis Child 91:520

Jaeken J, Matthijs G (2007) Congenital disorders of glycosylation: a rapidly expanding disease family. Annu Rev Genomics Hum Genet 8:261–278

Jissendi-Tchofo P, Kara S, Barkovich AJ (2009) Midbrain-hindbrain involvement in lissencephalies. Neurology 72:410–418

Kasprian G, Brugger PC, Weber M, Krssák M, Krampl E, Herold C, Prayer D (2008) In utero tractography of fetal white matter development. Neuroimage 43:213–224

Kasprian G, Langs G, Brugger PC, Bittner M, Weber M, Arantes M, Prayer D (2010) The prenatal origin of hemispheric asymmetry: an in utero neuroimaging study. Cereb Cortex [Epub ahead of print]

Kier EL, Truwit CL (1997) The lamina rostralis: modification of concepts concerning the anatomy, embryology, and MR appearance of the rostrum of the corpus callosum. AJNR Am J Neuroradiol 18:715–722

Kjaer I, Hansen N, Becktor KB, Birkebaek N, Balslev T (2001) Craniofacial morphology, dentition, and skeletal maturity in four siblings with Seckel syndrome. Cleft Palate Craniofac J 38:645–651

Klein O, Pierre-Kahn A, Boddaert N, Parisot D, Brunelle F (2003) Dandy-Walker malformation: prenatal diagnosis and prognosis. Childs Nerv Syst 19:484–489

Koenigkam-Santos M, de Castro M, Versiani BR, Diniz PR, Santos AC (2010) Kallmann syndrome and mirror movements: white matter quantitative evaluation with magnetic resonance imaging. J Neurol Sci 15:40–44

Kostovic I, Vasung L (2009) Insights from in vitro fetal magnetic resonance imaging of cerebral development. Semin Perinatol 33:220–233

Levine D, Trop I, Mehta TS, Barnes PD (2002) MR imaging appearance of fetal cerebral ventricular morphology. Radiology 223:652–660

Lim CC, Yin H, Loh NK, Chua VG, Hui F, Barkovich AJ (2005) Malformations of corticaldevelopment: high-resolution MR and diffusion tensor imaging of fiber tracts at 3T. AJNR Am J Neuroradiol 26:61–64

Limperopoulos C, Robertson RL, Estroff JA, Barnewolt C, Levine D, Bassan H, du Plessis AJ (2006) Diagnosis of inferior vermian hypoplasia by fetal magnetic resonance imaging: potential pitfallsand neurodevelopmental outcome. Am J Obstet Gynecol 194(4):1070–1076

Longman C, Mercuri E, Cowan F, Allsop J, Brockington M, Jimenez-Mallebrera C, Kumar S, Rutherford M, Toda T, Muntoni F (2004) Antenatal and postnatal brain magnetic resonance imaging in muscle-eye-brain disease. Arch Neurol 61:1301–1306

Maeda T, Akaishi M, Shimizu M, Sekiguchi K, Anan A, Takano T, Imai K, Suenobu S, Korematsu S, Izumi T (2009) The subclassification of schizencephaly and its clinical characterization. Brain Dev 31:694–701

Malinger G, Lev D, Kidron D, Heredia F, Hershkovitz R, Lerman-Sagie T (2005) Differential diagnosis in fetuses with absent septum pellucidum. Ultrasound Obstet Gynecol 25:42–49

McInnes M, Fong K, Grin A, ter Brugge K, Blaser S, Halliday W, Shannon P (2009) Malformations of the fetal dural sinuses. Can J Neurol Sci 36:72–77

Mighell AS, Johnstone ED, Levene M (2009) Post-natal investigations: management and prognosis for fetuses with CNS anomalies identified in utero excluding neurosurgical problems. Prenat Diagn 29:442–449

Mitchell LA, Simon EM, Filly RA, Barkovich AJ (2000) Antenatal diagnosis of subependymal heterotopia. AJNR Am J Neuroradiol 21:296–300

Mühler MR, Rake A, Schwabe M, Schmidt S, Kivelitz D, Chaoui R, Hamm B (2007) Value of fetal cerebral MRI in sonographically proven cardiac rhabdomyoma. Pediatr Radiol 37:467–474

Nanni L, Ming JE, Du Y, Hall RK, Aldred M, Bankier A, Muenke M (2001) SHH mutation is associated with solitary median maxillary central incisor: a study of 13 patients and review of the literature. Am J Med Genet A 102:1–10

Noronha LD, Medeiros F, Martins VD, Nones RB, Sepulcri RP, Prevedello LM, Sampaio GA, Serapião MJ, Torres LF (2001) The neuropathology of neonatal period: analysis of 1616 autopsies. Arq Neuropsiquiatr 59:411–416

Oi S (2003) Diagnosis, outcome, and management of fetal abnormalities: fetal hydrocephalus. Childs Nerv Syst 19: 508–516

Ozanne A, Alvarez H, Krings T, Lasjaunias P (2007) Pediatric neurovascular malformations: vein of Galen arteriovenous malformations (VGAM), pial arteriovenous malformations (pial AVM), dural sinus malformations (DSM)]. J Neuroradiol 34:145–166

Parisi MA (2009) Clinical and molecular features of Joubert syndrome and related disorders. Am J Med Genet C Semin Med Genet 15:326–340

Parisi MA, Dobyns WB (2003) Human malformations of the midbrain and hindbrain: review and proposed classification scheme. Mol Genet Metab 80:36–53

Pasquier L, Marcorelles P, Loget P, Pelluard F, Carles D, Perez MJ, Bendavid C, de La Rochebrochard C, Ferry M, David V, Odent S, Laquerrière A (2009) Rhombencephalosynapsis and related anomalies: a neuropathological study of 40 fetal cases. Acta Neuropathol 117:185–200

Patel S, Barkovich AJ (2002) Analysis and classification of cerebellar malformations. AJNR Am J Neuroradiol 23: 1074–1087

Pavone L, Corsello G, Pavone P, Iannetti P (2010) Lissencephalic syndromes: brain and beyond. Front Biosci 2:85–95

Perkins L, Hughes E, Srinivasan L, Allsop J, Glover A, Kumar S, Fisk N, Rutherford M (2008) Exploring cortical subplate evolution using magnetic resonance imaging of the fetal brain. Dev Neurosci 30:211–220

Pilu G, Falco P, Gabrielli S, Perolo A, Sandri F, Bovicelli L (1999) The clinical significance of fetal isolated cerebral borderline ventriculomegaly: report of 31 cases and review of the literature. Ultrasound Obstet Gynecol 14: 320–326

Poretti A, Huisman TA, Cowan FM, Del Giudice E J, Jeannet PY, Prayer D, Rutherford MA, du Plessis AJ, Limperopoulos C, Boltshauser E (2009) Cerebellar cleft:confirmation of the neuroimaging pattern. Neuropediatrics 40:228–233

Prayer D, Barkovich AJ, Kirschner DA, Prayer LM, Roberts TP, Kucharczyk J, Moseley ME (2001) Visualization of nonstructural changes in early white matter development on diffusion-weighted MR images: evidence supporting premyelination anisotropy. AJNR Am J Neuroradiol 22: 1572–1576

Prayer D, Kasprian G, Krampl E, Ulm B, Witzani L, Prayer L, Brugger PC (2006) MRI of normal fetal brain development. Eur J Radiol 57:199–216

Rankin J, Cans C, Garne E, Colver A, Dolk H, Uldall P, Amar E, Krageloh-Mann I (2010) Congenital anomalies in children with cerebral palsy: a population-based record linkage study. Dev Med Child Neurol 52:345–351

Raybaud C (2010) The corpus callosum, the other great forebrain commissures, and the septum pellucidum:

anatomy, development, and malformation. Neuroradiology 52:447–477
Raybaud C, Di Rocco C (2007) Brain malformation in syndromic craniosynostoses, a primary disorder of white matter: a review. Childs Nerv Syst 23:1379–1388
Richards LJ, Plachez C, Ren T (2004) Mechanisms regulating the development of the corpus callosum and its agenesis in mouse and human. Clin Genet 66:276–289
Righini A, Fiori L, Parazzini C, Doneda C, Arrigoni F, Riva E, Triulzi F (2010) Early prenatal magnetic resonance imaging of glutaric aciduria type 1: case report. J Comput Assist Tomogr 34:446–448
Rorke LB, Fogelson MH, Riggs HE (1968) Cerebellar heterotopia in infancy. Dev Med Child Neurol 10:644–650
Ross ME, Swanson K, Dobyns WB (2001) Lissencephaly with cerebellar hypoplasia (LCH): a heterogeneous group of cortical malformations. Neuropediatrics 32:256–263
Saito K (2006) Prenatal diagnosis of Fukuyama congenital muscular dystrophy. Prenat Diagn 26:415–417
Saleem SN, Zaki MS (2010) Role of MR imaging in prenatal diagnosis of pregnancies at risk for Joubert syndrome and related cerebellar disorders. AJNR Am J Neuroradiol 31:424–429
Saleem SN, Said AH, Abdel-Raouf M, El-Kattan EA, Zaki MS, Madkour N, Shokry M (2009) Fetal MRI in the evaluation of fetuses referred for sonographically suspected neural tube defects (NTDs): impact on diagnosis and management decision. Neuroradiology 51:761–772
Schell-Apacik CC, Wagner K, Bihler M, Ertl-Wagner B, Heinrich U, Klopocki E, Kalscheuer VM, Muenke M, von Voss H (2008) Agenesis and dysgenesis of the corpus callosum: clinical, genetic and neuroimaging findings in a series of 41 patients. Am J Med Genet A 146A: 2501–2511
Schmook MT, Brugger PC, Weber M, Kasprian G, Nemec S, Krampl-Bettelheim E, Prayer D (2010) Forebrain development in fetal MRI: evaluation of anatomical landmarks before gestational week 27. Neuroradiology 52: 495–504
Schrander-Stumpel C, Vos YJ (2004, updated 2006) L1 syndrome. In: Pagon RA, Bird TC, Dolan CR, Stephens K (eds) Genereviews. University of Washington, Seattle
Schumacher GH (2004) Teratology in cultural documents and today. Ann Anat 186:539–546
Senat MV, Bernard JP, Delezoide A, Saugier-Veber P, Hillion Y, Roume J, Ville Y (2001) Prenatal diagnosis of hydrocephalus-stenosis of the aqueduct of Sylvius by ultrasound in the first trimester of pregnancy. Report of two cases. Prenat Diagn 21:1129–1132
Simioli S, Napolitano R, Quaglia F, Mazzarelli LL, Agangi A, Milanes GM, Tessitore G, Iannaccone A, Maruotti GM, Martinelli P (2009) Fetal borderline cerebral ventriculomegaly: clinical significance and management. Minerva Ginecol 61:109–112
Slavotinek AM (2004) Fryns syndrome: a review of the phenotype and diagnostic guidelines. Am J Med Genet A 124A:427–433
Sommer IE, Smit LM (1997) Congenital supratentorial arachnoidal and giant cysts in children: a clinical study with arguments for a conservative approach. Childs Nerv Syst 13:8–12
Soto-Ares G, Delmaire C, Deries B, Vallee L, Pruvo JP (2000) Cerebellar cortical dysplasia: MR findings in a complex entity. AJNR Am J Neuroradiol 21:1511–1519
Spadoni AD, McGee CL, Fryer SL, Riley EP (2007) Neuroimaging and fetal alcohol spectrum disorders. Neurosci Biobehav Rev 31:239–245
Spampinato MV, Kraas J, Maria BL, Walton ZJ, Rumboldt Z (2008) Absence of decussation of the superior cerebellar peduncles in patients with Joubert syndrome. Am J Med Genet A 146:1389–1394
Starkman SP, Brown TC, Linell EA (1958) Cerebral arachnoid cysts. J Neuropathol Exp Neurol 17:484–500
Takanashi J, Arai H, Nabatame S, Hirai S, Hayashi S, Inazawa J, Okamoto N, Barkovich AJ (2010) Neuroradiologic Features of CASK Mutations. AJNR Am J Neuroradiol 31:1619–1622
ten Donkelaar HJ, Wesseling P, Semmekrot BA, Liem KD, Tuerlings J, Cruysberg JR, de Wit PE (1999) Severe, non X-linked congenital microcephaly with absence of the pyramidal tracts in two siblings. Acta Neuropathol 98: 203–211
ten Donkelaar HJ, Lammens M, Wesseling P, Thijssen HO, Renier WO (2003) Development and developmental disorders of the human cerebellum. J Neurol 250: 1025–1036
ten Donkelaar HJ, Lammens M, Wesseling P, Hori A, Keyser A, Rotteveel J (2004) Development and malformations of the human pyramidal tract. J Neurol 251:1429–1442
Tilea B, Delezoide AL, Khung-Savatovski S, Guimiot F, Vuillard E, Oury JF, Garel C (2007) Comparison between magnetic resonance imaging and fetopathology in the evaluation of fetal posterior fossa non-cystic abnormalities. Ultrasound Obstet Gynecol 29:651–659
Tilea B, Alberti C, Adamsbaum C, Armoogum P, Oury JFCD, Sebag G, Kalifa G, Garel C (2009) Cerebral biometry in fetal magnetic resonance imaging: new reference data. Ultrasound Obstet Gynecol 33:173–181
Tortori-Donati P (2005) Pediatric neuroradiology. Springer, Berlin/Heidelberg/New York
Utsunomiya H, Takano K, Ogasawara T, Hashimoto T, Fukushima T, Okazaki M (1998) Rhombencephalosynapsis: cerebellar embryogenesis. AJNR Am J Neuroradiol 19: 547–549
Utsunomiya H, Yamashita S, Takano K, Okazaki M (2006a) Arrangement of fiber tracts forming Probst bundle in complete callosal agenesis: report of two cases with an evaluation by diffusion tensor tractography. Acta Radiol 47: 1063–1066
Utsunomiya H, Yamashita S, Takano K, Ueda Y, Fujii A (2006b) Midline cystic malformations of the brain: imaging diagnosis and classification based on embryologic analysis. Radiat Med 24:471–481
van de Kamp JM, Lefeber DJ, Ruijter GJ, Steggerda SJ, den Hollander NS, Willems SM, Matthijs G, Poorthuis BJ, Wevers RA (2007) Congenital disorder of glycosylation type Ia presenting with hydrops fetalis. J Med Genet 44:277–280
Vilain C, Mortier G, Van Vliet G, Dubourg C, Heinrichs C, de Silva D, Verloes A, Baumann C (2009) Hartsfield holoprosencephaly-ectrodactyly syndrome in five male patients: further delineation and review. Am J Med Genet A 149A:1476–1481

Volpe P, Campobasso G, De Robertis V, Rembouskos G (2009) Disorders of prosencephalic development. Prenat Diagn 29:340–354

Wagner C, Batiz LF, Rodríguez S, Jiménez AJ, Páez P, Tomé M, Pérez-Fígares JM, Rodríguez EM (2003) Cellular mechanisms involved in the stenosis and obliteration of the cerebral aqueduct of hyh mutant mice developing congenital hydrocephalus. J Neuropathol Exp Neurol 62:1019–1040

Wahl M, Strominger Z, Jeremy RJ, Barkovich AJ, Wakahiro M, Sherr EH, Mukherjee P (2009) Variability of homotopic and heterotopic callosal connectivity in partial agenesis of the corpus callosum: a 3T diffusion tensor imaging and Q-ball tractography study. AJNR Am J Neuroradiol 30: 282–289

Widjaja E, Blaser S, Miller E, Kassner A, Shannon P, Chuang SH, Snead OC 3rd, Raybaud CR (2007) Evaluation of subcortical white matter and deep white matter tractsin malformations of cortical development. Epilepsia 48:1460–1469

Widjaja E, Geibprasert S, Blaser S, Rayner T, Shannon P (2009) Abnormal fetal cerebral laminar organization in cobblestone complex as seen on post-mortem MRI and DTI. Pediatr Radiol 39:860–864

Widjaja E, Geibprasert S, Mahmoodabadi SZ, Blaser S, Brown NE, Shannon P (2010a) Alteration of human fetal subplate layer and intermediate zone during normal development on MR and diffusion tensor imaging. AJNR Am J Neuroradiol 31: 1091–1099

Widjaja E, Geibprasert S, Mahmoodabadi SZ, Brown NE, P S (2010b) Corroboration of Normal and Abnormal Fetal Cerebral Lamination on Postmortem MR Imaging with Postmortem Examination. Am J Neuroradiol [Epub ahead of print]

Winter TC, Kennedy AM, Byrne J, Woodward PJ (2010) The cavum septi pellucidi: why is it important? J Ultrasound Med 29:427–444

Zalel Y, Yagel S, Achiron R, Kivilevich Z, Gindes L (2009) Three-dimensional ultrasonography of the fetal vermis at 18 to 26 weeks' gestation: time of appearance of the primary fissure. J Ultrasound Med 28:1–8

Acquired Brain Pathology

Daniela Prayer, Ulrika Asenbaum, Peter C. Brugger, and Gregor Kasprian

Contents

Abstract

› Acute brain injury is rarely seen, but salient features include acute hemorrhage, thrombosis, and localized or general edema. Findings are rarely specific with regard to etiology. In addition to maternal disease, risk factors for acquired brain lesions include disorders of the placenta and/or umbilical cord, exposure to toxic agents, metabolic disease, iatrogenic hazards, fetal cardiovascular disease, and space-occupying lesions. Most often, defective stages are found, characterized by local or diffuse tissue loss, and/or hemorrhagic residuals, and/or calcification. In order to describe an acquired lesion most accurately, in addition to T2-weighted sequences, T1-weighted, diffusion-weighted, and echoplanar (or T2*) information is necessary. In case of suspected infection, the whole fetus and the extrafetal structures must be screened for pathological changes.

D. Prayer (✉)
Department of Diagnostic Radiology, University Hospital Vienna, Waehringer Guertel 18-20, 1090 Vienna, Austria
e-mail: daniela.prayer@meduniwien.ac.at

U. Asenbaum
Department of Diagnostic Radiology,
University Hospital Vienna, Waehringer Guertel 18-20
1090 Vienna, Austria
e-mail: ulrika.asenbaum@meduniwien.ac.at

P.C. Brugger
Center of Anatomy and Cell Biology, Medical University Vienna, Waehringerstrasse 13, 1090 Vienna, Austria
e-mail: peter.brugger@meduniwien.ac.at

G. Kasprian
Department of Diagnostic Radiology, University Hospital Vienna, Waehringer Guertel 18-20,
1090 Vienna, Austria
e-mail: gregor.kasprian@meduniwien.ac.at

D. Prayer (ed.), *Fetal MRI*, Medical Radiology,
DOI: 10.1007/174_2010_118, © Springer-Verlag Berlin Heidelberg 2011

1 Introduction

Acquired fetal brain lesions are a consequence of damage to a previously normally formed structure. These lesions must be differentiated from malformations (where a structure is not normally formed), and from disruption, where maldevelopment occurs because of early damage (Reardon and Donnai 2007). The true incidence of acquired fetal brain injury is unknown; in a neuropathological series of intrauterine or neonatal deaths, 20.4% showed evidence of prenatal ischemic brain damage (Gaffney et al. 1994). However, the incidence of intravitam observations may be higher: unspecific ventriculomegaly may be the result of periventricular leukomalacia (PVL) that occurred earlier (van Gelder-Hasker et al. 2003). Fetal MRI may help to recognize acquired brain injury by visualizing different blood breakdown products, recent or residual stages of ischemia, and/or thrombosis of the venous sinus (Prayer et al. 2006a).

2 Risk Factors

Risk factors for acquired fetal brain injury include:

2.1 Maternal Disease

Maternal disease, such as coagulation disorders, and others (see Chapter 28).

2.2 Acute Maternal Impairment

Acute maternal impairment, as, for instance, cardiovascular collapse, anaphylactic reaction, and preeclampsia (see Chapter 28).

2.3 Disorders of the Placenta and/or Umbilical Cord

Disorders of the placenta and/or umbilical cord. Placental insufficiency leads to compensatory mechanisms, in which some organs are better supplied at the expense of others. The brain experiences an increased flow in such situations, called the "brain sparing" effect. However, it has been shown that the brain might still experience chronic hypoxic-ischemic injury (Roza et al. 2008). Placental abruption (leading to an acute interruption of materno-fetal perfusion) and chorioamniotic hemosiderosis, reflecting a chronic deficiency of maternally caused insufficient fetal blood supply, have been identified as reasons for postnatal cerebral palsy in mature newborns (Redline and O'Riordan 2000). Other underlying factors are chronic villitis and perivillous fibrin deposition that increase the diffusion distance between the maternal and fetal circulation (Redline and O'Riordan 2000). Large fetal vessels may be affected by meconium-associated vascular necrosis and fetal chorioamnionitis via cytokine-mediated damage of the vessel wall. Such findings have been associated with white matter damage in newborns (Nelson 2008). Chorionic vessel thrombosis, usually associated with a great number of avascular villi, may lead to upstream vascular occlusion. In addition, such conditions may predispose to vasospasm (Nelson 2008). Avascular villi may be due to inherited thrombophilia, chronic villitis, and/or chronic stasis, as a consequence of fetal positioning and umbilical cord compression. Elongation of the umbilical cord is associated with fetal thrombotic vasculopathy (FTV), especially when the cord is longer than 70 cm (excessively long umbilical cord) (Taweevisit and Thorner 2010). FTV is a chronic vasoocclusive disorder of the placenta, with focal or widespread villous involvement. Thromboembolic events in any fetal organ may be the consequence. Brain involvement will cause cerebral palsy postnatally (Redline and O'Riordan 2000).

2.4 Exposition to Toxic Agents

Exposition to toxic agents, such as alcohol, cocaine, cannabis, CO, warfarin (Girard et al. 2003; Prayer et al. 2006). Alcohol intake by the pregnant woman may cause a variety of craniofacial abnormalities, summarized under the term fetal alcohol syndrome (FAS). Brain involvement comprises malformative changes, as well as loss of substance, appearing in the most severe form as hydranencephaly. In addition, changes in the ventricular size and/or shape, abnormalities in the basal ganglia, the diencephalon, the cerebellum, the brainstem, the optic

nerve, the olfactory bulb, the hippocampus, the pituitary, and pathological cortical organization have been reported (Reinhardt et al. 2010). From postnatal diffusion-tensor (DTI) studies, there is evidence that FAS includes damage to the white matter, in particular, compromising the white matter integrity in cortical areas associated with visual processing (Fryer et al. 2009). The prenatal effect of cocaine on the developing brain has been identified as twofold: mechanisms that regulate neuronal growth are altered; and vasoconstrictive effects are thought to act indirectly on the brain via an impact on placental vessels (Derauf et al. 2009). Postnatally, volume reductions of certain gray matter structures, especially the basal ganglia, and the corpus callosum, were seen in children whose mothers consumed cocaine during pregnancy (Derauf et al. 2009). Endocannabinoids have a functional role in early brain development (Downer and Campbell 2010). Exencephaly, spina bifida, and body edema have been reported to be caused by cannabinoid intake during pregnancy (Downer and Campbell 2010). As cannabinoid is frequently taken in combination with other drugs, it is not possible to differentiate which of these drugs may be responsible for developmental changes, such as, for instance, a reduction of the white matter (Derauf et al. 2009; Downer and Campbell 2010). Carbon monoxide expossure has been described to have caused hemorrhagic infarctions (Abboud et al. 2001). Intracranial hemorrhage might also be the result of Warfarin therapy (Ville et al. 1993). In cases of cerebral hemorrhage in the second trimester, a schizencephalic cleft may develop (Pati and Helmbrecht 1994).

2.5 Metabolic Disease

Metabolic disease. Most inborn errors of metabolism do not lead to any pathological changes in the fetal brain, as the respective metabolic defect is compensated for by maternal enzymes. However, some of these diseases may lead to prenatal morphological changes that can be recognized on MRI (Prasad et al. 2009).

2.6 Iatrogenic Hazards

Iatrogenic hazards during amniocentesis and placental puncture.

2.7 Feto-Fetal Transfusion Syndrome

Feto-fetal transfusion syndrome. In cases of feto-fetal transfusion syndrome, both fetuses, or the surviving twin, may suffer brain damage (Fichera et al. 2009). Twinning has been recognized for a many years as a 5–10-fold increased risk for cerebral palsy of predominantly prepartal origin (Pharoah and Dundar 2009). It was thought that, in monochorionic twins, the death of one might cause the migration of emboli into the surviving twin via placental anastomoses (Pharoah and Dundar 2009). However, as such emboli could not be proved, other mechanisms, such as changing blood pressure gradients, for instance, are more likely to occur. In cases of feto-fetal transfusion syndrome, perturbations in inter-fetal blood flow dynamics associated with placental vascular anastomoses have been identified as possible reasons for cerebral pathology (Pharoah and Dundar 2009).

2.8 Fetal Coagulation Disorders

Fetal coagulation disorders, such as, for instance, alloimmune thrombocytopenia, may predispose to hemorrhage (Carletti et al. 2009).

2.9 Disorders of the Fetal Circulation

Disorders of the fetal circulation comprise changes in placental vascular resistance, the peripheral fetal vascular bed, vessel compliance, and blood viscosity (Limperopoulos 2009). Consequently, neurovascular malformations can also lead to an impairment of the oxygen supply of the developing white matter (Ozanne et al. 2007).

2.10 Cardiac Malformations

Cardiac malformations restrict the amount of oxygenated blood arriving at the brain (Mlczoch et al. 2010). Microcephaly, frequently seen in newborns with congenital heart disease, may be interpreted as the

sequelae of chronic undersupply (McQuillen and Miller 2010). Stroke was seen in one series of studies, with transposition of the great vessels and white matter injury in newborns with a hypoplastic left ventricle or a single ventricle (McQuillen and Miller 2010). In fetuses with Fallot's tetralogy, microcephaly was interpreted as a consequence of deoxygenated blood, arriving at the brain (Barbu et al. 2009). Those fetuses with an absence of antegrade blood flow through the aorta, in particular, were found to have smaller brain volumes than normal fetuses (Limperopoulos et al. 2010).

2.11 Space-Occupying Lesions

Space-occupying lesions, including mainly cysts that compress adjacent tissue, and, in rare cases, also brain tumors (Prayer et al. 2006).

2.12 Infection

See Sect. 5.

3 MR Sequences to Visualize Acquired Brain Pathology

While T2-weighted fast spin-echo sequences suffice in most brain malformations to gain enough information, this is not true in case of screening for an acquired injury (Brugger et al. 2006; Prayer et al. 2006). In particular, the full extent of an intracranial hemorrhage may not be depicted by T2-weighted sequences. Moreover, in cases of ventriculomegaly, blood breakdown products of a frequently underlying intraventricular hemorrhage are rarely detected by ultrasound or conventional fetal MR sequences. Thus, EPI or gradient echo sequences, and T1-weighted sequence information is needed. Also calcification, a hallmark of several infections, can be detected most sensitively by using T1-weighted sequences. In addition, it has been shown that laminar necrosis and PVL lesions may present with T1-weighted hyperintense signals (Garel et al. 2004). Diffusion-weighted sequences allow the identification of recent ischemic changes (Righini et al. 2007), and may depict gliosis in chronic alterations (Guimiot et al. 2008). In addition, diffusion-tensor-based tractography (Kasprian et al. 2008) helps to identify preserved or destroyed brain connectivity in cases of destructive lesions.

4 Morphological Manifestations of Acquired Fetal Brain Injury

Generally, the morphological appearance of an acquired lesion depends on the time of occurrence of an insult with respect to the gestational age, and on the time interval between the examination and the occurrence of the event.

4.1 Acute Manifestations

4.1.1 Intracranial Hemorrhage

Intracranial hemorrhage may manifest itself as subdural, intracerebral, and/or intraventricular bleeding. Intrauterine subdural hematomas have been observed in case of maternal coagulation disorder/anticoagulation medication (Bauder et al. 2009), and after trauma (Piastra et al. 2009). In intraventricular hemorrhages, blood-fluid levels may be detected. T2* and echoplanar sequences are most sensitive for detecting deoxyhemoglobin. T1-weighted images are necessary to visualize the methemoglobin content of a hemorrhage, and T1-weighted FLAIR sequences may show similar signals (Kang et al. 2001) (Fig. 1). Postnatal experience is not akin to the prenatal situation in terms of the temporal time course of signal changes of blood breakdown products (Zuerrer et al. 1991). Underlying reasons include the different composition of the fetal hemoglobin molecule, which has a different binding of oxygen than adult hemoglobin. T2-weighted hypointensity, ascribed to the presence of intracellular deoxyhemoglobin, persists for longer periods in vitro than that known from hemorrhages in adults (Prayer et al. 1999). Furthermore, blood breakdown products are actively removed by a specific transport mechanism (Johansson et al. 2008). Consequently, hemorrhages may no longer be proven after several weeks.

Brain regions with high vascular density, such as the ganglionic eminences of the ventricular zones, are the

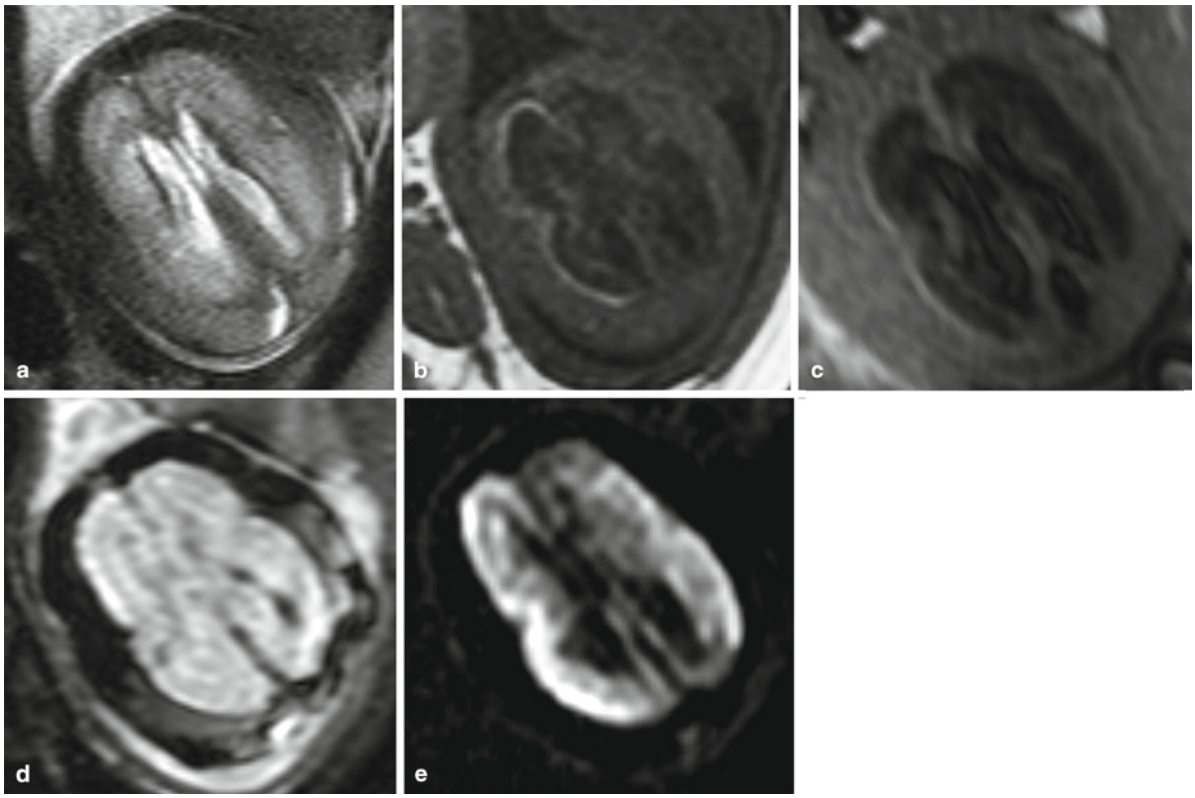

Fig. 1 GW 24 axial T2 (**a**), T1 (**b**), T1-FLAIR (**c**), EP (**d**), and DW (**e**) images. Subdural and intraventricular hemorrhages. Additional signs of ischemic transformation of the cortical plate as well as diffuse edema of the parenchyma

main site of bleeding. Grade I hemorrhages may be difficult to identify: as the cellular density of the ganglionic eminence leads to a low signal on T2-weighted images, further signal loss, as a consequence of a hemorrhage and deoxyhemoglobin formation, may be missed. However, size differences may give a clue to the unilateral presence of hemorrhage within the germinal matrix. Intraventricular bleeding may not only be the consequence of a hemorrhage grade II–IV, but may also originate from the choroid plexus. In contrast to postnatal findings, a higher grade hemorrhage is not necessarily associated with an adverse outcome (Asenbaum et al. 2009). As a possible complication of supratentorial ventricular hemorrhage, blood clots may obstruct the aqueduct and cause severe hydrocephalus. Blood that reaches the posterior fossa may lead to a consecutive disruptive cerebellar development (Messerschmidt et al. 2005). This is especially true in the vulnerable phase between GW 26–30 (Messerschmidt et al. 2005). With regard to the overall prognosis, associated findings (such as edema, extracerebral lesions, and/or placental pathology) must be considered, as well. Generally, typical sites of hemorrhages include the following structures: the ganglionic eminences, the ventricular zone, the ependyma, the choroid plexus, and the cortical plate. These locations are frequently involved in hemorrhage primarily associated with hypoxic-ischemic events (frequently seen in cases of feto-fetal transfusion syndrome), infections, or disorders of coagulation. In cases of "atypical" sites of prenatal hemorrhages, an underlying lesion or traumatic event should be suspected. In rare cases, a hemorrhage may be a sign of an underlying brain tumor.

4.1.2 Local Edema

Local edema, visible on DWI sequences only (Baldoli et al. 2002), may occur as a sign of acute infarction (Fig. 2). However, this is a very rare prenatal finding. More often, residuals of such infarctions are seen in the form of cystic lesions or enlargement of one or both lateral ventricles, which may show an irregular delineation of the borders.

4.1.3 Global Brain Edema

The first sign of global brain edema in fetuses up until GW 28/30 may be a loss of normal lamination in the brain parenchyma on T2-weighted and/or diffusion-weighted sequences (Fig. 3). Frequently, edematous changes are combined with various degrees of hemorrhage.

4.1.4 Venous Thrombosis

Venous thrombosis may occur in isolation or in combination with metabolic disease, intoxication, infection, trauma, or malformations that are associated with pathological venous drainage, such as venous malformations or lymph(hem)angiomas (Fig. 4). Isolated venous

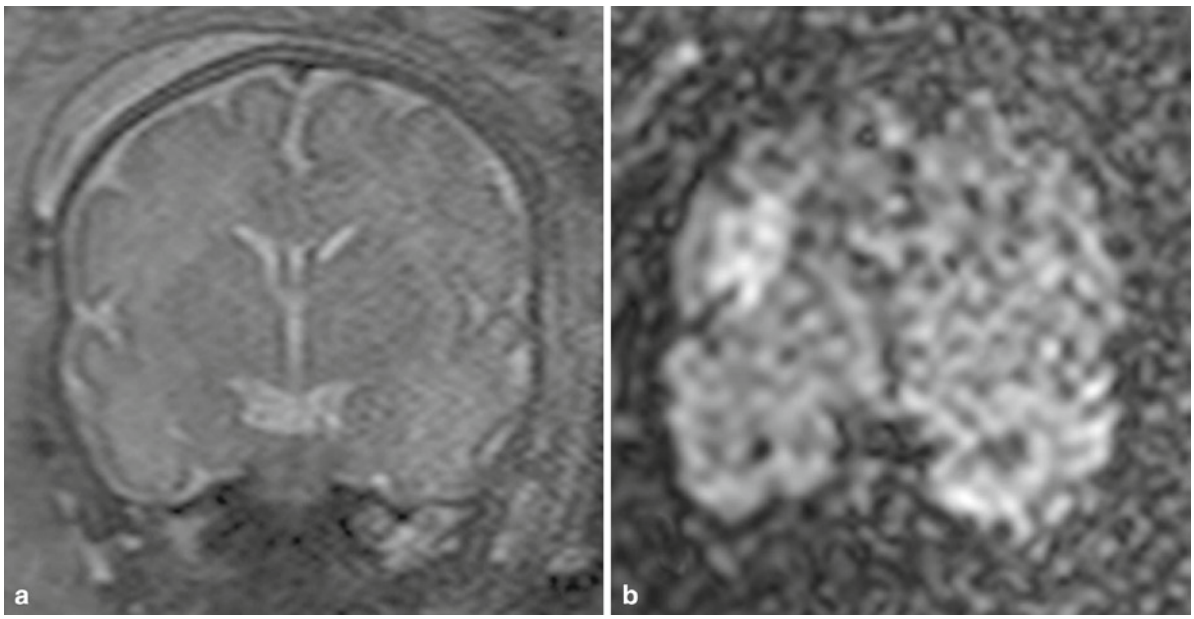

Fig. 2 GW 33+4: Fetus with pathological Doppler values of medial cerebral artery. (**a**) Coronal T2-weighted image without detectable abnormalities. (**b**) The corresponding DWI image showing a hyperintense lesion in the frontal white matter with preserved cortex

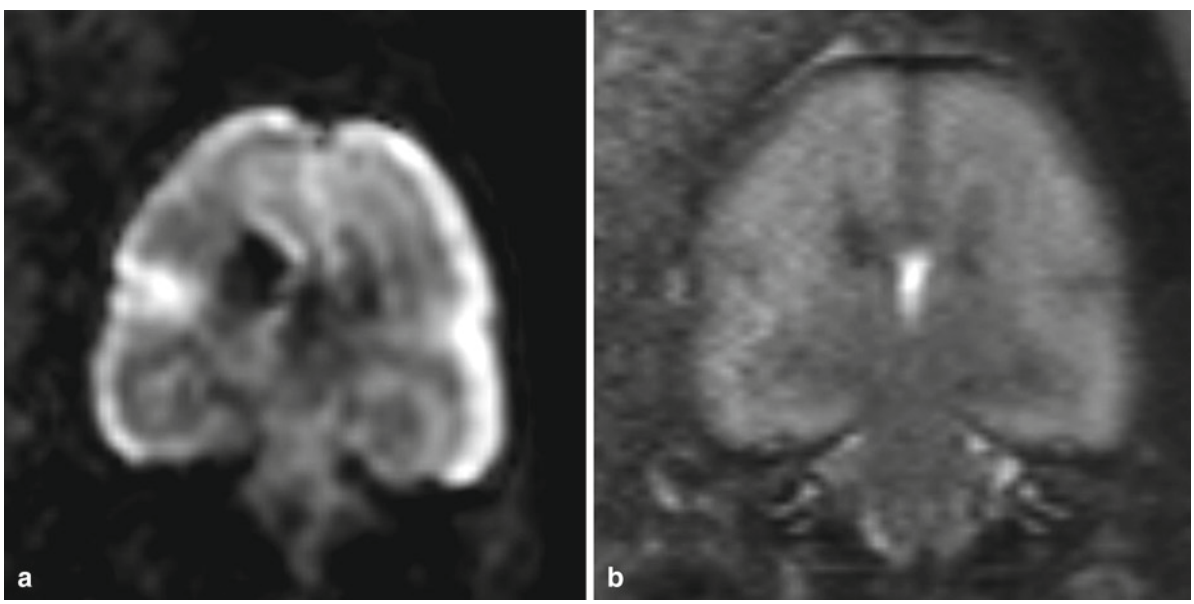

Fig. 3 GW 25: Coronal T2-weighted sequence (**a**) showing massive brain edema and consecutive missing lamination and consummation of inner and outer CSF spaces. Restricted diffusion of the cortical plate on diffusion-weighted sequences (**b**)

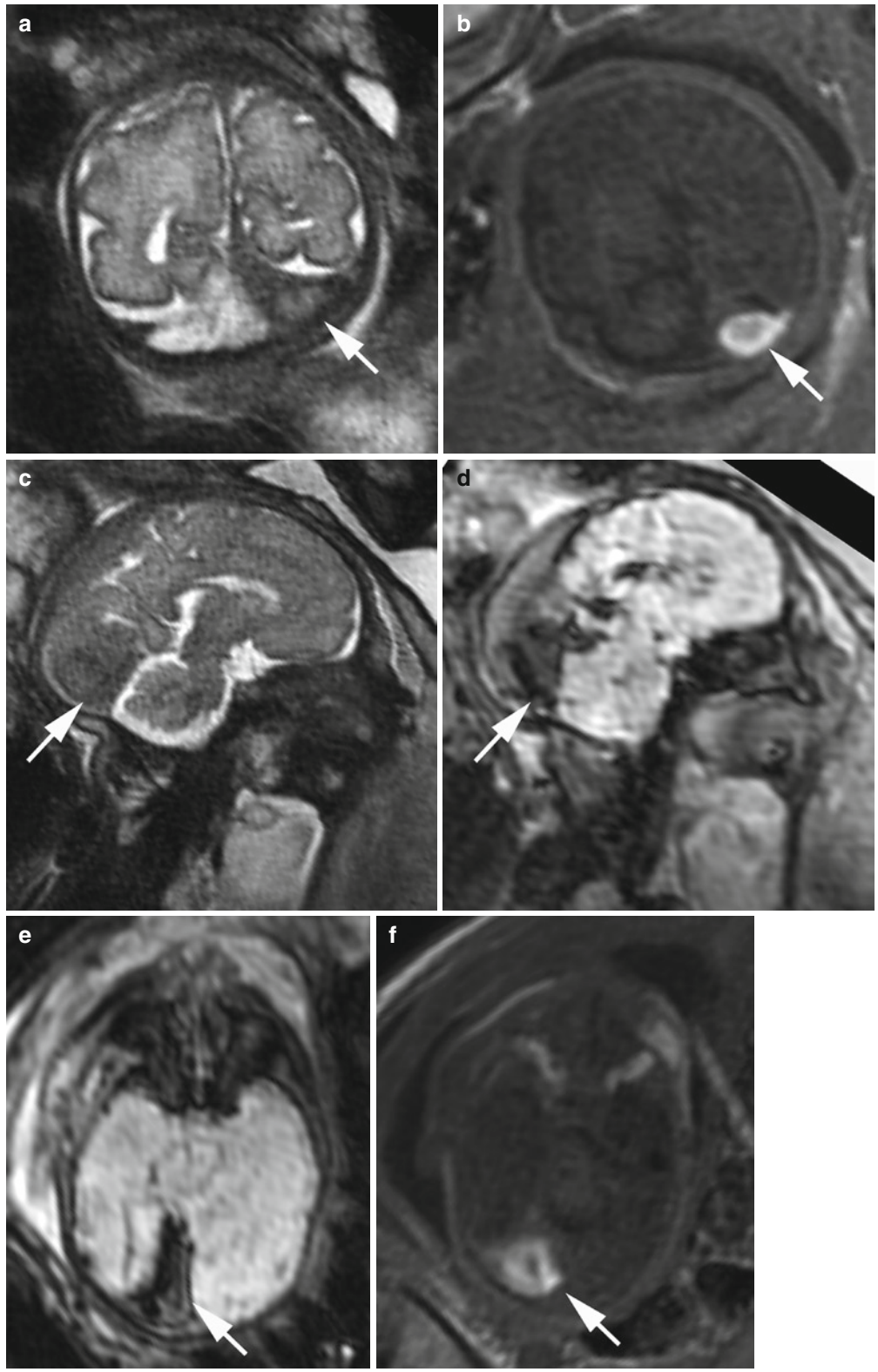

Fig. 4 GW 29+3, coronal T2 (**a**), T1 (**b**) weighted, sagittal T2 (**c**), EPI (**d**) weighted, axial EPI (**e**), and T1-FLAIR (**f**) weighted sequences. A fetus with a large lymphangioma of the neck shows a T1-weighted hyperintense and T2- and EPI weighted hypointense signal alteration of the left transverse sinus (*arrows*), representing sinus vein thrombosis without associated parenchymal damage

thrombosis is usually not associated with a poor outcome (Laurichesse Delmas et al. 2008). Dural malformations with arteriovenous shunts may lead to congestive cardiac failure (Laurichesse Delmas et al. 2008). On fetal MRI, thrombi display signals comparable to those seen postnatally on the respective sequences. It has been suggested that fetal MRI should be performed in cases of suspected dural sinus thrombosis on ultrasound and normal brain. In cases where no cerebral lesions are apparent on MRI either, the prognosis is usually favorable (Laurichesse Delmas et al. 2008).

4.2 Defective States

4.2.1 Loss of Substance

Loss of substance will occur if a structure is destroyed, resulting in symmetric or asymmetric enlargement of the inner and/or outer cerebrospinal fluid (CSF) spaces. Ventricles may display irregular borders and/or may be distorted. Parenchymal defects can be seen in various locations and sizes, ranging from small defects to destruction of both hemispheres, as in hydranencephaly. Periventricular leukomalacia (PVL) is associated with prematurity and/or a birth weight of fewer than 1,500 g. While almost 90% of these children survive the neonatal period, 10% of this group will develop motor deficits, and up to 25% will develop cognitive and/or behavioral deficits (Volpe 2001). Two forms of PVL have been described: a circumscript type, consisting of lesions that can be delineated on imaging studies, and a diffuse white matter injury that results from damage to the oligodendrocyte precursors (Volpe 2001). The sensitive age for PVL lies between gestational weeks 26 and 32. However, intrauterinely, PVL has only been reported rarely (Garel et al. 2004), and mainly in pregnancies characterized by the feto-fetal transfusion syndrome (Righini et al. 2004). In this setting, surviving twins have been found to be at the most risk to acquire PVL (Simonazzi et al. 2006). Diffuse changes and/or gliosis may be difficult to recognize (Garel et al. 2004; Guimiot et al. 2008) (Fig. 5). On ultrasound, the evolution of cysts occurs about 2 weeks after the first detection of increased periventricular echodensities (van Gelder-Hasker et al. 2003). On MRI, the evolution to cysts takes 3 weeks (Barkovich 2005).

In cases of congenital cystic PVL, a prenatal manifestation must be postulated. As a result, this condition is probably unrecognized in an uncertain number of cases, which may be due to the fact that diffusion-weighted sequences are not used routinely at all institutions.

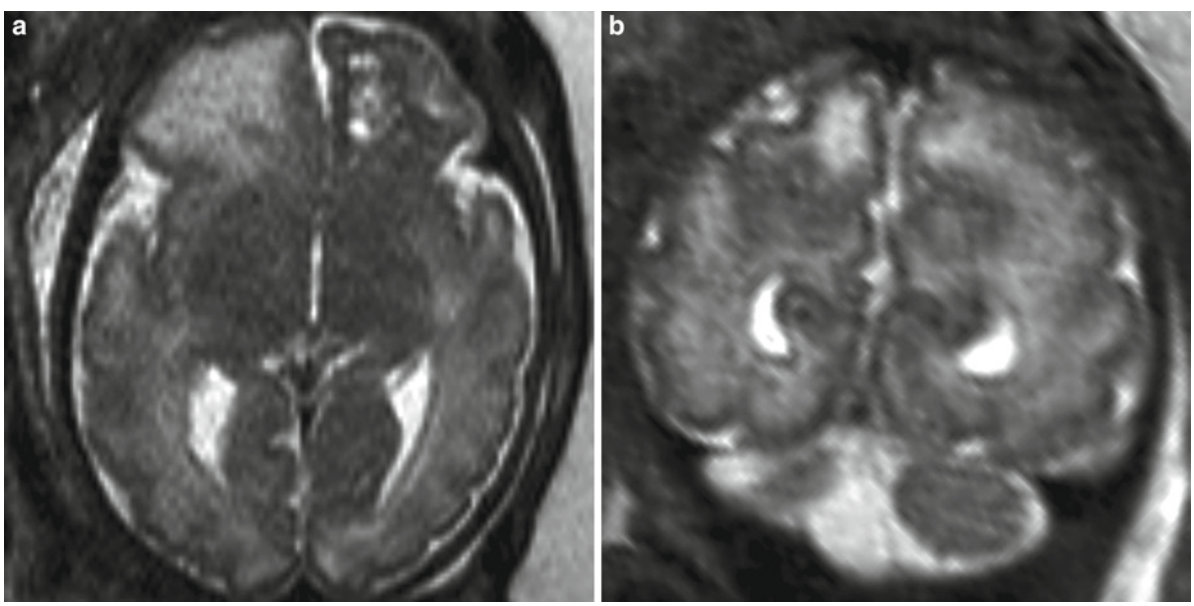

Fig. 5 GW 26+4, axial (**a**) and coronal (**b**) T2-weighted sequences: Hyperintense parasagittal infarctions corresponding to late PVL and hemorrhagic transformation of the left frontal lesion

The shape, location, and delineation of a defect may indicate the underlying etiology: Classic porencephaly is thought to be the sequelae of an arterial infarction of the anterior or medial cerebral artery. Hydranencephaly is the consequence of bilateral internal cerebral artery occlusion: this condition may be difficult to differentiate from hydrocephalus, lissencephaly type II (in the second trimester), and holoprosencephaly. However, hemorrhagic residuals, separated thalami, the presence of the falx, and remaining brain tissue in regions that are not supplied by the medial cerebral artery may help with the differential diagnosis. Unilateral striatal or thalamic cavities can be seen after the occlusion of perforating branches (Govaert 2009). Venous infarctions may be seen together with germinal matrix hemorrhages. Hemosiderin residuals in such cavities are seen inconsistently.

However, periventricular or subependymal cysts may have a variable underlying background. In addition, the nomenclature of such changes is incongruent. In newborns, frontal horn cysts, described as thin-walled cysts located at the superolateral angle of the frontal horn of the lateral ventricles, have been described as transient manifestations and are usually associated with a good outcome (Unger et al. 2010) (Fig. 6). As they are histologically not lined by ependyma, they are called pseudocysts (van Baalen and Versmold 2007). Differential diagnostic considerations are based on the exact location of these pseudocysts (Malinger et al. 2002). When located in the caudothalamic groove, or the germinal matrix (Chang et al. 2006), they may represent posthemorrhagic residuals. When these cysts are an isolated finding (regardless of whether they are unilateral or, more frequently, bilateral), the prognosis is usually good (Makhoul et al. 2001). However, they are seen in a number of malformative as well as acquired pathologies, such as, for instance, Zellweger syndrome (Mochel et al. 2006), Wolf–Hirschhorn syndrome (Verbrugge et al. 2009), congenital Rubella syndrome (Beltinger and Saule 1988), and CMV (Guibaud et al. 2004). In addition, they may be found in fetuses with cardiac anomalies (Mlczoch et al. 2010). A differential diagnosis of PVL is based on location (while frontal horn cysts are located at the external angle below the level of the lateral ventricles, periventricular leukomalacia cysts extend above this level) (de Vries et al. 2004). In utero tractography may delineate potentially involved adjacent tracts, and may help to further differentiate the origin of the cysts (ganglionic eminence, medially vs. parenchyma, laterally). Tractography may also provide information about the involvement of functionally important pathways, such as the corticospinal tract (Fig. 7).

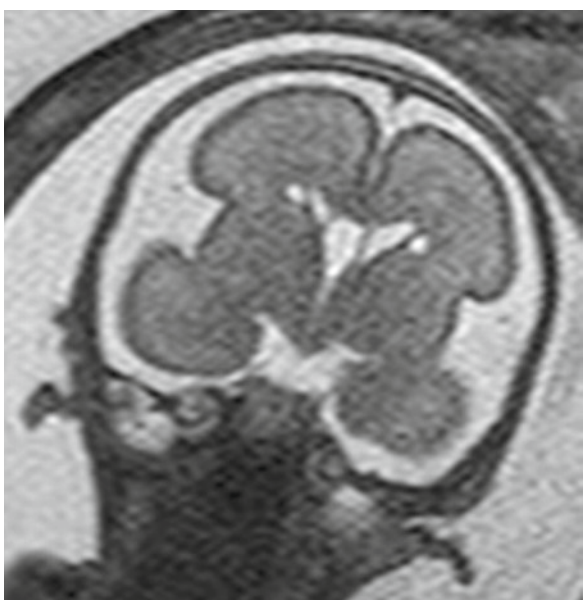

Fig. 6 GW 26+4. Coronal T2-weighted image demonstrates bilateral cystic lesions on adjacent to the frontal horns

Widening of the outer CSF spaces has been seen, for instance, in fetuses with cardiac problems (Mlczoch et al. 2010). Identification of this condition may require a comparison with normal values.

4.2.2 Pathological Signals

Pathological signals within the brain parenchyma may correspond to blood-breakdown products, calcification, CSF (in case of a defect or a cyst), or gliosis. The latter is difficult to diagnose in vivo, as T2-weighted FLAIR sequences are not practical. However, the use of diffusion-weighted imaging methods seems to be promising for the detection of gliosis in vivo (Guimiot et al. 2008). With regard to calcification, MRI is inferior to ultrasound. Calcification may show signals similar to blood breakdown products on the respective sequences.

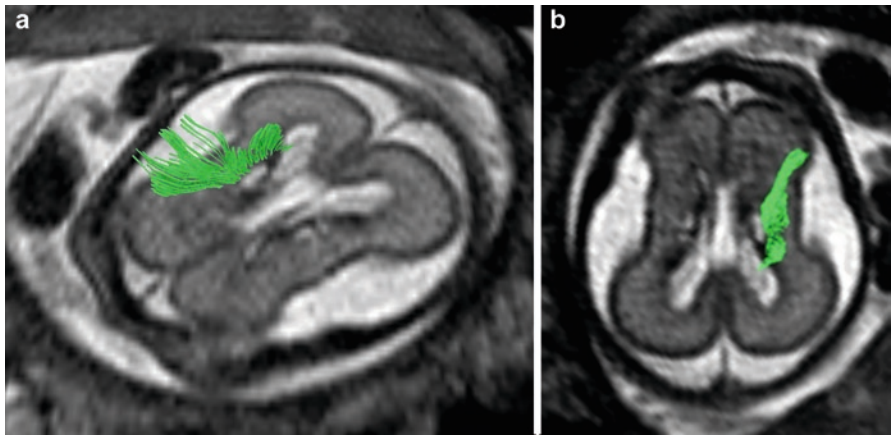

Fig. 7 GW 24+4. Diffusion-tensor-imaging-based tractography and coregistered axial T2-weighted images (**a**, **b**) showing the preserved cortical spinal tracts (*green*) lateral to the cystic lesions

4.2.3 Irregular Gyration

Irregular gyration, especially polymicrogyria, with or without schizenzephalic clefts, has been interpreted as the sequelae of previous vascular or infectious events that interfere with cortical formation (Leventer et al. 2010). Consequently, these changes might not be detectable until the third trimester. Loss of lamination refers to a pathological presentation of the laminar zones that are detectable within the fetal brain up to GWs 28/30 (Prayer et al. 2006b). Laminar necrosis, seen as a T1- weighted hyperintensity, has been interpreted as a change in the protein content of the respective lamina (Garel et al. 2004). Germinolysis leads to a failure to confirm the presence of the ganglionic eminences or to lesions in these regions (Prayer et al. 2006). While the cytomegalovirus is known to involve the vessels of the ganglionic eminence, and consequently, interferes with cell formation, other events may also lead to premature germinolysis, the pathological significance of which is not yet fully understood (Prayer et al. 2006).

4.2.4 Space-Occupying Lesions

Most space-occupying lesions are cysts that are usually of malformative origin. In some cases, they may obliterate CSF spaces, leading to CSF circulation problems, or causing tissue damage because of mechanical pressure. Brain tumors are only rarely seen. Congenital brain tumors account for 0.5–1.9% of all pediatric tumors (Isaacs 2009). Teratomas, followed by astrocytomas and craniopharyngeomas, occur most frequently. Usually, these types of tumors show rapid growth, leading to macrocephaly, and have a poor prognosis (Vazquez et al. 2009). Prenatally, they present as intracranial masses that may impair CSF circulation, they may have hemorrhagic parts, and they may lead to hydrops and/or intrauterine death. Usually, brain tumors are not diagnosed before the third trimester. Using MRI, different signal intensities on the various sequences will give a clue to solid/cystic/necrotic, and/or hemorrhagic parts of the lesions (Fig. 8). In addition, it is possible to differentiate solid tumors from low-flow vascular structures.

However, without contrast-media information and equivocal results of spectroscopy (as a high choline peak is physiological prenatally), differential diagnostic decisions may be difficult.

Teratomas, which are composed of tissue elements derived from the germinal layers of the embryo, can be found primarily in the location of the cerebral hemispheres, replacing normal brain tissue there. They can extend into the facial sinus. Furthermore, extracranial teratomas of the neck region may also grow into the skull. On MRI, teratomas show solid and cystic parts, hemorrhages, and calcifications.

Astrocytomas occur with different degrees of malignancy. They are more frequently found in supratentorial regions, but may also be located infratentorially. The morphological hallmark of rapidly growing glioblastomas is often a large hemorrhage.

Giant cell astrocytomas in the context of Bourneville–Pringle syndrome, may be detected as T1-weighted hyperintense, and T2- weighted hypointense nodules in the ventricular wall at the caudothalamic groove. Postnatally, they may occlude the intraventricular foramen, sometimes leading to unilateral ventriculomegaly.

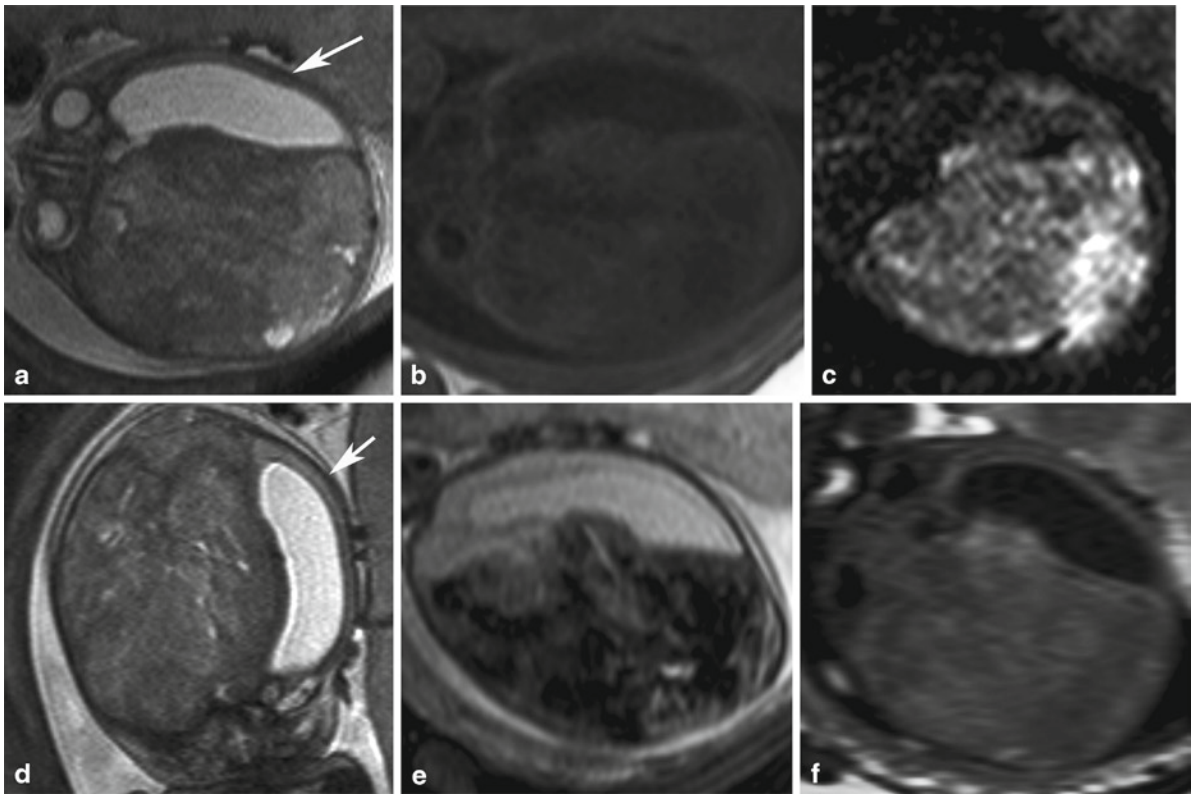

Fig. 8 GW 27, axial T2 (**a**), T1 (**b**), DW (**c**), coronal T2 (**d**), EP (**e**), and axial T1-FLAIR (**f**) weighted images and coronal T2-weighted image. Space-occupying lesion on the right side with consecutive impairment of CSF circulation at the level of the left foramen Monroi and widened left ventricle leading to increased head size. Remains of the left parenchyma see (*arrows*)

In contrast to other fetal brain tumors, giant cell astrocytomas may remain stable prenatally (Fig. 9).

Craniopharyngiomas tend to calcify and are consequently reliably detected by ultrasound. As midline processes, they tend to occlude the third ventricle, leading to supratentorial hydrocephalus, and subsequent head enlargement (Isaacs 2009).

Primitive neuroectodermal tumors (PNET) are rarely seen. Prenatal MR descriptions are not yet available, and the morphology may overlap with that of glioblastoma.

Plexus papillomas originate more frequently from the glomus of the choroid plexus in the lateral ventricles than from the fourth ventricle. Hemorrhage and hydrocephalus are the most common consequences.

As a consequence of their origin from the ependymal lining of the ventricles, ependymomas cause early hydrocephalus. The prenatal MR appearance has not been described. At birth, in some cases, CSF seeding has been reported (Isaacs 2009).

Tumors derived from meningeal structures may lead to asymmetric enlargement of the fetal head.

4.2.5 Congenital hydrocephalus

Congenital hydrocephalus is seen in about 1/1,000 newborns (Nomura et al. 2009). However, this number includes only those that survive until birth, and does not differentiate between the origins. Prenatal hydrocephalus may have a malformative origin (as in x-linked hydrocephalus, Dandy–Walker complex malformations, and Chiari II malformations). Acquired conditions comprise posthemorrhagic hydrocephalus, and occlusion of the ventricles. Hydrocephalus that is understood as an enlargement of parts of the ventricular system, following an impairment of CSF circulation, must be differentiated from ventriculomegaly. The latter is due to a loss of tissue. The following MR features can be used for (differential) diagnosis: delineation of the aqueduct on thin (2–3 mm thick) T2-weighted or SSFP sequences. If this is not possible, the shape of the third ventricle might provide a clue about whether the aqueduct is open. In the case of stenosis or occlusion of the acqueduct, it will be widened. Assessment of the shape of the lamina quadrigemina, which is malformed in cases of X-linked

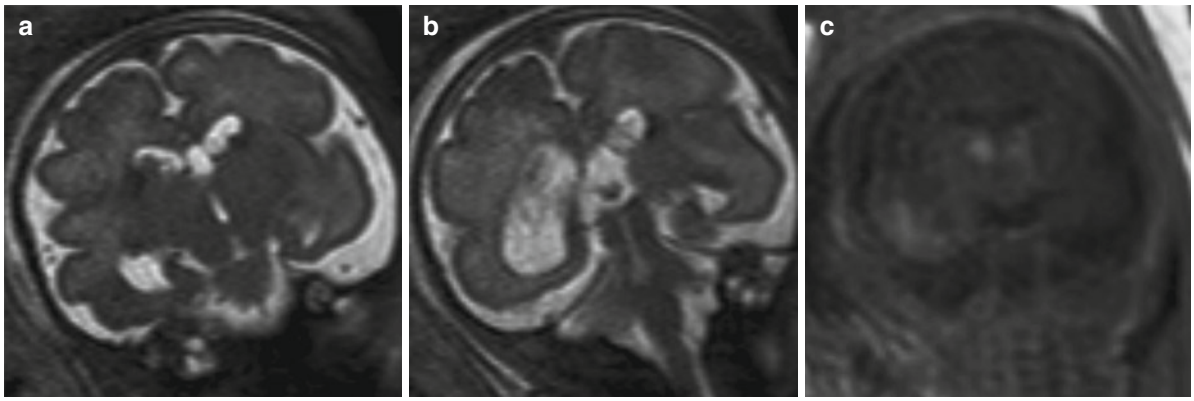

Fig. 9 GW 29, coronal T2-weighted images (**a**, **b**), and coronal T1- weighted image (**c**). Giant cell astrocytomas in location of the foramen Monroi

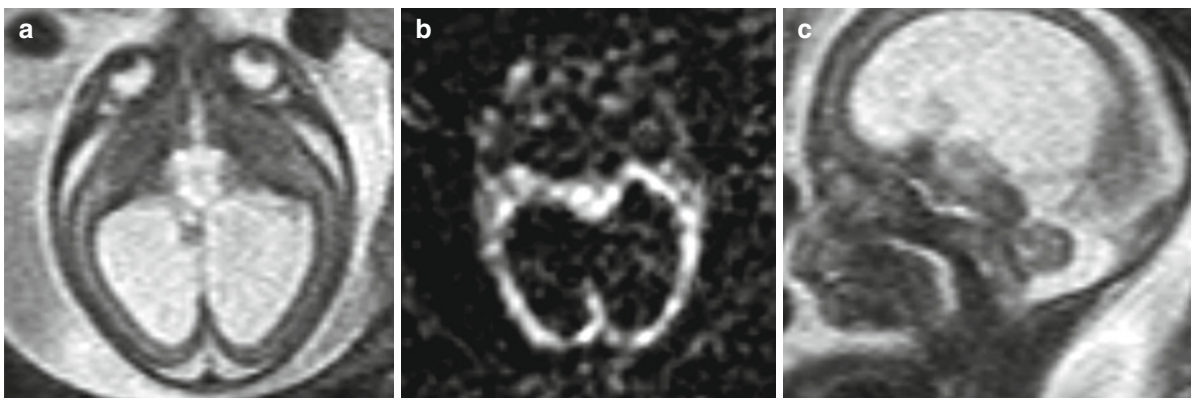

Fig. 10 GW 21, axial and sagittal T2-weighted (**a**, **c**) and DW (**b**) images. Occlusion of the acqueduct without detectable blood breakdown products and consecutive hydrocephalus. Mild consummation of the outer CSF spaces and thinning of the parenchyma with loss of lamination on DW sequences

aqueduct obliteration, may help to recognize or exclude this condition (Fig. 10). Blood breakdown products clinging to the ventricular wall will indicate a posthemorrhagic hydrocephalus. Intraventricular cysts originating from the choroid plexus may also lead to impairment of CSF circulation. These cysts may be difficult to delineate from subependymal (pseudo-)cysts, combined with CMV and Zellweger'syndrome. Differentiating ventriculomegaly from hydrocephalus may be difficult. Symmetrical ventriculomegaly may occur with agenesis of the corpus callosum ("colpocephaly"), where the ventricles will have a characteristic teardrop shape, with a Chiari II malformation, usually associated with pointed posterior horns of the lateral ventricles, and with holoprosencephaly, where separation of the lateral ventricules is at least partly absent. Unilateral ventriculomegaly is also not specific for acquired pathology, but may be seen in certain conditions, such as disorders of cortical development, that involve only one hemisphere, as, for instance, hemimegalencephaly. The prognosis of acquired hydrocephalus, defined as "secondary" hydrocephalus by Oi (2003), is largely unknown. However, it might be suspected that, as in primary or so-called dysgenetic hydrocephalus (Oi 2003), the following factors should be considered:

1. The onset of hydrocephalus (the earlier the onset, the more developmental steps will be impaired).
2. The extent of ventriculomegaly and thinning of the cortical mantle. In this case, ventriculomegaly up to 15 mm without progression is thought to be associated with a better prognosis. A thickness of the cortical mantle of less than 1.5 mm has been reported to be associated with an adverse outcome (Levitsky et al. 1995).

3. Our own observations have shown that a loss of lamination of the cerebral parenchyma on T2 weighted and/or diffusion-weighted sequences (in fetuses up to 28/30 GWs) indicates a poor outcome.
4. In acquired hydrocephalus, the underlying pathology is most important for prognosis: A one-time event, such as a hemorrhage, for instance, will have a better outcome than continued exposure to hypoxia, for example, or an infectious agent.

5 Infection

Depending on the time when MRI is performed, with respect to the onset of an infection, acute or chronic changes may be observed in the fetal brain (Barkovich and Girard 2003). Some patterns allow a conclusion about the underlying agent, but, in most cases, morphological presentation will be unspecific. With regard to polymicrogyria, for instance, the etiological background includes previous vascular events, as well as genetic disorders (Leventer et al. 2010). Even features that are regarded as highly characteristic for infections, such as calcifications and microcephaly, may have a genetic, and not infectious, background (Abdel-Salam et al. 2008). Prenatal infection may be acquired via ascending agents from the maternal vagina, hematogeneous spread via the placenta, retrograde from the abdominal cavity, or iatrogenic (at amniocentesis). An infection will lead to the so-called fetal inflammatory response syndrome (FIRS), a condition characterized by systemic activation of the fetal innate immune system (Gotsch et al. 2007). FIRS may lead to hematologic abnormalities, endocrine activation, cardiac dysfunction, pulmonary injury, renal dysfunction, and enzymatic digestion, and may also involve skin and brain. On MRI, pathological signals may be found, in such cases, in the placenta (consisting of edematous changes with or without thickening of the placenta), premature aging, infarctions, and hemorrhages (Pătraşcu et al. 2009) (Fig. 11). Various infections are associated with ocular involvement, as known

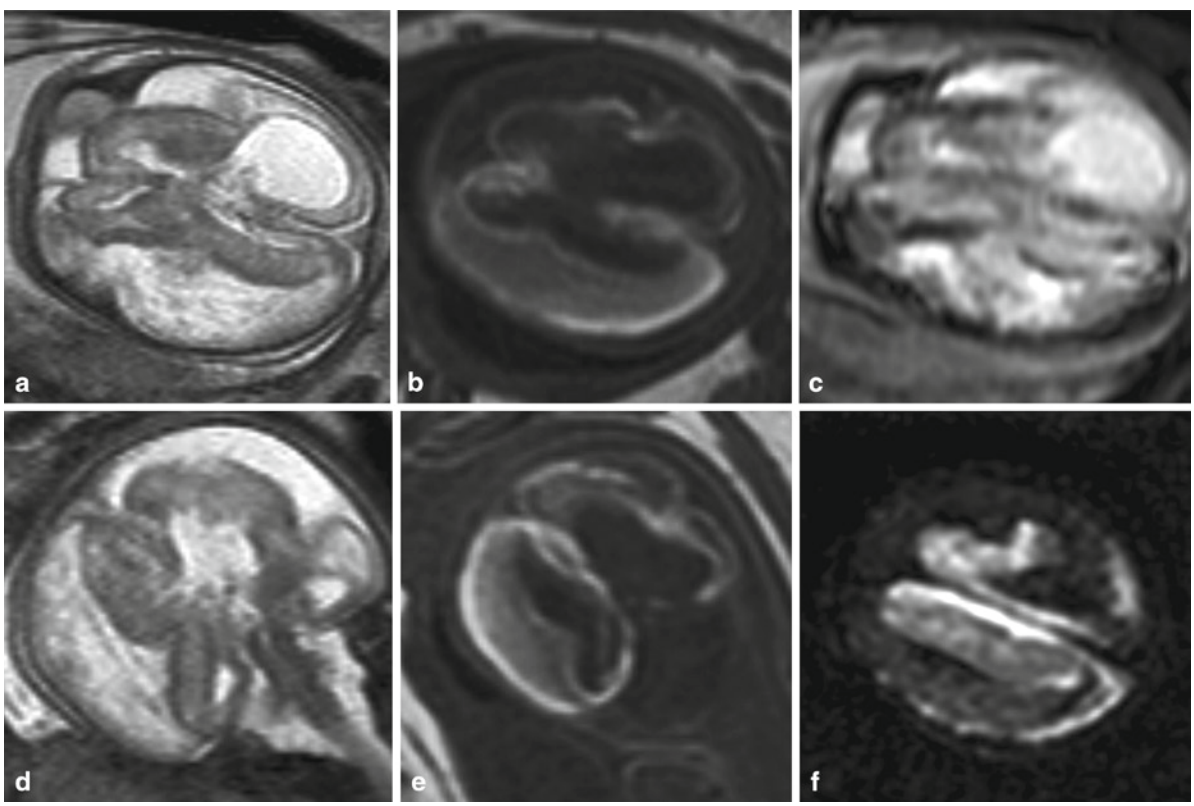

Fig. 11 Parenchymal bleeding in GW 29, axial T2 (**a**), T1 (**b**) EPI (**c**) DWI (**f**) weighted images and coronal T2 (**d**), and T1 (**e**) weighted sequences. MRI showing multicompartment hemorrhage and large tissue destruction

from postnatal studies in congenitally blind children (Mets and Chhabra 2008). Intracerebrally, any manifestation of acute or chronic injury may be seen. Characteristic findings may be present, mostly in the chronic stages. Tissue loss may manifest in the form of parenchymal cysts or defects, with or without signs of old hemorrhage. Indirect markers of tissue loss are thinning of the corpus callosum, the brainstem, widening of the inner/outer CSF spaces, and microcephaly in variable combinations. To narrow the differential diagnoses of such unspecific findings, screening for the possible involvement of extra-CNS structures should be performed. In addition to the morphological changes associated with FIRS (see above), other organs may also be affected during an infection. On ultrasound, hyperechogenic bowel loops that may also be seen in a variety of underlying conditions may indicate the presence of inflammation (Oboh et al. 2006). The MRI-correlate is not completely clear, to date, but seems to be associated with a higher amount of meconium filling (appearing hyperintense on T1-weighted images) than would be expected for the respective fetal age. Hepatosplenomegaly and/or calcifications in these organs may occur. Hemorrhages may be seen in any part of the fetal body.

5.1 Cytomegalovirus

CMV infection has been found to affect up to 2.5% of newborns (Engman et al. 2010). In particular, infections during the first and second trimesters will lead to disorders of cortical development, as CMV damages the subventricular and ventricular zones, where neurons and glia cells are formed. Subependymal cysts and calcifications can be seen. Signal changes in the temporal lobes (Doneda et al. 2010) have been described as almost certainly specific for CMV. Extracerebral findings comprise hepatomegaly with or without ascites, or "echogenic" bowel on ultrasound, the MR correlate of which is not yet fully understood.

5.2 Toxoplasmosis

Toxoplasmosis may lead to hydrocephalus as a consequence of aqueduct obliteration, and hydranencephaly has also been described (Laure-Kamionowska and Dambska 1992). Calcifications may be seen not only intracerebrally, but also in the meninges or in the eye (Barkovich and Girard 2003) (Fig. 12).

5.3 Parvovirus

Susceptibility to parvovirus B19 infection is present in up to 60% of pregnant women, depending on the parts of the world in which they reside (Enders et al. 2004). Fetal anemia and hydrops have been described in parvovirus B19 infection (Al-Khan et al. 2003). With regard to the brain, polymicrogyria was found in a case that was infected with parvovirus B19 before GW 16 (Pistorius et al. 2008). In other cases, cerebellar hemorrhages have been described (Glenn et al. 2007).

5.4 Herpes Simplex Virus

Herpes simplex virus in utero, via hematogeneous spread or ascending infection, occurs in only 5% of fetuses (Duin et al. 2007). Cerebral tissue loss and polymicrogyria have been reported (Duin et al. 2007).

5.5 Varicella-Zoster Virus

The varicella-zoster virus has an affinity for the spinal cord ganglia, and, when these structures are affected, may lead to shortening and/or malformation of the limbs and scarring of the skin associated with the respective segment (Auriti et al. 2009). Cerebral manifestations consist of ventriculomegaly, calcifications, and microcephaly (Degani 2006).

5.6 Rubella

Rubella infection is seen only rarely. White matter lesions and parenchymal calcifications have been described (Tang et al. 2009).

In most cases, metabolic defects of the fetus are compensated for by maternal enzymes and do not become apparent until after birth. However, inborn errors of metabolism may affect the intrauterine milieu and may disrupt brain development (Nissenkorn et al. 2001). It is

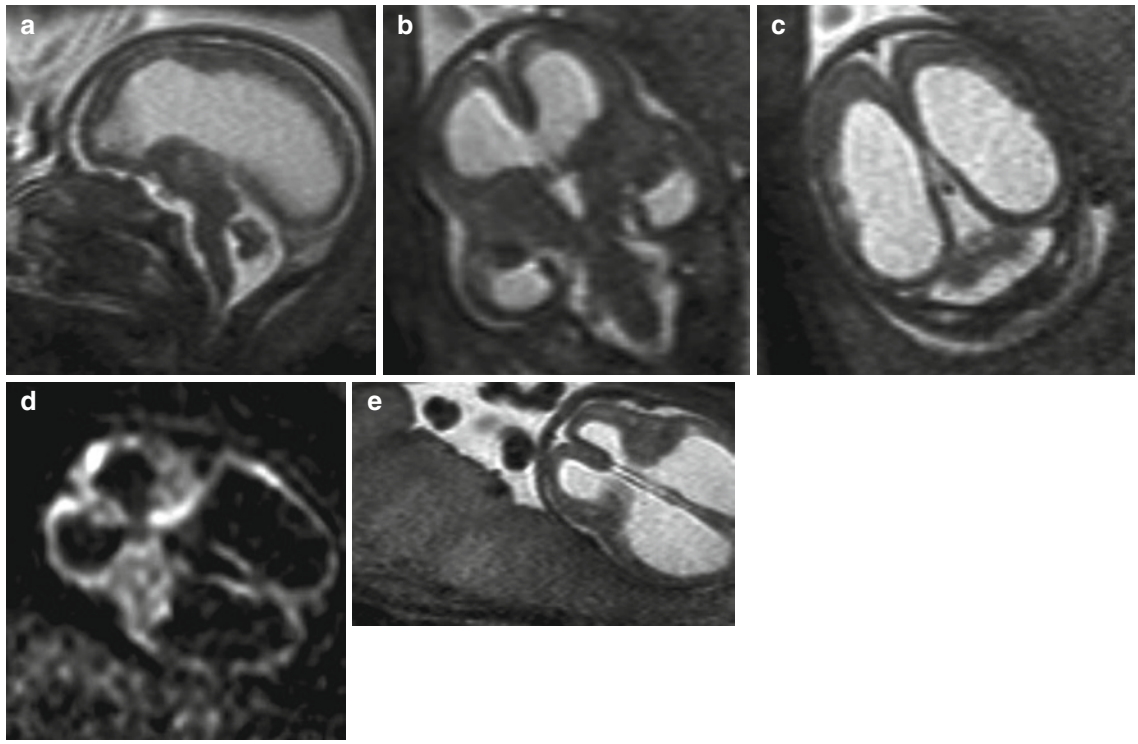

Fig. 12 GW 22, sagittal (**a**), coronal (**b**), axial (**c**, **e**) T2-weighted sequence, and DW sequence (**d**). Occlusive hydrocephalus, parenchymal lesions, missing lamination, irregular delineation of the ependyma, and edema of the placenta (in **e**)

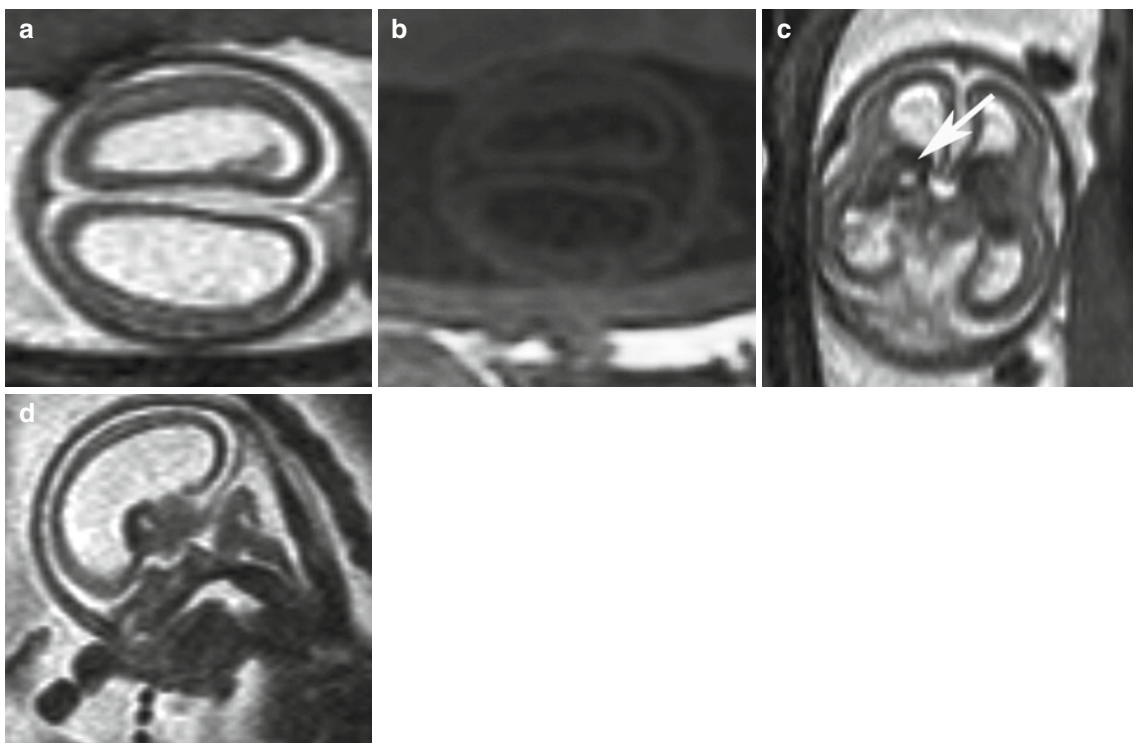

Fig. 13 Fetus in GW 20, axial T2 (**a**) T1-FLAIR (**b**) weighted, coronal (**c**) and sagittal T2-weighted sequence (**d**). Wide ventricles without any signs of obstruction of the CSF spaces or hemorrhage. Callosal agenesis and thinning of the parenchyma. Cystic lesion in the *right* thalamus in (**c**) (*arrow*) and (**d**)

Table 1 Malformations as a consequence of a metabolic disease

Neural tube defect	Folic acid metabolism, ethyl malonic aciduria
Holoprosencephaly (Smith–Lemli–Opitz syndrome)	Cholesterol metabolism
Disorders of cortical development	Peroxisomal disorders, Refsum disease, chondrodysplasia punctata, glutaric acidemia II
Corpus callosum agenesis/ dysgenesis	Pyruvate dehydrogenase deficiency (Robinson et al. 2001), maternal phenylketonuria, peroxisomal disorders, organic acidurias
Hypoplastic temporal lobes	Glutaric acidemia II (Righini et al. 2010)
Subependymal pseudocysts	Peroxisomal disorders

thought that energy depletion or the presence of a toxic agent, or impairment of signaling mechanisms, at a particular time, may lead to malformations, such as, for instance, callosal agenesis (Prasad et al. 2007). Mitochondrial disorders, for instance, may lead to a shortage of energy that is necessary to fuel developmental steps such as cell migration. Malformations have been described in disorders such as Zellweger's syndrome (Mochel et al. 2006), carnitin palmitoylransferase 2 deficiency, glutaric aciduria type 2, pyruvate dehydrogenase deficiency (Fig. 13), or fumarase deficiency. Some of the disorders in which malformations have been found prenatally are summarized in Table 1. (Nissenkorn et al. 2001; Prasad et al. 2007, 2009). In addition, cystic white matter lesions can be found in fetuses with pyruvate dehydrogenase deficiency, at least in the third trimester.

In addition to malformations, unspecific signs, such as wide inner and/or outer CSF spaces, deviations of normal head size, restricted movement, and IUGR, may be associated with metabolic diseases.

6 Conclusion

To date, only a few cases of fetal brain injury are on record. Consequently, descriptions of typical findings with regard to etiological background are only rarely available. A detailed history with respect to maternal diseases, especially infections or chronic illnesses, is required to narrow the differential diagnoses. A variety of available MR sequences must be used for accurate visualization of the specific pathology.

References

Abboud P, Mansour G, Lebrun JM, Zejli A, Bock S, Lepori M, Morville P (2001) Acute carbon monoxide poisoning during pregnancy: 2 cases with different neonatal outcome. J Gynecol Obstet Biol Reprod (Paris) 30:708–711

Abdel-Salam GM, Zaki MS, Saleem SN, Gaber KR (2008) Microcephaly, malformation of brain development and intracranial calcification in sibs: pseudo-TORCH or a new syndrome. Am J Med Genet A 146A:2929–2936

Al-Khan A, Caligiuri A, Apuzzio J (2003) Parvovirus B-19 infection during pregnancy. Infect Dis Obstet Gynecol 11: 175–179

Asenbaum U, Brugger PC, Kasprian G, Ulm B, Messerschmidt A, Prayer D (2009) MRI of fetal intracerebral hemorrhage. Neuroradiology 51:51

Auriti C, Piersigilli F, De Gasperis MR, Seganti G (2009) Congenital varicella syndrome: still a problem? Fetal Diagn Ther 25:224–229

Baldoli C, Righini A, Parazzini C, Scotti G, Triulzi F (2002) Demonstration of acute ischemic lesions in the fetal brain by diffusion magnetic resonance imaging. Ann Neurol 52:243–246

Barbu D, Mert I, Kruger M, Bahado-Singh RO (2009) Evidence of fetal central nervous system injury in isolated congenital heart defects: microcephaly at birth. Am J Obstet Gynecol 201(43):e41–47

Barkovich AJ (2005) Pediatric neuroimaging. Lippincott Williams & Wilkins, Philadelphia

Barkovich AJ, Girard N (2003) Fetal brain infections. Childs Nerv Syst 19:501–507

Bauder F, Beinder E, Arlettaz R, Albisetti M, Boltshauser E, Gessler P (2009) Intrauterine subdural hemorrhage in a preterm neonate possibly associated with maternal low-molecular weight heparin treatment. J Perinatol 29:521–523

Beltinger C, Saule H (1988) Sonography of subependymal cysts in congenital rubella syndrome. Eur J Pediatr 148:206–207

Brugger PC, Stuhr F, Lindner C, Prayer D (2006) Methods of fetal MR: beyond T2-weighted imaging. Eur J Radiol 57:172–181

Carletti A, Colleoni GG, Perolo A, Simonazzi G, Ghi T, Rizzo N, Pilu G (2009) Prenatal diagnosis of cerebral lesions acquired in utero and with a late appearance. Prenat Diagn 29:389–395

Chang CL, Chiu NC, Ho CS, Li ST (2006) Frontal horn cysts in normal neonates. Brain Dev 28:426–430

de Vries LS, Gunardi H, Barth PG, Bok LA, Verboon-Maciolek MA, Groenendaal F (2004) The spectrum of cranial ultrasound and magnetic resonance imaging abnormalities in congenital cytomegalovirus infection. Neuropediatrics 35:113–119

Degani S (2006) Sonographic findings in fetal viral infections: a systematic review. Obstet Gynecol Surv 61:329–336

Derauf C, Kekatpure M, Neyzi N, Lester B, Kosofsky B (2009) Neuroimaging of children following prenatal drug exposure. Semin Cell Dev Biol 20:441–454

Doneda C, Parazzini C, Righini A, Rustico M, Tassis B, Fabbri E, Arrigoni F, Consonni D, Triulzi F (2010) Early cerebral lesions in cytomegalovirus infection: prenatal MR imaging. Radiology 255:613–621

Downer EJ, Campbell VA (2010) Phytocannabinoids, CNS cells and development: a dead issue? Drug Alcohol Rev 29:91–98

Duin LK, Willekes C, Baldewijns MM, Robben SG, Offermans J, Vles J (2007) Major brain lesions by intrauterine herpes simplex virus infection: MRI contribution. Prenat Diagn 27:81–84

Enders M, Weidner A, Zoellner I, Searle K, Enders G (2004) Fetal morbidity and mortality after acute human parvovirus B19 infection in pregnancy: prospective evaluation of 1018 cases. Prenat Diagn 24:513–518

Engman ML, Lewensohn-Fuchs I, Mosskin M, Malm G (2010) Congenital cytomegalovirus infection: the impact of cerebral cortical malformations. Acta Paediatr 99(9): 1344–1349

Fichera A, Zambolo C, Accorsi P, Martelli P, Ambrosi C, Frusca T (2009) Perinatal outcome and neurological follow up of the cotwins in twin pregnancies complicated by single intrauterine death. Eur J Obstet Gynecol Reprod Biol 147:37–40

Fryer SL, Schweinsburg BC, Bjorkquist OA, Frank LR, Mattson SN, Spadoni AD, Riley EP (2009) Characterization of white matter microstructure in fetal alcohol spectrum disorders. Alcohol Clin Exp Res 33:514–521

Gaffney G, Squier MV, Johnson A, Flavell V, Sellers S (1994) Clinical associations of prenatal ischaemic white matter injury. Arch Dis Child Fetal Neonatal Ed 70: F101–106

Garel C, Delezoide AL, Elmaleh-Berges M, Menez F, Fallet-Bianco C, Vuillard E, Luton D, Oury JF, Sebag G (2004) Contribution of fetal MR imaging in the evaluation of cerebral ischemic lesions. Am J Neuroradiol 25: 1563–1568

Girard N, Gire C, Sigaudy S, Porcu G, d'Ercole C, Figarella-Branger D, Raybaud C, Confort-Gouny S (2003) MR imaging of acquired fetal brain disorders. Childs Nerv Syst 19:490–500

Glenn OA, Bianco K, Barkovich AJ, Callen PW, Parer JT (2007) Fetal cerebellar hemorrhage in parvovirus-associated nonimmune hydrops fetalis. J Matern Fetal Neonatal Med 20:769–772

Gotsch F, Romero R, Kusanovic JP, Mazaki-Tovi S, Pineles BL, Erez O, Espinoza J, Hassan SS (2007) The fetal inflammatory response syndrome. Clin Obstet Gynecol 50: 652–683

Govaert P (2009) Prenatal stroke. Semin Fetal Neonatal Med 14:250–266

Guibaud L, Attia-Sobol J, Buenerd A, Foray P, Jacquet C, Champion F, Arnould P, Pracros JP, Golfier F (2004) Focal sonographic periventricular pattern associated with mild ventriculomegaly in foetal cytomegalic infection revealing cytomegalic encephalitis in the third trimester of pregnancy. Prenat Diagn 24:727–732

Guimiot F, Garel C, Fallet-Bianco C, Menez F, Khung-Savatovsky S, Oury JF, Sebag G, Delezoide AL (2008) Contribution of diffusion-weighted imaging in the evaluation of diffuse white matter ischemic lesions in fetuses: correlations with fetopathologic findings. Am J Neuroradiol 29:110–115

Isaacs H (2009) Fetal brain tumors: a review of 154 cases. Am J Perinatol 26:453–466

Johansson PA, Dziegielewska KM, Liddelow SA, Saunders NR (2008) The blood-CSF barrier explained: when development is not immaturity. Bioessays 30:237–248

Kang BK, Na DG, Ryoo JW, Byun HS, Roh HG, Pyeun YS (2001) Diffusion-weighted MR imaging of intracerebral hemorrhage. Korean J Radiol 2:183–191

Kasprian G, Brugger PC, Weber M, Krssak M, Krampl E, Herold C, Prayer D (2008) In utero tractography of fetal white matter development. Neuroimage 43:213–224

Laure-Kamionowska M, Dambska M (1992) Damage of maturing brain in the course of toxoplasmic encephalitis. Neuropatol Pol 30:307–314

Laurichesse Delmas H, Winer N, Gallot D, Lopes K, Perrotin F, Fluncker S, Geissler F, Beaufrere AM, Vendittelli F, Couture C, Lemery D (2008) Prenatal diagnosis of thrombosis of the dural sinuses: report of six cases, review of the literature and suggested management. Ultrasound Obstet Gynecol 32:188–198

Leventer RJ, Jansen A, Pilz DT, Stoodley N, Marini C, Dubeau F, Malone J, Mitchell LA, Mandelstam S, Scheffer IE, Berkovic SF, Andermann F, Andermann E, Guerrini R, Dobyns WB (2010) Clinical and imaging heterogeneity of polymicrogyria: a study of 328 patients. Brain 133:1415–1427

Levitsky DB, Mack LA, Nyberg DA, Shurtleff DB, Shields LA, Nghiem HV, Cyr DR (1995) Fetal aqueductal stenosis diagnosed sonographically: how grave is the prognosis? Am J Roentgenol 164:725–730

Limperopoulos C (2009) Disorders of the fetal circulation and the fetal brain. Clin Perinatol 36:561–577

Limperopoulos C, Tworetzky W, McElhinney DB, Newburger JW, Brown DW, Robertson RL Jr, Guizard N, McGrath E, Geva J, Annese D, Dunbar-Masterson C, Trainor B, Laussen PC, du Plessis AJ (2010) Brain volume and metabolism in fetuses with congenital heart disease: evaluation with quantitative magnetic resonance imaging and spectroscopy. Circulation 121:26–33

Makhoul IR, Zmora O, Tamir A, Shahar E, Sujov P (2001) Congenital subependymal pseudocysts: own data and meta-analysis of the literature. Isr Med Assoc J 3: 178–183

Malinger G, Lev D, Ben Sira L, Kidron D, Tamarkin M, Lerman-Sagie T (2002) Congenital periventricular pseudocysts: prenatal sonographic appearance and clinical implications. Ultrasound Obstet Gynecol 20:447–451

McQuillen PS, Miller SP (2010) Congenital heart disease and brain development. Ann NY Acad Sci 1184:68–86

Messerschmidt A, Brugger PC, Boltshauser E, Zoder G, Sterniste W, Birnbacher R, Prayer D (2005) Disruption of cerebellar development: potential complication of extreme prematurity. Am J Neuroradiol 26:1659–1667

Mets MB, Chhabra MS (2008) Eye manifestations of intrauterine infections and their impact on childhood blindness. Surv Ophthalmol 53:95–111

Mlczoch E, Brugger PC, Hanslik A, Ulm B, Salzer-Muhar U, Pollak A, Prayer D (2010) Prenatal brain pathology in

congenital heart disease - does oxygen saturation of cerebral blood influence its occurrence? Ultrasound Obstet Gynecol 35:627–635

Mochel F, Grebille AG, Benachi A, Martinovic J, Razavi F, Rabier D, Simon I, Boddaert N, Brunelle F, Sonigo P (2006) Contribution of fetal MR imaging in the prenatal diagnosis of Zellweger syndrome. Am J Neuroradiol 27:333–336

Nelson KB (2008) Causative factors in cerebral palsy. Clin Obstet Gynecol 51:749–762

Nissenkorn A, Michelson M, Ben-Zeev B, Lerman-Sagie T (2001) Inborn errors of metabolism: a cause of abnormal brain development. Neurology 56:1265–1272

Nomura ML, Barini R, De Andrade KC, Milanez H, Simoni RZ, Peralta CF, Machado IN, Zambelli H, Maio KT (2009) Congenital hydrocephalus: gestational and neonatal outcomes. Arch Gynecol Obstet 282:607–611

Oboh AE, Orsi NM, Campbell J (2006) Amniotic fluid cytokine profile in association with fetal hyperechogenic bowel. Eur J Obstet Gynecol Reprod Biol 128:86–90

Oi S (2003) Diagnosis, outcome, and management of fetal abnormalities: fetal hydrocephalus. Childs Nerv Syst 19: 508–516

Ozanne A, Alvarez H, Krings T, Lasjaunias P (2007) Pediatric neurovascular malformations: vein of Galen arteriovenous malformations (VGAM), pial arteriovenous malformations (pial AVM), dural sinus malformations (DSM). J Neuroradiol 34:145–166

Pati S, Helmbrecht GD (1994) Congenital schizencephaly associated with in utero warfarin exposure. Reprod Toxicol 8:115–120

Pătraşcu A, Berceanu S, Popescu CF, Gheorman V, Berceanu C (2009) Clinical and histopathological correlations of the modifications of fetal membranes in amniochorial infection. Rom J Morphol Embryol 50:67–72

Pharoah PO, Dundar Y (2009) Monozygotic twinning, cerebral palsy and congenital anomalies. Hum Reprod Update 15:639–648

Piastra M, Pietrini D, Massimi L, Caldarelli M, De Luca D, Del Lungo LM, De Carolis MP, Di Rocco C, Conti G, Zecca E (2009) Severe subdural hemorrhage due to minimal prenatal trauma. J Neurosurg Pediatr 4:543–546

Pistorius LR, Smal J, de Haan TR, Page-Christiaens GC, Verboon-Maciolek M, Oepkes D, de Vries LS (2008) Disturbance of cerebral neuronal migration following congenital parvovirus B19 infection. Fetal Diagn Ther 24:491–494

Prasad AN, Bunzeluk K, Prasad C, Chodirker BN, Magnus KG, Greenberg CR (2007) Agenesis of the corpus callosum and cerebral anomalies in inborn errors of metabolism. Congenit Anom (Kyoto) 47:125–135

Prasad AN, Malinger G, Lerman-Sagie T (2009) Primary disorders of metabolism and disturbed fetal brain development. Clin Perinatol 36:621–638

Prayer D, Kuhle S, Prokesch R et al (1999) In vitro MR imaging of blood containing fetal hemoglobin (abstr). Radiology 213:144

Prayer D, Brugger PC, Kasprian G, Witzani L, Helmer H, Dietrich W, Eppel W, Langer M (2006a) MRI of fetal acquired brain lesions. Eur J Radiol 57:233–249

Prayer D, Kasprian G, Krampl E, Ulm B, Witzani L, Prayer L, Brugger PC (2006b) MRI of normal fetal brain development. Eur J Radiol 57:199–216

Reardon W, Donnai D (2007) Dysmorphology demystified. Arch Dis Child Fetal Neonatal Ed 92:F225–229

Redline RW, O'Riordan MA (2000) Placental lesions associated with cerebral palsy and neurologic impairment following term birth. Arch Pathol Lab Med 124:1785–1791

Reinhardt K, Mohr A, Gartner J, Spohr HL, Brockmann K (2010) Polymicrogyria in fetal alcohol syndrome. Birth Defects Res A Clin Mol Teratol 88:128–131

Righini A, Salmona S, Bianchini E, Zirpoli S, Moschetta M, Kustermann A, Nicolini U, Triulzi F (2004) Prenatal magnetic resonance imaging evaluation of ischemic brain lesions in the survivors of monochorionic twin pregnancies: report of 3 cases. J Comput Assist Tomogr 28: 87–92

Righini A, Kustermann A, Parazzini C, Fogliani R, Ceriani F, Triulzi F (2007) Diffusion-weighted magnetic resonance imaging of acute hypoxic-ischemic cerebral lesions in the survivor of a monochorionic twin pregnancy: case report. Ultrasound Obstet Gynecol 29:453–456

Righini A, Fiori L, Parazzini C, Doneda C, Arrigoni F, Riva E, Triulzi F (2010) Early prenatal magnetic resonance imaging of glutaric aciduria type 1: case report. J Comput Assist Tomogr 34:446–448

Robinson JN, Norwitz ER, Mulkern R, Brown SA, Rybicki F, Tempany CM (2001) Prenatal diagnosis of pyruvate dehydrogenase deficiency using magnetic resonance imaging. Prenat Diagn 21:1053–1056

Roza SJ, Steegers EA, Verburg BO, Jaddoe VW, Moll HA, Hofman A, Verhulst FC, Tiemeier H (2008) What is spared by fetal brain-sparing? Fetal circulatory redistribution and behavioral problems in the general population. Am J Epidemiol 168:1145–1152

Simonazzi G, Segata M, Ghi T, Sandri F, Ancora G, Bernardi B, Tani G, Rizzo N, Santini D, Bonasoni P, Pilu G (2006) Accurate neurosonographic prediction of brain injury in the surviving fetus after the death of a monochorionic cotwin. Ultrasound Obstet Gynecol 27:517–521

Tang PH, Bartha AI, Norton ME, Barkovich AJ, Sherr EH, Glenn OA (2009) Agenesis of the corpus callosum: an MR imaging analysis of associated abnormalities in the fetus. Am J Neuroradiol 30:257–263

Taweevisit M, Thorner PS (2010) Massive fetal thrombotic vasculopathy associated with excessively long umbilical cord and fetal demise: case report and literature review. Pediatr Dev Pathol 13:112–115

Unger S, Salem S, Wylie L, Shah V (2010) Newborn frontal horn cysts: cause for concern? J Perinatol 8 July doi:10.1038/jp.2010.79

van Baalen A, Versmold H (2007) Non-haemorrhagic subependymal pseudocysts: ultrasonographic, histological and pathogenetic variability. Ultraschall Med 28:296–300

van Gelder-Hasker MR, van Wezel-Meijler G, de Groot L, van Geijn HP, de Vries JI (2003) Peri- and intraventricular cerebral sonography in second- and third-trimester high-risk fetuses: a comparison with neonatal ultrasound and relation to neurological development. Ultrasound Obstet Gynecol 22:110–120

Vazquez E, Castellote A, Mayolas N, Carreras E, Peiro JL, Enriquez G (2009) Congenital tumours involving the head, neck and central nervous system. Pediatr Radiol 39: 1158–1172

Verbrugge J, Choudhary AK, Ladda R (2009) Tethered cord, corpus callosum abnormalities, and periventricular cysts in Wolf-Hirschhorn syndrome. Report of two cases and review of the literature. Am J Med Genet A 149A:2280–2284

Ville Y, Jenkins E, Shearer MJ, Hemley H, Vasey DP, Layton M, Nicolaides KH (1993) Fetal intraventricular haemorrhage and maternal warfarin. Lancet 341:1211

Volpe JJ (2001) Neurobiology of periventricular leukomalacia in the premature infant. Pediatr Res 50:553–562

Zuerrer M, Martin E, Boltshauser E (1991) MR imaging of intracranial hemorrhage in neonates and infants at 2.35 Tesla. Neuroradiology 33:223–229

Diagnosis of Congenital Diaphragmatic Hernia

Mieke Cannie and Jacques Jani

Contents

Abstract

› With advances in ultrasound technology, congenital diaphragmatic hernia (CDH) is easily diagnosed prenatally. In contrast, prenatal prognostication remains a challenge. In view of the current availability of fetal therapy this becomes even more important. To date, one of the most studied markers is the lung-area to head circumference ratio and has been shown in large studied to be predictive of postnatal outcome in terms of survival and also morbidity. Since the fetal lung is a fluid filled structure hence has high signal intensity on T2-WI, it can be easily discernible from the surrounding structures using fetal magnetic resonance imaging (MRI). This remains so even in case of oligohydramnios and obesity, conditions that make appropriate ultrasound evaluation difficult and inaccurate. The advantage of prenatal assessment in CDH using fetal MRI is that both lungs can be measured accurately, prediction can be adjusted to fetal biometry using the fetal body volume and intrathoracic position of the liver can be quantified, given a more accurate prediction of postnatal survival rather than the simple semiquantitative assessment of liver position. Further research using fetal MRI is directed towards the assessment of lungs at the microstructural level.

1 Introduction

Congenital diaphragmatic hernia (CDH) occurs in about 1/2,500–1/5,000 of newborns, depending on whether stillbirths are included or not (Butler and Claireaux 1962),

M. Cannie (✉)
Department of Radiology, University Hospital Brugmann, Brussels, Belgium and
Departments of Radiology,
UZ Brussels, Vrije Universiteit Brussels,Belgium
e-mail: miekecannie@hotmail.com

J. Jani
Department of Obstetrics and Gynaecology, Section Fetal Medicine and Therapy, University Hospital Brugmann, Brussels, Belgium

D. Prayer (ed.), *Fetal MRI*, Medical Radiology,
DOI: 10.1007/174_2010_21, © Springer-Verlag Berlin Heidelberg 2011

and accounts for approximately 8% of all major congenital anomalies (Torfs et al. 1992). It is a surgically correctable, anatomical defect with unknown etiology. While the majority of cases are sporadic, less than 2% are familial (Enns et al. 1998), and recurrence rate of isolated CDH is known to be around 2% (Norio et al. 1984). The defect is believed to arise in the embryological period, and as a consequence lung development during further gestation is impaired (Keijzer et al. 2000). A genetic basis remains largely unidentified, but recent work points to the potential of gene discovery tools in CDH and also proves that the phenotypic spectrum of CDH may reflect mutations of different genes (Ackerman et al. 2005; Hara et al. 2005; Slavotinek 2005).

CDH is classified according to the location of the defect in the diaphragm. Most commonly, CDH are left-sided, however in 13% they are right-sided and in 2% they are bilateral (Torfs et al. 1992). Posterolateral defect, known as the Bochdalek hernia are the most common while the Morgagni hernia occurring at the anterior portion of the diaphragm are more rare.

In around 40% of the CDH patients, there are associated anomalies and these can be structural or chromosomal defects, and genetic syndromes. The structural anomalies associated with CDH are mainly congenital heart and central nervous system defects, but also include urogenital, gastrointestinal, musculoskeletal and respiratory anomalies (Crane 1979; Witters et al. 2001). The chromosomal anomalies associated with CDH are most commonly trisomy 21, 18 and 13. Other chromosomal abnormalities such as turner, tetrasomy 12p, partial trisomies 5 or 20 are rare. Genetic syndromes include Fryns syndrome, de Lange syndrome, Marfan syndrome and many others. Associated anomalies are independent predictors of survival, with less than 15% of babies surviving in this group (Skari et al. 2000; Stege et al. 2003).

Actual survival rates in isolated CDH are a matter of debate. Intuitively one would expect that, with advances in neonatal care, neonatal survival rates to improve accordingly. Larger surveys however rate mortality in antenatal diagnosed isolated and live born cases around 30%, still today (Stege et al. 2003; Colvin et al. 2005). Some series from postnatal surgical units report survival rates in excess of 80% (Bagolan et al. 2004; Downard et al. 2003). However, such results overlook the prenatal "hidden mortality" arising from fetal death or termination of pregnancies considered to have a poor prognosis (Harrison et al. 1978), or babies born in outreach hospitals and dying before referral for pediatric surgery (Scott 2004). A study from Western Australia, on 116 babies with CDH collected over a 10-year period, reported that prenatal diagnosis was made in 53% of cases and half of these underwent termination of pregnancy (Colvin et al. 2005). Although the survival in those cases that were selected for neonatal surgery was 92% and the overall survival of the prenatally diagnosed fetuses was only 16%. In another recent population-based study from France on 51 cases of CDH, the condition was isolated in 29 and 16 (55%) of these survived (Gallot et al. 2005).

Whatever the true mortality is, in the group with isolated CDH a high proportion of babies still die in the neonatal period due to pulmonary hypoplasia and/or hypertension. Antenatal prediction of likely postnatal outcome is a clinical need since we need to offer parents different management options including expectant management, termination of pregnancy and prenatal treatment. Nowadays, such a prediction is less of a challenge and the purpose of this chapter is to provide a review of the current imaging modalities available in the diagnosis and the assessment of prognosis of these cases.

2 Prenatal Diagnosis

The diaphragm is imaged by prenatal ultrasonography as an echo-free space between the thorax and abdomen. The diagnosis of CDH can be easily made on ultrasound by the demonstration of stomach and intestines (90% of the cases) or liver (50%) in the thorax and the associated mediastinal shift to the opposite side (Fig. 1). Herniated abdominal contents, associated with a left-sided diaphragmatic hernia, are easy to demonstrate because the echo-free fluid-filled stomach and small bowel contrast dramatically with the more echogenic fetal lung. In contrast, a right-sided hernia is more difficult to identify because the echogenicity of the fetal liver is similar to that of the lung, and visualization of the gall bladder in the right side of the fetal chest may be the only way of making the diagnosis. Polyhydramnios (usually after 25 weeks) is found in about 75% of cases and this may be the consequence of impaired fetal swallowing due to compression of the esophagus by the herniated abdominal organs. The main differential diagnosis is from cystic lung disease, such as cystic adenomatoid malformation (Fig. 2) where fetal magnetic resonance imaging (MRI) can be of help, or

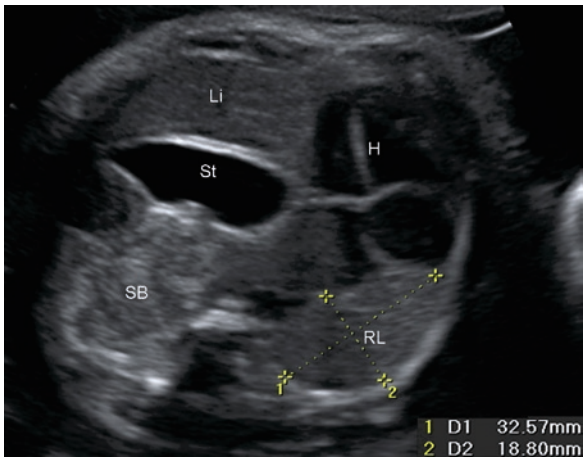

Fig. 1 Ultrasound image in an axial view of a fetus at 26 weeks of gestation at the level of the 4-chamber view of the heart showing a left-sided congenital diaphragmatic hernia (CDH) with massive mediastinal shift caused by intrathoracic herniation of the left lobe of the liver (Li), small bowels (SB) and stomach (St). Note the remaining right lung (RL) and the heart (H) shifted towards the right part of the thorax. The RL area is measured by multiplying the longest axis (D1) and that perpendicular to it (D2)

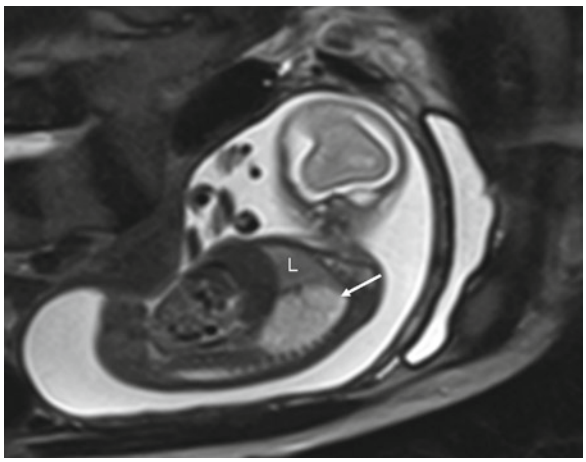

Fig. 2 T2-WI in a sagittal view of a fetus at 22 weeks of gestation showing a hyperintense mass of the inferior lobe of the right lung corresponding to a congenital cystic adenomatoid malformation type II (*arrow*). Note the remaining left lung with normal signal intensity (L)

mediastinal cystic processes, e.g., neuroenteric cysts, bronchogenic cysts and thymic cysts (Table 1) (Graham and Devine 2005). In these cases, a fluid-filled structure causing mediastinal shift may be present within the chest. However, in contrast to diaphragmatic hernia, the upper abdominal anatomy is normal.

Table 1 Differential diagnosis of CDH (adapted from Graham and Devine 2005)

Congenital cystic adenomatoid malformation
Bronchopulmonary sequestration
Diaphragmatic eventration
Bronchogenic cyst
Enteric and neurenteric cysts
Mediastinal teratoma
Bronchial atresia

3 Prenatal Prediction of Postnatal Survival

The main predictor of outcome is the presence of other major abnormalities that can be diagnosed by detailed ultrasonographic examination and fetal karyotyping.

In those with apparently isolated CDH prenatal prediction of outcome essentially relies on the assessment of the degree of lung compression by the herniated abdominal viscera. Many prognostic factors based on conventional 2D-ultrasound have been evaluated such as the left to right ventricle ratio (Sharland et al. 1992; Thebaud et al. 1997), lung diameter to thoracic circumference ratio (Bahlmann et al. 1999), amniotic fluid volume, mediastinal shift and stomach position (Hatch et al. 1992). A prognostic score combining sonographic features has also been proposed (Dommergues et al. 1996). Recently, new potential prognostic factors were reported, such as fetal pulmonary artery diameters (Sokol et al. 2002) or the use of Doppler ultrasound to measure impedance to flow in the pulmonary arteries (Fuke et al. 2003).

3.1 Prenatal Assessment with 2D-Ultrasound

3.1.1 The Lung to Head Ratio and Liver Herniation

The most widely studied prognostic factors using ultrasound are firstly, determination whether the herniated abdominal viscera in the fetal thorax include the liver and secondly, measurement of the contralateral lung area to head circumference ratio (LHR) (Fig. 1). The LHR was first proposed by Metkus et al., who observed

a relationship to survival (Metkus et al. 1996). Prediction is improved by combining parameters with another anatomical observation, such as the presence of liver herniation as assessed by ultrasound (Fig. 3) and/or by MRI (Fig. 4). Liver herniation was earlier shown to be closely related to survival chances (Bootstaylor et al. 1995; Albanese et al. 1998). In practice the population investigated is stratified based on the position of the liver and the LHR, with pivotal points below or above LHR = 1.0 and 1.4 (Table 2) (Metkus et al. 1996; Lipshutz et al. 1997; Harrison et al. 1998; Flake et al. 2000; Sbragia et al. 2000; Laudy et al. 2003; Heling et al. 2005; Jani et al. 2006a).

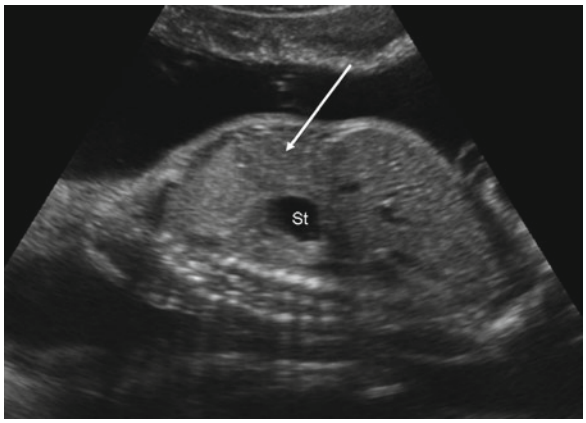

Fig. 3 Ultrasound image in a sagittal view of a fetus at 24 weeks of gestation with a left-sided CDH showing the massive intrathoracic herniation of the left lobe of the liver (*arrow*). Note the stomach (St) in an intrathoracic position

These considerations became clear in a recent study including several large referral centers. This retrospective chart review included 184 fetuses, diagnosed with isolated left-sided CDH and assessed between 22 and 28 weeks, expectantly managed and live born after 30 weeks between 1996 and 2004. Liver herniation had a clear effect on LHR. LHR on itself correlated to survival, but the predictive value of LHR became better when the liver was herniated. Using both variables, allows a clinical stratification of risk. In fetuses with liver herniation, which theoretically have a 50% chance to survive, survival can be predicted more accurately from LHR measured in the second trimester. When a fetus has a $1.0 \leq LHR < 1.6$ it has a 66% chance to survive. At 1.6 or higher this would increase to 83% or

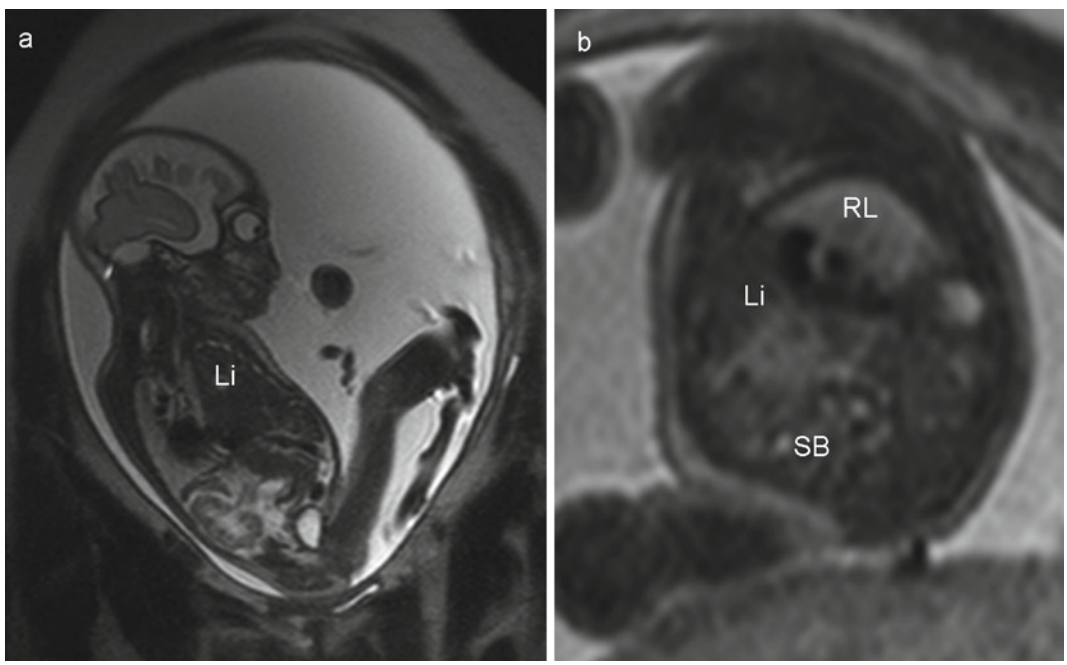

Fig. 4 T2-WI of fetuses with left-sided CDH: (**a**) in a sagittal view at 27 weeks of gestation showing massive intrathoracic herniation of the left lobe of the liver (Li) and (**b**) in an axial view at 26 weeks of gestation showing intrathoracic herniation of the small bowel (SB) and liver (Li). Note the remaining right lung (RL)

Table 2 Studies reporting on the value of fetal lung area to head circumference ratio (LHR) in the prediction of survival in isolated left-sided congenital diaphragmatic hernia (CDH). In the third column the percentage of patients with liver herniation in the series is displayed; in the fourth column the gestational age period at LHR measurement

References	*n*	Liver: intrathoracic herniation (%)	Gestation (weeks)	LHR cut-off	Survival (%)
Metkus et al. (1996)	38	≥80	≤25	<0.6 0.6–1.35 >1.35	0 57 100
Lipshutz et al. (1997)	15	Not given	24–26	<1.0 1–1.4 >1.4	0 38 100
Harrison et al. (1998)	13	100	20	<1.0 1.0–1.4	20 57
Flake et al. (2000)	47	Not given	23–25	<1.0 1–1.4 >1.4	0 56 85
Sbragia et al. (2000)	20	0	16–26	<1.4 ≥1.4	89 73
Laudy et al. (2003)	21	Not given	28–37	<1.0 1–1.4 >1.4	0 38 100
Heling et al. (2005)	22	64	16–38	<1.0 1.0–1.4 >1.4	67 60 40
Jani et al. (2006a)	184	47	22–28	0.4–0.5 0.6–0.7 0.8–0.9 1.0–1.1 1.2–1.3 1.4–1.5 >1.6	0 30 32 74 68 72 88

more (Jani et al. 2006a). In the past LHR = 1.0 has been considered as a pivotal point, and this is still so today, however a further refinement of prediction might be possible for fetuses under this threshold. In this multicenter study not a single patient with a $0.4 \leq LHR \leq 0.7$ survived. Three fetuses with $0.8 \leq LHR < 1.0$ survived (16%). This study certainly shows that the critical margin of viability in fetuses with liver herniation lies somewhere in the transition of 0.7–1.0, and while individual chances might vary from center to center, this might be the current limit. Furthermore, since LHR increased with gestation, we recently introduced the observed to expected (o/e) LHR which provides a gestation independent measurement of lung size (Jani et al. 2007b). In fetuses with isolated CDH, the o/e LHR represents at this stage the most validated method of 2D assessment of lung size in the prediction of postnatal survival.

3.1.2 Blood Flow and Resistance Measurements

Fetal echocardiography is able to assess repercussion of pulmonary hypoplasia on right and left ventricular proportions. It can measure branch pulmonary artery diameters, later shown to correlate to lung mass. In CDH, a larger contralateral diameter and discrepancy between contra- and ipsilateral diameters have been shown to predict neonatal death and morbidity indicators such as later oxygen requirements (Sokol et al. 2002). Next to determination of the size of vessels, Doppler interrogation of the pulmonary circulation or

ductus arteriosus may be a proxy of vascular resistance. Pulmonary vascular resistance is indirectly related to hypoplasia in some diseases (Laudy and Wladimiroff 2000; Fuke et al. 2003; Mahieu-Caputo et al. 2004). Although theoretically promising, it is not likely that large enough changes in peak systolic and end diastolic velocities would be detected, as they are already minimal during pregnancy to start with. This adds to other limitations, such as the difficulty to insonate at perpendicular angles to the vessel in the presence of abnormal anatomy, and the variability of the waveform along the proximal or distal vasculature.

3.2 Prenatal Assessment with 3D-Ultrasound

In the assessment of lung size by LHR only the contralateral lung area in a single transverse section of the thorax is measured. Therefore, it seemed logic to investigate whether the measurement of total lung volume either by 3D ultrasound (Fig. 5) or MRI (Fig. 6) may provide better prediction of outcome than the LHR measurement.

Three-dimensional technology is now widely available and several studies have published normograms for multiplan or rotational volume 3D ultrasound acquisitions. Moeglin et al. demonstrated that both 3D techniques are interchangeable in normal patients (Moeglin et al. 2005). Much less data are available on 3D volumetry in patients at risk for lung hypoplasia (Kalache et al. 2003; Ruano et al. 2004).

In a recent study involving 47 fetuses with CDH evaluated between 21 and 36 weeks of gestation, we found that the prediction obtained using the o/e LHR-tracing method was better than the contralateral lung volume measured by 3D ultrasound (Jani et al. 2007c). A possible explanation for our finding that o/e LHR-tracing is better in predicting outcome than volume, is that maximum compression of the contralateral lung occurs laterally rather than longitudinally. Therefore, the knowledge of the third dimension of the contralateral lung is of no use in improving the prediction of postnatal survival. This has been shown in another study comparing LHR with contralateral lung volume in fetuses with CDH (Jani et al. 2006b). Consequently, in fetuses with expectantly managed isolated CDH, there is currently less focus in 3D ultrasound volume assessment in the prediction of postnatal outcome.

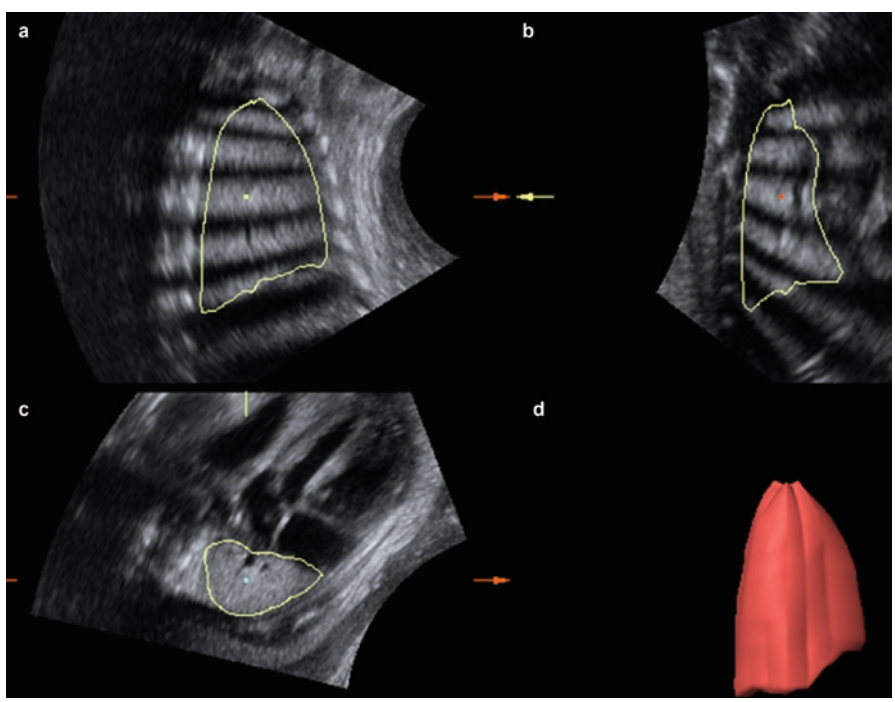

Fig. 5 Volume calculation of the contralateral lung in a left-sided CDH at 28 weeks of gestational age by the virtual organ computer-aided analysis technique. (**a**) Corresponds to the starting plane of rotation, (**b**, **c**) are the two other perpendicular planes and (**d**) corresponds to the final volume

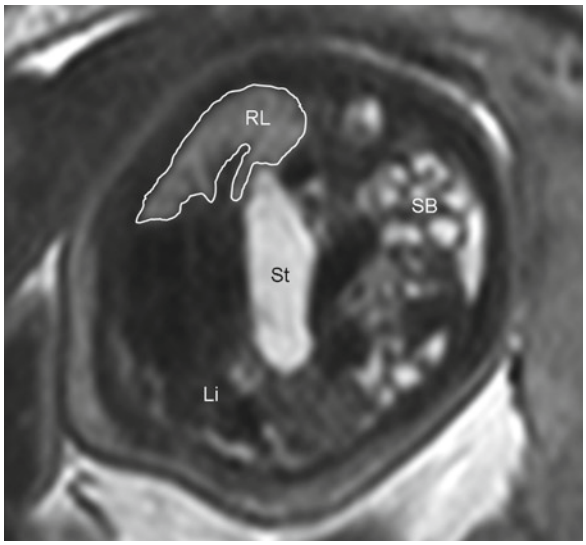

Fig. 6 T2-WI in an axial view of a fetus with left-sided CDH at 26 weeks of gestation showing the freehand region of interest (line) drawn on the right lung. Note the organs herniated into the thoracic cavity: left lobe of the liver (Li), small bowels (SB) and stomach (St)

3.3 Prenatal Assessment with Fetal MRI

3.3.1 Prenatal Assessment of Lungs Based on Gestational Age

Superior tissue contrast, a large field of view and relative operator independence enables fetal MRI to provide information that can supplement the information obtained by prenatal ultrasound examination. The advantage with MRI is that both the ipsilateral and contralateral lungs can be visualized and measured reliably, whereas with 3D ultrasound it is not possible to examine the ipsilateral lungs in nearly half of the cases (Jani et al. 2007a). Relatively few studies have examined the potential value of total fetal lung volume (TFLV) as measured by MRI, in the prediction of outcome (Table 3) (Cannie et al. 2006; Gorincour et al. 2005; Mahieu-Caputo et al. 2001; Paek et al. 2001; Walsh et al. 2000; Williams et al. 2004). So far, the number of patients examined was too small to draw definite conclusions, let be allowing assessment of confounding factors such as intrathoracic herniation of the liver or gestation at delivery which have a profound impact on survival. Furthermore, no studies have compared the value of the volume assessment by MRI as compared to LHR in the prediction of postnatal survival in fetuses with CDH.

None of all the previous studies has taken into account other variables than the TFLV in the prediction of postnatal survival, some of them being consistently shown to be major predictors such as intrathoracic liver herniation (Jani et al. 2006a; Kitano et al. 2005; Hedrick et al. 2007). The largest study by Gorincour el al., although being a prospective study on 77 fetuses with isolated CDH, failed to integrate intrathoracic liver herniation as a determinant of postnatal survival. Furthermore, in the same study, gestation at diagnosis was shown to be predictive of postnatal survival and the prediction by lung size was not corrected for it making the conclusions less reliable.

Table 3 Studies reporting on the value of fetal observed to expected (o/e) total fetal lung volume (FLV) in % in the prediction of survival in isolated CDH. In the third column the percentage of patients with liver herniation in the series is displayed; in the fourth column the gestational age period at o/e total FLV measurement

References	*n*	Liver: intrathoracic herniation (%)	Gestation (weeks)	o/e Total FLV cut-off (%)	Survival (%)
Cannie et al. (2006)	8	25	24–26	<35 ≥35	50 100
Gorincour et al. (2005)	77	Not given	24–37	<25 >25	19 60
Williams et al. (2004)	25	Not given	21–36	Not proposed	Not given
Paek et al. (2001)	11	73	21–28	≤40 >40	25 100
Mahieu-Caputo et al. (2001)	11	45	28–37	<35 ≥35	0 67
Walsh et al. (2000)	41	51	20–39	Not proposed	59

[a]Out of 28 at high risk for pulmonary hypoplasia, 25 had CDH

In a recent study on 148 fetuses with isolated CDH assessed at 22–38 weeks of gestation, the o/e TFLV was found to be a strong predictor of postnatal survival (Jani et al. 2008). Unlike many other studies, a large part of our population was assessed at the end of the second trimester which is important when considering termination of pregnancy where in some countries it becomes illegal after 24 weeks of gestation and most importantly fetal therapy that should better be offered before 29 weeks of pregnancy.

It was shown that both o/e TFLV and intrathoracic herniation of the liver as determined by MRI provided independent prediction of subsequent postnatal survival at discharge from the hospital but not side of CDH, gestation at diagnosis and delivery, nor year and institution at which the patient was managed.

In the group with intrathoracic herniation of the liver there was an inverse linear correlation between o/e TFLV and subsequent survival. Essentially, the survival rate increased from 12% for those with o/e TFLV of 25% or less, to about 40% for o/e TFLV of 26–35, 60% for o/e TFLV of 36–45% and more than 70% for o/e TFLV of 46% or more. In the group with no intrathoracic herniation of the liver, the survival rate was about three times higher in the group of o/e TFLV of 25% or less with a 40% survival rate; however this was substantially smaller than the survival rates of at least 80% in all groups with o/e TFLV above 25%.

Finally, in nearly half of the cases, fetuses were assessed within 2 weeks of each other with both MRI and 2D ultrasound with measurement of o/e LHR using the longest method. The study showed that there was a trend towards a better prediction with TFLV measurement by MRI rather than a 2D measurement with ultrasound, however it was underpowered to show any significance.

3.3.2 Quantification of Intrathoracic Liver

In fetuses with CDH, prenatal assessment of intrathoracic liver position using ultrasound and/or MRI is a strong predictor of subsequent survival in the neonatal period (Walsh et al. 2000; Kitano et al. 2005; Hedrick et al. 2007), and some authors have also suggested that it was better than estimation based on the lung size as measured by LHR (Hedrick et al. 2007). Most of the studies reporting on intrathoracic liver in the prediction of survival in CDH have done so in a nonquantitative manner. The position of the liver is reported as a categorical variable as "liver up" or "liver down."

Although for all studies intrathoracic liver was defined the same way, this has not necessarily been the case with studies where only a fraction of the liver would qualify as liver up, whereas others would only consider massive liver herniation. It is clear that standardization of the definition for liver herniation would help, but more importantly a more quantitative method for liver herniation is required, which would also permit better comparison of studies. This concept was already introduced by Walsh et al. (2000) obtaining the liver/diaphragm ratio in a single dimension on MR images and unlike lung volumes, the liver/diaphragm ratio was shown to be predictive of postnatal survival.

In a recent study and in fetuses with expectantly managed isolated CDH, the potential of volumetric quantification of intrathoracic liver herniation using MR imaging in the prediction of postnatal survival was evaluated (Cannie et al. 2008a). On axial T2-weighted images (T2-WI) the degree of intrathoracic liver herniation using the xyphoid process and thoracic apex as landmarks was defined (Fig. 7). Both of these are easily recognizable and unequivocal landmarks. The ratio of the liver to the thoracic cavity was calculated, further referred to as LiTR. It was demonstrated that measurement of LiTR is reproducible and that LiTR is larger in fetuses that subsequently died as compared to those that survived. Further, it was shown that LiTR provided independent prediction of survival from lung size as measured by o/e TFLV.

3.3.3 Prenatal Assessment of Lungs Based on Fetal Biometry

To date, the most available normal ranges of TFLV are typically calculated based on gestational age and would exclude multiplets or fetuses under the fifth and above the 95th weight percentile as determined by ultrasound (Mahieu-Caputo et al. 2004; Rypens et al. 2001). Several biometric markers that can be obtained through the ultrasound or the MR examination, such as head circumference, femur length, liver volume or the combination of all markers have been proposed as an alternative to calculate relative lung volume in fetuses with normally developed lungs and those affected by pulmonary

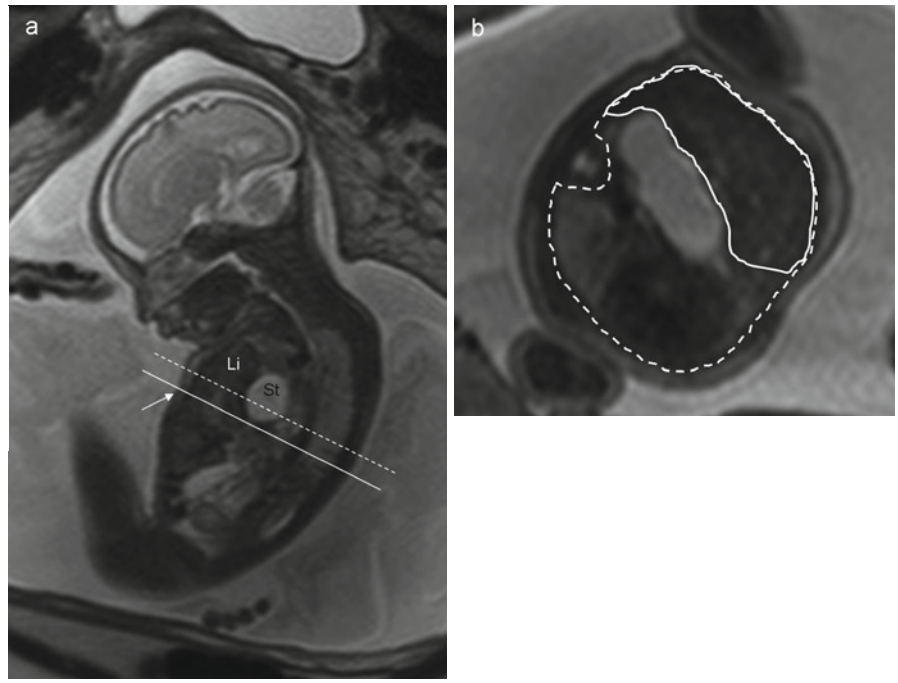

Fig. 7 T2-WI of a fetus with left-sided CDH at 28 weeks of gestation (**a**) in a sagittal view showing the landmark at the xyphoid process (*arrow*) for the first plane of measurement (*continuous line*) and another plane higher into the thorax (*interrupted line*). Note the left lobe of the liver (Li) and stomach (St). Same fetus in an axial view at the level of the stomach (**b**) with delineation of the liver (*continuous line*) and the thoracic cavity (*interrupted line*)

hypoplasia (Coakley et al. 2000; Williams et al. 2004). It was recently demonstrated that in normal fetuses, TFLV correlated better with such biometric markers than with GA. The advantage of the above biometric markers is their application irrespective of the actual fetal growth percentile or in multiple pregnancies.

As an alternative to such a complex process, we introduced the fetal body volume (FBV) as a single biometric variable which can be obtained throughout only one examination (Fig. 8). FBV has been earlier shown to be superior to ultrasound in predicting fetal weight at term, and our idea was to use it in an algorithm in order to improve postnatal prediction of survival in fetuses at risk for pulmonary hypoplasia.

In a recent study, we have built normal ranges of 200 fetuses between 16 and 40 weeks of gestation of TFLV vs. liver volume but also vs. FBV (Cannie et al. 2008c). This study confirmed earlier studies from Coakley that TFLV correlated better with biometrical markers rather than with gestational age.

In another study and in fetuses with CDH, the benefit of predicting lung volume with FBV rather than with gestational age was shown (Cannie et al. 2008b). The study included 53 fetuses with isolated CDH and showed that the prediction of survival based on gestational age vs. that based on FBV depends on fetal biometry and that there was a trend towards a better

Fig. 8 T2-WI in a sagittal view of a fetus at 25 weeks of gestation showing the delineation of the total fetal body volume

prediction when calculation was based on FBV rather than on gestational age. Clearly, correction for fetal biometry seems logical and very promising, but larger multicenter studies are still needed before wider use of fetal biometry in the prenatal prediction of postnatal survival in fetuses with CDH.

3.3.4 Prenatal Microstructural Assessment of Lungs

Microstructural assessment of the pulmonary system is less well developed. A leading study done by Osada et al. evaluated the lung/spinal fluid signal intensity ratio (Osada et al. 2004) and Brewerton et al. used another approach evaluating the lung/liver signal intensity ratio (Brewerton et al. 2005). However these studies are still small or methodologically flawed which needs to be solved before large implementation (Keller et al. 2004).

Studies on the evaluation of the human fetal lung using diffusion-weighted (DW) MRI are equally scarce. DW MRI is quantitatively expressed using the apparent diffusion coefficient (ADC). The first study by Moore et al. was conducted on 26 fetuses with normally developed lungs between 19 and 39 weeks of gestation (Moore et al. 2001) and showed an increase in the calculated ADC values with gestation. The second study by Balassy et al. was conducted on 53 fetuses with normally developed lungs between 20 and 37 weeks of gestation (Balassy et al. 2008) and was not able to identify a pattern of changes in the ADC values that correlate with lung maturation. They concluded that ADC cannot be used as an indicator of lung maturity. The most recent study was conducted by Manganaro et al. on 50 fetuses with normally developed lungs between 18 and 36 weeks of gestation (Manganaro et al. 2008). They found a significant correlation between ADC and gestational age and concluded that ADC can be considered as a new parameter for studying lung maturity.

The contradictory results between these studies confirms the fact that DWI in the fetal lungs needs certainly to be further explored in larger numbers and later on in the group of interest meaning fetuses at risk for pulmonary hypoplasia such as those with CDH.

Furthermore, both for DWI and T2 signal intensity of fetal lungs, results should be compared to functional studies performed using ultrasound on the vascular bed but also to histological findings in fetuses with termination of pregnancy in order to better understand the pathophysiology, behind the changes that are found.

4 Prenatal Prediction of Postnatal Morbidity

It is important to realize that survivors are not free of morbidity on the long term. They may suffer from serious long term morbidity, including chronic respiratory, feeding, hearing and neurodevelopmental problems (Muratore et al. 2001a, b; Jaillard et al. 2003; Trachsel et al. 2005; Crankson et al. 2006; Davis et al. 2004). Some newer neonatal strategies, like permissive hypercapnea and tolerance of lower oxygen saturation, may actually contribute to the latter, although they might improve survival. Morbidity may thus not be only related to the underlying condition but also to the postnatal therapy and can certainly not be ignored (Cortes et al. 2005; Stefanutti et al. 2004; Jaillard et al. 2003).

In severe cases, which are the targets of prenatal intervention (Deprest et al. 2004; Jani et al. 2005), one should be even more cautious not to substitute mortality by morbidity. For all these reasons, it is obvious that a proper long term multidisciplinary follow up program of CDH survivors is needed. High volume centers may be the best place to run such a program, caring for the kids and young adults even long time after discharge (West and Wilson 2005). Studies on prenatal prediction of postnatal morbidity in CDH are scarce although this became a clinical need for counseling parents, not only interested on the chances of their unborn child to survive but also on their quality of life.

A recent multicenter study on 100 survivors of expectantly managed isolated CDH was conducted to assess the prenatal measurement of o/e LHR and liver position in the prediction of postnatal morbidity events (Jani et al. 2009). O/e LHR and intrathoracic position of the liver were found to be independent significant predictors of the need for prosthetic patch repair. The incidence of gastroesophageal reflux was also related to the need for prosthetic patch repair. The o/e LHR predicted the need for postnatal assisted ventilation, supplemental O_2 at 28 days – which may increase risk for longer term respiratory morbidity – and the postnatal age at full enteral feeding. This study established that in isolated CDH the prenatally assessed size of the contralateral

lung is a significant predictor of the severity of the diaphragmatic defect, the functional consequences of impaired lung development and incidence of feeding problems. There are today no such studies based on fetal MRI in the prenatal prediction of postnatal morbidity in fetuses with isolated and expectantly managed CDH.

References

Ackerman KG, Herron BJ, Vargas SO, Huang H, Tevosian SG, Kochillas L, Rao C, Pober BR, Babiuk RP, Epstein JA, Greer JJ, Beier DR (2005) Fog2 is required for normal diaphragm and lung development in mice and humans. PLos Genet 1:58–65

Albanese CT, Lopoo J, Goldstein RB, Filly RA, Feldstein VA, Calen PW, Jennings RW, Farrell JA, Harrison MR (1998) Fetal liver position and prenatal outcome for congenital diaphragmatic hernia. Prenat Diagn 18:1138–1142

Bagolan P, Casaccia G, Crescenzi F, Nahom A, Trucchi A, Giorlandino C (2004) Impact of a current treatment protocol on outcome of high-risk congenital diaphragmatic hernia. J Pediatr Surg 39:313–318

Bahlmann F, Merz E, Hallermann C, Stopfkuchen H, Kramer W, Hofmann M (1999) Congenital diaphragmatic hernia: ultrasonic measurement of fetal lungs to predict pulmonary hypoplasia. Ultrasound Obstet Gynecol 14:162–168

Balassy C, Kasprian G, Brugger PC, Csapo B, Weber M, Hörmann M, Bankier A, Bammer R, Herold CJ, Prayer D (2008) Diffusion-weighted MR imaging of the normal fetal lung. Eur Radiol 18:700–706

Bootstaylor BS, Filly RA, Harrison MR, Adzick NS (1995) Prenatal sonographic predictors of liver herniation in congenital diaphragmatic hernia. J Ultrasound Med 914:515–520

Brewerton LJ, Chari RS, Liang Y, Bhargava R (2005) Fetal lung-to-liver signal intensity ratio at MR imaging: development of a normal scale and possible role in predicting pulmonary hypoplasia in utero. Radiology 235:1005–1010

Butler N, Claireaux AE (1962) Congenital diaphragmatic hernia as a cause of perinatal mortality. Lancet 1:659–663

Cannie M, Jani JC, De Keyzer F, Devlieger R, Van Schoubroeck D, Witters I, Marchal G, Dymarkowski S, Deprest JA (2006) Fetal body volume: use at MR imaging to quantify relative lung volume in fetuses suspected of having pulmonary hypoplasia. Radiology 241:847–853

Cannie M, Jani J, Chaffiotte C, Vaast P, Deruelle P, Houfflin-Debarge V, Dymarkowski S, Deprest J (2008a) Quantification of intrathoracic liver herniation by magnetic resonance imaging and prediction of postnatal survival in fetuses with congenital diaphragmatic hernia. Ultrasound Obstet Gynecol 32:627–632

Cannie M, Jani J, Meersschaert J, Allegaert K, Done' E, Marchal G, Deprest J, Dymarkowski S (2008b) Prenatal prediction of survival in isolated diaphragmatic hernia with observed over expected total fetal lung volume determined by magnetic resonance imaging based either on gestational age or fetal body volume. Ultrasound Obstet Gynecol 32:633–639

Cannie M, Jani J, Van Kerkhove F, Meerschaert J, De Keyzer F, Lewi L, Deprest J, Dymarkowski S (2008c) Fetal body volume at MR imaging to quantify total fetal lung volume – normal ranges. Radiology 247:197–203

Coakley FV, Lopoo JB, Lu Y, Hricak H, Albanese CT, Harrison MR, Filly RA (2000) Normal and hypoplastic fetal lungs: volumetric assessment with prenatal single-shot rapid acquisition with relaxation enhancement MR imaging. Radiology 216:107–111

Colvin J, Bower C, Dickinson J, Sokol J (2005) Outcomes of congenital diaphragmatic hernia: a population-based study in Western Australia. Pediatrics 116:e356–e363

Cortes R, Keller R, Townsend T, Harrison MR, Farmer DL, Lee H, Piecuch RE, Leonard CH, Hetherton M, Bisgaard R, Nobuhara KK (2005) Survival of severe congenital diaphragmatic hernia has morbid consequences. J Pediatr Surg 40: 36–45

Crane JP (1979) Familial congenital diaphragmatic hernia: prenatal diagnostic approach and analysis of twelve families. Clin Genet 16:244–252

Crankson SJ, Al Jadaan SA, Namshan MA, Al-Rabeeah AA, Oda O (2006) The immediate and long-term outcomes of newborns with congenital diaphragmatic hernia. Pediatr Surg Int 22:335–340

Davis PJ, Firmin RK, Manktelow B, Goldman AP, Davis CF, Smith JH, Cassidy JV, Shekerdemian LS (2004) Long-term outcome following extracorporeal membrane oxygenation for congenital diaphragmatic hernia: the UK experience. J Pediatr 144:309–315

Deprest J, Gratacos E, Nicolaides KH, on behalf of the FETO task group (2004) Fetoscopic tracheal occlusion (FETO) for severe congenital diaphragmatic hernia: evolution of a technique and preliminary results. Ultrasound Obstet Gynecol 24:121–126

Dommergues M, Louis-Sylvestre C, Mandelbrot L, Oury JF, Herlicoviez M, Body G, Gamerre M, Dumez Y (1996) Congenital diaphragmatic hernia: can prenatal ultrasonography predict outcome? Am J Obstet Gynecol 174:1377–1381

Downard C, Jaksic T, Garza J, Dzakovic A, Nemes L, Jennings RW, Wilson JM (2003) Analysis of an improved survival rate for congenital diaphragmatic hernia. J Pediatr Surg 38: 729–732

Enns GM, Cox VA, Goldstein RB, Gibbs DL, Harrison MR, Golabi M (1998) Congenital diaphragmatic defects and associated syndromes, malformations and chromosomal anomalies. Am J Med Genet 79:215–225

Flake AW, Crombleholme TM, Johnson MP, Howell LJ, Adzick NS (2000) Treatment of severe congenital diaphragmatic hernia by fetal tracheal occlusion: clinical experience with fifteen cases. Am J Obstet Gynecol 183:1059–1066

Fuke S, Kanzaki T, Mu J, Wasada K, Takemura M, Mitsuda N, Murata Y (2003) Antenatal prediction of pulmonary hypoplasia by acceleration time/ejection time ratio of fetal pulmonary arteries by Doppler blood flow velocimetry. Am J Obstet Gynecol 188:228–233

Gallot D, Coste K, Francannet C, Laurichesse H, Boda C, Ughetto S, Vanlieferinghen P, Scheye T, Vendittelli F, Labbe A, Dechelotte PJ, Sapin V, Lemery D (2005) Antenatal detection and impact on outcome of congenital diaphragmatic hernia: a 12-year experience in Auvergne (France). Eur J Obstet Gynecol Reprod Biol 125:202–205

Gorincour G, Bouvenot J, Mourot MG, Sonigo P, Chaumoitre K, Garel C, Guibaud L, Rypens F, Avni F, Cassart M, Maugey-Laulom B, Bourliere-Najean B, Brunelle F, Durand C, Eurin D, Groupe Radiopediatrique de Recherche en Imagerie Foetale (GRRIF) (2005) Prenatal prognosis of congenital diaphragmatic hernia using magnetic resonance imaging measurement of fetal lung volume. Ultrasound Obstet Gynecol 26:738–744

Graham G, Devine PC (2005) Antenatal diagnosis of CDH. Semin Perinatol 29:69–76

Hara A, Chapin CJ, Ertsey R, Kitterman J (2005) Changes in fetal lung distension alter expression of vascular endothelial growth factor and its isoforms in the developing rat lung. Pediatr Res 58:30–37

Harrison M, Bjordal R, Langmark F, Knutrud O (1978) Congenital diaphragmatic hernia: the hidden mortality. J Pediatr Surg 13: 227–230

Harrison MR, Mychaliska GB, Albanese CT, Jennings RW, Farrell JA, Hawgood S, Sandberg P, Levine AH, Lobo E, Filly RA (1998) Correction of congenital diaphragmatic hernia in utero IX. Fetuses with poor prognosis (liver herniation and low lung-to-head ratio) can be saved by fetoscopic temporary tracheal occlusion. J Pediatr Surg 33:1017–1023

Hatch EI, Kendall J, Blumhagen J (1992) Stomach position as an in utero predictor of neonatal outcome in left-sided diaphragmatic hernia. J Pediatr Surg 27:778–779

Hedrick HL, Danzer E, Merchant A, Bebbington MW, Zhao H, Flake AW, Johnson MP, Liechty KW, Howell LJ, Wilson RD, Adzick NS (2007) Liver position and lung-to-head ratio for prediction of extracorporeal membrane oxygenation and survival in isolated left congenital diaphragmatic hernia. Am J Obstet Gynecol 197(422):e1–e4

Heling KS, Wauer RR, Hammer H, Bollmann R, Chaoui R (2005) Reliability of the lung-to-head ratio in predicting outcome and neonatal ventilation parameters in fetus with congenital diaphragmatic hernia. Ultrasound Obstet Gynecol 25:112–118

Jaillard SM, Pierrat V, Dubois A, Truffert P, Lequien P, Wurtz AJ, Storme L (2003) Outcome at 2 years of infants with congenital diaphragmatic hernia: a population-based study. Ann Thorac Surg 75:250–256

Jani J, Gratacos E, Greenough A, Piero JL, Benachi A, Harrison M, Nicolaides K, Deprest J, FETO Task Group (2005) Percutaneous fetal endoscopic tracheal occlusion (FETO) for severe left sided congenital diaphragmatic hernia. Clin Obstet Gynecol N Am 48:910–922

Jani J, Keller RL, Benachi A, Nicolaides KH, Favre R, Gratacos E, Laudy J, Eisenberg V, Eggink A, Vaast P, Deprest J (2006a) Prenatal prediction of survival in isolated left-sided diaphragmatic hernia. Ultrasound Obstet Gynecol 27:18–22

Jani J, Peralta CFA, Van Schoubroeck D, Deprest J, Nicolaides KH (2006b) Relation between lung-to-head ratio and lung volume in normal fetuses and fetuses with diaphragmatic hernia. Ultrasound Obstet Gynecol 27:545–550

Jani J, Cannie M, Peralta CFA, Deprest J, Nicolaides KH, Dymarkowski S (2007a) Lung volumes in fetuses with congenital diaphragmatic hernia: comparison of 3D US and MR Imaging assessments. Radiology 244:575–582

Jani J, Nicolaides KH, Keller RL, Benachi A, Peralta CFA, Favre R, Moreno O, Tibboel D, Lipitz S, Eggink A, Vaast P, Allegaert K, Harrison M, Deprest J; on behalf of the antenatal-CDH-Registry group (2007b) Observed to expected lung area to head circumference ratio in the prediction of survival in fetuses with isolated diaphragmatic hernia. Ultrasound Obstet Gynecol 30:67–71

Jani J, Peralta CFA, Ruano R, Benachi A, Done E, Nicolaides KH, Deprest J (2007c) Comparison of fetal lung area to head circumference ratio with lung volume in the prediction of postnatal outcome in diaphragmatic hernia. Ultrasound Obstet Gynecol 30:850–854

Jani J, Cannie M, Sonigo P, Robert Y, Moreno O, Benachi A, Vaast P, Gratacos E, Nicolaides K, Deprest J (2008b) Prenatal prediction of survival in diaphragmatic hernia by fetal lung volume measured by magnetic resonance imaging. Ultrasound Obstet Gynecol 32:793–799

Jani J, Benachi A, Nicolaides KH, Allegaert K, Gratacós E, Mazkereth R, Matis J, Tibboel D, van Heijst A, Storme L, Rousseau V, Greenough A, Deprest JA; and the antenatal-CDH-Registry group (2009) Prenatal prediction of neonatal morbidity in survivors with congenital diaphragmatic hernia: a multicenter study. Ultrasound Obstet Gynecol 33:64–69

Kalache KD, Espinoza J, Chaiworapongsa T, Londono J, Schoen ML, Treadwell MC, Lee W, Romero R (2003) Three-dimensional ultrasound fetal lung volume measurement: a systematic study comparing the multiplanar method with the rotational (VOCAL) technique. Ultrasound Obstet Gynecol 21:111–118

Keijzer R, Liu J, Deimling J, Tibboel D, Post M (2000) Dual-hit hypothesis explains pulmonary hypoplasia in the nitrofen model of congenital diaphragmatic hernia. Am J Pathol 156:1299–1306

Keller TM, Rake A, Michel SC, Seifert B, Wisser J, Marincek B, Kubik-Huch RA (2004) MR assessment of fetal lung development using lung volumes and signal intensities. Eur Radiol 14:984–989

Kitano Y, Nakagawa S, Kuroda T, Honna T, Itoh Y, Nakamura T, Morikawa N, Shimizu N, Kashima K, Hayashi S, Sago H (2005) Liver position in fetal congenital diaphragmatic hernia retains a prognostic value in the era of lung-protective strategy. J Pediatr Surg 40:1827–1832

Laudy JA, Wladimiroff J (2000) The fetal lung 2: pulmonary hypoplasia. Ultrasound Obstet Gynecol 16:482–494

Laudy JAM, Van Gucht M, Van Dooren MF, Wladimiroff JW, Tibboel D (2003) Congenital diaphragmatic hernia. an evaluation of the prognostic value of the lung-to-head ratio and other prenatal parameters. Prenat Diag 23:634–639

Lipshutz GS, Albanese CT, Feldstein VA, Jennings RW, Housley HT, Beech R, Farrell JA, Harrison MR (1997) Prospective analysis of lung-to-head ratio predicts survival for patients with prenatally diagnosed congenital diaphragmatic hernia. J Pediatric Surg 32:1634–1636

Mahieu-Caputo D, Sonigo P, Dommergues M, Fournet JC, Thalabard JC, Abarca C, Benachi A, Brunelle F, Dumez Y (2001) Fetal lung volume measurement by magnetic resonance imaging in congenital diaphragmatic hernia. BJOG 108:863–868

Mahieu-Caputo D, Aubry MC, El Sayed M, Joubin L, Thalabard JC, Dommergues M (2004) Evaluation of fetal pulmonary vasculature by power Doppler imaging in congenital diaphragmatic hernia. J Ultrasound Med 23:1011–1017

Manganaro L, Perrone A, Sassi S, Fierro F, Savelli S, Di Maurizio M, Tomei A, Francioso A, La Barbera L, Giancotti A, Ballesio L (2008) Diffusion-weighted MR imaging and apparent diffusion coefficient of the normal fetal lung: preliminary experience. Prenat Diagn 28:745–748

Metkus AP, Filly RA, Stringer MD, Harrison MR, Adzick NS (1996) Sonographic predictors of survival in fetal diaphragmatic hernia. J Ped Surg 31:148–151

Moeglin D, Talmant C, Duyme M, Lopez AC, CFEF (2005) Fetal lung volumetry using two- and three-dimensional ultrasound. Ultrasound Obstet Gynecol 25:119–127

Moore RJ, Strachan B, Tyler DJ, Baker PN, Gowland PA (2001) In vivo diffusion measurements as an indication of fetal lung maturation using echo planar imaging at 0.5T. Magn Reson Med 45:247–253

Muratore C, Kharasch V, Lund D, Sheils C, Friedman S, Brown C, Utter S, Jaksic T, Wilson J (2001a) Pulmonary morbidity in 100 survivors of congenital diaphragmatic hernia monitored in a multidisciplinary clinic. J Pediatr Surg 36:133–140

Muratore C, Utter S, Jaksic T, Lund D, Wilson J (2001b) Nutritional morbidity in survivors of congenital diaphragmatic hernia. J Pediatr Surg 36:1171–1176

Norio R, Kaariainen H, Rapola J, Herva R, Kekomäki M (1984) Familial CDH defects: aspects of etiology, prenatal diagnosis and treatment. Am J Med Genet 17:471–483

Osada H, Kaku K, Masuda K, Iitsuka Y, Seki K, Sekiya S (2004) Quantitative and qualitative evaluations of fetal lung with MR imaging. Radiology 231:887–892

Paek BW, Coakley FV, Lu Y, Filly RA, Lopoo JB, Qayyum A, Harrison MR, Albanese CT (2001) Congenital diaphragmatic hernia: prenatal evaluation with MR lung volumetry-preliminary experience. Radiology 220:63–67

Ruano R, Benachi A, Joubin L, Aubry MC, Thalabard JC, Dumez Y, Dommergues M (2004) Three-dimensional ultrasonographic assessment of fetal lung volume as prognostic factor in isolated congenital diaphragmatic hernia. BJOG 111:423–429

Rypens F, Metens T, Rocourt N, Sonigo P, Brunelle F, Quere MP, Guibaud L, Maugey-Laulom B, Durand C, Avni FE, Eurin D (2001) Fetal lung volume: estimation at MR imaging-initial results. Radiology 219:236–241

Sbragia L, Paek B, Filly RA, Harrison MR, Farrell J, Farmer D, Albanese CT (2000) Congenital diaphragmatic hernia without herniation of the liver: does the lung-to-head ratio predict survival? J Ultrasound Med 19:845–848

Scott L (2004) Ontario Congenital Anomalies Study Group. Apparent truth about congenital diaphragmatic hernia: a population-based database is needed to establish benchmarking for clinical outcomes for CDH. J Pediatr Surg 39:661–665

Sharland GK, Lockhart SM, Heward AJ, Allan LD (1992) Prognosis in fetal diaphragmatic hernia. Am J Obstet Gynecol 166:9–13

Skari H, Bjornland K, Haugen G, Egeland T, Emblem R (2000) CDH: a meta-analysis of martoality factors. J Ped Surg 35:1187–1197

Slavotinek AM (2005) The genetics of congenital diaphragmatic hernia. Sem Perinatol 29:77–85

Sokol J, Bohn D, Lacro R, Ryan G, Stephens D, Rabinovitch M, Smallhorn J, Hornberger LK (2002) Fetal pulmonary artery diameters and their association with lung hypoplasia and postnatal outcome in congenital diaphragmatic hernia. Am J Obstet Gynecol 186:1085–1090

Stefanutti G, Filippone M, Tommasoni N, Midrio P, Zucchetta P, Moreolo GS, Toffolutti T, Baraldi E, Gamba P (2004) Cardiopulmonary anatomy and function in long-term survivors of mild to moderate congenital diaphragmatic hernia. J Pediatr Surg 39:526–531

Stege G, Fenton A, Jaffray B (2003) Nihilism in the 1990s: the true mortality of congenital diaphragmatic hernia. Pediatrics 12:532–535

Thebaud B, Azancot A, de Lagausie P, Vuillard E, Ferkadji L, Benali K, Beaufils F (1997) Congenital diaphragmatic hernia: antenatal prognostic factors. Does cardiac ventricular disproportion in utero predict outcome and pulmonary hypoplasia? Intensive Care Med 23:10062–10069

Torfs CP, Curry CJ, Bateson TF, Honoré LH (1992) A population-based study of congenital diaphragmatic hernia. Teratology 46:555–565

Trachsel D, Selvadurai H, Bohn D, Langer JC, Coates AL (2005) Long-term pulmonary morbidity in survivors of congenital diaphragmatic hernia. Pediatr Pulmonol 39:433–439

Walsh DS, Hubbard AM, Olutoye OO, Howell LJ, Crombleholme TM, Flake AW, Johnson MP, Adzick NS (2000) Assessment of fetal lung volumes and liver herniation with magnetic imaging in congenital diaphragmatic hernia. Am J Obstet Gynecol 183:1067–1069

West S, Wilson J (2005) Follow up of infants with congenital diaphragmatic hernia. Semin Perinatol 29:129–133

Williams G, Coakley FV, Qayyum A, Farmer DL, Joe BN, Filly RA (2004) Fetal relative lung volume: quantification by using prenatal MR imaging lung volumetry. Radiology 233:457–462

Witters I, Legius E, Moerman P, Deprest J, Van Schoubroeck D, Timmerman D, Van Assche FA, Fryns JP (2001) Associated malformations and chromosomal anomalies in 42 cases of prenatally diagnosed diaphragmatic hernia. Am J Med Genet 103:278–282

Treatment of Congenital Diaphragmatic Hernia

Jan Deprest, Roland Devlieger, Maissa Rayyan, Chris Vanhole, Najima El handouni, Filip Claus, Steven Dymarkowski, Marc Van de Velde, Kypros Nicolaides, and Eduardo Gratacos

Contents

Abstract

› Congenital diaphragmatic hernia (CDH) can be associated with genetic or structural anomalies that render the prognosis overall poor. In isolated cases, survival is dependent on the degree of lung hypoplasia and potentially also liver position. Isolated CDH remains today, fatal in around 30% of prenatally diagnosed cases. Cases should be referred in utero to tertiary care centers familiar with this condition for comprehensive assessment, prediction of individual outcome as well as timed delivery. Individual prognosis can be estimated based on lung size measurement as well as documentation of the degree of liver herniation into the thorax. The use of imaging to document pulmonary vascularization is promising, but is at present still under investigation. Based on the predicted survival rate, parents can be counseled about their options. In those with a poor prognosis, termination of pregnancy can be considered. Antenatal intervention, aiming to stimulate lung growth, has become an alternative for these cases. Lung growth is triggered by temporary fetal endoscopic tracheal occlusion (FETO). Growing experience has demonstrated the feasibility and safety of the technique, and survival has increased from around 15% to over 50% in this group. In Europe a trial has now started, documenting the place of FETO in moderate cases (predicted survival rate 50%), and soon also in severe cases. It is hypothesized that prenatal intervention might decrease oxygen dependency in survivors (moderate), or increase survival (severe).

J. Deprest (✉), R. Devlieger, M. Rayyan, C. Vanhole, and N. El handouni
Division of Woman and Child, University Hospitals Leuven, 3000 Leuven, Belgium
e-mail: jan.deprest@uz.kuleuven.ac.be

F. Claus and S. Dymarkowski
Division of Medical Imaging, Unit of Radiology, University Hospitals Leuven, 3000 Leuven, Belgium

M. Van de Velde
Division of Critical Care, Unit of Anaesthesiology, University Hospitals Leuven, 3000 Leuven, Belgium

K. Nicolaides
King's College Hospital, Denmark Hill, London SE5 9RD, UK

E. Gratacos
Dept. Obstetrics & Gynaecology, Fetal Medicine Unit Hospital Clinic, Sabino de Arana 1, Barcelona 08028, Spain

D. Prayer (ed.), *Fetal MRI*, Medical Radiology,
DOI: 10.1007/174_2010_22, © Springer-Verlag Berlin Heidelberg 2011

1 Introduction

Congenital diaphragmatic hernia (CDH) occurs sporadically with an incidence of 1–2/5,000 of newborns, depending on whether stillbirths are included or not. CDH does not designate one single clinical entity, and outcomes are diverse. The embryology, molecular and genetic mechanisms behind this anomaly are beyond the scope of this chapter, for which we refer to the literature. The majority of lesions are left sided (84%), 13% right sided, and bilateral lesions, complete agenesis, eventration and other rare malformations can also occur. Associated anomalies occur in up to 40% of cases. They are an independent predictor of neonatal death, with less than 15% of babies surviving in this group. As a consequence, the majority of cases are apparently isolated although they might still be part of a yet unidentified spectrum of a polygenic disease affecting perhaps multiple organs.

CDH essentially points to an anatomical and surgically correctable defect in the diaphragm. However, the clinical relevance lays in the abnormal lung development that accompanies the condition. The changes in the lung are usually seen as a direct consequence of compression by herniating viscera during pregnancy, although this is probably only partly true. Some even argue that CDH actually arises in the lung. In essence, lungs in fetuses with CDH have a reduced number of conducting airways as well as vessels. There are fewer alveoli, thickened alveolar walls, increased interstitial tissue, markedly diminished alveolar air space and gas-exchange surface area. There are a reduced number of vessels, adventitial thickening, medial hyperplasia and peripheral extension of the muscle layer into the smaller intraacinary arterioles. CDH lungs are not surfactant deficient. It is important to realize that both lungs are affected, but the one that is on the side of the lesion is indeed more affected than the contralateral one. There may be other anatomic aberrations present in the diaphragm and in the upper gastrointestinal tract, such as the position of the liver, lower esophagus and stomach.

Today, screening programs allow prenatal detection of the condition, at least in two cases out of three (Garne et al. 2002). Normal chest findings (Chap. 16) and the typical presentation as well as differential diagnosis of CDH (Chap. 23) are discussed more in detail elsewhere in this book. Herein, only the essentials of the prenatal prediction of outcome will be summarized, as this is highly relevant to perinatal management, including fetal therapy.

2 Clinical Presentation and Natural History

The above *morphologic* changes become obvious when the lung becomes *functional* at birth. These lead to variable degrees of respiratory insufficiency and pulmonary hypertension (PH). Reduction of the available air space and vascular bed leads to hypoxia, hypercarbia as well as PH. The aberrant vasculature is also more sensitive to pulmonary vasoconstriction, which worsens PH, further increasing the right-to-left shunt. This leads to a vicious cycle preventing gas exchange of the shunted blood, increasing acidosis and hypoxia (Fig. 1). Before the 1990s the cornerstone of neonatal management was aggressive hyperventilation and hyperoxygenation, together with other measures for controlling PH, and *emergency* repair of the defect. These two tenets have been questioned and today "gentle ventilation" followed by delayed surgery has improved results. Gentle ventilation protocols or spontaneous breathing, with permissive hypercapnea and minimal sedation reduce baro- and volutrauma (Boloker et al. 2002). High frequency oscillatory ventilation (HFOV) has been suggested as a *primary* ventilation mode in cases of lung hypoplasia, but most centers use it as *rescue* therapy prior to the eventual use of extra corporeal membrane oxygenation (ECMO) (Smith et al. 2005). The so-called VICI-trial is designed to determine the place of HFOV and has been initiated in Europe. PH is treated by early administration of inhaled nitric oxide (iNO) (Kinsella et al. 2003). Also it has been suggested that, keeping the ductus arteriosus patent by administration of prostaglandins PGE_1 in case of severe secondary left ventricular cardiac dysfunction may be beneficial (Kinsella et al. 2005). Some centers are proponents of a liberal use of ECMO (Khan and Lally 2005), but its role has been criticized because of unproven benefits, its inherent complications and because it is not widely available.

With advances in neonatal therapy one would expect to continue seeing increasing survival rates. Reported survival rates vary widely for a number of reasons. Some series include cases with associated anomalies,

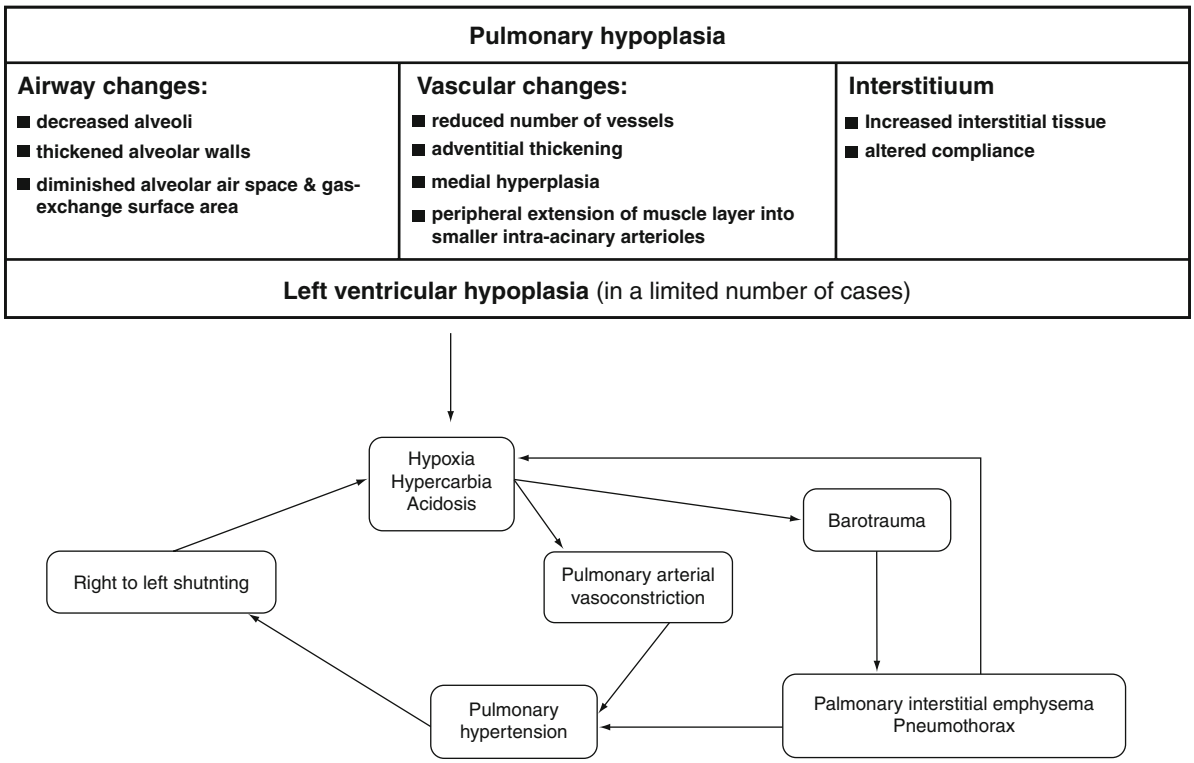

Fig. 1 Pathophysiology of neonatal lung function in congenital diaphragmatic hernia (CDH). (From: Done et al. (2008) – with permission from Wiley)

while others do not. Some studies only consider cases from birth onwards, but that may be inborn cases, or only those who survive transfer to the tertiary unit (outborn). Further, there is other so-called "hidden mortality," i.e., termination of pregnancy in case of prenatal diagnosis, which may cause an apparent improvement in survival (Stege et al. 2003). In the UK, termination rates range from 9% for isolated CDH to 51% in case of associated anomalies (Tonks et al. 2004). To that adds a spontaneous intrauterine fetal death rate of 1–2%, which is often forgotten (Gallot et al. 2007).

Statistics may also be influenced by in utero referral to a tertiary centre with more experience. For example, in France this policy significantly increased survival from 41 to 66% ($p = 0.03$) (Gallot et al. 2007). Centralized management, with increased case load and using consistent neonatal protocols has also lead to increased survival rates in Canada, high volume centers being defined as >12 CDH admissions over a 22 months, resulting in a 13% higher survival rates than low volume centers (Javid et al. 2004). All these factors make it difficult to define the "natural history" of isolated CDH, i.e., outcome with best reasonable postnatal management. Despite this uncertainty, recent statistics from large centers on both sides of the ocean keep on facing a survival rate for isolated CDH of 50–70% (Stege et al. 2003; Gallot et al. 2005; Sartoris et al. 2006; Hedrick et al. 2007; Yang et al. 2007; Datin-Dorriere et al. 2008). This number coincides with that from the world wide registry of the CDH study group (60–70% survival rate). Occasionally, rates in excess of 80–90% are quoted, usually claiming this is a result of a certain management protocol, but most such statements remain unsubstantiated.

Survivors may have significant morbidity, including pulmonary, nutritional (gastro-esophagal reflux and feeding problems), orthopedic, hearing and neurodevelopmental problems. For this reason survivors should remain in long-term specialized multidisciplinary follow up programs.

3 Prenatal Diagnosis and Prediction of Outcome

In the last 20 years, prenatal detection rates significantly improved, from 15% in the mid-eighties to around 60% today (Garne et al. 2002). In cases of suspected CDH, parents should be referred to a tertiary centre used to managing serious congenital anomalies both in the prenatal and postnatal period. They will make a comprehensive diagnostic and prognostic assessment, including advanced structural evaluation, and genetic testing. We refer to Chap. 23 for the features of CDH itself as well as the differential diagnosis. Associated and/or genetic or syndromal anomalies must be ruled out. Once the assessment is complete, parents are to be counseled by the various specialists who will be involved in perinatal care. They can base their decisions on the individualized prognostic estimation. Again this is explained in detail in Chap. 23, but the essentials of that process are briefly summarized, as they are key to the planning of therapy in the prenatal period.

3.1 2D-Ultrasound of the Contralateral Lung Area and Liver Herniation

Both position of the liver and lung size have been long time recognized to be important predictors. The best validated prediction method is by 2D ultrasound measurement of the lung area contralateral to the lesion, which is related to the head circumference of the fetus. This is the so-called lung-to-head ratio (LHR) and is most accurate by tracing the lung contours (Metkus et al. 1996; Peralta et al. 2005) (Fig. 2). LHR is a function of gestational age, as the normal lung area increases four times more than the head circumference between 12 and 32 weeks. That effect can be discounted by expressing what is measured as LHR (called *observed*) as a proportion to what LHR is *expected* in a normal fetus at the same gestational age (Peralta et al. 2005). Normative curves for LHR are available for all measurement methods; for instance, when tracing a lefts sided hernia it can be easily calculated as left LHR = −1.4815 + 0.1824 × gestation (weeks) −0.0023 × gestation (weeks)^2. In view of the trials described below, an easy tool to calculate a lung areas and O/E LHR with the different methods and for left and right sided cases will be available on the website of the TOTAL-trial (www.totaltrial.eu).

Several recent studies have confirmed that both LHR and liver position relate to survival (Hedrick et al. 2007; Yang et al. 2007; Datin-Dorriere et al. 2008). Numerically most important are the data from the "antenatal CDH registry," that first looked at outcomes of 184 consecutive fetuses with isolated left-sided CDH, managed at ten tertiary centers (Jani et al. 2006). In a second report on 354 cases over a wider range of gestation, the O/E LHR was used, this time including a reasonable number of right sided lesions (Jani et al. 2007a, b, c). In that study, the position of the liver was no longer an independent predictor of outcome. Prediction was better late in gestation, as earlier suggested by others (Jani et al. 2008a, b; Yang et al. 2007). More importantly, O/E LHR also correlates with short term morbidity indicators such as oxygen and ventilatory needs as well as the requirement for patch repair (Jani et al. 2009).

Based on the consistency of these observations, we proposed to stratify fetuses with isolated left sided CDH according to prenatal measurements and expected survival (Deprest et al. 2009a, b; Fig. 3) when counseling parents in the prenatal period. In order to predict survival, both O/E LHR and the position of the liver were used, given the uncertainty whether these are independent predictors. Postnatal survival chances correspond with the perceived severity, ranging from extreme (those without reasonable hope for survival) to mild cases (those with an over 80% survival rate).

- *Extreme* hypoplasia allows with the current state of affairs, virtually no survival chances. This corresponds with fetuses with an O/E LHR ≤ 15%, their liver is typically up. Early morbidity rates in these are not known because of lack of observations.
- *Severe* hypoplasia corresponds with a survival rate of <20%, and more than 70% of fetuses are oxygen dependent at 1 month of life, in other words having bronchopulmonary dysplasia (BPD). This corresponds with an O/E LHR of 16–25%, irrespective of the liver position.
- *Moderate* hypoplasia corresponds with an overall survival rate of 50%. This includes fetuses with an O/E LHR 26–35% (irrespective of the liver position) or with an O/E LHR 36–45% and the liver up. The rate of BPD is around 30%.
- *Mild* hypoplasia is likely to result in survival (>75%). These are fetuses with an O/E LHR

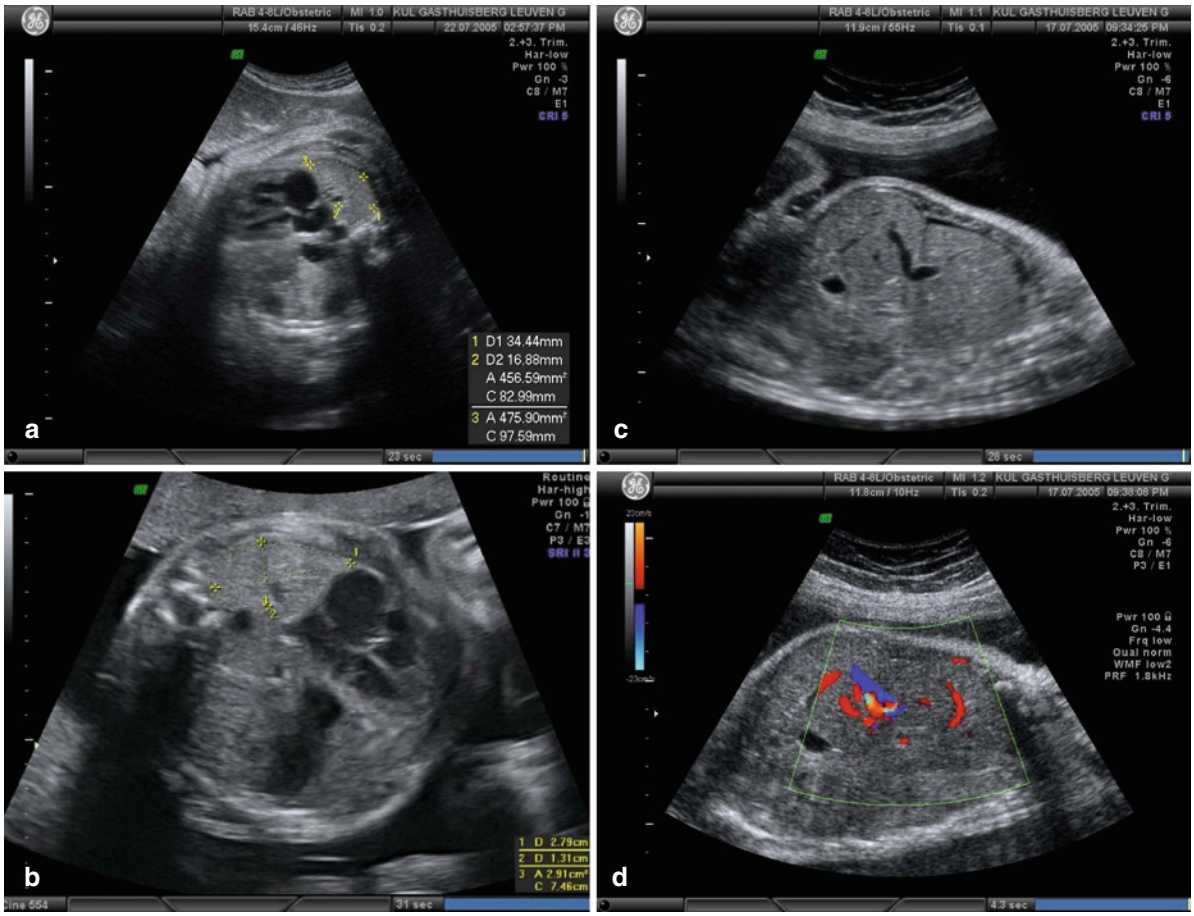

Fig. 2 Fetus with CDH on 2D ultrasound before and after fetal therapy. (**a**) measurement of the lung in a section through the four chamber view with the so-called "longest axis method" as well as "tracing method." These dimensions will be used to calculate the lung-to-head ratio. (**b**) Measurement of the lung 1 day after balloon insertion, with changed echogenicity and dimensions. (**c**) Herniation of the liver. (**d**) Visualization of the major vessels helps in its identification

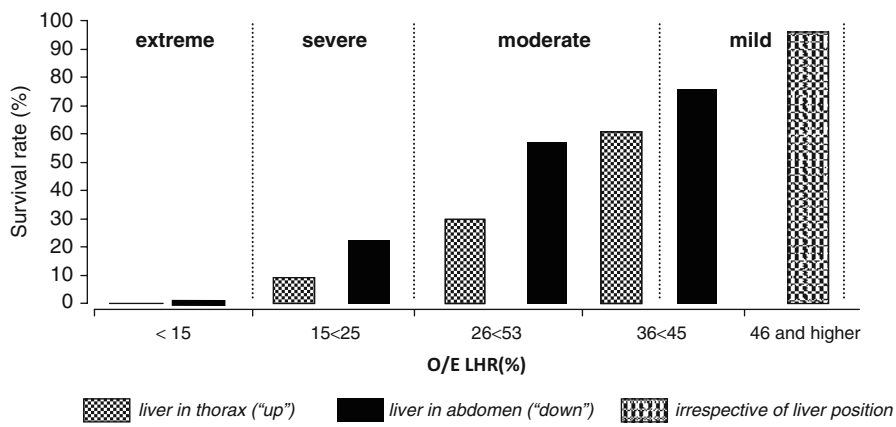

Fig. 3 Survival rates of fetuses with isolated left-sided CDH, depending on measurement of the observed/expected lung:head ratio (O/E LHR) measurements and liver position as in the antenatal CDH registry. (From Deprest et al. (2009a, b))

36–45% and the liver down, and those with an O/E LHR >45%. In this group, the rate of BPD is around 10%.

- The antenatal CDH registry study is also one of the few prenatal studies reporting outcomes of 25 fetuses *right*-sided lesions, which have overall poorer outcomes (44% survival only). Along the same lines, an O/E LHR < 45% would be classified as severe hypoplasia, because of predicted poor survival chances.

3.2 3D Volumetric Assessment of Lung Size and Liver Herniation

2D-ultrasound is widely available and the method is well standardized. For that reason, it will probably remain the most used clinical method for quite a while. LHR however measures only one lung in one section, while volumetric methods are these days available as well and can measure both lungs. It is here that MRI plays an important role, much more so than 3D ultrasound, which theoretically has the same potential. Again, we refer for details to Chap. 23 and would summarize the status as follows. With 3D ultrasound, one fails to measure the ipsilateral lung in 40% of cases. This is not the case when using MRI (Jani et al. 2007b). Compared to ultrasound, MRI offers a superb tissue contrast, allowing accurate volumetric measurements, even in case of obesity and reduced amniotic fluid volume.

MRI lung measurements of the index cases must also be expressed as a function of what is expected in a normal fetus. Historically, matches were chosen based on gestational age (Coakley et al. 2000), or biometric variables such as liver volume (Williams et al. 2004), and more accurately, fetal body volume (Cannie et al. 2006) (Fig. 4). This discounts the effect of unknown gestational ages and growth differences (Cannie et al. 2008a, b). We expect MRI volumetry to become the method of choice, when others validate preliminary European findings, which coincide with the earlier observed relationship of lung size using ultrasound, and survival (Jani et al. 2008a, b). However, it will be virtually impossible to demonstrate statistically the superiority of 3D-volumetry over 2D-area measurement (Cannie et al. 2008a, b).

MRI can also be used to quantify the degree of liver herniation as a continuous, rather than a categorical variable. Again different landmarks and subsequent methods have been proposed. Walsh et al. (2000) was the first to propose to use the distance between the most apical part of the liver and the dome of the chest which is then divided by the distance between the diaphragmatic remnant and the thoracic apex. Cannie proposed to consider cases as "liver up" when the liver was above a reference line between the lower tip of the xyphoid and the corresponding vertebral body (Cannie et al. 2008b) (Fig. 5). The volume of the herniated liver can be subsequently quantified and expressed as a proportion of the thorax, the so-called liver to thorax ratio (LiTR). In a first report on 40 patients from Lille and Leuven, the herniated liver volume was compared to total lung volume. At first glance, LiTR and lung volume are inversely related, but in reality they are independent in cases with liver up (LiTR > 0).

3.3 Prediction of Pulmonary Arterial Hypertension

Next to ventilatory insufficiency, PH is a major neonatal problem. It is believed to find its origins in structural vessel changes, which in theory might be documented during fetal life. One can measure number of branches, vessel diameters and flow velocimetry or flow volume with 2D or 3D techniques. There has been recently a lot of work done in this field, as recently summarized by Gucciardo et al. (2008). The validation status of these techniques is at this moment more limited, both in terms of numbers as well as reproducibility among centers. The most important work comes according to us from Toronto resp. Paris. Hornberger et al. demonstrated that the ipsilateral branch main pulmonary vessel diameter is related to outcome. Ruano established nomograms for branch main pulmonary artery (PA) diameters (Ruano et al. 2007), but the Necker group (Paris) also used 3D power Doppler to assess the entire lung vasculature for the prediction of survival as well as the occurrence of PH (Ruano et al. 2006). Recently, we studied the value of the peak early-diastolic reversed flow (PEDRF) and a number of other Doppler indices in proximal arterial branches in the controlateral lung, but also in three out of four ipsilateral lungs (Moreno-Alvarez et al. 2008). We observed a strong correlation of PEDRF with o/e LHR, but the added value of this parameter in prediction needs to be determined. We have further studied

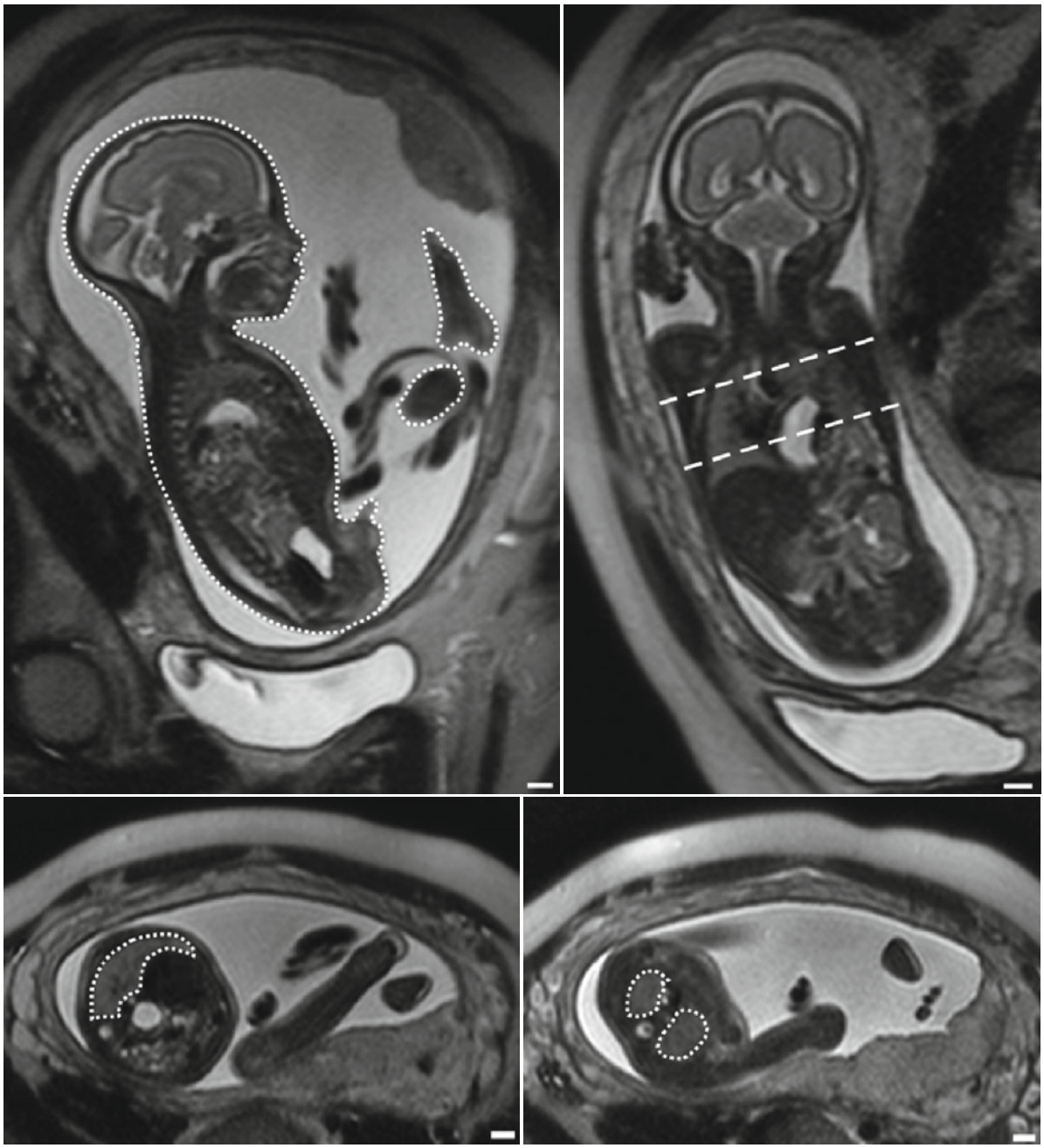

Fig. 4 T2-weighted images of fetus with left sided CDH at 26 weeks without liver herniation. *Top left*, sagittal section with tracing of the body contours. *Top right*: coronal view of the fetus demonstrating the level at which the two axial images are made (*bottom*). Lung tracing (*dotted line*) on the two axial views. Scale: *white bar* in *right lower corner* is 1 cm

pulmonary artery reactivity following maternal hyperoxygenation (Fig. 6). The so-called hyperoxygenation test involves Doppler measurements of the pulsatility index (PI) in the first branch of the contralateral pulmonary artery, before and after maternal administration of 60% O_2 by mask. A decrease of ≥20% of the PI-value after O_2 exposure is considered reactive (Broth et al. 2002). In an initial study on 22 fetuses with severe CDH evaluated after 30 weeks, a reactive test was predictive of survival, whereas a negative test predicted an

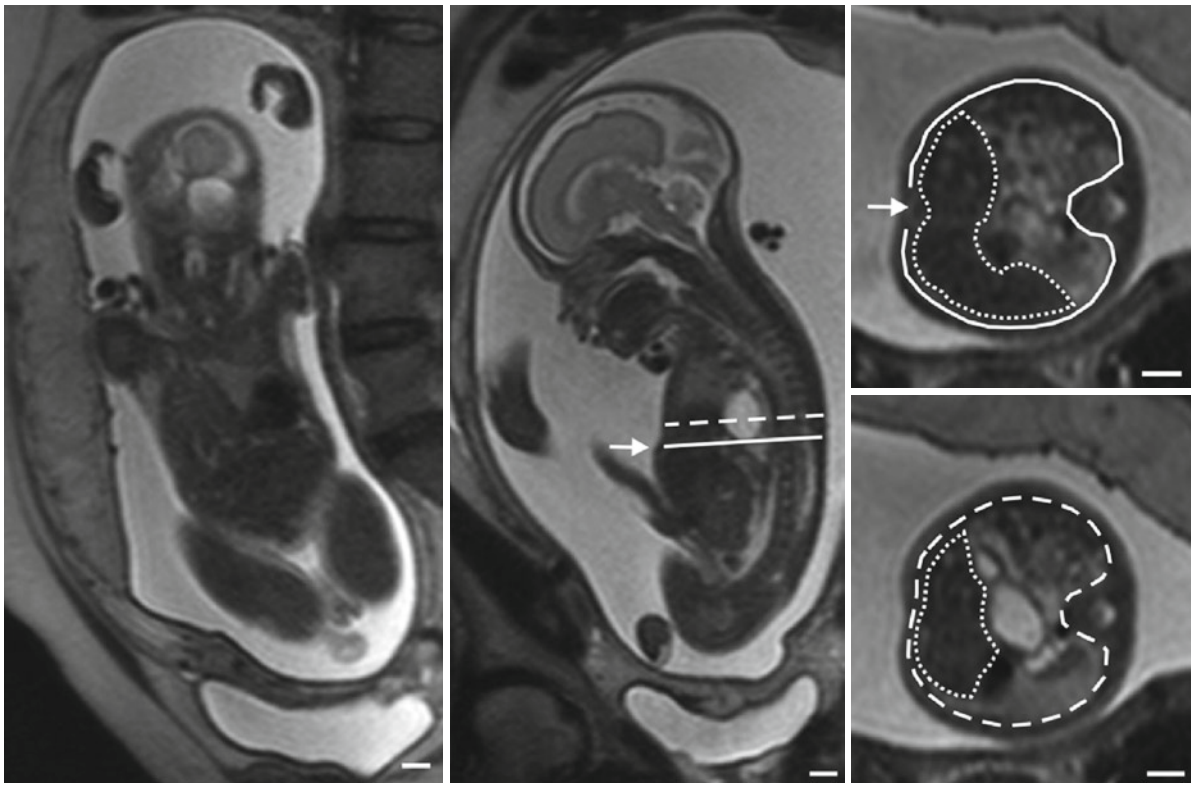

Fig. 5 T2-weighted images of fetus with left sided CDH at 26 weeks with liver herniation, as best shown on coronal view (*left image*). Sagittal view (*middle*) demonstrating the reference line (*full line*) at the level of the xyphoid process (*white arrow*) and above (*dashed line*), which correspond to the axial images on the *right*. Liver tracing (*dotted line*) and contours of the thoracic cavity (*full* and *dashed lines*) shown on both axial views. Scale: *white bar* in *right lower corner* is 1 cm

increased risk for severe PAH and neonatal death (Done et al. 2010). Unfortunately, this test can only be done in late gestation so that it may not be that useful for prenatal decision making, unless for instance referral to an ECMO center – once validated.

4 Clinical Fetal Tracheal Occlusion

4.1 The Concept of Fetal Therapy and Rationale of Tracheal Occlusion

Under the assumption that a population who cannot be salvaged postnatally, can be identified before birth, one may attempt an *antenatal* intervention that restores the pulmonary hypoplasia. In analogy to postnatal repair, in utero anatomical correction of the defect was first considered. It would even allow improved lung development, but it technically requires open fetal surgery. Neither can it be offered to fetuses with liver herniation, which is present in the worst cases, because reduction of the liver kinks the vital umbilical circulation (Harrison et al. 1993). As an alternative, lung growth can be triggered by tracheal occlusion (TO) (DiFiore et al. 1994). We refer to the specialized literature for the experimental basis of TO (Nelson et al. 2006; Khan et al. 2007). Normal lung growth and maturation is steered through a process of cyclical pressure changes in the airways. During fetal life the lung secretes fluid, that cannot escape as long as the glottis is closed, therefore acting as a stenting force within the fetal airways. During fetal breathing movements, the glottis opens and the pressure gradient is leveled. Prenatal TO increases airway pressure by entrapped fluid, causing proliferation, increased alveolar airspace and it also interferes with pulmonary vascular development. Sustained TO reduces surfactant expression, which is in part solved by release of the occlusion

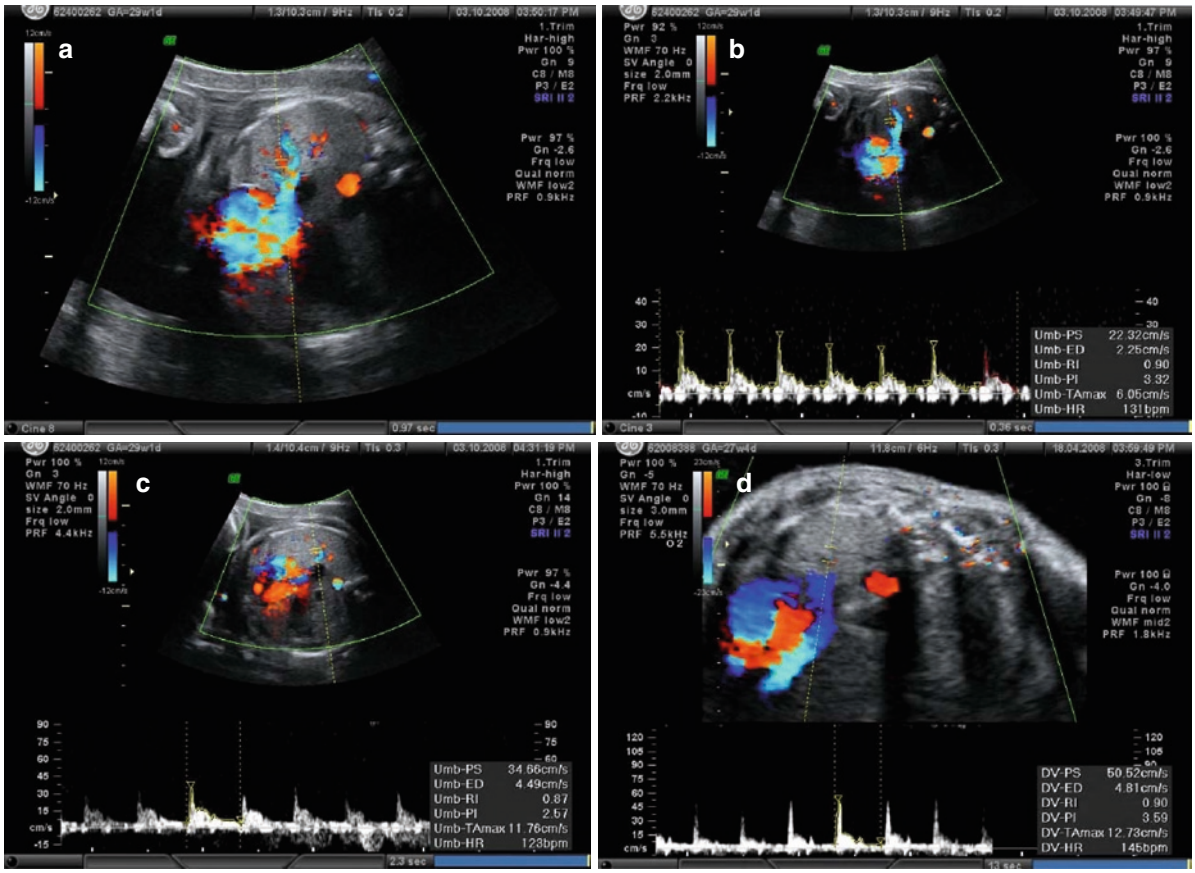

Fig. 6 Fetus with CDH at 29 weeks during a maternal hyperoxygenation study. (**a**) The first branch of the pulmonary artery contralateral to the lung lesion is identified with Doppler examination. (**b**) The pulsatility index is measured during inhalation of room air, in this case it is 3.32. (**c**) A second measurement is done after inhalation of 60% oxygen for 10 min. In this case the PI dropped to 2.57. Since the decrease is more than 20%, the test is considered positive. (**d**) Same as **c**, but in a case with negative test at 27 weeks, with a measurement at baseline of 3.88 (not shown) and after oxygen of 3.59 (7% drop). Images: courtesy Elisa Done'

before birth. We captured this two step intervention under the name "plug–unplug sequence" (Flageole et al. 1998). Based on experimental findings in sheep and extrapolation to human lung developmental phases, the balloon is inserted at 26–28 weeks and removed at 34 weeks, at least in severe cases (Deprest et al. 2006a, b). Also other prenatal factors may improve the ultimate pulmonary architecture, lung function, mechanics and hemodynamic, such as antenatal injection of steroids or postnatal administration surfactant, as well as factors beyond control, like gestational age at birth, the initial severity of lung hypoplasia and lung response to TO.

Clinical TO was first achieved through maternal laparotomy, hysterotomy, neck dissection and clipping (Flake et al. 2000). We first described the use of an endoluminal balloon to be inserted by fetoscopic route, which accommodates the increasing diameter of the fetal trachea during gestation, and has the potential for ultrasound guided puncture (Flageole et al. 1998). This was clinically first applied through hysterostomy and 5 mm equipment (Harrison et al. 2003a, b). We proposed a procedure today referred to as fetoscopic endoluminal tracheal occlusion (FETO), which can be done percutaneously via a 3.3 mm cannula and under local or loco-regional anesthesia (Deprest et al. 2004). Until 2008, the FETO-consortium has been offering FETO only to fetuses with severe or extreme pulmonary hypoplasia. This consortium groups fetal medicine units of Leuven, London and Barcelona. That will change now: a trial in moderate cases has been proposed and it is estimated that the group will be soon embracing other high volume fetoscopic units who are training in this procedure.

4.2 Percutaneous Fetoscopic Endoluminal Tracheal Occlusion with a Balloon

4.2.1 Instruments

The instrumentation for this operation has been purposely designed by Karl Storz Endoskope (Tuttlingen, Germany), with support from the European Commission within the "Eurostec" R&D project (Deprest et al. 2006a, b; Klaritsch et al. 2009). For balloon insertion we use a 1.3 mm fiber endoscope (11630 AA; Fig. 7c),within a 3.3 mm outer diameter sheath with three side openings, allowing for amnioinfusion, a forceps or puncture needle and the microcatheter-system (Fig. 7d). This sheath is slightly curved and blunted at its tip. The cannula is the same as what is used for fetoscopic laser coagulation, i.e., a 10 Fr (3.3 mm) Teflon cannula (Check-Flo Performer® Introducer Set, Cook Medical Inc., Bloomington, Fig. 7a), loaded with an appropriately sized pyramidal trocar (11650 TG) or to be inserted over a guide wire (Seldinger technique). The detachable latex balloon is one borrowed from interventional radiology (Goldbal 2, Balt, Paris, France), which is first tested by filling with 0.6 mL isotonic contrast agent fluid. (Fig. 7b). This volume and balloon provides dimensions in proportion to the third trimester fetal trachea. For fetoscopic retrieval a 3 Fr (1 mm) forceps (11510C) or puncture needle (11506P) is used. For retrieval during an EXIT procedure we use a shorter and wider, double flow tracheoscopic instrument (26161 CN/CD) of 4.3 mm in diameter and a working channel for the needle or forceps. This sheath is loaded with a rod lens 2 mm telescope (26008 AA). A laryngoscopic set is under development.

The fetoscope is connected to a high quality cold light source (e.g., Xenon light 300 CB) via an adapted small diameter (2.5 mm) light cable that matches the light transmission bundle. It is useful to choose the longer cables (e.g., 230 cm) to allow different positions of the equipment to the patient. Cameras are no different

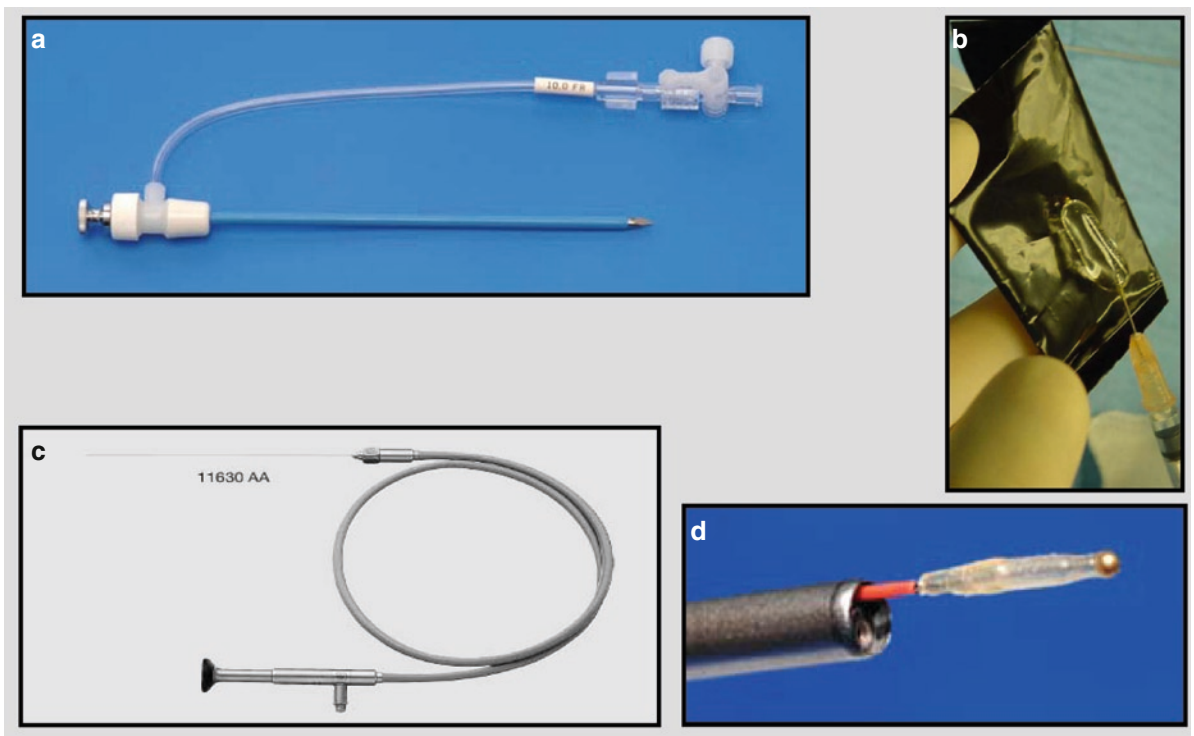

Fig. 7 Instrumentation for fetoscopic endoluminal tracheal occlusion (FETO). (**a**) Cannula for uterine access, which can be loaded with a pyramidal trocar or inserted over a guide wire. (**b**) Testing of the balloon, prior to insertion. It is inflated via a blunt needle with 0.8 mL isotonic fluid. (**c**) Semirigid fetoscope with deported eyepiece (**d**) fetoscope within sheath, through which a catheter with balloon is inserted. Note the blunted tip of the sheath

from those used in laparoscopy, but the generated image is not the only one that is relevant to the operative team. Half if not more of the manipulation is guided by US and therefore the operator must be able to see both images during the entire operation. Images can be displayed separately or as a "Picture in Picture" generated by software within modern screens or a video mixer. We use modern high resolution ultrasound offering the possibility of 2D and 3D ultrasound as well as Doppler examination (Voluson 730 Expert, GE Medical Systems, Zipf, Austria). Whether 3D-ultrasound is of any relevant role is very doubtful.

4.2.2 Procedure and Perioperative Care

The time point in pregnancy balloon insertion will take place is depending on severity of the hypoplasia, or in cases with late diagnosis, at the earliest convenience (Sect. 3.2). We do our operations under loco-regional or local anesthesia, in sterile conditions within a fully equipped and staffed operation theatre. When the fetus is judged viable, everything is ready for operative delivery and a neonatologist is on standby. Perioperative tocolysis consists of either indomethacin or tractocile, antibiotic coverage (cefazolin 2 g I.V. preoperatively; in case of allergy: erythromycin) and gastric acid reductors. Steroids (bethamethasone; two intramuscular injections of 12 mg over 24 h) are only administered in case of fear of preterm delivery; they have no other established role in the treatment of CDH as surfactant deficiency has recently been revoked. On ultrasound examination, the position of the fetus and placenta is determined, and whenever required an external version is done. The purpose is to have a smooth ultrasound guided access of the cannula towards the mouth. In that position the fetus is medicated with a mixture of fentanyl (15 μg/kg, for pain relief), pancuronium (0.2 mg/kg, for immobilization), and atropine (20 μg/kg, for the prevention of bradycardia, as has been described for other intrafetal procedures (Van de Velde et al. 2006)).

Following sterile draping the trocar is inserted under ultrasound guidance towards or into the mouth, whenever possible coming from a slightly cranial direction, so that the cannula will ultimately parallel as much as possible the course of the trachea. The philtrum and lips, the alveolar ridges and the ciliated upper part of the tongue, the raphe of the palate, the uvula and epiglottis, and the vocal cords are subsequent fetoscopic landmarks. The balloon is positioned between the carina and vocal cords, which is the narrowest part of the trachea. Intra-operative dislodgment can occur, so that a new one needs to be inserted. These balloons may also dislodge later (<5%), probably because their manually made valves, leak (which is not a problem for their actual indication but in this indication will prompt reinsertion). At the end of the procedure any redundant amniotic or infusion fluid is drained. Fetoscopic balloon retrieval is not much different from the above. At that time, the balloon is either withdrawn fetoscopically, or punctured under ultrasound guidance. In case of oligohydramnios because of rupture, prior amnioinfusion may help (Fig. 8).

4.2.3 Care During the Occlusion Period

In Europe patients undergoing fetoscopic surgery typically are admitted for 1–2 days, while kept on prophylactic tocolytics. Postoperative ultrasound examination for fetal wellbeing, balloon position and lung size is done during that period. Ultrasound follow up is further empirically set for every 2 weeks. We determine balloon position, measure lung response (LHR and volume, perfusion and pulmonary reactivity), amniotic fluid volume (deepest vertical pocket), and screen for occurrence of membrane separation and measure cervical length. We have not seen an abnormally vigorous lung response prompting the need for earlier balloon removal, but this has been reported by Flake et al. (2000). In the absence of any problems elective removal is planned at 34–35 weeks, where after the patient is transferred back to the referring tertiary institution. When there is membrane separation or shortening of the cervix, the risk of preterm prelabour rupture of the membranes (PPROM) and preterm delivery increases. Whether admission or any other measure can prevent this, remains to be demonstrated.

In Europe it is very uncommon that patients travel very far and stay over for longer periods, even for advanced care. There are a number of countries where some degree of centralization of care for CDH babies is present, however for the FETO baby, there is now a new problem. The baby has until removal of the balloon occluded airways and cannot be ventilated in a centre not prepared for this situation. This is definitely the Achilles' heel of the current occlusion device. In our experience we have seen dramas of patients who where

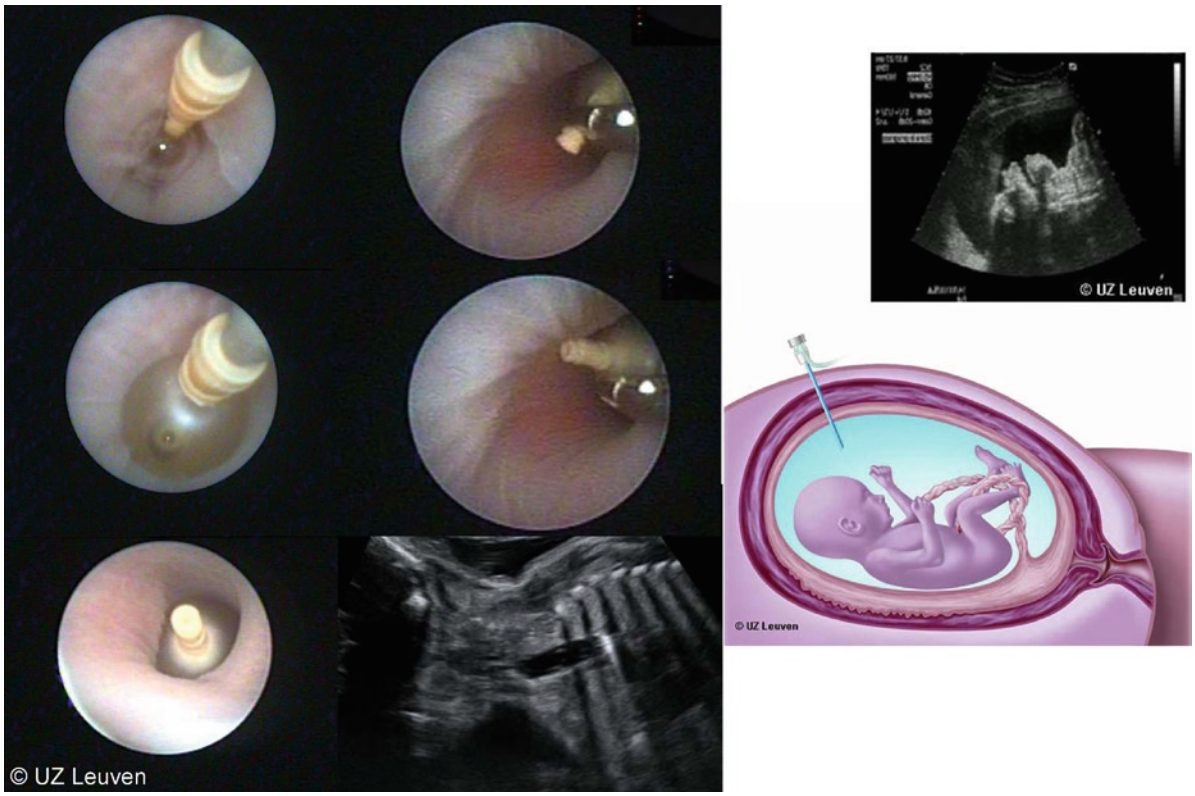

Fig. 8 *Left*: fetoscopic images of balloon insertion. The catheter, loaded with the balloon is inserted, the balloon inflated between carina and vocal cords and then detached. *Middle*, *bottom*: ultrasound image of the balloon in place. *Middle*, *upper two images*: balloon is being retrieved by fetoscopic extraction, using a 1 mm forceps. *Right*: schematic drawing of cannula insertion towards the mouth (*upper corner*). (From Gucciardo et al. 2008 – with permission from authors and Elseviers)

(purposely or involuntary) managed outside the FETO centers, eventually leading to a situation that the balloon could not be safely or not at all removed. We as a group have taken the commitment to organize ourselves with a 24/24 service of 3–4 operators able to remove the balloon in the peripartal period. This includes fetal medicine specialists (in utero fetoscopic or ultrasound guided removal or EXIT) and neonatologists and anesthesiologists (EXIT or postpartum retrieval). We also now have a support program funded by the Flemish Government (Instituut voor Wetenschap en Technologie, IWT 070715) that covers costs for stay over in a family room nearby the hospital as long as the balloon is in place. This is our preferential management during the occlusion period. Many patients prefer to travel home, which they must understand they are doing at their own risk. Although that risk seems completely out of proportion to the effort they have done to have the surgery per se, other psycho-emotional factors play a role in this decision, and we respect it. Patients at higher risk for earlier delivery, e.g., those with membrane separation, shortened cervix, polyhydramnios, are more than encouraged to stay on campus.

Amniorrhexis usually indicates iatrogenic membrane rupture but does not immediately lead to preterm labor. In that case, the patient is admitted and the balance of elective removal versus sustained occlusion, is daily made on an individual basis. If labor unexpectedly starts, the team is on site and EXIT services can be offered around the clock without any problem.

4.3 Initial Results with FETO for Extreme and Severe Hypoplasia

The initial results of this procedure were published in some overlapping reports (Jani et al. 2005). In brief, there were no maternal complications but iatrogenic preterm rupture of the membrane (iPPROM) remains a

major obstacle: around 20% rupture prior to 34 weeks. More than 75% of patients deliver beyond 34 weeks (mean GA at birth = 36 weeks), which is significantly more than the 31 weeks observed by Harrison et al. (2003b). This has an impact on survival, which in the early period can be as high as 75%.

Survival till discharge continues to be around 50–55% (Jani et al. 2006). Neonatal survival was higher with prenatal versus perinatal balloon retrieval (83.3 vs. 33.3%; $p = 0.013$), a trend persisting till discharge (67 vs. 33%; NS). Major other predictors of survival are gestational age at delivery and lung size prior to FETO (Table 1) (Jani et al. 2006). In other words, fetuses with the smallest lungs are less likely to respond to fetal therapy than those with larger lungs. Apart from that, the individual increase in lung area or volume after FETO is an independent predictor of survival (Jani et al. 2006; Peralta et al. 2008). Furthermore, the pulmonary vascular reactivity changes following FETO can be used for that purpose and is predictive of survival as well as the occurrence of PH (Done et al. 2010). Conversely the inability of the lung to respond to TO indicates that the neonate is highly likely to die from (persisting) pulmonary hypoplasia, which remains the leading cause of death.

Most babies require patch repair, indicating the size of the defect in this selected group. Short term morbidity in survivors is actually better than expected from the severity of lung hypoplasia. We showed that it is comparable to that of cases with moderate pulmonary hypoplasia, which were expectantly managed during pregnancy (Jani et al. 2007d). We have not been able so far to report on long term morbidity, partly due to the fact that most babies are not born at one of the FETO centers, making standardized follow up more difficult. Information via other tertiary centers is neither standardized and difficult. Based on the available feedback from those centers the nature of the morbidity in survivors is what one expects in babies with CDH. To date we are only aware of one baby with severe developmental delay following TO. The Flemish government (IWT 070715) is now partly supporting the recall of patients for such long term evaluation in Belgium and collaboration with Dutch and French centers should make evaluation of a reasonable number possible. This will be reported in due course in the medical literature.

5 The European Program in 2009 and Beyond

5.1 Does FETO Have a Place for Severe Hypoplasia?

Many have argued against fetal therapy for CDH, even for selected cases, but the FETO consortium continues to do so for fetuses with severe lung hypoplasia (Deprest et al. 2009a, b; Willyard 2008). Our strategy is based on a number of observations. First, current neonatal management has not dramatically changed the limits of viability. The published mortality rates remain virtually unchanged with pulmonary hypoplasia as a leading cause of death in up to 30% of patients (Datin-Dorrière et al. 2007; Hedrick et al. 2007; Yang et al. 2007; Sartoris

Table 1 Neonatal outcome as a function of LHR in fetuses with left sided isolated CDH and liver herniation, expectantly managed (left) or after FETO (right) (From Jani et al. 2006)

Degree of pulmonary hypoplasia	LHR	O/E LHR[a]	*n*	Expectant management (Jani et al. 2006)	*n*	FETO (Jani et al. 2006)
Extreme	0.4–0.5	15–19	2	0 (0%)	6	1 (16.7%)
Severe	0.6–0.7	20–23	6	0 (0%)	13	8 (61.5%)
	0.8–0.9	24–27	19	3 (15.8%)	9	7 (77.8%)
	LHR < 1.0	15–27	27	3 (11.1%)	28	16 (57.1%)
Moderate	1.0–1.1	28–31	23	14 (60.9%)		n a
	1.2–1.3	32–35	19	13 (68.4%)		n a
Mild	1.4–1.5	36–39	11	8 (72.7%)		n a
	≥1.6	≥41	6	5 (83.3%)		n a
	Total		86	43 (50%)		

n.a. not applicable since these fetuses were not eligible for FETO in current protocols
[a]Percentage conversion rounded

et al. 2006). Second, a growing number of studies show that survival chances can be predicted based on lung size and/or liver position. As a consequence, one can pick up before birth candidates for fetal intervention which reverses pulmonary hypoplasia. Third, current instrumentation and experience has made FETO a reproducible procedure with acceptable invasiveness, without identified maternal risks so far.

Another often heard argument against fetal therapy is that Harrison et al. (2003a, b) already demonstrated in a randomized, single centre trial that there is no benefit from fetal therapy for this condition. This is however not precise enough as a statement. This randomized trial was not conclusive at all for the population who is *currently* offered FETO in Europe, i.e., with severe or extreme hypoplasia. In the study by Harrison, only three cases with an LHR < 1.0 (=O/E LHR 27%) and liver up were included, one of them was surviving. The European program also differs substantially in technique (Table 2). The FETO procedure is a single, 3.3 mm port and completely percutaneous procedure. The use of a balloon avoids neck dissection, accommodates tracheal growth and makes reversal easier. Whereas preterm rupture of the membranes remains a problem, it is far less frequent than what was reported by Harrison et al. (2003a, b). In our experience, 20% instead of 100% rupture membranes prior to 34 weeks. Over 75% of patients deliver ≥34 weeks, whereas none in the trial. This may be due to reduced diameter of instruments, our growing experience and short operation times (Deprest et al. 2005). In brief, maternal and obstetric side effects seem to compare favorably to the results using general anesthesia, laparotomy and 5 mm access to the uterus.

Therefore the FETO consortium has not hesitated to continue its program in severe cases. Over the last years we have attempted to set up a randomized trial in this severity group, because indeed evidence for this intervention remains poor. Our outcomes can only be positioned to those in historical or contemporary controls. Apart from other, more logistic and financial restrictions against such trial, we experienced an unexpected resistance from patients and physicians to a trial with an expectant management arm (Deprest et al. 2009a, b). They found it difficult to accept that a pregnant mother, faced with an expected mortality as high as 80%, and a pulmonary morbidity rate as high as 75% when managed in the postnatal period, would have a one in two chance to be randomized to a treatment arm with exactly that poor perspective. Since FETO had for all those years been offered for that precise reason, patients would perceive this as a "no therapy" and the pressure for out of protocol treatment would be high. We admit that this objection is debatable, because it is clear that the assumption of an extremely poor survival chance may afterwards turn out not to be necessarily true because of a trial effect (Harrison et al. 2003a, b). Validity of prenatal selection is obviously a condition sine qua non for a fetal therapy trial, and many still debate this. However, in the absence of a consensus on a trial design for severe hypoplasia, the FETO consortium is still offering fetal therapy to this group. We consider a trial testing the

Table 2 Fetal surgery for CDH – trends in clinical experience

	Harrison et al. (2003a, b)	FETO consortium (ongoing)
Criteria for surgery	LHR < 1.4 and liver "up"	LHR < 1.0 and liver "up"
Anesthesia	General	Loco-regional or local
Access through abdominal wall	Laparotomy	Percutaneous
Access diameter	5 mm cannula	3.3 mm cannula
Occlusive device	Clip or endoluminal balloon	endoluminal balloon
Reversal of occlusion	EXIT delivery	In utero reversal
PPROM <34 weeks (%)	100	20
Mean gestational age at birth (weeks)	30.8 (28–34)	35 (27–38)
Survival following TO (LHR < 1.4)	73% ($n = 11$) (controls: 77%)	Those fetuses not eligible so far
Survival following TO (LHR < 1.0)	33% ($n = 3$)	50% (uncontrolled)[a]

[a]In the antenatal CDH registry survival in this group is under 15%. In the studies by Harrison, LHR was used and therefore those values are used as a reference

hypothesis whether TO at different time points prior to 29 weeks, may increase survival and/or decrease morbidity (Deprest et al. 2006a, b, 2009a, b). Occlusion as late as 30 weeks (saccular phase) is not considered for this group because our clinical experience is that later occlusion is in this group, at the expense of lung growth (Deprest et al. 2006a, b).

5.2 Moderate Hypoplasia: the TOTAL (Tracheal Occlusion to Accelerate Lung Growth) Trial

The above objections led us to reconsider a trial in case of moderate hypoplasia. We propose to randomize patients to either expectant management during pregnancy or insertion of a balloon at a FETO center at 30–32 weeks, and its removal to take place at 34–35 weeks. In both groups, this would be followed by standardized postnatal management at a high volume tertiary care center. Patients randomized to FETO will be offered stay on campus for as long as the trachea is occluded, so that optimal facilities are available for balloon removal in an emergency. This is a multicenter trial, where mothers return to their own tertiary referral center, either following removal of the balloon, or when randomized to expectant management. The main outcome measure for this trial will be a neonatal morbidity indicator. We hypothesize that fetal intervention decreases BPD (the need for O_2-supplementation at 28 days) by 20%. The potential for TO to reduce morbidity is based on two independent clinical observations. Keller et al. demonstrated in survivors from the NIH trial, that TO had several beneficial effects on pulmonary function including an improvement in alveolar-arterial oxygen difference and lung compliance, and this despite premature birth at around 30 weeks (Keller et al. 2004). In our experience, which pertains more severe cases, the occurrence of BPD was around 30% lower than what was expected in same severity controls (Jani et al. 2007a, b, c).

The current trial design will allay fears that studies have focused too long on mortality whereas the morbidity in survivors is clinically even more relevant. Power calculations have demonstrated that such study is realistic so that all now depends on the disciplined attitude of the fetal medical community not to offer FETO outside this (or other) trials to allow sufficient patient recruitment. First patients were recruited already in October 2008 in Leuven, later joined by the Barcelona group. (www.TOTALtrial.eu). Following the success of the Eurofoetus study on TTTS (Senat et al. 2004), we are now defining criteria for trial participation by high volume fetoscopy centers, who have gained meanwhile sufficient FETO-experience, and can ensure around the clock services of a team familiar with emergency balloon extraction and neonatal management of babies with CDH. Although far from ideal, the multicenter setting accounts for a European reality, with limitations of national boundaries for certain patients or insurance companies, but also the availability of a few pioneers with consistent experience in fetoscopy (Deprest et al. 2006a, b).

5.3 Standardization of Postnatal Management

Such trial would obviously be meaningless without standardization of postnatal management which is done at a tertiary care center with proven track record. Ideally these will be high volume centers (≥7 admissions/year), based on the Canadian experience that using consistent neonatal protocols and experience, improves infant survival (Javid et al. 2004). Prior to entry in the trial as a postnatal treatment center, vital statistics of the last years will be documented, and they must adhere in written to standardization guidelines, which were drafted within the framework of the CDH-EURO consortium. This is a consortium 16 centers in eight European countries, in which all follow the same protocol of postnatal therapy with regards to ventilatory approach and therapy from the moment of birth, including the period in the delivery room. The same holds true for analgesia and sedation, fluid regimen and adjustment of the ventilation based on preductal arterial PaO_2 values. Preceding the institution of this standardized postnatal management, protocol site visits were performed by the principal investigator (Dick Tibboel, Erasmus Medical Centre, Rotterdam) to discuss actual and adjusted management reaching ultimately a consensus (Table 3). Needless to say that the level of evidence of the different management modalities cannot be higher than consensus, due to the absence of properly designed RCT in any aspect of therapy in CDH till now. This consortium approach will reveal over the years solid morbidity data to fill the gap of knowledge on injury and repair (Castro et al. 2008) of

Table 3 Summary of the most important item in the postnatal treatment of patient with CDH according, based on the consensus statement of the CDH-EURO consortium

Treatment in the delivery room	No bag masking Immediately intubation Peak pressure below 25 cmH_20 Nasogastric tube
Treatment on the NICU/PICU	Adapt ventilation to obtain preductal saturation between 85 and 95% pH > 7.20, lactate 3–5 mmol/L Conventional ventilation (CMV) or high frequency oscillation (HFO) maximum peak-pressure 25–28 cmH_20 in CMV and mean airway pressure 17 cmH_20 in HFO Targeting blood pressure : normal value for gestational age Consider of inotropic support
Treatment of pulmonary hypertension (PH)	Perform echocardiography Inhaled nitric oxide (iNO) first choice in case of non response stop iNO In the chronic phase : phosphodiesterase – inhibitors, endothelin antagonist, tyrosine kinase inhibitors
ECMO (extracorporeal membrane oxygenation	Only starting if the patient is able to achieve a preductal saturation >85% Inability to maintain preductal saturation above 85% Respiratory acidosis Inadequate oxygen delivery (lactate>5 mmol/L) Therapy resistant hypotension
Surgical repair	Fraction of inspired oxygen (FiO_2) below 0.5 Mean blood pressure normal of gestational age Urine output >2 mL/kg/h No signs of persistent PH

these susceptible lungs and the relationship between prenatal variables, postnatal management (with detailed knowledge of neonatal demographics) and outcome. This consensus is currently in press, but its summary can be found at the trial website (www.totaltrial.eu).

Acknowledgment The European Commission supports our workinitssixthFramework(EuroSTEC;LSHC-CT-2006-037409). The Flemish Community of Belgium supports the clinical trial (IWT/070715). J.D. is the recipient of a "Fundamental Clinical Researcher" grant of the Fonds Wetenschappelijk Onderzoek-Vlaanderen (1.8.012.07.N.02). The collaborating centers from the antenatal CDH registry group and our colleagues from the FETO-task force or referring doctors are acknowledged for their contribution to the clinical program.

References

Boloker J, Bateman D, Wung J, Stolar C. Congenital diaphragmatic hernia in 120 infants treated consecutively with permissive hypercapnea/spontaneous respiration/elective repair. J Pediatr Surg. 2002;37(3):357–366

Broth RE, Wood DC, Rasanen J, Sabogal JC, Komwilaisak R, Weiner S, Berghella V. Prediction of lethal pulmonary hypoplasia: the hyperoxygenation test for pulmonary artery reactivity, Am J Obstet Gynecol 2002; 187 (4): 940–945

Cannie M, Jani JC, De Keyzer F et al (2006) Fetal body volume: use at MR imaging to quantify relative lung volume in fetuses suspected of having pulmonary hypoplasia. Radiology 241(3):847–853

Cannie M, Jani J, Chaffiotte C, Vaast P, Deruelle P, Houfflin-Debarge V, Dymarkowski S, Deprest J (2008a) Quantification of intrathoracic liver herniation by magnetic resonance imaging and prediction of postnatal survival in fetuses with congenital diaphragmatic hernia. Ultrasound Obstet Gynecol 32(5):627–632

Cannie M, Jani J, Meersschaert J, Allegaert K, Done' E, Marchal G, Deprest J, Dymarkowski S (2008b) Prenatal prediction of survival in isolated diaphragmatic hernia using observed to expected total fetal lung volume determined by magnetic resonance imaging based on either gestational age or fetal body volume. Ultrasound Obstet Gynecol 32(5):633–639

Castro M et al (2008) Strategic plan for pediatric respiratory diseases research: An NHLBI Working Group Report. Pediatr Pulmonol 2008:1–12

Coakley FV, Lopoo JB, Lu Y et al (2000) Normal and hypoplastic fetal lungs: volumetric assessment with prenatal single-shot rapid acquisition with relaxation enhancement MR imaging. Radiology 216(1):107–111

Datin-Dorriere V, Rouzies S, Taupin P et al (2008) Prenatal prognosis in isolated congenital diaphragmatic hernia. Am J Obstet Gynecol 198(1):80.e1–80.e5

Deprest J, Gratacos E, Nicolaides KH (2004) Fetoscopic tracheal occlusion (FETO) for severe congenital diaphragmatic

hernia: evolution of a technique and preliminary results. Ultrasound Obstet Gynecol 24(2):121–126

Deprest J, Jani J, Gratacos E et al (2005) Fetal intervention for congenital diaphragmatic hernia: the European experience. Semin Perinatol 29:94–103

Deprest J, Jani J, Gratacos E, Nicolaides K, Nelson S (2006a) Reply to a letter. J Pediatr Surg 41(7):1345–1346

Deprest J, Jani J, Lewi L, Ochsenbein-Kölble N, Cannie M, Doné E, Roubliova X, Van Mieghem T, Debeer A, Debuck F, Sbragia L, Toelen J, Devlieger R, Lewi P, Van de Velde M (2006b) Fetoscopic surgery: encouraged by clinical experience and boosted by instrument innovation. Semin Fetal Neonatal Med 11(6):398–412

Deprest J, Flemmer A, Gratacos E, Nicolaides K (2009a) Antenatal prediction of lung volume and in-utero treatment by fetal endoscopic tracheal occlusion in the severe isolated congenital diaphragmatic hernia. Semin Fetal Neonatal Med 14:8–13

Deprest JA, Hyett JA, Flake AW et al (2009b) Current controversies in prenatal diagnosis 4: should fetal surgery be done in all cases of severe diaphragmatic hernia. Prenat Diagn 29:15–19

DiFiore JW, Fauza DO, Slavin R, Peters CA, Fackler JC, Wilson JM (1994) Experimental fetal tracheal ligation reverses the structural and physiological effects of pulmonary hypoplasia in congenital diaphragmatic hernia. J Pediatr Surg 29(2):248–256, discussion 56–57

Done E et al (2008) Prenatal diagnosis, prediction of outcome and in utero therapy of isolated congenital diaphragmatic hernia. Prenat Diagn 28:581–591

Done E, Allegaert K, Lewi P, Jani J, Gucciardo L, Van Mieghem T, Gratacos E, Devlieger R, Van Schoubroeck D, Deprest J. Maternal hyperoxygenation test in fetuses treated for severe isolated congenital diaphragmatic hernia. Ultrasound Obstet Gynecol 2010 (in press)

Flageole H, Evrard VA, Piedboeuf B, Laberge JM, Lerut TE, Deprest JA (1998) The plug-unplug sequence: an important step to achieve type II pneumocyte maturation in the fetal lamb model. J Pediatr Surg 33(2):299–303

Flake AW, Crombleholme TM, Johnson MP, Howell LJ, Adzick NS (2000) Treatment of severe congenital diaphragmatic hernia by fetal tracheal occlusion: clinical experience with fifteen cases. Am J Obstet Gynecol 183(5):1059–1066

Gallot D, Boda C, Ughetto S, et al. 2007. Prenatal detection and outcome of congenital diaphragmatic hernia: a French registry-based study. Ultrasound Obstet Gynecol 29(3): 276–83

Garne E, Haeusler M, Barisic I, Gjergja R, Stoll C, Clementi M, Euroscan Study Group (2002) Congenital diaphragmatic hernia: evaluation of prenatal diagnosis in 20 European regions. Ultrasound Obstet Gynecol 19:329–333

Gucciardo L, Deprest J, Done E et al (2008) Prediction of outcome in isolated congenital diaphragmatic hernia and its consequences for fetal therapy. Best Pract Res Clin Obstet Gynaecol 22(1):123–138

Harrison MR, Adzick NS, Flake AW et al (1993) Correction of congenital diaphragmatic hernia in utero: VI. Hard-earned lessons. J Pediatr Surg 28(10):1411–1417, discussion 17–18

Harrison MR, Keller RL, Hawgood SB et al (2003a) A randomized trial of fetal endoscopic tracheal occlusion for severe fetal congenital diaphragmatic hernia. N Engl J Med 349(20): 1916–1924

Harrison MR, Sydorak RM, Farrell JA, Kitterman JA, Filly RA, Albanese CT (2003b) Fetoscopic temporary tracheal occlusion for congenital diaphragmatic hernia: prelude to a randomized, controlled trial. J Pediatr Surg 38(7):1012–1020

Hedrick HL, Danzer E, Merchant A et al (2007) Liver position and lung-to-head ratio for prediction of extracorporeal membrane oxygenation and survival in isolated left congenital diaphragmatic hernia. Am J Obstet Gynecol 197(4):422.e1–422.e4

Jani J, Gratacos E, Greenough A, et al. 2005. Percutaneous fetal endoscopic tracheal occlusion (FETO) for severe left-sided congenital diaphragmatic hernia. Clin Obstet Gynecol 48(4):910–922

Jani J, Keller RL, Benachi A et al (2006) Prenatal prediction of survival in isolated left-sided diaphragmatic hernia. Ultrasound Obstet Gynecol 27(1):18–22

Jani JC, Cannie M, Peralta CF, Deprest JA, Nicolaides KH, Dymarkowski S (2007a) Lung volumes in fetuses with congenital diaphragmatic hernia: comparison of 3D US and MR imaging assessments. Radiology 244(2):575–582

Jani J, Nicolaides KH, Keller RL et al (2007b) Observed to expected lung area to head circumference ratio in the prediction of survival in fetuses with isolated diaphragmatic hernia. Ultrasound Obstet Gynecol 30(1):67–71

Jani J, Nicolaides K, Gratacos E et al (2007c) Short term neonatal morbidity in severe left-sided congenital diaphragmatic hernia treated by tracheal occlusion before 30 weeks. Am J Obstet Gynecol 197(6):S162

Jani J, Nicolaides K, Gratacos E, et al Allegaert K, Greenough A, Moreno O, Deprest J (2007d) Short term neonatal morbidity in severe left-sided congenital diaphragmatic hernia treated by tracheal occlusion before 30 weeks. Am J Obstet Gynecol; 197(6):S162

Jani J, Cannie M, Sonigo P, Robert Y, Moreno O, Benachi A, Vaast P, Gratacos E, Nicolaides KH, Deprest J (2008a) Value of prenatal magnetic resonance imaging in the prediction of postnatal outcome in fetuses with diaphragmatic hernia. Ultrasound Obstet Gynecol 32(6):793–799

Jani J, Nicolaides KH, Benachi A et al (2008b) Timing of lung size assessment in the prediction of survival in fetuses with diaphragmatic hernia. Ultrasound Obstet Gynecol 31(1):37–40

Jani JC, Benachi A, Nicolaides KH, Allegaert K, Gratacós E, Mazkereth R, Matis J, Tibboel D, Van Heijst A, Storme L, Rousseau V, Greenough A, Deprest JA, the Antenatal CDH Registry group (2009) Prenatal prediction of neonatal morbidity in survivors with congenital diaphragmatic hernia: a multicenter study. Ultrasound Obstet Gynecol 33:64–69

Javid P, Jaksic T, Skarsgard E, Lee S (2004) Survival rate in congenital diaphragmatic hernia: the experience of the Canadian Neonatal Network. J Pediatr Surg 39:657–660

Keller R, Hawgood S, Neuhaus J et al (2004) Infant pulmonary function in a randomized trial of fetal tracheal occlusion for severe congenital diaphragmatic hernia. Pediatr Res 56: 818–825

Khan PA, Cloutier M, Piedboeuf B (2007) Tracheal occlusion: a review of obstructing fetal lungs to make them grow and mature. Am J Med Genet C Semin Med Genet 145C(2): 125–138

Khan A, Lally K. The role of extracorporeal membrane oxygenation in the management of infants with congenital diaphragmatic hernia. Semin Perinatol. 2005; 29(2):118–22

Kinsella J, Parker T, Dunbar I, Abman S. Noninvasive delivery of inhaled nitric oxide therapy for late pulmonary hypertension

in newborn infants with congenital diaphragmatic hernia. J Pediatr. 2003; 142(4):397–401

Kinsella J, Dunbar I, Abman S. Pulmonary vasodilator therapy in congenital diaphragmatic hernia: acute, late, and chronic pulmonary hypertension. Semin Perinatol. 2005; 29(2):123–8

Klaritsch P, Albert K, Van Mieghem T, Gucciardo L, Done' E, Bynens B, Deprest J (2009) Instrumental requirements for minimal invasive fetal surgery. BJOG 116(2):188–197

Metkus AP, Filly RA, Stringer MD, Harrison MR, Adzick NS (1996) Sonographic predictors of survival in fetal diaphragmatic hernia. J Pediatr Surg 31(1):148–151, discussion 151–152

Moreno-Alvarez O, Hernandez-Andrade E, Oros D, Jani J, Deprest J, Gratacos E (2008) Association between intrapulmonary arterial Doppler parameters and degree of lung growth as measured by the lung-to-head ratio in fetuses with congenital diaphragmatic hernia. Ultrasound Obstet Gynecol 31:164–170

Nelson SC, Cameron AD, Deprest J (2006) Fetoscopic surgery for in utero management of congenital diaphragmatic hernia. Fet Mat Medicine Rev 17(1):69–104

Peralta CF, Cavoretto P, Csapo B, Vandecruys H, Nicolaides KH (2005) Assessment of lung area in normal fetuses at 12-32 weeks. Ultrasound Obstet Gynecol 26(7):718–724

Peralta CF, Jani JC, Van Schoubroeck D, Nicolaides KH, Deprest JA (2008) Fetal lung volume after endoscopic tracheal occlusion in the prediction of postnatal outcome. Am J Obstet Gynecol 198(1):60.e1–60.e5

Ruano R, Aubry MC, Barthe B, Mitanchez D, Dumez Y, Benachi A. Quantitative analysis of pulmonary vasculature by 3D-power Doppler ultrasonography in isolated congenital diaphragmatic hernia. Am J Ojbstet Gynecol, 2006; 195: 1720–28

Ruano R, de Fatima Yukie Maeda M, Ikeda Niigaki J, Zugaib M. Pulmonary artery diameters in healthy fetuses from 19–40 weeks gestation. J Ultrasound Med 2007; 26:309–316

Sartoris J, Varnholt V, Dahlheim D, Schaible T (2006) CDH in Mannheim – algorithm and results. Monatschr Kinderheilkd 153:717

Senat MV, Deprest J, Boulvain M, Paupe A, Winer N, Ville Y (2004) Endoscopic laser surgery versus serial amnioreduction for severe twin-to-twin transfusion syndrome. N Engl J Med 351(2):136–144

Smith N, Jesudason E, Featherstone N et al. Recent advances in congenital diaphragmatic hernia. Arch Dis Child. 2005; 90(4):426–8

Stege G, Fenton A, Jaffray B (2003) Nihilism in the 1990s. The true mortality of CDH. Pediatrics 112: 532–535

Tonks A et al. Congenital malformations of the diaphragm: findings of the West Midlands Congenital Anomaly Register 1995 to 2000. Prenat Diagn. 2004 Aug;24(8):596–604

Van de Velde M, Jani J, De Buck F, Deprest J (2006) Fetal pain perception and pain management. Semin Fetal Neonatal Med 11(4):232–236

Walsh DS, Hubbard AM, Olutoye OO, Howell LJ, Crombleholme TM, Flake AW, Johnson MP, Adzick NS (2000) Assessment of fetal lung volumes and liver herniation with magnetic resonance imaging in congenital diaphragmatic hernia. Am J Obstet Gynecol 183:1067–1069

Williams G, Coakley FV, Qayyum A, Farmer DL, Joe BN, Filly RA (2004) Fetal relative lung volume: quantification by using prenatal MR imaging lung volumetry. Radiology 233(2):457–462

Willyard C (2008) Tinkering within the womb: the future of fetal surgery. Nat Med 14(11):1176–1177

Yang SH, Nobuhara KK, Keller RL et al (2007) Reliability of the lung-to-head ratio as a predictor of outcome in fetuses with isolated left congenital diaphragmatic hernia at gestation outside 24-26 weeks. Am J Obstet Gynecol 197(1): 30.e1–30.e7

MRI of the Pathological Fetal Thorax

Gregor Kasprian

Contents

Abstract

› Prenatal sonography provides a sensitive detection of most fetal thoracic pathologies. However, the specificity and reliability in the diagnosis as well as prediction of postnatal outcome may be further optimized by fetal MR imaging. Due to the excellent tissue contrast of fetal MRI and the ability to provide information on the chemical composition of certain lung lesions using different MR sequences, this imaging modality can add further diagnostic information, which may be even superior to the commonly used postnatal imaging procedures. Thus, fetal MR of thoracic pathologies finally constitutes a valuable preoperative imaging tool. This chapter generally reviews the most frequently encountered thoracic pathologies of the fetus focusing on pulmonary hypoplasia and cystic lung lesions and describes their MR imaging appearance on a variety of MR sequences.

1 Pulmonary Hypoplasia

Because the occurrence of primary pulmonary hypoplasia is rare, this entity can be considered a secondary abnormality, associated with different extrathoracic or intrathoracic pathologies (Table 1). The pathological definition of fetal pulmonary hypoplasia is based on the detection of an abnormally small lung, characterized by an abnormally small lung-to-body-weight ratio (Wigglesworth and Desai 1981; De Paepe et al. 2005).

G. Kasprian
Department of Radiology, Medical University of Vienna,
Währinger Gürtel, 18-20
e-mail: gregor.kasprian@meduniwien.ac.at

D. Prayer (ed.), *Fetal MRI*, Medical Radiology,
DOI: 10.1007/174_2010_98, © Springer-Verlag Berlin Heidelberg 2011

In addition, the reduction in alveolar number can be quantified by the radial alveolar count (Askenazi and Perlman 1979), which further specifies the postmortem diagnosis of pulmonary hypoplasia. Finally, the DNA content of the fetal lung can be determined, and the gestational age-specific reduction serves as an additional source of information about the grade of severity of pulmonary hypoplasia (Wigglesworth and Desai 1981). Clinically, pulmonary hypoplasia presents as an immediate postnatal onset of respiratory insufficiency, complicated by pulmonary hypertension and recurrent pneumothoraces, which requires intensive respiratory support.

Particularly, in cases of pathologies known to be associated with a high risk for pulmonary hypoplasia (Table 1), the prenatal prediction of the postnatal risk for respiratory insufficiency is of great clinical interest, and a confident prognosis would support the choice of further therapeutic and perinatal management. The fetal MR techniques that are currently available, in addition to prognostic sonographic markers (Lauria et al. 1995; Laudy and Wladimiroff 2000), are described in Chap. 15. In this chapter, the MR imaging strategy and appearance of the main extra- and intrathoracic causes of pulmonary hypoplasia are described.

Table 1 Common intrathoracic and extrathoracic origins of pulmonary hypoplasia (After Sherer et al. 1990)

Intrathoracic	Extrathoracic
Congenital diaphragmatic hernia (CDH)	Oligohydramnios (renal and nonrenal)
Hydrops fetalis and/or pleural effusion	Intrauterine growth restriction
Cystic adenomatoid malformations	Skeletal dysplasia
Bronchogenic cysts	Neuromuscular disease
Cardiac lesions/anomalies	Central nervous system abnormalities and fetal akinesia
Intrathoracic masses (other)	Abdominal wall defects

1.1 Oligohydramnios

Renal and nonrenal reduction of amniotic fluid is known to be the most frequent extrathoracic cause of pulmonary hypoplasia. Generally, the most common cause of oligohydramnios is premature rupture of membranes (PROM), which occurs in 10% of all pregnancies. The high prevalence and reported pulmonary hypoplasia-associated mortality rate between 29% and 58% (reviewed in (Laudy and Wladimiroff 2000)) emphasizes the high clinical relevance of this condition.

The pathogenesis of oligohydramnios-associated pulmonary hypoplasia is believed to relate mainly to the mechanic compression of the fetal thorax and the fetal lungs. Thus, chronic compression results in a reduced intra- to extrapulmonary pressure gradient (generated by the fetal lung fluid production), and thus, to loss of a significant growth stimulus for the fetal lung (see Chap. 15).

One week of existing oligo- or anhydramnios may lead to a significant reduction in lung volume and critical pulmonary hypoplasia (Moessinger et al. 1986). Particularly in midtrimester premature rupture of membranes, the gestational age of onset remains the most important risk factor and predictor for lethality (Lauria et al. 1995; van Teeffelen et al. 2010). However, the exact time point of onset is often unknown. In addition, the grade of amniotic fluid reduction, which is routinely assessed by indirect sonographic amniotic fluid pocket measurements, and the time of persistence of pulmonary hypoplasia are important risk factors.

1.1.1 Imaging Appearance of Oligohydramnios-Associated Pulmonary Hypoplasia

The image quality of prenatal sonography is often significantly limited by the absence of amniotic fluid as an acoustic window. In contrast, both the reduced maternal abdominal circumference and the immobile position of the fetus are particularly convenient for fetal MR imaging.

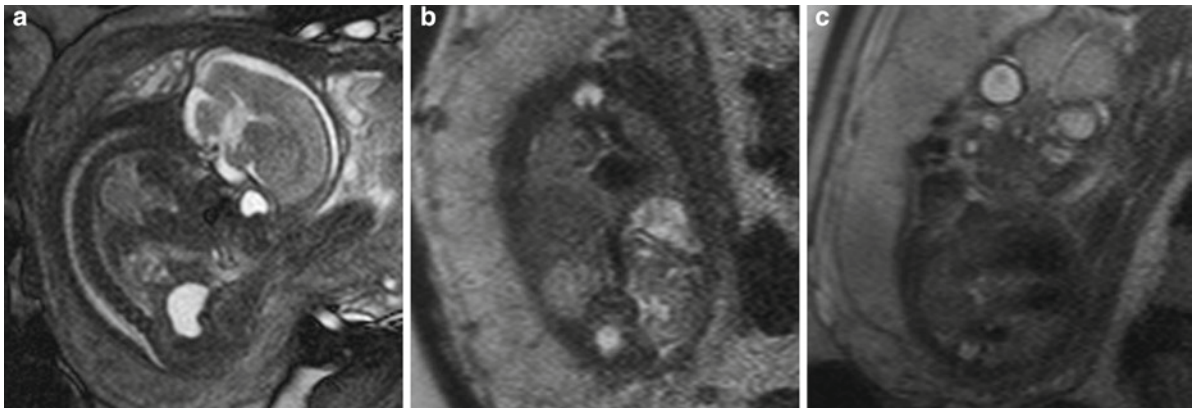

Fig. 1 (**a**–**c**) Lethal pulmonary hypoplasia in a case of PROM and anhydramnios. A sagittal balanced angiography sequence (**a**) shows the increased flexion of the thoracic spine. A coronal T2-weighted sequence (**a**) and axial T2-weighted sequence (**b**) (TE = 100 ms) depict the hypointense fetal lungs with fluid-marked main bronchi and trachea (**b**)

When imaging any fetus with signs of reduced amniotic fluid volume, a dedicated MR imaging protocol to rule out or detect pulmonary hypoplasia must be applied. This includes an axial T2-weighted lung volumetry sequence (preferable slice thickness: 3–5 mm) that covers the fetal thorax. Preferably, echo times of 100 ms to assess the signal intensity of the fetal lungs should be used. In the presence of severe pulmonary hypoplasia and consecutive reduction of lung fluid, the fetal lungs appear profoundly hypointense on T2-weighted images (Kuwashima et al. 2001) (Fig. 1), and are, therefore, often difficult to differentiate from other intrathoracic organs during volumetry. In contrast to the indirect approximate determination of amniotic fluid volume by sonographic amniotic fluid pocket measurements, MRI provides detailed data about the exact amount of amniotic fluid. Depending on the grade of amniotic fluid reduction, thoracic compression can be also indirectly assessed by the pronounced flexure of the thoracic spine (Albuquerque et al. 2002) (Fig 1). Fig. 2 shows the presence of a congenital cystic adenomatoid malformation in a fetus with anhydramnios and illustrates the considerable T2-w signal difference between the cystic and hyperintense lung lesion and the hypointense signal characteristics of the hypoplastic contralateral lung. The combination of T2-w hypointensity of the fetal lung and markedly reduced lung volumes (<10mL) is a strong indicator of clinically severe pulmonary hypoplasia. Finally, fetal MR may also help to elaborate the exact origin of an-/oligohydramnios. In the setting of infection and fetal inflammatory response syndrome and premature rupture of membranes, placental abnormalities (for instance, infarction and hemorrhage) are a frequent finding. In renal oligohydramnios, the pathology of the urogenital system can be specifically evaluated (Fig. 3).

1.2 Hydrothorax

Hydrothorax, as an isolated (uni- or bilateral) pathology, or in the condition of fetal hydrops, frequently leads to lethal pulmonary hypoplasia, and is associated with an overall mortality of 53% (Longaker et al. 1989). Pleural effusions prevent the proper expansion and growth of the fetal lung. However, the clinical course of hydrothorax is generally unpredictable, with spontaneous regression in some cases. Current guidelines recommend invasive prenatal therapy for this condition in cases of hydrops without additional abnormalities (NICE Guidelines 2006).

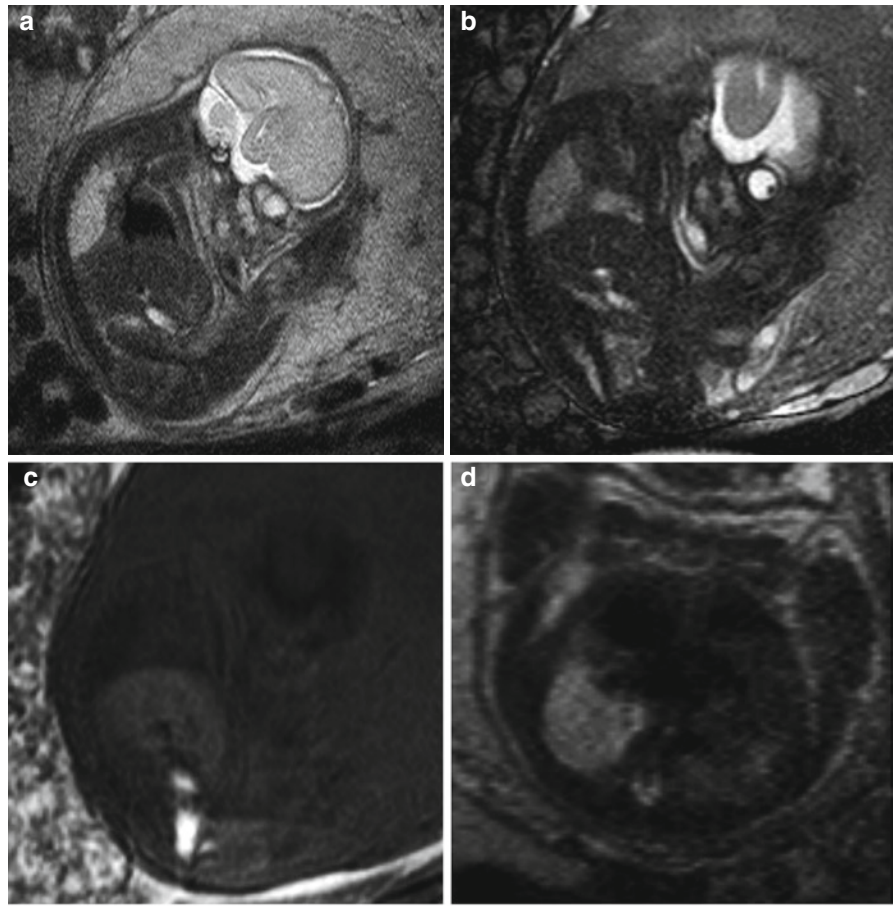

Fig. 2 (**a**–**d**) Anhydramnios in a fetus with pulmonary hypoplasia at 27GW: unexpectedly high T2-weighted signal of the lower lobe of the right lung, depicted using sagittal T2-weighted sequences (TE = 140 ms) (**a**), balanced angiography (**b**), and T1-weighted sequences and T1-weighted sequences (**c**). The axial T2-weighted sequence (TE = 149 ms) (**d**) indicates the expected low T2-weighted signal of the left hypoplastic lung, and suggests the presence of a cystic lung lesion (CCAM type 3) of the right lung

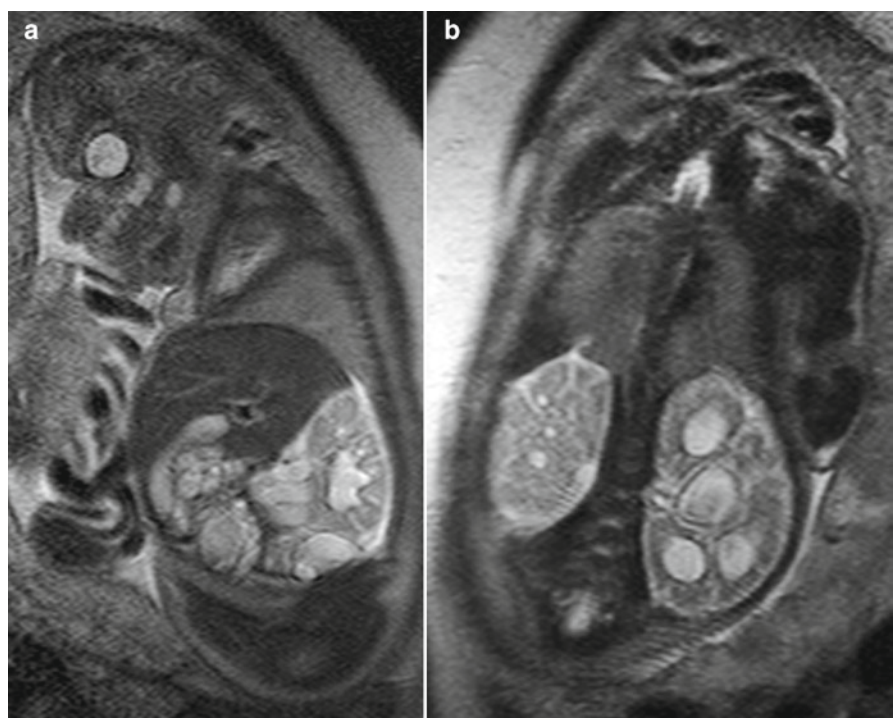

Fig. 3 (**a**, **b**) Sagittal and coronal T2-weighted sequences from a fetus with bilateral posterior urethral valves and hydroureter at 28GW showing markedly reduced amniotic fluid volume and compression of the fetal thorax due to the abdominal mass effect of the enlarged fetal kidneys. The signal intensity of the fetal lungs is consequently slightly reduced, which is another sign of pulmonary hypoplasia

1.2.1 Imaging Appearance of Hydrothorax

Hydrothorax-related pulmonary hypoplasia appears as a T2-weighted profound hypointensity or muscle-isointensity of the fetal lungs. MR volumetry is facilitated by the exact differentiation between the bright pleural effusion and dark lung tissue. Often, even the anatomical identification of the oblique pulmonary fissure (Fig. 4), which cannot be delineated in healthy conditions, is possible. Another task for fetal MRI, when evaluating fetal hydrothorax, is the exclusion of associated anomalies, which occur in up to 40% of cases (Hubbard and Crombleholme 1998). Finally, fetal MR may be used as a follow-up imaging modality to assess the success of a prenatal intervention (for instance, thoracoamniotic shunting or pleurodesis) qualitatively and quantitatively (Fig 4).

1.3 Cystic Lung Lesions

1.3.1 Cystic Adenomatoid Malformation – CCAM

After the initial description of a solid-appearing lung mass, consisting of small cyst-like structures, by Ch'In and Tang (1949), Stocker et al. (1977) reported a variety of neonatal/stillborn lung lesions that shared a characteristic pathologic and microscopic features. Generally, the size of the cysts and the type of cellular lining were used to assign the lesions to a specific type.

Thus, CCAM Type 1 lesions are pathologically characterized by rather large cysts (0.5–10 cm) lined by a cuboidal to a ciliated pseudostratified epithelium (Stocker 2009), and sometimes containing mucogenic cells, the presence of which has been attributed to the

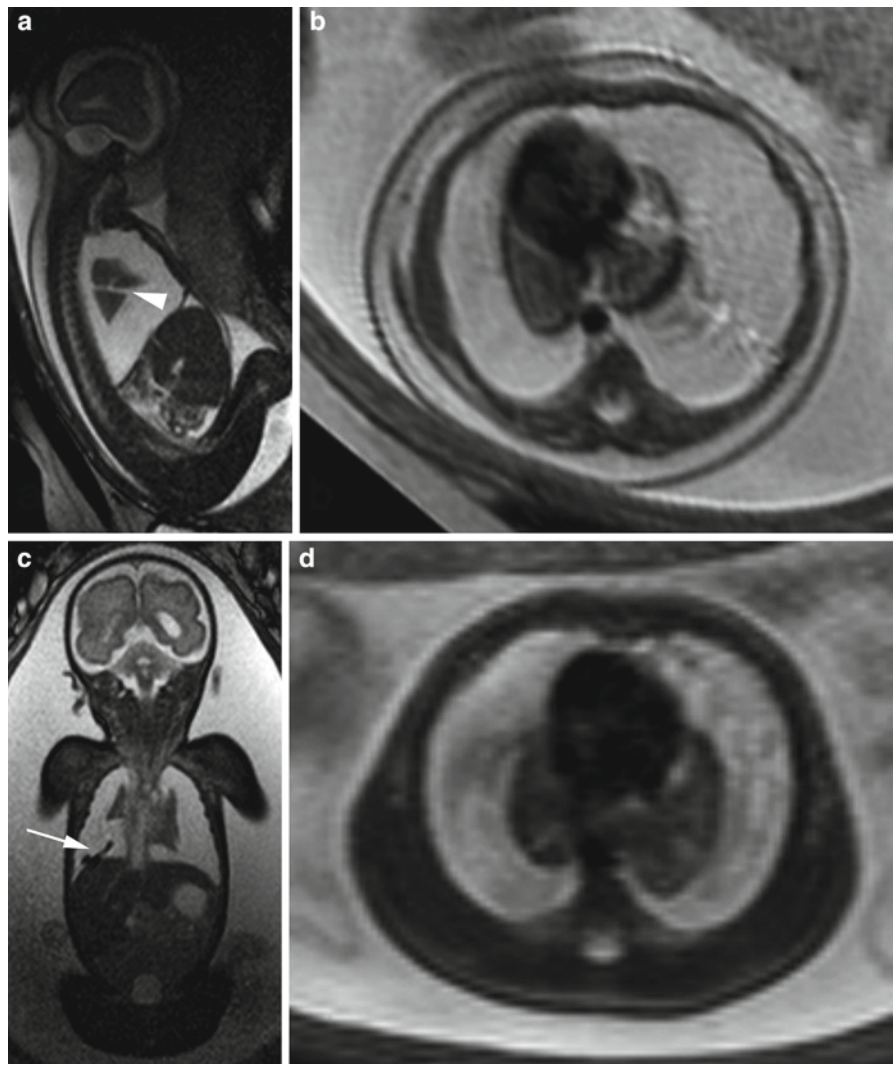

Fig. 4 (**a**–**c**) Follow-up MRI in a fetus with hydrops and bilateral pleural effusions (**a**, **b**). The contours of the fetal lungs are easily delineable with the oblique fissure clearly visible. After the placement of a thoracoamniotic shunt (b, *arrow*), the hydrops resolved. However, the compression of the fetal lung remained, as indicated by the profoundly hypointense fetal lung on T2-weighted images (**c**, **d**)

occurrence of bronchoalveolar carcinoma in postnatal/adult life.

CCAM Type 2 lesions show rather smaller cysts (up to 2 cm), and are often encountered in association with other abnormalities (congenital diaphragmatic hernia, cardiac malformations, bilateral renal agenesis, etc.). Histologically, a columnar epithelial lining is found, often surrounded by fibrovascular tissue, and sometimes, containing mature skeletal muscle (Stocker 2009).

The original description by Ch'In and Tang probably best fits CCAM Type 3, which is characterized by a rather bulky solid mass that contains glandular tissues and structures that resemble bronchioles.

The developmental origin of these lesions remains unclear; however, an abnormal interaction between the mesenchymal and epithelial or vascular components has been proposed (Cangiarella et al. 1995). Additionally the occasional description of a blind atretic bronchus in CCAM, as well as the mechanical obstruction of bronchi during fetal development, may contribute to the pathogenesis of these lung lesions (Morotti et al. 1999).

Imaging Appearance of CCAM

Several attempts have been made to classify cystic lung lesions on the basis of their in vivo imaging appearance. Based on the large histological and morphologic overlap of different CCAM types and appearances, and particularly due to the common coexistence of CCAM and bronchopulmonary sequestrations – "hybrid lesions" – a unified imaging classification system for cystic lung lesions has to be further elaborated (Adzick et al. 1985; Achiron et al. 2004a, b).

CCAM lesions are usually detected by ultrasound at about 20GW (Cavoretto et al. 2008), and appear as cystic or solid echogenic lung masses. Generally, the specificity of the sonographic diagnosis for these lesions is high. Occasionally, CCAM may be mistaken for CDH and vice versa (Quinn et al. 1998). However, in most cases, experienced prenatal sonographers can be certain in their diagnosis of CCAM. Moreover, duplex sonography offers the possibility to examine the intralesional vascular anatomy in great detail, and may identify abnormal feeding vessels in order to identify sequestrations or hybrid lesions more confidently. Because there is a lack of results of large prospective comparative studies between ultrasound and fetal MRI (Quinn et al. 1998; Matsuoka et al. 2003), it is unclear which modality depicts the extent of these lesions with greater detail. Thus, the true sensitivity of MRI in detecting CCAM prenatally is not known, but is of specific clinical/surgical interest, especially in those cases where the lesions seem to be apparently resolved on the ultrasound images, but are still detectable on postnatal CT scans (Khosa et al. 2004; Illanes et al. 2005).

Still, fetal MR can contribute to the preoperative characterization of the lesion and may add multiplanar imaging data, which aids in the surgical planning. In addition, fetal MRI is valuable in situations where the quality of the sonographic evaluation is limited (oligohydramnions, maternal factors, etc.). Finally, the clear delineation of CCAM on MR images enables a volumetric assessment of normal and lesional pulmonary parenchyma and helps to quantify and monitor the growth or resolution of the lesions (Liu et al. 2010).

As a rule, CCAM share one specific imaging feature on MR, which allows their discrimination from normal lung parenchyma: they appear bright on T2-weighted sequences (Figs. 2, 5, and 6). This most probably relates to the specific composition of the accumulated fluid/mucus and the reduced density of mesenchymal tissue components within the cystic lesions (Fig. 6). Thus, T2-weighted TSE sequences are the most suitable sequences for the detection and the assessment of the size of CCAM. Choosing longer echo times (TE > 140 ms) helps to further optimize the contrast between normal and affected lung tissue (Figs. 5 and 6). Due to the limited in-plane resolution of these sequences (0.7 × 0.7 mm), the microcysts themselves are not visible in CCAM type 3 lesions, whereas, larger cysts can be easily identified. Finally, it should be noted that, due to the increase of overall T2-weighted lung signal intensity (see Chap. 15), the contrast between the lesion and the lung parenchyma may be less pronounced in the third trimester than in earlier gestational stages (Fig 8).

Thick-slab T2-weighted sequences can help to visualize the gross aspect of the lesion and its relation to the normal lung tissue, and sometimes, help to visualize smaller cystic components, and should, therefore, be included in the protocol (Table 1). SSFP sequences can depict CCAM lesions. However, this may lead to an underestimation of the true lesional size, but SSFP sequences often remain the only artifact-free imaging strategy, especially in cases complicated by polyhydramnios and fetal movement.

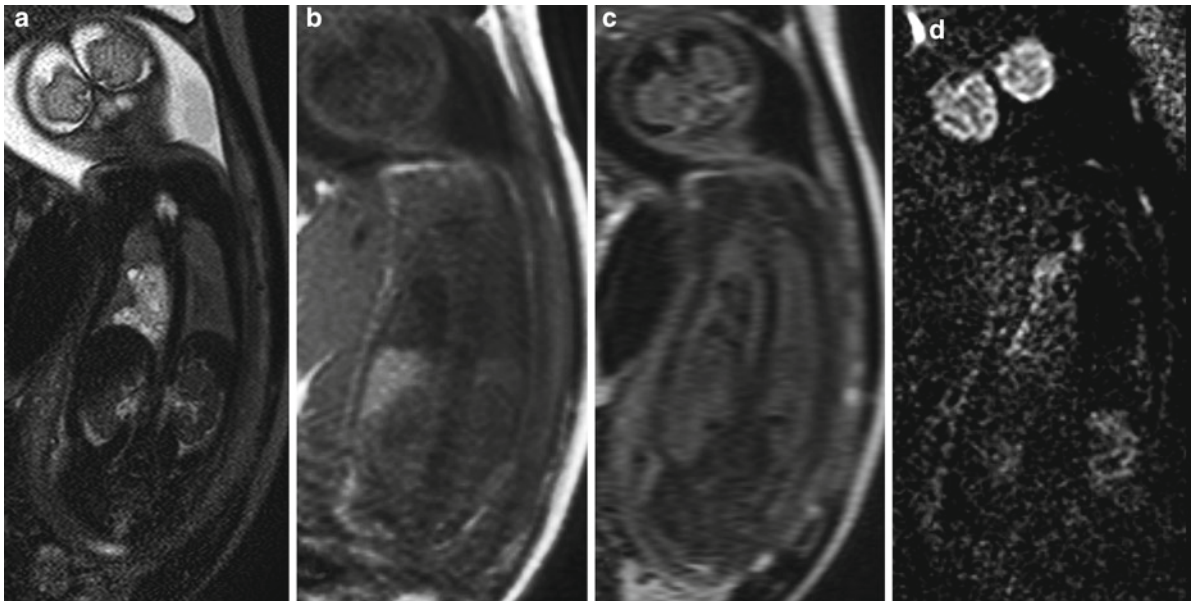

Fig. 5 (**a**–**d**) Coronal T2-weighted (**a**), T1-weighted (**b**), FLAIR (**c**), and diffusion-weighted (**d**) sequences from a fetus at 30GW with CCAM type 2. The coronal T2-w (**a**) shows a hyperintense (TE = 140 ms) lesion of the right lower pulmonary lobe with larger (2 cm) and smaller (<1 cm) cysts. The lesion appears T1-weighted (**b**) and FLAIR hypointense, indicating low protein content. On diffusion-weighted sequences, the lesion appeared with an intermediate signal on the $b = 700$ anisotropy image

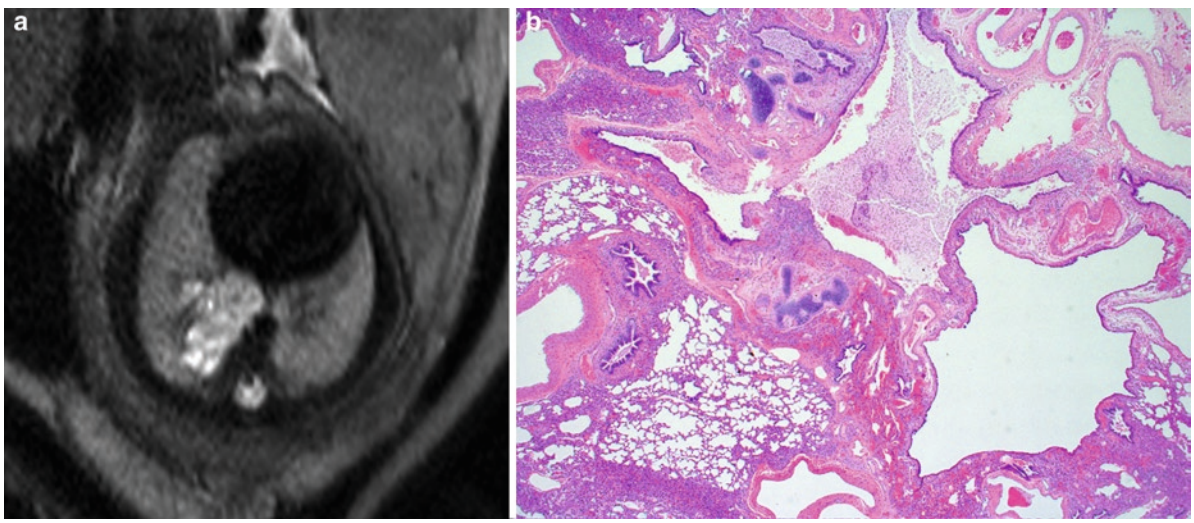

Fig. 6 (**a**, **b**) The same patient as in Figure 5: The well-delineated cystic lesion is clearly visible on axial T2-weighted sequences with a long echo time (TE = 140). Histology shows cysts lined with respiratory epithelium and some cartilage, as well as bronchi, leading to the diagnosis of CCAM type 2 (Courtesy of Gabriele Amann and Anke Koller)

T1-weighted information is generally not needed for the specific diagnosis of CCAM, but, may further characterize the fluid content of the cyst. Thus, CCAM cysts typically appear hypointense on T1-weighted sequences (Fig 5). Due to the mesenchymal tissue structures and the cyst walls of the microcysts, CCAM type 3 lesions show higher T1-weighted signal intensities than the large cysts of CCAM 1, which appear homogeneously dark.

In case of reduced fetal motion, FLAIR sequences may also be helpful. Typically, the cysts appear dark on FLAIR sequences with the surrounding lung tissue

having a higher signal intensity (Fig 5). In case of cysts with moderately bright content, a high amount of protein/lipid should be suspected (Table 2).

In addition to tissue characterization using different sequences, the clear reproducible anatomical visualization of the lesion is possible with MRI. Mediastinal shifting, or compression of the adjacent lung tissue, can be easily identified. Finally, axial T2-weighted sequences can be used to determine the absolute size of the lesion and the size of the nonlesional lung tissue by volumetry (see Chap. 15), providing detailed information on the relative lesion size in order to monitor further lesion growth.

Prognosis of CCAM

Originally, CCAM were thought to frequently lead to prenatal death, and are often associated with early postnatal demise. However, after all lesions with associated anomalies (mostly Stocker type 2 lesions) were excluded from the analysis, it became evident that the prognosis of isolated CCAM (independent of histological type) is good, with an overall survival of over 97% of cases (Cavoretto et al. 2008).

The most important prognostic factor in the assessment of isolated CCAM is the presence or absence of signs of fetal hydrops. Pathophysiologically, CCAM may compress the fetal heart and inferior vena cava, and consequently, lead to a reduction in cardiac contractility and impairment of venous return (Nishibayashi et al. 1981; Moerman et al. 1982; Adzick et al. 1985; Rosado-de-Christenson and Stocker 1991). More than 90% of expectantly managed cases with CCAM and hydrops die before birth (Adzick et al. 1998; Grethel et al. 2007).

Other factors, such as the presence of a significant mediastinal shift and polyhydramnios, seem to have a certain negative impact on overall survival (Thorpe-Beeston and Nicolaides 1994; Bunduki et al. 2000); however, these factors were not found to be significantly associated with outcome (Cavoretto et al. 2008). There is a certain prognostic influence of the histological subtype of the lesion, with type 1 lesions showing better outcomes and often being less associated with hydrops (Thorpe-Beeston and Nicolaides 1994; Bunduki et al. 2000).

Since the common treatment strategy after birth is the surgical excision of "significant" CCAM, it may be of interest to assess the prenatal growth characteristics of these lesions as the phenomenon of "disappearing" CCAM is widely known. In larger series, it has been reported that up to 50% of cystic fetal lung lesions show a resolution during prenatal ultrasound follow-up (summarized in (Cavoretto et al. 2008)). Typically, larger lesions (>84% of total lung volume) show an incomplete resolution, while smaller lesions (<57% of total lung volume) may show a complete resolution (Liu et al. 2010). Generally, the rather high rate (about 64%) of apparently resolved lesions, still detectable after birth by CT scans (Illanes et al. 2005), may reflect a certain methodologic limitation of ultrasound in monitoring CCAM. Based on the overall increase in lung signal, and consequently, the loss of contrast between the lesional and nonaffected tissue, MRI may also have some limitations in its diagnostic sensitivity at later gestational stages, but may still be more sensitive than ultrasound. Due to its multiplanar capabilities, MRI is also more comparable to postnatal follow-up CT scans (Figs. 7 and 8), and thus, MRI can provide more appropriate information to establish a definite indication for a surgical intervention (Table 2).

Table 2 Fetal MR sequences used for the characterization of cystic lung lesions

Sequence	Orientation	Characterization
T2 TSE (TE > 140 ms)	Three orthogonal planes	Delineation of lesion (hyperintense), volumetry
T2 TSE (TE = 100–120 ms), slice thickness: 3 mm	Axial/coronal	Abnormal arterial supply
Thick slab T2-weighted	Coronal/sagittal	General aspect, cyst characterization/size
T1-weighted	Coronal	Fluid composition
FLAIR	Coronal	Protein content of cysts
Diffusion	Coronal	Restricted diffusion (low ADC, high FA) as potential hint toward lesional vascularization

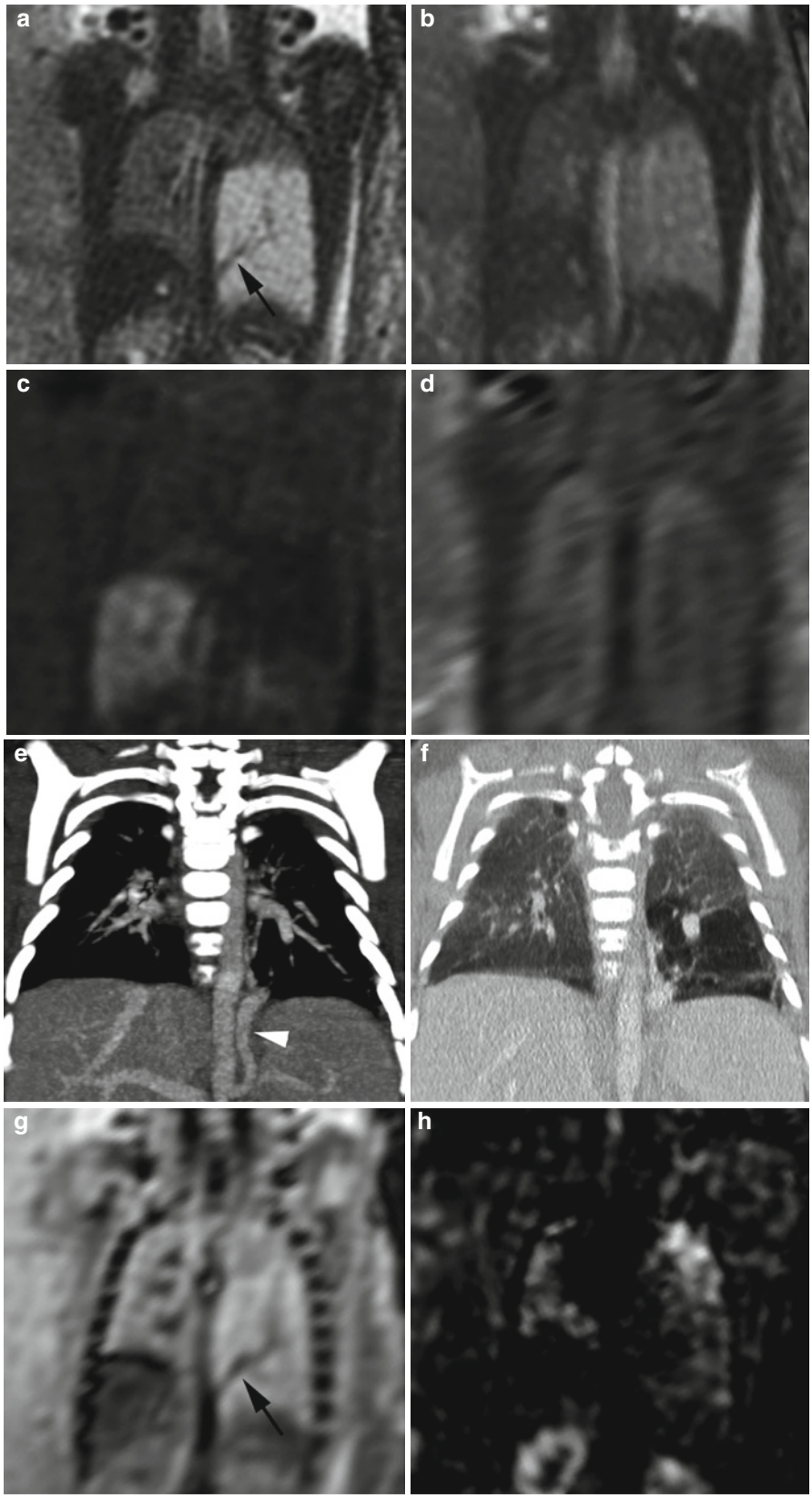

Fig. 7 (**a**–**g**) Coronal MR (**a**–**d**, **g**, **h**) of a fetus with a intrapulmonary sequestration and postnatal contrast-enhanced preoperative CT images (**e**, **f**). Coronal T2-weighted (**a**, TE = 140 ms) and echo planar sequences (**g**) depict the aberrant systemic artery supply (*black arrow*) originating from the abdominal aorta (**e**, *white arrow*), whereas, the balanced angiography sequence (**b**) does not show any vessel structure in the corresponding region. T1-weighted (**c**) and FLAIR (**d**) sequences depict the lesion as a hypointense, poorly identifiable structure. The lesion does not show a significantly different appearance on diffusion-weighted anisotropy images ($b = 700$, h). Postnatal CT scan (**f**) shows a hypertransparent change in the left lower lobe

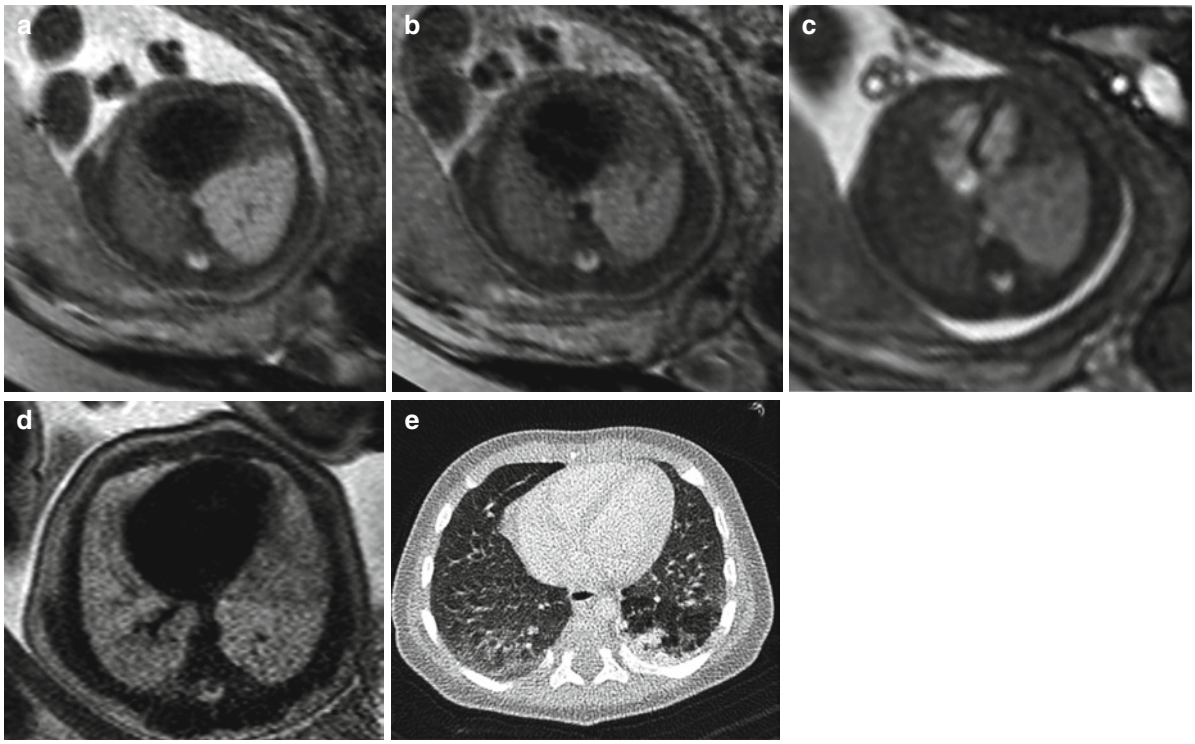

Fig. 8 (**a**–**e**) Axial series in the same case as in Figure 7: The delineation of the intrapulmonary sequestration is more distinct on T2-weighted images with longer echo times (TE = 140, **b**, compared to TE = 100, **a**). Balanced angiography images (**c**) may depict the intrinsic details of the fetal heart, but, fail to show intrinsic vascular structures of the lesion. Follow-up examination at 34GW (**d**): the difference between the pulmonary parenchyma and the lesion becomes less evident due to the increasing signal intensity of the normal lung parenchyma. Axial postnatal CT (e) showing the partly cystic, partly consolidated lesion of the left lower lobe

1.3.2 Sequestration, Hybrid Lesions

After CCAM, bronchopulmonary sequestration (BPS) is the second most common prenatally detected lung lesion. Depending on its pleural investment, it can be classified as intrapulmonary or extrapulmonary (Stocker 1986). The common feature of both types is the abnormal arterial supply of a nonfunctioning lung segment, with or without the connection of tracheobronchial airways and/or abnormal venous drainage (Clements and Warner 1987). Again, due to the great diversity in the involvement of the different pulmonary tissue compartments (systemic/pulmonary arterial/venous vascular, tracheobronchial), the entity of BPS should be generally regarded as a "spectrum" (Stocker 1986; Clements and Warner 1987; Cass et al. 1997; Achiron et al. 2004; Davenport et al. 2004).

Pathologically, the classic types of intrapulmonary BPS are rarely diagnosed prenatally and are mostly encountered in adults (Zylak et al. 2002). The true developmental origin of BPS is problematic, since there are frequently inflammatory tissue changes on histology that may be the result of parasitisation of normally occurring pulmonary ligament arteries, which results in a systemic artery supply to the infected area of the lung (Savic et al. 1979a, b; Stocker 1986). However, fetal intrapulmonary lesions with abnormal arterial supply, mostly demonstrating the histologic features of CCAM, are more frequently reported and often referred to by the term "hybrid lesion" (Cass et al. 1997; Zeidan et al. 2009) (Fig 6).

Due to its pleural investment, fetal extrapulmonary BPS can be more consistently defined and characterized. Macroscopically, extrapulmonary BPS are located between the diaphragm and the left lower

lobe in over two-thirds of cases (Savic et al. 1979). Rarely (in less than 10%), they can be encountered subdiaphragmatically, and here, almost exclusively in the left suprarenal region (Fig 10) (Laje et al. 2006). Sometimes, they are found in the mediastinum/paracardially. In some cases, fistulous connections from bronchi to structures, which are embryologically derived from the primitive foregut (esophagus and stomach), have been described. Histologically, extralobar BPS appear as frequently cystic, sometimes solid masses with thick-walled systemic arteries, which represent the persistent primitive splanchnic vessels that supply the early foregut (Savic et al. 1979). These features may indicate the etiologic developmental origin of these lesions as ectopic accessory buds of the foregut. Frequently, more than one systemic artery serves as a feeding vessel (Clements et al. 1987). In half of all cases, the systemic arterial supply originates from the thoracic aorta, and, in 30%, from the abdominal aorta, particularly in infradiaphragmatic BPS (Shanmugam et al. 2005). Rarely, an atypical origin of the feeding vessel from the intercostal, pulmonary, subclavian, gastric, or splenic arteries has been described. In the majority of cases, venous drainage occurs to the hemiazygos and azygos system, and occasionally, also to the pulmonary veins (Savic et al. 1979).

1.3.3 Imaging Appearance of BPS

Again, ultrasound can usually detect BPS during the second trimester (Cavoretto et al. 2008), because of the increased echogenicity, partly cystic components of BPS, and sometimes, because of space-occupying effects. The further clinical and surgical evaluation of BPS requires the confident identification and detailed description of the abnormal systemic artery supply, independent of the exact pathohistological classification of the lesion. Feeding vessels can be identified by Doppler sonography; however, the potential and sensitivity of this method has not been well-documented in larger study cohorts (Becmeur et al. 1998; Cavoretto et al. 2008).

Similarly, the exact potential and sensitivity of MRI in detecting the abnormal vessel (particularly in cases where it does not arise from the fetal aorta) has not been addressed systematically (Dhingsa et al. 2003). Currently, both methods are useful in localizing the abnormal arterial supply. However, because of the multiplanar capabilities of fetal MRI, this technique may offer a more standardized view of the pathology.

Again, T2-weighted sequences in three orthogonal planes, with a preferable slice thickness between 3 and 5 mm, may be the most appropriate for characterizing BPS. Due to the flow-void, the systemic arterial supply usually appears as a T2-weighted hypointense vascular structure, arising from the thoracic or abdominal aorta (Figs. 7 and 10). Smaller feeding vessels that originate from other systemic arteries may be too small to be sufficiently visualized and sensitively detected by MRI. Compared to the surrounding pulmonary parenchyma, BPS and hybrid lesions are generally hyperintense on T2-weighted sequences, and hypointense on T1-weighted sequences (Figs. 7, 8, and 10–12). Commonly, cystic components are found within the lesions (Figs. 9 and 10). Again, BPS have been reported to regress and may "disappear" during pregnancy in 50% of cases, with no need for postnatal surgery (Cavoretto et al. 2008). The most important differential diagnoses constitute congenital diaphragmatic hernia, and, particularly in cases of infradiaphragmatic lesions (Figs. 11 and 12) in the suprarenal region, neuroblastomas.

Generally, BPS, independent of their subtype, have an excellent prognosis. In contrast, the majority of cases with hydrops and pleural effusions are associated with a lethal course. Mediastinal shift and pulmonary hypoplasia are additional indicators of a lethal outcome (Dolkart et al. 1992).

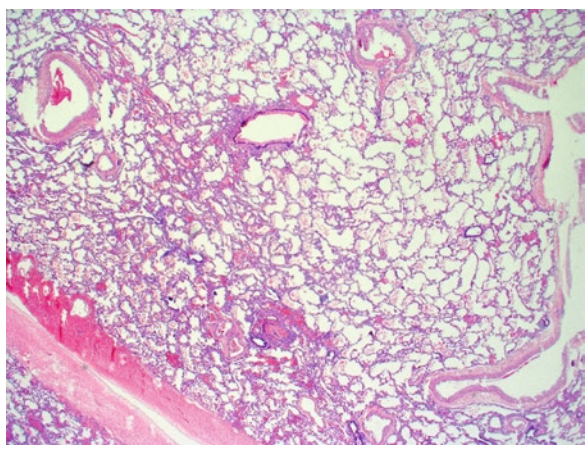

Fig. 9 Histology of the lesion in Figures 7 and 8. Systemic arteries with thick muscular walls appear as an indication of the vascular malformation within the microcystic lesion/bronchopulmonary sequestration (Courtesy of Gabriele Amann and Anke Koller)

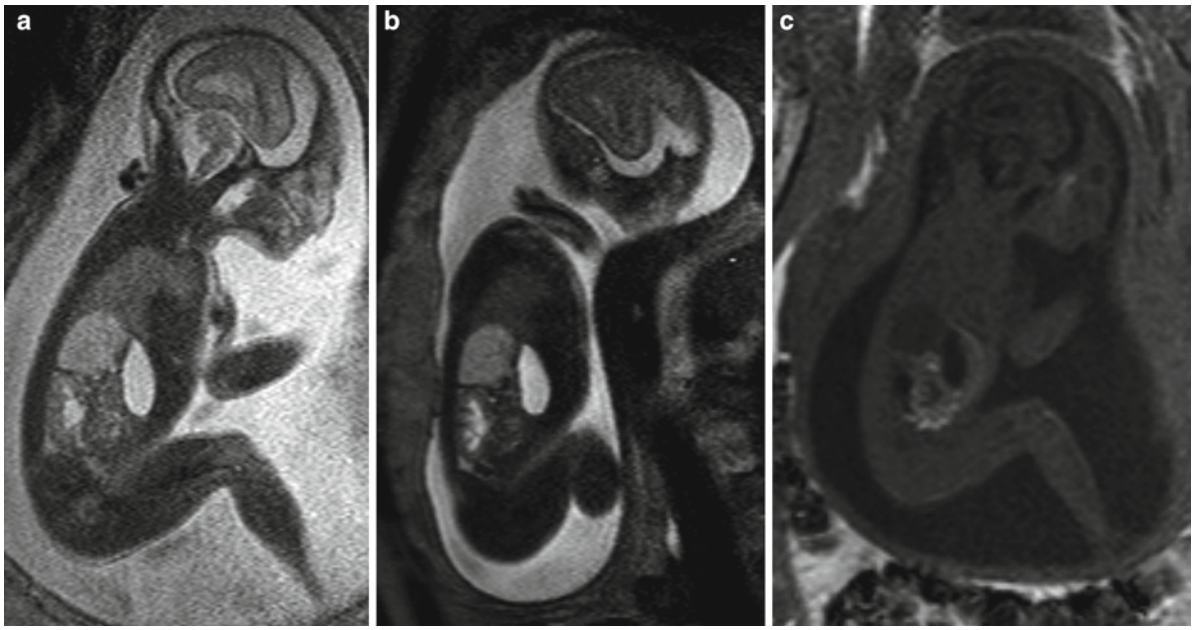

Fig. 10 (**a**–**c**) Infradiaphragmatic bronchopulmonary sequestration at 24GW: Well-demarcated infradiaphragmatic lesion in the left suprarenal region. The better contrast of T2-weighted sequences with TE > 140 ms (**b**) is visible (compared to TE = 100 ms, (**a**). The T1-weighted image shows a homogenous, hypointense lesion

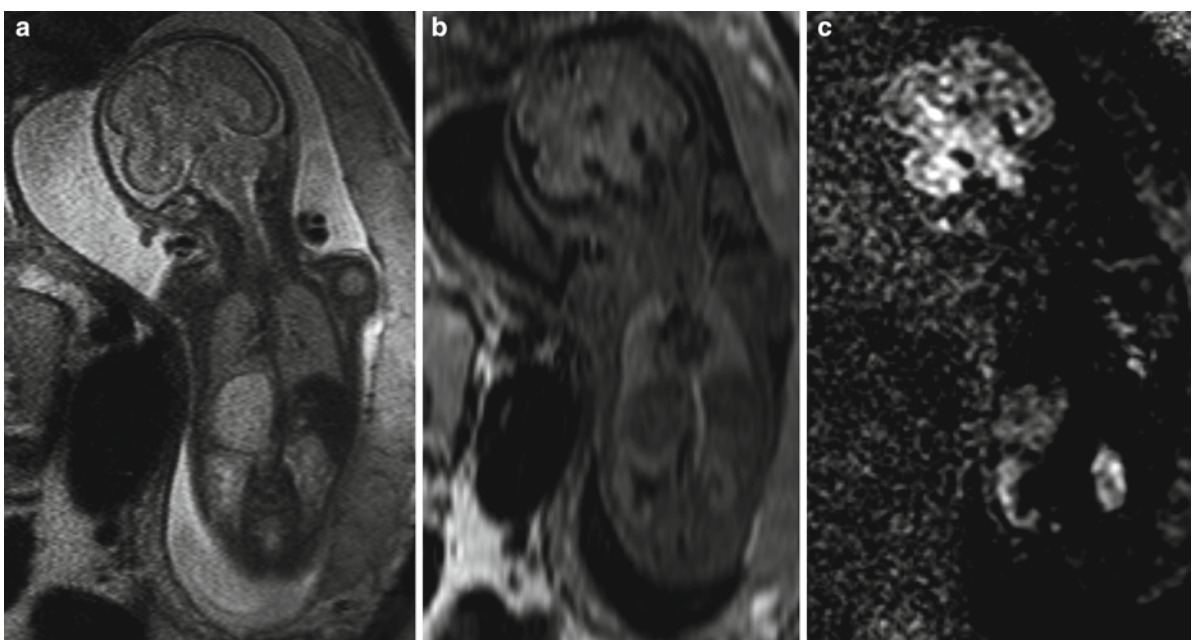

Fig. 11 (**a**–**c**) Coronal T2-weighted (**a**), FLAIR (**b**), and diffusion-weighted (**c**) sequence in the same case as in Figure 10: the low signal on FLAIR indicates low protein content and few cellular structures of the lesion. As occasionally observed by others, DWI shows diffusion restriction of the sequestration ($b = 700$ s/mm², **c**)

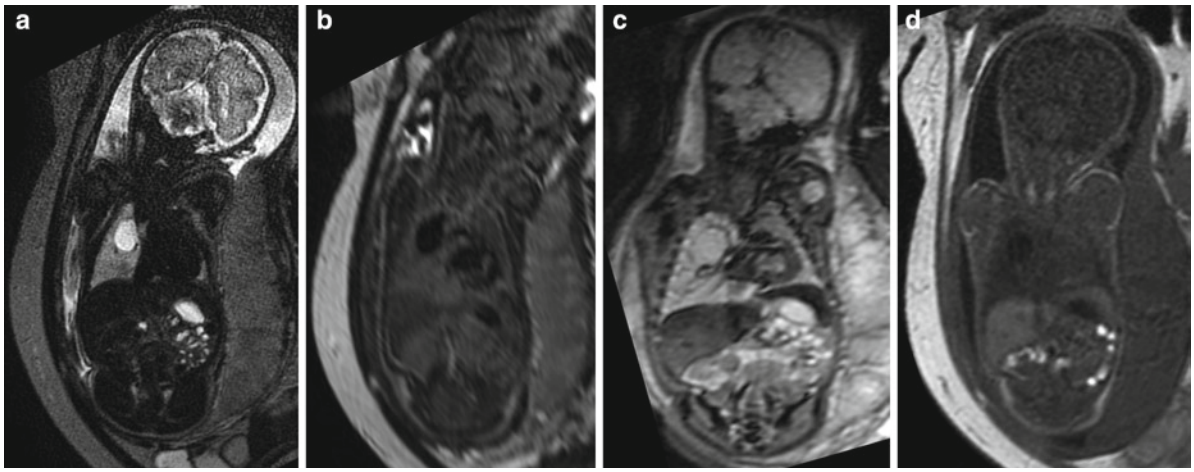

Fig. 12 (**a**–**d**) Bronchogenic cyst in a fetus at 30GW: Coronal T2-weighted (**a**) show a homogenously hyperintense, sharply demarcated cystic lesion in the area of the right upper lobe/parahilar region. Echo planar (**c**) sequences show a subtle hypointense rim of the lesion (potentially relating to the hyaline cartilage found by histology – see Figure 14). On FLAIR (**b**) and T1-weighted (**d**) sequences, the lesion appears homogenously hypointense, excluding hemorrhage or protein-rich content

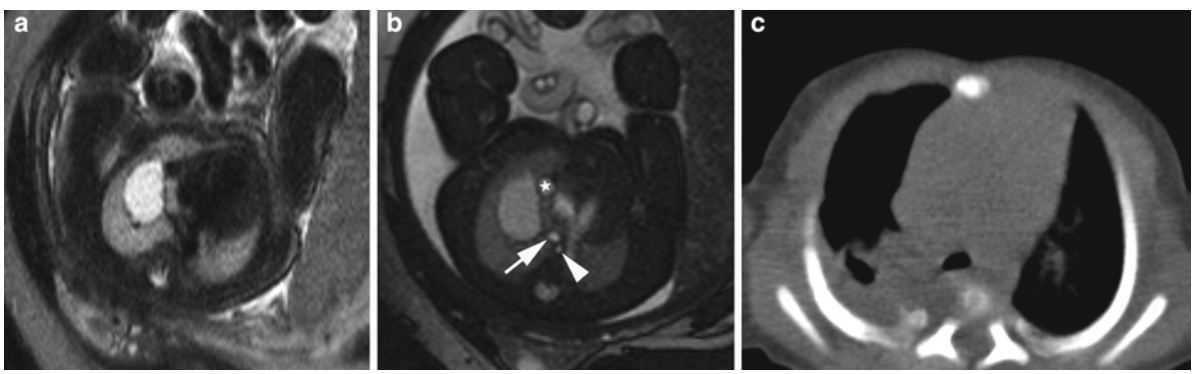

Fig. 13 (**a**–**c**) Axial T2-weighted (**a**) and balanced angiography (**b**) sequences of a bronchogenic cyst at 30GW (same as in Figure 12). Note the detailed anatomical information on the topographical relationship of the superior vena cava (*star*), the esophagus (*arrowhead*), and the tracheal bifurcation (*arrow*), which could not be provided by the postnatal noncontrast CT in the same patient

1.3.4 Bronchogenic Cysts, and Solitary Cystic Lesions of the Fetal Thorax

The most common solitary cystic lesions encountered in the fetal thorax are bronchogenic cysts. Based on their developmental origin, as an abnormal budding of the laryngotracheal groove (see Chap. 15), they are classified within the spectrum of the bronchopulmonary foregut malformations (Gerle et al. 1968). Thus, the location of bronchogenic cysts is mostly in close anatomical proximity to the trachea and/or esophagus, at the level of the trachea, the tracheal bifurcation, or the hilum, on the right side more often than on the left (Takeda et al. 2003). Only few lesions are found below the hilar level (Ribet et al. 1995). They are filled with mucoid, clear or yellow, turbid or purulent, and rarely, a hematic content (postnatal observations), and show either a squamous or respiratory epithelium (Ribet et al. 1995). Postnatally, they can sometimes cause bronchial obstruction, particularly if located adjacent to the left main bronchus.

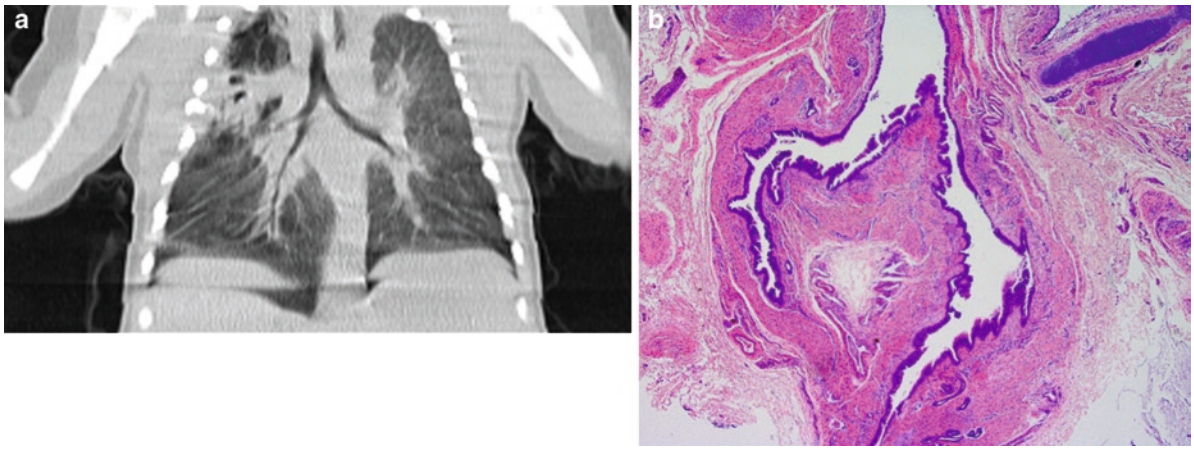

Fig. 14 Coronal reconstruction of the postnatal CT in the same patient as in Figures 12 and 13. A partly cystic, partly consolidated lesion appears in the right upper lobe (*left image*). After surgical resection, histology (*right image*) shows the cystic lesion, lined by a pseudostratified cylindrical epithelium and hyaline cartilage within its wall (Courtesy of Gabriele Amann and Anke Koller)

Other types of thoracic cysts comprise thymic, pericardial, pleural, and finally, esophageal duplication cysts (Takeda et al. 1999). Anterior meningoceles constitute another important differential diagnosis of cystic lesions in the posterior mediastinum. They are associated with neurofibromatosis type 1, and generally communicate with the spinal canal.

Imaging Appearance of Bronchogenic Cysts

The true benefit of fetal MR lies in the clear delineation of the location of the cyst and its anatomical relationships in a multiplanar fashion (Figs. 12–14). Most importantly, *axial* T2-weighted and balanced angiography sequences seem to provide imaging data that is equivalent to postnatal CT scans, and may therefore provide valuable information for the pediatric surgeon since most cysts are resected postnatally (Figs. 13 and 14). Moreover, fetal MRI may detect bronchial obstruction caused by the mass effect of some cysts, with the obstructed lung (lobe) appearing hyperintense on T2-weighted images, due to fluid accumulation (Levine et al. 2001). By using different MR sequences, useful information about the content of the cyst (high amount of protein – FLAIR, T1w and EPI hyperintense; hemorrhagic component – FLAIR, T1w hyper-, EPI hypointense) can be obtained (Fig. 12). Finally, follow-up with fetal MR allows an objective evaluation of the growth dynamics of the cyst.

References

Achiron R, Hegesh J, Yagel S (2004a) Fetal lung lesions: a spectrum of disease. New classification based on pathogenesis, two-dimensional and color Doppler ultrasound. Ultrasound Obstet Gynecol 24:107–114

Achiron R, Zalel Y, Lipitz S, Hegesh J, Mazkereth R, Kuint J, Jacobson J, Yagel S (2004b) Fetal lung dysplasia: clinical outcome based on a new classification system. Ultrasound Obstet Gynecol 24:127–133

Adzick NS, Harrison MR, Crombleholme TM, Flake AW, Howell LJ (1998) Fetal lung lesions: management and outcome. Am J Obstet Gynecol 179:884–889

Adzick NS, Harrison MR, Glick PL, Golbus MS, Anderson RL, Mahony BS, Callen PW, Hirsch JH, Luthy DA, Filly RA et al (1985) Fetal cystic adenomatoid malformation: prenatal diagnosis and natural history. J Pediatr Surg 20:483–488

Albuquerque CA, Smith KR, Saywers TE, Johnson C, Cock ML, Harding R (2002) Relation between oligohydramnios and spinal flexion in the human fetus. Early Hum Dev 68:119–126

Askenazi SS, Perlman M (1979) Pulmonary hypoplasia: lung weight and radial alveolar count as criteria of diagnosis. Arch Dis Child 54:614–618

Becmeur F, Horta-Geraud P, Donato L, Sauvage P (1998) Pulmonary sequestrations: prenatal ultrasound diagnosis, treatment, and outcome. J Pediatr Surg 33:492–496

Bunduki V, Ruano R, da Silva MM, Miguelez J, Miyadahira S, Maksoud JG, Zugaib M (2000) Prognostic factors associated with congenital cystic adenomatoid malformation of the lung. Prenat Diagn 20:459–464

Cangiarella J, Greco MA, Askin F, Perlman E, Goswami S, Jagirdar J (1995) Congenital cystic adenomatoid malformation of the lung: insights into the pathogenesis utilizing quantitative analysis of vascular marker CD34 (QBEND-10) and cell proliferation marker MIB-1. Mod Pathol 8:913–918

Cass DL, Crombleholme TM, Howell LJ, Stafford PW, Ruchelli ED, Adzick NS (1997) Cystic lung lesions with systemic arterial blood supply: a hybrid of congenital cystic adenomatoid malformation and bronchopulmonary sequestration. J Pediatr Surg 32:986–990

Cavoretto P, Molina F, Poggi S, Davenport M, Nicolaides KH (2008) Prenatal diagnosis and outcome of echogenic fetal lung lesions. Ultrasound Obstet Gynecol 32:769–783

Ch'In KY, Tang MY (1949) Congenital adenomatoid malformation of one lobe of a lung with general anasarca. Arch Pathol (Chic) 48:221–229

Clements BS, Warner JO (1987) Pulmonary sequestration and related congenital bronchopulmonary-vascular malformations: nomenclature and classification based on anatomical and embryological considerations. Thorax 42:401–408

Clements BS, Warner JO, Shinebourne EA (1987) Congenital bronchopulmonary vascular malformations: clinical application of a simple anatomical approach in 25 cases. Thorax 42:409–416

Davenport M, Warne SA, Cacciaguerra S, Patel S, Greenough A, Nicolaides K (2004) Current outcome of antenally diagnosed cystic lung disease. J Pediatr Surg 39:549–556

De Paepe ME, Friedman RM, Gundogan F, Pinar H (2005) Postmortem lung weight/body weight standards for term and preterm infants. Pediatr Pulmonol 40:445–448

Dhingsa R, Coakley FV, Albanese CT, Filly RA, Goldstein R (2003) Prenatal sonography and MR imaging of pulmonary sequestration. AJR Am J Roentgenol 180:433–437

Dolkart LA, Reimers FT, Helmuth WV, Porte MA, Eisinger G (1992) Antenatal diagnosis of pulmonary sequestration: a review. Obstet Gynecol Surv 47:515–520

Gerle RD, Jaretzki A 3rd, Ashley CA, Berne AS (1968) Congenital bronchopulmonary-foregut malformation. Pulmonary sequestration communicating with the gastrointestinal tract. N Engl J Med 278:1413–1419

Grethel EJ, Wagner AJ, Clifton MS, Cortes RA, Farmer DL, Harrison MR, Nobuhara KK, Lee H (2007) Fetal intervention for mass lesions and hydrops improves outcome: a 15-year experience. J Pediatr Surg 42:117–123

Hubbard AM, Crombleholme TM (1998) Anomalies and malformations affecting the fetal/neonatal chest. Semin Roentgenol 33:117–125

Illanes S, Hunter A, Evans M, Cusick E, Soothill P (2005) Prenatal diagnosis of echogenic lung: evolution and outcome. Ultrasound Obstet Gynecol 26:145–149

Khosa JK, Leong SL, Borzi PA (2004) Congenital cystic adenomatoid malformation of the lung: indications and timing of surgery. Pediatr Surg Int 20:505–508

Kuwashima S, Nishimura G, Iimura F, Kohno T, Watanabe H, Kohno A, Fujioka M (2001) Low-intensity fetal lungs on MRI may suggest the diagnosis of pulmonary hypoplasia. Pediatr Radiol 31:669–672

Laje P, Martinez-Ferro M, Grisoni E, Dudgeon D (2006) Intraabdominal pulmonary sequestration. A case series and review of the literature. J Pediatr Surg 41:1309–1312

Laudy JA, Wladimiroff JW (2000) The fetal lung. 2: Pulmonary hypoplasia. Ultrasound Obstet Gynecol 16:482–494

Lauria MR, Gonik B, Romero R (1995) Pulmonary hypoplasia: pathogenesis, diagnosis, and antenatal prediction. Obstet Gynecol 86:466–475

Levine D, Jennings R, Barnewolt C, Mehta T, Wilson J, Wong G (2001) Progressive fetal bronchial obstruction caused by a bronchogenic cyst diagnosed using prenatal MR imaging. AJR Am J Roentgenol 176:49–52

Liu YP, Chen CP, Shih SL, Chen YF, Yang FS, Chen SC (2010) Fetal cystic lung lesions: evaluation with magnetic resonance imaging. Pediatr Pulmonol 45:592–600

Longaker MT, Laberge JM, Dansereau J, Langer JC, Crombleholme TM, Callen PW, Golbus MS, Harrison MR (1989) Primary fetal hydrothorax: natural history and management. J Pediatr Surg 24:573–576

Matsuoka S, Takeuchi K, Yamanaka Y, Kaji Y, Sugimura K, Maruo T (2003) Comparison of magnetic resonance imaging and ultrasonography in the prenatal diagnosis of congenital thoracic abnormalities. Fetal Diagn Ther 18: 447–453

Moerman P, Fryns JP, Goddeeris P, Lauweryns JM (1982) Nonimmunologic hydrops fetalis. A study of ten cases. Arch Pathol Lab Med 106:635–640

Moessinger AC, Collins MH, Blanc WA, Rey HR, James LS (1986) Oligohydramnios-induced lung hypoplasia: the influence of timing and duration in gestation. Pediatr Res 20:951–954

Morotti RA, Cangiarella J, Gutierrez MC, Jagirdar J, Askin F, Singh G, Profitt SA, Wert SE, Whitsett JA, Greco MA (1999) Congenital cystic adenomatoid malformation of the lung (CCAM): evaluation of the cellular components. Hum Pathol 30:618–625

NICE Guideline I (2006) Insertion of pleuro-amniotic shunt for fetal pleural effusion. National Institute for Health and Clinical Excellence, London

Nishibayashi SW, Andrassy RJ, Woolley MM (1981) Congenital cystic adenomatoid malformation: a 30-year experience. J Pediatr Surg 16:704–706

Quinn TM, Hubbard AM, Adzick NS (1998) Prenatal magnetic resonance imaging enhances fetal diagnosis. J Pediatr Surg 33:553–558

Ribet ME, Copin MC, Gosselin B (1995) Bronchogenic cysts of the mediastinum. J Thorac Cardiovasc Surg 109: 1003–1010

Rosado-de-Christenson ML, Stocker JT (1991) Congenital cystic adenomatoid malformation. Radiographics 11:865–886

Savic B, Birtel FJ, Knoche R, Tholen W, Schild H (1979a) Pulmonary sequestration. Ergeb Inn Med Kinderheilkd 43:57–92

Savic B, Birtel FJ, Tholen W, Funke HD, Knoche R (1979b) Lung sequestration: report of seven cases and review of 540 published cases. Thorax 34:96–101

Shanmugam G, MacArthur K, Pollock JC (2005) Congenital lung malformations – antenatal and postnatal evaluation and management. Eur J Cardiothorac Surg 27:45–52

Sherer DM, Davis JM, Woods JR Jr (1990) Pulmonary hypoplasia: a review. Obstet Gynecol Surv 45:792–803

Stocker JT (1986) Sequestrations of the lung. Semin Diagn Pathol 3:106–121

Stocker JT (2009) Cystic lung disease in infants and children. Fetal Pediatr Pathol 28:155–184

Stocker JT, Madewell JE, Drake RM (1977) Congenital cystic adenomatoid malformation of the lung. Classification and morphologic spectrum. Hum Pathol 8:155–171

Takeda S, Miyoshi S, Inoue M, Omori K, Okumura M, Yoon HE, Minami M, Matsuda H (1999) Clinical spectrum of congenital cystic disease of the lung in children. Eur J Cardiothorac Surg 15:11–17

Takeda S, Miyoshi S, Minami M, Ohta M, Masaoka A, Matsuda H (2003) Clinical spectrum of mediastinal cysts. Chest 124:125–132

Thorpe-Beeston JG, Nicolaides KH (1994) Cystic adenomatoid malformation of the lung: prenatal diagnosis and outcome. Prenat Diagn 14:677–688

van Teeffelen AS, van der Ham DP, Oei SG, Porath MM, Willekes C, Mol BW (2010) The accuracy of clinical parameters in the prediction of perinatal pulmonary hypoplasia secondary to midtrimester prelabour rupture of fetal membranes: a meta-analysis. Eur J Obstet Gynecol Reprod Biol 148:3–12

Wigglesworth JS, Desai R (1981) Use of DNA estimation for growth assessment in normal and hypoplastic fetal lungs. Arch Dis Child 56:601–605

Zeidan S, Hery G, Lacroix F, Gorincour G, Potier A, Dubus JC, Guys JM, de Lagausie P (2009) Intralobar sequestration associated with cystic adenomatoid malformation: diagnostic and thoracoscopic pitfalls. Surg Endosc 23:1750–1753

Zylak CJ, Eyler WR, Spizarny DL, Stone CH (2002) Developmental lung anomalies in the adult: radiologic-pathologic correlation. Radiographics 22 Spec No: S25–43

MRI of the Fetal Abdomen

Peter C. Brugger

Contents

P.C. Brugger
Integrative Morphology Group, Center of Anatomy and Cell Biology, Medical University of Vienna, Waehringerstrasse 13, 1090 Vienna, Austria
e-mail: peter.brugger@meduniwien.ac.at

D. Prayer (ed.), *Fetal MRI*, Medical Radiology,
DOI: 10.1007/174_2010_23, © Springer-Verlag Berlin Heidelberg 2011

Abstract

› Fetal abdominal MRI is a comparatively recent branch of fetal MRI. Like other organ systems, the abdominal viscera also show considerable changes during the time period covered by fetal MRI. This leads to a different appearance of the fetal abdomen on MRI, depending on gestational age. The changes observed in the gastrointestinal tract relate to the distribution of swallowed amniotic fluid and meconium within the intestines, which is characteristic of both developmental stages as well as of certain pathologies. Organs such as the spleen or adrenal glands change their signal characteristics during development. This chapter summarizes the current knowledge of the prenatal development of the abdominal organs, correlates it with imaging findings, and reviews the MRI appearance of fetal abdominal pathologies.

1 Introduction

Fetal abdominal MRI is a comparatively relative recent branch of fetal MRI. With the emergence of ultrafast sequences, fetal MRI studies were primarily designed to assess the fetal central nervous system (CNS) (Girard et al. 1995; Garel et al. 1998). Organ systems other than the CNS were dealt with rather infrequently (Levine et al. 1998; Amin et al. 1999; Shinmoto et al. 2000; Trop and Levine 2001a). However, much emphasis had been placed on the fetal lungs by then.

More recently, interest has shifted to the abdomen and gastrointestinal tract (Benachi et al. 2001; Saguintaah et al. 2002; Verswijvel et al. 2002; Shinmoto and Kuribayashi 2003; Barnewolt 2004; Veyrac et al. 2004; Daltro et al. 2005; Farhataziz et al. 2005; Hill et al. 2005; Brugger and Prayer 2006; Garel et al. 2006; Inaoka et al. 2007; Huisman and Kellenberger 2008).

2 Normal Fetal Abdominal Anatomy

Although the major steps in the development of the abdominal organs are over around 18 gestational weeks (GW), the fetal abdomen differs in many respects from the adult. These differences are mainly due to different proportions and topographical relationships. The large and symmetric liver occupies a considerable part of the upper abdomen and nearly reaches the iliac crests. Due to the small size of the fetal pelvis, the greater part of the fluid-filled urinary bladder is situated cranially to the symphysis, with its apex at the level of the umbilicus in older fetuses.

As the time period covered by fetal MRI is characterized by further growth and differentiation of organ structures, it seems appropriate to briefly summarize the relevant anatomy and developmental changes in each subchapter. Fetal age will be given in gestational weeks postmenstruation.

3 MR Imaging of the Fetal Gastrointestinal Tract

Imaging protocols to study the fetal abdomen include T2-weighted TSE with short echo time (~100 ms) sequences and/or steady-state free-precession (SSFP) sequences in three orthogonal planes of the fetal body. The field-of-view (FOV), adjusted to fetal size and maternal body habitus, ranges from 200 to 350 mm, with a 3–5-mm slice thickness. Frontal planes cover the whole fetus with the fewest number of slices. In addition, frontal and/or sagittal T1-weighted fast, low-angle shot sequences (TR/TE: shortest/4.6 ms; FOV 265–325 mm; slice thickness 4–5 mm; gap 0–0.5 mm; performed during maternal breath-hold; 15 slices in 16 s) are routinely used. Echo-planar sequences (TR/TE: 3,000/53 ms; slice thickness 4.0 mm) are acquired in the sagittal or frontal planes and dynamic SSFP sequences may be used to demonstrate abnormal bowel motility. To further evaluate the content of cystic lesions, FLAIR and diffusion-weighted sequences may be helpful.

Fetal MRI of the gastrointestinal tract is based on the presence of "natural" contrast media: swallowed amniotic fluid passed to the intestines and meconium. The fetus begins to swallow amniotic fluid by 9–10 GW (Grand et al. 1976; Dumont and Rudolph 1994); however, except for the stomach, it is not until 25 GW that significant amounts of fluid enter the fetal intestines to serve as a natural contrast medium. The swallowed amniotic fluid volume increases steadily, with the term fetus swallowing as much as 750 mL/day (Dumont and Rudolph 1994). Meconium starts to accumulate in the fetal rectum by 18–20 GW and subsequently fills up the oral parts of the colon. Because the presence and distribution of natural contrast media within the fetal gastrointestinal tract are age-dependent, a different appearance of the normal gastrointestinal tract results at different gestational ages (Fig. 1).

3.1 Stomach

3.1.1 Anatomy

The fetal stomach is adult-shaped and continuously increases in size with advancing gestation. By 11–12 GW, three muscle layers can be distinguished (Liebermann 1966), with the fetal pyloric region being more muscular than the remainder of the stomach (Koyuncu et al. 2009). The muscles of the pyloric region achieve a complete adult form by 27 GW (Bremner 1968). As early as 14 GW, sporadic peristalsis of the stomach can be demonstrated (Sase et al. 1999). Gastric motility parallels the maturation of gastric innervation, with pyloric innervation reaching an adult-like profile by 23–23 GW (Abel et al. 1998). By that time, grouped peristalsis can be seen in all fetuses, which is considered to be responsible for gastric emptying (Sase et al. 1999, 2000).

3.1.2 Imaging

The variable fluid-filled stomach should always be recognizable in the upper left abdomen on T2-weighted sequences (Fig. 1). The stomach wall itself is already visible by 20 GW, and the pyloric

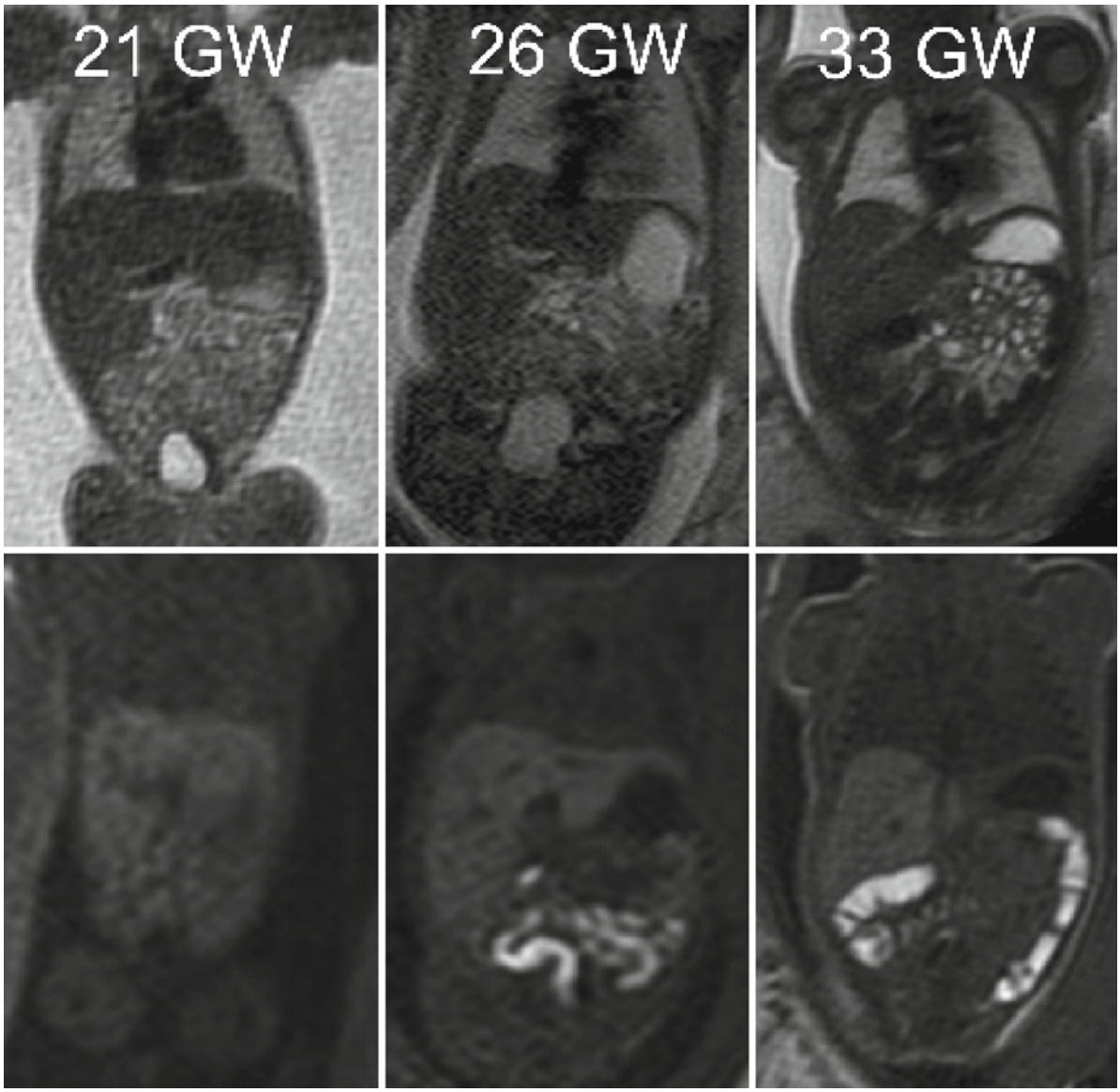

Fig. 1 Varying appearance of the normal fetal abdomen at different gestational weeks. Frontal T2-weighted images (*upper row*) and corresponding T1-weighted images (*lower row*). Increased fluid-filling of the small intestines is seen on the T2-weighted images, and accumulating meconium within the colon is recognizable on the T1-weighted images

region can occasionally be identified. With advancing gestation (>29 GW), mucosal folds also become visible. As the fluid within the stomach mostly consists of swallowed amniotic fluid, the hyperintense T2-weighted signal corresponds to T1-weighted hypointensity. However, gastric fluid may show T1-weighted hyperintensity in the presence of intraamniotic bleeding, when the fetus swallows amniotic fluid with diluted blood. Reflux of the intestinal contents into the stomach in case of proximal jejunal atresia (Fig. 3) may also lead to increased T1-weighted signal intensity of the gastric content.

3.1.3 Anomalies

Abnormal intraabdominal position of the stomach heralds situs anomalies. An intrathoracic stomach is seen in most cases of left-sided congenital diaphragmatic hernias (CDH). Less frequently, this may be due to

gastric herniation (Shinmoto et al. 2000; Al-Assiri et al. 2005).

An extracorporeal stomach may sometimes be found in omphaloceles (Fig. 14).

Little fluid-filling of the stomach, together with polyhydramnios, should raise the suspicion of esophageal atresia. Demonstration of an esophageal pouch sign is diagnostic in such cases (see Chap. 8 , Fig. 13). While a fistula per se cannot be demonstrated, increasing stomach size after several attempts to swallow may be taken as an indirect sign for the presence of a fistula. In fact, fluid-filling of the small intestines is reduced, but this may only be evident in fetuses older than 25/26 GW (vide infra). However, in small fetuses, concomitant duodenal atresia may lead to a normal-appearing, fluid-filled stomach.

A small midline stomach (microgastria) may been seen in the right-sided isomerism (Biyyam et al. 2009).

Marked dilation of the fetal stomach is present in case of duodenal or proximal jejunal stenosis/atresia, as well as in megacystis-microcolon intestinal hypoperistalsis syndrome.

Gastric duplication cysts present as thick-walled cystic masses dorsal to the stomach (Levine et al. 1999; Granata et al. 2003; Okamoto et al. 2008). According to Levine et al. (1999), the signal intensity of the cystic content is slightly lower than that of the fluid within the stomach on both T1- and the T2-weighted sequences. While distinguishing between gastric duplication and pancreatic cysts may be difficult or impossible, distinction from infradiaphragmatic bronchopulmonary sequestration is possible based on the different intrinsic structures and the presence of a feeding vessel in the latter.

3.2 Small Intestines

3.2.1 Anatomy

By 20–21 GW, the small intestines measure 93–98 cm in length (Blumenthal et al. 1980; Shanklin and Cooke 1993) and have mean diameters of 3 mm, which will steadily increase in the following weeks, with the jejunum showing larger dimensions (Malas et al. 2003). The duodenum becomes fixed in its retroperitoneal position early in fetal development (12–14 GW), and by that time, develops an ascending part (Kanagasuntheram 1960). Maturation of the intestinal mucosa occurs in the cranio-caudal direction, and by midgestation (20–25 GW), the intestinal architectural and functional features are highly similar to those of the neonate (Ménard 1994; Vachon et al. 2000).

3.2.2 Imaging

In fetuses younger than 24/25 GW, the small intestines have intermediate to hypointense T2-weighted signal intensity, as they usually are not fluid-filled. Depending on the sectional plane, they present as dot-like or vermiform structures with a 2–3 mm in diameter in cross-section (Figs. 1 and 10). An exception to that rule is the duodenum, which is usually seen partly fluid-filled before 25 GW, with maximum diameters ranging from 2 to 4 mm.

As the proximal and distal small intestines show similar signal intensities, differentiation between them is only possible by their location within the abdomen. Owing to increasing amounts of swallowed amniotic fluid and the rapid development of gastric emptying after 25 GW, more fluid appears within the intestines, primarily in the left abdomen. With advancing gestation, the diameter and number of fluid-filled jejunal loops increase. The maximum jejunal diameter increases in a linear fashion from 2–3 mm by 24 GW to 5–7 mm by 35 GW.

While the fluid within the proximal small intestines appears hyperintense on T2-weighted and SSFP sequences, it usually presents with an intermediate T1-weighted signal intensity that is similar to muscle or liver. This is probably due to the fact that secretions of the liver, pancreas, and jejunum mix with the swallowed amniotic fluid.

The content of the distal small intestines shows intermediate to low T2-weighted signal intensity that corresponds to moderate T1-weighted hyperintensity. After 25 GW, these T1-weighted hyperintense ileal loops are seen predominantly in the lower right quadrant of the abdomen and may be distinguished from the ascending colon by their topography and smaller cross-sectional diameters (3–4 mm).

3.2.3 Anomalies

Anomalies in position include intrathoracic small bowel in CDH and extracorporeal small intestines in gastroschisis and omphalocele. In case of severe

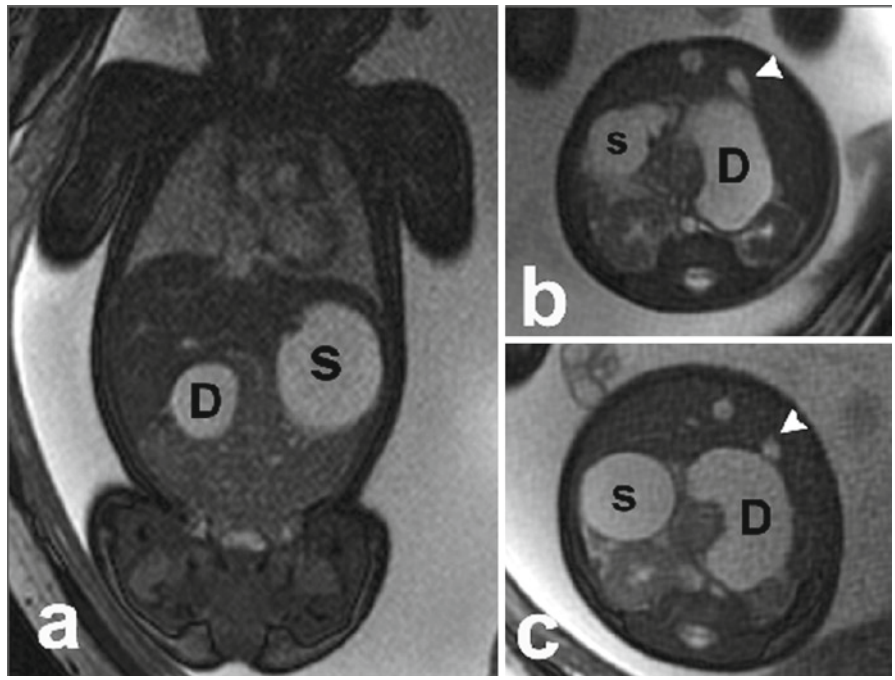

Fig. 2 Fetus at 32+0 GW with duodenal atresia. (**a**) Frontal SSFP image shows distended stomach (S) and duodenum (D) (*double bubble sign*). Note also the absence of fluid-filled jejunal loops. (**b**, **c**) Axial SSFP images. *Arrowheads* denote the gallbladder

oligohydramnios, the fetal small bowels are somewhat fluid-filled and display a more pronounced T1-weighted hyperintensity than usual. This is also the case in the presence of intra-amniotic bleeding.

Atresia or stenosis of the small intestines leads to dilation of the bowel proximal to the site of obstruction. Duodenal stenosis or atresia is easily recognized by the presence of the characteristic "double bubble" sign: proximal to the obstruction, the distended duodenum may have similar dimensions as the stomach, which is also dilated (Fig. 2). The content of the distended duodenal loop shows the same T2- and T1-weighted signal intensities as the stomach. Peristalsis is evidenced by flow voids on T2-weighted sequences or can be demonstrated using dynamic SSFP sequences.

Depending on the site of atresia/stenosis, the content of the dilated bowel loops displays different signal intensities. In proximal jejunal atresia/stenosis, the dilated intestinal loops may present with variable T1-weighted hyperintensity that corresponds to high or intermediate signals on T2-weighted and SSFP sequences (Fig. 3). However, these signal intensities are variable and may change with advancing gestation. Hyperperistalsis is usually present and can be visualized with dynamic SSFP sequences. In cases of proximal intestinal stenosis or atresia, meconium filling of the colon is less conspicuous or absent. However, the postatretic bowel may be detected (Fig. 3c).

While atresia or stenosis of the duodenum or proximal jejunum is usually associated with polyhydramnios, this may not be the case in distal atresias. In distal ileal atresia, the content of the dilated prestenotic bowel reportedly presents with a meconium-like signal intensity (Saguintaah et al. 2002).

According to Carcopino et al. (2006), it is possible to differentiate ileal atresia from meconium ileus: in the former, the dilated bowel loops show hyperintense T1-weighted and hypointense T2-weighted signal intensity, while in the latter the dilated bowel loops appear moderately hyperintense on T1-weighted sequences and have intermediate T2-weighted signal intensity.

In bowel dilatation associated with cystic fibrosis, the content of the dilated bowel loops reportedly shows unusual hyperintense T1-weighted and intermediate T2-weighted signal intensities (Carcopino et al. 2006).

Small bowel stenosis may rarely be caused by a too narrow ventral abdominal wall defect in gastroschisis. Another uncommon cause of bowel obstruction is midgut volvulus. In a third trimester fetus, Miyakoshi et al. (2001) reported multiple dilated bowel loops. The mildly dilated bowel with hyperperistalsis showed high T2-weighted signal intensity, while the enlarged

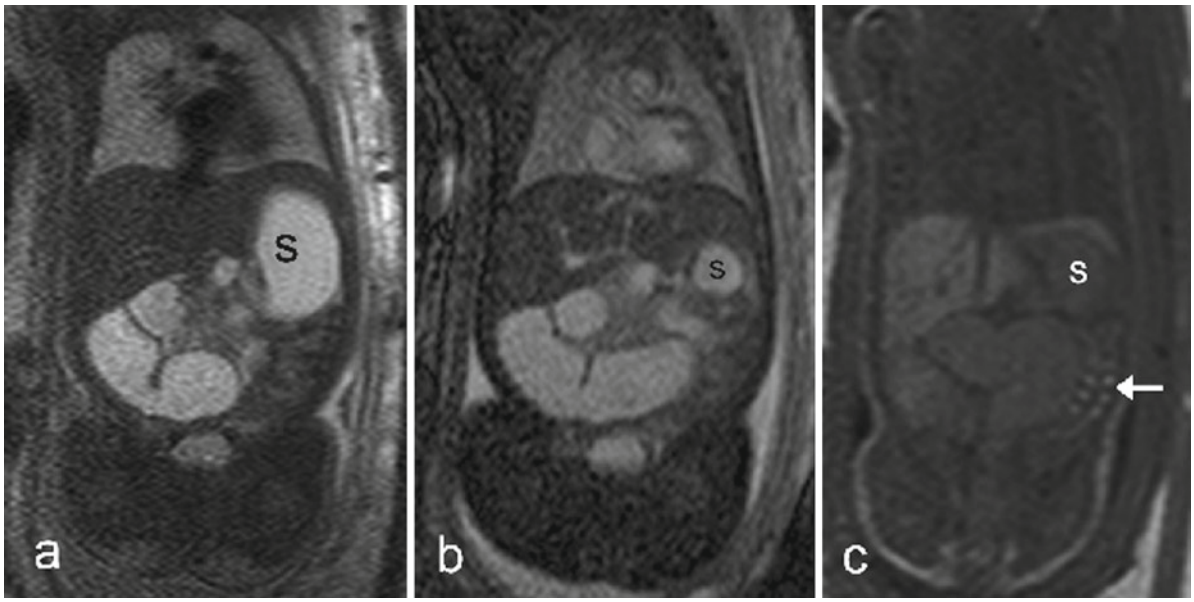

Fig. 3 Fetus at 28+0 GW with jejunal atresia type IIIb. (**a**) Frontal T2-weighted; (**b**) SSFP; and (**c**) T1-weighted image. *S* stomach. The distended jejunal loops display hyperintense signal intensity on T2 and SSFP images, corresponding to a slight increase of T1-weighted signal intensity. The stomach shows the same signal as the jejunum. The postatretic bowel (*arrow*) is clearly visible on the T1-weighted image

bowel loops that lacked peristalsis were homogeneous, with an intermediate T2-weighted signal intensity.

A unique type of bowel dilatation is present in congenital chloride diarrhea. Although of rare occurrence, it is easily diagnosed by its very typical appearance (Fig. 4). The whole gastrointestinal tract, including the colon and rectum, is distended and filled with fluid that appears as hyperintense T2-weighted and hypointense T1-weighted signal intensity. Meconium cannot be demonstrated in any segment of the fetal intestines.

Intestinal atresias may be complicated by perforation of the small bowel, which results in meconium peritonitis. A different prenatal course of fibroadhesive and cystic meconium peritonitis has been reported (Kuroda et al. 2004). Meconium pseudocysts may present with internal septations, high signal on T2-weighted images, variable T1-weighted signal characteristics (Saguintaah et al. 2002; Veyrac et al. 2004; Wong et al. 2006; Šimonovský and Lisý 2007), and no restriction of water diffusion on DWI (Wong et al. 2006). However, meconium cysts with high T1-weighted signal and intermediate T2- (Garel et al. 2006; Zizka et al. 2006), or very low T2-weighted signal intensity (Carcopino et al. 2007), have also been reported.

In terms of signal intensity, similar findings have been reported in segmental ileal dilatation and small bowel duplication cyst. In a case of segmental ileal dilatation, the dilated bowel loop had heterogeneous low T2-weighted and high T1-weighted signal intensity, with the remainder of the small bowel and colon appearing normal (Waters et al. 2007). In duplication of the small bowel near the cecum, the lesion also presented with meconium-like signal (high T1- and low T2-weighted signal intensity) and the colon and rectum were normal (Carcopino et al. 2007).

3.3 Colon

3.3.1 Anatomy

The left colonic flexure and descending colon have achieved their retroperitoneal position by 18–19 GW (Fröber et al. 1991; Richer and Sakka 1994). By that time, the transverse and ascending colon, together with the cecum, form a diagonal limb that courses from the left colonic flexure to the right iliac crest (Fitzgerald et al. 1971; Harris et al. 1976; Fröber et al. 1991).

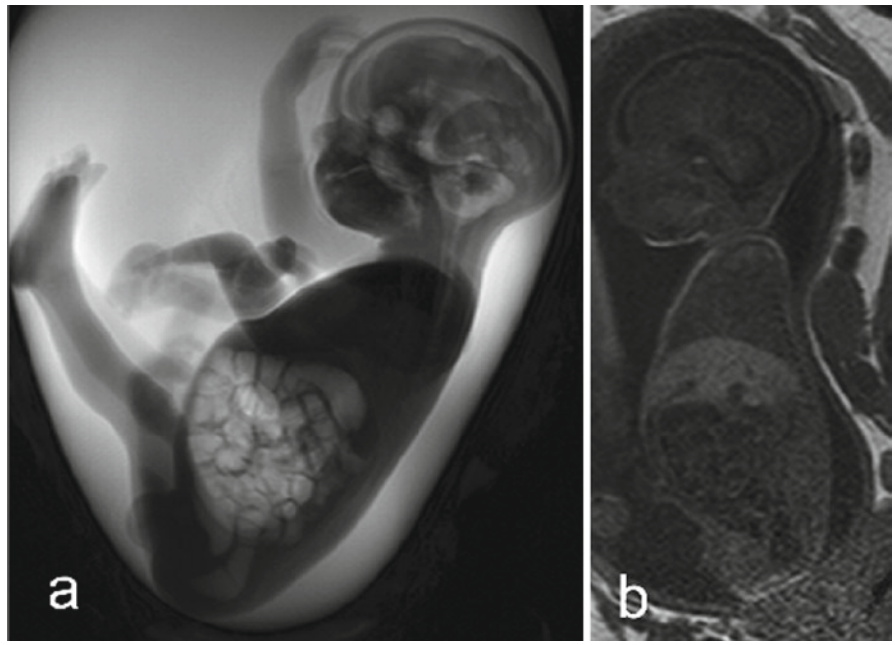

Fig. 4 Fetus at 27 + 3 GW with congenital chloride diarrhea. (**a**) Thick-slab T2-weighted image demonstrates the distended fluid-filled bowel loops. (**b**) Sagittal T1-weighted image showing no trace of meconium within the fetal bowels

The future right colonic flexure is foreshadowed by a kink ventral to the descending part of the duodenum (Hunter 1928; Fröber et al. 1991). In the fifth fetal month, the ileocecal region becomes fixed (Fröber et al. 1991), and the cecum is positioned at the level of the right iliac crest (Fitzgerald et al. 1971). Its final position within the right iliac fossa is reached later in development.

The maximum diameter of the colon increases from 3–4 mm by 20 GW to 8–15 mm at term (Malas et al. 2004). As in adults, the length and position of the sigmoid and transverse colon are quite variable (Malas et al. 2004).

The circular muscles of the colon are already present at the beginning of the fetal period. The longitudinal muscle layer differentiates somewhat later in a caudo-cranial fashion (Lineback 1920). The taeniae begin to appear around 11 GW (Pace 1971) and are evident along the whole colon by 15 GW (Lineback 1920; Pace 1971). Corresponding to the development of the taeniae, colonic haustra can histologically be demonstrated as early as 10–11 GW (Pace 1971). They first appear in the ascending colon and develop toward the sigmoid, becoming more conspicuous in the third trimester (Malas et al. 2004).

The development of the anal sphincter complex starts at the beginning of the fetal period and the three muscles become fully mature between 28 and 30 GW (Bourdelat et al. 2001). However, anal continence is present by 22 GW, as evidenced by the fact that digestive enzymes are no longer present in the amniotic fluid subsequently (Bourdelat et al. 2001). This finding may be attributed to the increasing viscosity of the meconium.

During development, the fetal colon becomes filled with meconium, which consists of intestinal secretions, desquamated intestinal epithelium, swallowed amniotic fluid, and epidermal cells (Schmidt 1971). Therefore, the colon is composed of approximately 72% water and mucosubstances make up nearly 80% of its dry weight (Grand et al. 1976).

3.3.2 Imaging

Visualization of the fetal colon with MRI depends on the signal characteristics of meconium.

Meconium usually appears more or less hypointense on T2-weighted and echo-planar sequences and usually has intermediate signal intensity on SSFP sequences. Its T1-weighted hyperintense signal properties allow selective demonstration of the meconium-filled parts of the colon.

These signal characteristics are most likely due to either the high protein content and/or the presence of

paramagnetic minerals (iron, copper, manganese) in the meconium (Saguintaah et al. 2002). However, there is considerable variation in the signal intensity of the meconium, probably reflecting differences in its composition and/or concentration. Different segments of the colon may show different T1-weighted signal intensities (Fig. 5a), and the meconium signal on SSFP sequences may occasionally become markedly hypointense.

Visualization of the parts of the colon depends on gestational age. As meconium collects in the ileum and subsequently accumulates in the fetal colon from 19 GW onward, the rectum becomes filled first and is seen as a T1-weighted hyperintense column between the urinary bladder and sacrum on sagittal images (Fig. 4b).

Although there is basically a successive "filling up" from distal to proximal, variable progression from the rectum into the descending colon obviously depends on the varying length of the sigmoid. Frequently, gaps may be found, as some parts of the colon may be devoid of meconium. A continuous filling of the whole colon will only be seen closer to term. By 22/23 GW, the left colonic flexure becomes recognizable by its cranial and dorsal position. The transverse and ascending colon become meconium-filled next, usually showing a transverse or oblique course.

Following 25 GW, the whole colon is usually meconium-filled and maximum intensity projections of T1-weighted images allow colonography that produces enema-like images (Brugger et al. 2005) (Fig. 4c). The topography, flexures, and parts of the fetal colon, including the variable sigmoid, can be identified. With MRI, colonic haustra become apparent with advancing age (>30 GW). While the colon wall itself cannot be identified on T2- or T1-weighted images, this is usually possible on SSFP sequences, since the intermediate signal intensity of the meconium contrasts with the hypointense-appearing wall, allowing demonstration of the colonic haustra as well.

With fetal MRI, the maximum colonic diameter may be found in either part of the colon and increases continuously from 4 mm at 21 GW to 18 mm at term. In contrast, an increase in the maximum diameter of the rectum is less pronounced: from 4–5 mm at 21 GW to 12 mm by 38 GW. However, the sagittal and transverse diameters of the rectum are influenced largely by the filling of the urinary bladder. Massive filling of the

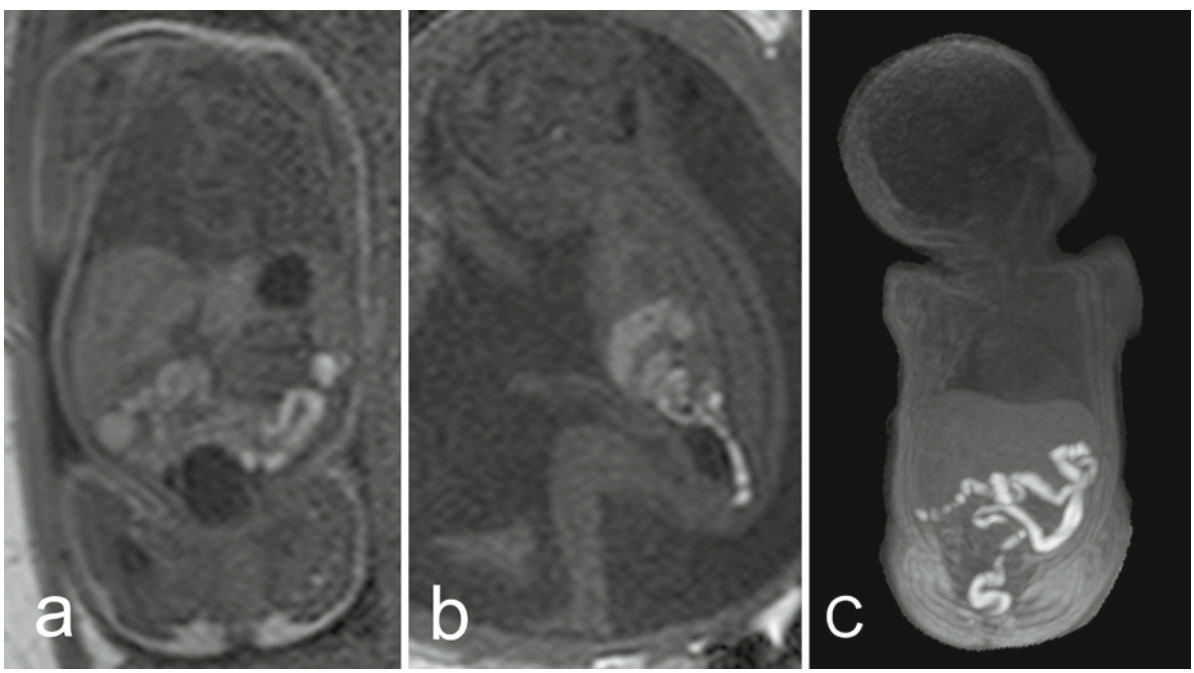

Fig. 5 (**a**) Fetus at 32+4. Frontal T1-weighted image demonstrates different signal intensities of meconium within the descending colon and ascending/transverse colon, the latter showing signal intensity similar to that of the small intestine. (**b**) Sagittal T1-weighted image (fetus at 21+1 GW) showing the meconium-filled rectum dorsal to the hypointense-appearing urinary bladder. (**c**) Colonography in a 31 GW fetus. The different parts of the colon can be distinguished. Note the gaps of filling in the sigmoid and the discontinuous filling of the ascending colon, making it look like a rope of pearls

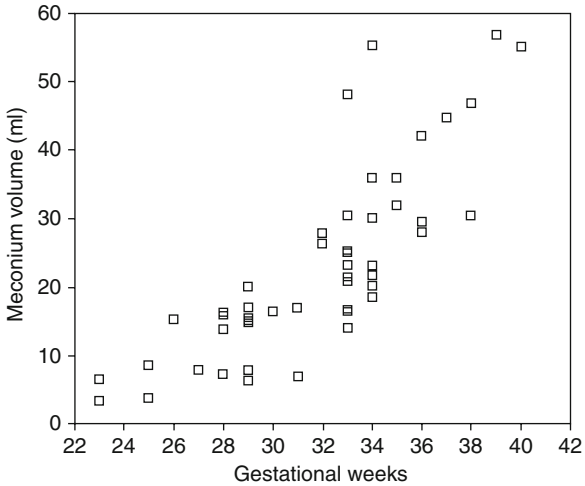

Fig 6 Increase in meconium volume as a function of gestational age (personal data on 49 fetuses). Note the considerable variation at a given gestational week: e.g., at GW 33, the minimum is 14 mL and the maximum 48 mL

urinary bladder may "squeeze" out the meconium of the rectum. This is especially true in older fetuses, where the rectum may not be circular in cross-section.

The meconium content of the fetal colon increases with gestational age (Rubesova et al. 2009).

As can be seen in Fig. 6, the total meconium content of the fetal large intestine is subject to considerable variation, becoming more pronounced with advancing gestation.

3.3.3 Anomalies

In left-sided CDH, the left colonic flexure and distal segments of the colon are in situ, while parts of the transverse and the whole ascending colon are displaced into the left hemithorax. Later in gestation, the diameters of the intrathoracic colon usually exceed those of the intraabdominal parts and show very bright T1-weighted signal intensity.

The greater part of the colon is usually extracorporeal in gastroschisis (Fig. 7). Only the sigmoid and rectum are intracorporeal. Toward the end of the third trimester, the maximum diameter of the extracorporeal colon loops usually becomes greater than normal intraabdominal colon of the same gestational age.

A malrotated or nonrotated colon can be demonstrated by its atypical position (Fig. 8). Malrotation is usually found in heterotaxy syndromes and may be present together with large intraabdominal masses.

Fig. 7 Sagittal T1-weighted image of a fetus at 30+4 GW with gastroschisis, demonstrating the extracorporeal bowel with T1-weighted hyperintensity. Note the change in diameter of the colon entering the abdomen (*arrow*)

Fig. 8 Colonography in a fetus at 28+6 GW showing malrotated colon. This finding was associated with a mesenteric cyst in the cecal region and left-sided renal agenesis

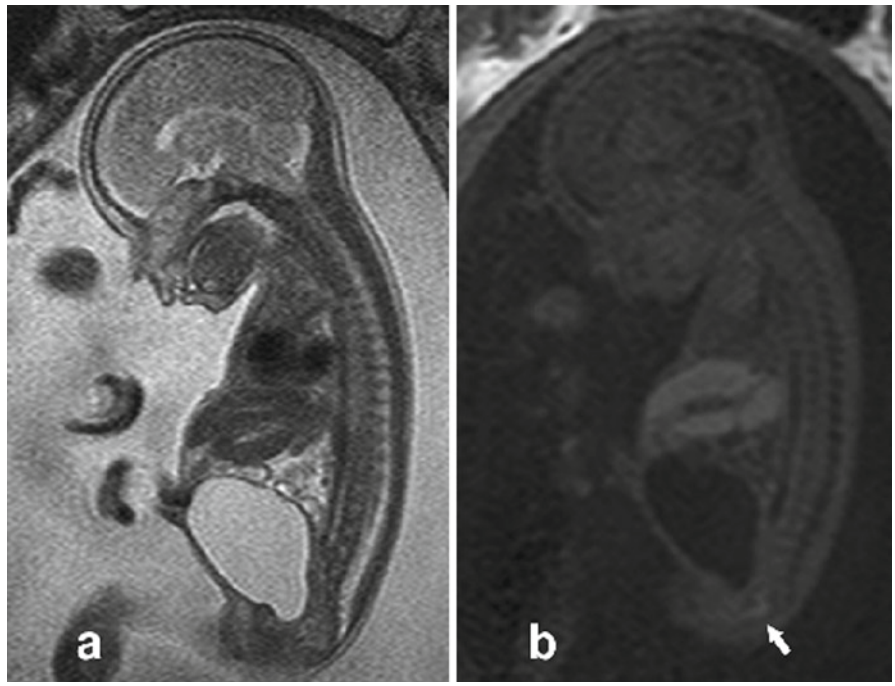

Fig. 9 Fetus at 23 + 5 GW with microcolon-megacystis-intestinal hypoperistalsis syndrome. (**a**) Sagittal T2-weighted image demonstrates dilated urinary bladder and fluid-filled jejunal loops. (**b**) Corresponding T1-weighted image shows only faint meconium signal in the small rectum (*arrow*), which is less than 3 mm in diameter

In microcolon-megacystis-intestinal hypoperistalsis syndrome, the enlarged urinary bladder is the most conspicuous finding. Before 24 GW, very small amounts of meconium are present, with only intermediate T1-weighted hyperintensity being traceable in the small rectum (Fig. 9). Only later in gestation does more meconium accumulate, and the microcolon, as such, can be seen.

Atresias of the large bowel other than those involving the rectum are an uncommon finding. Atresia of the transverse colon (Fig. 10) presents with dilated colon and a sudden cessation of meconium filling the colon. No meconium is detectable in the remainder of the colon, and the dilated bowel loop shows no peristalsis. Similarly, the case of cecal atresia reported by Hill et al. (2005) also showed the distended cecum with meconium-like signal. In addition, the terminal ileum also was dilated and showed meconium-like signal intensity.

In a fetus with Hirschsprung's disease, Ohgiya et al. (2001) reported that the dilated rectum showed intermediate T2-weighted signal intensity.

Low forms of isolated anal atresia may go undetected by fetal MRI, while high forms are easy to recognize (Fig. 11). Such cases may occur together with cloacal malformations, and the content of the rectum may present with abnormal low T1-weighted and high T2-weighted signal intensity (Saguintaah et al. 2002; Garel et al. 2006) due to a rectourethral fistula. In contrast, the content of the urinary bladder may become hyperintense on T1-weighted images. However, in case of a fistula too small to permit a significant exchange of fluid, no changes in signal intensity may be found (Garel et al. 2006).

4 Liver

4.1 Anatomy

Since the physiological left hepatic lobe is larger than the right-sided lobe from the fifth to ninth fetal month, the fetal liver is rather symmetric. This difference is, in part, explained by the different blood supply: the left hepatic lobe is supplied with highly oxygenated blood from branches of the umbilical vein, while the right hepatic lobe receives blood with lower oxygen saturation from the portal vein (Emery 1963; Lind 1963).

The fetal liver is a hemopoietic organ from 6 to 8 GW onward, with the right lobe showing greater

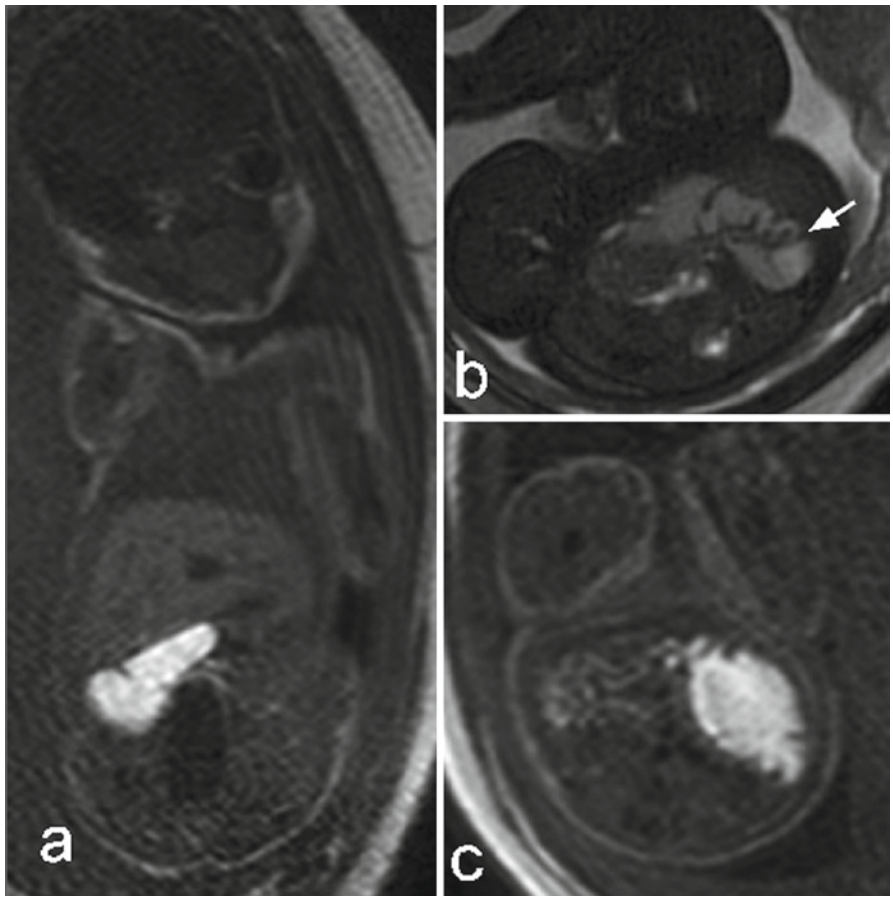

Fig. 10 Atresia of the transverse colon in a fetus at 32+0 GW. (**a**) Frontal T1-weighted image shows meconium-filled transverse colon. No meconium was seen distal to the site of atresia. (**b**) Axial SSFP image showing ileocecal junction (*arrow*). (**c**) Axial T1-weighted image

hemopoietic activity than the left (Emery 1963). In the last trimester, hepatic hemopoiesis decreases progressively as it is shifted to fetal bone marrow. In addition, the fetal liver is an important site of (non-heme) iron storage, which may be as high or even higher than in adults. Paralleling organ growth, the total iron content increases with advancing gestational age (Singla et al. 1985), but considerable variation of the liver iron storage content is present in fetuses of comparable gestational age and body weight (Chang 1973).

By the time hepatic bile secretion begins (around 12 GW), there is already a patent passage to the alimentary canal, as the lumina of the primitive ductal plate structures are continuous with the maturing tubular biliary tree and the extrahepatic biliary system (Crawford 2002). During fetal life and continuing into the neonatal period, a remodeling process toward a mature tubular biliary tree takes place, beginning at the porta hepatis and proceeding centrifugally into the periphery (Crawford 2002).

4.2 Imaging

The hepatic parenchyma appears hypointense on SSFP and T2-weighted sequences and shows moderate inhomogeneous T1-weighted hyperintensity. On echo-planar sequences, the fetal liver is usually hypointense, but marked differences in signal intensity may be seen (Fig. 12). Changes of the hepatic signal intensities on echo-planar sequences between 20 and 26 GW are believed to reflect changes in fetal liver erythropoiesis (Duncan et al. 1997).

Intrahepatic vessels (umbilical and hepatic veins, ductus venosus) are best visualized using SSFP sequences (Fig. 12), since flow void within these vessels usually provides little contrast to the surrounding liver on T2-weighted sequences. Visualization of hepatic vessels on T2-weighted sequences depends on flow velocity and acquisition plane. Laminar flow may lead to a target sign. On T1-weighted sequences, the umbilical vein and major branches of the hepatic veins are seen as hypointense tubular structures, which become more clearly visible in larger fetuses.

Fig. 11 Frontal T1-weighted image in a female fetus at 36 + 1 with cloacal malformation and colon malrotation shows high anal atresia. The colon (*arrow*) tapers off toward the rectum and could not be demonstrated further caudally. In addition, there was left-sided renal agenesis, a hydronephrotic right kidney (*asterisk*) and moderate hydrocolpos

In third trimester fetuses, the portal vein and its tributaries may occasionally be visualized on SSFP sequences.

The intrahepatic bile ducts cannot be demonstrated under normal circumstances.

4.3 Anomalies

In CDH, a hepatic lobe, or part of it, is frequently displaced into the thorax. The intrathoracic liver is best demonstrated using T1-weighted sequences (Fig. 13), which also show the meconium-filled intrathoracic bowels. On sagittal images, the ventrally situated diaphragmatic remnant is frequently seen to cause a notch on the ventral hepatic surface.

In omphaloceles, the fetal liver may be found partly or totally protruding through the ventral abdominal wall defect (Fig. 14). In the latter case, the infrahepatic segment of the inferior vena cava is often absent.

While the fetal liver is rather symmetric, enlargement in case of isomerism can be diagnosed when the associated findings (spleen(s), stomach, bowels) are taken into consideration.

Hepatomegaly is characterized by protrusion of the upper abdomen beneath the costal arch and may be associated with splenomegaly (Fig. 19).

In cirrhosis, the bumpy hepatic surface may be recognized when this condition is associated with ascites. The absence or hypoplasia of one hepatic lobe is a rare finding (Fig. 15) that may be associated with abnormal position of the gallbladder. Bowel loops are found in place of the hepatic lobe.

Persistence of the right umbilical vein results in a left-sided gallbladder and a right-convex course of the intrahepatic part of the vein.

In congenital hemochromatosis, hepatic iron overload may be demonstrated using T2* sequences (Marti-Bonmati et al. 1994; Coakley et al. 1999; Quarello et al. 2008). However, since there is considerable variation of hepatic signal intensity on T2* and echo-planar sequences, relating to both gestational age and sequence parameters, the absence of T1-weighted hyperintensity may be considered to be more reliable in diagnosing this condition.

Currently, intrahepatic calcifications cannot be depicted with fetal MRI.

Fetal liver tumors are an uncommon finding and, to date, only a few cases have been reported using fetal MRI. Hepatoblastoma may present as a space-occupying lesion with a spoke-wheel appearance, showing T2-weighted and T1-weighted hypointense signal intensity when compared to the surrounding liver (Fig. 16). A case of hepatic cavernous hemangioma presented as a solid mass with heterogeneous T2-weighted and low T1-weighted signal intensity (Hill et al. 2005). Shinmoto et al. (2000) found it difficult to differentiate an infantile hemangioendothelioma from other solid tumors of the liver, as it appeared as an inhomogeneous mass with intermediate T2-weighted signal intensity on MRI.

In very rare cases, extensive metastases into the liver may be seen in cases of congenital neuroblastoma. The massively enlarged liver may then show inhomogeneous signal intensities on both T2- and T1-weighted sequences, with its characteristic hyperintense T1-weighted signal intensity being lost in the affected areas.

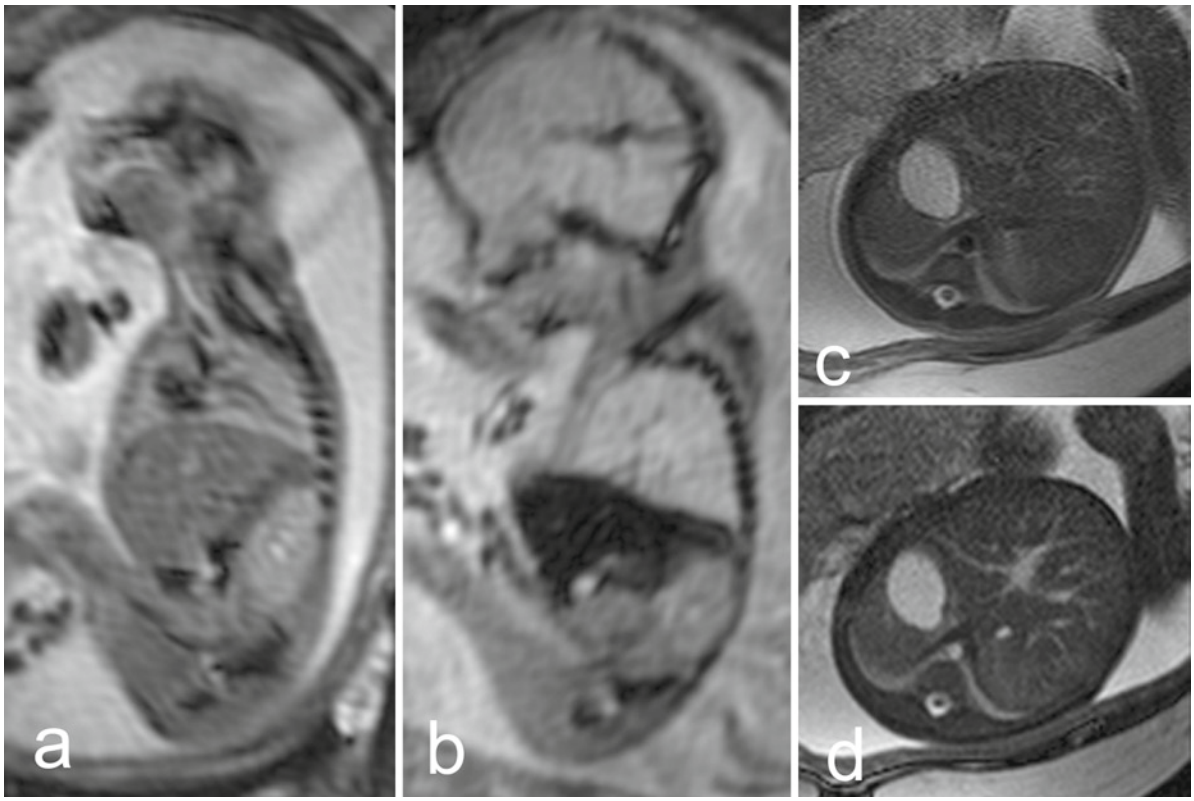

Fig. 12 (**a**, **b**) Fetuses of the same age showing marked differences in hepatic signal intensity on the echo-planar sequence. (**a**) Sagittal image of a fetus at 23+3 GW (Chiari II malformation) displays only intermediate signal intensity. (**b**) Sagittal image of a fetus at 23+4 GW with congenital cystic adenomatoid malformation shows the more typical hypointense signal of the liver. (**c**, **d**) Corresponding axial images through the upper abdomen of a fetus at 32+0 GW. The umbilical vein and its branches and the tributaries to the hepatic veins are hardly recognizable on the T2-weighted image (**c**), but are clearly depicted on the SSFP image (**d**)

5 Gallbladder and Extrahepatic Bile Ducts

5.1 Anatomy

The fetal gallbladder is nearly entirely embedded within the inferior surface of the liver up to 16–17 GW. Following 18 GW, the gallbladder bed becomes more shallow and the biliary bladder increasingly projects below the inferior hepatic surface with advancing gestation. However, the fundus of the fetal gallbladder normally does not protrude beyond the inferior hepatic margin (Haffajee 2000). Gallbladder size increases with gestational age (Chan et al. 1995; Tanaka et al. 2000) and is subject to a daily sinusoidal contractility cycle (Tanaka et al. 2000).

The development of the gallbladder epithelium passes through three stages and gains an adult morphology by the sixth lunar month (Laitio and Nevalainen 1972). The major bile ducts at the porta hepatis are fully formed by 16 GW (Tan and Moscoso 1994).

5.2 Imaging

The fetal gallbladder presents as a right-sided, elongated, pear-shaped structure on the inferior surface of the liver and is consistently demonstrated from 18 GW onward. The hyperintense T2-weighted signal intensity of fetal bile usually corresponds to T1-weighted hypointensity. However, after 30 GW, the T1-weighted hypointense signal intensity frequently becomes iso or hyperintense to liver Brugger et al (2010)?

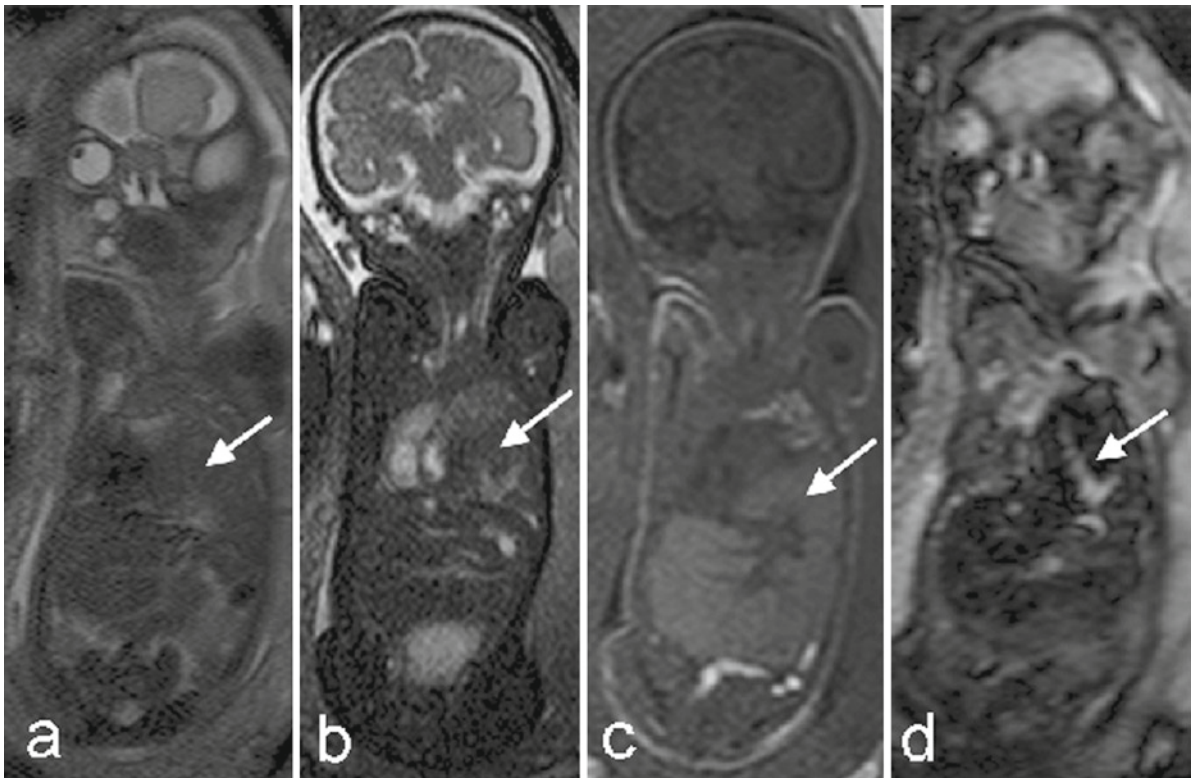

Fig. 13 Corresponding frontal images from a fetus at 30+2 GW with left diaphragmatic hernia and intrathoracic left hepatic lobe (*arrow*). (**a**) T2-weighted image; (**b**) SSFP image; (**c**) T1-weighted image; (**d**) Echo-planar image. The intrathoracic left hepatic lobe is best seen in (**c**, **d**)

Under normal conditions, the extrahepatic biliary ducts may rarely be demonstrated in fetuses older than 30 GW.

5.3 Anomalies

In case of left-sided diaphragmatic hernias with an intrathoracic left hepatic lobe, the gallbladder is usually found to the left of the midline or even intrathoracically. In contrast, in right-sided CDH, the gallbladder may be located in the right hemithorax. In either case, its relationship to the umbilical vein is normal.

In addition to situs inversus and heterotaxy syndromes, left-sided gallbladders are seen together with persistent right umbilical vein (Hochstetter 1886) and may be associated with other anomalies (Bronshtein et al. 1993).

Suprahepatic or retrohepatic positions of the gallbladder may be encountered in hypoplasia of the right hepatic lobe (Fig. 15) (Faintuch et al. 1980).

Since absence of the gallbladder is rare, its nonvisualization on T2-weighted sequences in fetuses older than 30 GW is most likely due to the presence of sludge or gallstones. Corresponding T1-weighted images will then show a hyperintense signal of the gallbladder bile.

Choledochal cysts present as subhepatic cystic masses to the right of the midline, lined by a clearly visible smooth wall (Fig. 17). Being positioned within the hepatoduodenal ligament, they have typical topographical relationships. In the region of the porta hepatis, dilated bile ducts in continuity with the cyst can be demonstrated and dilated intrahepatic ducts are visible on T2-weighted sequences. In younger fetuses, the homogeneous content of the cyst corresponds to amniotic fluid on all sequences (T2, T1, SSFP, FLAIR), while in older fetuses T1-weighted signal intensity may become hyperintense to amniotic fluid and similar to the lungs.

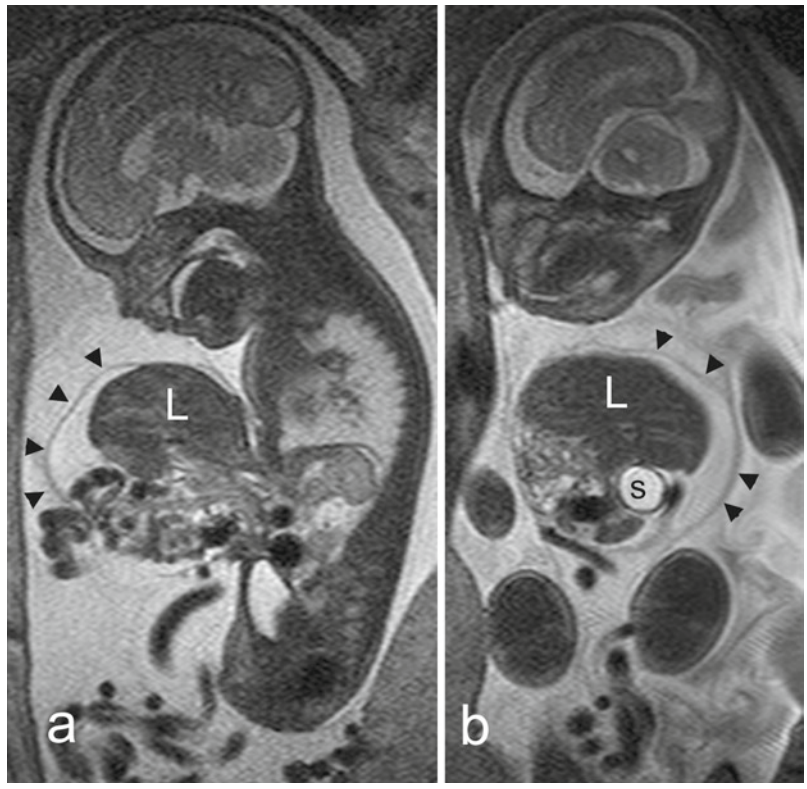

Fig. 14 Omphalocele in a fetus at 29+5 GW with extracorporeal liver. Sagittal (**a**) and frontal **(b)** T2-weighted images demonstrate protrusion of the liver (L) and bowel into the hernial sac (*arrowheads*). *s* stomach. The fetal abdomen is much reduced in the sagittal diameter because of the extracorporeal organs

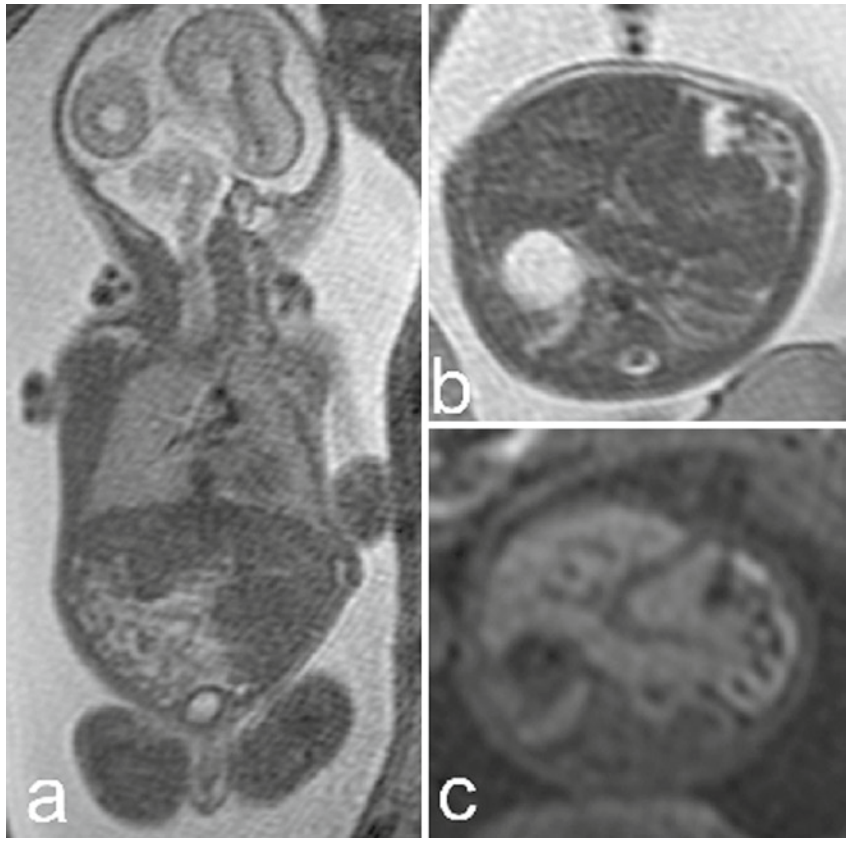

Fig. 15 Fetus at 20+3 GW with hypoplastic right hepatic lobe. (**a**) Frontal T2-weighted image. (**b**) Axial T2-weighted image. (**c**) Corresponding T1-weighted image

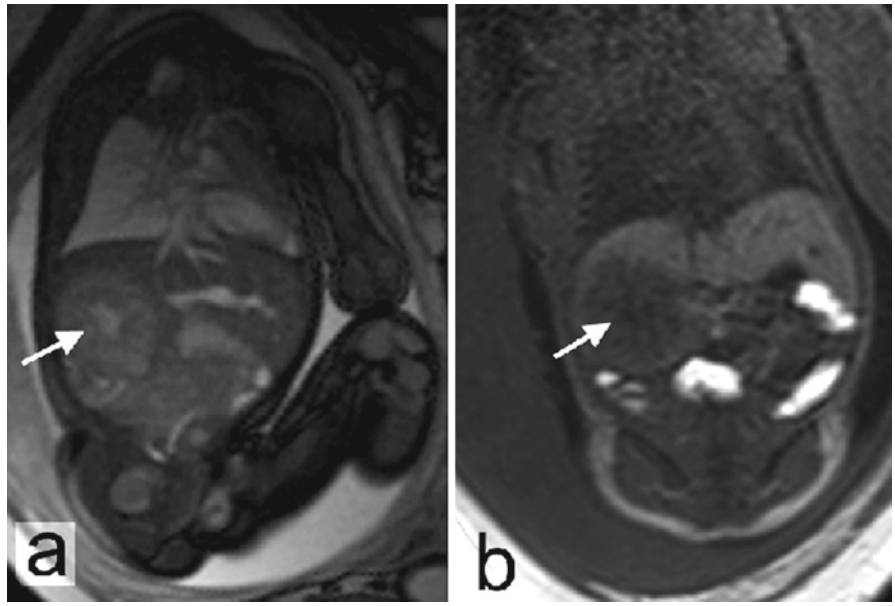

Fig. 16 Hepatoblastoma (*arrow*) in a fetus at 35 + 5 GW. (**a**) Frontal SSFP image demonstrates well-demarcated mass in the right hepatic lobe with spoke-wheel appearance and central hyperintensity. (**b**) Frontal T1-weighted image shows hypointense signal intensity of the lesion compared to the liver

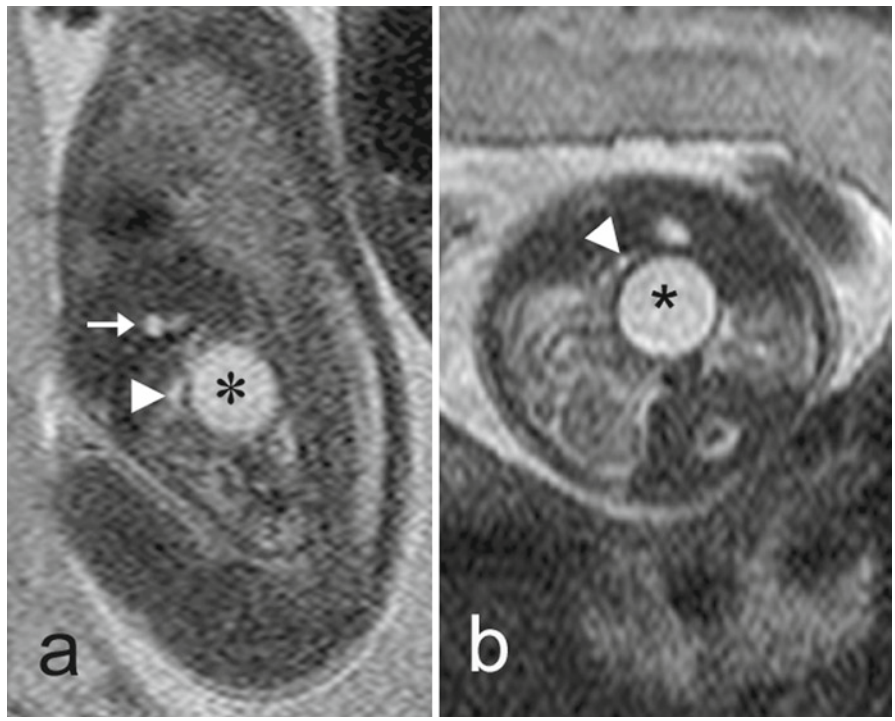

Fig. 17 Fetus (22 + 2 GW) with choledochus cyst (*asterisk*). (**a**) Sagittal T2-weighted image shows dilated intrahepatic bile duct (*white arrow*). (**b**) Axial T2-weighted image. *Arrowheads* denote the duodenum

6 Spleen

6.1 Anatomy

By 20 GW, the fetal spleen weights 0.5–0.6 g and measures about 7×10×17 mm in diameter (Üngör et al. 2007). Splenic growth is allometric during the second and third trimester, with steadily increasing mean weight from 27 GW to term (Barzanji and Emery 1979; Aoki et al. 1992; Hansen et al. 2003). In contrast to the adult condition, the fetal spleen usually is in contact with the left hepatic lobe (Üngör et al. 2007).

Differentiation into red and white pulp takes place between 13 and 19 GW (Weiss and Chen 1974; Timens et al. 1987), and splenic lobules begin to form between 15 and 17 GW, with lymphocytic accumulations around the central arteries recognizable by 19–20 GW (Vellguth et al. 1985).

Extension of the white pulp begins at 20 GW, and by 24 GW, the white pulp occupies about half the organ volume. This contrasts with the situation in the postnatal spleen, where the red pulp makes up more than 80% of the volume (Vellguth et al. 1985).

Although the human fetal spleen is commonly referred to as a hemopoietic organ, there is accumulating evidence that no hematopoiesis takes place (Wolf et al. 1983; Ishikawa 1985; Vellguth et al. 1985; Wilkins et al. 1994; Thomas 1995; Calhoun et al. 1996).

6.2 Imaging

Despite its small size, the fetal spleen can be identified, by 20 GW, by its position dorsolateral to the stomach. The signal intensity of the homogeneous-appearing splenic parenchyma decreases with advancing gestation on T2-weighted and echo-planar sequences, while few changes are present on T1-weighted sequences (Fig. 18). These changes may relate to the increase in red pulp volume with advancing gestation.

Differentiation from the liver may be complicated in terms of signal intensity. Compared to the liver, the spleen usually is hypointense on T1- and hyperintense on T2-weighted sequences.

6.3 Anomalies

An intrathoracic spleen is seen in left-sided CDH with an intrathoracic stomach, but also when the stomach is in the abdomen. Because of its variable position and its small size, it may be hard to identify an intrathoracic spleen in younger fetuses with this condition.

Anomalies in number are typical for heterotaxy syndromes (Applegate et al. 1999). In left-sided isomerism, multiple spleens can be demonstrated in the upper left abdomen along the greater curvature of the stomach. With their number varying from two to nine, the

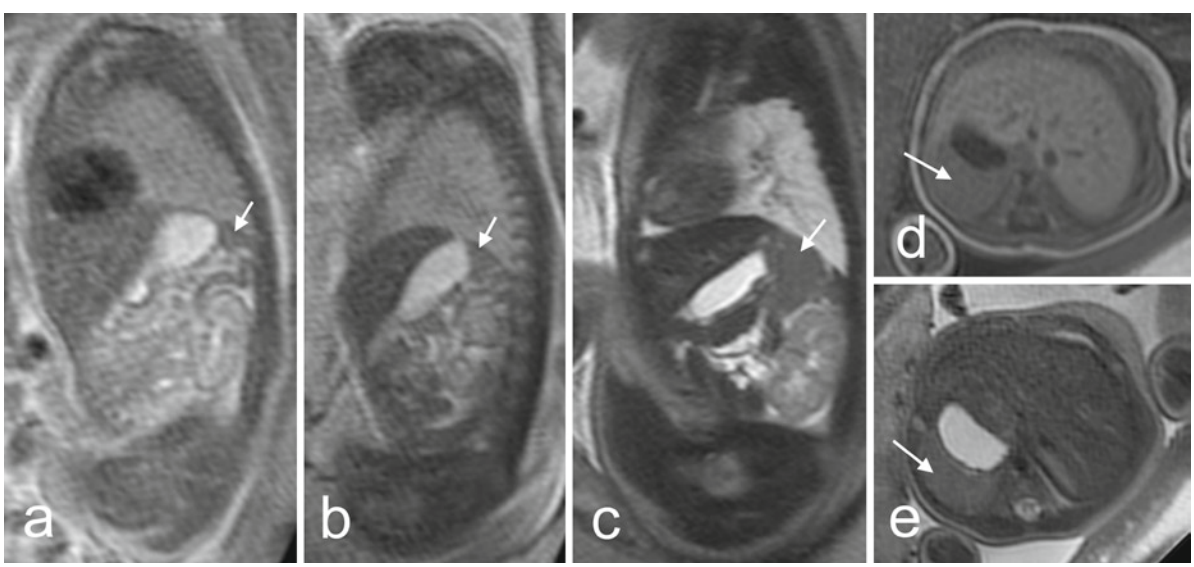

Fig. 18 (**a–c**) Sagittal T2-weighted images depicting the fetal spleen (*arrow*) at different gestational weeks. (**a**) Fetus at 22+0 GW; (**b**) fetus at 25+0; (**c**) fetus at 35+0 GW. (**d**) Axial T1-weighted image and (**e**) corresponding T2-weighted image in a fetus at 38+0 GW

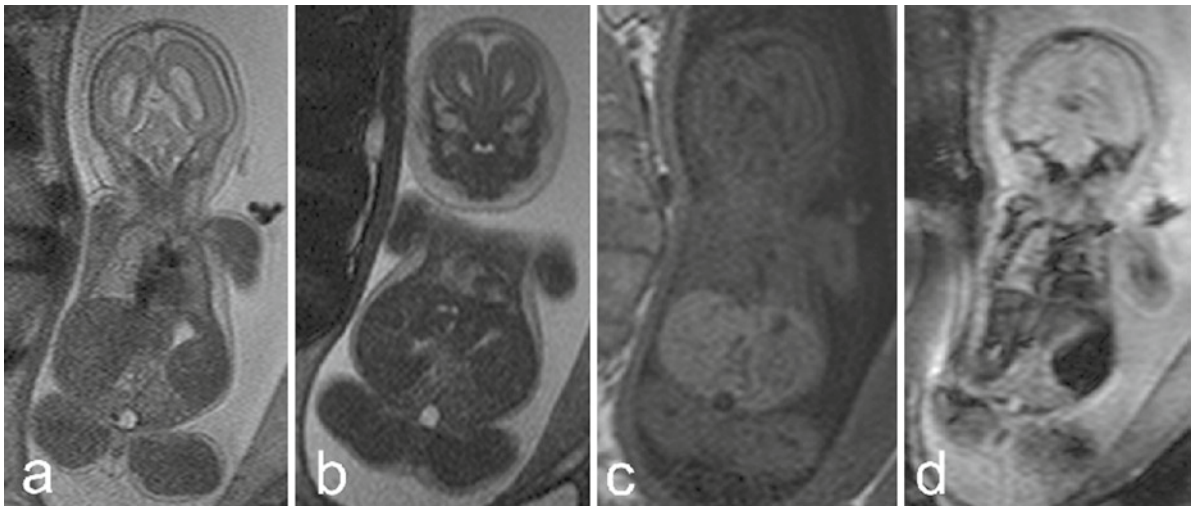

Fig. 19 Frontal images of a fetus at 21 + 1 GW with hepatosplenomegaly. On T2-weighted (**a**) and SSFP (**b**) sequences, the enlarged spleen can be identified by its position lateral to the stomach and shows little difference in signal intensity compared to liver. Signal differences are present on the T1-weighted (**c**) and echo-planar (**d**) image, with the spleen hypointense relative to the liver

relatively equal-sized spleens have a normal combined weight (Moller et al. 1967). Demonstration of multiple spleens with fetal MRI will depend on gestational age, but is usually possible in the third trimester.

Absence of the spleen is characteristic of right-sided isomerism and is usually associated with a small midline stomach.

Fetal splenomegaly (Fig. 19) may be seen in a variety of conditions, including anemia due to Rh-alloimmunization (Bahado-Singh et al. 1998), myeloproliferative disorders (Smrcek et al. 2001), or intrauterine infection (Chaoui et al. 2002).

Splenic cysts are rare and present as T2-weighted hyperintense lesions or masses, dorsolateral to the stomach (Fig. 20), with the cystic content hypointense on T1-weighted images.

Fig. 20 Sagittal T2-weighted image of a fetus at 26 + 3 GW. The septated splenic cyst (*arrow*) is seen dorsal to the fluid-filled stomach. The space caudal to the spleen is filled with bowel loops, as there was concomitant left-sided renal agenesis

7 Pancreas

7.1 Anatomy

The fetal pancreas shows the same topographical relationships as in the adult, and its growth during

the second and third trimester correlates well with age (Hata et al. 1988; Mandarim-de-Lacerda 1994; Krakowiak-Sarnowska et al. 2005). Development of the exocrine pancreas begins during the third month with the appearance of acini (Liu and Potter 1962; Laitio et al. 1974). In the fifth fetal month, significant numbers of zymogen granules are present (Conklin 1962; Laitio et al. 1974) and a complex acinar structure becomes evident (Fukayama et al. 1986). From 25 GW to term, the lobular arrangement becomes more accentuated and the acinar cell volume increases steadily (Carrere et al. 1992). With the exception of amylase, pancreatic enzymes are detectable from 15 GW onward, with lipase not present before 21 GW (Fukayama et al. 1986; Carrere et al. 1992).

The endocrine pancreas begins to develop shortly before the exocrine (Liu and Potter 1962) and grows most rapidly between 21 and 40 GW (Bouwens et al. 1997).

7.2 Imaging

The fetal pancreas may be identified by its topography and is ideally depicted when framed by the fluid-filled duodenum (Fig. 21). It displays intermediate signal intensity on T2-weighted sequences and appears somewhat inhomogeneous. On T1-weighted sequences, fetal pancreatic tissue shows hyperintense signal intensity, similar to the liver.

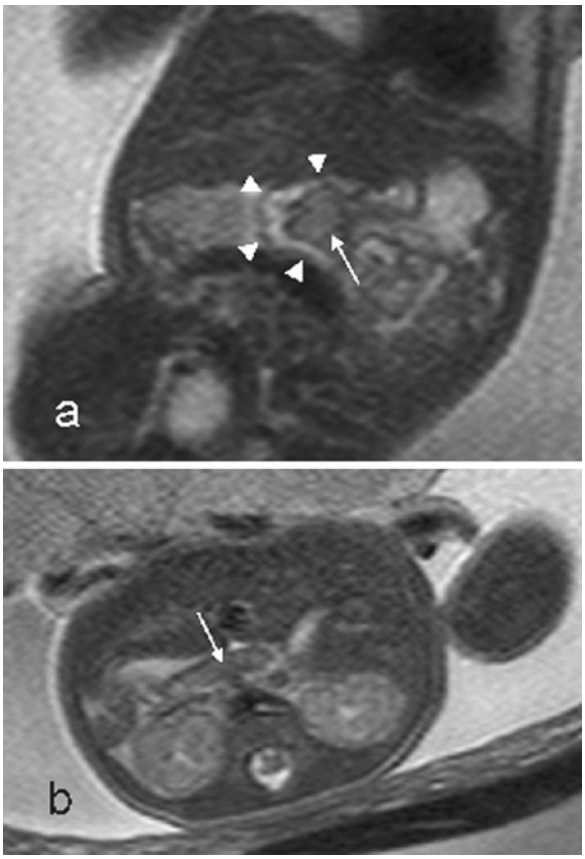

Fig. 21 Fetus at 27 + 1 GW. (**a**) Frontal T2-weighted image: the fluid-filled duodenum (*arrowheads*) allows differentiation of the pancreatic head (*arrow*) from the surroundings. (**b**) Axial T2-weighted image demonstrates the pancreatic body (*arrow*)

7.3 Anomalies

Congenital cysts of the pancreas are rare and present as T2-weighted hyperintense and T1-weighted hypointense cystic lesions dorsal to the stomach (Shinmoto and Kuribayashi 2003; Choi et al. 2007). An annular pancreas, which is often associated with, or may lead to, duodenal obstruction, can usually not be visualized with fetal MRI per se.

8 Adrenal Glands

8.1 Anatomy

The fetal adrenal glands are relatively large organs that show a marked increase in size during the second and third trimester (Gaillard et al. 1990; Chang et al. 2002) and achieve adult dimensions at birth (Barbet and Bargy 1987). This increase in size is mainly due to the presence of a well-developed inner zone of the adrenal cortex, the so-called "fetal zone." At birth, this zone comprises about 80% of the fetal

adrenal cortex (Johannisson 1968; Sucheston and Cannon 1968) or 85% of the total organ volume, but involutes within the first four postnatal months (Sucheston and Cannon 1968; Barbet and Bargy 1987).

Early in development, the fetal adrenals have no medulla as a distinct entity since medullary cells are scattered in small clumps and make up only 1% of the total gland volume (Swinyard 1943). Adrenal medulla volume increases slowly up to 20 GW and then grows more rapidly until 31 GW (Bocian-Sobkowska et al. 1996). This enlargement is mainly due to proliferation of medullary cells and the developing capillary sinusoids, which make up about 36% of the medullary volume in older fetuses (Bocian-Sobkowska et al. 1996). Medullary maturation continues after birth, and the adult type of architecture is present by 12–18 postnatal months.

8.2 Imaging

In young fetuses, the adrenals show marked hypointensity on T2-weighted sequences and can be distinguished from the adjacent organs by virtue of the surrounding hyperintense-appearing perirenal adipose tissues by 20 GW (Fig. 22). Depending on the sectional plane, they show a variable outline, appearing triradiate or lambda-shaped in the frontal or sagittal planes and comma-shaped in the axial plane. Notably, adrenals are more easily recognized in smaller fetuses. While growing larger and assuming a pyramidal shape that corresponds to a triangular cross-sectional appearance, their T2-weighted signal intensity increases and the glands become less conspicuous (Fig. 22). As their T2-weighted signal intensity becomes similar to the spleen, the right adrenal is usually better demarcated from the more hypointense-appearing liver.

On T1-weighted sequences, the fetal adrenals show hyperintense signal similar to that of the liver.

8.3 Anomalies

The absence of an adrenal gland has been reported to be a common condition in cases of unilateral renal agenesis (Ashley and Mostofi 1960). In cases of an empty renal fossa because of ectopic or agenetic kidney, the adrenal appears enlarged and more globular or discoid in shape (Fig. 23).

Enlargement of the adrenal glands may be encountered in Beckwith–Wiedemann syndrome (Fig. 24), in

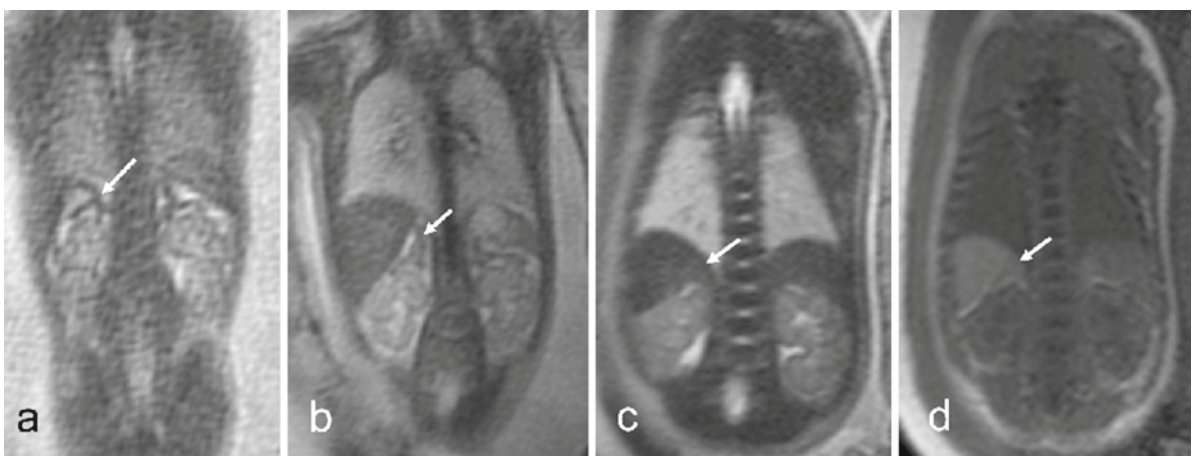

Fig. 22 Frontal images of normal adrenal glands at different gestational weeks. White arrows denote the left adrenal gland. (**a**) Frontal T2-weighted image of a fetus at 20 + 5 GW: the adrenals are seen as hypointense triradiate structures cranial to the upper renal pole. (**b**) Fetus at 25 + 0 with the adrenals appearing less hypointense. Due to the slightly oblique plane, the right adrenal presents with a different shape. (**c**, **d**) Fetus at 36 + 6 GW. T2-weighted image (**c**): the adrenals can hardly be delineated from the spleen or liver. (**d**) Corresponding frontal T1-weighted image shows the adipose tissue of the renal capsule intervening between the kidney and adrenal gland

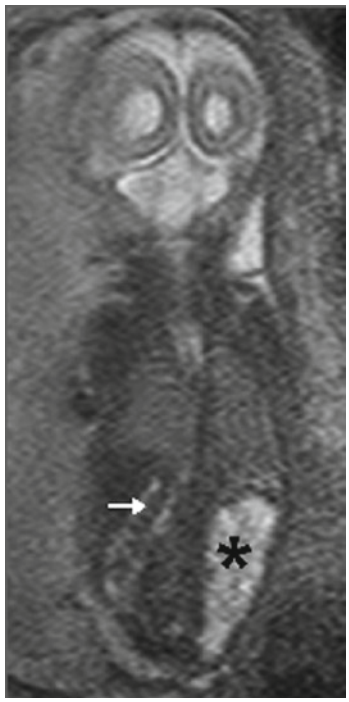

Fig. 23 Fetus at 20+0 GW with agenesis of the right kidney. Frontal T2-weighted image shows the elongated, discoid-shaped right adrenal (*arrow*) and the dysplastic left kidney (*asterisk*) showing abnormal T2-weighted hyperintensity

which visceromegaly may involve one or more intraabdominal organs.

Suprarenal masses in the fetus include a variety of conditions. Because of the polymorphous appearance, the diagnosis may be challenging. With fetal MRI, congenital neuroblastomas present as retroperitoneal, well-circumscribed cystic masses (Fig. 25), which may exhibit extensive areas of hemorrhage and necrosis that show different areas with low-signal intensity on SSFP sequences (Aslan et al. 2004). Intracystic fluid levels, as a consequence of hemorrhage, may be present (Hamada et al. 1999; Trop and Levine 2001b). On the other hand, neuroblastomas may also present as solid-appearing neoplasms with intermediate (Houlihan et al. 2004; McNamara and Levine 2005) or hypointense signal intensity on T2-weighted images (Shinmoto and Kuribayashi 2003). In exceptional cases, adrenal neuroblastomas may present together with massive fetal hepatomegaly, indicating liver involvement as well.

In adrenal hemorrhage, the content of the sharply delineated lesion presents with hyperintense signal intensity on both T1- and T2-weighted sequences (Zizka et al. 2006).

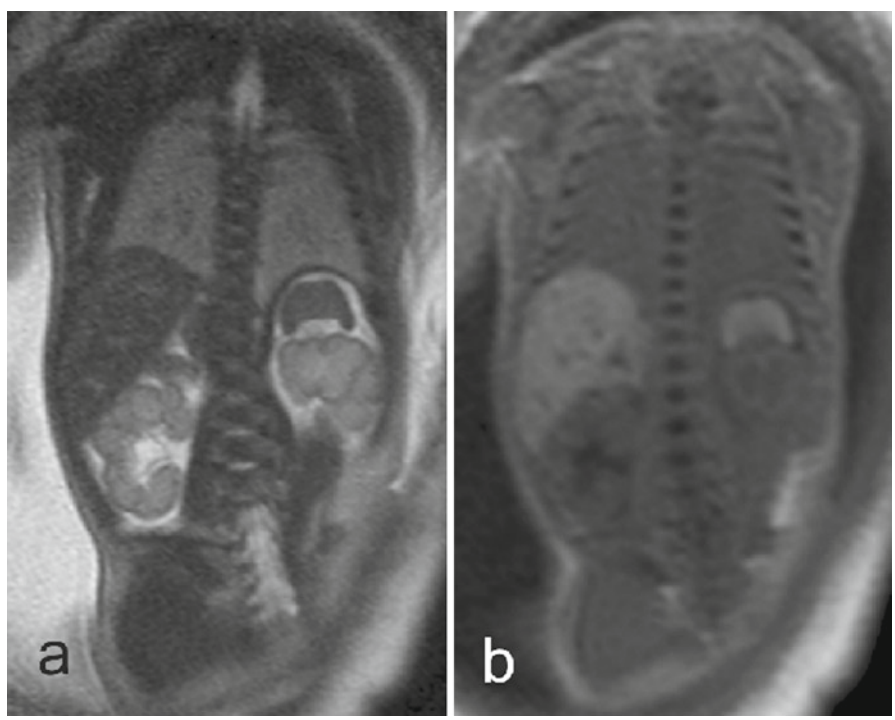

Fig. 24 Enlargement of the adrenals in a fetus (29+1 GW) with Beckwith–Wiedemann syndrome. (**a**) Slightly oblique frontal T2-weighted image. (**b**) Corresponding T1-weighted image. The hypointense appearance of the central part of the right adrenal is due to volume averaging with the perirenal fat, which has not yet gained T1-weighted hyperintensity by 30 GW. Note also the different appearance of the adrenals due to the oblique section plane

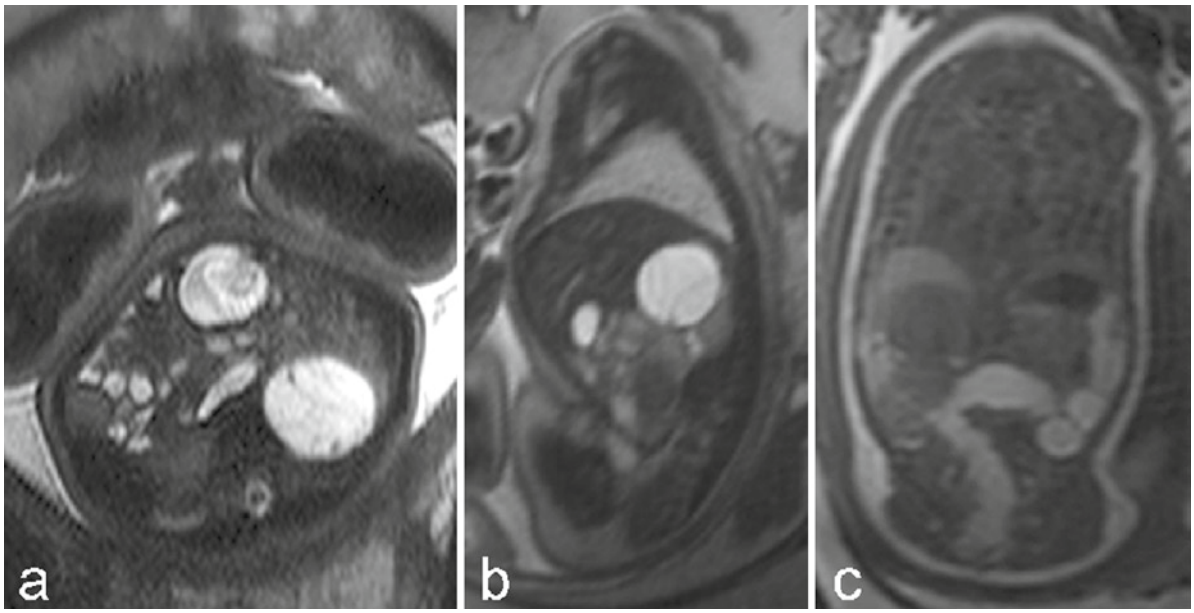

Fig. 25 Fetus at 39+4 GW with right-sided cystic neuroblastoma. (**a**) Axial T2-weighted image shows hyperintense signal intensity of the septated mass. (**b**) Sagittal T2-weighted image. (**c**) T1-weighted image demonstrates the homogenous intermediate signal intensity of the lesion

References

Abel RM, Bishop AE, Moscoso G, Spitz L, Polak JM (1998) The ontogeny of innervation of the human pylorus. J Pediatr Surg 33:613–618

Al-Assiri A, Wiseman N, Bunge M (2005) Prenatal diagnosis of intrathoracic stomach (gastric herniation). J Pediatr Surg 40:E15–E17

Amin RS, Nikolaidis P, Kawashima A, Kramer LA, Ernst RD (1999) Normal anatomy of the fetus at MR imaging. Radiographics 19(spec no):S201–S214

Aoki S, Hata T, Kitao M (1992) Ultrasonographic assessment of fetal and neonatal spleen. Am J Perinatol 9:361–367

Applegate KE, Goske MJ, Pierce G, Murphy D (1999) Situs revisited: imaging of the heterotaxy syndrome. Radiographics 19:837–852

Ashley DJB, Mostofi FK (1960) Renal agenesis and dysgenesis. J Urol 83:211–230

Aslan H, Ozseker B, Gul A (2004) Prenatal sonographic and magnetic resonance imaging diagnosis of cystic neuroblastoma. Ultrasound Obstet Gynecol 24:693–694

Bahado-Singh R, Oz U, Mari G, Jones D, Paidas M, Onderoglu L (1998) Fetal splenic size in anemia due to Rh-alloimmunization. Obstet Gynecol 92:828–832

Barbet JP, Bargy F (1987) Développement et régression du cortex foetal de la surrénale. Bull Assoc Anat (Nancy) 71: 37–44

Barnewolt CE (2004) Congenital abnormalities of the gastrointestinal tract. Semin Roentgenol 39:263–281

Barzanji J, Emery JL (1979) Changes in the spleen related to birth. J Anat 129:819–822

Benachi A, Sonigo P, Jouannic JM, Simon I, Revillon Y, Brunelle F, Dumez Y (2001) Determination of the anatomical location of an antenatal intestinal occlusion by magnetic resonance imaging. Ultrasound Obstet Gynecol 18:163–165

Biyyam DR, Dighe M, Siebert JR (2009) Antenatal diagnosis of intestinal malrotation on fetal MRI. Pediatr Radiol 39:847–849. doi:10.1007/s00247-00009-01226-00245

Blumenthal SG, Stucker T, Rasmussen RD, Ikeda RM, Ruebner BH, Bergstrom DE, Hanson FW (1980) Changes in bilirubins in human prenatal development. Biochem J 186: 693–700

Bocian-Sobkowska J, Wozniak W, Malendowicz LK, Ginda W (1996) Stereology of human fetal adrenal medulla. Histol Histopathol 11:389–393

Bourdelat D, Muller F, Droulle P, Barbet JP (2001) Anatomical and sonographical studies on the development of fecal continence and sphincter development in human fetuses. Eur J Pediatr Surg 11:124–130

Bouwens L, Lu WG, De Krijger R (1997) Proliferation and differentiation in the human fetal endocrine pancreas. Diabetologia 40:398–404

Bremner CG (1968) Studies on the pyloric muscle. S Afr J Surg 6:79–85

Bronshtein M, Weiner Z, Abramovici H, Filmar S, Erlik Y, Blumenfeld Z (1993) Prenatal diagnosis of gall bladder anomalies – report of 17 cases. Prenat Diagn 13:851–861

Brugger PC, Prayer D (2006) Fetal abdominal magnetic resonance imaging. Eur J Radiol 57:278–293

Brugger PC, Weber M, Prayer D (2010) Magnetic resonance imaging of the fetal gallbladder and bile. Eur Radiol, DOI: 10.1007/s00330-010-1856-x?

Brugger PC, Mittermayer C, Herold CJ, Prayer D (2005) Virtual colonography of the fetal colon. Eur Radiol 15, Suppl 1: B-892

Calhoun DA, Li Y, Braylan RC, Christensen RD (1996) Assessment of the contribution of the spleen to granulocytopoiesis and erythropoiesis of the mid-gestation human fetus. Early Hum Dev 46:217–227

Carcopino X, Chaumoitre K, Shojai R, Panuel M, Boubli L, D'Ercole C (2006) Use of fetal magnetic resonance imaging in differentiating ileal atresia from meconium ileus. Ultrasound Obstet Gynecol 28:976–977

Carcopino X, Chaumoitre K, Shojai R, Akkawi R, Panuel M, Boubli L, D'Ercole C (2007) Foetal magnetic resonance imaging and echogenic bowel. Prenat Diagn 27:272–278

Carrere J, Figarella-Branger D, Senegas-Balas F, Figarella C, Guy-Crotte O (1992) Immunohistochemical study of secretory proteins in the developing human exocrine pancreas. Differentiation 51:55–60

Chan L, Rao BK, Jiang Y, Endicott B, Wapner RJ, Reece EA (1995) Fetal gallbladder growth and development during gestation. J Ultrasound Med 14:421–425

Chang LL (1973) Storage iron in foetal livers. Acta Paediatr Scand 62:173–175

Chang CH, Yu CH, Chang FM, Ko HC, Chen HY (2002) Assessment of fetal adrenal gland volume using three-dimensional ultrasound. Ultrasound Med Biol 28:1383–1387

Chaoui R, Zodan-Marin T, Wisser J (2002) Marked splenomegaly in fetal cytomegalovirus infection: detection supported by three-dimensional power Doppler ultrasound. Ultrasound Obstet Gynecol 20:299–302

Choi SJ, Kang MC, Kim YH, Lim JS, Lim SC, Chang JH (2007) Prenatal detection of a congenital pancreatic cyst by ultrasound. J Korean Med Sci 22:156–158

Coakley FV, Hricak H, Filly RA, Barkovich AJ, Harrison MR (1999) Complex fetal disorders: effect of MR imaging on management–preliminary clinical experience. Radiology 213:691–696

Conklin JL (1962) Cytogenesis of the human fetal pancreas. Am J Anat 111:181–193

Crawford JM (2002) Development of the intrahepatic biliary tree. Semin Liver Dis 22:213–226

Daltro P, Fricke BL, Kline-Fath BM, Werner H, Rodrigues L, Fazecas T, Domingues R, Donnelly LF (2005) Prenatal MRI of congenital abdominal and chest wall defects. AJR Am J Roentgenol 184:1010–1016

Dumont RC, Rudolph CD (1994) Development of gastrointestinal motility in the infant and child. Gastroenterol Clin North Am 23:655–671

Duncan KR, Baker PN, Gowland PA, Issa B, Moore R, Worthington B, Johnson IR (1997) Demonstration of changes in fetal liver erythropoiesis using echo-planar magnetic resonance imaging. Am J Physiol 273:G965–G967

Emery JL (1963) Functional asymmetry of the liver. Ann NY Acad Sci 111:37–44

Faintuch J, Machado MC, Raia AA (1980) Suprahepatic gallbladder with hypoplasia of the right lobe of the liver. Arch Surg 115:658–659

Farhataziz N, Engels JE, Ramus RM, Zaretsky M, Twickler DM (2005) Fetal MRI of urine and meconium by gestational age for the diagnosis of genitourinary and gastrointestinal abnormalities. AJR Am J Roentgenol 184: 1891–1897

Fitzgerald MJ, Nolan JP, O'Neill MN (1971) The position of the human caecum in fetal life. J Anat 109:71–74

Fröber R, Kleta U, Linss W (1991) Neue Aspekte zur ontogenetischen Entwicklung des menschlichen Colons. Anat Anz 173:215–223

Fukayama M, Ogawa M, Hayashi Y, Koike M (1986) Development of the human pancreas: immunohistochemical study of fetal pancreatic secretory proteins. Differentiation 31:127–133

Gaillard DA, Lallemand AV, Moirot HH, Visseaux-Coletto BJ, Paradis PH (1990) Fetal adrenal development during the second trimester of gestation. Pediatr Pathol 10:335–350

Garel C, Brisse H, Sebag G, Elmaleh M, Oury JF, Hassan M (1998) Magnetic resonance imaging of the fetus. Pediatr Radiol 28:201–211

Garel C, Dreux S, Philippe-Chomette P, Vuillard E, Oury JF, Muller F (2006) Contribution of fetal magnetic resonance imaging and amniotic fluid digestive enzyme assays to the evaluation of gastrointestinal tract abnormalities. Ultrasound Obstet Gynecol 28:282–291

Girard N, Raybaud C, Poncet M (1995) In vivo MR study of brain maturation in normal fetuses. AJNR Am J Neuroradiol 16:407–413

Granata C, Dell'Acqua A, Lituania M, Oddone M, Rossi U, Toma P (2003) Gastric duplication cyst: appearance on prenatal US and MRI. Pediatr Radiol 33:148–149

Grand RJ, Watkins JB, Torti FM (1976) Development of the human gastrointestinal tract. A review. Gastroenterology 70(5 pt 1):790–810

Haffajee MR (2000) The fetal gallbladder: morphology and morphometry by microdissection. Surg Radiol Anat 22:261–270

Hamada Y, Ikebukuro K, Sato M, Tanano A, Kato Y, Takada K, Hioki K (1999) Prenatally diagnosed cystic neuroblastoma. Pediatr Surg Int 15:71–74

Hansen K, Sung CJ, Huang C, Pinar H, Singer DB, Oyer CE (2003) Reference values for second trimester fetal and neonatal organ weights and measurements. Pediatr Dev Pathol 6:160–167

Harris PF, Jones PR, Robertson CS (1976) A radiological study of morphology and growth in the human fetal colon. Br J Radiol 49:316–320

Hata K, Hata T, Kitao M (1988) Ultrasonographic identification and measurement of the human fetal pancreas in utero. Int J Gynaecol Obstet 26:61–64

Hill BJ, Joe BN, Qayyum A, Yeh BM, Goldstein R, Coakley FV (2005) Supplemental value of MRI in fetal abdominal disease detected on prenatal sonography: preliminary experience. AJR Am J Roentgenol 184:993–998

Hochstetter F (1886) Anomalien der Pfortader und der Nabelvene in Verbindung mit Defect oder Linkslage der Gallenblase. Arch Anat Entwick 9:369–384

Houlihan C, Jampolsky M, Shilad A, Prinicipe D (2004) Prenatal diagnosis of neuroblastoma with sonography and magnetic resonance imaging. J Ultrasound Med 23:547–550

Huisman TA, Kellenberger CJ (2008) MR imaging characteristics of the normal fetal gastrointestinal tract and abdomen. Eur J Radiol 65:170–181

Hunter RH (1928) A note on the development of the ascending colon. J Anat 62:297–300

Inaoka T, Sugimori H, Sasaki Y, Takahashi K, Sengoku K, Takada N, Aburano T (2007) VIBE MRI for evaluating the normal and abnormal gastrointestinal tract in fetuses. AJR Am J Roentgenol 189:W303–W308

Ishikawa H (1985) Differentiation of red pulp and evaluation of hemopoietic role of human prenatal spleen. Arch Histol Jpn 48:183–197

Johannisson E (1968) The foetal adrenal cortex in the human. Its ultrastructure at different stages of development and in different functional states. Acta Endocrinol (Copenh) 58(suppl 130):7–107

Kanagasuntheram R (1960) Some observations on the development of the human duodenum. J Anat 94:231–240

Koyuncu E, Malas MA, Albay S, Cankara N, Karahan N (2009) The development of fetal pylorus during the fetal period. Surg Radiol Anat. doi:10.1007/s00276-008-0449-8

Krakowiak-Sarnowska E, Flisinski P, Szpinda M, Sarnowski J, Lisewski P, Flisinski M (2005) Morphometry of the pancreas in human foetuses. Folia Morphol (Warsz) 64:29–32

Kuroda T, Kitano Y, Honna T, Sago H, Hayashi S, Saeki M (2004) Prenatal diagnosis and management of abdominal diseases in pediatric surgery. J Pediatr Surg 39:1819–1822

Laitio M, Nevalainen T (1972) Scanning and transmission electron microscope observations on human gallbladder epithelium. II. Foetal development. Z Anat EntwicklungsGesch 136:326–335

Laitio M, Lev R, Orlic D (1974) The developing human fetal pancreas: an ultrastructural and histochemical study with special reference to exocrine cells. J Anat 117:619–634

Levine D, Barnes PD, Sher S, Semelka RC, Li W, McArdle CR, Worawattanakul S, Edelman RR (1998) Fetal fast MR imaging: reproducibility, technical quality, and conspicuity of anatomy. Radiology 206:549–554

Levine D, Barnes PD, Edelman RR (1999) Obstetric MR imaging. Radiology 211:609–617

Liebermann D (1966) Die Muskelarchitektur der Magenwand des menschlichen Foeten im Vergleich zum Aufbau der Magenwand des Erwachsenen. Gegenbaurs Morphol Jahrb 108:391–400

Lind J (1963) Changes in the liver circulation at birth. Ann NY Acad Sci 111:105–109

Lineback PE (1920) Studies on the longitudinal muscle of the human colon, with special reference to the development of the taeniae. Contrib Embryol 11:33–44

Liu HM, Potter EL (1962) Development of the human pancreas. Arch Pathol 74:439–452

Malas MA, Aslankoc R, Ungor B, Sulak O, Candir O (2003) The development of jejunum and ileum during the fetal period. Early Hum Dev 74:109–124

Malas MA, Aslankoc R, Ungor B, Sulak O, Candir O (2004) The development of large intestine during the fetal period. Early Hum Dev 78:1–13

Mandarim-de-Lacerda CA (1994) Croissance relative du pancréas chez le foetus humain. Bull Assoc Anat (Nancy) 78:27–29

Marti-Bonmati L, Baamonde A, Poyatos CR, Monteagudo E (1994) Prenatal diagnosis of idiopathic neonatal hemochromatosis with MRI. Abdom Imaging 19:55–56

McNamara A, Levine D (2005) Intraabdominal fetal echogenic masses: a practical guide to diagnosis and management. Radiographics 25:633–645

Ménard D (1994) Development of human intestinal and gastric enzymes. Acta Pediatr Suppl 405:1–6

Miyakoshi K, Ishimoto H, Tanigaki S, Minegishi K, Tanaka M, Miyazaki T, Yoshimura Y (2001) Prenatal diagnosis of midgut volvulus by sonography and magnetic resonance imaging. Am J Perinatol 18:447–450

Moller JH, Nakib A, Anderson RC, Edwards JE (1967) Congenital cardiac disease associated with polysplenia. A developmental complex of bilateral "left-sidedness". Circulation 36:789–799

Ohgiya Y, Gokan T, Hamamizu K, Moritani T, Kushihashi T, Munechika H (2001) Fast MRI in obstetric diagnoses. J Comput Assist Tomogr 25:190–200

Okamoto T, Takamizawa S, Yokoi A, Satoh S, Nishijima E (2008) Completely isolated alimentary tract duplication in a neonate. Pediatr Surg Int 24:1145–1147

Pace JL (1971) The age of appearance of the haustra of the human colon. J Anat 109:75–80

Quarello ER, Molho M, Ville Y (2008) The diagnostic value of fetal liver MRI in cases of congenital haemochromatosis. Ultrasound Obstet Gynecol 32:456

Richer JP, Sakka M (1994) Ontogénèse humaine du côlon gauche. Etape foetale. Bull Assoc Anat (Nancy) 78:31–35

Rubesova E, Vance CJ, Ringertz HG, Barth RA (2009) Three-dimensional MRI volumetric measurements of the normal fetal colon. AJR Am J Roentgenol 192:761–765

Saguintaah M, Couture A, Veyrac C, Baud C, Quere MP (2002) MRI of the fetal gastrointestinal tract. Pediatr Radiol 32:395–404

Sase M, Tamura H, Ueda K, Kato H (1999) Sonographic evaluation of antepartum development of fetal gastric motility. Ultrasound Obstet Gynecol 13:323–326

Sase M, Nakata M, Tashima R, Kato H (2000) Development of gastric emptying in the human fetus. Ultrasound Obstet Gynecol 16:56–59

Schmidt W (1971) Über den paraplacentaren, fruchtwassergebundenen Stofftransport beim Menschen. IV. Vernix caseosa und Meconium. Z Anat Entwicklungsgesch 135:222–241

Shanklin DR, Cooke RJ (1993) Effects of intrauterine growth on intestinal length in the human fetus. Biol Neonate 64:76–81

Shinmoto H, Kuribayashi S (2003) MRI of fetal abdominal abnormalities. Abdom Imaging 28:877–886

Shinmoto H, Kashima K, Yuasa Y, Tanimoto A, Morikawa Y, Ishimoto H, Yoshimura Y, Hiramatsu K (2000) MR imaging of non-CNS fetal abnormalities: a pictorial essay. Radiographics 20:1227–1243

Šimonovský V, Lisý J (2007) Meconium pseudocyst secondary to ileal atresia complicated by volvulus: antenatal MR demonstration. Pediatr Radiol 37:305–309

Singla PN, Gupta VK, Agarwal KN (1985) Storage iron in human foetal organs. Acta Paediatr Scand 74:701–706

Smrcek JM, Baschat AA, Germer U, Gloeckner-Hofmann K, Gembruch U (2001) Fetal hydrops and hepatosplenomegaly in the second half of pregnancy: a sign of myeloproliferative

disorder in fetuses with trisomy 21. Ultrasound Obstet Gynecol 17:403–409
Sucheston ME, Cannon MS (1968) Development of zonular patterns in the human adrenal gland. J Morphol 126:477–491
Swinyard CA (1943) Growth of the human suprarenal gland. Anat Rec 87:141–150
Tan CE, Moscoso GJ (1994) The developing human biliary system at the porta hepatis level between 11 and 25 weeks of gestation: a way to understanding biliary atresia. Part 2. Pathol Int 44:600–610
Tanaka Y, Senoh D, Hata T (2000) Is there a human fetal gallbladder contractility during pregnancy? Hum Reprod 15:1400–1402
Thomas DB (1995) Is the spleen a preferential site of blood cell production in the human fetus? Ital J Anat Embryol 100(suppl 1):245–251
Timens W, Rozeboom T, Poppema S (1987) Fetal and neonatal development of human spleen: an immunohistological study. Immunology 60:603–609
Trop I, Levine D (2001a) Normal fetal anatomy as visualized with fast magnetic resonance imaging. Top Magn Reson Imaging 12:3–17 (published in the February issue)
Trop I, Levine D (2001b) Hemorrhage during pregnancy: sonography and MR imaging. AJR Am J Roentgenol 176:607–615 (published in the March issue)
Üngör B, Malas MA, Sulak O, Albay S (2007) Development of spleen during the fetal period. Surg Radiol Anat 29:543–550
Vachon PH, Cardin E, Harnois C, Reed JC, Vezina A (2000) Early establishment of epithelial apoptosis in the developing human small intestine. Int J Dev Biol 44:891–898
Vellguth S, von Gaudecker B, Muller-Hermelink HK (1985) The development of the human spleen. Ultrastructural studies in fetuses from the 14th to 24th week of gestation. Cell Tissue Res 242:579–592
Verswijvel G, Gyselaers W, Grieten M, Van Robaeys J, Palmers Y (2002) Omphalocele: prenatal MR findings. JBR-BTR 85:200–202
Veyrac C, Couture A, Saguintaah M, Baud C (2004) MRI of fetal GI tract abnormalities. Abdom Imaging 29:411–420
Waters KJ, Levine D, Lee EY, Buonomo C, Buchmiller TL (2007) Segmental dilatation of the ileum: diagnostic clarification by prenatal and postnatal imaging. J Ultrasound Med 26:1251–1256
Weiss L, Chen LT (1974) The differentiation of white pulp and red pulp in the spleen of human fetuses (72-145 mm crown-rump lenght). Am J Anat 141:393–413
Wilkins BS, Green A, Wild AE, Jones DB (1994) Extramedullary haemopoiesis in fetal and adult human spleen: a quantitative immunohistological study. Histopathology 24:241–247
Wolf BC, Luevano E, Neiman RS (1983) Evidence to suggest that the human fetal spleen is not a hematopoietic organ. Am J Clin Pathol 80:140–144
Wong AM, Toh CH, Lien R, Chao AS, Wong HF, Ng KK (2006) Prenatal MR imaging of a meconium pseudocyst extending to the right subphrenic space with right lung compression. Pediatr Radiol 36:1208–1211
Zizka J, Elias P, Hodik K, Tintera J, Juttnerova V, Belobradek Z, Klzo L (2006) Liver, meconium, haemorrhage: the value of T1-weighted images in fetal MRI. Pediatr Radiol 36:792–801

Normal and Pathological Placental Development: MRI and Pathology

Sabine Dekan and Nina Linduska

Contents

S. Dekan (✉)
Clinical Institute of Pathology,
Medical University of Vienna, Austria
e-mail: sabine.dekan@meduniwien.ac.at

N. Linduska
Department of Pediatrics and Adolescent Medicine,
Medical University of Vienna, Austria
e-mail: nina.linduska@meduniwien.ac.at

D. Prayer (ed.), *Fetal MRI*, Medical Radiology,
DOI: 10.1007/174_2010_61, © Springer-Verlag Berlin Heidelberg 2011

Abstract

› The placenta is essential for fetal growth and development. Ultrasound and Doppler are still the standard methods of placenta investigation, but some pathologies such as placenta increta and infarction are better seen in magnetic resonance imaging (MRI). Due to the larger field of view and multiplanar capabilities, MRI has advantages especially in advanced gestational ages. The MRI appearance of the placenta can provide essential information about underlying pathologies contributing to fetal problems such as intrauterine growth restriction (IUGR) and may be helpful for making management decisions or in monitoring the severity of placental pathologies.

1 Introduction

The placenta serves as the organ providing oxygen and nutrition to the fetus. Placental pathologies can lead to disturbances in the exchange and are therefore often responsible for IUGR, prematurity, and intrauterine fetal death. Ultrasound and Doppler flow sonography are the gold standard in placental examination. But due to new MRI techniques and active research in this topic, the healthy and pathological placenta has been described in detail. This chapter provides an overview of the placenta and its pathologies, as well as used MRI sequences and differential diagnoses of placental findings in MRI.

2 Reporting on Placenta in Fetal MRI

Examination of the placenta and the gravid uterus is an integral part of any obstetric sonographic study. Sonographic visualization of the placenta can be difficult due to impaired sonographic conditions such as oligohydramnios, adipositas, or adverse fetal position and posterior placental location. Limited soft tissue contrast is a restriction of this method. MRI is a valuable adjunct technique to evaluate unclear diagnosis with ultrasound. The large field of view is an advantage to ultrasound, especially in the third trimester. The high spatial resolution of MRI, the multiplanar capabilities, the large field of view, and the high soft tissue contrast, which enables simultaneous visualization of fetal and maternal structures, have proven to be advantageous in antenatal examinations. MRI can demonstrate the uterine wall, placenta, amniotic fluid, and the fetus with excellent contrast (Blaicher et al. 2006). Due to greater availability of fetal MRI scans for various fetal or maternal reasons, more attention has been paid on placental lesions.

Documentation of the placenta in MRI should include an assessment of placental location, documentation of the amniotic fluid volume, alterations of the placenta form, alterations near the basal plate as placenta accreta or retroplacental hematoma, placenta parenchyma alterations in maturation or localized processes as for example infarctions or chorioangiomas, umbilical cord abnormalities, alterations of the membranes, and eventually uterine abnormalities.

3 Normal Placental Development

Some knowledge of placental development and structure is necessary to understand its MRI and certain pathology of the organ.

3.1 Development of the Placenta

The major component of the placenta is trophoblastic tissue.

During the first trimester, the basic gross morphology is established (Table 1). Trophoblasts derive from the external cells of the morula by 4–5 days after fertilization. The trophoblastic cells proliferate rapidly and surround the inner cell mass, covering the entire surface of the blastocyst. At day 5–6, attachment to the endometrial surface and implantation occur, usually in the upper part of the uterus. The bastocyst becomes totally embedded in the endometrium. The endometrial stroma undergoes decidual change. In the beginning, the entire gestational sac is covered by chorionic villi. As the sac grows, its surface thins, forming the peripheral membranes. These membranes are composed of decidua capsularis, atrophied chorion, and amnion. The definitive placenta is left at the base.

Table 1 Placental development – first 21 days postfertilization

4–5	Trophoblast derives from external cells of the morula Proliferation of trophoblasts, covering the entire surface of the blastocyst Blastocyst totally embedded in the endometrium Endometrium stroma becomes decidual Entire gestational sac covered by chorionic villi Thinning of the gestational sac, according to its growth, into membranes Membranes consisting from outside decidua capsularis, atrophied chorion, and inside amnion Definitive placenta on the base left Apposition of the membranes with the decidua vera without fusion
9	Fetal–placental circulation establishes with lacunae from syncytial trophoblast
10–12	Maternal blood vessels eroded by trophoblastic invasion (intermediate trophoblast)
14	Primary fetal villi, avascular, consisting of cytotrophoblast covered by syncytiotrophoblast Invasion of avascular extra-embryonic mesenchyma from the embryonic body stalk into the primary villi forming secondary villi
20	Capillaries developing in the villous stroma, forming networks -- tertiary villi
21	Functional circulation with the fetus through umbilical cord, large surface vessels and vessels differentiating from the chorion and the connecting stalk.

With continuous enlargement of the conceptus, it protrudes into the uterine cavity. There, apposition of the membranes with the decidua vera of the opposite side of the uterus takes place without fusion.

The fetal–placental circulation begins at about 9 days postfertilization when lacunae develop from the syncytial trophoblast, which link at day 10 to 12 with maternal blood vessels eroded by trophoblastic invasion. The intermediate trophoblastic cells are responsible for invasion into the uterine wall and maternal vasculature. At day 14 primary fetal chorionic villi have formed, consisting of cords of cytotrophoblast covered by syncytial trophoblast. Shortly after, an invasion of avascular extra-embryonic mesenchyma from the embryonic body stalk into these columns takes place, forming secondary villi. Capillaries develop within the villous stroma forming networks, so-called tertiary villi by day 20. These vessels communicate with the fetus through vessels differentiating from the chorion and the connecting stalk, the large surface vessels and umbilical cord. A functional circulation is established by the end of the third developmental week.

Table 2 Placental maturation

2nd trimester	Extensive growth through branching of the villous tree Primary, secondary and tertiary stem villi occur
GW 9–18	Membrane formation, peripheral expansion
GW 12–20	Late implantation, artery remodeling
GW 13–40	Placental growth
GW 22–30	Terminal villogenesis

In the second and third trimester, the placenta shows extensive growth (Table 2). The placenta grows through branching of the villous tree. Primary stem villi occur below the chorionic plate, secondary and tertiary stem villi and finally distal terminal villi develop (Kaplan 2007).

3.2 Anatomy of the Placenta

3.2.1 Basal Plate

The basal plate is defined as the maternal aspect of the intervillous space. It is the most intimate and most important contact zone of maternal and fetal tissues. The definitive basal plate is composed of extra villous trophoblast, decidua, fibrinoid, residues of degenerating villi, and maternal vessels. During gestation the basal plate grows laterally as well as in thickness. Placenta septa develop from a basal plate folding into intervillous space. Eighty to hundred spiral arteries perforate the basal plate to supply maternal blood to the intervillous space.

3.2.2 Functional Units of the Placenta

Placenta lobule

The placenta is built from subunits. These have been known under various names as, for example, lobules and placentomes.

The physiologic unit of maternal perfusion is called lobule. The opening of the spiral artery is in the center.

Anchoring villi and their distal branching villi constitute the periphery of the lobule.

Cotyledon

Cotyledon describes the functional unit of the fetal vascular tree, defined as that part of the villous tree that has arisen from a single primary stem villous (Ramsey 1959). One cotyledon may contain multiple lobules (Fig. 1).

3.2.3 Fetal Membranes and Surface

Fetal placental surface and the peripheral membranes are continuous. The layer of membrane closest to the fetus is the amnion, which is surrounded by the chorion. The chorion is minimal on the peripheral membranes and more extensive on the disk. Between amnion and chorion, the remnant of the yolk sac can be found.

3.3 Placental Function

Placental function includes nutrition and metabolic and endocrine activities. Maternal blood perfusing the intervillous space allows the transfer of oxygen, (steroid-) hormones, electrolytes, and nutrients from the mother to the fetus and the transfer of waste products and carbon dioxide back from the fetus to the mother.

Additionally, the placenta has endocrine activity, producing progesterone, which is necessary for maintaining the pregnancy, somatomammotropin/placental lactogen, which increases the amount of glucose and lipids in the maternal blood, and estrogen, relaxin, chorionic corticotropin, chorionic thyrotropin, and beta-HCG.

3.4 Placental Maturation

The placenta consists of many branching, treelike villi containing fetal blood and stroma, and bathed in maternal blood within the intervillous space. There is a progressive diminution in villous size and stromal content with increasing portion of the villous composed of blood vessels. During maturation branching increases the villous surface area. The syncytiotrophoblast nuclei become aggregated into "knots" and the cytoplasm thins over vessels, forming vasculo-syncytial membranes, while the originally prominent cytotrophoblastic layer disappears. Syncythial membranes develop; a greater exchange membrane surface is built.

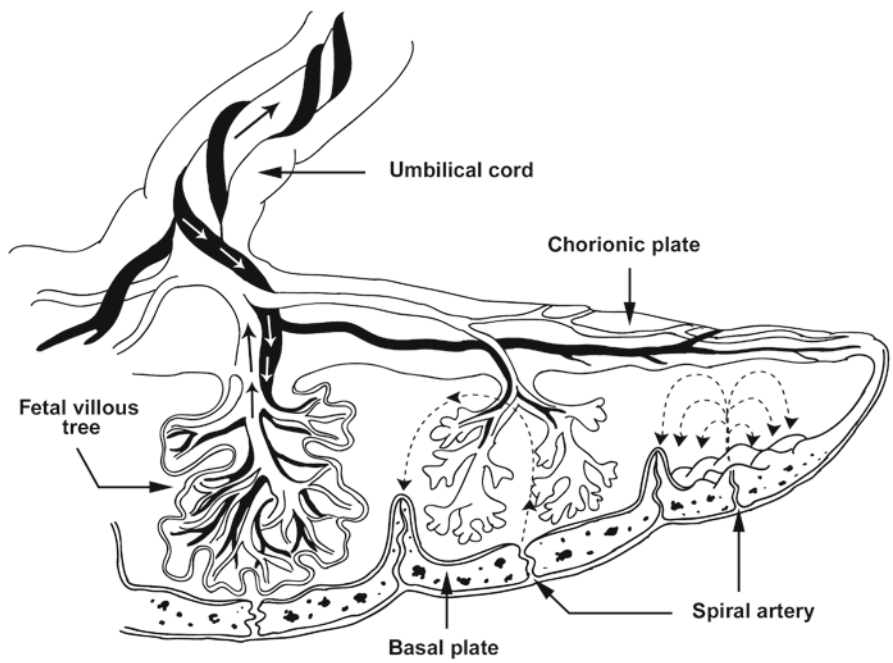

Fig. 1 Schematic placental architecture

Abnormal delayed maturation is commonly seen in inadequately treated gestational diabetes and fetal hydrops. It leads to a reduced surface of exchange membranes.

3.4.1 MRI – Placental Maturation

Placental Maturation in MRI Without Contrast Media

According to the sonographic classification of Grannum et al. (1979), four stages of placental maturation can be differentiated in MRI without contrast media use (Blaicher et al. 2006) (Table 3).

Grade 0 can be seen in the first and second trimester, while Grade I shows predominantly at 24–31 gestational weeks (GW). Grade II, which predominates at 32–35 GW, has been described till delivery at term. Calcifications appear along the basal plate in a Do-dash configuration. Grade III, which represents a mature placenta can develop from 36 GW on, but does not have to be reached necessarily. Grade III shows more irregular calcifications and has been associated with smoking, chronic hypertension, diabetes, and systemic lupus erythematosus (SLE).

The ratio of placenta/amniotic fluid signal intensity decreases significantly with gestational age.

T2-weighted (−w) images show the placenta as moderately hyperintense and allow differentiation between the placenta and the hypointense myometrium in most cases. It provides clear images from multiple angels.

Placental Maturation in MRI with Contrast Media

Marcos et al. (1997) studied the normal placenta with gadolinium-enhanced dynamic MRI using T1- and T2-w sequences. The placentas were of minimally higher signal intensity on T1- and T2-w images than the signal intensity of the myometrium. On immediately post-contrast, fat-suppressed, SPGR images, the placenta enhances early and intensely in an arterial phase. Myometrial enhancement is less and more delayed.

Lobular pattern of enhancement is shown in third trimester placentas, resembling the organization of the placenta into cotyledons, while second trimester placentas exhibit heterogeneous enhancement (Marcos et al. 1997).

Contrast media seem not to increase information according visualization of placental maturation in MRI.

3.5 Calcification of the Placenta

Calcification is mostly located at the maternal surface and the villous. It increases with gestational age with variable degree. The etiology is unclear. Calcifications are seen in term placentas most commonly in the fibrin and fibrinoid in the basal plate and the placental septa. Massive calcification of the placenta may occur but is not considered to be associated with any significant clinical abnormalities. Villous microcalcification shows microscopic deposits lining the villous basement membranes and are seen in abortions, hydramnios, and other conditions including fetal vascular thrombosis, anencephaly, trisomy 21, and others.

3.6 Placental Shape

Placental shape is quite variable, usually round to ovoid and about 18–20 cm in diameter, 1.5–2.5 cm thick at term (Kaplan 2008). Placental thickness over

Table 3 Grannum-Classification of Placenta Maturation in Ultrasound

Grade	Chorionic plate	Basal layer	Placental substance	GA in weeks
0	Straight well defined	No densities	Homogeneous	12–30
I	Subtle undulations	No densities	Few scattered EGAs	30–32
II	Indentations extending into the placenta but not to basal layer	Linear arrangement of small EGAs	Linear echogenic densities, comma-like	32–35
III	Indentations communicating with basal layers	Large, somewhat confluent basal EGSs	Circular densities with echosharped areas in center; irregular densities	From 36

EGA, echogenic area

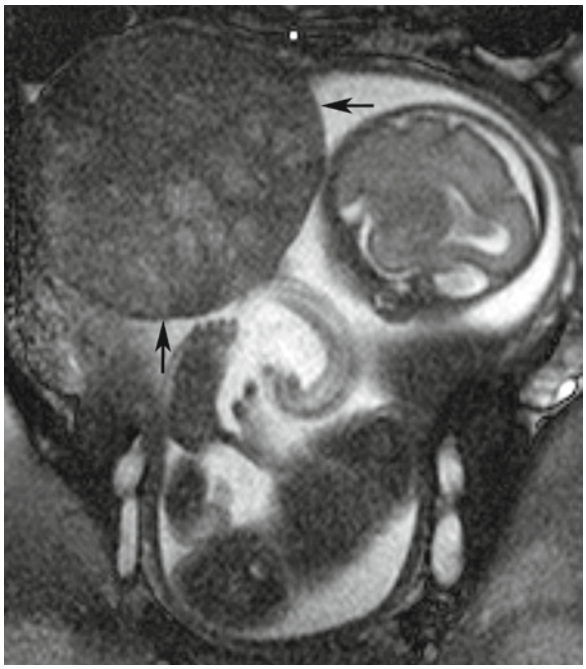

Fig. 2 Pathological placental shape, placenta to small, GW 29

5 cm is considered pathological (Elchalal et al. 2000; Salafia et al. 2008) (Fig. 2).

Failure of atrophy of capsular villi leads to succenturiate lobes (Kaplan 2008). Bilobate placentas with two roughly equal-sized lobes separated by a segment of membranes result from uterine sulcal implantation (incidence 2–8%).

Uterine cavity abnormalities often lead to unusually shaped, often multilobate placentas. Multilobated placentas are thought to arise due to implantation in areas of decreased uterine perfusion. Local factors as leiomyomas, areas of previous surgery or over the cervical os may lead to abnormal shapes as well.

Placenta membranacea, a diffuse thin placenta without free membranes is extremely rare and may represent a shallow implantation with persistence of virtually all the capsular villi.

4 Pathological Placenta Development

4.1 Intrauterine Growth Restriction and Preeclampsia

The current model of the pathogenesis of preeclampsia (PE) suggests that the trophoblastic invasion of spiral arteries is defective. Failure of transformation of these arteries to a low-pressure, high-flow system leads to placental hypoperfusion, the release of circulation factors, and consequent endothelial dysfunction. IUGR is a related complication. Multiple areas of infarction, reduced surface for molecular exchange, and lower volumes of placental parenchymal tissue may lead into a failure of the placenta to transfer oxygen and nutrients adequately to the fetus. IUGR is associated with low birth weight, increased risk of perinatal mortality, premature delivery, cerebral palsy, and even long-term effects on cardiovascular and renal function. In clinically routine use of Doppler ultrasound to monitor uterine artery blood flow representing the input blood flow of the whole placenta is standard and known to be reduced in PE.

In IUGR, the MRI placental appearance is more often a thickened globular structure, as opposed to the typical appearance of a flattened disk with tapering edges and significantly associated with an increased incidence of fetal or neonatal mortality. The maximal placental thickness to placental volume ratio and the percentage of placental volume affected by abnormal signal intensities correlate significantly with the severity of IUGR (Damodaram et al. 2010).

4.1.1 Spiral Artery Blood Volume Measurement by MRI

Intra Voxel Incoherent Motion (IVIM) has been used to measure placental blood flow at the basal plate (Moore et al. 2008). It can demonstrate local flow from the spiral arteries to the placenta. The blood flow per unit mass of the placenta might be relevant. Doppler results could be confounded by variations in the total volume of the placenta. The number of recruited spiral arteries remains constant during the second and the third trimester of pregnancy. No significant change of the moving blood fraction could be detected. With growth of the uterus, the number of spiral arteries per Voxel would be expected to fall. Together this implicates that the volume of blood contained in the spiral arteries in vivo must increase.

In PE, reduced lumen diameter in myometrial arteries could be demonstrated compared to normal pregnancies.

4.2 Mesenchymal Dysplasia

Mesenchymal dysplasia is a rare disorder of unknown etiology characterized by serpinginous surface blood vessels and large cystic villi, often resembling molar tissue in a cluster-like dissemination. The most common association is with Beckwith–Wiedemann Syndrome (H'Mida et al. 2008).

4.3 Placenta Shape Abnormalities

4.3.1 Extrachorial Placentation

The membranes normally insert at the peripheral margin of the villous tissue that is usually the outer limit of the vascular plate. Placenta extrachorialis is an extraordinary, rather rare type of placenta where the chorionic vascular plate is much smaller than the villous tissue, which is "uncovered" in the periphery. The etiology of extrachorial placentation is unclear. Two forms are morphologically described. The circumvallation form of this condition shows a redundant, double-back membrane fold with enclosed debris and old hemorrhage at the point of membrane insertion. The circummargination form contains a mostly small ride of fibrin only (Figs. 3–5).

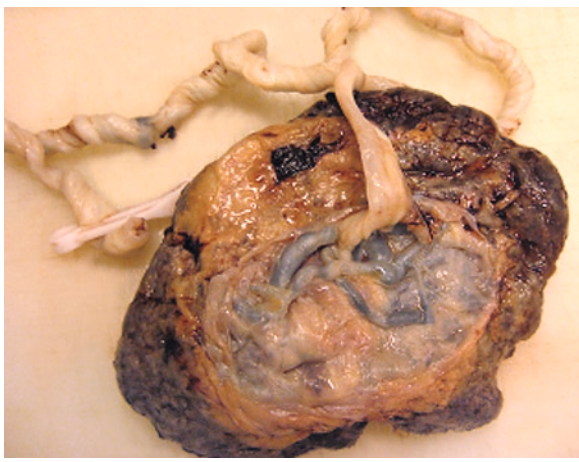

Fig. 3 Placenta extrachorialis with small chorionic plate not covering the whole placental disk

Fig. 4 Placental lamellar cross section through an extrachorial placenta with thick fibrinoid depositions over the uncovered placental surface

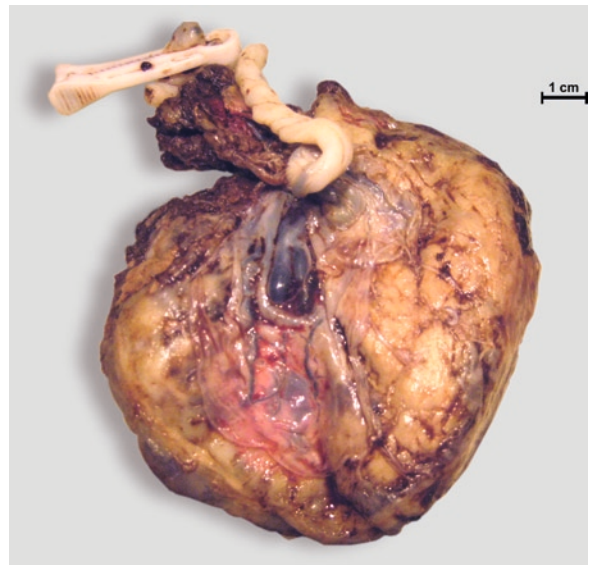

Fig. 5 Placenta extrachorialis

MRI Features of Extrachorial Placentation

Extrachorial placentation can be seen in MRI as a thickening of the placental surface without vessels of the chorionic plate (Figs. 6 and 7).

4.3.2 Placenta Bilobata

Bilobated placentas show two lobes separated by a segment of membranes. These membranes contain blood vessels which may imponate as vasa previa. Succenturiate lobes may occur singular or multiple and are often infarcted (Figs. 8 and 9).

Fig. 6 Placenta extrachorialis, in the placental periphery the chorionic plate is thickened without blood vessels (*arrows*). The covering membranes show a double contour, indicating fluid underneath. MRI scan in gestational week 33, T2-w sequence

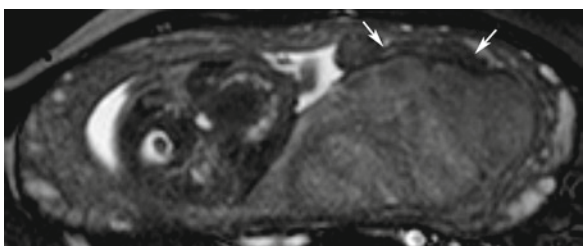

Fig. 7 Placenta extrachorialis, hypointense structure on placental surface presents the shrinked chorionic plate in addition to thickened edematous placenta. SSFP-sequence, GW 26

4.3.3 Placenta Membranacea

Placenta membranacea is a rare condition and may be associated with placenta accreta. The placental mass is thin, 1–2 cm thick, and often disrupted. If all, or nearly all the circumference of the fetal sac is covered by villous tissue, it is called placenta membranacea diffusa. This condition presents clinically frequently with vaginal bleeding and placenta previa (Fig. 10).

Fig. 8 Placenta bilobata, basal plate

Fig. 9 Placenta bilobata, fetal surface

Fig. 10 Lamellar cross section of a placenta membranacea with thinned parenchyma

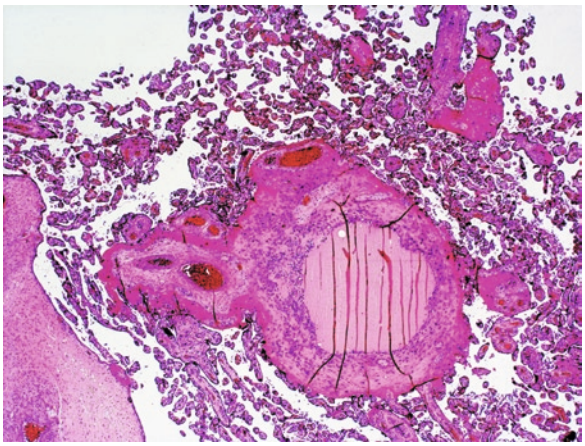

Fig. 12 Septal cyst histology H&E staining 20×

5 Circumscribed Pathologies of the Placenta

5.1 Septal Cysts

Septal cysts are located in the placental parenchyma often subchorionic and measure usually 5–10 mm in diameter. The cyst wall is formed by folding of the basal plate and septum with intermediate trophoblast. The cysts contend gelatinous material. Septal cysts are common, occurring in up to 20% of uncomplicated term placentas and are not associated with any clinical problem (Figs. 11 and 12).

5.2 Infarction

Villous infarctions are located paracentral or central in the area served by one single spiral artery and have usually a wedge-like shape affecting the full thickness of the placenta with rather linear-shaped margins. Small lesions less than 1 cm in diameter in the periphery are common and usually insignificant. Central and large marginal infarctions suggest maternal vascular disease, particularly if they are extensive or in preterm placentas. They are a consequence of uteroplacental disease and are associated with IUGR and PE. Sonographic sensitivity is low (Sebire and Sepulveda 2008). Fetal problems such as growth restriction are often present if 15% or more of placental tissue is affected. The adverse effect of extensive infarctions is further potentiated if the placenta is small, below the 10th percentile for the gestational age. Infarcts involving as much as 50% of placental mass in normal-sized placentas may cause a reduction of placental function enough to cause hypoxia and intrauterine fetal death (Kraus et al. 2004). Infarcts collapse and shrink over time with cystic changes and hemorrhage possibly seen (Figs. 13–17).

Massive inter-/perivillous fibrin depositions are quite common in the periphery of the placenta. Fibrin depositions aggregate to so-called gitter infarctions with an area less clearly circumscribed and more irregularly shaped. They occur suprabasal as maternal floor infarctions or subchorial. Maternal floor infarction recurrence in further pregnancies, association with IUGR and oligohydramnions, and related neurological impairment have been reported (Adams-Chapman et al. 2002) (Figs. 18 and 19).

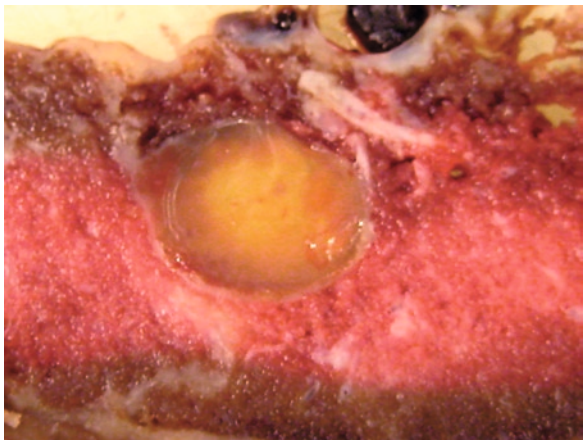

Fig. 11 Placental lamellar cross section with a septal cyst

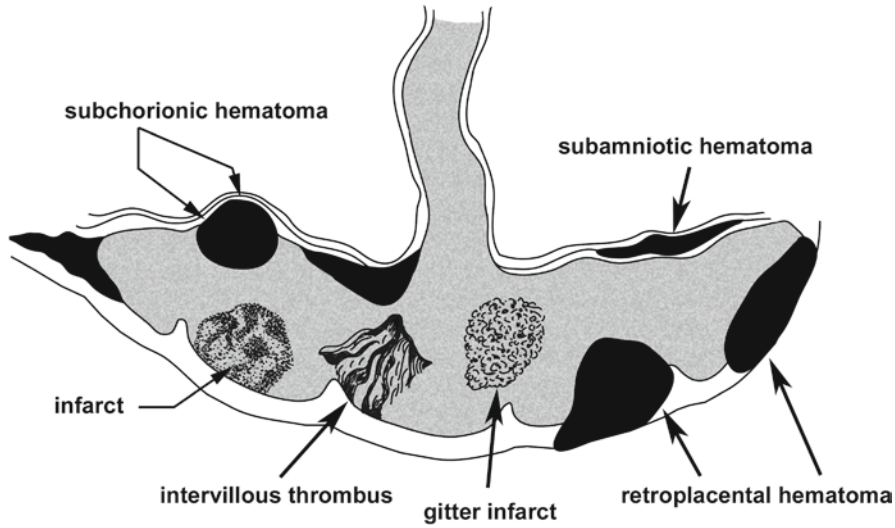

Fig. 13 Schematic location of circumscribed placental pathologies

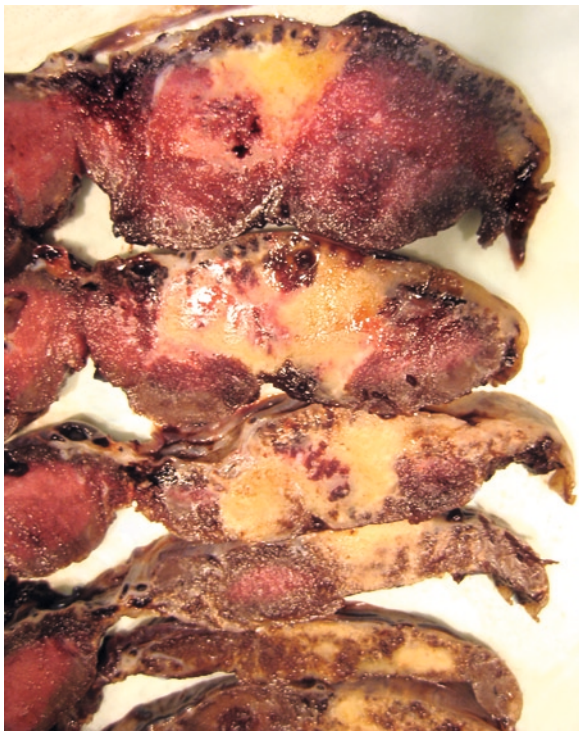

Fig. 14 Placental lamellar cross sections with multiple infarctions

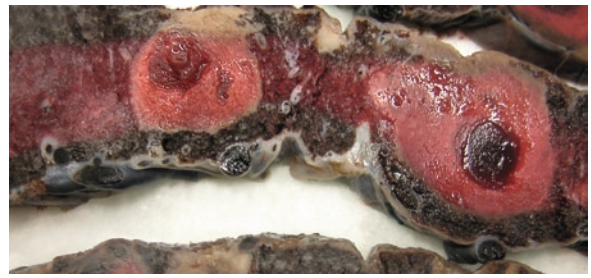

Fig. 15 Placental lamellar cross sections with multiple infarctions with central hemorrhage

Fig. 16 Placental lamellar cross section with circumscribed cotyledon-infarction in a suprabasal location

5.2.1 MRI Infarction

SSFSE T2-w and SSFP sequences have high sensitivity in detecting acute ischemic lesions and have been found useful in nonhemorrhagic placental pathologies as infarctions (Figs. 4–6). Ischemic infarctions present as hyperintense lesions in T2-w sequences. Hemorrhagic and thrombotic infarctions are seen as hyperintense lesions in T1-w sequences (Linduska et al. 2009) (Table 4, Figs. 20–22).

Fig. 17 Placental lamellar cross sections with a massive older infarction

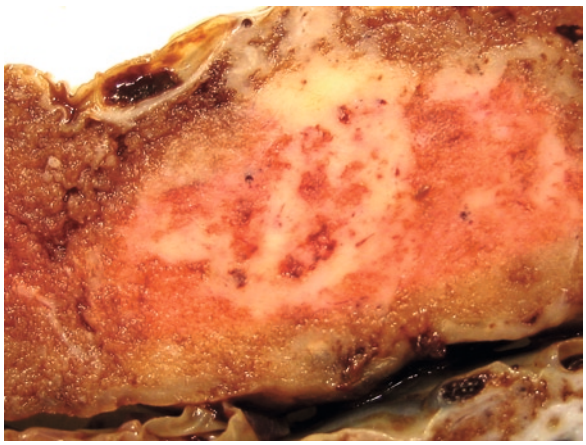

Fig. 18 Placental lamellar cross section with infarction in a gitter manner – so-called gitter infraction

Malian and Lee (2001) described placental infarctions in an extrauterine pregnancy not enhancing with contrast medium (gadolinium), hyperintense in T2-w and hypointense in T1-w.

5.3 Thrombi

Standards for detecting localized alterations in the placental parenchyma have been set up by comparing MRI scans with histopathological examination in a median time interval of 7 days in between scan and delivery. Interpretation standards have been found to categorize different pathologies

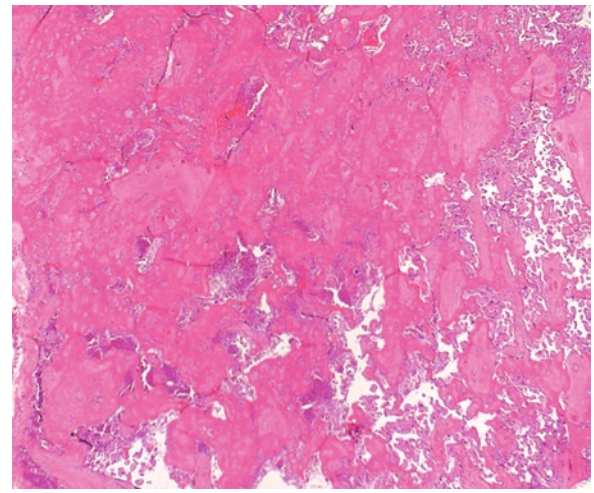

Fig. 19 Massive intervillous fibrin depositions, so-called gitter infarction, histology H&E staining 100×

but their impact on the developing fetus is outstanding (Linduska et al. 2009).

5.3.1 Intervillous Thrombi

Intervillous thrombi are common and present in 25% of all placentas and usually singular and small. They are localized clots in the intervillous space. There are thrombi of fetal origin occurring secondary to leakage from fetal capillaries and may manifest fetomaternal hemorrhage. Thrombi of maternal origin are due to an increased thrombosis in the maternal circulation occurring in maternal thrombophilia or PE. Multiple and large thrombi indicate a reduced maternal circulation of the intervillous space and may block further circulation and reduce exchange surface of the placenta. Recent hematomas have a layered appearance, older lesions evolve to clots as the hemoglobin is degraded (Figs. 23 and 24).

5.3.2 Subchorionic Thrombi

Subchorionic thrombi are located underneath the chorionic plate and consist of layers of blood cells and fibrin. The quantity of subchorionic fibrin has been associated with fetal activity. Unusually thick layers of subchorionic hemorrhage can be associated with chronic bleeding and prematurity (Figs. 25 and 26).

Table 4 Ischemic and hemorrhagic placental pathologies and their correlating signal relationship in different MR sequences

	T1-w	T2-w	SSFP	EPI DWI (0)	DWI ("i")	Localization	Morphological appearance
Ischemic infarction	–	+	+	=/+	+	Intraplacental	Diffuse/ circumscribed
Hemorrhagic infarction	+	–	–	–	+	Intraplacental	Diffuse/ circumscribed
Subchorionic hemorrhage	+	–	–	–	+	Subchorionic	Circumscribed
Intervillous hemorrhage	+	-	-	-	+	Intraplacental	Round
Thrombi	–	+	+	–	Variable	Intraplacental	Circumscribed
Retroplacental hematoma	+	–	–	–	+	Retroplacental	Circumscribed

DWI zero image (0), DWI isotropic image ("i"), hyperintense (+), hypointense (–), isointense (=)

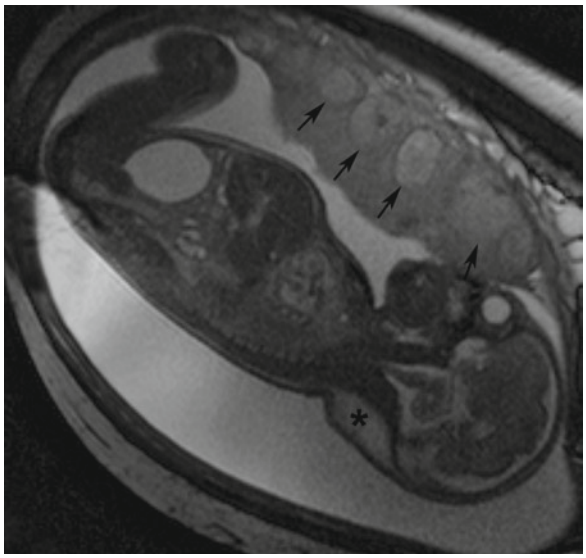

Fig. 20 Multiple ischemic lesions (*arrows*) on an SSFP sequence in GW 29. Polyhydramnios with extensively filled urinary bladder and hygroma (*asterisk*)

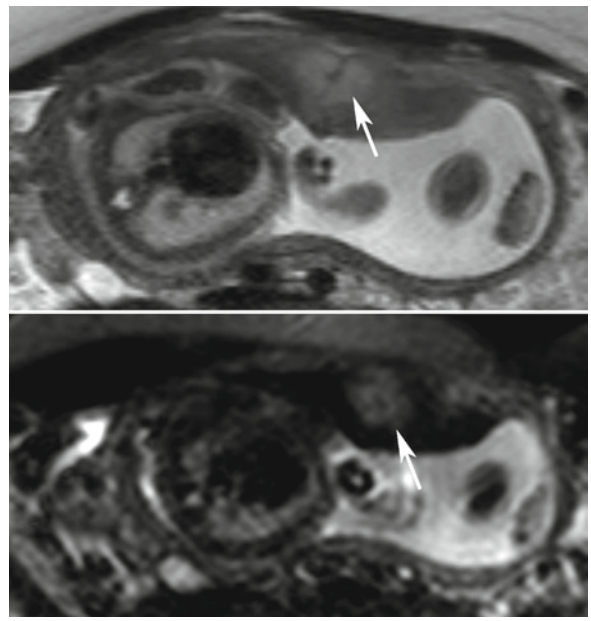

Fig. 21 Placental parenchyma on T2-w and DWI zero-image sequences in GW 27. Hyperintense circumscribed lesions representing ischemic infarction (*arrows*)

5.3.3 MRI Thrombi

While the normal placenta appears homogeneous on T1-w images, venous stasis and/or thrombotic changes may cause hyperintense signal changes (Brugger et al. 2006; Prayer et al. 2004; Verswijvel et al. 2002). Although recent intraplacental hematomas may have a layered or laminated appearance, older lesions evolve to clots as the hemoglobin is degraded. In ultrasound, an acute hematoma appears slightly hyperechoic, becoming hypoechoic and echolucent with time (Sebire and Sepulveda 2008). These changes could be seen in MRI as well (Table 4).

In MRI, intervillous thrombi imponate as hypointense in T2-w sequences, or hyperintense in T1-w images (Fig. 27).

Subchorionic thrombi present hypointense in T2-w and SSFP sequences (Fig. 28). Hemorrhage in T1-w sequences presents as hyperintense lesion, in the zero image of DWI it appears hypointense. Blood breakdown products, resembling hemorrhagic lesions can be demonstrated using zero images of the DWI or EPI.

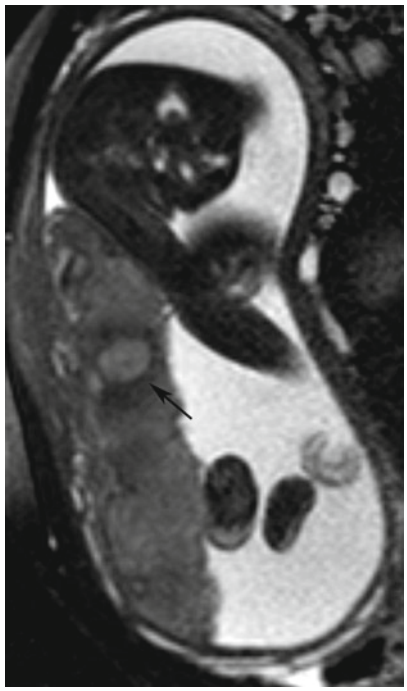

Fig. 22 SSFP sequence with fresh ischemic infarction (*arrow*), in the center already hyperintense (degraded blood), surrounded by a still hemorrhagic component (hypointense), GW 29

Fig. 23 Placental lamellar cross section with an older intervillous thrombus with lamellar appearance

5.4 Placental Lakes

Placental lakes are larger areas of villous free intervillious space within the placental parenchyma, due to intervillous reduced blood flow, thrombosis, or subchorionic fibrin depositions. The term "cavern" has previously been used synonymously. They are defined as homogeneous sonolucent lesions greater than 2 × 2 cm in diameter in ultrasound. The prevalence is reportedly 18% in mid gestation (Thompson et al. 2002) (Fig. 29).

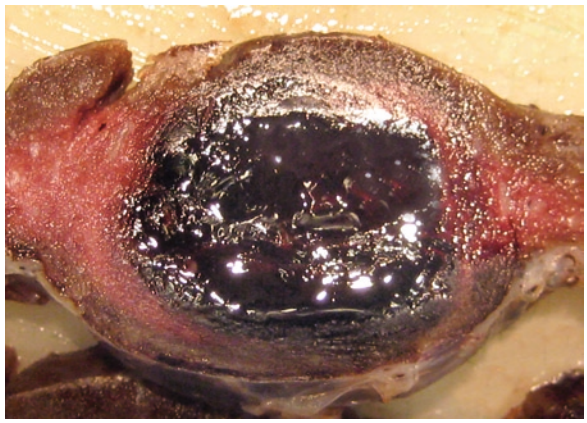

Fig. 24 Placental lamellar cross section with a fresher intervillous hemorrhage

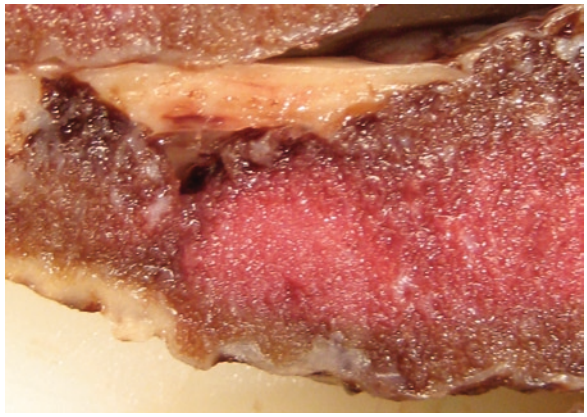

Fig. 25 Placental lamellar cross sections with circumscribed subchorionic thrombus

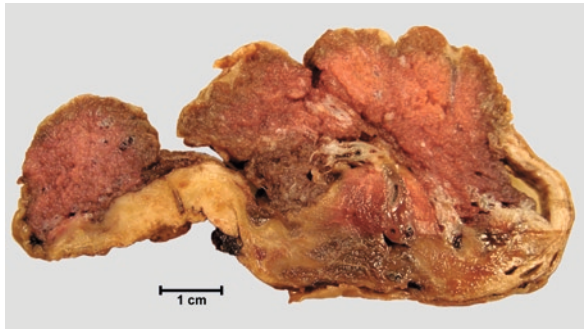

Fig. 26 Placental lamellar cross sections with massive older subchorionic thrombi

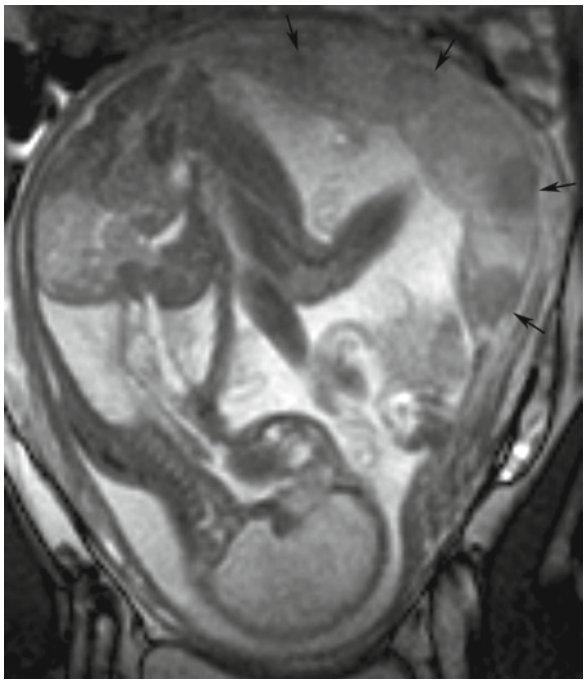

Fig. 27 Intervillous thrombi, SSFP sequence in GW 29, showing round hypointense lesions (*arrows*)

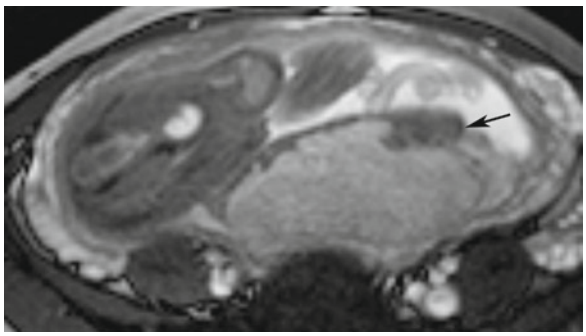

Fig. 28 Subchorionic thrombi (*arrow*), SSFP sequence, gestational week (GW) 30

Differential diagnosis includes subchorionic cyst, old subamniotic hematoma, centrocotyledonary cavity, septal cyst, and early stage of thrombosis formation and placenta form variations as placenta circummarginata.

5.4.1 MRI of Placental Lakes

According to a case report from Morikawa et al. (2005), placental lakes show low intense on T1-weighted and isointense on T2-weighted imaging suggesting that

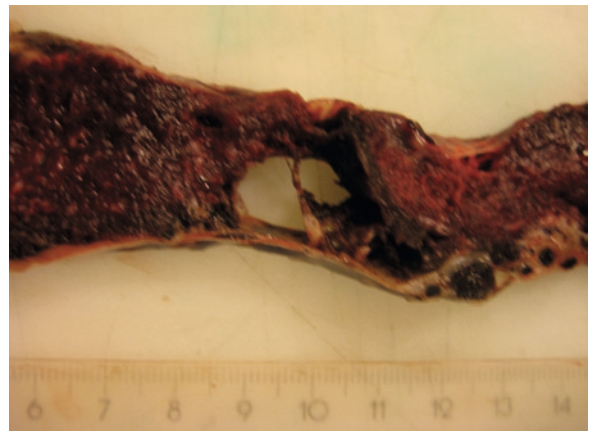

Fig. 29 Placental lamellar cross section with a hole, resembling a placental lake

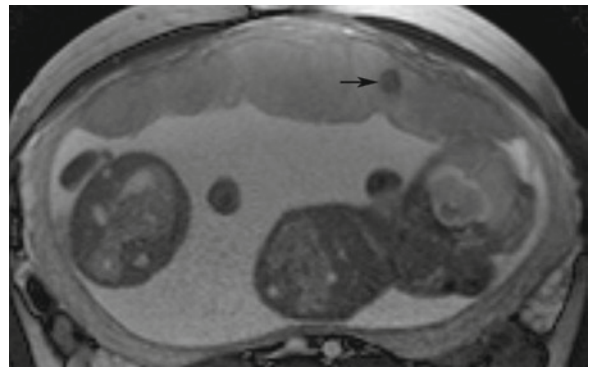

Fig. 30 Placental lake (*arrow*). Monochorionic twin pregnancy complicated by TTTS in GW 28

they contain fresh maternal blood. Real-time imaging revealed a turbulent blood flow generated by a pulsatile jet flow (pulse rate 40–69 beats per minute) (Fig. 30).

5.5 Retroplacental Hematoma and Abruptio Placentae

Abruptio placentae is defined as the detachment of the placenta from its decidual seat. Many causes are known including maternal vascular diseases, trauma, amniocentesis, uterine abnormalities, placenta previa, chorioamnionitis, smoking, and possibly cocaine. A retroplacental hematoma results from the clinical condition of abruption. Peripherally located retroplacental

Fig. 31 Placental lamellar cross sections with retroplacental hematoma

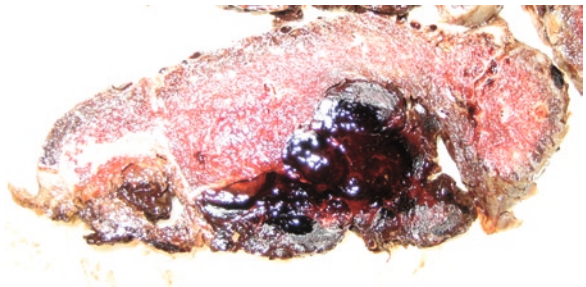

Fig. 32 Placental lamellar cross section with relatively fresh retroplacental hematoma

hematomas are not associated with major complications, while paracentral and centrally located retroplacental hematomas indicate an abruption of the placenta (Figs. 31 and 32). Compression of the underlying placental villous tissue occurs after a few hours and can result in infarctions (subacute abruption) (Fig. 33).

5.5.1 MRI Features of Retroplacental Hematoma and Abruptio Placentae

Retroplacental hematomas can be seen in MRI with high specificity in T1-w sequences as hyperintense and in SSFP sequences as hypointense retroplacental lesions (Fig. 34, Table 4). In 50% of cases of abruption, sonography is negative. MR can be utilized to visualize abruptions that are occult sonographically (Levine 2005).

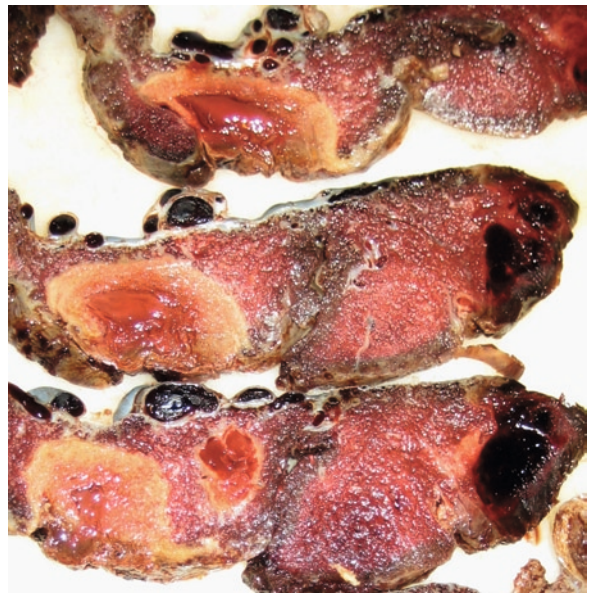

Fig. 33 Placental lamellar cross sections with older degenerated retroplacental hematoma

5.6 Hemorrhage During Pregnancy

Hemorrhage in pregnancy is associated mostly with placenta previa or lower placenta location. In MRI, a blood clot can be visualized at the inner cervical opening, on T1-w better than T2-w sequences (Trop and Levine 2001).

6 Tumors of the Placenta

Placental tumors are divided into trophoblastic tumors, non-trophoblastic tumors, and metastasis from other tumors as malignant melanoma.

6.1 Chorioangioma

Synonyms used are chorangioma, fibroma, and hemangioma.

Placental chorioangiomas are the most common benign and non-trophoblastic tumors of the placenta. Most are discovered incidentally. The incidence is about 1% to 1:9,000 births in literature. Whether

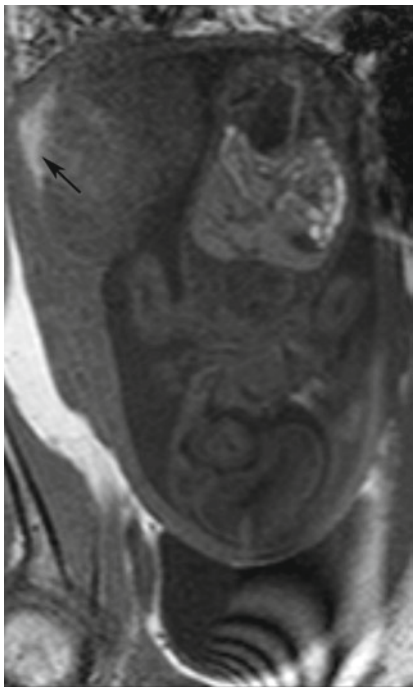

Fig. 34 Retroplacental hematoma (*arrow*); on a T1-w sequence between the placental basal plate and the uterine wall in the periphery of the placental disk, a retroplacental hyperintense lesion is seen

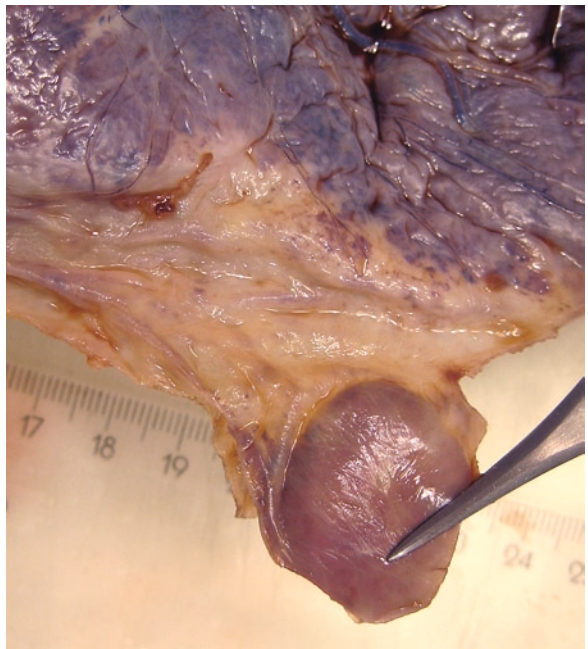

Fig. 35 Chorangioma

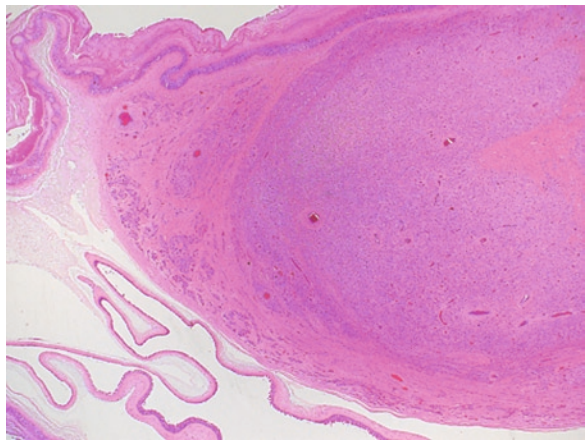

Fig. 36 Chorangioma histology H&E staining 20×: well-circumscribed tumor consisting from capillaries

chorioangiomas represent a true neoplasm or a hamartoma is not known. Three histopathologic patterns of chorioangiomas have been described: angiomatious, cellular, and degenerative. They are usually peripherally located and found protruding from the fetal surface (Figs. 35 and 36). The tumor size varies from a few millimeters in diameter to 10 cm and greater. Depending on size and location they can cause major complications. Large chorioangiomas, larger than 4 cm in diameter, are clinically significant and can cause polyhydramnions, hemolytic anemia, thrombocytopenia, cardiomegaly, IUGR, and hydrops in the fetus due to arteriovenous shunting. Differential diagnosis includes hydatidiform mole, chorioepithelioma, and tumors arising from the uterine wall.

6.1.1 MRI of Placental Chorangioma

Some cases of placental chorangioma have been visualized antenatally by MRI. Chorioangioma presents as a well-circumscribed placental tumor with relatively high signal intensity on proton density imaging and T2-w imaging like hemangioma and partly high signal rims on T1-w imaging. T1-w sequences are useful for anatomical localization and characteristics due to missing motion artifacts (Mochizuki et al. 1996).

Others described chorioangiomas in MRI as in T1-w mostly isointense to the placental tissue with an

area of high signal intensity near the base and at the periphery, suggestive of hemorrhage or hemorrhagic infarction. On T2 – HASTE images heterogeneous high signal intensity with an area of low signal intensity near the surface was seen. MR appearance may vary due to differences in used MR sequences and dependency on the composition of the lesion (Kawamotoa et al. 2000).

6.2 Teratomas

Teratomas are much less common than chorangiomas and should be differentiated from acardiac twins. If the lesion does not contain axial skeleton or umbilical cord, it is likely to represent a true tumor.

6.3 Gestational Trophoblastic Disease

Gestational trophoblastic disease (GTD) is a disorder characterized by an abnormal proliferation of trophoblastic tissue and includes diagnoses as hydatidiform mole, invasive mole, choriocarcinoma, and placental site trophoblastic tumor. The International Federation of Gynecology and Obstetrics (FIGO) has devised a staging system for GTD that has been revised to include the World Health Organization risk factor scoring system recently (Ngan et al. 2003). The scoring system has enabled simple stratification of patients into two therapeutic groups, those with low score (≤6) and high score (>6), which require multiagent chemotherapy. GTD is typically diagnosed by ultrasound. MRI can be useful for the evaluation of the extent and the complications (Jung et al. 2001).

6.3.1 Molar Pregnancy

Incidence of molar pregnancy is 1 in 1,000–2,000 pregnancies with ethnic and geographic differences. There are two types of molar pregnancies, the complete hydatidiform mole and the partial mole.

Complete Hydatidiform Mole

Hydatidiform moles are not neoplasms; however, they are associated with an increased risk of 16% for the development of neoplasms, especially choriocarcinoma. Genetically, the material is all androgenetic and paternally derived. This may result from an ovum that has lost its nucleus, an empty egg, followed by fertilization by a single sperm with subsequent duplication of the haploid spermatozoal component. Less frequently, fertilization of an empty egg by two sperms occurs. Grossly villous hydropic change with grapelike translucent vesicles up to 2 cm in diameter appears, usually not present until the second trimester. No embryonic or fetal tissue is present. The uterine cavity often is filled with molar tissue. Trophoblastic hyperplasia and atypia are universally present. Intervillous thrombi frequently occur due to aberrant intervillous circulation. Elevation of serum β-HCG is high. Clinical manifestation occurs usually between gestational week 11 and 25 often with genital bleeding. Because of a high association between a complete hydatidiform mole pregnancy and choricarcinoma, these patients should undergo surveillance.

MRI Features of the Complete Hydatidiform Mole

The abnormal placental tissue is mostly not seen before the second trimester in complete hydatidiform moles. It appears as a heterogeneous mass hyperintense in T2-w sequences, with a snow flurry like aspect, similar to sonographic findings (Fig. 37). Cystic spaces may be present within the mass (Wagner et al. 1996). On T1-w images molar tissue is typically of similar or higher signal intensity than the adjacent myometrium (Allen et al. 2006).

Partial Hydatidiform Mole

Partial hydatidiform moles are usually triploid, developing from an ovum fertilized by two sperms. Normal villous tissue is intermixed with hydropic changed tissue (Fig. 38). Embryonic tissue may be present. Clinically, vaginal bleeding suggestive of a missed abortion and moderate elevation of serum β-HCG is found. The risk for transformation into a malignant form of GTD is slightly raised, up to 0.5%.

Fig. 37 Complete hydatidiform mole (*asterisk*) in a dichorionic twin pregnancy in GW 27

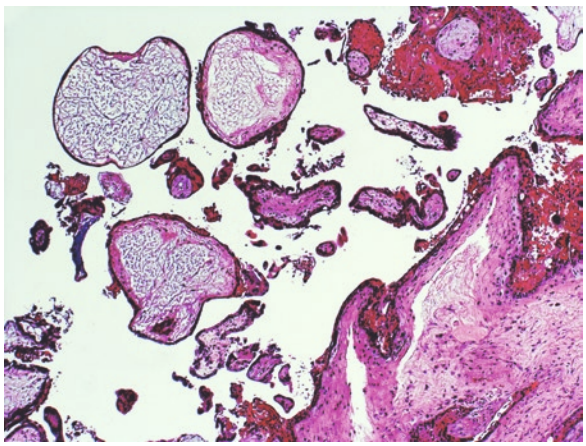

Fig. 38 Partial hydatidiform mole, histology H&E staining 100×

Invasive Hydatidiform Mole

Invasive hydatidiform mole is a rare entity composed of trophoblastic cells and molar villi, which invades the uterus/myometrium and has the potential for invasion of adjacent structures. Invasive mole pregnancy is defined as hydatidiform mole with abnormal villous tissue invading the myometrium or blood vessels. Metastasis to the lung or other organs may occur.

Invasive Mole in MRI

MRI is useful in detecting myometrial or parametrial invasion (Takeuchi et al. 2005). Contrast-enhanced dynamic MRI has potential for early detection of invasive disease postmolar pregnancy. Invasive disease is seen in T2-w imaging as hyperintense areas within the myometrium (Allen et al. 2006).

6.3.2 Choriocarcinoma

Choriocarcinoma is a highly malignant tumor of trophoblastic origin. Incidence is 1 in 25,000 to 40,000 pregnancies. It may develop after an abortion, a term or preterm pregnancy, an ectopic pregnancy, or a hydatidiform mole. Clinically abnormal vaginal bleeding is seen. Grossly choriocarcinoma may vary from a few millimeters to large tumors. It invades vasculature leading to hemorrhage and necroses. Metastases occur largely from hematogenous dissemination through the venous system to the lungs and sometimes into the systemic circulation. If a choriocarcinoma develops during a term or near-term pregnancy, an intraplacental lesion may be identified, classified as choriocarcinoma in situ. Fetomaternal hemorrhage may occur in these cases due to the tumor (Takai et al. 2000; Nagel et al. 2007).

Choriocarcinoma in MRI

Hemorrhage and necrosis are seen in MRI (Takeuchi et al. 2005).

6.4 Neoplasm's Metastatic to the Placenta

Maternal malignancies occur in approximately 1 in 1,000 pregnancies, but metastasis to the placenta is rare with less than 100 cases in the literature. The most common tumor to metastasize to the placenta is the malignant melanoma, but metastasis from breast, cervix, gastrointestinal tract, or lung cancer occurs less frequently. There exist reports of metastasis from pancreas, ovary, skin, as well as brain tumors. Many placental metastases occur in end-stage diseases.

Transplacental metastasis to the fetus is extremely rare. Cases of melanoma, lymphoma, leukemia, and pulmonary adenocarcinoma have been reported. Fetal congenital malignancies are rare but may have potential to metastasize to the placenta as well. This includes neuroblastoma, lymphoma, leukemia, sarcomas, brain tumors, hepatoblastoma, and teratomas. Only large metastasis can be seen grossly and should be distinguished from infarcts. The placenta may present enlarged.

7 Pathology of the Membranes

7.1 Cysts

Cysts on the surface of term placentas are common. They are usually only a few centimeters in diameter, occasionally much larger, and may show hemorrhage. Subchorionic cysts are most common, which are found in 5–7% of term placentas and are often multiple. Infrequently amniotic epithelial inclusion cysts are seen.

7.2 Retromembranous Hemorrhage

Retromembranous hemorrhage is quite common, particularly in multiple gestations and results from confined regions of hemorrhage in areas of decidual necrosis. They cause rarely significant problems (Fig. 39).

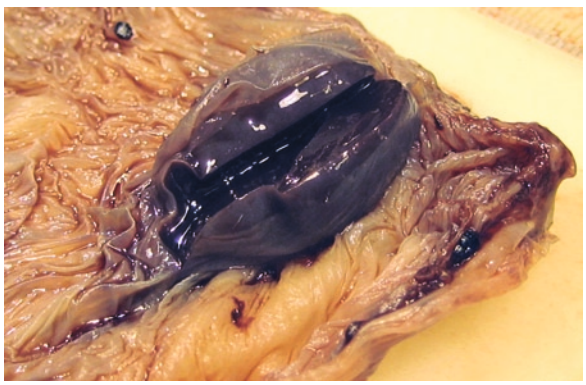

Fig. 39 Membranes with significant retroamniotic hemorrhage

7.3 Fetus Papyraceous

In multiple gestations with demission of one fetus in early pregnancy, the vanished twin may be present as compressed fetus papyrceous in the membranes (Fig. 40).

7.4 IUD

Retained intrauterine devices (IUD) may lay underneath the membranes and are visible in MRI.

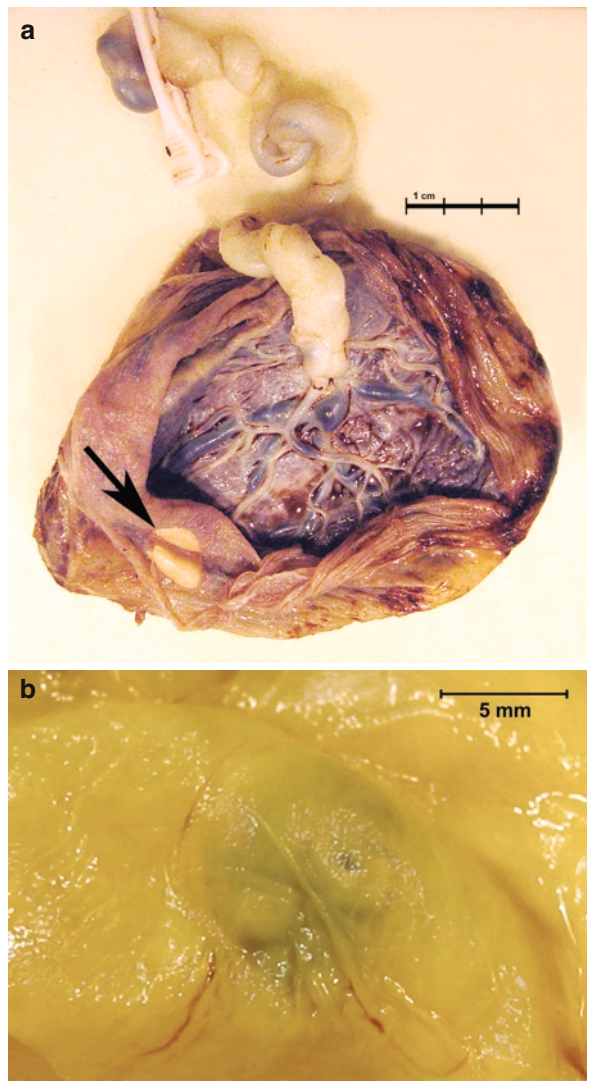

Fig. 40 Fetus papyraceous in the membranes

7.5 Amniotic Sheets

Amniotic sheets are benign and the accurate diagnosis including the differential diagnosis amniotic band syndrome is important. Amniotic sheets are shelflike structures, secondary to uterine synechia (Asherman's syndrome) with a part of placenta on it, dividing the uterine cavity.

7.5.1 Amniotic Sheets in MRI

MRI with excellent soft tissue contrast and three-dimensional observation shows septum-like structures without direct connections between the fetus and the septum-like membrane (Kato et al. 2005).

7.6 Vasa Previa

Fetal vessels run through the membranes, unprotected by placental tissue and Wharton's jelly. Vasa previa located below the fetal presentation part and close to the internal cervical os are linked to risk of fetal exsanguination and death when membranes rupture (Fig. 41).

Risk factors are multiple pregnancies, pregnancies resulting from IVF, velamentous cord insertion, succenturiate, or accessory placental lobes (Abramowicz and Sheiner 2007). Incidence of vasa previa has been estimated at 1 in 2,500 pregnancies. Prenatal diagnosis is important for a good outcome. Caesarean delivery of the fetus prior to rupture of the membranes is essential. Transvaginal sonography with color Doppler is the standard method to diagnose vasa previa, but MRI is useful in the evaluation of a posterior vasa previa, when sonographic evaluation may be difficult (Oyelese et al. 2003).

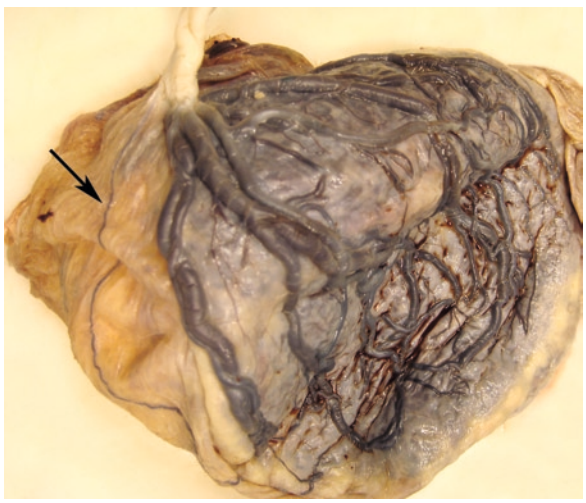

Fig. 41 Placenta with marginal cord insertion and aberrant vessels in the membranes

8 Infection: Chorioamnionitis

Chorioamnionitis due to ascending infections is common, especially in preterm premature rupture of membranes (pPROM) and preterm delivery (up to 67%). It has been implicated in the development of poor long-term neurologic outcome and cerebral palsy.

Hematogenous or continuous spread from plevic organs, or direct inoculation of organisms during diagnostic procedures, such as amniocentesis, can be a reason too. The cervicovaginal tract has a rich microbial flora, including transiently harbored organisms as group B streptococci, *Listeria monocytogenes* and the predominantly anaerobic flora associated with bacterial vaginosis, which have capacity to spread, and therefore to infect the fetus and placental tissue.

Most congenital infections in the first half of pregnancy are acquired hematogenously, and are a result of primary infection of the mother. Spirochetes (*Treponema pallidum*, *Borrelia burgdorferi*), parasites (*T. gondii*, *T. cruzi*, *P. falciparum*, *S. hematobium*), and viruses (CMV, HIV, Hepatitis B and C, Parvovirus B19, varicella zoster virus, herpes simplex virus, rubella virus, enterovirus) are the major causative agents. Organisms may elicit inflammation in the intervillous space as some parasites cross the placenta without eliciting an inflammatory response as most viruses, or infect both the fetus and the placenta. The clinically used acronym TORCH is standing for toxoplasmosis, (others), rubella virus, cytomegalovirus, and herpes simplex. Infants affected by TORCH infections have a number of common features including IUGR, hepatosplenomegaly, pancytopenia, and coagulopathy. Laboratory testing for IgM and PCR testing of fetal blood can help in the confirmation of diagnosis.

Fig. 42 Placental lamellar cross section with thickened chorionic plate due to chorioamnionitis

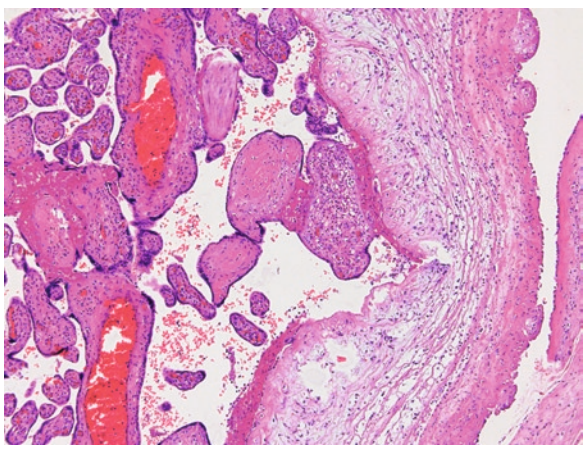

Fig. 43 Placenta with edematous thickened membranes and chorionic plate due to chorioamnionitis histology H&E staining 200×

Nevertheless, the majority of infections occur in the second trimester through ascension.

Pathologically maternal and fetal inflammatory responses should be separated. Maternal response is located in the chorion and amnion. Fetal response involves chorionic vessels and the umbilical cord, including arteritis.

The decidua capsularis is often hemorrhagic altered and detached, membranes may be edematously thickened (Figs. 42 and 43).

8.1 Infection in MRI

Although chorioamnionitis can complicate pregnancies after pPROM and has high mortality rates, detection by imaging is still not possible in a reliable fashion.

In some but not all studied cases with chorionic amnionitis, thickened edematous fetal membranes were seen in DWI and T2-w sequences. One case with extrachorionic placenta showed similar features without clinical or histopathological signs of inflammation or infection.

Chorionamnionitis might be detectable when membranes are edematous. Thickening of membranes can sometimes be seen, but is hard to differentiate from other pathologies like retromembranous hematoma or placenta extrachorialis in our experience.

9 Umbilical Cord

9.1 Normal Development of the Umbilical Cord

The umbilical cord is the lifeline of the fetus. It develops from the region of the body stalk where the embryo is attached to the chorion. This area consists of allantois, omphalomesenteric duct, vitelline vessels, and evolving umbilical arteries and vein. Those structures become covered by the expanding amnion, building the umbilical cord. The right umbilical vein disappears as most of the embryonic elements, leaving two arteries and one vein. Embryologic remnants are rarely seen grossly, but frequently on microscopy.

9.2 Pathologic Development of the Umbilical Cord

9.2.1 Single Umbilical Artery (SUA)

The incidence of SUA is about up to 1% in singleton deliveries and more frequently seen with twins (8.8%) and velamentous cord insertion. SUA has been associated with growth restriction, maternal diabetes, antepartum hemorrhage, polyhydramnios, and oligohydramnios. About 20% of infants missing one artery have other major congenital abnormalities (Kaplan 2008), which may involve any organ system, often associated with chromosomal aberrations. Renal and hollow organ abnormalities such as intestinal atresia are relatively frequent. Infants without malformations

are slightly growth retarded and have an increased perinatal mortality. Cord accidents have been reported unusually frequent in this group. In 73% the defect is located in the left artery and may occur as aplasia, or as the consequence of atrophy of one artery.

9.2.2 Twist/Hypercoiling

Umbilical cord twisting etiology is unknown and is usually a counterclockwise left twist. Excessive twisting is associated with fetal morbidity and mortality (Kaplan 2008). This is called hypercoiling synonymously and can be visualized by MRI (Figs. 44 and 45).

9.2.3 Length of the Umbilical Cord

Umbilical length increases throughout gestation. Fetal activity and stretch on the cord, as well as genetic factors are determining length. Abnormal measures of the cord can cause significant clinical correlates. Long cords are defined by longer than 75 cm and are associated with knots and fetal entanglements. They may correlate with fetal hyperactivity. For normal vaginal delivery, a minimum cord length of 32 cm is felt to be necessary. Uterine traction on the cord can cause fetal distress, cord tearing with hemorrhage, and possibly placental separation. Entanglement can lead to functionally short cord. Disorders with decreased fetal movement, for example, oligohydramnios are known to be associated with short cord.

Fig. 44 Hypercoiling of the umbilical cord

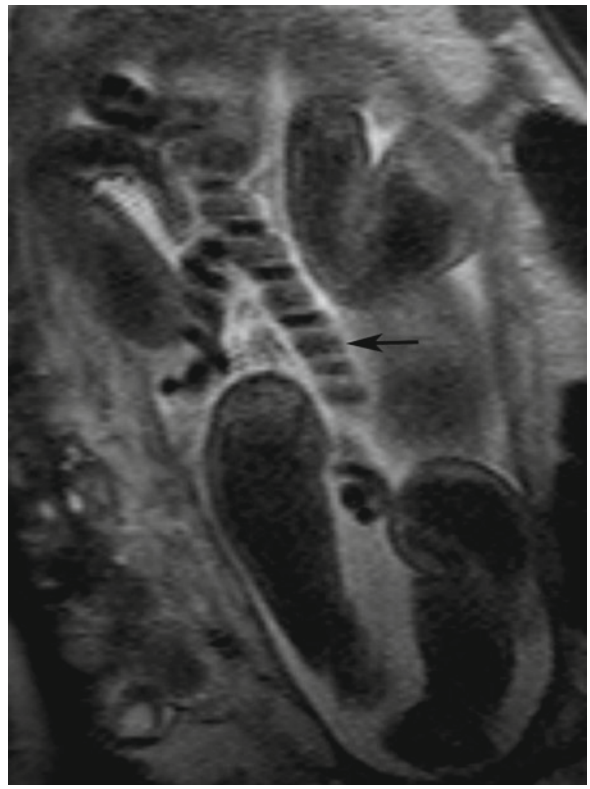

Fig. 45 Hypercoiling with narrowly twisting of the umbilical cord

9.2.4 Umbilical Cord Knots

True knots of the umbilical cord occur with a frequency of 0.4–0.5%. Tight true knots cause compression of Wharton's jelly at the site of knotting, congestion of the placental side of the knot, and tendency of the unknotted cord to coil (Fig. 46). Venous stasis can result in thrombosis of placental surface veins or even umbilical vein thrombosis and become clinically significant. This may cause intrauterine fetal death or lead to significant hypoxia with lasting neurologic damage in the infant. True knots have an overall mortality of about 10%.

False knots are actually local redundancies of the umbilical vessels, mostly the vein and should not be called knots (Fig. 47).

A case of umbilical cord constriction due to an amniotic band was described in MRI by Voss et al. (2007).

Fig. 46 True knot of the umbilical cord

Fig. 47 False knot of the umbilical cord

9.2.5 Umbilical Urachal Cysts

Umbilical cord cysts originate from an extra-abdominal urachal system and its failure of absorption. Cysts near the placenta are suspicious for fetal abnormalities, as trisomy 18 syndrome, and differential diagnosis includes hemangioma.

A cystic lesion in the umbilical cord, isointense to amniotic fluid on T1-w and T2-w sequences, and a relatively high signal intensity compared to amniotic fluid on DWI and echoplanar imaging was described as an umbilical urachal (allantoic) cyst filled with urine (Amano et al. 2003).

9.3 Umbilical Cord Insertion

The insertion is most likely in the center or slightly eccentric on the placental disk.

9.3.1 Locating the Umbilical Cord Insertion in MRI

In MRI, few flow voids within the placenta indicate usually the insertion point of the umbilical cord (Baughman et al. 2008) (Fig. 48).

SSFP sequences can be helpful to differentiate between insertion and adjacent cords.

Especially in multiple pregnancies, cord insertion as well as allocation can be difficult to evaluate.

9.3.2 Marginal or Velamentous Cord Insertion

Marginal or velamentous cord insertion is associated with complications including rupture of membranous vessels and vasa previa. These cords may be less mobile and more prone to compromise. Infants are slightly smaller on average. They are found more often in multiple gestations and in association with a singular umbilical artery. The frequency of velamentous cord insertion

Fig. 48 EPI-sequence, GW 30. The umbilical cord and its central insertion (*arrow*) are on this scan, the large vessels are dividing on the chorionic plate into the placental parenchyma

is about 1% in singletons and is seen more often in twins. Marginal cord insertion has a frequency of about 7% in singletons and may show membranous vessels as well. Vessels with a long membranous course are more vulnerable to injuries.

9.3.3 Furcate Cord Insertion

In furcate cord insertion, umbilical vessels separate from the cord prior to reaching the placental surface. This rare condition often is associated with complications.

9.3.4 Forked Umbilical Cord

In monoamniotic twins missing complete separation of the umbilical cord at developmental day 11–12 postfertilization is an extremely rare event.

In a rare case of monoamniotic twins, a forked umbilical cord was seen as partially fused at serial MRI scans (Figs. 49 and 50).

10 Pathologies of Placentation

Pathologies of placentation are abnormal placental locations in utero, namely placenta previa, and abnormal deep placenta implantation forms, such as placenta accreta, increta, or percreta.

Fig. 49 Monoamniotic twin placenta with forked umbilical cord

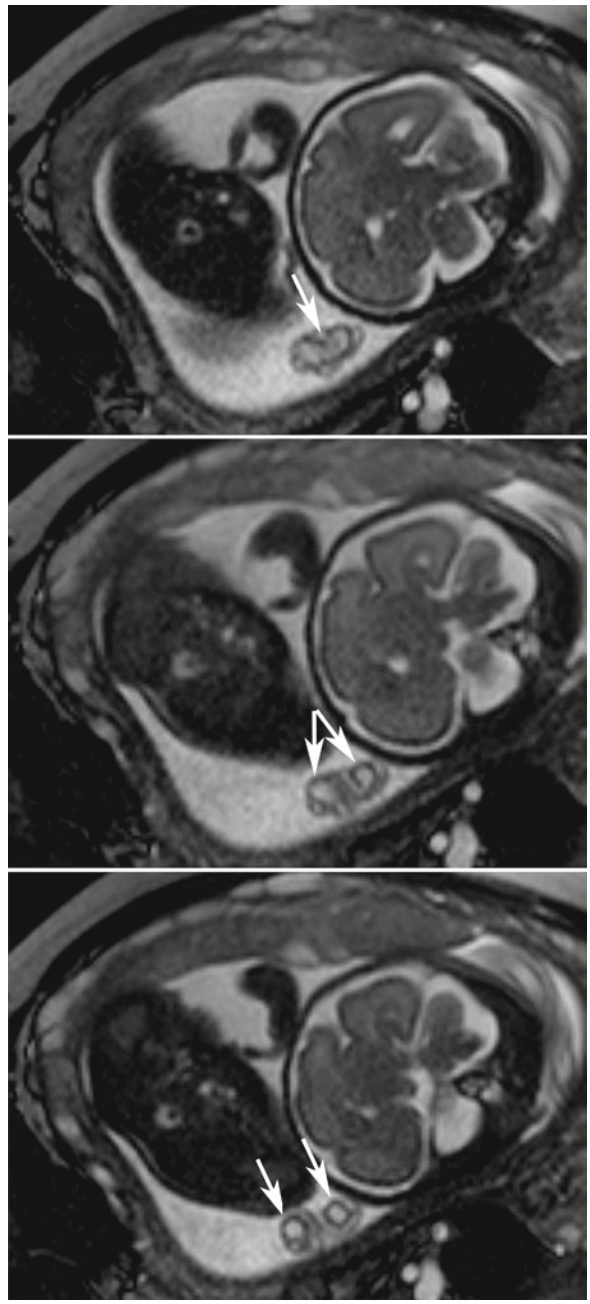

Fig. 50 Forked umbilical cord in a monochorionic monoamniotic twin pregnancy, GW 28. Arrows showing the fused umbilical cord and further two separated cords

10.1 Placenta Previa

Placenta previa is a placenta with low implantation when villous tissue covers the inner cervical opening. The incidence is between 0.3% and 1%. It has been shown by

serial ultrasound examinations throughout pregnancy that the placenta wanders. Dynamic placentation takes place by marginal atrophy on one side and growth and expansion on the other, called trophotropism. This would explain the higher incidence of placenta previa in early pregnancy. Placenta previa is associated with a higher risk for abruption, postpartum hemorrhage, fetal and perinatal mortality, fetal growth restriction and fetal abnormalities, and prolapsed umbilical cord. Complete placenta previa requires delivery by caesarean section. Placenta previa is often associated with placenta accreta.

Placenta previa is usually diagnosed by ultrasound, but can be visualized by sagittal-oriented MR in the plane of the cervix (Fig. 51).

10.2 Placenta Accreta/Increta/Percreta

Suspected placenta increta is the main indication for placental MRI.

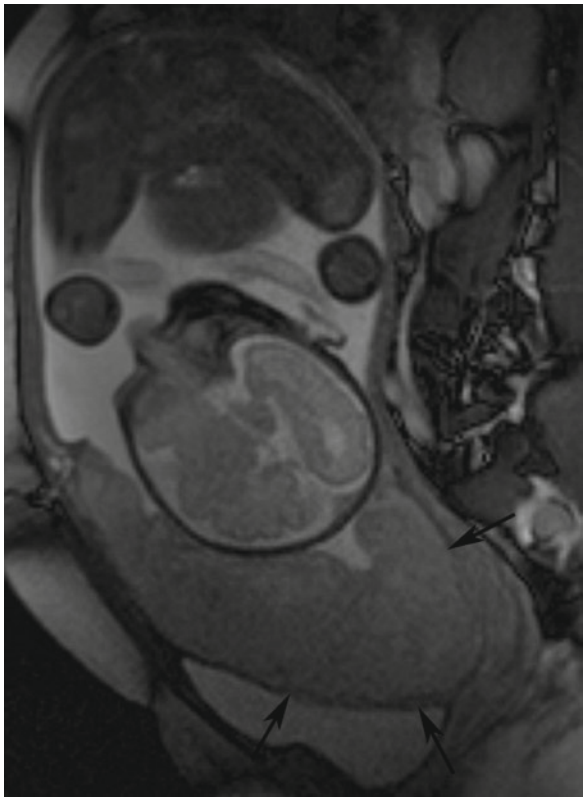

Fig. 51 Placenta previa, sagittal MRI scan through the gravid uterus at GW 32. The placenta is located in the lower part of the uterus, overlying the inner cervical os

In normal placentation, extravillous trophoblast invades the decidua controlled and converts the spiral arterioles of the endometrium to uteroplacental vessels. Decidual tissue apparently limits placental growth. In placenta accreta normal decidua fails to form, most times locally because the subjacent endometrium is deficient and cannot decidualize. The trophoblast invades and penetrates into the myometrium. Placenta accreta has been classified into placenta accreta, placenta increta, and placenta percreta, based on how deeply the trophoblastic tissue invades. In placenta accreta, the chorionic villi are implanted on the myometrium without intervening decidua. In placenta increta, the myometrium becomes invaded by the placental villous tissue. In placenta percreta, the chorionic villi penetrate the entire uterine wall. Placenta increta and percreta are diagnosed more frequently ante partum than placenta accreta.

10.2.1 Classification of Placenta Accreta (Table 5)

Palacios Jaraquemada et al. (2004) proposed a more detailed classification of placenta accreta, including topography (Table 6).

Ultrasound characterization for placenta accreta and its varieties was generally established according to Finberg and Williams (1992) diagnostic criteria.

Table 5 Classification of abnormal placental invasion

Classification	Depth of invasion
Placenta accreta	Villi attached to the myometrium but no invasion
Placenta increta	Villi partially invade the myometrium
Placenta percreta	Villi invade up to or beyond the uterine serosa

Table 6 Classification of placenta accreta

S1	Upper uterine segment
S2	Lower uterine segment
A	Partial myometrial invasion
B	Total myometrial invasion
C	Invasion involving the complete myometrium including one or both parametria

After Palacios Jaraquemada et al. (2004)

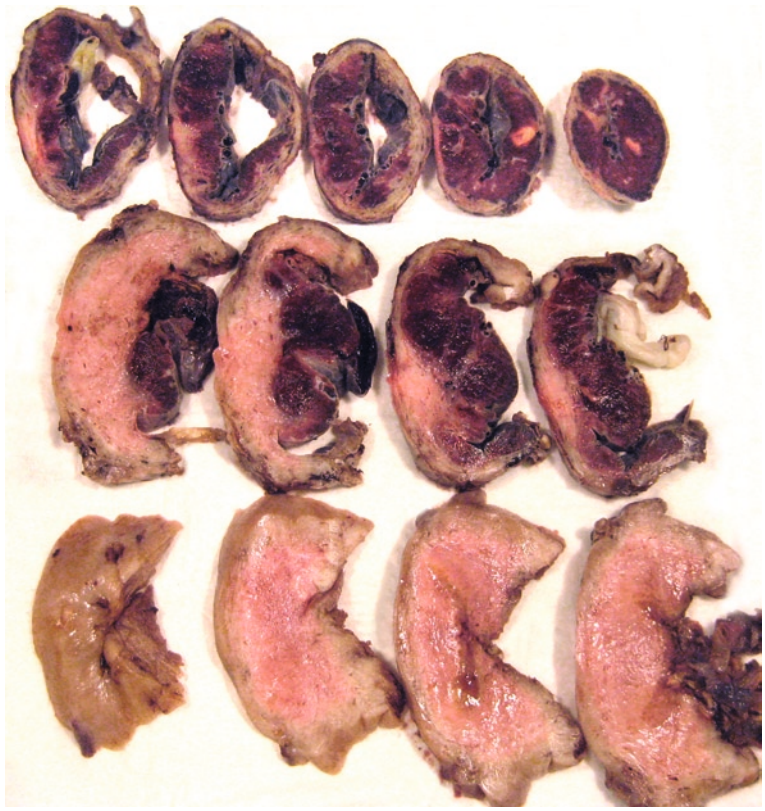

Fig. 52 Placenta percreta: cross section of the uterus with placenta invading through the myometrium

The division into S1 and S2 topographical areas is directly related to the degree of local irrigation. S2 B and C invasions imply a higher probability of using specific procedures and are at higher risk for severe hemorrhage due to difficulty to perform bloodless dissection within a vascular magma located deeply inside the pelvis. MRI can provide useful information for proper surgery planning and uterine conservation (Palacios Jaraquemada and Bruno 2005).

Patients at risk of placenta accreta are those with a scarred uterus, for example, after caesarean sections or conservative myom surgery and placenta previa. The risk of placenta accreta in patients with placenta previa is 5%. Patients who have undergone uterine surgery including multiple prior caesarean sections are also at higher risk of developing placenta accreta. The clinical consequence of placenta accreta is massive hemorrhage at the time of placental separation. Hysterectomy is often required. Placenta percreta can lead to the destruction of adjacent organs through invasion, most often into the bladder, or to uterine rupture (Figs. 52–54).

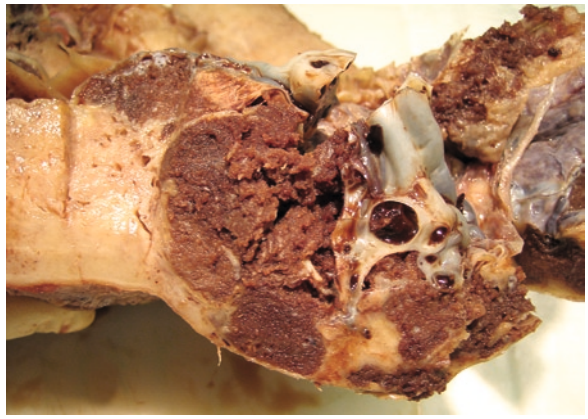

Fig. 53 Placenta percreta: cross section of the uterus with placenta invading through the myometrium

10.2.2 MRI of Placenta Accreta

Orientation of the placenta according to the cervix in placenta previa can be assessed by sagittal MRI (Fig. 55). MRI can also demonstrate other placental abnormalities as vasa previa or succenturiate lobes.

MRI is usually performed to proof placental adherence abnormalities when there is a strong clinical suspicion or ultrasound findings. MRI criteria for diagnosis of these abnormalities are similar to sonographic criteria and include:

- Thinning or irregularity of the myometrium
- Disruption of the interface between the placenta and myometrium
- Interruption of the tissue plane between the myometrium and the surrounding organs
- Mass effects of the placenta on the uterus causing an outer bulge

When uterine bulging is present, a focal outward contour bulge can be seen, or there can be disruption of the normal pear shape of the uterus, with the lower uterine segment being wider than the fundus. Heterogeneous signal intensity in the placenta can be seen as well. Sometimes it may be technically difficult to visualize the myometrium, as pregnancy progresses, it can become quite thin. However, when the myometrium can be well visualized, focal interruptions of the myometrial wall can be seen at the sites of placenta invasions. Focal thinning of the myometrium might not be a reliable sign of invasion on its own. Dark intraplacental band on T2-w imaging can be seen usually extending from the uterine–myometrial interface, having a variable thickness and random distribution. MRI can make diagnosis of placenta percreta confidently (Fig. 56). Differentiation between accreta and increta or exclusion of accreta may be more difficult (Bardo and

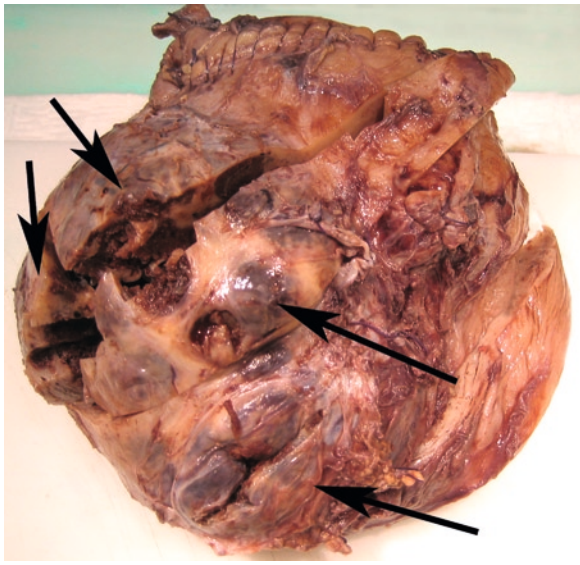

Fig. 54 Hysterectomy specism with placenta percreta

Fig. 55 Placenta previa totalis and percreta. SSFP sequence in GW 33. The placenta is located in the lower part of the uterus overlying the inner cervical os (*arrows*) and posterior uterine wall. The myometrial tissue is interrupted by placental tissue in the full circumference at the isthmic uterus

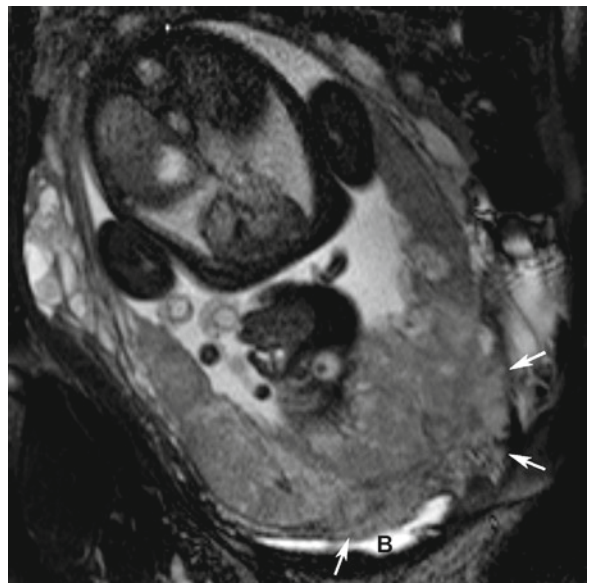

Fig. 56 Placenta previa with placenta percreta invading the urinary bladder (*B*) at GW 37. The myometrial tissue is interrupted by placental tissue; SSFP-sequence

Oto 2008; Laifer-Narin et al. 2007). Placental MRI provides a morphological description and topographical information that optimizes diagnosis and surgical management (Warshak et al. 2006; Palacios Jaraquemada and Bruno 2005).

MRI findings in Placenta Accreta (Bardo and Oto 2008)

- Placenta previa
- Uterine bulging
- Heterogeneous signal intensity within the placenta
- Dark intraplacental bands on T2-w
- Focal interruption in the myometrial wall
- Tenting of the bladder
- Direct visualization of the invasion of pelvic structures by placental tissue

In some cases, if no active major bleeding occurs postpartum, placenta percreta can be treated by methotrexate and fertility can be saved. On follow up of one of these cases, MRI showed a decrease of size after 5 weeks of therapy and on long-term follow-up a small calcificated transmural extension of 1 cm of the placenta throughout the uterus in the fundal area (Heiskanen et al. 2008).

Irregular-shaped placental lacunae signs ("Swiss cheese" appearance) represent vascular spaces (Abramowicz and Sheiner 2007). Thinning of the myometrium overlying the placenta, protrusion of the placenta into the bladder, increased vascularity of the uterine serosa–bladder interface, or in rare cases sacculation of the uterus as described by Defriend et al. (2000) are other signs for placenta percreta.

Placental Invasion

Three MRI features with good interrater reliability were seen in different proportions among those patients with placental invasion as compared with those with normal placentation. Although abnormal uterine bulging was seen in a few of the true negative subjects, it was much more common in the patient with placenta accreta. Perhaps the bulging is related to an abnormally tense myometrium created by the placental invasion or by the frequently thickened and hemorrhagic placenta seen in those cases. In placental invasion, a heterogeneous signal could be due to products of hemorrhage and/or artifacts from blood flow. Heterogeneous blood flow was found in none of the control group patients. Dark intraplacental bands on T2-w images were found in placenta accreta and some normal patients. In patients not showing those bands, placenta accreta is unlikely. Patients with dark bands are suspicious of invasion. The pathological correlate is not known but could possible represent abnormal bands of fibrous tissue. Interestingly some of the features that are used to diagnose placental invasion sonographically were not found to be useful in MRI evaluation (Lax et al. 2007). These features are thinned or absent retroplacental myometrial zone, presence of exophytic masses and the irregularity of the hyperechoic uterine serosa-bladder complex.

MRI has a very good interobserver agreement and allows a reproducible evaluation of placenta abnormalities, while ultrasound is strongly operator dependent (Masselli et al. 2008).

11 Multiple Gestations

Due to assisted reproductive techniques (ART), as in vitro fertilization, the incidence of multiple gestations increases. Twins are accounting for a disproportional percentage of perinatal morbidity and mortality.

11.1 Chorionicity

Dichorionic: two placentas have formed
Monochorionic: a single placenta is shared

11.2 Dichorionic Twin Placentas

Any gestation arising from two separate fertilized eggs will be dichorionic, as each conception forms it own placenta. These placentas may be totally separate or due to limitation of space in the uterus frequently fused to a single disk. There is no connection of circulations in such placentas. T-sections including the dividing membranes at the point where they meet the placental surface may show a wedge-shaped villous tissue in fused dichorionic placentas. Histologically in the dividing membrane chorionic tissue is present. In

ultrasound, chorionicity can be determined prior to the 16th gestational week by searching for the presence of the lambda-sign.

11.3 Monochorionic Twin Placentas

Monochorionic placentas occur only in monozygotic twins when the fertilized egg splits early in gestation and each portion develops separately. Chorionicity is dependent on the time separation occurs.

- Splitting before 3 days of development leads to gestations with totally separated dichorionic placentas.
- At about 3 days of development separation is incomplete and leads to two embryos and amnions developing within a single chorion – monochorionic placenta, as seen in two-third of monozygotic twins.
- Later splitting (>8 days) is unusual and leads to twins in a single amniotic sac – monoamniotic placenta with risk of umbilical cord entanglement (Fig. 57), or even to conjoined twins (splitting >12 days).

Monochorionic placentas virtually always show vascular anastomoses, which may lead to specific problems.

Histologically in the dividing membrane the amniotic membrane layers are in direct contact without chorionic tissue in between, presenting as T-sign in sonographic evaluation.

Fig. 57 Monoamniotic twin placenta with umbilical cord entanglement

11.4 Chorionicity and Dividing Membranes in MRI

According to ultrasound, the dividing membranes are good to evaluate by MRI in the first half of pregnancy.

11.4.1 Dichorionic Placentation in MRI

In dichorionic pregnancies, the membranes are thicker and sometimes two sheets of membranes are visible (Fig. 58). The lambda sign can be found before the 20th week of gestation. In later gestation, the dividing membrane is more difficult to visualize. In some cases with non-fused placentas, two placentas can be seen (Fig. 59).

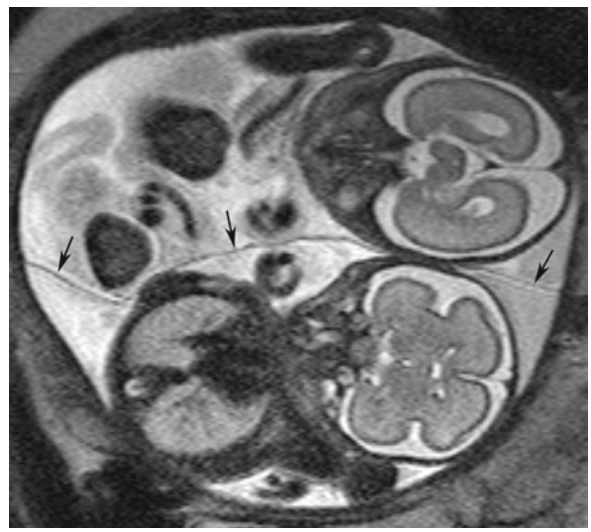

Fig. 58 Dichorionic diamniotic twin pregnancy in GW 27 with relatively thick dividing membranes (*arrows*), due to amnion-chorion-chorion-amnion structure

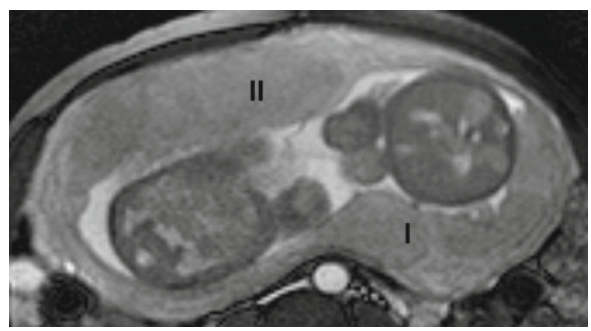

Fig. 59 Dichorionic twin pregnancy with two separated placentas, one anterior (II) the other posterior (I) located, in GW 29

Fig. 60 T2-w image of a monochorionic diamniotic twin pregnancy at GW 29, showing a thin dividing membrane (*arrows*), consisting of two amniotic sheets

11.4.2 Monochorionic Diamniotic Placentation in MRI

The dividing membrane in monochorionic twins is thin compared to dichorionic pregnancies (Fig. 60).

11.5 Twin-to-Twin Transfusion Syndrome

Twin-to-twin transfusion syndrome (TTTS) is a severe complication in monochorionic twin pregnancies that results from a hemodynamical imbalance of placental vascular anastomosis connecting the circulation of both fetuses. Unidirectional prenatal transfusion of blood through arteriovenous anastomosis is the specific etiology (Fig. 61). One twin serves as the donor, the other as the recipient. Discrepancy in size and development, particularly with respect to amniotic fluid and fetal fluid status is seen. Monoamniotic twins even with multiple large anastomoses are at lower risk of TTTS. High fetal morbidity and mortality are due to an oligo/polyhydramnion sequence. There may be microscopic differences in villous structure and maturation. The donor's placenta part presents larger, pale, and microscopically less mature with larger somewhat edematous chorionic villi. The recipient's part is smaller, more mature, and much more congested with blood (Fig. 62). Acute transfusion syndrome can complicate the course. Very premature delivery is common in sever chronic

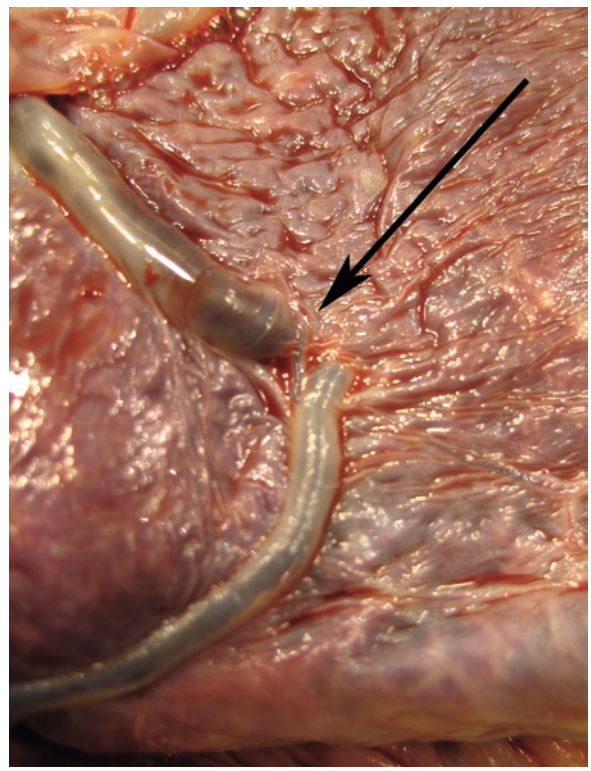

Fig. 61 Vascular anastomosis on the fetal surface of a monochorionic placenta

Fig. 62 Placental lamellar cross sections of a monochorionic twin placenta with TTTS showing differences in parenchyma

TTTS, often occurring in the second trimester. Mortality rates and risk of fetal demise of both twins are high.

11.5.1 MRI of Placenta Affected by TTTS

In monochorionic placentas affected by TTTS placental maturation according to Blaicher et al. (2006) presents pathological. Seldom two different compartments with differences in signaling in the placenta, representing the part of each fetus can be seen (Fig. 63).

11.5.2 MRI Evaluation of Placental Changes in TTTS after Laser Coagulation

Fetoscopic laser coagulation of the placental anastomoses can limit or prevent fetal injury (Figs. 64–66).

MRI is a postoperative imaging tool after fetoscopic laser coagulation therapy. In the studied cases of Huisman et al. (2005), the middle section of the placental surface showed on T2-w MRI hypointensity indicating postinterventional coagulation of anastomosis as well as an inhomogeneous signal within the placenta indicating partial placental infarction (Figs. 67 and 68).

12 Extrauterine Pregnancy

Extrauterine abdominal pregnancy is defined as the implantation of the fertilized ovum directly on the peritoneal surface of the abdomen. The risk of

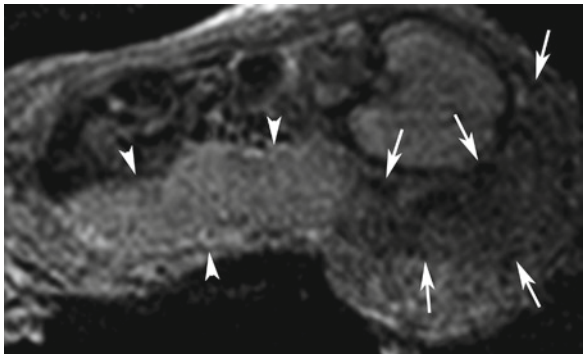

Fig. 63 Monochorionic diamniotic twin pregnancy in GW 25 with TTTS. Placental tissue shows differences in DW-signals (*arrows* vs. *arrow heads*)

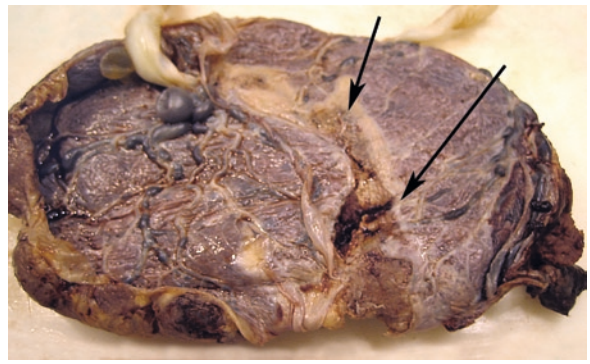

Fig. 64 Monoamniotic diamniotic twin placenta after laser coagulation of vascular anastomoses

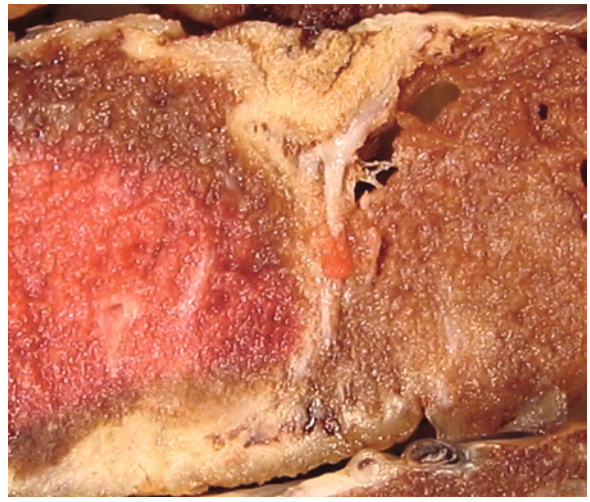

Fig. 65 Placental lamellar cross section of a monoamniotic diamniotic twin placenta after laser coagulation of vascular anastomoses with a scar in the placental tissue in V-shape

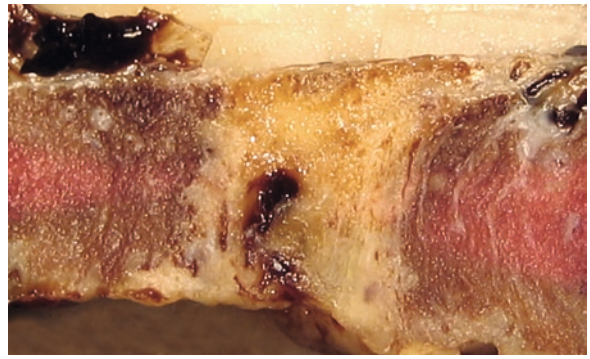

Fig. 66 Placental lamellar cross section of a monoamniotic diamniotic twin placenta after laser coagulation of vascular anastomoses with older necrotic placenta tissue over the full placental thickness

Fig. 67 Subchorionic hematoma on the placental surface; MRI after laser coagulation of vascular anastomosis because of TTTS in a T2-w sequence. A triangular area in the placental tissue underneath the dividing membranes appears hypointense due to fresh hemorrhagic infarction

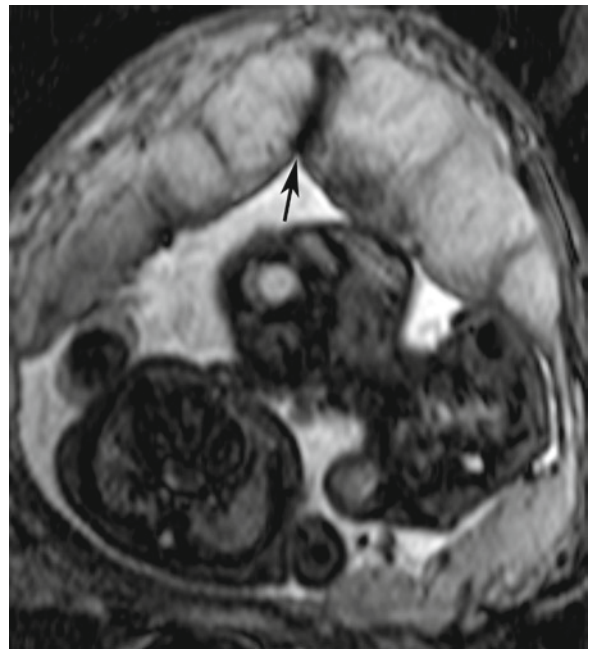

Fig. 68 Monochorionic diamniotic twin pregnancy affected by TTTS after laser coagulation therapy. DWI sequence in GW 29 showing a hypointense area in the placental tissue representing the ischemic scar

the mother dying from such an extrauterine pregnancy is 90 times greater than with a normal intrauterine pregnancy. The perinatal mortality is very high, from 5% to 25% due to prematurity, fetal growth retardation, and hemorrhage. Localization of the placenta in the abdominal cavity and the detection of placental adherence to solid organs, the bowel, and omentum can be problematic on ultrasound examination. Accurate intra-abdominal placental localization and morphological assessment of the fetus is necessary to plan management (Bertrand et al. 2009). Attempted removal of a placenta that is adherent to abdominal organs at the time of delivery can lead to torrential hemorrhage and rapid exsanguation of the mother.

Lockhat et al. (2006) reported on nine cases of extrauterine pregnancies, on average detected in the second trimester. T1- and T2-w sequences and magnetic resonance angiography (MRA) were performed without contrast media. Fetal position was most commonly found transverse subhepatic. The placenta was either attached to the fallopian tubes and broad ligament or the fundus of the uterus followed by the pouch of Douglas. Feeding arteries were correctly identified on MRA, the most common origins being branches of the internal iliac artery especially the uterine arteries. The presence of an empty uterine cavity with endometrial and myometrial thickening was detected in all patients. The management depends on the stage at which the extrauterine pregnancy is detected. Conservative management with maternal obstetric monitoring is available if diagnosis is made before 28 weeks of gestation and the placenta has implanted in the lower abdomen and not on the surface of the liver or spleen and a living fetus is present. After 28 weeks of gestation in the presence of a living normal fetus, immediate laparatomy and delivery of the fetus is recommended. In case of intrauterine fetal death (IUFT) immediate delivery is recommended. Management of the placenta after delivery is controversial. Follow-up MRI examinations demonstrated involution of the left in situ placentas over a 6-week period in those patients with adherent placenta.

Gadolinium-bolus MR angiography is useful to show location and vasculature supplying in extrauterine pregnancies and is a good tool for operative planning in ectopic pregnancies (Malian and Lee 2001).

13 Placental Pathology in Neurologically Impaired Infants

Clinically silent pathophysiological processes, which can directly cause CNS damage, decrease threshold for injuries, or serve as markers for deleterious in utero environment, may be seen in the placenta.

13.1 Premature Infants

In premature infants with very low birth weight (VLBW) (less than 1,500 g), CNS damage is related to immaturity of the developing brain and cardiopulmonary system. In these infants placental lesions may modulate the risk, but they usually are not the sole factor causing brain injury.

An association of clinical signs of acute chorioamnionitis and cerebral palsy has been found in premature infants. The relationship of histological acute chorioamnionitis to outcome is not clear yet. Severe maternal vascular disease secondary to abnormal artery remodeling in early pregnancy is the most common cause of IUGR. Severe IUGR has been demonstrated to be associated with increased prevalence of cerebral palsy and other neurodevelopmental disorders. In these severe cases, fetal blood flow in several vascular beds including the middle cerebral artery measured by Doppler is abnormal. Autopsy studies revealed a significant relationship between placental lesions as infarcts and neuronal necrosis in stillbirths. Villous edema is associated with low APGAR scores, and an increased risk of acute respiratory distress syndrome as well as an increased risk of neonatal death, cerebral palsy, and lung disease in VLBW infants. Multiple placental lesions have dramatically enhanced risk of neurodisability, each of which is by itself associated with adverse outcome.

13.2 Term Infants

In term infants underlying risk factors explaining CNS injury are much less clear than in premature infants. Placental pathology can identify processes, which either directly contributed to neurologic impairment or decreased functional reserve and adaptive changes indicating an abnormal intrauterine environment.

Sentinel events causing acute asphyxia less than 4–6 h prior to delivery are placental abruption presenting with a large retroplacental hematoma. Typical clinical signs and symptoms and sonographic diagnosis are associated with a significant number of false-positive and false-negative results. The strongest placental evidence of acute abruption is a central retroplacental blood clot with indentation of the placenta or rupture of the basal plate. Further complete umbilical cord obstruction due to tight cord knot, cord prolaps, and severe torsion related to cord entanglement or marginal/velamentous cord insertion might cause acute asphyxia. Intrapartum hemorrhage occurring due to placental vascular disruptions, for example, vasa previa, or rarely umbilical cord hematoma, can be another reason.

Subacute placenta injury may cause a pattern of brain injury related to sustained or repetitive periods of significant hypoxia or other systemic stress affecting the fetus over a period of many hours to days. Processes related to this are chorioamnionitis with severe acute fetal vasculitis, meconium staining with fetal vascular necrosis, chronic intermittent umbilical cord occlusion, subacute abruption, and fetomaternal hemorrhage.

Active chronic placental disease processes have their onset weeks prior to delivery and are progressive, continue to cause deterioration of placental function at an unpredictable rate until delivery. Fetal thrombotic vasculopathy has been strongly associated with neonatal encephalopathy, cerebral palsy, and other forms of neurological impairment. It can potentially cause brain injury directly via embolization of placental clots through the umbilical vein to the middle cerebral artery via the ductus venosus and foramen ovale or indirectly secondary to a fetal coagulopathy, sometimes accompanied by thrombocytopenia and thrombi in other fetal organs. Etiology of this condition includes abnormalities of the umbilical cord, cord entanglement, fetal thrombophilia, maternal antiphospholipid syndrome, and maternal diabetes. Chronic villitis with obliterative fetal vasculopathy, also known as villitis of unknown etiology, can cause obliterative fetal vasculopathy characterized by chronic vasculitis, luminal narrowing, and thrombosis. These rare but severe cases are related strongly with neurological impairment. This condition also has been associated with IUGR and recurrent reproductive loss. The etiology may be due to a maternal host versus graft reaction. Massive perivillous fibrin deposition (maternal floor infarction) is a

rare idiopathic condition characterized by progressive obliteration of the intervillous space by a combination of fibrin and a fibrinoid extracellular matrix. The etiology is still unclear but an association with autoimmune disease, maternal thrombophilia, and hypertensive disorders has been suggested. This condition may be recurrent and is related to spontaneous abortion, IUFD, severe IUGR, and premature delivery as well as increased adverse neurodevelopmental outcomes. Chronic peripheral separation (chronic abruption) is a recognized cause of premature delivery and the correlate of the chronic abruption-oligohydramnio sequence. Morphologically subchorionic hemorrhage, degenerated marginal blood clots, and circumvallated membrane insertion may be found. Clinically repetitive episodes of vaginal bleeding are seen, often in the third trimester. Affected infants show a specific pattern of lung disease but no association with neurological impairment could be proved even if chronical vaginal bleeding was shown to be a risk factor for cerebral palsy.

In chronic placental insufficiency placenta reserve capacity is reduced. It has been estimated that the placenta has an approximately 30% reserve capacity to maintain maternofetal gas exchange during times of stress. Conditions as maternal underperfusion or macrosomia and placentamegaly with distal villous immaturity, that reduce placental reserve by decreasing the volume or efficiency of placental tissue do not directly cause brain injury. Placentas with decreased ability to withstand significant stress occurring during the course of normal labor and delivery may be a risk factor for neurological impairment.

Stressful intrauterine environment is characterized by adaptive changes of the fetus and the placenta as increased circulating nucleated red blood cells or villous chorangiosis. These processes are indicators of the intrauterine status but do not cause placental insufficiency. They may occur due to decreased oxygen delivery associated to factors as high altitude, maternal anemia, and heavy smoking.

Multiple placenta lesions seem to act synergistically. Lesions occur at different time periods and each additional lesion significantly elevates the specificity of abnormal pathology for predicting adverse outcome. This sensation or preconditioning might reflect the effects of later lesions on compensatory mechanisms invoked by the initial process.

Knowing these facts investigation of the fetal brain in MRI should include a placenta scan as well, even if some of the pathologies listed above are microscopic and may not be seen in MRI. In utero diagnosis of fetal brain and placental conditions using modern imaging technologies have become an additional tool for the evaluation of the clinical management of a pregnancy and time and mode of delivery.

14 Postpartal Placenta Residuals – Placental Polyps

Intrauterine retained polypoid tissue after delivery or abortion is called placental polyp and may cause massive bleeding in late puerperal periods. Kurachi et al. (1995) reported on two cases where MRI has been performed before and after treatment with transcatheteral arterial embolization and local methotrexate injections.

14.1 Placental Polyps in MRI

T2- and contrast-enhanced T1-w images were studied by Suzuki et al. (1995). MRI features were polypoid masses, which appeared isointense on T1-w and hyperintense on T2-w images compared with myometrium. They might be accompanied by remarkable flow voids in the uterine cavity. Placental polyps were more intensely enhanced than the myometrium by the contrast media and indicated an adherent part to the myometrium. Follow-up was useful to image the reduction of size of the lesion and the blood flow after treatment.

Differential diagnoses on MRI are cirsoid aneurysms with increased flow void in the uterus and arteriovenous fistulas occurring in the myometrium, as well as choriocarcinoma and endometrial polyps.

15 The Uterus and the Placenta

Regarding the placenta in fetal MRI, some special uterine conditions and pathologies may be seen. It is helpful to know them for making differential diagnosis. Therefore, some of them will be discussed in this chapter.

The normal myometrium is visualized as a continuous band of soft tissue surrounding the gestational sac, which is at least 3 mm thick.

15.1 Uterine Dehiscence and Rupture

Uterine dehiscence is defined as the separation of the uterine musculature without extravasation of intraamniotic contents. Uterine rupture describes a defect in the uterine musculature with fetal parts or intraamniotic contents shift to the peritoneal cavity. The risk of uterine rupture is related to the thickness of the lower uterine segment.

Extremely thin myometrium may be seen in patients with prior caesarean section, especially in the third trimester and in the isthmic part of the uterus.

In MRI, it is visualized as a thin line hypointense in T2-w sequences (Levine 2006).

15.2 Congenital Abnormalities of the Uterus

Uterus arcuatus, subseptus, bicornis, and duplex are caused by persistence of the uterine septum and associated with higher risk for pPROM, abruption, as well as intrapartal and postpartal complications (Rossier et al. 2008), especially if placentation occurs at the septum.

In MRI location of the placenta at the septum can be seen (Fig. 69). The percentage of placental surface attached to the septum and to the uterine wall should be estimated.

15.3 Leiomyomas of the Uterus

Leiomyomas, although called fibroids, are well-circumscribed tumors derived from the smooth muscles of the myometrium. They can be located subserous, intramural, or in the submucosa and do occur singular or multiple. They may enlarge during pregnancy and may be confused with placental tumors. Rapid growth can lead to necrosis with hemorrhagic degeneration and pain, resulting in inflammation and stimulation of labor. Leiomyomas can lead into abruption of the placenta (Iwahashi et al. 2008).

In MRI, leiomyomas of the uterus are seen as well-circumscribed tumors, hypointense in native T2-w sequences, hyperintense if loaded with contrast agent (Figs. 70 and 71).

Fig. 69 On a frontal MRI scan (FLAIR sequence) of the gravid uterus in GW 23 a septum based on the uterine fundus is seen. The placenta is located in the right uterine horn and on the septum

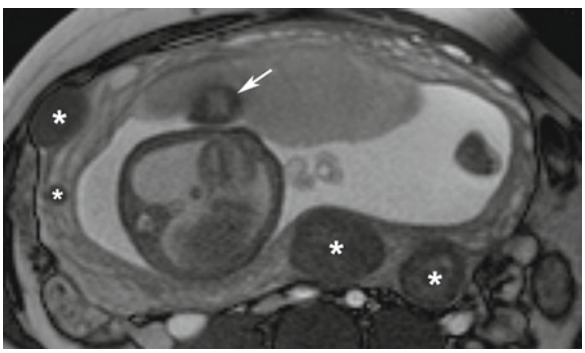

Fig. 70 Multiple intramural and subserosal leiomyomas of varying size in a pregnant uterus (*asterisks*). Arrow points at a fresh hemorrhagic infarction

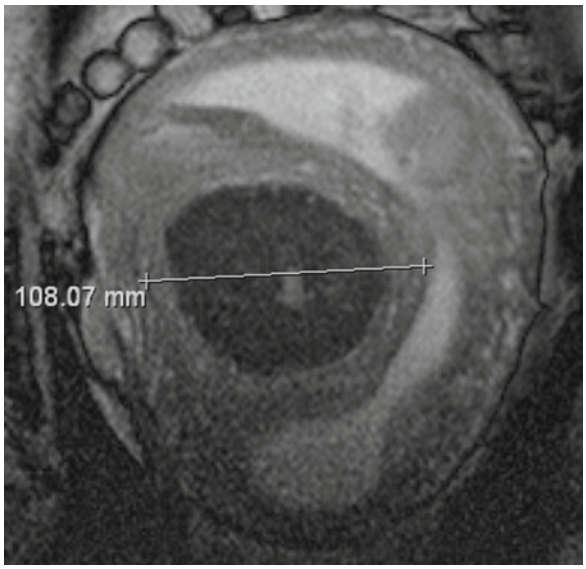

Fig. 71 A giant leiomyoma of 10.8 cm in diameter is located in the uterine wall and protubing into the uterine cavity

15.4 Uterine Contractions

Contractions of the uterus, as they randomly appear during pregnancy, can be visualized as thickened uterine wall and may be confused with leiomyoma or retroplacental hematoma (Fig. 72).

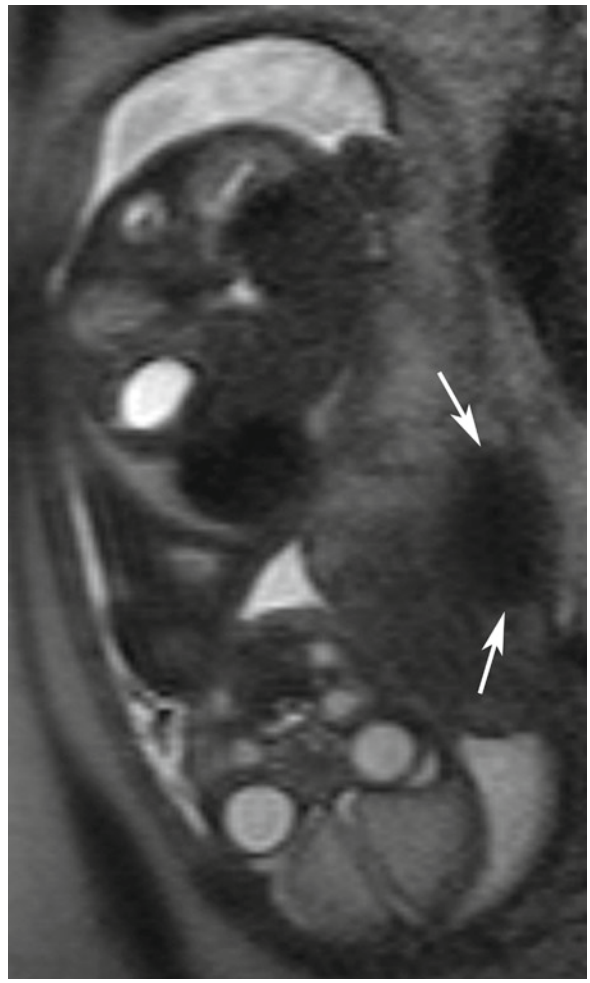

Fig. 72 The posterior uterine wall underneath the placenta is thickened and hypointense (*arrows*) due to uterine contraction

16 Special Methods and Techniques in MRI of the Placenta

In this chapter, special techniques of placental evaluation in MRI, which are not part of the routine fetal MRI scan evaluation, are described.

16.1 Use of Contrast Material in Placental MRI

Contrast medium is rarely used in antenatal MRI, as allergic reactions may occur and contrast media pass the placenta. A number of studies have evaluated the administration of gadolinium contrast during pregnancy and reported no obvious harmful effects, even if gadolinium passes through the placenta to the fetus. The only obstetric indication for gadolinium contrast material suggested is the evaluation of placenta accreta. Some centers use gadolinium-base contrast material for dynamic contrast-enhanced imaging in placenta accreta patients, assuming that the benefits overweigh the risks (Warshak et al. 2006; Palacios Jaraquemada and Bruno 2005).

16.2 Placental Volumetry by MRI

16.2.1 Placental Volume

Placental volume increases with gestational age. The volumetric estimates throughout the gestation correlate well with known fetal weight at these gestations (Williams et al. 1982). During pregnancy, blood volume increases.

Small placenta volumes indicate a restricted placental reserve and are seen in IUGR, chromosomal aberrations as trisomy 13, 18, and 21, and PE including HELLP syndrome.

16.2.2 MRI Volumetry Techniques

Volumetry using 3D reconstructions of MR data sets acquired in utero with T2-w SSFSE MRI was first described by Kubik-Huch et al. (2001). The segmentation has to be performed manually and is time consuming. Mean placental volume was 668 cm^3 ± 369 (range: 58–1.736 cm^3), but gestational age was 16–41 weeks. There are no reference standards for placental volumes published up to now. The mean amniotic fluid volume was 591 cm^3 ± 608 (range: 101–2.881 cm^3). Fetal motions make measurement slightly more difficult in smaller fluid volumes. In vitro tests showed a good agreement for volume calculations with a bias of 0.8% (Duncan 2001).

The technique of volumetry of fetal lungs in MRI, as described by Kasprian et al. (2006), can be possibly used for placental evaluation.

16.3 Placenta Perfusion Scan

Doppler ultrasound can detect changes in the velocity waveform of the uterine artery in established diseases and can identify a group at high risk (Moore et al. 2000).

DWI-based perfusion scans can separate good perfused placental areas from nonperfused areas and might be a diagnostic tool in future. Further studies are necessary to find optimal imaging protocols of the placental perfusion.

16.4 Intra Voxel Incoherent Motion – MRI

IVIM MRI is used to measure and portray blood movement in the placenta and obtains a more complete picture of the complex dynamics of placental blood flow. In normal pregnancies, different zones of blood movement within the capillaries (f) in the placenta were found. Variations in f have been related to the number of capillaries recruited to accommodate blood flow by Le Bihan et al. (1992) and the diameter of the vessels involved. In the placenta, maternal blood flow between intervillous spaces, unrestricted by maternal vessels, is resulting in turbulent blood flow over a wide range of velocities. An inner zone consisting mainly of fetal villi bathed in maternal blood, and an outer zone corresponding to areas consisting largely of maternal blood were identified. A difference in pressure between the maternal blood entering the intervillous space from low-resistance spiral arteries and the blood draining into the maternal venous system was shown.

In growth-restricted pregnancies, the placenta appears far more homogeneous, possibly indicating a reduction in the pressure gradient. The outer zone shows a significantly reduced proportion of moving blood compared to normal cases, indicating a reduction in volume or velocity of incoming maternal blood. Highest f values are generally recorded in the inner zone, possibly representing an adaptation of the fetal circulation in response to reduced maternal blood flow.

Placentas of pregnancies complicated by PE and the related pregnancy complication of fetal growth restriction are characterized by multiple areas of infarction, reduced surface areas for molecular exchange, and lower volumes of placental tissue (Moore et al. 2008).

Doppler ultrasound of the uterine arteries monitors the integrated flow of the whole placenta, whereas MRI measures the local flow from the spiral arteries to the placenta per unit area of the basal plate, which is more closely related to the blood flow per unit volume of the placenta. Early gestational ages are more difficult to study due to more fetal movement, and the small size of the placenta, making it hard to distinguish the basal plate.

IVIM may be clinically useful in identifying women at risk for developing PE and provides information for understanding the causes of compromised pregnancies (Ong et al. 2004).

16.5 Magnetization Transfer – Functional MRI In Vivo

Longitudinal studies show no alteration of values and R:T ratios calculated after quantifying the volumes of nonvascular and other tissue compartments by

stereological analysis of histological sections during normal or compromised pregnancies between 16 and 36 weeks of gestation. Vascular and nonvascular volumes alter proportionally during this period. Changes in intervillous and villous volumes and surfaces are attributable to IUGR and not to PE (Mayhew et al. 2004).

16.6 Magnetic Resonance Spectroscopy

Magnetic resonance spectroscopy (MRS) analyzes the energy levels of several elements and can help characterize metabolic processes and disturbances thereof. It can be used to determine chemical structure of molecules and study tissue biochemistry. It was hypothesized that the time from placental delivery to collection of tissues into liquid nitrogen may induce hypoxic changes and lead to metabolic changes compared to the in vivo situation. ATP concentrations decreased to 29% of the control levels within 25 min following placental delivery. No metabolite concentration differences in placentas obtained from vaginal deliveries and those from caesarean sections were found. In vivo analysis has been used extensively to study fetal organs like brain, heart, liver, and muscle, but there are few studies of the placenta. Most of these have analyzed the placenta in its normal physiologic state, but significant signal derangement has been observed when comparing normal with diseased placentas, such as those from IUGR pregnancies, suggesting the possibility that accurate diagnostic assessments of the severity of disease could be developed on the basis of nuclear magnetic resonance (NMR) spectroscopy findings. Uses of newer in vitro techniques could well suit to study the placenta and are probably the most valuable information about placental metabolism yet. A typical 31P (Phosphor isotope) NMR spectrum was described, containing a-ATP, b-ATP, g-ATP, inorganic phosphate (Pi), phosphomonoester (PME), and phosphodiester (PDE). Placentas from molar pregnancies showed higher signal intensity for PME than normal first trimester placentas. The PME signal intensity in normal pregnancies was highest when the tissue was undergoing its most rapid relative growth, that is, in the first and second trimesters. Placental ischemia has been found to decrease ATP and increase Pi (Mckelvey and Kay 2007).

16.7 PET-MR of the Placenta

PET-MR is a method that can provide information on maternal–fetal pharmacokinetics and pharmacodynamics in a primate animal model, but is not yet established for human beings (Benveniste et al. 2003).

References

Abramowicz JS, Sheiner E (2007) In utero imaging of the placenta: importance for disease of pregnancy. Placenta 21:S14–S22

Adams-Chapman I, Vaucher YE, Bejar RF et al (2002) Maternal floor infarction of the placenta: association with central nervous system injury and adverse neurodevelopmental outcome. J Perinatol 22:236–241

Allen SD, Lim AK, Seckl MJ et al (2006) Radiology of gestational trophoblastic neoplasia. Clin Radiol 61:301–313

Amano Y, Hayashi T, Takahama K et al (2003) MR imaging of umbilical cord urachal (allantoic) cyst in utero. AJR Am J Roentgenol 180:1181–1182

Bardo D, Oto A (2008) Magnetic resonance imaging for evaluation of the fetus and the placenta. Am J Perinatol 25:591–599

Baughman WC, Corteville JE, Shah RR (2008) Placenta accreta: spectrum of US and MR imaging findings. Radiographics 28:1905–1916

Benveniste H, Fowler JS, Rooney WD et al (2003) Maternal-fetal in vivo imaging: a combined PET and MRI study. J Nucl Med 44:1522–1530

Bertrand G, Le Ray C, Simard-Emond L et al (2009) Imaging in the management of abdominal pregnancy: a case report and review of the literature. J Obstet Gynaecol Can 31:57–62

Blaicher W, Brugger PC, Mittermayer C et al (2006) Magnetic resonance imaging of the normal placenta. Eur J Radiol 57:256–260

Brugger PC, Stuhr F, Lindner C et al (2006) Methods of fetal MR: beyond T2-weighted imaging. Eur J Radiol 57:172–181

Damodaram M, Story L, Eixarch E et al (2010) Placental MRI in intrauterine growth restriction. Placenta. doi:10.1016/j.placenta.2010.03.001

DeFriend DE, Dubbins PA, Hughes PM (2000) Sacculation of the uterus and placenta accreta: MRI appearances. Br J Radiol 73:1323–1325

Duncan KR (2001) Fetal and placental volumetric and functional analysis using echo-planar imaging. Top Magn Reson Imaging 12:52–66

Elchalal U, Ezra Y, Levi Y et al (2000) Sonographically thick placenta: a marker for increased perinatal risk–a prospective cross-sectional study. Placenta 21:268–272

Finberg HJ, Williams JW (1992) Placenta accreta: prospective sonographic diagnosis in patients with placenta previa and prior cesarean section. J Ultrasound Med 11:333–343

Grannum PA, Berkowitz RL, Hobbins JC (1979) The ultrasonic changes in the maturing placenta and their relation to fetal pulmonic maturity. Am J Obstet Gynecol 133:915–922

Heiskanen N, Kroger J, Kainulainen S et al (2008) Placenta percreta: methotrexate treatment and MRI findings. Am J Perinatol 25:91–92

H'Mida D, Gribaa M, Yacoubi T et al (2008) Placental mesenchymal dysplasia with beckwith-wiedemann syndrome fetus in the context of biparental and androgenic cell lines. Placenta 29:454–460

Huisman TA, Lewi L, Zimmermann R et al (2005) Magnetic resonance imaging of the feto-placentar unit after fetoscopic laser coagulation for twin-to-twin transfusion syndrome. Acta Radiol 46:328–330

Iwahashi M, Otani N, Umesaki N (2008) A giant placenta: the patient's placenta was growing quickly; the fetus was not. Am J Obstet Gynecol 199(712):e1

Jung SE, Byun JY, Lee JM et al (2001) MR imaging of maternal diseases in pregnancy. AJR Am J Roentgenol 177: 1293–1300

Kaplan C (2007) Color atlas of gross placental pathology, 2nd edn. Springer, New York

Kaplan CG (2008) Gross pathology of the placenta: weight, shape, size, colour. J Clin Pathol 61:1285–1295

Kasprian G, Balassy C, Brugger PC et al (2006) MRI of normal and pathological fetal lung development. Eur J Radiol 57:261–270

Kato K, Shiozawa T, Ashida T et al (2005) Prenatal diagnosis of amniotic sheets by magnetic resonance imaging. Am J Obstet Gynecol 193:881–884

Kawamotoa S, Ogawa F, Tanaka J et al (2000) Chorioangioma: antenatal diagnosis with fast MR imaging. Magn Reson Imaging 18:911–914

Kraus F, Redline R, Gersell D et al (2004) Placental pathology, 1st edn. American Registry of Pathology with the Armed Forces Institute of Pathology, Washington, DC, p 125

Kubik-Huch RA, Wildermuth S, Cettuzzi L et al (2001) Fetus and uteroplacental unit: fast MR imaging with three-dimensional reconstruction and volumetry–feasibility study. Radiology 219:567–573

Kurachi H, Maeda T, Murakami T et al (1995) MRI of placental polyps. J Comput Assist Tomogr 19:444–448

Laifer-Narin S, Budorick NE, Simpson LL et al (2007) Fetal magnetic resonance imaging: a review. Curr Opin Obstet Gynecol 19:151–156

Lax A, Prince MR, Mennitt KW et al (2007) The value of specific MRI features in the evaluation of suspected placental invasion. Magn Reson Imaging 25:87–93

Le Bihan D, Turner R, Douek P et al (1992) Diffusion MR imaging: clinical applications. AJR Am J Roentgenol 159: 591–599

Levine D (2005) Atlas of fetal MRI, 1st edn. Taylor & Francis, Boca Raton, 207

Levine D (2006) Obstetric MRI. J Magn Reson Imaging 24:1–15

Linduska N, Dekan S, Messerschmid A et al (2009) Placental pathologies in fetal MRI and pathohistological correlation. Placenta 30(6):555–559, Epub 2009 Apr

Lockhat F, Corr P, Ramphal S et al (2006) The value of magnetic resonance imaging in the diagnosis and management of extra-uterine abdominal pregnancy. Clin Radiol 61: 264–269

Malian V, Lee JH (2001) MR imaging and MR angiography of an abdominal pregnancy with placental infarction. AJR Am J Roentgenol 177:1305–1306

Marcos HB, Semelka RC, Worawattanakul S (1997) Normal placenta: gadolinium-enhanced dynamic MR imaging. Radiology 205:493–496

Masselli G, Brunelli R, Casciani E et al (2008) Magnetic resonance imaging in the evaluation of placental adhesive disorders: correlation with color Doppler ultrasound. Eur Radiol 18:1292–1299

Mayhew TM, Wijesekara J, Baker PN et al (2004) Morphometric evidence that villous development and fetoplacental angiogenesis are compromised by intrauterine growth restriction but not by pre-eclampsia. Placenta 25:829–833

McKelvey SS, Kay HH (2007) Magnetic resonance spectroscopy of the placenta. Placenta 28:369–377

Mochizuki T, Nishiguchi T, Ito I et al (1996) Case report. Antenatal diagnosis of chorioangioma of the placenta: MR features. J Comput Assist Tomogr 20:413–416

Moore RJ, Strachan BK, Tyler DJ et al (2000) In utero perfusing fraction maps in normal and growth restricted pregnancy measured using IVIM echo-planar MRI. Placenta 21: 726–732

Moore RJ, Ong SS, Tyler DJ et al (2008) Spiral artery blood volume in normal pregnancies and those compromised by pre-eclampsia. NMR Biomed 21:376–380

Morikawa M, Cho K, Kataoka S et al (2005) Magnetic resonance image findings of placental lake: report of two cases. Prenat Diagn 25:250–252

Nagel HT, Vandenbussche FP, Smit VT et al (2007) Intraplacental choriocarcinoma as an unexpected cause of intrauterine death at term. Int J Gynecol Cancer 17:1337–1339

Ngan HY, Bender H, Benedet JL et al (2003) Gestational trophoblastic neoplasia, FIGO 2000 staging and classification. Int J Gynaecol Obstet 83(Suppl 1):175–177

Ong SS, Tyler DJ, Moore RJ et al (2004) Functional magnetic resonance imaging (magnetization transfer) and stereological analysis of human placentae in normal pregnancy and in pre-eclampsia and intrauterine growth restriction. Placenta 25:408–412

Oyelese Y, Jha RC, Moxley MD et al (2003) Magnetic resonance imaging of vasa praevia. BJOG 110:1127–1128

Palacios Jaraquemada JM, Bruno CH (2005) Magnetic resonance imaging in 300 cases of placenta accreta: surgical correlation of new findings. Acta Obstet Gynecol Scand 84:716–724

Palacios Jaraquemada JM, Pesaresi M, Nassif JC et al (2004) Anterior placenta percreta: surgical approach, hemostasis and uterine repair. Acta Obstet Gynecol Scand 83: 738–744

Prayer D, Brugger PC, Prayer L (2004) Fetal MRI: techniques and protocols. Pediatr Radiol 34:685–693

Ramsey EM (1959) Vascular adaptations of the uterus to pregnancy. Ann N Y Acad Sci 75:726–745

Rossier MC, Bays V, Vial Y et al (2008) Congenital uterine anomalies: diagnosis, prognosis and management in 2008. Rev Med Suisse 4:2253–2254, 2256–2258, 2260

Salafia CM, Zhang J, Charles AK et al (2008) Placental characteristics and birthweight. Paediatr Perinat Epidemiol 22: 229–239

Sebire NJ, Sepulveda W (2008) Correlation of placental pathology with prenatal ultrasound findings. J Clin Pathol 61:1276–1284

Suzuki N, Suzuki M, Terada S et al (1995) Placental polyp: MR imaging findings. AJR Am J Roentgenol 165:1554

Takai N, Miyazaki T, Yoshimatsu J et al (2000) Intraplacental choriocarcinoma with fetomaternal transfusion. Pathol Int 50:258–261

Takeuchi M, Matsuzaki K, Uehara H et al (2005) Pathologies of the uterine endometrial cavity: usual and unusual manifestations and pitfalls on magnetic resonance imaging. Eur Radiol 15:2244–2255

Thompson MO, Vines SK, Aquilina J et al (2002) Are placental lakes of any clinical significance? Placenta 23:685–690

Trop I, Levine D (2001) Hemorrhage during pregnancy: sonography and MR imaging. AJR Am J Roentgenol 176:607–615

Verswijvel G, Grieten M, Gyselaers W et al (2002) MRI in the assessment of pregnancy related intrauterine bleeding: a valuable adjunct to ultrasound? JBR-BTR 85:189–192

Voss MK, Hansen LS, Rasmussen KL (2007) Umbilical cord constriction caused by amniotic band. Ugeskr Laeger 169: 3497–3498

Wagner BJ, Woodward PJ, Dickey GE (1996) From the archives of the AFIP. Gestational trophoblastic disease: radiologic-pathologic correlation. Radiographics 16:131–148

Warshak CR, Eskander R, Hull AD et al (2006) Accuracy of ultrasonography and magnetic resonance imaging in the diagnosis of placenta accreta. Obstet Gynecol 108: 573–581

Williams RL, Creasy RK, Cunningham GC et al (1982) Fetal growth and perinatal viability in California. Obstet Gynecol 59:624–632

Problems of Multiple Pregnancies Ultrasound and MRI

Elisabeth Krampl-Bettelheim

Contents

Abstract

- The number of multiple births is increasing. This is due to assisted reproduction and maternal age.
- It is crucial for management and prognosis to differentiate between monochorionic and dichorionic twin pregnancies by ultrasound in the first trimester.
- The outcome of multiple pregnancies is significantly worse compared to singleton pregnancies. Perinatal mortality is three to seven times higher, due to the higher incidence of preterm birth, intrauterine growth restriction, malformations, and to the complications specific for twin pregnancies.
- Management of twin pregnancies includes repeat ultrasound scans for screening for malformations, chromosomal abnormalities, and for assessing fetal growth and fetal circulation. Magnetic resonance imaging is used as additional tool from 18 weeks onward to further assess fetal malformations and placental pathology.

1 Zygocity and Chorionicity

Dizygotic twin pregnancies develop after fertilization of two different oocytes by two different sperms. Each of them develops into embryo and placenta, which are separated. Dizygotic twin pregnancies are therefore always dichorionic.

E. Krampl-Bettelheim
Department of Obstetrics and Gynecology,
Medical University Vienna, Vienna, Austria
e-mail: elisabeth.krampl-bettelheim@meduniwien.ac.at

D. Prayer (ed.), *Fetal MRI*, Medical Radiology,
DOI: 10.1007/174_2010_120, © Springer-Verlag Berlin Heidelberg 2011

In monozygotic twins, one fertilized oocyte splits up within 2 weeks. Depending on the time of splitting, there are three different types of placentations (Fig. 1).

- Splitting before the morula stage (day 1–3) occurs in about 30% of monozygotic pregnancies and leads to a dichorionic, diamniotic twin pregnancy. The separating membrane between the two fetuses consists of four layers: amnion – chorion – chorion – amnion.
- Splitting in the early blastocyst stage (day 4–8) occurs in about 65% of monozygotic pregnancies. It affects the inner cell mass (embryoblast) and leads to a monochorionic diamniotic pregnancy. The two embryos share one placenta and chorion, and the separating membrane consists of two layers: amnion – amnion.
- Splitting after day 9 (two germ layers), which occurs in about 5% of monozygotic twin pregnancies leads to a monochorionic, monoamniotic twin pregnancy. The two embryos share one chorion// placenta and one amnion.
- In very rare cases, splitting occurs after day 12, which leads to Siamese twins.

1.1 Implications of Knowing the Chorionicity

Chorionicity – not zygocity – is the major determinant of fetal outcome in twin pregnancies.

- Miscarriage rate and perinatal mortality are higher in monochorionic compared to dichorionic twin pregnancies (Derom et al. 1995; Hack et al. 2008)
- Intrauterine fetal death often leads to death or neurological handicap of the co-twin (Liu et al. 1992; Quarello et al. 2008; O'Donoghue et al. 2009). This is particularly important in severe intrauterine growth restriction (IUGR) and imminent intrauterine death, and in the technique for selective feticide in case of malformations.

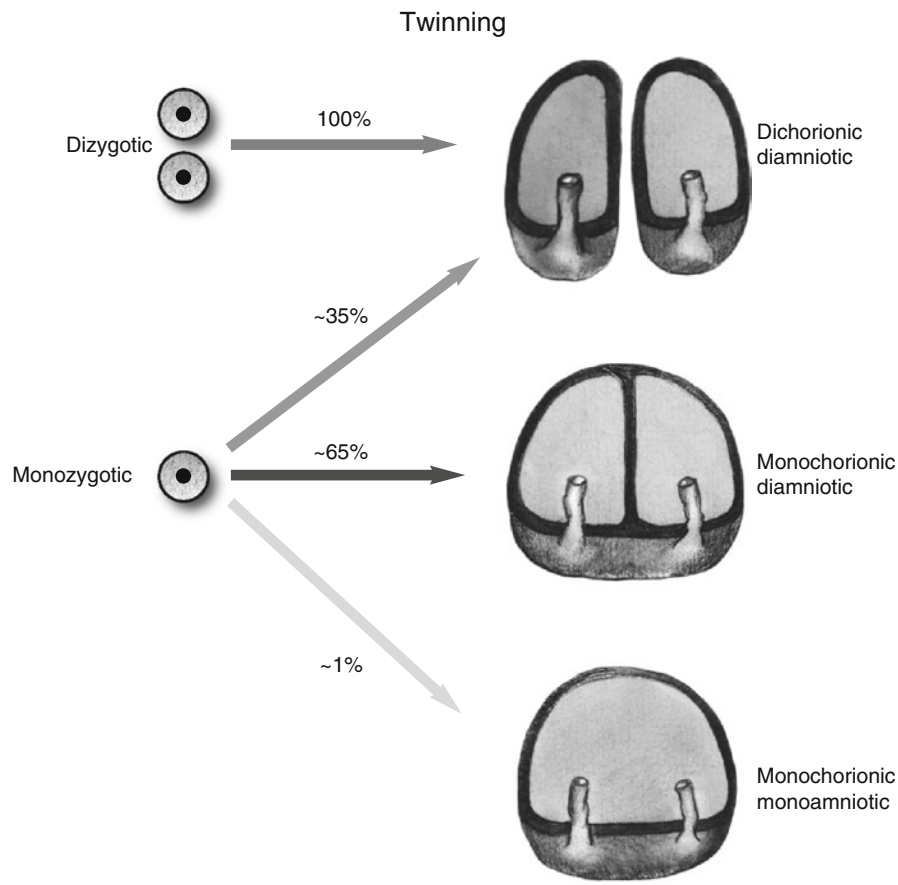

Fig. 1 Placentation dizygotic twins are always dichorionic; monozygotic twins can be monochorionic or dichorionic

- Chorionic villous sampling in monochorionic twins needs to be done from one fetus only in most cases, because they are genetically identical.

1.2 Determining Chorionicity

Chorionicity can be determined up to 14 weeks of gestation by ultrasound scan.

In dichorionic twins, there is chorion visible between the amniotic membranes. This is very obvious in early pregnancy (Fig. 2a), and up to week 14 or sometimes longer there is the so-called λ-sign.

In monochorionic, diamniotic twins, two very thin amniotic sacs can be seen. After fusion of the two amniotic sacs and of the amnion with the chorion, the so-called T-Sign is visible where the two amniotic membranes touch the chorion (Fig. 2b).

Monochorionic, monoamniotic twins can be diagnosed by cord entanglement, visible by the end of the first trimester (Sebire et al. 2000) (Fig. 2c). Since the membrane can be very thin in a monochorionic, diamniotic pregnancy, it may be misdiagnosed as monoamniotic (Weisz et al. 2005).

2 Special Aspects of Ultrasound Screening in Multiple Pregnancies

2.1 Chromosomal Abnormalities

Since monochorionic twins are always monozygotic, the age-related risk of aneuploidy of a singleton pregnancy applies to both fetuses. Considering that 90% of dichorial twins are dizygotic, the risk of aneuploidy of one of the two fetuses is doubled for mathematical reasons. Multiplying the risk of one fetus by the risk of the second fetus gives the risk that both fetuses are affected.

Screening for chromosomal abnormalities by measuring the nuchal translucency is a valid screening method also in twin pregnancies. The detection rate is 88% with a 7.7% false positive rate (Sebire et al. 1996b). The risk is assessed for each fetus separately, taking into account maternal age, gestational age, and nuchal translucency. In monochorionic twins, one has to take into consideration that an increased nuchal translucency may be an early sign of twin-to-twin transfusion syndrome. Screening by maternal serum biochemistry is possible in twin pregnancies. It does not increase the detection rate, but it reduces the rate of false-positive results in combination with nuchal translucency measurement (Spencer 2000).

2.2 Malformations

Multiple pregnancies have a higher risk for chromosomal and anatomical malformations. This is due to the higher number of fetuses and the increased malformation risk associated with monozygotic twins. Therefore, the overall malformation rate per child is about twice as high as in singleton pregnancies (Baldwin 1994).

Malformations are more frequent in monozygotic than in dizygotic twins. Hydrocephaly, anencephaly, holoprosencephaly, sacrococcygeal teratoma, and congenital heart defects are typical malformations. Irrespective of the type of malformation and chorionicity, only one fetus is affected in the majority of cases (80–90%).

Fig. 2 Chorionicity on ultrasound

3 Complications of Multiple Pregnancies

3.1 Intrauterine Death

The incidence of intrauterine fetal death in the second half of the pregnancy is 0.5–6.8% in twin pregnancies and 14–17% in triplet pregnancies. Death of one fetus does not lead to "poisoning" or coagulopathy as assumed in the past.

The outcome of the surviving twin is dependent on the chorionicity. In dichorionic twins, preterm labor and premature birth can occur; otherwise, there is no risk for the surviving twin. In monochorionic twins, the death of a fetus leads to acute episodes of hypotension and anemia of the second twin. This causes death or severe neurological damage in 25% of cases. The damage seems to occur within 24 h after fetal death (Senat et al. 2003). If there are no ultrasonograhic signs of anemia, fetal damage seems to be unlikely. Ischemic lesions can be sensitively detected by MRI (Fig. 3). In most cases there are hemorrhagic components. A review of studies and case reports shows that the risk of fetal death in the second twin is six times higher in monochorionic than in dichorionic twins (OR 6.04 [95% CI1.84–19.87]). Neurological damage was also increased (OR 4.07 [95% CI1.32–12.51]) (Ong et al. 2006).

In our twins clinic, the surviving monochorionic twin is monitored by CTG and Doppler for 24 h after intrauterine death of the second twin. The baby is delivered in case of signs of anemia. Fetal MRI is performed as soon as possible – ideally within 24 h – and a few weeks later to assess potential brain damage. Antenatal care of dichorionic twins does not change after intrauterine death of one fetus.

Intrauterine death of one twin always leads to considerable psychological stress. Particular to this situation is the fact that after birth the surviving child reminds the parents of the dead twin. For many parents, grief overshadows the joy with the healthy baby. Psychological support is therefore recommended.

3.2 Preterm Labor

A quarter of all children born premature are multiples, although only 3% of all children are twins and 0.1% are triplets. Compared to singletons birth weight is lower at every gestational age. Five percent of all twins have a birth weight of less than 1,000 g compared with about 0.5% of singletons (Kiely 1990). A large newborn database ($n = 51388$) shows that both mortality and morbidity are the same in singletons and in multiples at any gestational age. The determining factor for adverse outcome is prematurity (Garite et al. 2004). Eighty percent of all singletons are born by 40 weeks of gestation, whereas 80% of all twins are born by 37 weeks and 80% of all triplets by 34 weeks (Kiely 1990; Derom et al. 1995).

Higher order multiple pregnancies therefore are obligatory preterm.

Chorionicity plays a crucial role in predicting preterm births. The risk for spontaneous preterm birth is twice as high in monochorionic twins than in dichorionic twins (9% vs 5.5%). The probability for intrauterine growth restriction and perinatal mortality in monochorionic twins is also twice as high as in dichorionic twins (Sebire et al. 1997b).

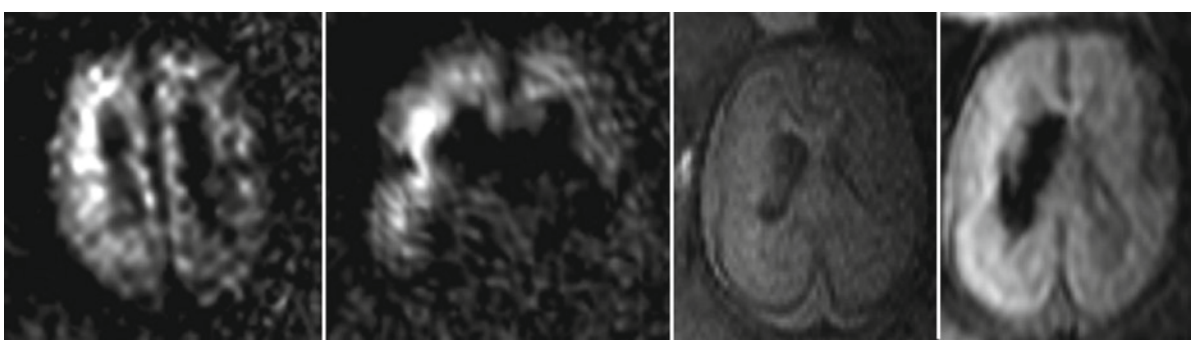

Fig. 3 GW24, acceptor in TTS: Axial and coronal diffusion-weighted images, showing bright signals in ischemic regions; T2-w and echoplanar images: revealing the signal loss in hemorrhagic components

Known risk factors for spontaneous preterm birth include smoking, conization, previous late miscarriage or premature delivery, and cervical length. A recent study including 1,200 twin pregnancies showed that in a multivariate analysis the only independent factor predicting preterm birth is the cervical length (To et al. 2006). The fetal fibronectin test in twin pregnancies is most accurate at 24–28 weeks of gestation (Wennerholm et al. 1997).

Preterm deliveries due to other pregnancy complications are also more frequent in multiple than in singleton pregnancies. A British study showed that the incidence of 6–27% for preeclampsia in twin pregnancies is significantly higher compared to singleton pregnancies. In triplet pregnancies, the incidence is 5–46% (Savvidou et al. 2001).

The rate of intrauterine growth restrictions is also increased. In 1.7% of dichorionic twins and 7.5% of monochorionic twins, birth weight is under the 5th centile for both children (Sebire et al. 1997a). The risk for premature rupture of membranes is twice as high in twin pregnancies than in singleton pregnancies (Myles et al. 1997).

Neonatal outcome is not improved by prophylactic bed rest and "homeuterine activity monitoring" (HUAM). A recent review showed that the rate of preterm delivery is doubled after cerclage (Berghella et al. 2005; Berghella 2009).

In a large placebo-controlled study of patients with a short cervix in both twin and singleton pregnancies, the incidence of preterm delivery was decreased significantly by daily vaginal application of progesterone (Fonseca et al. 2007). Several randomized trials showed a reduction of the preterm delivery rate in singleton pregnancies at high risk for preterm birth by injecting 17-alpha-hydroxyprogesterone (Tita and Rouse 2009). A possible effect in twin and triplets pregnancies (Caritis et al. 2009) has not been seen so far. However, several studies have finished recruiting and results are expected within the next years.

3.3 Intrauterine Growth Restriction

Birth weight of twins is lower than that of singletons, 800 g on average (Kiely 1990). This is due to preterm delivery and a higher rate of intrauterine growth restriction (IUGR). IUGR is a significant factor of neonatal morbidity in twins, and perinatal mortality is 2.5 times higher in twins with IUGR compared to normally grown twins. In up to one out of four twin pregnancies only, one fetus is affected by IUGR. In monochorionic twins, selective intrauterine growth restriction is one of the major complications (see Sect. 4.2).

4 Problems Specific to Monochorionic Twin Pregnancies

4.1 Twin-to-Twin Transfusion Syndrome (TTS)

At 16–24 weeks of gestations, the miscarriage rate of monochorionic twins is 12%, six times higher than in dichorionic twins. This is due to the twin-to-twin transfusion syndrome. Thirty percent of all monochorionic twin pregnancies show the following three signs of imbalance at 16 weeks of gestation:

- Folding of the separating membrane showing a double membrane at the free end on ultrasound
- Amniotic fluid discrepancy
- A discrepancy in the size of the fetal urinary bladder (Sebire et al. 1997b)

Half of these cases, this is 15% of all monochorionic twin pregnancies, will develop a twin-to-twin transfusion syndrome. This is defined by the anhydramnios-polyhydramnios sequence and can be classified in five stages (Quintero et al. 1999). In FFTS, mortality is 90% when untreated (Yamamoto and Ville 2005). This can be due to miscarriage, cardiac failure of the recipient, or consequences of hypotension in the donor. Figure 3 shows acute brain hemorrhage of the acceptor in a rapidly evolving TTS at 24 weeks of gestation.

Possible treatments include repeat amniodrainage or fetoscopic laser coagulation of the placental anastomoses. Prior to 26 weeks of gestation, the prognosis of TTS is significantly better after laser treatment compared to amniodrainage, regarding both survival and neurological damage. This was shown in a prospective, randomized trial (Senat et al. 2004). After 26 weeks of gestation, amniodrainage and delivery was considered the best option; however, recent reports suggest a

possible advantage in later fetoscopic laser ablation (Middeldorp et al. 2007).

Data regarding long-term outcome is scarce: A small study about the neurological development of children after laser treatment aged 6 months to 5 years using the Griffiths Score showed average values. The only significant difference was in the locomotor subscale where donor and recipient scored less than singletons. 13.3% of the twin survivors group suffered from cerebral palsy but none of the surviving singletons (Sutcliffe et al. 2001).

4.2 Selective Intrauterine Growth Restriction

The growth of two fetuses is rarely exactly the same; minor differences in size are common in almost all multiple pregnancies. If the difference in crown rump lengths is more than 10–14%, close follow-up is necessary to react appropriately to possible problems. A growth discrepancy in the first trimester has a considerably worse prognosis in monochorionic than a dichorionic twins. In dichorionic twins, a big difference in crown rump length can be a sign for trisomy 18, triploidy, or other malformations (Kalish et al. 2004; Salomon and Ville 2005). With normal chromosomes, mortality in dichorionic twins with growth discordance is low.

Growth discrepancy is not an early sign of twin-to-twin transfusion syndrome (Sebire et al. 1998), but mortality due to selective IUGR is high.

Severe selective intrauterine growth restriction is currently one of the major challenges in the management of monochorionic twins. Especially, cases with intermittent reverse flow in the umbilical artery have a poor prognosis. Sudden intrauterine death has been reported in 15%, and parenchymal brain lesions in 20% (Gratacos et al. 2007). Almost always this is associated with large arterio-arterial anastomoses. However, early mild ventriculomegaly may be associated with a favorable prognosis. Figure 4 shows both fetuses at GW22. The size differences can be depicted as well as the ventriculomegaly of the smaller fetus. The development at 22 years of age showed normal Bayle's scores.

4.3 Monoamniotic Twin Pregnancy

About 1% of all twin pregnancies, or 22 out of 10,000 pregnancies, are monoamniotic. Definitive diagnosis is possible by ultrasound from 12 weeks by cord entanglement (Fig. 2c). A characteristic of monoamniotic twin pregnancy is the high perinatal mortality, up to 75% in series with recruitment in early gestation. This is due to the high rate of malformations and sudden intrauterine death, and to failed splitting of the embryos (conjoined twins). The high rate of malformations results from the late separation of the embryonic area and the hemodynamic imbalance (Sebire et al. 2000).

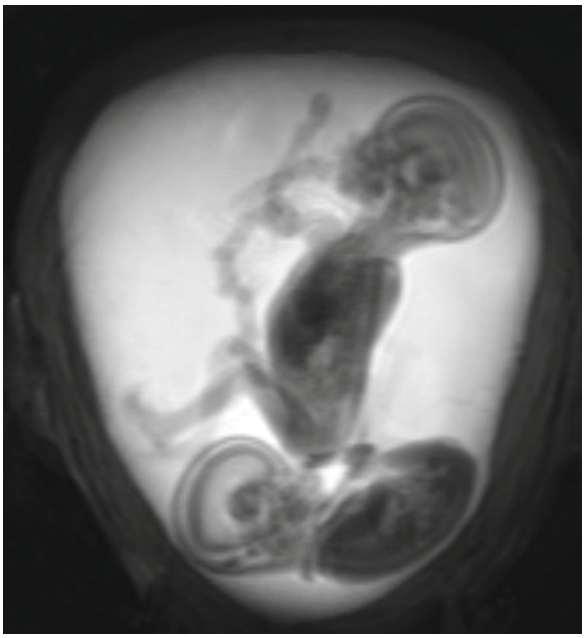

Fig. 4 GW22, thick slab steady-state free precession image: notice the size difference of the fetuses as well as the ventriculomegaly of the smaller one

Acute twin-to-twin transfusion syndrome or cord entanglement can lead to late intrauterine death. Chronic twin-to-twin transfusion syndrome is rarely described in monoamniotic twins. This is probably due to large superficial placental anastomosis. Observational studies showed that mortality may be reduced to 10% by close monitoring and early delivery (Durand-Reville et al. 2005; Ezra et al. 2005; Heyborne et al. 2005; DeFalco et al. 2006). Former methods such as reduction of amniotic fluid by giving sulindac (Pasquini et al. 2006) are not generally recommended. In the absence of large prospective trials, a widely accepted management strategy includes early diagnosis of malformations and education about prognosis. If the fetuses survive the first and second trimester, close monitoring from 26 weeks gestational age and elective delivery in pregnancy week 32 are associated with good outcome.

4.4 Twin Reverse Arterial Perfusion (TRAP)

The most extreme form of twin-to-twin transfusion is a development of one twin without heart, known as acardius corioangiopagus parasiticus. This malformation is also called twin reverse arterial perfusion (TRAP) to explain the underlying mechanism. Incidence is about 1% of all monochorionic twin pregnancies corresponding to about one in 35,000 pregnancies (Sogaard et al. 1999). For the acardic twin, the term parasite is used, because it is perfused by the normal twin ("pump twin"). This condition can lead to high output cardiac failure in the pump twin. Suspected causes are artery-to-artery and vein-to-vein anastomoses in the placenta combined with a delay in the development of the heart in early pregnancy (Benirschke and des Roches Harper 1977; Gibson et al. 1986). If one twin develops slower than the other twin, the imbalance in blood pressure leads to a retrograde perfusion of the weaker twin. The consequence is a mal development of the heart, often remaining in a rudimentary state.

Appearance of the acardiac twin varies. Generally, the upper part of the body fails to develop and frequently head, spine, and upper extremities are missing. Edema and cystic hygroma can often be found (Van Allen et al. 1983). This can be explained by the fact that the oxygen in the blood is used in the lower part of the body and the upper part is only supplied with deoxygenated blood (Sepulveda et al. 1995; Quintero et al. 1995). Another possible cause for a TRAP is the fertilization of the polar body by a second sperm (Bieber et al. 1981). However, DNA fingerprinting patterns were compared in nine sets of twins with TRAP and they were all identical, which means that they were monozygotic (Fisk et al. 1996).

On ultrasound scan, a normal twin and a twin that is growing but does not have a heart in a monochorionic, most often diamniotic pregnancy can be seen. Pathognomonic is a reversed arterial perfusion on Doppler ultrasound (Pretorius et al. 1988). Differential diagnosis includes selective IUGR in monochorionic twins, but in these cases, the smaller fetus has a heart. In case of a suspected intrauterine fetal death or severe malformations of one twin, TRAP has to be considered (Sepulveda et al. 1993; Petersen et al. 2001).

The acardiac twin is not viable: the other twin carries a high risk for intrauterine death because of heart failure or extreme preterm birth due to polyhydramnios (Moore et al. 1990). This risk is directly correlated with the size of the acardiac twin. If the acardiac twin is considerably smaller than the normal twin, expectant management is adequate. In case of a large acardiac twin the risk for the other twin is very high. Treatment possibilities include coagulation of the umbilical cord by laser at the end of the first trimester, fetoscopic laser coagulation of the placental vascular anastomoses, or occlusion of the umbilical cord via bipolar coagulation in the second trimester (Sepulveda et al. 1995; Robyr et al. 2005; Diehl and Hecher 2007).

4.5 Conjoined Twins

In case of a single zygote failing to separate completely after day 13 following fertilization the two fetuses remain conjoined. This condition is also known as Siamese twins. About 1 in 300 monozygotic twins are conjoined, this corresponds to 11 in 60,000 to 11 in 200,000 pregnancies. On average 3 out of 10 conjoined twins die before birth; therefore, only one pair of Siamese twins is born in about11 million live births.

Different organs may be affected:

- Thorax (Thoracopagus, about 70% of all cases)
- Hips (Ischiopagus, about 5% of all cases)
- Head (Craniopagus, cephalopagus, less than 2% of all cases)
  - Dicephaly: one body with two heads
  - Janiceps (after the two-faced god Janus): two faces on opposite sides of a single, conjoined head
- Lower chest to lower abdomen (Omphalopagus)
- Tailbone (Pygopagus)
- Fetal inclusion or fetus in fetus: one twin is absorbed by the other

Prognosis is dependent on the location and the extent of the fusion, most of the time it is dismal.

5 Invasive Procedures

Treatment of twin-to-twin transfusion syndrome by laser photocoagulation of the shunting vessels is possible.

5.1 Karyotyping

If parents opt for karyotyping there are two possibilities: chorionic villus sampling (CVS) from 11 weeks or amniocentesis (AC) from 16 weeks onward. Relative safety of both interventions, reliability to get

genetic material from both fetuses and further management should be taken into account when deciding between CVS and AC. In twin pregnancies, both interventions should take place in a specialized center. With ACs, it is important to make sure that amniotic fluid is gained from both amniotic sacs. Frequently the interventions are performed with two insertions, sometimes using methylene blue dye after the first sample. But the intervention is also possible with only one needle insertion (Antsaklis et al. 2002). There are no prospective trials, but observational studies show that the risk of miscarriage is slightly higher after chorionic villus sampling.

By chorionic villus sampling the risk of taking two biopsies from the same placenta is relatively high. The advantage of an early diagnosis is a lower miscarriage risk after early selective feticide. Therefore a CVS should be performed in case of high risk for chromosomal abnormalities, otherwise amniocentesis is advisable.

Selective feticide is the method of choice in case of trisomy 21 if the parents opt for termination. In case of trisomy 18, expectant management may be better.

5.2 Reduction of Higher Number Multiple Pregnancies

Higher number multiple pregnancies are almost always caused by assisted reproduction techniques. Triplets and higher order multiples have a high risk of miscarriage or preterm birth, and perinatal mortality is high. This risk can be decreased by embryo-reduction. A reduction to twins rather than to a singleton (or triplets) is commonly performed. The miscarriage rate of an experienced operator is dependent on the number of fetuses: It is 4.5% in triplets, 8% in quadruplets, 11% in quintuplets, and 15% in sextuplets or more (Evans and Britt 2008). In quadruplets and higher order multiple pregnancies, embryo-reduction improves the outcome considerably (Evans et al. 1996).

Iatrogenic death is achieved by an ultrasound-guided injection of potassium chloride into the fetal heart. The risk of a spontaneous miscarriage is relatively high in early pregnancy; therefore, it is worth delaying a reduction until 11 weeks of gestation. Furthermore, at the end of the first trimester, severe malformations and markers for chromosomal abnormalities can be seen by ultrasound scan. In some centers, karyotyping is always performed before a reduction; others perform high-level ultrasound screening and limit invasive testing to fetuses at increased risk. Determination of chorionicity is essential prior to reduction because in monochorionic twins the risk of intrauterine death of the other fetus after feticide is high.

5.3 Selective Feticide

If malformation or chromosomal abnormalities affect one fetus, the pregnancy may be terminated or a selective abortion of the affected fetus may be performed. If the malformation is not fatal but the parents decide for an abortion, selective feticide is possible. In case of fatal malformation, waiting is recommended unless the malformation poses a risk for the healthy fetus.

If the parents decide for the selective feticide because of a chromosomal or anatomical anomaly the miscarriage rate at 12 weeks is 8%. A quarter of these miscarriages occur within the first week after the procedure but the remaining 75% take place 6–8 weeks later. Selective feticide at 20 weeks carries a miscarriage risk of 20%. A substantial number of these occur after weeks 24 of gestation, leading to severe preterm delivery and the associated complications.

To keep the miscarriage risk low, chorionic villous sampling at 11–14 weeks is the method of choice if the risk for chromosomal abnormalities is higher than 1:50. If the karyotype turns out abnormal, the parents have the possibility of early embryo reduction (Sebire et al. 1996a, b).

In monochorionic pregnancies, death of one fetus leads to death of the other fetus or neurological damage due to hypotonia and anemia in about a third of all cases. Therefore, coagulation of the umbilical cord appears to be the safest technique (O'Donoghue et al. 2008; Rossi and D'Addario 2009).

In case of fatal malformation, selective termination should depend on the impact of the malformation. For example, 50% of all fetuses with anencephaly develop polyhydramnios leading to preterm birth and endangering the other twin. Retrospective analysis and literature show that in dichorionic twins the best management may be to wait and perform an amniodrainage and feticide only in case of polyhydramnios.

References

Antsaklis A, Souka AP et al (2002) Second-trimester amniocentesis vs. chorionic villus sampling for prenatal diagnosis in multiple gestations. Ultrasound Obstet Gynecol 20(5):476–81

Baldwin VJ (1994) Anomalous development of twins. In: Baldwin VJ (ed) Pathology of multiple pregnancy. Springer, New York, pp 169–197

Benirschke K, des Roches Harper V (1977) The acardiac anomaly. Teratology 15(3):311–6

Berghella V (2009) Novel developments on cervical length screening and progesterone for preventing preterm birth. BJOG 116(2):182–7

Berghella V, Ness A et al (2005) Cervical sonography in women with symptoms of preterm labor. Obstet Gynecol Clin North Am 32(3):383–96

Bieber FR, Nance WE et al (1981) Genetic studies of an acardiac monster: evidence of polar body twinning in man. Science 213(4509):775–7

Caritis SN, Rouse DJ et al (2009) Prevention of preterm birth in triplets using 17 alpha-hydroxyprogesterone caproate: a randomized controlled trial. Obstet Gynecol 113(2Pt1):285–92

DeFalco LM, Sciscione AC et al (2006) Inpatient versus outpatient management of monoamniotic twins and outcomes. Am J Perinatol 23(4):205–11

Derom R, Orlebeke J et al (1995) The epidemiology of multiple births in Europe. In: Keith LG, Papiernik E, Keith DM, Luke B (eds) Multiple pregnancy. Parthenon, Lancaster, pp 145–162

Diehl W, Hecher K (2007) Selective cord coagulation in acardiac twins. Semin Fetal Neonatal Med 12(6):458–63

Durand-Reville M, Schumacker-Blay C et al (2005) Monochorial monoamniotic twin pregnancies: targeted surveillance reduces the risks of cord entanglement. Eur J Obstet Gynecol Reprod Biol 119(1):130–1

Evans MI, Britt DW (2008) Fetal reduction 2008. Curr Opin Obstet Gynecol 20(4):386–93

Evans MI, Dommergues M et al (1996) International, collaborative experience of 1789 patients having multifetal pregnancy reduction: a plateauing of risks and outcomes. J Soc Gynecol Investig 3(1):23–6

Ezra Y, Shveiky D et al (2005) Intensive management and early delivery reduce antenatal mortality in monoamniotic twin pregnancies. Acta Obstet Gynecol Scand 84(5):432–5

Fisk NM, Ware M et al (1996) Molecular genetic etiology of twin reversed arterial perfusion sequence. Am J Obstet Gynecol 174(3):891–4

Fonseca EB, Celik E et al (2007) Progesterone and the risk of preterm birth among women with a short cervix. N Engl J Med 357(5):462–9

Garite TJ, Clark RH et al (2004) Twins and triplets: the effect of plurality and growth on neonatal outcome compared with singleton infants. Am J Obstet Gynecol 191(3):700–7

Gibson JY, D'Cruz CA et al (1986) Acardiac anomaly: review of the subject with case report and emphasis on practical sonography. J Clin Ultrasound 14(7):541–5

Gratacos E, Lewi L et al (2007) A classification system for selective intrauterine growth restriction in monochorionic pregnancies according toumbilical artery Doppler flow in the smaller twin. Ultrasound Obstet Gynecol 30(1):28–34

Hack KE, Derks JB et al (2008) Increased perinatal mortality and morbidity in monochorionic versus dichorionic twin pregnancies: clinical implications of a largeDutch cohort study. BJOG 115(1):58–67

Heyborne KD, Porreco RP et al (2005) Improved perinatal survival of monoamniotic twins with intensive inpatient monitoring. Am J Obstet Gynecol 192(1):96–101

Kalish RB, Gupta M et al (2004) Clinical significance of first trimester crown-rump length disparity in dichorionic twin gestations. Am J Obstet Gynecol 191(4):1437–40

Kiely JL (1990) The epidemiology of perinatal mortality in multiple births. Bull NY Acad Med 66(6):618–37

Liu S, Benirschke K et al (1992) Intrauterine death in multiple gestation. Acta Genet Med Gemellol (Roma) 41(1):5–26

Middeldorp JM, Lopriore E et al (2007) Twin-to-twin transfusion syndrome after 26 weeks of gestation: is there a role for fetoscopic laser surgery? BJOG 114(6):694–8

Moore TR, Gale S et al (1990) Perinatal outcome of forty-nine pregnancies complicated by acardiac twinning. Am J Obstet Gynecol 163(3):907–12

Myles TD, Espinoza R et al (1997) Preterm premature rupture of membranes: comparison between twin and singleton gestations. J Matern Fetal Med 6(3):159–63

O'Donoghue K, Barigye O et al (2008) Interstitial laser therapy for fetal reduction in monochorionic multiple pregnancy: loss rate and association with aplasia cutis congenita. Prenat Diagn 28(6):535–43

O'Donoghue K, Rutherford MA et al (2009) Transfusional fetal complications after single intrauterine death in monochorionic multiple pregnancy are reduced but not prevented by vascular occlusion. BJOG 116(6):804–12

Ong SS, Zamora J et al (2006) Prognosis for the co-twin following single-twin death: a systematic review. BJOG 113(9):992–8

Pasquini L, Wimalasundera RC et al (2006) High perinatal survival in monoamniotic twins managed by prophylactic sulindac, intensiveultrasound surveillance, and Cesarean delivery at 32weeks' gestation. Ultrasound Obstet Gynecol 28(5):681–7

Petersen BL, Broholm H et al (2001) Acardiac twin with preserved brain. Fetal Diagn Ther 16(4):231–3

Pretorius DH, Leopold GR et al (1988) Acardiac twin. Report of Doppler sonography. J Ultrasound Med 7(7):413–6

Quarello E, Stirnemann J et al (2008) Outcome of anaemic monochorionic single survivors following early intrauterine rescue transfusion in cases of feto-fetal transfusion syndrome. BJOG 115(5):595–601

Quintero R, Munoz H et al (1995) Fetal endoscopic surgery in a case of twin pregnancy complicated by reversed arterial perfusion sequence (TRAP sequence). Rev Chil Obstet Ginecol 60(2):112–6, discussion116-7

Quintero RA, Morales WJ et al (1999) Staging of twin-twin transfusion syndrome. J Perinatol 19(8Pt1):550–5

Robyr R, Yamamoto M et al (2005) Selective feticide in complicated monochorionic twin pregnancies using ultrasound-guided bipolar cord coagulation. BJOG 112(10):1344–8

Rossi AC, D'Addario V (2009) Umbilical cord occlusion for selective feticide in complicated monochorionic twins: a systematic review of literature. Am J Obstet Gynecol 200(2):123–9

Salomon LJ, Ville Y (2005) First-trimester crown-rump-length (CRL) discrepancy: much ado about nothing? Am J Obstet Gynecol 193(2):592–3, author reply 593-4

Savvidou MD, Karanastasi E et al (2001) Twin chorionicity and pre-eclampsia. Ultrasound Obstet Gynecol 18(3):228–31

Sebire NJ, Noble PL et al (1996a) Fetal karyotyping in twin pregnancies: selection of technique by measurement of fetal nuchal translucency. Br J Obstet Gynaecol 103(9):887–90

Sebire NJ, Snijders RJ et al (1996b) Screening for trisomy21in twin pregnancies by maternal age and fetal nuchal translucency thickness at10-14 weeks of gestation. Br J Obstet Gynaecol 103(10):999–1003

Sebire NJ, D'Ercole C et al (1997a) Dichorionic twins discordant for intrauterine growth retardation. Arch Dis Child Fetal Neonatal Ed 77(3):F235–6

Sebire NJ, Snijders RJ et al (1997b) The hidden mortality of monochorionic twin pregnancies. Br J Obstet Gynaecol 104(10):1203–7

Sebire NJ, D'Ercole C et al (1998) Intertwin disparity in fetal size in monochorionic and dichorionic pregnancies. Obstet Gynecol 91(1):82–5

Sebire NJ, Souka A et al (2000) First trimester diagnosis of monoamniotic twin pregnancies. Ultrasound Obstet Gynecol 16(3):223–5

Senat MV, Loizeau S et al (2003) The value of middle cerebral artery peak systolic velocity in the diagnosis of fetal anemia after intrauterine death of one monochorionic twin. Am J Obstet Gynecol 189(5):1320–4

Senat MV, Deprest J et al (2004) Endoscopic laser surgery versus serial amnioreduction for severe twin-to-twin transfusion syndrome. N Engl J Med 351(2):136–44

Sepulveda WH, Quiroz VH et al (1993) Prenatalultrasonographic diagnosis of acardiac twin. J Perinat Med 21(3):241–6

Sepulveda W, Bower S et al (1995) Ablation of acardiac twin by alcohol injection into the intra-abdominalumbilical artery. Obstet Gynecol 86(4 Pt2):680–1

Sogaard K, Skibsted L et al (1999) Acardiac twins: pathophysiology, diagnosis, outcome and treatment. Six cases and review of the literature. Fetal Diagn Ther 14(1):53–9

Spencer K (2000) Screening for trisomy21in twin pregnancies in the first trimesterusing free beta-hCG and PAPP-A, combined with fetal nuchal translucency thickness. Prenat Diagn 20(2):91–5

Sutcliffe AG, Sebire NJ et al (2001) Outcome for children born after inutero laser ablation therapy for severe twin-to-twin transfusion syndrome. BJOG 108(12):1246–50

Tita AT, Rouse DJ (2009) Progesterone for preterm birth prevention: an evolving intervention. Am J Obstet Gynecol 200(3):219–24

To MS, Fonseca EB et al (2006) Maternal characteristics and cervical length in the prediction of spontaneous early preterm delivery in twins. Am J Obstet Gynecol 194(5):1360–5

Van Allen MI, Smith DW et al (1983) Twin reversed arterial perfusion (TRAP) sequence: a study of14 twin pregnancies with acardius. Semin Perinatol 7(4):285–93

Weisz B, Pandya P et al (2005) Scanning for chorionicity: comparison between sonographers and perinatologists. Prenat Diagn 25(9):835–8

Wennerholm UB, Holm B et al (1997) Fetal fibronectin, endotoxin, bacterial vaginosis and cervical length as predictors of preterm birth and neonatal morbidity in twin pregnancies. Br J Obstet Gynaecol 104(12):1398–404

Yamamoto M, Ville Y (2005) Twin-to-twin transfusion syndrome: management options and outcomes. Clin Obstet Gynecol 48(4):973–80

Fetal/Perinatal Autopsy and MRI: Synthesis or Alternative?

Gabriele Amann

Contents

Abstract

› A complete fetal/perinatal autopsy includes external examination, dissection and examination of internal organs with consecutive histological sampling, microbiological and virological studies as well as the use of sophisticated techniques for cytogenetic and metabolic laboratory investigation. Additional post-mortem X-ray is essential in cases of skeletal abnormalities. Sufficient clinical information and specification of clinical questions is especially important in cases where macroscopic performance may be limited due to small size and/or autolysis. Apart from the most obvious, namely to explain causes and mechanisms of death and disease, the still undisputed manifold benefits obtained from an autopsy in case of fetal perinatal and neonatal death include assurance and improvement of medical quality as well as teaching and research. However, a worldwide decline in autopsy rates over the past decades resulted in a drop of fetal/perinatal autopsies below the level of 75%, which is considered the minimal requirement for quality assurance. Since difficulties in obtaining parenteral consent for a complete autopsy was felt to represent a major reason for this decline, post-mortem MRI was brought up as a possible alternative method, as part of the concept of so called less/minimally invasive autopsies. Systematic and evidence based reviews of studies comparing post-mortem MRI with conventional autopsies however showed that diagnostic accuracy of this method is still insufficient to replace autopsies. Among the reasons for the decline in autopsy rates,

G. Amann
Department of Pathology Medical University of Vienna
e-mail: gabriele.amann@meduniwien.ac.at

D. Prayer (ed.), *Fetal MRI*, Medical Radiology,
DOI: 10.1007/174_2010_70, © Springer-Verlag Berlin Heidelberg 2011

misconceptions about autopsies by parents and clinicians are mentioned in the literature. Rehabilitation of the autopsy as a tool of surveillance, teaching and research therefore also seems to require reeducation of the professionals, which should be based on better interdisciplinary communication. On the other hand, places with still adequate autopsy rates, like we have in Vienna, should establish large scale studies, to clearly demonstrate the position pm MRI examination has in the performance of a fetal/perinatal autopsy.

1 Introduction

1.1 Viennese Preamble

In the Institute of Clinical Pathology at Vienna Medical University Hospital, pediatric pathology has the status of a subspeciality, similar to hematopathology, uropathology, or bone pathology for example. This means that the respective specialized pathologists are also involved in the institute's routine general pathology diagnosis, whereas gynecopathology has a kind of subdepartmental state with staff pathologists dealing solely with this speciality, which includes reporting curettages and abortions before 14 weeks of gestation. This is in contrast to the use in Anglo-American countries where perinatal and pediatric pathology most often represent independent pathology units/institutes of women's or children's hospitals. Since more than 30 years postmortem examinations of fetuses older than 14 weeks, like all other pediatric autopsies, are performed in the mortuary unit of the Institute of Pathology. This implies that, whether or not an autopsy took place, an essentially cost-free burial will be undertaken by the official Viennese funeral furnishers, employed by the city of Vienna. Thereby the fetuses are buried at a special area of Viennese Central Cemetery, unless the parents or relatives expressed the special wish of a private burial at their own expenses. This represents an exceptional way of postmortal handling of small fetuses with birth weights below 500 g, which is very much appreciated by not only the parents but also psychologists and organizations assisting parents who experienced fetal loss.

Presumptions under which a clinical autopsy has to be performed by pathologists are defined by the Viennese "Krankenanstaltengesetz" § 40 as follows:

> On the corpses of patients who died in a public hospital an autopsy has to be performed when this is necessary for safeguarding of public or scientific interest, in particular because of diagnostic obscurities or because of an operative intervention. The definition of corpse includes not life born fetuses and parts of a corpse. In the absence of such instances, the relatives have to be asked for permission. (Wiener Krankenanstaltengesetz 1987)

Thus, with the exception of autopsy refusal for religious reasons, by law, more weight is placed on clinical than on personal interest. In daily practice, however, the clinicians try to reach a consensus with the parents and, apart from cases with uncertain cause of death, the parent's wish to restrain from autopsy will be respected.

1.2 General Background

In the preface of his textbook on fetal and perinatal pathology, Jonathan Wigglesworth in 1991 put the increasing popular and medical interest in embryonic, fetal, and neonatal well-being in context with recent cultural changes in developed countries (Wigglesworth 1991). In his opinion, the main change is expressed in the prevalence of small families and of older mothers, which leads to high expectations of a successful outcome of each pregnancy. Medical technical advances in obstetric, pre- and perinatal as well as in neonatal medicine not only fortified this interest but also the importance of fetal and perinatal autopsies. It is thus understandable that in contrast to adult autopsies, fetal and perinatal autopsy rates remained higher and remained fairly stable until the early 1990s (Khong 1996b). Nevertheless, a strong decline in autopsy rates during the last two decades has been noted worldwide (Gordijin et al. 2002; Okah 2002; Brodlie et al. 2002; Kumar et al. 2000 Jan; Adappa et al. 2007 Jan). The varying extents to which different countries have been affected can be partially explained by the respective medicolegal backgrounds (Gordijin et al. 2002; Burton & Underwood 2007). Since these drops are of major concern especially in terms of quality assurance, quite some studies, trying to trace possible causes, have been published and reviewed (Cartlidge et al. 1995; Khong

et al. 2001; Burton 2003 Dec; Snowdon et al. 2004 May; Gordijn et al. 2007 May; McDermott 2004 May). Apart from the parents' refusal of an autopsy, one main factor seems to be the attitude of the clinicians towards the necessity of an autopsy. This may be influenced by decreasing knowledge about the procedure, combined with a strong belief in medical technical advances, thereby overestimating the diagnostic quality and sensitivity of pre- and postnatal investigations. In addition to these factors, which mainly are based on misconceptions by parents and medical staff, questionable clinical relevance and delay of autopsy reports as well as poor quality of the autopsy performance are quoted causes.

The still undisputed manifold benefits obtained from an autopsy in case of fetal perinatal and neonatal death can be summarized in three main aspects (Laing 2004; Porter & Keeling 1987; Goldman et al. 1983; Dahms 1986; Lundberg 1983; Putman 2007 Dec) (Fig. 1).

1. The most obvious reason is establishing/defining the cause of death, illness, or maldevelopment (degree and type of deviation from normal development). This information not only is of importance as an aid in genetic counseling and managing future pregnancies, but also in reassuring or refuting parents helping them to cope with their loss. In this respect, negative results in one or the other point, like lack of fetal malformation or lacking evidence of maternal cause for the loss of pregnancy, may at least be equally or even more important for the family.
2. Another very important role fetal/perinatal autopsy plays is that of quality assurance. This not only concerns perinatal management and treatment, but also verification and identification of fetal anomalies diagnosed by prenatal real-time ultrasound or MRI, that may have led to termination of pregnancy. In this context, it seems worthy to note that in 1988 even in centers of prenatal ultrasound examination, 37% of fetuses with correctly diagnosed anomalies were found to have additional defects evidenced by autopsy not diagnosed before birth (Manchester et al. 1988). Even in the time of pre- and postnatal MRI diagnosis, studies reported in the years 2002 and 2004 have shown that in around 30% of cases, perinatal autopsy revealed significant clinical information not evident during life (Gordijin et al. 2002; Boyd et al. 2004). In 2007, Dickinson et al. published a study on 1,012 consecutive pregnancy terminations for fetal abnormalities over a period of 10 years, in 79% of which an autopsy was performed (Dickinson et al. 2007 Dec). For one, they reported that decline in autopsy rates in the given period was significantly higher in cases with fetal karyotypic anomalies (from 93.5% to 31.1%) compared to euploid cases (95–67.5%). In the latter, autopsy confirmed the diagnosis with no additional information in 63.5%. Additional contribution in the remaining 36.5% cases were divided between major (1.1%), significant (15.1%), minor (19.8%) added value, and not confirmed anomaly (0.5%).

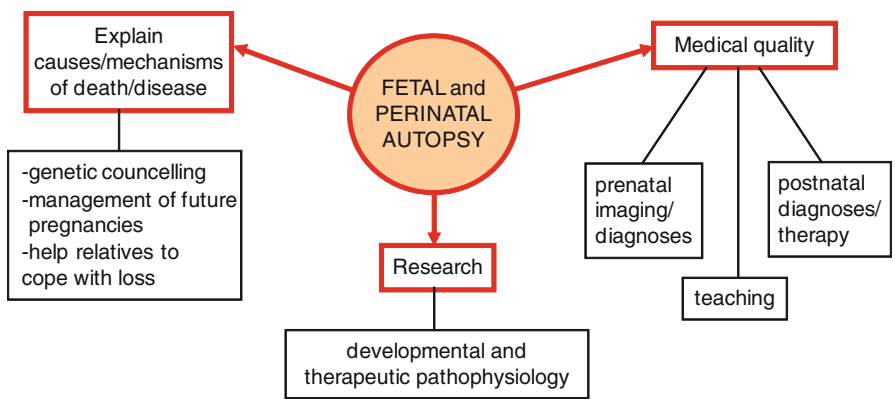

Fig. 1 Main benefits of fetal/perinatal autopsy. At first fetal/perinatal autopsy is important for the family in terms of efficient genetic counseling and optimization of future pregnancies by elucidating causes and mechanisms of illness and disease, which also assists in coping with the loss. These explanations together with autopsy reports, however, play an important role in improving medical quality by correlating postmortal findings with pre- and postnatal clinical diagnoses. Improving medical quality also includes controlling the effects of applied therapy and teaching students as well as medical doctors. Finally, better understanding of developmental and therapeutic pathophysiology is essential to induce further research, thereby promoting advances in modern medicine i.e., therapeutic modalities

3. In contrast to the two aspects discussed so far, which offer direct benefits for the family and the involved medical staff, the third major reason for perinatal postmortem examination may be called altruistic and somehow appears to be less popular nowadays, namely for research and educational purposes (Wigglesworth 1991; Gordijn et al. 2007 May; McDermott 2004 May). This simply results when pathologists, in doing a perinatal postmortem examination, leave the position of an observing reporter by trying to answer the always pending simple question "why" behind the obvious. This path not only leads to a better understanding of human perinatal pathophysiology which requires thorough tissue examination and cannot be fully obtained by creating animal models. It also is the path along which the many advances in perinatal and neonatal management and treatment have been achieved so far.

2 The Fetal/Perinatal Autopsy

2.1 General Remarks

In an ideal case, fetal/perinatal postmortem examination includes microbiological and virological studies as well as the use of sophisticated techniques for cytogenetic and metabolic laboratory investigation: (Khong 1996a; Kapur 2007) (Fig. 2). For this, the umbilical cord, placental blood, and/or pieces of the patient's skin or soft tissue may be used. For the sake of offering enough time to the relatives for leave-taking, at Vienna university hospital, the body will remain at the department of obstetrics for approximately 24 hours after death. At Vienna university hospital, it is the use that the body will be kept at the department of obstetrics for 24 h after death for the sake of offering enough time to the relatives for leave-taking. Therefore, these samples will be obtained by the obstetricians. Before starting a postmortem examination, the pathologist should receive all the clinical information necessary to undertake an efficient autopsy. To guarantee submission of the essential information, it may be useful to create a structured autopsy request form, adapted to the respective local circumstances, and to be filled in as easily as possible. Examples of relevant data are shown in Table 1. Medical records or a written summary of clinical data as well as information on prenatal imaging should be added and special questions should be stated.

Submission of the placenta, the complete umbilical cord, and membranes represents an absolute requirement in postmortem examination in fetal and perinatal death. In quite a number of cases, placental examination not only represents one piece of a puzzle but actually holds the clue to explain the cause of death (Kraus 2003; Roberts & Oliva 2006). Since placental weight (after stripping of the membranes and removing the cord) and length of the cord may represent risk factors to fetal outcome, comments as to their completeness have to be given on the autopsy request form. In case a piece of the cord was used for further diagnostic studies, the length of this piece has to be stated. Otherwise it may be impossible to identify risk factors such as long or short cord. Pieces from at least three different areas of the placenta are taken for histological examination together with samples from macroscopically conspicuous areas and at least three cross-sections of the cord. A roll is usually formed of the stripped membranes, of which slices can be easily cut after fixation in formalin.

2.2 Practical Performance *(Fig. 2)*

Postmortem examination itself starts with a thorough external examination, first judging on the development with respect to the given gestational age, including reporting on minor and major anomalies, preferably also using photodocumentation. The important measurements to document fetal growth, apart from body weight and CH as well as CR length, are the foot length, the circumferences of the head, thorax, and abdomen, with the latter two taken at the level of the mamillae and umbilicus, respectively.

In case of suspected skeletal anomalies, a postmortal X-ray is essential for the diagnosis of bone malformations and dysplasias, respectively (Gronvall & Graem 1989; van der Harten 2001).

Opening of the head and of the body cavities is usually achieved by skin incisions causing as little damage as possible to facilitate reconstruction and body closure at the end of the autopsy. In Vienna, no incisions are done in the face, the anterior and lateral neck, and, if possible, in the extremities. Already at this point it is important to have information on suspected

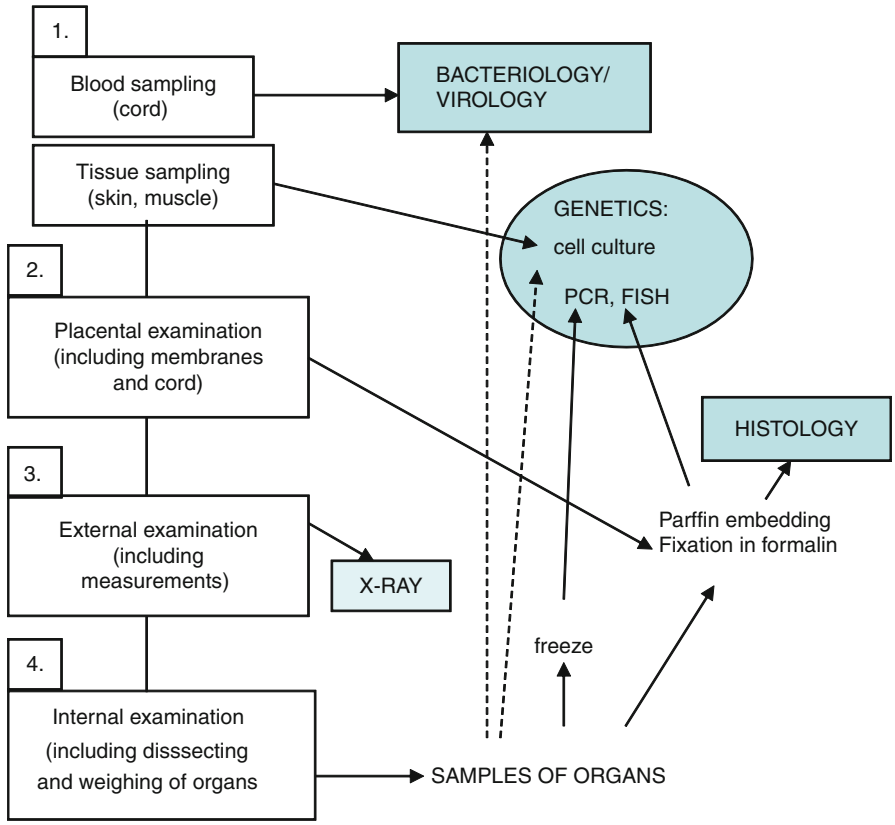

Fig. 2 Components of fetal/perinatal autopsy. Samples of blood and tissue should be obtained immediately after death. They may be used for bacterial, viral, and metabolic analyses, and to establish cell cultures for chromosomal analysis. Submission of the placenta with membranes and umbilical cord is obligatory in fetal autopsy cases. After macroscopical examination, representative pieces are fixed in formalin for further embedding in paraffin and final histological examination. External examination includes taking measurements of body lengths and weight, as well as circumferences of the head, the thorax, and the abdomen. Development has to be judged with relation to the given gestational age. In case of suspected skeletal anomalies and chondrosseous dysplasias, respectively, postmortal X-ray examination is essential for diagnosis. To report minor and major anomalies, additional photodocumentation is especially helpful for later evaluation. This also implies to internal examination and dissection. Sampling of organs should cover all functionally related systems. If necessary, also at this step, fresh pieces may be directly used for viral or genetic analysis, respectively. Especially in the case of suspected single gene defects, freezing of representative tissues is important: Although PCR and FISH analyses can also be done on paraffin-embedded material, frozen samples are more easily and more reliably analyzed by these methods

Table 1 Autopsy request form – essential data

Mother	Pregnancy	Birth	Infant	Placenta
Age	Multiple/single	Spontaneous/induced	Gestational age	Complete? (with membranes)
Underlying disease (hypertension, DM, etc.)	Complications	Duration complications	Time of birth	Umbilical cord (complete – length if not!)
Previous pregnancies			Prenatal interventions (IVF, CVS, etc.)	
			Prenatal investigations (US, MRI, etc.)	
			Postnatal investigations (blood sampling, CT, MRI, etc.)	

anomalies like the Arnold Chiari malformation, since special techniques have to be applied to prove the malposition and malformation of the cerebellar vermis (Fig. 3). An important step is the in situ examination of organs and organ systems, since position and shape of the organs often indicate certain anomalies, which can only be proven/diagnosed when the way of further dissecting and removing organs will be correspondingly adapted. This is especially important in diagnosing cardiovascular malformations. The configuration of the heart, the shape and position of the atrial appendages, and the course of the coronary arteries, i.e., the anterior and posterior ramus interventricularis in most cases indicate certain anomalies to which dissecting of the heart has to be adapted (Fig. 4). In fetal and perinatal autopsy, it is generally preferred to remove the thoracic and abdominal organs in one. This is most helpful in cases of esophageal atresia/esophagotracheal fistulas, and cardiovascular malformations like anomalous pulmonary venous return, where the pulmonary veins may join the caval and/or portal venous systems subdiaphragmatically. Removing the intestine by cutting the large bowel at the rectal level, followed by loosening the colonic mesentery and separating the intestine from the mesentery helps to view the retroperitoneal organs in situ (Fig. 5a). In cases with scoliosis, a section through the affected vertebra in frontal plane is ideal to visualize eventual vertebral anomalies (Fig. 5b). In cases with cystic dilatation of structures of the urogenital tract and/or the intestine, it is useful to fix the sometimes friable dilated parts by injecting formalin before final dissection. This also helps to trace eventually small fistulas, the presence or absence

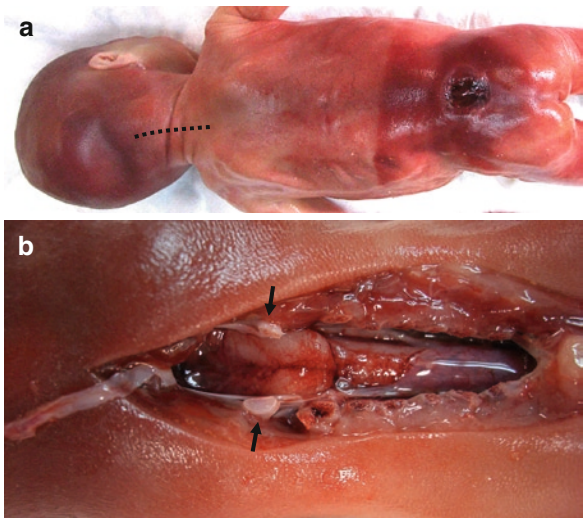

Fig. 3 Dissecting in a case of suspected Arnold Chiari malformation. (**a**) The lumbosacral spina bifida In this 18-week-old fetus may be part of an Arnold Chiari malformation type II. The associated malformation and malposition of the cerebellar vermis can only be proven with the brain and the spinal cord still in situ. Thus, before removing the brain, a short incision (*dotted line*) is made in the dorsal neck area. (**b**) After removal of several cervical arches and part of the atlas bone (*arrows*), the dural sack is opened to visualize the malformation

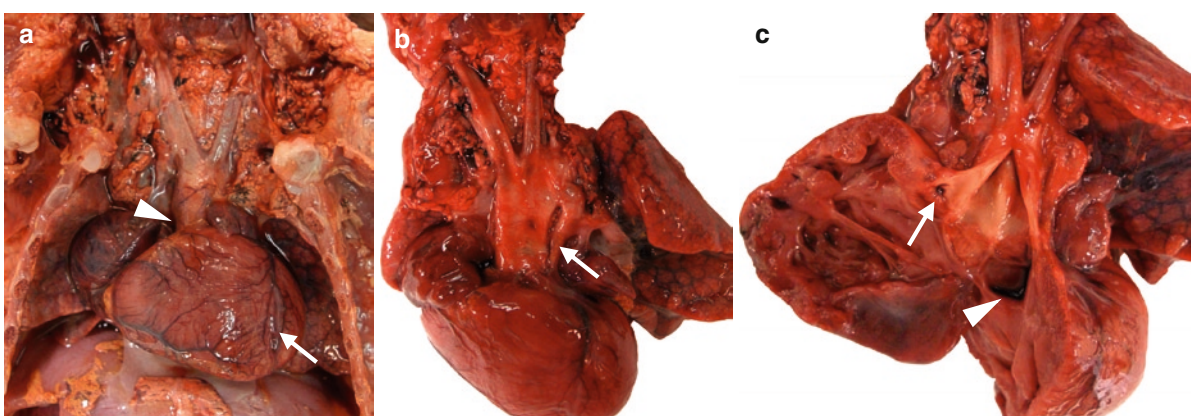

Fig. 4 Dissecting a complex cardiovascular malformation. (**a**) Seen in situ, the heart almost fills the thoracic cavity. The position of the ramus interventricularis anterior (*arrow*) indicates an enlarged right ventricle. At the base of the heart at first only one large vessel is seen, corresponding to the aorta (*arrowhead*). After removal of the thoracic organs, a further dissection in (**b**) a thread-like pulmonary artery (PA) becomes evident (*arrow*), with a slightly widening diameter close to the patent ductus arteriosus (PDA), connecting the PA to the enlarged aorta, the position of which indicates transposition of the great arteries (TGA). (**c**) Opening of the right ventricle proves the aorta (*coronary artery indicated by the arrow*) arising from the right outflow tract and in addition shows a large VSD, The final diagnosis of this complex malformation is d-TGA, pulmonary atresia, PDA, and VSD

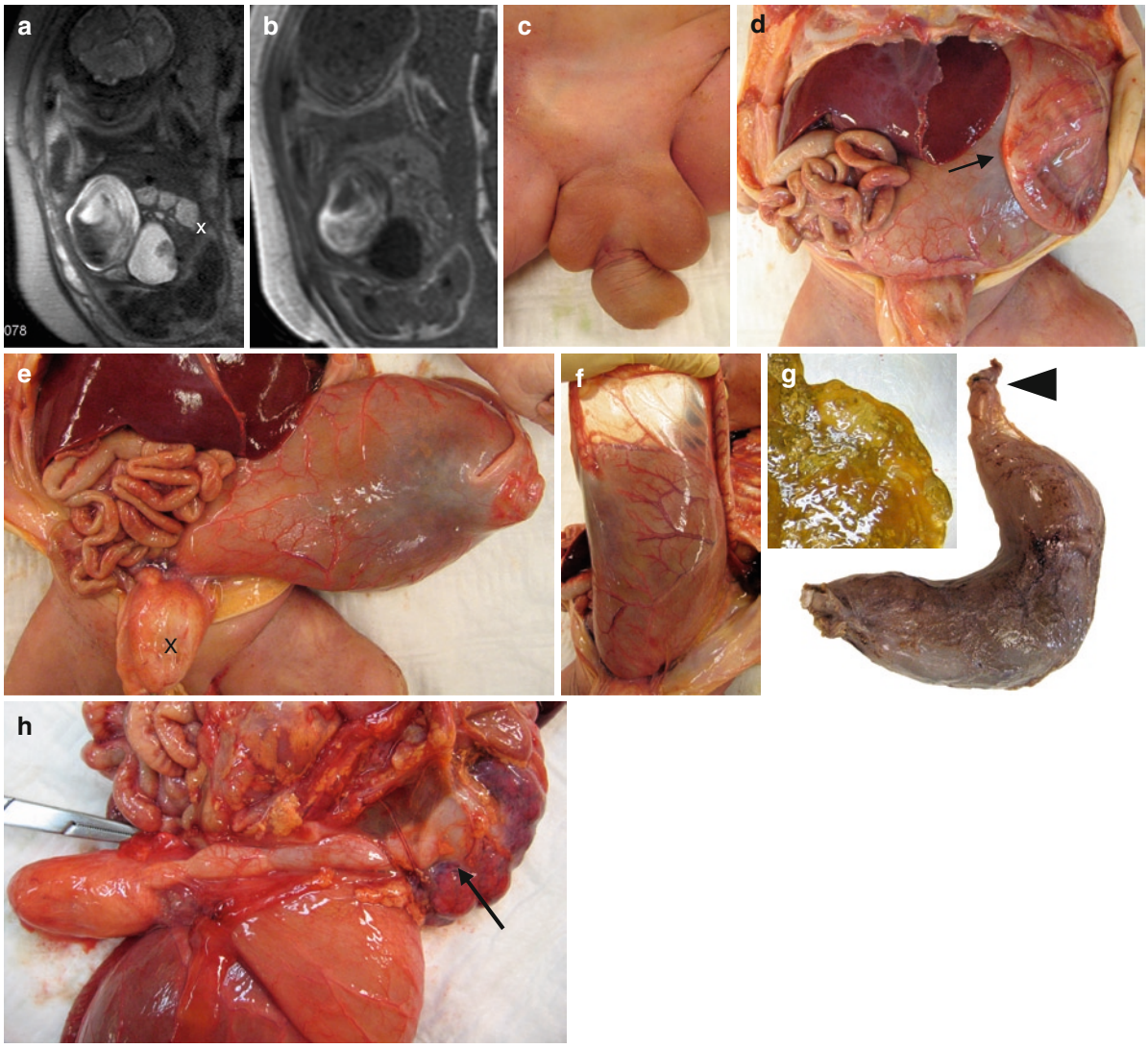

Fig. 5 "Cystic abdominal tumor" caused by cloacal anomaly. In this case, the suspected diagnosis on the autopsy request form was "cystic abdominal tumor," based on prenatal MRI. T2-weighed (**a**) and T1-weighed (**b**) coronal images show a cystic structure in the right upper abdomen with hyperintense contrast on both images, an abnormal hypointense T1-weighed signal in the colon, appearing hypointense in T2 (x). The T2-weighed hyperintense and T1-weighed hypointense urinary bladder is seen in the midline. No rectum was visible. (**c**) Dysplastic external genitalia with a bifid scrotum accompanying an imperforate anus suggest a cloacal anomaly. (**d**) A large cystic structure displaces the liver and most parts of the intestine. At its right upper part a flat colonic segment forms a cap-like covering (arrow) in questionable continuity with a thin colon. (**e**) After mobilization of the cystic structure, no continuity with the normal-sized bladder (x) was evident. (**f**) Lifted up, an extremely attenuated colonic wall becomes obvious at the upper pole of the cystic dilatation. The content (*insert in* (**g**)) is bile stained, but quite liquid, suggesting a dilution by urine through a persistent connection between rectum and bladder. However, formalin injection into the cystic rectum failed to prove an open fistula. Also, preparation and removal of the formalin-fixed dilated segment shown in (**g**) (*ligated and cut oral colonic end indicated by arrowhead*) did not reveal continuity, suggesting obliteration of a rectovesical fistula in this case of persistent cloaca. (**h**) Hydroureter and hydronephrosis (*arrow*), often accompanying cloacal anomalies, is present at the right side

of which may be difficult to prove even histologically (Fig. 6).

Most textbooks on fetal, perinatal, and pediatric pathology provide detailed information on the best way macroscopic examination and dissection could be performed (Siebert 2007; Macpherson & Valdes-Dapena 1998). However, as a rule it can be stated that any way of examination and dissection is right as long as no anomaly will be missed or destroyed. Optimizing the dissection in an individual case very often

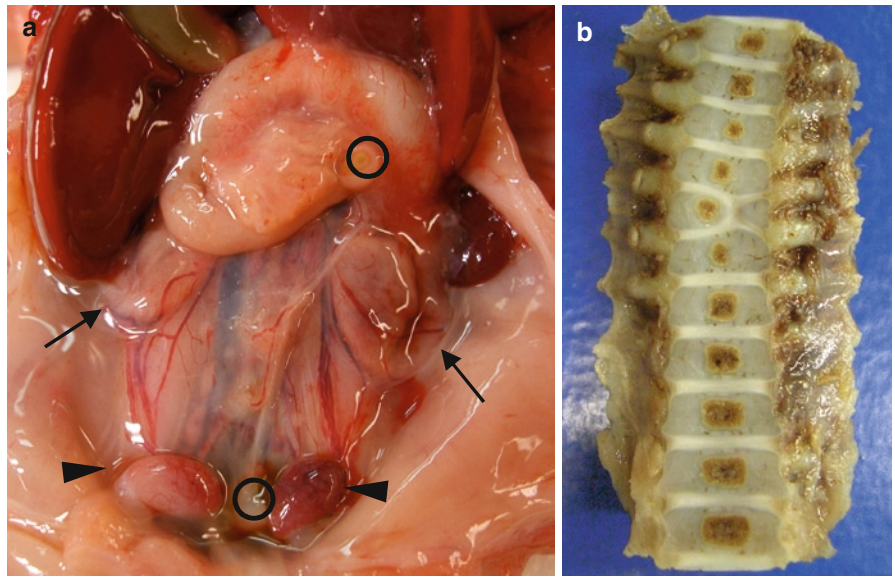

Fig. 6 Viewing the retroperitoneum and the vertebra. (**a**) After removal of the intestine (*cuts at rectal and duodenal level indicated by rings*), the retroperitoneum can be viewed, in this case demonstrating bilateral renal agenesis with flat adrenal glands (*arrows*). Undescended testes are also evident (*arrowheads*). (**b**) In another case, a frontal cut through a thoracolumbal segment of a vertebra demonstrates a hemivertebra, resulting in scoliosis

challenges manual skills and creativity of the involved pathologist, especially when dealing with complex situations like body stalk malformation or conjoined twinning. In the background of the timely limitation inherent to an autopsy performance, photodocumentation of critical and/or questionable/unclear findings is extremely important for later reevaluation and discussions with clinicians and/or geneticists.

Representative pieces of each organ should be taken for histological examination (Kapur 2007). Thereby, it is important that these specimens cover all functionally related organ systems in order to be able to solve questions that may have not been obvious at the time of macroscopic examination (e.g., special types of immunodeficiency). In addition, freezing of representative organ samples is useful in cases of suspected metabolic disease. Histological examination not only provides information on development and gestational age and may indicate a specific type of genetic disorder (Fig. 7), but is the most important assistant in sorting out timely relation of events, which is of profound importance in cases of peri- and neonatal death (Bendon 2004). Correctly interpreted, reading of histological slides may equal a written story of the infant's pre- and postnatal life. The histomorphology of the thymus and adrenal glands, respectively, reflects the quality and duration of stress. Especially in the context of prematurity and its consequences, histological examination is of crucial importance: in the background of multimorbidity, very often no single major cause of death can be identified. Histological examination, however, may point out the butterfly wing that pushed a highly sensitive equilibrium system over the edge. On the other hand, pathohistology may help to explain the influence certain malformations or anomalies have on a functionally associated organ when this is still developing. One example for this is the relation of urinary tract obstruction and primary or secondary (obstructive) renal dysplasia adding important information to human renal developmental research that are difficult to obtain from animal models or cell cultures. It may be of note that even in cases with advanced maceration/autolysis, infectious agents like toxoplasmosis and CMV can still be identified microscopically (Fig. 8).

2.3 Limitations and Problems of Fetal/Perinatal Autopsies

Most limitations of fetal/perinatal autopsies relate to small size and/or state of preservation, i.e., autolysis and maceration, the latter resulting from a longer time of postmortal intrauterine retention. The best way to minimize postmortal lyses or drying out is to keep the fetuses

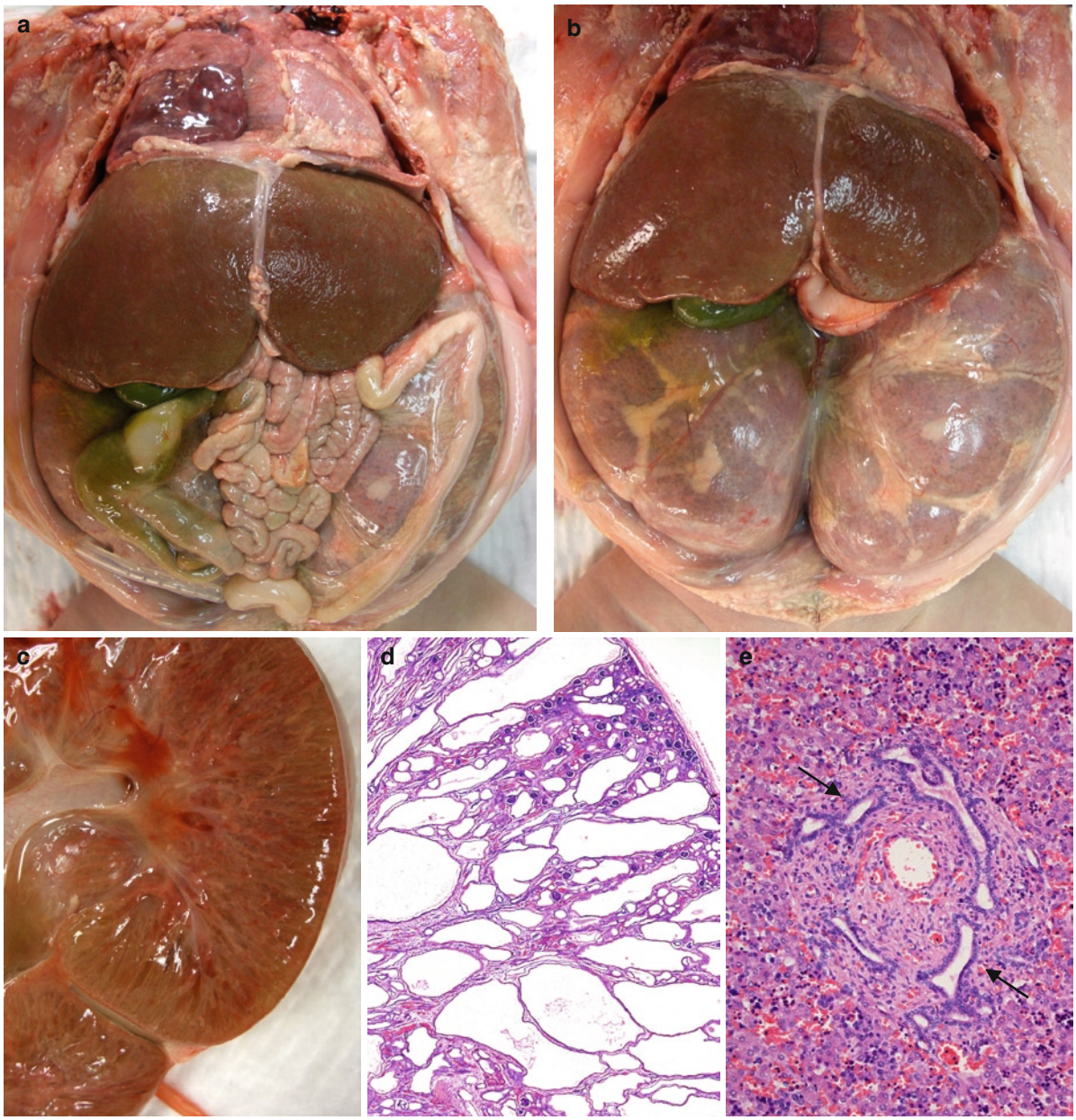

Fig. 7 A case of polycystic kidney disease. (**a**) The contents of an extremely distended abdomen are seen, compressing the thoracic organs caused by bulging kidneys, the symmetrical enlargement of which becomes more obvious after removal of the intestine (**b**). The cut surface (**c**) shows a radial spongy structure corresponding to longitudinal cystic dilatations of renal tubules seen in low magnification of the hematoxylin and eosin (H&E) stained section in (**d**). This feature is fairly typical for polycystic kidney disease (ARPKD). In this case, the surface of the firm liver in (**a**) and (**b**) suggests fibrosis. The H&E stained section, depicted in higher magnification in (**e**), shows bile duct anomalies presenting with irregularly shaped proliferations (*arrows*) in fibrotically widened portal tracts. This is in keeping with congenital hepatic fibrosis, often accompanying ARPKD, which presents a disease with a wide range of phenotypic expressions

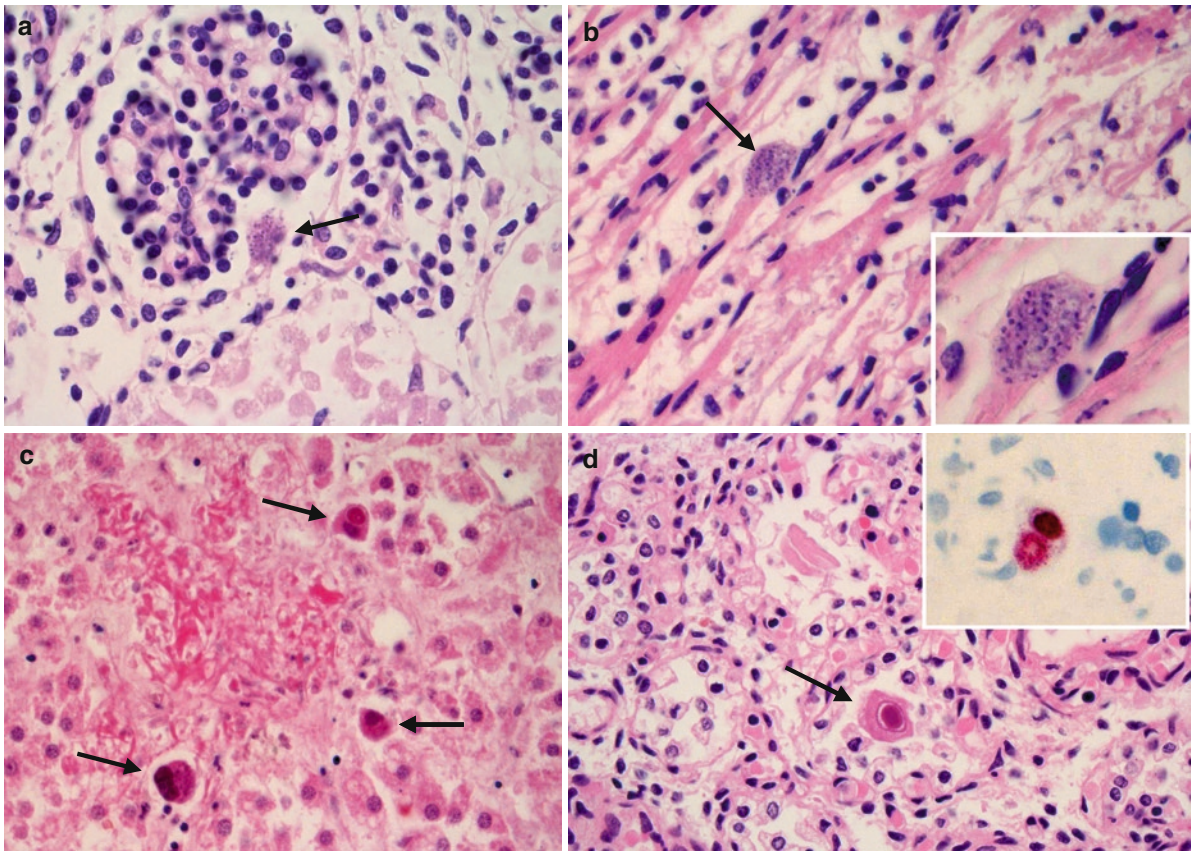

Fig. 8 Histology of specific infections in macerated fetuses. The histologic pictures show bad tissue preservation of the organs, originating from macerated fetuses, who were submitted for autopsy without any known clinical data. In one fetus (**a** and **b**), toxoplasmosis could be diagnosed by identification of the cyst (*arrows and insert in* **b**) in the kidney (**a**) and the heart (**b**) The other fetus (**c** and **d**) presented with hydrops. Due to maceration, no blood could be sampled for bacterial/viral investigations. Cells with viral inclusions (*arrows*) corresponding to CMV were found in histologic sections of many organs. (**c**) Demonstrates three cells with nuclear and cytoplasmic inclusions in the adrenal gland, although nuclear staining has almost vanished, due to maceration. (**d**) A characteristic nuclear inclusion is evident in this lung section, which is slightly better preserved. Immunohistochemical staining with CMV-antibody proved the type of infection (*insert*)

cool at about 4 C and to cover them with foil. Freezing at lower temperatures, however, must be avoided, because of the adverse effect consecutive thawing during the autopsy has on tissue preservation. Quite commonly, in medically induced abortions, there may be a delay of several days between fetal death and birth. With advanced lyses, the organs turn soft and friable, which makes them difficult to handle. In such situations, short formalin fixation for several hours is helpful, especially in dissecting the heart and vessels when cardiovascular malformations are suspected. Also in autolyzed fetuses, histological examination of the organs can no longer be done in a reliable way. Especially in a status with very advanced autolysis close to mummification, minor anomalies like facial anomalies may be impossible to recognize. Also smaller, skin-covered defects of the dorsal spine may be very hard to identify (Fig. 9). Such anomalies, if known, should therefore be indicated at the autopsy request form.

In addition to such secondarily imposed limitations there are other, primary ones that could be called "inherent to certain organ systems." The first one to be mentioned here is the skeletal system, where in cases of doubt about an underlying skeletal dysplasia, a postmortem X-ray examination represents the most important part of diagnosis (Fig. 10) (Olsen 2006 Feb). The second most important system with inherent limitations is the CNS. Not only are the developing structures of the incompletely myelinated CNS very friable per se and the first to be affected by maceration, they are also in association with fetocide for which potassium chloride is most commonly used (Carroll et al. 2000). Also, in

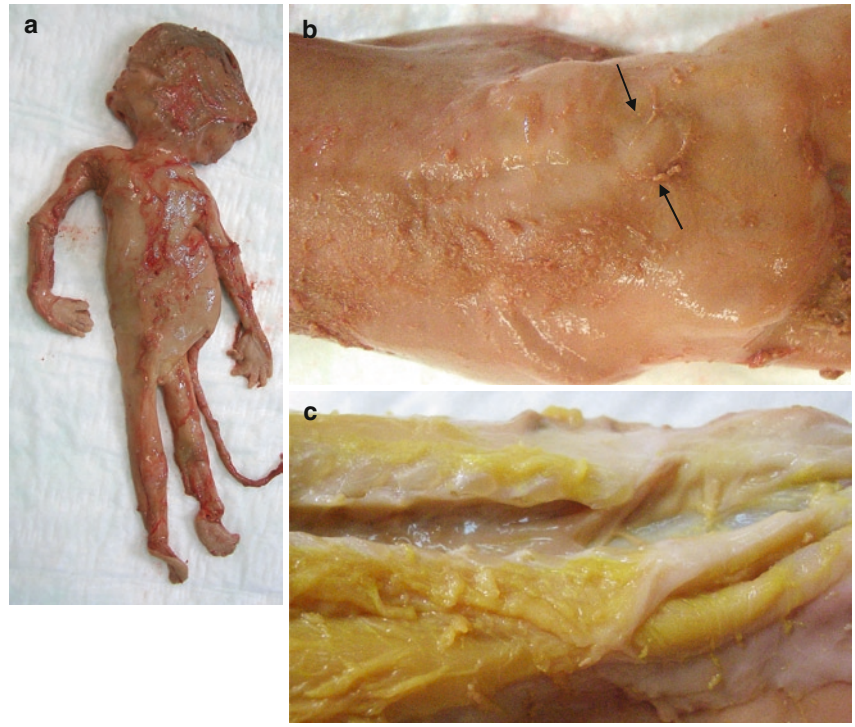

Fig. 9 Spina bifida four months after death. (**a**) This fetus died 4 months before birth. Severe intrauterine maceration, close to mummification, has led to massive alterations in shape. (**b**) Only a small bump in the dorsal lumbosacral region (*arrows*) indicates the spina bifida, which could be visualized (*arrow in* **c**) after appropriate dissection and removal of the vertebral arches. Even with adequate information in the autopsy request form it may be very difficult to identify malformations in severely macerated fetuses

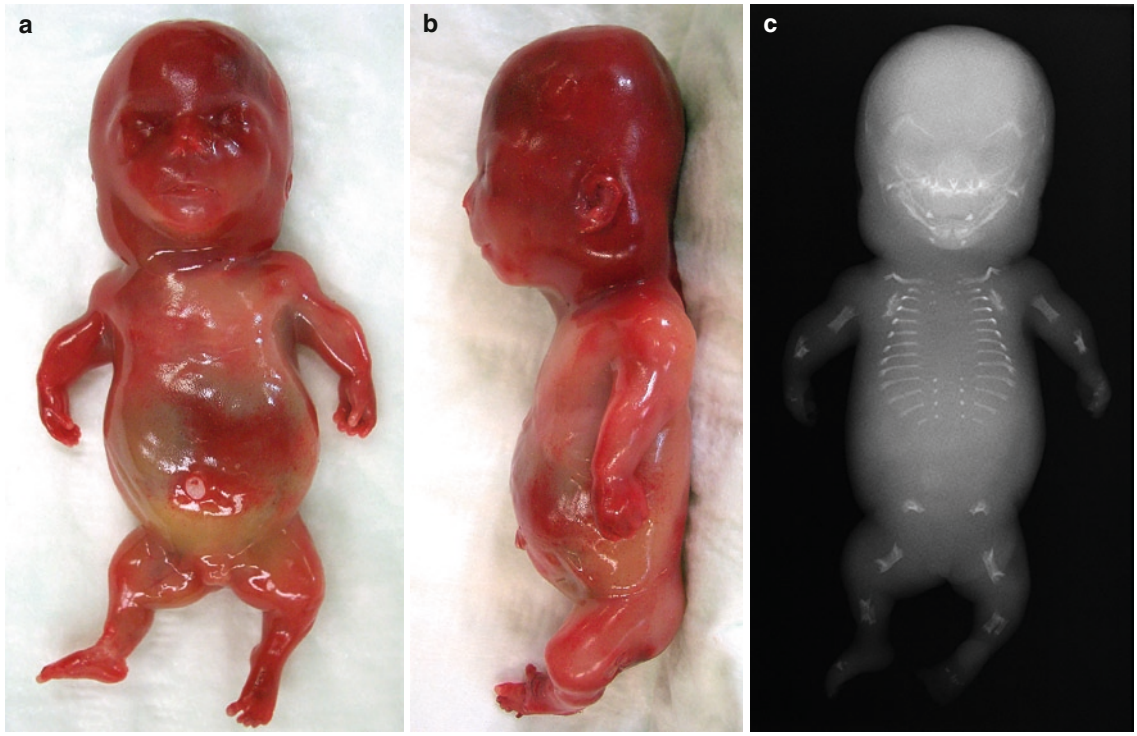

Fig. 10 A case of achondrogenesis. In this case, prenatally diagnosed skeletal dysplasia led to termination of pregnancy at 17 weeks. (**a, b**) Extremely short extremities are obvious, accompanied by a small thorax and a prominent abdomen. There also is evidence of slight generalized subcutaneous edema and hygroma. The small nose shows anteverted nostrils. To further distinguish between the type of achondrogenesis, suggested by these findings, an X-ray was performed. (**c**) Apart from absence of ossification in the ischia, pubis, and vertebral bodies, accompanying extremely short limb bones with spike-like metaphyseal spurs, irregularities of the short ribs, suggesting fractures, and lack of cranial bone ossification are indicative of achondrogenesis type IA (Houston-Harris)

the diagnosis of many CNS anomalies, the spatial relation to adjacent structures is important and may be destroyed by dissection or/and removal of the brain along with the medulla. In such situations, a postmortem MRI investigation can be of diagnostic help. Another problem arises when more extensive histological examination of the brain is needed for diagnosis, since this requires about 3 weeks of formalin fixation before adequately large slices can be cut and processed.

3 MRI and Fetal/Perinatal Autopsy

3.1 Background

Time-related statistics are ideal to point out certain trends or tendencies, and by identifying possibly correlating events not only help to explain these tendencies but also to disclose modalities to change them. In the background of a general complaint about decline of autopsy rates, it seems useful at this stage to look at the dynamics of fetal/perinatal autopsies performed in Vienna Medical University Hospital in the years from 1990 to 2009 (Fig. 11). Strictly viewed, the perinatal period only includes the first week of postnatal life. With technical advances in perinatal medicine, it appears reasonable that adding 1 week will more reliably cover deaths related to problems of intrauterine life, including anomalies, and of birth. Therefore, the data in Fig. 8 include all cases of fetal/perinatal death from 14 weeks of gestation to a postnatal age of 14 days. The graph starts with an autopsy rate of 98% in 1990 and shows a temporary drop between 1995 (97%) and 2000 (91%), which recovered to 93% in 2005. However, after 2005 a decline of 12% down to 81% occurred within 2 years, which in 2008 and 2009 kind of stabilized at the 80% level. The drop between 1995 and 2000 most likely can be explained consequences of the so-called organ retention scandal of Alder Hey, Liverpool, in the late 1990s, hitting Vienna with kind of an ebbing wave (Dewar & Boddington 2004 Oct). In this time, drops down to around 50% have been reported in the UK (Brodlie et al. 2002). The more severe decline of autopsy rates between 2005 and 2007 weighs more, because it already comes quite

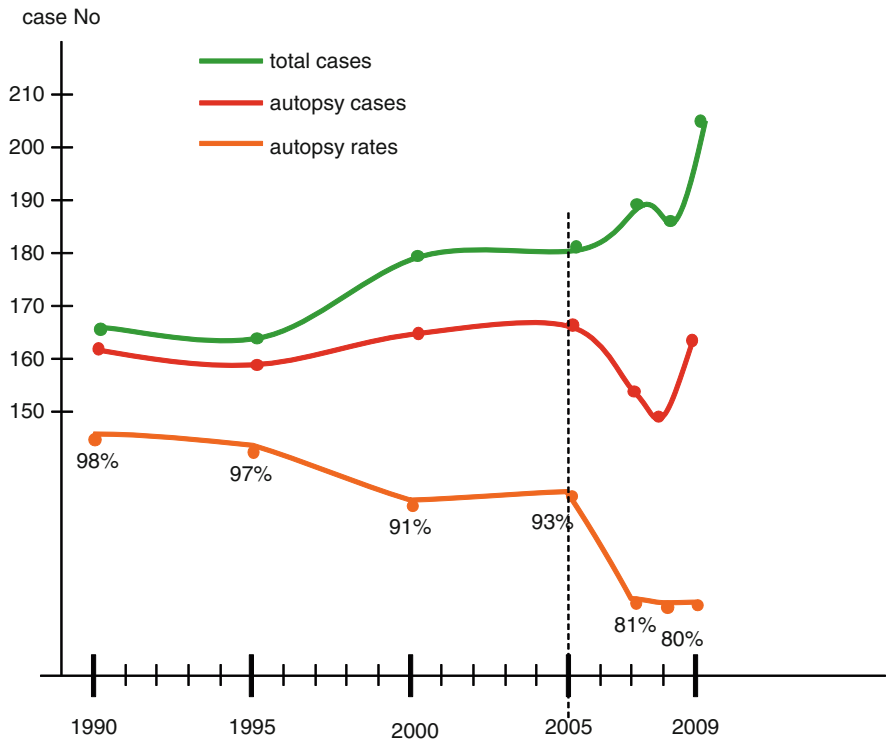

Fig. 11 Autopsy rates at Vienna University Hospital. Autopsy rates of fetuses older than 14 weeks and infants younger than 15 days at Vienna University Hospital show a decline of app. 25% within the last 20 years. The drop at 2000 with a slight recovery till 2005 may represent mitigated consequences of the so-called organ retention scandal at Alderhey Hospital in the late 1990s. The more severe decline of about 12% in the last 4 years possibly not by chance, with a slight timely transposition, coincidences with intensification of publications on the use of postmortem MRI starting around 2003

close to 75%, which has been recommended as the minimum level for quality control by a joint working party of the Royal College of Obstetricians and Gynaecologists and Royal College of Pathologists (Joint Working Party of Royal College of Obstetricians and Gynaecologists and Royal College of Pathologists 1988). This therefore needs to be analyzed more closely with respect to the possibly underlying mechanisms and reasons, if a further decline has to be avoided. Although at a much higher level, this decline essentially parallels the general trend. It therefore is quite likely that the causes already mentioned in the introduction also apply to the situation in Vienna (Cartlidge et al. 1995; Khong et al. 2001; Burton 2003 Dec; Snowdon et al. 2004 May; Gordijn et al. 2007 May; McDermott 2004 May). To some extent, the decline between 2005 and 2007 may represent a secondary consequence of what happened at Alder Hey, relating to the increasing use of postmortem MRI: In the legal background of autopsies only permitted with parenteral consent, the tremendous drop in autopsy rates in the UK urged a search for alternative methods to overcome this problem. Postmortem MRI examination obviously presented itself as the most appropriate tool. The first study of 6 cases (4 fetuses and neonates and 2 adults) suggesting postmortem MRI examination as possible alternative or adjunct to autopsies was published 1990 (Ros et al. 1990), followed by two larger studies on 20 and 26 cases reported by Brookes (1996) (Brookes et al. 1996) and Woodword (1997) (Woodward et al. 1997 Jan), respectively, in which whole body examinations were compared. Following recommendations of the Chief Medical Officer of the UK to assess less invasive ways of postmortem examination, more studies comparing postmortem MRI examination with autopsy results were published in shorter time intervals. It may be not by chance that after the publication of two reports by the Chief Medical Officer of the UK in 2000 and 2001 (Huisman et al. 2002 Jan-Feb; Alderliesten et al. 2003 Apr), wherein the assessment of less invasive ways of postmortem examination was recommended, more studies comparing postmortem MRI examination with autopsy results were published in shorter time intervals (Huisman et al. 2002 Jan-Feb; Alderliesten et al. 2003 Apr; Griffiths et al. 2003 Jan). This was already overlapping with publications discussing the usefulness of MRI as an adjunct or replacement of autopsy. (Whitby et al. 2005 Oct; Griffiths et al. 2005; Huisman 2004 Aug; Brookes & Hagmann 2006 Dec; Whitby et al. 2006 Feb) Larger series with more than 30 cases, however, were restricted to the brain and the spine, respectively, with the largest retrospective study on 100 brains reported in 2008 by Cohen (Cohen et al. 2008 Jan–Feb). The largest prospective study on the whole body included 30 cases and was published in 2006 (Breeze) (Breeze et al. 2006 Dec). This study reported 87.5% sensitivity and 95.5% specificity for detecting brain malformations, 62.5% sensitivity and 87% specificity for lung lesions, but poor utility for other organs. Problems that may arise in postmortem MRI examinations essentially parallel the limitations of conventional autopsy, namely small size of the fetus and autolysis. Part of the former can be overcome by the use of high-field MRI at 9.4 T (Thayyil et al. 2009). In a most recent systematic review of the comparison of postmortem MRI with conventional autopsy in fetuses, children and adults Thayyil found the published literature being limited to small and poorly designed studies (Thayyil et al. 2010 Jul). It was concluded that postmortem MRI still provides insufficient diagnostic accuracy to be used as an alternative for conventional autopsy.

3.2 Minimally/Less-Invasive Autopsy

In the background of autopsy rates of around only 50% in the UK and a study published by Berry (Berry et al. 1997), stating that noninvasive examinations would be sufficient for diagnosis in 40% of perinatal deaths, the concept of so-called minimally and less invasive autopsy was pushed forward (Whitby 2009; Sebire 2006 Dec). Although sometimes used synonymously, minimally invasive autopsy is defined as using X-ray, CT, and MR imaging with the disadvantage of lacking histological examination. The latter could be included in so-called less-invasive autopsies where percutaneous needle core and/or endoscopic biopsies are taken from the areas of interest as identified by MRI. In a review published in 2010, an evidence-based approach to less-invasive autopsy summarized the main studies on postmortem MRI in fetuses, newborns, and children (Thayyil 2010). For one, it was concluded that postmortem examination of the brain has proven sufficiently effective to be recommended in fetuses with

suspected brain malformation. Referring to studies on pediatric hospital deaths and coroner's cases with poor agreement of postmortem MRI and findings in conventional autopsies in as much as 67%, it was however also stated that less-invasive autopsy at the moment is still far away from the point at which it could be used systematically in clinical practice. It was again emphasized that minimal and less-invasive autopsy must not be interpreted as MRI examination on its own, but apart from external examination and histological examination of the placenta includes genetic and metabolic analyses, X-ray, CT, and percutaneous or endoscopic biopsies as well as skin and muscle biopsies. Whereas MR imaging in cases of brain malformation is recommended as an adjuvant, large-scale studies are still needed to possibly prove the effectiveness of less-invasive autopsy as an alternative method. In addition, this review touches aspects that do not turn up in many publications on pm MRI, namely the benefits conventional autopsies have in terms of medical education, science, public health, and even psychology, which are difficult to measure.

4 Summary

4.1 Momentary State

Before reasonable perspectives can be proposed, the momentary situation has to be analyzed. What we seem to be facing at the moment are steady advances in sophisticated medical diagnostic and therapeutic methods contrasting with a general decline in autopsy rates meanwhile also affecting fetal and perinatal autopsies, which in many countries reached levels far below the percentages necessary for quality assurance (Okah 2002; Brodlie et al. 2002; Kumar et al. 2000 Jan; Adappa et al. 2007 Jan; Dickinson et al. 2007 Dec). This in parts is due to difficulties in gaining parenteral consent. It also reflects the attitude of the society (including medical doctors), namely the tendency to more strongly believe in sophisticated than in simple techniques. Consequently, the benefits of an autopsy will be underestimated, although a review on published studies showed that perinatal autopsy provides important additional information, could reveal a new diagnosis, or change a diagnosis in 22–76% of cases (Gordijin et al. 2002). This seems to be fortified by a general decline in medical professionalists' understanding and knowledge about the value and procedure of an autopsy, respectively. In addition, most likely as a reaction to decades during which interests of the individual have been largely ignored for the sake of society, society now seems to be much in favor of the individual's personal interests. In this respect, autopsy rates of fetal/perinatal deaths in the background of in vitro fertilization (IVF) may be of interest: At Vienna University Hospital in all fetal/perinatal cases of death occurring in the background of IVF, an autopsy was performed in 2005, whereas this figure of 100% declined to 66% in 2009 (almost 20% lower than the general rate). The danger of following the individual's interests irrespective of global ones seems, however, already changing in terms of aspects of nature, where the connection between the individual's interests with the individual's responsibility has been brought to attention. The technical advances in medicine indeed are very tempting to believe in everything being feasible. However, what tends to be forgotten is that medical advances are and have to be based on two facts. One is research and the other quality assurance by control systems, which should not use the same method to be tested. In terms of the relation of postmortem MRI examination and fetal/perinatal autopsy, this means that actually much more autopsies should be performed in combination with MRI examination to prove this system. This has actually been emphasized by most publications on this topic. There also is the pending danger of entering a vicious cycle by further reducing autopsy rates and thereby losing the skills necessary to do an efficient fetal/perinatal autopsy and indirectly weakening the position and belief in pediatric pathology. One other point is that in general, the advances of sophisticated methods elevating medical costs are facing an economic situation in which money tends to be saved on social and research topics and the number of medical doctors also decline. Trying to save money by reducing the autopsy rates does not seem the right way when comparing the costs of an autopsy with those of modern medical therapy.

4.2 Perspectives

The decline in autopsy rates in part results from misconceptions about autopsies by parents and clinicians.

Better information and knowledge on the benefits and the procedure of an autopsy should be the right means to such change in attitudes and possibly add more altruistic aspects. At this point, it may be worth to quote a commentary by Lyon (Lyon 2004 Jul). There, reasons for the parents refusing permission, namely the combination of a dread of the child being mutilated and a wish not to have anything else done to a baby who had already been through so much, are argued with the following comment: "it is precisely because the baby has been through so much and yet the outcome is negative, that it is not only the parents but also the baby's right to have these investigations carried out to be sure to have the best chance to explain why he/she died." What also has to be considered is that any kind of unanswered questions represents the main motivation for performing an autopsy, from both parental and clinical aspects. With a more critical attitude, one would expect that advances and increasing complexity of diagnoses and therapy would result in more questions to be answered in case of death, thereby increasing autopsy rates. Better interdisciplinary communication seems to be the base for the reeducation of the professionals as suggested by Snowdon (Snowdon et al. 2004 May) necessary for rehabilitation of the autopsy also as a tool of surveillance, teaching, and research.

In the beginning of the twenty-first century, it seems to be time to add postmortem MRI examination to fetal/perinatal autopsies in a differentiated way, namely in areas where it has been proven to be of help. In forthcoming studies, it may also be important to clearly separate the use of pm MRI examination in anomaly-associated spontaneous/medically induced fetal death from cases of perinatal death due to immaturity or prematurity. In the latter, histological sampling is important not only to serve as a kind of quality control for neonatal therapy, but also to be able to timely correlate endogenous and exogenous events. Although histological sampling may be less important for diagnosis in cases with associated anomalies, the importance of a complete autopsy, including sufficient tissue sampling, still plays an important role to elucidate developmental pathophysiology and genetic correlations. To perform an autopsy only to prove a diagnosis and/or cause of death means regression by putting pathology back to the position of observantly reporting, albeit on a technically higher level. Also, the statement of the joint working party of the Royal College of Obstetricians and Gynaecologists and Royal College of Pathologists has to be kept in mind, wherein autopsy rates of 50% are considered as unacceptable, 75% as the border, 80–90% as acceptable, and 90–100% as ideal for quality control (Joint Working Party of Royal College of Obstetricians and Gynaecologists and Royal College of Pathologists 1988). This could be understood as direct order to places with still adequate autopsy rates like we have in Vienna, to establish large-scale studies, to clearly demonstrate the position pm MRI examination has in the performance of a fetal/perinatal autopsy. For sure, the success will depend on a close cooperation of gynecologists, pediatric pathologists, and radiologists for one to prove the necessity of such studies and for the other to prove to healthcare systems that such studies are worth to be funded.

References

Wiener Krankenanstaltengesetz 1987 – Wr. KAG, Fassung vom 16.11. 2009, LGB1 Nr 56/2009

Wigglesworth JS (1991) Role of pathology in modern perinatal medicine. In: Wigglesworth JS, Singer DB (eds) Textbook of fetal and perinatal pathology. Blackwell Scientific, Boston, pp 3–9

Khong TY (1996b) A review of perinatal autopsy rates worldwide, 1960s to 1990s. Paediatr Perinat Epidemiol 10(1): 97–105, discussion 106–109

Gordijin SJ, Erwich JJ, Khong TY (2002) Value of the perinatal autopsy: critique. Pediatr Dev Pathol 5:480–488

Okah FA (2002) The autopsy: experience of a regional neonatal intensive care unit. Paediatr Perinat Epidemiol 16:350–354

Brodlie M, Laing IA, Keeling JW, McKenzie KJ (2002) Ten years of neonatal autopsies in tertiary referral centr: retrospective study. Br Med J 324:761–763

Kumar P, Angst DB, Taxy J, Mangurten HH (2000 Jan) Neonatal autopsies: a 10-year experience. Arch Pediatr Adolesc Med 154(1):38–42

Adappa R, Paranjothy S, Roberts Z, Cartlidge PH (2007 Jan) Perinatal and infant autopsy. Arch Dis Child Fetal Neonatal Ed 92(1):F49–F50

Burton JL, Underwood J (2007) Clinical, educational, and epidemiological value of autopsy. Lancet 369(9571):1471–1480, 28 Apr 2007

Cartlidge PH, Dawson AT, Stewart JH, Vujanic GM (1995) Value and quality of perinatal and infant postmortem examinations: cohort analysis of 400 consecutive deaths. BMJ 310(6973):155–158, 21 Jan 1995

Khong TY, Turnbull D, Staples A (2001) Provider attitudes about gaining consent for perinatal autopsy. Obstet Gynecol 97(6):994–998

Burton JL (2003 Dec) Medical educators' personal attitudes towards the necropsy. J Clin Pathol 56(12):950–951

Snowdon C, Elbourne DR, Garcia J (2004 May) Perinatal pathology in the context of a clinical trial: a review of the literature. Arch Dis Child Fetal Neonatal Ed 89(3): F200–F203
Gordijn SJ, Erwich JJ, Khong TY (2007 May) The perinatal autopsy: pertinent issues in multicultural Western Europe. Eur J Obstet Gynecol Reprod Biol 132(1):3–7
McDermott M (2004 May) The continuing decline of autopsies in clinical trials: is there any way back? Arch Dis Child Fetal Neonatal Ed 89(3):F198–F199
Laing IA (2004) Clinical aspects of neonatal death and autopsy. Semin Neonatol 9:247–254
Porter HJ, Keeling JW (1987) Value of perinatal necropsy examination. J Clin Pathol 40:180–184
Goldman L, Sayson R, Robbins S, Cohn LH, Bettmann M, Weisberg M (1983) Value of autopsy in three medical areas. N Engl J Med 308:1000–1010
Dahms B (1986) The autopsy in pediatrics. Am J Dis Child 140:335
Lundberg GD (1983) Medical students, truth and autopsies. JAMA 50:1199–1200
Putman MA (2007 Dec) Perinatal perimortem and postmortem examination: obligations and considerations for perinatal, neonatal, and pediatric clinicians. Adv Neonatal Care 7(6):281–288
Manchester DK, Pretorius DH, Every C et al (1988) Accuracy of ultrasound diagnosis in pregnancies complicated by suspected fetal anomalies. Prenat Diagn 8:109
Boyd PA, Tondi F, Hicks NR, Chamberlain PF (2004) Autopsy after termination of pregnancy for fetal anomaly:retrospective cohort study. BMJ 328:137
Dickinson JE, Prime DK, Charles AK (2007 Dec) The role of autopsy following pregnancy termination for fetal abnormality. ANZ J Obstet Gynaecol 47(6):445–449

X.2

Khong TY (1996a) The contribution of the pathologist after a perinatal loss: what we should be telling the parents. ANZ J Obstet Gynaecol 36(1):15–17
Kraus FT (2003) Perinatal pathology, the placenta, and litigation. Hum Pathol 34(6):517–521
Roberts DJ, Oliva E (2006 May) Clinical significance of placental examination in perinatal medicine. J Matern Fetal Neonatal Med 19(5):255–264
Gronvall J, Graem N (1989) Radiography in post-mortem examinations of fetuses and neonates. APMIS 97:274–280
van der Harten HJ (2001) The skeletal system. In: Keeling J (ed) Fetal and neonatal pathology. Springer, London, pp 685–709
Siebert JR (2007) Perinatal, fetal and embryonic autopsy. In: Gilbert-Barnes E (ed) Potter's pathology of the fetus, infant and child, 2nd edn. Mosby, Philadelphia, pp 695–739
Macpherson TA, Valdes-Dapena M (1998) The perinatal autopsy. In: Wigglesworth JS, Singer DB (eds) Textbook of fetal and perinatal pathology. Blackwell Science, Malden
Kapur RP (2007) Use of ancillary tests in perinatal pathology. In: Gilbert-Barnes E, ed *Potter's Pathology of the Fetus, Infant and Child.*2nd Ed Mosby, Philadelphia 2007:871–82
Bendon RW, Coventry S (2004) Non-iatrogenic pathology of the preterm infant. Semin Neonatol 9:281–287
Olsen OE (2006 Feb) Radiography following perinatal death: a review. Acta Radiol 47(1):91–99
Carroll SG, Porter H, AbdelFattah S, Kyle PM, Soothill PW (2000) Correlation of prenatal ultrasound diagnosis and pathologic findings in fetal brain abnormalities. Ultrasound Obstet Gynecol 16:149–153

X.3

Dewar S, Boddington P (2004 Oct) Returning to the Alder Hey report and its reporting: addressing confusions and improving inquiries. J Med Ethics 30(5):463–469
Joint Working Party of Royal College of Obstetricians and Gynaecologists and Royal College of Pathologists (1988) Report on fetal and perinatal pathology. London: RCOG 1988
Ros PR, Li KC, Vo P, Baer H, Staab EV (1990) Preautopsy magnetic resonance imaging:initial experience. Magn Reson Imaging 8(3):303–308
Brookes JA, Hall-Craggs MA, Sams VR, Lees WR (1996) Non-invasive perinatal necropsy by magnetic resonance imaging. Lancet 348(9035):1139–1141, 26 Oct 1996
Woodward PJ, Sohaey R, Harris DP, Jackson GM, Klatt EC, Alexander AL, Kennedy A (1997 Jan) Postmortem fetal MR imaging: comparison with findings at autopsy. AJR Am J Roentgenol 168(1):41–46
Huisman TA, Wisser J, Stallmach T, Krestin GP, Huch R, Kubik-Huch RA (2002 Jan-Feb) MR autopsy in fetuses. Fetal Diagn Ther 17(1):58–64
Alderliesten ME, Peringa J, van der Hulst VP, Blaauwgeers HL, van Lith JM (2003 Apr) Perinatal mortality: clinical value of postmortem magnetic resonance imaging compared with autopsy in routine obstetric practice. BJOG 110(4):378–382
Griffiths PD, Variend D, Evans M, Jones A, Wilkinson ID, Paley MN, Whitby E (2003 Jan) Postmortem MR imaging of the fetal and stillborn central nervous system. AJNR Am J Neuroradiol 24(1):22–27
Whitby EH, Paley MN, Cohen M, Griffiths PD (2005 Oct) Postmortem MR imaging of the fetus: an adjunct or a replacement for conventional autopsy? Semin Fetal Neonatal Med 10(5):475–483
Griffiths PD, Paley MN, Whitby EH (2005) Post-mortem MRI as an adjunct to fetal or neonatal autopsy. Lancet 365(9466): 1271–1273, 2–8 Apr 2005
Huisman TA (2004 Aug) Magnetic resonance imaging: an alternative to autopsy in neonatal death? Semin Neonatol 9(4): 347–353
Brookes JS, Hagmann C (2006 Dec) MRI in fetal necropsy. J Magn Reson Imaging 24(6):1221–1228
Whitby EH, Paley MN, Cohen M, Griffiths PD (2006 Feb) Postmortem fetal MRI: what do we learn from it? Eur J Radiol 57(2):250–255
Cohen MC, Paley MN, Griffiths PD, Whitby EH (2008 Jan–Feb) Less invasive autopsy: benefits and limitations of the use of magnetic resonance imaging in the perinatal postmortem. Pediatr Dev Pathol 11(1):1–9
Breeze AC, Cross JJ, Hackett GA, Jessop FA, Joubert I, Lomas DJ, Set PA, Whitehead AL, Lees CC (2006 Dec) Use of a confidence scale in reporting postmortem fetal magnetic resonance imaging. Ultrasound Obstet Gynecol 28(7):918–924

Thayyil S, Cleary JO, Sebire NJ, Scott RJ, Chong K, Gunny R, Owens CM, Olsen OE, Offiah AC, Parks HG, Chitty LS, Price AN, Yousry TA, Robertson NJ, Lythgoe MF, Taylor AM (2009) Post-mortem examination of human fetuses: a comparison of whole-body high-field MRI at 9.4 T with conventional MRI and invasive autopsy. Lancet 374(9688): 467–475, 8 Aug 2009

Thayyil S, Chandrasekaran M, Chitty LS, Wade A, Skordis-Worrall J, Bennett-Britton I, Cohen M, Withby E, Sebire NJ, Robertson NJ, Taylor AM (2010 Jul) Diagnostic accuracy of post-mortem magnetic resonance imaging in fetuses, children and adults: a systematic review. Eur J Radiol 75(1):e142–e148

Berry PJ, Keeling JW, Wigglesworth JS (1997) Perinatal necropsy by magnetic resonance imaging. Lancet 349(9044):55, 4 Jan 1997, author reply 55–56

Whitby E (2009) Minimally invasive autopsy. Lancet 374(9688): 432–433, 8 Aug 2009

Sebire NJ (2006 Dec) Towards the minimally invasive autopsy? Ultrasound Obstet Gynecol 28(7):865–867

Thayyil S (2010) Less invasive autopsy: an evidenced based approach. Arch Dis Child. 1 Jun 2010 [Epub ahead of print]

Lyon A (2004 Jul) Perinatal autopsy remains the “gold standard”. Arch Dis Child Fetal Neonatal Ed 89(4):F284

Postmortem Magnetic Resonance Imaging of the Fetus

Elspeth Whitby, Martyn Paley, and Marta Cohen

Contents

Abstract

› Postmortem fetal MR imaging is regarded as a valuable adjunct or alternative method to autopsy. The latter is frequently denied by the parents of the deceased. In addition, autopsy may be impaired by tissue autolysis. High quality anatomical information and a permanent record of the information may be obtained from postmortem MRI. Most experience exists with postmortem MRI of the brain. An examiner with experience and knowledge of both fetal development and common artefacts from postmortem MR images is essential to ensure the accurate interpretation of the information obtained.

1 Background

Antenatal imaging has evolved rapidly over the last few decades, yet the role of the perinatal autopsy remains essential to confirm or refute the antenatal diagnosis (Picone et al. 2008; Sankar and Phadke 2006). There has been a general decline in autopsy numbers over the last 40 years (Burton and Underwood 2003 and 2007). This has been explained in several ways including religious beliefs, organ retention scandals, and reluctance of the clinicians to request the autopsy (Snowdon et al. 2004). Most recently, postmortem imaging has had a high profile in the medical literature and junior doctors perceive that it is easier to ask for imaging than autopsy when talking to bereaved relatives (Burton 2001; Snowdon et al. 2004).

E. Whitby (✉) and M. Paley
University of Sheffield, Glossop Road, Sheffield S10 2JF, UK
e-mail: whitby@sheffield.ac.uk;
m.n.paley@sheffield.ac.uk

M. Cohen
Sheffield Children's Hospital,
Western Bank, Sheffield, UK
e-mail: marta.cohen@sch.nhs.uk

D. Prayer (ed.), *Fetal MRI*, Medical Radiology,
DOI: 10.1007/174_2010_25, © Springer-Verlag Berlin Heidelberg 2011

Postmortem imaging has been established as an adjunct to the autopsy procedure for many years, but has consisted mainly of X-ray images for skeletal abnormalities. If no specific abnormalities are suspected, these are often just faxitron images (two views of the whole body for fetal, neonatal, and pediatric cases). Over the last two decades, there has been increasing interest in additional imaging modalities including CT, and more recently, MR. The initial interest in CT was driven by the forensic services, often to locate foreign bodies, e.g., gunshot wounds and track their course specifically if aided by 3D reconstruction (Levy et al. 2006). Forensic Pathologists have recently expanded their interest to include MR imaging too as this provides detailed imaging on soft tissues and intracranial pathology, which is not available in as much detail from CT (Thali et al. 2003; Roberts et al. 2007).

2 History

Full-body postmortem MR (PM MR) was first reported by Ros et al. (1990) trying to compensate for the declining autopsy rates in the United States and to maintain quality assurance. The study involved three fetal cases, one infant and two adult cases using a 0.15 T magnet, and concluded that MR imaging was as good as autopsy for identifying gross cranial, pulmonary, abdominal, and vascular abnormalities. A larger study focusing specifically on fetal anatomy was published 5 years later (Roberts et al. 1995); this did not compare the results with autopsy, but looked at signal characteristics of different tissues in each case. That study, done on a 1.5 T magnet, demonstrated the detail with which fetal anatomy could be depicted. Individual organs of the cardiovascular, pulmonary, gastrointestinal, endocrine, musculoskeletal, and genitourinary systems were seen in detail as early as 14-week gestational age. It is worth noting that the signal characteristics were different if the fetus was fixed or fresh. Brookes et al. in 1997 (Brookes and Hall-Craggs 1997) studied 20 fetuses (10 second trimester and ten third trimester). In eight cases the MR and autopsy were in agreement, in eight cases autopsy provided more information than MR, and in four cases MR provided more information than autopsy (two of these were central nervous system (CNS) abnormalities). The MR imaging time was restricted to less than 1 h, used a water bath technique, and immediately preceded the autopsy. T2-weighted images (TR 3,000, TE90) in sagittal and coronal planes were obtained, using a 1.5 T magnet and head coil. Larger fetuses needed to be repositioned to cover the entire body. The diagnostic sensitivity of MR was highest for CNS abnormalities, but was also good for the musculoskeletal system. It was less sensitive for cardiac abnormalities. At the time that Brookes et al. undertook that study, autopsy was performed in fewer than 60% of perinatal deaths in the UK. A joint working party of the Royal College of Pathologists and the Royal College of Obstetricians and Gynecologists states that "a perinatal necropsy rate of less than 75% is unacceptable" (Pathologists 1988). Previous research had suggested that when necropsy was undertaken it was below the minimum standards in almost 50% (Cartlidge et al. 1995). This has now been rectified resulting in autopsies above the minimum standard in 93% of cases; some of this improvement has been achieved by the centralization of services and by better awareness of the importance of good quality examinations (Vujanic et al. 1998). Uptake of the autopsy is still poor. Recent figures from the Confidential Enquiry into Maternal and Child Health (CEMCH) indicated that the percentage of postmortem examinations in stillbirths during 2006 fluctuated between 29% in Yorkshire and 62% in Northern Ireland (Cemach 2008).

In 1997, Woodward and colleagues imaged 26 fetuses (whole body). Three radiologists interpreted the results independently and these were compared to the formal autopsy which was done blinded to the MR results (Woodward et al. 1997). The abnormalities were divided into major (i.e., contributed to fetal death or caused or would cause morbidity in life) and minor (unlikely to cause morbidity and undetected throughout life). A detection rate of 79% (all reviewers detected it) or 91% (at least one reviewer detected it) was reported for major abnormalities. The minor abnormalities were not detected apart from one (undescended testes). However, MR was superior in two cases with major malformations (CNS abnormalities). As in the study by Brookes et al (Brookes and Hall-Craggs 1997), there was difficulty in detecting and defining cardiac abnormalities. Additional imaging planes and thinner slices could increase the sensitivity for cardiac abnormalities.

During the next few years adult postmortem imaging was investigated by a group in Manchester, UK, driven by the local Jewish community who for religious reasons would prefer imaging to autopsy. They produced several papers establishing the role of adult postmortem MR imaging (Bisset 1998; Bisset et al. 2002; Roberts et al. 2003).

The interest in fetal and neonatal imaging began in earnest in early 2000 when there was a significant decline in the fetal autopsy rate. Initially this decline was thought to be due to the organ retention issues that had blighted the pathology services in the UK (Burton and Underwood 2003), but despite increased legislation and improved training for pathologists so that a specialist pathologist performed the examination, the uptake has never reached the ideal of 100% (Cemach 2008). While parents are unwilling to grant consent for autopsy, important clinical information, which might be crucial to provide genetic counseling for the families, is lost. Initially, the idea of postmortem imaging was not welcomed in pathology circles as it was seen as a threat to their service. However, recent years have seen pathologists realize the potential of imaging and several of them are working alongside imaging departments to establish the value of imaging in the autopsy process (Alderliesten et al. 2003; Cohen et al. 2008; Dean and Whitby 2007; Evans et al. 2008; Vasudevan et al. 2006). In Sheffield, UK, postmortem MR is currently used in fetuses beyond 12-week gestation, in stillbirths and in neonatal deaths. To date, the unit has investigated over 450 fetuses and children by MRI prior to autopsy.

Our work has concentrated on the CNS. This is the main anatomical area of research interest where we have most experience based on in utero and neonatal imaging. It accounts for 20% of fatal congenital abnormalities (Grandjean et al. 1999) and is the most difficult area to investigate at autopsy as the fetal and neonatal brain is predominantly water which, once removed from the supporting CSF and skull, it collapses and the structure is lost. Parents are refusing to allow detailed studies because of the additional time needed to fix the brain with formalin and examine brain tissue. In addition, the two previous studies in 1997 (Brookes and Hall-Craggs 1997; Woodward et al. 1997) noted that PM MR was particularly useful in CNS abnormalities. In 2003, the results of our first 40 cases were published. In eight of these cases, there was no information available from the autopsy as the brain was too macerated to assess. Of the other 32 cases, there was complete agreement in 28. Review of the other four cases led to agreement in three additional cases and incorrect information from the MR in the final case (Griffiths et al. 2003).

In 2002, the Department of Health decided to investigate the role of imaging more formally and has funded two groups to investigate MR imaging in the pediatric and the adult groups. As yet there are no formal results from these groups, although small areas have been studied and published as part of the work (Thayyil 2008; Thayyil et al. 2008a, b, c). Meanwhile, other groups are also looking at different aspects of MR imaging as part of the autopsy procedure.

The publication of studies and the service for adults based in Greater Manchester has led to public knowledge of the possibility of imaging rather than autopsy (Bisset et al. 2002). The interest has been greatest in those groups where religious beliefs prevent formal autopsy. In many areas the local coroner is now aware of the use of MR imaging, but as yet it is not fully validated. Several coroners have enquired about MR imaging, and in some cases, have allowed imaging to replace autopsy. However, although MR imaging of the fetal and neonatal CNS has been shown to detect the cause of death or clearly define the malformation in 87% of cases when the information from cultures, cytology, radiology, and cytogenesis was included, there remains 13% where it would have not detected the cause or mechanism of death. Some of these would have a cause of death detected at autopsy (Cohen et al. 2008). The converse is also true. Autopsy identified the cause of death or defined the malformation in 73% of cases, but not the remaining 27% (Cohen et al. 2008).

The published papers are summarized in Table 1.

3 The MR Technique for Fetal Postmortem Imaging

The examinations are usually performed with a 1.5 T superconducting MR system. In our department, to image the CNS structures, we have used high-spatial resolution imaging in the three orthogonal planes using fast spin echo methods to produce T2-weighted images. Imaging with these sequences takes around 30 min. We have found these to be optimal owing to the absence of myelin at this stage of development. T1-weighted

Table 1 Each of the major published papers on postmortem imaging of the fetus is listed below, along with the reference, year of publication, strength of the MR scanner, and summary of the findings

References	Number of subjects	MR scanner strength (T)	Autopsy	Results
Ros et al. (1990)	3 Fetal 1 Infant 2 Adult	0.15	Yes	MR and autopsy were equivalent for gross pathology
Roberts et al. (1995)	20 Fetuses	1.5	No	Individual organs seen in detail as early as 14-week gestational age
Brookes and Hall-Craggs (1997)	20 Fetuses	1.5	Yes	8 MR equivalent to autopsy 8 Autopsy superior 4 MR superior
Woodward et al. (1997)	26 Fetuses	1.5	Yes	79% Major abnormalities detected but no minor Autopsy superior to MR
Griffiths et al. (2003)	40 Fetuses (CNS only)	1.5	Yes	8 No autopsy information 28 MR equivalent to autopsy 3 Consensus agreed 1 MR incorrect
Alderliesten et al. (2003)	26 Fetuses	1	Yes	56% Major malformations detected by MR
Hagmann et al. (2006, 2007)	6 Fetuses	1.5	Yes	5 MR equivalent to autopsy 1 MR incorrect
Huisman et al. (2002)	10 Fetuses	1.5	Yes	8 MR equivalent to autopsy 2 Autopsy superior
Breeze et al. (2006)	30	1.5	Yes	Autopsy was superior in all cases (kappa agreement scores were 0.83 brain, 0.33 heart, 0.56 lungs)
Cohen et al. (2008)	100	1.5	Yes (full in 90)	60% MR = autopsy 27% MR superior (if other ancillary investigations considered) 13% Autopsy superior

imaging tends to be flat with little inherent tissue contrast; however, it is useful in certain pathologies, e.g., when looking for hemorrhage, and ideally should be included in cases where the fetal autopsy is not performed. The sequence, which provides the "workhorse" for postmortem imaging of the brain of the fetus in our institute, as mentioned above, consists of a T2-weighted fast spin echo sequence in three orthogonal planes as detailed in Table 2. Comparable sequences in the sagittal plane and either axial or coronal plane depending on the expected or demonstrated abnormality are used to image the spine. Additional sequences have recently been introduced which are dependent on the pathology seen. The bodies are stored in a standard refrigerated environment before imaging. They should be returned to the refrigerator immediately postimaging and remain cool throughout.

In postmortem neonatal and pediatric imaging, the sequences need to be adapted depending on the age of

Table 2 This lists the typical imaging sequences used to obtain detailed T2-weighted images of the postmortem fetus. The parameters will need to be adapted slightly depending on the scanner manufacturer and the size of the fetus. We find it easier to use the knee or wrist coil, again depending on the size of the fetus to be imaged

TE 92
TR 15,662
Band width 20.8 kHz
NEX 4
Echo train length 32
Matrix 256 × 256
In plane resolution 0.5 mm
Slice thickness 2 mm, no gap

the neonate/child as the developing brain continues to myelinate and the inherent contrast will improve. In most cases it is useful to adapt the sequences used in clinical practice for the age group being imaged. As there are usually no time constraints to postmortem imaging, sequences that take longer to acquire but give additional detail are beneficial. There are now several groups using postmortem imaging in these age groups and they all are working on sequence development to determine the best sequences to use, but currently there are no published results (Thayyil 2008). These sequences will need to be adapted depending on the age and size of the fetus/neonate/child that is to be imaged.

Postmortem MR is not as sensitive in detecting cardiac abnormalities when compared with the detection of CNS abnormalities. The use of the 3D sequences has already been demonstrated to allow better organ detail such as the heart. Further development of sequences and radiology experience may enable all organs to be depicted easily and interpretation of pathology may then be more precise.

Higher field strength scanners have been reported to provide additional detail, especially in the early gestation fetus, and if available, have been recommended for imaging the postmortem fetus less than 20-week gestation (Thayyil 2008). If not available, a 1.5 T scanner can be used with a small imaging coil, e.g., a wrist coil. In our experience we have found the addition of a fluid-filled phantom into the coil, e.g., a bag of saline, helps with calibration and increases the detail achieved from the imaging process. In such cases the field of view can also be reduced.

4 Image Interpretation

The quality and value of the report will depend on the experience of both the radiographer and the radiologist. They will need to be experienced in the developmental stages of the fetus to ensure correct interpretation as illustrated by Hagmann et al. (2006, 2007), who looked at the role of MR imaging of the postmortem neonate with respect to the renal tract. The authors reported six cases with renal tract abnormalities. Comparable information was obtained from the MR and the autopsy for gross anatomical information; however, they had one false positive from imaging due to an incorrect understanding of the fetal renal anatomy at diagnosis/reporting.

Breeze et al. (2006) attempted to assess the confidence of radiologists in interpreting MR images of the postmortem fetus using a confidence scale. The reporting radiologist graded their level of confidence of normality or abnormality in the interpretation of the different body organs. For the majority of the organs, there was a high level of confidence; however, it was lower for cardiac abnormalities and some gastrointestinal structures. Several false positives were reported in all major organ groups, including a case where the kidneys were reported as abnormal on imaging but normal at autopsy. Interestingly, cardiac abnormalities are the ones reported by all groups using MR imaging of the postmortem fetus as the most difficult to interpret correctly. This may reflect experience and confidence.

4.1 Central Nervous System

A thorough understanding of normal development is particularly relevant to the interpretation of the CNS, especially the brain with respect to cortical development. There are now several bench books (Garel 2004; Adamsbaum et al. 2001) on the development of the fetal brain in utero as shown by MR imaging and these are useful in the interpretation of postmortem fetal MR imaging alongside the research papers (Garel et al. 2001, 2003; Prayer et al. 2006; Levine and Barnes 1999).

Early on in the establishment of in utero imaging, Levine et al. demonstrated the normal cortical development seen in vivo and compared this to the standard anatomical reports from specimens and textbooks (Levine and Barnes 1999). It was concluded from a sample of 53 normal fetuses that cortical maturation occurred in a predictable fashion that was only slightly delayed (0–8 weeks) compared to the anatomical studies; however, coexisting CNS pathology ($n=40$) delayed the cortical development. The French group led by Garel added to this work in 2001 (Garel et al. 2001). Fetuses from 22 to 38 weeks gestation ($n=173$) were studied. They confirmed that the sulcal and gyral pattern developed in a sequential order as expected; however, the mean lag time was only 1 week from the reported neuropathological studies by Chi et al. (1977). In general, there was a 2-week lag time from the first appearance of the sulci

and their presence in 75% of cases in utero at a specific gestational age. Excellent review articles summarize the cortical development as seen on in utero MR images (Fogliarini et al. 2005a, b, Girard et al. 2007), while Garel and her group have published a useful and widely used bench book on these findings which should be in every department performing in utero MR (Garel 2004). We have also found this a useful reference text for interpretation of postmortem imaging of the fetus as the majority of texts available on the neuropathological findings in the developing fetus have been based on fixed and dissected specimens. A bench book ideal for those performing both in utero fetal MR and postmortem fetal MR is that by Adamsbaum et al. (2001). This book includes images in utero (Magnetic resonance and ultrasound), ex utero (magnetic resonance), and photographs taken at the autopsy.

Premature infants have also been used to study the sulcal and gyral development, again reporting an orderly and predictable pattern to sulcal and gyral development (McArdle et al. 1987).

Postmortem scans take longer and provide more detail than in utero fetal imaging by MR. There are now several excellent papers detailing and illustrating the development of the fetal brain shown by both imaging and dissection.

The most detailed work on neuronal development of the fetal brain has been done in Croatia (Rados et al. 2006; Kostovic and Judas 2007; Kostovic et al. 2002). The work describes and illustrates, among other aspects of development, the laminar pattern seen at both histology and on MR images, most clearly seen in the coronal plane.

A thorough understanding of this work is beneficial to the interpretation of postmortem MR images.

Briefly, the laminar pattern consists of the following:

- At 10 postovulatory weeks, there is a trilaminar appearance to the cerebral wall, the ventricular zone (contains the germinal eminence), the intermediate zone, and the cortical plate.
- Weeks 15–22 fetal lamination pattern appears – marginal zone, cortical plate high cellular density, subplate zone, intermediate zone, subventricular zone, the ventricular zone prominent ganglionic eminence. These can be seen most clearly on the coronal images of the postmortem fetal brain as illustrated in Fig. 1.

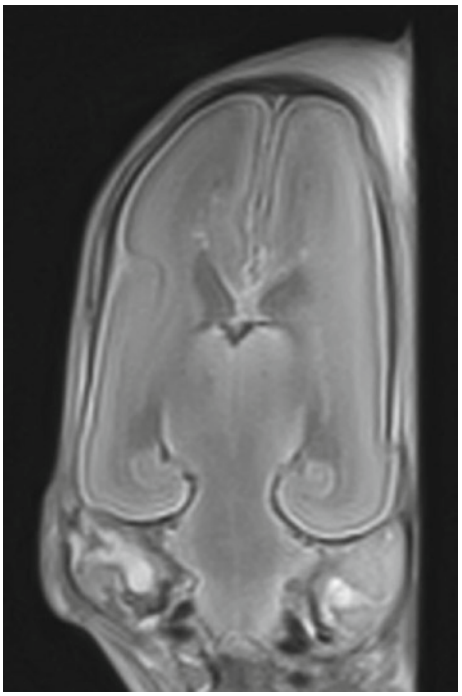

Fig. 1 Coronal MR image of a 19-week gestation fetus. The laminar structure can be seen clearly and consists of (from ventricle outwards) the dark signal ganglionic eminence, ventricular zone (intermediate signal), subventricular zone, intermediate zone, subplate zone (high signal), and cortical plate (dark signal). These appear as bands of different signal intensity

- Weeks 22–26 transient features due to cell migration (Fig. 2).
- Twenty-seven to thirty weeks loss of laminar structure and increased sulcal and gyral pattern (Fig. 3).

Bendersky et al. (2006) published detailed work on ten normal cases and assessed the cortical development as compared to Chi et al. (1977) for autopsy and previous in utero fetal MR papers for the MR images (Garel et al. 2001). Detailed postmortem MR images were compared with the anatomical and anthropometric measurements (crown rump length, frontal occipital length, and corporal weight).This comparison was performed as it is often difficult to ascertain if the fetal age given in gestational weeks is from the last menstrual period (standard in our institution) or from the day of conception or based on ultrasound measurements. The majority of the fetuses in the study were 23 weeks plus gestational age. The fetuses were fixed in formalin before imaging and dissection. Their MR imaging consisted of T1 inversion recovery and dual

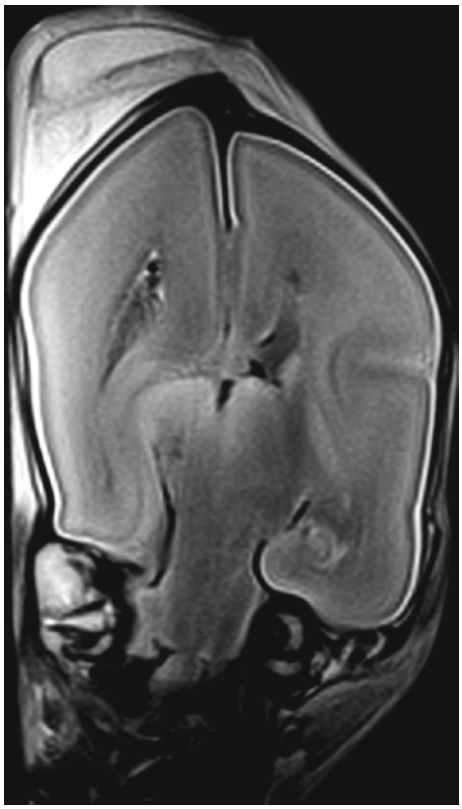

Fig. 2 Coronal MR image of a 23-week gestation fetus

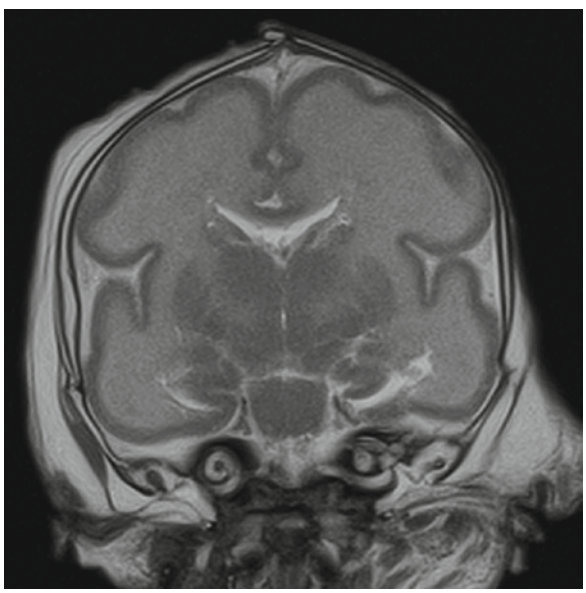

Fig. 3 Coronal MR image of a 31-week gestation fetus, the laminar structure is no longer visible

echo T2 with a small field of view, 120 and 3-mm thick slices. Autopsy consisted of 3–5-mm slices. The sulcal/gyral aging was based on a modified van der Knaap classification A to D. A was a wide and shallow sulcus, D deep and thin sulcus, and B and C between the two. Secondary and tertiary branchings were as expected with branching from the primary and secondary structures, respectively. They also assessed the grey white matter changes for signs of maturation. This was judged by looking at myelination in the brain stem, optic radiations, and posterior limb of the internal capsules. The established multilayer cortical pattern is due to myelination and hydration of the white matter and the migration of neurons in the grey matter from the ganglionic eminence adjacent to the lateral ventricle out to the cortical margins.

The sulcal and gyral pattern allowed estimation of the gestational age to within 1–2 weeks, while the grey white matter differentiation was less reliable with an error varying 3–8 weeks. They concluded that the multilayered pattern was not as accurate as the sulcal gyral pattern, was less defined by 27 weeks, and could be seen on postmortem images (Figs. 1–3).

Bendersky et al. produced a table ideal for use in everyday practice as seen in Table 3 (Bendersky et al. 2006).

Table 3 This details a clinically useful breakdown of the sulcal and gyral development and also grey white matter changes into gestational age groups to aid image interpretation (Bendersky et al. 2006)

Age (weeks)	Sulci and gyri	Grey–white matter
<23 (Fig. 1)	Sylvian fissure is still open, parietal occipital and hippocampic fissures develop	Multilayered cortex, myelin in brain stem, basal ganglia visible
24–26	Adds calcarine fissure	
27–29	Begins sylvian closure, adds pre and postcentral and superior temporal sulcus	Multilayered (less-defined)
29–35 (Fig. 3)	Central (rolandic) fissure well visible	Multilayered pattern disappears. Myelin in the internal capsule (posterior limb)
>35	Secondary and tertiary sulcation	Myelin in optic radiations

All the above and our own experience demonstrate that the sulcal and gyral pattern seen on postmortem imaging in the normal brain can be used to determine the gestational age at the time of death. However, the above mentioned studies have also shown that coexisting pathology will affect the development of the sulci and gyri. This in itself is important for diagnosis, and a thorough understanding of the sulcal and gyral development is essential for the interpretation of the images obtained.

5 Current Published Data on Postmortem Fetal Magnetic Resonance Imaging

The current published evidence includes:

- Comparison of MR imaging and autopsy of the fetal and neonatal CNS
- The use of MR imaging to predict organ weight by semiautomated methods
- MR imaging and biopsy compared to autopsy
- Limited autopsy
- Artifacts seen in postmortem imaging

In all cases the results will depend on the experience of both the radiographer, to obtain good quality images, and the radiologist for accurate interpretation.

5.1 Comparison of MR Imaging and Autopsy of the Fetus

Table 1 summarizes the results from the majority of the published papers comparing postmortem fetal imaging with conventional autopsy.

In almost all the studies the detail from the autopsy exceeds that from the MR imaging studies in some of the cases. What is not yet known is whether we can identify which cases require the formal autopsy, which can be fully assessed using imaging techniques only, and which cases require both investigations to obtain all the diagnostic information. The choice will have time and cost implications. It has been argued that imaging only provided information on the mode of death and not the causative event. This is important in the pediatric and adult population, but less so for fetal demise as the majority of cases have congenital malformations with structural abnormalities. In cases where there has been an intrauterine death or a stillbirth, assessment of the placenta and cord is essential. In these cases autopsy is superior to imaging alone.

Our own experience has shown that MR imaging is a useful adjunct to the autopsy process, but should only be used as a replacement when the family refuses autopsy. The current evidence supports this (Cohen et al. 2008). In cases where the family has refused autopsy, the imaging should always be seen as part of a minimally invasive autopsy, which should include analysis of the placenta, cultures, cytogenetics, and x-rays as well as the MR imaging (Cohen et al. 2008).

5.2 The Use of MR Imaging to Predict Organ Weight by Semiautomated Methods

There have been reports from two groups on the use of imaging to determine the organ weight. Both groups have used the knowledge of different tissue densities determined by MRI signal characteristics to calculate the factor required to multiply the tissue volume by in order to get a weight from a measured volume.

Breeze et al. (2008a) performed a manual selection of the fetal liver, brain, and lungs and applied the stereology package ANALYZE on the GE workstation to estimate the organ size by means of applying a grid to the image slice and counting the number of grid points overlying the organ. Breeze et al. concluded that the method was useful for cases where there was fetal death but no structural abnormality and may be used to detect IUGR or pulmonary hypoplasia, e.g., by organ weight changes. The fetal liver, lung, and brain weights estimated by their method correlated highly with the postmortem weights and other published data. However, the smaller the organs and the younger the fetuses, the more variable the results.

Thayyil et al. (2008b) used a semiautomated method to speed up the calculations and make it more likely to be used in clinical practice. Their study assessed all the body organs in 65 cases, but only 30 were fetuses. They included 5 newborns and 30 children.

They used a 3D turbo spin echo T2-weighted sequence. In this study all body organs were assessed, having previously established the feasibility and accuracy using animal organs. Image postprocessing software

was used that used pattern recognition and interpolation techniques to extrapolate the volume of the region of interest in 2D image data. This was based on the grey-scale values of images of the organs selected manually by the operator. The weights for the liver and spleen were obtained in all cases, but this was not the case for other organs. The rate of success decreased for kidneys and lungs and fell further for adrenal thymus and heart. The total time per case was still quite long at 54 min (mean time). When the volume was multiplied by the estimated density for each organ, an estimated weight was achieved. This weight was compared to the autopsy weight and the results showed a good correlation for liver, spleen, and kidney, but less so for other organs. The reliability was less for the younger fetuses (<20 weeks). Similarly, the inter and intraobserver variation was highest in those organs where the predicted weight was most variable. This may be due to the smaller size, difficulty in establishing the real density at younger gestational ages, especially for example in the lungs where the density would change with increasing alveolar development, and may alter in the time of storage between imaging and autopsy. Changes will also occur in cases with maceration and decomposition, so care must be taken when applying this technique in clinical practice.

Maroun and Graem (2005) have shown that there are changes in the weight of fetal organs when comparing macerated with nonmacerated fetuses from a large group of fetuses (796, 49% nonmacerated, 10% mildly macerated, 23% moderately macerated, and 18% markedly macerated). Weights of the liver, thymus, and spleen markedly decreased with increasing maceration, while weights of the lungs, kidneys, and adrenals decreased moderately. The weight of the heart and brain only changed slightly. This group produced detailed user-friendly charts from the nonmacerated fetuses with the aim of increasing the diagnostic quality of the fetal autopsy.

5.3 MR Imaging and Biopsy Compared to Autopsy

5.3.1 Autopsy and Biopsy

The idea is to limit the autopsy by using biopsy alongside imaging. This has been investigated with different degrees of success. Breeze et al. (2008b) deemed it unsatisfactory as the success rate for biopsy was less than 50%. However, the fact that the biopsies were not image-guided precluded a higher success rate.

Nicholl et al. (2007) used selective tissue biopsy and imaging in six cases with neonatal encephalopathy. Unfortunately, although they did selective biopsy, only one case had a formal autopsy with which to compare the results, so there is no real validation of the outcome in this study. In addition, the recorded pathologies were quite diverse.

Further work has been reported from Switzerland in the adult population where they have used CT guidance for the biopsies enabling accurate placement in all the tissues and with samples of sufficient quality for histology (Aghayev et al. 2007). There is no reason to suggest that this would not be possible in the fetus or under MR guidance as is done in clinical practice.

5.3.2 Angiography and Autopsy

Additional imaging techniques have been tried in the adult population, but the small size and fragility of the fetus may render these techniques unsuitable. However, CT angiography has been used successfully to perform postmortem whole body angiography to illustrate the vasculature, again by the forensic group based in Switzerland (Grabherr et al. 2006, 2007, 2008).

5.3.3 Normal Postmortem Findings and Artifacts Seen in Postmortem Imaging

Postmortem radiology is a rapidly growing area of interest, yet little is known about imaging changes after death. There have been numerous studies in the adult population aiming to acquire this knowledge and some of these can be extrapolated to the younger age group. However, there are currently no large studies in the fetus and neonate that detail the "normal" postmortem findings, although there are several groups working toward this goal. In our experience we have reviewed 250 cases of CNS abnormalities at autopsy after previous postmortem imaging. We also have experience, although less extensive, in imaging the postmortem fetus whole body. From this experience, we can state that a normal postmortem finding is small bilateral pleural effusions where as we do not see large effusions or blood stained effusions normally.

Sedimentation of the blood occurs in the venous sinuses resulting in an observed fluid level boundary. Studies performed by Jackowski et al. (2006) in adult cases suggested that the fluid level represents the position of the body around the time of death. In all our cases the fluid level represented the lividities seen at postmortem. In cases of termination of pregnancy (TOP) the fetus will not be in the supine position at the time of intrauterine death. This suggests that the fluid level does not reflect the position at death, but rather a time later when the blood is changing and decants by gravidity after death.

Sedimentation is seen universally after death resulting in the fluid level seen between the lighter serum and the heavier cellular component which is best seen on T2-weighted imaging (serum has high signal and cells have low signal). Sedimentation also occurs in the capillary system within the organs resulting in a change in the signal characteristics of the organ. The lower, more dependant, regions have a reduction in the T2 signal. The signal reduction was dependent on the specific organ studied and on the volume of blood in the body at the time of demise (Jackowski et al. 2006).

Clotting may not be seen in cases of sudden death and there have been several theories proposed including even that it does not occur. Postmortem clots are dissolved by fibrinolysis or, alternatively, both fibrinolysis and clotting can occur in parallel. Postmortem clots show sedimentation within the clot, whereas vital clots that occur antemortem do not (Jackowski et al. 2006).

Putrefaction also affects the imaging appearances and it would be expected that decomposition of the body would affect the imaging appearances. Unfortunately, there is no documented evidence for or against this. Our work suggests that MR should be beneficial in cases with decomposition and that the quality of both the MR and the autopsy will be reduced in cases with decomposition (Lavanya et al. 2008). Scanty evidence for specific effects of decomposition is available from animal studies, for example, D'Arceuil and de Crespigny (2007) USA have demonstrated the reduction in fiber tracts when the brain has partly decomposed as compared to the fresh brain. Autolysis occurs when the dead fetus is left in a warm moist environment, e.g., with TOP or intrauterine fetal death and this is retarded by cold. Bar et al. (1988), using a mouse model, have taken biopsies of the brain and shown that the microstructure is altered by autolysis. Twenty-four hours postdeath, glial cell axoplasm showed marked autolytic changes and advanced degenerative changes and myelin was also noted to breakdown. The changes occurred progressively from the time of death until fixation. The fiber tracts decreased, especially in the corpus callosum, and the body was more severely affected than the genu and splenium. The premortem state, e.g., hypoxia, hemorrhage, and hyperperfusion, may affect the PM appearances.

6 Advantages of Postmortem Imaging

Postmortem imaging has several advantages over the formal autopsy procedure. These include the fact that it is noninvasive, can be done remotely and reported at a distance by experienced staff, provides a permanent record of the findings available at any time point for review, and provides images of the body organs in situ. This is particularly useful in the fetal brain where imaging can provide an accurate account of the anatomy as it is still supported by the cerebrospinal fluid. This is of particular value in the early gestational age range and in macerated fetuses. It is also valuable where there is destruction of the brain tissue and little tissue left to visualize, e.g., severe ventriculomegaly (Fig. 4). In many cases the supporting cerebrospinal fluid is lost at autopsy and the ventricular size is difficult to determine. In some centers they inject contrast into the ventricles and image the fetus using X-rays (a ventriculogram) to accurately assess the ventricles. Magnetic resonance imaging can replace this and gives additional information on the quality and stage of development of the remaining cerebral tissue.

Similarly in cases with hydranencephaly (Fig. 5) and alobar holoprosencephaly (Fig. 6).

When imaging and autopsy are used as a combined procedure (the ideal scenario to maximize information), the imaging can guide the autopsy procedure. This applies to all methods of antenatal imaging (Dean and Whitby 2007) as well as postmortem imaging. We have found imaging a useful guide in cases of, for example, conjoined twins (Fig. 7a, b) where the imaging information can be used to plan the dissection without disruption to major organs.

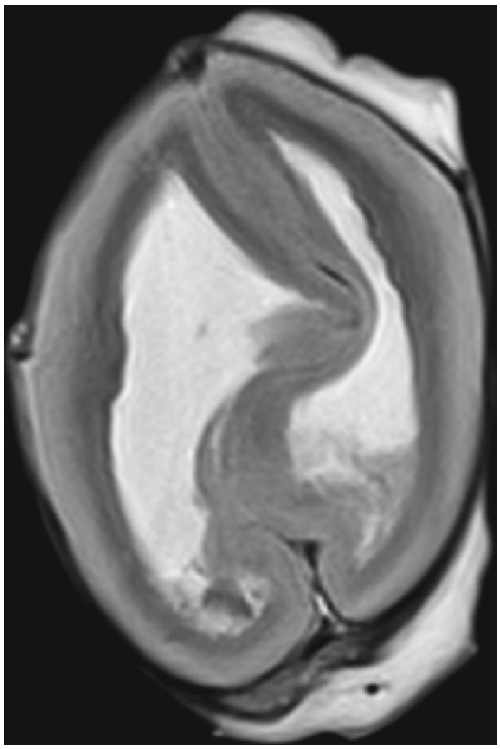

Fig. 4 Axial MR image of a 24-week gestation fetus with severe ventriculomegaly. The ventricles have "collapsed" at death, hence the folded appearance of the parenchyma. The MR image will underestimate the true extent of the antenatally diagnosed ventriculomegaly, but allows it to be visualized and shows the surrounding parenchyma clearly

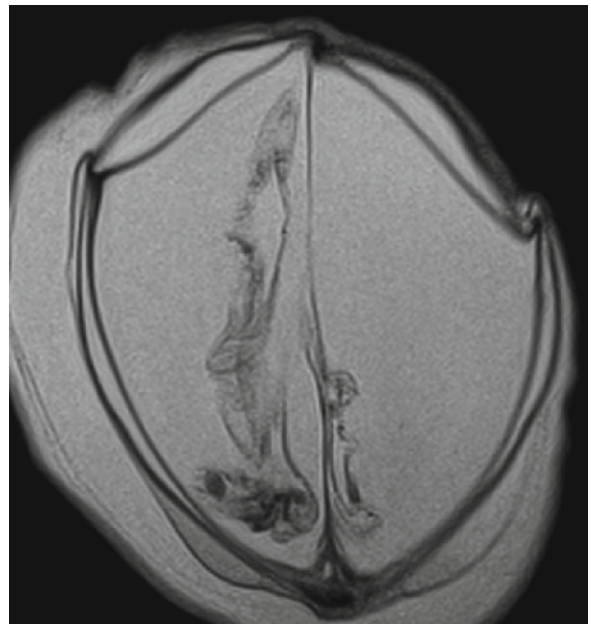

Fig. 5 Axial MR image of 28-week gestation fetus with hydranencephaly. There is no parenchyma visible on this section. The meninges are seen and the choroid plexus within a fluid-filled space. In most cases there will be a small amount of frontao and occipital lobe present, often connected by a "basket handle" distribution of parenchyma seen on the midline sagittal view only (not shown)

It is useful in cases with small encephaloceles, both intracranial and extracranial extension can be clearly defined, and in cases with distorted anatomy due to coexisting pathology (Fig. 8a, b). Again, the imaging helps plan the dissection to maximize the information obtained.

Imaging is also helpful in cases with small spinal lesions (Fig. 9a–d), which may be disrupted at autopsy, and to guide the pathologist to small areas of abnormality within a relatively normal looking brain (Fig. 10). This helps ensure that biopsies are obtained in the pertinent areas.

Imaging is also useful for other areas of the fetal body, but currently there has been less research on other areas and we have limited knowledge as to its value. We have used it to ascertain whether the fetal lungs contain air or fluid, essential in cases of infanticide; the images provide a permanent record (unpublished data).

7 Disadvantages of Postmortem Imaging Compared to Autopsy

There are several disadvantages to postmortem imaging compared to formal autopsy. The first and probably most important is the lack of histology from the tissues and, even if selected biopsy of tissues is allowed, this still depends on the correct identification of lesions or organs that are abnormal on the imaging process.

Cultures, cytogenetics, and X-rays are also essential to complete the autopsy and so should be included in any postmortem imaging if that is to be considered complete. We have shown that in the fetus where we are predominantly looking at structural malformations, the imaging should be part of the autopsy process; in some cases it can replace formal autopsy of the brain, but as yet is still inferior for other body organs. In the older patients where the malformation may be present but is not the cause of death, autopsy is essential to detect infections, toxicity, etc. and the role of imaging will be less.

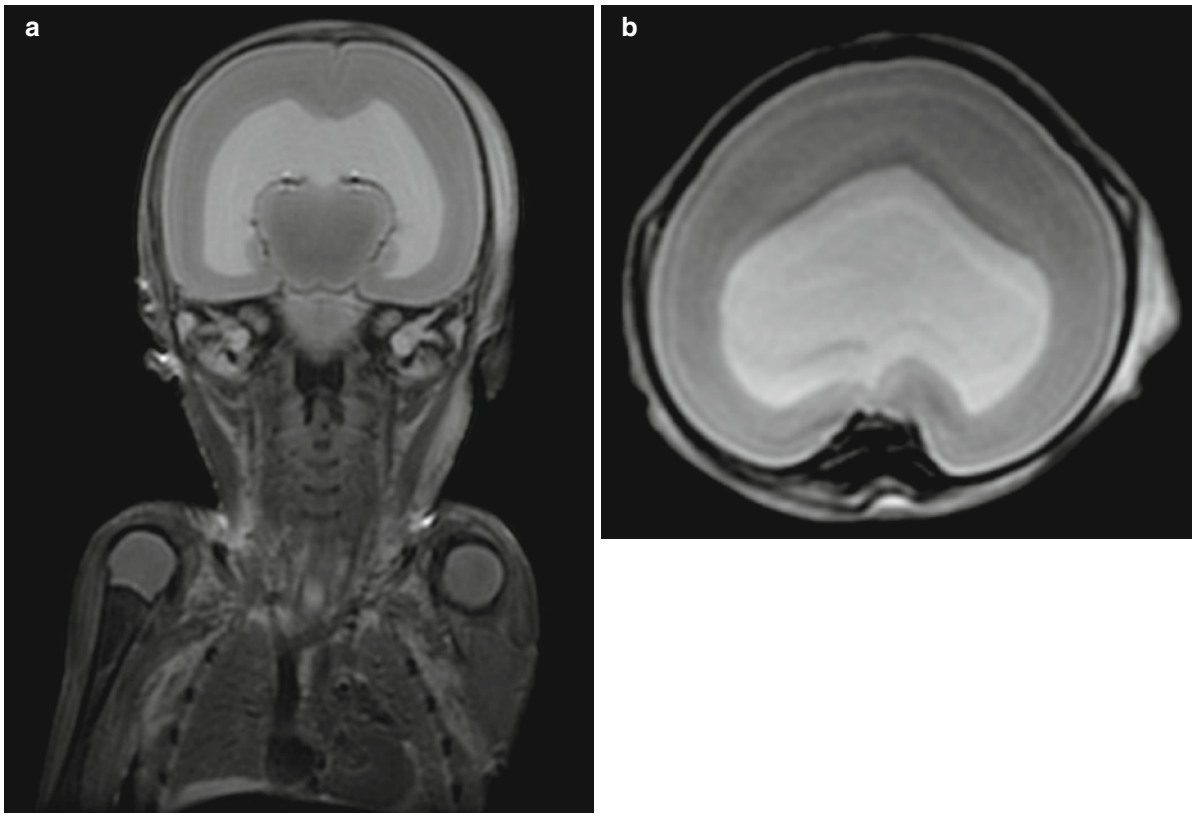

Fig. 6 (**a**) Coronal MR image, (**b**) axial MR image of a 22-week gestation fetus with holoprosencephaly. The coronal section shows the start of cleavage in the midline consistent with a semilobar holoprosencephaly. This is not visible on the axial section shown, which illustrates the single ventricle

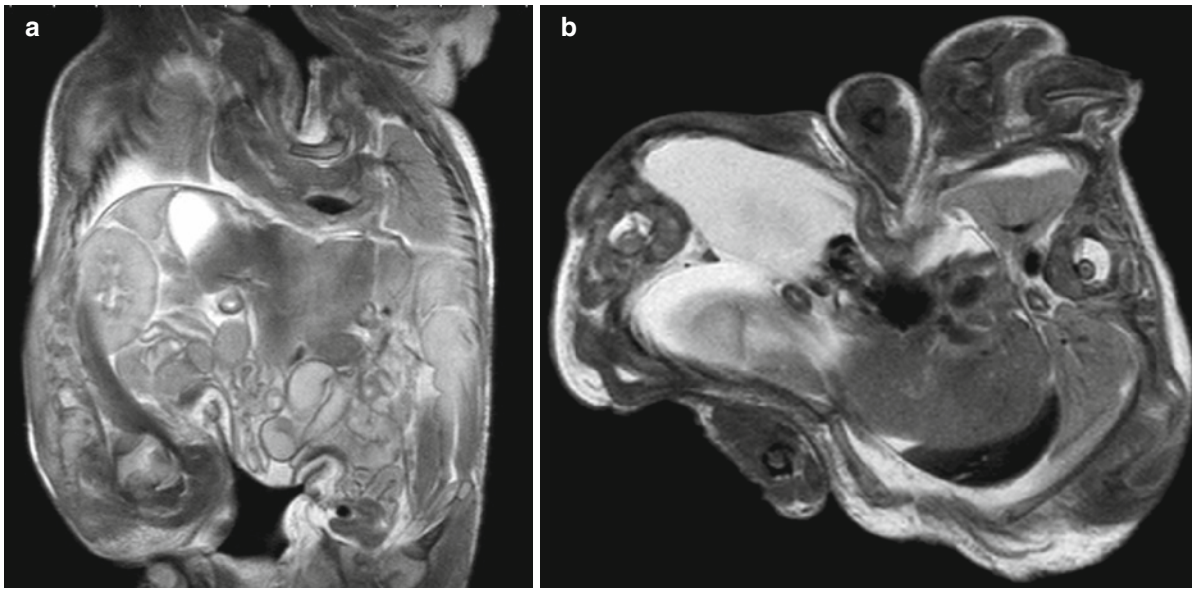

Fig. 7 (**a**) Sagittal section, and (**b**) axial section through conjoined thoracopagus twins. Joined from the xiphisternum down to the pubis. They share the heart, liver, and bowel. There are bilateral pleural effusions. That on the right side is pathological, while on the left is the amount often seen on postmortem imaging

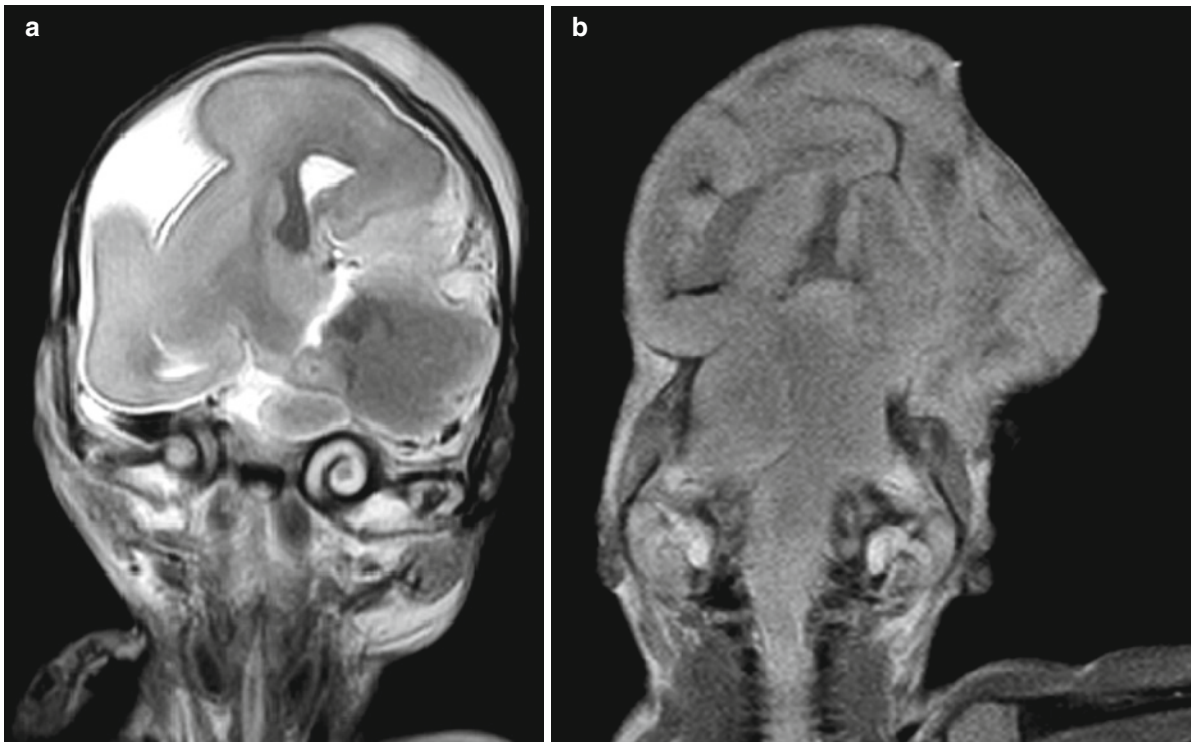

Fig. 8 (**a**) Coronal image of a fetus where there is dysgenesis of the left cerebral hemisphere. The right hemisphere is normal but has filled the space left from the abnormal development of the left. There was also a small sphenoidal encephalocele, not seen on this image. (**b**) Coronal section of a different fetus to (**a**). Here there is acrania (complete absence of the skull vault above the base) due to an abnormality in the membranous bone formation

Currently, the other major disadvantage is the lack of experienced radiologists working on postmortem imaging (Cohen et al. 2008; Hagmann et al. 2007; Breeze et al. 2006). We are essentially at the stage that the autopsy was in the 1990s when the overall quality of the fetal autopsy was poor due to the lack of qualified staff. We have since corrected that and yet are now looking at replacing the autopsy done by experienced staff with imaging interpreted by inexperienced staff. To provide the best service for patients and the best diagnostic test, we need to train staff in the technique and interpretation before changing clinical practice. A lot of the suggested imaging parameters and postprocessing to obtain 3D images of, e.g., the heart, and to estimate organ weight are time-consuming and need to be done by skilled operators. This does not preclude the use of postmortem magnetic resonance imaging in clinical practice, but it should be introduced with care and as part of the multidisciplinary team approach to investigating the demised fetus and neonate to maximize the information obtained. Care should be taken to ensure that the diagnosis made is also the cause of demise and not just an associated abnormality that may have predisposed the individual to the causative event.

Fig. 9 (**a**) Autopsy photograph illustrating the membrane over the lower sacral region, but no defect through the muscle layers was identified. (**b**, **c**) Faxitron images of the fetus, sagittal and coronal showing a normal vertebral column. (**d**) Sagittal MR image showing the spinal cord exiting through a defect in the muscles and entering into the membranous sac

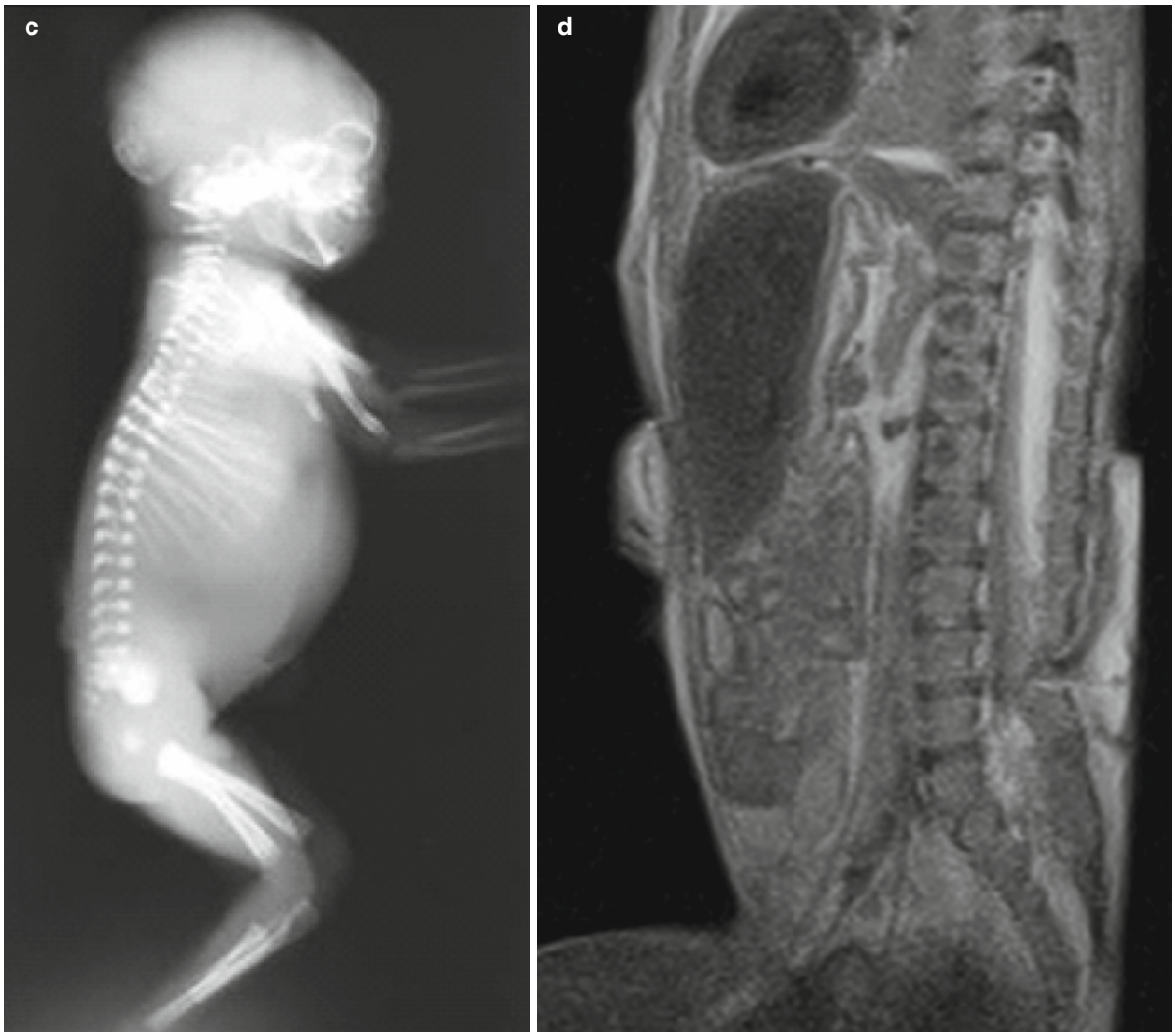

Fig. 9 (continued)

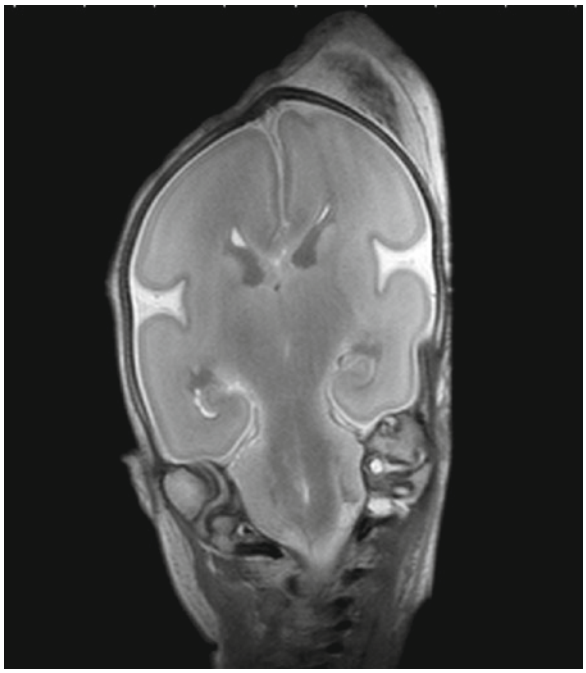

Fig. 10 Coronal section through the brain of a 24-week gestation fetus. A small dark band can be seen running from the left ventricular border out to the cortex where a "dimple" is seen. This area needs to be biopsied for histological analysis which confirmed an area of heterotopia

References

Adamsbaum C, Gelot A, Andre C, Baron JM (2001) Atlas d'IRM du cerveau foetal. Masson, Paris

Aghayev E, Thali MJ et al (2007) Post-mortem tissue sampling using computed tomography guidance. Forensic Sci Int 166(2–3):199–203

Alderliesten ME, Peringa J et al (2003) Perinatal mortality: clinical value of postmortem magnetic resonance imaging compared with autopsy in routine obstetric practice. BJOG 110(4):378–382

Bar W, Kratzer A et al (1988) Postmortem stability of DNA. Forensic Sci Int 39(1):59–70

Bendersky M, Musolino PL et al (2006) Normal anatomy of the developing fetal brain. Ex vivo anatomical-magnetic resonance imaging correlation. J Neurol Sci 250(1–2):20–26

Bisset R (1998) Magnetic resonance imaging may be alternative to necropsy. BMJ 317(7170):1450

Bisset RA, Thomas NB et al (2002) Postmortem examinations using magnetic resonance imaging: four year review of a working service. BMJ 324(7351):1423–1424

Breeze AC, Cross JJ et al (2006) Use of a confidence scale in reporting postmortem fetal magnetic resonance imaging. Ultrasound Obstet Gynecol 28(7):918–924

Breeze AC, Gallagher FA et al (2008a) Postmortem fetal organ volumetry using magnetic resonance imaging and comparison to organ weights at conventional autopsy. Ultrasound Obstet Gynecol 31(2):187–193

Breeze AC, Jessop FA et al (2008b) Feasibility of percutaneous organ biopsy as part of a minimally invasive perinatal autopsy. Virchows Arch 452(2):201–207

Brookes JS, Hall-Craggs MA (1997) Postmortem perinatal examination: the role of magnetic resonance imaging. Ultrasound Obstet Gynecol 9(3):145–147

Burton JL (2001) Getting consent for necropsies. Perhaps we should seek consent to show necropsies to students. BMJ 323(7326):1426

Burton JL, Underwood J (2007) Clinical, educational, and epidemiological value of autopsy. Lancet 369(9571):1471–1480

Burton JL, Underwood JC (2003) Necropsy practice after the "organ retention scandal": requests, performance, and tissue retention. J Clin Pathol 56(7):537–541

Cartlidge PH, Dawson AT et al (1995) Value and quality of perinatal and infant postmortem examinations: cohort analysis of 400 consecutive deaths. BMJ 310(6973):155–158

CEMACH (2008). CEMACH perinatal mortality 2006: England, Wales and Northern Ireland.

Chi JG, Dooling EC et al (1977) Gyral development of the human brain. Ann Neurol 1(1):86–93

Cohen MC, Paley MN et al (2008) Less invasive autopsy: benefits and limitations of the use of magnetic resonance imaging in the perinatal postmortem. Pediatr Dev Pathol 11(1):1–9

D'Arceuil H, de Crespigny A (2007) The effects of brain tissue decomposition on diffusion tensor imaging and tractography. Neuroimage 36(1):64–68

Dean A, Whitby EH (2007) Contribution of antenatal magnetic resonance imaging to diagnostic neuropathology. Curr Diagn Pathol 13(3):171–179

Evans C, Marton T, et al. (2008). Cranial vault defects: the description of 3 cases that illustrate a spectrum of anomalies. Pediatr Dev Pathol 1

Fogliarini C, Chaumoitre K et al (2005a) Assessment of cortical maturation with prenatal MRI. Part I: Normal cortical maturation. Eur Radiol 15(8):1671–1685

Fogliarini C, Chaumoitre K et al (2005b) Assessment of cortical maturation with prenatal MRI: part II: abnormalities of cortical maturation. Eur Radiol 15(9):1781–1789

Garel C (2004) MRI of the fetal Brain. Springer, Berlin

Garel C, Chantrel E et al (2001) Fetal cerebral cortex: normal gestational landmarks identified using prenatal MR imaging. AJNR Am J Neuroradiol 22(1):184–189

Garel C, Chantrel E et al (2003) Fetal MRI: normal gestational landmarks for cerebral biometry, gyration and myelination. Childs Nerv Syst 19(7–8):422–425

Girard N, Confort-Gouny S et al (2007) MR imaging of brain maturation. J Neuroradiol 34(5):290–310

Grabherr S, Djonov V et al (2006) Postmortem angiography after vascular perfusion with diesel oil and a lipophilic contrast agent. AJR Am J Roentgenol 187(5):W515–W523

Grabherr S, Djonov V et al (2007) Postmortem angiography: review of former and current methods. AJR Am J Roentgenol 188(3):832–838

Grabherr S, Gygax E et al (2008) Two-step postmortem angiography with a modified heart-lung machine: preliminary results. AJR Am J Roentgenol 190(2):345–351

Grandjean H, Larroque D et al (1999) The performance of routine ultrasonographic screening of pregnancies in the Eurofetus Study. Am J Obstet Gynecol 181(2):446–454

Griffiths PD, Variend D et al (2003) Postmortem MR imaging of the fetal and stillborn central nervous system. AJNR Am J Neuroradiol 24(1):22–27

Hagmann CF, Robertson NJ, et al. (2006). Postmortem MRI as an adjunct to perinatal autopsy for renal tract abnormalities. Arch Dis Child Fetal Neonatal

Hagmann CF, Robertson NJ et al (2007) Postmortem magnetic resonance imaging as an adjunct to perinatal autopsy for renal-tract abnormalities. Arch Dis Child Fetal Neonatal Ed 92(3):F215–F218

Huisman TA, Wisser J et al (2002) MR autopsy in fetuses. Fetal Diagn Ther 17(1):58–64

Jackowski C, Thali M et al (2006) Postmortem imaging of blood and its characteristics using MSCT and MRI. Int J Legal Med 120(4):233–240

Kostovic I, Judas M (2007) Transient patterns of cortical lamination during prenatal life: do they have implications for treatment? Neurosci Biobehav Rev 31(8):1157–1168

Kostovic I, Judas M et al (2002) Laminar organization of the human fetal cerebrum revealed by histochemical markers and magnetic resonance imaging. Cereb Cortex 12(5):536–544

Levine D, Barnes PD (1999) Cortical maturation in normal and abnormal fetuses as assessed with prenatal MR imaging. Radiology 210(3):751–758

Levy AD, Abbott RM et al (2006) Virtual autopsy: preliminary experience in high-velocity gunshot wound victims. Radiology 240(2):522–528

Maroun LL, Graem N (2005) Autopsy standards of body parameters and fresh organ weights in nonmacerated and macerated human fetuses. Pediatr Dev Pathol 8(2):204–217

McArdle CB, Richardson CJ et al (1987) Developmental features of the neonatal brain: MR imaging. Part I. Gray-white matter differentiation and myelination. Radiology 162(1 Pt 1): 223–229

Nicholl RM, Balasubramaniam VP et al (2007) Postmortem brain MRI with selective tissue biopsy as an adjunct to autopsy following neonatal encephalopathy. Eur J Paediatr Neurol 11(3):167–174

Pathologists, Joint Working Party Royal College Obstetricians and Gynaecologist and Royal College of Pathologists. (1988). Report of fetal and Perinatal pathology. London.

Picone O, Levaillant JM et al (2008) Correlation between referral ultrasound with suspected foetal anomalies and autopsy examination in two prenatal diagnosis centres. Impact of the routine use of 3D/4D scan. Prenat Diagn 28(3):191–196

Prayer D, Kasprian G et al (2006) MRI of normal fetal brain development. Eur J Radiol 57(2):199–216

Rados M, Judas M et al (2006) In vitro MRI of brain development. Eur J Radiol 57(2):187–198

Roberts IS, Benbow EW et al (2003) Accuracy of magnetic resonance imaging in determining cause of sudden death in adults: comparison with conventional autopsy. Histopathology 42(5):424–430

Roberts ISD, Benbow EW (2007). The non-invasive or minimally invasive autopsy. Recent Advances in Histopathology 22. The Royal Society of Medicine Press, London.

Roberts MD, Lange RC et al (1995) Fetal anatomy with magnetic resonance imaging. Magn Reson Imaging 13(4): 645–649

Ros PR, Li KC et al (1990) Preautopsy magnetic resonance imaging: initial experience. Magn Reson Imaging 8(3): 303–308

Sankar VH, Phadke SR (2006) Clinical utility of fetal autopsy and comparison with prenatal ultrasound findings. J Perinatol 26(4):224–229

Snowdon C, Elbourne DR et al (2004) Perinatal pathology in the context of a clinical trial: attitudes of neonatologists and pathologists. Arch Dis Child Fetal Neonatal Ed 89(3): F204–F207

Thali MJ, Yen K et al (2003) Virtopsy, a new imaging horizon in forensic pathology: virtual autopsy by postmortem multislice computed tomography (MSCT) and magnetic resonance imaging (MRI)–a feasibility study. J Forensic Sci 48(2):386–403

Thayyil S (2008) Magnetic resonance imaging of the post-mortem fetus – technical factors.(personal communication)

Thayyil S, Cleary JO, Price AC, et al (2008). Whole-body postmortem magnetic resonance imaging at 9.4T: a rapid and less invasive autopsy for small fetuses. ISMRM, Toronto Canada.

Thayyil S, Robertson NJ et al (2008b) Parental consent for research and sudden infant death. Lancet 372(9640):715

Thayyil S, Schievano S, et al. (2008) A semi-automated method for non-invasive internal organ weight estimation by postmortem magnetic resonance imaging in fetuses, newborns and children. Eur J Radiol.

Vasudevan PC, Cohen MC et al (2006) The OEIS complex: two case reports that illustrate the spectrum of abnormalities and a review of the literature. Prenat Diagn 26(3):267–272

Vujanic GM, Cartlidge PH et al (1998) Improving the quality of perinatal and infant necropsy examinations: a follow up study. J Clin Pathol 51(11):850–853

Woodward PJ, Sohaey R et al (1997) Postmortem fetal MR imaging: comparison with findings at autopsy. AJR Am J Roentgenol 168(1):41–46

Genetics of Fetal Disease

Maximilian Schmid and Wibke Blaicher

Contents

Abstract

The causes of congenital anomalies are genetic and nongenetic.

Genetic disorders include chromosomal disorder, single gene (monogenic) disorders, and multifactorial disorders that result from the interaction of multiple genes and environmental factors.

There is little experience with fetal magnetic resonance imaging (MRI) and genetic disorders.

However, fetal MRI, in addition to sonography and prenatal genetic testing, has been shown to improve prenatal diagnosis of certain genetic disorders in various cases.

While its definite role in diagnosis of genetic disorders remains to be determined, fetal MRI is currently mainly used as a second-line prenatal diagnostic method at larger centers.

It frequently enables differential diagnosis and determination of the extent of a certain genetic disorder.

In cases with suspected genetic disorders where the underlying genetic defect is not known, fetal MRI may be essential to exclude a certain disorder or find a diagnosis. Looking forward it will be of great importance to correlate different genotypes with fetal MRI data.

M. Schmid (✉) and W. Blaicher
Department of Obstetrics and Feto-maternal Medicine,
Medical University of Vienna General Hospital,
Waehringer Guertel 18–20, A-1090 Vienna, Austria
e-mail: maximilian.schmid@meduniwien.ac.at;
wibke.blaicher@meduniwien.ac.at

D. Prayer (ed.), *Fetal MRI*, Medical Radiology,
DOI: 10.1007/174_2010_62, © Springer-Verlag Berlin Heidelberg 2011

1 Introduction

Fetal MRI is a well-known useful adjunct to sonography, yet there is little experience with fetal MRI and genetic disorders. However if one takes into account that major structural or genetic birth defects still affect approximately 3% of births in the USA (Hoyert et al., 2006) and remain a major contributor to infant mortality (Yoon et al., 1997), it is mostly probable that fetal MRI will play a bigger role in the future. Nowadays, the most common clinical pathway to fetal MRI is the following: A fetal abnormality is detected during a routine ultrasound scan, karyotyping (and depending on suspected diagnosis molecular genetic testing) follows, and finally, fetal MRI is performed in order to substantiate the diagnosis. In cases with known underlying genetic defect, fetal MRI is not essential for diagnosis itself, but it may help to predict the extent of the disease and improve quality of counseling. Nonetheless, there are hereditary disorders where the underlying genetic defect is unknown. Under such circumstances, analysis of the family history may help to identify a suspected recurrence risk, but prenatal genetic testing as such is not available. If in addition due to technical or anatomical limitations sonography is also limited in detecting associated fetal abnormalities, prenatal diagnosis seems impossible. In some of these cases, fetal MRI may help to exclude a certain hereditary disorder or establish a diagnosis. Consequently knowing about the expected appearance of a certain well-defined hereditary disorder may prove helpful for professionals involved in fetal MRI. Therefore, we will give a brief overview of some of the most common hereditary disorders and discuss associated findings. We also want to outline possible indications for fetal MRI in cases of suspected hereditary disorders where the underlying defect is not known.

2 Diagnosis of Genetic Disorders

A genetic disorder is a condition caused by abnormalities in genes or chromosomes. Though individual genetic disorders are rare, collectively they comprise several thousand recognized genetic disorders with more being continuously discovered. Since genetic disorders are often associated with early fetal loss, the incidence of chromosomal abnormalities is dependent upon the population studied. They are most frequent in spontaneous abortions and less common in live births (Won et al., 2005). It is estimated that 7% of all stillborns and 0.5% of all newborns have a chromosomal abnormality and that 20–30% of all infant deaths are due to genetic disorders (Berry et al., 1987). In general, diagnosis of genetic disorders is rising not only due to advances in genetic research but also due to the increasing availability of genetic testing and prenatal screening for genetic disorders. Most common genetic disorders are associated with a specific pattern of congenital malformations. However, there is a significant clinical variability within groups of patients with the same chromosomal abnormality and in many cases what seems to be a certain pattern of congenital malformations does not point toward a specific genetic disorder.

2.1 Prenatal Screening

Today various screening tests for common genetic disorders are offered to pregnant women (Norton, 2008). Fetal MRI is not routinely used for screening purposes. Screening tests mainly rely on prenatal ultrasound and maternal blood sampling, while for prenatal diagnosis of genetic disorders invasive prenatal testing may be required. Screening tests are commonly classified according to the phase of pregnancy in which they are performed.

2.1.1 First Trimester Screening

In contrast to fetal MRI, prenatal sonography is a very common procedure. It has been estimated that a prenatal ultrasound examination was performed in two thirds of live births in the USA in 2002 (Martin et al., 2003). Today the early detection of genetic disorders is one of the major goals of widespread prenatal screening programs. First trimester screening programs for common genetic disorders usually combine (“Combined Test”) sonographic findings at 11+0 until 13+6 gestational weeks (e.g., nuchal translucency), maternal serum markers (i.e., PAPP-A, beta-hCG), and parental risk factors for genetic disease to determine the risk that the fetus is affected. The Combined Test detects approximately

90% of Down syndrome, one of the most frequent genetic disorders, with a false positive rate (FPR) of 5% (Nicolaides, 2005). Moreover, it has been found that first trimester combined screening also detected 78% of all non-Down syndrome numerical chromosomal aberrations (i.e., aneuploidy) with an overall FPR of 6% (Breathnach et al., 2007). However, even in the absence of a chromosomal aberration, nuchal thickening is clinically relevant because it is associated with an increase in adverse perinatal outcome caused by a variety of fetal malformations, dysplasias, deformations, disruptions, and genetic syndromes (Souka et al., 2005). For women who first present for prenatal care after 13+6 weeks of gestation, maternal serum markers ("quadruple test") can be used to screen for certain genetic disorders such as Down syndrome. The test usually involves measurement of alpha-fetoprotein (AFP), unconjugated estriol (uE3), human chorionic gonadotropin (hCG), and inhibin A and can be performed until 22 weeks of gestation (Wald et al., 1997).

2.1.2 Second Trimester Screening

While sonography continually improves and detection of fetal anomalies constantly shifts to earlier gestational weeks, ultrasound has its limits. Detection of fetal anomalies in the first trimester is limited by the small size of the fetus and ongoing fetal development. Markers suggestive of an underlying genetic disorder (e.g., hyperechogenic bowel in fetuses with cystic fibrosis) may develop after the first trimester. Hence, second trimester ultrasound scans for detection of anomalies are often part of prenatal screening programs usually offered at 18–20 weeks of gestation (Schwarzler et al., 1999). This is early enough to allow for additional diagnostic procedures while legal termination of pregnancy is mostly possible, if desired. Structural abnormalities that can be reliably diagnosed by an ultrasound examination in the second trimester include hydrocephalus, anencephaly, myelomeningocoele, dwarfing syndromes, spina bifida, omphalocele, gastroschisis, duodenal atresia and fetal hydrops, cleft lip, clubfoot, many urinary tract and renal abnormalities, and a variety of congenital cardiac abnormalities (Benacerraf, 2005). Some of these anomalies are associated with genetic disorders and may require further genetic testing. They may also be found in fetuses without genetic disorder but are more present in fetuses with genetic disorders.

2.2 Invasive Fetal Sampling

To confirm or rule out a certain genetic disorder, genetic testing of fetal tissue is often required. In general, invasive fetal sampling is offered to women identified at significant risk for genetic disorders by the screening methods described above or with a family history of genetic disease. Chorionic villus sampling (CVS) refers to a procedure for the prenatal diagnosis of genetic disorders in which small samples of the placenta are obtained for chromosome or DNA analysis. It is usually performed as an ambulatory procedure after ten completed weeks of gestation. CVS enables prenatal diagnosis of conditions in which diagnostic cytogenetic or DNA analysis is possible. Rapid karyotyping can be achieved within 24–48 h of sampling by examining cytotrophoblastic cells in metaphase (direct method). However, due to the risk of false positive results (about 0.04–0.12%) (Hahnemann and Vejerslev, 1997; van den et al. 2000), long-term cultures are usually performed concurrently. Prenatal diagnosis via DNA extraction from chorionic cells is performed primarily when there is a family history of a Mendelian disorder. CVS is the procedure of choice for first trimester prenatal diagnosis of genetic disorders. Alternatively, fetal cells can be obtained from amniotic fluid drawn from the uterine cavity by amniocentesis, usually performed between 15 and 17 weeks of gestation. Later procedures can be problematic if a termination of pregnancy is planned based upon abnormal results. Nonetheless, late procedures are performed in some cases, especially when fetal abnormalities are discovered late in gestation. CVS and Amniocentesis both carry a certain risk of fetal loss (0.6–2.0%), which needs to be weighed against the diagnostic value of the genetic test when the procedure is offered (Mujezinovic and Alfirevic, 2007). This usually is preformed as part of prenatal genetic counseling by expert genetic counselors.

2.3 Fetal MRI

While fetal MRI is rapidly gaining ground, its role in diagnosis of genetic disorders remains to be determined. Very little is known about MRI appearance of genetic disorders. So far mainly case reports on genetic disorders have been published. Little effort is being put

in larger investigative series. This is very much because its diagnostic advantages in comparison to ultrasound are still very much question of debate (Malinger et al., 2002). Currently, superiority in use of fetal MRI is mainly presumed for certain intracranial applications, such as diagnosis of Lissencephaly, a mainly hereditary malformation of the cortex and posterior fossa malformations often found in genetic disorders (Dill et al., 2009). The cost of fetal MRI further limits availability and stalls widespread research efforts. Consequently, the use of fetal MRI in diagnosis of genetic disorders is currently mainly limited to larger centers with experienced operators. In general, its main advantages have been pointed out to be its high soft-tissue contrast, presumed safety and independence of maternal anatomy as well as fetal position (Pugash et al., 2008). Fetal MRI is mainly used to elucidate equivocal findings on routine ultrasound or to further delineate some pathological entities. In respect to genetic disorders, fetal MRI is currently recommended if a genetic disorder has been suspected or diagnosed and additional information that is relevant for establishment of diagnosis, prognosis, or consequent treatment may be obtained. Looking forward new functional imaging methods and perfusion imaging will help to further differentiate fetal MRI from ultrasound and allow for further applications in diagnosis of genetic disorders.

3 Chromosomal Aberrations

Chromosomal aberrations are among the most important causes of congenital malformation and mental handicap. The prevalence of chromosomal abnormalities ranges from 2% to 35% in fetuses with congenital anomalies, with the highest rate in fetuses with multiple anomalies, as opposed to an isolated anomaly (Staebler et al., 2005). Therefore, when a major structural anomaly is identified, the likelihood of an abnormal karyotype rises dramatically. Chromosomal aberrations are disruptions in the normal chromosomal content of a cell. Human cells have 23 pairs of large linear nuclear chromosomes, giving a total of 46 per cell. Chromosomal aberrations may reflect an abnormality of chromosome number or structure. Only a few chromosomal aberrations can survive to term in an apparently nonmosaic state. These include trisomy 21, trisomy 13, trisomy 18, triploidy, and sex chromosome aneuploidy, with a combined incidence of 1 per 300 live births. Typical prenatal findings in fetuses with common chromosomal aberrations are listed in Table 1, 2, 3.

3.1 Numerical Chromosomal Aberrations

Numerical aberrations represent a significant proportion of chromosomal changes found in humans. They represent a significant cause of pregnancy loss as well as abnormalities found in live births. Numerical aberrations from the human number of 46 chromosomes are called aneuploidy. Aneuploidy is the most common genetic disorder detected by prenatal diagnosis. Most aneuploidy is caused by nondisjunction during cell division. One single additional chromosome is termed trisomy. The term monosomy refers to lack of one chromosome of the normal complement. Trisomy is an important cause of congenital malformations as well as of congenital mental retardation. Triploidy describes an extra set of chromosomes. Triploidy is estimated to be present in 1% of all clinically recognized pregnancies, with 6% of spontaneous abortions and 0.5% of stillborn infants affected. The extra haploid set of chromosomes in triploidy may come from either the mother (digynic) or father (diandric). Malformations and fetal loss are nearly universal in triploid fetuses because of the excess complement of chromosomes (McFadden and Langlois, 2000). In the rare cases of survival to the second trimester, fetal MRI may have some advantage over ultrasound in showing anatomical detail of triploid fetuses if oligohydramnios is present (Chen et al., 2007).

3.1.1 Autosomal Chromosomal Aberrations

Individuals with unbalanced autosomal aberrations have multiple congenital abnormalities that can involve one or more organ systems. Since most other trisomies end in early abortions, Down syndrome (Trisomy 21), Edwards syndrome (Trisomy 18), and Patau syndrome (Trisomy 13) are the most common frequently diagnosed trisomies involving autosomes, or nonsex chromosomes. Trisomy 21, is the most common genetic cause of mental retardation. The majority of Trisomy

21 is due to a nondisjunction event; however, approximately 5% of cases are associated with chromosomal translocations, some of which are inherited (Bandyopadhyay et al., 2003). Trisomy 21 in the fetal period shares some of the phenotypic features seen in infants. Dysmorphic facial features (flattened nasal bridge, upslanting palpebral fissures, and protruding tongue), cardiac anomalies (characteristically atrioventricular canal defect), and duodenal atresia are often found. The risk of having a child with Down syndrome increases with increased maternal age from 1 in 600 births for mothers under 30 years to 1 in 50 births for mothers over 40 years (Hook, 1981). As described earlier, the majority of pregnancies at high risk of Down syndrome can be identified based on a combination of ultrasound findings at 11+0 – 13+6 weeks gestation and maternal serum markers. Fetal MRI may be beneficial in evaluation of associated congenital malformations that need imminent surgical treatment after birth when termination of pregnancy is not desired. For example, fetal MRI aided diagnosis and surgical management of a case of Down syndrome with combined esophageal, duodenal, biliary, and pancreatic ductal atresia first diagnosed in the second trimester. It was able to show the entire extent of the lesion in a single cut and provided improved anatomic detail, particularly of the diaphragm and defect (Pameijer et al., 2000). Trisomy 13 is rare (incidence 1/5,000 to 1/20,000 births) and associated with more severe structural malformations than trisomy 21 or 18. Even when liveborn, trisomy 13 is considered a lethal condition and most affected persons die in early infancy. The trisomy 13 phenotype is characterized by a range of brain abnormalities, including absence of the corpus callosum and holoprosencephaly. Facial abnormalities mirror the extent of the forebrain abnormalities. There may be microphthalmia and hypotelorism or cyclopia. Bilateral cleft lip and palate are common. There are often extra digits on the ulnar side of the hand. Cardiac abnormalities are frequent and can include truncus arteriosus and tetralogy of Fallot. Intrauterine growth retardation is present in about half of infants with trisomy 13 (Lehman et al., 1995;Watson et al., 2007). Trisomy 18 is more common in live births than is trisomy 13 but is still rare (1/8,000 to 1/10,000 live births). It is only second to Down syndrome in being the most common autosomal trisomy detected in the second trimester. In the third trimester, fetuses with trisomy 18 often have both polyhydramnios and intrauterine growth restriction (IUGR), an unusual combination. It is especially likely when these findings are also associated with abnormal hand positioning (second and fifth fingers overlapping). Cardiac defects are particularly common, affecting more than 60% of fetuses. Omphalocele, defects in the diaphragm, and abnormalities of the genitourinary system are also common abnormalities. Survival beyond a few months after birth is rare (Watson et al., 2008).

3.1.2 Sex Chromosome Aberrations

Numeric sex chromosome imbalances are the cause of several clinical syndromes, such as Turner syndrome (45,X0) or Klinefelter syndrome (47,XXY) or triple X syndrome (47,XXX). Turner syndrome (45,X) is a common cause of early pregnancy loss, accounting for about 7% of spontaneous abortions. The liveborn frequency is estimated to be 1–2/10,000 (Hook and Warburton, 1983). Unlike the described trisomies, Turner syndrome is not associated with advanced maternal age and is caused by mechanisms other than nondisjunction. It is associated with lymphedema, which is often discovered during the first trimester screening. T2-weighted images of a fetus at 29+2 gestational weeks with Turner syndrome and a characteristic lymphedema of the neck are shown in Fig. 1. Congenital heart disease, particularly coarctation of the aorta and atrial septal defect, are present in 20% of cases (Wald et al., 1997). Renal malformations are also common. Klinefelter syndrome (46, XXY) is the most common cause of hypogonadism and male infertility, accounting for about 10% of infertile men. There is an increased frequency of a variety of nonspecific major and minor congenital abnormalities at birth. Clinodactyly is the most common minor anomaly, being found in about 74% of cases (Zeger et al., 2008). Most females with Triple X syndrome (47, XXX) are phenotypically normal, sometimes taller than average. In addition, the majority of affected females are fertile and produce chromosomally balanced offspring (Linden et al., 1996).

3.2 Structural Rearrangements

Structural rearrangements or aberrations of chromosomes include deletions, duplications, translocations, inversion, formation of ring chromosomes or isochromosomes. The gain or loss of chromosome material

Table 1 Typical prenatal findings in chromosomal aberrations -- Numerical chromosomal aberrations

Examples	Down Syndrome (Trisomy 21)	Edwards Syndrome (Trisomy 18)	Patau Syndrome (Trisomy 13)
Typical prenatal findings	Cardiac defects (VSD, ASD, AVC, Tetralogy of Fallot)	Clenched hands (overlapping fingers)	Holoprosencephaly
	Duodenal atresia	IUGR	Cleft lip or palate
	Thicked nuchal fold	Polyhydramnios	Microcephaly
	Ventriculomegaly	Club feet/rocker bottom feet	Polydactyly
	Absent nasal bone	Micrognathia	Sloping forehead
	Shortening of proximal long bones (humerus, femur)	Single umbilical artery	Dandy Walker Malformation
	Clinodactyly	Chorioid plexus cysts	Hydrocephalus
	Sandal gap deformity	Omphalocele	Omphalocele
	Pericardial effusion	Low set of ears	Agenesia of the corpus callosum
	Pyelectasis	Brain anomalies (Vermian hypoplasia, agenesia of the corpus callosum)	Rocker bottom feet
	Wide iliac angle	Shortened limbs	Neural tube defects
	Brachycephaly	Cardiac defects (Mitral or aortic atresias, pulmonic stenosis, APVR)	Genitourinary anomalies
	Midface hypoplasia	Renal anomalies (horseshoe kidney)	Cardiac defects (VSD, ASD, PDA, hypoplastic left heart, mitral or aortic atresia, pulmonary stenosis)
		Brachycephaly (Strawberry shaped head)	Pyelectasia
		Neural tube defects	Hypotelorism
		Congenital diaphragmatic hernia	Single umbilical artery
		Micropthalmus	Cyclopia
		Hydrocephalus	Lymphangiectasia
		Esophageal atresia and/or fistula	Midline dysmorphic features
		Radial aplasia	IUGR
		Cleft lip or palate	
		Lymphangiectasia	
		Hypertelorism	
		Decreased fetal activity	
Comment	Incidence approx. 1:800 -1:2000 live births	Incidence aprox. 1:6000-1:8000 live births	Incidence approx. 1:8000-1:15000 live births
	Major anomalies seen in 20% of Fetuses	In utero death occurs in more than 95% of affected fetuses	In utero death occurs in more than 95% of affected fetuses
	Many live to adulthood	Major anomalies seen inmore than 80% of fetuses	Median survival 89 days
	Mental handicap	50% die within 1 week of birth, 90% within 5 months	Severe Retardation
	Risk of leukemia and other malignancies	Mental retardation	Both sexes equally affected
	Reduce muscle tone	3:1 fenale to male predominance	

Triploidy	Turner Syndrome (45,X0)	Klinefelter Syndrome (47,XXY)	Triple X Syndrome (47,XXX)
IUGR	Genitourinary anomalies (ovarian dysgenesis, hydronephrosis, horseshoe kidney, renal agenesia, renal malrotation)	Hypospadia	Phenotypically normal
Placenta malformations (partial hydatidiform mole)	Cardiac defects (coarctation, bicuspid aortic valve)	Small phallus	
Oligohydramnios	Nonimmune hydrops	Cryptorchidism	
Major facial defects	Lymphedema (neck)	Clinodactyly	
Central nervous system anomalies (eg, ventriculomegaly, holoprosencephaly, Dandy-Walker anomaly)	Protuberant ears with upturned lobules		
Neural tube defects	High arched palate		
Renal anomalies	Large septate cystic hygromata, usually noted in the second trimester		
Syndactyly of the third and fourth digits	Total body lymphangiectasia (fetal hydrops)		
Clubbed feet	Cardiac defects (eg, coarctation)		
Two vessel umbilical cord	Nuchal thickening		
Nuchal thickening	Short femur		
Incidence aprox. 1:50000 live births	Incidence approx. 1:5000 live births	Prevalence approx. 1:500 males	Prevalence approx. 1:1000 girls
Usually lost through early miscarriage	Highly lethal in embryonic life	Most common sex chromosome disorder	Many have no or only mild symptoms (learning disabilities)
Those that are born alive usually die shortly after birth	Most survive after birth	40% of concepti survive the fetal period	Most have normal sexual development (no infertility)
Two distinct phenotypes depending on the origin of the extra haploid set	Normal intelligence	After birth mortality rate is not significantly higher	
Not associated with a mother's age	Usually ovarian failure and infertility	Little to no signs of affectedness in adults (infertility, gynaekomastia)	
		Expressive language skills may be impaired	

VSD=ventriculoseptal defect, ASD=atrioseptal defect, PDA=patent ductus arteriosus, APVR=Anomalous pulmonary venous return, AVC=Atrioventricular canal

Table 2 Typical prenatal findings in chromosomal aberrations -- Structural Rearrangements

Examples	Wolf-Hirschhorn Syndrome (Deletion, 4p-)	Robertsonian translocation	Ring chromosome 13 Syndrome (r13)
Typical prenatal findings	Microcephaly	Phenotypically normal	Microcephaly
	Hypertelorism		IUGR
	Cleft-lip palate		Hand, foot or toe abnormalities
	Congenital heart defects		CNS malformations
	CNS malformations		Urogenital malformations
	Dysplastic ears		Distal limb deformities
	Urogenital malformations		Heart defects
Comment	Prevalence approx. 1:50000	Prevalence approx. 1:1000 individuals	Constitutional ring chromosomes occur in 1:50000 human fetuses
	Distinctive craniofacial phenotype	Common form of chromosomal rearrangement	Chromosome whose arms have fused together to form a ring
	Mental retardation and seizures frequent	Formed by fusion of long arms of two acrocentric chromosomes	Very heterogeneous
	Most die in early infancy	Involves the acrocentric chromosomes 13, 14, 15, 21, 22	Type and severity of symptoms is determined by the amount and location of genetic material missing
		Individuals with a balanced translocation are usually phenotypically normal	Mental and growth retardation are common in affected individuals
		Carriers may have unbalanced offspring with multiple malformations	

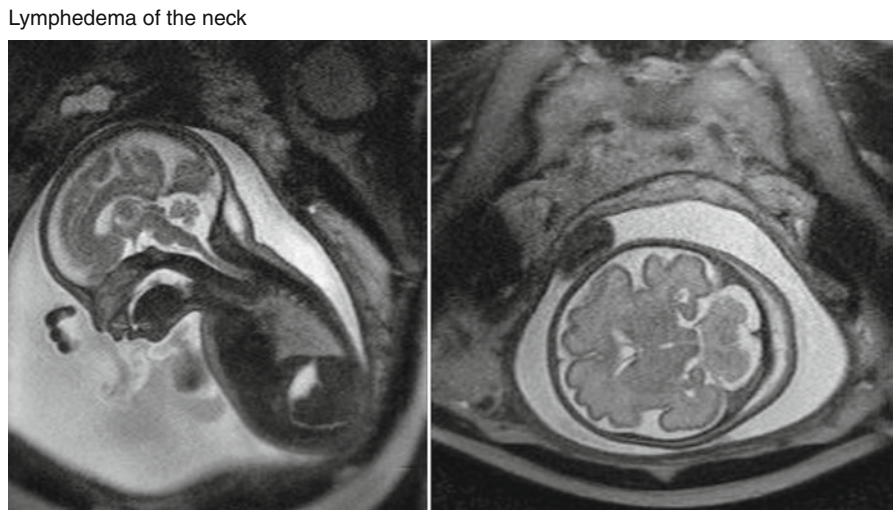

Fig. 1 Fetus at 29+2 gestational weeks with Turner Syndrome (T2-weighted images)

Table 3 Typical prenatal findings in chromosomal aberrations -- Uniparental Disomy and Imprinting

Examples	Prader Willi Syndrome (del 15q11-13 paternal)	Angelman Syndrome (del 15q11-13 maternal)	Beckwith Wiedemann (UPD 11p15 paternal)
Typical prenatal findings	Genital hypoplasia, Cryptorchidism	Gnerally, no major congenital defects	Macrosomia
	Hypotonia, decreased fetal movement		Macroglossia
	Scoliosis and/or kyphosi		Visceromegaly
	Labia minora and/or clitoral hypoplasia		Hemihypertrophy
	Polyhydramnios		Abdominal wall defects
	Frequent abnormal fetal position		Polyhydramnios
			Placental mesenchymal dysplasia
			Cardiac defects
			Hemangiomata
			Embryonal tumors (heart)
Comment	Prevalence approx. 1:10000-1:20000	Prevalence approx. 1:12000	Incidence approx. 1:13700 live births
	Obesity, Hyperphagia (over-eating) from age 2 - 4 years	Characteristic facial features and happy demeanor	Most cases are sporadic
	Delayed psychomotor development	Delayed psychomotor development	Usually development of embryonal tumors (Wilms' tumor or nephroblastoma)
	Short stature and characteristic facial features	Speech impairment, unique beahvior	Frequent neonatal hypoglycemia
	Severe hypotonia during the neonatal period	Seizures, onset usually < 3 years of age	Mental development appears to be normal to very slightly decreased
	Usually learning difficulties, behavioral problems or severe psychiatric problems	Normal prenatal and birth history	Children who survive infancy are usually healthy
	Life-span near average	Life-span near average	

can lead to a variety of genetic disorders. If no genetic material is lost or gained, structural aberrations do usually not cause disease in carriers, such as balanced translocations, or chromosomal inversion, although they may lead to a higher chance of having a child with a chromosome disorder. Examples of genetic disorders due to loss of chromosome material are the Cri du Chat syndrome, which is caused by a deletion on the short arm of chromosome 5 (5p-) and the Wolf–Hirschhorn syndrome, which is caused by deletion on the short arm of chromosome 4 (4p-). Both genetic disorders are very rare and associated with severe mental and physical retardation (Battaglia et al., 2001;Cerruti, 2006). Structural defects such as heart defects, hypospadia, and midline defects are also found when chromosome material is lost. Fetal MRI has been shown to be helpful in diagnosis of brain anomalies in a fetus with Wolf–Hirschhorn syndrome (De et al., 2002). T2-weighted images of a fetus with Wolf–Hirschhorn syndrome at 29+2 gestational weeks are shown in Fig. 2. Some chromosomal deletions cannot be readily seen by microscopy because they only involve a few neighboring gene loci. Contiguous gene syndromes (CGS) are characterized by multiple, apparently unrelated, clinical features caused by deletion of the multiple adjacent genes. Important member of this kind of

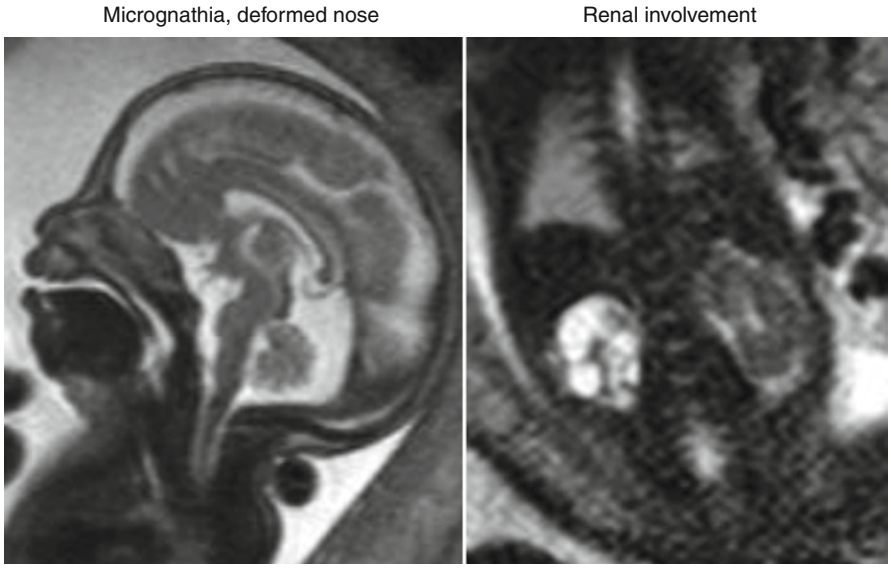

Fig. 2 Fetus at 29+2 gestational weeks with Wolf–Hirschhorn syndrome (T2-weighted images)

genetic disorders is the Di George Syndrome. It is associated with a microdeletion on the long arm of chromosome 22 (22q11). It is characterized by abnormalities in the development of the third and fourth brachial arches, resulting in hypoplasia of the thymus and/or parathyroid gland, conotruncal cardiac defects, and facial dysmorphism (Kobrynski and Sullivan, 2007). Fetal MRI has been shown to facilitate diagnosis of Miller-Dieker syndrome (MDS), characterized by classical lissencephaly, which is associated with a deletion at the short arm of chromosome 17 (17p13.3). The detection or confirmation of MDS and associated cranial as well as extracranial abnormalities has been shown to be possible in the second trimester (Fong et al., 2004). Less known CGS are the Rubinstein-Taybi and the Williams-Beuren syndromes.

3.3 Uniparental Disomy and Imprinting

In some cases, it is essential whether a gene is inherited from a person's mother or father. Uniparental disomy (UPD) occurs when a person receives two copies of a chromosome, or part of a chromosome, from one parent and no copies from the other parent. Prader–Willi syndrome and Angelmann syndrome are the most common of several genetic disorders resulting from UPD or a disruption of normal genomic imprinting. Both disorders most commonly involve a small deletion on the long arm of chromosome 15 (del 15q11–q13). In Prader–Willi syndrome, it involves the chromosome of paternal origin; in Angelmann syndrome, it involves the chromosome of maternal origin. Both disorders are associated with severe motoric and mental retardation and lead to abnormal social behavior (Horsthemke and Wagstaff, 2008). Beckwith-Wiedemann syndrome has been associated with Microduplication of on the short arm of chromosome 11 (11p15). It is a congenital overgrowth condition with an increased risk of developing embryonic tumors, such as Wilms' tumor. The cardinal features are abdominal wall defects, macroglossia, and gigantism (Enklaar et al., 2006). Parental imprinting appears to play a significant role in the development of this disorder. Affected individuals have been shown to have a duplication of 11p15 in the gene of paternal origin or paternal uniparental disomy of chromosome 11. T2-weighted images of a fetus with Beckwith-Wiedemann syndrome at 32+6 gestational weeks are shown in Fig. 3. In many cases, UPD likely has no effect on health or development. Because most genes are not imprinted, it doesn't matter if a person inherits both copies from one parent instead of one copy from each parent (Kotzot, 2008).

4 Single Gene Disorders

Genes are complete, functional units of DNA. Typical genes include a coding region whose sequence directs the synthesis of a polypeptide chain. Genes are

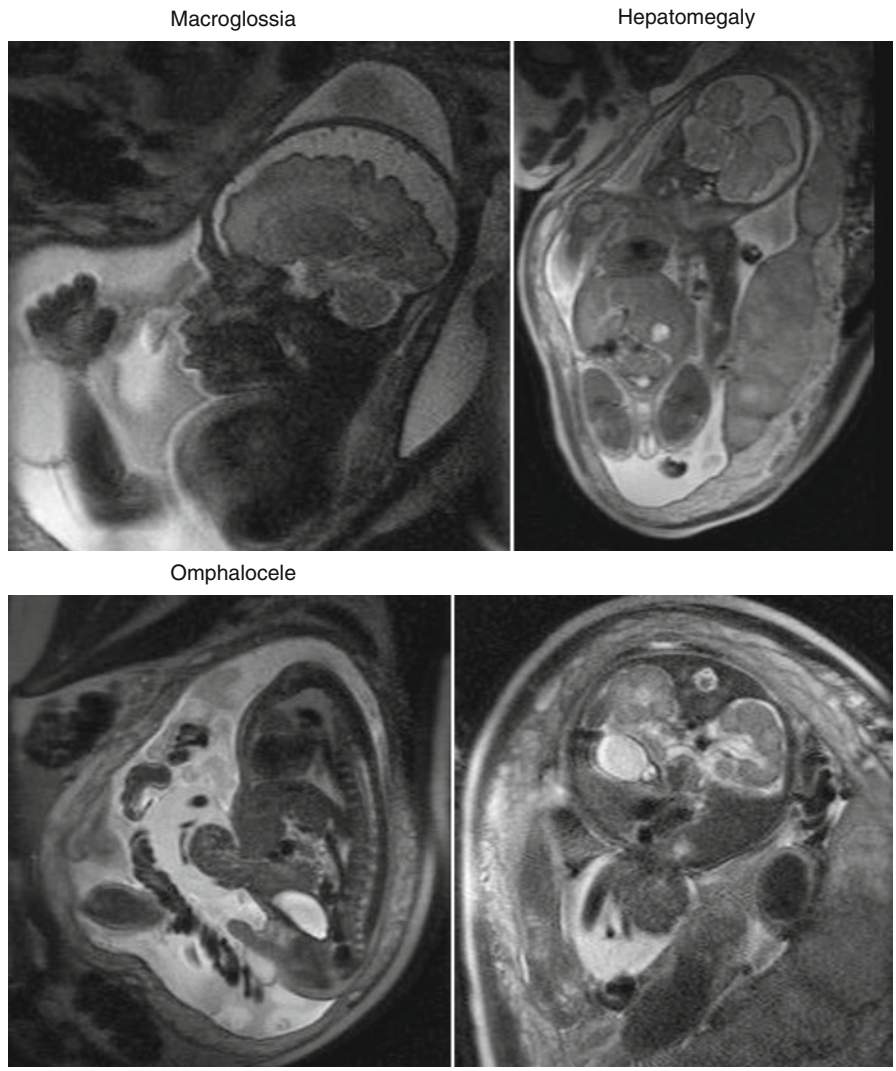

Fig. 3 Fetus at 32+6 gestational weeks with Beckwith-Wiedemann syndrome (T2-weighted images)

arranged in a linear order on the chromosomes. Each chromosome harbors many genes, and a gene can be defined by a specific genomic location or locus. As opposed to chromosomal abnormalities, single gene disorders are usually inherited. Also called Mendelian or monogenic diseases, they are caused by mutations in one gene and can be passed on to offspring in several ways. They may be inherited in one of the following patterns: autosomal dominant, autosomal recessive, X-linked (usually recessive, rarely dominant), and mitochondrial. The overall frequency was estimated to be 1%, with 0.7% as dominant conditions, 0.25% as recessive conditions, and 0.04% as X-linked conditions (Baird, 1987). These patterns of inheritance can often be worked out from a family tree. Recurrence risks of single gene disorders are predictable based on the pattern of inheritance. However if the disorder is not known in advance, with over 380 human genes linked to single gene disorders, single gene defect screening in the prenatal setting can be challenging (South et al., 2008). Examples of experience with fetal MRI and Single gene disorders may be seen in Table 4.

4.1 Autosomal Dominant

Humans have two copies of each chromosome and consequently of all genes (with the exception of an X and Y in males). Only one mutated copy of the gene will be necessary for a person to be affected by an

Table 4 Examples for Fetal MRI in Single Gene Disorders

Type/ Inheritance	Genetic disorders	Findings	Value of fetal MRI
Autosomal dominant	Tuberous Sclerosis Complex (TSC)	Cardiac rhabdomyomas, cerebral tubers	Sufficient for the detection of cerebral lesions in TSC; TSC Consensus Conference criteria can also be applied to fetal MRI (Muhler MR et al., 2007)
	Neurofibromatosis type I	Neurofibromas, skeletal abnormalities	Provides significant additional information, facilitating prenatal diagnosis (McEwing RL et al., 2006)
	Sotos syndrome	Overgrowth, Macrocephaly, ventriculomegaly, hypertelorism	Aids in confirmation of the diagnosis (Chen CP et al., 2002)
	Pfeiffer syndrome type II	Cloverleaf skull, dilated lateral ventricles, hypertelorism, broad thumbs	Helps in diagnosis and differentiation of syndromatic craniosynostosis, such as Pfeiffer syndrome (Itoh S et al., 2006)
	Apert syndrome	Craniosynostosis, midfacial hypoplasia and bilateral syndactyly	Demonstrates the whole characteristic craniofacial shape (Pooh RK et al., 1999)
Autosomal recessive	Autosomal Recessive Polycystic Kidney Disease (ARPKD)	Loss of normal renal architecture, enlarged kidneys	Serves as an adjunctive method for diagnosing ARPKD (Nishi T et al., 1995)
	OIsteogenesis Imperfecta type II	Limb dwarfism, unusually large fontanels, numerous bone fractures	Complements sonography, further differentiating clinical and sonographic findings (Teng SW et al., 2003)
	Zellweger syndrome	Abnormal cortical gyral patterns, hepatosplenomegaly, renal hyperechogenicity, enlarged ventricles	Facilitates the prenatal diagnosis of complex polymalformative syndromes such as Zellweger syndrome (Mochel F et al., 2006)
	Walker-Warburg syndrome	Congenital muscular dystrophy, lissencephaly, eye abnormalities	Aids in timely prenatal diagnosis, management, and counseling (Low AS et al., 2005)
	Muscle-Eye-Brain Disease	Congenital muscular dystrophy, structural eye abnormalities, lissencephaly	Helps to evaluate cortical abnormalities which may be difficult to identify otherwise as the major sulci are only beginning to form (Longman C et al., 2004)
	Joubert syndrome	Hypoplastic cerebellar vermis and hemispheres, molar tooth sign (brainstem), polydactyly	Enables prenatal diagnosis of Joubert syndrome in the second trimester (Poretti A et al., 2008)
X-linked	X-linked hydrocephalus	Hydrocephalus without aqueductal stenosis	Allows differentiation between the various etiologies of ventriculomegaly: hydrocephalus, congenital malformation, and destructive processes (Zimmerman RA et al., 2005)
Mitochondrial	Complex I deficiency	IUGR, various multisystemic findings (oxygen dependent tissue: heart, brain, muscle, kidney)	Helps in the diagnosis of mitochondrial disorders (Gire C et al., 2002)
Multifactorial and polygenetic	Non-syndromic isolated cleft palate	Isolated cleft palate	Allows detailed assessment of the midline structures, providing accurate diagnosis of isolated cleft palate (Kazan-Tannus JF et al., 2005)

autosomal dominant disorder. Each affected person usually has one affected parent. The likelihood of transmitting a dominant trait from parent to child is usually 50%. The phenotype of an individual carrying a gene with an autosomal dominant mutation may vary based upon the penetrance and expressivity of the mutation. Conditions often have a high intrafamiliar variability in clinical course. Examples of autosomal dominant disorders include Huntington's disease, Neurofibromatosis I, Autosomal Dominant Kidney Disease (ADPKD) and Marfan syndrome. T2-weighted images of a fetus with ADPKD at 22+9 gestational weeks are shown in Fig. 4. There is some evidence that fetal MRI may prove useful for some

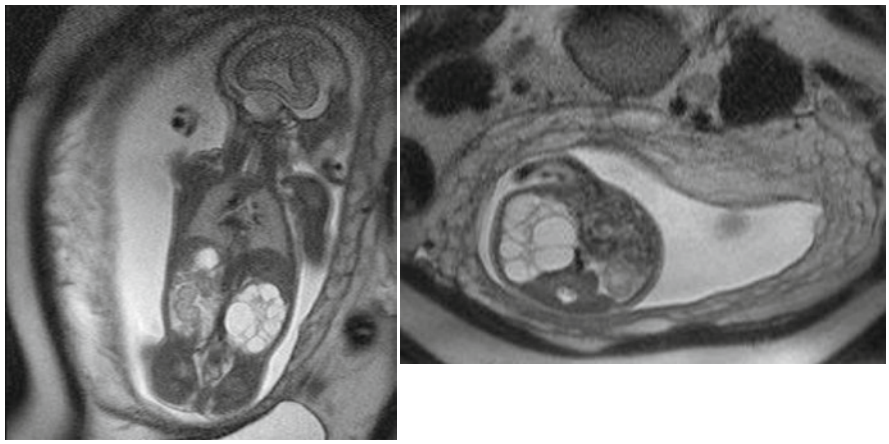

Fig. 4 Fetus with autosomal dominant kidney disease (ADPKD) at 22+9 gestational weeks (T2-weighted images)

autosomal dominant disorders such as Tuberous Sclerosis Complex (TSC), an autosomal dominant phakomatosis associated with intracardiac rhabdomyomas. Fetal MRI has been shown to be of value for the detection of cerebral lesions in TSC (Muhler et al., 2007). Also fetal MRI examination provided significant additional information, facilitating prenatal diagnosis in a case of neurofibromatosis (McEwing et al., 2006). Perinatal MRI studies aided in confirmation of the diagnosis of Sotos syndrome, which most likely also follows an autosomal dominant mode of inheritance in another case (Chen et al., 2002). However, in other autosomal dominant disorders, such as Apert syndrome, fetal MRI provided no significant additional information compared to ultrasound (Pooh et al., 1999).

4.2 Autosomal Recessive

Autosomal recessive single gene diseases occur only in individuals with two mutant alleles of the disease-associated gene. An affected person usually has unaffected parents who each carry a single copy of the mutated gene (and are referred to as carriers). The usual likelihood that carrier parents will have affected offspring is 25%. Because recessive genes are relatively rare, autosomal recessive conditions are found more commonly in ethnic groups who marry within the group or in consanguineous relationships. They are mostly metabolic disorders, such as Zellweger syndrome, a rare autosomal recessive peroxisomal biogenesis disorder. The high level of resolution of fetal MRI allows for analysis of cerebral gyration and myelination and facilitates the prenatal diagnosis of complex polymalformative syndromes such as Zellweger syndrome (Mochel et al., 2006). Other examples of rare neurodevelopmental disorders where fetal MRI provides useful information are the Walker-Warburg syndrome (Low et al., 2005), MDS (Fong et al., 2004), Muscle Eye Brain Disease (Longman et al., 2004) and other Lissencephalies, some of which are autosomal recessive. It has been suggested that fetal MRI may prove useful as screening method for families at risk for these kind of disorders as long as genetic screening is not available (Le et al., 2005; Rubod et al., 2005). However sometimes diagnosis is tricky and can only be made very late in pregnancy. For example, prenatal diagnosis of Joubert syndrome and related autosomal recessive disorders has been shown to be possible with fetal MRI from 29 weeks' gestation (Poretti et al., 2008). Nevertheless, fetal MRI has not always been shown to be superior. It was not useful in further differentiating the diagnosis and cerebral findings in a case of Pena-Shokeir syndrome type I, an autosomal recessive form of neurogenic arthrogryposis (Persutte et al., 1988). Some well-known examples of autosomal recessive diseases are Cystic Fibrosis (CF), Phenylketonuria, Sickle Cell Anemia, Tay Sachs, Albinism, and Galactosemia. The role of fetal MRI in these more common autosomal recessive disorders is unclear. Currently, it mainly helps to further evaluate sonographic findings of specific associated malformations. For example, fetal MRI provided additive information with regard to bowel dilatation in cases of echogenic bowel often found in fetuses with CF (Carcopino et al., 2007). In a fetus with Osteogenesis Imperfecta, type II fetal MRI revealed additional diagnostic information on the extent of bone fractures and affected internal organs (Teng et al., 2003). Use of functional MRI techniques, such as MR spectroscopy, may prove

useful in diagnosis of autosomal recessive metabolic disorders in the future. One could even imagine that a metabolic profile obtained by functional MRI could make the need of invasive genetic testing expendable. However, preliminary reports, such as in the evaluation of Pyruvate Dehydrogenase Deficiency, have been disappointing (Robinson et al., 2001).

4.3 X-linked

Single-gene diseases that involve genes found on the sex chromosomes have somewhat different inheritance patterns than those described above. Relatively few X-linked dominant conditions have been identified. These include Rett syndrome, Incontinentia Pigmenti, and Vitamin D-resistant Rickets. X-linked recessive disorders are also caused by mutations in genes on the X chromosome. However, while in X-linked dominant conditions the presence of one single mutated copy of the gene is sufficient to result in expression in females, X-linked recessive conditions require two alleles for expression in females. Since males have no second X-chromosome, one mutated copy is sufficient to cause an X-linked recessive disease. Hence they are more frequently affected. Examples of X-linked recessive disorders include: Duchenne Muscular Dystrophy, Hemophilia A and B, and Wiskott–Aldrich syndrome. Also in X-linked disorders it appears that fetal MRI is currently primarily helpful in evaluating associated malformations. Craniosynostosis, for example, is found in Vitamin D-resistant Rickets, and it has been suggested that fetal MRI is of diagnostic value when synostosis is suspected on ultrasonography. Especially in the detection of associated brain abnormalities, an important prognostic issue, it proved helpful (Fjortoft et al., 2007).

4.4 Mitochondrial

Mitochondrial disorders can be caused by mutations of nuclear DNA or mitochondrial DNA (DiMauro and Schon, 1998). Since only the mother contributes mitochondria to the developing embryo, mitochondrial DNA defects are transmitted by maternal inheritance. Because usually varying numbers of mitochondria are affected, transmission and severity are difficult to predict. Risk of recurrence among the offspring of affected women has been estimated to be 4% (Chinnery et al., 2004). Mitochondrial deletion disorders include Kearns–Sayre syndrome, Chronic Progressive External Ophthalmoplegia, and Pearson Bone-marrow Pancreas syndrome. Mitochondrial point mutation disorders include Leber Hereditary Optic Neuropathy, Myoclonic Epilepsy with Ragged Red Fibers (MERRF), and Leigh syndrome (ataxia, hypotonia, spasticity, and optic abnormalities). Mitochondrial disorders that are based on nuclear gene defects may be inherited in an autosomal recessive manner or an autosomal dominant manner. Prenatal diagnosis of such mitochondrial disorders is difficult. Antenal presentation is highly variable. The combination of intra uterine growth restriction and developmental anomalies during pregnancy in an at-risk family is suggestive of a recurrence of the disease (von Kleist-Retzow et al., 2003).

5 Multifactorial and Polygenic (Complex) Disorders

Traditionally, genetic disorders have been classified as monogenic (involving one gene) or polygenic (complex). Complex, multifactorial, or polygenic genetic disorders are likely associated with the effects of multiple genes in combination with lifestyle and environmental factors (Badano and Katsanis, 2002). Although complex disorders often cluster in families, they do not have a clear-cut pattern of inheritance. This makes it difficult to determine a person's risk of inheriting or passing on these disorders. Complex disorders are also difficult to study and treat because the specific factors that cause most of these disorders have not yet been identified. Examples of multifactorial disorders include asthma, autism, diabetes, inflammatory bowel disease, and many more. Most of these disorders have not been associated with typical congenital malformations or significant fetal disease, and therefore currently only play a minor role in prenatal diagnosis of genetic disorders. However, isolated anomalies, such as non-syndromic cleft lip and palate, may have polygenic basis which is not fully understood.

6 Link to Further Literature

An in-depth discussion of all genetic syndromes is beyond the scope of this article. The reader is referred to the many excellent available literature that cover genetic syndromes in detail and depth. Up-to-date information on genetic syndromes and diagnostic options can also be found online. We recommend the following websites:

- *Online Mendelian Inheritance in Man* (*OMIM*). OMIM is a comprehensive, authoritative, and timely compendium of human genes and genetic phenotypes. The full-text, referenced overviews in OMIM contain information on all known Mendelian disorders and over 12,000 genes. OMIM focuses on the relationship between phenotype and genotype. Website: www.ncbi.nlm.nih.gov/Omim/
- *Orphanet.* Orphanet is the European portal dedicated to information on rare diseases and orphan drugs for patients and their families, health professionals, and researchers. It provides an encyclopedia of rare diseases, a directory of services in Europe including specialized clinics, clinical laboratories, research projects, registries, clinical trials and support groups concerning rare diseases and publishes an online newsletter. Website: www.orpha.net
- *Genetests.* Genetests provides information about molecular genetic testing options for inherited disorders. The website also offers "GeneReviews," which provides disease descriptions focused on the use of currently available molecular genetic testing in diagnosis, management, and genetic counseling. Website: www.genetests.org

7 Outlook

The use of new techniques in research and diagnostics of genetic disorders is leading to the identification of many new syndromes, elucidates the genomic bases of well-established clinical conditions, and expands our knowledge about the phenotypic spectrum of genetic disorders. The development of microarray-based comparative genomic hybridization (array CGH) methods and new fast molecular sequencing techniques represent such new advances. At the same time, the progress of MRI as a clinical tool proves to be extraordinary. The use of fetal MRI will be expanding, even faster sequencing will allow for better images, new powerful magnets will help to even more detailed snapshots of anatomic structures and visualization of metabolic as well as structural pathways. The vast potential of such new functional MRI techniques, MRI perfusion, and other applications unique to MRI will help it to further differentiate from ultrasound. While ultrasound is likely to remain the method of choice for early prenatal screening for genetic disorders, MRI will likely gain more importance once a certain condition has been suspected. As our knowledge of human genetics is expanding, the definite role of fetal MRI in diagnosis of genetic disorders will depend on correlation of its imaging capabilities with the outcome of genetic testing. Since some genetic disorders are very rare, a concerted effort is needed to correlate phenotypes, seen in fetal MRI, and the genotype obtained by genetic testing (Hengstschlager, 2006). Eventually it may help to replace the need for invasive fetal sampling for certain conditions. Diagnosis of a genetic metabolic disorder by visualization of metabolic pathways using fetal MRI could, for example, void the need for invasive testing and associated risks for the fetus. However the extent to which fetal MRI will help to further improve the outcome of affected fetuses will largely depend on the development of new treatments for fetal anomalies.

References

Badano JL, Katsanis N (2002) Beyond Mendel: an evolving view of human genetic disease transmission. Nat Rev Genet 3:779–789

Baird PA (1987) Measuring birth defects and handicapping disorders in the population: the British Columbia Health Surveillance Registry. CMAJ 136:109–111

Bandyopadhyay R, McCaskill C, Knox-Du BC, Zhou Y, Berend SA, Bijlsma E, Shaffer LG (2003) Mosaicism in a patient with Down syndrome reveals post-fertilization formation of a Robertsonian translocation and isochromosome. Am J Med Genet A 116A:159–163

Battaglia A, Carey JC, Wright TJ (2001) Wolf-Hirschhorn (4p-) syndrome. Adv Pediatr 48:75–113

Benacerraf BR (2005) The role of the second trimester genetic sonogram in screening for fetal Down syndrome. Semin Perinatol 29:386–394

Berry RJ, Buehler JW, Strauss LT, Hogue CJ, Smith JC (1987) Birth weight-specific infant mortality due to congenital anomalies, 1960 and 1980. Public Health Rep 102:171–181

Breathnach FM, Malone FD, Lambert-Messerlian G, Cuckle HS, Porter TF, Nyberg DA, Comstock CH, Saade GR, Berkowitz RL, Klugman S, Dugoff L, Craigo SD, Timor-Tritsch IE,

Carr SR, Wolfe HM, Tripp T, Bianchi DW, D'Alton ME (2007) First- and second-trimester screening: detection of aneuploidies other than Down syndrome. Obstet Gynecol 110:651–657

Carcopino X, Chaumoitre K, Shojai R, Akkawi R, Panuel M, Boubli L, D'ercole C (2007) Foetal magnetic resonance imaging and echogenic bowel. Prenat Diagn 27:272–278

Cerruti MP (2006) Cri du Chat syndrome. Orphanet J Rare Dis 1:33

Chen CP, Chang TY, Liu YP, Chern SR, Wang W (2007) Prenatal magnetic resonance imaging evaluation of a digynic triploid fetus. Taiwan J Obstet Gynecol 46:284–285

Chen CP, Lin SP, Chang TY, Chiu NC, Shih SL, Lin CJ, Wang W, Hsu HC (2002) Perinatal imaging findings of inherited Sotos syndrome. Prenat Diagn 22:887–892

Chinnery PF, DiMauro S, Shanske S, Schon EA, Zeviani M, Mariotti C, Carrara F, Lombes A, Laforet P, Ogier H, Jaksch M, Lochmuller H, Horvath R, Deschauer M, Thorburn DR, Bindoff LA, Poulton J, Taylor RW, Matthews JN, Turnbull DM (2004) Risk of developing a mitochondrial DNA deletion disorder. Lancet 364:592–596

De KB, Albert M, Hillion Y, Ville Y (2002) Prenatal diagnosis of brain abnormalities in Wolf-Hirschhorn (4p-) syndrome. Prenat Diagn 22:366–370

Dill P, Poretti A, Boltshauser E, Huisman TA (2009) 2009. Fetal magnetic resonance imaging in midline malformations of the central nervous system and review of the literature J Neuroradiol 36(3):138–146

DiMauro S, Schon EA (1998) Nuclear power and mitochondrial disease. Nat Genet 19:214–215

Enklaar T, Zabel BU, Prawitt D (2006) Beckwith-Wiedemann syndrome: multiple molecular mechanisms. Expert Rev Mol Med 8:1–19

Fjortoft MI, Sevely A, Boetto S, Kessler S, Sarramon MF, Rolland M (2007) Prenatal diagnosis of craniosynostosis: value of MR imaging. Neuroradiology 49:515–521

Fong KW, Ghai S, Toi A, Blaser S, Winsor EJ, Chitayat D (2004) Prenatal ultrasound findings of lissencephaly associated with Miller-Dieker syndrome and comparison with pre- and postnatal magnetic resonance imaging. Ultrasound Obstet Gynecol 24:716–723

Hahnemann JM, Vejerslev LO (1997) Accuracy of cytogenetic findings on chorionic villus sampling (CVS)–diagnostic consequences of CVS mosaicism and non-mosaic discrepancy in centres contributing to EUCROMIC 1986–1992. Prenat Diagn 17:801–820

Hengstschlager M (2006) Fetal magnetic resonance imaging and human genetics. Eur J Radiol 57:312–315

Hook EB (1981) Rates of chromosome abnormalities at different maternal ages. Obstet Gynecol 58:282–285

Hook EB, Warburton D (1983) The distribution of chromosomal genotypes associated with Turner's syndrome: livebirth prevalence rates and evidence for diminished fetal mortality and severity in genotypes associated with structural X abnormalities or mosaicism. Hum Genet 64:24–27

Horsthemke B, Wagstaff J (2008) Mechanisms of imprinting of the Prader-Willi/Angelman region. Am J Med Genet A 146A:2041–2052

Hoyert DL, Mathews TJ, Menacker F, Strobino DM, Guyer B (2006) Annual summary of vital statistics: 2004. Pediatrics 117:168–183

Kobrynski LJ, Sullivan KE (2007) Velocardiofacial syndrome, DiGeorge syndrome: the chromosome 22q11.2 deletion syndromes. Lancet 370:1443–1452

Kotzot D (2008) Prenatal testing for uniparental disomy: indications and clinical relevance. Ultrasound Obstet Gynecol 31:100–105

Le GM, Doret M, Pasquier JC, Till M, Lebon P, Buenerd A, Escalon J, Gaucherand P (2005) Prenatal diagnosis of Aicardi-Goutieres syndrome. Prenat Diagn 25:28–30

Lehman CD, Nyberg DA, Winter TC III, Kapur RP, Resta RG, Luthy DA (1995) Trisomy 13 syndrome: prenatal US findings in a review of 33 cases. Radiology 194:217–222

Linden MG, Bender BG, Robinson A (1996) Intrauterine diagnosis of sex chromosome aneuploidy. Obstet Gynecol 87:468–475

Longman C, Mercuri E, Cowan F, Allsop J, Brockington M, Jimenez-Mallebrera C, Kumar S, Rutherford M, Toda T, Muntoni F (2004) Antenatal and postnatal brain magnetic resonance imaging in muscle-eye-brain disease. Arch Neurol 61:1301–1306

Low AS, Lee SL, Tan AS, Chan DK, Chan LL (2005) Difficulties with prenatal diagnosis of the Walker-Warburg syndrome. Acta Radiol 46:645–651

Malinger G, Lev D, Lerman-Sagie T (2002) Is fetal magnetic resonance imaging superior to neurosonography for detection of brain anomalies? Ultrasound Obstet Gynecol 20: 317–321

Martin JA, Hamilton BE, Sutton PD, Ventura SJ, Menacker F, Munson ML (2003) Births: final data for 2002. Natl Vital Stat Rep 52:1–113

McEwing RL, Joelle R, Mohlo M, Bernard JP, Hillion Y, Ville Y (2006) Prenatal diagnosis of neurofibromatosis type 1: sonographic and MRI findings. Prenat Diagn 26: 1110–1114

McFadden DE, Langlois S (2000) Parental and meiotic origin of triploidy in the embryonic and fetal periods. Clin Genet 58:192–200

Mochel F, Grebille AG, Benachi A, Martinovic J, Razavi F, Rabier D, Simon I, Boddaert N, Brunelle F, Sonigo P (2006) Contribution of fetal MR imaging in the prenatal diagnosis of Zellweger syndrome. AJNR Am J Neuroradiol 27: 333–336

Muhler MR, Rake A, Schwabe M, Schmidt S, Kivelitz D, Chaoui R, Hamm B (2007) Value of fetal cerebral MRI in sonographically proven cardiac rhabdomyoma. Pediatr Radiol 37:467–474

Mujezinovic F, Alfirevic Z (2007) Procedure-related complications of amniocentesis and chorionic villous sampling: a systematic review. Obstet Gynecol 110:687–694

Nicolaides KH (2005) First-trimester screening for chromosomal abnormalities. Semin Perinatol 29:190–194

Norton ME (2008) Genetic screening and counseling. Curr Opin Obstet Gynecol 20:157–163

Pameijer CR, Hubbard AM, Coleman B, Flake AW (2000) Combined pure esophageal atresia, duodenal atresia, biliary atresia, and pancreatic ductal atresia: prenatal diagnostic features and review of the literature. J Pediatr Surg 35:745–747

Persutte WH, Lenke RR, Kurczynski TW, Brinker RA (1988) Antenatal diagnosis of Pena-Shokeir syndrome (type I) with

ultrasonography and magnetic resonance imaging. Obstet Gynecol 72:472–475

Pooh RK, Nakagawa Y, Pooh KH, Nakagawa Y, Nagamachi N (1999) Fetal craniofacial structure and intracranial morphology in a case of Apert syndrome. Ultrasound Obstet Gynecol 13:274–280

Poretti A, Brehmer U, Scheer I, Bernet V, Boltshauser E (2008) Prenatal and neonatal MR imaging findings in oral-facial-digital syndrome type VI. AJNR Am J Neuroradiol 29: 1090–1091

Pugash D, Brugger PC, Bettelheim D, Prayer D (2008) Prenatal ultrasound and fetal MRI: the comparative value of each modality in prenatal diagnosis. Eur J Radiol 68: 214–226

Robinson JN, Norwitz ER, Mulkern R, Brown SA, Rybicki F, Tempany CM (2001) Prenatal diagnosis of pyruvate dehydrogenase deficiency using magnetic resonance imaging. Prenat Diagn 21:1053–1056

Rubod C, Robert Y, Tillouche N, Devisme L, Houfflin-Debarge V, Puech F (2005) Role of fetal ultrasound and magnetic resonance imaging in the prenatal diagnosis of migration disorders. Prenat Diagn 25:1181–1187

Schwarzler P, Senat MV, Holden D, Bernard JP, Masroor T, Ville Y (1999) Feasibility of the second-trimester fetal ultrasound examination in an unselected population at 18, 20 or 22 weeks of pregnancy: a randomized trial. Ultrasound Obstet Gynecol 14:92–97

Souka AP, Von Kaisenberg CS, Hyett JA, Sonek JD, Nicolaides KH (2005) Increased nuchal translucency with normal karyotype. Am J Obstet Gynecol 192:1005–1021

South ST, Chen Z, Brothman AR (2008) Genomic medicine in prenatal diagnosis. Clin Obstet Gynecol 51:62–73

Staebler M, Donner C, Van RN, Duprez L, De MV, Devreker F, Avni F (2005) Should determination of the karyotype be systematic for all malformations detected by obstetrical ultrasound? Prenat Diagn 25:567–573

Teng SW, Guo WY, Sheu MH, Wang PH (2003) Initial experience using magnetic resonance imaging in prenatal diagnosis of osteogenesis imperfecta type II: a case report. Clin Imaging 27:55–58

van den BC V, OD BH, Wildschut HI, den Hollander NS, Pijpers L, Jan HG, Los FJ (2000) Accuracy of abnormal karyotypes after the analysis of both short- and long-term culture of chorionic villi. Prenat Diagn 20:956–969

von Kleist-Retzow JC, Cormier-Daire V, Viot G, Goldenberg A, Mardach B, Amiel J, Saada P, Dumez Y, Brunelle F, Saudubray JM, Chretien D, Rotig A, Rustin P, Munnich A, De LP (2003) Antenatal manifestations of mitochondrial respiratory chain deficiency. J Pediatr 143:208–212

Wald NJ, Kennard A, Hackshaw A, McGuire A (1997) Antenatal screening for Down's syndrome. J Med Screen 4:181–246

Watson WJ, Miller RC, Wax JR, Hansen WF, Yamamura Y, Polzin WJ (2008) Sonographic findings of trisomy 18 in the second trimester of pregnancy. J Ultrasound Med 27: 1033–1038

Watson WJ, Miller RC, Wax JR, Hansen WF, Yamamura Y, Polzin WJ (2007) Sonographic detection of trisomy 13 in the first and second trimesters of pregnancy. J Ultrasound Med 26:1209–1214

Won RH, Currier RJ, Lorey F, Towner DR (2005) The timing of demise in fetuses with trisomy 21 and trisomy 18. Prenat Diagn 25:608–611

Yoon PW, Olney RS, Khoury MJ, Sappenfield WM, Chavez GF, Taylor D (1997) Contribution of birth defects and genetic diseases to pediatric hospitalizations. A population-based study. Arch Pediatr Adolesc Med 151:1096–1103

Zeger MP, Zinn AR, Lahlou N, Ramos P, Kowal K, Samango-Sprouse C, Ross JL (2008) Effect of ascertainment and genetic features on the phenotype of Klinefelter syndrome. J Pediatr 152:716–722

Maternal Diseases with Possible Impact on Pregnancy

Harald Leitich

Contents

Abstract

› In this chapter, the most relevant maternal diseases with possible adverse effects on pregnancy are briefly reviewed. The choice of maternal disorders covered in this chapter reflects the chances that they may be encountered in daily practice and that they may exhibit prominent features on fetal MR examinations. The topics covered in this chapter are: hypertensive disease, diabetes mellitus, thromboembolic disease, Rhesus alloimmunization, intrauterine infection, syphilis, *Listeria monocytogenes* infection, rubella, Parvovirus B19 infection, Cytomegalovirus infection, Varicella-zoster virus infection, and toxoplasmosis. Genetic diseases will be covered in a specific chapter of this volume and (with the exception of inherited thrombophilias) are not reviewed in this chapter.

H. Leitich
Department of Obstetrics and Gynecology, Medical University of Vienna, Währinger Gürtel 18–20, 1090 Vienna, Austria
e-mail: harald.leitich@meduniwien.ac.at

D. Prayer (ed.), *Fetal MRI*, Medical Radiology,
DOI: 10.1007/174_2010_26, © Springer-Verlag Berlin Heidelberg 2011

1 Hypertensive Disease

1.1 Definition

Arterial hypertension is a symptom of several distinct disorders in pregnancy: Preeclampsia is defined as systolic blood pressure ≥140 mmHg and/or diastolic blood pressure ≥90 mmHg and proteinuria of ≥0.3 g in 24 h with an onset after 20 weeks gestational age, whereas "gestational hypertension" is hypertension without proteinuria. The term "chronic hypertension" is used for hypertension that has been present before 20 weeks gestational age. Preeclampsia may also be superimposed upon chronic hypertension or chronic renal disease.

Severe preeclampsia is defined as systolic blood pressure ≥160 mmHg and/or diastolic blood pressure ≥110 mmHg or as preeclampsia occurring with any of the following signs: proteinuria of ≥5 g in 24 h, neurological symptoms (e.g., vision disturbance, headache), hepatic symptoms (e.g., right upper quadrant pain or elevated liver enzymes), renal symptoms (oliguria), hematological symptoms (thrombocytopenia), or fetal symptoms (growth restriction).

HELLP syndrome is a severe form of hypertensive disease and is characterized by (h)emolysis, (e)levated (l)iver enzymes, and a (l)ow (p)latelet count. HELLP syndrome may develop from preexisting preeclampsia, but may also occur in patients without preceding hypertension.

1.2 Pathogenesis

Preeclampsia appears to originate in early pregnancy from a disturbed invasion of the cytotrophoblast cells into the myometrium, leading to an insufficient remodeling of the spiral arteries and consecutive malperfusion of the placenta (Fig. 1a). As a consequence of placental hypoperfusion, several factors are released into the maternal blood resulting in generalized maternal endothelial dysfunction. Endothelial dysfunction in the kidneys, liver, or central nervous system leads to the typical symptoms of preeclampsia. Placental malperfusion may also lead to fetal growth restriction. Microangiopathic changes include increased turnover of platelets resulting in thrombocytopenia and microangiopathic hemolysis.

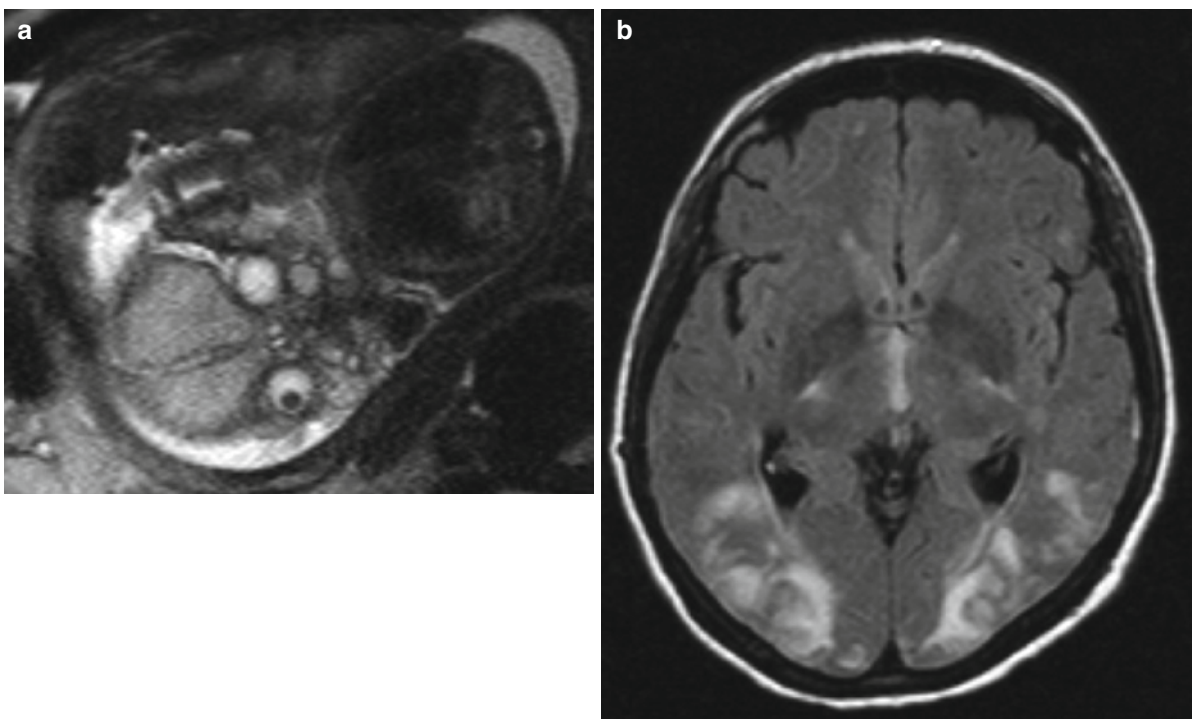

Fig. 1 HELLP syndrome in gestational week 25+1: (**a**) T2-weighted MR image of the placenta, showing hypointense (*dark*) lesions corresponding to venous stasis in some parts of the otherwise normal placenta, (**b**) axial fluid-attenuated inversion recovery MR image of the maternal head: typical hyperintense (*bright*) lesions in the occipital lobes can be detected

1.3 Incidence

Two to eight percent of all pregnancies are complicated by preeclampsia, although large variations exist between different populations (World Health Organization 1988). The course of preeclampsia will be mild in the majority of patients and severe in about a quarter. HELLP syndrome occurs in <0.2% of all pregnancies.

1.4 Clinical Manifestations

Apart from proteinuria, renal findings include decreased glomerular filtration rate, oliguria, elevated plasma creatinine concentration, and hyperuricemia. Epigastric or right upper quadrant pain and elevated transaminases suggest hepatic involvement. The involvement of the central nervous system is suggested by vision disturbances or headache. Radiologically, on MR images manifestations of a posterior reversible leukoencephalopathy syndrome (PRES) may be detected (Fig. 1b). Hematological signs include hemolysis (with elevated lactate dehydrogenase and lowered haptoglobin levels) and thrombocytopenia. Endothelial damage leads to the development of edema and hemoconcentration. Fetal symptoms include intrauterine growth restriction and oligohydramnios.

1.5 Maternal Outcome

The mild forms of hypertensive disease do not pose a threat to maternal health, and only the progression to severe forms with multiorgan involvement may have serious consequences.

In its severest forms, the generalized endothelial dysfunction of maternal blood vessels may lead to hemorrhage and ischemia in target organs, resulting in stroke, intracerebral hemorrhage, subcapsular hepatic bleeding with possible rupture, or renal failure.

1.6 Fetal Outcome

Mild forms of hypertensive disease usually do not compromise fetal well-being.

Fetal risks associated with severe disease include growth retardation, the consequences of prematurity in preterm deliveries, and more rarely, placental abruption.

1.7 Management

The ultimate therapy of hypertensive disease in pregnancy is delivery to avoid progression to more severe forms of hypertensive disease and the increasing probability of fetal and maternal complications associated with severe disease. The exact timing of delivery will depend on the severity of disease and the gestational week. Around term, patients will usually be delivered in due course. In patients remote from term, the risks associated with preeclampsia must be weighed against the risks associated with prematurity. The most severe forms of hypertensive disease, however, will not allow prolongation of pregnancy beyond the 48 h needed to complete fetal lung maturation with corticosteroids.

Fetal surveillance includes serial ultrasound to assess fetal growth and Doppler velocimetry studies and nonstress tests to assure fetal well-being. If fetal compromise is suspected, immediate delivery is indicated except in gestational weeks at or before the threshold of fetal viability.

Antihypertensive treatment does not alter the natural course of hypertensive disease and the treatment of mild hypertension does not improve outcome (Abalos et al. 2007). The primary goal of antihypertensive treatment is to prevent serious cerebral complications in the mother, e.g., cerebral hemorrhage or stroke.

Magnesium sulfate is the drug of choice to prevent eclamptic seizures (Altman et al. 2002).

2 Diabetes Mellitus

2.1 Definition

Glucose tolerance is physiologically diminished in pregnancy, predisposing pregnant women to diabetes mellitus. Diabetes mellitus in pregnant women may be preexisting type 1 or type 2 diabetes or may be first diagnosed in pregnancy ("gestational diabetes mellitus"). Some cases of gestational diabetes may in fact be preexisting type 2 diabetes that was first recognized in pregnancy.

2.2 Pathogenesis

If diabetes is already present in the first trimester, unrecognized hyperglycemia may have teratogenic effects, resulting in an increased rate of miscarriages and congenital anomalies (especially cardiac or central nervous system malformations). Teratogenic effects will almost exclusively occur in women with preexisting diabetes, as gestational diabetes usually does not occur before the second trimester. If diabetes remains untreated during the second and third trimesters, insufficient glycemic control in the mother ultimately leads to fetal hyperglycemia and fetal hyperinsulinemia, i.e., fetal diabetes mellitus (HAPO Study Cooperative Research Group 2008).

2.3 Incidence

Around 1–14% of all pregnancies are affected by gestational diabetes mellitus, depending on the population and diagnostic procedure used (American Diabetes Association 2004), whereas the incidence of women with preexisting disease is much lower.

2.4 Clinical Manifestations and Diagnosis

Maternal manifestations suggesting unrecognized diabetes include obesity, polyuria, and polydipsia. Women with suspected undiagnosed type 2 diabetes should be evaluated as early as possible in pregnancy because of the risk of congenital malformations associated with untreated disease. In women at low risk for diabetes mellitus, screening is recommended between 24 and 28 weeks of gestation. Screening is done with a 75-g oral glucose tolerance test. The upper limit of normal fasting serum glucose concentration is 95 mg/dL, and the limits for serum glucose concentration at 1 or 2 h after the test are 180 or 155 mg/dL, respectively (American Diabetes Association 2004). It should be noted, however, that tests and test thresholds are not uniformly standardized.

2.5 Maternal Outcome

Restoration of adequate glycemic control will avoid many possible adverse consequences of diabetes mellitus and serious efforts should be made to reach this goal. Diabetic mothers are more likely to develop preeclampsia than women with normal glucose tolerance (for details see Sect. 1). Long-term risks include persistent obesity and an increased likelihood to develop type 2 diabetes after pregnancy (Kim et al. 2002).

2.6 Fetal Outcome

The consequences of fetal hyperinsulinemia are macrosomia and polyhydramnios due to fetal polyuria. Fetal macrosomia is a risk factor for an increase in operative deliveries, birth traumata, e.g., shoulder dystocia, and perinatal mortality (HAPO Study Cooperative Research Group 2008; Kjos and Buchanan 1999). On fetal MRI, fetuses of diabetic women may show a thicker subcutaneous fat layer in the third trimester than those of normoglycemic women (Fig. 2). In women with accompanying preeclampsia placental insufficiency may also result in fetal growth restriction. The presence and amount of coexisting vascular damage is a major determinant of fetal outcome. As the most serious consequence, hypoxemia in patients with untreated diabetes may lead to fetal demise. Long-term fetal risks of diabetes in pregnancy include childhood obesity and an increased likelihood to develop type 2 diabetes (Vohr et al. 1999).

2.7 Management

Nutritional advice and prescription of a diet by a professional dietitian are recommended for all women with diabetes mellitus. Also, moderate exercise should be encouraged (Hu et al. 2001). Women with diabetes mellitus should monitor fasting glucose levels in the morning and glucose levels 1-h after each meal, and levels should be below 95 mg/dL (preprandial) or 130 mg/dL (postprandial) (De Veciana et al. 1995). If diet and exercise alone do not keep glucose levels below these thresholds, insulin therapy is recommended (Crowther et al. 2005).

Serial ultrasound examinations are recommended to detect congenital anomalies, macrosomia or growth restriction, and poly- or oligohydramnios. Nonstress tests or Doppler velocimetry examinations are done to assure fetal well-being.

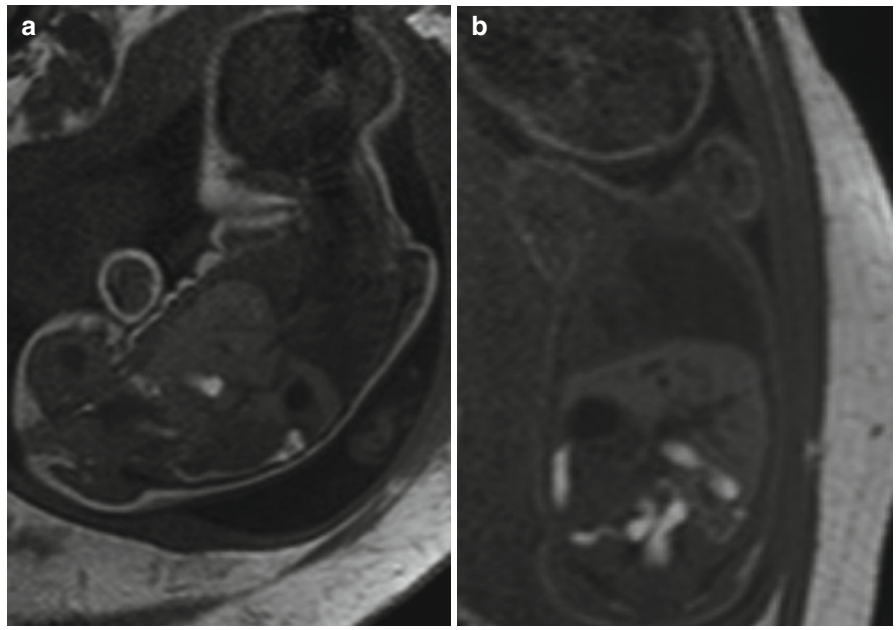

Fig. 2 T1-weighted coronal sections in gestational week 30. (**a**) Fetus of a diabetic woman, (**b**) Fetus of a normoglycemic woman. The hyperintense (*bright*) subcutaneous fat layer is thicker in (**a**) than in (**b**)

Delivery is indicated in cases with macrosomia or nonreassuring fetal tests, with the exact timing of delivery depending on the week of gestation. In general, pregnancies should not be extended beyond 40 weeks of gestation.

3 Thromboembolic Disease

3.1 Pathogenesis

Pregnancy and the associated changes in several coagulation factors induce a procoagulable state predisposing pregnant women to venous thromboembolism (VTE). The risk of VTE is further increased in the presence of inherited thrombophilias or minor risk factors, such as the presence of dilated varicose veins, obesity, smoking, age over 35 years, reduced mobility, and reduced fluid intake. Other major metabolic risk factors include the presence of antiphospholipid antibodies and hyperhomocysteinemia. Known inherited thrombophilias are Factor-V-Leiden mutation, prothrombin gene mutation, protein C and S deficiency, and antithrombin deficiency.

3.2 Incidence

The risk of VTE is estimated to be 5–30-fold in pregnant compared to nonpregnant women, and the total incidence of VTE is between 1:300 and 1:2,500 pregnancies (Heit et al. 2005). VTE is more common after birth than during pregnancy and in patients with cesarean section than in women with vaginal deliveries (Stein et al. 2004). The risk of VTE in patients with inherited thrombophilias or antiphospholipid antibodies is much higher than that in the general population.

3.3 Screening

Women with previous venous or arterial thromboembolism, recurrent miscarriages, stillbirth, severe preeclampsia, HELLP syndrome, or preterm delivery of a small-for-gestational-age infant should be offered diagnostic workup for inherited thrombophilias and the presence of antiphospholipid antibodies. Also, in patients without VTE, but with first-degree relatives with VTE occurring <50 years, genetic workup should be considered (Bates et al. 2008).

3.4 Maternal Outcome

Deep vein thrombosis and pulmonary embolism are the classical manifestations of VTE. Although serious thromboembolic events leading to permanent maternal injury are rare today, they are one of the remaining leading causes of maternal death during pregnancy and the postpartum period. Women with inherited thrombophilias may have an increased risk to develop preeclampsia with its potential consequences (see Sect. 1). Women with antiphospholipid syndrome are predisposed to both venous and arterial thromboembolism in multiple organs, preeclampsia, and HELLP syndrome.

3.5 Fetal Outcome

Spontaneous miscarriages and stillbirths occur more frequently in women with inherited thrombophilias or with antiphospholipid antibodies. Fetal growth restriction (Fig. 3) with or without preeclamsia and placental abruption (Fig. 4) is also found more frequently in this population.

3.6 Management

General recommendations to avoid VTE in pregnancy include adequate fluid intake, avoidance of immobilization, and compression stockings.

Women with previous life-threatening thromboembolism, antiphospholipid syndrome, antithrombin deficiency or previous VTE, and inherited thrombophilias should be offered VTE prophylaxis with low-molecular weight heparin in prophylactic doses from the beginning of pregnancy until 6 weeks after birth (Bates et al. 2008). Heparin prophylaxis is also recommended in patients delivered by cesarean section. Heparin prophylaxis in therapeutic doses may be necessary in patients with previous thromboembolism and antiphospholipid syndrome or multiple inherited thrombophilias. The decision to recommend medical prophylaxis in pregnant women with combinations of minor risk factors will be made on an individual basis.

Fig. 3 Asymmetrical growth restriction, as a consequence of placental dysfunction in gestational week 19. Sagittal echo-planar-weighted section: the misshaped proportions of the fetus (large head and small body) can be recognized. In addition, the placenta shows hypointense (*dark*) regions of venous stasis

4 Rhesus Alloimmunization

4.1 Definition

Rhesus alloimmunization can result from any antigen in the Rhesus system, i.e., the C, c, D, E, and e antigens. Of these, Rhesus(D) alloimmunization is the most important form and will be reviewed in this chapter.

4.2 Pathogenesis

If the immune system of a Rh(D)-negative person is exposed to Rh(D)-positive red blood cells, Rhesus(D) alloimmunization can occur. Rh(D)-positive blood

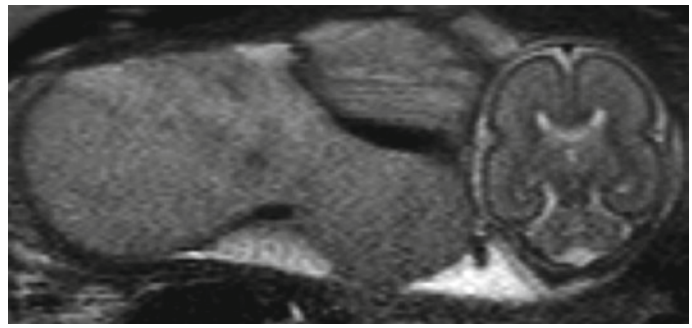

Fig. 4 Placenta abruption in gestational week 23. T2-weighted axial section: an inhomogeneous region with a fluid level, corresponding to hemorrhage, can be seen between the placenta and the uterine wall

cells in women are usually of fetal origin, but may also be the consequence of exposure to Rh(D)-positive cells in blood transfusions or in other circumstances. From 7 gestational weeks onwards, the D antigen is expressed on embryonic red blood cells. Significant amounts of fetal blood cells have been found in maternal blood after situations leading to feto-maternal hemorrhage (see the Sect. 4.6, below). In all of these circumstances, Rhesus(D) alloimmunization may occur.

4.3 Incidence

With the introduction of immunoprophylaxis in Rh(D)-negative women (see the Sect. 4.6, below), the incidence of Rhesus(D) alloimmunization dropped to 0.1% of all pregnancies (Bowman 1988). However, immunoprophylaxis is not universally performed, and effective rates of Rhesus(D) alloimmunization will be substantially higher in some populations.

4.4 Diagnosis

In early pregnancy, maternal blood tests should be done to perform Rh(D) typing and to detect the presence of anti-erythrocyte antibodies. In Rh(D)-negative women, antibody tests should be repeated at least once during the second and third trimester. Rh(D) alloimmunization is diagnosed when anti-Rh(D) antibodies are found in maternal serum.

4.5 Fetal Outcome

Transplacental passage of maternal anti-Rh(D) antibodies into the fetal circulation results in hemolytic anemia in the Rh(D)-positive fetus. As a result of severe anemia in untreated Rhesus(D) alloimmunization, fetal cardiac insufficiency may lead to hydrops fetalis (Fig. 5), and ultimately, fetal demise. If pregnancies with Rhesus(D) alloimmunization are carefully monitored and appropriate interventions are performed in time, the general long-term outcome is favorable.

Fig. 5 Sagittal steady-state free-precession-sequence image showing a fetus in gestational week 22 with hydrops fetalis, consisting of pleural effusions, ascites, and subcutaneous fluid collections. Notice the increased amount of amniotic fluid

4.6 Prevention

Serious efforts should be made to avoid Rh(D) alloimmunization in Rh(D)-negative women, although even the best efforts will not prevent Rh(D) alloimmunization in all situations. Specific recommendations include:

- At 28 weeks of gestation, immunoprophylaxis with anti-D-hyperglobulin is recommended in Rh(D)-negative women (Crowther and Keirse 2000).
- Immunoprophylaxis will be repeated after birth in Rh(D)-negative women, if the child is Rh(D)-positive, because significant feto-maternal hemorrhage occurs during birth (Crowther and Middleton 2000).
- Immunoprophylaxis is also recommended during pregnancy in Rh(D)-negative women if feto-maternal hemorrhage is suspected. Feto-maternal hemorrhage is usually suspected in any invasive procedure during pregnancy (e.g., amniocentesis or chorion biopsy), vaginal bleeding of intrauterine origin, abdominal trauma, miscarriage, pregnancy termination, or ectopic pregnancy (American College of Obstetricians and Gynecologists 1999).

Immunoprophylaxis is not necessary in Rh(D)-negative women, if the fetus is known to be Rh(D)-negative. However, the only way to determine the fetal Rh(D) genotype used to be the collection of fetal cells by amniocentesis or chorion biopsy. New tests that determine the fetal Rh(D) genotype from free fetal DNA circulating in maternal serum will probably change the concept of immunoprophylaxis in the near future.

4.7 Management

Anti-D-titers should be carefully monitored in women with Rhesus(D) alloimmunization. Rising titer levels indicate an increased risk of severe fetal anemia. The best method to predict fetal anemia is the measurement of fetal middle cerebral artery peak systolic velocity by Doppler ultrasound (Moise 2008). The rationale for this method is that the fetus increases cerebral blood flow to ensure sufficient oxygen delivery to the brain. The detection of hydrops fetalis by ultrasound is a definite marker of very severe hemolytic anemia in the fetus. If severe fetal anemia is suspected, the direct measurement of anemia in fetal blood sample by chordocentesis, followed by intrauterine transfusion of blood to the fetus, will be necessary. In the late third trimester, the definite choice of obstetric management of suspected severe fetal anemia will usually be delivery, followed by neonatal treatment of the anemic child.

5 Bacterial Infections

5.1 Intrauterine Infection

5.1.1 Definition

The term “intrauterine infection” is used to describe infection of the placenta, the decidua, the amniotic membranes, the amniotic fluid, or the fetus itself.

5.1.2 Diagnosis

Uterine infection is diagnosed clinically in the presence of maternal fever >38°C, positive laboratory signs of maternal infection, maternal or fetal tachycardia, uterine tenderness, and foul-smelling vaginal discharge. Although the clinical diagnosis of intrauterine infection using these criteria is reliable, most cases of intrauterine infection will remain subclinical. Subclinical intrauterine infection may be diagnosed by performing tests with amniotic fluid gained by amniocentesis. A positive amniotic fluid culture remains the definite proof of intrauterine infection, but other tests, such as Gram stain, glucose concentration, white blood cell concentration, and measurement of cytokines, are helpful too (Gomez et al. 1995).

5.1.3 Incidence

Intrauterine infection is rare in uncomplicated pregnancies at term, but is present in one-third of patients with preterm labor and in one-half of patients with preterm premature rupture of membranes (Yoon et al. 2001).

5.1.4 Pathogenesis

Microorganisms frequently detected in amniotic fluid culture include *Ureaplama urealyticum*, *Mycoplasma hominis*, *Gardnerella vaginalis*, and a mixture of anaerobic bacteria. The presence of bacteria inside the uterine cavity may result in direct damage by bacterial products or in indirect damage by cytokines produced in reaction to bacterial colonization. Also, the presence of bacteria may stimulate preterm labor and lead to premature rupture of the membranes, resulting in preterm birth.

5.1.5 Maternal Outcome

Although the incidence of perinatal maternal infection has decreased dramatically with the introduction of modern antibiotics and severe complications such as septic shock have become rare, intrauterine infection remains one of the leading causes of maternal morbidity and mortality associated with pregnancy and birth. Intrauterine infection may result in postpartum hemorrhage due to uterine atony, postpartum endometritis, or wound infections after cesarean sections.

5.1.6 Fetal Outcome

Infants born after intrauterine infection are prone to develop neonatal infections, such as pneumonia, sepsis, and meningitis. In preterm infants, the production of cytokines, especially tumor necrosis factor, by the fetus itself, appears to induce fetal brain injury, e.g., intraventricular hemorrhage or periventricular leukomalacia. Neurodevelopmental delay and long-term neurological sequelae, such as cerebral palsy, are more common in preterm infants after intrauterine infection (Morales et al. 1987).

5.1.7 Management

Broad spectrum antibiotic therapy is indicated in mothers with intrauterine infection. In women with preterm labor or preterm premature rupture of membranes, there is a high risk of preterm delivery. Therefore, corticosteroid therapy to induce fetal lung maturation is indicated. Careful fetal surveillance with regular nonstress tests is necessary to detect signs of fetal compromise. Delivery is usually indicated when fetal heart rate patterns are not reassuring or if maternal health is threatened. The exact timing of delivery in intrauterine infection is controversial because the neonatal consequences of prematurity associated with earlier delivery must be weighed against the risk of fetal infection with expectant management.

5.2 Syphilis

Although the incidence of syphilis has dropped dramatically with the introduction of penicillin after the Second World War, this chronic infection with *Treponema pallidum* is of particular importance to obstetrics because of the possibility of vertical transmission. Untreated syphilis in pregnancy may result in fetal infection leading to severe adverse outcome, including perinatal death, fetal growth restriction, preterm delivery, and congenital syphilis. It is recommended that all pregnant women are screened for syphilis and that women with syphilis are treated with penicillin regimens appropriate for the respective disease stage.

5.3 Listeria monocytogenes Infection

Pregnant women, especially during the third trimester, are susceptible to be infected by *L. monocytogenes*. Most often, infection is the result of oral ingestion of contaminated food, usually farm products. Unspecific flu-like symptoms, such as fever, chills, and back pain may be the only clinical signs indicating maternal infection. Whereas the infection is usually unproblematic for the mother, vertical transmission to the fetus may have serious consequences. The most severe form of infection, granulomatosis infantiseptica, is characterized by the formation of multiple abscesses in the fetus and usually results in stillbirth. Other adverse effects on pregnancy are an increased risk of preterm birth and listerial infection in the surviving infants. It is recommended that all pregnant women with flu-like symptoms of unknown origin are tested for listerial infection and receive appropriate antibiotic therapy, if necessary.

6 Viral Infections

6.1 Rubella

Rubella infection is generally mild and self-limiting. Symptoms include a characteristic exanthema, preceded by flu-like symptoms, and tenderness of the suboccipital, postauricular, or cervical lymphatic nodes, sometimes followed by rheumatic symptoms. Maternal rubella infection may be transmitted to the fetus with potentially catastrophic consequences. Fetal rubella infection can lead to fetal growth restriction, miscarriage, or stillbirth. In surviving fetuses, classical manifestations are described as congenital rubella syndrome, including growth restriction, microcephaly, cardiac malformations, damages of eyes and ear including cataract and deafness, and mental retardation with persistent deficits. Congenital rubella syndrome only occurs in the first 16–20 weeks of gestation, and fetal Rubella infection in the second half of pregnancy is usually limited to fetal growth restriction (Miller et al. 1982) The incidence of rubella infection has declined dramatically after the introduction of universal Rubella vaccination. Immunity to Rubella, however, is far from universal in pregnant women. All women should be screened for Rubella seroconversion in pregnancy. If Rubella infection is suspected by maternal serologic tests, fetal infection should be confirmed or excluded by direct detection of Rubella virus by PCR in fetal specimen obtained with amniocentesis, chorion biopsy, or chordocentesis. Because fetal infection cannot be treated, pregnancy termination should be offered if fetal infection in the first half of pregnancy has been confirmed.

6.2 Parvovirus B19 Infection

The clinical manifestations of Parvovirus B19 infection are usually mild, but may also be severe in immunocompromised individuals and in patients with hematological disorders. In most cases, Parvovirus B19 infection is a mild childhood disease. Symptoms include a characteristic rash (“erythema infectiosum”), arthralgia, and flu-like symptoms, but infection will often be subclinical. Parvovirus B19 has cytotoxic effects on erythroid progenitor cells. The infection is problematic in pregnancy because transplacental passage may result in fetal infection. Parvovirus B19 appears not to have teratogenic effects, but may damage the fetus seriously by inducing severe fetal anemia. As a result of severe fetal anemia, fetal hydrops and stillbirth may occur. Fetal Parvovirus B19 infection appears to be dangerous if it occurs <20 weeks of gestation and will only rarely lead to stillbirth after this time (Enders et al. 2004). If pregnant women are having symptoms of Parvovirus B19 infection or were exposed to infected individuals, antibody tests from maternal serum should be performed to confirm or exclude maternal infection. If maternal infection is confirmed, fetuses should be carefully monitored for signs of hydrops or fetal anemia (for details on monitoring for and management of fetal anemia see Sects. 4 and 4.7). Because fetal effects of maternal Parvovirus B19 infection may slowly evolve, fetal monitoring should be continued for 8–10 weeks.

6.3 Cytomegalovirus Infection

Cytomegalovirus (CMV) infections are very common and asymptomatic in the majority of cases. If symptoms are present, they are usually unspecific, “flu-like.” CMV virus is only transmitted by direct contact with body fluids of infected persons. CMV may be transmitted vertically to the fetus of infected pregnant women. Long-term outcome of congenital CMV infection is unfavorable. The most severe sequelae result from damages to the fetal central nervous system resulting in poor general neurodevelopmental outcome, hearing and vision loss. If maternal CMV infection is confirmed by serological tests, fetal infection should be ruled in or out by performing amniocentesis for PCR of CMV DNA. Ultrasonographic and/or MR signs of fetal infection include microcephaly, fetal growth restriction, intracranial calcifications, hydrocephalus, hepatomegaly, ascites, and hyperechogenic bowel. The treatment options for fetal CMV infection are limited. Passive immunization is an option, but has not been evaluated in controlled trials yet (Nigro et al. 2005). Because CMV virus is only transmitted by direct contact, all pregnant women should know basic hygienic measures to prevent horizontal transmission. Special emphasis should be put on good personal hygiene, especially hand washing after direct contact with body fluids of children.

6.4 Varicella-Zoster Virus Infection

Primary infection with varicella-zoster virus (VZV), resulting in varicella (chickenpox), is a highly contagious, but usually self-limiting, mild, childhood disease. Clinical features include a typical rash, and preceding unspecific symptoms, like fever and myalgia. Most pregnant women have a history of childhood infection, so that varicella in pregnant women occurs only rarely. If present, maternal varicella may complicate pregnancies in two different ways:

- The classical consequences of fetal infection in pregnancies <24 weeks are summarized as "congenital varicella syndrome," including growth retardation, multiple ocular abnormalities, anomalies of the lower extremities, and mental retardation. Maternal herpes zoster, resulting from reactivation of VZV, does not result in congenital abnormalities (Enders et al. 1994).
- Another, potentially lethal, consequence of fetal VZV infection is neonatal varicella as a result of fetal infection around birth.

If pregnant women get in contact with persons with varicella, maternal immunity should be evaluated by performing serological tests. Patients susceptible for VZV infection should receive passive immunoprophylaxis if the gestational age is <24 weeks. The occurrence of varicella in pregnancy should become rarer in the future with the introduction of varicella vaccine into general vaccination programs.

7 Other Infections

7.1 Toxoplasmosis

Contact with *Toxoplasma gondii*, a common protozoan parasite, occurs mainly in childhood. Primary infection will usually be asymptomatic or with unspecific symptoms, e.g., fever, myalgia, headache, or lymphadenopathy and results in a chronic infection. Although the parasite will never be eliminated in chronically infected persons, it usually remains in a dormant form and will not cause further harm. When primary infection with *Toxoplasma gondii* occurs during pregnancy, maternal-fetal transmission may cause fetal infection. The risk of transmission increases with advancing gestational age and is highest in the third trimester. Fetal infection may cause chorioretinitis, intracranial lesions with calcification, and serious neurological impairment in infancy. Diagnosis of maternal infection is based on serological tests. If maternal infection has been serologically confirmed, amniocentesis to confirm or exclude fetal infection is recommended. The rationale for diagnosing fetal infection is to make the choice between different treatment regimens, e.g., spiramycin vs. pyrimethamine and sulfadiazine. In some European countries, serological tests for *Toxoplasma gondii* are part of a general screening program. General screening, however, is not universally performed because doubts about the long-term benefits of such a screening program persist. Serious efforts should be made to prevent women from acquiring an infection during pregnancy. The main sources of infection are contact with contaminated soil or ingestion of undercooked meat products. Simple preventive measures would, therefore, be careful personal hygiene, especially hand washing after gardening or outdoor activities, and avoidance of eating undercooked meat products.

References

Abalos E, Duley L, Steyn DW et al (2007) Antihypertensive drug therapy for mild to moderate hypertension during pregnancy (Cochrane Review). Cochrane Database Syst Rev (1):CD002252

Altman D, Carroli G, Duley L, Magpie Trial Collaboration Group et al (2002) Do women with pre-eclampsia, and their babies, benefit from magnesium sulphate? The Magpie Trial: a randomised placebo-controlled trial. Lancet 359: 1877–1890

American Diabetes Association (2004) Gestational diabetes mellitus. Diabetes Care 27:s88–s90

Bates SM, Greer IA, Pabinger I et al (2008) American College of Chest Physicians. Venous thromboembolism, thrombophilia, antithrombotic therapy, and pregnancy: American College of Chest Physicians Evidence-Based Clinical Practice Guidelines (8th Edition). Chest 133:S844–S886

Bowman JM (1988) The prevention of Rh immunization. Transfus Med Rev 2:129–150

Crowther CA, Keirse MJ (2000) Anti-D administration in pregnancy for preventing rhesus alloimmunisation. Cochrane Database Syst Rev (2):CD000020

Crowther C, Middleton P (2000) Anti-D administration after childbirth for preventing Rhesus alloimmunisation. Cochrane Database Syst Rev (2):CD000021

Crowther C, Hiller J, Moss J et al; for the Australian Carbohydrate Intolerance Study in pregnant women (ACHOIS) Trila

Group (2005) Effect of treatment of gestational diabetes mellitus on pregnancy outcomes. N Engl J Med 352: 2477–2486

De Veciana M, Major CA, Morgan MA et al (1995) Postprandial versus preprandial blood glucose monitoring in women with gestational diabetes mellitus requiring insulin therapy. N Engl J Med 333:1237–1244

Enders G, Miller E, Cradock-Watson J et al (1994) Consequences of varicella and herpes zoster in pregnancy: prospective study of 1739 cases. Lancet 343:1548–1551

Enders M, Weidner A, Zoellner I et al (2004) Fetal morbidity and mortality after acute human parvovirus B19 infection in pregnancy: prospective evaluation of 1018 cases. Prenat Diagn 24:513–518

Gomez R, Ghezzi F, Romero R et al (1995) Premature labor and intra-amniotic infection. Clinical aspects and role of the cytokines in diagnosis and pathophysiology. Clin Perinatol 22:281–342

American College of Obstetricians and Gynecologists (1999) Prevention of Rh(D) alloimmunization. American College of Obstetricians and Gynecologists Practice Bulletin No 4. American College of Obstetricians, Washington

HAPO Study Cooperative Research Group (2008) Hyperglycemia and adverse pregnancy outcomes. N Engl J Med 358: 1991–2002

Heit JA, Kobbervig CE, James AH et al (2005) Trends in the incidence of venous thromboembolism during pregnancy or postpartum: a 30-year population-based study. Ann Intern Med 143:697–706

Hu FB, Manson JE, Stampfer MJ et al (2001) Diet, lifestyle and the risk of type 2 diabetes mellitus in women. N Engl J Med 345:790–797

Kim C, Newton KM, Knopp RH (2002) Gestational diabetes and the incidence of type 2 diabetes. A systematic review. Diabetes Care 25:1862–1868

Kjos S, Buchanan T (1999) Gestational diabetes mellitus. N Engl J Med 341:1749–1756

Miller E, Cradock-Watson JE, Pollack TM (1982) Consequences of confirmed maternal rubella at successive stages of pregnancy. Lancet 2:781–784

Moise KJ Jr (2008) The usefulness of middlecerebral artery Doppler assessment in the treatment of the fetus at risk for anemia. Am J Obstet Gynecol 198(161):e1–e4

Morales WJ, Washington SR, Lazar AJ (1987) The effect of chorioamnionitis on perinatal outcome in preterm gestation. J Perinatol 7:105–110

Nigro G, Adler SP, La Torre R et al (2005) Passive immunization during pregnancy for congenital cytomegalovirus infection. N Engl J Med 353:1350–1362

Stein PD, Hull RS, Kayali F et al (2004) Venous thromboembolism in pregnancy: 21-year trends. Am J Med 117: 121–125

Vohr BR, McGarvey ST, Tucker R (1999) Effects of maternal gestational diabetes on offspring adiposity at 4-7 years of age. Diabetes Care 22:1284–1291

World Health Organization International Collaborative Study of Hypertensive Disorders of Pregnancy (1988) Geographic variation in the incidence of hypertension in pregnancy. Am J Obstet Gynecol 158:80–83

Yoon BH, Romero R, Moon JB et al (2001) Clinical significance of intra-amniotic inflammation in patients with preterm labor and intact membranes. Am J Obstet Gynecol 185: 1130–1136

Index

D. Prayer (ed.), *Fetal MRI*, Medical Radiology,
DOI: 10.1007/174_2010, © Springer-Verlag Berlin Heidelberg 2011